

AD A 279242

PROCEEDINGS OF 42ND INTERNATIONAL WIRE AND CABLE SYMPOSIUM

—Sponsored by
International Wire and Cable Symposium, Inc. (IWCS)
Eatontown, New Jersey

With Participation by
US Army Communications-Electronics Command (CECOM)
Fort Monmouth, New Jersey

ADAM'S MARK HOTEL
ST. LOUIS, MISSOURI
NOVEMBER 15, 16, 17 and 18, 1993

Accession For	
NTIS	CRA&I <input checked="" type="checkbox"/>
DTIC	TAB <input type="checkbox"/>
Unannounced <input type="checkbox"/>	
Justification _____	
By _____	
Distribution /	
Availability Codes	
Dist	Avail and/or Special
A-1	

APPROVED FOR PUBLIC RELEASE: DISTRIBUTION UNLIMITED

94-13676
905 PG

94 5 05 13 4

**Best
Available
Copy**

MISSION

The International Wire and Cable Symposium provides a forum for the exchange of technical information amongst suppliers, manufacturers, and users on technological advancements in materials, processes, and products used for voice, data and video signal transmission systems.

TECHNICAL PAPERS

Tuesday, November 16, 1993

9:00 am	SESSION 1	Cable User's Needs in an Increasingly Competitive Environment
		<i>Track 1—Fiber Optic Cables</i>
1:00 pm	SESSION 2	Fiber Optic Cable Design
1:00 pm	SESSION 3	Materials Processing & Manufacturing
		<i>Track 2—Copper Cables</i>
1:00 pm	SESSION 4	Manufacturing & Testing of High Performance Copper Cable I
1:00 pm	SESSION 5	Coaxial & Power Cables

Wednesday, November 17, 1993

8:00 am	SESSION 6	<i>Track 1—Fiber Optic Cables</i>
8:00 am	SESSION 7	Fiber Optic Cable Design & Installation
		Fiber Optic Connectors
		<i>Track 2—Copper Cables</i>
8:00 am	SESSION 8	Manufacturing & Testing of High Performance Copper Cable II
8:00 am	SESSION 9	Future Architecture of the Outside Plant
		<i>Track 1—Fiber Optic Cables</i>
2:15 pm	SESSION 10	Extended Fiber Performance & Survivability
		<i>Track 2—Copper Cables</i>
2:15 pm	SESSION 11	Fire Resistance I
2:15 pm	SESSION 12	Copper Durability
4:00 pm	SESSION 13	Poster Papers

Thursday, November 18, 1993

		<i>Track 1—Fiber Optic Cables</i>
8:30 am	SESSION 14	Polarization Mode Dispersion (PMD): Effects on System Performance
8:30 am	SESSION 15	Fiber Optic Coatings I
8:30 am	SESSION 16	Submarine Cables
		<i>Track 2—Copper Cables</i>
8:30 am	SESSION 17	Fire Resistance II
		<i>Track 1—Fiber Optic Cables</i>
1:00 pm	SESSION 18	Fiber Optic Testing & Monitoring
1:00 pm	SESSION 19	Fiber Optic Coatings II

PAPERS

The papers in this volume were printed directly from unedited reproducible copies prepared by the authors. Responsibility for contents rests upon the authors and not the symposium committee or its members. All rights reserved by the International Wire and Cable Symposium, Inc., 174 Main Street, Eatontown, New Jersey 07724.

PROCEEDINGS/PUBLICATIONS

INTERNATIONAL WIRE AND CABLE SYMPOSIUM (IWCS)

Proceedings – Bound – Available from IWCS

31st IWCS Proceedings – 1982 – \$8.00
 32nd IWCS Proceedings – 1983 – \$8.00
 33rd IWCS Proceedings – 1984 – \$10.00
 34th IWCS Proceedings – 1985 – \$10.00

35th IWCS Proceedings – 1986 – \$15.00

39th IWCS Proceedings – 1990 – \$25.00

40th IWCS Proceedings – 1991 – \$35.00

41st IWCS Proceedings – 1992 – \$40.00

42nd IWCS Proceedings – 1993 – \$50.00

Publications – Bound – Available from IWCS

Index of IWCS Papers (1983–1990); PUB #1001RP-1991 – \$15.00

PIC Insulation Testing & Field Experience; PUB #1003RP-1992 – \$25.00

Fiber Optic Cables; PUB #1004RP-1992 – \$25.00

Extra Copies of the 1993 Proceedings: 1–3, \$50.00 per copy; 4–10, \$40.00 per copy;

11 and above \$30.00 per copy

Shipping/Handling:

Proceedings

\$ 7.00 per copy USA only

\$15.00 per copy Surface Mail

(overseas – 4 to 6 weeks)

\$35.00 per copy Airmail (Europe)

\$40.00 per copy for (Asia)

Publications

\$ 3.00 per copy USA Only

\$ 5.00 per copy Surface Mail

(overseas – 4 to 6 weeks)

\$10.00 per copy Airmail

(Europe and Asia)

Payment: Make a check or bank draft payable in U.S. Dollars drawn on U.S. Bank only to the INTERNATIONAL WIRE & CABLE SYMPOSIUM, INC. or use your VISA/MasterCard/AMEX by providing number and expiration date and forward request to: International Wire and Cable Symposium, Inc., 174 Main Street, Eatontown, NJ 07724. Telephone inquiries may be directed to Pat Hudak (908) 389-0990. Prices are subject to change.

Photocopies are available for complete sets of papers for 1964 thru 1992. Information on prices and shipping charges should be requested from the:

US Department of Commerce

National Technical Information Service (NTIS)

Springfield, Virginia 22151

Telephone: (703) 487-4650

Include Title, Year and "AD" Number

13th Annual Wire & Cable Symposium (1964)	— AD 787164
15th Annual Wire & Cable Symposium (1966)	— AD A006601
16th International Wire & Cable Symposium (1967)	— AD 787165
17th International Wire & Cable Symposium (1968)	— AD 787166
18th International Wire & Cable Symposium (1969)	— AD 787167
19th International Wire & Cable Symposium Proceedings 1970	— AD 714985
20th International Wire & Cable Symposium Proceedings 1971	— AD 733399
21st International Wire & Cable Symposium Proceedings 1972	— AD 752908
22nd International Wire & Cable Symposium Proceedings 1973	— AD 772914
23rd International Wire & Cable Symposium Proceedings 1974	— AD A003251
24th International Wire & Cable Symposium Proceedings 1975	— AD A017787
25th International Wire & Cable Symposium Proceedings 1976	— AD A032801
26th International Wire & Cable Symposium Proceedings 1977	— AD A047609
27th International Wire & Cable Symposium Proceedings 1978	— AD A062322
28th International Wire & Cable Symposium Proceedings 1979	— AD A081428
29th International Wire & Cable Symposium Proceedings 1980	— AD A096308
30th International Wire & Cable Symposium Proceedings 1981	— AD A110859
31st International Wire & Cable Symposium Proceedings 1982	— AD A125662
32nd International Wire & Cable Symposium Proceedings 1983	— AD A136749
33rd International Wire & Cable Symposium Proceedings 1984	— AD A152119
34th International Wire & Cable Symposium Proceedings 1985	— AD A164384
35th International Wire & Cable Symposium Proceedings 1986	— AD A180828
36th International Wire & Cable Symposium Proceedings 1987	— AD A189610
37th International Wire & Cable Symposium Proceedings 1988	— AD A200903
38th International Wire & Cable Symposium Proceedings 1989	— AD A216023
39th International Wire & Cable Symposium Proceedings 1990	— AD A233634
40th International Wire & Cable Symposium Proceedings 1991	— AD A244038
41st International Wire & Cable Symposium Proceedings 1992	— AD A259235
Kwic Index of Technical Papers, International Wire & Cable Symposium (1952–1982)	— AD A027588



MESSAGE FROM THE PRESIDENT/DIRECTOR

Another year has swiftly passed and again it's my pleasure on behalf of the International Wire and Cable Symposium (IWCS) Committee and CECOM, Fort Monmouth, New Jersey to welcome each one to what should be another exciting and enlightening experience. I am pleased to report that last year's symposium in Reno, Nevada, attracted more than 1000 attendees, including over 300 from 34 countries outside the USA. In addition, the attendance to the Suppliers Forum and Educational Short Courses were outstanding and the Poster Session as always was a major attraction for nearly all the attendees.

This year's symposium should be just as exciting as last years, with more than 120 papers scheduled for presentation. The two track program with a large number of papers covering both optical and copper cables and the special invited sessions should provide all attendees the opportunity to attend sessions on a variety of subjects of interest. The opening session with four excellent speakers, addressing the subject of "Cable Users Need in an Increasingly Competitive Environment" should be of major interest to all attendees, since the use or non-use of wires and/or cables in a variety of applications will be covered.

Ten education short course are being offered this year, covering subjects that continues to be of interest and several new subjects such as wireless communication and ISO 9000. The suppliers forum and the ever popular poster session completes the program.

The IWCS Committee accepted an invitation to hold its June Meeting in Europe. Several Cable Manufacturers and user organizations in France and Italy were visited. It was an exciting and very successful meeting. This was the committee's third year of accepting an invitation to hold a meeting outside of the USA. Last year the committee held a meeting in Australia and Canada, and prior to that, one was held in Germany. All the meetings have been extremely interesting and informative. The committee plans to visit several cable manufacturers and/or user organizations in Japan next year (1994).

Three members are retiring from the committee this year, namely Dr. Robert Baboian of Texas Instruments, Inc., Dave Fischer of Superior TeleTec and Manuel Santana of AT&T Bell Laboratories. The three have been great workers and strong supporters of the symposium's objectives. I extend to each, the committee's sincere thanks and appreciation for their dedication, cooperation and contribution to the symposium during their four year tenure.

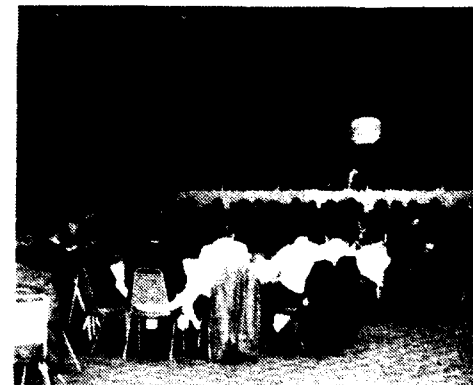
The symposium cannot continue to prosper without the sustained participation and attendance of representatives from the various industrial organizations and government activities. This continued support and financial contributions, has nourished the symposium from its meager beginnings in 1952 to its present prestigious position in the worldwide wire and cable community. Therefore, the committee needs and still solicits the financial support and suggestions from all wire/cable manufacturers-users and material suppliers.

Included on the last page of these proceedings is a Call for Papers for next year's symposium, scheduled for November 14-17 at the Atlanta Hilton Hotel, in Atlanta, Georgia. All authors are encouraged to submit their abstracts early for the committee's review.


ELMER F. GODWIN
President/Director, IWCS

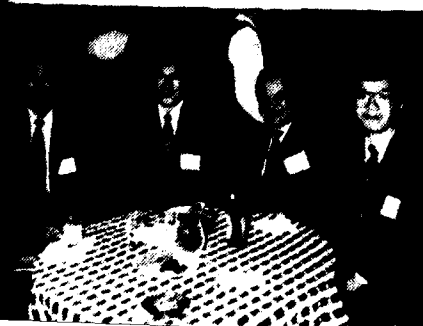
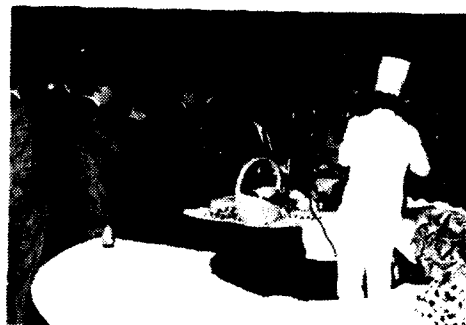
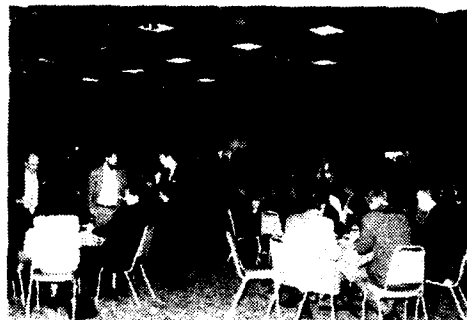


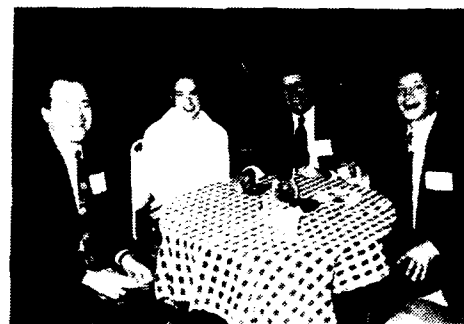
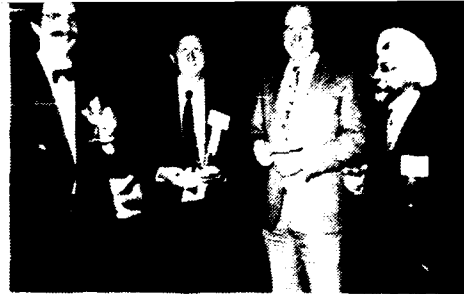
AWARDS





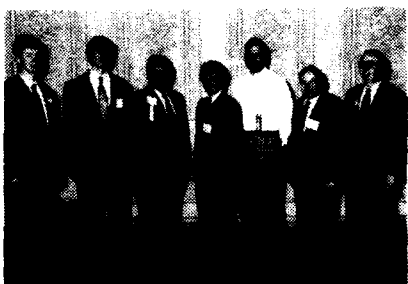
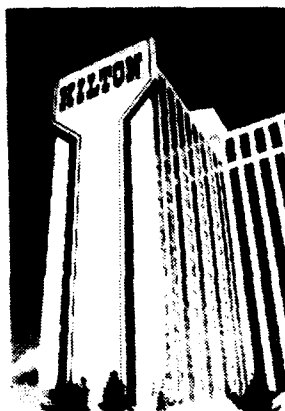
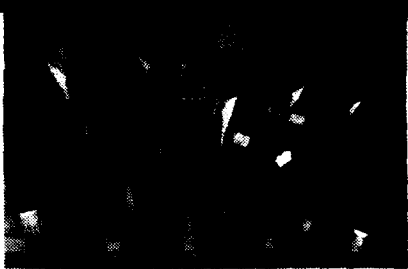
HOSPITALITY HOUR



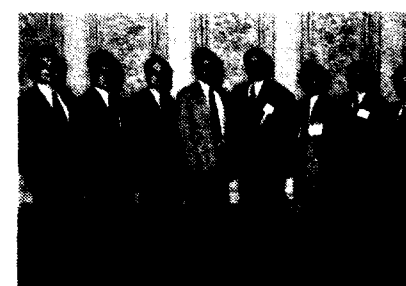
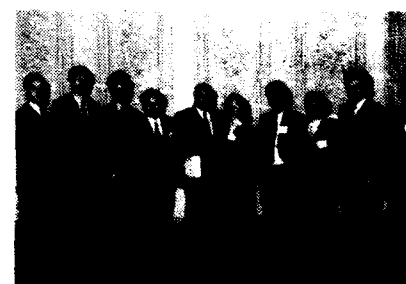
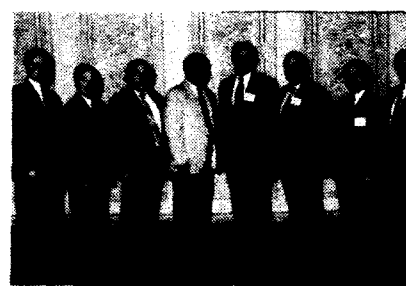


HOSPITALITY HOUR



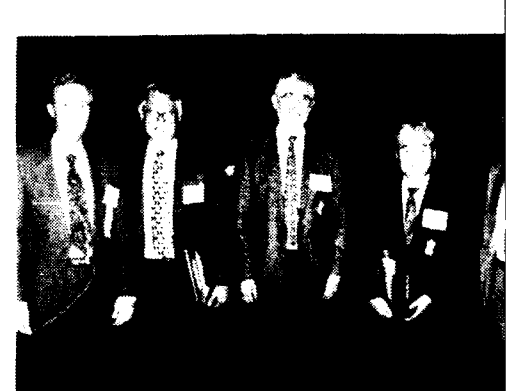


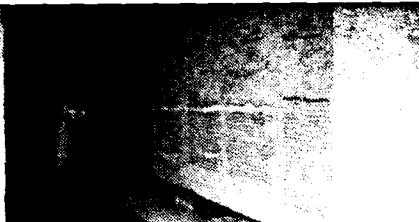
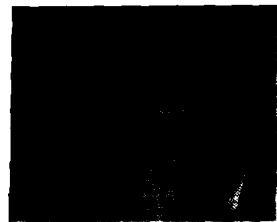
SESSIONS



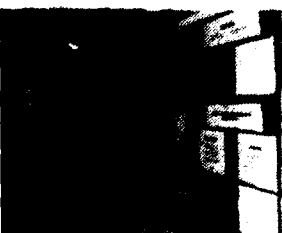
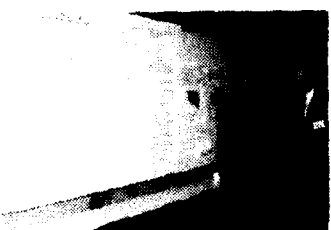
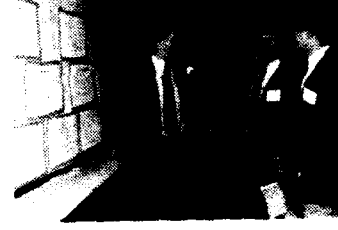
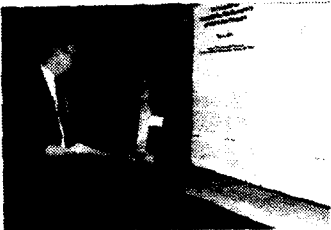
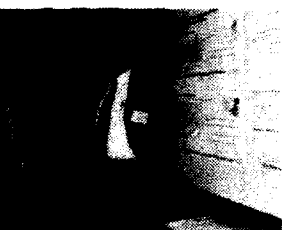
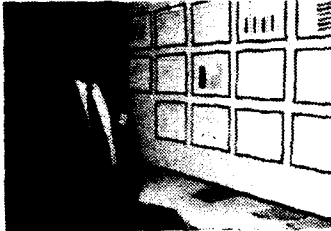
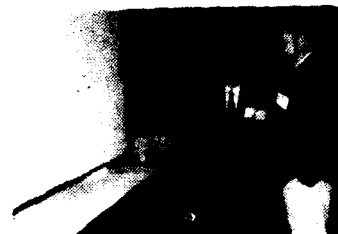


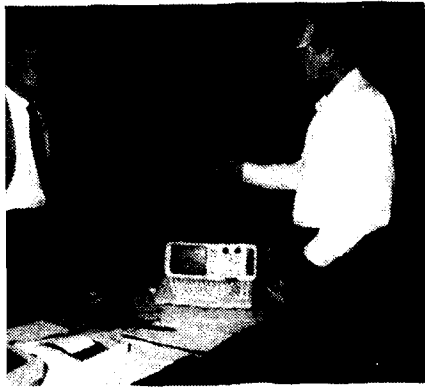
TUTORIAL



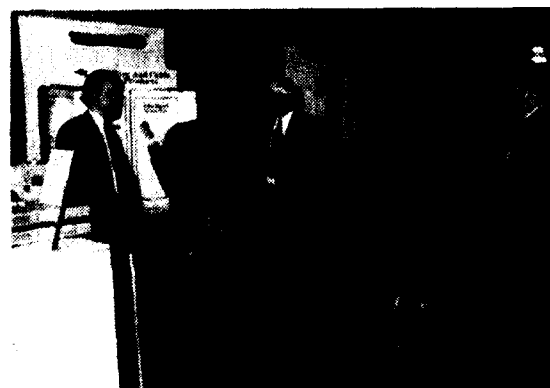


**POSTER
PAPERS**





SUPPLIERS FORUM



AWARDS

Outstanding Technical Paper

- | | |
|--|------|
| H. Lubars and J. A. Olszewski, General Cable Corp. — "Analysis of Structural Return loss in CATV Coaxial Cable" | 1968 |
| J. P. McCann, R. Sabia and B. Wargotz, Bell Laboratories — "Characterization of Filler and Insulation in Waterproof Cable" | 1969 |
| D. E. Setzer and A. S. Windeler, Bell Laboratories — "A Low Capacitance Cable for the T2 Digital Transmission line" | 1970 |
| R. Lyenger, R. McClean and T. McManus, Bell Northern Research — "An Advanced Multi-Unit Coaxial Cable for Toll PCM Systems" | 1971 |
| J. B. Howard, Bell Laboratories — "Stabilization Problems with Low Density Polyethylene Insulations" | 1972 |
| Dr. H. Margin, Kabelmetal — "High Power Radio Frequency Coaxial Cables, Their Design and Rating" | 1973 |
| D. Doty, AMP Inc. — "Mass Wire Insulation Displacing Termination of Flat Cable" | 1974 |
| T. S. Choo, Dow Chemical U.S.A. — "Corrosion Studies on Shielding Materials for Underground Telephone Cables" | 1975 |
| N. J. Cogelia, Bell Telephone Laboratories and G. K. LaVoie and J. F. Glahn, US Department of Interior — "Rodent Biting Pressure and Chemical Action and Their Effects on Wire and Cable Sheath" | 1976 |
| T. K. McManus, Northern Telecom Canada Ltd. and R. Beveridge, Saskatchewan Telecommunications, Canada — "A New Generation of Filled Core Cable" | 1977 |
| F. Suzuki, S. Sato, A. Mori and Y. Suzuki, Sumitomo Electric Industries, Ltd. Japan — "Microcoaxial Cables Insulated with Highly Expanded Polyethylene By Chemical Blowing Method" | 1978 |
| S. Masaki, Y. Yamazaki and T. Ideguchi, Nippon Telegraph and Telephone Public Corporation, Japan — "New Aluminum Sheath Cable Used for Electromagnetic Shielding" | 1979 |
| P. Kish and Y. BeBorgne, Northern Telecom Canada Limited, Montreal, Canada — "General Crosstalk Model For Paired Communication Cables" | 1980 |
| C. J. Arroyo, N. J. Cogelia, Bell Laboratories, and B. J. Darsey, Western Electric — "Thermal Behavior of Experimental Plenum Cable Sheaths Determined in a Radiant Heat Chamber" | 1981 |
| R. H. Whiteley, Raychem Ltd. — "A Comprehensive Small Scale Smoke Test" | 1982 |
| V. A. Gentress, Raychem Corp. and D. V. Nelson, Stanford University — "Fracture Mechanics Evaluation of the Static Fatigue Life of Optical Fibers in Bending" | 1983 |
| M. Fujise and Y. Iwamoto, KDD Research & Development Laboratories, Tokyo, Japan — "Self-Core-Alignment Arc-Fusion Splicer Based on a Simple Local Monitoring Method" | 1984 |
| James A. Krabec and John W. Kincaid, Jr., Belden Technical Research Center — "Advances in the Optimization of Multi-Layer Shield Design" | 1985 |
| Simon D. Dadakarides and Bruce B. Lusignam, Stanford University — "Magnetically Loaded Cables" | 1986 |

Best Presentation

- | | |
|--|--|
| N. Dean, B.I.C.C. — "The Development of Fully Filled Cables for Distribution Network" | |
| J. D. Kirk, Alberta Government Telephones — "Progress and pitfalls of Rural Buried Cable" | |
| Dr. O. Leuchs, Kable and Metalwerke — "A New Self-Extinguishing Hydrogen Chloride Binding PVC Jacketing Compound for Cables" | |
| S. Nordblad, Telefonaktiebolaget L. M. Ericsson — "Multi-Paired Cable of Nonlayer Design for Low Capacitance Unbalance Telecommunications Network" | |
| N. Kojima Nippon Telegraph and Telephone — "New Type Paired Cable for High Speed PCM Transmission" | |
| S. Kaufman, Bell Laboratories — "Reclamation of Water-Logged Buried PIC Telephone Cable" | |
| R. J. Oakley, Northern Electric Co., Ltd. — "A Study Into Paired Cable Crosstalk" | |
| G. H. Webster, Bell Laboratories — "Material Savings by Design in Exchange and Trunk Telephone Cable" | |
| J. E. Wimsey, United States Air Force — "The Bare Base Electrical Systems" | |
| Michael DeLucia, Naval Ship Research and Development — "Highly Fire-Retardant Navy Shipboard Cable" | |
| William L. Schmacher, AMP Inc. — "Design Considerations for Single Fiber Connector" | |
| Richard C. Mondello, Bell Labs. — "Design and Manufacture of an Experimental Lightguide Cable For Undersea Transmission Systems" | |
| I. Wadehra, IBM Corporation — "Performance of Polyvinyl Chloride Communication Cables in Modified Steiner Tunnel Test" | |
| J. J. Refi, Bell Laboratories — "Mean Power Sum Far-End Crosstalk of PIC Cables as a Function of Average Twist Helix Angle" | |
| G. S. Anderson, Belden Corporation — "Installation of Fiber Optic Cable on 457 Meter Tower" | |
| A. Yoshizawa, The Furukawa Electric Co., Ltd. — "Structure and Characteristics of Cables for Robots" | |
| J. R. Bury, Standard Telecommunication Laboratories, Ltd., Hallow, England — "Development of Flame Retardant, Low Aggressivity Cables" | |
| William E. Dennis, Dow Corning Corporation, Midland, Michigan — "Hydrogen Evolving Tendencies of Cable Fillers and Optical Fiber Coatings" | |
| Stephen Hornung, British Telecom Research Laboratories — "Manufacture and Performance of Fibre Units for Installation by The Viscous Drag of Air" | |
| Dave Fischer, Superior Cable Corp. — "Progress Towards the Development of Lighting Test for Telecommunication Cables" | |
| John C. Chamberlain, Siecor Corp. — "Zero Halogen Fire Retardant Fiber Optic Shipboard Cable" | |

Outstanding Technical Paper

1987

Stephen B. Pierce—Conel Laboratories—"Digital Transmission on Customer Premises Wiring"

1988

Martin C. Light Jr., James A. Moses, Mark A. Sigmon and Christopher A. Story—Siecor Corp.—"Design and Performance of Telecommunication Cable Optimized for low Fiber Count"

1989

Michel Plasse, Lise Desroches and Paul-Andre Guilbert - Northern Telecom Canada Limited - "High Performance Twisted-Pair Cable for LAN Systems"

1990

Trevor N. Bowmer, Russell J. Miner, Irene M. Plitz, Joseph N. D'Amico and Lal M. Hore - Bellcore - "Thermal Stability Tests for Polyolefin Insulations"

1991

Shigeru Tomita, Michito Matsumoto, Tetsuro Yabuta and Takuya Uenoya - NTT - "Preliminary Research into Ultra High Density and High Count Optical Fiber Cables"

1992

Nathan E. Hardwick III and Kris Kathiresan - AT&T Bell Laboratories and J.G. Hartley - Georgia Institute of Technology - "Analysis of Fiber Optic Cable Design Conditions in Vicinity of Steam Lines - Ruptured and Pristine"

Outstanding Poster Paper

William Wood—Bell Communication Research—"Performance Analysis of Optic Fiber Cleavers"

Dr. R. Raman - Contel Laboratories—"Loss at Dissimilar Fiber Splices"

Werner Bernard and Susan C. Grant - Siecor Corporation - "Fiber Optic Drop Cables in the Subscriber Loop"

Steve Lischynsky, Helmut Lukas, Robin McIntyre and Grant Pacey - Bell-Northern Research Ltd. - "New Technology for a Single Mode Mechanical Splice"

G. Scott Glaesemann - Corning Inc. - "The Effect of Proof Testing on the Minimum Strength of Optical Fiber"

Svend Hopland and Albert Klykken - Norwegian Telecom - "Installation of Submarine Fiberoptic Cables in Rugged Coastal Terrain"

Best Presentation

Richard Rossi—General Cable Company—"Cable Sheathing Design and Performance Criteria"

Janice B. Haber - AT&T Laboratories—"Single-Mode Media and Apparatus for Fiber to the Home"

Michel de Vecchis - Les Cables de Lyon - "Results on a Large Scale Installation of a Fibre Optic Distribution Network"

Harold W. Friesen - AT&T Bell Laboratories - "An Improved Characteristic Impedance Measurement Technique"

Sue V. Wolfe - STC Submarine Systems - "Structure and High Voltage DC Behaviour of Submarine Cable Mouldings"

Peter Latoszynski - Telecom Australia - "Development of Co-Extruded Polyethylene/Polyamide 12 Insect Resistant Telecommunications Cable"

42ND INTERNATIONAL WIRE AND CABLE SYMPOSIUM (IWCS)

SYMPOSIUM COMMITTEE

ELMER F. GODWIN
(President/Director)
GEF Associates
3A Buttonwood Drive
Shrewsbury, NJ 07702
Office: (908) 389-0990
Fax: (908) 389-0991
Home: (908) 741-8864

Dr. Robert Baboian
Texas Instruments, Inc.
34 Forest Street
MS 10-13
Attleboro, MA 02703
Tel: (508) 699-1350
Fax: (508) 699-3476

Dave Fischer
Superior TeleTec
Suite 300
150 Interstate North Parkway
Atlanta, GA 30339
Tel: (404) 953-8338
Fax: (404) 984-3218

Rene G. Freeman
(Secretary)
Union Carbide Chemicals and Plastics
Company, Inc.
505 North 51st Avenue
Phoenix, AZ 85043
Tel: (602) 233-5904
Fax: (602) 233-5905

Brian D. Garrett
Comm/Scope, Inc.
P.O. Box 879
Claremont, NC 28610
Tel: (704) 459-5003
Fax: (704) 459-5097

IRVING KOLODNY
(Director's Assistant)
80-56 230th Street
Bellerose Manor, NY 11427
Tel & Fax: (718) 464-9197

Dr. Koichi Inada
Fujikura Ltd.
Opto-Electronics Laboratory
1440 Mutsuzaki, Sakura-shi
Chiba-ken, 285 Japan
Tel: 011-81-43-484-3940
Fax: 011-81-43-484-3988

Dr. Felix P. Kapron
Bellcore
445 South Street, MRE- 2K140
Morristown, NJ 07960-6438
Tel: (201) 829-5225
Fax: (201) 829-5965

Dr. Joyce P. Kilmer
Optotec, N.A.A.
21 East 26 St.; Suite 300
New York, NY 10010
Tel: (212) 696-1966
Fax: (212) 696-1961

Inge B. Kovacs
Neste Polymers, Inc.
RR#2, Box 274A
Rockport and Thomas Roads
Port Murray, NJ 07865
Tel: (908) 850-6219
Fax: (908) 850-6268

Xavier Mann
(Vice Chairman)
AT&T Fitel
P.O. Box 486
Carrollton, GA 30117
Tel: (404) 830-6616
Fax: (404) 836-8820

HOMERO VELA
(Chairman)
AT&T Network Cable Systems
505 North 51st Avenue
Phoenix, AZ 85043
Tel: (602) 233-5552
Fax: (602) 233-5798

Dieter S. Nordmann
Kabelmetal Electro
P.O. Box 260
Kebelkamp 20
D30002 Hannover
Germany
Tel: 011-49-511-676-2020
Fax: 011-49-511-676-2664

Richard Rossi
(Treasurer)
General Cable Corp.
160 Fieldcrest Avenue
Edison, NJ 08837
Tel: (908) 417-3132
Fax: (908) 225-3185

Manuel R. Santana
AT&T Bell Laboratories
2000 NE Expressway; Rm 1D32
Norcross, GA 30071
Tel: (404) 798-2754
Fax: (404) 798-4654

Roland H.W. Watkins
Anixter Bros., Inc.
4711 Golf Road
Skokie, IL 60076
Tel: (708) 677-2600
Fax: (708) 677-8557

ADVISORY

Dr. Peter R. Bark
Siecor Corporation
P.O. Box 489
489 Siecor Park
Hickory, NC 28603
Tel: (704) 323-6205
Fax: (704) 323-6264

Leo Chattler
DCM Industries, Inc.
2930 Faber Street
Union City, CA 94587
Tel: (510) 429-9500
Fax: (510) 429-1250

Michael A. DeLucia
Naval Surface Warfare Center
Carderock Div., Annapolis Detach.
Energy R&D Office, Code 859
Annapolis, MD 21402-5067
Tel: (410) 267-3825
Fax: (410) 267-2875

Dave Fallowfield
AGT Limited
Floor 18-H
10020 100 St.
Edmonton, Alberta
Canada T5J 0N5
Tel: (403) 493-5880
Fax: (403) 493-5357

CONSULTANTS

Dr. Reiner J. Gerdes
Gerdes Consulting
812 Oakdale Rd., N.E.
Atlanta, GA 30307-1210
Tel: (404) 377-8608
Fax: (404) 378-5658

Dr. Raymond E. Jaeger
SpecTran Corporation
50 Hall Road
Sturbridge, MA 01566
Tel: (508) 347-2261
Fax: (508) 347-2747

Hans A. Mayer
Olex Cables A Division of Pacific
Dunlop Ltd.
207 Sunshine Road
Tottenham, VIC 3012
Melbourne, Australia
Tel: 011-61-3-316-2240
Fax: 011-61-3-314-1436

TABLE OF CONTENTS

TUESDAY MORNING—9:00 AM—12:00 PM (NOON) St. Louis Ballroom

Announcements/Greetings

Elmer F. Godwin, President/Director, IWCS, Inc., Eatontown, NJ
 Homero Vela, AT&T Network Cable Systems, Phoenix, AZ, Chairman, IWCS
 Joseph J. Pucilowski, Jr., Director, Space and Terrestrial Communications, U.S. Army CECOM, Fort Monmouth, NJ

SESSION 1: CABLE USER'S NEEDS IN AN INCREASINGLY COMPETITIVE ENVIRONMENT

Chairperson: Dr. Joyce P. Kilmer, Optotec, N.A.A., New York, NY

Panelists (Invited Presentations):

Ahmed Laouyane, Chief, Policies, Strategies & Programming, Telecommunications Development Bureau (BDT), Geneva, Switzerland
 Dr. Walter S. Ciciora, Vice President, Technology, Time Warner Cable, Stamford, CT
 Phyllis Cosentino, Technical Manager of International Wireless Systems Engineering, AT&T Bell Laboratories, Naperville, IL
 Kenneth Goodsell, Contract Manager for Fiber Cable, Associated Apparatus and Fiber-in-The-Loop, Southwestern Bell Telephone, St. Louis, MO

TUESDAY AFTERNOON—1:00 PM—5:00 PM

Promenade Ballroom

Salon B

Track 1—Fiber Optic Cables

SESSION 2: FIBER OPTIC CABLE DESIGN

Chairperson: Dr. Peter R. Bark, Siecor Corporation, Hickory, NC

Ultra High-Density Optical Fiber Cable with Thin Coated Fibers and Multi-Fiber Connectors—*S. Tomita, M. Matsumoto, S. Nagasawa, T. Tanifuji*, NTT Telecommunication Corp., Ibaraki, Japan 5

16-Fiber Ribbon for Ultra-High-Density and High-Count Optical Fiber Cable—*M. Saito, S. Okagawa*, The Furukawa Electric Co., Ltd., Chiba-ken, Japan .. 16

A Modular Ribbon Design for Increased Packing Density of Fiber Optic Cables—*K. W. Jackson, M. R. Santana, N. W. Sollenberger*, AT&T Bell Laboratories, Norcross, GA; and *R. J. Brown, K. M. Kroupa, S. H. Webb*, AT&T Network Systems, Norcross, GA 20

The Effect of Fiber Ribbon Component Materials on Mechanical and Environmental Performance—*K. W. Jackson, T. L. Parker, J. R. Petisce, N. W. Sollenberger, C. R. Taylor*, AT&T Bell Laboratories, Norcross, GA 28

Evolving New Technologies for the Italian Optical Cable Plants—*F. Montalti, F. Nanni*, SIP, Roma, Italy; and *F. Caviglia, D. Suino*, CSELT, Torino, Italy. 36

Optical Ground Wire a Worldwide Technical Survey and Comparison—*J. P. Bonicel, S. Pouilly, O. Tatat*, Alcatel Cable, Bezons, France; *C. G. Cortines*, Alcatel Cable Iberica, Maliano, Spain; *J. C. Delomel*, Câbleries de Lens, Lens Cedex, France; and *G. Hög, P. E. Zamzow*, Kabel Rheydt AG, Monchengladbach, Germany 42

TUESDAY AFTERNOON—1:00 PM—5:00 PM Promenade Ballroom

Salon C

SESSION 3: MATERIALS PROCESSING & MANUFACTURING

Chairperson: Mr. Rene G. Freeman, Union Carbide Chemicals and Plastics Company, Incorporated, Phoenix, AZ

Moderator: Mr. Jay Warmke, Building Industry Consulting Service International (BICSI) Tampa, FL

Developing Optimal Processing of Hydrolytically Stabilized PBT for Fiber Optic Cable Core Components—*G. N. Griswold*, GE Plastics, Pittsfield, MA 48

Evaluation of Creep Effects on Jointed and Unjointed Non-Metallic Strength Members in Optical Communication Cables—*V. E. Watson*, Pirelli Cables, Gwent, UK; and *D. Rees, G. White*, University of Glamorgan, Mid Glamorgan, UK 56

Degradation of PP in Jelly-Filled Cables—*P. Hasløv, N. H. Skovgaard*, NKT Elektronik A/S, Broendby, Denmark 65

A Study of Thermal Oxidative Deterioration of Foam-Skin Insulation—*B. D. Oh, Y. S. Kim, J. Y. Hah*, Taihan Electric Wire Co., Ltd., Kyungki-Do, Korea 71

Limitations and Applications of Oxidative Induction Time (OIT) to Quality Control of Polyolefins—*J. R. Pauquet, R. V. Todesco, W. O. Drake*, Ciba-Geigy Ltd., Basel, Switzerland 77

Cable Compounds of Silane-Crosslinkable PVC—*R. Dahl, M. Rogstedt*, Hydro Plast AB, Stenungsund, Sweden 87

TUESDAY AFTERNOON—1:00 PM—5:00 PM

Promenade Ballroom

Salon D

Track 2—Copper Cables

SESSION 4: MANUFACTURING AND TESTING OF HIGH PERFORMANCE COPPER CABLE I

Chairperson: Mr. Brian D. Garrett, Comm/Scope, Incorporated, Claremont, NC

Copper Cables for Local Area Networks With Very High Bit Rate Data Transmission—*S. Richter*, Kabelmetal Electro GmbH, Nürnberg, Germany; and *K. Lehan*, Kabel Rheydt AG, Monchengladbach, Germany 97

Automated Transmission Line Characterization of Balanced Pair Cables—*T. M. Hayes*, Comm/Scope, Inc., Claremont, NC 106

Electronic Drawing Management (Imaging) System in a Copper Cable Manufacturing Facility—*J. E. Maloney*, Butler Service Group, Phoenix, AZ; and *H. Vela*, AT&T Network Cable Systems, Phoenix, AZ ... 113

A Decade of Experience—Review of Polyethylene Insulation Performance Above Ground Installations in Australia—*P. Boes, P. Latoszynski*, Telstra Corp. Ltd., Melbourne, Australia 117

The Temperature of Aerial Plant and Its Effect Upon Foam-Skin Insulation Life—*T. Dougherty*, AT&T Network Cable Systems, Phoenix, AZ; and *E. Gurney*, GTE Telephone Operations, Irving, TX 126

TUESDAY AFTERNOON—1:00 PM—5:00 PM
Promenade Ballroom
Salon E

SESSION 5: COAXIAL & POWER CABLES

Chairperson: Mr. Hans A. Mayer, Olex Cables, A Division of Pacific Dunlop Ltd., Melbourne, Australia

A Contribution to Better Knowledge of RF Coaxial Cables— <i>O. Verbich</i> , VUKI, Bratislava, Slovakia	135
A New High-Power Segmented Semiflexible Coaxial Transmission Line for Use at HF— <i>H. R. Nudd</i> , Andrew Corp., Orland Park, IL	141
Influence of Frequency on the Temperature Rise of Short Circuited Electric Conductors— <i>W. Z. Black</i> , George W. Woodruff School of Mechanical Engineering, Atlanta, GA; and <i>B. B. McWhorter</i> , Thiokol Corp., Brigham City, UT	148
Temperature Monitoring System Using Optical Fiber Sensors for Underground Power Cables— <i>M. Asakawa</i> , <i>Y. Yoshida</i> , Tokyo Electric Power Co., Tokyo, Japan; <i>Y. Ozawa</i> , International Superconductivity Technology Center, Tokyo, Japan; and <i>S. Osawa</i> , <i>H. Kawakami</i> , <i>S. Yamazaki</i> , Hitachi Cable Ltd., Hitachi, Japan	155
Development of Overhead Water Blocked Covered Aluminum Conductors for MV Distribution— <i>E. Buczma</i> , <i>A. Fragale</i> , Olex Cables a Division of Pacific Dunlop Ltd., Melbourne, Australia	164
Submarine Electric Power-Optical Communications Composite Cable— <i>S. Camps</i> , <i>C. Osorio</i> , <i>R. Vasquez</i> , <i>J. A. Olszewski</i> , CABEL Industria Venezolana de Cables Electricos C.A., Valencia, Venezuela	174

WEDNESDAY MORNING—8:00 AM—11:45 AM
Promenade Ballroom
Salon B
Track 1—Fiber Optic Cables

SESSION 6: FIBER OPTIC CABLE DESIGN & INSTALLATION

Chairperson: Mr. Manuel R. Santana, AT&T Bell Laboratories, Norcross, GA

Design and Test of a New Metallic Fibre-Optic Cable for Aerial Cable Ways— <i>A. Fargahi</i> , <i>C. Zehnder</i> , <i>A. Banfi</i> , <i>H. Hagmann</i> , <i>W. Nägele</i> , <i>H. Zimmermann</i> , Brugg Telecom AG, Brugg, Switzerland; <i>D. Schoepke</i> , Brugg Drahtseil AG, Birr, Switzerland; and <i>C. Theodossi</i> , Laser Armor Tech Corp., San Diego, CA	182
Development of a Compact High Fiber Count Intrabuilding Cable— <i>D. Tatarka</i> , <i>E. O. Shiflett</i> , <i>M. R. Ferrell</i> , <i>G. E. Alls</i> , <i>R. C. Roman</i> , Alcoa Fujikura Ltd., Duncan, SC	189
Long-Distance Optical Fiber Cable Installation System Using Automatic Control Puller— <i>S. Genno</i> , <i>S. Yamaguchi</i> , <i>T. Furumiya</i> , NTT Telecommunication, Ibaraki, Japan	194
Cable Installation by Hydrodynamic Drag: Theory and Practice— <i>D. L. Walters</i> , <i>M. J. Parry</i> , BNR Europe Ltd, Essex, England; and <i>C. J. W. Thomson</i> , <i>D. F. Harrison</i> , NT Integrated Networks, Essex, England	202
Mass Fusion Splicing Parameters for Optical Fiber Ribbons— <i>M. Morooka</i> , <i>H. Kawasaki</i> , <i>I. Suzuki</i> , <i>M. Yoshinuma</i> , Fujikura Ltd., Chiba-ken, Japan	212

Protection and Reliability of Single-Fiber and Ribbon-Fiber Fusion Splices—*E. Serafini*, SIRT S.p.A., Milano, Italy

218

WEDNESDAY MORNING—8:00 AM—11:45 AM
Promenade Ballroom
Salon C

SESSION 7: FIBER OPTIC CONNECTORS

Chairperson: Dr. Felix P. Kapron, Bellcore, Morristown, NJ

16-Fiber Optical Connector— <i>J. Yamakawa</i> , <i>H. Yamada</i> , <i>T. Shigematsu</i> , <i>H. Yanagase</i> , <i>K. Kanai</i> , The Furukawa Electric Co., Ltd., Chiba-ken, Japan ..	225
Low-Loss Molded Plastic 16-Fiber Single-Mode Connector— <i>D. O. Harris</i> , <i>D. L. Dean, Jr.</i> , <i>J. R. Merriken</i> , <i>O. I. Szentesi</i> , Siecor Corp., Hickory, NC ..	231
High Fiber Count Optical Connectors— <i>Y. Kikuchi</i> , <i>Y. Nomura</i> , <i>H. Hirao</i> , <i>H. Yokosuka</i> , Fujikura Ltd., Chiba-ken, Japan	238
Development of 16-Fiber Connectors for High-Speed Low-Loss Cable Connection— <i>T. Ueda</i> , <i>H. Ishida</i> , <i>I. Tsuchiya</i> , <i>T. Kakii</i> , <i>T. Yamanishi</i> , Sumitomo Electric Industries, Ltd., Yokohama, Japan	244
Filter-Embedded Optical Connector and Fan-out Cord with High-backreflection— <i>H. Hosoya</i> , <i>K. Asano</i> , <i>M. Akiyama</i> , <i>H. Yokosuka</i> , Fujikura Ltd., Chiba-ken, Japan	250
Fiber Motion in Ceramic-Ferrule Optical Connectors— <i>L. A. Reith</i> , <i>R. A. Frantz</i> , <i>W. W. Wood</i> , Bellcore, Morristown, NJ; and <i>I. M. Plitz</i> , Bellcore, Red Bank, NJ	256
Development of a Non-Blocking Opto-Mechanical Switch— <i>Y. Hayashi</i> , <i>H. Naidu</i> , <i>Y. Nomura</i> , <i>H. Yokosuka</i> , Fujikura Ltd., Chiba-ken, Japan	265

WEDNESDAY MORNING—8:00 AM—11:45 AM
Promenade Ballroom
Salon D
Track 2—Copper Cables

SESSION 8: MANUFACTURING AND TESTING OF HIGH PERFORMANCE COPPER CABLE II

Chairperson: Mr. Roland H. W. Watkins, Anixter Brothers, Inc., Skokie, IL

Performance of Current Local Cable Designs in High Bit Rate Applications— <i>G. D. Maltz</i> , <i>Ch. Chojetzki</i> , <i>J. Schulte</i> , <i>G. Verdenhalven</i> , <i>K. Verlande</i> , Kabelmetal Electro GmbH, Hannover, Germany	270
Transmission Performance of Quadded Wire and Cable for T1 and High Speed Data Services— <i>J.-H. Walling</i> , <i>P. Kish</i> , <i>D. Mercier</i> , Northern Telecom Canada Ltd., Quebec, Canada; and <i>P. S. V. Maddali</i> , Telesector Resources Group, New York, NY	283
TMP Implementation: Can the Program Survive Cost Cutting and Down Sizing?— <i>D. W. Holley</i> , AT&T Network Cable Systems, Phoenix, AZ	296
Assuring the Overall Performance of Copper Cabling Systems— <i>N. A. Sigmon</i> , AMP Inc., Winston-Salem, NC	304
Total Quality Management—A Practical Approach Towards Implementation of a CIM Based Quality Programs in a Modern Telecommunication Cable Plant— <i>M. J. Khan</i> , Saudi Cable Co., Jeddah, Saudi Arabia	310

Advanced Twisted Pair Cable Designs: Field Trial
Validations—*W. Reichert, K. St. Cyr*, Champlain
Cable Corp., Colchester, VT 323

WEDNESDAY MORNING—8:00 AM—11:45 AM
Promenade Ballroom
Salon E

**SESSION 9: FUTURE ARCHITECTURE OF THE OUT-
SIDE PLANT**

Chairperson: Mr. Homero Vela, AT&T Network Cable
Systems, Phoenix, AZ

Local Loop Evolution – Emerging Technologies—*G.
L. Sparks*, GTE Telephone Operations: Irving, TX 329

To Make the Economical Deployment of Subscriber
Networks—*T. Nakayama, H. Okabayashi, S.
Matsushashi*, NTT Telecommunication, Ibaraki,
Japan; and *E. Kondo*, NTT Telecommunication,
Chiba-ken, Japan 339

Network Components and Cables for Effective Fiber
Handling of Star Topology in FTTH Field Trial in
Ballerup, Copenhagen—*H. Olofsson*, Ericsson
Cables AB, Hudiksvall, Sweden; and *J. Meyer*,
Ericsson Telecom AB, Stockholm, Sweden 346

First Large Scale FITL Installation: Experience
From Opal '93—*W. Wenski, H. Dominik, W. Liese,
H. Schönfeld*, Kabelmetal Electro GmbH, Hannover,
Germany 353

Wireless LANs Complement Wired LANs With
Flexible, Mobile Network Solutions—*A. Alavi*,
Motorola, Inc., Schaumburg, IL 365

WEDNESDAY AFTERNOON—11:45 AM—2:15 PM
Awards Luncheon
St. Louis Ballroom
Salons C, D, & E

Admission by badges issued to all registrants

WEDNESDAY AFTERNOON—2:15 PM—5:00 PM
Promenade Ballroom
Salon B

Track 1—Fiber Optic Cables

**SESSION 10: EXTENDED FIBER PERFORMANCE AND
SURVIVABILITY**

Chairperson: Mr. Dave Fischer, Superior TeleTec,
Atlanta, GA

Moderator: Mr. Vasilios E. Kalomiris, US Army CECOM,
Fort Monmouth, NJ

Characteristics of Carbon-Coated Optical Fibers and
Structural Analysis of the Carbon Film—*H. Aikawa,
M. Nakamura, H. Ishikawa, I. Fujita, T. Danzuka*,
Sumitomo Electric Industries, Ltd., Yokohama,
Japan 374

Hermetic Product Performance: Ensuring the
Uniformity of the Carbon Layer—*M. R. Tuzzolo, A.
E. Allegretto*, Corning Inc., Wilmington, NC; and *E.
H. Urruti*, Corning Inc., Corning, NY 381

Study of Microbending Loss in Thin Coated Fibers
and Fiber Ribbons—*K. Kobayashi, J. Baldauf, N.
Okada, K. Ishida, S. Araki, M. Miyamoto*, Opto-
Electronics Laboratory Fujikura Ltd., Chiba-ken,
Japan 386

A Zero-Stress Aging Relationship for Optical Fiber—
J. J. Carr, Corning Inc., Painted Post, NY 394

WEDNESDAY AFTERNOON—2:15 PM—5:00 PM
Promenade Ballroom
Salon D

Track 2—Copper Cables

SESSION 11: FIRE RESISTANCE I

Chairperson: Ms. Inge B. Kovacs, Neste Polymers, Inc.,
Port Murray, NJ

Reduced Corrosive and Lower Smoke Flame
Retardant W&C Formulations—*R. L. Markezich, D.
G. Achbacher*, Occidental Chemical Corp., Grand
Island, NY 400

Testing of Corrosivity of Smoke From Cable
Pyrolysis—*G. Målhammar*, Ericsson Telecom AB,
Stockholm, Sweden; and *C.-G. Ekroth*, Ericsson
Cables AB, Hudiksvall, Sweden 404

Ultraviolet and Oxidative Thermal Degradation
Studies on Flame Retardant Cable Sheathing
Compounds—*S. Rampalli*, Andrew Corp., Orland
Park, IL 410

A Study on Fire-retardant Optical Cable II—*H.
Kanzaki, S. Shimizu, A. Otake*, The Furukawa
Electric Co., Ltd., Chiba-ken, Japan 430

Halogen Versus Non-Halogen Materials for
Telecommunications Wire & Cable. . . What are the
Pros and Cons?—*C. A. Glew*, Gary Corp.,
Leominster, MA 435

WEDNESDAY AFTERNOON—2:15 PM—5:00 PM
Promenade Ballroom
Salon E

SESSION 12: COPPER DURABILITY

Chairperson: Dr. Robert Baboian, Texas Instruments, Inc.,
Attleboro, MA

Corrosion and Corrosion Control of the
Communication Cable Plant—*G. Schick*, Bell
Communications Research, Morristown, NJ 446

Laboratory Test and Field Trial Data of Copper
Cable Protected With Water Absorbent Thixotropic
Gel—*L. E. Davis*, WaterGuard Cable Products, Inc.,
Houston, TX 451

Corrosion Tests for Shielding Materials in Copper
Cable—*G. Haynes, R. Baboian*, Texas Instruments
Inc., Attleboro, MA 458

Corrosion in Submarine Systems and Test Methods
for Evaluation of Long Term Performance—*C. J.
Brown, G. McGurk*, STC Submarine Systems, Ltd.,
Western Docks, Southampton; and *F. C. Walsh, B.
D. Barker*, University of Portsmouth, Portsmouth,
UK 463

WEDNESDAY AFTERNOON—4:00 PM—6:30 PM
St. Louis Ballroom
Salons E & F

SESSION 13: POSTER PAPERS

Chairpersons: Dr. Reiner J. Gerdes, Gerdes Consulting,
Atlanta, GA and Mr. Dieter S. Nordman,
Kabelmetal Electro, Hannover, Germany

Mechanical Lifetime of Optical Fibers—*W. Griffioen*,
PTT Research, Leidschendam, The Netherlands 471

Reliability Testing of Fiber Optic Loose Buffer
Tubes—*J. Eickholt*, Marl, Germany 476

Preform Manufacturing by FCVD (Furnace C.V.D.)
Using Very Large and Precisely Bored Synthetic
Silica Ingots—*G. Le Noane, I. Hardy, P. Grosso, D.
Le Droumaguet*, Lannion, France 479

Keyfactors to Determine the Optimum Balance Between Central and Peripheral Reinforcement of Dielectric Optical Fiber Cables— <i>Th. Bijker, J. J. Bensink, AKZO Aramid Fibers, Arnhem, The Netherlands</i>	487	Performance of Improved Air Blown Fiber System— <i>H. Sano, S. Takaoka, S. Tanaka, N. Suzuki, T. Kumakura, Sumitomo Electric Industries, Ltd., Yokohama, Japan</i>	570
Application of Solvent to the Cure Degree Measurement of UV Curable Optical Fiber Coating— <i>N. Inoue, T. Seki, T. Shiono, H. Matsuura, Showa Electric Wire & Cable Co., Ltd., Kanagawa, Japan</i>	491	Effect of Waterproofing Compound on the Performance of Optical Fiber Ribbon— <i>T.-C. Chang, J.-M. Hsiao, W.-J. Chen, D.-M. Fann, K-y Chen, Y-c Lin, Telecommunication Labs, MOC, Taiwan, Republic of China</i>	578
New Directions in Fiber Optic Splice Storage— <i>W. W. Jones, G. S. Cobb, AT&T Bell Laboratories, Norcross, GA</i>	496	Improved Automatic OTDR Measurement of Fiber-Ribbons or Fiber Bundles Using Ribbon Handling Techniques— <i>J. Piffaretti, B. Jenzer, Cabloptic S.A., Cortaillod, Switzerland</i>	586
A Submarine Fiber Optic Splice Closure for Intermediate Water Depths— <i>G. S. Cobb, W. H. Bensei, H. O. Lindstrom, P. M. Thomas, AT&T Bell Laboratories, Norcross, GA</i>	502	High Durability Couplers— <i>S. Endo, T. Ide, T. Hattori, T. Morrison, T. Wakinosono, Sumitomo Electric Industries, Ltd., Yokohama, Japan</i>	591
Monitoring Accelerated Aging of Polyester Buffer Tubes in Fiber Optic Cables— <i>O. S. Gebizlioglu, I. M. Plitz, Bellcore, Red Bank, NJ</i>	509	New Wide Bandwidth Microwave Leaky Coaxial Cables— <i>K. Watanabe, J. Baldauf, M. Miyamoto, Y. Suzuki, K. Ogawa, Fujikura, Ltd., Chiba-ken, Japan</i>	596
Steel Tube Armoured Fiber Optic Cable Design— <i>D. Lachmann, T. Rödder, Nokia Kabel GmbH, Köln, Germany</i>	516	A Device for Making Connection to MDF Terminating Blocks and Pair Identification System Without Interrupting Data Services on Copper Cables— <i>S. Asakawa, K. Ishikawa, T. Sakaguchi, S. Matsushashi, NTT Telecommunication Corp., Ibaraki, Japan</i>	601
A Study on Reverse Lay Stranding Loose Tube Cable Containing Ribbon Fibers— <i>M. Yamanaka, N. Okada, H. Sawano, M. Miyamoto, Fujikura Ltd., Chiba-ken, Japan</i>	521	Improved Cure Test Techniques for Controlling Wire and Cable Compound Consistency— <i>J. A. Jerdonek, Monsanto Company, Akron, OH</i>	606
Microbend Loss of Colored Optical Fibers Measured Over Extended Temperature Range— <i>Z. Pasturczyk, C. Saravanos, Northern Telecom Canada Ltd., Saskatchewan, Canada</i>	527	Modern Wire and Cable Factor Automation: An Integrated Solution— <i>G. E. Smith, Comm/Scope, Inc., Claremont, NC</i>	611
Effect of Curing Temperature and Thermal History on Mechanical Properties of UV Curable Polyurethane Acrylate for Optical Fiber Coatings— <i>Z. Komiya, Y. Takasugi, T. Ukachi, Japan Synthetic Rubber Co., Ltd., Kawasaki, Japan; and G. Paternack, DSM Desotech, Inc., Elgin, IL</i>	531	Addressing Current and Future Global Requirements for Environmentally Sealed Telecommunications Terminal Systems— <i>J. Pinyan, M. Grice, D. Swan, Raychem Corp., Fuquay-Varina, NC</i>	616
A Non-Rigid Pre-Terminated Closure System for Fiber-in-the-Loop (FITL)— <i>R. G. Sember, J. A. Aberson, Raychem Corp., Fuquay-Varina, NC</i>	536	Cost-Effective Cables for LAN- and FTTH-Applications— <i>B. Behr, P. Brehm, F. Brode, M. Emmerich, H.-U. Müller, KWO Kabel GmbH, Berlin, Germany</i>	621
The Effect of Prolonged UV Exposure on the Properties of Low Smoke, Zero Halogen, Fire Retardant Sheathing Compounds— <i>J. Taylor, J. Preston, D. Sawyer, L. P. Cheng, Lindsay & Williams Ltd., Manchester, England</i>	541	Development of a Jointing/Repair Facility for High Reliability Submarine Cables— <i>S. C. Beech, R. Maxted, STC Submarine Systems Ltd., Southampton, UK</i>	625
Multicomponent Quantitative Determination of Two Antioxidants in ETPR Cable Filling Compound Using Factor Analysis Based on Fourier Transform-Infrared (FTIR) Spectroscopy and the Correlation of Antioxidant Concentrations to the Oxidation Induction Time (OIT)— <i>W. J. Thalman, A. Debska, A. Eckard, J. A. Weaver, Witco Corp., Oakland, NJ</i>	547	<p align="center">THURSDAY MORNING—8:30 AM–12:00 PM (NOON) Promenade Ballroom Salon B Track 1—Fiber Optic Cables</p>	
Effect of Environmental Aging on Optical Fiber Color Codings— <i>J. R. Petisce, M. D. Kinard, S. Siddiqui, C. Taylor, AT&T Bell Laboratories, Norcross, GA</i>	552	SESSION 14: POLARIZATION MODE DISPERSION (PMD): EFFECTS ON SYSTEM PERFORMANCE	
Development of Electronic Wire Harness With Laminated Flexible Flat Cable— <i>T. Yamamoto, T. Ohnuma, T. Enami, H. Yoshinaga, H. Komatsuda, C. Tracey, Fujikura Ltd., Atlanta, GA</i>	557	<i>Chairperson:</i> Dr. Koichi Inada, Fujikura Limited, Chiba-ken, Japan	
Nondestructive Evaluation and Failure Analysis of Mechanical Splices— <i>T. Wei, B. T. Devlin, GTE Laboratories Inc., Waltham, MA</i>	562	PMD Characterization of Production Cables for Critical Lightwave Systems— <i>A. F. Judy, W. T. Greene, J. B. Haber, AT&T Bell Laboratories, Norcross, GA</i>	630
Thermal Strippability of 4- and 12-Fiber Ribbons— <i>J. W. Botelho, Corning Inc., Corning, NY</i>	566	Relation Between Polarization Mode Dispersion and Fiber Core Ovality in Long DSF— <i>K. Kashiwara, S. Aoyagi, H. Nakamura, O. Aso, The Furukawa Electric Co., Ltd., Chiba-ken, Japan</i>	635
		Polarisation Mode Dispersion Measurements and Relevant Theoretical Evaluations on Optical Fibre Ribbon Cables— <i>G. Carones, F. Donazzi, R. Gaspari, A. Ginocchio, Pirelli Cavi S.p.A., Milano, Italy</i>	639

- Extrinsic Stress Effects on Polarization Mode Dispersion in Optical Fiber Cables—*S. Grindstaff, J. Hill, O. Daneshvar*, AT&T Fitel Co., Carrollton, GA ... 647
- PMD Reduction of Optical Fiber Cables for Transoceanic Optical Amplifier Submarine Cable Systems—*Y. Namiyama, T. Kawazawa*, KDD R&D Laboratories, Saitama, Japan; and *N. Norimatsu*, KDD Co. Ltd., Tokyo, Japan 655

THURSDAY MORNING—8:30 AM—12:00 PM (NOON)

**Promenade Ballroom
Salon C**

SESSION 15: FIBER OPTIC COATINGS I

Chairperson: Mr. Xavier Mann, AT&T Fitel, Carrollton, GA

- New Developments in Ultra-Violet Curable Optical Fiber Coatings Based on Vinyl Ether Technology—*J. R. Snyder, G. D. Green, R. J. Swedo*, AlliedSignal Inc., Des Plaines, IL; *C. M. Srivastava*, AlliedSignal Inc., Morristown, NJ; *A. C. Levy, R. J. Kovac*, Alvin Levy & Assoc., Chamblee, GA; and *P. R. Foy*, Rutgers University, Piscataway, NJ 665

- Blends Based on Thermotropic Liquid Crystalline Polymers (TLCP) as Primary Coating of Optical Fibers—*F. Cocchini, I. Ferri, G. Sabbato*, Fos-Fibre Ottiche Sud, Battipaglia, Italy; and *A. Apicella*, University of Naples, Naples, Italy 674

- Liquid Crystal Polymer Coated Fibers With Thermally Stable Delay Time Characteristics—*A. Sano, A. Mogi, K. Suzuki, M. Miyamoto*, Fujikura Ltd., Chiba-ken, Japan 680

- Coating Design of Thin Coated Fiber for Ultra-High-Count Optical Fiber Cable—*K. Oishi, W. Katsurashima, T. Kakuta, Y. Matsuda, S. Tanaka*, Sumitomo Electric Industries, Ltd., Yokohama, Japan 687

- Development and Characterization of Novel UV-Curable Optical Fiber Coatings—*C. P. Chawla, E. S. Poklacki*, DSM Desotech Inc., Elgin, IL 694

- Designing an Optical Fiber Dual Coating System for Loose Tube and Ribbon Cable Long Line and Local Loop Applications—*R. J. Overton, A. R. Lopez*, Alcatel Telecommunications Cable, Roanoke, VA; *C. Lasne*, Alcatel Alsthom Recherche, Marcoussis, France; *H.-M. Michaud*, Alcatel Fibres Optiques, Bezons, France; and *R. G. Sommer*, Kabel Rheydt AG, Moenchengladbach, Germany 701

THURSDAY MORNING—8:30 AM—12:00 PM (NOON)

**Promenade Ballroom
Salon D**

SESSION 16: SUBMARINE CABLES

Chairperson: Mr. Dieter S. Nordmann, Kabelmetal Electro, Hannover, Germany

- Development of a 100-Fiber Submarine Cable—*N. Yoshizawa, T. Tanifuji*, NTT Telecommunication, Ibaraki-ken, Japan 708

- Dispersion Management in Long-Haul Optically Amplified Submarine Systems—*J. N. Russell*, STC Submarine Systems Ltd., Southampton, UK; *N. H. Taylor*, STC Submarine Systems Ltd., London, UK; *K. C. Byron*, BNR Europe Ltd., Harlow, UK; and *I. J. Blewett*, Heriot Watt University, Edinburgh, UK 716

- The Design and Manufacture of Fiber and Cable for Undersea Optical Amplifier Systems—*R. E. Frantz, K. S. Kim, L. J. Marra, M. Spalding Stix, R. D. Tuminaro*, AT&T Bell Laboratories, Holmdel, NJ; and *D. L. Philen*, AT&T Bell Laboratories, Norcross, GA 721

- Expendable Miniature Fiber Optic Cable for Underwater Communications—*J. Rosko, G. Loehfelm, K. Cotton*, Berk-Tek, Inc., Fuquay-Varina, NC 729

- Investigation of Cable Behaviour in Water During Laying of Fiberoptic Submarine Cables—*S. Hopland*, Norwegian Telecom, Oslo, Norway 734

- Plough-Towing Analysis in Submarine Cable Laying—*J. Fang, J. A. Witz*, University College London, London, UK 740

- Development of Fiber Splicing Method for Optical Submarine Cable—*T. Shimobachi, S. Suzuki, H. Hisata*, Ocean Cable Co., Ltd., Yokohama, Japan; and *Y. Tokumaru, T. Yanagi, K. Kashima*, Sumitomo Electric Industries, Ltd., Yokohama, Japan 749

THURSDAY MORNING—8:30 AM—12:00 PM (NOON)

**Promenade Ballroom
Salon E
Track 2—Copper Cables**

SESSION 17: FIRE RESISTANCE II

Chairperson: Mr. Richard Rossi, General Cable Corporation, Edison, NJ

Moderator: Ms. Grace Waag, Union Carbide Corporation, Danbury, CT

- Low Fire Hazard Cables - The European Experience—*J. R. Barker*, BICC Cables, Indianapolis, IN; and *D. E. M. Ness*, BICC Energy Cables, Prescott, UK 757

- Cone Corrosimeter Testing of Fire Retardant and Other Polymeric Materials for Wire and Cable Applications—*D. S. Malin*, Quantum Chemical Corp., Cincinnati, OH 765

- Non-Halogen, Low Smoke Insulation for Low Voltage Telecommunications Power Wire Applications—*F. F. Mekan*, AT&T Power Systems, Dallas, TX 780

- Nonthermal Damage Associated with Wire and Cable Fires—*A. Tewarson*, Factory Mutual Research Corp., Norwood, MA 783

- Performance Characteristics of Low Smoke/Zero Halogen Cables—*B. C. Gentry, T. Cene, J. M. Hesterlee*, Southwire Co., Carrollton, GA 792

THURSDAY AFTERNOON—1:00 PM—5:00 PM

**Promenade Ballroom
Salon B
Track 1—Fiber Optic Cables**

SESSION 18: FIBER OPTIC TESTING AND MONITORING

Chairperson: Dr. Joyce P. Kilmer, Optotec, N.A.A., New York, NY

- 1625 nm Monitoring Systems Design for the Preventive Maintenance of Fiber Optics Plants—*E. Cottino, D. Delleria, S. De Paoli*, AET Telecomunicazioni, Torino, Italy 799

Increasing Productivity of Single and Mass Optical Fiber Splicing When Testing with One-Way OTDR—*W. E. Beasley*, Sumitomo Electric Fiber Optics Corp., Research Triangle Park, NC

Low-Coherence Reflectometer Using Multimode Light Source and Elastic Optical-Fiber Delay Line for Testing Optical-Fiber Connectors—*M. Kobayashi, N. Kuwaki, K. Yoshida*, NTT Telecommunication, Tokyo, Japan

New Technique for Optical Fiber Outside Diameter Measurement and Calibration—*C. Brehm, P. Darbon, B. Minvielle*, Alcatel Alsthom Recherche, Marcoussis, France; and *H. Gagnaire*, Université de St-Etienne, Saint-Etienne, France

Measuring the Endurance of Optical Fibers—*Z. Pasturczyk, M. Ruiz-Vidal, C. Saravanos*, Northern Telecom Canada Ltd., Saskatchewan, Canada

Improvement of the Support System for Subscriber Optical Fiber Cable Operations—*T. Isomura, H. Suzuki, M. Arai, N. Atobe*, NTT Telecommunication, Chiba-shi, Japan

Fiber Optic Measurement Techniques for Improved Product and System Quality Control—*R. G. Gravely III, S. R. Stokes, E. L. Buckland*, Sumitomo Electric Fiber Optics Corp., Research Triangle Park, NC

THURSDAY AFTERNOON—1:00 PM—5:00 PM
Promenade Ballroom
Salon C

SESSION 19: FIBER OPTIC COATINGS II

Chairperson: Dr. Raymond E. Jaeger, SpecTran Corporation, Sturbridge

The Effects of Environment on Ultra-Violet Curable Optical Fibre Coatings—*E. Cressan, P. Andre, D. Crespel, O. Fournier, A. Morgand, A. Peraudeau, Y. Ruello*, France Telecom, Lannion, France

The Effects of Aging on the Discernibility of the Color Identification of Optical Fibers—*R. A. Frantz*, Bellcore, Morristown, NJ; and *I. M. Plitz*, Bellcore, Red Bank, NJ

The Mechanical Performance of Aged Dual-Coated Fibers with Varying Extents of Coating Cure—*H. H. Yuce, R. A. Frantz*, Bellcore, Morristown, NJ; *O. S. Gebizlioglu, I. M. Plitz*, Bellcore, Red Bank, NJ; and *T. T. Volotinen*, Ericsson Cable, Hudiksvall, Sweden

Solvent Swelling of Optical Fiber Coatings as a Diagnostic Measure of Crosslinking—*P. Wiltzius, E. Helfand, D. A. Simoff*, AT&T Bell Laboratories, Murray Hill, NJ; and *D. Tull*, Northwestern University Technological Institute, Evanston, IL

Toward a Zero Loss Change Outside Plant Cable—*S. R. Stokes, P. E. Neveux, Jr., R. G. Gravely, E. L. Buckland*, Sumitomo Electric Fiber Optics Corp., Research Triangle Park, NC

OPENING SPEAKERS



Homero Vela

Manager of Engineering, Phoenix Works
AT&T Network Cable Systems
Phoenix, Arizona

Homero Vela was born in 1951 in Brownsville, TX. He received a Bachelor of Science Degree in Industrial Engineering at the University of Houston in 1978, and began working for AT&T in that same year.

After a series of assignments in Maintenance and Engineering, he became Manager of Engineering in 1989. In this capacity he has been responsible for new product and process developments for the Copper Telephony Business Unit.

Mr. Vela received a Master of Technology Degree from Arizona State University in 1992. His office is located at AT&T Phoenix Works, 505 N. 51st Avenue, Phoenix, Arizona.



Joseph J. Pucilowski, Jr.
Director, Space and Terrestrial
Communications, RD&E Center
U.S. Army Communications-
Electronics Command
Fort Monmouth, New Jersey

Mr. Joseph J. Pucilowski, Jr. was appointed as Director for Space and Terrestrial Communications, U.S. Army Communications-Electronics Command (CECOM), Research, Development and Engineering Center (RDEC) on 27 December 1992. He has command responsibility for formulating, coordinating, managing and implementing internal and external research, development, engineering and support programs to provide the Army with seamless communications across the tactical battlefield, while also providing full technical support to U.S. Army Program Executive Officers and Project Managers in communications.

He was awarded a Bachelor of Arts in Physics, with a minor in mathematics from Rutgers University, and a Master of Science in electrical engineering from Fairleigh Dickinson University. He was appointed by the Secretary of the Army to the Senior Executive Service in November 1986.

Mr. Pucilowski was appointed Acting Deputy Chief of Staff for Concurrent Engineering at the U.S. Army Materiel Command Headquarters from February 1991 to September 1991. In that capacity he had command responsibility for Concurrent Engineering planning and implementation as well as test and evaluation, production base planning and product assurance for AMC.

Mr. Pucilowski began his government career in 1963 as a physicist for the U.S. Atomic Energy Commission. He transferred to Fort Monmouth in 1967 and has held various technical and managerial assignments at Fort Monmouth to include: Director of the Center for Command, Control and Communications (C3) Systems, CECOM RDEC; Director of Product Assurance and Test; Associate Director for Research & Technology, CECOM RDEC; Associate Technical Director for Automation, CECOM RDEC; Associate Director for Information Processing Technology, Center for COMM/ADP; and Deputy Director and Acting Director of the Center for Tactical Computer Systems.

He has served on various NATO panels. Mr. Pucilowski served as President of the Armed Forces Communications-Electronics Association (AFCEA) Fort Monmouth Chapter and as the Chairman of the 14th and 17th Annual AFCEA Symposia. He also serves as an Honorary Advisor Member of the Board of AUSA, Fort Monmouth Chapter. He has been a member of the NJ Dept of Higher Education's Panel on Faculty Development in Telecommunications and Army Member of the Joint Directors of Laboratories Technology Panel on C3.

He has published or presented over thirty-five technical papers. He was recipient of the Presidential Meritorious Rank Award in 1991.

A native of New Jersey, Mr. Pucilowski currently resides in Howell with his wife Maryann. They have six children...Adam, Joseph, Linda Ann, Mary, Kristin and Francine.

TUTORIAL SPEAKERS



Dr. Joyce P. Kilmer
Optotec, N.A.A.
New York, New York

Dr. Joyce P. Kilmer received the Ph.D. degree in electrical engineering from the University of Florida and joined Bellcore as Member Technical Staff of the Optical Cables District in the Fiber Optic Technology Division in 1984. In 1988, he was temporarily reassigned to Fiber Optic Systems District to study the effects of reflections on fiber optic system performance. In 1989, he was promoted to District Manager of the Optical Connector, Splicing and Closures District. In 1990, he became Director of the Optical Cables & Distribution Terminals/Closures Group. In his capacity he was responsible for writing generic requirements, performing product and post-mortem analyses, and developing long term reliability testing of optical fiber, optical fiber cable, and distribution terminals for Fiber-in-the-Loop (FITL). Currently, Dr. Kilmer is the North American agent for Optotec.



Ahmed Laouyane
Chief, Policies, Strategies & Programming
Telecommunications Development Bureau (BDT)
Geneva, Switzerland

Ahmed Laouyane is Chief of the Policies, Strategies and Programming Department within the BDT at the International Telecommunications Union (ITU). A graduate in

mathematics and physics (1962), and telecommunications (1964) he has had a wide national and international career in the engineering, management and development of telecommunications. Ahmed Laouyane served in the Tunisian PTT 1957-1973 as Chief of the Switching Department. In 1972 he joined the ITU as Regional Telecommunications Advisor for West Africa, and in 1977 was transferred to the ITU Headquarters, serving as Head of the Asia Pacific Division and then as Head of the Europe and Middle East Division.

In 1986 he was elected as Deputy Executive Director of the CTD and assumed his current position in January 1991 with the creation of the BDT.



Dr. Walter S. Ciciora
Vice President, Technology
Time Warner Cable
Stamford, CT

Dr. Ciciora is Vice President of Technology at Time Warner Cable. Walt joined American Television and Communications, the predecessor to Time Warner Cable, in December of 1982 as Vice President of Research and Development. Prior to that he was with Zenith Electronics Corporation since 1965. He was Director of Sales and Marketing, Cable Products, from 1981 to 1982. Earlier at Zenith he was Manager, Electronic System Research and Development specializing in Teletext, Videotext and Video Signal Processing with emphasis on digital television technology and ghost canceling for television systems.

He has nine patents issued. He has presented over one hundred papers and published about fifty, two of which have received awards from the Institute of Electrical and Electronic Engineers. Walt wrote a monthly column for Communications

Engineering and Design magazine and for Communications Technology magazine for three years each.

He currently serves on the Executive Committee of the Montreux Television Symposium, and is a member of the board of directors of the Society of Cable Television Engineers, SCTE. He was Chairman of the Technical Advisory Committee of CableLabs for four years and Chairman of the National Cable Television Association, NCTA, Engineering Committee also for four years. He was president of the Institute of Electrical and Electronic Engineers, IEEE, Consumer Electronics Society for two years and is a past chairman of the IEEE International Conference on Consumer Electronics. He chaired the Joint Engineering Committee of the NCTA and the Electronic Industry Association for eight years. He has served on several industry standard-setting committees.

Walt is a Fellow of the IEEE, a Fellow of the Society of Motion Picture and Television Engineers, and a Senior Member of the SCTE. Other memberships include Tau Beta Pi, Eta Kappa Nu, and Beta Gamma Sigma.

Current interests center on competitive technology, the consumer electronics interface with cable, Digital Video Compression, and High Definition Television.

Walt received the 1987 NCTA Vanguard Award for Science and Technology and was named "1990 Man of the Year" by Communications Engineering and Design magazine.

Walt has a Ph.D. in Electrical Engineering from Illinois Institute of Technology dated 1969. The BSEE and MSEE are also from IIT. He received an MBA from the University of Chicago in 1979. He has taught Electrical Engineering in the evening division of IIT for seven years.

Hobbies include helping his wife with her horses, reading, wood working, photography, skiing, and a hope to someday become more active in amateur radio (WB9FPW).



Phyllis Cosentino
Technical Manager of International
Wireless Systems Engineering
AT&T Bell Laboratories
Phoenix, Arizona

Phyllis Cosentino is the Technical Manager of International Wireless Systems Engineering at AT&T Bell Laboratories. She has been involved in the development of wireless registration capabilities, billing features and intersystem networking. She is now responsible for wireless system engineering work for the Asia Pacific and Latin America regions. She received both a Bachelor's and Master's Degree in Electrical Engineering from the University of Michigan. Ms. Cosentino recently received the distinction of being selected Honorable Mention for Eta Kappa Nu's Outstanding Young Electrical Engineer Award. She is a member of the Society of Women Engineers and the I.E.E.E. and joined AT&T Bell Laboratories in 1986.



Kenneth W. Goodsell
Contract Manager
Southwestern Bell Telephone
St. Louis, Missouri

Kenneth W. Goodsell was born in Sioux City, Iowa in 1951. He attended the University of Nebraska. Mr. Goodsell joined Southwestern Bell Telephone in 1973. He has worked in a number of departments over his twenty year career, including coin collection, line work, splicing, Outside Plant Engineering and wire center forecasting.

He is currently the Contract Manager for fiber cable, associated apparatus and Fiber-in-The-Loop. He has been involved in the procurement of fiber products for five years. He has made fiber related presentations at the National Forecasting Conference in 1989 and 1991.



Elaine Viets
St. Louis, Missouri

Pulitzer prize nominee Elaine Viets, who was nominated for her investigative writing, is not just a columnist ... but a humorist as well.

Viets, who resides in St. Louis, Missouri writes a humor column that is distributed to 300 newspapers throughout the Nation. For years, while her column was running, Elaine also did a syndicated travel show on radio. She has traveled throughout the world - doing spots on places to visit and people she has met. Her humor land warm-hearted approach to any issue - whether in newsprint, on radio or during personal appearances - always holds an audience's interest!

Her offbeat look at men and women has ingratiated her to audiences all over the country. Viets speaks about the clothing-impaired male who can't throw away any old clothes. ("My husband was staring at an eighteen-year-old. I said, "aren't you ashamed? Your sweater is older than she is!")

Elaine is presently preparing a prime time television special to be aired on KMOV T.V. She has written three books, including The Viets Guide to Sex, Travel and Anything Else That Will Sell This Book.

When Viets speaks, you'll laugh. You'll also learn about life and yourself.

Ultra High-Density Optical Fiber Cable with Thin Coated Fibers and Multi-Fiber Connectors

Shigeru TOMITA, Michito MATSUMOTO,
Shinji NAGASAWA and Tadatoshii TANIFUJI

NTT Telecommunication Field Systems R & D Center
Tokai, Naka, Ibaraki, 319-11 JAPAN

Abstract

We present the structures and characteristics of five ultra-high density cables with thin coated fibers. These cables can contain stacked 16-fiber ribbons. Most of the cabled fiber characteristics are good except for the attenuation in the corner fibers in the stacked ribbons. When the cables are on a reel, the attenuation of the corner fibers is slightly high compared with that of other fibers. However, when the cables are straightened, this loss is reduced.

Next, we present multi-fiber connectors with 16-fiber ribbons. We measured the connection loss of two kinds of 80-fiber connector. The stacked type connector shows the almost same connection loss as the 16-fiber connector which was presented at the 41st IWCS. The unit type connector has a slightly higher connection loss than the stacked type.

In addition, we present a pre-connectorized cable end which can contain 4000 fibers.

1. Introduction

Fiber To The Home (FTTH) network construction is the biggest problem facing telephone companies. We think that the Single Star (SS) Network which consists simply of optical fibers and connectors, is the most suitable for providing all the various services required by subscribers who use broadband signal services such as B-ISDN (Broadband Integrated Services Digital Network).[1] When we construct this network, very high count optical fiber cables and connectors are needed. We presented the design and performance of a 1500-fiber U-groove unit cable which contains 12-fiber ribbons at the 41st IWCS.[2] However, the fiber count in this cable is not sufficient for FTTH Networks. Therefore, we studied new cables which are designed to contain 4000-

fibers less than 39 mm in diameter. These cables contain ribbons which consist of sixteen thin coated fibers.

Next, we describe the structure and performance of 80-fiber connectors which will be used for the pre-connectorized cable end of high-count cables. There are two kinds of 80-fiber connector called the stacked type and the unit type.

In addition, we present a 4000-fiber cable joint which employs unit type 80-fiber connectors.

2. High-count cable design

The largest optical fiber cable currently used by NTT is 40 mm in diameter. This value should not be exceeded if we wish to continue to use conventional conduits and installation tools.

There are three possible ways of reducing cable diameter. One is to reduce the fiber coating diameter, another is to increase the fiber count in a ribbon and the third is to change the cable design. The third way has already been described in the proceedings of the 41st IWCS. In this paper, we describe cables composed of thin-coated fibers and 16-fiber ribbons.

2.1 Thin-coated fiber

Recently, several studies on thin coated fibers have been published.[3],[4] Major problems with these fibers are their mechanical strength and micro-bending characteristics and we think

that more detailed investigations will be necessary before they can be solved. However, these studies have indicated that it is difficult to use fiber whose coating is less than 0.18 mm in diameter. Therefore, we used fiber with a 0.18 mm diameter coating in this work. The structure is shown in Fig. 1. We adopted a double coating (soft and hard) to reduce the micro-bending sensitivity. The outer diameter of the primary coating was from 0.15 to 0.16 mm. The Young's modulus of the secondary coating was from 2 to 2.5 times higher than that of conventional material to improve the micro-bending and mechanical characteristics.

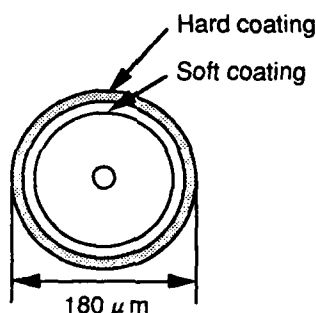


Figure 1 Thin coated fiber

2.2 16-fiber ribbon

The second way to reduce cable diameter is to increase the fiber count in a ribbon. The highest fiber count currently used, is twelve.[5] We manufactured a 16-fiber ribbon (Fig. 2) which consists of thin coated fibers 0.18 mm in diameter as described above. We measured the lateral pressure characteristics of these fiber ribbons. Figure 3 shows that the characteristics are the same as those of conventional fiber ribbons.

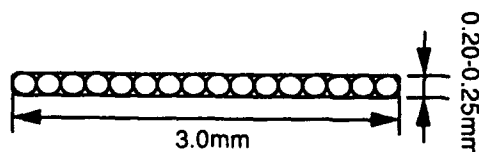


Figure 2 16-fiber ribbon

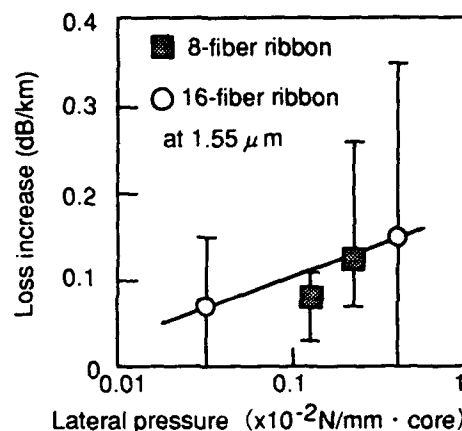


Figure 3 Lateral pressure characteristics of fiber ribbons

2.3 Model cable structure

We studied four cable structures designed to contain 4000 fibers, as shown in Fig. 4(a) to (d).

Figure 4(a) shows a U-groove unit cable as described at the 40th and 41st IWCS.[1],[2] Ten stacked 16-fiber ribbons are contained in one U-groove. Ten U-grooves are stranded in the inner layer and fifteen are stranded in the outer layer.

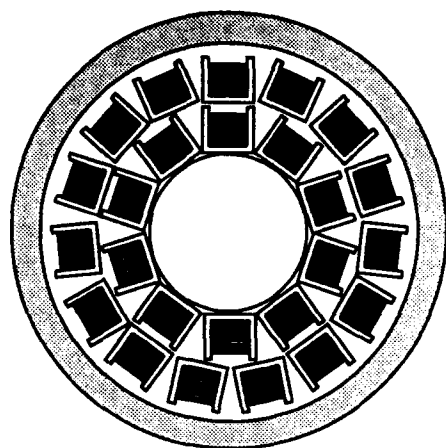
Figure 4(b) shows a slotted-rod cable. Each slotted-rod has five slots which contain ten stacked 16-fiber ribbons. Five slotted-rods are stranded around a central member.

The cable shown in Fig. 4(c) is composed of plastic rods which have only one helical slot and a central member. Ten rods are stranded in the inner layer and fifteen are stranded in the outer layer.

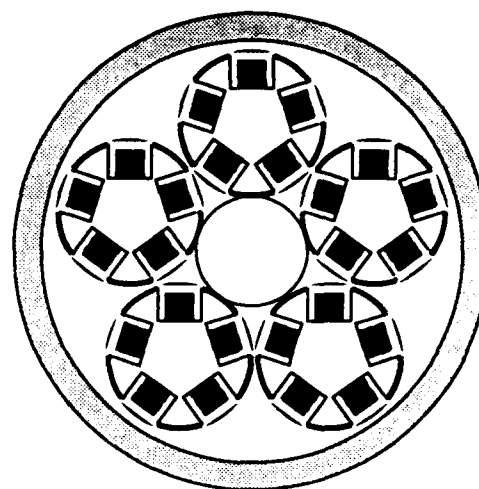
The cable shown in Fig. 4(d) has large U-shaped trays. Fourteen stacked 16-fiber ribbons are stranded in each tray.

The best way to evaluate a cable design is to fabricate actual cables and measure their characteristics. However, it is difficult to manufacture entire cables, because of the limits of currently available manufacturing equipment and resources.

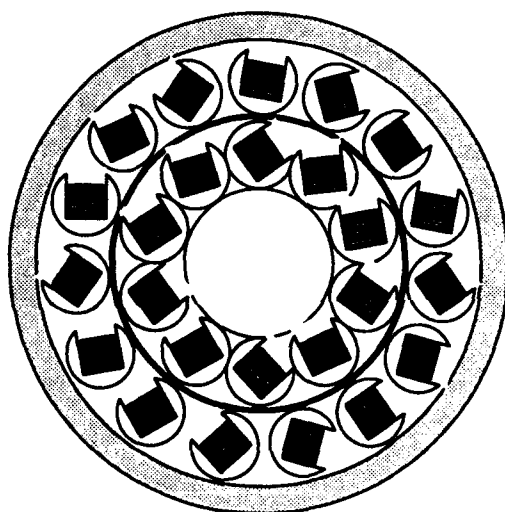
Therefore, we constructed and measured model cables as shown in Fig. 5(a) to (d), which are composed of fundamental components of the 4000-fiber cables shown in Fig. 4.



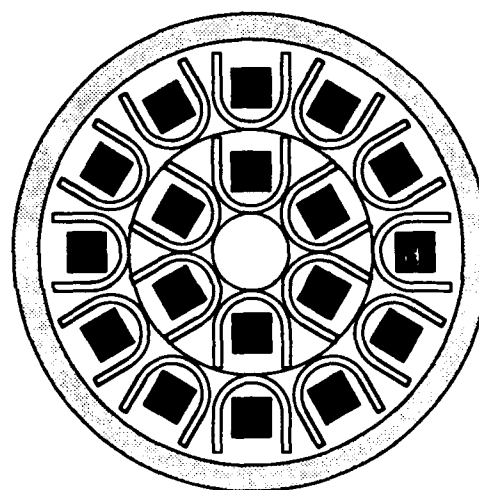
(a) U-groove unit cable



(b) Slotted-rod cable



(c) One slot in a rod cable



(d) Large U-shaped tray cable

Figure 4 Structures of 4000-fiber cables

2.3.1 U-groove unit cable

U-groove unit cable as shown in Fig. 5(a) can contain 1600 fibers and the U-grooves are stranded uni-directionally. We filled two U-grooves with ten stacked 16-fiber ribbons, and measured the attenuation on a reel, lateral pressure, temperature, bending, elongation and squeezing characteristics. The measurement conditions and measured results are shown in Table 1. We carefully examined the attenuation

of the four corner fibers in the ten stacked 16-fiber ribbons. This was because the mechanical forces caused by stranding and cable bending are concentrated in these fibers. At 1550 nm, the attenuation of corner fibers in a cable on a reel is slightly higher than other fibers in the stack.

We also measured an SZ-stranded U-groove unit cable, and found that the results were almost the same as those of the uni-directional stranded cable.

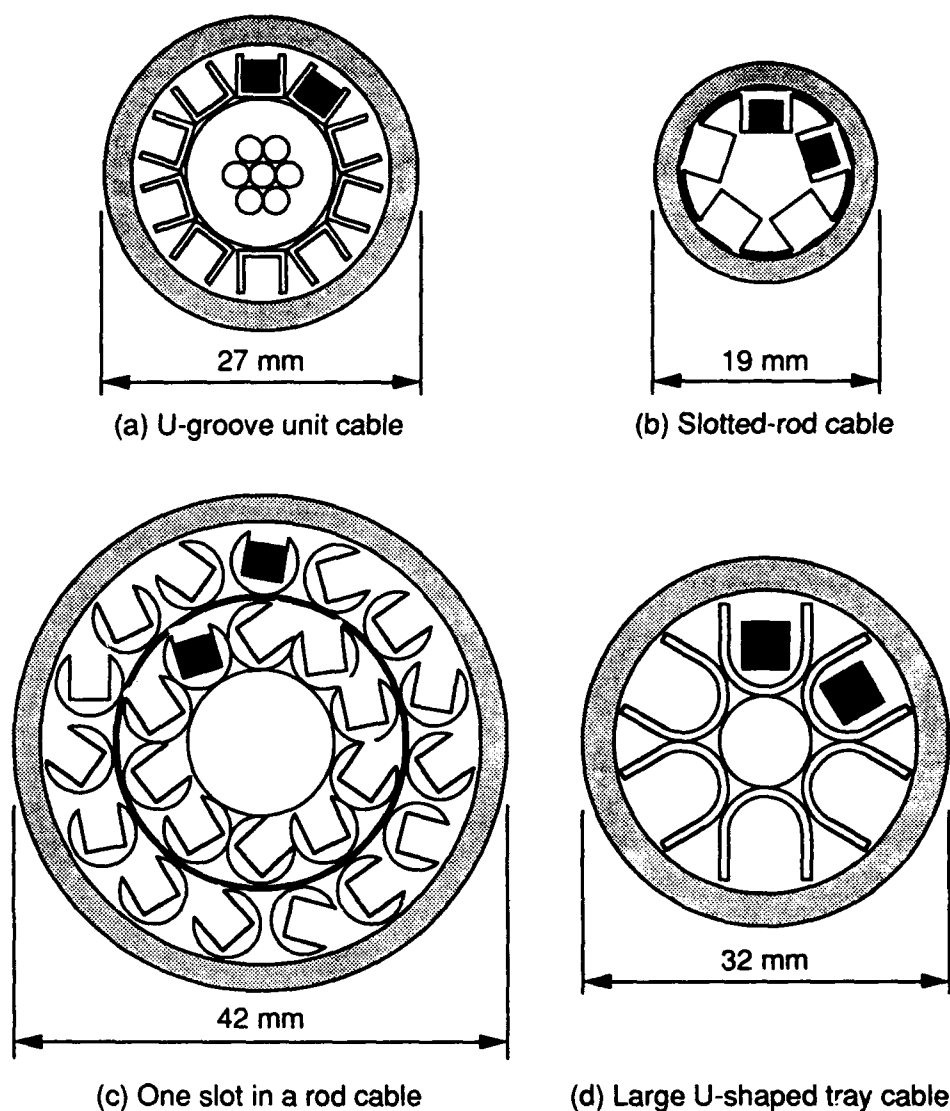


Figure 5 Structures of trial cables

2.3.2 Slotted-rod cable

Figure 5(b) shows a slotted-rod cable which can contain 800 fibers. We filled two slots with ten stacked 16-fiber ribbons, and measured the same characteristics as described in 2.3.1. At 1550 nm, the attenuation of the corner fibers in a cable on a reel was also slightly higher, however these values were lower than those of the U-groove unit and other cables. In Japan, this cable design is the most widely used, therefore the cabling technique has been well developed.[6] This is why the attenuation of this

cable is good.

2.3.3 One slot in a rod cable

Figure 5(c) shows a cross section of another slotted-rod cable which can contain 4000 fibers. The rod in this cable, has only one helical slot. We filled two rods with ten stacked 16-fiber ribbons, and performed the measurements described in 2.3.1. At 1550 nm, again the attenuation of the corner fibers on a reel was slightly higher than that of the other fibers.

Table 1 Characteristics of trial Cables

Test Items			U-groove	Slotted rod	One slot	Large U
Attenuation at 1310 nm (1 km)	on the reel	except corners	0.35 dB (ave.)	0.33 dB (ave.)	0.35 dB (ave.)	0.35 dB (ave.)
		corner fibers	0.40 dB (ave.)	0.36 dB (ave.)	0.39 dB (ave.)	0.34 dB (ave.)
	off the reel	except corners	0.33 dB (ave.)	0.30 dB (ave.)	0.31 dB (ave.)	0.31 dB (ave.)
		corner fibers	0.35 dB (ave.)	0.32 dB (ave.)	0.33 dB (ave.)	0.35 dB (ave.)
Attenuation at 1550 nm (1 km)	on the reel	except corners	0.24 dB (ave.)	0.20 dB (ave.)	0.24 dB (ave.)	0.19 dB (ave.)
		corner fibers	0.40 dB (ave.)	0.23 dB (ave.)	0.33 dB (ave.)	0.27 dB (ave.)
	off the reel	except corners	0.22 dB (ave.)	0.20 dB (ave.)	0.23 dB (ave.)	0.23 dB (ave.)
		corner fibers	0.27 dB (ave.)	0.22 dB (ave.)	0.23 dB (ave.)	0.22 dB (ave.)
Temperature characteristics (from -20 to 60 °C)			increase in loss < 0.1 dB/km	increase in loss < 0.1 dB/km	maximum loss increase 2.0 dB/km	increase in loss < 0.1 dB/km
Bending (at 300mm radius)			increase in loss < 0.1 dB	increase in loss < 0.1 dB	increase in loss < 0.1 dB	increase in loss < 0.1 dB
Lateral pressure (10000N/500mm)			increase in loss < 0.1 dB	increase in loss < 0.1 dB	increase in loss < 0.1 dB	increase in loss < 0.1 dB
Tensile (0.2% elongation)			increase in loss < 0.1 dB	increase in loss < 0.1 dB	increase in loss < 0.1 dB	increase in loss < 0.1 dB
Squeezing (0.2% elongation, 600mm radius)			increase in loss < 0.1 dB	increase in loss < 0.1 dB	increase in loss < 0.1 dB	increase in loss < 0.1 dB

2.3.4 Large U-shaped tray cable

The cross section of another high-density cable is shown in Fig. 5(d). Fourteen stacked 16-fiber ribbons are stranded and contained in a large U-shaped tray. We filled two such trays, and performed the measurements described in 2.3.1. We again found that the corner fiber attenuation on a reel was slightly higher than that of the other fibers.

2.4 4000-fiber cable with U-groove units

Although we found that fibers at the four corners exhibit slightly high attenuation, the characteristics of the slotted-rod cable indicated that these losses will be reduced by improving manufacturing techniques. Of the

four structures described above the U-groove unit cable offers the highest fiber density. Therefore, we manufactured a U-groove unit cable which can contain 4000 fibers as shown in Fig. 6. We filled one U-groove unit in the outer and inner layers with ten stacked 16-fiber ribbons. The measured characteristics are shown in Figs. 7 and 8 and in Table 2.

(1) Attenuation

As shown in Fig. 7, the attenuation of the four corner fibers is also slightly high, because the cabling technique has yet to be optimized.

(2) Temperature

Figure 8 shows the loss variation due to temperature change. The loss variation is less than 0.05 dB/km in the -30 to +60 °C

temperature range. This value is almost same as that of conventional optical fiber cables.

(3) Bending

The cable was bent with a radius ranging from 200 to 600 mm and the loss increase and maximum elongation were measured. There were no loss increases in this bending radius range.

(4) Crushing

There was no loss increase with a crushing force of up to 10000 N applied to 500 mm of cable.

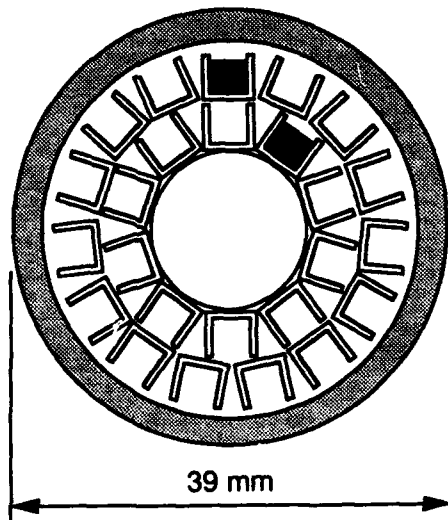
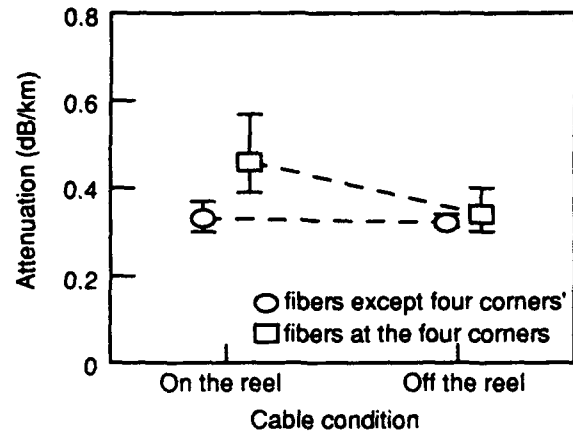


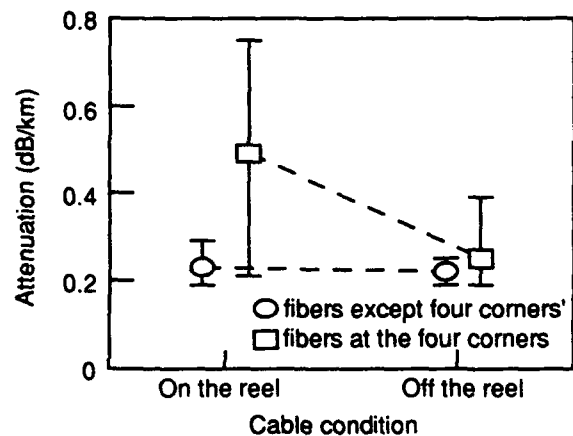
Figure 6 4000-fiber trial cable

Table 2 Characteristics of 4000-fiber cable

Test Items	Results
Bending (at 300mm radius)	increase in loss < 0.1 dB
Lateral pressure (10000N/500mm)	increase in loss < 0.1 dB
Tensile (8000N)	increase in loss < 0.1 dB
Squeezing (8000 N, 600 mm radius)	increase in loss < 0.1 dB



(a) Attenuation at 1310 nm



(b) Attenuation at 1550 nm

Figure 7 Optical attenuation of 4000-fiber trial cable on and off the reel

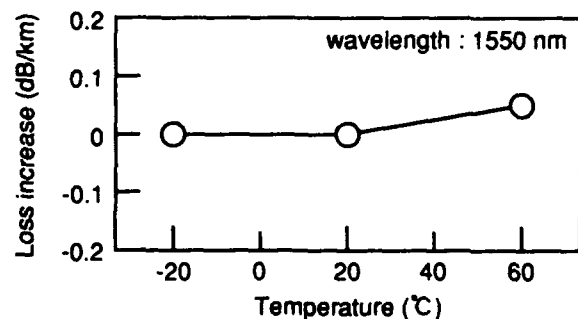


Figure 8 Temperature characteristics of 4000-fiber cable

(5) Tension

There was no loss increase, when a 36 m long cable was subjected to a pulling force of up to 10000 N.

(6) Squeezing

There was no loss increase when the cables were squeezed across a mandrel with a radius of 600 mm and a pulling force of up to 8000 N.

2.5 Next step

There were no problems with the 4000-fiber U-groove unit cable other than the loss in the fibers at the four corners of stacked ribbons. As mentioned above, this problem is closely related to cabling techniques. Therefore, we believe that it will be possible to overcome this problem and manufacture in the near future.

There is another problem related to thin coated fibers. Because their coating is very thin, they are more easily damaged during the manufacturing process than conventional fiber with a 0.25 mm coating diameter. This may pose problems in terms of the economical production of thin coated fiber. Therefore, when we decide on the coating diameter, both fiber density and mechanical strength must be taken into the consideration. In the future, we plan to manufacture trial cables to find an answer to these problems.

3. 80-fiber connector

Based on our study of a 16-fiber connector presented at the 41st IWCS,[2] we fabricated and evaluated two types of 80-fiber connector.

3.1 Structure

Figure 9(a) and (b) show the structures of the two types of 80-fiber connector.

(1) Stacked type

The 80-fiber connector shown in Fig. 9(a), is called a stacked type connector.[7] Five 16-fiber connectors of the type reported at the last IWCS, are stacked and fixed together with two binder pins. Because there is some clearance

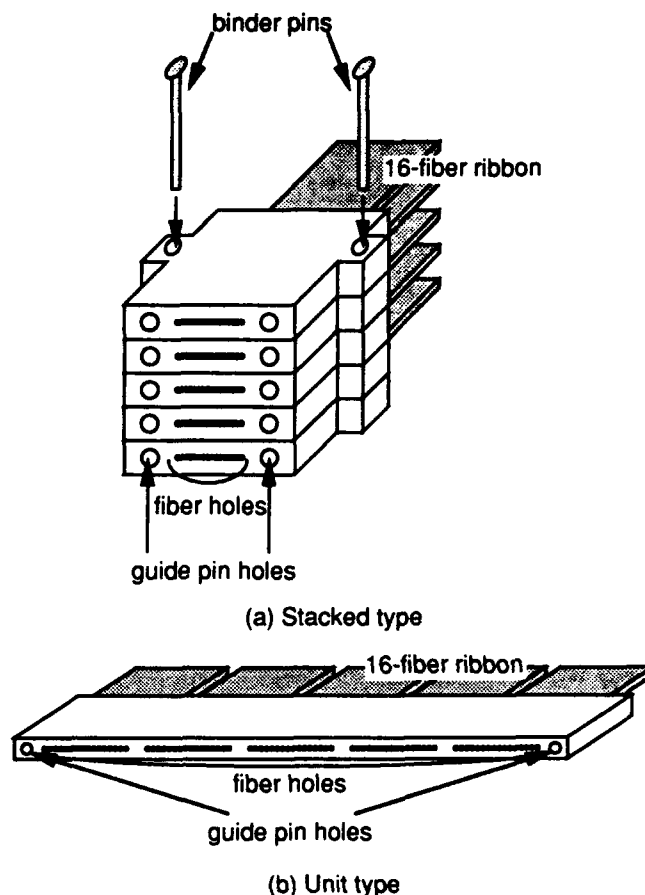


Figure 9 80-fiber connector

between the binder pins and the binder pin holes, each connector is aligned by using its own guide pins and guide pin holes. This mechanism guarantees the same connection loss as that of a 16-fiber connector.

(2) Unit type

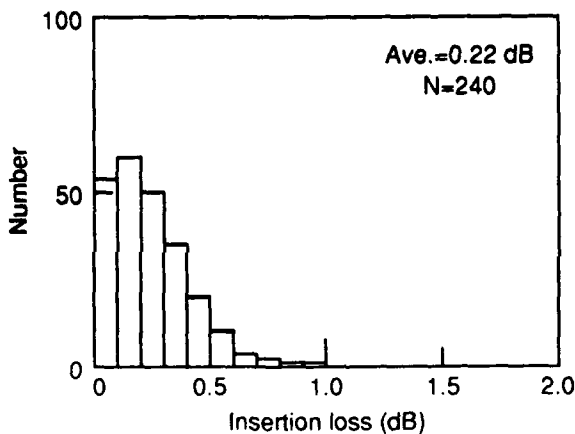
Figure 9(b) shows the structure of a unit type 80-fiber connector. 80 fiber holes are aligned in a straight line between two guide pin holes.

The benefit of this connector is that 80 fibers can be connected using only five elements, two ferrules, two guide pin and a spring. Therefore, the cost per fiber connection is very low and connection time is very short. However, the ferrules are much larger than that of the 16-fiber connector, and the molding condition must be controlled carefully to eliminate the heat shrinking effect.

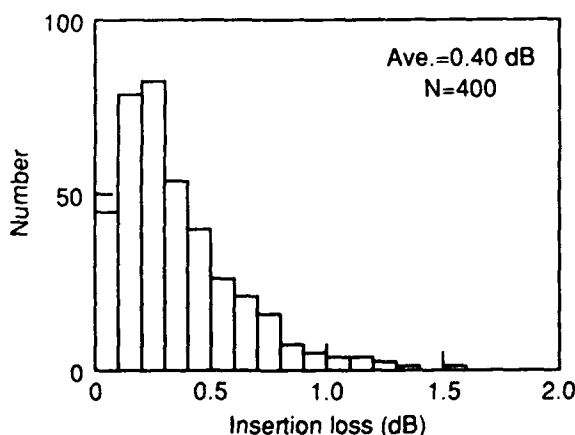
3.2 Performance

Figure 10(a) and (b) show the connection loss distribution of the stacked type and unit type 80-fiber connectors, respectively. Table 3 shows other performance of both connectors. In the stacked type, the connection loss was approximately the same as in the 16-fiber connector. The loss of the unit connector was slightly higher than that of the stacked type. This is because the fiber alignment is inaccurate owing to the large ferrule size.

The connection time is shorter with the unit type connector than with the stacked type, because of the smaller number of connector parts. The unit connector has a higher fiber density for the same reason.



(a) Stacked type



(b) Unit type

Figure 10 Connection loss of 80-fiber connectors

Each connector has its own advantages, therefore, we must select the connector type based on requirements.

Table 3 Characteristics of 80-fiber connector

Items	Stacked type	Unit type
Average connection loss (dB)	0.22	0.40
Connection time (sec.)	90	50
Fiber density (core/mm ²)	0.53	0.80

4. 4000-fiber pre-connectorized cable ends and enclosures

We constructed enclosures for 4000 fibers using 80-fiber unit type connectors.

4.1 Structure

Figure 11 shows a pre-connectorized cable end and its cover which provides protection during installation. The cable end is designed to contain fifty 80-fiber unit type connectors. A pulling force of 800 kgf can be applied to this cable end.

Fifty 80-fiber unit connectors are contained in the enclosure as shown in Figs. 12 and 13. There are stacked trays at the center of this enclosure which can hold fifty 80-fiber connectors. Two hundred and fifty 16-fiber ribbons are packed in the spaces on each side of the enclosure and there is also some remaining space to house excess cable.

4.2 Performance

The connection time and connection loss of the enclosure are shown in Fig. 14. The connection time of 3 hours satisfies the requirement of connecting 4000 fibers in one work-day [8 hours]. The average connection loss of 0.4 dB is the same as that of the unit connectors described in section 3.2. This

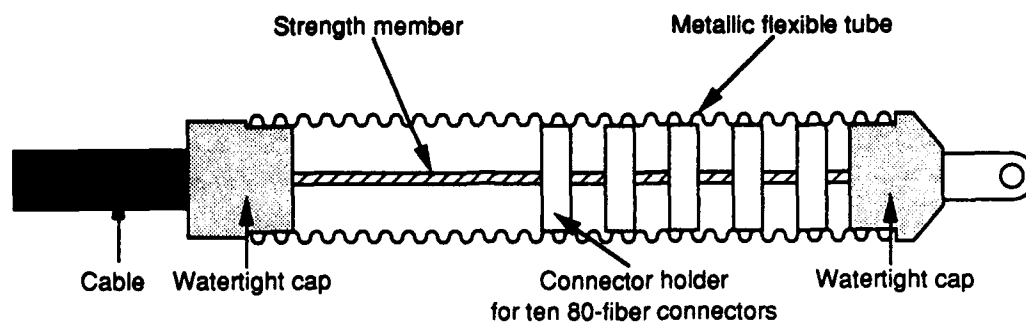


Figure 11 Structure of connectorized cable and its cover



Figure 12 Enclosure for 4000-fiber connection

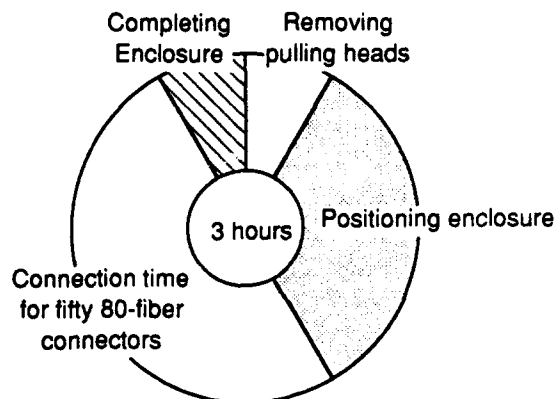


Figure 13 80-connector trays in 4000-fiber enclosure

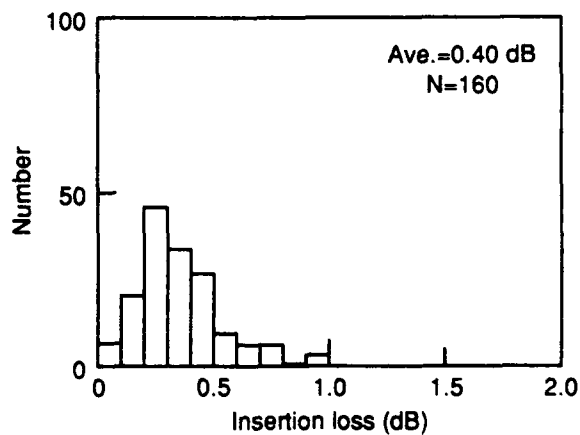
shows that installing the connectors and housing the excess fiber ribbon in the enclosure has no effect on attenuation.

5. Conclusions

In the last three years, we have been studying high-count and high-density cables and



(a) Connection time



(b) Insertion loss

Figure 14 Characteristics of the 4000-fiber enclosure

connectors, in order to construct optical subscriber cable networks for FTTH. We have made the following progress.

(1) Cable

We have developed ultra high-density cables with thin coated fibers. Their performance

makes them suitable for installation in subscriber networks except for remaining slight loss in the corner fibers of the stacked ribbons. We think that this loss can be reduced by refining the cabling procedure, which is our current goal.

(2) Connectors

The mean connection loss of the stacked type 80-fiber connector is about 0.2 dB. The fiber density of the unit type 80-fiber connector is about 0.8 core/mm². This value is 1.5 times higher than that of the stacked type. The connection time is about 50 seconds, which is half of that of the stacked type.

(3) Pre-connectorized cable end

We have fabricated and evaluated pre-connectorized ends and enclosures for 4000-fiber connection. The total connection time is 3 hours for unit type connectors.

Our ultimate goal is to complete a 4000-fiber pre-connectorized cable, by combining and refining the above technologies.

6. References

- [1] S. Tomita, M. Matsumoto, T. Yabuta and T. Uenoya "Preliminary Research into Ultra High Density and High Count Optical Fiber Cables", 40th IWCS, pp.8-15, 1991
- [2] S. Tomita, M. Matsumoto, T. Tanifuji, S. Nagasawa and T. Uenoya; "Preliminary Research into High-count Pre-connectorized Optical Fiber Cable", Proc. of 41st IWCS pp. 5-12, 1992.
- [3] W. Katsurashima, Y. Kitayama, K. Oishi, T. Kakuta and N. Akasaka "Microbending Loss of Thin Coating Single Mode Fiber for Ultra-High-Count Cables", 41st IWCS, pp. 13-19, 1992
- [4] M. Hara, S. Okagawa, and A. Otake "Design of Downsized Coated Optical Fibers to Minimize Microbending Loss", 41st IWCS, pp.20-24, 1992
- [5] K. W. Jackson M. L. Pearsall "Design and Performance of a Compact 204-Fiber Ribbon Cable", OFC'90, p. 107, 1990
- [6] M. Kawase, T. Fuchigami, M. Matsumoto, S. Nagasawa, S. Tomita, and S. Takashima "Subscriber Single-Mode Optical Fiber Ribbon Cable

Technologies Suitable for Midspan Access", J. of Lightwave Technology, Vol.7, No.11, November, 1989.

[7] T. Haibara, S. Tomita, M. Matsumoto and T. Yabuta "High-Speed Low-Loss Connection Techniques for High Count Pre-Connectorized Cables", 40th IWCS, pp.296-302, 1991



Shigeru TOMITA

Telecommunication Field
Systems R&D Center
Tokai, Ibaraki,
319-11, JAPAN

Shigeru Tomita is a Senior Research Engineer.

He was born in 1960 and received B.E. and Ph.D degrees in electronics engineering from Nihon University in 1983 and 1993 respectively.

He joined NTT in 1983. Since 1990 he has been engaged in research on High-density and Pre-connectorized optical fiber cable.

Dr. Tomita is a member of IEEE.



Michito MATSUMOTO

NTT
Telecommunication Field
Systems R&D Center
Tokai, Ibaraki,
319-11, JAPAN

Michito Matsumoto is an Executive Research Engineer. He was born in 1952 and received B.E. degree in electrical engineering from Kyushu Institute of Technology. He received M.E. and Ph.D. degrees in electronics engineering from Kyushu University in 1977 and 1987, respectively.

He joined NTT in 1977. Since 1990 he has been engaged in research on High-density and Pre-connectorized optical fiber cable.

Dr. Matsumoto is a member of IEEE.



Shinji NAGASAWA

NTT
Telecommunication Field
Systems R&D Center
Tokai, Ibaraki,
319-11, JAPAN

Shinji Nagasawa is an Executive Research Engineer. He was born in 1950 and received B.E. degree in electrical engineering from Chiba University in 1974 and 1976, respectively.

He joined NTT in 1976. Since 1990 he has been engaged in research on multi fiber connectors.

Mr. Nagasawa is a member of IEEE.



Tadatoshi TANIFUJI

NTT
Telecommunication Field
Systems R&D Center
Tokai, Ibaraki,
319-11, JAPAN

Tadatoshi Tanifuji is the leader of high count optical fiber cable research group. He was born in 1949. He received B.E. and M.E. degrees in electronics engineering from Hokkaido University in 1972 and 1974, respectively.

He joined NTT in 1974. Since 1991 he has been engaged in research on High-density and Pre-connectorized optical fiber cable.

Dr. Tanifuji is a member of IEEE.

16-FIBER RIBBON FOR ULTRA-HIGH-DENSITY and HIGH-COUNT OPTICAL FIBER CABLE

M. SAITO, S. OKAGAWA

THE FURUKAWA ELECTRIC CO., LTD.
6, YAWATA KAIGAN-DORI, ICHIHARA, CHIBA, 290, JAPAN

Abstract

The authors produced 16-fiber ribbons using downsized coated optical fibers, and evaluated their lateral pressure characteristics with long span high tension bobbin winding test. Bobbin winding loss increase was evaluated with a multi-regression analysis. And we introduced an empirical formula with two parameters, stiffness of fiber ribbon and buffer effect of ribbon coating. It suggested the minimum ribbon fiber height was approximately 0.25mm for ultrahigh density optical fiber cable.

1. Introduction

For the construction of optical fiber network to the whole subscribers, the development of an ultrahigh density optical fiber cable is required. A cable structure composed of U-groove units is one of the cable structures proposed for an ultrahigh density optical fiber cable. In this cable structure, ten 16-fiber ribbons, each of which is composed of 16 downsized coated optical fibers, are tightly layered over one another in one U-groove unit¹⁾. Because of thin coating of fiber and ribbon, the 16-fiber ribbon seems to be sensitive to lateral pressure. Therefore it is desirable to improve the lateral pressure characteristics of 16-fiber ribbon in order to realize a high density optical fiber cable.

To determine the optimum coating structure of 16-fiber ribbon, we investigated the lateral pressure characteristics with a multi-regression analysis on four types of fiber ribbons and introduced an empirical equation. Using the derived empirical equation, we estimated the optimum height of a fiber ribbon for ultrahigh density optical fiber cable.

2. Experimental

2-1. Transmission Loss and Temperature Characteristics

We produced some types of 16-fiber ribbons as shown in Table 1 to evaluate the effect of Young's modulus and thickness of ribbon coating on the lateral pressure characteristics of fiber ribbon. The fiber parameters are also shown in Table 1.

Table 1 Structure of 16-fiber ribbon

Fiber parameter	M.F.D λ_c	$9.2 \pm 0.1 \mu\text{m}$ $1.25 \pm 0.02 \mu\text{m}$
Fiber structure	Diameter E_s	0.18mm $\geq 100 \text{kgf/mm}^2$
Ribbon fiber structure	Height E_r	0.20~0.25mm 30~150kgf/mm ²

M.F.D : mode field diameter

λ_c : cut off wavelength

E_s : Young's modulus of secondary coating

E_r : Young's modulus of ribbon coating

In this experiment, we used downsized coated optical fibers only (Diameter 0.18mm).

Table 2. shows the transmission losses and temperature characteristics of the produced fiber ribbons.

Table 2 Characteristics of 16-fiber ribbon

Item	Condition	Result
Transmission loss	Wavelength : 1.55 μm Diameter of bobbin : 280mm Tension : 2N/rib.	ave. 0.20dB/km max. 0.23dB/km
Temperature characteristics	Wavelength : 1.55 μm Temperature : -40~80°C Sample : free coil	Loss increase $\leq 0.03 \text{dB/km}$

The transmission losses and temperature characteristics were favorable. The maximum transmission loss was 0.23 dB/km and the maximum loss increase from -40 to 80 °C was 0.03dB/km (at Young's modulus of ribbon coating is 150kgf/mm² and height of ribbon was 0.25mm).

2-2. Lateral Pressure Characteristics

To investigate the effect of the fiber ribbon coating structure on its lateral pressure characteristics, four fiber ribbons were used. As can be seen in Table 3, their structures were upper and lower limit of Young's modulus and height of ribbon in Table 1.

Table 3 Structure of 16-fiber ribbon used for bobbin winding test

No	Height (mm)	Young's modulus (kgf/mm ²)
1	0.20	30
2	0.20	150
3	0.25	30
4	0.25	150

We estimated lateral pressure characteristics with long span bobbin winding test. 16-fiber ribbons were wound around a plastic bobbin (Diameter 280mm) at a tension of 2N and then were wound again at a tension of 6N. Bobbin winding loss increase is defined as the difference between the transmission loss at tension of 6N and 2N.

3. Parameter

Gloge expressed the microbending loss of optical fiber with parameter H (stiffness of optical fiber) and D (rigidity of optical fiber)²⁾. In this paper, parameter H and B expressing the structure and mechanical characteristics of fiber ribbon. H means stiffness of fiber ribbon and B means buffer effect of ribbon coating. H , stiffness of 16-fiber ribbon, can be represented by equation (1).

$$H = E_f \times I_f + E_p \times I_p + E_s \times I_s + E_r \times I_r \quad (1)$$

E_f, E_p, E_s, E_r : Young's modulus of optical fiber, primary coating, secondary coating and ribbon coating

I_f, I_p, I_s, I_r : moment of inertia of optical fiber, primary coating, secondary coating and ribbon coating

And I_r is calculated by the 16-fiber ribbon structure:

$$I_r = \frac{1}{12} W T^3 - 16 \times \pi \times \frac{d^4}{64} \quad (2)$$

W : width of fiber ribbon

T : height of fiber ribbon

d : diameter of optical fiber

On the other side, B , buffer effect of fiber ribbon, can be expressed by equation (3), (4).

$$B = \frac{E_r}{R} \quad (3)$$

$$R = \frac{T - d}{2} \quad (4)$$

With these parameters, the bobbin winding loss increase was evaluated by multi-regression analysis.

4. Result

4-1. Analysis with Parameter H and B

Fig 1. shows the correlation between parameter H and bobbin winding loss increase. The correlation coefficient of Fig.1 was 0.31. So we can say bobbin winding loss increase has very little correlation with parameter H .

Fig.2 shows the correlation between parameter B and bobbin winding loss increase. The correlation coefficient was 0.78. So it can be said that bobbin winding loss increase has correlation with parameter B .

Bobbin winding loss increase couldn't be expressed successfully with parameter H or B only. We obtained the optimum regression equation (Equation (5)) by using both H and B .

$$\alpha = C \times \frac{B^{1.7}}{H^{4.75}} \quad (5)$$

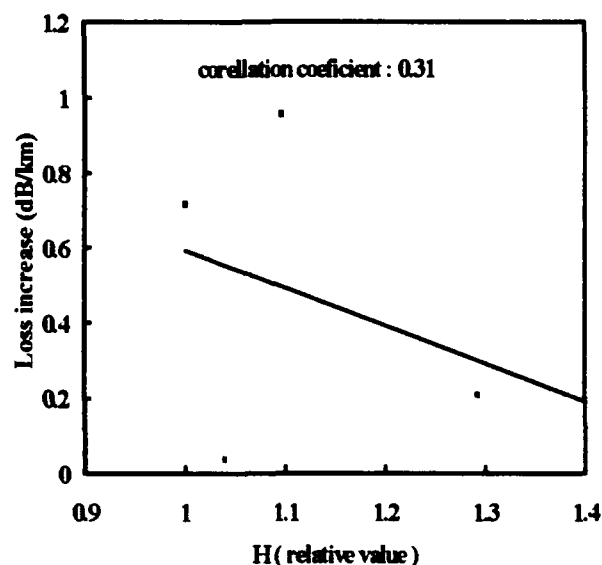


Fig.1 Correlation between bobbin winding loss increase and H

wavelength: 1.55 μ m

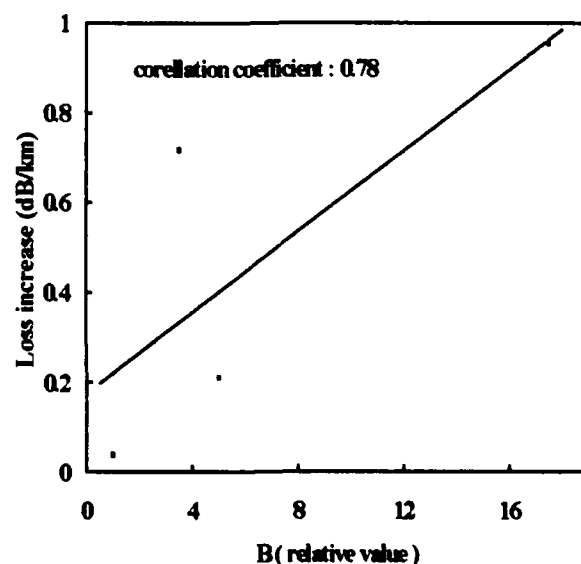


Fig.2 Correlation between bobbin winding loss increase and B

wavelength: 1.55 μ m

Fig 3. shows the correlation between the estimated value from equation (5) and the experimental value.

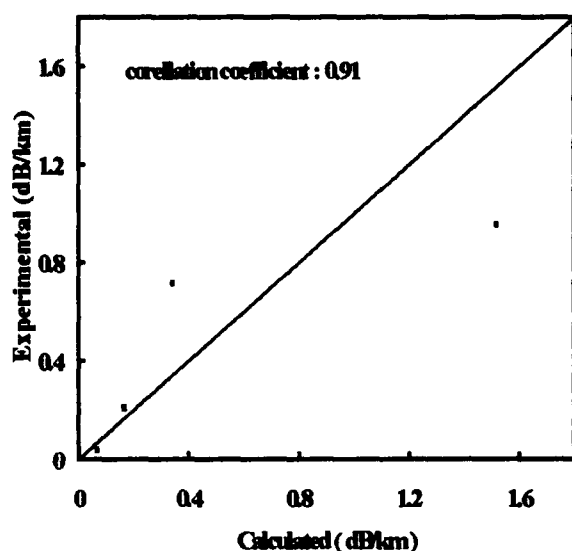


Fig.3 Correlation between the calculated and experimental loss increase

wavelength:1.55um

The correlation coefficient of Fig.3 was 0.91, so equation (5) represents the bobbin winding loss increase accurately. From equation (5), we can say that the bobbin winding loss increase depends upon both H and B . Small B and large H decrease bobbin winding loss. Because a smaller B means a greater buffer effect of fiber ribbon coating and larger H means a greater stiffness of fiber ribbon and as a result microbending loss decrease.

4-2. Estimation of Bobbin Winding Loss Based on Multiple Regression Analysis

Fig. 4 and 5 shows the calculated value of bobbin winding loss increase to Young's modulus and height of ribbon coating. As can be seen in Fig.4, at a thin fiber ribbon, bobbin winding loss increase changed very well with Young's modulus of ribbon coating.

In particular, it can be seen that there is a prominent bobbin winding loss increase for a fiber ribbon of high Young's modulus. Therefore thin fiber ribbon needs to be coated with soft material.

As can be seen in Fig.5 bobbin winding loss increase approached the minimum value at around 0.25mm height of fiber ribbon.

As a result, although downsizing of ribbon coating thickness was needed for high density cable, Fig. 5 showed that minimum height of fiber ribbon was approximately 0.25mm in view of lateral pressure characteristics of optical fiber ribbon.

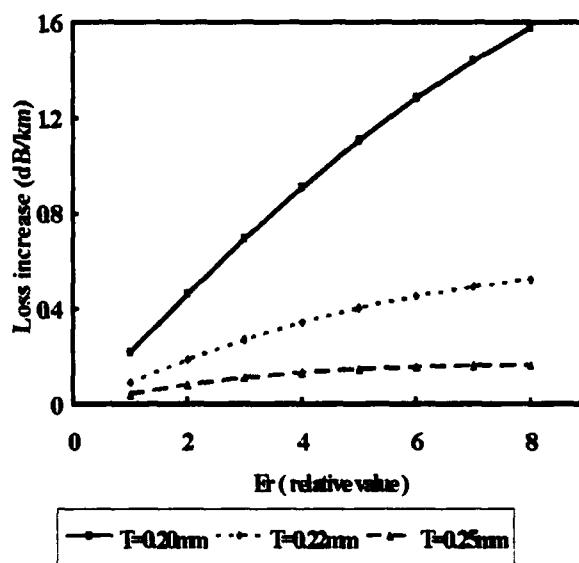


Fig.4 Correlation between bobbin winding loss increase and Young's modulus of fiber ribbon(relative value)
wavelength:1.55um

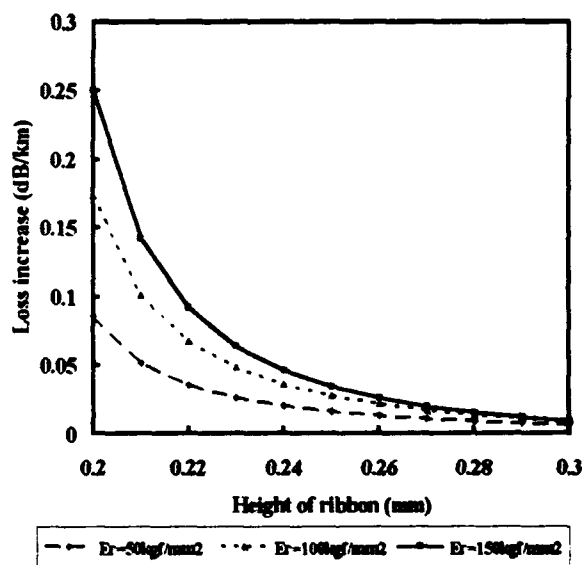


Fig.5 Correlation between bobbin winding loss increase and height of ribbon

wavelength:1.55um

5. Conclusion

Using downsized coated optical fibers with optimum coating structure, we produced 16-fiber ribbons with superior lateral pressure and temperature ($-40 \sim 80^{\circ}\text{C}$) characteristics. The lateral pressure characteristics was estimated by long span bobbin winding test and evaluated by multi-regression analysis. As a result, bobbin winding loss increase was expressed by an empirical equation. Although thin fiber ribbon is desirable for high density cable, it was found that the height of ribbon should be no thinner than around 0.25mm in the view of the lateral pressure characteristics of optical fiber ribbon.

Reference

- 1) S.Tomita et al., IWCS(1991) pp.8-15
- 2) D.Gloge, B.S.T.J., Vol.54, Feb, 1975, pp.245-262



Minoru SAITO

The Furukawa Electric
Co., Ltd.

6, Yawatakaigandori,
Ichihara, Chiba, 290,
Japan

Mr. Saito graduated from Kyushu University in 1992 with a M.E. in chemistry. Then he joined The Furukawa Electric Co., Ltd., Chiba, Japan, and has been engaged in research and development of optical fiber cables.

He is now a research engineer of Optical Fiber Transmission Section, Opto- Technology Laboratory, The Furukawa Electric Co, Ltd.



Shuji OKAGAWA

The Furukawa Electric
Co., Ltd.

6, Yawatakaigandori,
Ichihara, Chiba, 290,
Japan

Mr. Okagawa graduated from Osaka University in 1981 with a M.Sc. in chemistry. Then he joined The Furukawa Electric Co., Ltd., Chiba, Japan, and has been engaged in research and development of plastic materials and manufacturing methods for optical fiber cables.

He is now a major of reliability engineering section, The Furukawa Electric Co., Ltd.

A MODULAR RIBBON DESIGN FOR INCREASED PACKING DENSITY OF FIBER OPTIC CABLES

K. W. Jackson, M.R. Santana, N.W. Sollenberger
AT&T Bell Laboratories
2000 NE Expressway Norcross, Georgia 30071

R.J. Brown, K.M. Kroupa S.H. Webb
AT&T Network Systems
Norcross, Georgia 30071

ABSTRACT

In this paper we examine the limits to which fiber packing density in cables can be increased without reducing the diameter of the fiber's protective coating. We demonstrate the feasibility of increasing the fiber packing density of existing cable designs by 30 to 50 percent with a modular design concept for ribbons. The design concept is flexible in that it can accommodate 4-, 6-, or 8-fiber ribbon modules in a single linear array and provides for an organized structure for high fiber count cables. We present experimental data and a simple analytical model that clarify the physical mechanisms associated with packing density, stack geometry, ribbon stresses and environmental added loss.

INTRODUCTION AND BACKGROUND

Global interest in high density, small size cables and the high productivity of mass splicing is positioning ribbon-based cables as a bellwether for Fiber in the Loop (FITL) and Community Antenna Television (CATV) applications. For CATV aerial installations, small, high fiber count cables are attractive because of the high premium on available aerial space. Different network architectures require functional flexibility as well as the availability of diverse fiber counts per ribbon. Evidence for the trend toward high fiber count cables is found in the many technical papers being published on ribbon-based cables, associated apparatus and also in the emergence of international standards for ribbons (1,2).

Advances in materials and process technology, as well as increased demand for improved functionality have accelerated ribbon-based cable development and deployment for FITL and CATV applications. Higher fiber count cables and higher fiber packing densities continue

to be the leading performance metrics. For example, 4000 fiber cables that use downsized fiber coating designs have been proposed and are actively being investigated (3). Although downsizing of the protective coating on the fiber offers the potential for increasing the fiber packing density, the long term reliability, engineering and operational implications remain to be fully understood. Thus, the need for achieving higher fiber counts and densities with standard fiber coating dimensions continues to exist. The modular ribbon design described in this paper can satisfy this need and it offers operational advantages to the user.

BASIC CABLE DESIGN

The design uses the ribbon building block approach to increase the packing density of a central tube type cable. As shown in Figure 1, the cable consists of a core tube with diameter, D_c , that contains an array of n ribbons.

Each ribbon comprises modules with a repeating color code sequence and a printed identifier as shown in the photograph of Figure 2a.

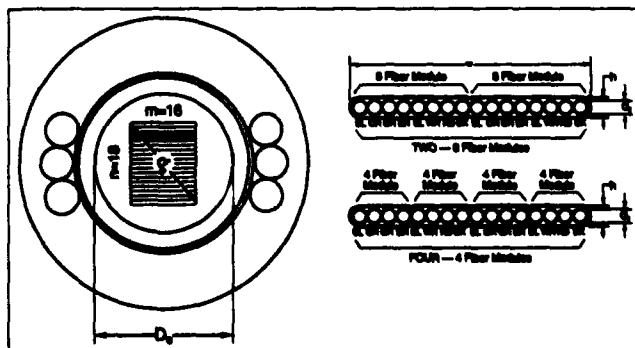


Figure 1. 288 Fiber Ribbon Cable with 16-Fiber Modular Ribbons.

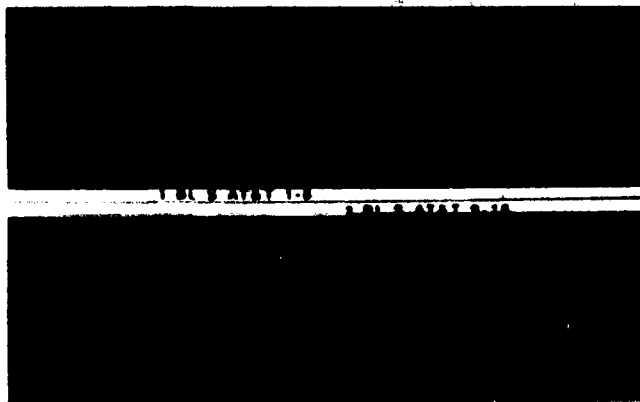


Figure 2a.

Modules are important for many applications to provide splicing flexibility. As shown in the photograph of Figure 2b, the modules can easily be separated from the main ribbon.

Typical modules comprise 4, 8, or 12 fibers. For generality, each ribbon is considered to have thickness, h and to comprise m fibers of diameter, d_f .

PACKING DENSITY ANALYSIS

There are several measures of fiber packing density. In this paper (unless noted otherwise) fiber packing density is defined to be the ratio of total fiber area (including the fiber coating) to total core tube internal area. High fiber counts and high fiber packing density are important for achieving small lightweight cables that are easy to handle and optimally utilize available space for installation. For a loose fiber bundle core the theoretical packing density is about 80%; however, less than 20% is attained practically with desired optical performance (4). Although ribboned fibers give a somewhat lower theoretical packing density of 50%, the practically achieved packing density is much closer to the theoretical maximum.

For a fixed core tube ID, the theoretical packing density of loose fiber bundle cores, can be increased only by reducing the fiber diameter. However, for ribbon-based cores, both the coated fiber diameter and the ribbon thickness contribute to packing density. The total packing density depends on the fiber packing density of the fibers in the ribbons themselves and the packing density of the ribbons in the core through the following expressions:

$$P_{fc}^* = 4P_{fc}/\pi d_f^2 \quad (1)$$

$$P_{fc} = P_{fr} \cdot P_{rc} \quad (2)$$

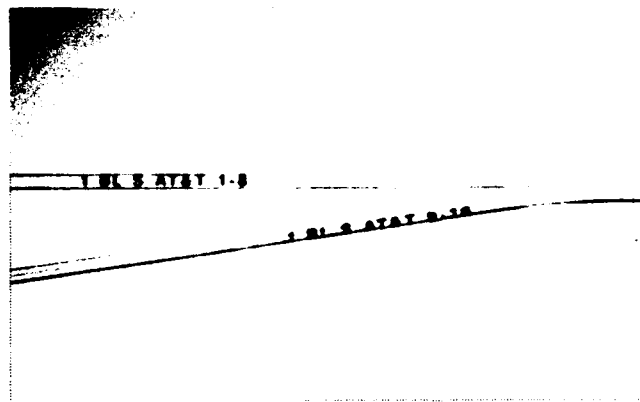


Figure 2b.

where

P_{fc}^* is the number of fibers per unit of core area

P_{fc} is the area of fibers per unit of core area

P_{fr} is the area of fibers per unit of ribbon area

P_{rc} is the area of ribbon per unit of core area

d_f is the diameter of the coated fiber

For a core tube of inside diameter, D_c , containing an $n \times m$ array of fiber ribbons as shown in Figure 1,

$$P_{rc} = \{4nm(1+\beta)d_f^2\}/\pi D_c^2 \quad (3)$$

$$\text{where} \quad (1+\beta) = h/d_f \quad (4)$$

Also,

$$P_{fr} = \pi/4(1+\beta) \quad (5)$$

The relation between the stack diagonal, d_s , and the core tube diameter can be approximated by the empirical relation:

$$d_s/D_c = K \approx K_R \cdot (m/n)^\gamma \quad \text{for } n > m \text{ and} \quad (6)$$

$$d_s/D_c \approx K_R \quad \text{for } n \leq m$$

where

$$\gamma \approx 0.3 \text{ for } n > m \text{ and}$$

$$d_s^2 = d_f^2 \{n^2(1+\beta)^2 + m^2\} \quad (7)$$

Equation (6) takes into account the minimum radius of fiber curvature resulting from the excess ribbon length in the core tube. (For strain relief, the ribbons are slightly longer than the longitudinal axis of the core. The per cent by which the ribbon length exceeds the core length is the excess ribbon length.)

Figure 1 and Equations 2-7 give

$$P_{fc} = \{K_R^2 \cdot X^{1-2\gamma}\} / \{X^2 \cdot (h/d_f)^2 + 1\} \quad (8)$$

where $X = n/m$ is an index of stack symmetry

Figure 3 shows the dimensionless packing density, (P_{fc}/K^2) as a function of the symmetry index, X with h/d_f as a parameter.

Figure 3 illustrates the negative effect of both stack asymmetry and increased ribbon thickness on fiber packing density. The curves illustrate a basic design principle that optimum packing density of the core is attained with a square array of ribbons where each ribbon has a thickness equal to the fiber diameter. In this case, the upper bound of packing density is seen to be 0.5. In practice, this principle must be modified to provide for excess fiber length and fiber counts that are common multiples of the standard number of units/fibers that are used in the field.

Figure 4 shows a plot of normalized packing density $(\pi P_{fc} \cdot 4/K_R^2)$ for a square array as a function of d_f with h/d_f as a parameter. Figure 4 demonstrates that two routes exist for achieving the same packing density while offering comparable levels of polymer buffer protection for the glass fiber: the fiber diameter can be decreased

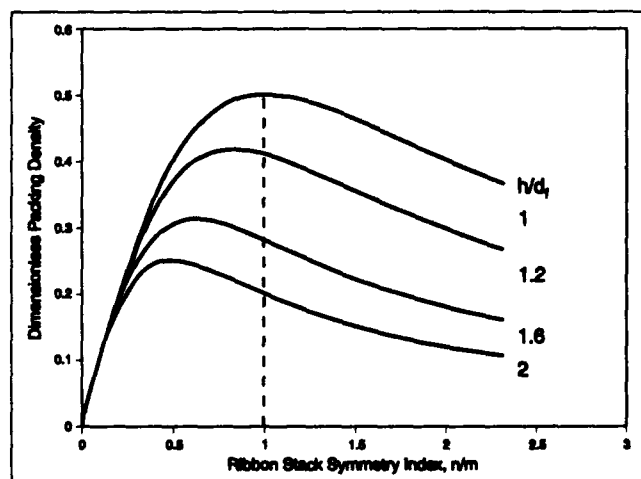


Figure 3. Dimensionless Packing Density as Related to Ribbon and Stack Geometry.

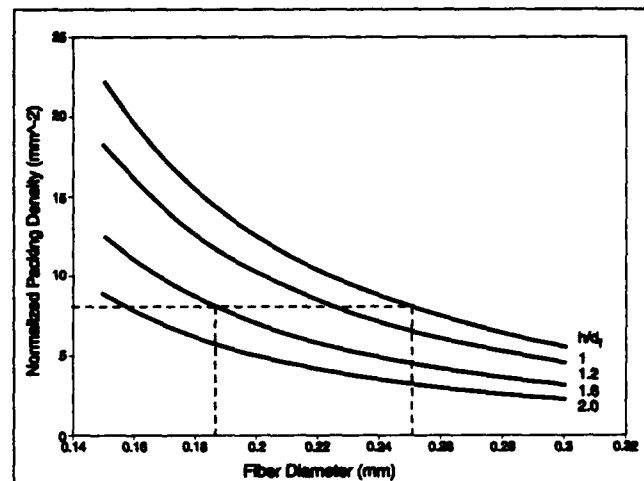


Figure 4. Normalized Packing Density as Related to Fiber Diameter and Ribbon Thickness

and the ribbon thickness increased; or keep the fiber diameter constant and use a ribbon of thickness, d_f .

As a numerical example, consider the case where a normalized packing density of 8 mm^{-2} is desired. This packing density can be achieved with fiber having the standard 0.25 mm diameter if $h/d_f = 1$; however, if $h/d_f = 1.6$, the fiber diameter must be reduced to about 0.185 mm .

The use of the foregoing principles for optimum ribbon cable design must account for fiber excess length, potential fiber stresses induced during stranding or cable bending, the mechanical robustness of the ribbon, and stripping and splicing considerations.

MECHANICAL ROBUSTNESS OF RIBBONS

In the loop environment there is more routing, handling, reconfiguring, and repair with an ensuing increase in ribbon bending and twisting. It is important that ribbons be designed to retain their mechanical integrity under a variety of loadings. Ribbon structures need to be sufficiently robust to withstand routine handling yet provide easy breakout of single and multiple fiber modules from a ribbon. Implicit in this user need is both a maximum and a minimum ribbon strength. A suitable test for characterizing the strength range of a ribbon is the torsion test (2). In this test, a length of ribbon is clamped at both ends under tension and rotated until matrix failure. Ironically, the structure does not fail primarily due to torsional shear stresses but because of transverse bending and buckling instability.

In this section we examine the mechanical robustness of a ribbon structure as it relates to loading and geometry.

A ribbon can be modeled as a lamina of unidirectional fibers in a matrix as illustrated in Figure 5.

In the terminology of composite materials the ribbon is an orthotropic body; it has material properties that are different in three mutually perpendicular directions and it has three perpendicular planes of material symmetry (5). In contrast to an isotropic material, the strength of an orthotropic material is not a function of the principal stresses because the highest stresses are not typically the ones which cause failure. Thus, the strength is a function of the **orientation** of the stresses in the ribbon. For fiber ribbons, the strength and stiffness of the glass fibers are several orders of magnitude greater than that of the viscoelastic matrix material that supports and aligns them. Moreover, the strength of the structure is different in the principal material directions. In particular, the strength in the transverse direction is several orders of magnitude less than that in the longitudinal direction.

Early work on the deformation mechanics of twisted ribbon structures demonstrated a "barrel-type" distortion of the cross section from the applied stresses (6). The foregoing reference also provides a qualitative description of the mechanism associated with this distortion. For a twisted ribbon, the fibers experience a longitudinal stress and follow a helical path with curvature given by

$$C_i = 1/\rho_i = \omega^2 R_i / (1 + \omega^2 R_i^2) \quad (9)$$

where

ω is the twist angle per unit length

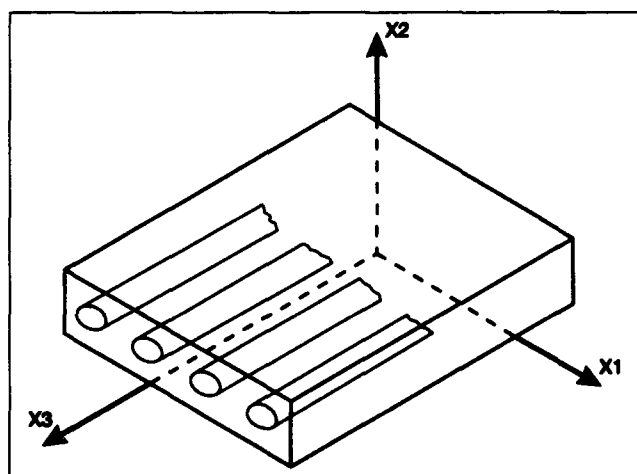


Figure 5. Orthotropic Structure; Lamina with Unidirectional Fibers.

R_i is the distance from the center of the ribbon to the i th fiber

ρ_i is the radius of curvature

The fiber curvature and longitudinal stresses necessitate that the fibers exert transverse forces, P_i , per unit length on the ribbon (6). These forces are directed toward the center of the ribbon and can induce bending, buckling and fracture of the ribbon matrix along the longitudinal axis of the ribbon.

Considering the ribbon as section of plate subject to uniform **lateral** compressive stress, σ , leads to consideration of the typical equation for plate buckling (7):

$$\begin{aligned} \sigma_{cr} &= P_{cr}/A \\ &= \{(K\pi^2 E)/12(1-\mu^2)\}(t/b)^2 \end{aligned} \quad (10)$$

where

t is the plate thickness

b is the plate width

In Equation (10), the pertinent variable is the critical buckling stress, σ_{cr} , which is proportional to $(t/b)^2$.

The maximum **longitudinal** stress in an outer filament of the plate is given by (8)

$$\sigma = E\omega^2 b^2 / 12 \quad (11)$$

Thus,

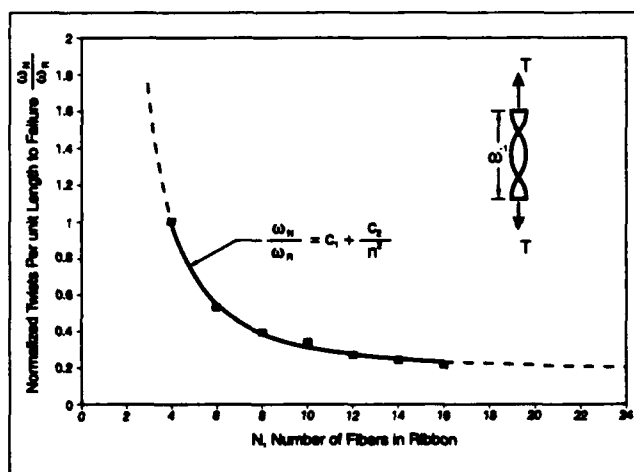


Figure 6. Ribbon Torsional Robustness as Related to Number of Fibers per Ribbon.

$$\omega^2 b^2 \sim (v/b)^2 \quad \text{or}$$

$$\omega \sim (v/b^2)$$

For a ribbon where $t = h = d_f$ and $b = m \cdot d_f$, the twist angle to failure would be expected to vary as $1/m^2$ where m is the number of fibers per ribbon.

Figure 6 shows a normalized plot of torsion test data for twist angle to failure as a function of m for a typical ribbon structure. The data correlate well with $1/m^2$.

CABLING AND ENVIRONMENTAL PERFORMANCE OF MODULAR RIBBON CABLE

Table I shows representative loss data for a 288 fiber cable consisting of eighteen, 16-fiber modular ribbons comprising both matched clad and depressed clad fibers. The mean and median cable losses are approximately equal and the mean added loss is negligible at both 1310 nm and 1550 nm. Table I shows similar results for the loss performance at -40°C .

By increasing the symmetry of the stack, the packing density has been increased by 33% (relative to contemporary 18x12 central tube ribbon cable designs) without decreasing the diameter of the fiber coating. With optimum stack symmetry (for example, 24x24), the potential exists for increasing the packing density by as much as 50% without decreasing the diameter of the coated fiber.

MASS FUSION SPLICING PERFORMANCE OF RIBBON MODULES

To realize the benefits of the modular ribbon concept, the modules must retain their mechanical integrity after being broken out from the main ribbon, strip in commer-

cial stripping tools, and exhibit suitable mass splicing performance. The mechanical robustness of 4, 6, 8, and 12-fiber modules broken out from a 16 fiber ribbon was characterized with the torsion test described earlier. The data shown in Figure 6 demonstrate that the ribbon modules retain mechanical integrity after break-out from the main ribbon. Figure 7 shows photomicrographs of the stripped end portions of 4, 8 and 12-fiber ribbon modules that have been broken out from the 16 fiber ribbon. The fibers are clean and free of residue following a single wipe with an alcohol moistened pad.

The ribbon modules were then mass fusion spliced and the performance compared to that of a 12 fiber ribbon. Figures 8-9 show empirical quantile-quantile plots of both machine estimated and actual average splice loss for 4, 8 and 12 fiber ribbon modules (9).



Figure 7. Stripped 12 Fiber Ribbon and 4 and 8 Fiber Modules.

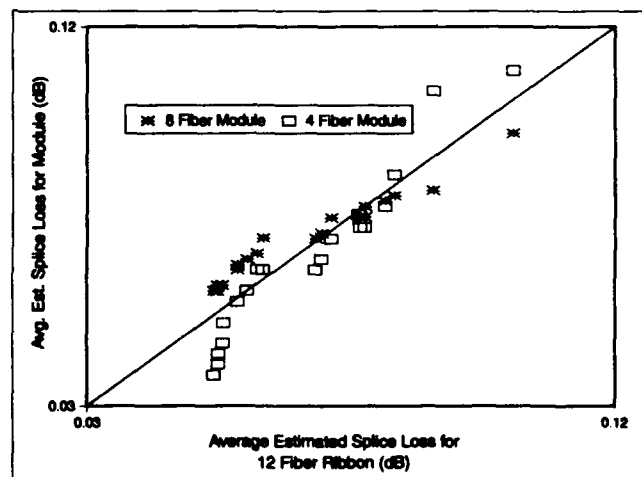


Figure 8. Q-Q Plot for Average Estimated Splice Loss for Ribbon Modules.

TABLE I
LOSS PERFORMANCE OF 288 FIBER CABLE

TEMPERATURE		CABLE LOSS dB/km			
		DC		MC	
		1310	1550	1310	1550
25°C	MEAN	0.35	0.20	0.36	0.20
	MEDIAN	0.35	0.20	0.36	0.20
-40°C	MEAN	0.36	0.26	0.37	0.26
	MEDIAN	0.35	0.22	0.36	0.23

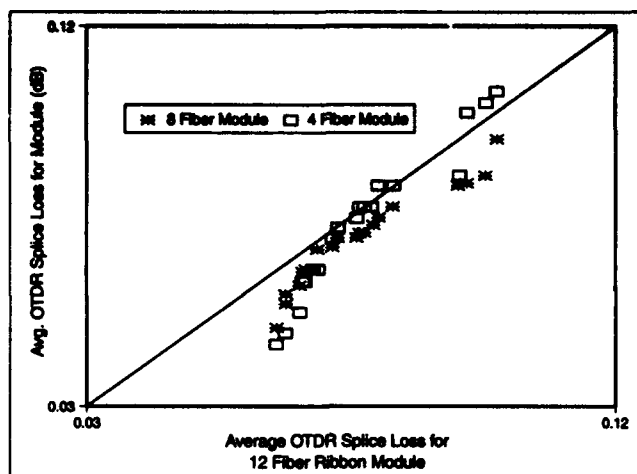


Figure 9. Q-Q Plot for Average OTDR Splice Loss for Ribbon Modules.

These plots demonstrate that the distributions' average splice loss for 4 and 8 fiber ribbon modules are comparable to that of a 12 fiber ribbon.

Additional insight into the splicing performance can be gleaned from the distributions of maximum splice loss as related to fiber count per ribbon. Figure 10 and 11 show quantile-quantile plots for the maximum splice loss (machine estimated and actual) of 4 and 8 fiber ribbon modules compared to that of a 12 fiber ribbon. Here we see that the maximum splice loss generally increases as the fiber count per ribbon increases. This is to be expected from basic statistical considerations because equal numbers of ribbon splices do not reflect equal numbers of fiber splices unless the fiber counts per ribbon are the same. An unbiased comparison must compare equal numbers of fiber splices.

CONCLUSION

The analytical and experimental results of this investigation indicate that the fiber packing density of central tube cables can be increased by about 33% without decreasing the diameter of the protective fiber coating. Design curves that illustrate how packing density relates to fiber, ribbon and core tube geometry are presented. A modular ribbon design that provides more operational flexibility is presented and the torsional robustness of the ribbon structure is demonstrated to vary inversely as the square of the number of fibers per ribbon. The fusion splice performance of ribbon modules is demonstrated to be similar to that of the parent ribbon. The modular ribbon cable provides increased packing density and enhanced features for FITL and CATV applications.

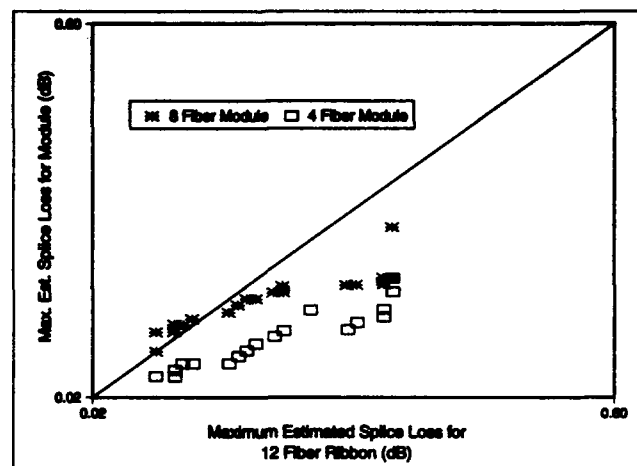


Figure 10. Q-Q Plot for Maximum Estimated Splice Loss for Ribbon Modules

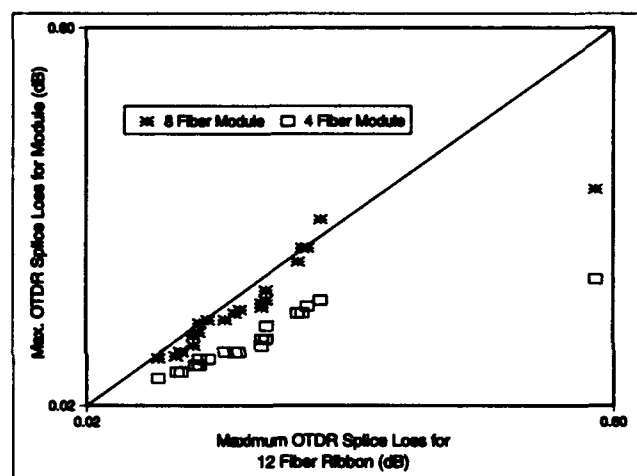


Figure 11. Q-Q Plot for Maximum OTDR Splice Loss for Ribbon Module.

ACKNOWLEDGMENTS

We acknowledge the contributions of H.P. Debban, P.D. Patel, W.J. Pauke, W.H. Ficke, K.W. Jackson Jr, S.C. Mettler and S. Sanchez.

REFERENCES

1. Proceedings of the Forty-First IWCS, Nov. 16-19 1992.
2. Product Specification for Optical Fiber Ribbon, IEC86A(SEC)239.
3. Tomita, S., Matsumoto, M., Yubata, T. and T. Uenoya; "Preliminary Research into Ultra High Density and High Count Optical Fiber Cables," 40th IWCS 1991, pp. 8-15.

4. Jackson, K.W., Sollenberger, N.W., Gentry, S.P., Brown, R.J., Petisce, J.R., Santana, M.R., Taylor, C.R. and S.H. Webb. "Optimizing Ribbon Structures for Performance and Reliability", 9th National Fiber Optic Engineers Conference, June 13-17, 1993 pp. 205-222.

5. Jones, R.M., Mechanics of Composite Materials, 1975, pp. 59-63.

6. Eichenbaum, B.R., M.R. Santana; "Analysis of Longitudinal Stress Imparted to Fibers in Twisting an Optical Communication Cable Unit", B.S.T.J., Vol 56, No.8, Oct. 1977, pp. 1503-1512.

7. Seely, F.B., J.O. Smith, Advanced Mechanics of Materials, 2nd. Ed., 1961, pp. 620-623.

8. Timoshenko, S., Strength of Materials, Part II, Advanced Theory and Problems, 1958, pp. 286-291.

9. Chambers, J.M., Cleveland, W.S., Kleiner, B. and P.A. Tukey; Graphical Methods of Data Analysis, 1983, pp. 48-56.

BIOGRAPHY



Kenneth W. Jackson is a Distinguished Member of Technical Staff in the Fiber Optic Cable and Materials Development and Engineering Department at AT&T Bell Laboratories, Norcross GA. He is responsible for the design and development of outside plant cables. He joined the Western Electric Co. in 1970 having received a B.S.M.E. from Auburn University. He joined AT&T Bell Laboratories in 1981 having received an M.S.M.E. and Ph.D. in Mechanical Engineering from the Georgia Institute of Technology. Since 1981 he has worked in the areas of Optical Fiber Fabrication, Fiber Optic Connector Design and Development, Materials' Design and Fiber Optic Cable Design and Development. He has been awarded 7 patents and has 9 publications. He is a Registered Professional Engineer in the state of Georgia.



M.R. Santana is a supervisor of the Outside Plant Cable Group with research, development and manufacturing responsibility for fiber optic cables used in the outside plant. He has been involved in research and product development in fiber optic cable and he has been awarded 12 patents and has 27 publications.

Mr. Santana joined AT&T Bell Laboratories in 1970 having received his B.S.M.E. from the University of Hartford and his M.S.M.E. from the Georgia Institute of Technology. He is a senior member of the IEEE.



Neil W. Sollenberger is a Member of Technical Staff in the Outside Plant Fiber Group at AT&T Bell Laboratories in Norcross, Georgia. He is responsible for various aspects in the design and development of outside plant fiber optic cables. Prior to his current assignment, his responsibilities have included the design and development of

both copper and fiber optic closures and terminals, as well as cabinets for loop electronics. Neil Sollenberger joined AT&T Bell Laboratories in 1978. He has a B. S. degree in Agricultural Engineering from University of Georgia, and he has a M. S. degree in Mechanical Engineering from Georgia Institute of Technology.



R.J. Brown is a Member of Technical Staff in the Outside Plant Group of the Fiber Optic Cable Development Engineering Department at AT&T Network Systems in Norcross, GA. After obtaining a BS in Mechanical engineering from The University of Maryland in 1969, he began his Western Electric

career in 1970 in Atlanta. While working in copper cable development he received an MSME from Georgia Tech in 1978 and has been involved in product design, process design and the manufacture of fiber optic cable since 1984.



high University in 1973 and a MBA from the University of New Hampshire in 1977. Since 1980, he has had

Kenneth M. Kroupa is a member of Technical Staff in the Fiber Optic Cable Packaging Department at AT&T Network Systems in Norcross GA. He joined the Western Electric Company in 1969 having received a B.S.M.E. from the University of Illinois. Subsequently, he received an MS in Metallurgy and Materials Science from Le-

production engineering responsibilities in the areas of fiber optic preform manufacturing, final cable inspection, connectorization, and ribbon manufacturing.



1986 having received an MBA from Mercer University. Since joining the PLM group, she has worked as both Fiber Product Manager and Fiber Optic Cable Product Manager.

Stephanie H. Webb is a Senior Product Manager in the Fiber Optic Cable Product Management Group at AT&T Network Cable Systems, Norcross GA. She joined the Western Electric Company in 1977 having received a B.S.I.E. from the Georgia Institute of Technology. She joined the Product Management Group in

THE EFFECT OF FIBER RIBBON COMPONENT MATERIALS ON MECHANICAL AND ENVIRONMENTAL PERFORMANCE

K.W. Jackson, T.L. Parker, J.R. Petisce, N.W. Sollenberger, C.R. Taylor

AT&T Bell Laboratories, Norcross, Georgia 30071

Abstract

Fiber optic ribbon designs are being more widely used in all areas of telecommunication applications. A series of ribbons have been evaluated to determine the effect of fiber coatings, color codings and matrix material on splicing and reliability which are of importance in all telecommunication ribbon applications. Since splicing requires rapid and easy removal of ribbon matrix and fiber coatings, the relation of the ribbon stripping tool environment to strippability was developed. Primary and secondary coatings were found to have the greatest impact on strippability.

Introduction

Migration of optical fiber to the loop plant has caused an evolution of cable designs which are adaptations to the end-user's special needs. Since its introduction in 1977, optical fiber ribbon has provided an ideal technology platform to satisfy the growing need for compact, high fiber count cables which favor the productivity advantages of mass splicing (1,2,3). In 1989, AT&T introduced an enhanced ribbon design based on UV coating technology similar to that used for fibers which is 40% more compact and can provide the largest number of fibers available in a 0.7 inch sheath (4).

Optimization of ribbon structures for performance and reliability has been a recent focus of attention (5). For example, the dependence of ribbon fiber strength retention and single fiber strippability on ribbon matrix material has been reported (6). Additionally, the effect of optical fiber coating system properties on ribbon strippability has been demonstrated (7). Ribbon strippability has become a common focus of UV bonded ribbon performance evaluation due to the end-user's desire to fully realize the potential productivity advantages of mass splicing in all commercially available ribbon products.

In order to fully understand ribbon strippability, we have characterized commercially available ribbon stripping tools which are commonly used today in mass splicing. Specifically, the ribbon strippability dependence on tool design and tool temperature setting has enabled us to define the ribbon stripping environment. Extension of single fiber stripping mechanisms (8,9) to ribbon stripping has been used as a mechanistic probe to evaluate the effect of ribbon components on ribbon strippability.

Experimental Ribbons

Three optical fiber ribbons were prepared with different primary and secondary coatings, designated ribbons A, B, and C. No two primary coatings or secondary coatings were identical. Each ribbon contained twelve color coded dual coated fibers edge-bonded with matrix material. The same inks and matrix were used on all ribbons. The physical properties of the cured coatings used in each system are shown in Table 1. Coatings properties (on fiber) before ribboning are presented in Table 2.

Ribbon Stripping Procedure

Commercial ribbon stripping tools have been developed to remove the coatings, color code and matrix from the end of the fiber array. Typically, tools contain matched cutting blades on the lid and base of the right side of the clam-shell design shown in Figure 1. Heating is provided from the right bottom surface only.

A fine wire thermocouple was used to calibrate the closed tool at the desired set point, then the lid was opened and allowed to return to ambient temperature. The ribbon was first arranged in a separate holder 30 mm back from the ribbon end, then the holder was placed into the tool base groove with the ribbon positioned over the heated base platen. The tool was closed and held firmly shut; after 10 seconds it was pulled apart to strip the polymer matrix off the end of the ribbon and leave the twelve fibers individually accessible for splicing. The

Table 1
FIBER COATING PROPERTIES

Ribbon	Equilibrium E' (eq) Primary Coating psi	Equilibrium Modulus Secondary Coating psi	TMA Tg Primary Coating C	Tan δ Tg Primary Coating C	TMA Tg Secondary Coating C	Tan δ Tg Secondary Coating C
A	95	4400	-43	-19	48	71
B	107	3000	-34	-6	-	55
C	120	7300	-39	-10	-	70

TMA Tg = Onset of Transition in TMA
Tan δ Tg = Peak in Tan δ in DMA

Table 2
FIBER PROPERTIES

Ribbon	23°C Pull Out Load lbs	23°C Pull Out Energy lb-in	90°C Pull Out Load lbs	90°C Pull Out Energy lb-in	23°C Strip Force lbs
A	1.85	0.217	0.224	0.0265	0.43
B	2.35	0.406	0.66	0.078	0.45
C	3.43	0.366	0.562	0.079	0.40

tool was subsequently cleaned by removing the stripped ribbon and any coating. The lid was left open between strips. A summary of the stripping procedure is shown below.

Ribbon Stripping Procedure

- Step 1
Equilibrate tool temperature
- Step 2
Place ribbon in holder with 30 mm protruding from end
- Step 3
Set holder in stripping tool slot
- Step 4
Align ribbon in heated groove in tool base
Close lid, hold firmly 10 seconds
- Step 5
Pull tool apart, removing matrix assembly from ribbon end
- Step 6
Open tool, remove stripped fiber, discard coating, and clean tool

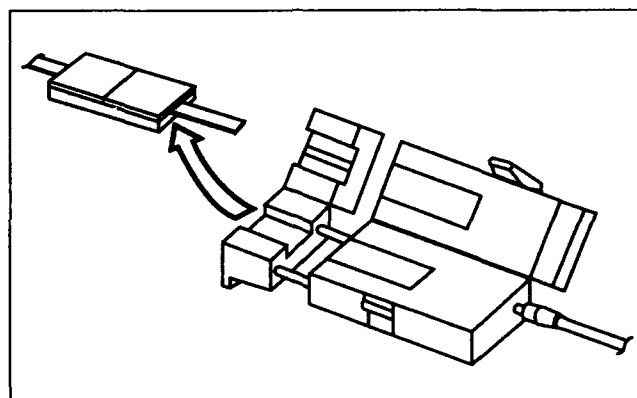


Figure 1.

In the ribbon stripping process, the two opposing blades cut through the matrix and color code to the region of the primary/secondary coating interface. As the tool is pulled apart, the blades act as a locus for initial coating tensile failure. Both the compressional push of the blades and the gripping frictional pull through the closed cover allows extraction of the fiber array and removal of the coating assembly intact. Any slippage of the ribbon in the cover clamp results in greater plowing action of the blades and consequent fraying and undesirable residue buildup on the stripped fiber surfaces. In worst case

stripping failure, the blade rides over the matrix leaving portions of scraped color code which is difficult to remove, even with several wipes of an alcohol saturated pad.

Characterization of Stripping Tools

A key characteristic of a particular ribbon stripping tool is the equilibrium temperature reached in the stripping zone at the original factory temperature setting. Two commercial tools, designated Tool A and Tool B, were examined by first following the temperature rise during heat-up with a fine wire J-type thermocouple. The closed tool was started cold and heating continuing until a steady equilibrium value was reached. The heating rate traces shown in Figure 2 indicate equilibrium temperatures of 166°C and 97°C for Tool A and Tool B, respectively, in a 5-6 minutes time period. Stability at the equilibrium level was $\pm 3^\circ\text{C}$ for Tool A and $\pm 2^\circ\text{C}$ for Tool B. Because of the great difference in factory pre-set conditions, the actual temperature of the ribbon will be quite different for the two tools after equal heating times before stripping. In fact, the factory recommended residence times of 1 second and 10 seconds for Tool A and Tool B, respectively, seem designed to give similar temperature ranges within the ribbon structure during stripping.

In both tools, heating is only on one side, in the lower body ribbon groove. The cover is unheated. With a system A ribbon placed in the closed tool, the temperature at both the heated bottom (tool base) side and top (tool cover) side of the ribbon was monitored (factory pre-sets maintained). In bottom measurements the ther-

mocouple was positioned between the heated platen and the bottom ribbon surface, while for top side measurements it was positioned between the top ribbon surface and a thin layer of paper insulating the unheated tool cover. Temperatures at the ribbon bottom were found to rise to the equilibrium value after only 5 seconds heating. The equilibrium values observed were $154 \pm 3^\circ\text{C}$ for Tool A and $88 \pm 2^\circ\text{C}$ for Tool B, both about 10°C below those observed without ribbon in the tool and the cover temperature equilibrated. These data suggest that the ribbon acts to dissipate heat from the tool. For the top side temperatures, however, the initial 5 second reading was 20-30°C lower than the equilibrium values previously observed without ribbon, but temperature continued to slowly increase over time. Plots of top side temperature versus heating time are shown in Figure 3. Since in normal operation the tool cover is left open and cool between ribbon strips, it can provide a thermal sink during ribbon heating that has the net result of creating a temperature gradient across the ribbon thickness.

Effect of Tool on Stripping Performance

Required performance attributes of a fiber ribbon are compatibility in mass fusion, single fiber break out, and mid-span entry connectorization processes. Mass fusion splicing is a popular technique used in commerce today. This method requires a clean glass fiber surface for precise fiber alignment to achieve low splice loss. A clean fiber surface is obtained by complete removal of all polymer material surrounding the fiber in the ribbon which includes primary and secondary coating, color code and bonding matrix. Any residual polymer material is undesirable and must be removed by wiping with an

Figure 2.

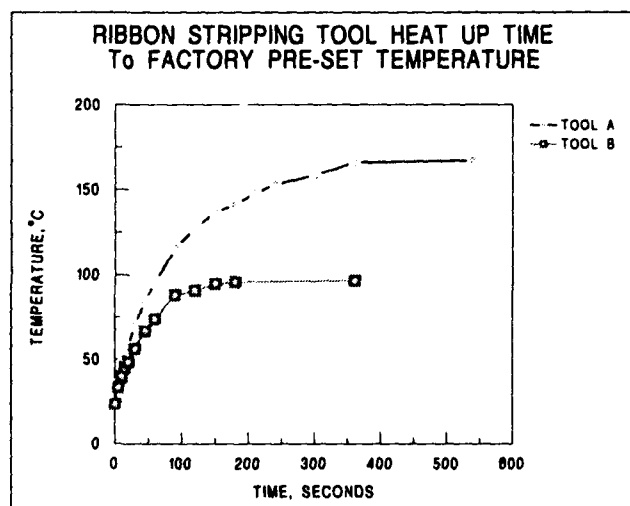
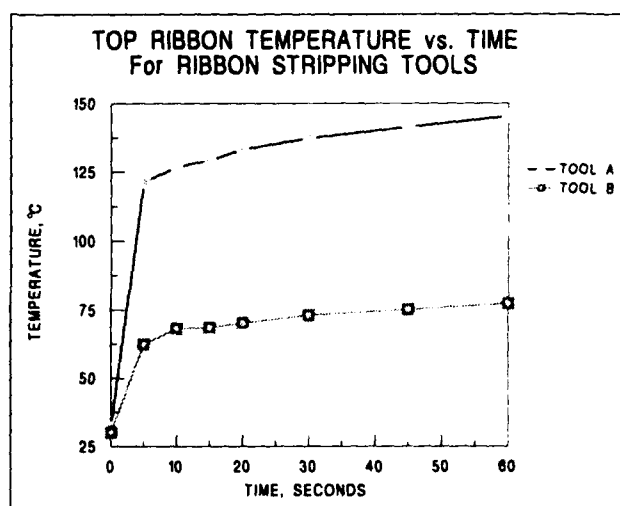


Figure 3.



alcohol saturated pad. No fibers can be damaged.

The ability of a tool to cleanly strip a 12 fiber ribbon was determined by its characteristic stripping profile over a wide temperature range. Stripping yield is the success of stripping a particular ribbon under a given set of temperature/time conditions. Ten 30 mm long ribbon samples were stripped by hand with a given tool after a fixed 10 second residence time at a given tool temperature. Stripping yield characteristics for the three 12 fiber ribbons at five stripping tool temperatures are shown in Tables 3 and 4 for Tool A and Tool B, respectively. The percentages reflect complete removal of coating, color code, and matrix with little or no residue and no broken fibers. The temperatures reported are the closed cover equilibrium values, which are somewhat higher than that actually experienced at the ribbon.

As shown in Table 3, Tool A was found to be more limited in its ability to strip ribbon. Specifically, only ribbon system A could be stripped well across the temperature range. The B ribbon system was marginal; much of the assembly came off frayed and fractured on many samples. Markedly better performance was found using Tool B on ribbon systems A and B over the same 60°C temperature range. Polymer layers on most ribbon system B specimens at or below 105°C could be removed as a single piece. When fraying occurred, it was limited to the first 5 mm of the removed polymer assembly that had been closest to the blades. Ribbon system A gave excellent performance across the range; ribbon system

C could not be adequately stripped with either tool at any temperature examined. Thus, choice of tool has a profound effect on the success of ribbon stripping, even under the same temperature range.

The ability to strip the fiber array cleanly with little or no polymeric material visible on the fiber surface after stripping is a highly desirable attribute of both ribbon and tool because it causes misalignment due to transverse offset. Additionally, polymeric residues can be charred during fusion splicing which can reduce fusion splicing strength. The matrix assembly of ribbon A was stripable as single pieces using Tool B. The level of residual material on ribbon A at all temperatures as readily removed with a single alcohol wipe, as shown in Table 5. Ribbon B had residue that could be removed with a single wipe at or below 90°C, but levels that were difficult to remove increased substantially at higher temperatures. The pattern of residue was heaviest on the central fibers of the ribbon array and towards the ends. Fiber C was unsatisfactory with portions of matrix and color code adhering tenaciously to many samples even after two alcohol wipes.

One design difference that could affect the performance of the tool with respect to stripping and residues is the elastomeric pad on the cover opposite the heated platen. In Tool A it is harder and less able to translate clamping pressure into frictional force on the ribbon. For ribbons requiring higher stripping forces, the frictional characteristics of the pad would become insufficient to hold the

Table 3
STRIPPING YIELD WITH TOOL A

RIBBON SYSTEM	75°C	90°C	105°C	120°C	135°C
A	100	90	100	100	100
B	10	70	80	80	50
C	0	0	0	0	0

Table 4
STRIPPING YIELD WITH TOOL B

RIBBON SYSTEM	75°C	90°C	105°C	120°C	135°C
A	100	100	100	100	100
B	90	100	90	-	40
C	0	0	0	0	0

Table 5
RESIDUE LEVEL WITH TOOL B

RIBBON SYSTEM	75°C	90°C	105°C	120°C	135°C
A	2	2	2	2	2
B	2	2	3	-	4
C	4	4	4	4	4

RESIDUE LEVEL: 1 NONE
 2 CLEAN 1 WIPE

3 CLEAN 2 WIPES
4 CANNOT CLEAN

ribbon in place and blade plowing would occur. The pad on Tool B was softer and more tacky. Additionally, the heated platen in Tool A stopped a few mm short of the blade so the matrix assembly was not heated directly where the initial cut was made.

Force and Energy of Stripping

The peak load experienced during fiber stripping has been used as a metric for compositional and processing variables. Generally, successful stripping has been associated with lower strip forces. This concept has been extended to obtain an understanding of the events occurring in ribbon stripping. Load versus displacement curves characterize the entire ribbon stripping process. The results for ribbon systems A-C at 90°C and 40 inches/minute using Tool B mounted in an Instron machine are shown in Figure 4. The curve shape for the most successful ribbon system, A, differed from that of the other two: for ribbon A there was an increase in load that peaked at a low displacement then decreased as the polymer assembly was removed intact, while for B and C peak load occurred over a large range of displacement and/or at greater displacement. The observation of a broad plateau or rising force in the load/displacement curve after an initial was always correlated with poor coating removal and heavy residuals.

Although the peak load observed was lower for ribbon system A than for B or C, peak force is not the sole consideration for good stripping. More importantly, all three systems behave similarly (as reflected in curve shape) up to a displacement of about 0.4 inches (10 mm). The best performing system, A, required successively less force for a given coating displacement while the inferior systems, B and C, required more. The physical phenomena associated with the 10-30 mm displacement

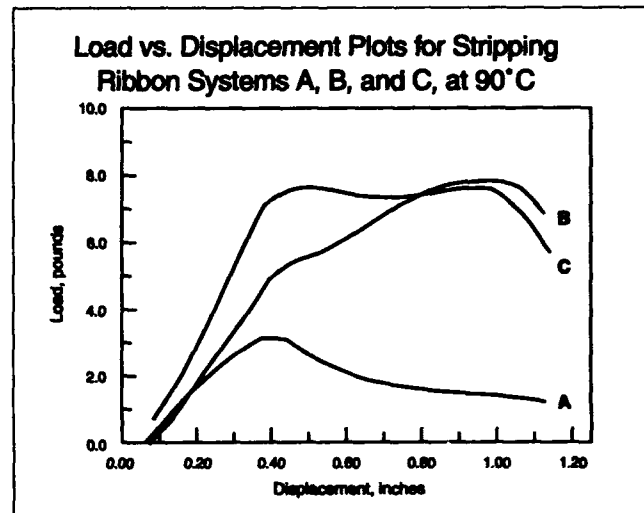


Figure 4.

region was intact coating/matrix removal in the good ribbon A system, and fraying, fiber spreading, and/or residue generation in the poor B and C systems. The former process would be expected to require successively less force as the total tube area sliding decreased with translation, while the latter deformations will cause continued resistance, maintaining or increasing the energy input needed to strip the coating.

The area under the force displacement curves was used as a metric to compare the performance of the ribbon systems at different strip temperature conditions and with each other. This energy was found to generally correlate with subjective "strippability". Values below 45 kg-mm nearly always correlated with good results, 45-60 kg-mm values with marginal results, and values above about 65 kg-mm nearly always with poor results. However, this relation was a better predictor of ribbon behavior with respect to removal of the coating/matrix

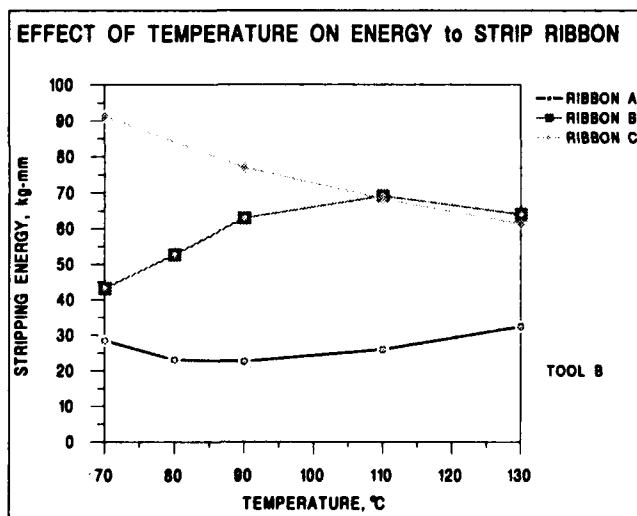
polymer assembly as a unit than of residue levels.

Using Tool B on the Instron (at 40 inches/minute and 10 second ribbon pre-strip residence time), the stripping energy for ribbons A-C was determined at five temperatures in the range 70-130°C; sample profiles are shown in Figure 5. The ribbon/conditions parameter combination with the absolutely lowest energy value obtained on the Instron was not always also judged to give the best strippability in the manual stripping mode typically used in the field. For example, ribbon B has the lowest stripping energy at 70°C, but the best stripping yield and lowest residues at 90°C. The stripping energy is, however, a general metric for hand stripping success and can guide the selection of the optimum stripping conditions. The flatter profile for ribbon A indicates tool variability in the field would be less of a problem than for ribbon B which could have limitations on the high temperature ends. The profile for ribbon C was decreasing, indicating it may enter a strippable temperature region somewhere above 135°C.

Correlation of Coating Properties with Ribbon Stripping Performance

The three ribbon systems, A-C, examined were prepared from fibers with different combinations of primary and secondary coatings, and no two of the primary or secondary coatings were identical. All fibers were color coded in the same manner, then formed into a twelve fiber edge-bonded ribbon structure using the same matrix material and process. Physical properties of the coatings and pull out and strip force properties of the pre-ribboned fibers are presented in Table 1 and Table 2, respectively.

Figure 5.



The equilibrium modulus is directly proportional to coating cross link density. The glass transition temperature was measured either by the onset of the transition in the TMA (Thermal Mechanical Analysis) plot or by the peak in Tan δ in the DMA (Dynamic Mechanical Analysis) scan. The Pull Out Test results reflect the maximum force and energy necessary to pull a 1 centimeter length of fiber out of the primary/secondary coating sheath.

The strippability of the three ribbon systems, based on stripping yield and residue level, was judged to follow the order $A > B \gg C$. There seems to be no discernible relation between the inherent cured properties of equilibrium modulus or T_g for either primary or secondary coating and strippability (Table 1). Certain coated fiber properties, however, were found to correlate with the energy under the stripping load-displacement curves (Table 2), which, as discussed above, was generally related to stripping performance. The energy required to remove the fiber from the coating in the fiber Pull Out Test done at 90°C was linearly related to the ribbon stripping energy also done at 90°C. The correlation coefficient was 0.946. Pull out energy measured at 23°C showed a reduced correlation to ribbon stripping energy at 90°C (coefficient 0.808), as shown in Figure 6. Since fiber strip force showed essentially no relation to ribbon stripping force or energy, it was a poor predictor of ribbon strippability. Thus, the sequence of events in ribbon stripping seems to more closely model fiber pull out where shear forces are concentrated at the glass/coating interface and smooth delamination is required, than fiber stripping where coating is continuously plowed away by the translation of the blade. Since pull out strength is associated with adhesion of the primary coating to the glass fiber surface, a balance must be obtained between good ribbon strippability and high adhesion.

Summary and Conclusions

This paper identifies several factors which affect performance and reliability of ribbon structures. Stripping tool design affects the ability to cleanly strip a ribbon to afford a fiber array with low polymer residuals required for mass splicing. The ribbon stripping energy measured under a load-displacement curve is a predictor of ribbon strippability. Pullout values at ribbon stripping temperatures correlate well with ribbon stripping energy.

Identification of other factors which affect performance and reliability of ribbon structures is continuing in our laboratory.

Acknowledgments

The authors thank Kenneth J. Jackson, Jr., Brian Dritschler, Claire Plaganis and Daniel Harper for ribbon stripping and in-situ coating measurements. Technical discussions with Steven Mettler are acknowledged. The authors thank Jim True for layout of this manuscript for publication.

References

1. Standley, R.D.; "Fiber Ribbon Optical Transmission Lines", B.S.T.J., Vol. 53, No. 6, July-August 1974, pp. 1183-1185.
2. Schwartz, M.I., Keenstra, W.A., Mullins, J.J. "The Chicago Lightwave Project", B.S.T.J., Vol. 57, No. 6, July-August 1978, pp. 1181-1188.
3. Tomita, S., Matsumoto, M., Yubata, T., Uenoya, T., "Preliminary Research into Ultra High Density and High Count Optical Fibers," 40th IWCS 1991, pp. 8-15.
4. Jackson, K.W., Patel, P.D., Pearsall, M.L., Petisce, J.R., Lochkovic, G.A.; "An Enhanced Ribbon Structure for High Fiber Count Cables in the Loop", 38th IWCS 1989, pp. 569-574.
5. Jackson, K.W., Sollenberger, N.W., Gentry, S.P., Brown, R.J., Petisce, J.R., Santana, M.R., Taylor, C.R., Webb, S.H.; "Optimizing Ribbon Structures for Performance and Reliability", Proceeding of the National Fiber Optics Engineer's Conference, 1993, pp 205-222.
6. Yuce, H., Wiczorek, C.J., Varachi, J.P.; "Mechanical Reliability of Ribbon Fibers", Proceedings of the National Fiber Optics Engineer's Conference, 1993, pp. 307-313.
7. Overton, R.J., Olson, T.C.; "Designing an Optical Fiber Dual Coating System for Loose Tube and Ribbon Cable Long Line and Local Loop Applications", Proceedings of the National Fiber Optics Engineer's Conference, 1993, pp. 149-167.
8. Shea, J.W., Turnipseed, J.M., Taylor, C.R., Petisce, J.R., Overton, B.J.; Material Research Society Proceedings, Vol. 224, 1992, p 85.
9. Chandan, H.C., Petisce, J.R., Shea, J.W., Taylor, C.R., Blyler, L.L., Inniss, D., Shepherd, L.; "Fiber Protective

Coating Design for Evolving Telecommunication Applications", 41st IWCS, 1992, 239-248.

Biography



Kenneth W. Jackson is a Distinguished Member of Technical Staff in the Lightguide Technology Department at AT&T Bell Laboratories, Norcross, GA. He joined the Western Electric Company in 1970 having received a B.S.M.E. from Auburn University. He joined AT&T Bell Laboratories in 1981 having received a M.S.M.E. and Ph.D. from the Georgia Institute of Technology. Since 1981, he has worked in the areas of Lightguide Fiber Fabrication, Lightguide Connectors, Materials Design, and Lightguide Cable Design and Development.



Ted L. Parker is a Member of Technical Staff in the Materials Engineering Department at AT&T Bell Laboratories in Norcross, Georgia. After receiving a BS in Chemistry from Duke University in 1971, he received a Ph.D. in Physical Organic Chemistry (Photochemistry) from the University of California-Los Angeles in 1976. For 16 years he worked in the field of polymer science for The Dow Chemical Co., developing thermoset composite matrices, latent cure film adhesives, polymeric optical fibers, and permselective membrane technology. Since joining Bell Laboratories, he has worked on the design of optical fiber coatings and the effect of aging on fiber and cable component properties.

James R. Petisce is a Member of Technical Staff in the Materials Engineering Department at AT&T Bell Laboratories in Norcross, Georgia. After receiving a BA/MA in Chemistry from Boston University in 1980, he received a Ph.D. in Organic Chemistry (Photochemistry) from Northwestern University (Evanston, IL.) in 1984.



Since joining Bell Laboratories in 1984, he has worked on the design and development of optical fiber coatings, bonded ribbon matrix materials, UV curable adhesives, index matching compounds, optical fiber color codings, and polyimide optical fiber coating. His present responsibilities include design and development of

materials for optical fiber and cable.



Neil W. Sollenberger is a Member of Technical Staff in the Outside Plant Fiber Group at AT&T Bell Laboratories in Norcross, Georgia. He is responsible for various aspects in the design and development of outside plant fiber optic cables. Prior to his current assignment, his responsibilities have included the design and development of

both copper and fiber optic closures and terminals, as well as cabinets for loop electronics. Neil Sollenberger

joined AT&T Bell Laboratories in 1978. He has a B. S. degree in Agricultural Engineering from University of Georgia, and he has a M. S. degree in Mechanical Engineering from Georgia Institute of Technology.



Carl R. Taylor is currently Supervisor of the Materials Technology and Quality Group at AT&T's main Fiber Optic Manufacturing site in Atlanta. The group has responsibility for the design and engineering of materials used in fiber optic cable and apparatus products as well as responsibility for the quality of all incoming materials

and components. He has previously been Supervisor of the Plastics Engineering and Characterization Group in Atlanta and Supervisor of the Polymer Materials Research Engineering Group at AT&T Bell Laboratories in Murray Hill, NJ. Prior to joining AT&T Bell Laboratories in 1977, he earned a B.S. in Chemistry from the College of Wooster in Ohio and a Ph.D. in Physical Chemistry from the University of Wisconsin in Madison. His graduate work focused on the physical and viscoelastic properties of polymers.

EVOLVING NEW TECHNOLOGIES FOR THE ITALIAN OPTICAL CABLE PLANTS

F. Montalti, F. Nanni (*)
F. Caviglia, D. Suino (**)

(*) SIP Società Italiana per l'Esercizio delle Telecomunicazioni, Roma ITALY

(**) CSELT Centro Studi E Laboratori Telecomunicazioni, Torino ITALY

ABSTRACT

The latest development in the components designed and specified for the optical network implemented in Italy by SIP are reviewed and the results of some year experience are reported. The attention is mainly devoted to the subscriber loop optical network and to the following components: ribbon optical cables, joints, connectors.

INTRODUCTION

Since 1986 optical fibre cables are exclusively deployed in the Italian interoffice transmission network (trunk and junction). At present more than 1 million km-fibre are laid down, and the annual growth is one of the highest among the industrialized countries: it is foreseen that about 2.5 million km-fibre will be reached by 1996 ¹.

The use of optical fibres in the subscriber loop network by SIP (the Italian Telecommunication Operating Company) has extensively started in 1991 and is progressing in accordance to the following strategy:

- deployment of optical Digital Loop Carriers to gradually replace the copper in the feeder plant. Both low-capacity DLC (30 POT channels) and high-capacity DLC (480 POT channels) are used.
- provision of an optical loop to the largest business customers, where flexible multiplexer are used for different services. Usually a double routing (ring topology) is provided. A special project has been recently launched for connecting some thousands large business customer sites in the next few years, providing advanced and high quality services through a centralized management; the first sites in Rome, Milan, Turin and Naples were served in 1992.

To push the fibre in the loop network, SIP is engaged since 1988 with a great technological effort to optimize all the network components in term of cost

and performances. This led to the development of a set of components, named "Cable System", consisting on an integrated system of modular elements (ribbon cables, fan-outs, connectors, cabinets, distribution frames, etc...) assembled as much as possible in the controlled environment of a factory.

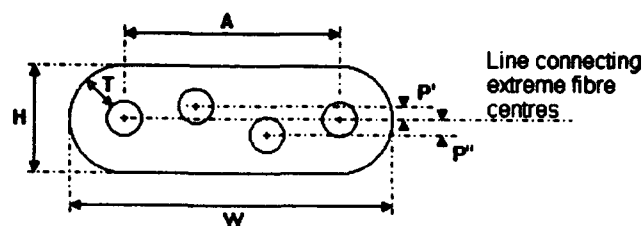
A survey of the main components of the SIP "Cable System" and the results of their first trial in field were previously given ^{2,3}. In this paper the latest technological developments in the "Cable System", are reviewed, and the results of a two year experience are reported.

FIBRES, RIBBONS AND CABLES

The fibre ribbon cable is a good solution for the subscriber network application in which the high number of fibres involved requires a low cost and an easy way to separate the fibres in groups, to identify and to splice them. Moreover design of high fibre density cables is necessary to keep small their outer dimensions for installation into conduits.

The cables designed for the SIP subscriber network (and used in the junction network as well) are ribbon cables, with four fibre ribbons inserted in a slotted core. They have a double plastic sheath, steel tape protection and aramidic yarns as strength member ². Cables of 4, 8, 20, 60, 100 and 400 fibres are used (the first two are drop cables). Both the ribbons and cables are designed and manufactured in Italy in compliance with the existing European standards.

A significant effort is devoted to the quality of the ribbon, because of its determining importance for the cable performances. The ribbon is of "encapsulated" type, the fibres are univocally coloured for identification and can be easily separated. The ribbon geometrical specification, and the actual values measured on a typical production sample are reported in Fig. 1.



	Spec. range	Mean value	Stand. deviat.	Max. value	Min. Value
H (μm)	380 ± 30	381	8	397	364
W (μm)	130 ± 5	1130	10	1133	1107
T (μm)	> 25	60	3	91	26
A (μm)	765 ± 30	754	5	763	745
P' (μm)	± 30	2	11	26	-17
P'' (μm)	± 30	1	11	28	-19

Fig. 1 Ribbon geometrical specification and values measured on a typical production sample

To optimize the ribbon performances, a new optical fibre named "Z1", with a special coating has been developed by FOS, the Italian fiber manufacturer. The new coating gives to the fibres better characteristics particularly in terms of reduced microbending and water sensitivity⁴. In Fig. 2 microbending test result on ribbons with Z1 fibres and standard fibres is reported.

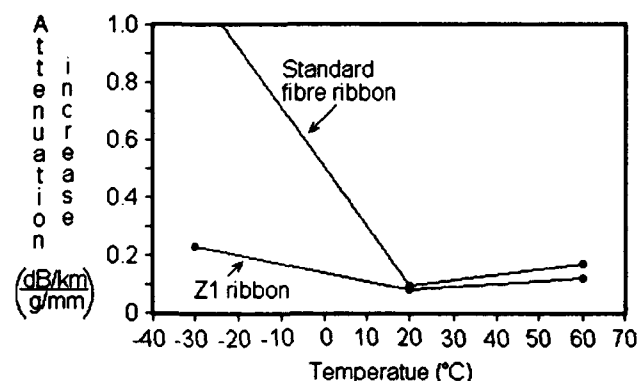


Fig. 2 Expandable bobbin test result, showing the Z1 better microbending performances at low temperature,

As for water sensitivity, reference is mainly made to water soak on ribbons at 20 °C. The ribbons with standard fibres generally show appreciable attenuation increase versus time yet after few days. On the contrary the ribbons with Z1 fibre, within the test time so far examined (more than one year), do not show any significant attenuation increase. A typical behaviour is represented in Fig. 3.

Test at higher temperature (60 °C) are now in progress; the first results broadly confirm such a trend

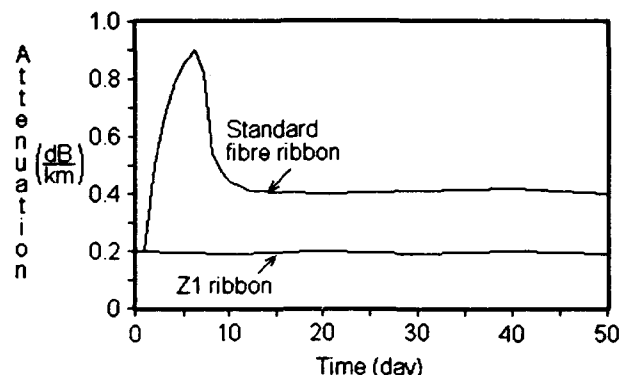


Fig. 3 A typical attenuation behaviour at 1550 nm of ribbons with standard and Z1 fibres during water immersion at 20 °C.

The uncabled ribbon is characterized and qualified with severe environmental tests (e.g. temperature, water immersion, side pressure).

The cables are characterized in the temperature range -30 °C to 60 °C, where the allowed loss increase is: 0.05 dB/km average value, 0.1 dB/km maximum value, while no loss increase is allowed in the range -15 °C to 40 °C. The tensile resistance of the cables is quite high (e.g. 450 kg for the 100 fibre cable) in order to allow the laying of long cable factory length in the existing conduits.

The cables used in the long distance network have a similar structure, but with fibre bundles on slotted cores (ten fibres in each slot). The maximum capacity is 100 fibres.

The data collected during the acceptance tests on the uncabled fibres and on the cables are stored in a database developed by SIP and CSELT⁵. This allows to analyze the cable production and to perform comparisons between products from different manufacturers.

Fibre loss data relevant to ribbon cables and to cables with fibres bundles in slots are reported in Tab. 1. Comparison between uncabled and cabled fibres and between ribbon cables and bundle cables shows no difference.

The results obtained during the cable installation and after more than three year lifetime are positive in terms of optical and mechanical performances.

		λ (nm)	Data count	Aver. (dB/km)	t. dev (dB/km)
Cable with fibre ribbons	Uncabled fibre	1310	2741	0.34	0.010
		1550	2741	0.19	0.007
	Cabled fibre	1310	585	0.34	0.014
		1550	2744	0.20	0.010
Cable with fibre bundles	Uncabled fibre	1310	22362	0.34	0.010
		1550	22362	0.19	0.007
	Cabled fibre	1310	7430	0.34	0.013
		1550	22236	0.20	0.009

Tab. 1 Statistics for the attenuation coefficient measured on bundle and ribbon slotted core cables.

MULTIPLE FIBRE JOINTING

One of the advantages in using the ribbon cable technology are the savings offered by the multiple splicing of the fibres.

The multiple fusion jointing technique is extensively used in the SIP network. The losses performances are fully satisfactory, as already reported ², the quoted results have been confirmed by further experiences, as reported in Tab. 2.

	Averag. (dB)	St. dev. (dB)	Percent over 0.3 dB
Monitoring the joint losses	0.06	0.04	0
Without monitoring the joint losses	0.15	0.10	10

Tab. 2 Typical loss values obtained in jointing by fusion 4 fibre ribbons. When the losses are monitored during the splicing, poor splices are repeated (max two time).

Another multiple jointing technique used in the SIP network is the well known MT mechanical joint ^{2,3}. This is used mainly at the central office terminations to access the "fan-out", that is the device for splitting the ribbon in four single connectorized fibres. Its performances are fair, but its convenience over the fusion splicing is still under consideration. Other mechanical joints will be experimented as well.

In the standard configuration a four fibre ribbon (two pairs of fibres) is provided to each business customer. To increase the connection reliability, from the central office to the distribution point the routings of the two pairs are different. To allow the connection

of a customer to the distribution point by simple ribbon splicing, a special cross-connect device has been developed (Fig. 4). This device is assembled in factory by single fibre fusion splices protected by an enclosure, and it is designed to guarantee high reliability and absence of modal noise.

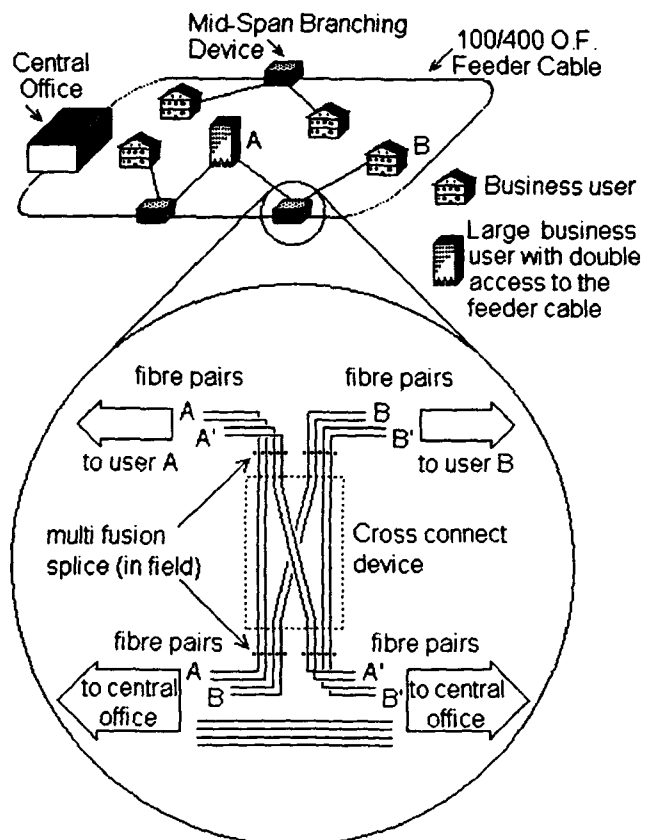


Fig. 4 Ring network structure and use of the cross-connect device.

SC CONNECTOR

In optimizing the optical network from the economical and performance point of view, connectors play a primary role for both the high number of used devices and the performances required by the use in a flexible network. Consequently a considerable effort has been devoted by SIP to this component, as outlined below.

The first type of connector used in the SIP single-mode optical network (1985) was the biconic connector, at that time widely used all around the world and whose performances were in line with the system requirements. Starting from 1988, the network evolution toward higher bit-rate system and the available interconnecting technologies suggested a revision of the network structure and components,

including the connector as well (see Fig. 5). A careful analysis of the connector market and technical comparisons among the different typologies led to the choice of the SC connector that was introduced for experimental use in 1989 on both the trunk and distribution networks.

Since 1991 the SC connector was definitely adopted in all SIP network. The connector is mostly manufactured in Italy from beginning of 1992.

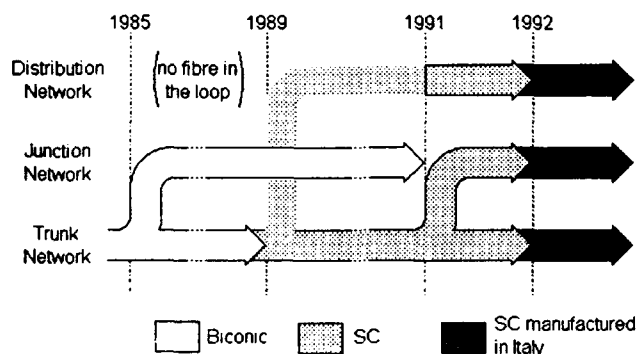


Fig. 5 Evolution of optical connectors used in the SIP network.

The actions undertaken to assure the quality of the SC connectors to be used in the SIP network include:

- the preparation of a detailed Technical Specification, based on the reference international specification (IEC, CECC),
- the setting up (at CSELT and at the manufacturers premises) of laboratories able to characterize and qualify the connectors,
- detailed studies on critical qualification and measurements aspects,
- an extensive testing procedure for the connectors supplied to SIP.

As the third point is concerned, mention can be done to the work devoted to the return loss qualification for the connector plugs and to fibre withdrawal measurement.

A problem with the return loss qualification rises if it is required to evaluate the characteristics of a single plug and not of a complete connector (two plugs mated together). The problem is solved using a "master" plug to be mated to the plug under test during the measurement. The characteristics to be required to the master plugs and their influence on the measured return losses were investigated. A method for qualifying the return loss masters and defining an "intrinsic return loss" for a single plug was developed ⁶.

Fibre withdrawal in respect to the polished end ferrule surface is a critical parameter in a physical contact optical connector like the SC. This parameter

is fairly difficult to measure due to its extremely small value (according the SIP Technical Specification the withdrawal must be less than 50 nm; an algorithm is therein indicated to derive in an univocal way the withdrawal from the plug surface profile). The measurement is usually done by mechanical profile analyzers, but interferometry can be used as well, giving some advantages. Interferometric measurement systems developed at CSELT for these parameters are described in [7].

Several qualification and acceptance tests are performed on the finished connectors and on the single components, to assure the product quality. This extensive measuring activity allows to have at present a good deal of data, showing the performance of the mass produced connector, in terms of insertion loss, return loss and geometrical parameters.

A particular attention is devoted to the intermateability among the products of different manufacturers.

In Fig. 6 and 7 examples of typical distributions of insertion and return losses measured on couples of plugs by different manufacturers and suppliers (both Italian and Japanese) are given.

NETWORK INFRASTRUCTURES AND CABLE LAYING

A complete serie of installation accessories (closures, boxes, etc...) were developed, in order to optimize the advantages offered by the use of ribbon cables in term of both technical and economical results.

The new accessories developed have been successfully tested in field and are currently used in the network. Figures. 8 and 9 show two examples.

Moreover attention is devoted to the cable installing procedures with the purpose to minimize direct and indirect costs. In particular the following techniques are object of experimental work:

- underground radar surveying to speed up the digging and to choose the best path;
- microtunneling (that is horizontal pipe pushing under the ground);
- pushing cable in conduits by the action of air or water.

CONCLUSIONS

The telecommunication network evolution toward the use of fibre-optic advanced technique is highly engaging SIP, as the other major telecommunication operating companies, in order to cope with the different user needs and with the availability of a modern, reliable, advanced and high quality telecommunication network.

Optical fibres are now widely used in the network, it is expected that the following years will be characterized by a large use of fibre optic techniques in the local loop.

The importance of using technologies that permit both savings and high network quality is a matter thoroughly investigated.

As reported, the SIP activities in optimizing the use of optical fibres in the local loop have been intensive; a particular emphasis was given to materials like connectors, splices and accessories.

The results from more than three years experience in the use of fibre ribbon cables in field are satisfactory, their use will proceed extensively in the following years.

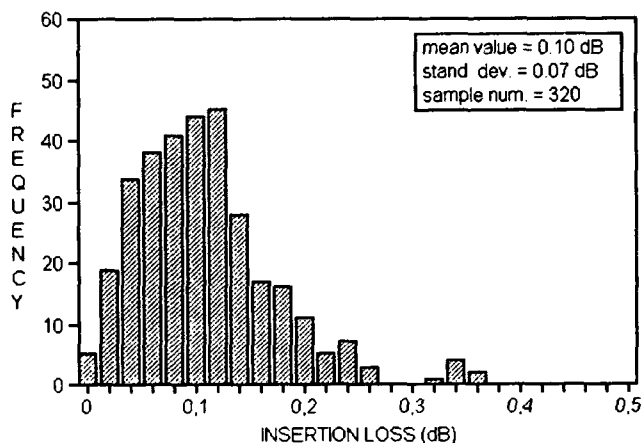


Fig. 6 Distribution of the insertion loss measured on connectors formed mating plugs of different manufacturers. The SIP Technical Specification require a mean value < 0.2 dB and a max value < 0.5 dB.

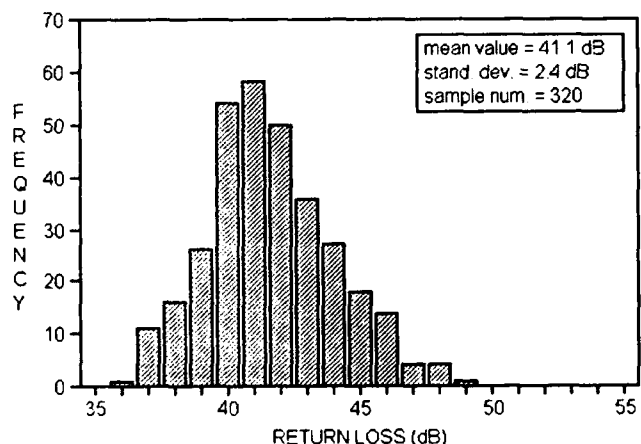


Fig. 7 Distribution of the return loss measured on connectors formed mating plugs of different manufacturers. The SIP Technical Specification requires a minimum value > 35 dB.



Fig. 8 Subscriber termination box.

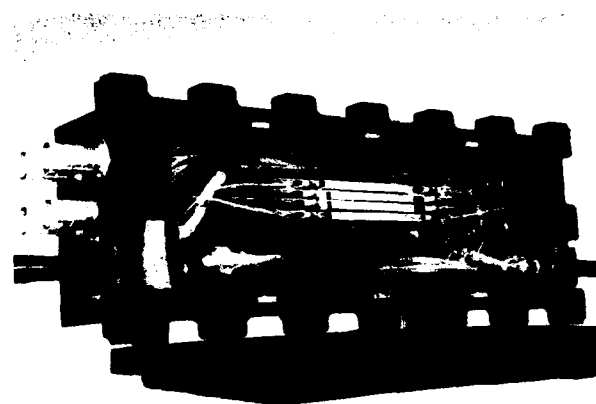


Fig. 9 Splice enclosure for mid-span branching.

REFERENCES

1. F. Esposto, F. Lombardi and A. Gambaro, "Optical Systems in the Italian Telecommunication Network", to be published in Fiber and Integrated Optics.
2. F. Esposto, F. Montalti and F. Nanni, "O. F. Ribbon Cable System Technology: the Italian Experience", 1991 International Wire and Cable Symposium Proceedings, pp 749-757.
3. A. Calantoni, G. Cerquozzi, F. Esposto, F. Montalti and F. Nanni, "Field Trials in Italy with the Ribbon Cable System", 1992 EFOC/LAN'92 Proceeding, pp 238-244.

4. G. Carones, A. Pannullo and A. Zuccala, "A Novel Optical Fibre for Ribbon Application" 1993 EFOC&N'93, pp 222-228.
5. R. Bortot, F. Esposto, G. Galliano, A. Giavelli and F. Nanni, "A Data Base for the Acceptance Test Results on SIP Optical Cables", 1993 EFOC&N'93, pp 277-280.
6. F. Caviglia, F. Esposto, G. Galliano, F. Nanni and D. Suino, "Assessing the Return Loss Performance in Physical Contact Optical Connectors", 1992 EFOC/LAN'92 Proceeding, pp 61-64.
7. A. Bollero, F. Caviglia, F. Esposto, M. Guglielmina, F. Nanni and D. Suino, "Interferometric Analysis of Optical Connector End Surface", 1993 EFOC&N'93, pp 68-71.



Francesco Montalti was born in Florence, Italy, in 1953. He received his doctorate in Physics from the University of Rome in 1976. In 1979 he joined Face Standard Research Center where he did research on optical fibres, optical components and thin film technologies.

In 1985 he joined SIP (Italian Telecommunication Operating Company) Headquarters where after being involved in the optical and copper cables specifications, is now in charge of the Cable Group in the "Outside Plant Technologies" section. His responsibilities include the activities of CCITT Comm. VI, IEC TC86B, CECC WG26. He lectures at "Scuola Superiore Guglielmo Reiss Romoli".



Francesco Caviglia was born in Turin, Italy, in 1943. He received his doctorate in Physics from the University of Turin in 1968.

He joined CSELT (Centro Studi e Laboratori Telecomunicazioni) in 1962, since then he has been engaged in: voice-frequency

and FDM transmission systems, cable and cable plants (formerly coaxial and then optical), electromagnetic compatibility.

At present he is responsible for the Physical Carrier Qualification group, dealing mainly with optical cable plants and their components (cables, connectors, etc..).

He lectures at "Scuola Superiore Guglielmo Reiss Romoli" on measurement methods and systems for optical cables and cable plants.



Fabrizio Nanni was born in Rome, Italy, in 1960. He received his doctorate in Physics from the University of Rome. During his studies from 1986 he has collaborated with a laboratory of research on optical communications: Fondazione "U. Bordoni" in

Rome working on photoconductivity ultrafast phenomena, semi-conductor laser and ultrafast photodiodes characterization.

In 1988 he joined SIP (Italian Telecommunication Operating Company) Headquarters where he has been engaged in the study and development of optical and copper cables and in optical cable specification and characterization both in laboratory and field. Moreover his present responsibilities include CCITT Com.XV, ETSI-TM1, CECC-WG28 and COST 246 activities.



Diego Suino was born in Turin, Italy, in 1962. He received his doctorate in Physics from the University of Turin. In 1989 he joined CSELT (Centro Studi e Laboratori Telecomunicazioni) where he works in the Physical Carrier Qualification group engaging at the study

and development of measurement technique on optical fibre and passive optical component.

His activity includes also passive optical component specification and characterization.

Moreover his present responsibilities include CCITT Comm. VI, and ETSI-TM1, activities.

OPTICAL GROUND WIRE A WORLDWIDE TECHNICAL SURVEY AND COMPARISON

J.P. BONICEL*, C.G. CORTINES**, J.C. DELOMEL*, G. HÔG**, S. POUILLY*, O. TATAT*, P.E. ZAMZOW**

*Alcatel Cable, **Alcatel Cable Iberica, °Câbleries de Lens, °°Kabel Rheydt AG

ABSTRACT

For approximately 25 years, telecommunication ground wires have been largely used on aerial, high and very high voltage lines. After the first generation of copper ground wires (quad or coaxial) a new generation, the optical ground wires, have been used during the last 10 to 15 years.

There are numerous parameters to be taken into account for the design of OPGW (optical fiber, electrical line characteristics, climatic environment, OPGW accessories, specific Power Utilities requirements and laying conditions...). Several OPGW structures have been developed, tested and some of them are installed.

Taking into account all the above mentioned parameters and considering the key problem of long term reliability, this paper presents the main OPGW structures used around the world with their advantages and what could be the best structures associated with accessories to guarantee a high reliability.

1. INTRODUCTION

A large number of different OPGW structures have been developed, tested and installed, considering optical fiber characteristics (lifetime vs strain, macro and microbending sensitivity, thermal stability), line mechanical characteristics (towers, spans, sags...), line electrical parameters (voltage, short circuit current, lightning), local climatic environment (wind, ice load, low temperature, corrosive atmosphere), coupling OPGW and its accessories, specific requirements of different Power Utilities (maximum pulling tension on the cable without stress on the fibers, maximum cable diameter, number of fibers, accessories, sag, cable laying under mechanical tension, maximum of cable length...), OPGW lifetime....

All of these structures have advantages and disadvantages but for the Power Utilities reliability and lifetime are the key problems, because the OPGW are widely used today in the modern high voltage power networks for telemonitoring, telecontrol... and also for Telecommunication.

The influence of the main requirements on the cable design are briefly discussed.

2. OPTICAL GROUND WIRE REQUIREMENTS

2.1. General considerations

Taking into account the different OPGW specifications already available around the world, it is not possible to meet the different requirements using only one product. So in this way, we have developed different cables with different optical cores, metallic sheaths and armors compatible with the available accessory systems. During these developments the guideline was cable reliability.

Figures 1 and 2 give an overview of typical OPGW constructions with their main advantages and disadvantages. The OPGW are often used in a harsh environment (short circuit current, lightning, climatic overload) and their lifetime must be long (25 years or more); so it is necessary to be very careful on choosing the cable design.

Element	Structure	Comments	Quotation
Optical core	Tight structure	Fiber always under stress or strain and particularly during overload	(---) reliability
		Difficult to guarantee a low attenuation ($\leq 0,22$ dB/Km) at 1550 nm	(-)
		Compactness (small optical core)	(+ +)
	Loose structure with stranded plastic tubes or plastic slotted core	Fiber exhibits a very low stress or strain level up to a very high overloading (up to 70 % of the cable UTS)	(+++) reliability
		Low attenuation at 1550 nm	(+ +)
		Crush resistance	(-)
	Loose structure with central plastic tube	Requires an optical core larger than tight structure	(-)
		Fiber exhibits a very low stress or strain level up to a high overloading	(+ +) reliability
		Low attenuation at 1550 nm	(+ +)
	Loose structure with stranded or central steel tube	Fiber exhibits a very low stress or strain level up to a high overloading	(+++) reliability
		Low attenuation at 1550 nm	(+ +)
		Compactness (small optical core)	(+ + +)
	Loose structure with stranded plastic tubes in aluminium slotted core	Radial water tightness	(+ + +) (+ + +) reliability
		Fiber exhibits a very low stress or strain level up to high overloading (up to 70 % of the cable UTS)	
		Low attenuation at 1550 nm	(+ + +)
	Compactness	(+ +)	
	Crush resistance	(+ + +)	

Figure 1 : Overview of typical OPGW constructions (optical core)

Note : On some optical cores it is possible to add an aluminium tube to improve core protection.

Element	Structure	Comments	Quotation
Armor	1 layer	- Possible to get small cable	(+ + +)
		- Necessary to use ACS Wires and the aluminium layer of the wires may be damaged during installation ====> ACS sensitive to corrosion if damaged	(- - -)
		- The cable is not anti torque (installation difficulties)	(- -)
		- Lower crush resistance than with 2 layers	(- -)
		- Short current capacity : low compared to double armored cables	(- -)
	2 (or 3) layers	- Larger cable than with 1 layer	(- -)
		- Galvanized steel wires or ACS wires or GALFAN wires are used in the first layer ====> corrosion problem, are very low	(+ + +)
		- Crush resistance improved compared to one layer armor	(+ +)
		- The cable is nearly anti torque	(+ +)
		- The short current capacity is improved compared to one layer cable	(+ + +)

Figure 2 : Overview of typical OPGW constructions (armour)

2.2. State of standardization

In most industrialized countries there are national specifications for the Power Utilities with large differences between each country's test procedures and recommended equipment. Taking into account the problem created by this situation, particularly in the case of an international market, it has been decided to start some standardization works in the IEC TC7/WG8 (1). Basically this IEC draft specification will establish the test procedures for the following items that are under consideration in the WG 8 :

- Tensile performance
- Crush
- Torsion
- Sheave test
- Aeolian vibration
- Galloping
- Creep
- Temperature cycling
- Short circuit
- Lightning
- Water penetration
- Highest allowable temperature.

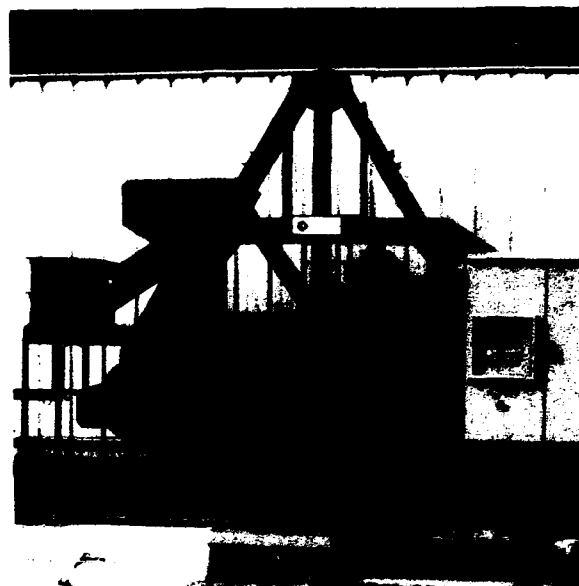
Most of our cables have been exposed to these tests with same or similar test procedures. Most of these tests are very important to give some guarantees on the cable's reliability. Figure 3 gives an example of the sheave test and the pulling test as performed on the OPGW in our laboratories.

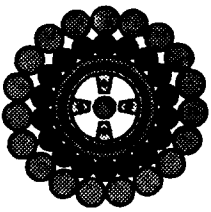
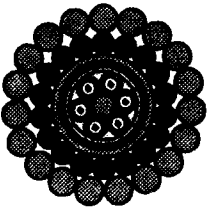
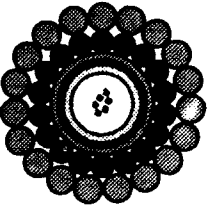
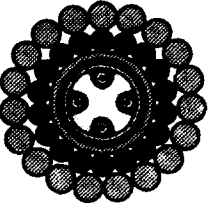
3. INFLUENCE OF THE MAIN REQUIREMENTS ON THE CABLE DESIGN

About 15 years ago some Power Utilities started to use the OPGW after different laboratory investigations. A lot of presentations have been made on the different cable structures. One of the most recent works in this area have been made by the CIGRE study committee 35 (2), who dedicated a part of the CIGRE booklet to the OPGW. Some standardizations have been also conducted by the IEEE organization (3).

Most of cables structures presented in the CIGRE booklet have been developed and tested in Alcatel Cable Group and some of them are in current production.

Figures 4.1 and 4.2 (4) give an overview of some cable designs in different families and present their main characteristics. Obviously the cross section of the armor on each cable may be modified (nature of the wires, wire diameter, number of armor layers, with or without flooding compound on the inner layers, stranding pitch...). So here we cannot present all the different products, but only a few in order to give some trends.



Cable structure with armor : 1st layer : steel wires (*) 2nd layer : aluminium alloy	Units	A	B	C	D
					
		references (5), (6), (7), (8), (9)			
- Tensile performance without stress on fibers	daN %	8260 0.7	8260 0.7	8260 (**)	8260 0.7
- Crush performance for a $\Delta\alpha$ at 1550 nm ≤ 0.1 dB	daN/100 mm	1500	1000	1400	5000
- Sheave test according to fig. 3 with a $\Delta\alpha$ at 1550 nm ≤ 0.1 dB	cycles	10 (60 bendings test) with cable ovalization	10 (60 bendings test) with cable ovalization	10 (60 bendings test) with cable ovalization	10 (60 bendings test) without cable ovalization
- Temperature cycling, change in attenuation at 1550 nm between -40°C/+80°C	dB/km	≤ 0.1	≤ 0.1	≤ 0.1 for -20/+70°C range	≤ 0.1
- Short circuit temperature without change in attenuation (**)	°C	170	170	170	170

(*) : galvanized steel wires or GALFAN or ACS (**) : limitation given by aluminium alloy wires and cable sag

Figure 4.1 : Overview of some cables designs

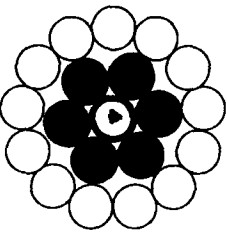
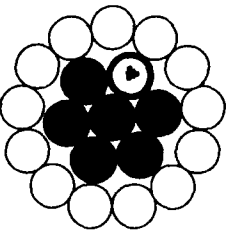
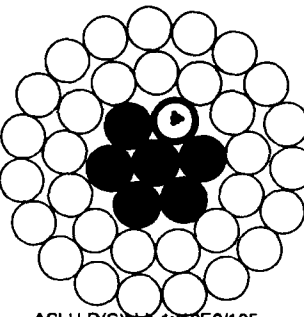
Cable structure with armor	Units	E	F	G
				
		ASLH-D(S)bb 1x6E9/125 (AyAw 52/29-5,5)	ASLH-D(S)bb 1x12E9/125 (AyAw 52/30-5,5)	ASLH-D(S)bb 1x12E9/125 (AyAw 147/13-14,4)
- Tensile performance without stress on fibers	daN %	4000 0.6	4800 0.8	7600 0.8
- Crush performance for a $\Delta\alpha$ at 1550 nm ≤ 0.1 dB	daN/100 mm	5000	5000	5000
- Sheave test according to fig. 3 with a $\Delta\alpha$ at 1550 nm ≤ 0.1 dB	cycles	under test	under test	under test
- Temperature cycling, change in attenuation at 1550 nm between -40°C/+80°C	dB/km	≤ 0.05	≤ 0.05	≤ 0.05
- Maximum temperature during short circuit without change in attenuation or birdcaging	°C	400	350	under test
- Maximum allowable temperature according to IEC 73	°C	200	200	200

Figure 4.2 : Overview of some cables designs

On these seven cable structures presented in figure 4 we can see the following trends :

- It is easy to obtain a large fiber overlength in the stranded structures with slotted core or loose tube (A, B and D structures).
- It is more difficult to obtain a large fiber overlength in an unitube structure (straight or helically extruded, structure C).
- The thermoplastic slotted core gives some improvements in the crush resistance compared to the loose tube structure, but it is not very significant. In comparison the aluminium slotted rod with loose tube inside the slots (structure D) gives a large improvement in the crush resistance performance. Depending on the accessories used and the technique utilized for the installation it could be very important to have a high crush resistant cable. In this case fibers are very well protected against lateral stress.
- On the unitube structure it could be difficult to have simultaneously a large fiber overlength (0.7 %) and a good attenuation stability at low temperature (- 40 °C).
- With the steel tube construction it is possible to make OPGW with similar diameter as the standard earth rope without fibers optics.

These are the main conclusions we have on these families of OPGW. We have results on other cable families and we are still working on them; we will present further results in the near future.

4. SHORT CIRCUIT CURRENT

The short circuit current is an important point for OPGW. This kind of cable must support high current levels depending on the line characteristics and electrical network response time (for example 0,25 or 0,5 or 0,75 or 1 s). Figure 5.1 gives the increase in temperature vs intensity and short circuit time for cables as presented in figure 4.1 and for an initial temperature of 25 °C.

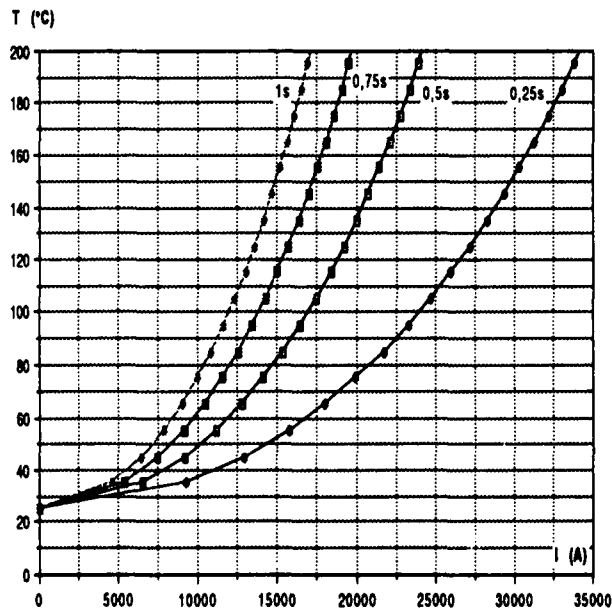


Figure 5.1 Increase in temperature vs intensity and short circuit time

Figure 5.2 gives the thermal load in % of the nominal value vs temperature for a short circuit current of 1s duration and for cables as presented in figure 4.2 F.

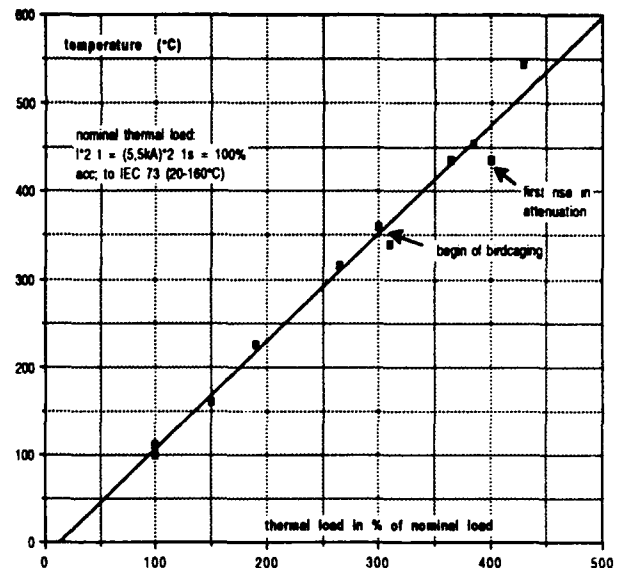


Figure 5.2 Thermal load in % of the nominal value vs temperature

Figure 6.1 and 6.2 give the sag increase vs the cable temperature and wind speed for a span of 500 m and a cable type as presented in figure 4.1.

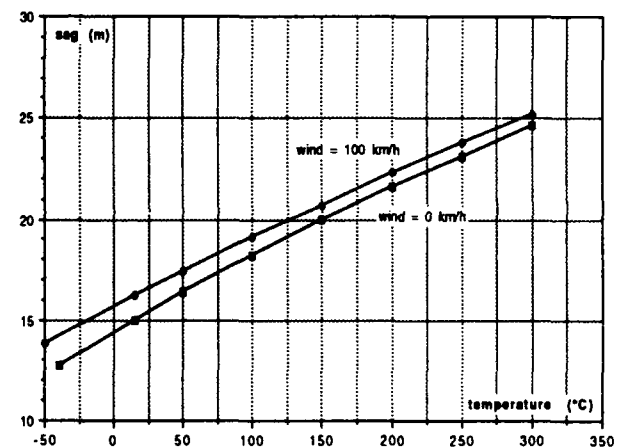


Figure 6.1 Sag increase vs cable (according to fig. 4.1) temperature

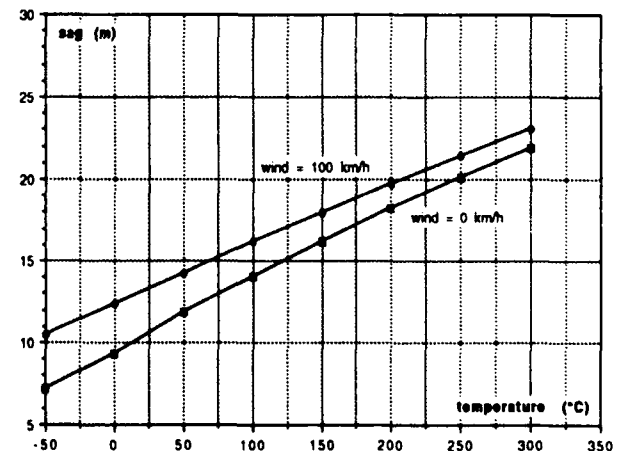


Figure 6.2 Sag increase vs cable (according to fig. 4.2 E or F) temperature

Figure 7.1 and 7.2 give the cable elongation vs cable temperature and wind speed for a span of 500 m and for the same cables of figures 6.1 and 6.2.

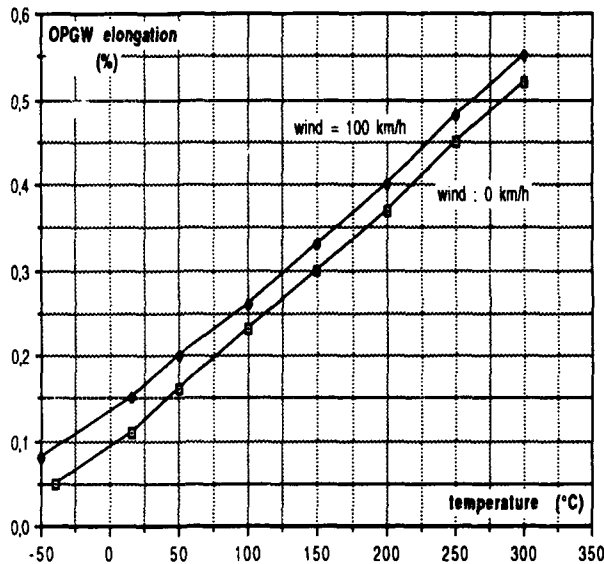


Figure 7.1 Cable elongation vs cable (according to fig. 4.1) temperature

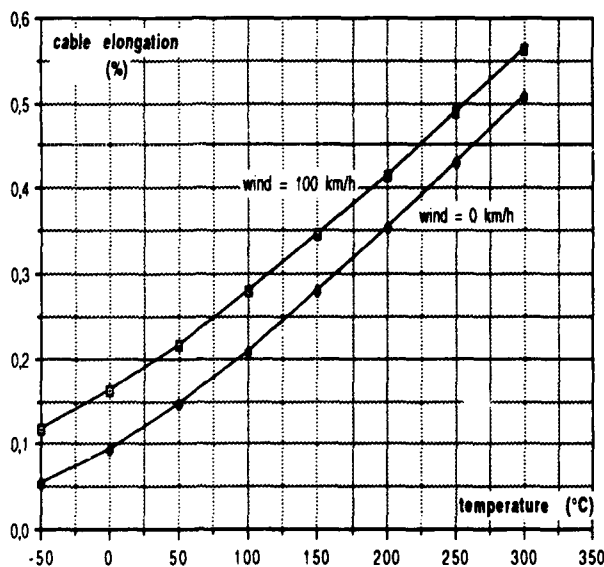


Figure 7.2 Cable elongation vs cable (according to fig. 4.2 E or F) temperature

From figures 6.1 and 6.2 we can see that the sag increase is very high when the cable reaches high temperatures: the sag increase is approximately 10 meters when the temperature rises from 25°C to 300°C. This large sag increase can create big problems, for example contact with the phase conductors. Also in figures 7.1 and 7.2 the elongation is near 0.5 % at 300°C, and due to this so high temperature most of the aluminium alloy wires loose a part of their mechanical characteristics. All these points are very bad for the high voltage line reliability, so it is recommended to limit the maximum temperature to around 170°C and to adjust the cable design to make it compatible with the short circuit current level.

5. CONCLUSIONS

This paper presents results obtained on different families of OPGW. The guide line of our works has been the reliability of the cable and of the high voltage line. In this way we have improved some cable characteristics such as crush resistance and we have preserved a high fiber freedom in the cable so as to keep the fibers nearly free of stress in all circumstances of cable utilization. Based on our different test results and calculations, and to ensure a good guarantee of cable reliability, we conclude that the maximum temperature in the cable during the short circuit current must be limited to an upper limit of around 170°C.

Since a complete control of all specific points during cable installation is not possible, the cable structure must be selected taking into account the different strains that could be applied to the cable, particularly:

- the crush resistance
- the strains at the suspension or anchoring points
- the abrasion of the outside armoring layer
- the bending and torsion
- the splice abilities (cable or optical core bending without risk for the fibers).

Other families of OPGW have been developed including other cable designs which are still under test; the results will be presented in the future and compared to the results included in this paper.

REFERENCES

- (1) IEC OPGW standard < 2nd Draft > May 1993
- (2) Optical Fiber Planning Guide for Power Utilities, CIGRE Study Committee 35/Working Group 4, September 1992
- (3) IEEE (Institute of Electrical and Electronics Engineers), Standard P 1138 for short circuit test.
- (4) H. Haag, G. Hög, and al. by AEG Kabel, Self Supporting Optical Fiber Aerial Cable Constructions..., IWCS 1991, pages 206 - 217.
- (5) A. Vicaud, P. Koutevnikoff, P. Trombert, P. Chéron «Optical ground wire communications on high voltage transmission lines», OPTO 85, Paris.
- (6) F. Duchateau, T. Hamet, P. Koutevnikoff, N. Recrosio «Silica optical fiber lins at EDF», Revue Générale d'Electricité, 1989, n° 5, pp 18-25.
- (7) P. Koutevnikoff, M. de Vecchis, JP. Bonicel «Single mode FOGW using dispersion shifted fibers». EFOC/LAN 88 Amsterdam, 27 July to 1 Aug 1988.
- (8) «Natural site mechanical tests «LAB'ECHO Vol 1, n° 3, April 1983.
- (9) P. Koutevnikoff, M. Pays, Y. Moller, A. Pannier, JP. Bonicel P. Trombert «Optical Fiber Telecommunications on the Electricity Transmission Network (Teleprotection, Teleoperation, Telecontrol) Equipment and Operating Experience», CIGRE 35-103/1990 session.

AUTHORS

Jean-Pierre BONICEL
Alcatel Cable
35 rue Jean Jaurès 95871 Bezons, France

Jean-Pierre BONICEL was born in 1952. He received his engineering degree from the Institut des Sciences de l'Ingénieur de Montpellier (ISIM) in 1976. He joined Les Câbles de Lyon now Alcatel Câble in 1977 where he was in charge of material and mechanical problems for telecommunication cables. Now he is the head of telecommunication cables laboratory and the manager for the Alcatel Optical Fiber Cable Competence Center.



Carlos G. CORTINES
Alcatel Cable Iberica
 39600 Maliaño - Cantabria, Spain

Carlos G. Cortines has received his Master Degree in Physics from Valladolid University in 1968. He joined Standard Electrica, ITT, today Alcatel, and worked in the Engineering Department of the Telecommunication Cable Division. Since 1982 he was the head of the Optical Fiber Development Group in Alcatel Standard Electrica cable factory in Maliaño-Cantabria. At present he is the Technical Director of Alcatel Cable Iberica.



Serge POUILLY
Alcatel Cable
 35 rue Jean Jaurès 95871 Bezons, France

Serge Pouilly was born in 1948. He has been graduated by Institut Universitaire de Technologie in 1971. He joined Les Câbles de Lyon in 1974 in the Submarine Division; now he is in charge of cable and machinery development in the Alcatel Cable Fiber Optic Competence Center in Bezons.



Jean-Charles DELOMEL
Câbleries de Lens
 B.P. 29 - 62301 Lens Cedex, France

Jean-Charles Delomel is the technical manager of the metallurgy department of Câbleries de Lens, a french company specialized in the production of copper, aluminium alloy rods, overhead conductors and low voltage cables.



Olivier TATAT
Alcatel Cable
 35 rue Jean Jaurès 95871 Bezons, France

Olivier TATAT was born in 1959. He received his engineering degree from the Institut des Sciences de l'Ingénieur de Montpellier (ISIM) in 1982. He joined Les Câbles de Lyon in 1985 where he was in charge of material and mechanical problems for telecommunication cables. He is now working as project engineer in the Optical Fiber Cable Competence Center at Alcatel Cable.



Georg HÖG
Kabel Rheydt AG
 Mönchengladbach, Germany

Georg Hög (42) is head of the Development Group for Optical Fiber Cables. He obtained his Dip.-Ing.-Degree from the University of Aachen and joined AEG Kabel in 1977. After being engaged in the development of symmetrical telecommunications cables he became responsible for this group in 1980. He is in his present position since 1985.



Peter E. ZAMZOW
Kabel Rheydt AG
 Mönchengladbach, Germany

Peter E. Zamzow (53) is director of the Telecommunication Development Division. After finishing his postgraduate studies in telecommunications in München and Graz as Dip.-Ing. he joined AEG Kabel in 1970. He has been engaged in development and production of telecommunication cables. In 1980 he became head of the fiber optic division at AEG Kabel and in 1982 he was nominated as a



DEVELOPING OPTIMAL PROCESSING OF HYDROLYTICALLY STABILIZED PBT FOR FIBER OPTIC CABLE CORE COMPONENTS

GARY N. GRISWOLD

GE PLASTICS
1 PLASTICS AVENUE
PITTSFIELD, MA 01201
(413) 448-4952

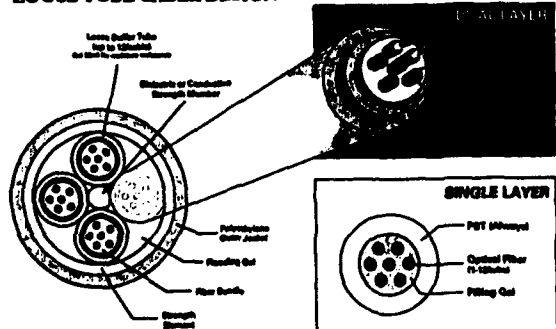
ABSTRACT

Fiber Optic (FO) Cables of the Loose Tube design typically use Polybutylene Terephthalate (PBT) in the core components (e.g. - buffer tubes). Enough concerns about the ability of PBT to resist hot, humid environments in the termination pedestal have been raised, over the past few years, to justify the specification of improved Hydrolytic Performance. This paper is a result of a multi year effort to understand the material characteristics and optimal processing conditions of a modified PBT designed to give improved hydrolytic performance. This Hydrolysis Resistant PBT (HR PBT) is unique in that its chemistry is dynamic and continues to reduce its carboxyl end groups (COOH) during processing and to some extent during cable life. In PBT, improved hydrolytic stability is achieved by reducing the number of COOH endgroups and if possible providing a mechanism to reduce the endgroups during hydrolysis.

INTRODUCTION

Below its glass transition temperature (~60 C) PBT shows fairly good resistance to the effects of moisture. However at higher temperatures, especially in the presence of various environmental factors, degradation can accelerate. If an unprotected PBT buffer tube is exposed to a hot humid environment the water present will act to hydrolyze the PBT resulting in loss of molecular weight. With sufficient loss of molecular weight, hydrolyzed PBT is typically brittle, loses its flexibility and readily cracks. The FO Industry is being required to improve the hydrolytic performance of its FO cables.

LOOSE TUBE CABLE DESIGN



Hydrolysis Resistant PBT offers the FO cable manufacturers a cost effective opportunity to significantly improve their cable performance. In today's manufacturing environment the trends are towards increasing productivity and quality while reducing costs in the effort to meet increased competitive pressures from other manufacturers.

Whenever a change must be implemented costs are involved to insure that the change will not result in lost production, reduced quality or field failures. In this case of introducing a new PBT, numerous aspects of a New Product Introduction must be evaluated. The Engineering and Production Departments must first understand the new materials properties and have enough confidence that the expense of evaluation and qualification will be justified.

This paper involves the evaluation of Hydrolysis Resistant PBT to understand its unique processing and performance characteristics. This study concentrated on evaluating only improved PBT for numerous reasons:

1. PBT is well established as a FO Cable Core Component.
2. HR PBT is a more economical upgrade over other materials (e.g. Nylon 12).
3. The HR PBT evaluated offers similar Hydrolytic performance as Nylon 12.

The methodology used in this evaluation included:

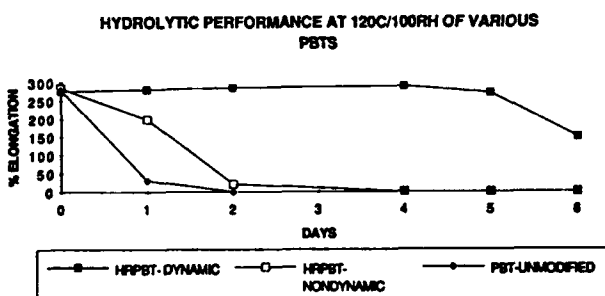
1. Material Characterization.
Understanding the material characteristics of the HR PBT.
2. Processing Capabilities.
Determining initial process conditions within the 30 mm extrusion lab line's capabilities.
3. Hydrolytic Stability Test Method.
Developing a test method for Hydrolytic Performance.

4. Process Optimization.
Conducting process optimization experiments to define the processing window of this HR PBT.
5. Continuous Improvement.
Reevaluate test methods for ways to improve accuracy.
6. Future Work.
Consider areas for further process evaluations.

FO Cable Suppliers can hopefully benefit from this experience and gain confidence that their investment in HR PBT will maximize their potential return in the form of enhanced FO cable performance and customer satisfaction.

1. MATERIAL CHARACTERIZATION

Before any process optimization can take place the processor must first understand the material's properties. The HR PBT used in this study has unique characteristics in that it is a high viscosity (~13,000 poise @ 250C) dynamic PBT. In developing this HR PBT, for extrusion applications, it was found that optimum hydrolytic performance came from this type of resin system. This HR PBT was also developed to minimize potential hazards to the production personnel. (e.g. - no potential for isocyanate fumes)



Once the rheology, drying characteristics and thermal stability are understood the initial process conditions can be determined. The search then starts for a stable linear screw design. Once a stable output is achieved, process optimization can begin. Before the process optimization is discussed the material's characteristics, drying characteristics, thermal stability and screw design selection will be reviewed.

MATERIAL CHARACTERISTICS

HR PBT DATA SHEET

The following data sheet gives typical physical properties of the HR PBT.

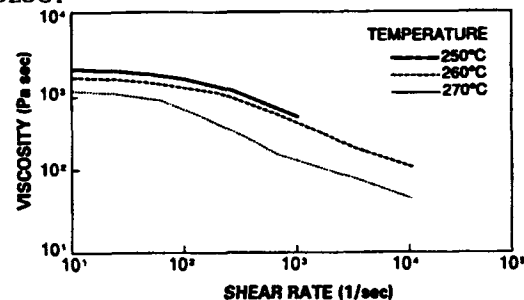
PROPERTY	TYPICAL DATA	UNIT	REFERENCE
Mechanical			
Tensile Strength, yield, Type I, 0.115"	7200	psi	ASTM D 256
Tensile Strength, yield, Type I, 0.115"	1200	psi	ASTM D 256
Tensile Strength, yield, Type I, 0.115"	1200	psi	ASTM D 256
Tensile Strength, yield, Type I, 0.115"	1200	psi	ASTM D 256
Tensile Strength, yield, Type I, 0.115"	1200	psi	ASTM D 256
Hardness, Rockwell R	115		
Impact			
Isod Impact, notched, 73F	1.0	ft-lb/in	ASTM D 256
Thermal			
MVT, 34 psi, 0.250" unannealed	265	deg F	ASTM D 256
MVT, 34 psi, 0.115" unannealed	125	deg F	ASTM D 256
CTE, flow, -40 to 100F	4.1 E-5	in/in-F	ASTM D 256
CTE, flow, -40 to 200F	4.1 E-5	in/in-F	ASTM D 256
Wire Sizing (estimated)	105		ASTM D 256
Physical			
Specific Gravity, solid	1.31		ASTM D 792
Water Absorption, 24 hours @ 73F	0.080		ASTM D 792
Water Absorption, equilibrium, 73F	0.08		ASTM D 792
Electrical			
Volume Resistivity	2.3E16	ohm-cm	ASTM D 257
Surface Resistivity	>1E14	ohm-cm	ASTM D 257
Dielectric Strength, in oil, 125 mils	44.7	kV/mil	ASTM D 149
Dielectric Constant, 25 Hz	2.96		ASTM D 150
Dielectric Constant, 60 Hz	2.96		ASTM D 150
Dissipation Factor, 60 Hz	0.011		ASTM D 150
Dissipation Factor, 1 MHz	0.0130		ASTM D 150

In addition to the standard data sheet properties this HR PBT is controlled to:

Melt Index (flow rate) : 10 - 14 g/10 min.
ASTM D1238 (2)

Carboxyl end group: 11.5 max. meq/ kg
GE Test method
VR- 5

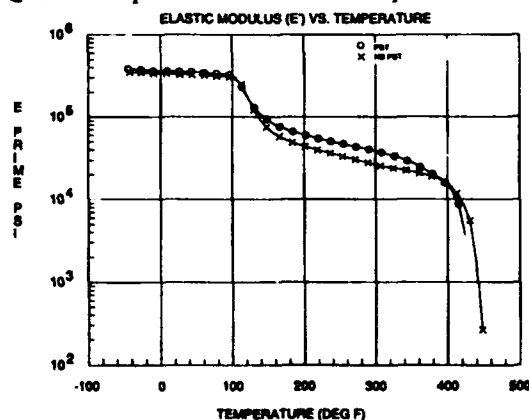
RHEOLOGY



Viscosity curves were generated with a capillary rheometer. This HR PBT extrudes well at the typical temperatures and shear rates used in FO Buffering. Although as shear rates increase and temperatures decrease the product becomes more difficult to extrude. Additional HR PBTs are under development for higher shear applications.

DYNAMIC MECHANICAL ANALYSIS

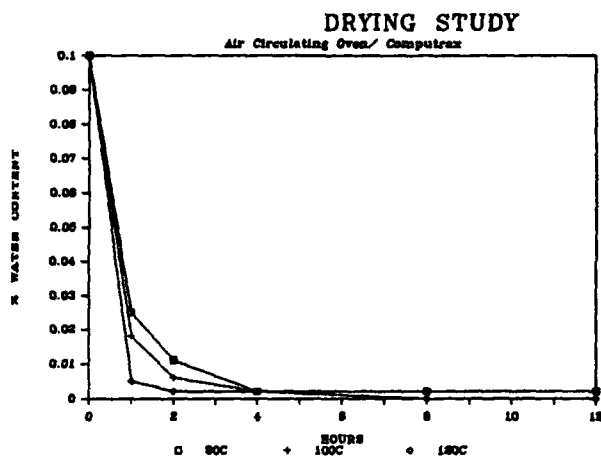
The Elastic Modulus versus Temperature portion of DMA analysis was used to determine the Drying, Melt and Quench temperatures for the initial process conditions.



The Drying temperature was selected as 250 F (121 C) maximum to avoid the pellets sticking together and to minimize the drying time. The Melt temperature was selected to be over 465 F (240 C) to develop a complete melt. The initial Quench temperature was selected to be around 100 - 150 F (38 - 66 C) to avoid thermal shocking the tubes. Upon consulting various FO cable producers it was found that substantially lower quenches are being used. Therefore the Process Optimization trials evaluated lower quench temperatures.

DRYING CHARACTERISTICS

The drying characteristics of the HR PBT were tested by first determining the material's equilibrium moisture content. (0.08 - 0.12%) Then exposing the HR PBT to 80, 100, 120 C conditions in an air circulating oven. The moisture content of samples were measured at various drying times to determine how quickly the PBT would dry. It was found that at every temperature tested the moisture content would fall below 0.04% after 1 hour. It was later found that drying should be extended to 4 hours to gain more consistent processing.

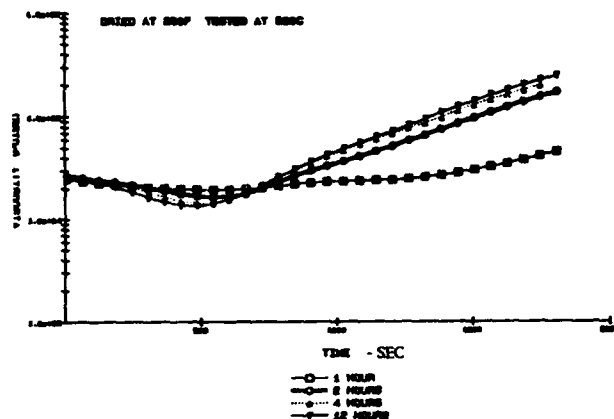


THERMAL STABILITY

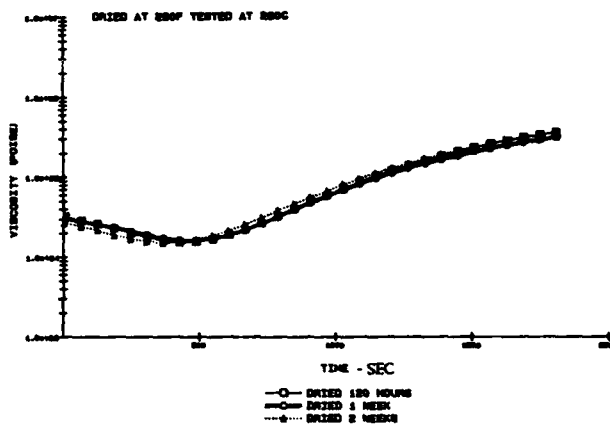
Thermal stability was evaluated by running the HR PBT in a parallel plate rheometer at 260C and 1 radian/ sec for 30 minute residence time. These test parameters were chosen because it was felt that they would accentuate any changes in viscosity with residence time versus the higher shear rates normally run in buffer tube production. The HR PBT's viscosity was measured versus residence time. This test showed the material to be, as designed, dynamic. The Melt Viscosity builds and the Melt Flow decreases with residence times up to 30 minutes.

This test was run with a few variations:

1. The viscosity build was measured to determine the effect of various drying times. It was found that the viscosity build profile would change from 0 - 4 hours but remains relatively constant after 4 hours. At this point it was determined to increase the drying time to 4 hours minimum at 250 F/ 120 C.

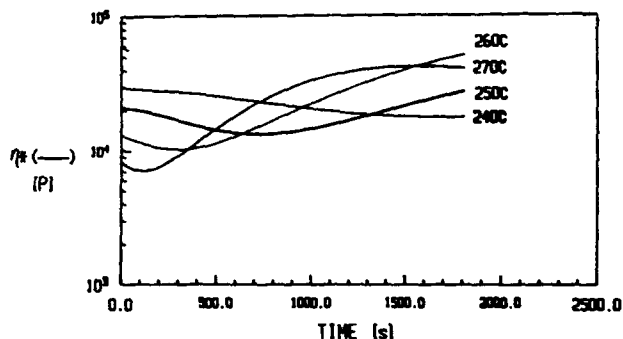


2. The viscosity build was also measured to determine the effect of extended drying up to 2 weeks (although drying at 2 weeks is not recommended). The Thermal Stability curves were similar to the curves measured at 4 and 12 hours. Therefore, the process conditions between 4 and 2 weeks of drying should be similar.



3. The viscosity build was also monitored at different melt temperatures to understand if processors would have to be concerned about excessive viscosity build during extruder downtime. All samples were dried at 250 F (121 C) for 6 hours. It was found that the viscosity profile was relatively flat at a temperature of 240 C. At higher temperatures the viscosity profile did not runaway and stayed within extrudable limits.

VISCOSITY TIME SWEEP AT VARIOUS TEMPERATURES



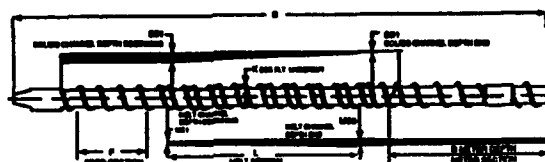
The Thermal Stability characteristics were confirmed by running an extruder at a 260 C (500 F) melt point then shutting it down and leaving it at temperature to simulate extruder downtime. After 1/2 hour the extruder was started again and the pressure, amperage and extrudate quality monitored. The pressures and amperage were substantially higher with poor extrudate quality during startup but returned to normal levels as fresh material purged the extruder.

To confirm the lack of viscosity build at below 240 C (464F) the extruder was run at a 260 C (500 F) melt stopped and temperatures reduced to 200 C and left for various times up to 3 days. Each time the extruder was restarted with the temperatures returned to 260C (500F) the extrudate was clean after a short purge of about 10 minutes at 20 - 30 RPMs.

SCREW DESIGN SELECTION

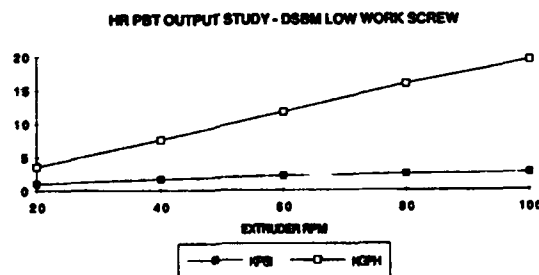
Determining the most stable screw design was done by first evaluating barrier and single flighted screws typically supplied to the FO Industry. Unfortunately, an unacceptable amount of instability and non linearity was experienced with two barrier designs and some limitations in mixing with the single flighted screws.

The best results for output stability and mixing were achieved when a Davis Standard Barrier Maddock (DSBM™) screw was evaluated.

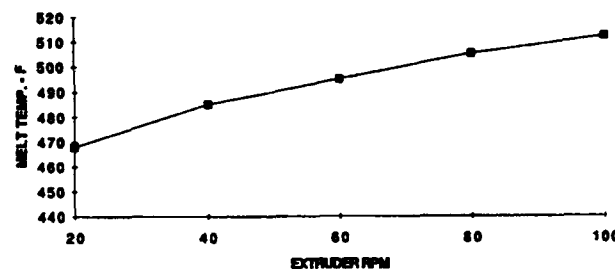


DSBM™ SCREW

The output stability could be held to around +/- 2 % with good linearity in the 20 - 100 rpm range using typical tube tooling (5.0 mm tip/ 7.0 mm die). A reverse temperature profile gave the best output stability. At RPMs over 100 the melt became slightly hazy. Since the HR PBT used in this study has a Melt Viscosity around 13,000 poise at 250 C, the melt temperature during extrusion will tend to rise with rpm. For this reason a Low Work DSBM screw was designed to help keep the melt temperature under control but still effect good mixing of color concentrates.



HR PBT - DSBM LOW WORK SCREW



2. PROCESSING CAPABILITIES

To summarize, the Material Characterization indicated the initial process conditions should be:

Drying: 4 hours minimum at 250 F (121 C).

Screw Design: DSBM™ Low Work.

Melt Temperature: 450F (235C) Minimum.

Quench Temperature: 100 - 150 F (38 - 66 C).

These studies were conducted by extruding unfilled tubes .100" (2.54 mm) OD x .070" (1.75mm) ID using an extrusion line consisting of:

1. 30 mm diameter, 24/1 L/D extruder - 120 RPM Max, 7.5 HP motor.
2. Fixed Center Crosshead - 5.0 MM Tip/ 7.0 MM Die.
3. Moveable quench trough
50 - 150 F (10 C - 65 C) capabilities.
4. Fixed trough - plant water
5. Air and Vacuum wipes.
6. Diameter Monitor - single plane.
7. Belt Wrap Capstan 18" Diameter
200 FPM (60 MPM) Max.
8. Reel Type Take Up - Tension Controlled.

During the initial trials, it was found that the capstan being limited to 200 FPM (60 MPM) the extruder was limited to 60 RPM. It is understood that the FO industry is moving well beyond this line speed but the evaluation was continued in spite of the limitation.

3. HYDROLYTIC STABILITY TEST METHOD

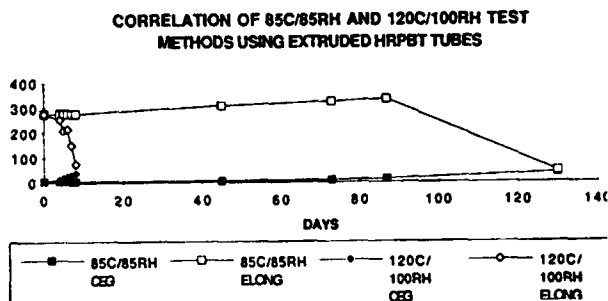
This HR PBT study required a Hydrolytic Stability test method be developed to:

1. evaluate an extruded tube sample which is similar to what the industry runs in production.
2. expose the samples to an environment and test conditions similar to what the specifying agency may require of the industry and if possible find a method to minimize testing time.
3. provide consistent repeatable results.
4. provide a means to determine if the tubes were processed to give optimum hydrolytic performance.

During manufacturing, the HR PBT pellets were tested analytically for as made properties such as Melt Viscosity, Melt Flow Index, and Carboxyl End Groups.

The Hydrolytic Stability test method developed used the .100" (2.5mm) OD x .070" (1.75mm) ID tubes extruded on the 30 mm diameter extrusion line.

The extruded tubes were tested analytically for changes in MV, MFI and CEG. The tubes were also physically tested for hydrolytic performance in both 85 C/ 85 RH (environmental chamber) and 120 C/ 100 RH (saturated steam - sterilizer) environments. The 85 C/ 85 RH was used to duplicate the controlling agencies anticipated testing and the 120C/ 100 RH testing was conducted as a means to effect accelerated aging. A good correlation was found between both exposure conditions which allowed the 120 C/ 100 RH to become the predominant test environment.



Hydrolytic Stability was determined by the extruded tube's ability to retain its original elongation after exposure to the hot humid environments. The Tensile and Elongation properties were obtained as follows:

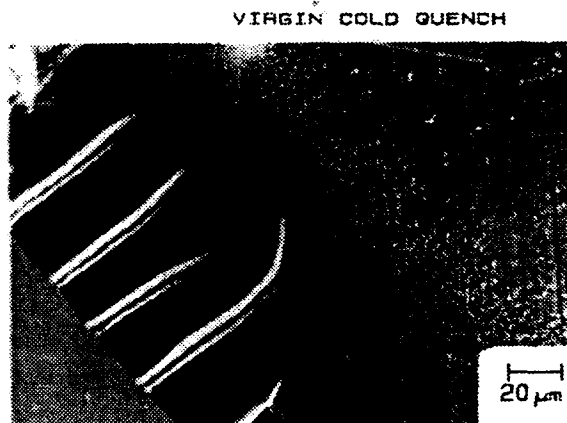
1. An extruded tube sample was cut into 2 1/2 - 2 3/4" length and measured for OD and ID.
2. Each end of the tube (~ 1/4 ") was then clamped into an air operated serrated jaws of a T&E test machine set up for a 2 inch jaw separation and 2 inch per minute head speed.

3. The tube was pulled and would typically yield at one of the jaws and continue to elongate towards the other jaw. The tube would be allowed to elongate until it reached the other jaw or it broke. The elongation at that point would be recorded as the Ultimate elongation with Yield and Ultimate Strength calculated. Five samples were pulled for each set of conditions.

Test Method Limitations. It was seen that if the tube was allowed to elongate beyond the opposite jaw the tube would slip in the jaws and cause erratic results. Since the Ultimate Elongation in this test method is not a true Ultimate Elongation it was understood that the data would be censored and difficult to statistically analyze but accurate enough to understand processing trends. It was also found that the Ultimate Strength could not be accurately measured due to the method of recording Ultimate Elongation.

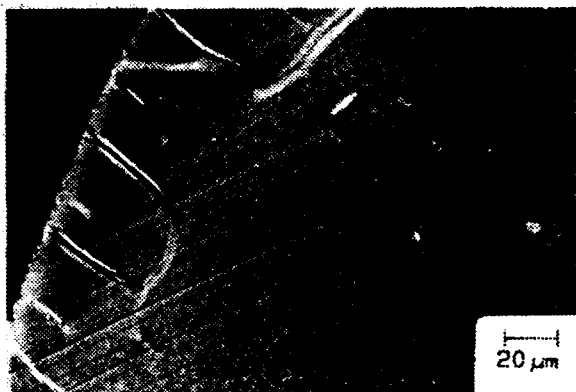
Note: Machining the tube, to allow a true Ultimate Elongation to be recorded as per the controlling agencies anticipated specification, was considered but not implemented due to:

1. The outer skin that would be removed has a unique crystal structure from the inner tube wall. The Skin-Core effect is well known in injection molding. [Ref. 8] The following micrographs show the relatively amorphous layer on the outside of the tube with a larger crystal size developing towards the center of the tube. **NOTE: The "fingers" seen perpendicular to the surface of each tube are an artifact of the sample preparation and do not reflect any discontinuity in crystal structure.**



650x

COLORED COLD QUENCH



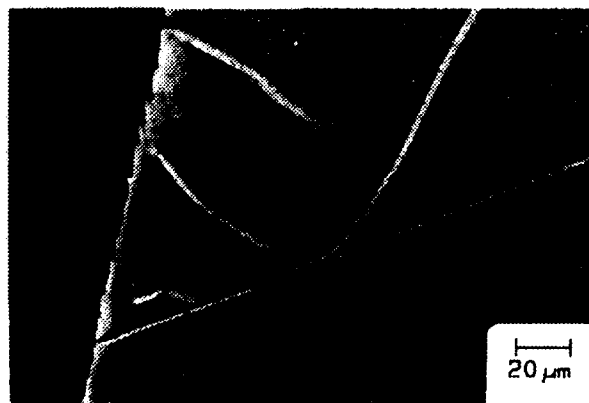
650x

VIRGIN HOT QUENCH



650x

COLORED HOT QUENCH



650x

2. An unmachined tube gives a better representation of the finished application.

3. Difficulty of machining and excessive time for sample preparation.

4. The unmachined test method provided a repeatable average initial elongation with low standard deviations. As aging occurred, the average elongation would decrease with a rise in the standard deviation.

4. PROCESS OPTIMIZATION STUDIES

The overall goal of the process optimization studies was to determine a processing window which would give optimum hydrolytic performance of extruded tubes.

The process conditions varied were:

Drying Times (0 - 24 hours at 250 F/ 120 C)

Extruder Temperatures (450 - 550 F/ 235 C - 285C)

Extruder RPM (20 - 60 RPM) 60 MPM limit @ 60 RPM.

Quench Temperature (10 C - 65 C)

Natural and with Color Concentrate (10 colors)

The processing trends that this study produced were as follows:

Drying Time showed little effect on hydrolytic performance but drying above 4 hours at 250 F (120C) gave more consistent processing.

Extrusion Temperatures:

Temperatures below 480F/ 250 C produced tubes with unmelted materials which caused low average elongations and high standard deviations.

Temperatures above 520 F/ 270 C caused two problems:

1. Degradation which gave reduced elongation during hydrolytic aging.
2. Die lip build up which is unacceptable for FO Buffer tube extrusion.

Extruder RPM showed that

1. Low Rpm and High Temperatures led to degradation.
2. High Rpm and Low Temperatures led to unmelts.

Quench Temperatures showed that a cold, close quench (~10 C, < 1" from the die) produced low elongation after hydrolytic aging.

Taking into account the difficulty in analyzing the data statistically, confidence in the processing trends is high since they are readily duplicated. The following section gives typical results seen when the processing trends are taken into consideration.

PROPERTY		PELLETS	TUBES
MELT VISCOSITY (POISE)		~13,000	13,000+
MELT FLOW (GMS/10MIN)		10 - 14	<10 - 14
CARBOXYL END GROUPS (MEQ/KG)		11.5 MAX.	1 - 6
ELONGATION	INITIAL	-	~300 %
85C/85RH Exposure	45 Days	-	~300 %
	60 Days	-	~300 %
	90 Days	-	~300 %
	120+ Days	-	<100 %
120C/100RH Exposure	4 Days	-	~300%
	5 Days	-	~275%
	6+ Days	-	<150%

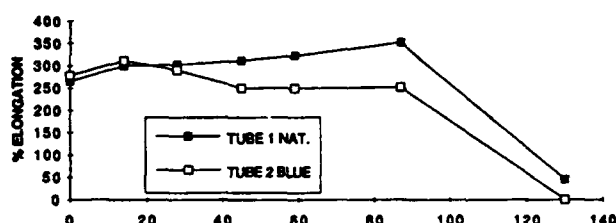
Natural versus Colorant. Initial work with colorants at 3 % loading of a colorant made of the same base resin showed little change in elongation at 30 days exposure to 85 C / 85 RH.

**85 Deg. C 85% Relative Humidity
Testing Per GEP Interpretation of TA-NWT.000020. Issue 8**

COLOR	YIELD STL. PSI	% STRAIN STD. DEV.	STL. @ MAX STRAIN PSI	% Strain Reduction vs. Natural Under Same Condition	% Strain Reduction vs. Unaged Control (30 Days)	Effects of Natural vs. 30 Days-10% Magnification Based on a 2" Standard
Natural	8200	410/9.4	4275		113.9	NO EFFECT
Blue	5660	400/36.0	4450	97	102.6	NO EFFECT
Red	5830	415/2.0	4100	101.2	106.4	NO EFFECT
Rose	5600	430/11.2	4850	104.9	110.3	NO EFFECT
Brown	5225	420/3.9	4600	116.7	107.7	NO EFFECT
Green	5300	435/10.8	4100	111.5	106.1	NO EFFECT
Violet	5000	410/2.1	4250	105.1	102.5	NO EFFECT
Yellow	5200	410/5.5	4300	100	105.1	NO EFFECT
Aqua	5350	415/6.3	4225	101.2	109.2	NO EFFECT
White	5050	420/4.5	4125	102.4	107.7	NO EFFECT
Slate	5900	415/9.2	4425	101.2	108.2	NO EFFECT
Orange	5475	395/7.9	4125	96.3	101.3	NO EFFECT

But further work at 85 C/ 85 RH showed that the addition of colorant tends to lower the elongation during long term hydrolytic aging versus natural tube.

HYDROLYTIC AGING AT 85C / 85 RH OF NATURAL VERSUS BLUE TUBES



5. CONTINUOUS IMPROVEMENT

The test method developed for Hydrolytic Stability in conjunction with the analytic testing gave very good insight into its processing window via processing trends. To improve the test methods ability to be statistically analyzed the following improvements should be considered.

1. Reduce the number of initial tubes pulled to 3. The average and standard deviation are so repeatable that three (3) pulls will give an adequate indication of initial elongation.
2. Eliminate the elongation check at 4 days exposure at 120C/ 100RH due to its similarity to the elongation at 5 days exposure.
3. Increase the number of pulls done at 5 and 6 days exposure to 10 to increase the samples size and get a better indication of average and standard deviation.

Note: The ability to obtain consistent, repeatable test results is greatly dependent on good temperature control of the test environment.

6. FUTURE WORK

This processing evaluation gave good insight in how to process a HR PBT tube. There are many other questions that could be investigated to fully understand the effects of processing HR PBT in a FO buffer tube. Some areas for additional processing studies could be:

1. The effects of processing on post extrusion shrinkage. This study would involve running buffer tubes with various drawdown ratios, quench temperatures, line speeds, etceteras. The excess fiber length would be measured as extruded and at various time intervals to determine how much shrinkage occurs and at what time does it stop.
2. Determining the production limits of the HR PBT in FO buffering and implementing improvements as needed.

7. CONCLUSIONS

Optimal Hydrolytic Performance (5 - 6 X Improvement over unmodified PBTs) of this HR PBT evaluated in this study can be achieved when .100" OD x .070" ID tubes are extruded within the following process conditions:

DRYING

4 Hours at 250 F/ 120 C (preferable in a dehumidifying dryer)

SCREW DESIGN

DSBM™ Low Work Screw.

SCREENS

60 - 100 - 100 - 40 mesh screen pack.

EXTRUDER TEMPERATURES

Water Cooled feed throat.

Barrel Zone 1:	520 F	(270 C)
Zone 2:	510 F	(265 C)
Zone 3:	500 F	(260 C)
Zone 4:	490 F	(255 C)
Clamp:	480 F	(250 C)
Head:	480 F	(250 C)
Die:	480 F.	(250C)
Melt:	480 - 520 F	(250 - 270 C).

NOTE: Due to the HR PBT's ability to build viscosity at temperatures over 240 C the extruder should not be left idle for more than 30 minutes without reducing the temperatures below 200 C.

TOOLING

Tube Tooling with Draw Down Ratio of 6.25 - 16.
Draw Ratio Balance close to 1.0.

QUENCH

20 - 25 C minimum no closer than 2 inches to die for speeds up to 60 MPM.

COLORANTS

Use color concentrate at levels no greater than 3 %.
Use color concentrates only made with same base resin.
Dry color for 4 hours at 250F / 120C to aid in mixing.

REFERENCES

1. GE Test Method VR-5. Test Method for PBT Carboxyl End Groups.
2. Characterization of Alternate Resins for Fiber Optic Loose Tubes, L. Baccaro, et. al., Wire Journal International, October 1992.
3. Bellcore TA-NWT-000020 - Issue 8, December 1991. Section 5.3.4 Cable Material Compatibility

4. ASTM D348-90 Standard Test Methods for Rigid Tubes Used for Electrical Insulation.

5. GE Test Method VFOATM - 16D. Determination of Melt Flow of PBT Resins by Using Gottfert Instruments.

6. Statistics for Experimenters. G. Box, W. Hunter, J.S. Hunter

7. The Effects of Temperature and Humidity on the Long Term Performance of PBT Compounds. W.F.H. Borman. Polymer Engineering and Science, Mid-October, 1982, Vol. 22, No. 14.

8. The Effects of Skin-Core Morphology on the Impact Fracture of PBT, S.Y. Hobbs and C.F. Pratt. Journal of Applied Polymer Science, 1975, Vol. 19.

AUTHOR PROFILE



Gary N. Griswold is a Process Development Engineer with GE Plastics, Pittsfield, MA. He holds a B.S. in Mechanical Engineering from Clarkson College of Technology, Potsdam, N.Y. - 1980 and a Masters in Business Administration from Western New England College, Springfield, MA - 1991.

ACKNOWLEDGMENTS

This paper represents the cumulative efforts of a dedicated team of Product Developers, Product Engineers, Plant Production and Quality Assurance Personnel, Analytic and Physical Testing Technicians and Extrusion Development Technicians. I want to express my deepest thanks and appreciation for their commitment and responsiveness to understanding this HR PBT. We hope the Fiber Optics Industry will benefit from our work and apply the findings to raise the bar of excellence in Fiber Optic cable performance.

**Evaluation of Creep Effects on Jointed and Unjointed
Non-Metallic Strength Members in Optical Communication Cables.**

V.E. Watson - Pirelli Cables^{*}
D. Rees, G. White - University of Glamorgan^{**}

^{*}Pirelli Cables, CCD, Newport, Gwent, UK.
^{**}Treforest, Mid Glamorgan, UK.

1. Abstract

A comprehensive comparative study of the creep properties of five yarn non-metallic strength members has been undertaken. A comparison of the creep properties of jointed aramid with unjointed aramid is included. Creep testing based on accurate LASE (Load At Specified Elongation) data were made possible by the use of a modified strain gauge arrangement. The method incorporated a mechanical contact method of creep measurement. The creep behaviour of the materials is assessed in the light of contemporary creep mechanism theories. Creep in material yarns is compared with creep in finished cables containing the same yarn as strength members. Creep data are considered in the light of a number of parameters that affect creep rate. Material yarn secondary creep rates and cable secondary creep rates were found to be constant and the same. The constant secondary creep rate of a jointed aramid material was greater than the constant secondary creep rates of two unjointed aramid materials.

2. Introduction

This paper is concerned with comparing creep expressed as percentage length increase with time in both finished non-metallic strength member yarns and finished cables containing the same yarn. The material types considered are two commercial brands of high modulus para-aramid yarn, one commercial brand of Ultra High Molecular Weight Polyethylene (UHMWPE), and one commercial brand of E-glass yarn. One of the brands of para aramid yarn is also included in jointed form and is considered as a separate material type.

By improving the understanding of the changes that take place within communication cables with time, product lifetimes will be better understood. An understanding of creep affecting parameters is necessary to enable product optimisation at the cable design stage. The creep rate dependant factors considered are temperature, creep activation energy, humidity, ageing effects and mechanical abrasion.

The secondary creep rate of a material is proportional to the applied mechanical stress to a power n , where n is a material constant. If individual yarn fibres are damaged due to chemical ageing, fatigue or abrasion the constant loading is shared between the reduced number of surviving fibres. Consequently the stress applied to each remaining fibre is increased and so correspondingly is the creep rate. The product lifetime is then reduced. Steenbakkers and Wagner [1] have reported variation in aramid fibre linear density, Young's modulus, diameter and tensile strength from fibre to fibre. No variation was reported in a longitudinal along fibre direction. The physical variations act as a source of variation in mechanical properties including creep properties.

The testing procedure is based on initial Load At Specified Elongation (LASE) testing data. Each yarn material was subjected to the same LASE test. The value of load at 0.5% strain was used as the basis for creep testing. The chosen strain represents a typical value possible under normal service conditions. Similar LASE testing was performed on lengths of finished cable.

Upon creep testing of non metallic strength member yarns two distinct types of secondary creep behaviour were evident. The three aramid yarn types (two brands and one jointed type) and the glass yarn displayed low and constant secondary creep rates. The polyethylene yarn displayed a high and increasing secondary creep rate. An assessment of the reasons for the observed macroscopic creep behaviour in terms of microscopic creep processes is given.

Cable LASE data differs from that of untwisted yarn material in that a small initial strain is required before the yarn contributes fully to the tensile performance of a cable. This feature is as a result of loss of back tension in short laboratory lengths of cable, and is not observed to any extent in large scale cable tensile testing. Cable creep follows a pattern where creep rates slow down then increase then slow down again. Cable creep rates after the initial creep

rate changes settle down to become the same as those of individual constituent material yarns. The strain is however greater in cables than material yarns due to the initial cable strain required to achieve full yarn strength contribution.

The importance of the research lies in its relevant application to cable design. The application of testing methods modified so as to reflect cable making practice has resulted in an improved knowledge of cable behaviour and lifetime. The result is optimisation of material usage.

3. Testing Procedures

3.1 LASE Testing

LASE testing was carried out prior to creep testing to determine the constant loads required for creep testing. Ten samples of each material type were taken from a single bobbin source. It is recognised that LASE, creep performance, creep lifetime, tensile strength and other mechanical properties vary from bobbin to bobbin and fibre to fibre [2]. A variation in impurity content also occurs [3]. Accurate LASE data was essential as the load required to strain each material yarn by an initial 0.5% formed the basis of yarn creep testing. The most suitable method of LASE testing yarn was to apply a soft rigid heat shrink polymer tube over the yarn so allowing the use of a 0-2.5% clip on extensometer without slippage (Figure 1).

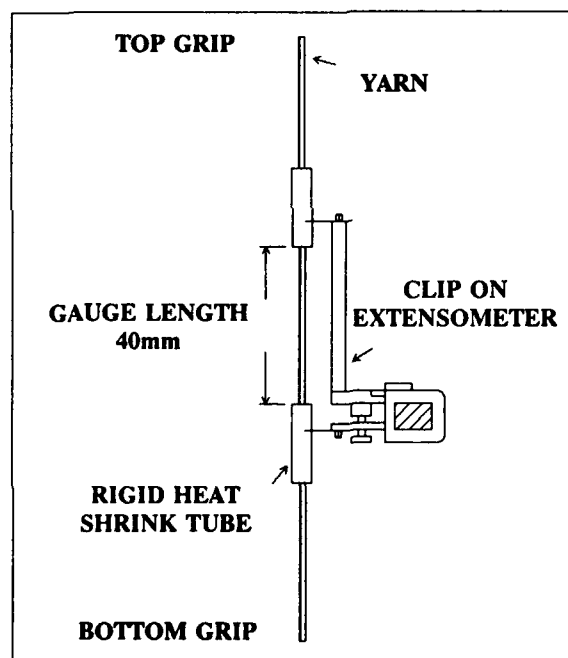


Figure 1. Yarn LASE Test Diagram

All yarn materials were LASE tested using the same test conducted under the same conditions (40mm gauge length, testing speed 40mm/min @ 23°C, 60 R.H.). Cable LASE data was produced using a 500mm gauge length Inductive Displacement Sensor (IDS), (70mm/min @ 20°C ± 2°C, 65% R.H.). It is further recognised that test parameters affect test results and that highly orientated polymeric materials such as aramid yarns generally are insensitive to changes in testing conditions and test parameters [4,5].

The LASE test results are given in Table 1.

Name	Type	Linear Density (decitex)	Load @ 0.5% Strain (N)
Yarn A	Aramid	1662 ± 100	63
Yarn B	Aramid	1648 ± 99	62
Yarn C	Jointed aramid B	1714 ± 103	62
Yarn D	UHMWPE	1739 ± 104	66
Yarn E	E-glass	7784 ± 467	88

Table 1. LASE Test Results

From the table a LASE value of 66N corresponds to a creep test loading of 6.6Kg for that material. A loading of 8.8kN was applied to cable samples.

3.2 Creep Testing

The most suitable method of supporting yarn creep specimens was found to be a combination of adhesive heat shrink tubes and cyanoacrylate adhesive to provide a loop at each end of the creep test specimen. A plastic bobbin placed inside the loop served to allow top and bottom support (Figure 2).

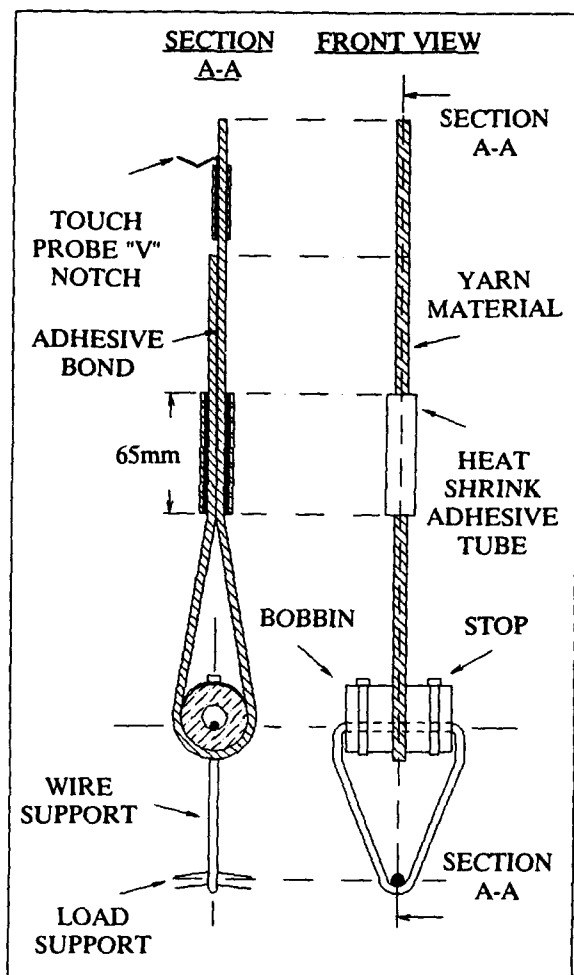


Figure 2. Yarn Creep Test Diagram

Figure 2 shows one end only of a creep test specimen, both ends are the same. Knots were found to be unsuitable as the stress concentration gave rise to premature sample failure. Heat shrink adhesive tubes containing rigid steel rods in a "v" shaped configuration provided accurate top and bottom locating points for a sensitive touch probe activated height gauge with an accuracy of $\pm 5\mu\text{m}$. The initial unstrained material creep test gauge length was 400mm. Ten samples of each of the five yarn material types were tested making a total of fifty material test specimens. The results shown represent an average value for the ten samples of each material type. The testing environment was $23^\circ\text{C} \pm 3^\circ\text{C}$ and 60% R.H. Results were collected over a period of eight months.

Cable creep tests were performed at $20^\circ\text{C} \pm 2^\circ\text{C}$ and 65% R.H (Figure 3).

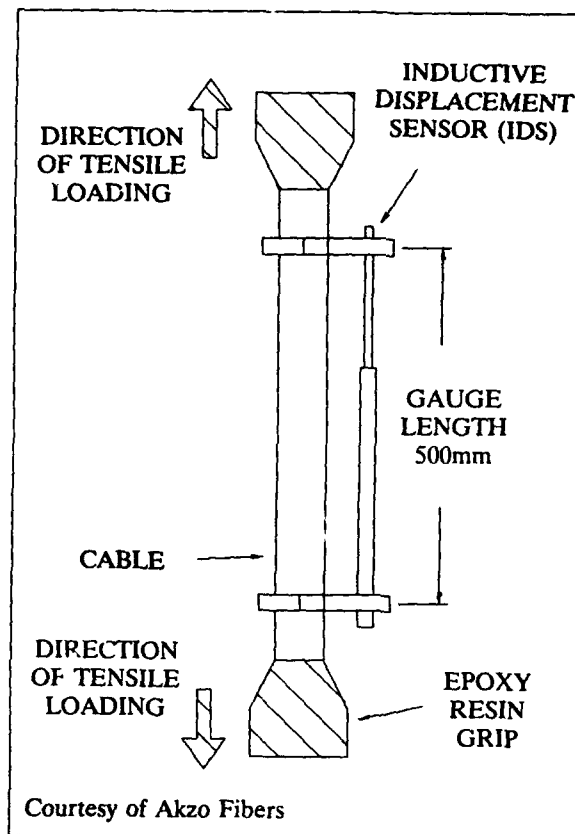


Figure 3. Cable Creep Test Diagram

Tests were performed at a load value corresponding to 25% of the breaking load of cable. Aramid yarn and a central strength member rod were encapsulated in epoxy resin. The IDS was clamped on the cable in such a way as to register aramid yarn length changes.

The material yarn creep test results (Figure 4), show that all materials increased in length with time. The results show only material creep. The total elongation is the material creep plus 0.5%, as the total elongation is the sum of the material creep and the initial strain due to loading. All materials exhibited a primary creep phase typically lasting less than 500 hours. Secondary creep results indicate that the materials fall broadly into two groups. The glass and aramid materials had constant low secondary creep rates. The UHMWPE results show a different type of creep behaviour whereby the secondary creep rate was higher than that of the other material yarns and increased with time. The value of creep rate for UHMWPE is an average value over the period of testing.

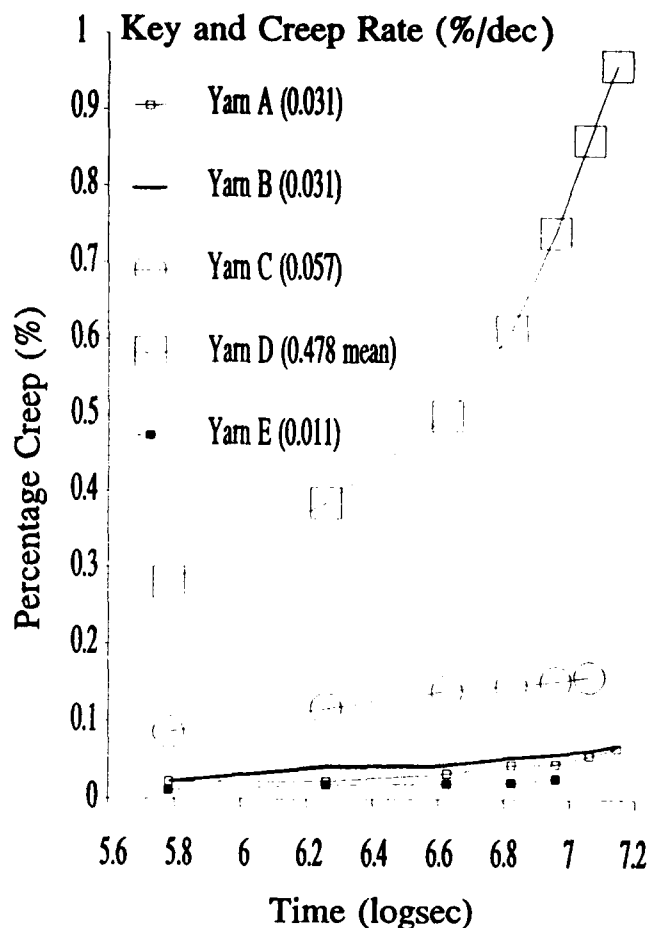


Figure 4. Yarn Creep Test Results

The jointed material yarn showed a higher initial strain upon loading than the unjointed material yarn. The jointed material yarn also possessed a higher creep rate than the unjointed material yarn. The reasons for differences in creep behaviour are discussed in Section 4.2.

Creep tests on three samples taken from the same cable length show that during the primary creep phase the creep rate is very low indeed and approaches zero (Figure 5). The creep rate then increases to a value significantly greater than that quoted by the manufacturers for the material yarn [6,7,8]. A rapid slowing down of the creep rate follows until the creep rate of the cable remains constant and the same as the manufacturers quoted value for the material yarn. No further fluctuations in creep rate are then observed over the ten day period of testing.

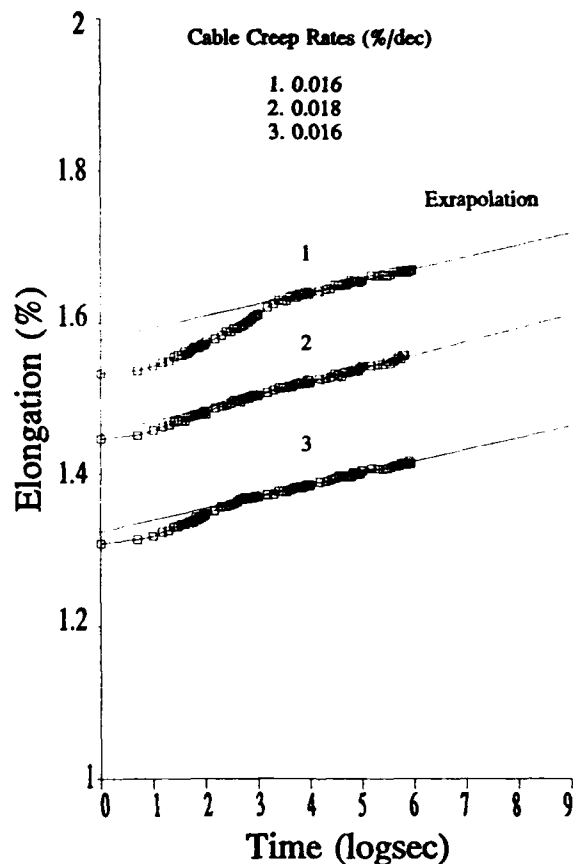


Figure 5. Cable Creep Test Results

3.3 Fatigue Testing

The configuration of the fatigue test used on material yarns is shown in (Figure 6). The yarns were wrapped around 60mm diameter aluminium alloy capstans and clamped between two 40mm aluminium alloy plates. A gauge length of 500mm was used. Six specimens of each yarn material were subjected to fatigue cycling with a sinusoidal displacement at each of 1, 10, 100, 1,000, 10,000, 100,000 and 1,000,000 cycles, making a total of forty two samples per yarn type. The machine was operated in load control mode. The load was taken from the LASE data and was the load that gave an initial 0.5% strain. The maximum cyclic loading was the same as the creep test loading. The six samples of each yarn material at each number of cycles were tensile tested after fatigue cycling.

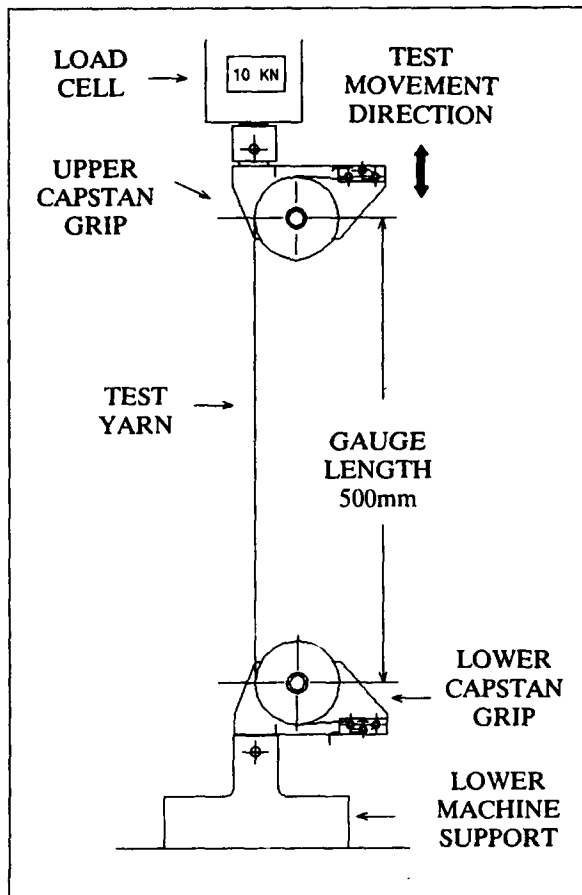


Figure 6. Fatigue Test Diagram

The tensile strength of the yarns is shown as a percentage of the mean strength of non fatigue cycled yarn (Figures 7 a,b and c). The results shown in three parts for clarity give a clear indication of loss of mechanical strength due to mechanical abrasion around the capstans. Mechanical abrasion of yarn against yarn and fibre breakage at the clamps was clearly visible during and after testing. The glass samples failing completely during the test through abrasion. The jointed aramid yarn also suffered from abrasion at the clamps but failure was due to pulling apart of the joint. The implications are that mechanical abrasion serves to reduce the number of surviving fibres such that the remaining fibres are subjected to an increased mechanical stress.

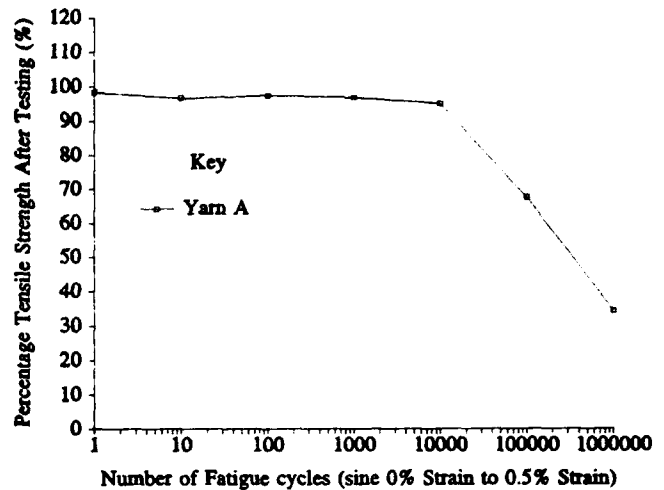


Figure 7a. Yarn A Fatigue Test Results

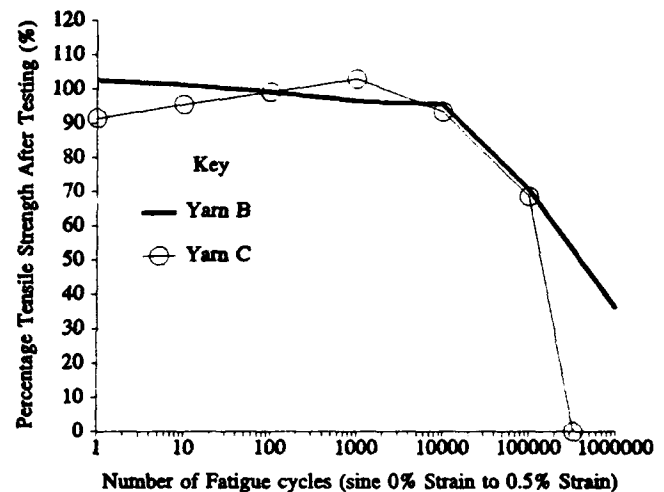


Figure 7b. Yarn B and Jointed Yarn C Fatigue Test Results

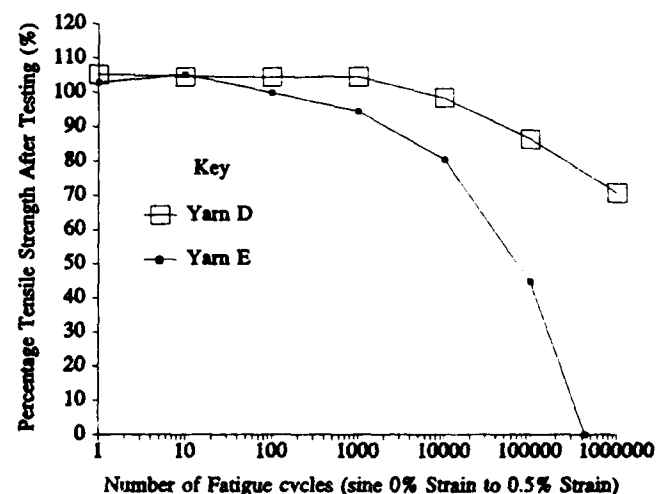


Figure 7c. Yarn D and Yarn E Fatigue Test Results

4. Discussion

4.1 Discussion of Material Yarn Creep

The material yarn creep test results show that samples from single bobbins of the two brands of aramid tested possessed the same creep rate. The UHMWPE creep rate was appreciably higher than the four other material types. The creep rate of UHMWPE increased with time. The jointed yarn material had a creep rate 54% greater than the unjointed material. The glass yarn material possessed the lowest creep rate of all at 0.011 dec/%. In contrast to the creep rate data, the yarn fatigue test percentage strength loss data shows that UHMWPE suffered least from the strength reducing effects of mechanical abrasion and the glass yarn suffered the most. It was observed that the smoothest material yarn (UHMWPE) suffered least from the effects of mechanical abrasion and the roughest yarn (E-glass) suffered most.

The material yarn creep test results identify two distinct groups of rigid non-metallic strength member materials. The aramid and E-glass materials tested as stated, possess low and linear creep rates. It has been suggested by Wagner et al [9] that the dominant creep mechanism of materials like aramid and E-glass is molecular chain scission. In the case of aramid materials breakage of carbon-nitrogen bonds is suggested as the likely main cause of creep [10]. On this basis it would seem likely that the main cause of creep in glass yarns is breakage of silicon-oxygen bonds in short range silica tetrahedra networks. Breakage of bonds results in an increased stress and consequently increased straining of neighbouring bonds in the rigid long chain molecular systems. The increased strain is observed as an increase in fibre length.

It has also been suggested by Wagner et al [9] that the creep behaviour of UHMWPE is dominated by molecular chain slippage leading to the observed high creep rates that increase with time. It is the creep activation energy (H) which must be overcome to cause either chain slippage or chain scission in a material. Chain slippage is the process whereby the aligned molecules slide past each other under load, material creep activation energy is low. Chain scission is the process by which aligned molecular chains break under load at the weakest link, material creep activation energy is high. A high creep activation energy indicates a material with a high degree of resistance to mechanical creep. Differences in mechanical properties from bobbin to bobbin would suggest some variation in activation energy and therefore creep rate from bobbin to bobbin [11]. It would seem probable that the creep activation energy

is not a true material constant. Scope for further work exists, whereby the calculation of creep activation energies based on creep testing of yarn materials over a range of mechanical stresses and temperatures would give a clear indication as to whether creep activation energy is a production related variable or a material constant.

The creep rates recorded as part of independent testing are significantly higher than those published by aramid yarn manufacturers. Published values are less than 0.02 %/dec for aramid. The values recorded as part of the authors testing are 0.031 %/dec. The increased creep rate is believed to be due to exposure to ultra violet radiation causing degradation. This view is supported by an observed darkening in colour of aramid yarn materials.

It is apparent that total cable strain after a nominal twenty or thirty years will be close to that of the material yarn. This conclusion will hold true since with full length cable sample tests the initial strain required to tension the aramid yarn in the cable is not present. It is recognised that creep lifetimes and extrapolated data are subjects to considerable scatter and should be treated with caution.

Wetting of previously dry material yarns with water during creep testing has been shown by Cook and Howard [12] to initially give rise to an increase in the creep rate of aramid yarn followed by a return to a creep rate very close to the original dry creep rate even though the yarn remained wet. The result was an increased strain without an increase in the creep rate. In the future failure of aramid and UHMWPE yarns in tension will occur at points of stress concentration. Points such as fibre surface defect sites. Splitting and peeling of aramid by the process of surface fibrillation will take place at points of stress concentration until failure in tension occurs [13].

4.2 Discussion of Creep in Jointed Aramid Yarn

Creep in jointed aramid is comprised of two separate components. The extension is the sum of true mechanical material yarn creep and some tightening or pulling together of the joint. The end effect is that the extension upon loading is greater than that of unjointed yarn and the creep rate is higher.

Cable LASE measurements like those of jointed yarn are gauge length dependant whereby the total extension required to tension a joint or short cable sample is constant irrespective of the length of the yarn or cable. In very short cable samples such as the ones used for LASE and creep testing the back tension of the yarn generated during stranding is relieved such that the yarn strength members may slacken. In commercial lengths of cable the back tension will tend to be fixed in place by the constraining effects of length. Therefore, the longer the gauge length the less the amount of tensioning is as a percentage of total cable length.

The LASE performance of jointed yarn is significantly less than that of unjointed yarn when using very short gauge lengths. In a 100m long cable no difference in LASE performance can be detected. For example, if there is 1mm take up of slack within a joint upon tensioning that equates to 2% strain in a 50mm gauge length. If a 100m gauge length is used the 1mm take up equates to one millionth of one percent strain and so the effect is not detectable.

4.3 Discussion of Creep in Cables

The cable creep samples consisted of aramid strength members and a central strength member embedded in epoxy resin at both ends. The cable LASE and creep test data therefore relates to this combination of strength contributing materials. The overall strength contribution was dominated by the aramid and so the creep rate of the cable is that quoted by the aramid manufacturer. This would suggest no progressive straightening out of lay length took place after the initial settling down of the creep rate.

It can be seen from Figure 5 that the initial cable creep rate is low, increases, then reduces to a value the same as that of the material yarn. This process is not clearly understood. Further work on this phenomena would need to take into consideration the effects of stranding including lay length, the contribution of the central strength member and creep test gauge length.

The work has shown that differences in creep performance between material yarns and cables exist. Only cables exhibit high initial strains and creep rate fluctuations. The work has identified that the secondary creep rates of material yarn and cable containing the same material yarn as strength members were the same. The total elongation of the cable samples was greater than the total elongation of material yarn. A twisting effect may occur when a load is applied to an aramid stranded cable where there is torque imbalance.

4.4 Creep Equation Discussion

The equation given below [14], gives an indication of the effects of mechanical stress, creep activation energy and absolute temperature on secondary creep rates. It is known that secondary creep rates are closely related to the Arrhenius equation :-

$$c_s = K \sigma^n e^{-H/RT} \dots\dots\dots(1)$$

c_s is the secondary creep rate (%/dec)
 K is a scaling constant.
 σ^n is the engineering stress (Pa).
 n is a material constant
 H is the creep activation energy ($J \text{ mol}^{-1}$).
 R is the universal gas constant ($8.314 J \text{ mol}^{-1} K^{-1}$).
 T is the absolute temperature (K)

$$c_s \propto \sigma^n \dots\dots\dots(2)$$

From equation 2 the secondary creep rate of any given material yarn is proportional to the engineering stress to the power n , and therefore load to the power n as well. Providing the cross sectional area and the temperature remain constant.

$$c_s \propto e^{-H} \dots\dots\dots(3)$$

From equation 3 the secondary creep rate of any given material yarn is proportional to the inverse exponential of the activation energy for creep. Providing the temperature and engineering stress remain constant.

$$c_s \propto e^{-1/T} \dots\dots\dots(4)$$

From equation 4 the secondary creep rate of any given material is proportional to the inverse exponential of the reciprocal of absolute temperature, providing the engineering stress remains constant.

It is seen that from equation 2, an increase in strain or load on any individual fibre for what ever reason will serve to increase the secondary creep rate. Consequently the net effect of fibre damage due to mechanical abrasion will be to increase the secondary creep rate.

Ageing of cables and material yarn may result in weak, broken or a reduced Young's moduli of fibres. Fibre failure will result in an increased creep rate as described. A reduced Young's modulus will result in increased elongation at any given load thereby shortening cable product lifetime. From equations 3 and 4, usage of materials with reduced creep activation energies, or an increase in temperature will serve to increase material secondary creep rates [15].

4.5 Justification

This work has shown how an assessment of creep and creep related effects combine to give a better understanding of cable properties with time. This type of work provides valuable input at the design stage leading to better cable design and material optimisation.

5. Conclusions

On the basis of the testing presented in this paper, the secondary creep rate of aramid material yarn and aramid stranded finished cables have been found to be the same under the same conditions. The total percentage length increase of short cable samples under tensile loading will be greater than that of constituent yarn tested independently under the same conditions. This difference is due to the strain required to restore back tension in cable yarn strength members. The material yarns with the lowest creep rates have the highest creep activation energies. The dominant process in low creep rate yarn materials is believed to be chain scission. The creep rates are likely to increase if yarn non metallic strength members are subjected to certain types of chemical ageing, and mechanical damage under load. It is suggested that the aramid creep rates recorded by the authors are higher than those recorded by manufacturers due to the degrading effect of ultra violet radiation during testing.

Appendices

References

1. Steenbakkens, L.W., Wagner, H.D., **Elasticity and Mechanical Breakdown of Kevlar 149 Aramid Fibres by a Probabilistic Approach**, J. Mater. Sci. Lett., 7(11), pp 1209-1212, 1988.
2. Cook, R., **A Simple Kinetic Approach to Fibre Failure : 2. Lifetime Distributions**, Engineered Material Abstracts 8708, 27(12), pp 1895-1898, 1986.
3. Pruneda, C.O., Morgan, R.J., et al., **Impurities in Kevlar 49 Fibres**, 21(5), pp 17-20, 1985.
4. Wagner, H.D., **Stochastic Concepts in the Study of Size Effects in the Mechanical Strength of Highly Orientated Polymeric Materials**, Jnl. Polym. Sci., 27(B), pp 115-149, 1989.
5. Wagner, H.D., **Ultimate Behaviour of Advanced Polymeric Fibres and Whiskers : A Stochastic Study of Size Effects**, Engineered Material Abstracts 8903, pp 623-632, 1988.

6. **Twaron Technical Documentation**, Enka bv, Product Group Industrial Fibres, 1985.

7. **Twaron Info Note QET004**, Akzo Fibers and Polymers Division, 1992.

8. **Kevlar for Communication Cables**, DuPont de Nemours International S.A., 1992, pp 33-35.

9. Wagner, H.D., Schwartz, P., Phoenix, S.L., **Lifetime Statistics for Single Kevlar 49 Filaments in Creep Rupture**, J. Mater. Sci., 21(6), pp 1868-1878.

10. Phoenix, S.L., Wu, H.F., **Lifetime Statistics for Single Kevlar 49 Filaments in Creep Rupture at Elevated Temperature**, I.C.C.M. and E.C.C.M., 4, pp 278-286, 1987.

11. Wagner, H.D., Phoenix S.L., Schwartz, P., **A Study of the Lifetime of Aramid Fibres Under Constant Stress**, 5th I.C.C.M. San Diego Calif., 5, pp 245-275, 1985.

12. Cook, J., Howard, A., **Creep, Stress Rupture and Degradation Effects in Organic Fibres**, R.A.R.D.E. Waltham Abbey, NP4.

13. Wagner, H.D., **A Model for Longitudinal Splitting From Surface Defects in Anisotropic Filaments**, J. Mater. Sci. Lett., 5(2), pp 229-230, 1986.

14. Gere, J.M., Timoshenko, S., **Mechanics of Materials**, Chapman and Hall, 3rd edition, pp 859-862, 1991.

15. Wu, H.F., Phoenix, S.L., Schwartz, P., **Temperature Dependence of lifetime Statistics for Single Kevlar 49 Filaments in Creep Rupture**, Jnl. Mater. Sci., 23(5), pp 1851-1860, 1988.

Disclaimer

Testing of commercial non-metallic strength member yarn type materials in no way represents endorsement or criticism of those materials or jointing processes applied to them. Other suitable materials not included here may be available.

Acknowledgements

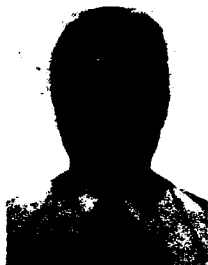
The authors would like to express their thanks to the Teaching Company programme between Pirelli Cables and the DTI/SERC for their support of this paper.

Appreciation is extended to Martin Davies for his help and advice in the preparation of this paper.

Also the authors would like to thank Akzo Fibers for creep testing carried out on company cable samples, and the supply of creep test data.

Biographies

Vincent Watson attained a B.Sc.(Hons) Degree in Applied Science from Staffordshire Polytechnic in 1989, and a P.G.C.E. from Bristol University in 1990. He is presently working on a two year Teaching Company project leading to an M.Phil degree supported by Pirelli Cables and the University of Glamorgan/DTI.



David Rees is the Associate Head of the Department of Electronics and Information Technology at the University of Glamorgan. He gained the Degree of B.Sc in Electrical Engineering from the University College of Swansea in 1967, and a Ph.D in 1976. His industrial experience includes five years with British Steel and two years with Imperial Chemical Industries. Over the past twelve years he has managed a SERC/DTI Teaching Company programme between the University of Glamorgan and Pirelli Cables. He is a fellow of the IEE and past Chairman of the IEE Control Applications Professional group.



Graham White is a senior Lecturer in the Department of Mechanical and Manufacturing Engineering at the University of Glamorgan, specialising in engineering materials. He graduated from the Department of Metallurgy, University of Sheffield with the Degrees of B.Met(Hons), M.Met and Ph.D. He spent a year as a visiting scientist in the Department of Materials Science and Engineering, Massachusetts Institute of Technology on a Rotary Foundation Fellowship. He has extensive experience of industrial consultancy.



DEGRADATION OF PP IN JELLY-FILLED CABLES.

Peter Haslöv

Niels H. Skovgaard

NKT Elektronik A/S
NKT Alle 85, 2605 Broendby, Denmark.

ABSTRACT.

The long term stability of PP-copolymers for use in slotted core optical cables was studied alone and in contact with different jellies using oven ageing and residual OIT as test methods. Silicone jelly resulted in shorter lifetimes than when using dry PP alone but longer than with hydrocarbon jellies. Oven ageing to brittleness at 100-140°C gave more reliable lifetime predictions than residual OIT. Care should be taken when combining HALS (hindered-amine-light-stabilizer) with thioester co-stabilizer as a negative effect on oven life has been observed. The accumulated test results and a theoretical treatment of the Arrhenius extrapolation method underline the importance of using the right environment and temperatures in accelerated testing.

1. Oxidation (consumption of stabilizers).
2. Migration and evaporation of stabilizers.
3. Reactions between stabilizers.

In order to take all such processes into account it is necessary that the test conditions are as close to reality as possible.

A good example of such a practical test is the Bellcore pedestal test [1] for lifetime estimation of HDPE insulated copper telecom cables which simulates field conditions well. It was found necessary to develop and later refine this complicated test method because of extensive field failures in the warmer parts of USA which necessitated more reliable lifetime tests.

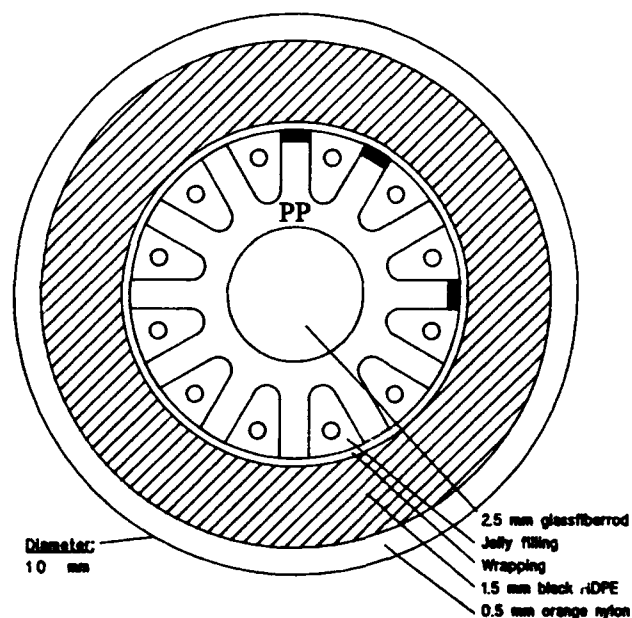
1. INTRODUCTION.

Polypropylene homo- and copolymers are successfully used for a wide variety of applications because of its high stiffness, low density, low price and excellent chemical resistance. Virgin polypropylenes are however rather unstable resins, prone to oxidation, but their resistance to oxidative degradation can be improved greatly by the addition of suitable stabilizer packages. The cable industry makes out one of the most demanding applications for PP because of the requirement for long lifetimes, typically above 25 years.

For cable applications it is therefore imperative that highly stabilized versions of PP are selected.

For the introduction of a new cable material knowledge of the types and amounts of stabilizers is however no guarantee against failures, meaningful lifetime tests should always be developed and carried out. This in itself presents a serious problem because of the complex environment inside a cable where several degradation mechanisms can occur at the same time :

FIG. 1
SLOTTED CORE OPTICAL CABLE.



In this paper a series of tests is described which has been carried out to ensure the reliability of our slotted core cable, schematically shown on fig. 1. The PP slotted core is in direct contact with a fairly large amount of filling compound and consequently migration reactions should be accounted for.

2. EXPERIMENTAL.

2.1 Raw materials tested.

PP-1 : PP-copolymer, MFI (230°C, 2.16 kg) 0.5, stabilized with Irganox 1010 and PS 802 (DSTDP), conc. not given by supplier.

PP-2 : Same as PP-1, but 0.3% Chimassorb 944 (HALS) added.

PP-3 : PP-copolymer, MFI (230°C, 2.16 kg) 0.4, stabilized with Ca-stearate and Irganox PS 802, conc. not given by supplier.

Si : Silicone jelly.

HC1 : Hydrocarbon jelly (conventional type, non polar).

HC2 : Hydrocarbon jelly (polar type)

PP binder tape (no special long term stabilisation).

2.2 Oven ageing.

Oven ageing was carried out in Hereaus Electronic ovens with constant temperature recording. The temperatures used were :

100, 120, and 140°C, all $\pm 1^\circ\text{C}$.

As failure criterion brittleness was chosen. This requires only small amounts of test material and can be easily evaluated manually in contrast to tensile testing. Thus more frequent inspections can be made and more precise life times determined.

The test samples were hot pressed plaques of PP cut into 0.5mm x 5mm x 50mm pieces used for the "dry" ageing of PP. For the ageing in cable environment 70mm pieces of the jelly filled slotted core (fig. 1) were used, only without the PE/PA jacket.

2.3 Oxidation induction time (OIT).

Instrument : Perkin Elmer Differential Scanning Calorimeter.

Procedure : 10 mg of the test piece was placed in an aluminium cup which was closed with a steel net. Heating from 30°C to the desired temperature at 20°C per min in a nitrogen atmosphere. After this temperature was kept constant and oxygen was supplied instead of nitrogen.

The OIT was determined as the time from the introduction of oxygen till the onset of the oxidation peak (crossing of baseline and deflection tangent to the peak).

3. RESULTS AND DISCUSSION

3.1 OIT versus oven ageing

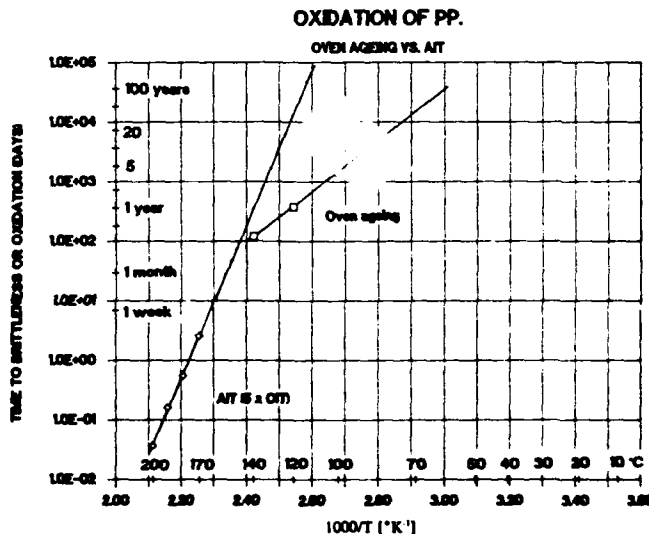
The oxidation induction time of PP-1 was measured at 170, 180, 190 and 200°C and the oven ageing time to embrittlement of identical samples was measured at 100, 120 and 140°C.

After multiplying the OIT's by 5 to correct for the 21% content of oxygen in the atmosphere, an approach proved valid in a parallel test with the same PP, the Arrhenius diagrams on Fig. 2 could be constructed.

If the "Air Induction Times" are used as basis for life time estimation a life time of more than 100 years at 110°C is obtained. This is in contrast to the oven ageing which gave a "real" life time of approximately 2 years. A 50-fold error, which will be even more pronounced at practical temperatures.

This conclusion has been made previously [2] and it is by now agreed that high temperature OIT is a reasonable QC test for a known stabilisation system, but of no use in life time determinations.

FIG. 2



3.2 Effect of HALS addition

It soon became clear that PP-1 life time was shortened considerably in contact with jelly (see Table 1) and therefore the effect of adding a more migration stable stabilizer was tested. Chimassorb 944 (HALS) was recommended because of the high molecular weight and 0.3% of this HALS was added to the PP which already contained Irganox 1010 (phenolic antioxidant) and Irganox PS 802 (thioester). The results of the oven ageing tests are shown in Table 1 together with OIT values at 180°C. At all three temperatures dry PP-1 performs better than the jelly filled slotted core, no doubt because of migration of stabilizer from PP-1 to the jelly.

Much more surprising, however, the addition of HALS had a significant negative effect on life time at all temperatures. The most probable explanation for this is that the thioester and the HALS react with each other and thereby a decreasing stability is obtained. This unfortunate effect has previously been observed by the supplier of stabilizers, but only in the case of light stability, not heat ageing [3].

Table 1. Oven ageing and OIT values

Time to Brittleness, Days			
Ageing Temp., °C	PP-1, dry	PP-1, jelly filled slotted core	PP-2 (with HALS), dry
140	140	70	11
120	380	270	95
100	1460	1110	930
OIT, 180°C	150 min.		8 min.

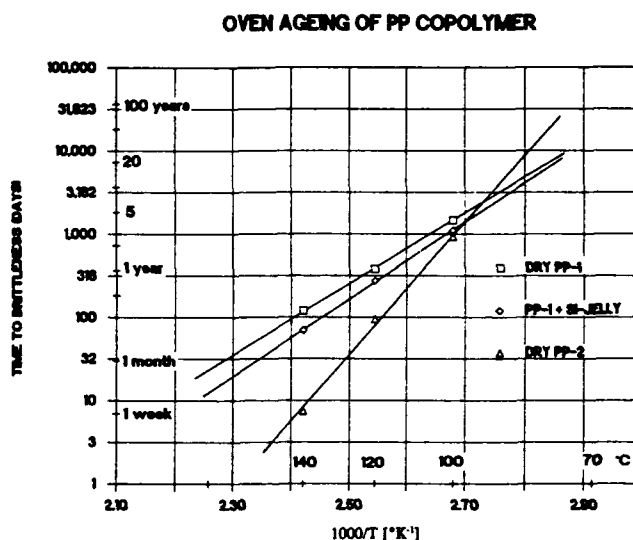
The corresponding Arrhenius plot on Fig. 3 shows an excellent relationship in the temperature interval 100-140°C for all the systems but with large differences in slope (activation energy).

Extrapolation of the life time curves to lower temperatures gives the best prediction for PP-2, regardless of the short oven life times measured.

However, for all three systems long life times can be extrapolated, at least 40 years at 70°C.

We will revert to the problems of selecting materials based on Arrhenius extrapolations in section 4.

FIG. 3



3.3 Effect of filling compounds

Traditional optical hydrocarbon jellies are absorbed in PP-copolymer to such an extent (App. 10% after one week at 80°C) that it was considered safer to use a silicone jelly which is not absorbed at all. The jelly influence on residual stability is shown in Table 2 together with the absorption in PP-copolymer.

Table 2. Effect of filling compound extraction and evaporation.

Jelly	Absorption in PP, 7 days, 80°C	OIT (180°C) for fresh PP-1, min	OIT for PP-1 after ageing in jelly, 28 days, 80°C, min		OIT after 21 days in air at 80°C, min
			180°C	150°C	
Si	0%	150	10	140	65
HC1	10%		1	20	
HC2	0%				

It is obvious that even for a silicon jelly which is not absorbed in PP, there is a significant migration of stabilizer to jelly but the silicone is performing much better than the absorbable hydrocarbon HC1 which facilitates the migration. The right column shows that evaporation of stabilizer is small compared to migration into jelly.

At a later stage of this test programme a new polar type of hydrocarbon jelly (HC2) with an absorption in PP close to zero was tested. The influence on the life time of PP-3 by this jelly was tested in oven ageing experiments (Table 3).

Table 3. Oven stability of PP in non-absorbable hydrocarbon and silicone jelly.

Time to Brittleness, Days. Jelly filled slotted cores		
Temperature	PP3/HC2	PP3/Si
140°C	30	125
120°C	90	>630

A considerable lowering of the thermal stability of the PP-3 with the polar HC2 is noted. The reason is not absorption but more likely a lower heat stability of the jelly. A possible free radical degradation of the jelly may then spread to the polymer and speed up stabilizer consumption. Severe degradation of the HC2 jelly was always observed together with embrittlement of the PP.

3.4 Residual OIT

Because of the very long times necessary for the oven tests we have investigated the possibility of using residual OIT as a measure of the residual life time [4]. At regular intervals during the oven ageing of PP-1 Si-jelly filled cores, samples were cut out for measuring OIT.

The results are shown on Fig. 4. We observe a rapid decline at all temperatures. At 140°C embrittlement (marked with a "B") occurs soon after the decline, but at 120°C embrittlement was not observed until after 270 days after a level of a constant OIT of app. 5 min. from 120 to 270 days. So in this case the residual OIT was of no use. Also at 100°C the shape of the curve does not encourage the use of this method.

3.5 Stability improvement through migration of stabilizer

For securing the optical fibres in the slotted core during processing, a binder tape is wound around the slotted core. The tape is a PP with a short oven life containing only base stabilisation. One could imagine that early degradation of the unstable PP (Table 4) would spread to the slotted core and reduce life time, however, this is not the case. In our tests the tape always had the same long lifetime as the slotted core. The reason for the improved stability of the tape can only be uptake of stabilizer that has migrated from the core through the jelly and into the tape. First when all stabilizer has been used both polypropylenes will start oxidizing.

FIG. 4

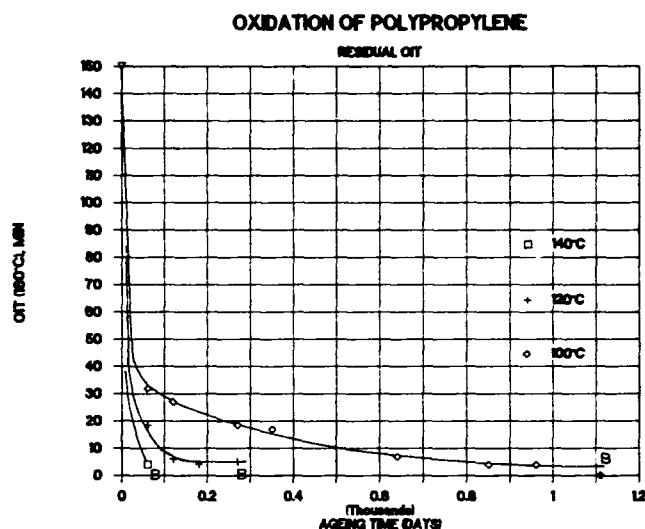


Table 4.

Oven ageing of PPs in air and cable environment.

Time to Brittleness at 140°C, Days	
PP-1, in air	140
Binder Tape, in air	10
PP-1 in cable	70
Binder Tape in cable	70

OIT measurements on aged samples taken from a submarine slotted core cable with a hermetic barrier keeping out oxygen illustrate this mechanism (Table 5). At the same time as PP-1's OIT decreases to 20% of the original value, the OIT of the tape was increased by a factor close to 3.

Table 5.

OIT of PPs after ageing in submarine cable.

	OIT (160°C) Binder Tape	OIT (180°C) Slotted Core
Fresh	44	150
Aged 70 days at 95°C	150	30

4. USING THE ARRHENIUS LAW

4.1 Single reaction

The temperature dependence of the reaction rate for a thermally activated n 'th order chemical reaction is described by the Arrhenius Equation:

$$-\frac{dA}{dt} = A^n \cdot k \cdot e^{-\frac{Q}{RT}} \quad (1)$$

Q is the constant activation energy for the reaction

k the rate constant

R the gas constant

A is the concentration of the compound consumed by the reaction, e.g. stabilizer.

If the life time of the item studied is defined as $t_{1/2}$ (when A is half of the original value A_0), the following "life time" equation can be deduced :

$$\ln t_{1/2} = -K + \frac{Q}{RT} \quad (2)$$

with K constant which is the well known linear relationship between the logarithmic life time and the inverse reciprocal absolute temperature commonly used for extrapolating accelerated test results to practical temperatures.

If only the same reaction is occurring in the relevant temperature window reliable life time estimates will be obtained.

4.2 Competing reactions

If A is consumed by more than one reaction the situation is more complex. If for example two competing n 'th order reactions with different activation energies, Q_1 and Q_2 are involved, the following equations will substitute (1) and (2) respectively:

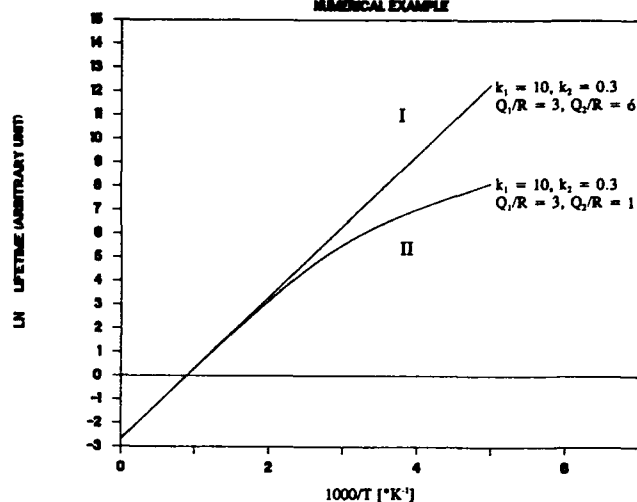
$$\text{Rate: } -\frac{dA}{dt} = A^n \cdot [k_1 \cdot e^{-\frac{Q_1}{RT}} + k_2 \cdot e^{-\frac{Q_2}{RT}}] \quad (3)$$

and

$$\text{Lifetime: } \ln t_{1/2} = C - \ln [k_1 \cdot e^{-\frac{Q_1}{RT}} + k_2 \cdot e^{-\frac{Q_2}{RT}}] \quad (4)$$

In (4) C is a constant. For three or more reactions with the same reactant A , equations analogous to (4) can be deduced.

FIG. 5
ARRHENIUS DIAGRAM
NUMERICAL EXAMPLE



To describe (4) more closely two situations must be considered:

I : $k_1 > k_2$ and $Q_1 < Q_2$

II: $k_1 > k_2$ and $Q_1 > Q_2$

In Fig. 5 the two situations are illustrated by a numerical example in an Arrhenius plot.

In situation I process 1 will dominate at all temperatures, but in situation II process 1 will dominate at high temperatures and process 2 at low temperatures. It can be stated that out of two competing processes the dominating process at the lowest temperature will be the one with the lowest activation energy.

4.3 Discussion.

This fact makes life time estimation much more difficult, but it can also explain unexpected results. The transition in slope on fig. 2 may be due to oxidative degradation dominating at (170-200°C) and evaporation of antioxidant dominating at (100-140°C) or opposite.

In Fig. 3 different activation energies characterize PP-1, PP-2 and jelly filled PP-1. This indicates that different reactions with different reactants are taking place, such as oxidation, migration, evaporation and reactions between stabilizers. Thus, uncritical extrapolation is dangerous, one cannot be sure that processes with lower activation energies will not take over at low temperatures and result in decreased real life times.

So even after more than three years thorough testing we cannot categorically rank the low temperature ageing stabilities of the two PP's tested. We can only say they both have a reasonably long life time at 100°C, which is important in itself.

CONCLUSIONS

Following conclusions can be drawn from the work carried out:

- Attempts to improve oven life times of PP by adding HALS to the primary antioxidant/thioester system gave unexpectedly much shorter oven life at temperatures above 100°C
- Residual OIT (measured at high temperature) was of no use for prediction of residual life time.
- Dry samples showed better stability than jelly filled PP-cores.
- Lifetimes acceptable for use in silicone jelly filled cables were obtained with the three polypropylenes selected.
- Silicone jelly performed better than hydrocarbon jellies regardless of absorption level of the latter.
- Excellent Arrhenius relationship was obtained for all three systems tested but nevertheless
- Arrhenius plots should be used with utmost care when extrapolating to low temperatures because processes with low activation energy may dominate at low temperatures and shorten service life.
- Accelerated tests should be made at lowest acceptable temperatures and in the actual cable environment to take as many effects as possible into account.
- Stabilizer migration from highly stabilized PP can improve stability of a poorly stabilized PP in a cable.

References :

1. T.N. Bowmer, R.J. Miner, I.M. Plitz, J.N. D'Amico and L.M. Hore: Thermal Stability Tests for Polyolefin Insulations. Proc. of IWCS (1990), 316-326.
2. F.Gugumus: The Use of Accelerated Tests in the Evaluation of Antioxidants and Light Stabilizers. Developments in Polymer Stabilisation-8, 239-287.
3. F. Gugumus: "Private Communication".
4. E. Kramer and J. Koppelman: Thermo-oxidative Degradation of Polyolefins Observed by Isothermal Long-Term DTA. Polymer Engineering and Science, July 1987, Vol. 27, No. 13, 945-953.



Peter Hasløv

NKT Elektronik A/S
NKT Alle 85
2605 Broendby
Denmark

Peter Hasløv (M.Sc.Chem.Eng.) graduated from DTH in 1974 with polymer technology as special subject. After 13 years in the plastics industry, he joined NKT Elektronik A/S in 1987 and is responsible for selecting, testing and processing polymers for telecommunication cables. He is also engaged in lifetime estimation of optical fibres.



Niels H. Skovgaard

NKT Elektronik A/S
NKT Alle 85
2605 Broendby
Denmark

Niels H. Skovgaard was born in Copenhagen, Denmark, in 1952. He received his M. Sc. Degree in Mechanical Engineering in 1981. From 1981 he worked as researcher at the Technical University of Denmark. In 1984 he joined NKT working with research and development of optical fibre cables. Since 1986 he has been the manager of the design and development department of NKT Elektronik A/S.

A STUDY ON THERMAL OXIDATIVE DETERIORATION OF FOAM-SKIN INSULATION

Byung D. Oh

Youn S. Kim

June Y. Hah

TAIHAN ELECTRIC WIRE CO., LTD.

785, KWANYANG-DONG, ANYANG CITY, KYUNGKI-DO, S-KOREA

ABSTRACT

Several years ago insulation failures in foam-skin insulated cable began to appear in field installations. The rate of insulation failure as well as changes in cracking behavior as oxidation progress have been discussed in many countries.

The resistance of insulation in mechanical damage during processing and termination will influence the life of insulations. Conductors with foam-skin insulation require considerably more careful attention than solid insulations on high speed extrusion.

The long term stability of polyethylene insulations can be predicted by thermal oxidative aging tests. This paper is on the analysis of causes for thermal cracking failures in high speed extrusion process. Also, factors other than field installations environment can affect the life of insulations.

INTRODUCTION

Foam-skin insulated local telephone cables had been installed in the Korea telecommunication network in 1985. Recently since 1988, with the introduction of a high speed telephone wire extrusion line in Korea, the insulations processed at a high speed of 2200 m/min. or higher have revealed a big problem in terms of the thermal oxidative deterioration.

It was found that the embrittlement of insulation occurring after 5~8 years exposure in ground jointing box was due to the depletion of antioxidant by copper-catalysed air-oxidation, at the elevated temperatures existing within the enclosures.

It was also considered that the oxidation process was accelerated by the presence of a processing aid and the pigment titanium dioxide in the color master

batch, and a reduction in the concentration of antioxidant by migration.

The findings of our comprehensive study on the factors affecting the thermal oxidation stability suggested that not only the types and characteristics of the insulation materials including the insulation compound and the Color Master Batch but also various conditions at the time of extrusion process such as mixing condition of the extruder, setting of production condition according to the type of compound, cooling condition, insulation surface, adhesive strength of the conductor and the insulation, and even the test conditions cause a significant influence upon the results of the thermal oxidative deterioration.

Thermal stability test of PIC insulation is applied as telephone insulation lifetime prediction method. Until now, oxidation induction time tests are used to physically measure cracking intervals of telephone wire insulation.

The OIT is obtained by heating the sample at 200 °C under oxygen. Using a thermal analyzer, time to degradation is observed as an exothermic reaction in the calorimeter plot. It is widely believed that the single most important factor that affects insulation oxidation is temperature. But, this test is a qualitative measure of the amount of remaining stabilizer in wire insulation. According to the results and observations of our studies, OIT has no relation with long term thermal stability.

The currently accepted test method for evaluating longevity of polyethylene wire insulation is the BELLCORE or IEC thermal oxidative stability test, because the most important factors for PIC cracking are temperature and stress, humidity, ultraviolet radiation, etc.

The loss has been caused by a number of competing and interacting factors. The oxidation process was accelerated by the presence of a processing aid and the pigment in the polymer, and a reduction in the concentration of antioxidant by migration. Accordingly, we have studied the testing method as well as polyethylene compound, color pigment and extrusion processing conditions. So cable manufacturers must study and keep the following facts to achieve above mentioned thermal oxidation cracking problem before making wire insulation at a high speed.

Table-1 shows the basic factors.

1. Experiment

1) Material

The characteristics of thermal oxidation stability are mostly affected by the physical properties of polyethylene compound as shown in Table 2 and 3. When the density of polyethylene and MWD are appropriate, the long term stability of the insulation can be reliable only when the stabilizers such as antioxidant and metal deactivator are properly mixed.

The mixing rate should be decided in consideration of the following ;

① Loss in the manufacturing process.

② Loss due to reaction to other additives including the Color Master Batch.

③ Loss migrated due to oxidation from the polymer surface after installation, and loss due to reaction to copper conductor.

The thermal stability has a correlation with the production condition or the test method. However, when these two conditions are the same, the mutual blending methods for the intrinsic physical properties of the polyethylene and the stabilizer have a significant effect as shown in the data of Table 3 and 5.

In addition, the Color Master Batch used as a color pigment also serves as an important factor. As the C-M-B is a kind of foreign material, its content in the insulation should be minimized to the degree of meet the standard colors in the cable specification. In consideration of the dispersibility of the color, it is advisable to use a C-M-B of low density polyethylene. However, as the low melting temperature of LDPE has a negative effect upon the thermal oxidation stability, it is a good idea to use MDPE or HDPE to the degree of easy dispersibility.

Table 4. show the test result from type of color master batch.

TABLE 1.

ITEM	FACTOR	DISCUSSION	RESULT & ANALYSIS
Materials	① Insulation polymer	① Influence for density of polyethylene compound ② Influence for temperature ③ Stabilization system	(a) To improve physical properties of the insulation (b) Depletion of an antioxidant (c) Chemical loss and physical stress (d) To improve the thermal oxidative resistance of polymer (e) Content of antioxidant
	④ Color Master Batch	④ Color pigment ④ Base resin	(a) To improve the concentration in the insulation (b) Migration to the polymer surface (c) Content of antioxidant system
Cable Type	① Insulation construction	① Type of insulation ② Wall thickness	(a) Relation of susceptibility of foam layer (b) Relation between foam layer and skin thickness
Production Condition	① Extrusion machine and Operating condition	① Mixing condition ② Balance of screw RPM and extruder temperature profile ③ During the conversion by the extrusion process	(a) Lead to differences in stabilizer percentage and distribution between wires (b) Subjected to high shear stress (c) Chemical and physical loss occurs (d) Stabilizer lost
	② Conductor surface ② Insulation adhesion	② Influence of conductor oxidizing and alien substance ③ Relation between conductor and insulation adhesion	(a) Interaction of oxidation by the copper conductor and dirt (b) Interaction with blowing agents
	② Concentricity of insulation ② Insulation defect ② Poor foam structure	② Concentricity of skin layer ② Influence of pin hole and surface smoothness ③ Influence of open cell construction	
Test Method	② Air oven condition ② Testing temperature ② Test method	② Critical temperature of thermal aging test ② Round robins ② Compare air exchanges and temperature ③ Incorporate OIT and long term aging test	

2) Production Condition

The foam-skin insulation has much more variables in the high speed extrusion compared with the solid insulation, and thus it is not stable.

As the insulation diameter and the coaxial capacitance value fluctuate depending upon the volume of extrusion output and the degree of foaming ratio, selection of optimum die size and setting of the extruder temperature range and temperature profile, and balance of the screw RPM serves as important factors for fluctuation. Basically, the cellular insulation is affected by the head pressure, temperature, and residual time. Therefore, setting of production condition for these three factors apparently has influence upon the thermal oxidation stability.

The jelly filled cable may be weaker than the air filled cable due to the occurrence of jelly compound absorption caused by migration into the insulation. But, use of the jelly compound of polybuten type instead of petroleum jelly results in lower level occurrence of swelling, and it shows a great resistance force against the thermal oxidation stability because it has a thicker insulation than the air filled cable.

As shown in Table 6, the foam-skin air filled insulation with $\phi 0.4\text{mm}$ conductor diameter shows the lowest level with regard to the thermal oxidation stability. It was also revealed that the result of thermal oxidation stability was not stable when the adhesive force of the inner conductor and the foam layer was strong rather than when it is weak.

When heat is applied to the insulation, shrinkage of the insulation occurs, thus decreasing the speed of thermal oxidation. When the adhesive force is strong, the metal ion of the conductor is activated, which in turn accelerates the oxidation of the insulation. Comparative testing of the original specimen and the specimen with tensioned conductor to assess their thermal oxidation stability in the same condition and specifications showed that the tensioned specimen had a long service life six times greater than the original specimen.

3) Test Method

Even the same insulated conductor may show

different results depending upon the condition of the test oven. Specially, the thermal oxidation stability may not be the same depending upon the air displacement volume and the rotation in the oven at the same test temperature as shown in Table 7.

This suggests that as the oven used to test the thermal oxidation stability is subject to the test similar to the pedestal test, the comparison and judgement on the thermal oxidation stability should be made based upon the results of execution of the air displacement and the rotation of the specimen in the oven in accordance with the specified conditions.

2. Results and Discussion

According to the results of this study, the stability and instability of thermal oxidation is affected by not only a few factors but also the correlation between the material in use and the production condition. In particular, in case of the foam-skin air filled cable with 0.4 mm conductor mentioned in this paper, control of such elements is much more important.

1) Relations between material and production condition

The thermal oxidation stability of polyethylene insulations is influenced by the density and melt index of insulation materials. Usually, we consider that the higher the density is, the better the thermal stability. But the above thinking was found not correct. It should be noted that the MDPE shows good stability equal to that of the HDPE.

And it is most stable to use the same base resin for the Color Master Batch as the insulation material to the degree of satisfying the color dispersion.

And, basically the insulation material should contain suitable stabilizers.

During the conversion of polyethylene compound to insulation on wire by the extrusion process, the polyethylene compound is subjected to very high shear stress and temperatures. Stabilisers are added to protect the polymer from degradation during extrusion process, and the amount of stabilizer lost in providing protection depends on variables associated with the extruder and operating conditions such as temperature profile, screw RPM etc.

Therefore, production condition also affects the stability. Then, the optimum condition shall be obtained by considering the characteristics of insulation material.

2) Condition of Insulated conductor

(a) Cable type

Irrespective of the material or production condition, the thermal oxidation stability increases when the insulation thickness becomes thickening. Therefore, the foam-skin jelly cable is more stable compared to the foam-skin air filled cable, and the foam-skin insulation cable is less stable than the solid insulation cable.

(b) Surface quality and foam structure

Good surface condition (smooth surface) and uniform cell construction contribute to the thermal oxidation stability.

(c) Concentricity and insulation defect

The thickness of the skin layer should be uniform. The occurrence of the spark fault is detrimental to the thermal oxidation stability.

(d) Adhesive strength

Excessive adhesive force of the conductor and the insulation has a negative effect upon the thermal oxidation stability.

3. Conclusion

As explained in the foregoing results and discussion, various factors combine to affect the thermal oxidation stability. Therefore, it is suggested that the cable manufacturer should maintain a periodic and consistent control for quality assurance over the selection of materials, changing trend of the physical properties for the material, and production condition, thus fulfilling the reliability for the long term service life of the cable.

Reference

- 1) H. J. Ruddel, D. J. Adams, B. A. Chisholm, "Deterioration of solid Polyethylene Insulation in service", *Plastics in Telecommunications* ■.

- 2) E. D. Nelson, 40th IWCS proceedings, 1991.

- 3) J. Y. Hah, Y. S. Kim, 40th IWCS proceedings, 1991.



Byung-Dan Oh
Taihan Electric Wire Co., Ltd.
785, Kwanyang-Dong, Anyang
-city Kyungki-Do, KOREA

Byung D. Oh received his B. S. degree in electronic communication engineering from Kwangwoon University in 1990.

He joined Taihan Electric Wire Co., Ltd. in 1990. He has been engaged in production engineering of communication cables. He is now a engineer of the communication cable engineering section.



Youn-Soo Kim
Taihan Electric Wire Co., Ltd.
785, Kwanyang-Dong, Anyang
-city Kyungki-Do, KOREA

Youn S. Kim received his B. S. degree in metallurgical engineering from Sungkyunkwan University in 1983. He joined Taihan Electric Wire Co., Ltd. And he has been engaged in communication cable production and technical departement.

He is now a assistant manager of the communication cable engineering section.



June-Young Hah
Taihan Electric Wire Co., Ltd.
785, Kwanyang-Dong, Anyang
-city Kyungki-Do, KOREA

June Y. Hah received his B. S. degree in electrical engineering from Hanyang University in 1978. And then joined Taihan Electric Wire Co., Ltd. and worked on the development of CATV coaxial cable and foam-skin insulated cables.

He is now general manager of the communication cable engineering department.

Table 2. Characteristics of Insulation Materials

PROPERTY	SAMPLE	A	B	C	D	E	REA SPEC. (PE-200)
Melt Flow Rate (M.I.)	g/10min.	0.58	0.70	0.25	0.76	0.78	0.2~2.0
Flow Ratio	MI ₁₀ /MI	14.9	12.7	10.1	17.2	15.2	
	MI _{21.0} /MI	107.7	91.4	76.8	84	85.2	
Density (Nominal)	g/cm ³	0.943	0.945	0.932	0.948	0.948	0.941~0.959
Mw	×10 ⁴	10.5	13.8	9.1	12.3	13.2	
Mn	×10 ⁴	1.4	1.3	0.73	0.97	0.96	
Mw/Mn	-	7.5	10.6	12.6	12.7	13.8	
Melting Temp.	°C	132	134	125	132	134	
Content of Antioxidant	%	0.12	0.16	0.13	0.15	0.21	
Content of Metal Deactivator	%	0.34	0.13	0.28	None	0.17	

Table 4. The Thermal Oxidation Stability and Type of C-M-B

PARAMETER	KIND OF C-M-B	1	2	3	4
Insulation Material		SAME			
Production Machine		SAME			
Conductor Dia.	mm	φ 0.4			
Insulation Dia.	mm	φ 0.64			
Base Resin of C-M-B		* HDPE	MDPE	LDPE	** HDPE
Thermal Oxidation Stability Test		> 74 Days	> 59 Days	< 25 Days	> 55 Days

[Remark] * : Of the same base resin as used for the skin layer
 ** : Not the same base resin as the skin layer

Table 5. Relations between Stability and Production Condition

PARAMETER		PRODUCTION CONDITION	I	II	III	IV
Conductor Dia.		mm	φ 0.4			
Insulation Dia.		mm	φ 0.64			
Line Speed		m/min	2200			
Ext. Temp.	Main	℃	161~184	161~182	163~187	163~189
	Aux.		199~240	199~240	199~240	199~240
Ext. RPM	Main	-	36	36	32	33
	Aux.		54	54	54	55
Capacitance Tolerance		pF/m	< ±1.5	< ±1.5	< ±2.5	< ±2.5
Spark Failure		No./Bo.	1~2	1~2	5~7	< 10
Foam Construction		-	Good	Good	Bad	Bad
Surface Roughness		-	Matt/Smooth	Matt/Smooth	Matt/Rough	Matt/Rough
Essentricity		%	About 92	About 80	About 92	About 80
Thermal Oxidative Stability Test.		-	> 72 Days	> 52 Days	< 45 Days	< 16 Days
Insulation Material		-	SAME			

Table 3. The Thermal Oxidation Stability and Materials

PARAMETER		SAMPLE	A	B	C	D	E
Conductor Dia		mm	0.4				
Insulation Dia		mm	0.64				
Production machine		-	SAME				
Line speed		m/min	2300	2200	2200	2200	2200
Ext. Temp	Main	℃	163~197	160~187	165~189	163~196	162~192
	Aux.		194~250	180~230	195~255	194~245	205~250
X-Head Pressure	Main	kg/cm ²	423	450	590	405	565
	Aux.		560	600	710	590	630
Capacitance		pF/m	< ±1.5	< ±1.5	< ±1.5	< ±1.5	< +2.0
Spark Voltage		kV	1.2	1.2	1.2	1.2	1.2
Spark Failure		No./Bo.	1~2	3~4	1~2	> 20	> 30
Foam Construction		-	Good	Good	Good	Bad	Bad
Surface Smoothness		-	Matt/Smooth	Smooth	Matt/Smooth	Rough	Matt/Rough
O.I.T test		Minute	Min. 55	Min. 38	Max. 67	Min. 38	Min. 85
* Thermal oxidation Stability test		-	> 61 Days	> 100 Days	> 93 Days	< 63 Days	< 48 Days

[Remark] Medium density cellular polyethylene compound was used for the foam insulations.

* : The test was made in accordance with Bell Standard testing methods designated. (110℃, Min. 45 days)

Table 6. Relations between Stability and Cable Insulation Type

CABLE TYPE PARAMETER		Foam-Skin Insulation				Solid Insulation	
		Air filled		Jelly filled		Air filled	
		φ 0.4	φ 0.5	φ 0.4	φ 0.5	φ 0.4	φ 0.5
Insulation Material		SAME				SAME	
Production Machine		SAME					
Insulation Thick.	mm	0.12	0.14	0.16	0.20	0.16	0.20
Skin Thickness	mm	0.05					
Thermal Oxidation Stability Test		> 52 Days	> 54 Days	> 66 Days	> 74 Days	> 90 Days	> 142 Days

Table 7. Relations between Stability and Test Method

CABLE TYPE PARAMETER		Air change and circulation		No air change and circulation	
		Round robin	Fix	Round robin	Fix
Insulation Material		SAME			
Production Machine		SAME			
Conductor Dia.	mm	φ 0.4			
Insulation Dia.	mm	φ 0.64 (Foam-Skin insulation)			
Thermal Oxidation Stability Test		> 71 Days	> 45 Days	> 52 Days	> 39 Days

LIMITATIONS AND APPLICATIONS OF OXIDATIVE INDUCTION TIME (OIT) TO QUALITY CONTROL OF POLYOLEFINS

J.R. Pauquet, R.V. Todesco, W.O. Drake.

Ciba-Geigy Ltd., Basel, Switzerland

Abstract

With phenolic antioxidants an linear relationship exists between the stabilizer concentration and the Oxidative Induction Time (OIT) of polyolefins. Thus, OIT can be used as an analytical method for determining the concentration of sterically hindered phenol. The development of automated DSC apparatus has allowed the technique to be used in quality control. The easy sample preparation and short measurement time make the method attractive. With multifunctional stabilizer molecules, it offers the advantage over other methods by determining the effective concentration of the active functional groups. OIT is generally not an appropriate method to predict the long-term thermal stability of polyolefins. It can be particularly misleading when used as a screening test to assess the relative performance of stabilizers. Correlation with other accelerated tests such as oven aging rarely exists.

Introduction

Oxidative Induction Time (OIT) measured by DSC/DTA on molten polymer samples has long been used in the plastics industry to assess the thermal stability of polyolefins. Its simplicity and speed makes the method attractive. Extrapolation to end use temperatures (usually below 80°C) by plotting induction time vs. reciprocal temperature (Arrhenius) was always tempting. It is striking that particularly those industries which have to guarantee their products for 30 to 50 years lifetime have specified OIT for quality purposes and screening tests. It is the case for the pipe as well as for the wire and cable industry.

The validity of the method as accelerated test method to predict behavior at normal temperatures has always been questioned. Extensive studies done with polyolefins for cable insulation in the early 1970's,

particularly at Bell Laboratories, have shown that the extrapolation of DSC/DTA OIT data leads to considerable over-estimation of life-time compared with data deduced from oven aging data in a draft air oven [1,2,3]. The relative efficiency of stabilizers can also be different from one test to the other. Tests conducted with samples in the solid state and at temperatures as close as possible to the end use conditions are the most reliable method for performance assessment of antioxidant systems and for life-time prediction of polymers. But the life-time can not be predicted by oven aging experiments alone. Extraction of additives by water or other extractive media or contact with copper and other transition metals are some of the factors that greatly influence the oxidative stability of polyolefins.

The rate of stabilizer loss is expected to be the determining factor for the stabilization efficiency at lower temperatures, particularly if the additives are supersaturated in the polymer [4,5]. The effects of crystallisation, causing changes in the oxidation mechanism (discontinuity in Arrhenius plot) [4,6] and redistribution of the additives in the polymer matrix complicate the extrapolation of OIT results below the melting point of the polymer. However, in some limited cases, the method was reported to be valid [7].

The development of high performance additives such as HALS and the increasing use of polyolefin compounds requiring effective processing stabilizers such as organophosphites have added further reasons to review the significance of this test.

The present paper discusses the relationship between the OIT value and the concentrations of different stabilizers and stabilizer combinations in polyolefins. Special attention will be given to the effect of phosphites and HALS on the OIT. The influence of polymer type and production process as well as the

presence of antacids or costabilizers are also included in the discussion. The lack of correlation between OIT and other accelerated tests will be addressed.

Experimental

The following polyolefins were used in this work :

HDPE (Cr): MF [190°C/10kg] = 4.9 g/10 min., density = 0.953.
HDPE (Ti): MF [190°C/5kg] = 1.5 g/10 min., density = 0.944.
PP: MF [230°C/2.16kg] = 3.2 g/10 min., density = 0.894.

Additives were dry blended with the resin powder in a high speed mixer and the samples were extruded on a 25 mm extruder, 100 rpm max. 260°C or mixed in a Brabender plastograph (10 min. at 180°C for HDPE and 190°C for PP).

Compression molded sheets of 0.5mm were prepared (6 min. at 190/230°C).

Oxidative induction time was measured with Du Pont TA2100 with Dual Sample DSC and autosampler or with a Mettler DSC20 system. A disc of 5 mm diameter was punched from a 0.5 mm thick compression molded sheet. The sample weight was approximately 7 mg. The polymer discs were placed in clean aluminum pans, using a empty pan as reference and heated at a rate of 10°C/min to the test temperature under nitrogen (50ml/min.). After thermal equilibration, at the preset temperature, the sample was exposed to pure oxygen at a flow rate of 50 ml/min until the exotherm occurred. The OIT value was taken as the time at the intersection of the extended baseline with the extrapolated slope of the exotherm. A minimum of 2 replicates were measured.

HPLC analysis of the additives was done on a Spectra Physic equipment using a UV/VIS detector and a hyperchrome 125 x 4.6 mm column filled with Nucleosil C18 5 micron. The eluent was a gradient with methanol, water and ethylacetate. Polyethylene was dissolved in hot toluene and polypropylene in hot chlorobenzene. After cooling and precipitation of the polymer with methanol, the solution was directly injected.

The additives used are given in Appendix 1.

Primary antioxidants and OIT

The autoxidation of polyolefins is an exothermal process and is, due to the branched chain nature of the oxidation reactions characterized by an induction period. The sudden change in evolved heat

or temperature of a polymer sample at the end of the induction period can be easily detected with commercial DSC/DTA equipment.

The effect of antioxidants on a polymer exposed to oxygen at high temperature is to inhibit the oxidation so that no observable changes occur. Thus, the length of the induction period increases with increasing antioxidant concentration. Polyolefins we generally gave a linear relationship between oxidative induction time (OIT) and the concentration of non-volatile phenolic antioxidants [8,9], at least in the concentration range of commercial interest. Figure 1 shows the correlation between the oxidative induction time of three different polyolefins and the concentration of AO-4. At very low concentrations (below 100 ppm) the linearity is not always observed [10]. This deviation from linearity at low antioxidant concentrations can be due to the relative insensitivity of the method at the given temperature or to consumption of stabilizer during sample preparation.

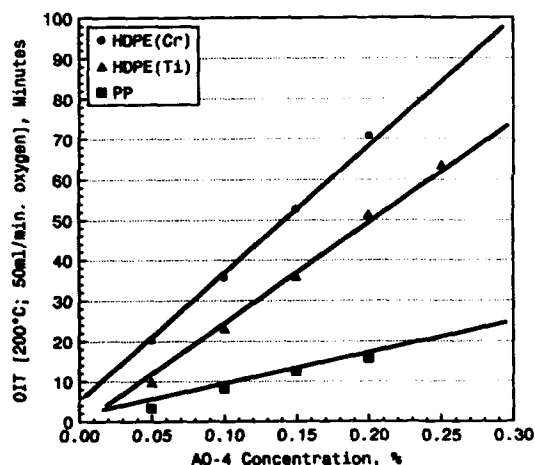


Figure 1: OIT of different polyolefins as a function of the concentration of AO-4.

Experience has shown that the OIT response is a function of the antioxidant used, as shown in Figure 2. The differences in stabilizing efficiency as determined by OIT is related to the chemical structure of the additives [11] but might also result from physical limitations or from interactions of the additives with impurities.

Within experimental error the concentration dependence of OIT is unaffected by the test temperature [4,9] and thus the temperature can be adjusted to give results in a reasonable time

frame. Therefore the OIT has been recommended for quality control purposes [3,12], the advantages being the easy sample preparation and measurement as well as the short response time. To further improve the response time and the test capacity, equipment with multiple sample holder have been built [8], and programmable robot system have been developed for commercial DSC/DTA equipment.

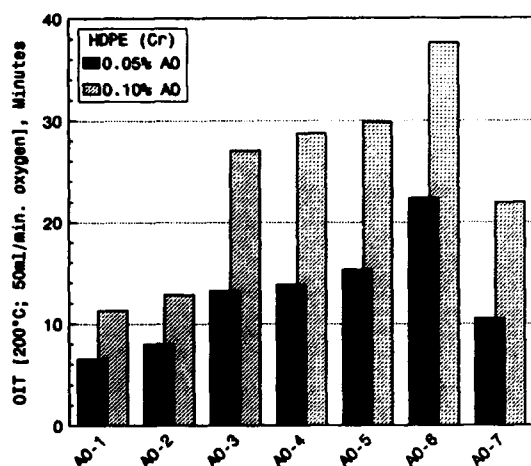


Figure 2: OIT of different phenolic antioxidants in HDPE (Cr).

Compared with other analytical methods, the thermal analysis method has the advantage of determining the active part of phenolic stabilizers [13]. This can be particularly useful with multi-functional antioxidants such as AO-4. It has been shown [11] that for anti-oxidants derived from 3, 5-di-(tert-butyl)-4 hydroxyphenyl propionate such as AO-1 and AO-4, the OIT values fall on a same curve when plotted as a function of the concentration of phenolic groups. Thus one line can be used as a calibration curve for both phenols in a given polymer. In Table 1 the results obtained from liquid chromatography analysis are compared with the results obtained from thermal analysis on HDPE (Cr) samples extruded at 260°C on a lab extruder.

Antioxidant	Theoretical Concentration	HPLC Analysis	Thermal Analysis
AO-1	0.10%	0.092 %	0.090 %
AO-4	0.05%	0.026 %	0.047 %

Table 1: Comparison between HPLC and thermal analysis result for AO-1.

There is a good agreement between both methods in case of AO-1 whereas the concentration of AO-4 found by HPLC is

significantly lower than the value found by thermal analysis.

The reason for this discrepancy is that the HPLC method detects only the unmodified AO-4 molecules - specifically when only one phenolic group of AO-4 has reacted during processing or aging of the material, the total molecule is consumed as far as the LC method is concerned. The remaining groups are still active as can be seen from the values obtained via the OIT calibration curve. The same arguments can be used to question failure prediction based on additive depletion measured with HPLC, particularly when multifunctional additives are used.

Influence of Phosphites on OIT

Combinations of sterically hindered phenols and hydrolytically stable organophosphites function synergistically to prevent molecular degradation in polyolefins and currently represent the state-of-the-art in processing stabilization of polyolefins [14]. However, little has been published about the effect of organophosphites on oxidative induction time. The opinion that predominated over years in industry was that phosphites did not influence the OIT [9,11]. Recently, some OIT data have been reported [15,16,17] suggesting that the induction time is not only a function of the concentration of phenolic antioxidant.

Some of the results published by Moss and Zweifel [15] are plotted in Figure 3. Using the same polymer resin further experiments were done particularly with AO-1, a monofunctional antioxidant. These results are also illustrated in Figure 3. The OIT decreases significantly with increasing number of extrusion passes at 260°C. This was first assumed to be due to the consumption of antioxidants during processing, because the phosphite used alone had never shown any effect on the induction time. The increasing OIT value with increasing ratio of phosphite PS-1 to antioxidant AO-1 or AO-4 were believed to result from the better protection of the phenolic antioxidants and of the polymer. The HPLC analysis of the samples showed indeed a reduced consumption of the AO-4 when increasing concentration of phosphite PS-1 was used and the molecular degradation of the polymer was also significantly reduced.

However, additional analytical work using HPLC on the extruded samples containing the monofunctional AO-1 showed that the consumption of phenolic antioxidant could only account for a small fraction of the

OIT drop observed. This is illustrated in Table 2, which summarizes the HPLC analysis results of AO-1 and PS-1.

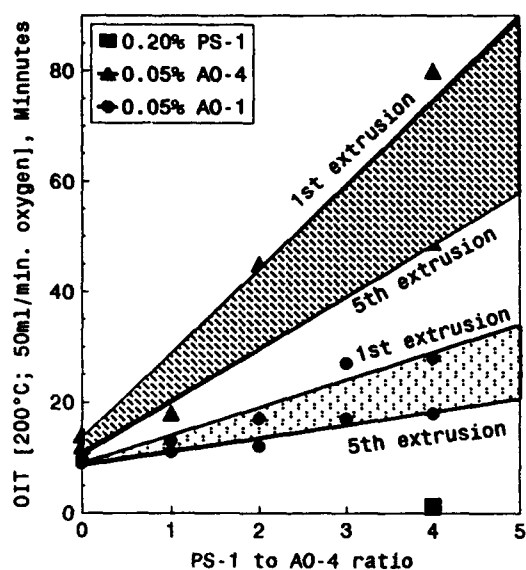


Figure 3: OIT after multiple extrusion at 260°C of HDPE (Cr).

Using a calibration line the OIT was calculated (OIT_c) based on the concentration of AO-1 found by LC analysis on samples extruded one and five times at 260°C, compared to the actual OIT measured (OIT_m). It is clear that the OIT can not be predicted by the sole concentration of phenolic antioxidant AO-1.

	1 Extrusion at 260°C			5 Extrusions at 260°C		
	HPLC [%]	OIT _c [min.]	OIT _m [min.]	HPLC [%]	OIT _c [min.]	OIT _m [min.]
0.05% AO-1	0.043	7	10	0.037	6	9
0.05% AO-1	0.045	8	17	0.042	7	12
0.10% PS-1	0.079	8	28	0.044	7.5	18
0.05% AO-1	0.046	8	29	0.095	16	25
0.20% PS-1	0.16	16		0.10		
0.10% AO-1	0.099			0.042		
0.10% PS-1	0.081					

Table 2. OIT of HDPE (Cr) after multiple extrusion at 260°C.

In order to verify some of these findings, all data available in our laboratories generated in the same polymer used by Moss and Zweifel [15] were assembled and are shown in Figure 4. The primary antioxidants are expressed in percent of hindered phenol group (2,6 di-tert-butyl phenol) and increase along the X-axis. Connecting the points at constant phosphite concentration, a family of lines were obtained. The slope increases with

increasing phosphite concentration. These lines obtained for different PS-1 concentrations in combination with AO-1 or AO-4 explain the drop in OIT observed between the 1st and the 5th extrusion by comparing the consumption measured for PS-1 by HPLC.

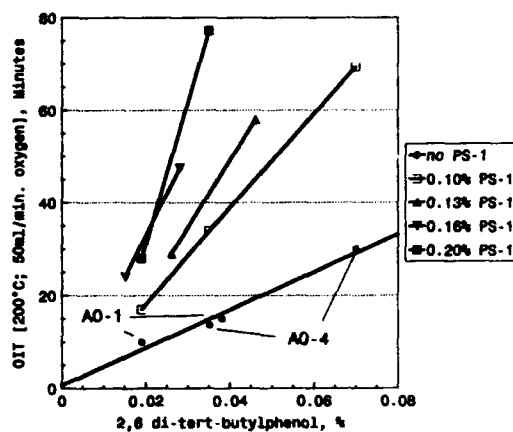


Figure 4: OIT of HDPE (C) as a function of the antioxidants AO-1 and AO-4 and the phosphite PS-1.

Similar experiments were repeated with different polyolefins. As examples Figure 5 shows the results obtained with a Ziegler-Natta HDPE and Figure 6 for polypropylene. In polypropylene and in some L-LDPE tested the phosphite PS-1 only significantly increased OIT when approximately 500ppm of AO-4 was present. This suggests that a certain threshold concentration of phenolic antioxidant is necessary to enable the phosphite to extend the oxidative induction time.

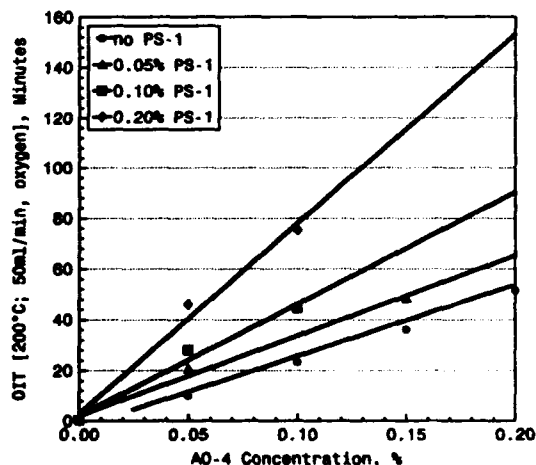


Figure 5: OIT of HDPE (Ti) as a function of the antioxidant AO-4 and the phosphite PS-1.

To test this suggestion, a series of compounds based on HDPE (Cr) similar to the one previously used, containing lower concentrations of AO-4 and PS-1 were prepared. The OIT values of these samples are given in Figure 7. The existence of a threshold concentration is not obvious.

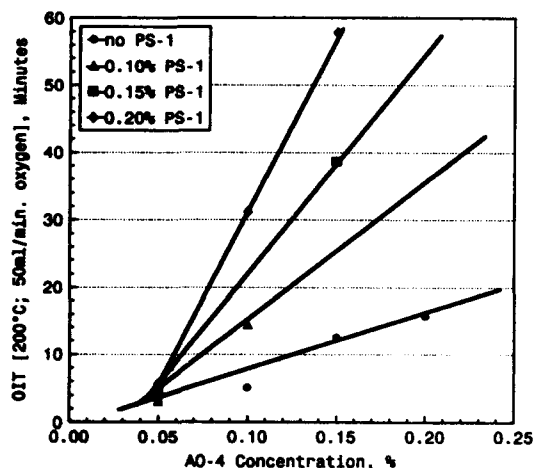


Figure 6: OIT of polypropylene as a function of the antioxidants AO-4 and the phosphite PS-1.

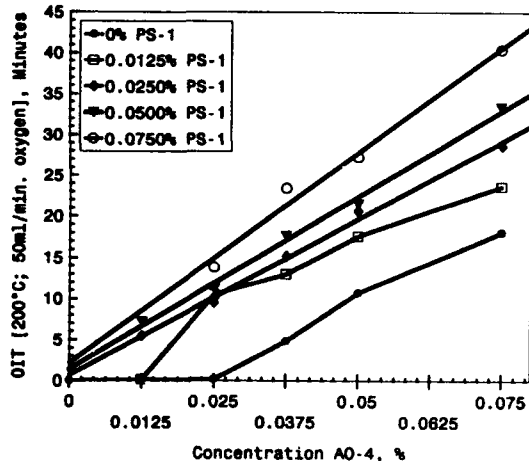


Figure 7: OIT of HDPE (Cr) as a function of AO-4 and the phosphite PS-1 at lower concentrations.

It seems that the lines intercept the Y-axis at the origin, representing the OIT of the unstabilized resin. In absence of phosphite 375ppm of AO-4 are necessary to increase the OIT of the resin at 200°C. Below, too much AO-4 is probably consumed during melt compounding of the samples. But 250ppm AO-4 combined with 125ppm PS-1 or 125ppm AO-4 combined with 250ppm PS-1 gave OIT values differing from the unstabilized resin. This suggests that 375ppm of the stabilizers, independently of the ratio used seems necessary to obtain the first significant increase in

OIT at 200°C. However, the ratio cannot be infinite since 0.20% PS-1 alone did not increase the induction time. Figure 8 shows the same results plotted as lines of same total concentration, the X-axis gives the percentage of phenolic antioxidant AO-4 in the blend. This figure suggests that one could replace up to 50% of AO-4 by PS-1 without losing OIT performance, at least under the test conditions used here.

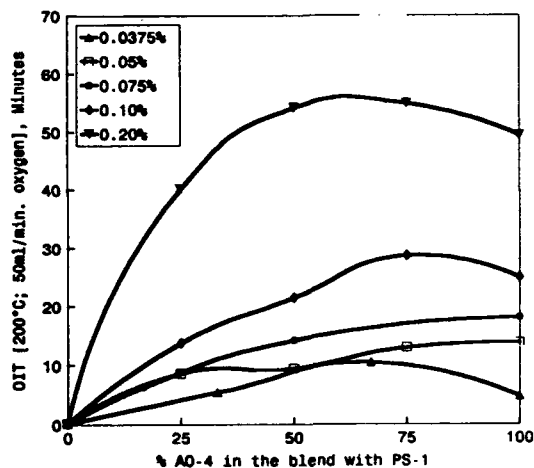


Figure 8: Influence of the AO-4 to PS-1 ratio on OIT of HDPE (Cr) at different total concentrations.

It might well be that the apparent threshold observed for PP is due to the insensitivity of the method at this temperature. Tests at lower temperatures should be able to confirm this.

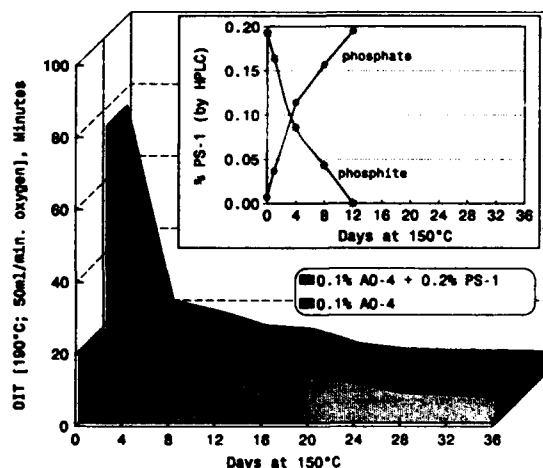


Figure 9: OIT after oven aging at 150°C of 1 mm PP compression molded plaques. Influence of PS-1.

Additional proof for the contribution of the phosphite PS-1 to OIT are the results plotted in Figure 9. OIT was measured after different time intervals on 1mm

samples aged in a draft air oven at 150°C. A rapid decrease in induction time is observed during the first 12 days of aging followed by a slow, but gradual decrease of OIT value until the samples failed mechanically. This initial decrease coincides with the conversion of phosphite to phosphate determined by HPLC of the samples. A reference sample containing the same amount of phenolic antioxidant without phosphite PS-1 had a lower initial OIT value which also gradually decreased at about the same rate over the entire aging time. It is remarkable that in this polymer the two samples failed after the same exposure time within experimental error. Long-term thermal stability predicted on the basis of the initial OIT would have lead to a different answer!

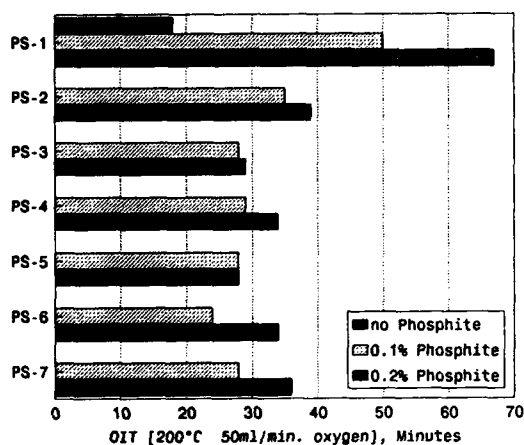


Figure 10: Influence of phosphites on OIT of HDPE (Cr). All samples contain 0.05% AO-4.

PS-1 is not the only organophosphite processing stabilizer that might boost OIT of polyolefins. Figure 10 gives the OIT obtained with a number of commercial phosphites, tested in combination with AO-4 at two different concentrations. In this particular polyethylene the results obtained with PS-1 are outstanding. However, the ranking found here is not always identical and is largely dependent on the polyolefin substrate. The same holds true for the extent of the OIT boost one can expect from a given phosphite at a given concentration.

Furthermore, the effect of phosphite on OIT is not restricted to a particular class of phenolic antioxidants, as shown in Figure 11.

The linear relationship between stabilizer concentration and OIT is also found for combinations of phenolic and phosphite stabilizers. The method can thus still be used for quality control purposes,

provided the stabilization system is known. However, the information given by such a test is basically only a go/no-go answer because deviation from the specified value might result from different causes: incorrect level of AO or PS, wrong AO/PS ratio or excessive consumption of processing stabilizers during melt processing. The possibility of passing specifications with a formulation inadequate for end use application is real, since a same OIT can be achieved with different AO/PS ratios of which only the AO portion is particularly effective as long-term thermal stabilizer.

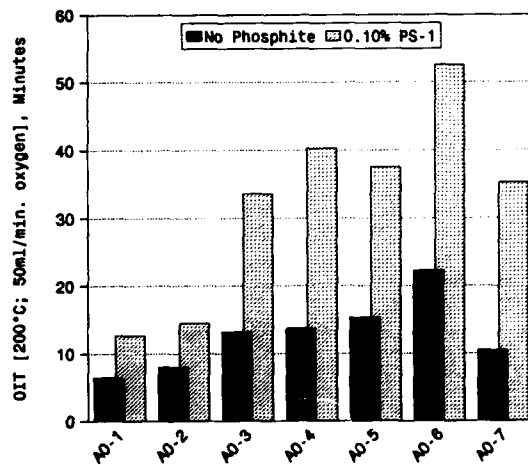


Figure 11: Combinations of PS-1 with different phenolic antioxidants in HDPE (Cr).

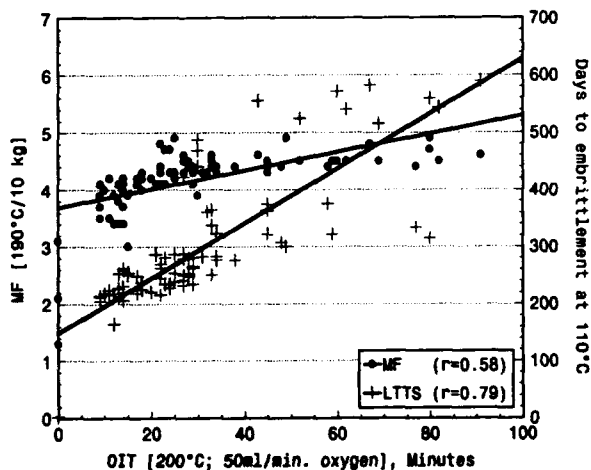


Figure 12: Correlation between OIT, melt flow and oven aging results for HDPE (Cr) extruded at different temperatures.

No correlation was found between OIT, either with oven aging at 100°C or with melt flow in HDPE (Cr) stabilized with AO-1 or AO-4 and PS-1 combinations of varying

ratio as shown in Figure 12. Oxygen deficient conditions and shear are most probably the reason why OIT cannot predict processing stability behavior of the polymer even though the test temperature is realistic.

HALS and OIT

Hindered amine light stabilizers (HALS) have been very successfully used for almost 20 years as light stabilizers in polyolefins [18]. More recently a number of publications have shown that the high molecular weight HALS are also outstanding long-term thermal stabilizers [19,20]. The great resistance to extractive media could be of great interest for pipe, geomembrane and wire and cable applications. However, one of the drawbacks encountered with this new concept are the accelerated test methods in use. Typical examples are the OIT specifications for pipe, geomembrane, and wire and cable applications. It has been known for years that high molecular weight HALS alone do not give appreciable OIT values even though their contribution to long-term thermal stability is tremendous. This is illustrated in Figure 13 for 200 micron blown LDPE films used in construction applications. These results provide a major argument for rejecting the OIT test as a screening method for long-term thermal stabilizer systems, because of the obvious lack of correlation between the two tests. Moreover, the OIT results would rather suggest not to use the combination of HALS with the phenolic AO-4. When oven aging results at 80°C and 100°C are considered, this is serious mistake, since the longest embrittlement times were achieved using combinations of HALS and AO-4.

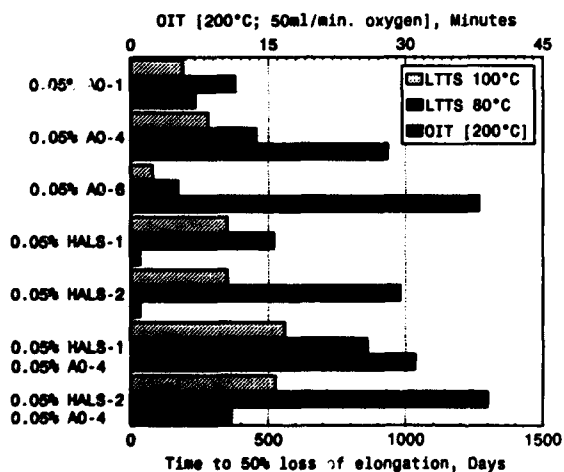


Figure 13: Comparison of oven aging results and OIT of 200 micron LDPE films.

Usually HALS are not used alone but are associated with antioxidants, processing stabilizers, antacids, pigments etc. Unpredictable OIT results have been observed with HDPE compounds containing high molecular weight HALS, as shown in Figure 14. The resins are both produced by chrome catalysts and the HALS concentrations are the same. The differences are the processing stabilizers, antacid or lubricants and pigmentation. A reason for this erratic behavior is the high test temperature, which gave results that are irrelevant to actual end-use conditions, as is clearly shown in Figure 13.

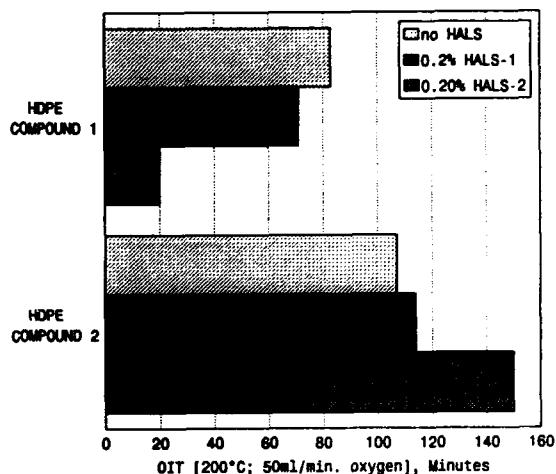


Figure 14: Influence of HALS on OIT of HDPE.

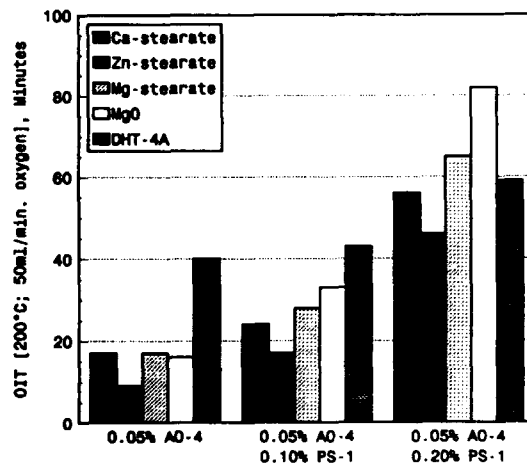


Figure 15: Influence of antacids on OIT of HDPE (Cr).

Not only antioxidant stabilizers, but also other additives such as antacids used as corrosion inhibitors in polyolefins polymerized with Ziegler-Natta catalysts

influence the oxidative induction time of a polymer [21]. It is also true for polymers, that do not need acid scavengers to neutralize catalyst residues, such as Phillips HDPE. This is illustrated in Figure 15 for different antacids in two HDPE resins of different technology. With Zn-stearate a serious reduction in OIT was systematically found, particularly when combinations of phenolic antioxidants and PS-1 were used. The effect observed in long-term thermal stability as judged by oven aging tests conducted at temperatures much closer to end use conditions were less significant [21].

Conclusions

OIT measured by DSC/DTA can be used as quality control method in polyolefins stabilized with phenolic antioxidants to verify the antioxidant concentration. The method is quick and easy and determines the concentration of active stabilizer, which is of particular interest when multifunctional stabilizers are used.

With organophosphite processing stabilizers, the slope of the calibration line established with a phenolic antioxidant alone increases with increasing phosphite concentration. Phosphite used alone does not increase the induction time of polyolefins in the temperature range of 180 to 210°C. It is still possible to use the method for quality control purposes but no conclusion can be drawn about the actual concentrations of both components in the stabilizer blend.

OIT cannot be used to predict long-term thermal or processing stability of polyolefin compounds. Particularly in the presence of HALS, the OIT measured bears no relation to the actual thermal stability of the polymer at lower test temperatures. Although OIT specifications were initially intended to improve the quality of manufactured plastics, they are now actually an obstacle to further technological improvements, because they yield misleading results about the effectiveness of new stabilizer systems under actual end use conditions.

A general consensus exists in the plastic industry on the lack of relevance of OIT as a predictive tool for long-term stability of polyolefins but still a great number of OIT specifications exist. Unfortunately, far too much product development time and effort is expended trying to make a formulation meet an OIT specification instead of generating more useful data under realistic conditions.

Acknowledgments

The authors are grateful to Dr.H.Zweifel for the encouragement and fruitful discussion during the course of this work. The authors would also like to thank Mrs. M.P.Meyer, Mr. B.Rein and Mr. R.Roggwiller for the innumerable OIT measurements run over last three years.

References

- [1] Howard, J.B. and Gilroy, H.M., Polym. Eng. Sci., 15 (1975), p. 268-271.
- [2] Kotka, E.T., Proc. 24th Int. Wire and Cable Symp. (Nov. 1975), p. 220-224.
- [3] Bernstein, B.S. and Lee, P.N., Proc. 24th Int. Wire and Cable Symp. (Nov. 1975), p. 202-212.
- [4] Billingham, N.C., Bott, D.C. and Manke, A.S. in Developments in Polymer Degradation - 3, Ed. N.Grassie (1981), p. 63-100, Applied Science Publishers, London.
- [5] Howard, J.B., Polym. Eng. Sci., 13, (1973), p. 429-434.
- [6] Kramer, E. and Koppelman, J., Polym. Degrad. Stab. 16 (1986), p. 261-275.
- [7] Steiner, G. and Koppelman, J., Polym. Degrad. Stab. 19 (1987), p. 307-314.
- [8] Marshall, D.I., George E.J., Turnipseed, J.M. and Glenn, J.L., Polym. Eng. Sci., 13 (1973), p. 415-421.
- [9] Foster, G.N., in Oxidation Inhibition in Organic Materials, Vol. 2, Ed. J.Pospisil and P.K.Klemchuk (1990), CRC Press, Boca Raton, Florida.
- [10] Schwarz, T., Steiner, G. and Koppelman, J., J. Appl. Polym. Sci., 37,(1989), p. 3335-3341.
- [11] Gugumus, F., in Developments in Polymer Stabilisation - 8, Ed. G.Scott (1988), p. 244-257, Applied Science Publishers, London.
- [12] Sebesta, E.C. and Rase, H.F., Ind. Chem Prod. Res. Dev. 6 (1967), p.150-154.
- [13] Bair, H.E., in Thermal Characterization of Polymeric Materials, Ed. E.A.Turi (1981),

Academic Press, Orlando, Florida,
p.871.

- [14] Drake, W.O., Pauquet, J.R., Todesco, R.V. and Zweifel, H., *Angew. Makromol. Chem.*, 176/177 (1990), p.215-230.
- [15] Moss, S. and Zweifel, H., *Polym. Degrad. Stab.*, 25 (1989), p. 217-245.
- [16] Chen, Y.L. and Ranby, B., *J. Polym. Sci., Part A*, 28 (1990), p. 1847-1859.
- [17] Uhniat, M. and Latocha, C., *Polym. Degrad. Stab.*, 35 (1992), p. 163-170.
- [18] Gugumus, F., in *Plastics Additives*, 3rd Ed., Ed. R. Gächter and H. Müller (1990), C.Hanser Publishers, Munich, p. 129-270.
- [19] Gugumus, F., 34th Annual Technical Conference of Soc. Plast. Eng., (1988), p. 1447-1450.
- [20] Drake, W.O., 14th Int. Conference on Advances in Stabilization and Degradation of Polymers (1992), Lucerne, Switzerland.
- [21] Todesco, R.V., SP'92 Conference, (1992), Zurich, Switzerland.

APPENDIX 1

- AO-1 : Octadecyl-3-(3,5-di-tert-butyl)-4-hydroxy-phenol propionate (Irganox 1076)
- AO-2 : 1,3,5 -Tris-(3',5'-di-tert-butyl-4'-hydroxybenzyl) isocyanurate (Irganox 3114)
- AO-3 : 2,4,6 -Tris-(3',5'-di-tert-butyl-4'-hydroxybenzyl) 1,3,5-tri-methyl benzene (Irganox 1330)
- AO-4 : Tetrakis-[methylene-3-(3,5-di-tert-butyl-4-hydroxyphenyl)-propionate] methane (Irganox 1010)
- AO-5 : (2,2'-Thiodiethylbis-[3-(3,5-di-tert-butyl-4-hydroxyphenyl)-propionate]) (Irganox 1035)
- AO-6 : (4,4'-Thiobis-(3-methyl-6-tert-butylphenol) (Santonox R)

- AO-7 : 1,2-Bis-[3,3-bis-(4'-hydroxy-3-tert-butylphenyl) butanate] ethane (Hostanox 03)
- PS-1 : Tris-(2,4-di-tert-butyl)phenyl phosphite (Irgafos 168)
- PS-2 : Tetrakis-(2,4-di-tert-butyl-phenyl)-4,4'-biphenyldiphosphonite (Sandostab, Irgafos P-EPQ)
- PS-3 : Tris-(nonylphenyl)-phosphite (TNPP)
- PS-4 : Di-(2,4-di-tert-butyl-phenol) pentaerythrityl diphosphite (Ultranox 626)
- PS-5 : Distearylpentaerythrityl diphosphite (Weston 618)
- PS-6 : Bis(2,6-di-tert-butyl-4-methylphenyl) pentaerythritol diphosphite (Mark PEP-36)
- PS-7 : 2,2'-Ethylidenebis-(4,6-di-tert-butylphenyl) fluorophosphite (Ethanox 398)
- HALS-1: Poly-(N-b-hydroxyethyl-2,2,6,6-tetramethyl-4-hydroxy-piperidyl succinate) (Tinuvin 622)
- HALS-2: Poly-([6-[(1,1,3,3-tetramethylbutyl)-imino]-1,3,5-triazine-2,4-diyl][2-(2,2,6,6-tetramethylpiperidyl)-amino]-hexamethylene-[4-(2,2,6,6-tetramethylpiperidyl)-imino]) (Chimassorb 944)



J.R. Pauquet is a member of the Technical Service Group of the Polyolefin Additives Laboratories of Ciba-Geigy, Limited, Basle, Switzerland. He received his degree as Chemical Engineer from the University

of Liege, Belgium in 1985 and joined Ciba in 1987. At present he is involved in the development and application of stabilizers for polyolefins.

W.O.Drake PhD has over 30 years experience in the areas of polymers and polymer additives, including managerial responsibilities in R&D, polymer production and technical service. He is currently Manager of Polyolefin Additives Application Laboratories of Ciba-Geigy, Limited, Basel, Switzerland, where he is responsible for the activities of the group involved in Screening, Development and Technical Service as well as Compounding and Fabrication.

R.V.Todesco PhD received his degree from The Catholic University of Leuven, Belgium. He then completed a post-doctoral research study concerning light degradation of polymers at the Radiation Laboratories, University of Notre Dame, USA. In 1988, after two years research experience involving stabilization of polymers at a major European polymer producer, Roberto joined Ciba-Geigy Limited, Basle, Switzerland, as manager of the Technical Service Laboratories for Polyolefin Additives.

CABLE COMPOUNDS OF SILANE-CROSSLINKABLE PVC

R. Dahl and M. Rogestedt

Hydro Plast AB, S-444 83 Stenungsund, Sweden

A new approach to crosslinkable plasticised PVC-compounds (Norvinyl DX-compounds) is introduced by Norsk Hydro. A reactive PVC-resin is used in combination with organosilanes. The compounds are extrudable on conventional cable extruders. Crosslinking is performed in hot water, steam bath, oven or by storing. The improvements compared with corresponding conventional plasticised PVC-compounds are better mechanical properties at high temperatures, better heat ageing performance, better abrasion resistance and better chemical resistance. This unique combination of improvements gives compounds made with this technology which are a viable alternative to irradiation-crosslinked PVC, XLPE, and different kinds of elastomers.

Introduction

Flexible PVC is one of the most versatile materials in the modern world. The outstanding processing properties in combination with innumerable possibilities to vary the mechanical properties have made PVC-based compounds to the most used insulation material within the cable industry. Although the properties of a PVC-material can be varied to such a great extent, it has of course its ultimate limitations. The most serious ones are mechanical properties at high temperatures in combination with a moderate upper service-temperature limit.

For overcoming the problem with mechanical properties at high temperatures, crosslinking is an obvious measure.

Crosslinking of PVC has been known for a long time. Examples of

processes for this are crosslinking via irradiation with¹ or without² reactive plasticisers, with dithiol triazines^{3,4}, aromatic dithioles⁵, diamines⁶.

The only process that seems to have reached some commercial importance is crosslinking via irradiation together with reactive plasticisers. The further growth of this process is limited due to several disadvantages being introduced when crosslinking this way. The material will stiffen when crosslinking, the thermostability will decrease due to the irradiation, and maybe the most important factor, the cost for the irradiation equipment is very high. The upper service temperature will not be improved by this crosslinking method.

The other processes all suffer from decreased thermostability and/or problems due to crosslinking when processing.

Silane crosslinking

An attractive alternative to the above-mentioned methods is the silane-crosslinking method. Polyethylene has for many years been crosslinked in this way, the so called Sioplas-method⁷. In this method vinyltrimethoxysilane is grafted to the polymer, via a free radical mechanism when processing. The crosslinking is then fulfilled under influence of moisture via hydrolysis and condensation.

Several attempts to crosslink PVC with organosilanes^{8,9,10} have been described in the literature. Due to different reasons these have not shown the same success as for polyethylene. Several workers have tried the use of aminosilanes for crosslinking. This suffers from the weakness that the aminosilane is too aggressive and reduces the thermostability of the

PVC-resin. Other workers have tried to use mercaptosilanes. The problem with this is, according to our experience, a poor grafting efficiency.

Silane-crosslinking of PVC with Norvinyl DX-technology

This process differs from earlier attempts by using a combination of a reactive PVC and organosilanes. In this way it is possible to use organosilanes which do not reduce the thermostability of the PVC-resin and still show a high grafting efficiency during appropriate compounding conditions.

Processing

In this paper three different grades of Norvinyl DX will be discussed:

Norvinyl DX 550; Shore A 90 moderately crosslinkable.
Norvinyl DX 750; Shore A 95, moderately crosslinkable
Norvinyl DX/PJ 92128; Shore A 78, highly crosslinkable. Will be renamed when commercially released.

The process consists of three important steps:

- * Compounding
- * Extrusion
- * Crosslinking

This is illustrated in Figure 1.

Compounding.

At present, the Norvinyl DX-compounds are compounded at Norsk Hydro's compounding plants only. The compounding is a key process, where the grafting of the organosilanes to the reactive PVC must occur to a high degree but the gelation degree must be kept low, to achieve good processing properties when extruding.

Extrusion

The compounds can be extruded on conventional cable extruders. Normally the same temperature profile and speed can be used, which would have been used for a conventional plasticised PVC with the same basic formulation. Extrusion lines from 30-90 mm screw diameter have been used,

with a production speed of 30-600 m/minute.

It is, however, necessary to be aware that processing of crosslinkable materials will always give a potential risk of early crosslinking during processing, i.e. scorching. Care should therefore be taken to avoid standstills in the extruder, especially when a catalyst is added during the extrusion. (For more information on catalysts, see below).

The extrusion will of course give a second chance for grafting of the organosilane on the reactive PVC-resin. Our experience is, however, that it is not possible to compensate for poor compounding by any adjustments of the extrusion conditions (on a conventional extruder).

The compounds of moderately crosslinkable formulations show good extrusion properties after storage of up to 1 year. For the more highly crosslinkable formulations like Norvinyl DX/PJ 92128 the storage stability is about 6 months. There is however not a very clear definition of when a compound is extrudable or not. It is to a great extent depending on how it is extruded. We have found that even a compound that apparently seems to be useless due to very poor extrudates on a laboratory extruder, can still give excellent extrudates simply by increasing the screw speed or changing to an extruder with greater shear (Table 1). The tendency is for the mechanical properties to be improved by ageing as long as they are extrudable.

Crosslinking.

Crosslinking is performed by exposing the cable to hot water or steam. Uncatalysed, the material needs around 48h to crosslink at 80°C. When increasing the water or steam temperature the crosslinking time decreases. By adding a catalyst masterbatch when extruding, the crosslinking times can be reduced down to 4-16h at 80°C water or steam.

When using catalyst the crosslinking can be performed in an oven or by storing at ambient conditions.

In Figures 2-4, the crosslinking efficiency is shown at different conditions with or without an addition of a catalyst masterbatch.

Properties

In Table 3 there is a summary from a test according to the automotive cable standard Volvo STD 7611.131 class R3. This study includes Norvinyl DX 750 and "PVC-R2", a commercial non-crosslinkable automotive cable compound close in basic formulation to DX 750 in use for the Volvo class R2 as well as two TPE-materials.

The strength of the Norvinyl DX-technology is that, as long as similar basic formulations are used, all the outstanding processing and mechanical properties which have given plasticised PVC such a wide-spread use within the cable industry are maintained except for some key properties that are improved.

Comparing Norvinyl DX 750 and "PVC-R2", shows that electrical properties, stripping, friction between cables, flexibility, shrinkage by heat and flammability were similar and within the standard.

The four main improvements¹¹ with Norvinyl DX-technology compared to "normal PVC" are as shown in the Appendix as the difference between Norvinyl DX 750 and "PVC-R2".

- * Improved mechanical properties at elevated temperatures. Norvinyl DX 750 passed the indentation at 120°C; PVC-R2 failed.
- * Better flexibility after ageing Norvinyl DX 750 passed cold-bending tests at -30°C after ageing 6h at 170°C and 1000h at 120°C; PVC-R2 failed.
- * Better abrasion resistance Norvinyl DX 750 774 cycles; PVC-R2, 282 cycles.
- * Better chemical resistance Norvinyl DX 750 max 13% swell, PVC-R2 max 17% swell in washer fluid and fuels.

Chemical resistance, abrasion resistance and mechanical properties at elevated temperatures are properties that improve by formulating stiffer compounds. Our technology gives therefore the possibility to formulate softer compounds for

meeting specific requirements.

Flexibility after ageing, on the other hand, improves by formulating softer compounds. In this case our technology allows stiffer formulations for meeting specific requirements.

While this may seem contradictory it may in some cases play an important synergistic role. For many advanced automotive cable standards for continuous use at high temperatures the properties discussed above are specified, so that it is not possible to fulfill all requirements with one formulation with conventional PVC-technology.

The use of our technology, makes it possible to formulate compound which fulfills cable standards where it is not possible with conventional PVC-technology which is illustrated in Figure 5.

The improved mechanical properties at elevated temperatures and the improved heat ageing resistance will be discussed in more detail below.

Mechanical properties at elevated temperatures

At room temperature the mechanical properties do not differ much from corresponding non-crosslinked formulations. This can be explained by the fact that conventional plasticised PVC already is physically crosslinked by crystallite structures. The magnitude of this physical network and the "silane"-network is of the same order. A chemical network like the silane-network and the physical network can also work synergistically towards each other¹².

The difference between crosslinked and non-crosslinked material will gradually increase, when temperature increases due to melting of the crystallites.

Mechanical properties at high temperatures can be measured, for example, as penetration resistance. The above mentioned increase in difference of crosslinked and non-crosslinked material with increasing temperature is very clearly illustrated in Figure 6.

In many European cable standards for crosslinked insulation and sheathing materials, there is a hot-set test at 200°C, at different loads.

One parameter that has been shown to be very important for the hot-set test is temperature of the copper wire when extruding. As indicated in Table 2, when extruding Norvinyl DX/PJ 92128, there was an extreme difference in performance during the hot-set depending on the copper wire temperature, although the crosslinking density was the same.

The importance of the copper wire temperature is a matter of orientation. The copper wire is very effective in cooling down the insulation right after extrusion. The mixed results with breaks and negative remaining elongation for the cable extruded with the wire at room temperature is very strong support for this statement. When using a hot wire the insulation material will have more time for relaxation. It might also be of importance that one crosslinks in a state as near the random coil conformation as possible so that one not only gets support from crosslinks but also from entanglements when making the hot-set.

Entanglements may play an important role at 200° C since the physical network is completely melted, so there is no support to be expected from that in this test.

Flexibility after ageing. The crosslinked material shows a slight tendency towards stiffening after crosslinking, (approximately 1-2 Shore A units). But after ageing at elevated temperatures the Norvinyl DX-compounds are more flexible than their corresponding non-crosslinkable formulations.

As seen in the appendix DX 750 withstood the cold-bend at -30°C after ageing 1000 h at 120°C. This is outstanding for a PVC-compound, especially taking into consideration that it has Shore A hardness of 95.

Even better for real long-term ageing is Norvinyl DX 550, which has shown to exhibit an excellent heat ageing resistance. In Figure 7, the ageing properties for crosslinked and non-crosslinked DX 550 and crosslinked DX 750 in a ventilated oven at 125°C are

shown.

To achieve these good long-term ageing properties it is not necessary to crosslink the material before ageing. At these high temperatures the material will self-crosslink early in the test. It seems from the curve that it is, at least initially, an advantage not to crosslink the material before the test, to get the best ageing properties. The comparison is, however, not absolutely fair, due to the fact that 3% of a catalyst masterbatch, plasticised with DOP, was used in the crosslinked samples. This means that the amount of high-temperature plasticisers has been reduced by 3%.

Comparisons with other materials. The success on the market of a new type of material will of course depend on how it performs in comparison with existing material in price and properties. Norvinyl DX is not a true alternative to normal PVC, where it meets requirements, due to the fact that Norvinyl DX materials are higher priced, but it is an interesting alternative to many other materials.

Comparing with irradiation-crosslinked PVC, the Norvinyl DX-compounds come out very strong, and show the following advantages:

- * Better thermostability
- * Higher use-temperature
- * Better low-temperature properties
- * No or very moderate stiffening after crosslinking
- * No expensive after-treatment

The only obvious disadvantage, the higher compound price, is in most cases more than compensated by cheaper crosslinking. Since the irradiation cost is paid per kilometer, the calculation is strongly affected by the thickness of insulation/sheathing. For cable manufacturers renting irradiation-capacity, the calculation will, in almost any case, be in favour of Norvinyl DX.

Crosslinked polyethylene (XLPE) has had success on the market for many years. The advantages for Norvinyl DX-materials will in principle be the same as for uncrosslinked PVC in comparison to uncrosslinked polyethylene, meaning the same advantages that have made PVC and not polyethylene the most preferred insulation and sheathing material.

- * Better flexibility
- * Lower flammability
- * Better processing properties
- * Better printability
- * Easier stripping
- * Easier to joint (glueing, welding, casting)

XLPE has better electrical properties, and has also a lower density if it is not filled for flame retardancy. The price is also lower.

The biggest improvements compared to most thermoset rubbers are an easier and faster processing, as well as ageing resistance.

In some applications such as automotive "under the bonnet" cables in Europe, Norvinyl DX competes with thermoplastic elastomers. For example polyether-ester elastomers and polyester elastomers. As can be seen in the Appendix Norvinyl DX is favoured by better flexibility, self-extinguishing properties, stripping and maybe the most important, the price is approximately half of the mentioned TPE:s.

The elastomers are favoured by the fact that they are not chemically crosslinked which facilitates recycling, and some of them can also reach a higher temperature-rating.

Applications

We have found a large potential for this technology within the cable industry such as:

- * Automotive cable
- * Flexible iron cordage
- * Cables for other domestic appliances
- * Heating cables
- * Power transmission cables
- * Tele communication cables

Recycling

Recycling of crosslinked materials is of course more difficult than for thermoplastics. There are however some possibilities. For the moderately crosslinked Norvinyl DX-grades there is possible to thermoform plates with good surface finish by mixing with small amounts of non-crosslinkable material.

When milled, the crosslinked material can work as a filler in normal or crosslinkable PVC.

We are also studying the possibilities to chemically break the crosslinks to make it reprocessible.

Conclusion

With the Norvinyl DX-technology, crosslinked PVC can be made with conventional equipment. Although flexibility at low temperatures is hardly affected, chemical resistance, abrasion resistance, mechanical properties at elevated temperatures and heat ageing resistance are improved by this technology.

This makes the Norvinyl DX a strong alternative to materials like irradiation-crosslinked PVC, crosslinked polyethylene, and different kinds of elastomers.

Acknowledgement

Alcatel IKO Kabel of Grimsås, Sweden is acknowledged for their permission to use their results from testing according to the norm Volvo Std 7611.131.

Å. Rynningen and M. Lundquist at the PVC-technical Department in Porsgrunn for valuable discussions and contribution.


Our colleagues at the Research Laboratory and at the Technical Service laboratory for carrying out the experimental work.

Our colleague Alan Fowler, at the PVC-technical department in Porsgrunn, Norway, is acknowledged for his correction of the English in this manuscript.

References


1. T. N. Bowner, M. Y. Hellman, W. I. Wroom, J. Appl. Polym. Sci. 28, 2083 (1983)
2. S. H. Pinner, Large Radiation Sources in Ind. Proc. Conf. Warsaw 2, 273, (1960)
3. K. Mori and Y. Nakamura, J. Macromol. Sci. Chem., A12 (2), 209 (1978)
4. T. Hjertberg, R. Dahl and E. Sörvik, J. Appl. Pol. Sci., 37, 1239 (1989)

5. V. Ducházek and A. Kuta, J. Appl. Pol. Sci., 27, 1549 (1982)
6. H. Kojima, Japan Plastics, 3 (2), 11 (1969)
7. M. Narkis, A. Tzur, A. Vaxman, and H.G. Fritz, Pol. Eng. Sci., 25 (13), 857 (1985)
8. M. S. Hearn, J. D. Baird, L. P. Nethsinghe and M. Gilbert, Polym. Commun., 31 (5), 194 (1990)
9. I. Kelnar and M. Schätz, J. Appl. Pol. Sci., 48, 657 (1993)
10. I. Kelnar and M. Schätz, J. Appl. Pol. Sci., 48, 669 (1993)
11. R. Dahl, Å. Rynningen, M. Lundquist and M Rogestedt, PVC 93, The Future, Inst. of Mat., 378-387 (1993)
12. T. Hjertberg and R. Dahl, J. Appl. Pol. Sci., 42, 107 (1991)



Roger Dahl, Lic. techn. Born 1956. M.Sc in Chemical Engineering at Chalmers Univ. of Techn 1981. Licentiate of technology in polymer technology 1985. Joined Ciba-Geigy Plastics & Additives Division in Sweden 1984-88. Since 1988 RD has worked for Norsk Hydro in Norway and Sweden within R&D, as Technical Service Manager and since 1992 as Project Manager for reactive PVC.

R Dahl is inventor or co-inventor to 5 patents within the reactive PVC-area.



Mikael Rogestedt. Born 1963. M.Sc in Chemical Engineering 1987. Between 1987-1992 he has been doctor student at Dep. of Polym. Techn. at Chalmers Univ. of Techn. Joined Norsk Hydro in beginning of 1993.

Table 1. Appearance of aged extrudates from extrusion of Norvinyl DX/PJ 92128 after ageing, with no protection against humidity.

Age	Extruder	Screw Speed	Result
Fresh	30 mm 25 D Collins, strips	10,30,60,100	Good
3 months	"	10	Poor
"	"	30,60,100	Good
6 months	"	10,30	Poor
"	"	60,100	Good
9 months	"	10,30,60,100	Poor
"	Maillefer, 30 mm 25 D, 2.0 mm cable.	50	Good

Table 2. Hot-set values for 0.75 mm², 2.3 mm cable insulated with Norvinyl DX/PJ 92128, extruded with a temp.profile 140..160°C with different temperatures on the copper wire.

Copper wire Temperature	Load MPa	Degree of cross- linking	Elong. after 15 min	Rem.elong. after unloading
Room temp	0.1	94%	break or 20%	- or -5%
"	0.2	"	break	-
100°C	0.1	95%	41%	-1%
"	0.2	"	break	-
150°C	0.1	94%	43%	2%
"	0.2	"	72%	8%

Appendix

Volvo STD 7611.131 class 3. Test with 0.75 mm² Cu, 1.8 mm cable (0.35 mm insulation).

	Norvinyl DX 750	PVC-R2	Polyeter- ester elastomer	Polyester elastomer
Volume resistivity. Requirement: $> 1 \cdot 10^9$ ohm.mm	$2.0 \cdot 10^{11}$	$2.6 \cdot 10^{11}$	$2.8 \cdot 10^{11}$	$6.1 \cdot 10^{11}$
30 min. voltage and breakdown voltage test. Requirement: No breakdown below 5kV.	OK	OK	OK	OK
Intendation test at 120°C.	OK	<u>failed</u>	OK	OK
Cold bending at -30°C after ageing 6h at 170°C.	OK	<u>failed</u>	OK	OK
Cold bending at -30°C after ageing 1000h at 120°C.	OK	<u>failed</u>	OK	OK
Wear strength. Requirement: > 250 cycles.	774	282	385	1124
Flexibility: Requirement: $F = \max 2.2$ N.	1.8	2.2	<u>2.7</u>	<u>2.3</u>
Friction between cables. Requirement: $\tan(\alpha) < 0.4$	0.21	0.20	<u>0.49</u>	0.18
Resistance to thermal shock, winding test.	OK	OK	OK	OK
Shrinkage by heat. Requirement: max 0.5%.	0.2	0.2	0.1	0.0
Adhesion of insulating layer to conductor. Requirement: $10 < F < 35$ N.	28	23	<u>> 100</u>	<u>90</u>
Properties under fire conditions. Requirement: Flame extinguish within 30 s after removal of bunsen flame.	3	1	16	18
Resistance to ASTM oil in 48 h at 110°C. Requirements: No cracks when winding at room temp., max 13% swell.	Winding: OK Swell -15%	Not tested	Winding: OK Swell: 6%	Winding: OK Swell: 7%
Resistance to brake fluid in 48h at 110°C. Requirements: No cracks when winding at room temp., max 13% swell.	Winding: OK Swell: <u>25%</u>	Not tested	Winding: OK Swell: <u>15%</u>	Winding: OK Swell: <u>34%</u>
Resistance to 4 different fuel and washer fluid in 10 min at room temp. Requirements: No cracks when winding, max 19% swell	Winding: 4xOK Swell: 2-13%	Winding: 4xOK Swell: 2-17%	Winding: 4xOK Swell: 4-10%	Winding 4xOK Swell: 2-10%

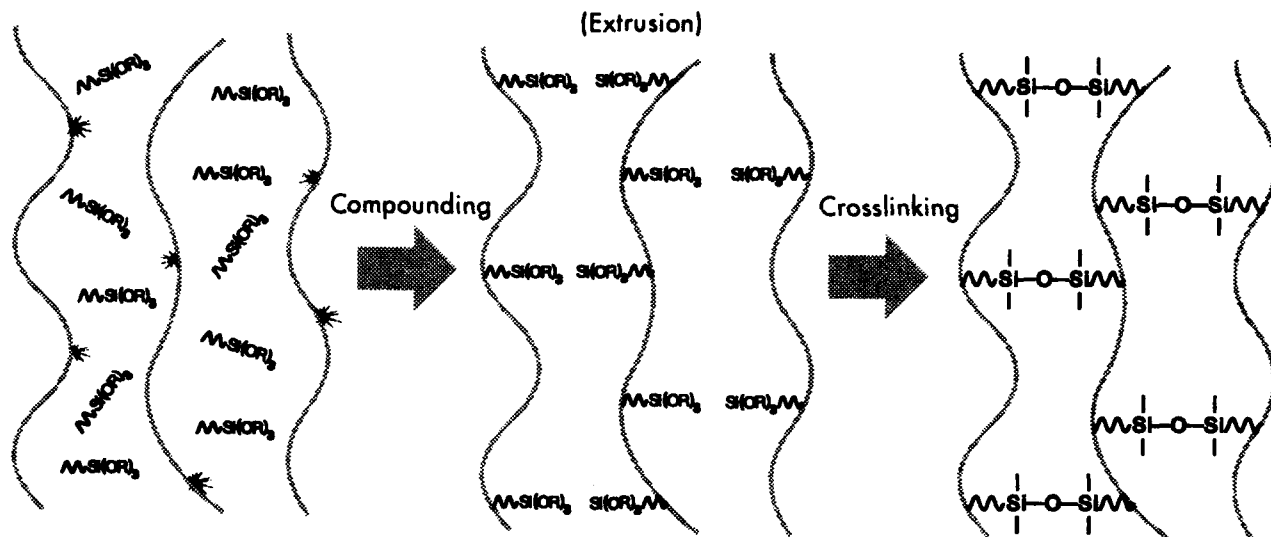


Figure 1: Scheme of Norvinyl DX-technology.

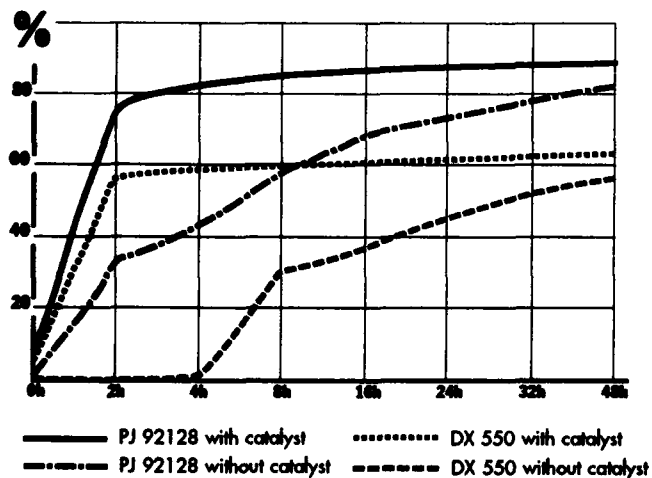


Figure 2: Degree of crosslinking (gel content) as function of crosslinking time at 80°C in water.

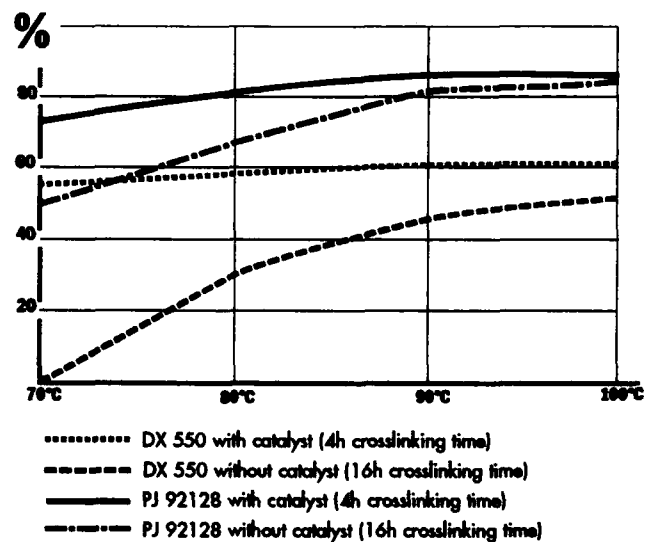


Figure 3: Degree of crosslinking as function of temperature of water when crosslinking.

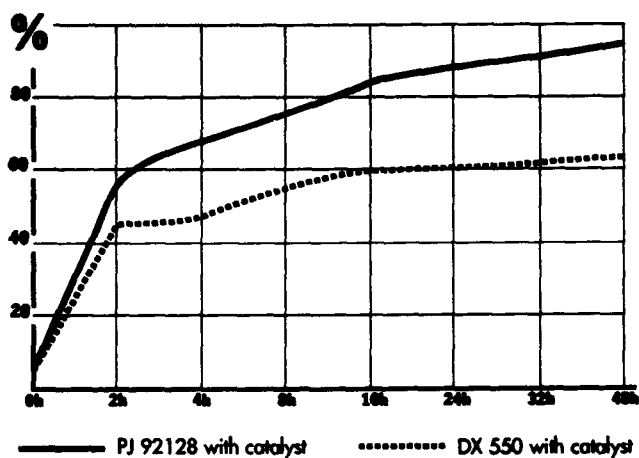


Figure 4: Degree of crosslinking (gel content) as function of crosslinking time at 100°C in an oven.

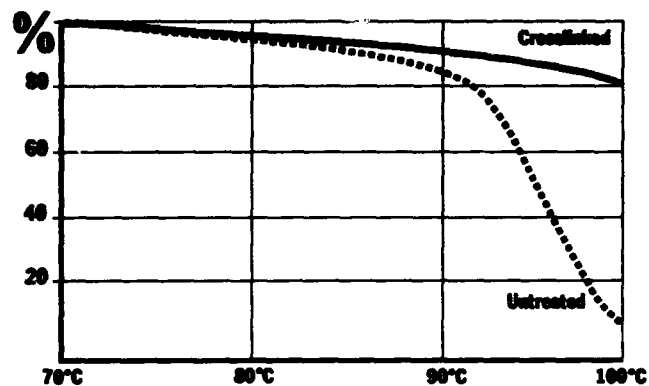


Figure 6: Penetration as function of temperature in a TMA-experiment for untreated and crosslinked Norvinyl DX 550.

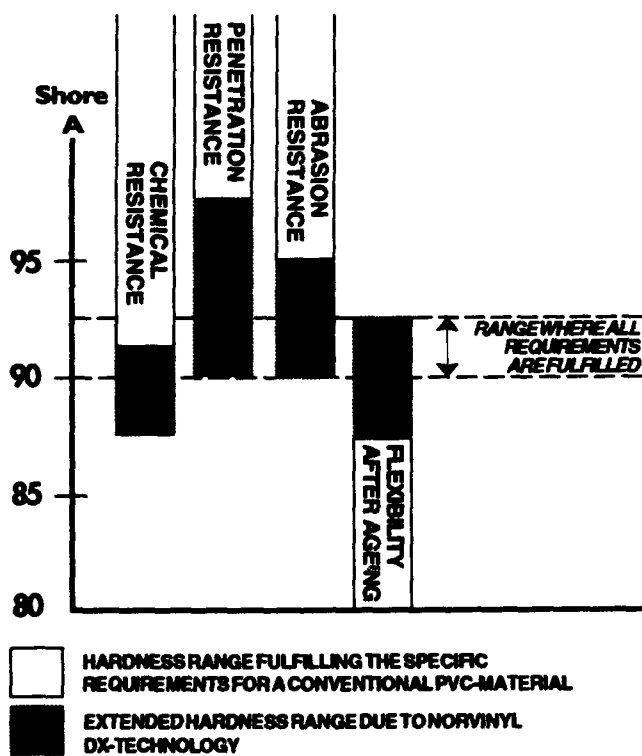


Figure 5: Example of hardness range fulfilling specific requirements of an automotive cable standard.

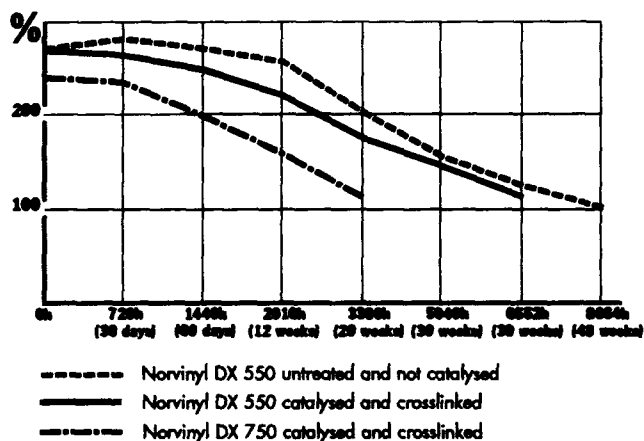


Figure 7: Elongation at break after ageing at 125°C in a fan-ventilated oven.

Copper Cables For Local Area Networks With Very High Bit Rate Data Transmission

Siegfried Richter Klaus Lehan

kabelmetal electro GmbH, Nürnberg, Germany
KABEL RHEYDT AG, Mönchengladbach, Germany

Summary

To date the requirements for high performance data cables are not described in public international standards. This is in particular true for the test methods. Therefore it is very time and cost consuming to compare different cables.

The following report compares the transmission properties and the EMC behavior of shielded and unshielded level 5 data cables.

The use of high performance data cables is far ahead of the test procedures. Some of the cables used today are not suitable for an undisturbed operation up to 100 Mbit/s. Unshielded cables failed in some of the EMC-tests and it was not possible to use them with the specified length of 90 m. The reason for the latter is not yet clear.

The ACR of cables having individually shielded pairs is about 10 dB better than for unshielded pairs. This guarantees safety for the advanced future LAN-systems with bit rates above 100 MBit/s.

Introduction

The increased utilization of personal computers in business systems has created new network structures with the demand of higher transmission bit rates. The transition from previous networks capable to transmit 10 M bit/s to high performance networks with rates of 100 Mbit/s cannot be viewed as an extension of the standard cable technology, but represents a quantum step into a new cable technology.

Public standards for the new data cables are currently not available. This is specifically true for the test methods. Today there are different test methods in use, which provide different results and a comparison of these results among each other is very difficult or almost impossible.

In the following test results are presented, which were carried out on different cables from major manufacturers. According to the manufacturers all three cables should fulfil the specifications of level 5, UL subject 444 and 13. All cables were randomly taken from the market.

The following factors have been investigated :

- changes of cable performance after mechanical handling, simulating the handling during installation.
- susceptibility to EM interference

Cable Types Investigated:

The cable types which have been investigated are :

- | | |
|-------|---|
| No. 1 | unshielded pair
4 x 2 x AWG 24 |
| No. 2 | unshielded pairs with common shield
4 x 2 x AWG 24 |
| No. 3 | individually shielded pairs
with additionally common shield
4 x 2 x .6 mm |

Installation Behavior Of High Performance Data Cables

Test Methods :

At present public standards for data cables for transmission rates up to 100 Mhz, which would guarantee reliable and reproducible performance evaluation are still not available.

Experiences has shown, that it is not sufficient to standardize the test method and the equipment only, but also the connection of the cables to the test set, viz. plugs, the length of the stripped cable ends and the geometrical layout for connection to the test set, the characteristics of the baluns and terminators and furthermore all calibration procedures. These details may have an important influence on the test results. Particularly sensitive in this respect are the characteristic impedance and the near-end crosstalk.

Finally, the number of test points to be used over the frequency range or frequency steps have to be defined. Large interval steps may hide sharp resonances if the measurements happen to be taken just before and after these events. These peaks, however, may disturb the network performance considerably. It is therefore suggested to require a minimum of 200 test points or intervals with a maximum of 500 kHz for all transmission tests in the range from 1 MHz to 100 MHz.

In order to obtain steady and reproducible results the minimum length of the cables shall be not less than 100 m.

In the following sections only the least favorable test result are presented for each cable tested.

Characteristic Impedance

Today the test methods for impedance are based on one of the following principles:

- resonance
- return loss
- open - short circuit performance

For this test program the open-short circuit measurement has been selected. The measurements were carried out in the frequency range from 1 MHz to 100 MHz at intervals of 500 kHz.

The calibrations were carried out following the S11-procedure with open end, shorting and a load connected to the symmetrical side of the balun.

The validity of the test results were controlled with equivalent measurement setups elsewhere. All measurements agreed within less than $\pm 3\%$.

Longitudinal Attenuation

The test for longitudinal attenuation is the easiest of the cable performance tests. A high output level at the balun and good impedance match at the input of the test set are all what is required for a trouble free test.

The measurement were carried out within the frequency range from 1 MHz to 100 MHz and with frequency intervals of 125 kHz.

Near-end Crosstalk Attenuation (NEXT)

The near-end crosstalk is very sensitive to changes in frequency therefore it is important to measure with high frequency resolution, e.g. small intervals. The measurements covered the frequency interval from 1 MHz to 100 MHz at intervals of 125 kHz.

Attenuation Unbalance

The evaluation of attenuation unbalance is already a standard practice for telecommunications cables. A test method for these cables is specified in the CCITT standards, but only the frequency range up to 4 MHz is there required. It is absolutely necessary for high performance data cables to extend the range up to 100 MHz.

Attenuation Crosstalk Ratio (ACR)

The Attenuation Crosstalk Ratio is calculated from the maximum longitudinal attenuation and the minimum crosstalk attenuation of the cable.

Installation Test:

It was supposed, that the transmission performance of data cables would suffer through the mechanical stresses, e.g. pull forces, torsion and bending, during installation. Therefore these stresses were reproducibly modelled in a test. The cable properties before and after the mechanical test have been determined.

Test Procedure:

In this test simultaneously well defined tension, torsion and bending loads are applied to the cable. The procedure is adopted from the European Harmonization Document CENELEC HD 22 S2.10 for flexible cables.

During the test the cables are pulled with constant tension through a set of rollers, which is made from three rollers of identical diameter, see Fig.: 1. This test set applies two S-shape bends and two torsions in the cable during the test run. The results show good reproducibility. The pull force applied to the cables was $75 \text{ N/mm}^2 - 80 \text{ N/mm}^2$. The diameter of the rollers was 60 mm.

The performance was measured on cable samples 100 m in length before and after mechanical loading in the frequency range from 1 MHz to 100 MHz with the following resolution:

- characteristic impedance	500 kHz
- longitudinal attenuation	125 kHz
- crosstalk attenuation	125 kHz
- attenuation unbalance	50 kHz
(only up to 4 MHz)	

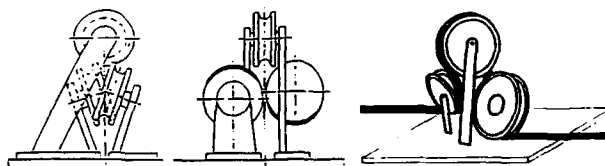


Fig.: 1 Bending equipment for installation test

Test Results:

Characteristic Impedance:

The upper part of Fig.: 2 shows the impedance as function of frequency. The measurements were carried out on cable 2, with twisted pairs and a common shield, before mechanical loading. The characteristic impedance curve approaches asymptotically the infinite cable impedance. The curve of measured values shows clearly some steps and peaks, deviating from theory's smooth curve. These affects are caused by the manufacturing process. The steps and peaks in this curve create on the interface cards of the computers a phase jitter during the signal processing.

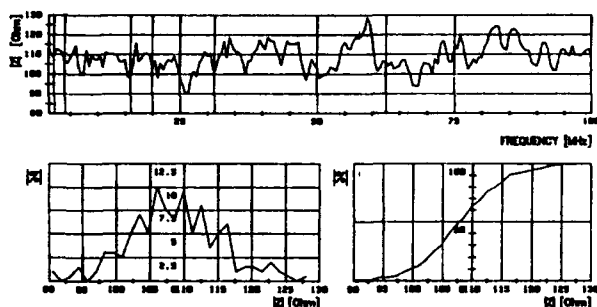


Fig.: 2 Characteristics impedance UTP-S cable before installation test

The following values have been measured at the frequencies specified for level 5 cables.

frequency MHz	impedance (Ohm)
1	114
2	108
4	105
10	107
16	98
20	103
25	99
31.25	102
62.5	106
100	110

All measurements were performed on the same pair of a cable and all impedances measured at these frequencies agree with the requirements of 100 Ohm ± 15 Ohm for level 5 cables, but in Fig.: 2 upper part, are significant discrepancies to be seen, if the whole frequency range is considered. The mean value of the impedance evaluated from the frequency intervals of Fig.: 2 is 107 Ohm - which meets the specification. However, a significant portion of the measurements (15 %) are exceeding the upper tolerated limit of 115 Ohm. Comparing the distribution of the measurements with the normal distribution of random events it can be supposed, that non-random processes (as e.g. periodic events) are responsible for these effects.

Jitter free operation is supported best by a normal distribution with small standard deviation. That means, to specify maximum and minimum values for the impedance at fixed frequencies is not sufficient to provide error free data transmissions in networks cascading several computers in the network, there should also a requirement for the standard deviation, to be sure, that all values are within the limits.

Fig.: 3 shows the cable impedance for cable 3, a cable with individually shielded pairs and an additional common shield over all pairs. The curve over the whole frequency range shows less severe peaks and steps, also the Gauss distribution is smaller than for the cables with unshielded pairs. All values are within the limits.

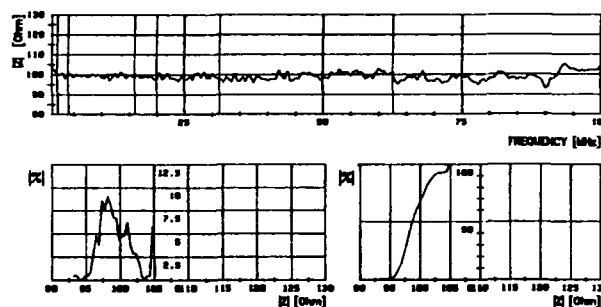


Fig.: 3 Characteristic impedance STP-S cable before installation test

As to be seen in Fig.: 4 the tests indicate, that mechanical loading, simulating the installation, changes the cable impedance to higher and lower values, giving a broadening of the distribution. In this respect are unshielded pairs more sensitive than shielded pairs.

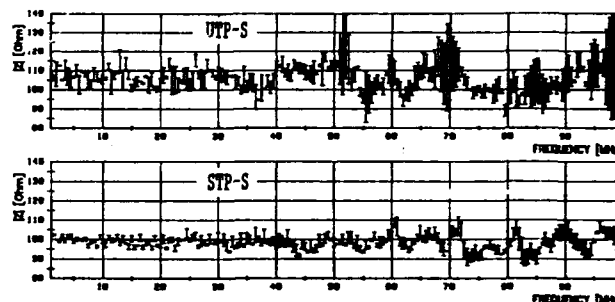


Fig.: 4 Characteristic impedance UTP-S and STP-S before and after installation test.

Longitudinal attenuation

The longitudinal attenuation is much less sensitive to mechanical loading than the impedance. All measured test-points fall within acceptable limits before and after applying the forces. All cables show a steady attenuation against frequency. It can therefore be expected, that non-linear distortions will not be significant. In some cases mechanical loading even improved the cable attenuation performance. Apparently the cable core became more relaxed and more homogeneous due to the test procedure.

In Fig.: 5 the changes implied by the mechanical test on cable attenuation are shown for the cables 1 and 3.

Crosstalk:

It is surprising, that the crosstalk performance of all cables after mechanical loading was unchanged or even improved. For the cable performance evaluation only the smallest values of all possible combinations have been selected because only these conditions determine the cable performance in operation.

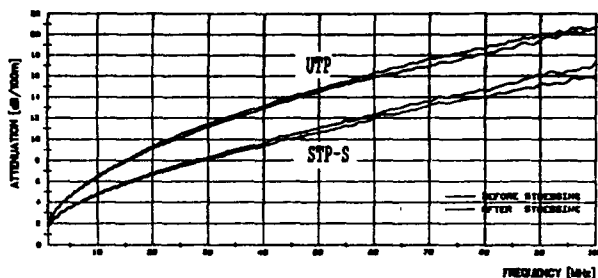


Fig.: 5 Maximum attenuation of any sides UTP and STP-S cables before and after installation test

Fig.: 6 shows the changes of crosstalk performance due to the simulated installation loads for the cables 1 and 3.

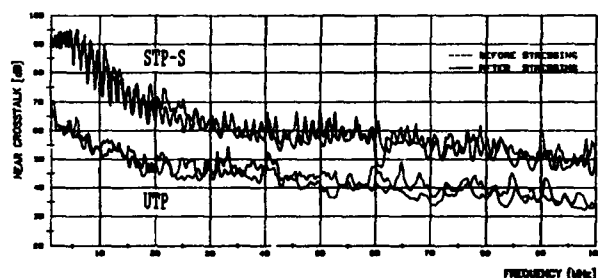


Fig.: 6 Minimum near end crosstalk of any pair UTP and STP-S cables before and after installation test

Attenuation Unbalance

The test methods used today permit cable performance evaluation for the attenuation unbalance only for frequencies up to 4 MHz. The level of asymmetry remained unchanged for the frequency range under investigation for all cables before and after loading.

Fig.: 7 shows the changes in the attenuation unbalance cable performance due to the simulated installation loads for the cables 2 and 3. Because there is no shield, for cable 1 no stable measurement was possible.

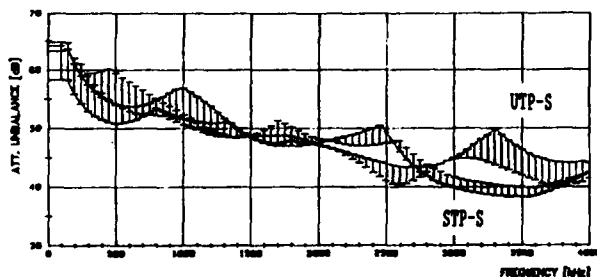


Fig.: 7 Minimum attenuation unbalance of any side UTP-S and STP-S cables before and after installation test.

Attenuation Crosstalk Ratio (ACR)

Longitudinal attenuation and crosstalk attenuation are only slightly affected by the mechanical loading at the installation simulation. Therefore it is no surprise to see only slight changes in the ACR performance of the cables before and after loading.

Fig.: 8 shows therefore no changes of the ACR performance of the cable 1 and 3.

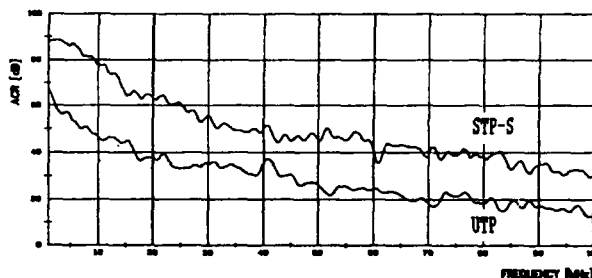


Fig.: 8 Smooth calculated maximum attenuation crosstalk (ACR) UTP and STP-S cables before and after installation test.

Evaluation of the results from simulated installation test:

The test results from the installation simulation show significant differences for the cable performance of the three investigated cable constructions. Most sensitive to this test are unshielded twisted pair cables followed by twisted pair cables with a common shield. The best results are achieved with individually shielded twisted pairs with an additional common shield.

The impedance is more sensitive than all other performance parameters investigated.

The influence of simulated load during installation on longitudinal attenuation, crosstalk and attenuation unbalance is only slight.

Further tests with cables of different constructions have been carried out, which are not reported here. These tests suggest, that cables with a loose cable core construction show higher sensitivity to mechanical loading than those with a tight core. This behavior is in line with the observed higher sensitivities of many cables assembled from unshielded twisted pairs without or with a common shield if compared to cables with individually shielded pairs. The tight winding on individually shielded pairs with metallized plastic foils provides more mechanical stability to the individually shielded pairs and resists any attempt to shift the positions of adjacent pairs relative to each other. This latter effect is responsible for the mechanically induced changes observed in impedance, crosstalk and attenuation unbalance.

EMC – Performance of Data Cables

Introduction

The requirements for the transmission technology are already largely fixed in international standards. The EMC performance of the systems, however, is not sufficiently considered. Looking at international standards you find only EN 55022, class B and IEC 801, parts 3 and 4, for interference voltages. In addition there are some national Standards on EMC, but there are no specific requirements for the influence on data cables operating in LAN-systems.

To evaluate EMC performance of a LAN-system a small cable installation operating with

10 MBit/s Ethernet
100 MBit/s CDDI System

have been tested. Currently there is no consent which 100 MBit/s systems have to be used for standardized tests. The same is valid also for the frequency spectrum of the individual LAN-systems. At present the CDDI-system with a main frequency of 62,5 MHz recommended in the Green book presents the most stringent requirements for cabling systems. Therefore it has been evaluated for these tests. Other bit sequences may have an other spectral distribution, however, the main frequency components are stable and changes in the bit sequences will not lead to a significant changes of the emitted level.

Special focus was put on reliable system performance. The large dimension of the test object "cable", and the desire to discriminate between EM interference originating from environment, the terminal equipment and the cables operating conditions requires all tests to be performed in a completely shielded absorbing hall.

Since international standards are based on lobe lengths of 90 m, for this investigations also cables 90 m in length have been used. The cables are of the same types as used in the installation test.

Test procedure

EM Performance According to EN 55022

In these tests all other passive components are intentionally excluded from the evaluation and placed outside the absorbing test hall.

The cable was connected with DSUB 9 - pin connectors directly to the concentrator next to the absorbing hall, so that only the emissions from the cable have been measured. Fig.: 9 shows the principle of the measurement.

From both cable ends LAN-systems were operated simultaneously and the emitted power was picked up by antennas.

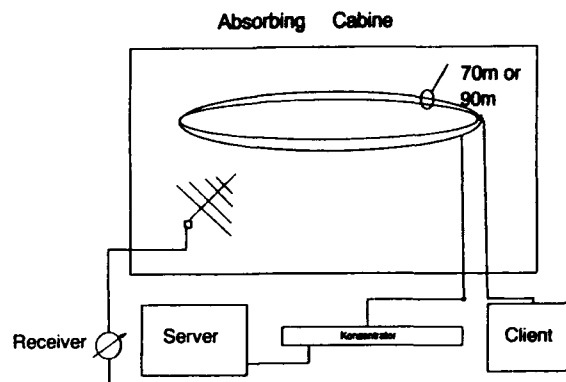


Fig.: 9 EM-performance according to EN 55022
Principle of test

Susceptibility to Interference (IEC 801-3)

For industrial applications IEC 801-3 is relevant. The test evaluate the impact of EM interference from external sources on the cable performance and maximum transmission rate of the system. In the frequency range from 100 kHz to 500 MHz an electrical field strength of 10 V/m is specified, which has been applied to the cable by an antenna. The LAN-system operates simultaneously. Fig.: 10 shows the principle of the test.

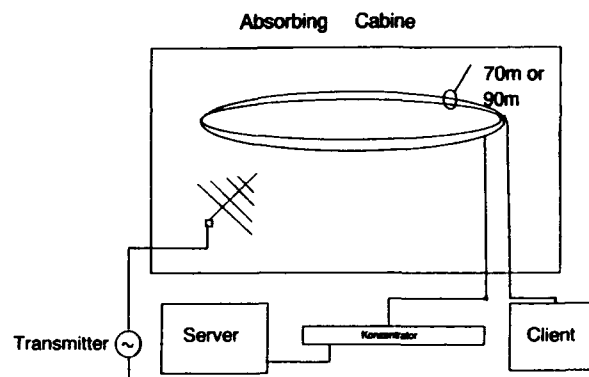


Fig.: 10 Susceptibility to interference
according to IEC 801.
Principle of test

Susceptibility to Interference (IEC 801-4)

In a LAN-system the signal is cascading from one station to the next. Therefore this electronic system is very sensitive to continuous or sudden or periodic disturbances. The test according to IEC 801-4 shows the limits of the max. load for each cable type operating in a LAN-system.

For the test a defined burst was directed to the investigated cable. There are 4 classes between level 500 V and level 2000 V and an extra class "X" for higher voltages, if required. The burst was coupled into the cable by means of a tube electrode covering the cable.

At the balun the asymmetric residual voltage was measured. This test gives quantitative information through recordings of the time resolved signals, which have been measured asymmetrically at the balun against the grounded conductors. This signal gives information on the attenuation of the burst induced signal by the cable symmetry and the transfer impedance. The Figs.: 11 and 12 show the principle of the test method.

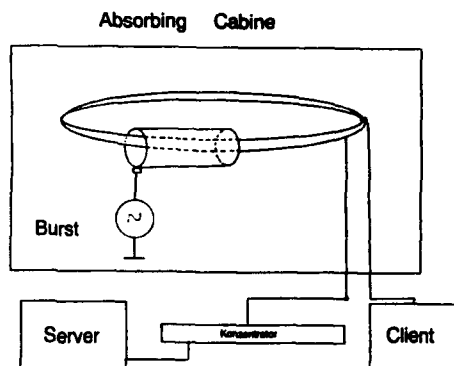


Fig.: 11 Susceptibility to interference according to IEC 801-4
Principle of test

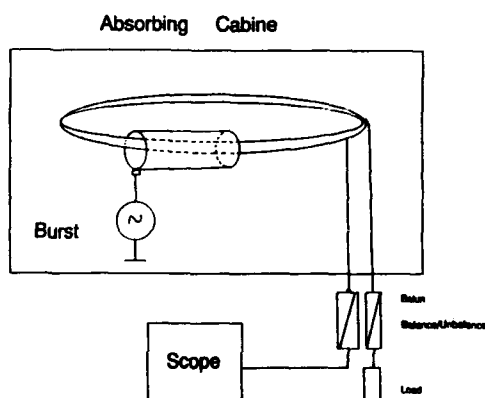


Fig.: 12 Measurement of residual voltage caused by burst
Principle of test

Evaluation of the results from the EMC-tests

Each cable type have been evaluated on its own (residual voltage) and operating under the above described LAN-systems (bit errors).

Results from UTP cables

Performance with 10 MBit/s – Ethernet

In Fig.: 13 is to be seen, that there are disturbances exceeding the limits given in EN 55022 class B. It can not be proofed whether these disturbances are caused by the cable itself or by the connected LAN-system, because UTP cables propagate all signals without discrimination of its origin, viz. signals from

data coding, transmission or interference signals from external noise sources. Therefore it is not possible to discriminate the sources of the disturbances, due to the fact that there is no shield.

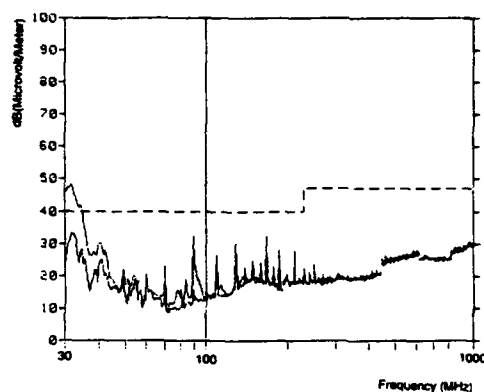


Fig.: 13 EM-performance according to EN 55022 UTP cable in 10 Mbit/s system

Performance with 100 MBit/s – CDDI

It was surprising that it was not possible to log the cable, having the standardized length of 90 m, in the systems. This became possible only when the cable was cut down to a length of 70 m. This can not be explained by the mismatch of the 100 Ohm cable impedance and the 150 Ohm impedance of the systems input. Probably the reason was that the resulting signal to the noise level was insufficient for the data transmission.

The level of the emitted signals are higher than the permitted values according to EN 55022, see Fig.: 14.

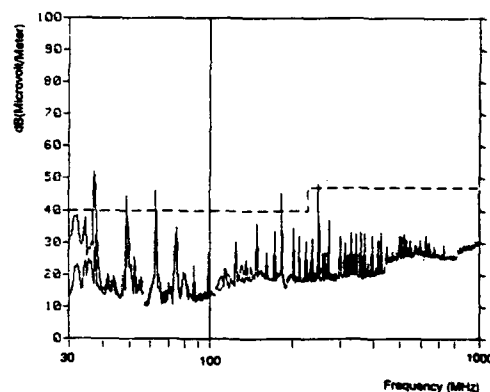


Fig.: 14 EM-performance according to EN 55022 UTP-cable in 100 Mbit/s system

Asymmetrical cables can attenuate interfering fields only through their own symmetry properties. Therefore it was no surprise, that under the Benchmark test the effective data transmission rate of the system dropped down to 55 % of the original rate.

For burst interference the IEC recommended level 3 (1 kV burst) was considered as the minimum level to be passed. The test showed however, that even the much weaker conditions of level 2 (500 V burst) are sufficient to disrupt the system and disengaged the server. The inherent problems of UTP cables becomes obvious here, demonstrating, that only the symmetry of twisted pairs is not sufficient to provide any protection from interference under these conditions

The Figs.: 15 shows the effect of the burst on a UTP cable, which is not suitable when used under influence of EM. It do not pass the requirements of IEC 801-3 and -4.

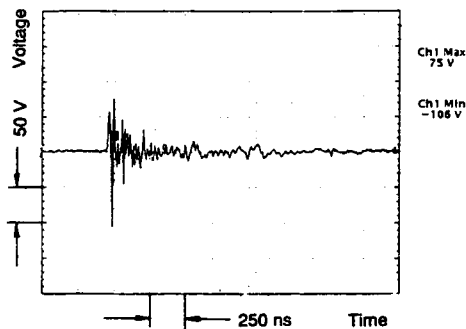


Fig.: 15 EM-performance burst impulse UTP cable in 100 Mbit/s system

Results from UTP-S cables

Performance with 10 MBit/s - Ethernet

The performance of this cable demonstrates, that the introduction of a common shield in the UTP construction stabilizes the operation conditions. Now the discrimination between radiated and emitted signals is possible. A good connection to the ground at the bushings into the absorbing hall eliminate the disturbing high frequency signals from the environment.

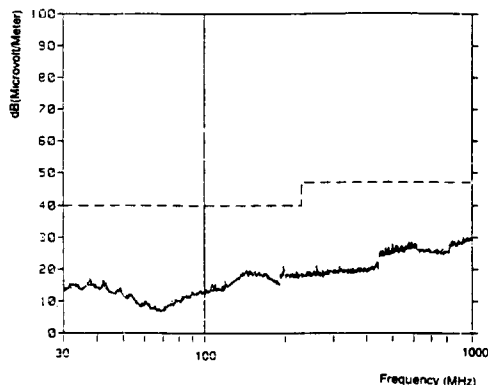


Fig.: 16 EM-performance according to EN 55022 UTP-S cable in 10 Mbit/s system

At the tests with the 10 MBit/s LAN-system all measured values have been within the limits. No peaks caused by radiation were observed, see Fig.: 16. The cable is suitable for use under the EM influences described in IEC 801-3 and -4.

Performance with 100 Mbit/s - CDDI

Also for this cable the length had to be reduced from 90 m to 70 m before the CDDI system accepted the client on the network. So the question raised again : what is the reason for these problems of cables 1 and 2 when used up to the reference length of 90 m ? Both cables meet the limits of the crosstalk attenuation, specified for level 5 cables.

The measurements for the emitted radiation, see Fig.: 17, show a clear peak at 62,5 MHz, which remains however well below the limits, therefore this cable meets the requirements of EN 55022.

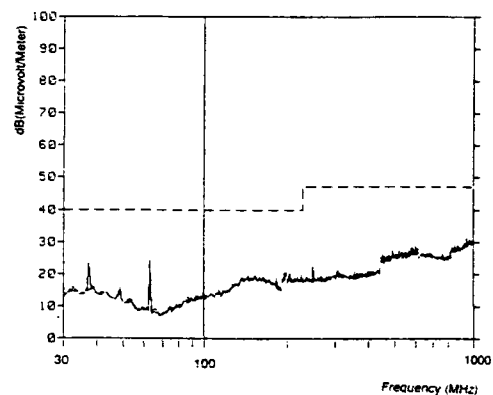


Fig.: 17 EM performance according to EN 55022 UTP-S cable in 100 Mbit/s system

Also the Benchmark test have been carried out. No performance reduction was observed. It can be assumed that the bit error rate will not be effected.

Furthermore the 100 Mbit/s system was tested under the exposure to burst interference fields. Even the burst level of 4 kV (level X according IEC 801-4) did not cut the system out of service and the effective transmission rate was only reduced by 5 %. These results demonstrate clearly the function and efficiency of a common shield in data cables.

In order to receive more detailed informations of the effects of interfering burst load on the cable performance the resolved response signal was measured again as described above. The signals for this cable are some decades smaller than for the unshielded UTP cable, see Fig.: 18.

Results from STP-S cables

Performance with 10 MBit/s - Ethernet

This cable is designed with individually shielded pairs and an additional common shield, which will reduce

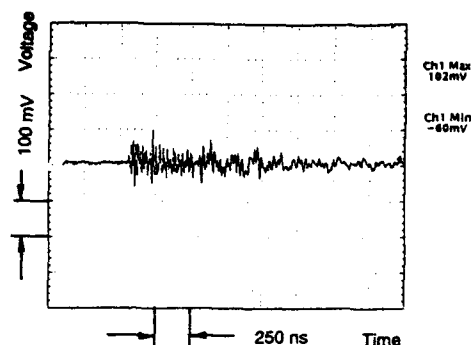


Fig.: 18 EM performance burst impulse
UTP-S cable in 100 Mbit/s system

the effects of radiated interference on the signal transmission path. Simultaneously transmission performance will be generally enhanced. All test in the 10 Mbit/s system indicated no peaks and the radiation performance meets fully class B of EN 55022. This cable is suitable to use under EM-influences.

Performance with 100 Mbit/s - CDDI

Evaluating the level of radiated interference the observation shows no significant peak and all measured values are far below the limit specified in EN 55022. The connected operating network system did not have further impact on the emitted interference of the complete system. The test result is shown in the Fig.: 19.

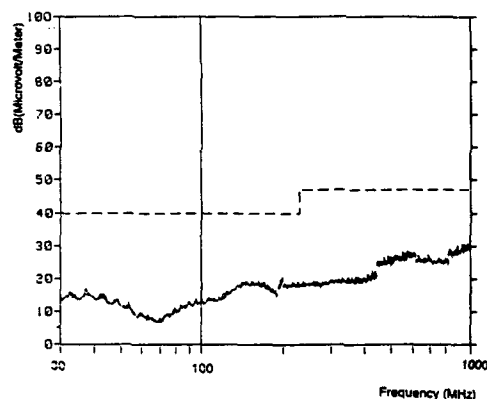


Fig.: 19 EM performance according to EN 55022
STP-S cable in 100 Mbit/s system

Also for this cable the Benchmark test was applied. No drop out was observed for this STP-S cable and the transmission rate was not reduced at all.

During the burst test at level X (4 kV) when the system was in operation no disturbance was indicated and the data transmission rate was still more than 95 % of the undisturbed rate.

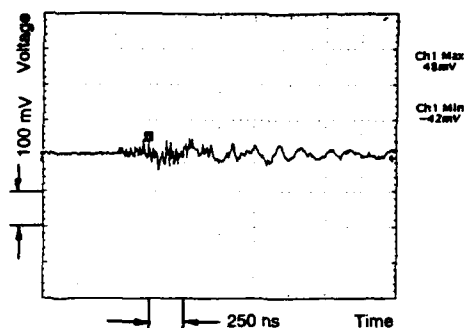


Fig.: 20 EM performance burst impulse
STP-S cable in 100 Mbit/s system

The time resolved cable response signal was recorded (Fig.: 20). The observed values being the smallest of the three cables under test. The maximum amplitude of these signals is reduced by a factor exceeding 1000, when compared with the unshielded UTP cable.

In this way the double screen demonstrates its superior EM performance. These effects will be even more important for the systems with 300 Mbit/s and 600 Mbit/s which are already under discussion.

Conclusion

The use of data cables in high performance LAN-systems is far ahead of the development of suitable standardized test methods. The technology innovation in LAN transmission has progressed rapidly over the last few years without simultaneously developing the relevant cable technology.

It is the intention of this paper to evaluate the influence of the cable installation to the performance of the data cables and to present some facts for the discussion on the EM performance of today's backbone cables in LAN-networks.

The investigations reported in this paper show clearly that the operation in networks with lower bit rate transmission, e.g. 10 Mbit/s differs significantly from the operation of LAN-systems with higher bit rates such as 100 Mbit/s. The observation, that the cables without individually shielded pairs, could not be logged in at the specified standard length of 90 m is an important fact which needs to be noticed.

Table 1 demonstrates clearly the advantages of screened data cables, in particular the superior advantages of individual screened cables.

The requested values for the impedance and the ACR may be met by the cable for selected frequencies, but it seems that this is not sufficient for trouble free operation. The requirements had to be more stringent. International consents for standardization should be reached as soon as possible.

Test methods for transmission characteristics have to be re-evaluated for the higher frequency ranges which are now requested. Also the development of standard test methods for EM susceptibility requires immediate attention. Action is required to define this in standards. Furthermore the development of a suitable test methods for the attenuation unbalance requires more activity. In this area progress has been made by the developments of suitable baluns.

Experiences from operating networks show that the physical layer of the network is the origin of most of the troubles. Here high performance components should be selected. The improved ACR-values provided by individually shielded pairs, more than 10 dB compared with UTP cables, and the substantially reduced susceptibility to interferences is a fringe benefit, in particular with view to future advanced LAN-systems with bit rates above 100 Mbit/s.

Application	UTP	UTP-S	STP-S
10 MBit/s			
VDE 0878, Conducted Emission	not passed*	passed	passed
EN 55022, Class B	not passed*	passed	passed
IEC 801-4, 4 kV Burst, unbalance voltage	Uss = 181 V	Uss = 162 mV	Uss = 90 mV
100 MBit/s			
VDE 0878, Conducted Emission	not passed	passed	passed
EN 55022, Class B	not passed	passed	passed
IEC 801-3, E = 10 V/m	0,45 * Umax	passed	passed
IEC 801-4, 1kV Burst	not passed	passed	passed
IEC 801-4, 4kV Burst, Level X	not passed	0,95 * Umax	> 0,95 Umax

Umax = maximal reading velocity from client to server

* system or cabling

Table 1: Properties of high performance data cables

Acknowledgment

The authors wished to thank the DASA (Deutsche Aerospace AG) which gave us the possibility to use the absorbing hall in their Hamburg plant for our measurements of the EM influence on data cables and company Schneider & Koch & Co in supporting the 100 Mbit/s measurements.



Siegfried Richter was born in 1929.

He studied Electrical Engineering and received an engineering degree in 1952. Until 1958, he developed power cables in the East German cable industry. In 1958, he joined Hackethal Draht- und Kabelwerke in Hannover which is now a part of

Kabelmetal-Electro. There he worked in cable design and production planning for power and telecommunication cables. In 1985, he moved to the Nürnberg plant of Kabelmetal electro where he is responsible for the development of special cables.

Richter is involved in national and international standardization for power and data-cables. He is a delegate for numerous committees of VDE, CENELEC and IEC.



Klaus Lehan was born in 1963.

Klaus Lehan (30) is an engineer in the Development Department for Telecommunication Cables. He finished his studies at the Fachhochschule Düsseldorf in 1987 as Dipl.-Ing. In 1988 he joined KABEL RHEYDT. Since this time he is engaged in the development of symmetrical cables and special measurement techniques.

Lehan is German delegate in the European CENELEC standard committee for data and control cables.

AUTOMATED TRANSMISSION LINE CHARACTERIZATION OF BALANCED PAIR CABLES

Trent M. Hayes
Comm/Scope, Inc.
Claremont, NC 28610

ABSTRACT

Today, with the increasing popularity of unshielded twisted pair (UTP) cabling as a transmission medium for local area networks, these UTP cables are tasked with ever higher transmission frequencies and more stringent specifications. As a result, both manufacturers and end users are demanding individual reel and statistically representative electrical performance certification reports. This paper reviews the following design considerations for the development of automated testing equipment: relay matrix configuration for 25 pair testing, return loss and insertion loss repeatability, bandwidth, and isolation. A model for implementation of an automated test apparatus including hardware, software, and fixtures will be developed. In addition, measurement error correction through calibration coefficients and measurement throughput will be addressed.

INTRODUCTION

Local Area Networks are employing higher and higher frequencies and using UTP as the transmission medium of choice. Because of the non-uniform nature of twisted pairs, each cable should be characterized to insure its adequacy to support these requirements. However, manual testing of each cable is prohibitively expensive. To increase throughput and lower testing costs, an automated testing apparatus with an appropriate sampling plan would be an invaluable tool to

both the manufacturer and the end user.

THEORY

The TEM wave solution of Maxwell's equations for a two-wire transmission line is well known and leads to transmission line equations of electric and magnetic fields. From these equations, an equivalent circuit model for a differential length two conductor transmission line can be developed.¹ It follows that a balanced pair transmission line can be described in terms of 2-port network theory. Any set of 2-port parameters are equally valid, however, S parameters are especially well suited because successive measurements with input and output ports open and short circuited are not necessary. Illustrated in figure 1, a_i and b_i are variables of normalized complex (magnitude and phase) voltage waves incident and reflected from the input and output ports of a 2-port network.²



Figure 1: Two - Port Network

The following table represents the input/output relationships of a 2-port network using the S parameter set.

$a_1 = v_{i1}/\sqrt{Z_0} \Rightarrow$ normalized voltage wave incident on port 1

$a_2 = v_{i2}/\sqrt{Z_0} \Rightarrow$ normalized voltage wave incident on port 2

$b_1 = v_{r1}/\sqrt{Z_0} \Rightarrow$ normalized voltage wave reflected or emanating from port 1

$b_2 = v_{r2}/\sqrt{Z_0} \Rightarrow$ normalized voltage wave reflected or emanating from port 2

$$b_1 = S_{11}a_1 + S_{12}a_2$$

$$b_2 = S_{21}a_1 + S_{22}a_2$$

$$S_{11} = b_1/a_1 |_{a_2=0} \quad \text{Note: } m \text{ } \text{hed load on port } 2 \text{ } a_2 = 0$$

$$S_{22} = b_2/a_2 |_{a_1=0}$$

$$S_{21} = b_2/a_1 |_{a_2=0} \Rightarrow \text{forward transmission gain}$$

$$S_{12} = b_1/a_2 |_{a_1=0} \Rightarrow \text{reverse transmission gain}$$

Table 1: S Parameter Relationships

As seen from the above relationships, only a matched load is necessary on port 2 to measure the input complex reflection coefficient and the complex transmission forward gain. This fact will be exploited later with the development of a relay matrix model. Typically, the UTP transmission line parameters of interest for measurement and performance certification include: input impedance, return loss, attenuation, and near end cross-talk. The following formulas relating transmission line parameters to S parameters will be useful in determining measurement configurations.

$$S_{11} = \Gamma = \text{complex reflection coefficient} \\ = \rho \angle \sigma = v_r/v_i$$

$$\text{return loss} = 20 \log_{10}(\rho)$$

$$\text{SWR} = (1+\rho)/(1-\rho)$$

$$\text{normalized input impedance } Z_n = (1+\Gamma)/(1-\Gamma)$$

$$\text{attenuation \& cross-talk} \Rightarrow 20 \log_{10}(S_{21})$$

Input impedance, return loss, reflection coefficient, and SWR are all mathematically related to the measured 2 port parameter S_{11} . Similarly, attenuation and near end cross-talk are related to S_{21} .

APPLICATION

The task ahead is to automate the testing of multipair balanced pair category 5 cables. Network analysis is a common solution to the problem of characterizing the behavior of a linear network. In addition, an S-Parameter test set, coupled with a network analyzer, measures the S-parameters of the 2-port device under test. Network Analyzers and S Parameters commonly available have 50Ω or 75Ω coax test ports. In order to measure a cable in balanced mode, it is necessary to use a balun (balanced to unbalanced transformer) to provide a balanced signal from the test equipment. In addition to providing a balanced signal, the balun matches the cables impedance to the analyzer. Also, a switch matrix and cable interface ports will be necessary to individually connect the multiple pairs of the cable to the measurement equipment. In order for these components to have a negligible effect on the measurement, a budget for return loss, insertion loss, bandwidth, and isolation for the sum of these components will be developed in a later section. As a top down approach to designing a testing system, it is first necessary to understand the various measurements and their configurations. The illustrations below indicate the test configurations necessary to perform the four transmission measurements. Notice that resistive terminations are required on the far end of the pair(s) under test for reflection and

cross-talk measurements and on both ends of the pairs not being tested.³ This practice minimizes the effects of a finite length line

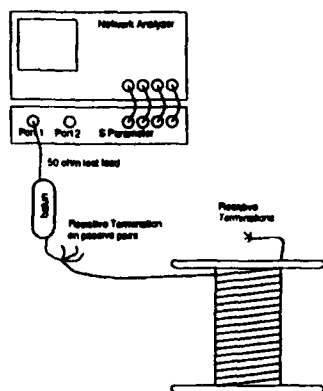


Figure 2: Return Loss and Input Impedance Measurement Configuration

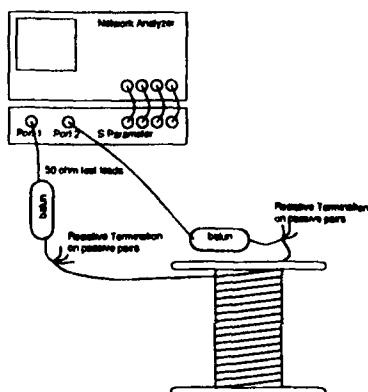


Figure 3: Attenuation Measurement Configuration

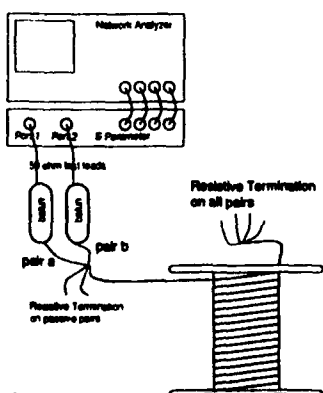


Figure 4: Near End Cross-Talk Measurement Configuration

Consider the n pair case:

Input impedance and return loss require the near end of the pair under test be terminated to port 1 of the test equipment while the far end be terminated in its characteristic

impedance. Additionally, the remaining passive pairs need be terminated on both ends.

Attenuation requires both ends be connected to the analyzer, as defined by the measurement of S_{21} .

Near end cross-talk specifies that two pairs (from the near end) be connected to the test equipment, their far ends and both ends of the remaining pairs be terminated.

From this set of measurement guidelines, it is desired to design an relay matrix such that all possible measurement configuration are satisfied and that it has negligible effects on the measurement itself. Figure 5 represents one possible relay configuration, other potential configurations exists and may be better suited for a given realization.

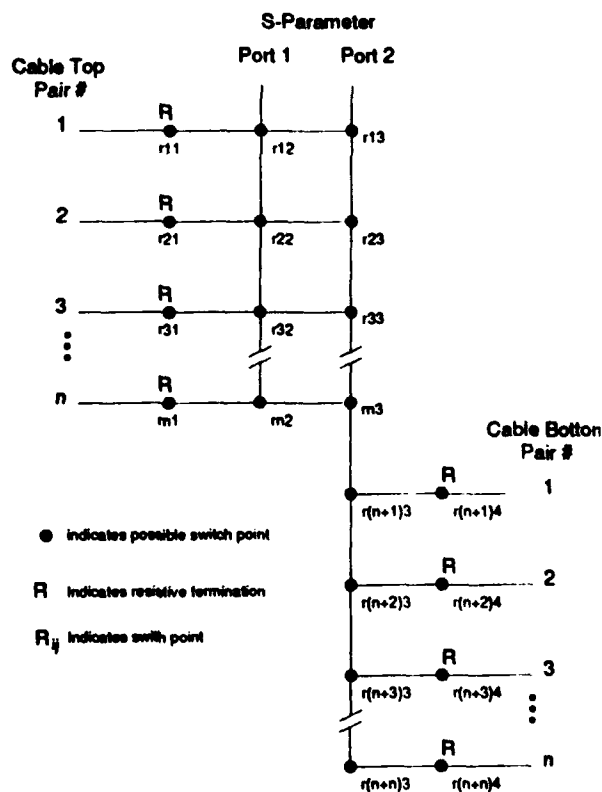


Figure 5: Possible RF Matrix for n Pair Cable Testing

Example:

Consider the following scenarios:

1) measure S_{11} on pair 2

r_{22} connects top of pair 2 to port 1 of analyzer

$r_{(n+2)4}$ terminates far end of pair 2

$r_{11}, r_{31}, \dots, r_{n1}$ terminate top of pairs 1, 3, ..., 4

$r_{(n+1)4}, r_{(n+3)4}, \dots, r_{(n+n)4}$ terminate bottom of pairs 1, 3, ..., n

2) measure S_{21} of pair 3

r_{32} connects top of pair 3 to port 1 of analyzer

$r_{(n+3)3}$ connects bottom of pair 3 to port 2 of analyzer

$r_{11}, r_{21}, r_{41}, \dots, r_{n1}$ terminate top of pairs 1, 2, 4, ..., n

$r_{(n+1)4}, r_{(n+2)4}, r_{(n+4)4}, \dots, r_{(n+n)4}$ terminate bottom of pairs 1, 2, 4, ..., n

3) measure S_{21} between pairs 1 and 3

r_{12} connects top of pair 1 to port 1 of analyzer

r_{32} connects top of pair 3 to port 2 of analyzer

$r_{(n+1)4}, r_{(n+3)4}$ terminates bottom of pairs 1 and 3

$r_{21}, r_{41}, \dots, r_{n1}$ terminates top of pairs 2, 4, ..., n

$r_{(n+2)4}, r_{(n+4)4}, \dots, r_{(n+n)4}$ terminates bottom of pairs 2, 4, ..., n

Notice that any matrix that satisfies all the possible measurement configurations is equally valid, but discretion should be used as to the realization of the switch matrix due to dimensional, isolation, and bandwidth limitations.

Additionally, a connection interface must be devised that allows all pairs from both ends of the cable to be connected to the relay matrix. This interface must adhere to the same guidelines of negligible contribution to the measurement. In order to develop design specifications for the entire system, electrical performance expectation must be clearly defined. In this case, Category 5 UTP performance establishes these boundaries.

PERFORMANCE REQUIREMENTS

Cable Specifications:

The specification for 100 Ω , 24AWG, extended frequency Category 5 cable

measurement	freq (MHz)	Spec
Impedance (Ω)	.772	102 \pm 15%
	1.0 - 100.0	100 \pm 15%
Return Loss (dB)	1.0 - 20.0	-23
	20.0 - 100.0	-23+10log(f/20)

where f = frequency in MHz

Attenuation (dB/1000 ft.)	.772	5.5
	1.0	6.3
	4.0	13
	10.0	20
	16.0	25
	20.0	28
	31.25	36
	62.5	52
	100.0	67

Cross-talk (dB)

$$.772-100.0 \quad -64 + 15\log(f/0.772)$$

where f is frequency in MHz

Table 2: Category 5 Cable Specifications^{4,5}

These specs will serve as a guideline for the performance requirements of the sum of the components. These components shall include network analyzer, S parameter, relay matrix, baluns, cable interface, cabling and connectors. While an upper cutoff of 100 MHz is considered in this case, the same design concerns apply to higher frequency systems.

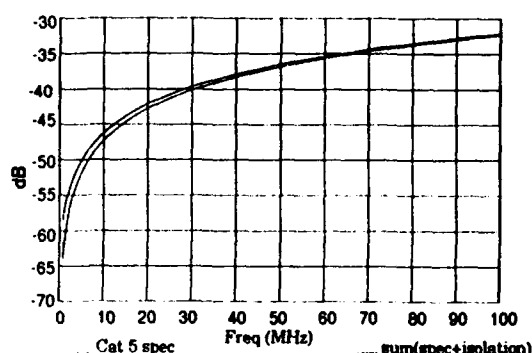
Isolation

Isolation is a measure of electrical separation. Within the cable, the most stringent cross-talk is 64dB @ 0.772 MHz. This value dictates that the isolation of the test equipment should be sufficiently superior as not to contribute to the

measurement. The following three graphs illustrate the effects of finite isolation on the cross-talk measurement.

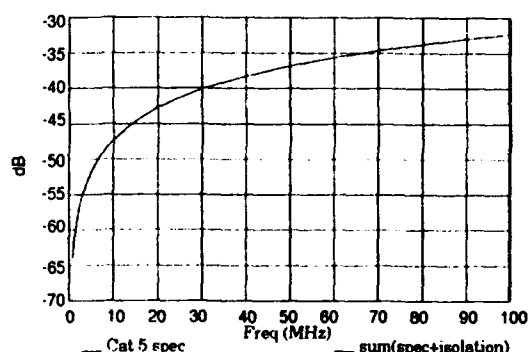
EFFECT OF ISOLATION ON XTALK

Isolation = 65dB



EFFECT OF ISOLATION ON XTALK

Isolation = 100dB



The following table reflects the worst case cross-talk measurement degradation for a given margin of isolation.

isolation (dB)	% effect on xtalk @.772 MHz
-100	0.21
-90	0.66
-80	2.00
-70	5.51
-65	8.65

Table 3: Dependence of Cross-Talk on Isolation

Dynamic Range & Bandwidth

Clearly the bandwidth of all components of the test system must be 0.772 - 100 MHz or greater.

Generally stated, the dynamic range of the analyzer and S parameter minus the loss due to the interconnect equipment must be greater than the attenuation @ 100MHz of the longest cable to be tested.

Standing Wave Ratio

It is not necessary that the SWR of the interconnect equipment have a flat frequency response. The key importance is that the analyzer has a dynamic accuracy sufficient enough to resolve the reflection coefficient through the interconnect equipment.

ERROR CORRECTION

Error correction models have been developed such that systematic errors can be removed from the measurement. All the cable interface hardware should have sufficient repeatability in terms of insertion loss, return loss, and isolation so as not to invalidate the calibration. The calibration will remove the systematic error (within the limits of the error model chosen) introduced by the finite isolation, attenuation, and return loss on the interconnect equipment. Residual errors remain from sources such as imperfect calibration standards and limitations of the analyzer itself. In addition, random sources of error such as noise, connectors, cabling, and switch matrix repeatability introduce measurement uncertainty.

Finally, drift is a source of measurement error caused by temperature swings and equipment instability over time. In order to minimize these errors, a recalibration schedule should be established. This schedule could be developed by a history of measuring a calibration standard and plotting its measured value deviation from actual.

Cable Connection Interface

A cable connection interface should allow all pairs (both ends) of the cable to be connected simultaneously. The main concern is to obtain a high degree of isolation between pairs without sacrificing the cable integrity. As a general rule, the pair twist must not be disturbed more than $\lambda_{\min}/20$ (λ_{\min} = wavelength at 100MHz). Reflection measurements would otherwise be adversely affected as a result.

COMPUTER INTERFACE/CONTROL

In addition to the testing hardware, it is necessary to use a computer/controller to facilitate cable testing. The computer will serve as the information interface for the operator and controller for the analyzer and relay matrix. Also, the computer will collect the data from the associated measurements, perform statistical analysis, and generate reports.

Measurement Throughput

Each measurement configuration has a different set of calibration coefficients. Depending on the error model chosen, each discrete frequency sample may have as many as twelve correction coefficients associated with it. As a result, each measurement requires an appreciable amount of time to perform the correction. Two possible methods for error correction include loading the error correction coefficients to the analyzer for data correction or alternatively, collecting raw data from the analyzer and performing the correction in the main processor. The previous method has the advantage of corrected data displayed on the analyzer for easy visual interpretation however, measurement through-put will be sacrificed due to the bottle neck of the analyzer interface bus and the "real-time" correction. In a multitasking environment, error correction using the latter method can be done simultaneous to other operations so measurement throughput can be maximized.

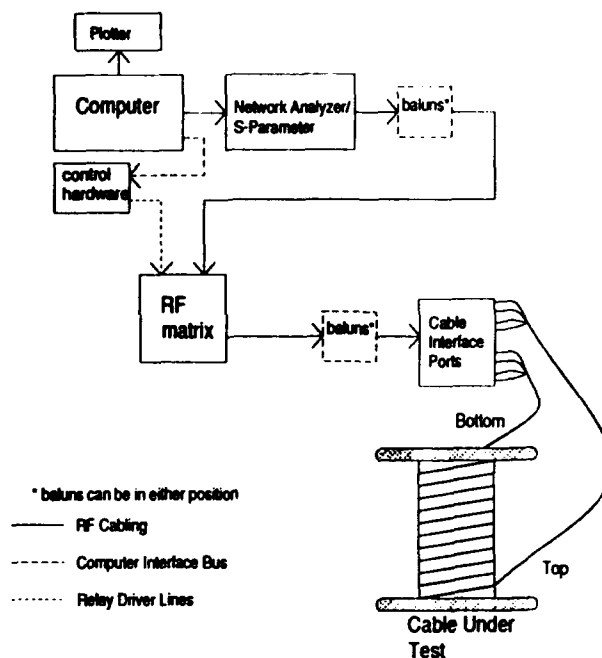


Figure 6: Automated Test Set Diagram

CONCLUSION

Accurate automated transmission and reflection characterization of multipair balanced pair cables can be achieved with an appropriately designed RF matrix, interconnection hardware, and the use of a network analyzer, s-parameter, relays, baluns, computer, computer control/acquisition software, and statistical analysis software. Because the computer handles all the instrumentation configurations for various measurements, the necessary operator expertise is minimized. Errors are subsequently reduced and time efficient testing of multiple pair cables is viable. Large samples of data can be collected from standard production, experimental trials, material lots, etc. and powerful analysis can be computed to determine trends and gain understanding of process variation.

REFERENCES

1. *Field and Wave Electromagnetics*, David K. Cheng, copyright 1989 by Addison-Wesley Publishing Company, Inc.
2. "S-Parameter Techniques for Faster, More Accurate Network Design", Hewlett Packard Application Note 95-1, February 1967.
3. "Standard Test Methods for Electrical Performance Properties of Insulations and Jackets for Telecommunications Wire and Cable", ASTM D 4566-90
4. NEMA Standard for "Performance Standard for Premise Telecommunications Cables", NEMA WC 63-19XX, July 1992
5. EIA/TIA Standard for "Commercial Building Telecommunications Wiring Standard EIA/TIA - 568 TSB 36", EIA/TIA July 1991



Trent. M. Hayes

Comm/Scope, Inc.
Claremont, NC 28610

Trent holds a Bachelor of Electrical Engineering from the Georgia Institute of Technology and a Master of Science in Electrical Engineering from Clemson University. He joined Comm/Scope, Inc. in 1991 and has worked primarily in test set design and product development.

ELECTRONIC DRAWING MANAGEMENT (IMAGING) SYSTEM in a COPPER CABLE MANUFACTURING FACILITY

John E. Maloney* & Homero Vela**

*Butler Service Group, Phoenix, Arizona

**AT&T Network Cable Systems, Phoenix Arizona

ABSTRACT To solve the problems associated with drawings being unavailable to the maintenance personnel on all shifts changes had to be made in our central filing methods. Through computerization of the drawings required by the maintenance organizations we have reduced costs, decreased machinery down time and increased the productivity of manufacturing equipment, maintenance technicians and engineers. Finding the proper solution to our problem required a two year feasibility study and careful evaluation of our requirements for drawing availability.

INTRODUCTION About four years ago a team of maintenance people brought to our attention their need for drawing availability on all shifts. They expressed the concern that our central filing arrangement did not provide drawing copies on the off shifts, which caused unnecessary down time of machinery and losses in manpower. The problem of drawing availability was given to the engineering and design organizations for a solution. Through our study other problems were identified and solutions sought.

IDENTIFYING A BOTTLENECK As indicated in Figure 1, our design organization was using both manual and computerized methods to create and change the drawings required by engineering and maintenance. With about 6,000 drawings per year being worked on, a bottleneck developed in the central files area due to the labor intensive and costly method of filing, reproducing and distributing large numbers of drawing copies. The storage of those copies throughout the plant was also a problem. Drawings were being stored in filing cabinets, machinery cabinets, supervisor's and engineer's desks and in the tool boxes of maintenance personnel. This led to the possibility of old drawing copies not being replaced by updated ones and therefore the possibility of machinery being repaired without the most current information. One drawing that was revision eight was found in a tool box. The original drawing stored in central files is revision 12. This indicated four changes to the machine were made and recorded but some earlier copies were still used to repair the machine. This could have resulted in higher scrap output or costlier repairs and higher down time for the machine.

GATHERING SOLUTIONS Several solutions were considered, such as, putting microfilms of the drawings in key areas of the plant for use by the maintenance people. This idea was rejected because we would have to ensure that the microfilms were filed properly after use, replaced when worn or changes were made to the original also, some prints made from the microfilms are too small to be usable for equipment repairs. Another idea was to convert all of our drawings to our Computer Aided Design and Drafting (CADD) system. A study of this showed that it would take five or more years and cost from 1.5 to over five million dollars to complete using current methods and technology. This method would not answer our needs for distribution since drawings generated by the CADD system are in a proprietary format requiring either expensive computers or software to view them and CADD drawings require large amounts of electronic storage space.

COMPUTERIZATION The studies and investigations on methods of drawing management indicated that computerization of all drawings pertaining to the manufacturing equipment in use was the key to the

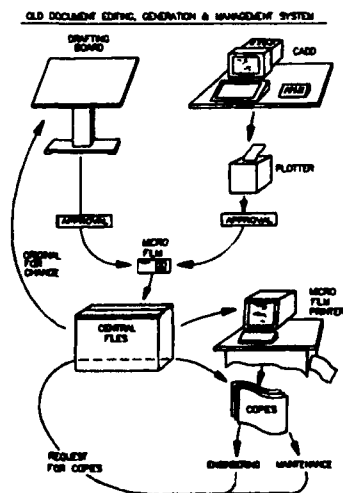


Figure 1

solution of our problems. New technology was available to allow for the conversion of hand drawn drawings into an electronic format. This format is easily compressible therefore not requiring the large electronic storage space as is required by the CADD system. Drawings can be easily transmitted to those requiring them over our current Local Area Network (LAN) to the existing personal computers connected to it. Also it does not require expensive software or hardware to view or modify the drawings. It was determined, the design group, through computerizing all of our drawings could reduce the number of designers and thus fund the project by reducing costs of the design contract. The system proposed and purchased was the result of a two-year feasibility study on drawings, methods of distribution and vendors who offered packaged systems for managing and distributing engineering documents that would be compatible with our computer network. The Electronic Drawing Management (IMAGING) system that was purchased and installed solves the problems and allows the most current machinery drawings to be available at all times as originally requested by the maintenance people.

TIME SAVINGS With all of the design organization trained and working on the CADD system, we realized changes to drawings were quicker and better in quality when done electronically. Although the design organization was reduced in size they continue to service the needs for designs and drawings with no reduction in production or increases in time. Studies have suggested that a 25 to 30 percent reduction in time can be attained for drawing changes when they are completed electronically. By purchasing and installing editing software for the IMAGING system computers used by the designers, this reduction in time for drawing changes is being realized.

AVAILABILITY Under the old system, when a drawing was checked out for manual changes, the original was no longer available to maintenance or engineering for reference if full size copies were required and no method was in place to tell the requester that a drawing was subject to change. The only copy available was from microfilm, which when printed resulted in a copy up to 50% smaller than the original. In some cases these microfilm copies were not usable due to the illegibility of the smaller size. The IMAGING system answers this problem by allowing full size copies of all drawings to be plotted when needed. If a designer is working on a drawing, on the IMAGING system anyone requesting the drawing receives a message indicating the drawing is subject to change and should be used with caution. By electronically transmitting drawings throughout the facility, down time of machinery and losses in manpower are reduced through fewer trips to central files.

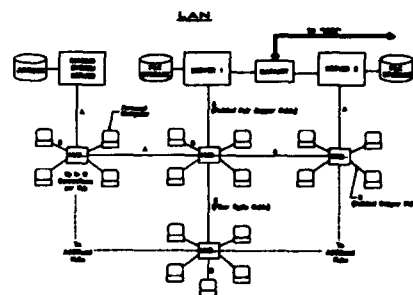


Figure 2

NETWORK The systems that we considered were required to be compatible with the twisted copper pair network that was already in place. This was done to insure that the costs would remain within those we proposed. Figure 2 above shows the configuration of the network as it is installed today. The only addition to the network that was required was the addition of a fiber optic leg that was necessary to overcome the recommended maximum distance between network hubs of 100 meters. The other option available to us was to add hubs every 100 meters. This would have resulted in down time of the network while the cabling was spliced and electricity was provided to power the hubs. Although this method would have made available more hubs through the facility they would not be utilized as their locations were in areas that did not require a computer system. With the addition of this fiber hub we are now able to connect those areas of our facility requiring drawings to our personal computer network and the IMAGING system.

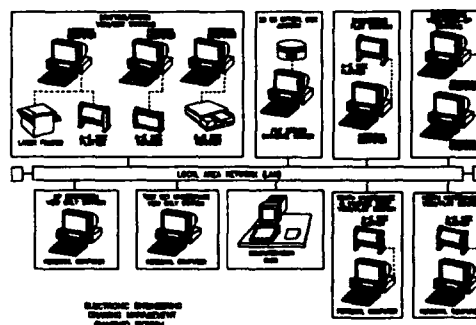


Figure 3

SYSTEM CONFIGURATION Figure 3 shows the configuration of the system as it is used today. There is a computer, used as a file server, and an optical disk jukebox that are located in the computer room. There are

twenty-five personal computers for viewing or marking up drawings and one for plotting in the engineering organization connected to the file server, through the local area network. A personal computer in each of two major maintenance areas of the plant is used for viewing and plotting drawings. Personal computers in the test set maintenance and the machinery parts (M.P.) storeroom area are used for viewing drawings. Test set maintenance and M.P. storeroom can plot drawings to either of the two major maintenance areas when drawing copies are needed. Three computers are connected in the design area for viewing and editing drawings. The design organization has a computer plot station as well as scanners for adding drawings to our drawing system. The CADD system is connected to the network to allow for the semiautomatic electronic transfer of drawings from CADD files to the IMAGING systems files.

FILE STORAGE CADD drawings are in vector format requiring each line, circle, square or any other piece of information on the drawings to be filed together with information defining its length, size, relation to other items, etc. This results in an electronic file that is large and not easily compressible with our present software, requiring large electronic storage space and devices. The IMAGING system uses files in a raster format which consists of a series of dots similar to a photograph in the newspaper. This raster format does not have any intelligent information associated in the files. Raster files are more compressible than CADD vector files therefore requiring less electronic storage space and are decompressed only for viewing and plotting. With the large numbers of drawings in use today this compression allows for the storage to be accomplished in a device no larger than a two drawer filing cabinet. This is compared to the near 500 square foot space required to store all of the original drawings.

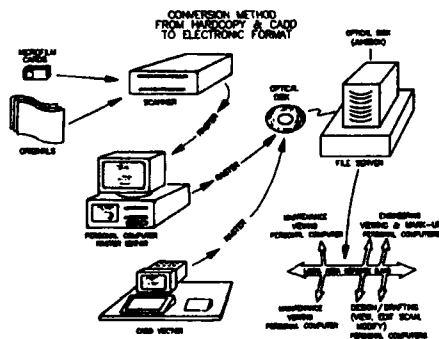


Figure 4

CONVERSION METHOD Figure 4 shows the method used to convert drawings to the electronic format used by the IMAGING system. The initial 40,000 drawings, targeted for placement on the system, were scanned by an outside vendor. Time and money were saved on this project by scanning microfilm aperture cards instead of the original drawings. The cost of scanning full size drawings would have been four times as expensive due to the time and labor involved. The scanned drawings included those that were generated on the CADD system, this was done so we could start the conversion before the IMAGING system was in place and to save the time and manpower that would have been required to separate the CADD drawings from the manual drawings. Once the IMAGING system was in place, the scanned image files were indexed by drawing and sheet number, titles and revisions and then linked to their associated information in a data base on the file server. This association between the data base and the image allow users to search and retrieve drawings in a short time, using "key" words when the drawing and sheet number is not known or when known by using the drawings part numbers. The electronic images, generated through scanning and after indexing, have been stored on thirteen optical disks. All of the optical disks are stored in the jukebox allowing users to view each drawing after the information is found in the data base without the need to manually change disks. An average of 8,000 drawings is stored on each disk in the jukebox that has a total capacity of thirty-two disks and is about the size of a two drawer filing cabinet. The ability to store this amount of information on each disk is due to the format of the images and their ability to be compressed.

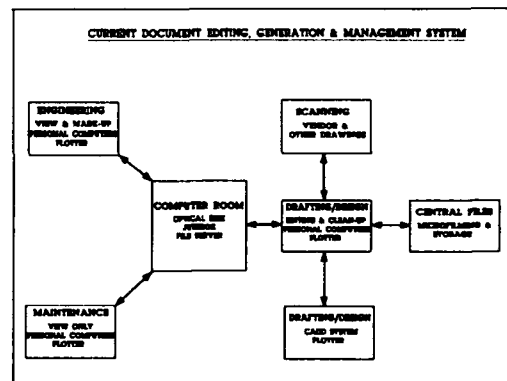


Figure 5

TODAY Figure 5 shows the current method of generating, storing, and distributing drawings. As shown here, central files is no longer a bottleneck but instead is utilized for storage of hand drawn originals and microfilming all drawings ensuring that a backup system

exists if there are problems with the LAN or computer system. Drawings requiring extensive changes are redrawn on the CADD system but the changes to hand generated drawings, when not extensive, are completed on the IMAGING system. All changes to drawings originally created on the CADD system are completed on the CADD system to ensure the intelligence and integrity of the CADD files. Vendor drawings and drawings from other locations are added to our system through scanning of the hard copies. The design organization now uses both the CADD and IMAGING system to complete projects and little or no manual drafting is done today. The IMAGING system was designed to compliment the CADD system not to replace it.

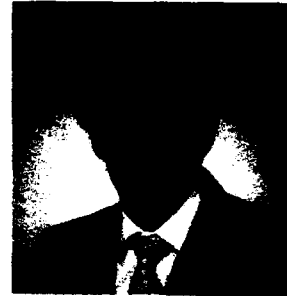
This current method of drawing revision and creation allows almost immediate availability of all drawings after their approval. This is accomplished through a check out/check in procedure on the IMAGING system and through semiautomatic electronic means from the CADD system. Through computerization, our design to maintenance shop time has been reduced, the bottleneck in central files has been eliminated and there is a reduction in down time as a result of quick drawing availability when required.

SAVINGS Although Electronic Drawing Management or IMAGING systems are relatively new, they provide a leading edge technology that offers time and labor savings over manual methods of drawing management and distribution. Some of these savings cannot be readily seen on a daily basis but will be felt when a critical piece of equipment requiring repairs breaks down and central files does not have an attendant on duty. If the machinery can be put back in service faster with the drawings available on the personal computer network, the IMAGING system soon becomes an asset to the maintenance shops and our production schedules.

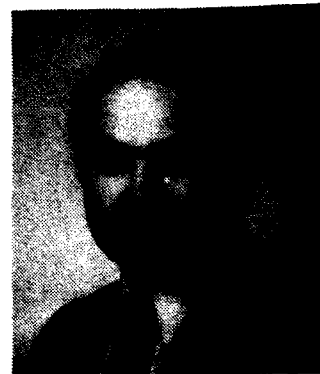
WHAT'S NEW The IMAGING system is on the forefront of technology and because it is relatively new technology all is not perfect with it. While connecting the system to our network, we were required to add a fiber optic extension to overcome the limitation of distance that the twisted copper pair network imposed. The speed of retrieving drawings is relatively slow due to the format of the files. The IMAGING system vendor is updating our software to increase the speed of viewing drawings. A Windows version of the viewing software is being added to the engineering computers to give them the capability of copying parts of drawings and using them in other computer generated documents such as operating and maintenance instructions.

THE FUTURE After a year of operation our IMAGING system is at less than half its designed capacity. As we utilize the power and versatility of the system, we expect to find new uses for our ability to quickly transfer information from one area of the manufacturing facility to

another whenever it is required. Someday, maybe even transferring drawings from one manufacturing facility to another - **ELECTRONICALLY - ACROSS COUNTRY - OR AROUND THE WORLD** - so that we may share our technology with others without using paper.



John Maloney started working at AT&T in 1973 as a contract employee in the engineering design organization. Starting as an engineering draftsman and leading to the position that he holds today as the Supervisor and Representative of the contract design organization. In 1989 he lead a team of Designers and Engineers that proposed and implemented the Electronic Engineering Drawing Management (IMAGING) System that is used today at the AT&T Phoenix Works. Mr. Maloney received his Associates in Arts Degree in Drafting and Design from Glendale Community College in 1978. His office is currently located at AT&T Phoenix Works, 505 N. 51st Avenue, Phoenix, Arizona 85043.



Homero Vela was born in 1951 in Brownsville, Texas. He received a Bachelor of Science Degree in Industrial Engineering at the University of Houston in 1978, and began working for AT&T in that same year. After a series of assignments in Maintenance and Engineering, he became Manager of Engineering in 1989. In this capacity he has been responsible for new product and process developments for the Copper Telephony Business Unit. Mr. Vela received his Master of Technology Degree from Arizona State University in 1992. His office is located at AT&T Phoenix Works, 505 N. 51st Avenue, Phoenix, Arizona 85043.

A DECADE OF EXPERIENCE - REVIEW OF POLYETHYLENE INSULATION PERFORMANCE IN ABOVE GROUND INSTALLATIONS IN AUSTRALIA

Mr. P. Boes and Mr. P. Latoszynski
Telstra Corporation Limited
Melbourne, Australia

ABSTRACT

The Australian telecommunications network, like most networks world-wide, retains a heavy dependence on the existing polyolefin insulated conductor (PIC) cable technology, irrespective of the substantial advances in optical fibre communications. Historically, one disadvantage of these external plant PIC systems has been their susceptibility to thermo-oxidative deterioration. From the time the problem first became evident in the USA in the mid 1960's the phenomenon has been the subject of extensive investigation. Not surprisingly, Australian systems which are exposed to comparable, if not harsher environmental conditions to that found in the USA, have to some extent reflected the US experience. This paper reviews the experiences of a decade of field and laboratory investigation in Australia into the performance of cellular polyethylene insulation in above ground installations. It outlines the various material, environment and design/work practice approaches that can be adopted to enhance the performance of future systems and those under threat in existing above ground installations.

INTRODUCTION

The Australian telecommunications network despite having a sizeable commitment to optical fibre technology does have a significant reliance on the existing polyolefin insulated conductor (PIC) cable network. It is estimated that in excess of 50 million pair kilometres (pkm) of below ground and, to a lesser extent, aerial PIC cable service the telecommunications needs throughout Australia. Its performance is therefore critical to the overall network operation.

Approximately 7.5 million pkm is used in the rural subscriber distribution network which is dependent on a substantial level of above ground cable jointing, in either above ground jointing posts (AGJP's), akin to the US pedestal, or pole mounted untailed terminal boxes (UTB's). The AGJP is used

widely in rural areas whereas the UTB is predominantly designated for urban distribution cable. The performance of the cable insulation systems within these above ground joints is highly dependent on the prevailing thermal climatic conditions which, in Australia, are quite varied, ranging from tropical and arid through to cooler temperate conditions. In the more harsh thermal environments of central and northern Australia, where air temperatures within closures approach 60°C, the oxidative stability of the total polymeric insulation system is of critical importance.

Over many years thermo-oxidative deterioration of insulation in above ground closures has been witnessed and addressed to varying degrees. This was particularly evident with the premature failure of the solid low density polyethylene insulations of the pre-1970's era in Australia and the USA¹⁻⁶. With the knowledge gained from the extensive investigations into oxidative degradation and thermal stability testing, the ensuing development of high density polyethylene solid and cellular insulation systems was expected to reduce the incidence of failure of insulation in above ground situations. This expectation was in part supported by subsequent field investigations⁷. However, recently reported premature insulation deterioration of foam skin 'jelly' filled cable systems in the USA, which occurred within a short period of service exposure⁸, has raised concerns with all current and future installations. The contribution of cable filling compound interactions to the degradative process, although referred to over recent years⁹⁻¹¹, were not envisaged to reduce the life expectancy of PIC cable systems to such a degree.

Although no such related failures have been witnessed in Australia to date, the US experience prompted a more comprehensive evaluation and

review of fully filled cable performance in the Australian environment.

This paper discusses both the results of a recent investigation into in-service filled cable performance in the Australian network, and a decade of field and laboratory investigations into the performance of cellular polyethylene insulation in above ground installations. It highlights the critical relationships between the materials used, the environment, joint closure design and work practices issues, all of which impinge on strategies both for improvement of future systems and the rehabilitation of existing plant.

REVIEW OF FIELD AND LABORATORY INVESTIGATIONS

The focus of the investigations was on the performance of cellular high density polyethylene (HDPE) insulations, of both dry core and filled cable constructions, when subjected to extremes of thermal exposure in controlled field trials and in true field situations. With the expectation that deterioration of filled cable would be more prevalent, emphasis was also placed on laboratory investigations into stabiliser/filling compound interactions and the resultant influence they may have on the overall performance in the field.

Field Exposure Trials

The controlled field trials centred on determination of insulation performance as a function of:

- stabiliser system (Table 1)
- cable filling compound contact
- insulation environment

All systems were exposed to thermal environments representative of the harsher climatic scenarios typical of many parts of Australia. The trial sites were the hot, dry environment of Cloncurry, inland northern Australia (latitude 20 40' South), and the hot, humid environment of Innisfail, coastal north-eastern Australia (latitude 17 31' South). The summer mean maximum temperatures at these sites are 38°C and 30°C respectively. The site at Cloncurry also experiences a greater number of sunshine days than that at Innisfail making it more thermally severe on above ground installations.

Stabiliser Code	Stabiliser System (Trade Names)	Insulation Polymer
A	Hostanox 03/Eastman OABH	Cellular HDPE
B	Permanax WSP/Eastman OABH	Cellular HDPE
C	Irganox 1010/Eastman OABH	Cellular HDPE
D	Cyanox 1790/Eastman OABH	Cellular HDPE
E	Irganox 1035/Irganox MD 1024	Cellular HDPE
F	Permanax WSP	Solid MDPE

Table 1. Insulation Stabiliser Systems Tried.

The stabilised insulation samples in the trials were exposed to the thermal conditions within:

- standard galvanised metal AGJP's
- standard AGJP's with reflective PVC covers
- complete cable sections.

The parameter used to follow the performance or the extent of deterioration of insulation was the well recognised Oxidation Induction Time (OIT) at 200°C, which effectively measures the oxidative stability of the insulation systems.

Experimental Results and Discussion

Stabiliser Variation

Figure 1 indicates the dependence of insulation stability on the stabiliser system used with dry core cable insulation. The decrease in this cellular insulation stability in the above ground posts can differ markedly, as observed with the stabiliser systems A and D, where the retention of stabiliser effectiveness was 50% and 29% respectively after 8 years exposure. With identical stabiliser levels present it is evident that the selection of the appropriate hindered phenolic antioxidant is critical for improved insulation life expectancy.

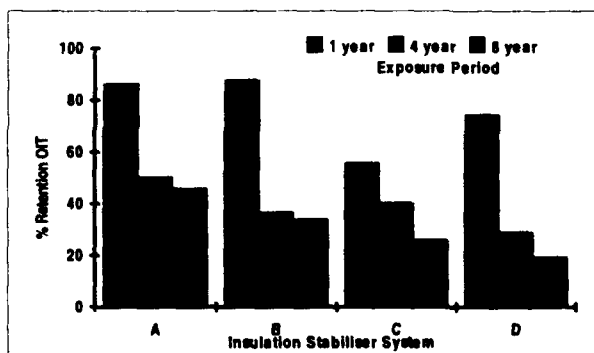


Figure 1. Retention of OIT of Dry Core Cable Insulation on Ageing in AGJP's at Cloncurry

Filling Compound Contact

Where insulation is in contact with filling compound the selection of an appropriate stabiliser system is more critical. The majority of stabilisers investigated exhibited considerable interaction with the filling compound and as a result the respective insulation oxidative stabilities were reduced in a relatively short time (Figure 2). This was particularly evident with the more traditionally used stabiliser systems of C and E. However, with the availability of stabilisers less prone to filler interaction, such as the antioxidant of system A, the detrimental effect of filling compounds can be markedly reduced.

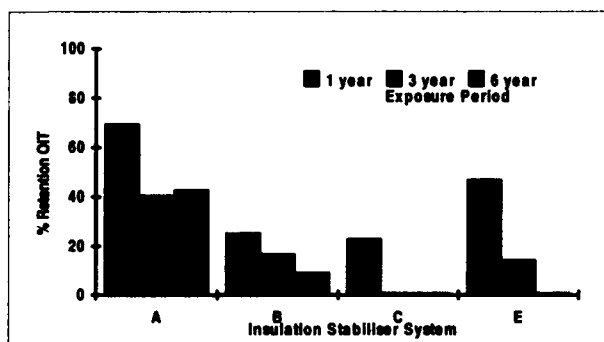


Figure 2. Retention of OIT of Filled Cable Insulation on Ageing in AGJP's at Cloncurry.

Complementary to stabiliser selection is the selection/development of filling compound formulations which interact to a lesser extent with stabilisers, an area discussed in more detail in subsequent sections of this paper.

Insulation Environment

It is well established that the thermal environment of the joint closure, due to both the general climatic conditions external to the joint and to the joint design itself, has a significant influence on the life expectancy of the insulation within^{8,12,13}. Figure 3 exemplifies the performance variation that can be observed with climatic variation. Exposure of the same insulation system in closures at Cloncurry and Innisfail predictably resulted in a significant difference in life expectancy. This pattern was found to be consistent with all dry core and filled cable systems trialed.

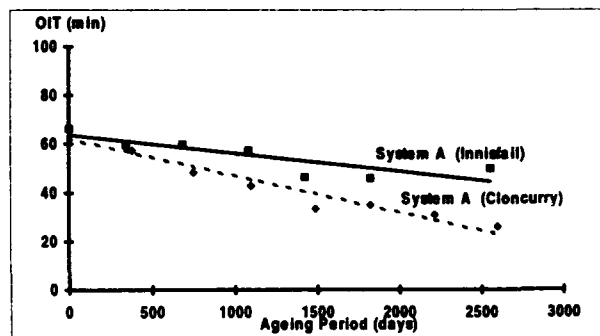


Figure 3. Impact of Climatic Variation on Oxidative Stability of Insulation in AGJP's.

The positive effect of reduction of temperature is again evident in Figure 4 where the immediate thermal environment at the joint was modified by applying a protective/reflective white PVC cover over the existing metal AGJP. This approach reduced the temperature of the internal closure environment by up to 10°C, which in turn decelerated the oxidative degradation process to the extent where insulation life increased twofold.

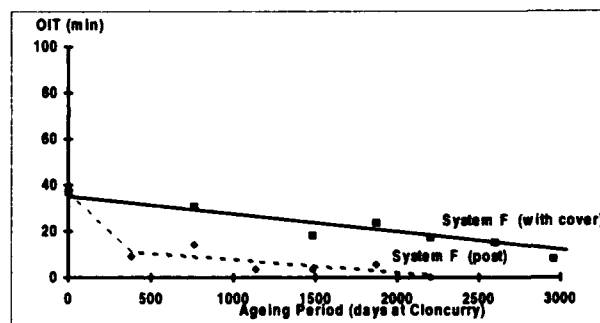


Figure 4. Variation in Insulation Oxidative Stability due to Joint Closure Temperature Reduction by Application of Reflective White PVC Cover.

A further environment modifying aspect that became evident in the trials was associated with the exposure of fully sheathed cable to direct sunlight. This test simulates the exposure typical of cable storage in the line yard and, to a lesser extent, the sheathed portion of cable in jointing posts. The oxidative stability of the insulation within the exposed cable samples was considerably less affected than the identical insulation in the unsheathed state within the AGJP (Figure 5). It is thought that the reduction of air space around the insulation, due to the presence of filling compound, in combination with the thermal shielding effect by

the sheath contributes to the reduction of the thermo-oxidative processes of insulation systems. This observation is further supported by observations of insulation performance in true field situations discussed in subsequent sections of the paper.

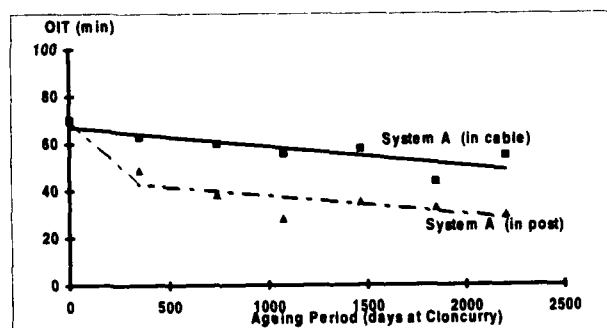


Figure 5. Comparison of Filled Cable Insulation Oxidative Stability when Exposed as Sheathed and Unsheathed Cable.

It should be stressed that the trends observed relate to specific Australian systems and some variance in performance may occur subject to use of differing polymer systems, filling compound formulations and stabiliser levels. It is, however, clear that consideration of these factors together with the intended exposure environment is necessary for the enhancement of life expectancy of polyethylene installations.

In - Service Performance Survey

In light of the generally poor performance of filled cable insulation observed in the above trials and the report of premature failure of similar systems in the USA, a comprehensive survey of above ground, in-service jointing systems was carried out. The areas surveyed were inland regions of South - West Queensland and South Australia which lie between latitudes of 25° and 35° South and have similar climatic conditions to Cloncurry in both temperature and sunshine exposure.

Cellular polyethylene insulated tilled cables were introduced into the Australian network in the late 1970's so at the time of the survey the oldest cables examined had been exposed for approximately 10 years. The results of the survey, summarised in Table 2, confirmed that the insulations exposed in

above ground joints had been adversely affected irrespective of the stabiliser systems used. The OIT values for the 1978/79 cable installations were of particular concern as they indicated little, if any, stabiliser was present and therefore these systems are the most likely to fail within the near future. However, unlike the experiences of the USA where failures were observed within 10 years⁸, no insulation failures have been observed with the Australian filled cable network after 15 years exposure. The life expectancy of these systems is expected to be further extended in the case where the white PVC covers were placed over the metal jointing post. The OIT values in these joints were, in some instances, double that of the non protected joints, which confirms the benefits of temperature reduction within the closure.

Year of Installation	OIT @ 200°C (exposed insulation)	OIT @ 200°C (with cover)	OIT @ 200°C (pre-installation)	Stabiliser Code
1978/79	<5 min	N/A	40	C
	<5 min	N/A	75	E
1980/83	10-15 min	N/A	40	C
	10-15 min	N/A	75	E
1984/86	10-15 min	20-25	55	B

N/A = Not Available

Table 2. Oxidative Stability of Field Insulations Examined.

As previously mentioned the extent of insulation deterioration can be minimised by retaining as much totally sheathed cable as practicable to isolate the insulation from the external environment. This factor is further highlighted in Figure 6 which shows the OIT distribution of filled cable insulation throughout typical joint closures, similar to that observed in the USA⁸. A substantial increase in oxidative stability is observed for the unexposed insulation in the sheathed cable in the jointing post and below ground, for both the 1983 cable (system C) and 1979 cable (system E) examples cited.

Laboratory Investigations

As shown by field trials and the in-service cable survey, the presence of filling compound reduces the life expectancy of the insulation, particularly when it is exposed to the higher thermal regimes

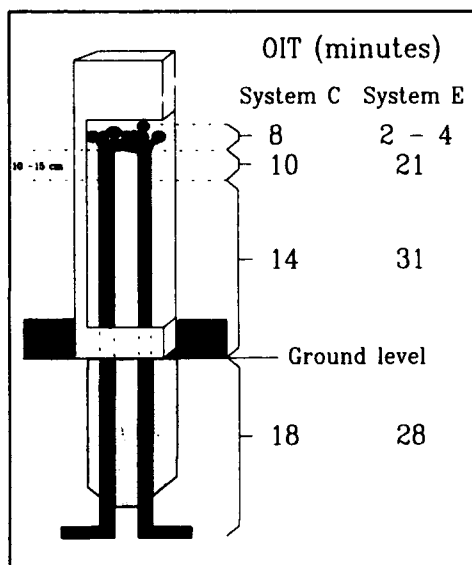


Figure 6. Distribution of OIT's of Filled Cable Insulation in Above and Below Ground Post Situation.

of above ground closures. The laboratory investigation, an adjunct of previously reported work⁹, focused on the definition of the mechanism of stabiliser/filling compound interaction and potential procedures for the retardation of this process.

Figure 7 shows the extent of reduction in insulation oxidative stability on contact with 'unstabilised' filling compound for a short period at 60°C and at 23°C. The extent of reduction in oxidative stability is dependent on the propensity for stabiliser interaction with the filling compound. This interaction is primarily linked to the solubility/extractability characteristics of stabilisers with the oil fraction of the filling compound.

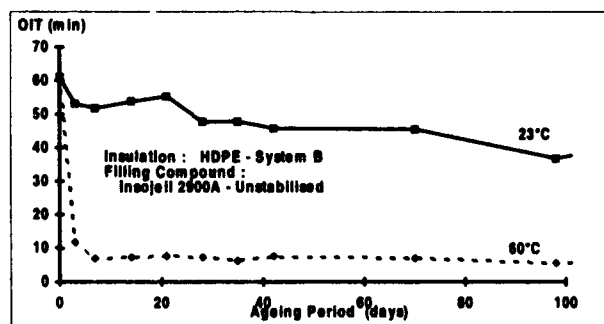


Figure 7. Ageing Characteristics of Cellular Insulation in Contact with Unstabilised Filling Compound.

The varying extractability characteristics of individual stabilisers is also evident in Figure 8, with the insulation stabilised with system A proving the least prone to filling compound interaction.

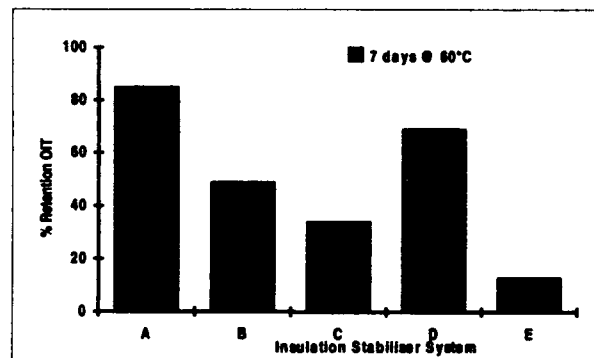


Figure 8. Retention of OIT's after 7 Days Ageing at 60°C in Unstabilised Filling Compound.

It was further observed that the incorporation of antioxidants into the filling compound retarded this extraction process. The exact mechanism, although not fully defined, is considered to involve the attainment of an equilibrium of stabiliser concentration between the filling compound and the insulation material. The effectiveness of this retardation process is dependent on both the antioxidant type and its concentration. Figure 9 shows the improved insulation performance for different antioxidants in the filling compound. Likewise, Figure 10 indicates that with increased levels of antioxidant in the filling compound the insulation retains a high level of oxidative stability.

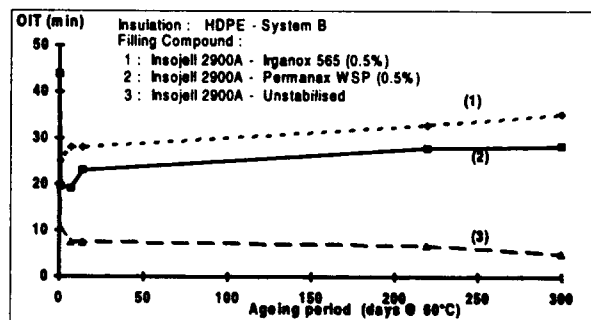


Figure 9. Filling Compound Stabilisation Effects on Ageing Characteristics of Cellular Insulation

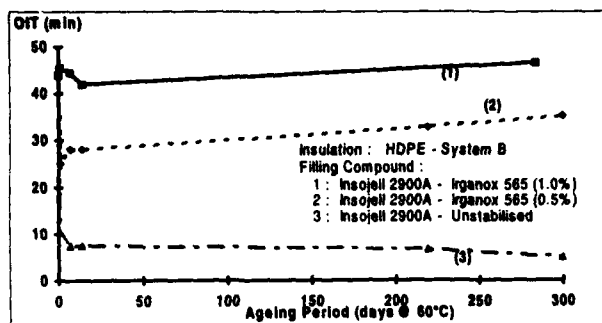


Figure 10. Filling Compound Stabiliser Concentration Effects on Ageing Characteristics of Cellular Insulation.

In addition to the prospect of retarding stabiliser extraction from insulation by using stabilised filling compound, the potential for a reverse process of diffusion of filling compound stabiliser into a stabiliser deficient insulation was examined.

A sample of insulation first exposed to an unstabilised filling compound to reduce its oxidative stability, was then exposed to a stabilised filling compound at an elevated temperature. After a short time a significant increase in oxidative stability of the insulation was observed (Figure 11), indicating that stabiliser from the filling compound had diffused into the cell structure of the insulation.

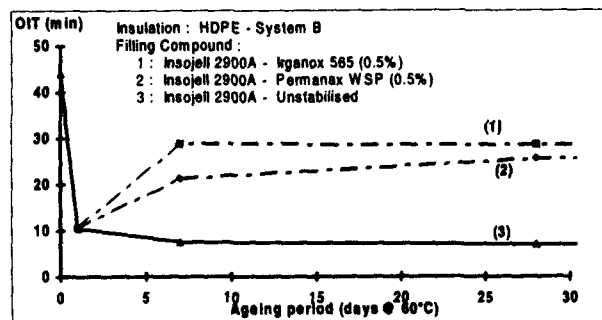


Figure 11. Insulation Oxidative Stability Enhancement on Contact with Stabilised Filling Compound.

A further test was carried out to observe if this reverse process would also take place with insulation that had no prior contact with filling compound and was deficient of stabiliser. Exposure of the unstabilised insulation to stabilised filling compounds resulted in a marked increase in OIT of the insulation (Figure 12). Even though this was carried out at 80°C it suggests that a similar

process may occur at temperatures closer to true operating conditions.

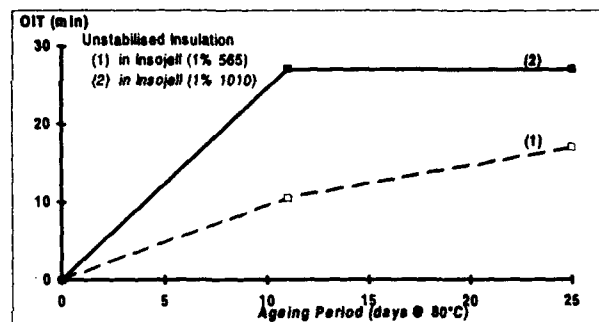


Figure 12. Insulation Oxidative Stability Enhancement of Unstabilised Insulation on Contact with Stabilised Filling Compound.

INSULATION PERFORMANCE ENHANCEMENT STRATEGIES

It should be noted that as the thermal environment of the insulation is the most critical parameter the most effective means of reducing the rate of oxidative degradation is to maintain the entire cable network below ground in the substantially cooler environment. However, as this approach in many instances is considered the least cost effective, in both hardware and manpower resources, particularly in the short term, alternative strategies need to be adopted for the above ground installations.

The approaches for the enhancement of cellular insulation in above ground installations are focused on three areas: materials formulation, joint closure design and work practices, each differing in the degree of complexity and ultimate effectiveness. The benefits and draw backs of each are summarised below.

Materials Formulation

The base material selections for both insulation compound and cable filling compound are reasonably well entrenched in all telecommunications networks world-wide and at present there does not appear to be the impetus for any alteration to this situation for both sound technical and commercial reasons.

Options	Advantages	Disadvantages
Insulation		
• higher stabiliser levels	• improved protection against oxidative deterioration	• marginal cost penalty
• alternative stabiliser systems		
a) primary and secondary antioxidant variations	• potential improved protection against oxidative deterioration	• limited information on proven systems
b) less oil-extractable stabilisers	• reduced premature depletion of stabilisers	• probable cost penalty
Filling Compound		
• total stabilisation	• reduced insulation stabiliser loss • improved oxidative protection for insulation and filling compound	• substantial cost penalty
• partial stabilisation (around joint)	• protection of most vulnerable part of network	• field application difficulties/inconvenience

Table 3. Material Focused Strategies for the Enhancement of Insulation Performance in External Plant Above Ground Installations.

Options	Advantages	Disadvantages
Work Practices		
• persist with current plant - repair / replace as required	• re-establish functional joint • accepted practices unchanged	• high cost
• minimise length of unsheathed cable in joint	• less exposed vulnerable insulation • in situ source of stabilised insulation for re-jointing	• none evident
• retain stabilised filling compound around joint	• reduction of moisture related faults • reduction in insulation stabiliser extraction	• field application difficulties
Joint Closure Design		
• white PVC covers	• simple, inexpensive • reduction of joint temperature	• cover life expectancy unknown
• white Plastics AGJP	• less expensive than metal designs • reduction of joint temperature	• construction life expectancy unknown • less robust
• re enterable sealed / encapsulated joints	• exclusion of environmental factors - moisture and air flow • reduction in insulation stabiliser depletion	• increased cost • variability in design possibilities • work practices difficulties

Table 4. Network Design and Work Practices Focused Strategies for the Enhancement of Insulation Performance in External Plant Above Ground Installations.

The strategy direction in Australia has therefore been focused on material stabilisation modification. The advantages and disadvantages of such approaches are outlined in Table 3.

Network Design and Work Practices

The design and practices options that are potential candidates for the enhancement of the network are

listed in Table 4 with their respective advantages and disadvantages.

The final adoption of any or all of the approaches is subject to their acceptance on the basis of performance expectation, economic factors and field implementation practicability.

CONCLUSION

Both the laboratory and field investigations into the performance of cellular insulation in external plant situations, particularly in the above ground installations, have isolated numerous factors that influence the rate of insulation deterioration. The options for performance enhancement that evolved were just as numerous ranging from the implementation of simple approaches, such as the use of white PVC covers on AGJP's, to the more sophisticated approaches associated with changes to material formulation and redesign of elevated joints. It is clear that each option cited will enhance the performance of above ground installations, but due to the degree of complexity or external commercial influences, many may not be cost effective in the short term. Of the options cited, the first to be implemented in the Australian network in the early 1980's were that of increased stabiliser concentration in insulation and the use of the white PVC cover. The absence of filled cable insulation failures to date may be indicative of the success of the actions taken. Many of the other options are currently under review, some of which may be adopted in the near future.

ACKNOWLEDGMENTS

The authors wish to acknowledge the assistance and co-operation of all parties within the Telstra organisation for their involvement in the preparation of trials, gathering of samples and carrying out the required analyses. The permission of the Group Managing Director, Network and Technology and the Director, Applied Research and Development, Telstra Corporation Limited, to publish and present this paper is also acknowledged.

REFERENCES

1. Pusey, B.B., Chen, M.T. and Roberts, W.L., 'Evaluation of Thermal Degradation in Polyethylene Telephone Cable Insulation', Proc. 20th. Int. Wire and Cable Symp. (1971), pp.209-218.
2. Hawkins, W.L., Chen, M.T. and Link, G.L., Polym. Eng. Sci., 11, 1971, p.377.
3. Howard, J.B., 'Stabilisation Problems with Low Density Polyethylene Insulation', Proc. 21st. Int. Wire and Cable Symp. (1972), pp.329-341.
4. Gilroy, H.M., 'Thermal Oxidative Cracking of Polyethylene Insulation on Telephone Conductors', Proc. 23rd Int. Wire and Cable Symp. (1974), pp.42-52.
5. Ance, L. and McCann, J.P., 'System Evaluation and Protection of Conductor Insulation in Outside Plant', Proc. 23rd. Int. Wire and Cable Symp. (1974), pp.82-90.
6. Board, B.L. and Ruddell, H.J., 'Investigation of Premature Depletion of Stabilisers from Solid Polyethylene Insulation', Proc. 31st. Int. Wire and Cable Symp. (1982), pp.300-312.
7. Englehart, W. and Hayes, R., 'An Analysis of Field Performance of Cellular Insulated Filled Telephone Cable after a Decade of Service', Proc. 35th. Int. Wire and Cable Symp. (1986), pp.252-258.
8. Bowmer, T.N., 'Cracking of Foam-Skin Polyethylene Insulations in Pedestals', Proc. 37th. Int. Wire and Cable Symp. (1988), pp.475-483.
9. Brown, G.D., 'Performance of HDPE Insulation Antioxidants in Filled Telephone Cable Applications', Proc. 36th. Int. Wire and Cable Symp. (1987), pp.337-343.
10. Aitken, H.S. and Mascarenhas, V.B., 'A Method for Evaluating Oxidative Stability and Performance of Polyolefin Insulations for Filled Telephone Cable', Proc. 37th. Int. Wire and Cable Symp. (1988), pp.442-448.
11. Beltz, L.P., 'Factors that Influence PIC Degradation of Filled Foamskin Telephone Cable', Proc. 38th. Int. Wire and Cable Symp. (1989), pp.123-131.
12. D'Amico, J.N. and Bowmer, T.N., 'Extending the life of Polyethylene Wire Insulation', Proc. 40th. Int. Wire and Cable Symp. (1991), pp.476-481.
13. Bowmer, T.N. and D'Amico, J.N., 'Remedial Strategies for Polyolefin Insulations in Outside Plant', Proc. 41st. Int. Wire and Cable Symp. (1992), pp.310-320.

Paul Boes

Access Product Group
Network and Technology
Telstra Corporation Limited
6/242 Exhibition Street
Melbourne Vic 3000
AUSTRALIA



Paul Boes joined Telstra in 1986 after graduating with a B.E. degree in communications engineering from the Royal Melbourne Institute of Technology. He is currently Principal Engineer in the Access Product Group, Network and Technology, responsible for the development, implementation and technical management of copper and optical fibre cable in the Telstra Customer Access Network.

Peter Latoszynski

Applied Research & Development
Telstra Corporation Limited
770 Blackburn Road
Clayton, Vic 3168
AUSTRALIA



Peter Latoszynski is an Applied Science Graduate of Footscray Institute of Technology (1975) and also gained post graduate qualifications in Analytical Chemistry from the Royal Melbourne Institute of Technology in 1980. Peter joined the Telstra Applied Research & Development in 1972 and has held a variety of technical positions prior to specialising in polymer technology. He is currently Principal Polymer Chemist responsible for network materials stabilisation, new cable materials and electro-active polymers.

THE TEMPERATURE OF AERIAL PLANT AND ITS EFFECT UPON FOAM-SKIN INSULATION LIFE

Tim Dougherty
AT&T Network Cable Systems
Phoenix, Arizona

Ed Gurney
GTE Telephone Operations
Irving, Texas

ABSTRACT

The temperatures of aerial filled cables and closures were measured at a test site in Phoenix, Arizona, and compared to pedestal temperatures. Aerial temperatures were dependent upon cable or closure size and design, an important aspect of which was color. The peak temperatures of insulations in black free-breathing closures were higher than in a typical light green PC-6 pedestal. The temperatures in sealed stainless steel closures were only slightly higher than in a PC-6 pedestal. The impact of higher temperatures upon insulation life was estimated by integrating measured temperature histories with an insulation life model. The insulation life model assumed compliance with a 260 day 90°C pedestal test which included cable preaging. The results indicated an acceptable life expectancy for foam-skin insulations in aerial closures.

INTRODUCTION

The high cost of maintaining nonpressurized air core PIC cables in aerial plant is a problem for many telephone companies due to their exposure to a variety of hazards. The common symptom is the presence of water in aerial spans caused by condensation or by sheath or closure damage from storms, birds, squirrels, tree abrasions and even bullets. GTE recognized that maintenance costs can be reduced through the use of 80°C ETPR filled cables in the air. Initial applications specified solid insulations because of their robust characteristics. Foam-skin insulations offered a 15% diameter reduction, a 15 to 20% weight reduction and lower cost to enhance overall savings. However, a major concern existed, the cracking of foam-skin insulations in closures due to high temperature exposure over extended periods. This had been a problem in pedestals in high temperature environments.

During the past 5 years, the U.S. telephone cable industry has been addressing the insulation cracking issue. A summary of the problem, the causes and the proposed specification changes can be obtained from papers published by Bellcore^[1,2,3]. Research demonstrated that the primary culprit reducing insulation life was the interaction between cable filling compounds and the stabilizers within the insulations. Cable stabilization requirements^[4] were modified through the addition of a 28 day 70°C cable preaging step to the qualifying pedestal test. The cable manufacturers and material suppliers responded by boosting the levels of stabilizers and copper deactivators in raw materials to compensate for stabilizer losses.

The advances in foam-skin stabilization led GTE to reconsider its use for aerial applications in 1991. Several concerns remained to be addressed because this was a new application for foam-skin insulation. The first was a need to understand the aerial temperature environment in detail, especially relative to pedestal temperatures, since the pedestal experience was the basis for stabilization specifications. A 1988 study in Las Vegas^[5] indicated maximum temperatures of 117°F in aerial closures which were surprisingly lower than pedestal temperatures measured by Bellcore^[6]. In addition, the aerial study did not provide an hourly temperature history to allow a calculation of the impact of temperature upon insulation life.

The second concern was the daily exposure of aerial cables to high temperatures, which could maximize filling compound-insulation interactions. If an aerial splice was added years after the initial installation to create a new drop, it would be important to prove that the insulations in the new splice would contain adequate levels of stabilizer to assure life performance.

A joint AT&T-GTE study was begun in 1991 to resolve these questions. A test site was established at the AT&T Phoenix Works because the high temperatures in Arizona would provide a worst case study.

EXPERIMENTAL FACILITIES

Two poles were spaced 50 feet apart in an east-west direction with support strands at 12, 15 and 18 foot levels as shown in Figure 1. A 50 pair 24 AWG foam-skin 80°C ETPR filled cable with alpeth sheath and 0.75 inch diameter was suspended



Figure 1. Phoenix Test Site

below the top strand. A 1200 pair cable of similar design but 2.7 inch diameter was placed at the mid level. The lowest level included 3 large commercial closures on a 25 foot section of the 1200 pair cable and 3 small closures of similar designs mounted on a 25 foot section of the 50 pair cable. The closures were spaced approximately 4½ feet apart. A variety of commercial pedestals were spaced approximately 4 feet apart below the aerial cables to allow temperature comparisons. All closures and pedestals included simulated splices. A summary of the hardware designs and dimensions is given in Table 1. For reference, the coordinates of the test site were 112° 10' 02" West, 33° 27' 04" North at an altitude of 1064 feet.

Table 1

Dimensions of Outside Plant Cable and Apparatus

Aerial Cables

50 Pair—24 AWG-Foam-Skin-80°C ETPR-Alpeth—.75" Diameter
1200 Pair-24 AWG-Foam-Skin-80°C ETPR-Alpeth-2.7" Diameter

Aerial Closures

	Diameter	Length
Large Black Free-Breathing	7.7"	29.5"
Large White Free-Breathing	7.7"	29.5"
Large Stainless Steel Sealed	9.8"	28.0"
Small Black Free-Breathing	3.5"	24.0"
Small White Free-Breathing	3.5"	24.0"
Small Stainless Steel Sealed	4.3"	25.8"

Pedestals

PC-6-----6" x 6"
PC-6+Dome-----6" x 6"
Dome = 2.7" Diameter x 14" Long Sealed
Black Plastic Bottle with Metalized Liner
Green Plastic Dual Sealed Chamber--
Outer Shell = 9.4" Diameter
Inner Chamber = 5.4" Diameter x 18" High
Green Plastic+Dome-----7.1" Diameter
PC-6+White Flood Cover--7" x 7" For Cover
Gray Plastic Flood Cover--7.5" x 7.5" At Top Of Cover
10" x 10" At Bottom Of Cover

Note: The Height Of All Pedestals Was 31" +/- 2" Above Ground.

INSTRUMENTATION

Two methods were used to measure the temperatures of the aerial cables. The first technique was based upon the temperature dependance of the resistance of copper conductors. Six conductors were spliced together at the ends of the cable so as to loop back and forth 6 times through a unit in the cable. This improved the measurement accuracy by providing a total resistance of approximately 8 ohms. A single measurement was made in the 50 pair cable and two measurements were made in the 1200 pair cable, one in an inner unit and one in an outer unit. Because the units are stranded and the core cabled, the resulting resistance, and hence temperature measurements, were an average for that layer. The resistances were measured at a known temperature in the laboratory before the cables were placed outside. A four wire measurement of resistance was made to minimize error. The standard technique for calculating temperature as a function of resistance and wire conductivity was applied^[7].

The second method of aerial cable temperature measurement was accomplished by inserting a 24 AWG bare junction type J thermocouple between the jacket and the aluminum shield on the top of the cable on the south side of the support strand to assure full sun exposure.

The closure and pedestal temperatures were measured using bare junction 24 AWG type J thermocouples. Typically 2 or 3 thermocouples were used depending upon the closure or pedestal size and configuration. The wire work inside the large closures was flared after cutting several units. One thermocouple was used to measure the temperature of the top surface of the plastic or metal closure and was located on the south side of the support strand. A second was placed at the top of the flared wire work within 1 inch of the cover and a third was located within the wires at the center of the closure.

Each pedestal contained sections of the 50 pair cable which extended from the bottom of the pedestal. The lower section of each pedestal was filled with fine gravel. The center section of sheath was removed and the wires were looped within 6 inches of the top. Again 2 or 3 thermocouples were installed. One was used to measure the top surface temperature, a second to measure the temperature on the top surface of any inner sealing dome or chamber and a third at the top of the wire work.

Fluke Hydra Data Loggers, Model 2625, were placed in an air conditioned structure which was located adjacent to one of the poles to collect and store 40 channels of resistance and thermocouple data. Connections were made to the individual thermocouples, which were only 3 feet long, using shielded 16 AWG iron-constantan thermocouple wire. The data were accessed by a PC via modems.

The temperature monitoring system was calibrated by inserting the thermocouple junctions in an ice bath. The maximum error was ±1°F. The accuracy of the temperature measurement via resistance was estimated to be ±2°F. The data were automatically recorded every 15 minutes and down loaded to a computer every second week over a period of 2 years for analysis.

TEMPERATURE DATA

As one can imagine, the quantity of data obtained from the above test site was overwhelming. Data were analyzed for a number and variety of days. The key issue was the relative differences between the temperatures of insulations in pedestals and those in the aerial plant. This can be illustrated by studying a very hot day. The day of June 24, 1992 was chosen because of its 112°F maximum air temperature and its proximity to the summer solstice, which maximized the height of the sun in the sky and the length of the daylight hours. Sunrise occurred at 5:20 am and sunset at 7:40 pm.

As will be seen, the apparatus temperatures are a balance between the radiant heat absorbed from the sun, the heat losses via convection to the air, the conduction losses to the cable or

to the earth and the heat capacity of the cable or apparatus. The combination of high ambient temperatures, low humidity and lack of wind in the desert during the day can produce high equilibrium temperatures.

Temperature data for a typical PC-6 light green pedestal are shown in Figure 2, which will serve as a reference. Note that maximum top surface temperature reached 140°F near noon, while the wire temperatures gradually increased to 130°F late in the afternoon. The air temperature is also shown.

Pedestal Temperatures PC-6/Phoenix-6/24/92

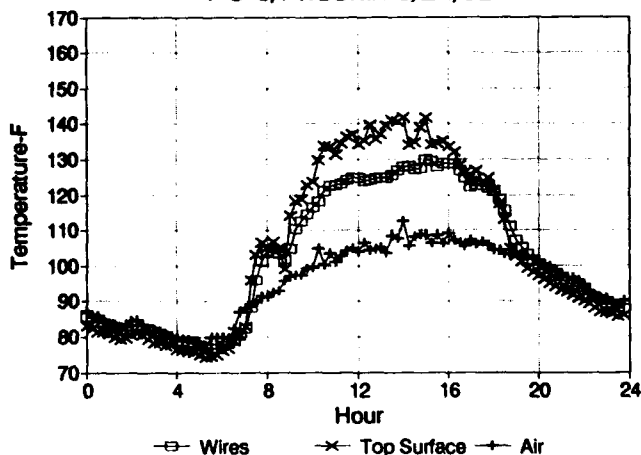


Figure 2

The aerial cable temperatures are shown in Figures 3 and 4. The 1200 pair cable internal wire temperatures and the jacket temperatures were equal, demonstrating the ability of the cable materials to rapidly transfer heat to equalize temperatures within the cable. The 2.7 inch diameter cable achieved a maximum temperature of 135°F. The same temperature uniformity was observed in the 0.75 inch diameter cable;

Aerial Cable Temperatures 1200 Pair-24 AWG/Phoenix 6/24/92

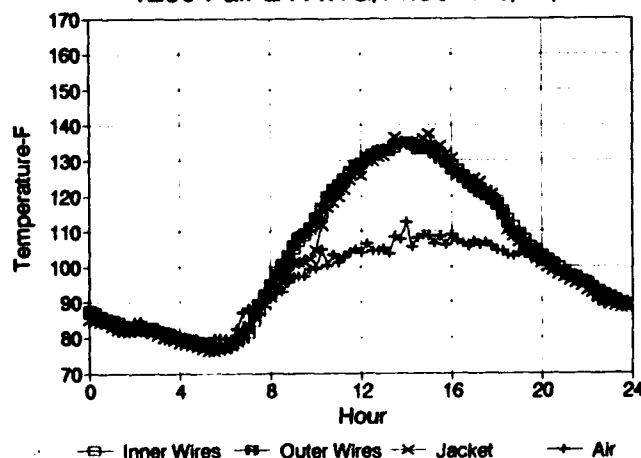


Figure 3

however, during June the resistance measurement was erratic due to a poor connection and so the data are not shown. The smaller cable temperature peaked at 125°F.

Aerial Cable Temperatures 50 Pair-24 AWG/Phoenix 6/24/92

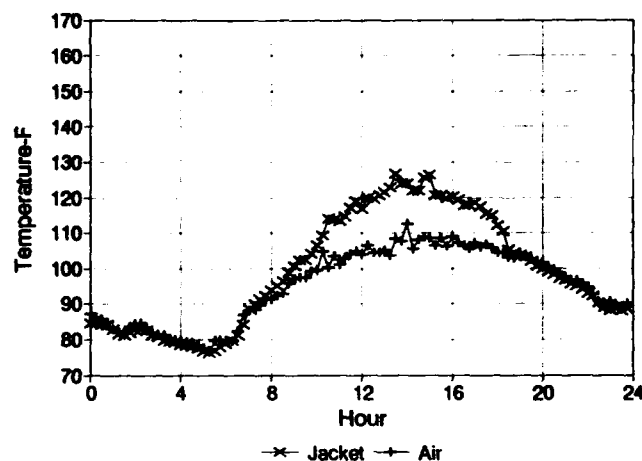


Figure 4

Temperatures in the large black free breathing closure are shown in Figure 5. The black plastic temperature reached 160 to 170°F while the wires approached 140°F, 10°F hotter than in the PC-6 pedestal. Simply painting that same closure white as suggested by Bellcore^[8] for pedestals, significantly lowered wire temperatures to within 10°F of ambient as shown in Figure 6. Before this is done, the longevity of a paint or of a white closure due to sun exposure would have to be investigated.

Aerial Closure Temperatures Large-Black/Phoenix 6/24/92

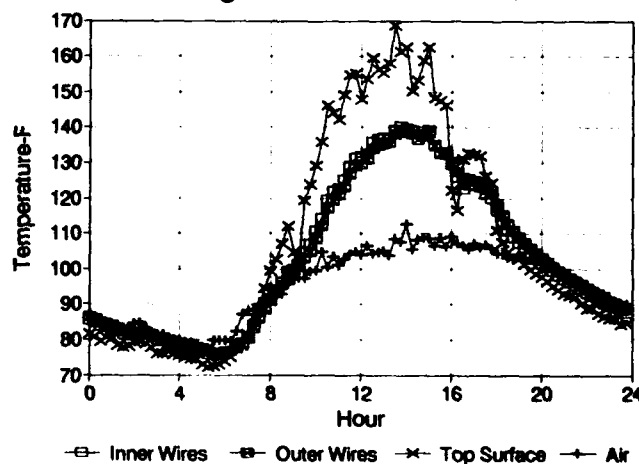


Figure 5

Temperatures in the large stainless steel sealed closure were between those of the black and the white closures as shown in Figure 7. The outer wires which were close to the cover

approached 135°F, while those in the center approached 125°F. Slightly lower temperatures were observed in the small closures. The maximum surface temperatures and the average and maximum wire temperatures are summarized in Table 2.

**Aerial Closure Temperatures
Large-White/Phoenix 6/24/92**

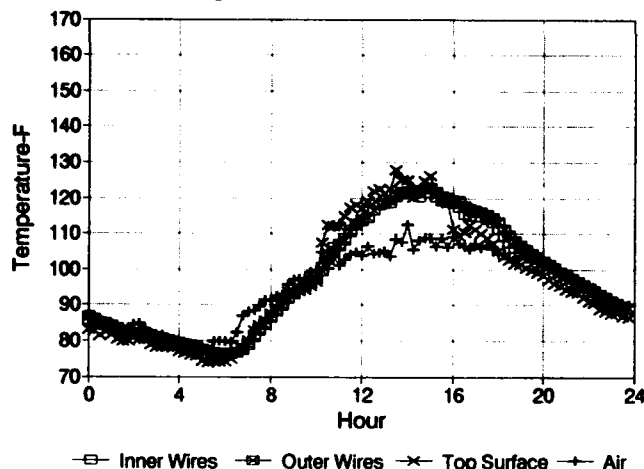


Figure 6

**Aerial Closure Temperatures
Large-SS-Sealed/Phoenix 6/24/92**

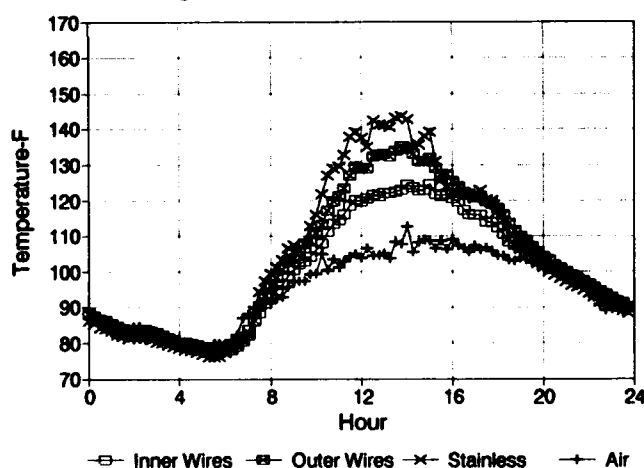


Figure 7

The temperatures in a variety of pedestal designs are shown in Figures 8 through 12. Several comments can be made relative to those data:

1. The use of a sealed dome around the wire work in a PC-6 pedestal did not lower the wire temperatures, although it did provide a protective environment (Figure 8).
2. The white flood cover over the PC-6 significantly reduced temperatures (Figure 9).

Table 2

**Outside Plant Temperatures
Phoenix 6/24/92**

Air = 112°F Maximum, 77°F Minimum, 95°F Average

Aerial Cables	Wires-Max.		
50 Pair	125°F		
1200 Pair	135		
Aerial Closures	Wires-Max.	Wires-Ave.	Top Surface-Max.
Large Black	140	103	165
Large White	122	97	125
Large Stainless	135	104	145
Small Black	134	102	158
Small White	120	97	125
Small Stainless	126	100	138
Pedestals			
PC-6	130	103	140
PC-6+Dome	130	102	140
PC-6+White Cover	115	96	115
Dual Sealed Chamber	131	103	140
Green Plastic+Dome	124	101	130
Gray Plastic	136	105	155

**Pedestal Temperatures
PC-6+Dome/Phoenix-6/24/92**

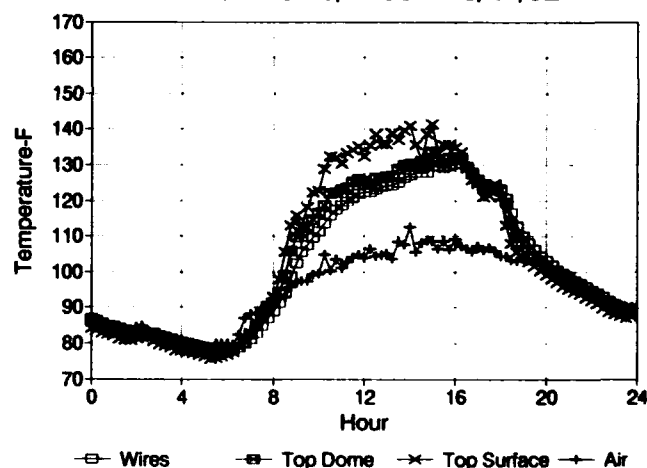


Figure 8

3. The green plastic pedestal with a sealed dome around the wire work experienced slightly lower temperatures. This may have been due to the whitening of the top surface via ultraviolet exposure (Figure 10).
4. The green plastic pedestal with integral sealed internal chamber did not reduce the maximum or average wire temperatures, but introduced a thermal lag during both heating and cooling (Figure 11).
5. The gray plastic pedestal with flood cover resulted in wire temperatures approximately 5°F hotter than the PC-6 (Figure 12).

Pedestal Temperatures
PC-6+White Cover/Phoenix-6/24/92

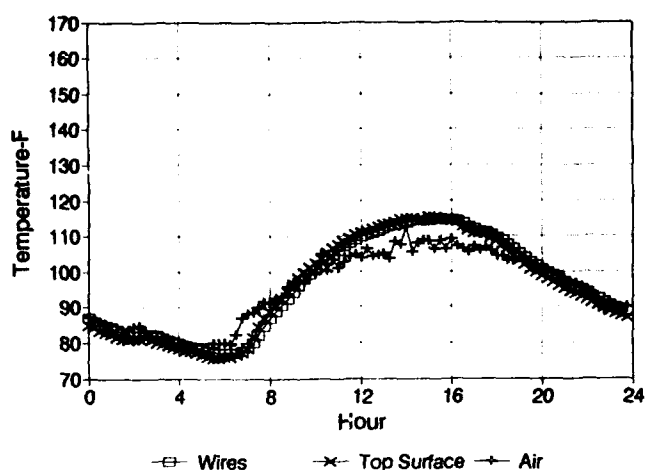


Figure 9

Pedestal Temperatures
Dual Sealed Chamber/Phoenix-6/24/92

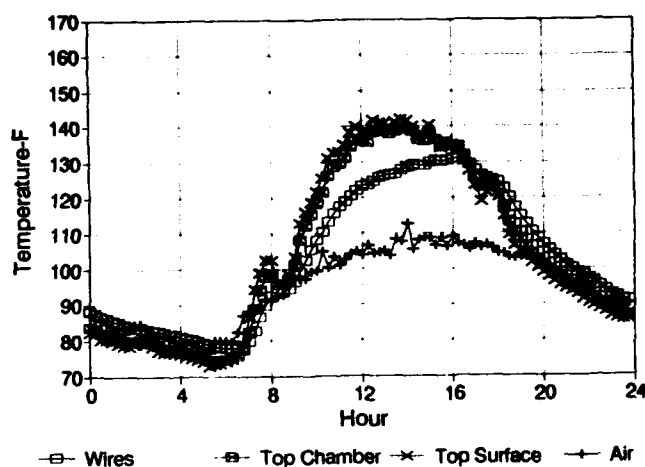


Figure 11

Pedestal Temperatures
Green Plastic+Dome/Phoenix-6/24/92

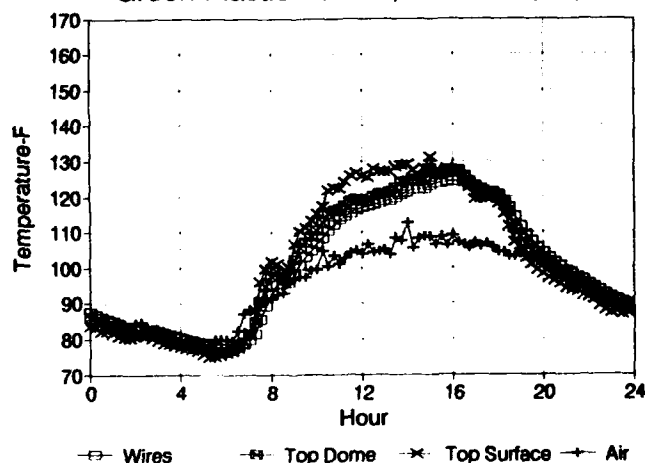


Figure 10

Pedestal Temperatures
Gray Plastic/Phoenix-6/24/92

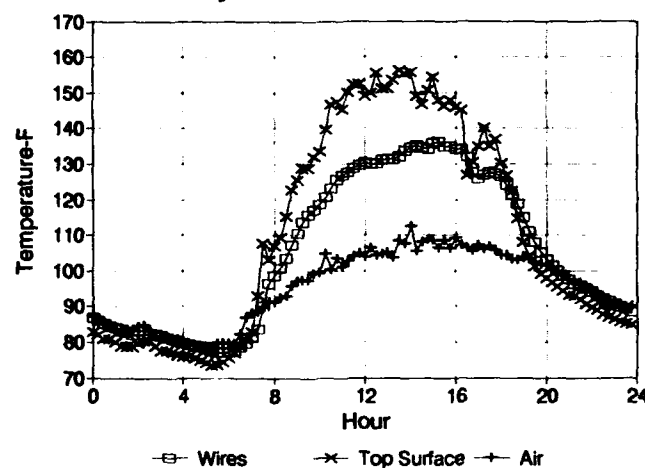


Figure 12

EFFECT OF TEMPERATURE ON LIFE

AT&T Bell Laboratories developed the pedestal test to not only accelerate insulation life testing, but to also provide data to allow life predictions. Tests were performed over a range of steady state temperatures, 110°C down to 40°C, to create Arrhenius plots. An example is given in Figure 13, which summarizes published AT&T data for a variety of insulation designs manufactured over the years. Before 1972, PIC insulation did not contain a copper deactivator and the stabilizer proved to be relatively volatile. Insulations cracked in the Southwestern U.S.A. after 4 to 5 years. Pedestal tests by H.M. Gilroy^[9] indicated a life expectancy of approximately 4 years at 40°C, an effective temperature for wires in pedestals in the Southwest. Those premature failures led to the

stabilization system used today, although the levels of stabilizer have increased over the years. The upward shift is demonstrated for a composite of PIC data between 1975 and 1977 by H.M. Gilroy and L.D. Loan^{[10][11]} with updated results by M.G. Chan of AT&T Bell Laboratories. Additional data by E.D. Nelson^[12] for foam-skin insulations manufactured before 1990, but with the 28 day 70°C preage step are also shown. All of this long-term historical data is valuable and can be used to predict insulation life by constructing parallel lines through the data. Note that insulation life increases by a factor of approximately 2.1 for each 10°C decrease in temperature.

To consistently comply with Bellcore's 260 day minimum pedestal test requirement at 90°C, it is necessary for manufacturers to assure test margins. The upper line in

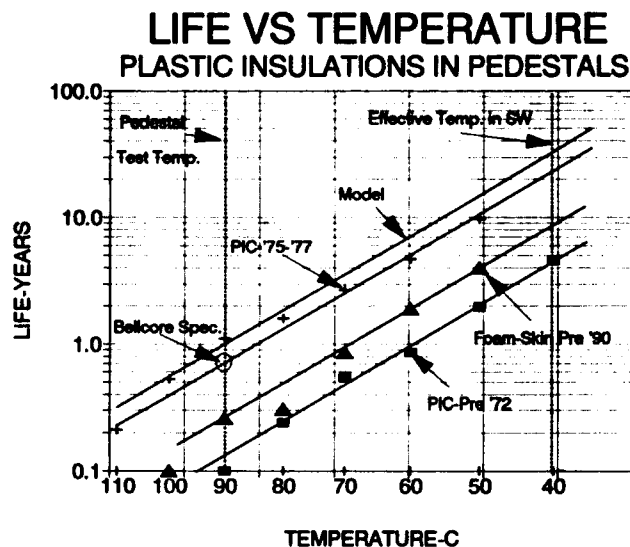


Figure 13

Figure 13 is an example of a manufacturing target which was used for a life model. The exponential equation for that line, Equation 1, was used in combination with measured wire temperatures to calculate relative differences in insulation lifetimes using a method proposed in 1971^[13].

L = Life in years

T = Temperature in °K

$$L = 2.96 \times 10^{-10} \times e^{7970/T} \quad (\text{Equation 1})$$

The useful life of an insulation is the time required to deplete its stabilizers. The rate of loss of those stabilizers is a function of the temperature which continuously varies. The rate of loss at a given temperature is inversely proportional to the lifetime at that temperature. Hence, the life model can be used to estimate stabilizer loss rates at different temperatures, which can then be averaged over a 24 hour day to determine relative lifetimes. An example of the procedure follows: The wire temperatures in the PC-6 pedestal, the large stainless steel sealed closure and the large black free-breathing closure are compared in Figure 14. At each data point or temperature, the insulation lifetime was estimated using Equation 1. This is the expected lifetime if the insulation were maintained at that constant temperature. The assumption is made that Equation 1 can be extrapolated below 40°C; i.e., that stabilizer reaction and diffusion rates do not change in relative proportion to one another. Any errors in this assumption will be small because reaction and diffusion rates at low temperatures are not significant when compared to rates at high temperatures.

Next, the inverse of the lifetimes were calculated to define the variation in the stabilizer loss rates over a 24 hour period as shown in Figure 15. Note that over a brief 4 hour period the

peak stabilizer loss rates differed by more than 50%. Finally, the average stabilizer loss rate was calculated over a 24 hour period. The inverse of that average is an estimate of the insulation lifetime if the insulation experienced a similar temperature cycle every day. The life predictions for all the closures and pedestals are summarized in Table 3. The slightly higher wire temperatures in the large aerial closures resulted in a slight decrease in the estimated time to first crack relative to a PC-6 pedestal. In addition, the white closures and the white pedestal lead to a significant improvement in life expectancies. Note that the predictions in this paper are based upon the latest techniques of accelerated testing. As such, they provide an indication of the useful service life of materials, but they do not constitute or imply any warranty on behalf of AT&T or GTE.

Comparison of Wire Temperatures Phoenix-6/24/92

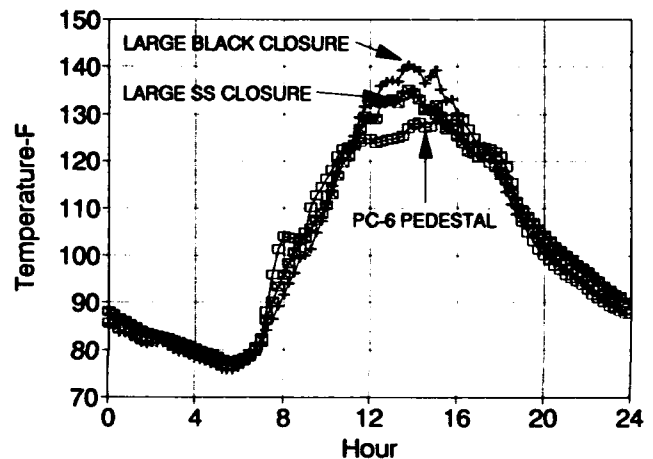


Figure 14

Comparison of Stabilizer Loss Rates Phoenix-6/24/92

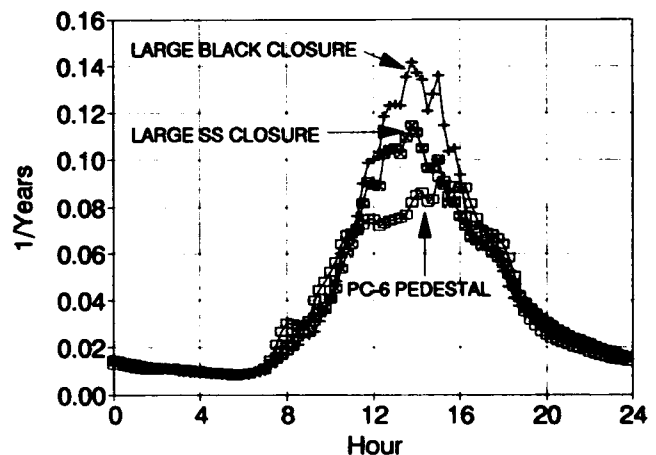


Figure 15

Table 3**Insulation Life Comparisons****Basis = 112°F Day at Phoenix on 6/24/92**

<u>Aerial Closures</u>	<u>Life-Years</u>
Large Black Free-Breathing	23
Large White Free-Breathing	36
Large Stainless Steel Sealed	25
Small Black Free-Breathing	27
Small White Free-Breathing	37
Small Stainless Steel Sealed	32
<u>Pedestals</u>	
PC-6	26 (Reference)
PC-6+Dome	26
PC-6+White Cover	40
Green Plastic Dual Sealed Chamber	25
Green Plastic+Dome	31
Gray Plastic Flood Cover	22

A similar analysis was performed for a day with a 102°F maximum air temperature, June 2, 1992. The temperatures are summarized in Table 4, and the impact of those temperatures upon life expectancies are shown in Table 5. Note the 35% increase in lifetime due to the lower ambient temperature. By coincidence, the 35 year life prediction for insulations in an actual PC-6 pedestal using this 102°F day nearly corresponded to the expected lifetime in a steady state pedestal test at 40°C or 104°F. Hence, this day proved to be more appropriate for making lifetime comparisons, while the 112°F day was an example of an extremely hot day. Again, the 5 to 10°F higher insulation temperatures in the large aerial closures had a slight negative effect upon life expectancy.

Table 4**Outside Plant Temperatures**
Phoenix 6/2/92**Air = 102°F Maximum, 74°F Minimum, 90°F Average**

<u>Aerial Cables</u>	<u>Wires-Max.</u>		
50 Pair	120°F		
1200 Pair	125		
<u>Aerial Closures</u>	<u>Wires-Max.</u>	<u>Wires-Ave.</u>	<u>Top Surface-Max.</u>
Large Black	132	97	155
Large White	114	92	118
Large Stainless	126	98	135
Small Black	125	96	150
Small White	111	92	115
Small Stainless	116	94	130
<u>Pedestals</u>			
PC-6	120	97	130
PC-6+Dome	121	97	130
PC-6+White Cover	108	91	108
Dual Sealed Chamber	121	98	130
Green Plastic+Dome	116	95	120
Gray Plastic	126	99	150

Table 5**Insulation Life Comparisons****Basis = 102°F Day at Phoenix on 6/2/92**

<u>Aerial Closures</u>	<u>Life-Years</u>
Large Black Free-Breathing	31
Large White Free-Breathing	49
Large Stainless Steel Sealed	34
Small Black Free-Breathing	37
Small White Free-Breathing	49
Small Stainless Steel Sealed	43
<u>Pedestals</u>	
PC-6	35 (Reference)
PC-6+Dome	36
PC-6+White Cover	53
Green Plastic Dual Sealed Chamber	35
Green Plastic+Dome	41
Gray Plastic Flood Cover	30

EFFECT OF CABLE AGING

As mentioned earlier, the daily exposure of aerial cables to high temperatures could increase stabilizer-filling compound interactions. To study this effect, 26 AWG solid and foam-skin cables filled with 80°C ETPR were preaged for 2, 4, 8, 12 and 16 weeks at 70°C. The insulations were removed from the cable, wiped and then analyzed via OIT and HPLC. The OIT was measured at 200°C in aluminum pans without the use of screens. The OIT's are shown in Figure 16. The solid insulations were tested with the conductor in place and the foam-skin insulations with the conductor removed as was the practice at the time of the test. Note the similarity of the curves. The data leveled off after 8 weeks. The difference in OIT between the 4 week preage used for pedestal testing and the 8 week preage was approximately 30%.

The levels of Ciba Additives' Irganox® 1010 and Irganox® MD 1024 were obtained by HPLC and are shown in Figure 17. After 2 weeks of preaging the Irganox® 1010 stabilizer was virtually undetectable in both the solid and the foam-skin insulations. The Irganox® MD 1024 stabilizer-copper deactivator content decreased for both solid and foam-skin insulations and also leveled off after 8 weeks.

Two pedestal tests were performed at 90°C after 4 weeks of preaging and another two after 16 weeks, which was double the equilibrium period. All samples have surpassed 1 year without cracking. They are still under test to determine any differences in the time to initial failures.

As a result of this new understanding of the aerial temperature environment, GTE is using foam-skin insulations in filled cables for all aerial and buried applications.

OIT vs Cable Aging Time 26 AWG-80C ETPR

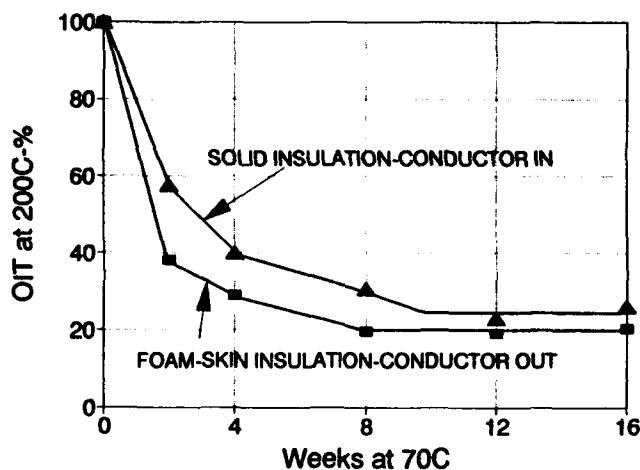


Figure 16

Stabilizer Levels vs Cable Aging Time 26 AWG-80C ETPR

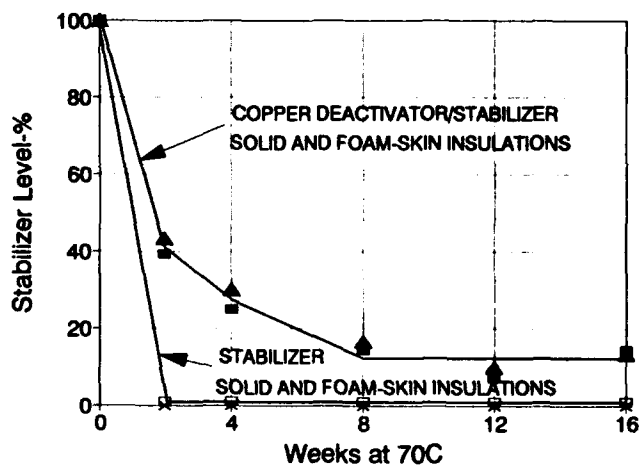


Figure 17

CONCLUSIONS

The following conclusions can be drawn from this experiment at the Phoenix test site:

1. The integration of field temperature data with insulation life models is a valuable tool which allows relative life predictions.
2. The temperatures of insulations in large aerial closures can exceed temperatures in typical pedestals for brief periods during the day.
3. The increased stabilizer loss during those brief high temperature periods has only a slight negative effect on overall lifetime.

4. The color of aerial closures has a significant effect upon insulation temperatures and life expectancies with white producing the best results.
5. Larger diameter cables or closures result in higher temperatures.
6. Insulation stabilizer levels approach equilibrium within cables aged for extended periods.
7. Robust insulation system stabilization performance provides a design safety factor to assure life performance in aerial and pedestal environments.

ACKNOWLEDGEMENTS

The authors wish to thank Bill McCoy and John Yunker of GTE and Maureen Chan of AT&T Bell Laboratories for their valuable advice on this project. Special thanks are also extended to the following AT&T personnel: Karen Dye and Cheryl Duffy for the OIT and HPLC measurements, Dick Rochford for the design of the data acquisition system and Richard Hill for the assembly of the pedestals and closures.

REFERENCES

1. T.N. Bowmer, "Cracking of Foam-Skin Polyethylene Insulations in Pedestals," *Proceedings of the Thirty-Seventh International Wire and Cable Symposium*, 1988, p.475.
2. T.N. Bowmer, E.P. Horth, R.J. Miner, O.S. Gebizlioglu, "Stability of Polyethylene Insulations in the Field and Laboratory," *Proceedings of the Thirty-Seventh International Wire and Cable Symposium*, 1988, p.490.
3. T.N. Bowmer, R.J. Miner, I.M. Plitz, J.N. D'Amico, L.M. Hore, "Thermal Stability Tests for Polyolefin Insulations," *Proceedings of the Thirty-Ninth International Wire and Cable Symposium*, 1990, p.316.
4. "Generic Requirements for Metallic Telecommunication Cables-Thermal Oxidative Stability Requirements for Cables with Polyolefin Insulated Conductors," *Bellcore Technical Reference TR-NWT-000421 Issue 3, September 1991, Revision 1, December 1992*.
5. E.A. Capadona, D. LaPointe, "An Examination of Temperature Rise Inside Aerial Splice Closures," *Outside Plant*, July, 1988, p.22.
6. T.N. Bowmer, R.J. Miner, R.C. Coker, "Field Temperatures in Outside Plant," *Proceedings of the Thirty-Ninth International Wire and Cable Symposium*, 1990, p.335.
7. "Copper Wire Tables," *National Bureau of Standards Handbook 100*, February 21, 1966, p.9.
8. J.N. D'Amico, T.N. Bowmer, "Extending the Life of Polyethylene Insulation," *Proceedings of the Fortieth International Wire and Cable Symposium*, 1991, p. 476.
9. H.M. Gilroy, "Thermal Oxidative Cracking of Polyethylene Insulation on Telephone Conductors," *Proceedings of the Twenty-Third International Wire and Cable Symposium*, 1974, p.42.
10. H.M. Gilroy, "Polyolefin Longevity for Telephone Service," *Proceedings of the Forty-Third ANTEC*, 1985, p.258.

11. L.D. Loan, "The Stabilization of Polyethylene for Long Term Use," *Proceedings of the Golden Jubilee Conference on Polyethylenes 1933-1983*, 1983, p.D11-1.
12. E.D. Nelson, "Methods of Determining Thermal Stability of Polyolefin Insulations," *Proceedings of the Fortieth International Wire and Cable Symposium*, 1991, p.277.
13. B.B. Pusey, M.T. Chen, W.L. Roberts, "Evaluation of Thermal Degradation in Polyethylene Telephone Cable Insulation," *Proceedings of the Twentieth International Wire and Cable Symposium*, 1971, p.209.



Tim Dougherty is a Distinguished Member of the Technical Staff for AT&T Network Cable Systems in Phoenix, Arizona. He received his B.S. in Mechanical Engineering from the University of Connecticut and his M.S. and Ph.D. in Mechanical Engineering from Rensselaer Polytechnic Institute. Tim joined AT&T in 1968 and has focused on foam-skin insulation development, copper cable design and insulation stabilization.



Ed Gurney is a Wire and Cable Outside Plant Standardization Manager for GTE Telephone Operations in Irving, Texas. He received his B.S. Degree in Mathematics from Elmhurst College in Elmhurst, Illinois. Ed joined GTE in 1966 and has an extensive laboratory testing background specializing in performance and quality testing of outside plant telephone equipment.

A contribution to better knowledge of RF coaxial cables

Otto Verbich

VÚKI a.s., Bratislava, Továrnská 14, Slovakia

ABSTRACT

Though it is possible to see very successful spreading of the optical cables, some of transmission lines are still better created with classical RF coaxial cables. Not all parameters of flexible coaxial cables are sufficiently known. Our paper should contribute some acknowledgements to ageing cables for receiver antenna feeders in CATV and a special view on attenuation of cables. There is described a offer how to look at complex losses in the RF coaxial cables. One of part is given to the application problems of metallic glasses on outer conductor of the screened cables.

Introduction

Though transmission properties of RF coaxial cables are well-known for a few generations of cable designers, we would like to comment some of contributions from Cables and Insulating Materials Research Institute as a centre for all cable industry in Czechoslovakia, now in Slovakia. We have been in very close cooperation with all cable makers in Eastern Europe.

In the present paper, we have studied the electrical properties of coaxial cables for CATV and LAN. The insulation is not only from polyethylene in solid and foam form, but in advanced balloon combination with tube, too. The orientation of our research analysis was focusing on ageing of RF cables, specially for higher ambient temperature, in the last years. Another research task has been very important for application of signal cables for EMC in transmission electronic systems. The screening of these type of cables has been realised from metallic glasses (or amorphous metals) and braiding of copper wires. Main effect of improving screening efficiency is for use the advanced designed cable near the power electric transmission lines in the same cable duct etc. For the technological experiments and evaluation of reduction factor we had chance to use not only metallic glasses from Germany, but new materials fabricated in scientific centre (SAV) of Slovakia, too.

All of our research experiences have very close continuity to the knowledge base of signal and RF cables and specifications of cables according to IEC, MIL, etc. The application of these experiences is not only in cable factories in former Czechoslovakia, but in more cable producers in Eastern Europe.

I suppose it was enough for the introduction of our not too much known activities in the field, which is presented in famous Cable and Wire Symposium, like in a Festival of the cable advanced production, every year.

How to look at the life time of RF coaxial cables

Many different opinions are on the ageing of RF coaxial cables for an external using. For example the feeders in CATV distribution or local computer networks. According to IEC 96-2 is increasing of the measured attenuation for 3 GHz the main response of the time instability of RF coaxial cables. But for the users is more important time dependence of attenuation in the typical frequency range 10 - 1000 MHz and ambient temperatures from +40 °C to the maximal limited temperature in the technical recommendation for cables with foam polyethylene insulation +65 °C and mechanical stress simulated like for TV receive antenna feeders.

For accelerating of ageing we have used temperatures 45, 55 and 65 °C. The lengths of cable samples have been more than 20 m. There have been focusing on two typical types of RF coaxial cables for CATV (RG 6) with the solid and the foam polyethylene and inner and outer conductors have been from copper. Before start of the testing in thermostats there have been exactly measured impedance matching in used connectors for next evaluating its influence upon results and after 7, 21, 35, 63 and 91 days there have been measured attenuation in the frequency range from 25 up to 1 000 MHz with application of the analog sweeping generator (SMLU, Rohde und Schwarz) and measuring reflectometer (ZRZ, R and S). There have been the minimal statistic collection of 3 samples from each cable type. We have taken about 100 detail frequency dependencies of the attenuation. The results are drawn in Fig. 1. Increasing values of attenuation $\Delta\alpha$ in dependence of ambient temperature are calculated from

$$\Delta\alpha = +\left(\frac{\bar{\alpha}_n}{\bar{\alpha}_0} - 1\right) \cdot 100 \quad (\%)$$

$\bar{\alpha}_n$ - arithmetic mean taken in the n -day of the testing

$\bar{\alpha}_0$ - arithmetic mean taken before start of the testing

Achieving life time attenuation dependencies show, that the cables with foam polyethylene insulation has a increasing more rapidly like on cables with the solid insulation. According to analysis of these phenomena it is due from increasing of the dielectric constant and carbonyl groups C=O with catalytic influence of the copper. There are two main solutions of these problems. The tinning or silvering the copper wires, or to use some antioxidant in polyethylene insulation against negative copper presenting. More detail informations are in [1].

There is very probably quite adequate to require in design of RF coaxial cables in the higher part of allowed temperatures special insulation with additives, or the limitation contacts with the copper conductors.

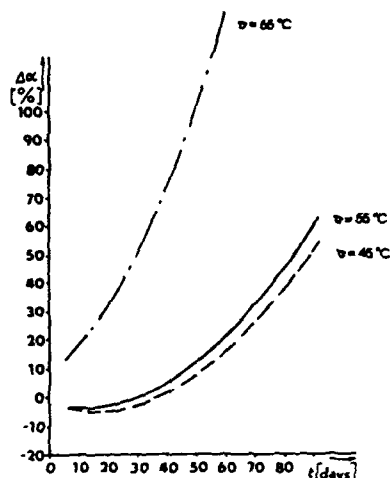
Some of producers have in their special offer RF coaxial cables with two layer jacket for receiving TV antenna feeders. Inner is from polyethylene and outer from PVC. After testing 5 months in moisturing of a few samples in vessels with water we had proved, that it is not necessary for the decreasing of diffuse of the water to the insulation and against a rapidly ageing of the cables to use the double jacket. The reason of these design is only in a better withstanding against a mechanical radial stressing.

The improving of the screening effectiveness

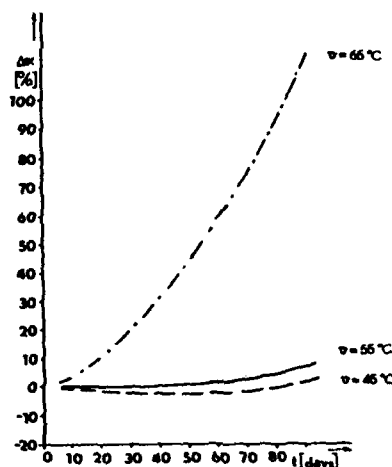
More pretending requirements to EMC and generally to the better screening effectiveness are necessary to solve with new design constructions of the outer conductor of RF coaxial cables. It has close coherence with the increasing of the ambient EMI and the higher sensitivity of a microelectronic receivers, too.

Typical design CATV flexible cables have the outer conductor from wire braiding. The cables for the improving screening effectiveness are completed with longitudinally overlapping metallic, or polymer + metal foil. It is the largest construction of the outer conductor for the all world. In the relationship to the classic braiding (covering 91%) it means the change in screening attenuation from 35-40 dB to about 70 dB. But according to the requirement, for example from Bundespost (Germany), is necessary to have minimal 75 dB in frequency range of the TV transmission channels. There is necessary to find some advanced constructions.

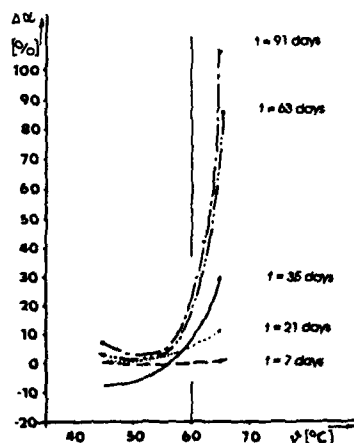
There have been evaluated many combinations with copper, aluminium, with PET foil and drain wires from copper and tinned copper. We have focused on improving of screening, but not with more and more density of wire braiding cover (more then 91%). The design solution with combination of two PET+Al foil and between them tinned copper longitudinally situated 24 wires has resulted to cables VCELY with very good values of the screening attenuation or a transfer impedance.



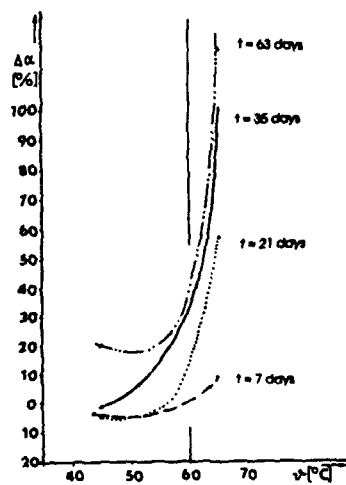
a) Foam PE



b) Solid PE



c) Solid PE



d) Foam PE

Figure 1: The ageing of the RF coaxial cables (modif. RG 6)

The last solution has been cable type VCEKY with sweeping wires along the axis of the cable and with "S fold" on outer PET+Al foil known from very good paper by Mr. Tsaliowich [2]. It is in Fig. 2.

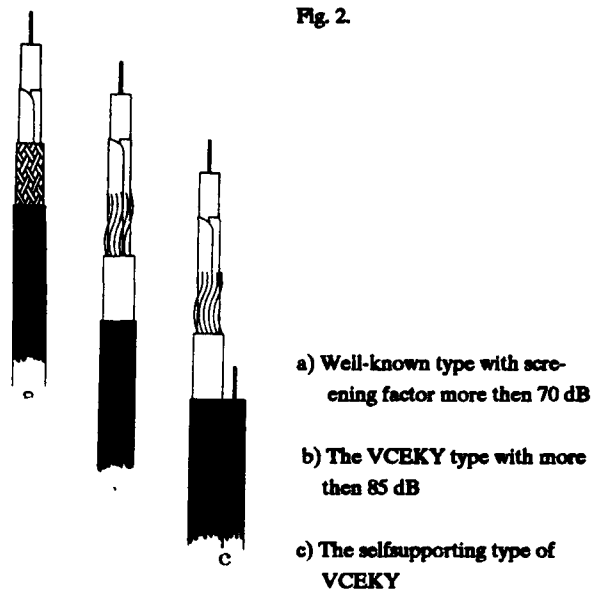


Fig. 2: The design construction of the cables with aim to the outer conductors

RG6:	VCJEY 75-4,8	VCELY 75-4,8	VCEKY 75-4,8
outer conductor	(Al/PET foil + Cu+Sn wires)	(2xAl/PET foils + longitudinally wires between)	(2xAl/PET foils + sweeping wires + „S fold“)
α_s	70 dB	75 dB	85 dB

Table 1: The comparing of known cable types according to the outer conductors

Much more complicated is the problem with EMC on the transmission lines arranged from coaxial cables in not to high frequencies. The electrostatic screening is usually realised by means of metals with good electric conductivity, occurring either in the form of braiding, or in the form of metallic tapes with drain wires. But magnetic permeability of Cu, Al, Sn and Ag is equal 1. In frequency ranges of tens and hundreds kHz is the signal part of the cable practically not screened. In more difficult conditions concerning magnetic screening for instance of signal cables situated near power cables it is usually used setting into the properly grounded cable ducts, or cable wrapped by the tapes with high value of magnetic permeability, such as MUMETAL, SONAPERME, PERMEDUR, etc. Their μ_r achieves values even in order of magnitude thousands. On the other side the higher heat or mechanical stress sensitivity is their great disadvantage.

All these deficiencies are eliminated by the tapes made from so-called "metallic glasses" or "amorphous metals". Their production consists of winding of the alloy (e.g. from Cr, Co, B, Si and Fe)

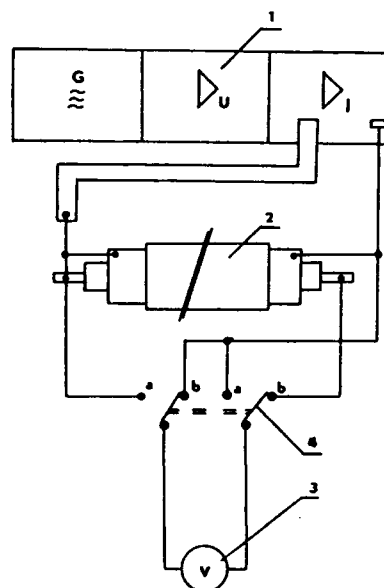
in plasmatic form and extremely rapidly temperature decreasing. These process is passing during winding tape on the rod in the strong magnetic field. It gives the opportunity to reach the tapes with μ_r about 130 000. Their width is from 5 to 25 mm and thickness about 0,4 mm. The tapes have relatively good mechanical properties, making their application in the cable industry possible without any important requirements. The only problem is represented by their nearly zero extensibility, what means that it is not possible to wrap them spirally around the cylindrical cable core with the overlapping, what leads to so-called "horn-like" effect. In order to reach applicable results in the further research have been successfully finished it was necessary to develop a method for the determination of minimal rising angle of the tape spiral wrapping for which following relation was derived

$$\varphi = \arcsin \frac{h+m}{\pi \cdot d}$$

where d ... diameter of the cable core [mm]
 h ... foil width [mm]
 m ... gap width [mm]
 φ ... wrapping angle [°]

Taking the last relation it is possible to set up tangential tape applicator according to tape width and cable core diameter in order to achieve the tight wrapping in open spiral along any cable length. For technological experiment we have had cable sample with 5 star-quads with PE insulation, the cable core was screened with Al tape and the sample had PVC sheet. The metallic glasses we had VITROVAC 6025 from Germany (Co, Fe, B, Si, Mo) and

VITROKOV 8116 from Slovak academy center in Bratislava. The second alloy was from Co, Cr, Fe, B and Si. For evaluation of EMC improving we have focused on measuring reduction factor. It is typical parameter for screening on signal cables near power electric cables. Detail informations are in [3].



- 1 - interference simulator
- 2 - cable sample
- 3 - voltmeter
- 4 - switch in position „a“ is measurement U_{sh}
in position „b“ is measurement U_{shh}

Figure 3: The block diagram of the measuring set

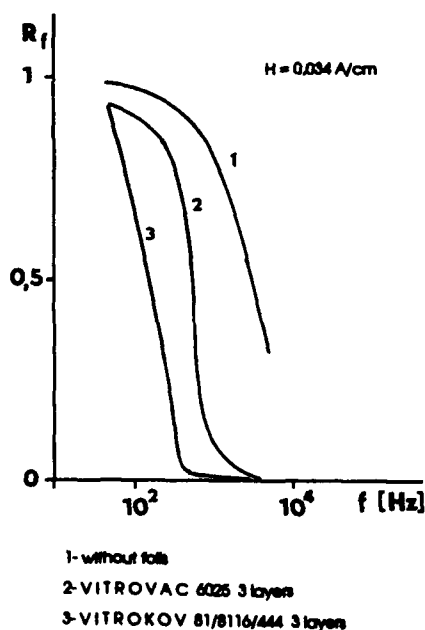
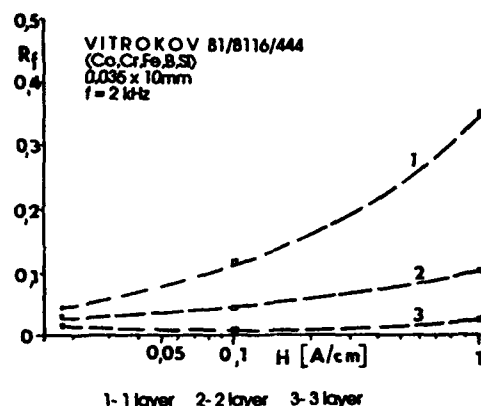
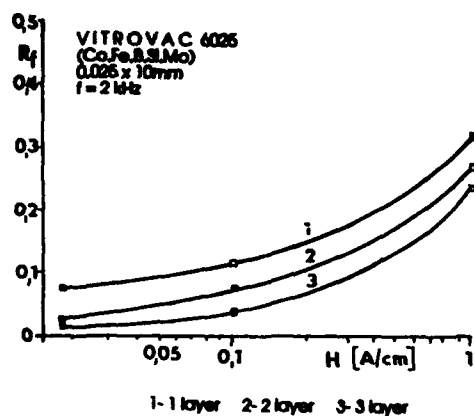


Fig. 4: The typical dependence of R_f on the frequency and the type of screening

According to these results it is in special cases, where is not possible to use optical fibre transmission system, without greater troubles to improve screening effectiveness for example on the control cables in power electric exchanges etc.

Advanced design of air insulating

There are some classical construction design in branch of telecommunication long distance coaxial cables. One of them is with balloon insulation with advantages in continuity of insulation layer between outer and inner conductors in a relationship to the well-known small distance disks construction, which is very wide-spread. And better parameters then the cables with foam polyethylene is in lower dielectric constant. We have tried to modified the balloon insulation design for using in frequency range of CATV cables and to find optimal combination of the balloons construction and foam polyethylene to the outer cavities, or another polyethylene tube by computer simulating on cables with diameter over dielectrics 7,25 - 11,5 and 17,3 mm. DOD is according to IEC. The variant with balloons and tight-fitting tube has been examined experimentally. The measured and calculated values have been in good accordance [4]. For exact calculating of the dielectric constant insulating combination in coaxial cables have been derived

$$\epsilon_r = \frac{2\pi\epsilon_p}{h} + \frac{\frac{d^1}{h} \ln \frac{D_1 + 2\tau_r}{d}}{\frac{1}{\epsilon_p} \ln \frac{D_1 + 2\tau_r}{D_1} + \ln \frac{D_1}{d + 2\tau} + \frac{1}{\epsilon_p} \ln \frac{d + 2\tau}{d}} + \frac{\frac{h - d^1 - 2\tau}{h} \ln \frac{D_1 + 2\tau_r}{d}}{\frac{1}{\epsilon_p} \ln \frac{D_1 + 2\tau_r}{D_1 - 2\tau} + \ln \frac{D_1 - 2\tau}{d}}$$

where D_1 ...diameter over outer conductor
 d ... diameter over inner conductor
 h ... lenght between neighbour small necks of balloon design
 d^1 ... longitudinal thickness of small neck
 τ ...thickness of balloon tube wall
 τ_r ... thickness of tight-fitting tube wall
 ϵ_p ... relative permittivity of PE material (according to IEC it is for solid PE 2,28)

D_1	d	τ	τ_r	h	ϵ_r
7,25	1,742	0,47	0,85	19,4	1,2986
11,5	2,880	0,62	1,00	26,5	1,2255
17,3	4,426	0,82	1,20	36,2	1,1867

Table 2: Optimum construction for selected variant (all dimensions are in mm)

A contribution to the problems of RF coaxial cables attenuation

The calculating relation for attenuation of RF coaxial cables is well-known, for example from IEC 96-0 (appendix 1). It is quite exactly calculating method for coaxial cable in ideal design construction, without impedance and other irregularities and without radiating of EMI to surrounding of the cable. It consists from the first part as losses in metallic conductors and the second part in dielectric losses of the cable.

But there is no ideal construction of outer conductor with 100% screening effectiveness in a real conditions. Considering with the fact that screening factor S is in relationship to screening attenuation

$$\alpha_s = 20 \cdot \log \frac{1}{|S|}$$

it is possible to imagine whole cable length from small samples in the cascade order with defined value of screening attenuation, but with to short length, that each measured attenuation is near zero. Than we can achieve for added part of attenuation relation

$$\alpha_3 = 10 \cdot \log \frac{n \cdot \Delta l}{1 - S^2}$$

The application with these theory has inevitable connection with no any external electric and a magnetic fields, or near any metallic grounded subjects and it has the domination influence for the cables with low losses of signals in conductors and insulation. There are no considering of an EMI from outside of the cable into them, but only from the transmission signal part of coaxial the cable to its surrounding.

The last part of growing to higher value of the attenuation on real coaxial cable is due its systematic small impedance irregularities along the cable [5 - 8]. It is only for very narrow frequency range and these increasing (pike) of attenuation is in many cases a few hundreds % in relation to value of attenuation for the same frequency, but without the pike. The value of the pike is depending on amount of irregularities, or better quantity of the sections between neighbouring changes of the local impedance. By the way attenuation is increasing with length of the cable sample, too. For some of the sample length is dominated only the influence of length and more and more quantity of the impedance unhomogeneity sections is without direct effect. For these l_{min} has been derived

$$l_{min} = \frac{10}{\alpha} \quad (\text{m, dB/m})$$

The repeatable value of pike is possible measured only on the lengths more then l_{min} . For example it is for cables RG 6 and frequency 208,3 MHz 51,2 m and for cables RG 11 and frequency 3,67 GHz 7,9 m. It was derived from real pikes on testing samples of cables for special using.

For the α_4 was derived following relation

$$\alpha_4 = 10 \cdot \log \frac{u}{1 - r^2}$$

where is u ... a quantity of the reflected sections created by distance of the neighbouring impedance irregularities

r ... reflection factor on one the systematic irregularity

The complex view on RF coaxial cable is possible to have according following relation

$$\alpha = \alpha_1 + \alpha_2 + \alpha_3 + \alpha_4$$

where is α_1 ... losses in metallic conductors

α_2 ... dielectric losses in insulation

α_3 ... losses due to EMI radiation through outer conductor

α_4 ... losses due to multireflections of transmitting signal

on systematic distributing impedance irregularities

The last two components of relation have not the same length dependence, like the first two! Frequency dependence α_3 is in range from 30 - 1000 MHz quite neglectable and for α_4 it is typical pike frequency characteristic the attenuation.

Conclusion and applicable of the described acknowledgments

This paper deals with problems of the ageing of RF coaxial cables, for example for CATV application, with some construction design innovation of outer conductors and special type of balloon insulation of RF coaxial cables and in the last part was brief focusing oriented on additional attenuation components on a coaxial cable with a braided outer conductor under operating conditions.

The long time dependence of attenuation increasing in temperature range recommended for using of the CATV cable types is quite surprising. The attenuation increasing more then 100% after already 90 days conducts to use less copper conductors, or to use antioxidant against the copper influence or rising C=O groups in PE.

Described construction design of foil and drain wires of outer conductor of the flexible RF coaxial cables has not only quite high value on the screening attenuation (more then 85 dB), but more higher productivity in relationship to the origin technological process, too. The analysis of the possibility of further use of the conventional balloon insulations of coaxial cables, e.g. in CATV, structure of power coaxial feeders, etc. is given. The variant with balloons and tight-fitting tube has been presented in details.

The contribution on attenuation of real RF coaxial cables is described in the last part of the paper. An increase in the loss due to the radiation of electromagnetic energy through the imperfect outer conductor as well as that caused by multiple reflection of the signal in the coaxial cable is derived. Special attention is paid to the minimum cable length from which the steep rise in the attenuation/frequency characteristic due to multiple reflection of the signal does not increase any longer.

References

- [1] Verbich, O. Job, P.: Recent knowledge on ageing of coaxial cables, EKT, 35, 1982, No.3, p.138-146
- [2] Tsaliowich, A.B.: Braided shield model: Shielding and transmission performance, optimal design, Wire and Cable Symposium, 1981
- [3] Verbich, O. Job, P. Gasparik, P.: A new approach to the possibility of the signal cables magnetic screening research, EMC 88, International Wroclaw Symposium on electromagnetic compatibility
- [4] Verbich, O. Kollarik, P.: Neue Moeglichkeiten der Verwendung von ballonfoermigen Isolierungen fuer Hochfrequenz- Koaxialkabel, ntzArchiv Bd. 9 (1987) H. 3
- [5] Lubars, H. Olisewski, J.A.: Analysis of Structural Return Loss in CATV Coaxial Cables, Seventeenth International Wire and Cable Symposium, Atlantic City (New Jersey) 1968
- [6] Karbowski A.E.: Investigation of Signal Distortion in Cables Caused by Imperfections in Cable Manufacture, Proceedings of the IEEE (June 1974), 1, no.6, 419-431
- [7] Dorezjuk, I.I. Popov, F.F.: RF cables of high uniformity, Svyaz Publisher, Moscow, 1979, 104 pp.
- [8] Verbich, O. Blanarik, M.: Koaxialkabel fuer den Frequenzbereich bis 12,4 GHz und ihre Herstellung in der CSSR, Nachrichtentech., Elektron., Berlin 39 (1989) 5
- [9] Verbich, O.: Erhoehte Wirksamkeit der Abschirmung bei biegsamen Koaxialkabeln, DRAHT UND KABEL PANORAMA, September/Okttober 1990



Otto Verbich received his Dipl.-Ing. degree (as M.S.E.) at the Telecommunication Department of State Technical University in Brno in year 1974. After ten years in Research Institute of Cables and Insulations in Bratislava he achieved PhD degree from Slovak Technical University. He has been working in telecommunication cables inclusive the optical ones in the last years. He is author and co-author of 19 patents and many publications. He had chance to spend in 1990 and 1991 more months in Tokyo Institute of Technology as visiting researcher and a few weeks in AT&T Labs in the last year. He is a member of IEEE and New York Academy of Sciences.

A NEW HIGH-POWER SEGMENTED SEMIFLEXIBLE COAXIAL TRANSMISSION LINE FOR USE AT HF

Hugh R. Nudd

HELIAX® Engineering Division
ANDREW CORPORATION, Orland Park, Illinois 60462, USA.

ABSTRACT

This paper describes the design process for a large (10" OD) coaxial cable for HF broadcast applications with transmitter powers up to 500kW. The new transmission line is semiflexible, and manufactured in flanged lengths which are packed and transported in standard 40 ft. shipping containers. Initial electrical, thermal and structural analyses were performed, and prototypes were built and tested. Electrical, mechanical and thermal tests were also performed on production lengths of the new transmission line, and results are presented. Installation and repair procedures are outlined.

INTRODUCTION

As transmitter powers in HF broadcast systems have increased, problems associated with traditional open-wire transmission lines (e.g. arcing, environmental and personnel safety issues, and coupling between transmission lines) have also increased. Coaxial transmission lines are free from these problems and have found increasing application. The coaxial lines used for high power HF broadcasting must be of large diameter to keep conductor temperatures within acceptable limits. For 500kW transmitters operating up to around 30 MHz, pressurized lines of 9 inch nominal diameter, or larger if unpressurized, are required. Until now, the alternative transmission lines available have been conventional rigid line, or continuous semiflexible line.

Rigid line, commonly used for connections within transmitter buildings, is not generally suitable for long runs to antennas over uneven terrain. Its rigidity makes it difficult and expensive to install, and it is also difficult to accommodate the thermal expansion and contraction which occurs as transmitters are turned on and off. Continuous semiflexible line, on the other hand, must be packed on very large reels of relatively limited capacity. It is inconvenient and expensive to transport to site, and awkward to handle during installation. Also, since typical feeder lengths between transmitter and antenna are of the order of 1km, it is usually

necessary to splice lengths together in the field, which is time-consuming and expensive. Repairs to damaged feeders require similar field splices.

This paper describes the development of a new type of transmission line^[1], designed to overcome these various limitations. The new transmission line is semiflexible, and manufactured in flanged lengths which are packed and transported in standard 40 ft. shipping containers. The outer conductors are annularly corrugated aluminum with welded flanges. The inner conductors are helically corrugated copper fitted with bolted joints, which provide high clamping forces when installed, thus ensuring high reliability. Connections to a 10 inch rigid line interface, employing conventional EIA-style joints, have also been produced.

DESIGN CONCEPT

In order to avoid the major logistical problems in transporting and installing large diameter semiflexible cable, a product was needed that was capable of being shipped in standard 40ft. containers. This, then, requires joints in both outer and inner conductors about every 40ft. Outer conductors are fitted with suitable bolted flanges, as has been done for example with rigid transmission lines for FM and TV broadcast for many years, which ensure high contact pressures at the joints, and suitably high current-carrying capacity. The inner conductor joint design, however, is more critical because of the higher current densities. The joints^[2] comprise threaded fittings at the end of each section. On installation, high torques are applied to the fittings, which provide high clamping forces and high contact pressures. This arrangement is adapted from standard connectorization techniques for semiflexible transmission lines.

The inner conductor and joint together must also accommodate the effects of differential thermal expansion. The inner conductor of any high power transmission line reaches quite high temperatures above the outer conductor because of the resistive losses in the line. For these large HF transmission lines, under extreme conditions of maximum incident power and maximum reflected power from the antenna, the inner conductor can reach a temperature of 150-C at the maximum

specified ambient of 50-C. The outer conductor temperature under these conditions is about 90-C, and the relative expansion of inner with respect to outer has to be accommodated. Semiflexible lines absorb the expansion in the corrugations of the inner conductor.

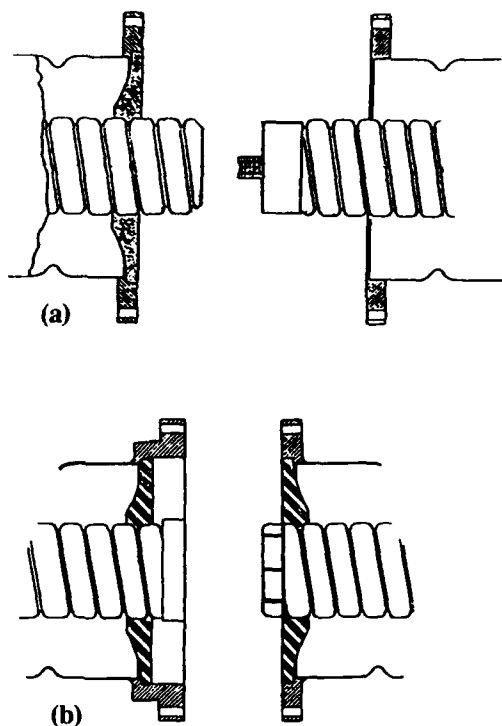


Figure 1
Schematic of (a) standard joint between sections and (b) "EIA" style joint at center of repair section

Now to minimise the loss contribution of the insulators, these large transmission lines have them spaced relatively far apart. With reduced lateral support, then, it is important to ensure that the differential expansion is absorbed evenly along the cable length, and does not all appear at critical locations, e.g. at a bend in the cable, causing electrical problems. For this reason in the new cable the inner conductor is mechanically locked to the outer conductor at each joint by a special insulator^[2]. This insulator, which is helically threaded to match the inner conductor, is also used to pre-tension the inner conductor, which further mitigates the effects of differential expansion.

Because the line is installed section by section, working from transmitter to antenna and fastening each new inner conductor length into the previous one, a special section is required in the event that a length somewhere in the middle of a run becomes damaged. This repair section has standard joints at each end, to connect with the previously installed segments, and an EIA style joint at the center to complete the connection.

The joints between standard sections of transmission line, and in the repair section, are shown schematically in Figure 1.

VSWR CONSIDERATIONS

As is well known in the high frequency transmission line industry, any series of repetitive discontinuities, occurring with a regular separation, will give rise to in-phase reflections, and a high total reflection, at the frequency where the spacing of the discontinuities is one half wavelength, and at harmonics of that frequency. The section length of the transmission line, then, is the appropriate separation for the (very small) electrical discontinuities at each flange joint. Now with the velocity for this type of line approaching 100%, the fundamental "reject" frequency associated with a nominal 40ft length is about 12 MHz, which is in the HF broadcast range (3.9 - 26.1 MHz). The second harmonic is also in the range.

However, not all frequencies in the total range are used. HF (shortwave) broadcast is confined to smaller bands within this range, as shown in Figure 2. It now becomes possible

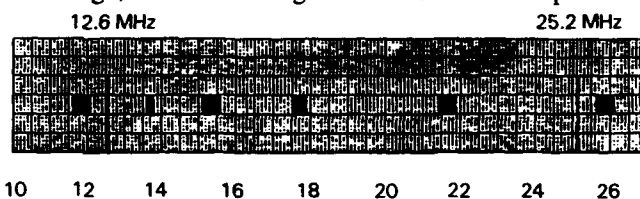


Figure 2
HF broadcast bands and section length reject frequencies

to adjust the section length, knowing the actual cable velocity, to avoid these bands with sufficient margin. With a velocity of 97.5% and section length of 38ft (11.58m) the reject frequencies are at 12.6 and 25.2 MHz. With appropriate electrical design (compensation) of the joint, individual reflections are made small enough so that the reject "spikes" comfortably avoid the operating bands, as predicted by analysis and confirmed in tests (see Section 6).

THERMAL CONSIDERATIONS

A coaxial cable has to be of a sufficient size to handle the required peak and average powers. The calculation of peak power handling from the maximum voltage withstand capability is straightforward. Average power handling capability is limited by dissipation arising from resistive loss in the transmission line, and consequent temperature rise of the conductors. Because in the equilibrium state any dissipation in the inner conductor has to be balanced by a heat flow from inner to outer conductor, the required temperature gradient means that the inner conductor is always the hottest point in the cable. The average power rating is thus the power which causes the maximum permissible inner con-

ductor temperature for long term stability of the dielectric for the stated conditions.

Because we do not readily have access to suitable high power RF transmitters to establish power ratings for large cables, these ratings are routinely established by performing heat tests (conductor temperature rise vs power dissipation) at 60 Hz. Using a suitable computer model, thermal parameters are established by the 60Hz tests, and the behaviour at RF is then calculated.

The basic model for the calculations is shown diagrammatically in Figure 3. The heat flows Q1 through Q5 are determined from dimensions, material characteristics (emissivities for radiation contribution) and the conductor and ambient temperatures using equations available in the literature^[3]. Also the inner and outer conductor dissipations are determined from the current flow, dimensions, frequency and conductivity at the operating temperatures. At HF and lower frequencies, dissipation in the dielectric can be neglected in comparison with that in the conductors. The

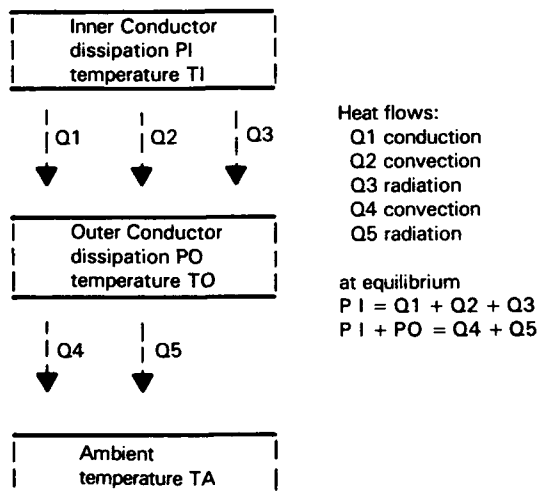


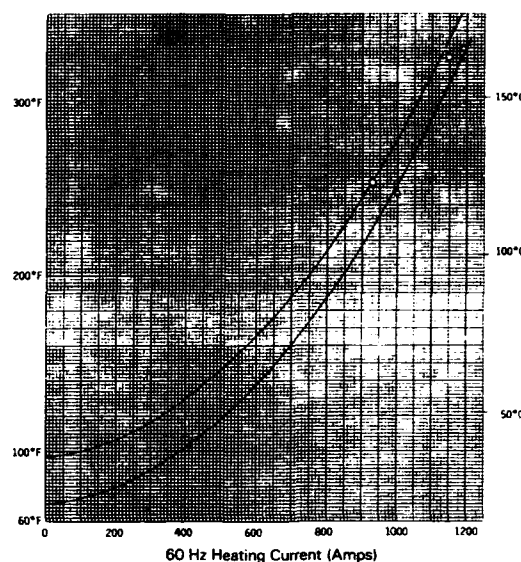
Figure 3
Thermal model

total heat flow between inner and outer conductors must then be equated to the inner conductor dissipation, and the total heat flow from outer conductor to ambient equated to the sum of the dissipations in inner and outer conductors. The various equations can now be solved iteratively by computer to find inner and outer conductor temperatures for given ambient temperature and current (i.e. average power).

Comparison of the calculations of inner conductor temperature with measurements for these 60Hz heat tests is shown for a prototype sample of the line in Figure 4.

CONSTRUCTION

The general construction of the transmission line is shown in Figure 5.



Calculated Curve and Measured Points for Δ 70° F Ambient
Calculated Curve and Measured Points for \circ 97° F Ambient

Figure 4
Experimental verification of thermal model

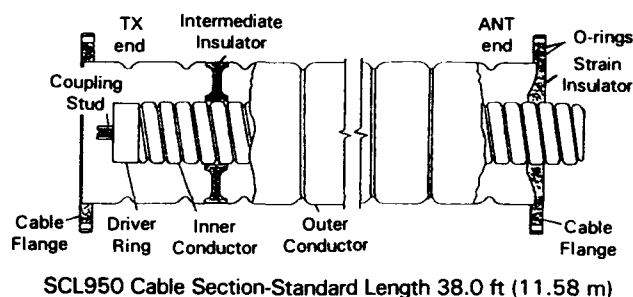


Figure 5
General construction of transmission line

The inner conductor is a seamwelded copper tube, helically corrugated for flexibility. Outer diameter is about 4 inches (100mm), and the tube is manufactured by a conventional seamwelding and corrugating process, similar to that used to make cables with outer conductors of about this size. Inner conductors are cut to length, and fitted at each end with inserts. The inserts are secured by forming the ends of the copper tube over the faces of the inserts, these formed ends thus being clamped between the inner joint parts as the sections are successively installed. The design of the parts provides very high clamping forces and contact pressures for a mechanically and electrically reliable joint, and very high frictional forces to prevent motion and subsequent loosening.

The outer conductor is an annularly corrugated aluminum tube, about 10" (250mm) in diameter, with aluminum flanges welded to the ends. The flange at one end contains grooves for two concentric "O" ring pressure seals. The second "O" ring is redundant, and is provided for increased

reliability since the line is ordinarily operated under quite high pressures (2.5 to 3 bar absolute, 23 to 30 psig) for increased power rating. Outer conductors are painted white to maximise the reflection of incident solar radiation, whilst giving good emissivities at the infrared wavelengths associated with normal temperatures. This maximises power ratings.

Ordinary "spacer" insulators are provided at intervals along each section. These are made from PTFE resin, and are restrained in position by the corrugations of the outer conductor. Special "strain" insulators are provided at each flange joint. These are also made from PTFE resin, and are designed to mechanically lock the inner and outer conductors at these points and to pre-tension the inner conductor, for control of differential expansion effects (see Section 2).

Connectors have aluminum outer bodies with machined aluminum flanges. Inner connector parts are silver-plated brass, and insulators are PTFE resin.

TESTS

The main test groups were mechanical and structural, low power electrical and high power electrical and thermal tests.

Mechanical and structural tests performed were pressure withstand, pressure sealing and fatigue resistance (a verification that repeated small dimensional changes resulting from pressure and temperature cycling would not cause fatigue of the outer conductors and failure). Pressure withstand and sealing tests were conducted on prototypes, and demonstrated acceptable performance with comfortable safety margins, and these tests are incorporated into the manufacturing process, as is usual with this type of product. Outer conductor fatigue tests were performed by building a suitable apparatus to generate the small longitudinal movements, and cycling over an extended period. No evidence of fatigue was found after a simulated exposure of 50 years, which is at least double the anticipated service life of the product.

Low power electrical tests performed were impedance (TDR), return loss (for VSWR), attenuation, and high voltage and leakage resistance. Expected values were confirmed, and return loss and attenuation results are shown in the plots of Figures 6 and 7 respectively. Measured return loss (ignoring the section length "spike" at 12.6 MHz) was better than 36dB for this length, and calculated attenuation was 0.76 dB/km at 26.1 MHz.

The final product testing involved confirmation of the average power handling capability using representative RF power levels from the appropriate transmitters. These tests were performed as part of first article testing of transmitters, switch matrices, and other transmission line components, at

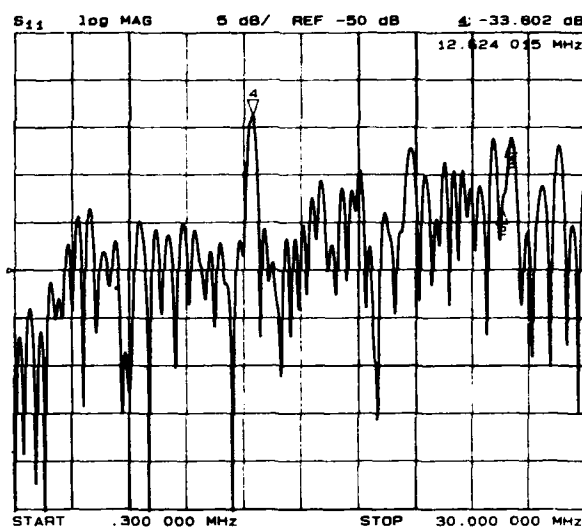


Figure 6
Return loss for prototype run of
31 sections (1178 ft)

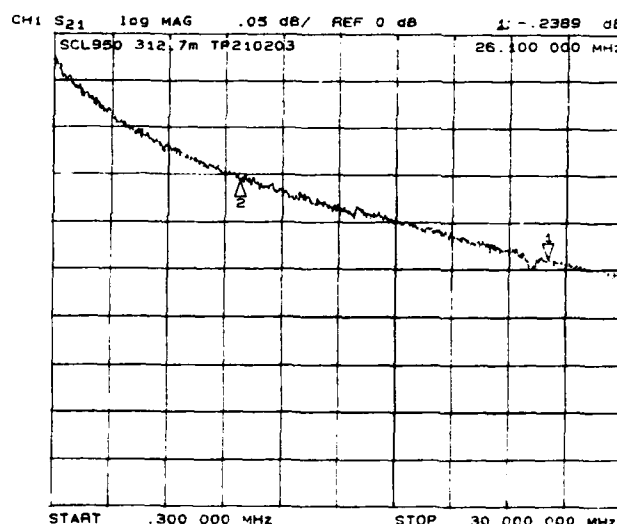


Figure 7
Insertion loss for run of 27 sections (1026 ft)

the premises of the transmitter manufacturer. As discussed in Section 4, a thermal model was established by which conductor temperatures could be determined for various conditions of applied 60Hz current, or applied RF power, and the model had been verified by 60Hz tests. Now the model was used to determine inner and outer conductor temperatures for the conditions of the RF test.

Before insertion of three sections of transmission line into the RF test assembly, adhesive temperature sensors were affixed at intervals to the inner conductors. These sensors have regions which darken successively as the temperature is raised, and the temperature reached can thus be sub-

sequently determined within a fairly close range. Temperature sensors were also fixed to the outer conductors at intervals. Then the transmitter was operated at known power into a known mismatch, i.e. significant RF power was reflected. In these conditions, the combination of currents associated with forward and reverse waves gives a current standing wave with maxima and minima at localised points along the line. This gives rise to conductor temperature maxima and minima, whose values can be calculated from the thermal model. Figure 8 shows the calculated conductor temperatures along the line, and the measurements subsequently determined from the sensors (to read the inner conductor sensors, it was necessary to disassemble the line). The odd shape of the calculated curve arises because it is a composite for two separate runs at different frequencies. The sensors monitor the maximum temperature reached in either run. The good agreement again verifies the thermal model, this time for the RF case, and establishes the average power ratings determined from it.

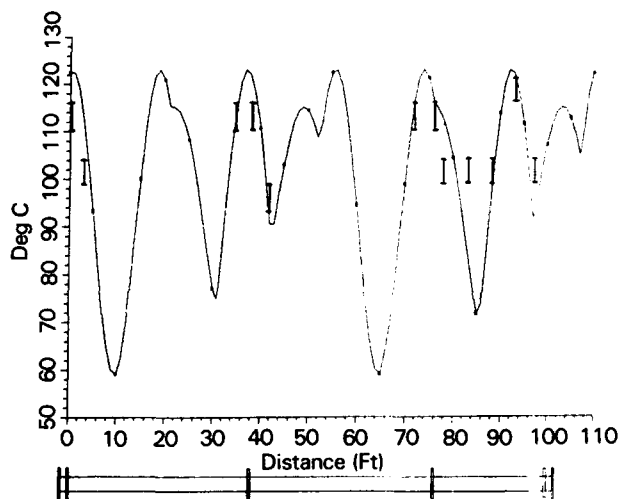


Figure 8
Measured on predicted inner conductor temperature along length of cable for RF heat test

SHIPPING

Suitable packaging was designed to store and ship the coaxial transmission line in standard 40 ft. containers. Depending on the internal structure, a single container can hold up to 34 or 36 sections (as six layers of six sections). Loading of a container is shown in process in the photograph of Figure 9.

Extensive tests of the packaging methods were performed by trucking container loads of transmission line sections over long distances, and over different road conditions. Lengths were shipped under pressure, which was subsequently monitored to verify that no leaks had developed. Additionally, mechanical inspection and electrical testing

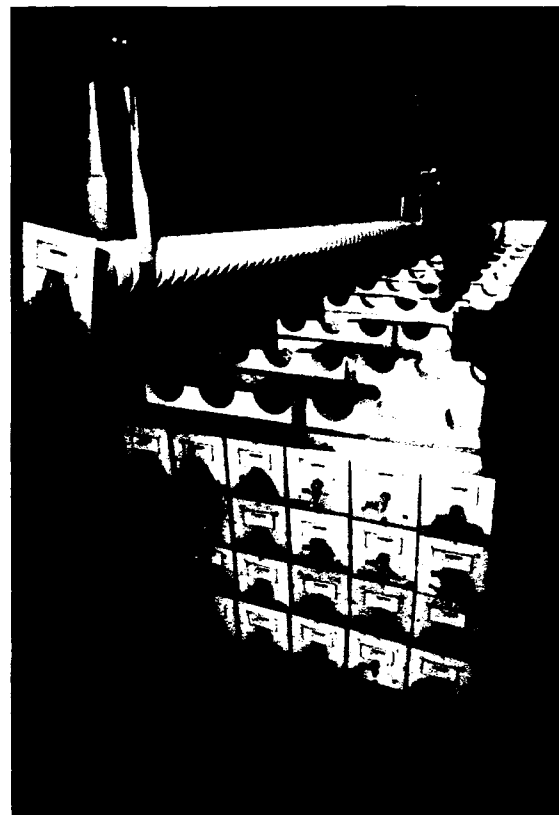


Figure 9
Loading a shipping container

before and after transportation confirmed the suitability of the packaging.

INSTALLATION

First installation experience with this new transmission line came in setting up trial runs of about 30 sections (350m) for VSWR and attenuation testing (see Section 6). Appropriate tools and procedures were developed, especially for the critical inner conductor joint. This run was set up as a large loop, to have the ends of the cable close together for attenuation measurement, and was configured as straight runs plus sections bent to the minimum bend radius. A portable tool to aid bending of the curved sections was devised, and use of this tool in the field installation is shown in Figure 10.



Figure 10
Bending tool

Also, before first shipment of the product, more formal trial installations were performed. Steelwork representative of high and low level supports at an HF broadcast station was set up, and sections comprising high and low level runs, and the flexed transition between them, were installed. These trials confirmed the suitability of the hangers and the support system.

A trial repair procedure, involving removal of a line section and replacement by the special repair section (see Section 2), was also performed using this installation. This involves cutting away a damaged section, unfastening the joints, and attaching the special repair section at both ends. Finally, the EIA style connector at the center of the section is mated to complete the repair.

Figure 11 shows installation in process for a number of runs at a high-to-low transition at a new HF broadcast site in Morocco, and Figure 12 shows part of the installation of



Figure 11
Cable runs on high-to-low transitions

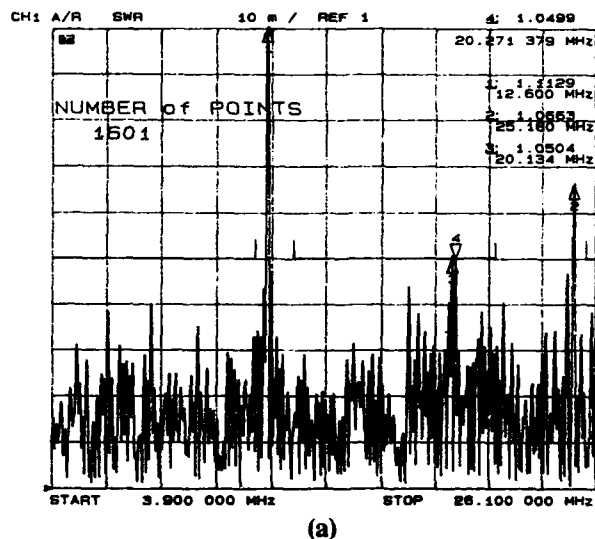


Figure 12
Cable runs on high level support
(installation in process)

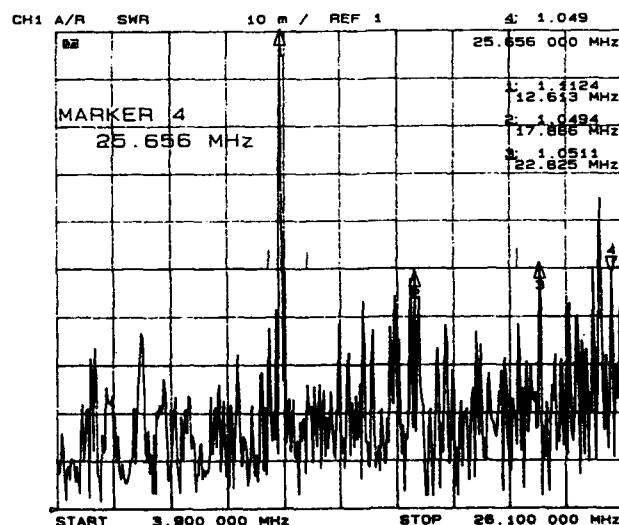
multiple runs on high level supports, again at the Morocco site.

SITE TESTS

After installation at site, all runs (about twenty in number, of average length about 800 m) were electrically tested. Performance after this large installation project was satisfactory, and as predicted from initial test data generated during development. Installed VSWR's for two of the longer runs is shown in Figure 13. The system requirement of 1.05 VSWR for the installed feeder (ignoring the section length "spikes") is met.



(a)



(b)

Figure 13
Measured VSWR's for installed runs
of (a) 1343m and (b) 1413m

CONCLUSION

A new large-diameter semiflexible coaxial transmission line for use at HF broadcast frequencies has been developed, manufactured and installed. This new line overcomes major problems of transportation, installation and repair to which conventional large diameter transmission lines are subject.

ACKNOWLEDGEMENTS

The successful conduct of a major development program such as this is the result of important contributions from many people. I would like, however, especially to mention Messrs Sid Bennett and Eric Brooker, who are largely responsible for the concept, and who gave much help and encouragement during the course of the project. Also, I would like to recognize the contributions of colleagues (and one ex-colleague) in the Engineering departments at Andrew Corporation; Messrs B.Burts, V.Chopra, B.Carlson, G.Frigo, J.Krabec, J.Midkiff, J.Paynter, H.Rosenmayer and J.Williamson. Finally, I would like to thank the management of Andrew Corporation, HeliAx Products, for supporting the publication of this paper.

REFERENCES

- [1]Andrew Corporation, Bulletin No 1623, "Andrew SCL semi-flexible coaxial cable for high power HF, MF and LF broadcasting stations", 1990
- [2]U.S. Patent No. 4,831,346
- [3]H.Martin. "High Power Radio Frequency Coaxial Cables; Their Design and Rating". Proceedings of the 22nd International Wire and Cable Symposium, 1973.



Hugh Nudd is Manager, Design Engineering, HELIAX® Products, with Andrew Corporation.

He graduated with honors degree in Physics from the University of Oxford, England in 1965 and joined the General Electric Company Ltd. (U.K.) to work on the design and development of microwave components, mainly for trunk radio systems. In 1975 he moved to Marconi Space and Defence Systems to work on microwave components and sub-systems for satellite communications.

He joined Andrew Corporation at their Lochgelly, Scotland, plant in 1978, transferring to the Orland Park, Illinois headquarters in 1982. Since 1983 he has been responsible for design engineering for the HELIAX® coaxial cable and waveguide product line.

INFLUENCE OF FREQUENCY ON THE TEMPERATURE RISE OF SHORT CIRCUITED ELECTRIC CONDUCTORS

W.Z. Black*

Bruce B. McWhorter**

* George W. Woodruff School of Mechanical Engineering
Georgia Institute of Technology
Atlanta, GA

** Thiokol Corporation
Brigham City, UT

ABSTRACT

When a conductor experiences a short-circuit waveform that has a high frequency, the current distribution can be highly non-uniform as a result of the skin effect in the conductor. In this situation the conductor can experience large variations in localized heating and temperature gradients across the conductor can be significant. This paper formulates a thermal model that accounts for spatial as well as time varying temperatures and compares the predicted temperature distributions as a function of current, frequency, short-circuit duration and conductor properties. The results show that for frequencies of 60 Hz and less, the traditional adiabatic thermal model based on uniform current density will give reasonable results for the maximum conductor temperature. However, at higher frequencies the uniform current density model can significantly underpredict the maximum temperature of the conductor. Temperature rise curves are presented for several common ACSR conductors as a function of the waveform frequency. As the frequency increases, the surface temperature rise of a conductor can significantly surpass the value predicted for the same conductor experiencing a short-circuit with the same value of I^2t but with a lower frequency. Therefore damage to a conductor as a result of excessive temperatures can be grossly underpredicted by the traditional equations if the conductor is shorted with a current waveform that contains high frequency components.

INTRODUCTION

Traditionally, the temperature rise of an electric conductor subjected to a short duration current surge has been calculated on the basis of a model that assumes all ohmic heating is distributed uniformly across the conductor and none of the heat is transferred from the surface of the conductor strands. These assumptions greatly simplify the calculation of the conductor temperature rise and they result in a very simple expression for the average temperature of the conductor cross-section. This type of model, often referred to as the adiabatic model, is a good one from the design standpoint, because it leads to a maximum calculated temperature rise. It therefore provides a conservative design standard so that a conductor can be selected that will not be damaged during a given short-circuit event.

This paper examines the problem of calculating the temperature rise in electric conductors when they are subjected to short-circuit events in which the current waveform has a variable frequency. At low frequencies the conductor skin effect is negligible and the current distribution is uniform across the conductor cross-section. Ohmic heating is therefore uniform at low frequencies and the traditional adiabatic temperature rise model provides a good estimate for the temperature as long as the duration is short enough so that a negligible amount of heat is transferred from the surface of the conductor. However, as the frequency of the current surge increases, the skin effect becomes appreciable and the heating within the conductor will begin to concentrate more toward the outer strands. Eventually a situation will arise in which the localized heating will result in a temperature rise near the surface that can significantly exceed the maximum temperature predicted by the adiabatic model.

The thermal model presented here has the capability of calculating the local temperature rise in a conductor when it carries a fault or overload current with a known frequency. The local current density in the conductor is first determined as a function of time and radial position in the conductor. These calculations can be made for any current waveform, provided a single dominating or fundamental frequency can be assumed for the given waveform. The model considers the skin effect as a function of frequency and it is capable of determining the temperature rise for two material conductors such as ACSR and SSAC, as well as single material conductors such as AAC and AAAC. Convection and radiation heat transfer are assumed to occur from the conductor during the short-circuit event. The equations which result from the application of the thermal model are solved numerically and the results are compared with the predictions of the traditional adiabatic model. The comparison reveals frequencies which result in localized heating and produce surface temperatures in excess of the maximum temperatures predicted by the adiabatic model.

THERMAL MODEL

The instantaneous, local temperature in a conductor can be determined by applying the principle of energy conservation to the stranded conductor. This process leads to the differential equation

$$\frac{1}{r} \frac{\partial}{\partial r} \left(kr \frac{\partial T}{\partial r} \right) + q_{gen}'''(r, t) = \rho c_p \frac{\partial T}{\partial t} \quad (1)$$

where $q_{gen}'''(r, t)$ is the heat generated within the conductor on a per unit volume basis. This equation assumes that the conductor temperature is only a function of radius r and time t . That is, it is not a function of axial position or angle around the conductor. This assumption implies that the model is unable to predict localized temperature at the point where the short may occur, because the temperature is assumed to be independent at distance along the conductor. The term q_{gen}''' is the rate that heat is generated in a unit volume of the conductor which is assumed to be a function of both radius and time. In this analysis the thermal conductivity k and the specific heat at constant pressure c_p of the conductor material are both assumed to be linear functions of temperature, but the conductor density ρ is assumed constant.

The Ohmic heating term per unit volume of conductor can be expressed as

$$q_{gen}''' = (I'')^2 \rho_{e20} [1 + \alpha_e (T - 20)] \quad (2)$$

where I'' is the current density, ρ_{e20} is the electric resistivity at 20°C and α_e is the temperature coefficient of resistance of the conductor material. The current density in the conductor is strongly influenced by the skin effect which in turn is a function of the frequency of the current waveform. At low frequencies the skin effect is negligible. At higher frequencies, the skin effect can be significant causing the

outer portion of the conductor to carry the majority of the current while the center strands carry practically no current.

The temperature rise experienced by a conductor that is subjected to a short-duration current transient is a function of the energy available in the current pulse. If the short-circuit current waveform is assumed to occur as a step function to a constant current I for a total time t , the energy in the pulse is simply proportional to $I^2 t$. Unfortunately most high current events can induce very complex current waveforms on overhead conductors. The waveform is rarely, if ever, one of constant current and many high current transients produce a current waveform that has multiple peaks. The complexity of the problem is further complicated by the fact that reflections of the waveform from structures such as towers can cause distortions of the current waveform. The model assumes a single or fundamental frequency can be selected from the waveform.

Once the current waveform and frequency have been selected, the distribution of current over the conductor cross-section must be calculated so that localized heating caused by the skin effect can be evaluated. Reference 2 gives a numerical procedure that can be used to determine the current density in a stranded conductor as a function of outer radius and frequency. The analysis presented here assumes that the current density is uniform in each layer of strands and the magnetic flux created by the spiraling of the strands is negligible compared to the flux resulting from the longitudinal current flow. Furthermore it assumes that there is no saturation of magnetic material of the conductor. The procedure first calculates the geometric mean radius d_i and self reactance x_i of each stranding layer i . These quantities can be determined from

$$d_i = [N_i a_i c_i^{(N_i-1)}]^{1/N_i} [\exp(-\mu_i / 4 N_i)] \quad (3)$$

and

$$x_i = 0.00466 f \log \left[\frac{\lambda^{(\mu-1)} r_c^\mu}{d_i^\mu} \right] \quad (4)$$

where the symbols are defined in the Nomenclature section. If no magnetic core is present in the conductor, Eq. 4 reduces to

$$x_i = 0.00466 f \log(r_c / d_i) \quad (5)$$

After the self reactance of each layer is determined, the resistance R_i of each layer is calculated from

$$R_i = \frac{\rho_{20}}{A_i} [1 + \alpha_s (T - 20)] \quad (6)$$

Assuming that there are no other current carrying conductors nearby, the total voltage drop for each conductor layer ($i = 0, 1, 2, \dots, n$; $i = 0$ represents the center strand) caused by the resistance and self-reactance of each layer is

$$V_i = \sum_{k=0}^i (R_k \delta_k + j x_k) I_k + \sum_{k=i+1}^n (j x_k) I_k \quad (7)$$

for $i = 0, 1, 2, 3, \dots, n$

The RMS currents in each layer are unknown quantities. Since each stranding layer in the conductor experiences the same voltage drop, $V_0 = V_1 = V_2 = \dots = V_n$. The series of equations (7) can now be expressed as

$$R_0 - m_i R_i + j(x_0 - x_i) + \sum_{k=1}^i m_k j(x_k - x_i) = 0 \quad (8)$$

$i = 1, 2, 3, \dots, n$

where

$$m_i = \frac{I_i}{I_0} \quad (9)$$

Equation 8 is a system of n algebraic equations and n unknowns $m_1 \dots m_n$. Once these values are calculated, the individual currents in each layer can be determined by using Eq. 9 and the following relation between I_0 and the total fault current I_T .

$$I_0 = \frac{I_T}{1 + m_1 + m_2 + \dots + m_n} \quad (10)$$

Once the variation of current with radius and time is determined, Eq. 1 can be used to predict the influence of localized heating on the conductor temperature.

The solution to Eq. 1 requires the application of two boundary conditions and a single initial condition. The first boundary condition requires that the centerline is an axis of temperature symmetry or

$$\frac{\partial T}{\partial r} = 0 \quad \text{at } r = 0 \quad (11)$$

and the second boundary condition results from the knowledge that the heat removed from the surface of the conductor at $r = r_c$ leaves via the radiative and convective modes.

$$-2\pi r_c k \frac{\partial T}{\partial r} = q_{\text{conv}} + q_{\text{rad}} \quad \text{at } r = r_c \quad (12)$$

Where q_{conv} and q_{rad} are the heat transfer rates per unit length in the conductive and radiative modes. The convective contribution at the surface of the conductor can be evaluated using standard Nusselt number correlations and the radiative flux can be determined by applying the Stefan-Boltzmann law. Details of these calculations can be found in Ref. 3.

Finally, the initial temperature distribution is assumed to be a known function of radius corresponding to the steady state temperature in the conductor for a known, constant current.

$$T(r, t) = T_0(r) \quad \text{at } t = 0 \quad (13)$$

The energy equation was solved in finite difference form by using a method consisting of a combination of a Crank-Nicolson method and a predictor-corrector routine. The error expected from this technique is on the order of $\Delta t^2 + \Delta r^2$. This method provides the temperatures as a function of total fault current, frequency, radius and time. Additional information that must be specified before the temperatures can be calculated are the conductor geometry, conductor thermal and electrical properties and the fault current frequency. The numerical procedure is an iterative one, because quantities such as k , c_p and both the radiative and convective heat fluxes from the surface are functions of the unknown conductor temperature. Furthermore the procedure allows the total fault current I_T to be incremented in time steps of Δt so that any current-time functionality can be approximated with a series of ramps and steps. Details of the numerical scheme used to solve Eq. 1 are given in Refs. 3 and 4.

The numerical results were verified by comparing the predicted temperatures with those resulting from similar problems with known solutions. The first check involved a comparison of the predicted temperatures with those of the adiabatic model. This comparison required that the convective and radiative heat losses from the surface were set to zero and that the effective thermal conductivity of the strands were set to a very high value so the model produced isothermal conditions across the conductor. The difference between the temperatures for the two models was less than 4% [4].

The second comparison was made with a known steady-state temperature distribution of a conductor which has a known surface temperature and a uniform current distribution (see Ref. 5 pg. 72). The difference between the known temperature distribution and the numerical results were less than 0.5% for all locations in the conductor [4].

A final check of the model consisted of a comparison of the temperature histories with those predicted by a program called DYNAMP which is part of the EPRI TLWorkstation software package [6]. The DYNAMP program ignores temperature gradients within the conductor, but it is capable of predicting the changes in conductor temperature as the current or weather conditions vary with time. The differences between the thermal model discussed here and the temperatures predicted by DYNAMP were negligible [4].

ADIABATIC MODEL

The adiabatic model assumes no heat loss from the surface of the conductor and it traditionally has been used to predict the maximum temperature rise of the conductor for a given value of I^2t [7]. The maximum average temperature rise of the conductor can be calculated from a special form of Eq. 1 because the adiabatic model results in an isothermal conductor. In this case there are no temperature gradients within the strands and the first term in Eq. 1 is zero. Therefore the adiabatic model energy balance reduces to

$$q_{gen} = \rho c_p \frac{dT}{dt} \quad (14)$$

where the energy generation per unit volume of conductor is given by Eq. 2. Substituting Eq. 2 into Eq. 14 followed by simplification results in a modified adiabatic energy equation of

$$I^2(C + BT) = m' c_p \frac{dT}{dt} \quad (15)$$

where m' is the mass of the conductor per unit length or

$$m' = \rho A_m \quad (16)$$

where A_m is the cross-sectional area of the metal in the conductor and the constants B and C are defined as

$$B = \frac{\rho_{e20} \alpha_e}{A_m} \quad (17)$$

and

$$C = \frac{\rho_{e20}}{A_m} (1 - 20\alpha_e) \quad (18)$$

The solution to the differential equation (15) subject to the initial condition

$$T = T_0 \text{ at } t = 0 \quad (19)$$

is

$$T_{max} = \frac{(C + BT_0)e^{(BI^2t/m'c_p)} - C}{B} \quad (20)$$

where the symbol T_{max} is used to denote the temperature of the conductor calculated by the adiabatic model and the constants B and

C are given in Eqs. 17 and 18. The definition of the remaining symbols is listed in the Nomenclature section. This equation is identical to Eq. 7 in Ref. 7 and it is the same equation used to develop the temperature curves in Chapter 6 of Ref. 8.

The temperature given by Eq. 20 shows that the maximum temperature in a shorted conductor is a function of the conductor design and the energy available in the short-circuit current. There are three important parameters relating to the design of the conductor: the two electrical characteristics given by the constants B and C and a thermal parameter given by the product $m'c_p$, which is a measure of the thermal capacitance of the conductor material. The energy available in the current is quantified by the single term I^2t as long as the frequency of the waveform is less than about 60 Hz. For higher frequencies the temperature rise in the conductor is also a function of the waveform frequency.

RESULTS

The model and procedure described above was formulated into a computer program that generated current and temperature distributions throughout the conductor as a function of total current and frequency. The procedure described in Ref. 2 was used to calculate the current density in stranded conductors and a set of typical current distributions is shown in Fig. 1 for a AAC Marigold (1113 kcmil) conductor and in Fig. 2 for an ACSR Curlew (1033 kcmil) conductor for 60 and 1000 Hz current waveform frequencies. The current waveform selected for these examples was a step change from 1000 amps to 150,000 amps. This example is presented not as a realistic fault but rather as a method of demonstrating the influence of frequency on the temperature profile in the conductor. The location of the various stranding layers is superimposed on Figs. 1 and 2 to illustrate the radial position where the current density changes in step-fashion. For both conductor designs, the current densities are nearly uniform at 60 Hz, but the skin effect is quite evident at a frequency of 1000 Hz. Regardless of frequency, the current density in the AAC conductor is more uniform than in the ACSR conductor due to the more uniform electric resistivity of the aluminum strands compared to the combination of steel and aluminum strands that exist in the ACSR design.

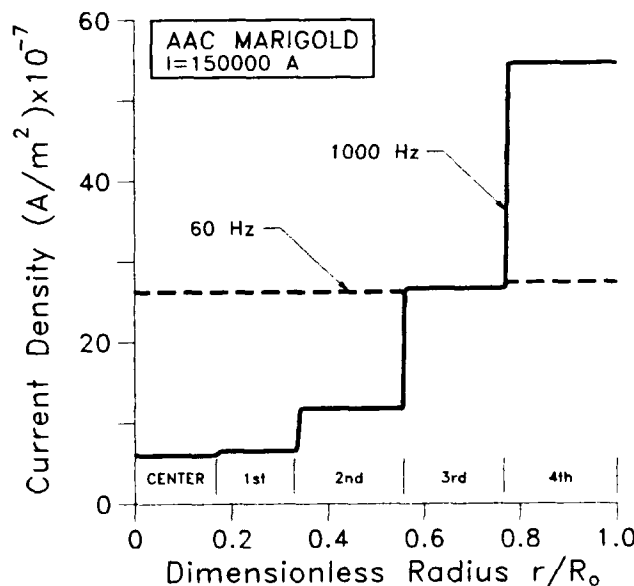


Figure 1: Current Density as a Function of Radial Position in an AAC Marigold Conductor for Frequencies of 60 and 1000 Hz

The non-uniform current density distributions shown in Figs. 1 and 2 lead to localized heating in the conductor which causes the conductor to be hotter on the outer surface than near the center. As long as the current is maintained over a relatively short period of time, the heat does not have sufficient time to transfer from the surface to the center, and localized hot regions will develop over the cross-section of the conductor. When the short-circuit exists over a longer period, there is a tendency to level the large temperature gradients that can exist early in the short-circuit event, and the temperature of the conductor becomes more uniform.

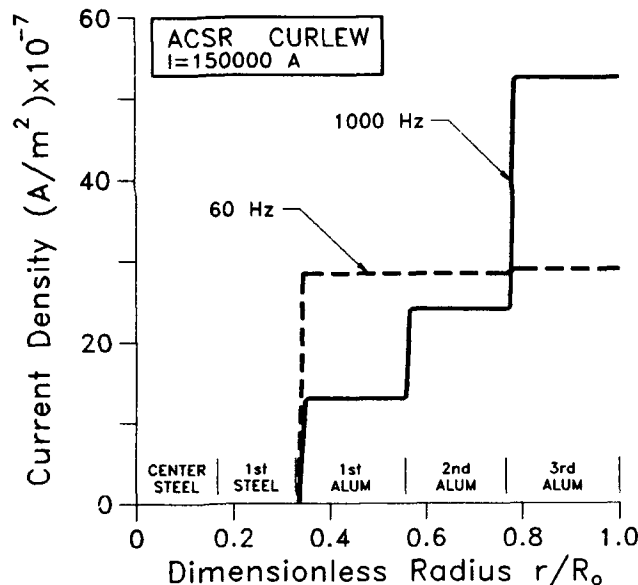


Figure 2 Current Density as a Function of Radial Position in an ACSR Curlew Conductor for Frequencies of 60 and 1000 Hz

Figures 3 and 4 show the type of temperature distributions that can exist in a stranded conductor when it experiences a low, medium and high frequency fault. The current is assumed to increase from 1000 to 150,000 amps in a step fashion and the curves reflect the conductor temperature after 0.0167 sec (1 cycle at 60 Hz). Results in Fig. 3 are the temperature rise for an AAC Marigold and Fig. 4 are for a ACSR Curlew. The uneven temperature distribution resulting from the skin effect is quite evident, and even at 60 Hz it is particularly strong for the ACSR Curlew conductor which has a high resistance steel core.

The adiabatic temperature curves are horizontal lines in Figs. 3 and 4, because the adiabatic model is able to predict only the average conductor temperature, and it assumes a constant current density across the cross-section of the conductor. At low frequencies, like 60 Hz, the adiabatic model does not seriously underpredict the conductor temperature. However, when the conductor experiences a high frequency fault the results are completely different. In the event of a high frequency fault, the adiabatic model can significantly underestimate the maximum surface temperature and therefore it is not an adequate model to warn of the damage to the conductor that may result during a high frequency event.

The thermal model was also used to develop a series of curves that predict the temperature rise of the conductor as a function of I^2t where the quantity is defined as

$$I^2t = \int_0^t I^2(t) dt$$

when the current during the short-circuit event is a function of time. Typical results of this exercise are shown in Fig. 5 for an ACSR

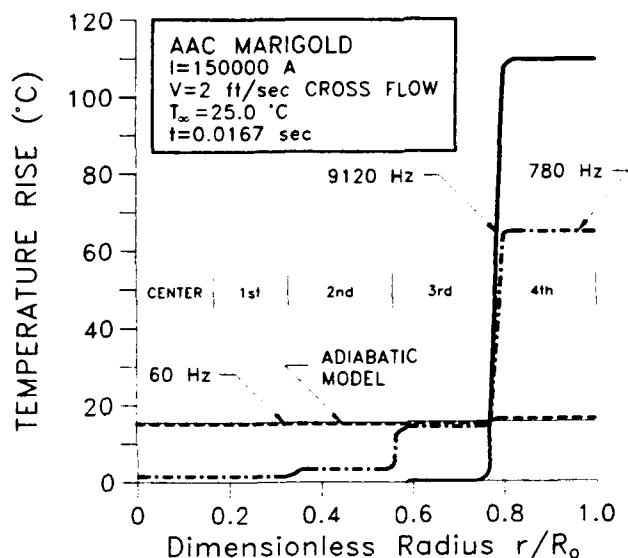


Figure 3 Temperature Distribution in an AAC Marigold Conductor Faulted with a Current of 150,000 Amps at Different Frequencies

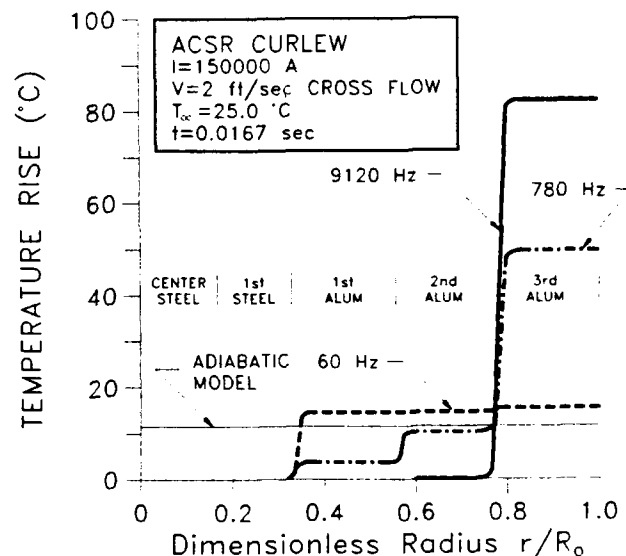


Figure 4: Temperature Distribution in an ACSR Curlew Conductor Faulted with a Current of 150,000 Amps at Different Frequencies

Conductor (795 kcmil) conductor faulted with a current that has a frequency of 1000 Hz. The various curves that appear in Fig. 5 are surface temperatures that result from different fault durations. The first curve applies to all faults that have a duration of less than one second regardless of current level. Faults with durations greater than about one second provide an opportunity for heat to be transferred from the outer strands to the cooler inner strands and to the environment, thereby reducing the magnitude of the temperature rise. Additional curves in Fig. 5 show that the temperature rise for a fault with a duration greater than one second is always less than the temperature rise for a fault with equal energy (equivalent value of I^2t) that lasts for less than one second. These results suggest that the adiabatic model can be used to accurately predict the temperature rise of a conductor as long as the fault duration is less than one second and as long as the skin effect is small enough to cause a uniform current

distribution. Faults that last greater than about one second provide sufficient time for heat transfer from the surface of the conductor to influence the temperature. Therefore for longer duration faults, a more complex thermal model than the simple adiabatic model must be used to accurately calculate the conductor temperature.

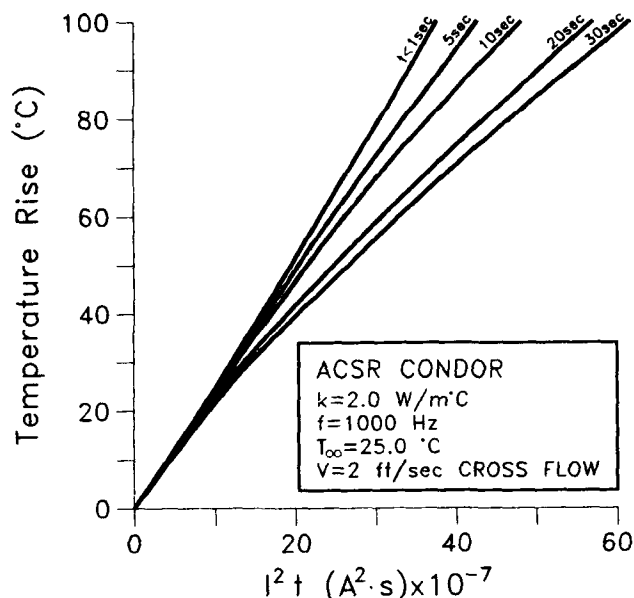


Figure 5: Surface Temperature Rise as a Function of I^2t for a ACSR Conductor Faulted with a 1000 Hz Current of Varying Duration

The curves in Fig. 6 illustrate the influence that the fault current frequency has on the surface temperature rise of three representative ACSR conductors. These curves can be used to determine the temperature rise of a conductor under a fault with a known frequency and a known value of I^2t . The influence of frequency is due solely to the uneven current density that becomes stronger at higher frequencies.

The thermal model can be used to predict the conductor temperature during the short-circuit event as well as after the current flow has ceased. The previous results (Figs. 3 and 4, for example) have shown that large temperature gradients can exist in a conductor during the short duration, high frequency fault. If the fault current ceases and the conductor is then allowed to cool, these large gradients will eventually disappear as heat is transferred through the high conductivity metal from the hot outer layer to the cool inner strands.

Figure 7 shows typical results of this cooling process for a Drake (795 kmil) conductor. The temperatures are plotted starting at $t = 0$ immediately after the fault current ceases resulting in a surface temperature that is 100° C greater than the central core. For this rather severe initial temperature difference, about one minute elapsed before the surface becomes cooler than the center and heat begins to be transferred from the center of the conductor to the surface where it is removed by radiation and convection to the surrounding air. Prior to this time the heat is conducted toward the center of the conductor, thereby smoothing the large temperature gradients that exist in the conductor immediately after the application of the fault current. These results show that the uneven temperature gradients in a faulted conductor can exist for several minutes depending upon conductor size, conductor type and fault current frequency. During this time interval damage to the conductor such as annealing and high temperature creep would result and both of these detrimental effects are not predicted by the adiabatic heating model.

The thermal model can be used to calculate the temperature rise of an overhead conductor that is hit by a lightning strike. The

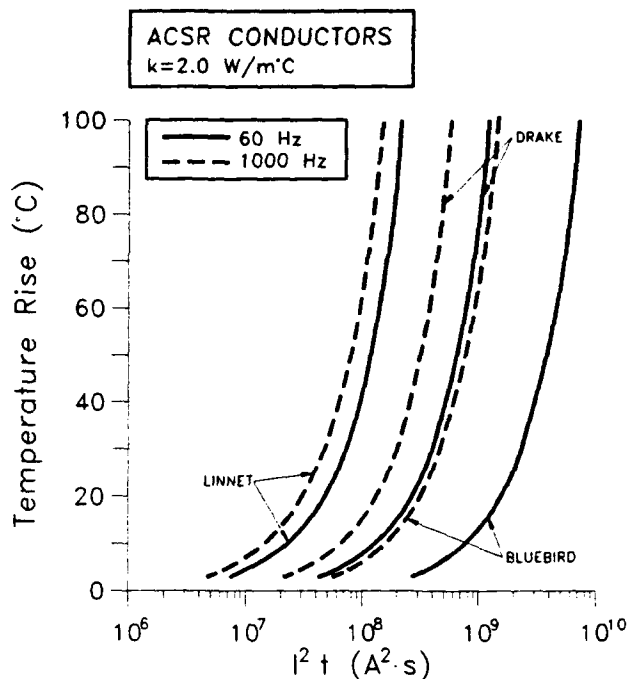


Figure 6: Surface Temperature Rises for Three ACSR Conductors as a Function of I^2t for 60 and 1000 Hz

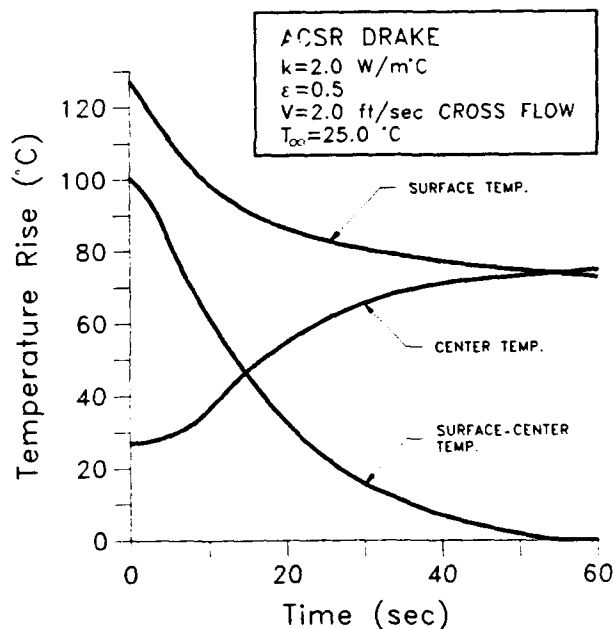


Figure 7: Cooling of an ACSR Drake Conductor Showing Temperature as a Function of Time

results presented here are representative of the temperature rise in the conductor a sufficient distance from the point where the lightning contacts the conductor such that the current distribution can be predicted by Eqs. 3-10. They are not intended to predict the temperature of the conductors at the point of contact. The current as function of time induced in the conductor must first be determined. For this analysis a simplified and ideal triangular waveform was

assumed and an estimate of the typical current frequency corresponding to the waveform equal to one-fourth the inverse of the rise time was used. This assumption provides an example of the single frequency that is necessary for the application of the thermal model. While this assumed waveform may seem over-simplified, it is commonly used to simulate the thermal, electrical and mechanical behavior of overhead lines when they are struck by lightning [1].

Rarely do lightning flashes induce currents greater than 200 kA and the rise time of most current waveforms is on the order of 1.0 - 2.0 μsec with the total duration of the waveform approximately 100-200 μsec [1]. In addition, most lightning strikes consists of multiple strokes with three strokes being a reasonable average [1]. Therefore, a reasonable current waveform on an overhead conductor that has been struck by a severe lightning strike is shown by the three multiple triangular curves shown in Fig. 8. Since waveforms with multiple current peaks are common, an induced current with three identical waveforms was selected to represent an upper limit for temperatures that can result in an overhead conductor which is struck by a very intense lightning bolt. Since the assumed rise time for the waveform is 2 μsec , the frequency of the waveform was estimated to be 125 kHz.

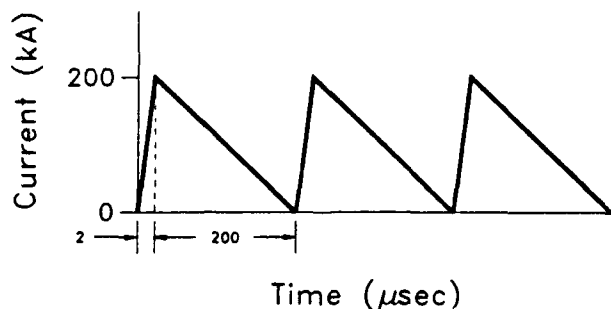


Figure 8: Idealized Current Waveform for Severe Lightning Strike

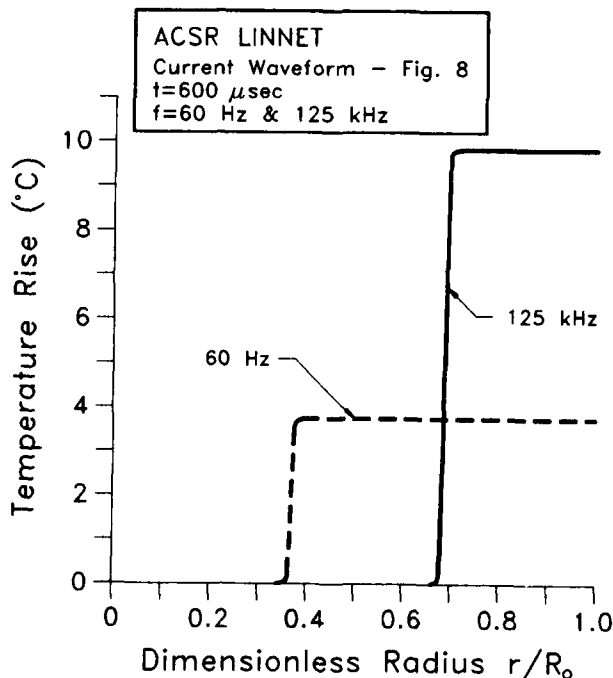


Figure 9: Temperature Distribution in an ACSR Linnet Conductor Subject to the Current Waveform Shown in Figure 8

In Fig. 9 the temperature rise resulting from the idealized lightning waveform shown in Fig. 8 is plotted as a function of position in an ACSR Linnet conductor (26/7, 336 kcmil). The curves show the influence of waveform frequency by plotting the temperature rise for 60 Hz and 125 kHz. Both curves show a moderate temperature rise resulting from the limited energy available even for the severely intense assumed waveform. The figure also shows the greater discrepancy between the surface and center temperatures that is produced when the frequency of the waveform is increased.

The temperature rise data for two conductors of different size is recast in a different format in Fig. 10. In this figure the surface temperature (the location of maximum temperature) is plotted as a function of time assuming the idealized current waveform in Fig. 8 has a frequency of 125 kHz. The curves show the rather small temperature rises that mirror the shape of the current waveform in Fig. 8 with the greater temperature rise occurring in the smaller Linnet conductor. These results reveal that the temperature rise in a typical conductor subjected to a relatively severe lightning strike is not severe.

CONCLUSIONS

The thermal model described in this paper is capable of predicting the short-circuit temperature history at all locations in a multi-component conductor. Temperatures predicted by this model lead to the following conclusions:

1. If the fault current has a frequency greater than approximately 60 Hz, the uneven current density in a conductor can produce temperature gradients in the conductor and at high frequencies the surface temperature rise in a faulted conductor can greatly exceed the temperature rise predicted by the traditional adiabatic heating model.
2. The uneven heating resulting from the skin effect is accentuated by the low resistivity outer strands and higher resistivity inner strands of composite conductors such as ACSR. These types of composite conductors have the potential for large temperature gradients which result from a combination of skin effect and uneven resistivity distribution.
3. If a short-circuit current at low frequency is maintained for greater than approximately one second, surface cooling can become significant producing conductor temperatures that are usually less than those predicted by the adiabatic heating model.
4. Large temperature gradients with surface temperatures exceeding the center temperature can exist for times up to about one minute when a conductor is shorted with a high frequency current. Depending upon the conductor and the surface cooling conditions, the large gradients disappear after approximately one minute as heat is transferred via conduction between the non-isothermal layers.
5. The temperature rise of a conductor contacted by a relatively severe lightning strike is small, although the temperature increase at the point of contact can be significant.

NOMENCLATURE

a_j	radius of each strand in layer i
A_j	cross-sectional area of strand layer i
A_m	cross-sectional area of metal in conductor
B	constant defined by Eq. 17
C	constant defined by Eq. 18
c_i	mean radius of strand layer i
c_p	specific heat at constant pressure for conductor
d_i	geometric mean radius of strand layer i

f	frequency of short-circuit current waveform
I	current
I_i	current through strand layer i
I_T	total fault current through conductor
I'	current per unit cross-sectional area of conductor
k	thermal conductivity
m'	mass of conductor per unit length
m_i	ratio of current in layer i to current in center strand layer
n	number of strand layer
N_i	number of conductor strands in layer i
q_{conv}	heat transfer per unit length of conductor by the convective mode
q''_{gen}	ohmic heating within a unit volume of conductor
q_{rad}	heat transfer per unit length of conductor by the radiative mode
r	radius measured from the center of the conductor
r_c	outer radius of conductor
R_i	electric resistance of strand layer i
t	time measured from start of short-circuit sequence
T	temperature
T_{max}	maximum, average temperature of conductor calculated by using the adiabatic assumption
T_{∞}	ambient air temperature surrounding the conductor
T_0	temperature of the conductor before the short-circuit
V_i	voltage drop per unit length of layer i
V	velocity of air circulated over the surface of the conductor
x_i	self reactance of conductor strand layer i

GREEK SYMBOLS

α_e	temperature coefficient of resistance of the conductor
ϵ	emissivity of the conductor surface
δ_{ik}	Kronecker delta
λ	ratio of total core diameter to total conductor diameter
μ_i	relative permeability of layer i
ρ	density of the conductor
ρ_{e20}	electric resistivity of the conductor at 20° C

REFERENCES

1. Transmission Line Reference Book 345KV and Above/2nd Ed. EPRI Palo Alto, CA. Chapter 12 Lightning Performance of Transmission Lines by J.G. Anderson.
2. Zaborszky, J., "Skin and Spiraling Effect in Stranded Conductors", *AIEE Trans.*, Vol. 72, pp 599, 1953.

3. Kakac, S., Yener, Y., *Heat Conduction*, Hemisphere Publ. Corp. 1985, pp. 325.
4. McWhorter, Bruce Burnett, "Transient Temperature Distribution in Short-Circuited Electrical Conductors", MS Thesis, School of Mechanical Engineering, Georgia Institute of Technology, June 1987.
5. Kreith, Frank and Black, William Z., "*Basic Heat Transfer*", Harper and Row, N.Y. 1980.
6. Black, W.Z. and Bush, R.A., "Conductor Temperature Research", EPRI Final Report for Project 2546-1, EL-5707, May 1988.
7. Walker, Mark, ed., *Aluminum Electrical Conductor Handbook*, Washington, D.C., The Alum. Assoc., 1982.
8. Black, W.Z. and Wells, Glenn M., "Temperature Rise of Optical Fiber Ground Wires Subjected to Short Duration-High Current Transients", *Trans. IEEE, Power Delivery*, Vol. 4, No. 3, pp. 1806-1815, July 1989.

BIOGRAPHY

W. Z. Black received his B.S. and M.S. in Mechanical Engineering from the University of Illinois and his Ph.D. in M.E. from Purdue University. He is currently Regents Professor and Georgia Power Distinguished Professor of Mechanical Engineering at Georgia Institute of Technology in Atlanta. His research effort is concentrated in the area of heat transfer from electrical and electronic equipment. He has been Principal Investigator for several EPRI ampacity projects and he is active in IEEE committee work relating to the thermal ratings of overhead and underground conductors.

Bruce McWhorter received his BSME and MSME from the Georgia Institute of Technology. His graduate study included heat transfer of electric power conductors. He now works for Morton Thiokol, Brigham City, Utah as a Systems Engineer. One of his duties is the study of lightning current through solid rocket motors.

TEMPERATURE MONITORING SYSTEM USING OPTICAL FIBER SENSORS FOR UNDERGROUND POWER CABLES

Masao Asakawa, Yasuo Yoshida, Yasuo Ozawa*,
Susumu Osawa**, Hiroshi Kawakami**, Shojiro Yamazaki**

Tokyo Electric Power Co., Tokyo, Japan

*International Superconductivity Technology Center, Tokyo, Japan

**Hitachi Cable Ltd., Hitachi, Japan

ABSTRACT

An innovative temperature monitoring system for underground power cables has been developed and practically applied. Optical fiber temperature sensors are used to detect the temperature profile over long cable runs. These sensors can measure the temperature distribution up to 10km within $\pm 1^\circ\text{C}$ and 1 meter spatial resolution. The optical fiber was laid along the outside of a power cable in the practical system. In addition, a 275-kV XLPE cable with integrated optical fiber sensors has been developed for future applications.

INTRODUCTION

To ensure the efficiency and reliability of electrical power systems, it is very important to monitor and supervise the operating conditions. In particular, a sensing system is needed that can continuously monitor the temperature distribution along long underground power cables under conditions of strong electromagnetic interference. Discrete sensors which use electronic and optical technologies have been developed, but they need electrical power sources and data transmitters to send their data over a long distance. This makes these systems complicated and expensive.

To overcome these problems, we have developed a fiber optic distributed temperature sensor. Its measurement distance was originally 2km,¹ but longer range measurements are needed for long cable runs. We therefore developed a long-range fiber optic temperature sensor that can measure the temperature distribution up to 10km.²

This paper describes the introduction of this sensor, its practical application to power cables, and the development of a 257-kV XLPE fiber optic sensors composite cable.

FIBER OPTIC DISTRIBUTED TEMPERATURE SENSOR

Principle

To obtain the temperature distribution along an optical fiber, it is necessary to locate the origin of the sensor signals and to determine the temperature from them.

Origin location is determined by measuring delay time t , which is composed of the time it takes an injection light pulse to reach the point where the transmitting light pulse generates a scattering light and return to the incidence end (Fig.1). The distance from the origin, x , is determined by

$$x = v \cdot t / 2 \quad (1)$$

where v is the velocity of light in an optical fiber.

The temperature at each point is derived from the intensity of the Raman scattering light in the backscattering light. The backscattering light consists mainly of: Rayleigh scattering light caused by elastic collisions with glass molecules in the fiber material and Raman scattering light, which is caused by nonelastic collisions and whose wavelength is different from the incident light.

The two components of Raman scattering light, anti-Stokes light and Stokes light, occur at the wave number shifts at around $+400\text{cm}^{-1}$ and -400cm^{-1} (Fig.2). The Raman scattering light intensity is very

weak, about 10^{-3} times that of the Rayleigh scattering light and about 10^{-6} times that of the incident light. However, the two components more strongly depend on temperature than Rayleigh scattering light. In addition, the intensity ratio of the two components depends only on the temperature, as shown in Eq.(2), if the wavelength of the incident light and the fiber material are fixed.³

$$I_a/I_s = \frac{(\tilde{\nu}_0 + \tilde{\nu}_k)^4}{(\tilde{\nu}_0 - \tilde{\nu}_k)^4} \exp(-h \cdot v \cdot \tilde{\nu}_k / k \cdot T) \quad (2)$$

- I_a : Intensity of anti-Stokes light
- I_s : Intensity of Stokes light
- $\tilde{\nu}_0$: Wave number of the incident light
- $\tilde{\nu}_k$: Wave number shift of glass
- h : Planck's constant
- v : Velocity of light in the optical fiber
- k : Boltzmann's constant
- T : Absolute temperature

Composition

The developed fiber optic temperature sensor consists of an optical fiber for temperature sensing and a measuring unit, which includes a personal computer, to calculate and display the temperature distribution (Fig.3). A high power LD-pumped solid-state laser is used for long-range measurement. This laser launches a peak power of about 100 W into a 50/125 multi-mode sensing fiber. An incident light pulse generates scattering light in the fiber, and part of this scattering light propagates back to the main measuring unit as back-scattering light.

After separating the anti-Stokes light and the Stokes light from the back-scattering light with an optical wavelength division demultiplexer, their intensities are converted to electrical signals. These signals are then amplified, sampled every 10 ns, converted to digital signals, and averaged by a high-speed digital averaging circuit to improve their signal-to-noise ratio. The 10-ns sampling interval corresponds to a 1-m interval. An external view of the sensor is shown in Fig.4.

Performance

The performance of the sensor is summarized in Table 1. The temperature measurement range depends on the temperature tolerance of the optical fiber itself, that is, on the fiber coating materials.

PRACTICAL APPLICATION TO POWER CABLE LINES

System Configuration

The first application of our long-range fiber optic distributed temperature sensor was to the Minami-Ikegami line of the Tokyo Electric Power Co. (Fig.5). This line is the first practical use of a 275-kV XLPE cable for a long transmission line.

The measuring unit was located at the Minami Kawasaki substation and the results were transmitted to the Kawasaki maintenance office over a telecommunication line, where they were stored.

Installation

Before laying the Minami-Ikegami line, we studied how to lay the optical fiber on the power cable to get the most accurate surface temperature measurements. Since there are many fixing cleats along the power cable, which the optical fiber must go around, the optical fiber is not always in close contact with the power cable. As a result, the temperature measured by the optical fiber may not be the actual surface temperature.

We conducted a trial implementation and checked for deviations between the measured temperature and the actual power cable surface temperature (Fig.6). The optical fiber measured temperatures were 3 to 5°C lower than those measured by thermocouples on the cable surface. The reason for this variance may be related to the spatial arrangement of the optical fiber. However, the variance was the same near the fixing cleats, so the fixing cleats have negligible effect. In practical application, the heat generated by the cable is estimated to about one quarter that of the trial setup. Therefore, the variance is a negligible 1 to 2°C.

After this preliminary trial, an optical fiber was laid on the surface of the power cable and joint boxes of the Minami-Ikegami 3rd circuit. It was fixed to the surface with fixing bands. To avoid excessive force, exclusive spacers were placed between the optical fiber and the fixing bands, and the exposed portions of the optical fiber were covered with tubes to protect against impacts. The composition of the optical fiber and the binding method are shown in Figs.7 and 8.

A double-core double-sheathed optical fiber cable

was used. One optical fiber was used as the sensor and the other was kept in reserve.

In addition to measuring cable temperature, the atmospheric temperature in the tunnel was measured at two points : on a bridge section of the tunnel affected by sunlight and in a underground section of the tunnel. At these points, the optical fiber was coiled and placed in a steel box installed on the ceiling.

Temperature Monitoring

The temperature distributions of the power cable surface and the inside conductor were displayed at the central station in the Kawasaki maintenance office. An example measured temperature distribution is shown in Fig.9. The conductor temperature was calculated from the surface temperature and the load current, taking thermal resistance and heat capacity into account. The surface and conductor temperatures were influenced by the laying conditions. For example, temperatures around manholes were lower than in other tunnel sections. The tunnel's maximum temperature was in the center of a shielded tunnel, between Kawadou #242 manhole and Kawakyou #509 manhole.

The monitoring system can also display the time dependence of these temperatures and load current (Fig.10). The time axis can be a day, a month, or a year, with up to 72 monitoring points depending on central station memory capacity.

275-kV XLPE/OPTICAL-FIBER COMPOSITE CABLE

Composition

In the practical application, optical fiber sensor cables were layed along the outside of the power cable. For future applications, we have developed a 275-kV XLPE cable with integrated optical fiber sensors (Fig.11). This composite cable eliminates the additional optical fiber cable and provides more accurate cable temperatures.

To determine the most suitable cable composition, optical fiber sensors were installed in three positions in the cable : in the center of the conductor, between the insulator and the aluminum(Al) sheath and between the Al sheath and the polyethylene(PE)

sheath.

The optical fiber sensor was placed in a metallic tube to protect it against mechanical force (Fig.12). Two types of metallic tubes were used. The tube placed in the conductor was made of copper, with an outer diameter of 2.1 mm and a wall thickness of 0.3 mm. The other was made of stainless steel, with an outer diameter of 1.8 mm and a wall thickness of 0.2 mm. Two stainless wires were installed on both sides of the stainless tube for reinforcement.

Test Results

Optical fiber sensors are subjected to mechanical stresses while the composite cable is being layed and during actual use. To examine the impact on the optical fiber sensors, we have conducted tension tests, compression tests, and thermal cycling tests.

The maximum strain on the optical fiber was 0.13% (allowable stain is 0.2%) at a tension of 25 tons (Fig.13). This is 2.5 times the allowable tension of cable laying. To test compression, we applied a load of 2 tons/m on the cable. The results confirmed that there was no increase in optical transmission loss.

To test temperature measurement consistency, we cycled the temperature daily for 30 days, with a maximum conductor temperature of 90°C. Fig.14 shows the arrangement of the cable and Fig.15 shows the temperature distribution of the cable, as measured using optical fiber sensors. The optical fibers were spliced at both ends of the cable in series. After 30 days of testing, there was no increase in optical transmission loss and no difference in the measured temperature from the initial one.

These test results show that all these sensor positions in the composite cable can be practically used. Considering cable splicing requirement and temperature measurement accuracy, however, the best location for the sensors is between the insulator and the Al sheath.

CONCLUSION

We have developed fiber optic temperature sensor

that can measure the temperature distribution up to 10km underground power cable. The measured temperature distribution of the cable surface and the estimated conductor temperature distribution were used for power cable line supervision.

For future application, we have developed 275-kV XLPE cable with integrated optical fiber sensors. This composite cable eliminates the separate optical fiber cable and provides more accurate cable temperatures.

In the future, the developed sensor will be applied to power cable control systems that include forced-cooling and load control, and will be used to power

cable fault location system based on the detecting of abnormal temperature rises.

REFERENCES

- (1) K.Ogawa, et al. : Fiber Optic Distributed Temperature Sensor with High Distance Resolution, OFS-6' 89, 1989
- (2) Y.Ozawa, et al. : Fiber-Optic Distributed Temperature Sensor for Long Range Remote Sensing, OEC, 92, 1992
- (3) D. A. Long: Raman Spectroscopy, McGraw-Hill International Book Co., 1977

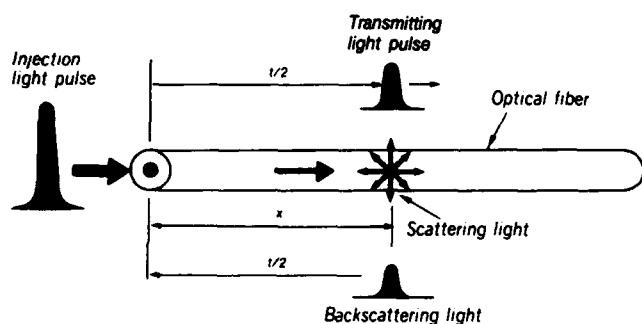


Fig.1 Model of backscattering light generation in an optical fiber

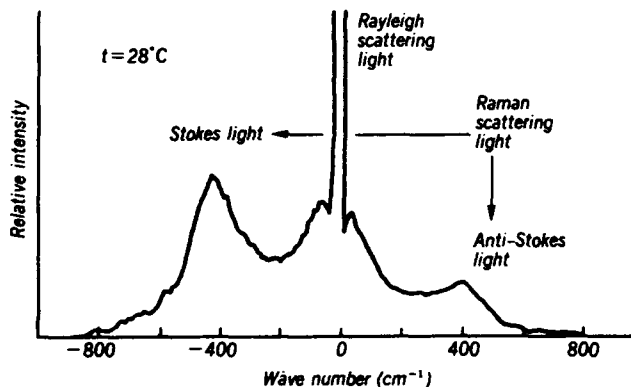


Fig.2 Raman scattering spectrum in optical fiber

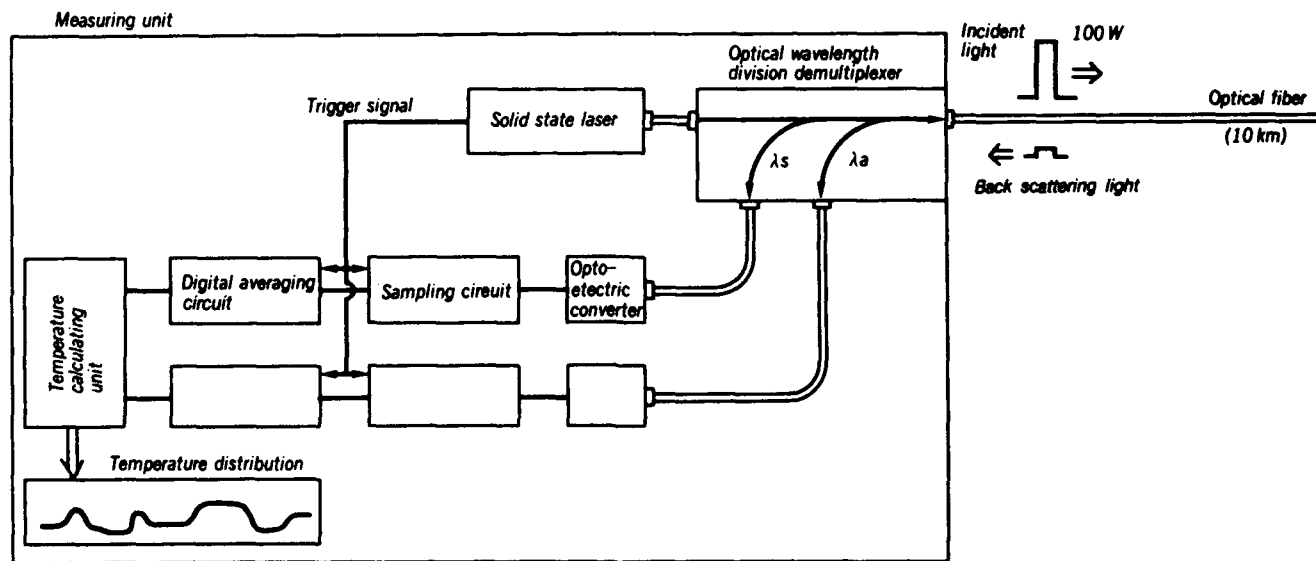


Fig.3 Fiber optic temperature sensor circuitry

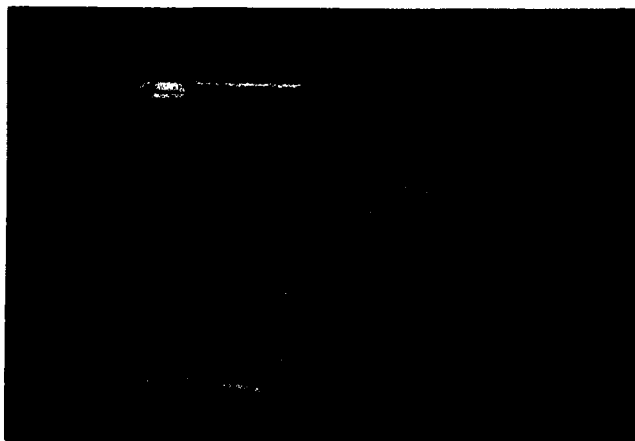


Fig. 4 External view of sensor system

Table 1 Sensor performance

Measurement distance	10 km
Spatial resolution	1 m
Temperature measurement accuracy	$\pm 1^{\circ}\text{C}$
Temperature measurement range	-50 to 150°C
Optical fiber sensor	50/125 μm GI

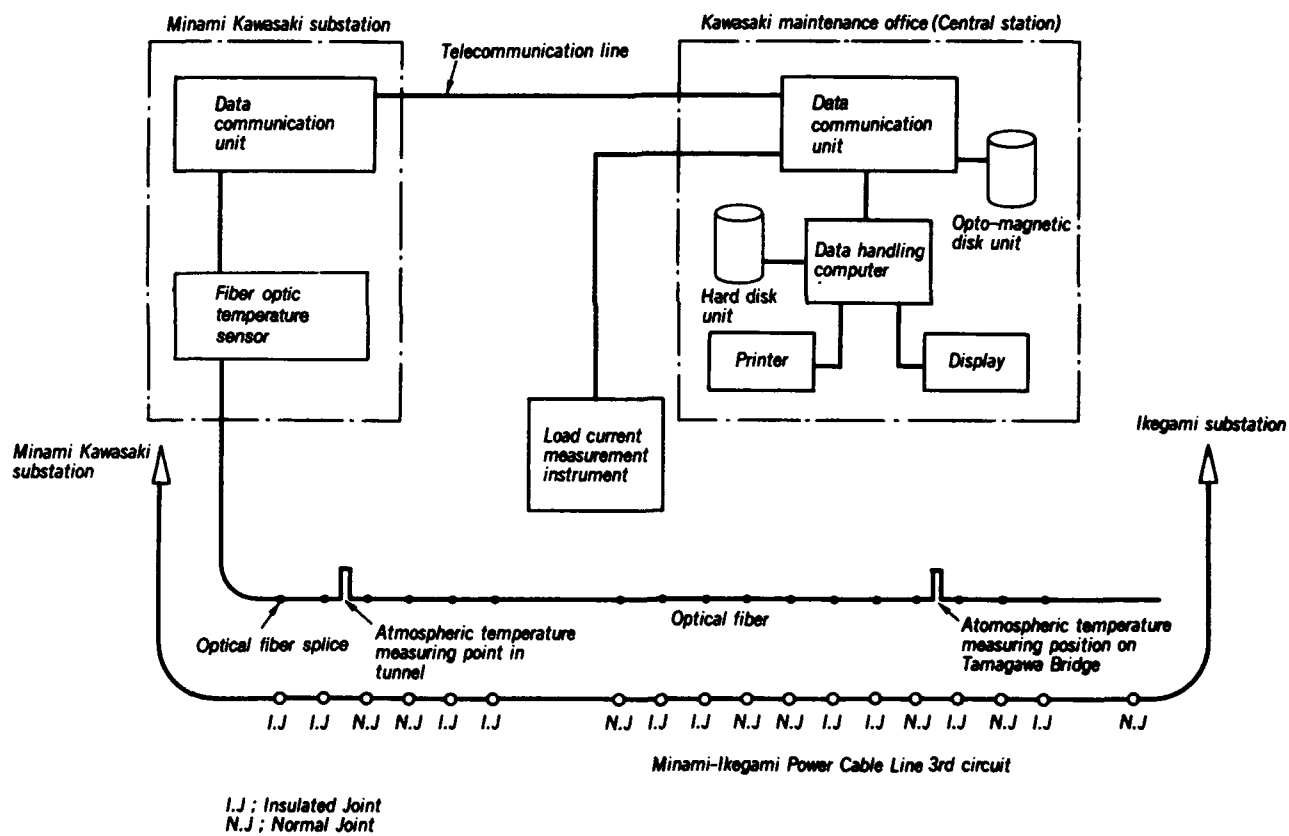


Fig.5 System configuration of the temperature monitoring system

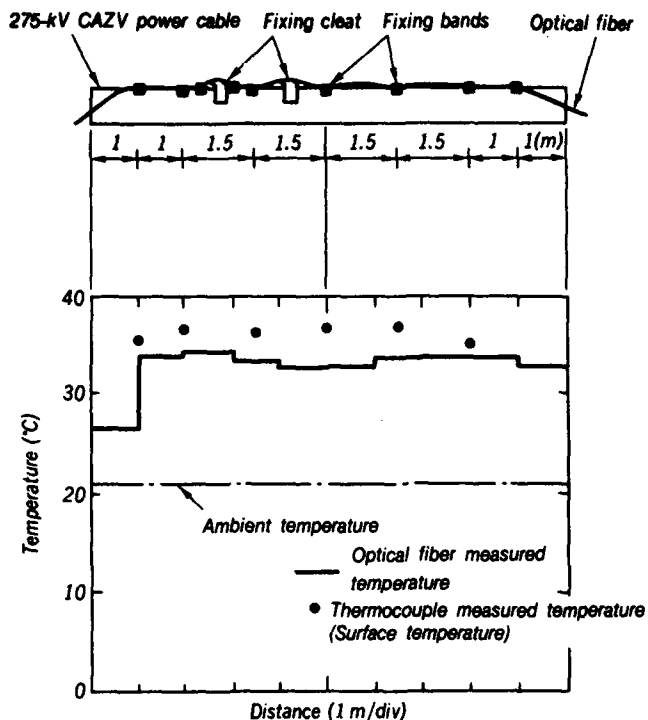


Fig.6 Difference in measured temperatures

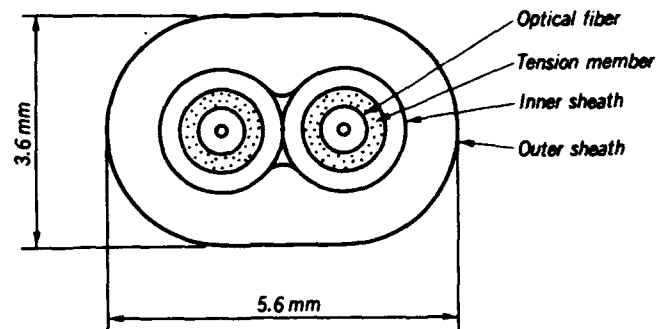
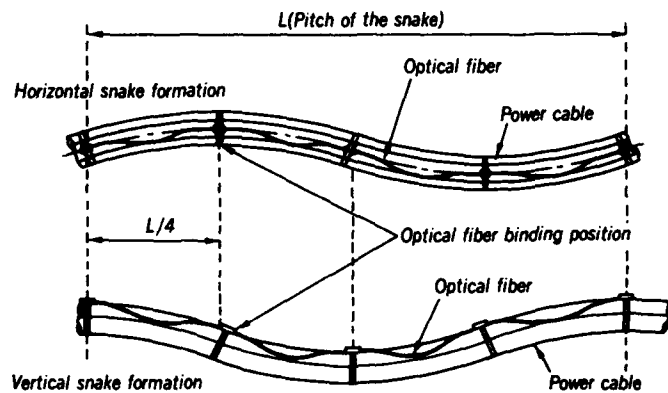
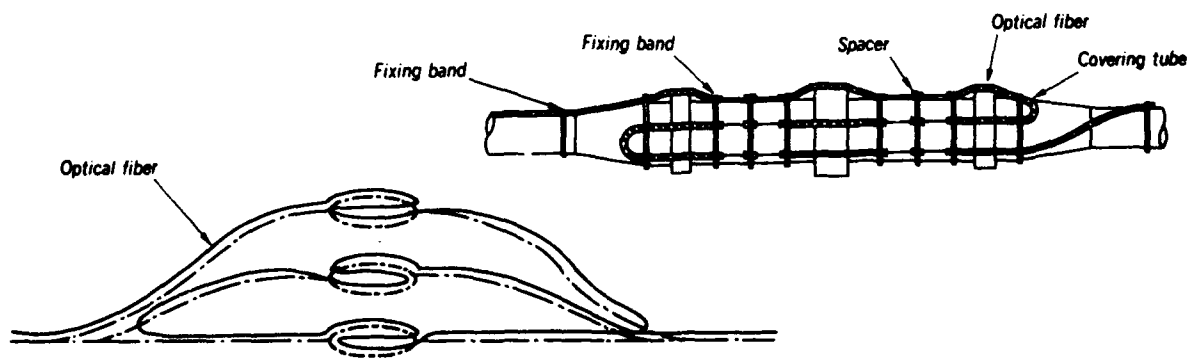
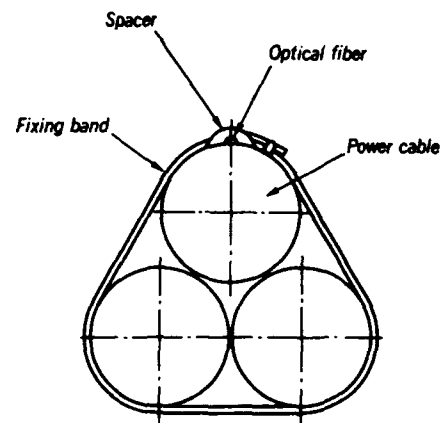


Fig.7 Optical fiber composition



(a) Cable section



(b) Joint section

Fig.8 Optical fiber binding method

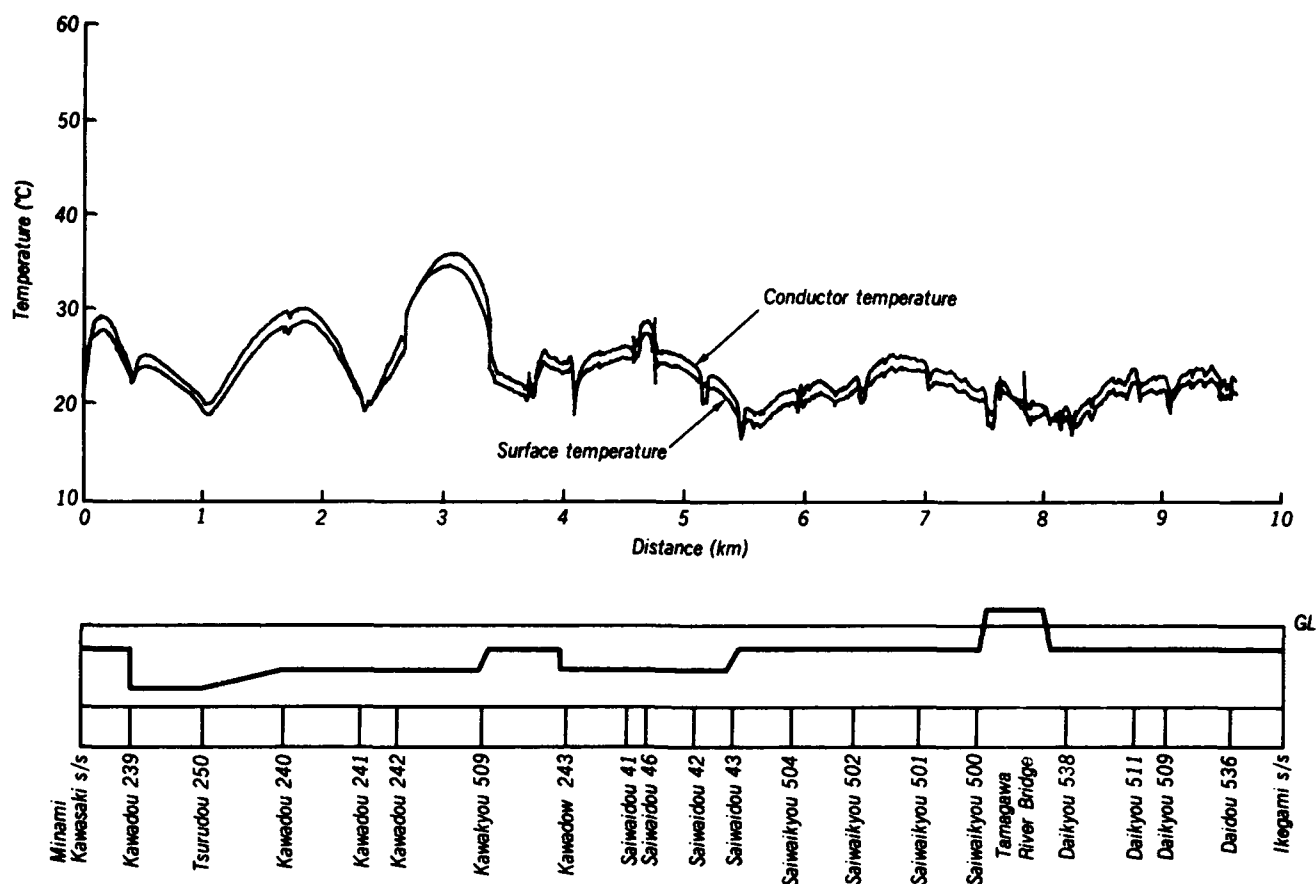


Fig.9 Temperature distribution

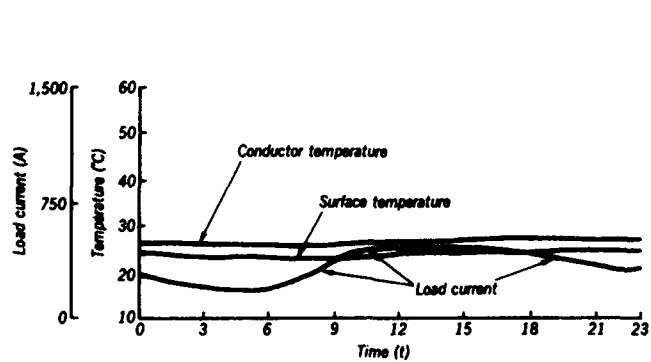


Fig. 10 Time dependence of temperature and load current

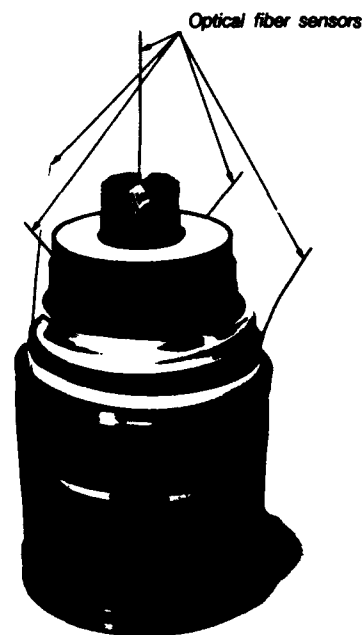


Fig.11 Composition of composite cable

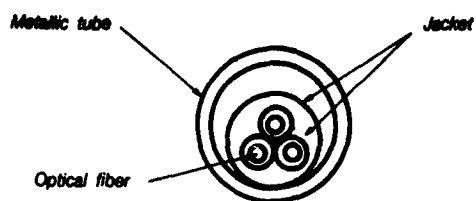


Fig.12 Composition of optical fiber sensor

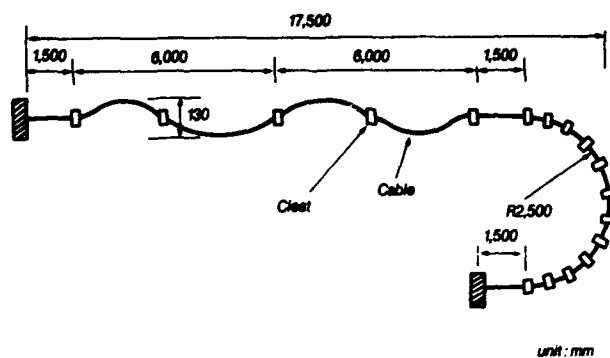


Fig.14 Arrangement of cable for thermal cycling test

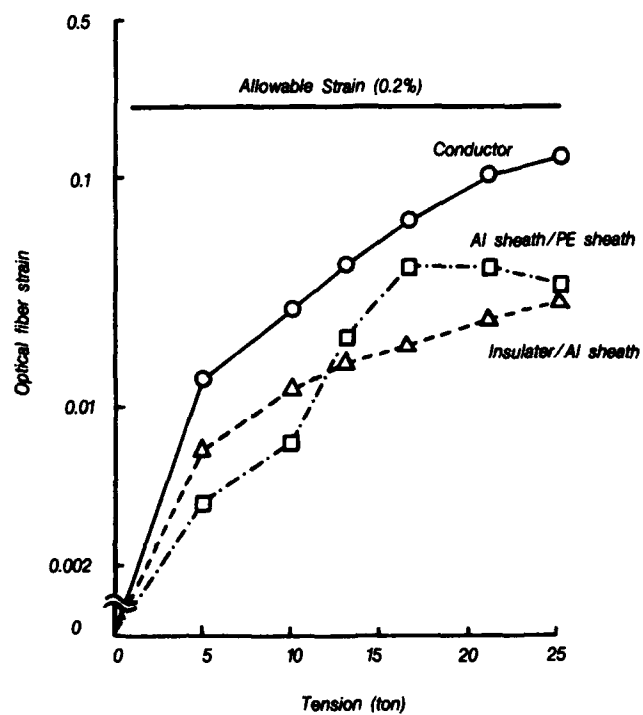


Fig.13 Tension test results

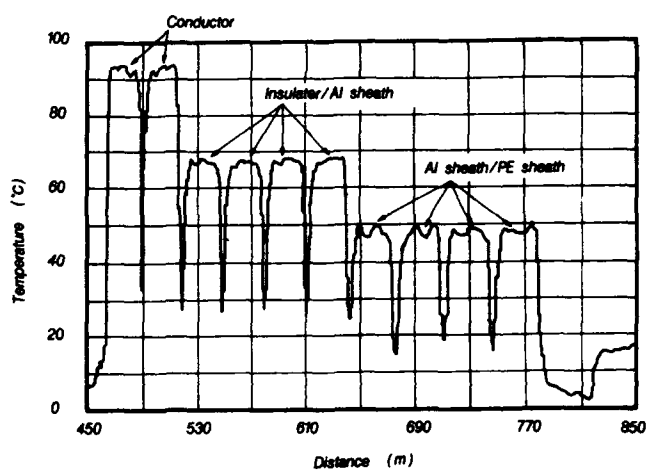


Fig.15 Cable temperature distribution



Masato Asakawa

Tokyo Electric Power Co.
2-2-30 Kandajinbo-cho,
Chiyoda-ku, Tokyo 101,
Japan

Mr. Asakawa received the M.E. degree in electrical engineering from Nihon University in 1986 and joined Tokyo Electric Power Co..
He is now a researcher of Engineering Development Center.



Susumu Osawa

Hitachi Cable Ltd.
880 Isagozawa-cho,
Hitachi-shi, Ibaraki
319-14, Japan

Mr. Osawa received the B.E. degree in mechanical engineering from Tokyo University in 1970 and joined Hitachi Cable Ltd..
He is now a senior engineer of Surveillance System Dept.



Yasuo Yoshida

Tokyo Electric Power Co.
1-1-3 Uchisaiwai-cho,
Chiyoda-ku, Tokyo 100,
Japan

Mr. Yoshida graduated Toden Educational Institute and joined Tokyo Electric Power Co..
He is now a engineer of Underground Transmission Div.



Hiroshi Kawakami

Hitachi Cable Ltd.
5-1-1 Hitaka-cho,
Hitachi-shi, Ibaraki
319-14, Japan

Mr. Kawakami received the B.E. degree in electrical engineering from Kyoto University in 1970 and joined Hitachi Cable Ltd..
He is now a senior researcher of Opto-electronic System Laboratory.



Yasuo Ozawa

International
Superconductivity
Technology Center

1-10-13 Shinonome,
Koto-ku, Tokyo 135,
Japan

Mr. Ozawa received the M.E. degree in electrical engineering from Nihon University in 1984 and joined Tokyo Electric Power Co..
He is now a associate director of Planning & Management Div. of Superconductivity Research Laboratory.



Shojiro Yamazaki

Hitachi Cable Ltd.
5-1-1 Hitaka-cho,
Hitachi-shi, Ibaraki
319-14, Japan

Mr. Yamazaki received the B.E. degree in electrical engineering from Osaka University in 1975 and joined Hitachi Cable Ltd..
He is now a senior engineer of Telecommunication Design Dept.

DEVELOPMENT OF OVERHEAD WATER BLOCKED COVERED ALUMINUM CONDUCTORS FOR MV DISTRIBUTION

E. Buczma

A. Fragale

Olex Cables a Division of Pacific Dunlop Limited
Melbourne, Victoria, Australia

ABSTRACT

The development of overhead water blocked covered aluminium conductors for an 11 kV medium voltage distribution system is described. The cables are non compacted conductors of the stranding configuration 7 wires 3.75 mm, 7 wires 4.75 mm and 19 wires of 3.5 mm of AAAC/1120 aluminium alloy each having a covering of 3.4 mm radial thickness of grey XLPE. A main characteristic of the product is that the conductor is fully water blocked using a developed polymeric non conductive compound such that no water penetration occurs. The developed cables also have good stripping properties such that the grey XLPE covering can be removed leaving a clean aluminium surface, good performance in interstrand conductivity and connectability of fittings tests, satisfactory performance of the dripping property of the water blocking compound and good adhesion properties in strain clamping tests.

INTRODUCTION

Covered conductors made of aluminium have been used in Australia for many years. The systems were introduced to improve reliability of supply through the prevention of the clouting of conductors by high winds, birds, animals or trees. The non water blocked conductors have been made with coverings at various times of PVC, high density polyethylene (HDPE) and black cross linked polyethylene (XLPE) containing a minimum of 2% well dispersed carbon black suitable for outdoor weathering performance.

Experience showed that where the covering was removed ingress of moisture occurred with subsequent corrosion of the aluminium either in the span or at a point where the covering was removed.

In Australia corrosion failure in overhead covered conductors occurred after 5-10 year service life in coastal areas and 20 year service life in inland areas.

In 1983 severe bushfires swept across a number of regions of Australia which resulted in a re-evaluation of overhead line construction using bare conductor. This resulted in further development of covered conductor systems.

One covered aluminium conductor cable system evaluated incorporated semi-conductive high temperature water blocking compound between the wire strands. It was used because overseas tests had shown it to be particularly suitable with connectors. However this system was later discontinued because the compound could not be used over the strand wires between the conductor and the covering. The system did not show the degree of water blocking required because a tight enough seal could not be obtained between the strand wires and the covering. Also there were some handling problems.

To overcome these deficiencies an Australian Power Authority requested that an 11 kV overhead distribution system be designed incorporating cable and accessories¹. The conductor was to have a polymeric non mastic type of water blocking material.

This paper describes the development of a suitable cable to meet these customer requirements.

CABLE SPECIFICATION

The cable specification by an Australian Power Authority² called for cross linked polyethylene covered conductors suitable for overhead lines operating at 11 kV, 50 Hz AC. The cable was to be filled with water blocking compound to inhibit migration of water along the conductor.

The conductors were required to be stranded circular non compacted and to comprise individual wires of Aluminium Alloy 1120.

The water blocking compound was required to completely fill the interstices of the conductor and to enclose the outer surface strands of the conductor. The compound was required to be pliant, non hygroscopic, non shrinking with age and not to present any toxicological or dermatological problems to persons. Also the compound should not affect the conductor nor the cross linked polyethylene covering when exposed to water or air or both at a continuous operating temperature up to 90°C. A compound which required activation by absorption of moisture was not allowed. On removal of the cross linked polyethylene covering any water blocking compound between the covering and the conductor had to peel away cleanly with the covering except that a small amount could remain at the extreme tip of the crevice between the individual wire strands.

The conductor and water blocking compound were to be covered with a grey cross linked polyethylene having a low carbon black content. The covering was to be concentric around the conductor to allow hand stripping with the aid of a stripping tool without preheating.

CABLE DESIGN

The cross section of the covered conductor is as shown in figure 1.

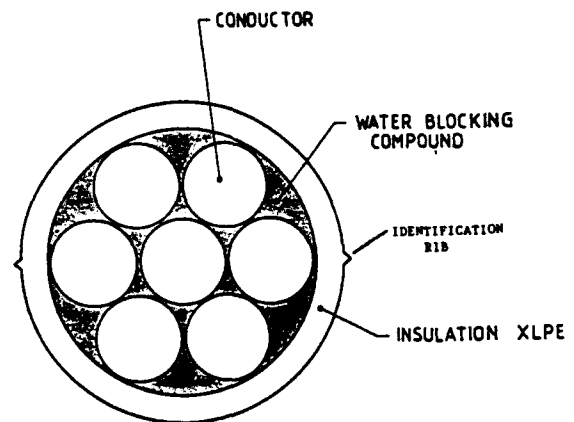


Figure 1 Cross section of the Covered Conductor

The covered conductor is identified using two longitudinal continuous raised ribs spaced 180° apart as shown in figure 1. Rib dimensions are, a base width of nominal 0.5 mm and a rib height of min 0.3 mm.

Table 1 Conductor Properties

No	Characteristic	Unit	Conductor Size		
1.	Standard Conductor Size	mm ²	80	120	180
2.	Conductor Stranding		7/3.75mm	7/4.75mm	19/3.5mm
3.	Conductor Type		All Aluminium Alloy Conductor AAAC/1120		
4.	Cross Sectional Area for Mechanical Purposes	mm ²	77.3	124.0	182.8
5.	Calculated Equivalent Aluminium Area ³	mm ²	73.7	118.2	173.5
6.	Calculated Minimum Breaking Load	kN	17.6	27.1	41.7
7.	Calculated DC Resistance at 20°C	ohm/km	0.384	0.239	0.163
8.	Approximate Mass	kg/km	436	619	848

There are three cables in the range 80 mm² of stranding 7 wires 3.75 mm, 120 mm² of stranding 7 wires 4.75 mm and 180 mm² of stranding 19 wires 3.5 mm. The conductors have the stranding characteristics and other properties shown in table 1.

Table 2 shows the dimensional requirements of the cables.

The thickness of the covering is the same as that used for a fully insulated underground cable of the same operating voltage and as such the cable has sufficient insulation thickness to withstand the electrical stresses encountered from extended contact with trees.

If this region was cut a lump of white corrosion product would be evident. Also in these samples white corrosion product was evident along the strands of the conductor between the conductor and the covering and also though the central strands of the conductor. This also occurred at locations some distance away from the moisture entrance point. If severe the corrosion could cause the individual wire strands to break especially at locations where some stress was evident.

With the non water blocked covered conductor designs corrosion of the conductor becomes a potential problem where the covering is removed or broken for whatever reason; installation of fittings, removal by birds, or damage.

Table 2 Dimensional Requirements

No	Characteristic	Unit	Conductor Size		
1.	Conductor Stranding		7/3.75	7/4.75	19/3.5
2.	Nominal Bare Conductor Diameter	mm	11.3	14.3	17.5
3.	Cross Linked Polyethylene Insulation Thickness Excluding Ribs				
	Minimum Average	mm	3.4	3.4	3.4
	Minimum at any Point	mm	3.0	3.0	3.0
	Maximum at any Point	mm	4.0	4.0	4.0
4.	Maximum Diameter Overall Excluding Ribs	mm	19.0	22.0	25.2

PREVIOUS DESIGNS

Previous designs of covered conductor were not water blocked but comprised a polymeric covering over the bare conductor of around 1.8 mm wall thickness. Because the thickness of the covering was insufficient to withstand sustained electrical stress and because of radio interference at pin insulation supports the covering was removed at the support points. This resulted in moisture going down the conductor strands and after a period of time resulting in corrosion of the aluminium conductor. The effect was exacerbated in regions close to the sea and in areas of high pollution.

Moisture could travel either through the conductor strands to the lowest part of the span where it could collect or between the outer wire strands and the covering. Over time corrosion would occur with severe corrosion where the water was trapped for longer periods. This could be seen in covered conductor samples where the covering had bulged.

Figures 2 and 3 show examples of corrosion in previous covered conductor designs.

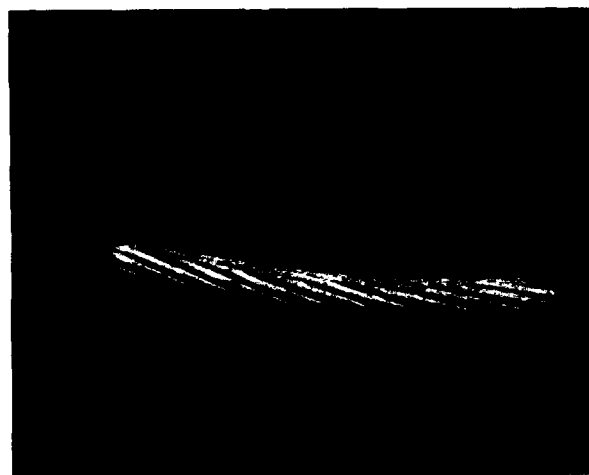


Figure 2 Corrosion in a Covered Conductor (previous design)

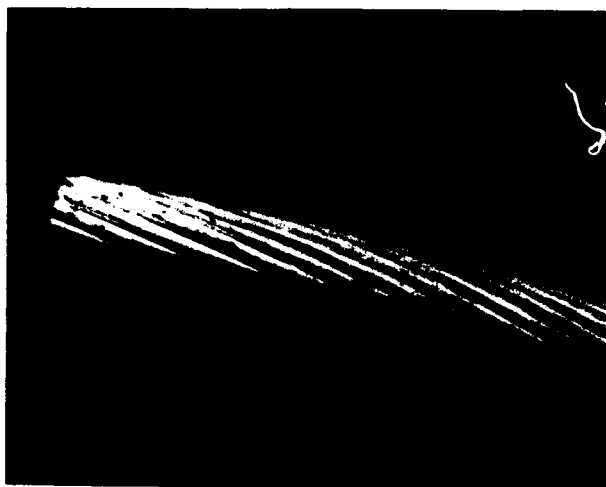


Figure 3 Corrosion on Conductor Surface (previous design)

MATERIALS

As shown in figure 1, the cable comprises a conductor made of aluminium alloy a water blocking compound and an outer covering.

The properties of the aluminium alloy, the wires and the conductor stranding configurations are covered in 3.

To meet the water blocking test performance requirements the water blocking compound has to fill in all the inner interstices of the conductor and also provide an interface between the surface of the conductor and the covering of cross linked polyethylene material. From earlier work it had been shown that it is very difficult to obtain the required degree of adhesion between the surface of the aluminium conductor and the cross linked polyethylene covering to meet the water blocking test requirements.

The water blocking material is polymeric from the polyolefin copolymer class. In this group of materials there are many different types and grades varying in their comonomer contents, flow properties, melting points, tensile properties and hardness characteristics. In selecting the materials for use as a water blocking compound for this application the method of application has to be considered and the application point to be used in the process. Also generally as the comonomer content increases so does the tendency for improved adhesion to the aluminium metal but the corresponding melting points, tensile properties and hardness values decrease.

The grey cross linked polyethylene covering is a mineral filled cross linkable polyethylene compound for low voltage cable insulation and contains additives for long term UV weathering performance. The mechanical and electrical performance data obtained from cable samples are shown in the section on type test results. Weathering test requirements for the material are covered in 2.

PROCESSING

The processing of the overhead covered conductors requires special attention at both the conductor manufacturing stage and at the insulation stage. The design and construction of these cables necessitates the selection of optimum processing conditions in order to have trouble free production.

Particular requirements at the conductor stage include selection of an optimum lay ratio within specified limits which will yield a tightly stranded conductor construction. Tight tolerances on wire and conductor size are important for successful manufacture.

Insulation is carried out on a Continuous Vulcanisation line. The water blocking compound is applied on line prior to the grey outer covering being extruded onto the conductor. This minimises the number of processes and improves the efficiency and productivity of the operation.

A nominal 3.4 mm wall of grey UV stabilised cross linked polyethylene compound is extruded over the conductor. The process conditions are selected to enable sufficient residence time within the curing tube to cross link the polyethylene compound to the appropriate degree. Also since the water blocking compound is thermoplastic, under the processing conditions used the material can flow and fill up all the inner interstices of the conductor. Under the temperatures and pressures encountered the water blocking compound can adhere to all the wires in the stranded conductor and also bond to the outer grey cross linked polyethylene covering.

Because of the specified sizes of the final product the water blocking compound has to be applied uniformly and within close tolerances.

EVALUATION

In order to optimise the performance of the water blocking compound formulation, the process and the final product performance, trial evaluations were carried out. For assessing the final product the following tests are important: water blocking compound drip test, static water blocking test, dynamic water blocking test, stripping test, adhesion test and interstrand conductivity test.

Water Blocking Compound Drip Test

The test is carried out by hanging vertically two cable samples 13 cm in length, both ends square cut with one of the samples having 3 cm of covering removed from one end, in an oven at $100 \pm 5^\circ\text{C}$ for 24 hours. At the end of the test period no compound should be present in trays placed under the samples at the start of the test.

Since the water blocking base materials used are thermoplastic resins with melting points below the drip test temperature this has implications for the formulation of the water blocking compound used and for the processing techniques used for the cable.

It is important to limit the amount of water blocking material in the cable yet it has to be filled to the correct level to meet the water blocking test requirements. The wires are stranded to give a tight conductor structure to limit the interstitial gaps between the wires. From the stranding configurations for the three conductor sizes the largest interstices will be present in the 7/4.75 mm product while the largest amount of water blocking material will be used in the 19/3.5 mm cable.

In order to meet the drip test requirements a proprietary water blocking compound was developed which was made up of a number of components with suitable melting points and adhesion properties to the aluminium.

The formulation of the water blocking compound depends on the method used to apply the water blocking compound to the conductor and also on its effect on the other required cable properties.

Water Blocking Tests

The product is required to meet two water blocking tests. The static water blocking test is shown in figure 4. Prior to preparation of the sample for the test a 0.5 metre length of the cable is subjected to three reverse bends around a mandrel of diameter $16(D + d)$ where D , d is the diameter of the cable and the conductor respectively. The sample for the test is then cut from the middle of the bend test piece, prepared and placed in the apparatus. The exposed conductor is subjected to an 800 mm head of water containing fluorescein at an ambient temperature for 24 hours.

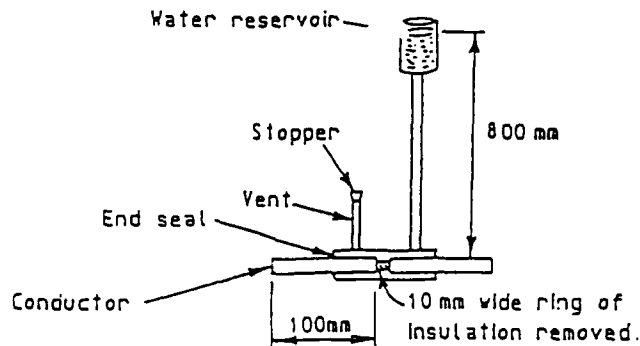


Figure 4 Static Water Blocking Test 2

To meet the test requirements no penetration of water is to occur either between the conductor surface and the covering or between the wires away from the 10 mm wide entry point. The examination is carried out under UV light at 254 nm wavelength.

For the dynamic water blocking test the same cable preparation and test arrangement is used except that after the 24 hour period at ambient temperature the cable sample is temperature cycled 10 times from ambient to $80^\circ\text{C} \pm 5^\circ\text{C}$. This is carried out by fitting a current transformer and correcting the ends of the conductor to form a closed loop. The test criteria are the same as for the static water blocking test.

To meet these severe requirements the water blocking compound must have good adhesion to the aluminium wires to cope with the initial bend test and also the expansion and contraction

during the temperature cycling test. Also the conductor has to be sufficiently filled with water blocking compound without any voids or gaps to meet the test requirements.

Stripping Test

The water blocking material should be easily removed from the outer surface of the conductor as the covering is removed leaving a clean aluminium surface. This requirement is to aid linesmen when attaching fittings. To test the product for this requirement a stripping tool as shown in figure 5 is used. Cable samples are conditioned in an oven at 20°C and 40°C after which a section of the outer covering is stripped using the tool. Figure 6 shows typical cable samples after the stripping test.

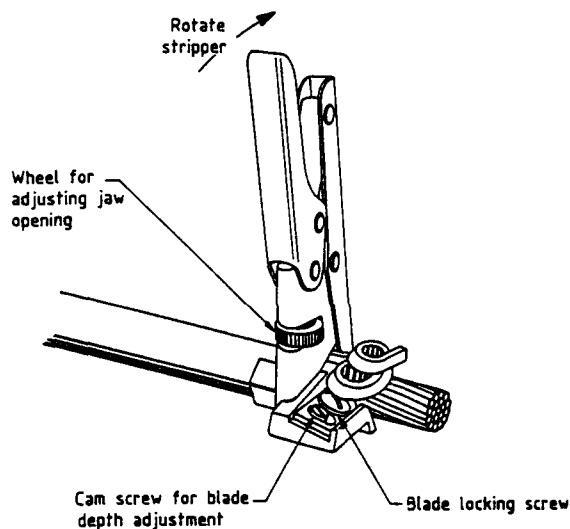


Figure 5 Stripping Tool 2

From the process side a tight conductor is required so that the web of water blocking material penetrating the outer strands of the conductor is very thin. From the material formulation/process point of view there is a balance between the degree of adhesion (between the water blocking material and the conductor) required for water blocking and the ease of removal of the water blocking material during the stripping test.

Also the water blocking material has to adhere to the cross linked polyethylene covering under the process conditions used.

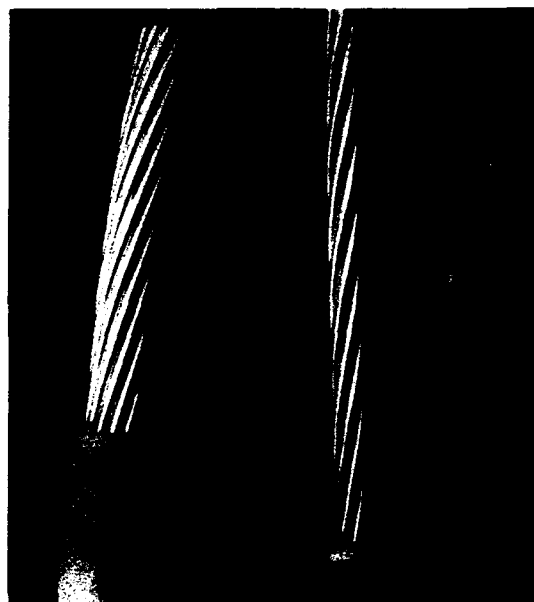


Figure 6 Cable After the Stripping Test

Adhesion Test

The test is carried out to determine the adhesion of the covering on the water blocked conductor when tension is applied to the cable. This information is required for stringing up of the covered conductor to ensure that no slippage of the covering over the conductor occurs at the stringing up tensions encountered.

The test is performed by anchoring a sample of the cable at one end while using a gripping device to grip the covering towards the other end. Tension is then applied to the gripping device.

The test arrangement is shown in figure 7. Tension is applied up to the required value over one minute then held for 10 minutes after which

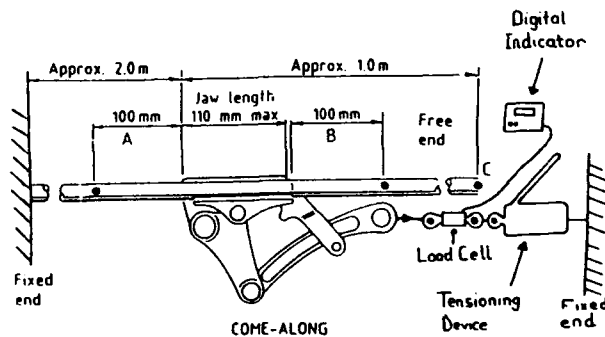


Figure 7 Adhesion Test Arrangement

it is increased until failure occurs. This is defined as section A > 105 mm or section B < 95 mm or the covering protruding 3 mm beyond the end of the conductor at C or the covering developing cracks.

The typical results obtained for the 7/3.75 mm cable are shown in figure 8. The required test tensions for the three sizes are shown in table 3.

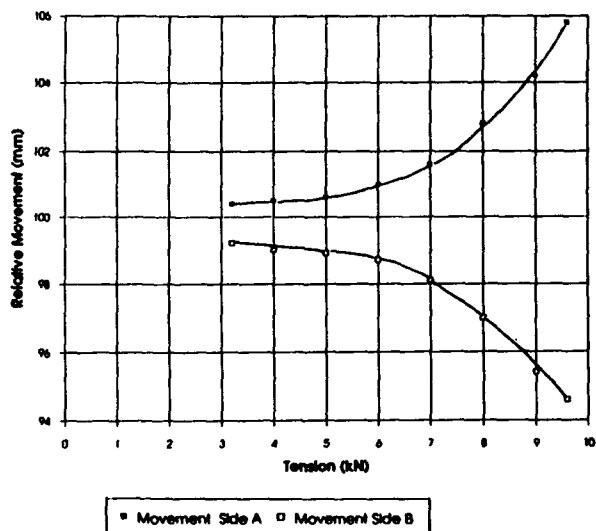


Figure 8 Adhesion Test Results for 7/3.75 mm Cable

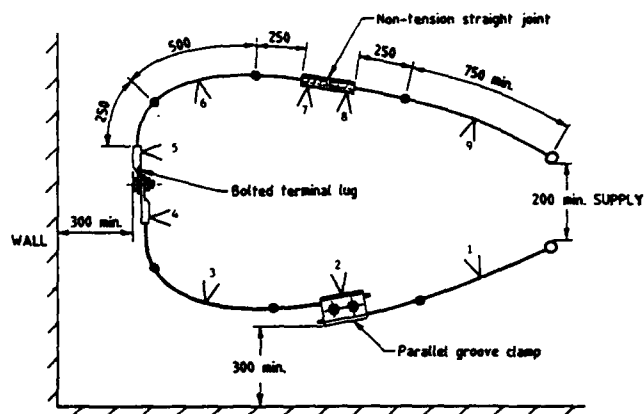
Interstrand Conductivity Test

The test is used to determine the effectiveness of electrical conductivity between the strands in the conductor and between the conductor and the line fittings.

A loop made up of the covered water blocked conductor joined with fittings to be used with the cable is temperature cycled under load and the temperature and resistance of various parts of the circuit monitored.

Table 3 Required Tensions (10 mins) for Adhesion Test

	Conductor Stranding		
	7/3.75 mm	7/4.75 mm	19/3.5 mm
Tension kN	3.2	4.9	7.5



NOTE: Dimensions are in millimetres

SYMBOLS

- potential measurement points
- > thermocouple (placed approx. mid-span in conductor length)
- lugs for point of connection of test loop supply

Figure 9 Interstrand Conductivity Test Arrangement 2

The test assembly with the fittings is shown in figure 9.

The temperature cycle consists of a test current passed through the test loop for two hours which raises the temperature of the reference conductor to $90 \pm 3^\circ\text{C}$ before the end of the two hour period. The reference conductor is taken as the section of cable in the test loop which reaches the highest temperature. After the heating cycle the assembly is allowed to cool to 5°C above ambient temperature. This is repeated 150 times. The temperature and electrical resistance monitoring points are shown in figure 9.

The requirements for the test are that the temperature of any fitting shall not exceed that of the conductor on either side of the fitting and that the final resistance after 150 cycles shall not exceed 115% of the initial value.

Results obtained for the 7/3.75 mm water blocked covered conductor cable are shown in tables 4 and 5.

The developed three sizes of covered water blocked conductor conformed to all the above test criteria.

Table 4 Final Temperature Measurements

Thermocouple Position as in Figure 9	1	2	3	4	5	6	7	8	9
Final Temperature (°C)	93	64	91	70	69	90	88	88	93

Track Resistance Test

The ability of the covering to resist electrical tracking was determined by the "Dip Track Test" technique outlined in 4. In this procedure the sample held vertically is immersed in a solution and then withdrawn. An electrode of Nichrome wire is sited on the sample. At the top of the stroke the electrode tip is one inch above the solution surface while the bottom of the sample is still in contact with the solution. The procedure is repeated

**Table 5 Resistance Measurements
Across Fittings (corrected to 20°C)**

Fitting	Resistances (m.ohm) - Cycling	
	Before	After
Parallel Groove Clamp	0.2333	0.2318
Bolted Terminal Lug	0.2416	0.2522
Non Tension Joint	0.2250	0.2375

four times per minute for a minimum of 10 and a maximum of 50 cycles. The severity of the test is controlled by the voltage applied to the electrode. Failure occurs when an arc is maintained for two consecutive cycles between the electrode and the solution across one inch (25.4 mm) of the test specimen. In the test, covering samples directly off cable can be evaluated.

**Table 6 Tracking Resistance of
Some Covering Materials**

Material (Thickness)	Tracking Test Result
Grey XLPE (3.4 mm)	No tracking or erosion at 3 kV
Grey XLPE (1.8 mm)	No tracking or erosion at 3 kV
Grey TR HDPE (1.9 mm)	No tracking to 2.6 kV, erosion 2.6 - 2.8 kV
Grey HDPE (1.9 mm)	No tracking to 2.4 kV, erosion 2.4 kV
Black 2.5% CB HDPE (3.5 mm)	No tracking to 1.2 kV, erosion 1.2 kV
Black 2% CB XLPE (1.8 mm)	No tracking to 1.8 kV, erosion 1.9 kV
Black TR MDPE (1.9 mm)	No tracking to 3 kV, erosion at 3 kV

CB - carbon black
TR - track resistant
MDPE - medium density polyethylene

The results obtained on some covering materials are shown in table 6.

The results in table 6 show that the grey cross linked polyethylene material used for the covered water blocked conductor is track resistant under the conditions of the test.

TYPE TESTS

Test results obtained on the grey cross linked covering material of the 19/3.5 mm water blocked covered conductor are shown in table 7.

**Table 7 Test Results of the Grey
XLPE Covering**

Test	Requirement	Result
Unaged Tensile strength	min 12.5 MPa	20.3
Elongation at break	min 200%	485
Aged 7 days 135°C Tensile strength	min 75% unaged	85
Elongation at break	min 75% unaged	91
Hot set, 15 min 200°C, 400 kPa Elongation under load	max 100%	50
Elongation after cooling	max 15%	0
Pressure test 6 hrs at 100°C Depth of indentation	max 50%	11
Shrinkage test 1 hr 130°C	max 4%	Pass

The 19/3.5 mm cable dimensional and electrical test results are shown in table 8.

The cable performance test results for the more critical tests are shown in table 9 for the 19/3.5 mm cable.

The test results show that the 19/3.5 mm water blocked grey XLPE covered conductor complied with all the requirements. Compliant results were also obtained for the other two cable sizes.

Table 8 19/3.5 mm Cable Dimensional and Electrical Test Results

Test	Requirement	Result
Covering thickness		
Minimum average	3.4 mm	3.4 mm
Minimum at any point	3.0 mm	3.2 mm
Maximum at any point	4.0 mm	3.6 mm
Maximum overall diameter	25.2 mm	25.0 mm
Insulation resistance constant, G.ohm.m		
at 20°C	min 3000	7700
at 90°C	min 3.0	162
Capacitance increase after immersion at 20°C		
between day 1-14	max 3%	Pass
between day 7-14	max 1.5%	Pass
Water absorption of insul. electrical method 5 days at 85°C, 2.5 kV DC	No breakdown	Pass
High voltage AC test 18 kV for 4 hr after 16 hrs immersion	No breakdown	Pass

density polyethylene is used as the outer layer because it generally has higher abrasion resistance than XLPE or LDPE. Therefore the cable as far as the abrasion property is concerned would be better in high tree contract areas.

The alternative design is shown in figure 10. The cable is manufactured

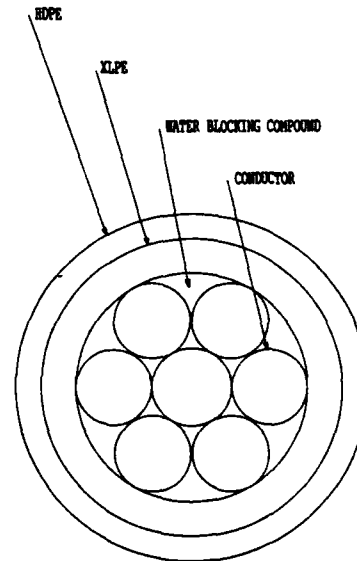


Figure 10 Alternative Design for the Water Blocked Covered Conductor

Table 9 Cable Performance Test Results

Test	Requirement	Result
Waterblocking tests		
(i) Static	No water penetration under the covering or along the interstices between the strands	Pass
(ii) Dynamic	as above	Pass
Stripping test at 20°C, 40°C	No water blocking compound left on outer surface of conductor	Pass
Interstrand conductivity test	During the test fittings at a lower temperature than conductor either side of the fitting. Final resistance of fittings after 150 cycles < 115% of initial value of each fitting	Pass Fittings clamp 101.4 bolted 102.8 non-tension 104.2
Dripping of compound test, 24 hours at 100 ± 5°C	No dripping of water blocking compound into tray	Pass
Adhesion test	Less than 5 mm slippage of covering on conductor	Pass - no failure at 17kN

using a similar process to that described earlier using the same water blocking compound except that the additional grey HDPE material is applied. Some materials for this application are shown in table 6.

Some type test data for the 7/3.75 mm water blocked cable with the XLPE and HDPE layers is shown in table 10.

From table 10 it can be seen that the cable with the HDPE outer layer has the same excellent water blocking characteristics and similar cable performance in the adhesion test, dripping of compound test and stripping test as the cable design with the single grey XLPE covering.

NEW DESIGN

An alternative design for the water blocked covered conductor has a 2.0 mm radial thickness of cross linked polyethylene (XLPE) followed by a further layer of 1.4 mm radial thickness of a UV stabilised grey high density polyethylene (HDPE) material. High

Conclusions

A range of water blocked grey XLPE covered conductors has been developed for an overhead medium voltage distribution system. The cables have excellent water blocking characteristics and also offer good performance in stripping tests, interstrand conductivity

**Table 10 Type Test Data for 7/3.75 mm
Water Blocked Covered
Conductor with HDPE Outer Layer**

Test	Requirement	Result
Static water blocking test	No water penetration under the covering or along the interstices between the strands	Pass
Dynamic water blocking test	As above	Pass
Stripping test at 20°C, 40°C	No water blocking compound left on outer surface of conductor	Pass
Dripping of compound test 24 hrs at 100 ± 5°C	No dripping of water blocking compound into tray	Pass
Adhesion test	Less than 5 mm slippage of covering on conductor	Pass-no failure at 8 kN
Grey HDPE		
Tensile strength	min 22 MPa	29 MPa
Elongation at rupture	min 400%	> 600%
ESCR (F1, Hrs)	min 250	> 250
Shore D hardness	-	62

tests and adhesion properties in strain clamping tests.

An alternative design comprising a second layer of a grey HDPE over the XLPE has also been presented. This cable shows similar performance in cable tests to the single layer grey XLPE design.

The advantages the water blocked covered conductors offer are reduced likelihood of conductor corrosion, possibility of reduced clearances between phases and the ability of the covered conductors to withstand in service clashing with other covered conductors in the same circuit and with conductive material between phases. The covered conductors described in the paper can remain in contact with tree branches for extended periods of time and give better performance in polluted environments.

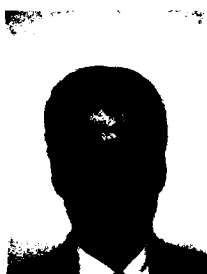
REFERENCES

- (1) Elford R.F., Kato K., et al "Development and Introduction of Aerial Insulated Unscreened Conductor (IUC) in South Australia" 8th. CEPSI, Singapore 1990.
- (2) ETSA Distribution Standard MDS 066/A.
- (3) Australian Standard AS 1531-1991.
- (4) ICEA S 66 524, NEMA WC7 - Track Resistance Test Method B.



Eugene Buczma graduated from the Department of Industrial Science Melbourne University in 1971, and received a Masters degree from the same University in 1980. In between he worked in the cable industry and with a plastics resin manufacturer carrying out

projects in cable materials development and in polymer resin and process development and Plastics Technical Service. In 1985 he joined Olex Cables where he became Manager Development Engineering and is now Materials and Process Technology Manager in the Communications Division.



Arturo Fragale received his B.E. degree in Chemical Engineering from Melbourne University in 1984 and an Associate Diploma of Engineering (Plastics Technology) from R.M.I.T. in 1991. In 1984 he joined Commercial Polymers Pty

Ltd with appointments in both Marketing and Technical Departments. In 1990 he joined Olex Cables as a Development Engineer, where he is engaged in product and process development.

Olex Cables, Melbourne
A Division of Pacific Dunlop Limited
207 Sunshine Road, Tottenham, 3012
Victoria Australia

SUBMARINE ELECTRIC POWER-OPTICAL COMMUNICATIONS COMPOSITE CABLE

Salvador Camps, Carlos Osorio, Richard Vasquez and J. A. Olszewski

CABEL Industria Venezolana de Cables Electricos C.A.
Valencia, Venezuela

ABSTRACT

The topic of this paper is the design and manufacturing technique of a series of high voltage power cables with a built-in multimode fibers complement for two-directional PCM voice or low speed data channels. These cables were made by Cabel C.A. and were installed for Freeport-McMoran Oil & Gas Company between different facilities in the Gulf of Mexico at the depth of up to about 90 meters (300 feet). As of this writing, the cables have been operational for about two years and have provided a satisfactory performance.

The construction was designed for dry operation or the cables cores were completely blocked either by pressure filling or extrusion. The power cable component was more or less standard, including triple extrusion XLPE conductors insulation and galvanized steel wires armor. Optical cable part, in spite of just 10 to 40°C water temperature range, had to contend with 90°C operation temperature design of the power conductors as well as 130°C and 250°C temperatures during 60 Hz power overload and short-circuit condition respectively. Since the cable temperature gradient was not provided by the customer, the improvised approach to the high temperature operation performance evaluation was required and is emphasized herein.

CONSTRUCTION OF CABLES

The submarine power-optical cables consisted of 3-phase, 15 kV, low resistance ground, power cable part with concentric-lay-stranded, copper conductors of 4/0 and No. 2 AWG sizes. The space between individual wire strands was filled with an asphaltic compound. The insulation was a triple, tandem extruded, steam cured XLPE compounds made by Union Carbide. The insulation level (IL) was 173% to minimize the likelihood of failures. A semi-conducting coated fabric tape was applied helically over the extruded insulation shield layer and a helically applied with overlap, 0.127 mm thick, bare copper tape completed the individual conductors.

The optical cable part was to carry 24 voice or data bi-directional channels on two fibers at the T1 carrier rate of 1.544 Mbps. Its construction was non-metallic. Corning's type CPC3, 62.5/125 μ m, multimode fibers coated with a low modulus inner and a high modulus outer dual acrylate coating to an overall diameter of 250 μ m. Oversized, color coded, polybutylene terephthalate tubes were employed as a secondary buffering for the fibers. A maximum of two fibers were inserted into each tube during their extrusion and the space inside the tube was filled with a thixotropic filling compound type Syncofox 280. Six or four fiber bearing tubes were stranded over 0.89 mm diameter glass-epoxy central strength members, with or without additional diameter build-up via extruded HDPE. Fiberglass core tape made by Chase & Sons was parallel folded in line with extrusion of LDPE inner jacket and the core spaces were filled with Syncoseal SCC-854 thermoplastic copolymer filling compound. A main reinforcement of Du Pont's Kevlar 49 aramid fibers was distributed over the outer circumference of the inner jacket in parallel application and the second LDPE jacket completed the assembly of the optical units.

Three insulated conductors of the specified size were cabled using a floating carriage machine. The required number and type of optical units were placed in their outer interstices. The space between insulated conductors was filled with a saturated polypropylene yarn. The inner space of composite cable core was pressure filled with amorphous polypropylene compound. The space around conductors and optical units assembly was then brought into a cylindrical configuration and made water tight by Cabel's proprietary pressure extruded PVC compound. Over it a layer of an extruded HDPE jacket was applied followed by a single layer rigid PVC coated galvanized steel wire armor, and the polyethylene jacket overall.

The cable construction details of main interest are as follows:

Table 1

Parameter	Cable Type		
	A	B	C
Cu power conductor, AWG	4/0	4/0	2
dia., mm	11.68	11.68	6.54
Dia. over metal insulation shield, mm	30.2	30.2	24.8
Number of multimode fibers ^a	12	6	3
Number of optical units	2	1	1
Number of PBT tubes			
per unit	6	6	4
Inner dia. of tubes, mm	1.0	1.0	1.0
Outer dia. of tubes, mm	2.0	2.0	2.0
Built-up dia. of central strength member, mm	2.11	2.11	0.89
Kevlar 49 content, 10 ³ denier			
per optical unit	89.46	89.46	25.56
per cable	178.9	89.46	25.56
Dia. of optical unit, mm	13.6	13.6	10.9
Stranding lay of tubes, cm	17.5 (LH)	17.5 (LH)	15 (LH)
Cabling lay of power & optical units, cm	89 (LH)	89 (LH)	74 (LH)
Galvanized steel wire armor:			
number of wires	32	32	32
size, BWG	6	6	8
overall dia. (1), mm	5.16	5.16	4.19
estimated zinc thickness ^b , mm	0.043	0.043	0.039
approx. steel wire dia., mm	5.07	5.07	4.11
lay length, cm	66 (RH)	66 (RH)	56 (RH)
Dia. of completed cable, mm	96.3	96.3	82.3
Composite cable weight, kg/m	15.79	15.84	10.12
Shipping reels size, cm			
flange	356	294	338
traverse	559	254	292
drum	163	163	152
Min. bending radius ^c , cm	122	122	107

^a 1 or 2 extra fibers per optical unit were inserted by Cabel C.A. as a precaution against fiber breakage in this complex cable construction.

^b Based on 7.14 specific gravity of zinc⁽²⁾ plus its 305 and 275 grams/m² coating on No. 6 and 8 BWG wires respectively⁽³⁾.

^c Empirically derived taking into account the minimum diameter of the power cables.

CABLE SERVICE ENVIRONMENT AND REQUIREMENTS

The cables were installed for Freeport - McMoran Oil & Gas Company by R. T. Casey Inc. either between a central facility or a power plant and the gas/oil/sulphur mine

platforms, at the depth of 61 - 84 meters, the latter due to subsidence during operation, in the Main Pass 299 field. The facility stretches to 1 mile in length and is located 16 miles east of the mouth of the Mississippi river in the Gulf of Mexico. The sea bottom was reported to be either sand or mud.



Figure 1

Due to relatively small distances between the individual facilities - see Figure 1 - the routes were designed to have no field joints nor communication repeaters. The critical nature of the application dictated this construction approach.

The ambient water temperature was established by the customer to be only 10 to 40°C, but normal continuous operating temperature of the conductors was given as 90°C with insulation shields being at about 85°C⁽⁴⁾. In addition, 130°C power conductors temperature was specified for emergency overload operation and 250°C for short-circuit fault condition. Neither the duration of overload and short-circuit fault condition nor the temperature distribution across the cables' cross-section were specified. Thus, having no specific guidelines, it was assumed that the temperature drop between the conductor and the shield will be directly proportional to the temperature of the conductor, namely, $5(130/90) = 7^\circ\text{C}$ for overload condition. As far as the short-circuit fault is concerned, it was assumed that such an event will most likely take place under the overload operation and will be dealt with quickly by a protection device. Consequently, the temperature of all three conductor shields during short circuit condition was assumed to remain unchanged at $(130 - 7) = 123^\circ\text{C}$. It was further assumed that the optical fibers and Kevlar reinforcement in the optical units will be 5°C below that of the insulation

shields.

The actual temperature of the steel wire armor during cable operation was another unanswered question of a major significance. Therefore, since the outer peripheries of three power conductor shields that were embedded in the pressure extruded PVC belt approached the cable armor more or less at the same distance as that between the circular layer of armor wires and the sea water, to be on the safe side it was assumed that the armor temperature will be at a mid point between that of shields and the sea water. Such cable temperature profile rather than exponential gradient, together with the sea water temperature being taken as 40°C, and ascribing the thermal effects totally to the cable components length change, was intended to represent the worst possible case scenario as far as optical fibers were concerned. In summary, the effect of the following assumed temperatures was studied:

Table 2

Cable Component	Temperature, °C		
	Normal Oper,n	Over- load	Short Circuit
Cu power conductors	90	130	250 ^a
Sea water (worst case)	40	40	40
Cu insulation shields	85	123	123
Optical fibers			
& Kevlar	80	118	118
Steel wire armor	62.5	81.5	81.5

^a One copper power conductor at this temperature if short-circuit fault to ground, two if fault between phases, etc.

DESIGN OF SECONDARY PACKAGING FOR OPTICAL FIBERS

It became obvious early in the development that expected by Freeport-McMoran Oil & Gas Company about 85°C normal operating temperature of the power cable's conductor shields will be a problem even in testing of finished cables. Similarly, 130°C and 250°C conductor temperatures during 60 Hz power overload and short-circuit condition respectively, somewhat arbitrary power industry limits for operation of extruded insulation cables⁽⁵⁾, while handleable by the thermoset XLPE power conductors insulation, at first glance appeared to present an extremely tough, if not impossible, design targets as far as optical fiber cable complement is concerned. It has to be realized though, that under normal conditions, overloads are of a limited time duration. To give an example, it was demonstrated⁽⁶⁾ that with 50% increase in current, it takes about 18 hours to change the normal operation conductor temperature of 90°C to

130°C. Of importance is also a fact that the short-circuit faults typically last seconds or just a fraction of a second and that while the specific heat of copper⁽²⁾ is 0.0921 calories/gram/°C, that of polyethylene, according to Union Carbide, is 0.500 calories/gram/°C. The overload, therefore, tends to be more problematic than the fault.

The cable design concerns stem from the fact that the commercially available fibers are coated with relatively low temperature acrylate material, which according to Corning are "conservatively rated for -60 to +85°C temperature range operation", and that no other coating materials were available. Additional concern was that the multimode fibers chosen by the customer were known to be more sensitive to light loss via microbending during their packaging into cables than the monomode fibers. As far as the oversized tubes fiber packaging is concerned, the polybutylene terephthalate (PBT), type Vestodur 3000 made by Huls Aktiengesellschaft, was decided upon primarily because of its high melting temperature of 221 - 226°C⁽⁶⁾ and other excellent physical properties, including high yield strength of 5.8 kgf/mm², 0.7x10⁻⁴ coefficient of linear expansion and just 0.5% water absorption⁽⁷⁾.

The length of fibers inside the tube was targeted to be longer than the length of the tube during its extrusion using typical industry approach. This operation causes the fiber to assume a helix that hugs the inner wall of the tube bore. The pitch of the so formed helix should be as short as possible without loss of guided light, or without stressing the fibers beyond a safe limit⁽⁸⁾ of not more than 30% of screen test value of 1070 kgf/cm² (10500 N/cm²). This condition is especially critical at the extreme cable length contraction by the operating environment's temperature drop and the resultant degree of fiber bending.

The actual effective fiber bend radius R_f due to its helical configuration in the tube is given below.

$$R_f = \frac{h_p^2}{4\pi^2(r_t - r_{cf})} + (r_t \cdot r_{cf}) \quad \text{----- (1)}$$

where h_p = helix pitch length
 r_t = tube bore radius
 r_{cf} = radius of coated fiber

Since the minimum fiber bend radius R'_t is stress limited and for 125 µm diameter fiber calculates to be about 110 mm, the minimum allowable fiber helix pitch h_p per equation (1) becomes strictly a function of r_{cf} and r_t as given for a straight tube by

$$h_p = 2\pi(r_t - r_{cf}) [110/(r_t - r_{cf}) - 1]^{1/2} \quad \text{---- (1a)}$$

where all dimensions are in mm.

Given high operating temperatures of the cable components but what had to be a relatively low steel wire armor temperature, an element that primarily controls thermally induced cable length changes, it was decided that with the use of one, or at the most two fibers per 1 mm inside diameter tubes, or $r_t = 0.5$ mm, should be adequate. Thus, with the diameter over fiber coating being 250 μ m, or $r_{cf} = 0.125$ mm, minimum permissible helix pitch h_p comes to 40.3 mm and became the process limit rather than the target minimum because of Cabel's observation of frequent and unavoidable, torsion induced, fiber helix direction reversals at a rather sharp radii.

Using the above design parameters, the excess fiber length or strain accommodation inside the straight 1 mm inside diameter tubes can be determined from a general relation

$$\Delta L_1 = \frac{\{[2\pi(r_t - r_{cf})]^2 + h_p^2\}^{1/2} - h_p}{h_p} 100, \% \quad (2)$$

and calculates to be 0.171% maximum.

Thus, since unlike the outside-plant communication cables that are required to operate at -40 to 70°C or just about $\pm 55^\circ$ C temperature excursions from ambient, the subject cables were to operate always at high temperatures, or at only positive temperature excursions, the required ΔL_1 had to be as high as possible and in practice was determined by measurements to be about 0.162% average. High temperatures operation also presented no particular problems in selection of the buffer tubes filling compound. Syncofox 280 thixotropic compound made by Synco Chemical Corporation was known to have good behavior at ambient and higher temperatures and Cabel C.A. had experience in its handling. This compound was adopted.

The second fiber strain consideration is its permissible safe residual value ΔL_2 in the operating cable. It is a function of the stress-strain in the fiber screen test which is typically performed at about 0.45 kgf (1 lbf) stress and resultant 0.50% strain during 125 μ m diameter fiber drawing. Since glass fibers are perfectly elastic and it was established⁽⁸⁾ that can be operated continuously at 1/3 of screen test value, $\Delta L_2 = 0.167\%$.

DESIGN OF OPTICAL UNITS

Small diameter glass-epoxy central strength member rods, one for each optical unit, were adopted primarily to enable safe stranding of the optical fiber bearing PBT tubes. The diameter of the rods had to be

adjusted (built up) to accommodate the desired number of tubes of a given (2.0 mm) outside diameter. The required center rod diameter D_r for L_s lay loosely stranded tubes of outside diameter d_{ot} can be shown to be:

$$D_r = \frac{d_{ot}(1 + \cos\psi)K}{\cos\psi \cos\theta} \quad (3)$$

where $\psi = (90 - 180/n)$ degrees, where n is the number of tubes in a single layer.

θ = tubes' lay angle

$$= \tan^{-1} \frac{\pi(D_r + d_{ot})}{L_s}, \text{ degrees}$$

and K = empirical constant enabling ease of filling compound penetration down to central rod.
= 1.05

It is known that the stranding lay of fiber bearing tubes L_s has to be relatively short in order to provide additional significant fiber strain accommodation with cable strain due to applied axial load or due to the thermally induced longitudinal cable expansion. In this case L_s was set at 175 mm for 6-tube and 150 mm for smaller diameter 4-tube optical units. This placed required central strength member diameter D_r per equation (3) at 2.11 and 0.87 mm for 6 and 4 tube constructions respectively. Because of convenience of supply, 4-tube construction employed readily available 0.89 mm diameter bare glass-epoxy rod while for 6-tube construction the rod diameter was built up by extrusion of HDPE.

It has to be realized that the additional fiber strain accommodation due to stranding is obtained by movement of already straightened fiber from tube center to the inner wall of the tubes in the direction of optical unit center. It is closely given by

$$\Delta L_3 = \frac{\{[\pi(D_r + d_{ot})]^2 + L_s^2\}^{1/2}}{\{[\pi(D_r + d_{ot} - d_t + d_{cf})]^2 + L_s^2\}^{1/2}} - 1 \quad (4)$$

multiplied by 100 if in per cent.

Thus, using chosen stranding lays and central rod diameters, the fiber strain accommodations due to stranding in Cabel's design of optical units calculates to be 0.083 and 0.090% for 4-tube and 6-tube unit constructions respectively.

It must be emphasized that short stranding lays of fiber bearing tubes are also required for their high mechanical coupling to the glass-epoxy central strength member. Good coupling tends to stabilize tubes' length with cable temperature changes to

that of glass-epoxy having thermal coefficient of linear expansion of $6.3 \times 10^{-6}/^{\circ}\text{C}$ versus $7.0 \times 10^{-5}/^{\circ}\text{C}$ for PBT tubes⁽⁷⁾. The former is more or less in line with other main strength materials used in the subject composite cable, i.e. $12.1 \times 10^{-6}/^{\circ}\text{C}$ for galvanized carbon steel wire armor and $16.9 \times 10^{-6}/^{\circ}\text{C}$ for copper power conductors⁽²⁾. It was felt that the above described combination of cable materials at lower temperatures will not cause local buckling or even occasional fractures of glass-epoxy rods that have been observed on typical, high polyethylene content (double jacketed), non-metallic, optical communication cables.

The use of Kevlar 49 reinforcement between inner and outer jackets of the optical units was of some concern in terms of pay-off tension controls for the individual bundles and the resulting stress-strain characteristics as well as the strength at break. It is known that the breaking strength per denier decreases with an increase of the bundle size and also for a increasing number of bundles when the latter have somewhat uneven pay-off tensions during cable manufacture. The main cause is Kevlar's low elongation at break⁽⁹⁾ of about 2.5%. Shortest bundle engages first, is first to fail with the increasing axial load and in turn leads to overall catastrophic break failure at abnormally low loads. This is especially true with the parallel application of the Kevlar bundles. Special tension controls were therefore, devised and an attempt was made to purchase larger bundles assembled by the specialists, namely, Du Pont. Tensile tests on completed fiber units yielded breaks essentially at about 80% average of the bundle nominal specified by Du Pont times the number of bundles employed.

COMPOSITE CABLE CONSIDERATIONS AND PERFORMANCE

Cable assembly, because of its large size and weight - see Figure 2 depicting loading one of the type A reels with 3.4 km length, 54 metric tons weight of cable onto a special truck - required heavy cable making machinery which typically has rather coarse tension controls. This was one reason for heavy reinforcement of optical units. Another problem was cable mechanical performance characterization by test. Large tensile machines were simply not available. The same was true for temperature and temperature cycling chamber. Optical attenuation testing was therefore performed at room temperature, while the bandwidth measurement was not required as it is known to improve with cable making operations due to the higher order modes stripping. Bandwidth of fibers as received from the supplier is virtually certain to improve in completed cables and an increase in optical loss of the multimode fibers in cable making opera-

tions attests to this phenomenon. Tests at higher temperatures of overload and short-circuit conditions were not even attempted because of certainty of damage to optical units.

The attenuation of optical fibers was measured with the aid of OTDR at 820 nm wavelength and the results at different stages of manufacture are given in Table 3.



Figure 2

Since the customer also needed to know the optical loss at 0.85 and 1.3 μm wavelength, these values were estimated from the spectral response curve of Figure 3 for CPC3 fibers that was supplied by Corning Inc.

Table 3

Optical Attenuation at 0.82 μm , dB/km		
Manufacturing stage	Min.	Max.
As received	2.71	2.94
After buffer coloring	2.94	2.99
After PBT tubing	2.86	2.91
After tubes stranding	2.87	2.91
After cable core assembly	3.12	3.20
Finished cable	3.12	3.21

Thus, assuming no local attenuation perturbations, and there were none as determined by the OTDR, Figure 2 shows that $\alpha_{0.85} = 0.869\alpha_{0.82}$ and $\alpha_{1.3} = 0.1314\alpha_{0.82}$. Therefore, based on 3.21 dB/km worst loss at 0.82 μm in completed cable; the maximum loss at 0.85 and 1.30 μm can be expected to be 2.79 and 0.42 dB/km respectively. Incidentally, the expected worst fiber loss at 1.55 μm estimates to be $3.21(0.15/3.12) = 0.15$ dB/km.

A theoretical high temperature attenuation performance estimate was undertaken in terms of thermally induced cable length

changes, but proved to be rather problematic because of not only temperature uncertainty of different cable main strength components, especially of the most critical

NOMINAL SPECTRAL ATTENUATION IN DB/KM OF CORNING 62.5/125 UM MULTIMODE FIBERS

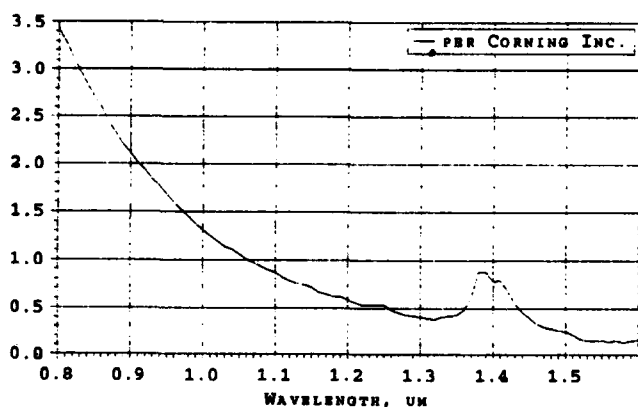


Figure 3

steel wire armor, but also because the temperature increase of conductors and armor could be expected to manifest itself in terms of an increase of their helices diameter rather than the pitch, etc.

Per reference 2, Table 4 gives the values of thermal coefficient of linear expansion α_0 and Young's modulus Y for cable components of interest.

Table 4

Cable Component	α_0 10 ⁻⁶ /°C	Y 10 ³ kg/mm ²
Steel armor	12.1	20.4
Cu power conductors	16.9	12.0
Kevlar 49* yarn		
reinforcement	2.0	11.6
Si optical fibers*	0.8	9.2

* Totally elastic material.

Since the maximum tensions of the cables are dictated by the optical fibers, Table 5 below gives the results of calculations for permissible cables' axial tension versus the design fiber strain accommodation for no increase in optical loss and permissible residual axial fiber stress-strain disregarding probability of optical loss rise. The derived values are based on just the main strength members and their listed in Table 4 values of Young's modulus, the definition of the latter being given by equation (5)

$$Y = \frac{F/A}{\Delta L/L_0}, \text{ kg/mm}^2 \quad \text{----- (5)}$$

where F is a force acting a on member that results in length change of ΔL and A is

the x-sectional area while L_0 is the initial length. Calculated tension forces F of the cables within the elastic limits of the components were obtained from this stress-strain slope relationship.

Table 5

Theoretical Cable Performance Results at Room Temperature			
Parameter	Cable A	Cable B	Cable C
<u>Fiber strain</u>			
accommodation, %			
tube helix (ΔL_1)	0.162	0.162	0.162
max. safe fiber strain (ΔL_2)	0.167	0.167	0.167
stranding (ΔL_3)	0.090	0.090	0.083
total cable strain for no increase in optical loss			
$\Delta L_0 = \Delta L_1 + \Delta L_3$	0.252	0.252	0.245
total cable strain for no fiber break failures			
$\Delta L_x = \Delta L_1 + \Delta L_2 + \Delta L_3$	0.419	0.419	0.412
<u>Cross-section area of cable main strength members A, mm²</u>			
steel armor ⁽¹⁾	646.0	646.0	424.5
Cu conductors ⁽¹⁾	321.4	321.4	100.8
Kevlar 49 ⁽⁹⁾	13.24	6.62	1.89
<u>Max. installation tension F, 10³ kgf</u>			
steel armor			
contribution	55.2	55.2	35.7
Cu conductors			
contribution	16.2	16.2	5.0
total			
$\Delta L_x (Y_{fe} A_{fe} + Y_{cu} A_{cu}) / 100$	71.4	71.4	40.7
<u>Max. installation tension F for no increase in optical loss, 10³ kgf</u>			
steel armor			
contribution	33.2	33.2	21.2
Cu conductors			
contribution	9.7	9.7	3.0
total			
$\Delta L_0 (Y_{fe} A_{fe} + Y_{cu} A_{cu}) / 100$	42.9	42.9	24.2

* Zinc coating excluded.

The cross-section area data show that the effect of Kevlar 49 can be neglected. Incidentally, its content calculation in different cables was based on Du Pont's figures for 4320 denier bundle of 0.737 mm diameter and 25% air content.

As far as cable tensions are concerned in general, it has to be kept in mind that from purely mechanical point of view the cables should not be stressed beyond the elastic limits of their components and that these limits are typically more broad than those permissible for optical fibers. Creep

under high continuous loads is yet another important factor.

In addition, Table 6 contains calculated per cent increases in cable length from a cable manufacturing temperature of 25°C to the operating temperatures versus different conditions of fiber strain accommodation. Since of the two main cable strength members, i.e. copper and steel, copper has higher α_{ocu} than that of steel α_{ofe} , a cable temperature rise of Δt in °C will put steel wire armor in tension and copper conductors into compression and the total temperature induced cable length increase in per cent ΔL_T should be given by the relationship derived below.

$$\Delta L_T = 100(\alpha_{ocu}\Delta t_{cu} - \alpha_{ofe}\Delta t_{fe}) \frac{Y_{cu}A_{cu}}{Y_{fe}A_{fe} + Y_{cu}A_{cu}} + 100(\alpha_{ofe}\Delta t_{fe}) \quad (6)$$

Table 6

Theoretical Cable Performance Results at Elevated Operating Temperatures for No Increase in Optical Loss

Parameter	Cable A	Cable B	Cable C
a) NORMAL OPERATION			
<u>Fiber strain accommodation, %</u>			
ΔL_o	0.252	0.252	0.245
linear thermal expansion, ΔL_{no}	0.004	0.004	0.004
total, $(\Delta L_o + \Delta L_{no})$	0.256	0.256	0.249
<u>Cable length increase, %</u>			
ΔL_T (based on Fe & Cu)	0.060	0.060	0.053
<u>Permissible cable strain & stress</u>			
strain, $\Delta L = (\Delta L_o + \Delta L_{no}) - \Delta L_T$, %	0.196	0.196	0.196
stress, $\Delta L(Y_{fe}A_{fe} + Y_{cu}A_{cu})/100$			
10^3 kg	33.4	33.4	19.3
b) OVERLOAD OPERATION			
<u>Fiber strain accommodation, %</u>			
ΔL_o	0.252	0.252	0.245
linear thermal expansion, ΔL_{oo}	0.007	0.007	0.007
total, $(\Delta L_o + \Delta L_{oo})$	0.259	0.259	0.252
<u>Cable length increase, %</u>			
ΔL_T (based on Fe & Cu)	0.093	0.093	0.082
<u>Permissible cable strain & stress</u>			
strain, $\Delta L = (\Delta L_o + \Delta L_{oo}) - \Delta L_T$, %	0.166	0.166	0.170
stress, $\Delta L(Y_{fe}A_{fe} + Y_{cu}A_{cu})/100$			
10^3 kg	28.3	28.3	16.9

c) SHORT-CIRCUIT CONDITION

<u>Fiber strain accommodation, %</u>			
ΔL_o	0.252	0.252	0.245
linear thermal expansion, ΔL_{sc}	0.007	0.007	0.007
total, $(\Delta L_o + \Delta L_{sc})$	0.259	0.259	0.252
<u>Cable length increase, %</u>			
ΔL_T (based on Fe & Cu)	0.139	0.139	0.107
<u>Permissible cable strain & stress</u>			
strain, $\Delta L = (\Delta L_o + \Delta L_{sc}) - \Delta L_T$, %	0.120	0.120	0.145
stress, $\Delta L(Y_{fe}A_{fe} + Y_{cu}A_{cu})/100$			
10^3 kg	20.4	20.4	14.3

Electrical testing of power conductors, of course, presented no particular problems. The conductors' insulation of all three cable types and lengths withstood 35 kV AC for 5 minutes and 70 kV DC for 15 minutes using rapid potential rise method. Corona inception voltage was determined to be greater than 20.0 kV AC worst case using 5 pC sensitivity apparatus; well above 15 kV operation. Typically, the partial discharge rose on an average to about 27.5 pC at 26 kV and 50 pC at 35 kV AC. The insulation resistance was in excess of 1 TΩ·km as measured with a 500 volts potential.

CONCLUSIONS

The estimates obtained in this study lead to the following conclusions:

1) The cables are very rugged and can take appreciable axial installation loads, i.e. about 70,000, 70,000 and 40,000 kg for types A, B and C respectively. Since with such loads the optical fibers will be under about 0.167% axial strain, the optical loss can be expected to be significantly higher throughout duration of these loads.

2) Cable types A, B and C can be installed without temporary increase in optical attenuation at axial loads of up to about 40,000, 40,000 and 25,000 kg respectively.

3) Taking into account cable temperatures during normal and overload operation as well as during short-circuit fault condition, all three cable types can be expected to operate satisfactorily, or without optical loss increase, if their axial loads will not be higher than:

a) 33,000, 33,000 and 19,000 kilograms for cables A, B and C respectively in normal operation.

b) 28,000, 28,000 and 17,000 kilograms for cables A, B and C respectively in overload operation.


c) 20,000, 20,000 and 14,000 kilograms for cables A, B and C respectively during short-circuit fault condition.

Since the optical fibers are expected to operate under all of the above listed conditions, the practical cable axial loads are limited to the values specified under (c). It has to be remembered however, that the creep of the main strength members will decrease these loads.


4) If the overload operation is limited to a few hours and a short-circuit fault condition is de-energized in a few seconds or less, no thermal damage of the acrylate coating on the optical fibers and other polymeric cable components will be expected. Days of overload operation will lead to problems even if the temperature of the conductors does not exceed 130°C.

REFERENCES


1. United States Department of Commerce, National Bureau of Standards, "Copper Wire Tables - Handbook 100", U.S. Government Printing Office, Washington, D.C., February 21, 1966.
2. Robert C. Weast, "CRC Handbook of Chemistry and Physics", 66th edition, CRC Press, Inc., Boca Raton, Florida.
3. ICEA Publication S-66-524/NEMA WC-7, 1988.
4. ICEA Publication P-45-482, "Short Circuit Performance of Metallic Shields and Sheaths of Insulated Cable", 2nd Edition, August, 1979.
5. Association of Edison Illuminating Companies, "Specifications for Thermoplastic and Crosslinked Polyethylene Insulated Shielded Power Cables Rated 5 Through 46 kV", 8th Edition, New York, 1982, (AEIC CS5-82).
6. C. Katz et al, "Emergency Overload Characteristics of Extruded Dielectric Cables Operating at 130°C and Above", IEEE Transactions on Power Apparatus and Systems, PAS-103, 3454-3463, December 1984.
7. Huls Aktiengesellschaft, "Polybutylene Terephthalate", Postfach 1320, D-4370 Marl, Germany.
8. S. T. Gulati, "Strength and Static Fatigue of Optical Fibers", Intelcom 77 Proceedings, Dedham, Mass., 1977.
9. Du Pont de Numours & Co. (Inc.), "Kevlar - Fiber Optic Database", Wilmington, Delaware.



Salvador Camps was born in Caracas, Venezuela and has a degree in electrical engineering. He joined Cabel in 1981 as a Technical Manager and at present holds the position of Operations Manager.



Carlos Osorio is a native of Camaguan, Venezuela and joined Cabel in 1968. He had assignments in product development as well as product engineering departments and at present holds the position of Technical Manager.



Richard Vasquez is a native of Maracay, Venezuela and a 1988 graduate of the University of Carabobo with a degree in electrical engineering. Upon graduation, he joined Cabel with assignment in application engineering, quality control and telephone cable production departments. At present, he holds the position of Telephone Plant Manager.

DESIGN AND TEST OF A NEW METALLIC FIBRE-OPTIC CABLE FOR AERIAL CABLE WAYS

Amir Fargahi*, Christoph Zehnder*, Angelo Banfi*, Daniel Schoepke**, Chambos Theodossi***, Hugues Hagmann*, Willibald Nägele* and Hubert Zimmermann*

* BRUGG TELECOM AG, CH-5200 BRUGG, SWITZERLAND

** BRUGG DRAHTSEIL AG, CH-5242 BIRR, SWITZERLAND

*** LASER ARMOR TECH CORP., SAN DIEGO, CA 92121, USA

Abstract

The aerial cable way operators in the mountains have increasing communication demands. In order to satisfy these needs in a cost-effective and environmental-friendly way, Brugg Telecom AG has developed and successfully tested a new generation of metallic fibre-optic aerial ropes.

The rope is especially designed to meet the required very high tensile performance and crush resistance. The tests have shown that the newly developed rope can withstand very high lateral loads.

During a long-term field-test we continuously monitored the attenuation of the optical signal, load and environmental conditions. The field-test has demonstrated the very good properties of the rope also in everyday use.

Thanks to its excellent mechanical and environmental performance the rope is as well best suited in the field of extreme and hazardous applications.

Introduction

In the Swiss mountains there are a lot of aerial cable ways, these installations show increasing communication demands. Optical fibres reveal to be the transmission media of choice to transmit video, TV, telephone and control signals. To comply with the requirements for this kind of installations, i.e. long spans, large altitude differences and high additional loads due to ice, snow and wind, an aerial cable with small diameter and high tensile strength is required.

The BRUGG group has a renowned experience in wire rope technology and is one of the major manufacturers of wire ropes for aerial cable ways worldwide. It was then a natural way to combine this experience with the know-how of fibre-optics, also available in the group, to offer a new innovative product to the aerial cable way operators.

The existing wire rope on top of the towers can be replaced by the new product. Therefore, we are able to provide a very value-effective and environmental-friendly solution in order to increase the information-carrying capacity of an existing installation, since it is not necessary to build new towers or other costly installation.

We didn't only develop the rope containing the optical fibres, but have set up as well the capability to plan and install turn-key installations.

Design and Manufacturing

The construction uses jelly-filled stainless steel tubes, which contain the optical fibres. These tubes are stranded together with zinc-coated steel wires, in a way that the fibres are protected against stress and lateral pressure also at the extreme mechanical loads (figure 1).

The design of the rope allows to fully exploit the mechanical longterm stability of the steel wires. Even at the maximum long-term cable load, the elongation of the optical fibres is insignificantly low.

To meet the different installation requirements, we developed ropes with different cross sections¹. The resulting ropes with diameters from 7 to 11.8 mm, weights from 190 to 550 kg/km and long-term tensile strengths from 15 to 45 kN are appropriate to cover the standard requirements of aerial cable way installations (table 1).

The ropes are suited to contain up to 36 single-mode (SM) or multi-mode (MM) fibres with the same fibre specifications as in standard outdoor cables¹. The optical specifications are according to Swiss PTT Telecom² and CCITT requirements.

The tube itself is made from a stainless steel strip which is formed into a tube through a precision forming mill. Optical fibres and thixotropic filling compound are introduced into the tube, which is then welded longitudinally with a CO₂ laser beam. The welded tube is then reduced in size through a set of diamond dies with the weld integrity continuously monitored and recorded.

The weld has a 100 % penetration, virtually indistinguishable to the naked eye and with a smooth inner surface at the welding area. The optical fibres are inserted into the tube with very little tension and with a slight excess length. The filling compound of the tubes is provided with a hydrogen getter.

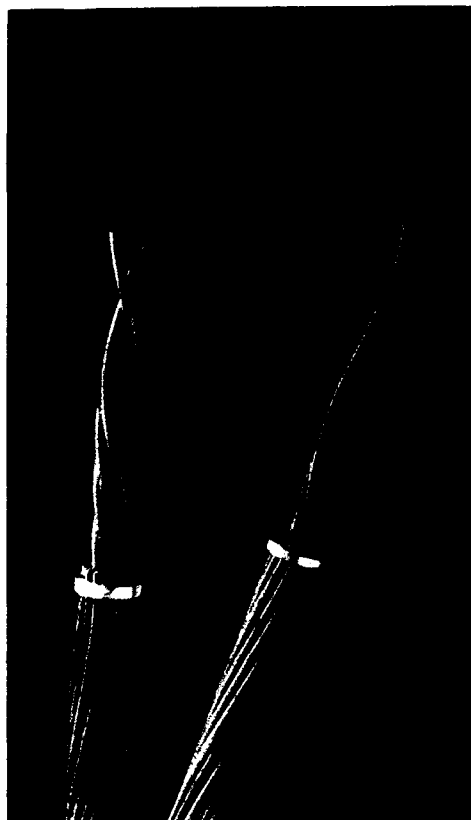


Figure 1: Wire ropes with optical fibres.

Diameter (mm)	7	9.2	11.8
Supporting cross-section (mm ²)	21	41	65
Weight (kg/km)	190	350	550
Min. breaking strength (kN)	33	64	100
Long-term tensile strength (kN)	15	29	45
E-Modulus (kN/mm ²)	158	158	158
Typ. spans (m)	300	600	900
Max. number of fibres	18	18	36

Table 1: Technical data of the wire ropes with optical fibres.

Mechanical and Environmental Performance

Prototype cables have been produced and tested to evaluate the optical, mechanical and environmental properties. The results obtained on different ropes with different diameter are summarized below.

Properties of the Tubes

To optimize the mechanical properties of the wire rope construction the crush resistance of the tubes has been evaluated in accordance with IEC 794-1-E3. The sample was placed between two metal plates of 100 mm length.

Figure 2 shows the excellent crush resistance of more than 700 daN/100 mm for the tubes used in the new product.

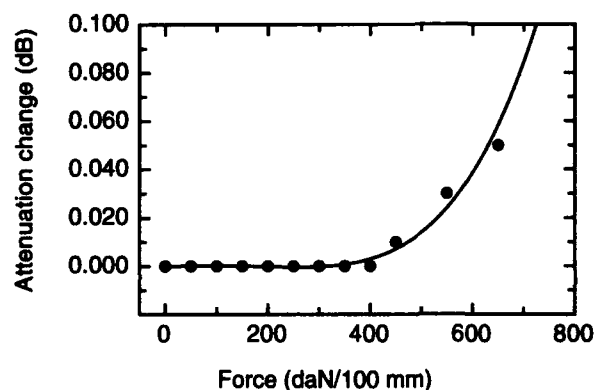


Figure 2: Crush resistance test of a 2.49 mm diameter tube. The attenuation change is measured on a 50 μ m fibre at 1300 nm.

The attenuation increase observed during crush testing is generally a micro bending induced loss, caused by pressing the fibres against the walls of the tubes and against neighbouring fibres³.

In the case of welded tubes the weld can be the weak element. The inspection of the tubes after crush testing has shown that the deformation is not significantly higher in the welded region. Therefore, we conclude that the weld of the evaluated tubes has a strength comparable to the used stainless steel.

In order to design a wire rope containing optical fibres, the bending performance of the tubes and fibres used has to be taken into account. The measurements have shown that using bending radii above 60 mm will not induce significant attenuation increase.

Another important point for an aerial installation with optical fibres is the migration of jelly and fibres due to the big height differences of the aerial cable way installations. Therefore the draw out force of the fibres has been measured and a jelly dropping test was performed for 6 days at 70 °C. With the presently used jelly a drawing force higher than 1 daN/m and no loss of jelly has been observed, showing that both tests have been passed successfully.

Tensile Performance

The rope is designed to have an elongation window of about 1 %, implying that no fibre elongation will occur at rope elongations below 1 %.

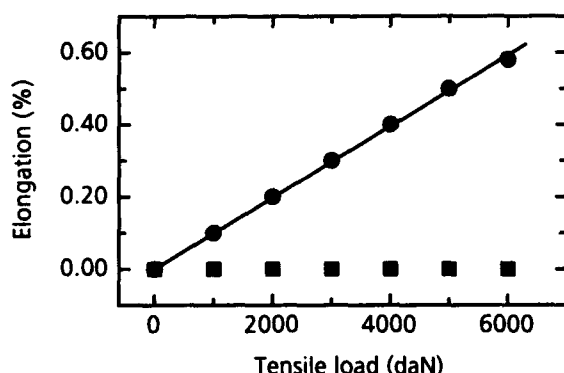


Figure 3: Rope (●) and fibre elongation (■) as a function of load, for the 11.8 mm diameter rope.

The fibre elongation was measured on a sample length of about 140 m in accordance with IEC 794-1-E1. Up to the highest applied load of 6000 daN, no fibre elongation was observed, confirming that the allowed longterm tensile stress of the steel wires is the limiting element and not the fibre elongation (figure 3).

Crush

Aerial ropes are subjected to high crushing forces all the time during service, because of the mounted clamps or come-alongs to hold the rope. Therefore the rope was designed paying special attention to the crush resistance.

A crush test was executed in accordance with IEC 794-1-E3. The experiment didn't show any significant attenuation change under crush load up to 3000 daN/100 mm (figure 4).

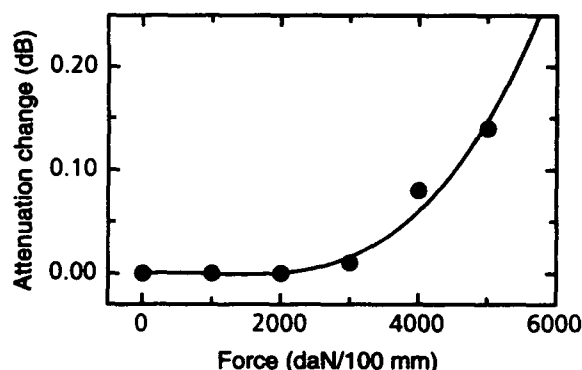


Figure 4: Attenuation change as a function of crushing force for a 50 µm MM fibre in a 9.2 mm diameter rope measured at 1300 nm.

This high crush resistance is owed to the rope construction and the excellent mechanical properties of the metallic tube, containing the optical fibres, itself. The newly developed rope can even withstand higher crush loads than the hollow rope construction of some OPGWs, which is often used with the goal to increase crush resistance.

Temperature Characteristics

A temperature cycling test was conducted in accordance with IEC 794-1-F1. MM and SM fibres were studied at different wavelengths (MM 1300 nm, SM 1310 nm and 1550 nm) in order to evaluate the thermal properties of the ropes. Results involved are shown in figure 5.

The attenuation as a function of temperature shows always an attenuation increase starting below -30 °C. As shown in Ref. 4 and 5 the observed attenuation increase at low temperature is micro-bending induced. The observed attenuation increase at low temperatures is below 0.1 dB/km down to -40 °C. Compared to the service temperatures down to -30 °C, there is big enough margin to ensure a safe operation in the field.

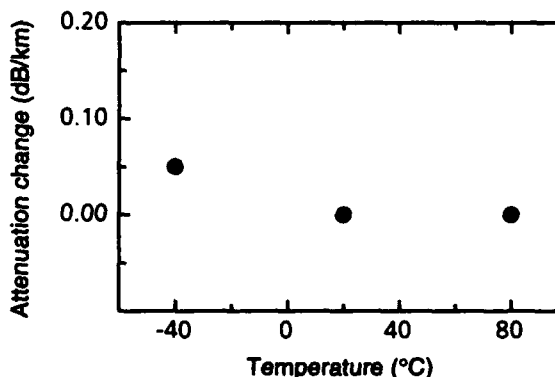


Figure 5: Worst case attenuation change of all measured fibres as a function of temperature for SM fibres measured at 1550 nm with an OTDR.

To gain information about the short-term temperature characteristics, 10 m of the rope was heated inductively up to 250 °C during 30 minutes. The attenuation change of a 50 µm MM fibre was below 0.02 dB at 1300 nm during this experiment.

The results obtained from mechanical and thermal tests are showing the excellent properties of the new developed product from a laboratory point of view. To guarantee the safe everyday operation of the whole installation, field-tests are needed, where load and performance of the product is monitored.

Field-test

We have conducted a field-test on an existing aerial cable way installation up in the Swiss mountains. During this long-term field-test, we continuously monitored the attenuation of the optical signal, rope load and the environmental conditions. The measurement set-up for the attenuation measurement is similar to Ref. 6 and 7 and is shown in figure 6.

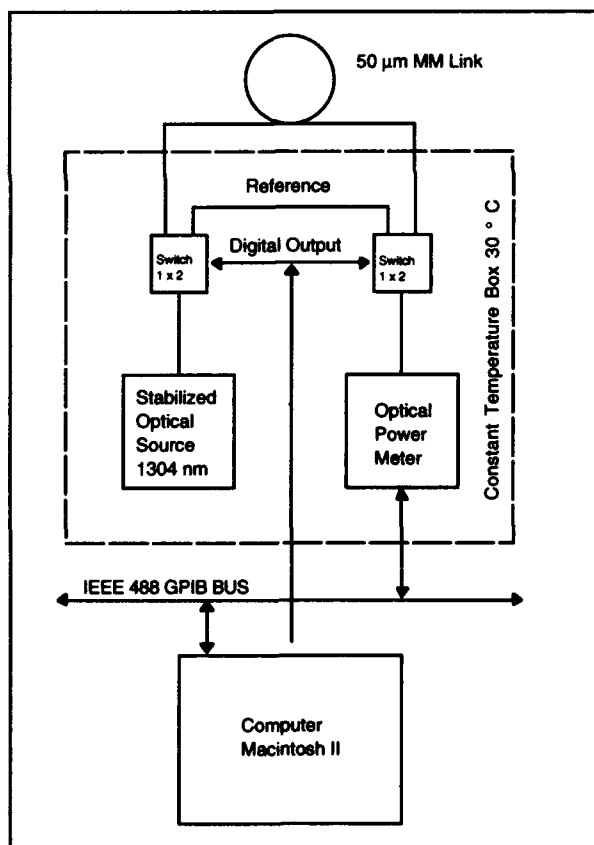


Figure 6: Attenuation measurement set-up for the field-test installation.

A LED source together with two optical switches and one power meter were used to measure the attenuation of the optical signal passing the MM fibre inside the rope at 1300 nm.

A reference fibre was alternatively measured to compensate the drifts of the set-up. To minimize thermal fluctuations, optical source, optical switches and power meter were hold at a constant temperature of 30 °C. A key issue to obtain high precise attenuation measurements is the repeatability of the optical switch, which is alternatively connecting the reference fibre and the transmission line. In the present set-up the repeatability of the attenuation measurement was increased with averaging techniques, finally the repeatability is better than 0.03 dB on a time scale of several weeks.

The tensile force is measured at the upper anchoring point with a load cell. The measured signal is transmitted through an optical fibre in the rope to the base station, where the data acquisition is done. The control of the whole set-up, data acquisition and calculations are done on a Macintosh personal computer with the program LabVIEW⁸.

Because of the extreme climatic conditions, ice loads of up to 2.3 kg/m as well as vibration, torsion and temperatures down to -30 °C have to be taken into consideration. The network planning calculations resulted in a required cross-section of 40 mm². The topographical data of the installation are shown in figure 7.

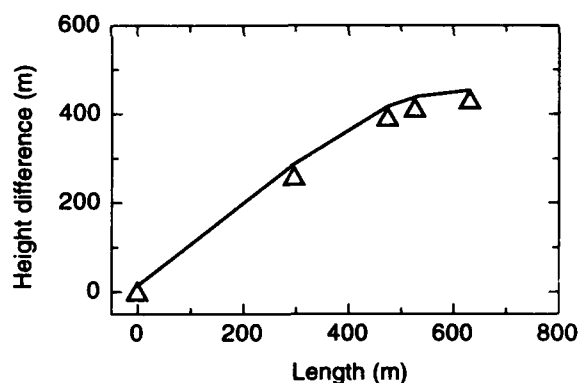


Figure 7: Topographical data of the field-test installation.

	Temperature (°C)	Tensile load (daN)
Mean value	-0.8	1391
Standard deviation	3.8	48.5
Minimum	-12.5	1253
Maximum	10.2	1512

Table 2: Statistical parameters of ambient temperature and tensile force at upper anchoring from February 23 to March 11 1993.

As an example, the attenuation change of a full bi-directional 50 μm MM link including the connectors is shown in figure 8, and the corresponding statistical data of ambient temperatures and measured tensile forces are listed in table 2.

This field-test has demonstrated that the new developed rope can entirely meet all requirements needed under practical conditions.

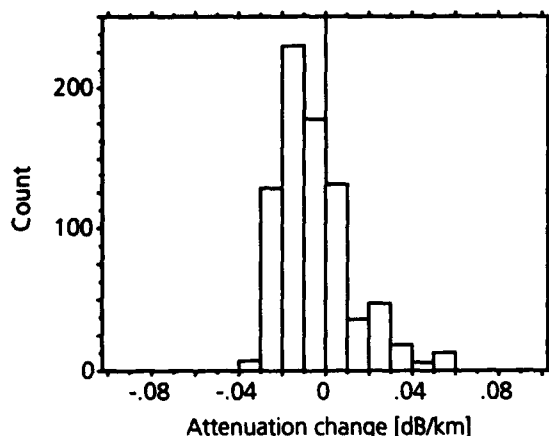


Figure 8: Attenuation change of a bi-directional MM link from February 23 to March 11 1993 measured at 1300 nm.

Conclusion

To draw a conclusion, Brugg Telecom AG has developed, manufactured and already successfully field-tested a new generation of optical fibre containing aerial ropes, the TELECOM ROPES. This newly developed product represents from a technical point of view a highly sophisticated and cost-effective solution, which meets entirely the multitude of requirements put forward by the aerial cable way operators. A special feature of the rope is the high crush resistance. The first installations have shown the very good qualification of the new product and proves to be the ideal product in the field of aerial cable way facilities.

But the newly developed product has much more application potential. Thanks to its hermetic sealed optical fibres containing tubes, it proves to be the right solution for use in security applications and in difficult climatic environment, i.e. high humidity, extreme temperatures and aggressive chemicals. With its high crush resistance and tensile load the rope is best suited in rough environments.

Therefore the TELECOM ROPE is not only applicable for aerial cable ways, but as well for installations in various kind of extreme and hazardous environment.

Acknowledgements

The authors would like to thank U. Boss and W. Rickhaus from the LSB Isenfluh-Sulwald for enabling and supporting our field-test and H. Müller, A. Gyger and S. Vogel from Brugg Telecom AG for their support.

References

- [1] BRUGG TELECOM AG, TELECOM ROPE Specification, (1993).
- [2] Dr. K. Vögtli, "Pflichtenheft für die Fabrikation und Lieferung von Glasfaserkabeln für die Netze der PTT", PTT 840.03, Bern (1991).
- [3] Hiroshi Murata, Handbook of optical fibres and cables, Marcel Dekker Inc, NY (1988).
- [4] P. Waegli, L. Fischer and H. Tschan, The effect of monomode fibre design on the temperature induced attenuation enhancement observed in loose tube fibre cables. Proceedings Fibre Optics 88, SPIE Vol. 949, 45, (1988).
- [5] L. Fischer, C. Huber and L. Rydskov, Designing Loose Tube Optical Cable for Increased Crush Resistance. Proceedings EFOC/LAN 90, 86, (1988).
- [6] DICON FIBREOPTICS INC, Berkeley, CA 94710, Switching system optical specification, (1992).
- [7] A.B. Bussard, M. Biller and D.A. Serfas, Multi-channel data acquisition system for assessing reliability of fibre-optic couplers, SPIE Vol. 1366, 380, (1990).
- [8] NATIONAL INSTRUMENTS, Austin, TX 78730-5039.



Amir Fargahi
BRUGG TELECOM AG
 CH-5200 Brugg
 Switzerland

Amir Fargahi graduated from Swiss Federal Institute of Technology, Zurich, with a Dipl.-Ing.-degree in Material Science. He joined Brugg Telecom AG in 1991 and has been engaged in the field of telecommunication cable development.



Christoph Zehnder
BRUGG TELECOM AG
 CH-5200 Brugg
 Switzerland

Christoph Zehnder received his Engineering degree from HTL Brugg in 1987. After three years working in the field of wireless communication, he joined Brugg Telecom AG in 1990. As product manager for optical signal transmission he is mainly engaged in aerial cable way projects.



Angelo Banfi
BRUGG TELECOM AG
 CH-5200 Brugg
 Switzerland

Angelo Banfi is head of the product management at Brugg Telecom AG. He received his degree in Mechanical Engineering in 1984. After R&D activities in the field of optical fibre sensors, he joined the marketing department of Brugg Telecom AG in 1987, where he covers the actual position since 1991.



Daniel Schoepke
BRUGG DRAHTSEIL AG
 CH-5242 Birr
 Switzerland

Daniel Schoepke (33) is the manager of the development and production department. He received his Mechanical Engineer BSc. from HTL Burgdorf in 1985. For the following two years he has been engaged in the design and development department of a generator manufacturing company. In 1987 he joined the development department of Brugg Drahtseil AG and since 1989 he covers the present position.



Chambos Theodossi
LASER ARMOR TECH
CORP.
 SAN DIEGO, CA 92121,
 USA

Chambos Theodossi is Director of Business Development at Laser Armor Tech Corporation. He received his degree in Electrical Engineering from Faraday House College, London England in 1958 and he has been involved in the field of telecommunications ever since.



Hugues Hagmann
BRUGG TELECOM AG
 CH-5200 Brugg
 Switzerland

Hugues Hagmann was born in 1965. After receiving his Electrical Engineering degree from HTL Brugg, Switzerland, he joined Brugg Telecom AG in 1991, where he is a development engineer for fibre-optic cables.



Willibald Nägele
BRUGG TELECOM AG
CH-5200 Brugg
Switzerland

Willibald Nägele (24) is a member of the product development department. He graduated in 1991 from the "Technikerschule Waldshut" with a degree in Electrical Engineering and joined Brugg Telecom AG in 1992, where he has been engaged in the field of telecommunication cables and computer assisted optical measurements.



Hubert Zimmermann
BRUGG TELECOM AG
CH-5200 Brugg
Switzerland

Dr. Hubert Zimmermann - head of product development - joined Brugg Telecom AG in 1991. He received his PhD. in Solid State Physics from University of Zurich, Switzerland, where he studied High- T_c -Superconductors.

DEVELOPMENT OF A COMPACT HIGH FIBER COUNT INTRABUILDING CABLE

D. Tatarka, E.O. Shiflett, M.R. Ferrell, G.E. Alls, and R.C. Roman

Alcoa Fujikura Ltd., Telecommunications Division,
Duncan, South Carolina.

ABSTRACT

With the rapid growth and expansion of high speed local area networks and intrabuilding communications central offices have become congested which places increasingly important roll on cable design. Higher fiber count, compact cable structures, and cable flexibility are some of the growing demands placed on cable designers. Continuing improvements in handling, installation, splicing, and connectorizing have become essential. Existing Riser cable designs typically use individual tight buffering, ribbon, or loose tube constructions. These cable designs have drawbacks such as bulky cable constructions, low fiber counts, and arduous cable preparation and installation.

To overcome the undesirable characteristics of these cables, a new type of fiber optic riser cable was developed which have tight buffered multi fiber units. The new design is dry, compact and easy to handle and splice.

INTRODUCTION

Fiber optic cable requirements for building premise systems have mechanical and environmental specifications defined by Bellcore's TR-NWT-000409 Issue 2 "Generic Requirements For Intrabuilding Optical Fiber Cable." Beyond these requirements, however, additional characteristics must be considered to fully utilize present technology in planning for future system upgrades. Addressing these characteristics will save time and expense during the cable installation.

Three characteristics to be recognized are cable diameter, ease of handling and routing, and splicing to outdoor cable.

Cable Diameter

Central office requirements are demanding higher fiber counts to meet future applications. Currently, cable diameters are influenced by fiber count and cable construction. As a result traditional cable designs are causing the central office to become more congested. Tight buffer cable designs are large and stiff for higher fiber count constructions. New designs have entered the market but materials and inherent design characteristics pose other problems during installation.

Handling and Routing

The routing of bundles of 6 to 12 fibers are typical for multiple rack locations. Traditional tight buffer constructions utilizing bundles of 6-12 individually buffered fibers subunits are bulky. Indoor loose tube designs have water blocking agents and gels which need to be cleaned and the gels can also migrate within the distribution frame. The plastic buffer tubes are also prone to kinking. Ribbon designs utilize a single sheath for protection and once removed expose the fiber ribbon and become vulnerable to damage during routing.

Splicing to Outdoor Cables

While the riser cables can be preterminated and patched into the distribution frame, the other end of the cable must be spliced (fusion or mechanically) to an outdoor cable in the cable vault or basement. The tight bound designs are typically buffered to 900 microns providing another opportunity chance to affect concentricity of the glass. Since some accuracy is lost the probability of nicking the fiber during stripping is increased. Further more, tight buffered products are not capable of mass splicing with existing systems. Ribbon designs typically utilize 12 fiber ribbons which must be separated when splicing in less than 12 fiber group.

NEW CABLE DESIGN

A new compact, high fiber count, intrabuilding cable has been designed and developed to address these concerns while meeting Bellcore's TR-409 specification. This cable consists of a stranded core of tight tube multi fiber units enclosed in a flame retardant sheath (Figure 2.). The key design concept of the cable is the tight tube unit which contains from 6 to 12 fibers and is less than 3.5 mm in diameter (Figure 1.). Table 1. summarizes the advantages of the tight tube unit over other designs.

The tight tube structure as shown in figure 1, consists of color coded fibers stranded around a fiber reinforced plastic (FRP) central member. Fibers are then encapsulated in a low modulus material to

cushion the fibers and covered with a high modulus material to protect the bundle. Multiple units can be stranded together to form a compact cable core construction as shown in figure 2, with fiber counts ranging from 6 to 216. Aramid yarn and an outer jacket surround the multiple unit core construction. The new design results in diameters that approach the smaller ribbon and indoor loose tube designs.

Additional advantages are that the cable design is dry, flexible and easy to handle and route. The cable design allows simple and quick breakout of units from the cable and of individual colored fibers from each unit.

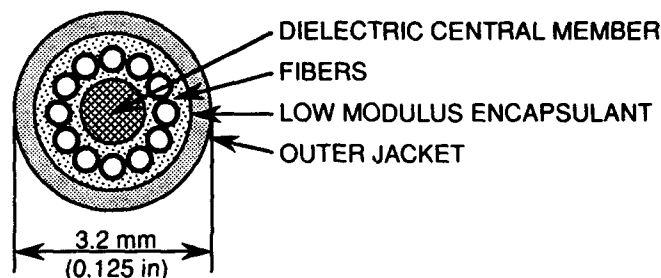


Figure 1. Cross-Sectional View of Tight Tube Unit

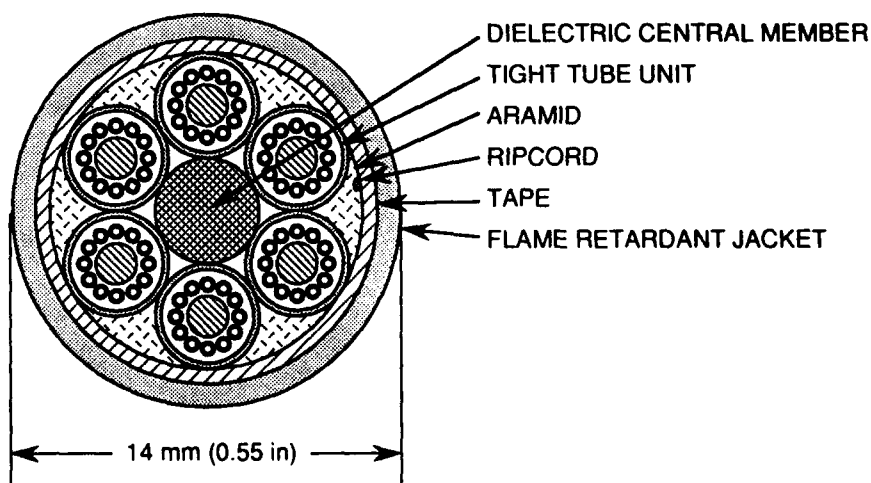


Figure 2. Cross Sectional View of Compact High Fiber Count Intrabuilding Cable (72 Fibers)

Table 1. Comparison of Intrabuilding Cables

ATTRIBUTE TYPE	Cable Size	Handling and Routing	Splicing to Outdoor Cables	Fiber Counts	Indoor & Outdoor
Tight Buffer	Large	Stiff Bulky	No Mass Splicing, Nicks Fiber	Low	No
Loose Tube	<i>Optimized</i>	Kinks, Gel Migration, cleaning Required	<i>Optimized</i>	High	Yes
Ribbon	<i>Optimized</i>	Needs Protection	<i>Optimized</i> (12 fiber groups only)	High	No
New "Tight Tube"	<i>Optimized</i>	<i>Optimized</i>	<i>Optimized</i>	High	Yes

CABLE PERFORMANCE CHARACTERISTICS

The compact high fiber count intrabuilding cable was tested in two configurations; a 12 fiber single "tight tube bundle" and a 144 fiber design in which 12 units of 12 fibers each were stranded around a central member. These designs were tested according to Bellcore TR-NWT-000409 as well as UL standard 1666 and CSA standard C22.2. The results were as follows:

Both cable designs performed adequately in temperature cycling and aging as specified by TR-409. Likewise, all designs passed the twist, flex, compressive strength, impact and tensile strength tests as shown in tables 2 and 3.

Aside from the targeted performance requirements addressed above, an extra test was added to the design qualification series as a result of a "problem" discovered in a field trial. Upon installation of the cable into a connector tray an unexplained increase in attenuation was observed. All of the test data indicated that the cable should have tolerated the bending required for installation. Further repeat testing confirmed this.

After extensive analysis by the cable design team, they discovered that a twist in combination with a bend was the source of the attenuation increase. This condition was encountered during installation

when the fiber tray was inverted to install the unit, returned to an upright position and inserted back into the cabinet. To assess this phenomenon a twist-bend test was devised and performed in which the tight tube unit was twisted 180° and then bent to reach a 60 mm diameter. The target performance for this test was 0.05 dB (or less) attenuation increase. With minor adjustment of the design and process the cable was improved to meet this criteria consistently.

The UL-1666 test for flame propagation height of electrical and fiber optic cables installed vertically in shafts resulted in a flame height and temperature measurement well below the maximum allowable levels. The CSA vertical tray flame test also yielded passing results well within the acceptable range.

CONCLUSION

A compact high fiber count cable design has been developed to address the congestion, handling, and installation requirements for distribution centers in central offices. The new design is dry, compact and easy to handle and splice. The cable has successfully passed all tests for Riser grade cable in Bellcore TR-NWT-000409 specification, the UL 1666 Cable Burn Test for an OFNR rating, the CSA C22.2 for an FT4 rating and a new "twist-bend" test which simulates installation practices.

Table 2. 12 Fiber TR-NWT-000409 Results

TEST NAME	CRITERIA	RESULT
High/ Low Temperature Bending	< 0.20 dB Loss Increase	0.00 dB Loss Increase
Impact Resistance	< 0.20 dB Loss Increase	0.01 dB Loss Increase
Compressive Strength	< 0.20 dB Loss Increase	0.05 dB Loss Increase
Tensile Strength	< 0.20 dB Loss Increase	0.04 dB Max Loss Increase
Cable Twist	< 0.20 dB Loss Increase	0.00 dB Loss Increase
Cable Cyclic Flexing	< 0.20 dB Loss Increase	0.02 dB Loss Increase
Temperature Cycling / Thermal Aging	< 0.30 dB Loss Increase	0.14 dB Max Loss Increase
Color Permanance	No Discernable Change	No Discernable Change

Table 3. 144 Fiber TR-NWT-000409 Results

TEST NAME	CRITERIA	RESULT
High/ Low Temperature Bending	< 0.20 dB Loss Increase	0.00 dB Loss Increase
Impact Resistance	< 0.20 dB Loss Increase	0.00 dB Loss Increase
Compressive Strength	< 0.20 dB Loss Increase	0.07 dB Loss Increase
Tensile Strength	< 0.20 dB Loss Increase	0.06 dB Max Loss Increase
Cable Twist	< 0.20 dB Loss Increase	0.00 dB Loss Increase
Cable Cyclic Flexing	< 0.20 dB Loss Increase	0.01 dB Loss Increase
Temperature Cycling / Thermal Aging	< 0.30 dB Loss Increase	0.11 dB Loss Increase
Color Permanance	No Discernable Change	No Discernable Change

ACKNOWLEDGEMENTS

The authors gratefully acknowledge the contributions of J. Lowe, H. Blumsack, M. Baker, T. Longshore, D. Bennett, T. Watts, A. Taylor, B. Creech, T. Robinson, B. Whitesell, G. Anderson and several other members of Alcoa Fujikura Ltd.

REFERENCES

1. Bellcore Technical Reference TR-NWT-000409, "Generic Requirements For Intrabuilding Optical Fiber Cable", Issue 2, September 1990.
2. Bell Canada's Specification "General Purpose In-Building F.O. Cables Performance Requirement Document (PRD)", Reference No. 626-241, October 1992.
3. National Electrical Code Article 770 "Optical Fiber Cables and Raceways", 1993.
4. Canadian Electrical Code, CSA Standard C22.1-1990, Section 56 "Optical Fiber Cables", Part 1, Sixteenth Edition, 1990.

AUTHORS PROFILES

Mr. Daniel Tatarka is manager of cable development at Alcoa Fujikura Ltd., Duncan, S.C. He is responsible for the design and development of fiber optic cables. He received a B.S. Degree in Applied Science, Manufacturing Engineering from Miami University, Oxford, Ohio. He joined Alcoa Fujikura Ltd., in 1988 as a development engineer and has been in his current position since 1990. Prior to his employment at AFL he has worked in engineering in fiber optic cable since 1982 for Siecor Corporation and Pirelli cable.

Mr. Gary E. Alls is a development technician at Alcoa Fujikura Ltd., Duncan, S.C. He is responsible for the design and processing of fiber optic cables. He's currently pursuing a Mechanical Engineering degree at Greenville Technical College. He joined Alcoa Fujikura Ltd. in 1989. Mr. Alls has been in the fiber optic industry for 17 years.

Mr. E. O. Shiflett is manager of systems engineering of Optical Fiber Systems Division at Alcoa Fujikura Ltd., Duncan, S.C. He received a B.S. Degree in Civil Engineering at Virginia Military Institute. He joined AFL in April of 1987 as a systems engineer for new product development and has been in his current position since 1990. Prior to his employment at AFL, he was director of cable design and development at Netek, Inc. and held various management positions at Siecor Corp.

Mr. Mack R. Ferrell is Development Technician of cable development at Alcoa Fujikura Ltd., Duncan, S.C. He is responsible for the implementation and testing of new fiber optic designs. He received a A.S. Degree in Applied Science, Industrial Electronics from Greenville Technical College, Greenville South Carolina and is presently pursuing a B.S. in Applied Science, Electrical Engineering Technology from South Carolina State University, Orangeburg, South Carolina. He joined Alcoa Fujikura Ltd., in 1985 and has been in his present position since 1988. Mr. Ferrell has been elected to the "Who's Who Registry of Outstanding Junior College Students of America-1992".

Mr. Robert C. Roman is Quality Assurance Manager for Alcoa Fujikura Limited's Cable facility in Duncan, SC. He is responsible for all quality related activities including test and measurement technology. He received a bachelor of arts degree from Newberry College, Newberry, SC in 1982. He received a Quality Engineering certification from the American Society for Quality Control in 1988 and has been a member of the society since 1986. He joined Alcoa Fujikura in 1985 and has been in his present position since 1989.

LONG-DISTANCE OPTICAL FIBER CABLE INSTALLATION SYSTEM USING AUTOMATIC CONTROL PULLER

Shuichi Genno, Shuichi Yamaguchi, Tadashi Furumiya

NTT Telecommunication Field Systems Research and Development Center,
Tsukuba, Ibaraki, 305, JAPAN

ABSTRACT

To fully make use of the merits of the optical fiber cable, which are a small outer diameter and light weight, it is urgent that long-distance optical fiber be installed effectively, when constructing optical communication networks.

However, current pullers in manholes require manual control to check the pulling situation. To do this, an optical fiber cable puller has been developed which detects loading tension on the cable by using sensors and automatically controls pulling speed so that the detection retains proper tension in the optical fiber cable installation.

This system installs cable effectively and safely, since the number of synchronized units that may be operated in manholes is unlimited and also since the puller stops automatically in case of an accident.

1. INTRODUCTION

In optical fiber cable installation in a conduit, to fully utilize of the merits of the optical fiber cable, which are low loss, small outer diameter, and light weight, it is important that the cable be installed in the longest possible unit lengths.

There are two specific types of cable pulling systems, namely. The first is a one-end cable pulling system which installs only one puller in the leading manhole. The second is a distributed cable pulling system which installs some pullers in intermediate manholes to distribute the cable pulling force. They are applied to the most suitable cable route according to the cable route configuration and cable structure.

In long-distance cable installation, the optical fiber cable has an allowable pulling force requires that the distributed cable pulling force must not exceed the cable allowable pulling force.

Because of this factor a distributed cable pulling system is generally applied.

However, in distributed pulling systems, the operator must synchronize each puller's pulling speed to prevent cable damage. With the self-control method by detecting overload, the current puller is limited to less than a few, which is the number of synchronized units is complicated set up for self-control. Also, current pullers in manholes require manual control to check the pulling situation.

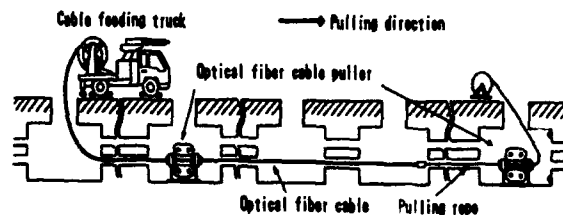


Fig. 1 Distributed pulling system

This thesis states an the automatic control puller which is suitable for long-distance cable installation and solves these problems. First, synchronized pulling speed of pullers in a dynamic model is investigated. Next, the control method of the puller developed in accordance with system is explained.

In conclusion, the trial test indicates that the automatic control puller is a practical system for long-distance cable installation.

2. AUTOMATIC CONTROL

2.1 Required function

For efficient long-distance cable installation the puller must have automatically controlled pulling speed to synchronize and no restriction on the number of synchronized units. So the pullers required the basic functions in the environment as follows.

Table.1
Required puller functions

Safety	Prevent cable damage and transmission characteristics loss Continuous speed to prevent cable surging
Work Efficiency	Ability to automatically pass joint between every kind of optical fiber cable and pulling rope Ability to safely pull every kind of cable and pulling rope
Flexibility	Ability to pull every kind of cable

2.2 Control method

2.2.1 Dynamical model

Every puller is required to steady to pull the cable by itself to prevent damage from a large tension, or a compressed force so that the pulling speed may be synchronized.

Therefore, it is important that every puller has ability to self-detect.

To investigate the dynamic model shown in Fig. 2, the following is assumed.

- ① To ignore inertia force because of small changes in the pulling speed
- ② To ignore electric and mechanical constants.

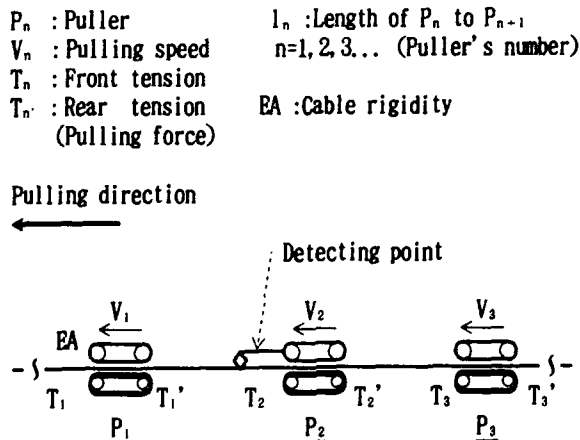


Fig. 2 Dynamical model

The pulling speed change and pulling force from balance can be expressed as ΔT_1 , ΔT_2 , ΔT_3 , ΔV_1 , ΔV_2 , ΔV_3 . In puller P_2 , the puller continuously detects tension T_2 and feeds the DC motor volts in proportion to ΔT_2 to synchronize the pulling speed. The change of the puller before puller P_1 's pulling speed is ΔV_1 and the change of the puller after puller P_3 's tension, ΔT_3 , is investigated as disturbance.

For the change of P_3 's tension, ΔT_3 , the motion equation is shown as follows.

$$d\Delta T_2/dt = EA (\Delta V_1 - \Delta V_2) / l_1 \quad [1]$$

$$\Delta V_1 = -q \Delta T_2 \quad [2]$$

$$\Delta l_2 = k \Delta T_2 \quad [3]$$

$$\Delta V_2 = m \Delta l_2 - q (\Delta T_3 - \Delta T_2) \quad [4]$$

$$m, k: \text{constant } (mk=p, L=EA/l_2)$$

$$q: \text{motor torque constant}$$

When Eqs. [1] ~ [4] are rearranged by the Laplace transform with $\Delta T_3(s)$, the result is shown as follows.

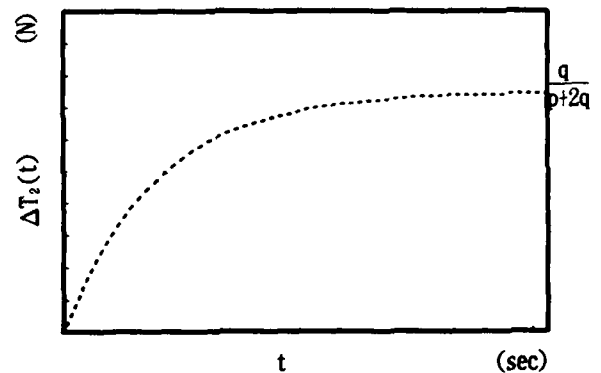
$$\Delta T_2(s) = Lq / [s + L(p + 2q)] \Delta T_3(s) \quad [5]$$

$$\Delta V_1(s) = -Lq^2 / [s + L(p + 2q)] \Delta T_3(s) \quad [6]$$

$$\Delta V_2(s) = (-qs - Lq^2) / [s + L(p + 2q)] \Delta T_3(s) \quad [7]$$

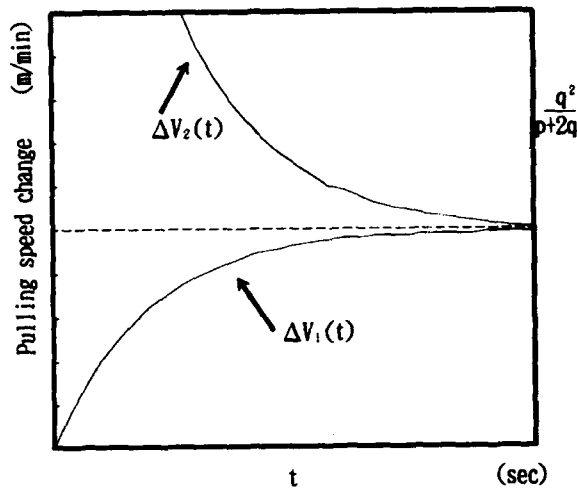
The time response given by unit step input for different $\Delta T_3(s)$ is derived by substituting $\Delta T_3(s) = 1/s$ and the inverse Laplace transform.

Fig. 3 shows the time response of Eq. [5], $\Delta T_2(t)$.



The time response of ΔT_2 with the change of T_3 , V_1
Fig. 3

Fig. 4 shows the time response of Eq. [6], $\Delta V_1(t)$ and Eq. [7], $\Delta V_2(t)$.



The time response of ΔV_1 , ΔV_2 with the change of T_2
Fig. 4

From Fig. 4, as time passes ΔV_1 and ΔV_2 corresponds to feed the volts in proportion to ΔT_2 . Therefore, whenever T_2 changes, the puller P_2 can synchronize pulling speed.

For the change of P_1 's pulling speed, ΔV_1 , the motion equation is shown as follows. On the other hand, it is assumed that P_2 's tension changes little with the pulling speed change of P_1 .

$$\Delta T_2/dt = EA(\Delta V_1 - \Delta V_2)/l_1 \quad [8]$$

$$\Delta V_2 = (p+q)\Delta T_2 \quad [9]$$

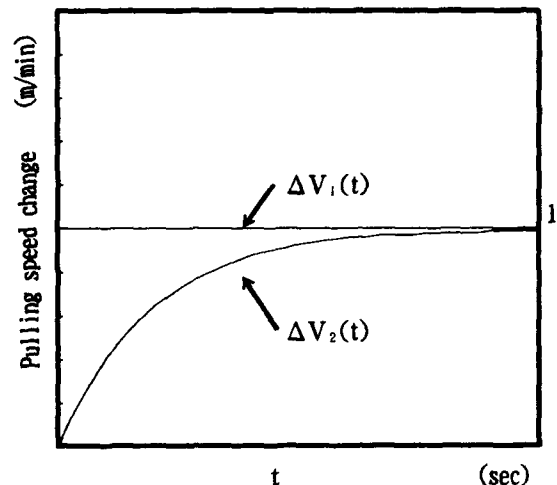
When Eqs. [8] ~ [9] are rearranged by the Laplace transform with $\Delta V_1(s)$, the result is shown as follows.

$$\Delta T_2(s) = L/[s+L(p+q)]\Delta V_1(s) \quad [10]$$

$$\Delta V_2(s) = L(p+q)/[s+L(p+q)]\Delta V_1(s) \quad [11]$$

The time response given by the unit step input for the different $\Delta V_1(s)$ is derived by substituting $\Delta V_1(s) = 1/s$ and the inverse Laplace transform.

Fig. 5 shows the time response of Eq. [10], $\Delta V_1(t)$ and $\Delta V_2(t)$.



The time response of ΔV_1 , ΔV_2 with the change of V_1
Fig. 5

From Fig. 5, as time passes, ΔV_1 and ΔV_2 corresponds to feed the volts in proportion to ΔT_2 . Therefore, whenever V_1 changes, the puller P_2 can synchronize pulling speed.

From Fig. 3, $\Delta T_2(t)$ has a steady state error. However, steady state error is cancelled by inputting the integral action into the circuit. The puller controls the pulling speed to maintain T_2 .

2.2.2 The Control system for the of automatic control puller

Fig. 6 shows the control system construction of the automatic control puller. It forms a closed loop transfer function which compares the mark value to the detection from the tension sensor and feeds the volts in proportion to the offset in terms of the difference.

(1) Control system

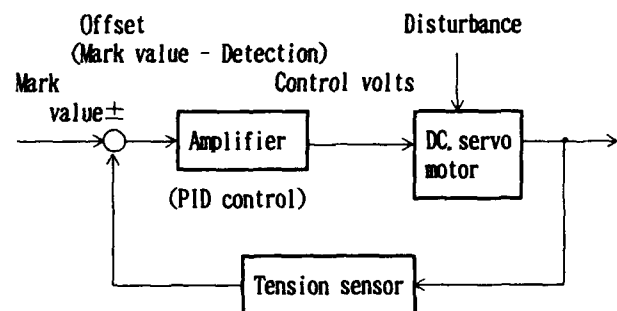


Fig. 6 Control system construction

(2)Control system smoothing A block diagram of the automatic control puller is shown in Fig. 7. The control depends on the proportion and integral action to the offset. When the parameters are set properly by the PID control, the control system functions smoothly. Consequently, the puller prevents the hunting action by cable rigidity and conduit and can stably pull the cable. Those following formula is generally referred to #1, #2 in control analysis.

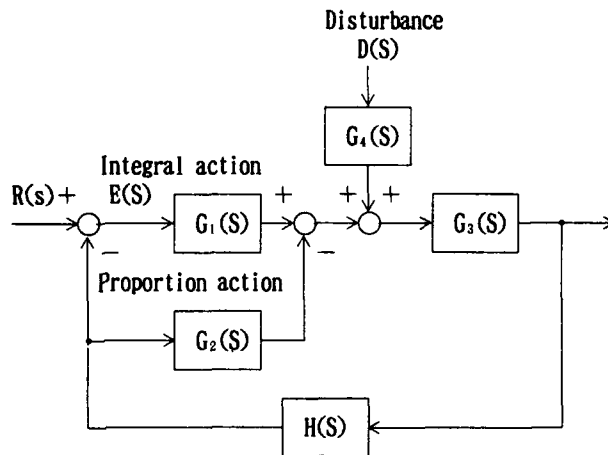


Fig. 7 Block diagram

The relationship between input and output is shown in Eq. [12] from Fig. 7.

$$Y(S) = \frac{G_1(S)G_3(S)R(s) + G_3(S)G_4(S)D(S)}{[1 + H(S)(G_1(S)G_3(S) + G_2(S)G_3(S))]} \quad [12]$$

$$\begin{aligned} G_1(S) &= K_1/S & H(S) &= 1 & G_2(S) &= K_2 \\ G_3(S) &= K_3/(1+TS) & G_4(s) &= K_4 \end{aligned} \quad [13]$$

When Eq. [12] is rearranged by substituting Eq. [13] and ω_n , ζ is defined by Eq. [15] and [16], the result is shown as Eq. [14].

$$Y(S) = \frac{\omega_n^2}{s^2 + 2\zeta\omega_n s + \omega_n^2} R(s) + \frac{\omega_n^2}{s^2 + 2\zeta\omega_n s + \omega_n^2} D(s) \quad [14]$$

$$\omega_n = (K_2 K_3 / T) \quad [15]$$

$$\zeta = 1/2 [(1 + K_1 K_3) / T] \quad [16]$$

The characteristic equation root is shown as follows.

$$s_1, s_2 = -\omega_n \zeta \pm \omega_n (\zeta^2 - 1) \quad [17]$$

The time response is derived by substituting $R(S)=1/s$, $D(S)=0$ and the inverse Laplace transform.

$$Y(t) = 1 + \frac{\omega_n^2}{s_1 - s_2} \left[\frac{1}{s_1} e^{s_1 t} - \frac{1}{s_2} e^{s_2 t} \right] \quad [18]$$

In $\zeta < 1$ the output of Eq. [18] shows vibration. Besides, in cable installation the puller occurs hunting action which is made the output added to vibration by cable rigidity and conduit situation. So the puller is controlled by over-braking in $\zeta > 1$. In the actual environment, with a slower starting time response, the puller increasingly loads previous puller. With a slower stopping time response, there is a greater fear of the cable damage from a loose cable. In addition, cable rigidity and the actual environment (conduit friction, pulling force, etc) are different for every installation. So, In the trial test in an actual environment, we set parameters K_1 , K_2 , K_3 , K_4 , T the vest value for control system smoothing.

2.2 Detection method

An automatic control puller detects the vertical force of the cable tension, T by using a tension sensor and controls the pulling speed to maintain the mark value set.

Fig. 8 shows the relationship between T and detection from the tension sensor F_v .

F_v : Detection from tension sensor
 T : Tension
 θ_1, θ_2 : Installation angle of the tension sensor

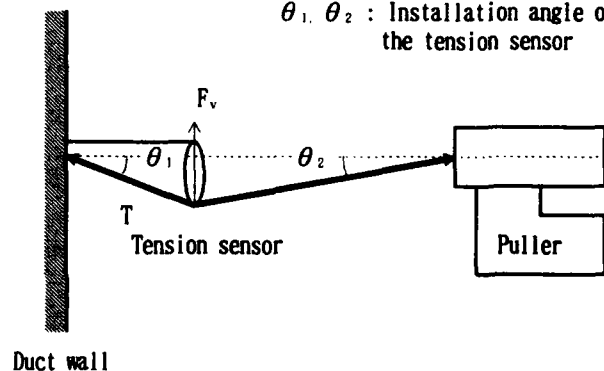


Fig. 8 Reactive force of the tension sensor

F_v is shown as follows.

$$F_v = T (\sin \theta_1 + \sin \theta_2) \quad [19]$$

Fig. 9 shows the relationship between T and F_v in the tension sensor experiment.

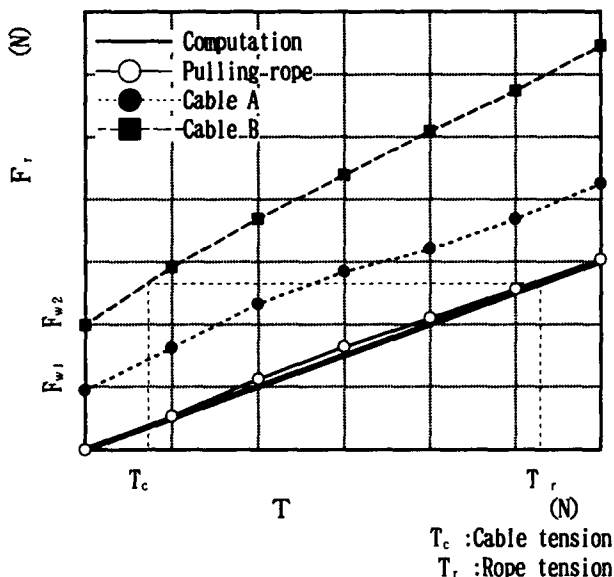


Fig. 9 Relationship between T and F_v

In Fig. 9, F_v is nearly proportional to T in all components. Pulling rope detection closely corresponds to the computation. However, every cable detection is larger than the computation by F_{w1}, F_{w2} since the cable rigidity, though the F_v -to- T ratio is closely corresponded. So, F_v is shown in Fig. 9, Eq. [19] as follows.

$$F_v = T (\sin \theta_1 + \sin \theta_2) + F_{wn} \quad (n=1, 2, 3, \dots) \quad [20]$$

Therefore, an automatic control puller employs $F_v - F_{wn}$ by subtracting F_v from F_{wn} as the mark value for every cable installation so that the puller can make T constant value. The pulling rope is connected and pulled with the cable. So, the set value can not be changed. In Fig. 9, when the puller controls pulling speed to maintain pulling tension T_c , the puller requires rope tension T_r in case of the pulling rope. The pulling force of the previous puller increases according to each component weight (ex. cable) and tension (ex. T_c) and the puller is installed at proper manhole span so that the cable pulling force is within allowable cable pulling force. If the rope pulling force exceeds the cable pulling force, the puller must be installed in a different manhole.

Therefore, T_r is set because the rope pulling force may exceed the cable pulling force.

The distance of the duct to the puller varies with every installation. So the puller sets the angle of the tension sensor θ_1 as a fixed unit, the other θ_2 varies with every installation. In addition the puller must set θ_2 larger than θ_1 , because the control detection may be influenced if θ_2 changes. However the larger θ_1 is, the more difficult it to set the cable within the allowable cable bending radius and the less smoothly the cable will pass. Therefore, trial tests in actual environment use θ_1 . In addition, the puller uses a bellmouse for the tension sensor setting so that θ_1 doesn't change with every cable installation.

2.4 Cancel volume setting

The control equipment of the automatic control puller cancels the output volts V_v in proportion to F_v by canceling volts V_c set in response to F_{wn} .

Fig. 10 shows the cancel block in the control equipment.

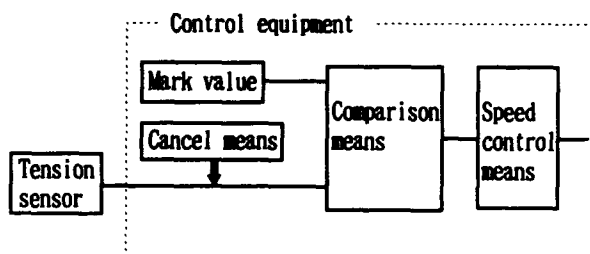


Fig. 10 Cancel block

Fig. 11 shows relationship between V_v and V_c .

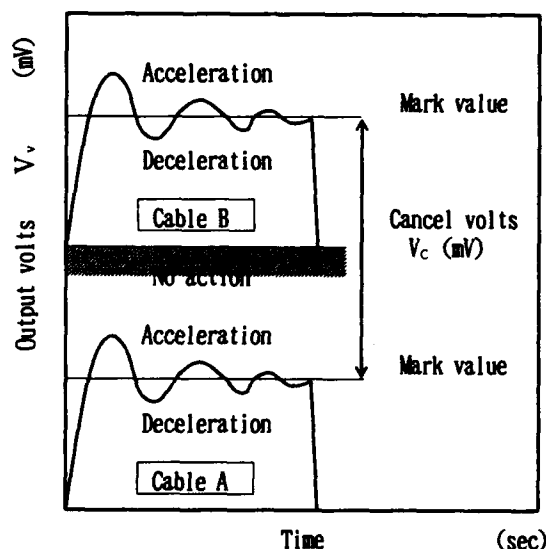


Fig. 11

Relationship between output volts and cancel volts

The puller continually controls pulling speed to maintain the mark value. For instance, for V_v excess of the mark value, the puller accelerates the pulling speed and for V_v less than the mark value, the puller reduces the pulling speed. On the other hand, if V_v drops below the threshold level, the puller automatically stops pulling. If V_v rises over the threshold level, the puller automatically starts pulling. Therefore, the V_c setting is important for control.

When the puller controls V_c not less than the required volts of F_{wn} , then the following is true.

- Cable tension T increases, and the cable pulling force of the previous puller increases.
- There is little cable loosening when stopping, and the danger of cable damage is reduced.
- V_c increases according to an increasing T , and the control characteristic doesn't depend on V_c .

When the puller controls V_c not more than the required volts of F_{wn} , the puller can't control the pulling speed to maintain the mark value and just stop pulling. Therefore, in trial tests in an actual environment set the mark value and cancel volts V_c vest value with respect to the above.

3. STRUCTURAL DESIGN

3.1 Reliability's progress of crawler

An automatic control puller must be able to pull the pulling rope (outer diameter, 8mm) and NTT's standard optical fiber cable (outer diameter 12mm~40mm). To grip these effectively, the puller has two belts whose sectional form is flat. Because the belts has no slits, there is little change of friction force between the belts and cable and continuously grip the cable. In addition, the core of the belt is made of Aramid fibers to prolong its durability.

As a result, the automatic control puller can consistently pull a cable, whether the cable is wet or not.

3.2 Crawler Auto-adjusting mechanism

When installing cable, the puller must adjust the gripping pressure of every component, optical fiber cable, pulling rope, etc, based on the diameter. An automatic control puller has an auto-adjusting mechanism that employs disc springs with a reactive force that is almost constant within a given range, irrespective of displacement changes. Therefore, there is no adjustment of gripping pressure during cable pulling.

3.3 Coping with accident

To cope with a situation when the cable slips on the belt or completely off of it, an automatic control puller detects the difference between the motor rotation speed and the sensor output speed. If the unit exceeds the proper value, the puller automatically stops pulling. When the previous puller stops, the puller begin to overload, but an automatic control unit automatically stops pulling if detects overload.

3.4 Outline of the automatic control puller

An outline of the automatic control puller is shown in Fig. 12 and its specifications are shown in Table 2.

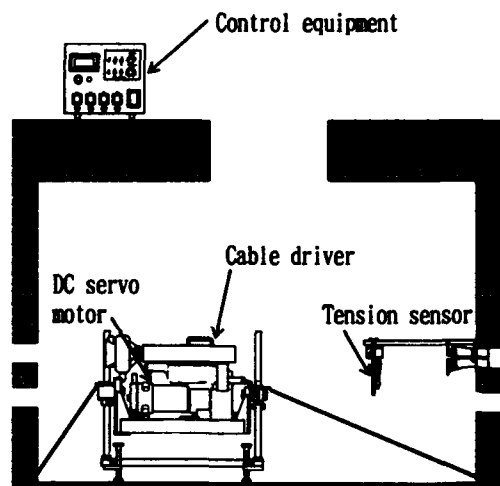


Fig. 12 Outline of the automatic control puller

Table. 2
Automatic control puller specification

Headings	Ability	Note
Pulling force	0 ~2kN	Enables operator to adjust Automatic stop at maximum
Pulling speed	0~20m/min	Adjusts automatically
Applicable cable diameter	8~56mm	Enables any diameter difference of less than 40mm to pass automatically
Power source	AC 100V	
Weight(Unit)	60kg	Can be divided into 4 pieces
Others	Stops automatically, displays messages, and checks unusual pulling. Permits an unlimited number of synchronized units	

4. TRAIL TEST

An automatic control puller was used in actual environment and was tested for synchronizing pulling speed. The basic configuration and puller layout is shown in Fig. 13.

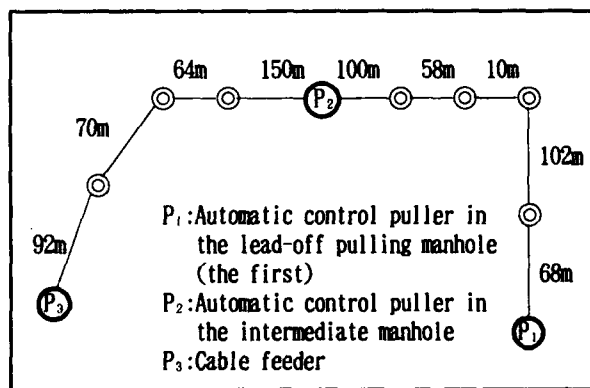


Fig. 13. Field test configuration

The automatic control puller in the intermediate manhole, P₂, is tested for synchronizing pulling speed, in which the automatic control puller in the first manhole, P₁, is started and has a varying pulling speed, and is then stopped. Fig. 14 shows the P₂ pulling speed change when P₁ has a varying pulling speed.

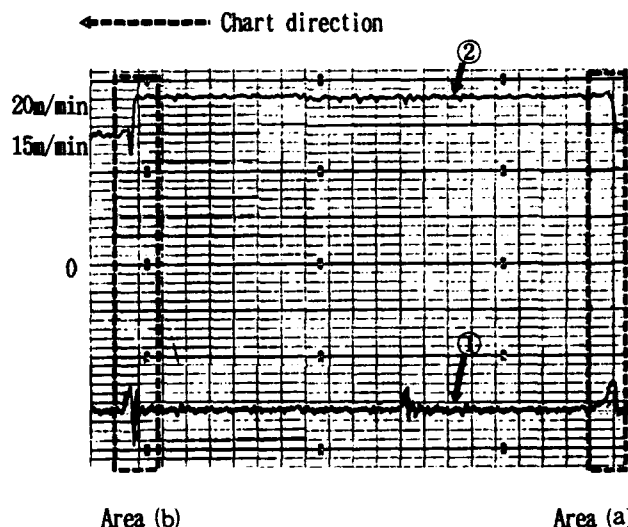


Fig. 14 P₂ pulling speed change

In Fig. 14, ① shows output of the tension sensor detection and ② shows the pulling speed. In area(a), when the sensor detection was over the mark value because of the P₁ pulling speed change (15m/min \Rightarrow 20m/min), P₂ adjusted the sensor detection to the mark value accelerating from 15m/min to 20m/min. In area (b), when the sensor detection was under the mark value because of the P₁ pulling speed change (20m/min \Rightarrow 15m/min), P₂ adjusted the sensor detection to the mark value, decelerating from 15m/min to 20m/min. It was also confirmed that P₂ controlled the pulling speed to synchronize better when P₁ was just starting and stopping.

4. CONCLUSION

An effective pulling method using a distributed cable pulling system has been discussed for the development of long-distance optical fiber cable installation.

To do this, an automatic control puller has been developed, which detects loading tension on the cable by using sensors and automatically controls the pulling speed to detect and retain the proper tension in the installing of the optical fiber cable. Also, field trial results confirm that the puller can realize control of synchronized pulling speed in this way, and as a result number of synchronized units, that may be operated in manholes becomes unlimited.

In conclusion, long-distance optical fiber installation using this puller reduce man-hours and makes the construction of digital networks, much more efficient.

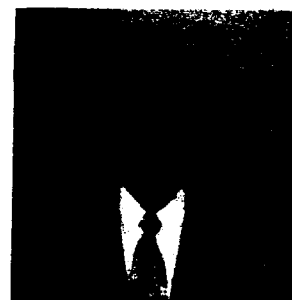
5. REFERENCES

- (1) H. Matsumura, "Automatic Control, 3rd ed." K. ASAKURA, 1986.
- (2) Society of little motor in Toshiba corporation, "Technique Utility Manual Of Control Motor, 3rd ed." T. TAKANO, 1988.
- (3) T. Watanabe, "An Efficient Optical Fiber Cable Installation System Using Self-Controlling Cable Pullers" International Wire & Cable Symposium Proceeding, 1986.



Shuichi Genno

Shuichi Genno is the Senior Manager of the Outside Plant Engineering Systems Development Project Group in the NTT Telecommunication Field Research and Development Center. He graduated from the Electronics of Engineering, Fukui University in 1976. He is presently engaged in development of optical fiber installation system and submarine technology.



Shuichi Yamaguchi

Shuichi Yamaguchi is an Engineer of the Outside Plant Engineering Systems Development Project Group in the NTT Telecommunication Field Research and Development Center. He graduated from the Mechanical of Engineering, MATZURU Collage of Technology in 1981. He is presently engaged in development of optical fiber installation system.



Tadashi Furumiya

Tadashi Furumiya is a Staff member of the Outside Plant Engineering Systems Development Project Group in the NTT Telecommunication Field Research and Development Center. He graduated from the Mechanical of Engineering, Ritsumeikan University in 1989. He is presently engaged in development of optical fiber

CABLE INSTALLATION BY HYDRODYNAMIC DRAG: THEORY AND PRACTICE

D.L. Walters*, M.J. Parry*, C.J.W. Thomson* & D.F. Harrison*

* BNR Europe Ltd, London Road, Harlow, Essex, England
+ NT Integrated Networks, Chester Hall Lane, Basildon, Essex, England

ABSTRACT

An analysis of the forces on a cable experiencing liquid drag in a mini-duct or pipeline has been carried out. This has shown that the use of hydrodynamic drag should enable cables to be installed rapidly in lengths of the order of 20km in a single operation. This is possible even with relatively low pressures (~10 Bar) and moderate flows (~0.8m/s). This theory has been confirmed, both by trials and actual installation, for cable lengths up to 16km.

A pipeline cable installation technique based on these principles has been patented and used over a number of years, utilising magnetic sensors, optical monitoring, and proven cable and mechanical technology.

INTRODUCTION

Because of the high costs associated with the jointing of optical cables, it is often economical to install cable links in as long continuous lengths as possible. For duct installation, the factors that limit this installable length are usually related to the force required to install the cable, rather than to drum sizes or weights. A number of novel installation techniques which do not depend solely on front-end force have therefore been proposed over the past decade^{2,3}, and some of these systems are now commercially available. In practice, however, installable lengths are still generally limited to a maximum of less than 2km, except where some form of tandemised blowing is used.

Within BNR and NT Europe (formerly STL and STC), the concept of installing a cable into a duct using hydrodynamic drag has been investigated and developed over a number of years. There are several advantages in using water, as opposed to air, to 'blow' a cable into a mini-duct, as described in detail in the next section. This technique was patented in 1986 and used by STC for installation of communications cable into ducts in part of the round-London water ring main. During 1992, a short installation test-bed and demonstrator was set up at BNR Harlow, and BNR acted as consultants to a cable supplier to the Hungarian PTT, who are using this

technique to install a significant part of their optical communications infrastructure.

It is only a small step to extend the concept of hydrodynamic installation to the insertion of cables into working pipelines, utilising the normal operational flow to provide the installing force. Northern Telecom Integrated Networks has had such a product for several years⁴ and has now gained considerable practical experience in carrying out these installations.

This paper describes the theory behind these techniques, and presents the results of practical trials and installations. The field results have enabled some unknown parameters in the theoretical model to be determined, and have highlighted the effectiveness of continuous monitoring of the cable during installations into pipelines.

FORCES ON THE CABLE

Installation by Front-End Force Alone

Any duct can be considered as a series of straight sections separated by bends. By using the usual formulae for friction and capstan effects and extending to the limit, the pulling force F_p in Newtons required to install a cable of length L km can be shown to be:

$$F_p = \frac{W \mu_s}{\phi \mu_b} (e^{\phi \mu_b L} - 1) \quad (1)$$

where W is the cable weight in N/km, ϕ the average 'bend frequency' in radians/km, and μ_s and μ_b are the coefficients of friction in straight sections and bends respectively. The equation ignores gradients and any additional cable/duct reaction due to cable flexural stiffness or set. This latter approximation is generally valid for ducts with a diameter much larger than the cable. For installation into mini-ducts, the cable flexural reactions can result in an even greater force being required than that predicted by equation (1).

It can be seen from the equation that the necessary pulling force increases exponentially with length so that, even with low friction, the installable length rapidly limits at a point beyond which the required pulling force becomes impracticably high. Inserting practical values into equation (1) for long-distance routes, we obtain the expected maximum figure for L of 1 to 2 km. In local area or access networks, shorter links are generally required, but in these cases the bend frequency ϕ is correspondingly larger, so that front-end force is again usually insufficient for installation of the optimum length.

Fluid Drag on Cable

From classical fluid mechanics, the fluid drag force F_D per unit length on a cable with diameter d_c is

$$F_D = 0.5 \Pi C_F \rho v^2 d_c \quad (2)$$

where ρ is the fluid density and v the net fluid speed with respect to the cable (i.e. the fluid speed minus the cable speed).

The drag coefficient, C_F is a slowly varying function of the appropriate Reynolds number Re , which is in turn a function of dimensions, speed and fluid properties. Formulae for C_F have been used for many years to predict the drag on cables moving in the sea, and the same formulae have, from direct measurement of drag forces and pressure drops, been found to be applicable to the case of fluid drag on a cable in a duct. For the dimensions and flows encountered in practice, C_F is of the order of 0.01.

Force Due to Pressure Gradient

In addition to the fluid drag force, there will be a 'pressure force' F_P per unit length on the cable given by

$$F_P = \frac{dp}{dl} \Pi d_c^2 / 4 \quad (3)$$

Where dp/dl is the pressure gradient in the duct with the cable present. For cable installation into mini-ducts, F_P is of comparable magnitude to F_D . When the duct diameter is much larger than that of the cable, as for pipeline cable installation, F_D is considerably larger and F_P can generally be ignored.

Approximation for Mini-Ducts

When the duct and cable diameters are comparable and the cable speed is low compared to the fluid speed, the pressure drop due to combined drag on cable and duct can be deduced from equations (2) and (3), and these can be combined to give the total positive force F_T per unit length of the cable:

$$F_T = \frac{dp}{dl} \Pi d_c d_D / 4 \quad (4)$$

where d_D is the duct diameter.

At first sight it may seem odd that the force on the cable can be increased by increasing the duct diameter. However, it must be remembered that this applies for a given pressure gradient, and the installing pump power is the pressure delivered multiplied by the volume flow rate. Since this volume flow is proportional to the square of d_D , the power needed for installation increases more rapidly with d_D than the installing force delivered. It is consequently advantageous to keep d_D as small as possible, subject to acceptable cable/duct reaction.

Resisting Force per Unit Length

Cable movement is opposed by frictional force F_F , which is simply the cable weight in the fluid multiplied by the cable/duct friction coefficient. This can be written as

$$F_F = \Pi d_c^2 \Delta \rho g \mu / 4 \quad (5)$$

Where $\Delta \rho$ is the cable-fluid density difference, g the acceleration due to gravity and μ the cable/duct friction coefficient.

Net Installing Force

The resultant force on the cable F_{NET} is the algebraic sum of the forces described in equations (3), (4) and (5).

$$F_{NET} = F_D + F_P - F_F \quad (6)$$

The cable can be installed if F_{NET} is always positive, i.e. the sum of the installing forces per unit length exceeds the resisting force.

For the case of a mini-duct, we use equations (4) and (5) to show that installation can take place provided:

$$\frac{d\phi}{dt} > \Delta\rho g \mu d_c/d_D \quad (7)$$

For the use of a pipeline cable, where equation (2) dominates the positive force, we obtain

$$V^2 > \frac{d_c \Delta\rho g \mu}{2 \rho C_f} \quad (8)$$

Equations (7) and (8) give us the criteria for installability in terms of pressure gradient and flow speed respectively. The key parameter in each case is $\Delta\rho$, the cable/fluid density difference: if this can be made small enough, then quite moderate pressures (~10Bar) and normal pipeline flow speeds (~0.8 m/s) will enable cables to be installed in very long (>20km) lengths.

This is the main advantage of using liquid, rather than pneumatic, drag to install a cable, since it is relatively easy to manufacture an optical cable with a density close to that of water.

Effect of Bends

Provided that the bend radius is not so small as to induce cable/duct flexural reaction effects, the tension in the cable will be reduced by a bend according to the familiar capstan effect formula:-

$$T_1 = T_0 e^{\mu_b \theta} \quad (9)$$

where T_0 and T_1 are the cable tensions before and after the bend respectively, μ_b is the cable/duct friction coefficient at the bend and θ the bend angle in radians. The effect of bends is therefore to reduce tension build-up in the cable, but provided the net force per unit length is positive (equation 6) bends will not, in themselves, prevent cable installation.

Front-End Force

Although hydrodynamic installation relies primarily on a net positive force acting equally along the whole length of the cable, it is essential that pipeline cables (or cables in any application where the duct diameter is large) are tensioned and centralised by a significant front-end force, to avoid 'looping' in the duct and to facilitate capture after deployment. In our

application, this is done by a drogue at the front end of the cable (see Fig. 5) which applies a force T_D where,

$$T_D = k\rho V^2 \quad (10)$$

and where k is a constant for a given duct. Direct measurements have shown T_D to be roughly equivalent to the force on 1 km of cable.

Cable Strain and Elongation

Equations (2) to (10) can be used to predict the tension distribution throughout the cable for any installation scenario, taking gradients into account where necessary. Dividing this by the cable tensile stiffness E gives the corresponding strain, and integrating this strain along the cable gives the total cable elongation El_{TOT} . For ducts or pipelines with low friction and/or negligible bends we obtain an expression for the total elongation of a cable of length L of

$$El_{TOT} = \frac{T_D L}{E} + \frac{F_{NET} L^2}{2E} \quad (11)$$

For ducts or pipelines with significant bends and high friction at these bends, the elongation becomes

$$El_{TOT} = \frac{T_D}{E\mu\phi} - \frac{F_{NET}}{E(\mu\phi)^2} + \frac{F}{E\mu\phi} L \quad (12)$$

Where ϕ is, as before, the bend frequency in radians per unit length.

HYDRAULIC DUCT TRIALS

To investigate the installation parameters associated with the hydraulic installation of cables into mini-ducts, a 300m trial was set up on site at BNR, Harlow.

Trial Configuration

Two 150m lengths of 20mm OD polyethylene duct, butt jointed using an external clamp, to maintain a smooth bore, were used for this trial. Attached to the input end of the duct was an injection head, fed with water from a storage tank, via a pump and flow transducer. Two pressure gauges were also installed to measure the water pressure at the pump and at the injection head.

The duct was laid as a loop directly on to the ground. At the far end of the loop, the duct swept through a 180° bend with a bend radius of 6 m. The duct then returned, sweeping through a second 180° bend of radius 3m before finishing above the water supply tank. This arrangement allowed the water to be recycled during the trials. Fig. 1 shows a schematic representation of the test layout.

The cable used for this trial was an 8mm OD, all dielectric, optical fibre cable, with a GRP strength member. This cable was chosen because its density of 1.03 gcm⁻³, minimised the density difference between water and the cable (equation 7).

The cable enters the injection head via a PTFE gland, with an 8.1mm clearance bore. This prevents excess leakage of water from the head.

Preliminary Trials

Before any installations were carried out, the cable entry gland was blocked and the pump switched on. The initial pressure on both gauges was 3.8 bar (60 psi) at a flow rate of 21 litres per minute. Installation of the cable then proceeded. Initially, the back pressure began to push the cable back out of the duct, rather than pull it in. However, by applying a gentle force, the cable was easily pushed into the duct. After 30m of cable had been installed, the back pressure no longer pushed the cable backwards, and it became much easier to install. The installation was then continued and no increase in installation force was needed even when the front of the cable negotiated the first bend. At 250m the flow was stopped and it was not possible to move the cable either in or out by hand. The flow was then switched back on, and the installation continued to completion. The whole operation took less than ten minutes.

To remove the cable from the duct, it was originally intended to continue the installation until all of the cable had passed completely through the duct. However, after ten metres of cable had emerged from the end of the duct, further installation became impossible, due to the front end of the cable 'stalling', causing the cable in the duct to form a sinusoidal wave. The reaction of the cable against the duct wall substantially increased the friction, preventing further installation of the cable. The application of a front end force to the cable, as it emerged from the end of the duct, straightened the cable, allowing it to pass all of the way through the duct. A similar effect to this was seen during a field trial. In that case, the cable had an aramid strength member, and was not as rigid as the cable with a GRP strength member. During production of this cable, a permanent set had been introduced. This set forced the cable against the duct walls, producing a flex reaction which rapidly stopped the installation. In this case, it was not possible to apply a front end force, and the cable could only be installed after it had been removed from the duct, and the permanent set removed.

Installation Parameters

In order to understand more fully the installation process, further trials have been carried out, with the following parameters being recorded as a function of installed length:

- Supply Pressure
- Head Pressure
- Flow Rate
- Installation Load at Zero Flow
- Installation Load at Half Flow
- Installation Load at Full Flow
- Pull-out Load at Zero Flow
- Pull-out load at Full Flow

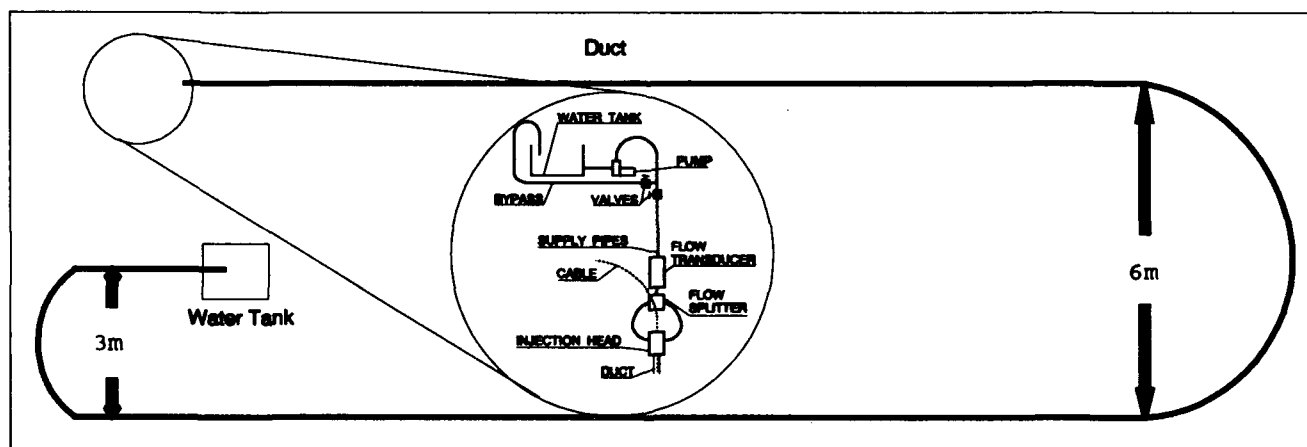


Figure 1
Schematic Diagram of Hydraulic Installation Test Layout

Half flow measurements were carried out, by opening the bypass valve. During these trials, the cable was removed from the duct either by reversing the water flow, or by blowing the line out with compressed air, which also removed all of the water from the duct. In both cases, the cable was recovered from the duct by fluid drag. No external force was required, as in this case there was no back pressure at the head to overcome.

Figs. 2 to 4 show these results graphically against installed length for installation load, flow rate and pull-out load respectively. These results show that with no flow it is possible to install approximately 100m of cable. This would be considerably less for standard telecoms cables, that do not have the high stiffness to weight ratio as the cable used for these trials.

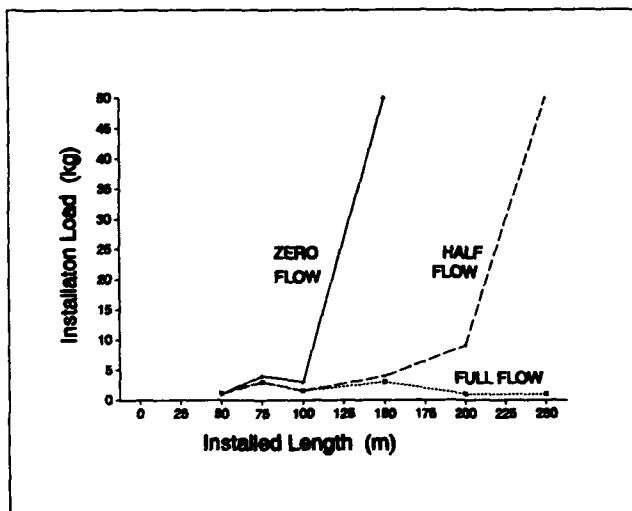


Figure 2
Installation Load vs Installed Length

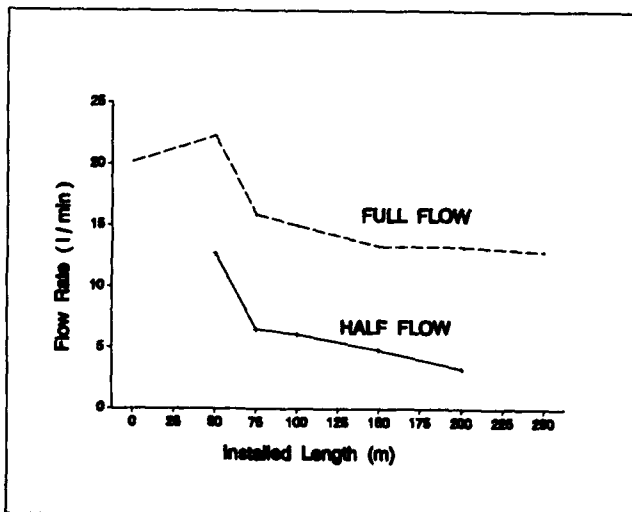


Figure 3
Flow Rate vs Installed Length

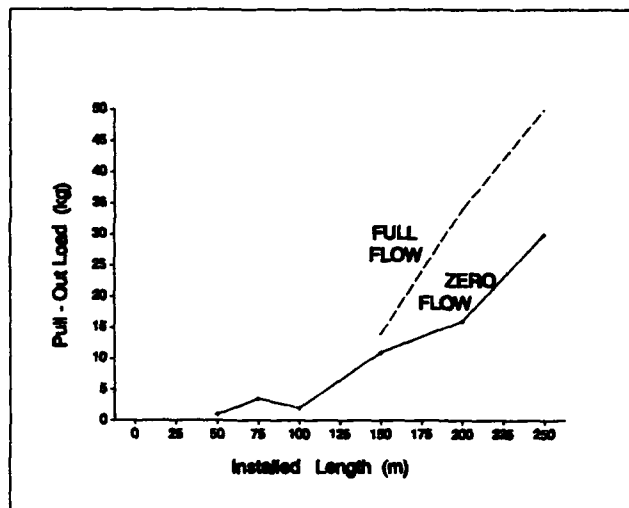


Figure 4
Pull-Out Load vs Installed Length

At half flow, the cable is easily installed up to the first bend. However, at this point the flexural reaction becomes significant and there is insufficient flow to keep the front end of the cable moving. This stalls the front end of the cable, forcing the rest of the cable into a sinusoidal wave. Increasing to full flow overcomes this problem, and the cable easily negotiates both bends in the system.

Fig. 3 showing flow rate vs installed length suggests that provided the flow rate in the system can be kept above 5-7 litres per minute, the cable can be installed in lengths approaching 10 km. Below this flow rate, installation will stop as the cable negotiates the next bend in the system. This figure also shows that flow rate decreases with installed length, this being due to the increase in resistance to flow caused by the increasing length of cable in the duct.

Measurements of the pull-out load at zero flow, and against full flow (Fig. 4) gives an indication of the installation force provided by the water flow.

Further Developments

In all of the early work carried out, the cables were fed manually into the duct, resulting in a typical installation time of 8 minutes for 300 m of cable (37.5 m/min). Further work has now been carried out, using a high speed caterpillar hauler to feed the cable into the duct. Using this system it is possible for a single operator to install 300 m of cable in 5-6 minutes (50-60 m/min).

PRACTICAL PIPELINE CABLE INSTALLATION

Overview

Installation of pipeline cables has now been carried out commercially for more than 5 years.

Pipeline cable installation is defined in three phases; Deployment, Installation, and Capture. Each phase can be considered separately as each has a developed, tried and tested procedure. In view of the special nature of the installation phase this is covered in the next section after the description of the deployment and capture.

Deployment Equipment

The basic components of the system consist of:

A transfer unit which is used to feed the fibre optic cable into the line. The forces developed by this transfer unit are just sufficient to overcome the back pressure of the fluid in the line.

The seal valve, this is the interface between the fluid and the atmosphere. It contains both static and dynamic seals within a steel casing as well as a chamber to contain the drogue prior to its deployment.

A gate valve, which is provided for safety. Its purpose is to seal the fluid in the line in the event of a catastrophic failure of the system. In all the years the installation technique has been employed, operation of these valves has never been required. A schematic of this equipment is shown in Fig. 5.

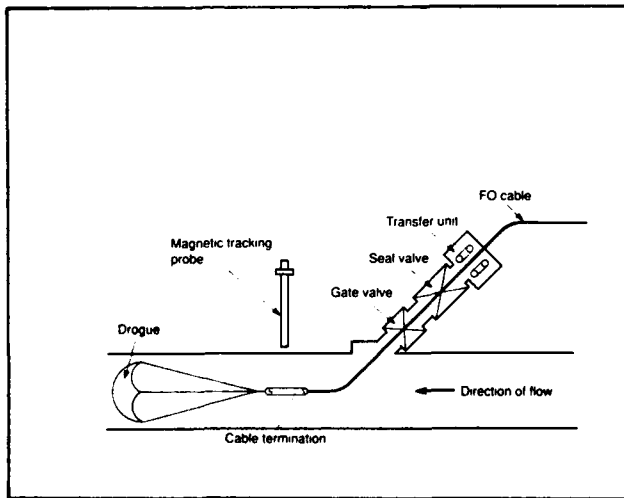


Figure 5
Deployment method - Start of Deployment

Deployment Method

Before the cable is passed through the transfer unit, a housing containing a series of magnets and a drogue is fitted to the front of the cable. The purpose of the magnets is to assist in locating the front end of the cable, whilst the drogue is needed to centralise the front of the cable in the line and to provide some front-end force. With the gate valve shut the cable is then threaded through the transfer unit and seal valve. An access port located in the body of the seal valve is opened to assist in the threading operation and to allow the drogue to be folded in order that it may drop smoothly into the line. When this operation is complete the access port is closed and the gate valve opened.

The cable is then driven into the line to a point directly beneath a magnetic detection probe located forward of the line access position in the direction of flow. By observation of the magnetic signature, verification that the drogue is inflated can be obtained. From this point on until the capture point is reached the cable is designated to be in the installation phase, and is continuously monitored optically.

Capture Equipment

The capture equipment consists of a transfer unit, seal valve and gate valve, as for deployment. For capture, a special type of lance assembly is bolted on to the top of the seal valve. The lance consists of a drive tube onto which a pressure tube and pneumatic cylinder are fitted. Within the pressure tube, a pneumatically-operated rod is located with a capture snare bolted on its end. A schematic is shown in Fig. 6.

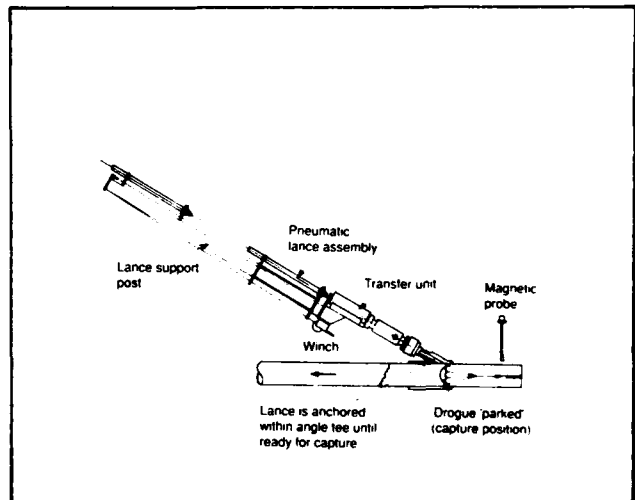


Figure 6
Pipeline Cables Capture Technique

Capture Method

On its arrival, the cable is detected by a magnetic tracking probe, and is then positioned with the drogue immediately under the line of capture lance. The lance tube complete with snare rod is driven into the line by the transfer unit. When in position the snare rod is extended from the lance tube by means of the pneumatic assembly. The magnetic tracking probe will indicate by means of a change to the magnetic signature that the snare has reached the drogue. When this change is observed the snare is retracted together with the drogue into the pressure tube.

The whole assembly can then be retracted from the line by means of the transfer unit until the end of the cable is above a dynamic seal contained within the seal valve. The dynamic seal is closed by means of a hydraulic pump and then the transfer unit, lance, drogue and magnetic housing are removed from the cable. Static seals are then fitted into the seal valve and the amount of cable that is required to reach the terminal equipment can be pulled down from the deployment end.

MONITORING OPTIONS FOR PIPELINE CABLES

The nature of pipeline deployments requires real-time monitoring of the cable, to ensure that the forces acting on the cable are sufficient to install the cable through the pipeline at all times.

Three methods of monitoring the installation have been developed. The types of pipeline and cable requirements will determine the most suitable method to be employed.

Video Camera

A video camera can be placed at the front of the cable. The progress of the deployment can then be monitored, together with the condition of the pipe. This requires the cable to have power lines for the camera, and optical fibre to carry the video information.

Loadcell Monitor

The front-end force T_D can be monitored by a loadcell at the front of the cable. The cable must have electrical wires to power the loadcell and relay the information. This is an effective method which can accurately determine the force and hence speed of the cable (equation 10).

Typical deployment speeds are around 0.2 m/s. An increase in speed will reduce the force on the cable, because this decreases the relative velocity of the fluid over the cable. When the original speed is resumed, the force should increase again. If the results are unsatisfactory a slowing of the deployment speed is required to increase the force and ensure the safety of the cable.

Elongation Measurement

The simplest method relies entirely on measuring the change in length of a fibre in the cable, caused by the net positive forces. An optical signal reflected from the front end of the cable can be used to measure the change in cable length, with an accuracy of 5 mm.

By correlating the strain measured with the length deployed, an indication is given of the force acting on the cable. From this information a safe speed of deployment can be determined.

As the system relies on the fluid forces stretching the cable, the start of any deployment gives negligible results. Typically, 1km must be deployed before the system can be relied upon. The individual pipeline and flow rates will determine the responses actually seen.

Simple theory suggests the general trend of the strain should be a quadratic curve (equation (11)). In practice this is modified by temperature, pressure and topographical effects, such as hills and bends, and the actual elongation corresponds more to equation (12).

External Monitoring

At predetermined locations the end of the cable can be identified using an external detector. Either a small radio transmitter is housed in the termination, or magnets as described in the last section. With a probe in position over the pipe the cable can be tracked as it passes through the line.

FIELD INSTALLATION RESULTS

For long-length cable installation into pipelines, the monitoring methods adopted were the elongation measurement, combined with intermittent external magnetic monitoring. While the video camera and loadcell techniques provide a great deal of information, they are not generally economically practical for the all-dielectric cables installed and captured through glands as described here.

CONCLUSION

Practical installations of optical cables into working pipelines, and installation trials into mini-ducts, have confirmed the theoretical prediction that cable lengths of the order of 20km can be installed in a single continuous operation by utilising liquid drag. The installation of such long lengths is possible because the cable can be manufactured so as to be close to neutral buoyancy in water, thereby drastically reducing its weight and frictional reaction.

In practice, pipeline cables have been installed in lengths up to 16km, which is the longest length which has so far been required. Procedures and techniques for such installations are now routine and mature.

An optical monitoring method has been developed to measure fibre elongation change during installation, and this has proved to be a very effective technique for instant detection of any problems and for optimising installation speed.

ACKNOWLEDGEMENTS

The authors thank the managements of NT Integrated Networks, BNR Europe, and the system customers for their support, and permission to publish this paper.

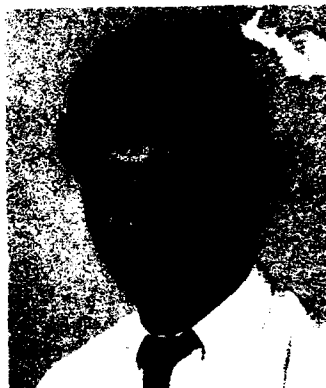
REFERENCE

- 1 Northern Telecom British Patent , 1982. 2171288
2. British Telecom European patent on Blown Fibre Installation, Reeve et al, 1983.
3. 'A Radically New, Ultra High Speed Method for the Installation of Cables' by Griffioen and Pins, IWCS 1991.
4. 'Telecommunications on Tap' by Smith & McDermott, IWCS 1988.
5. 'Accurate Determination of Optical Fibre Length From Measurements in the Frequency Domain' by D.L. Walters, US NBS Conference on Optical Fibre Measurements 1984.



David L. Walters
BNR Europe Ltd
London Road
Harlow
Essex
CM17 9NA

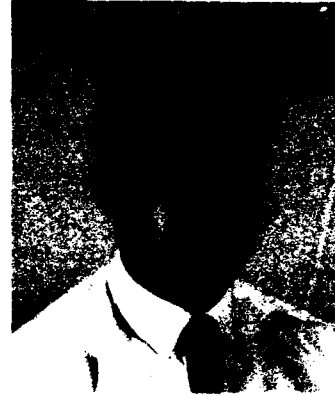
David L. Walters was born in Merthyr Tydfil, South Wales. He graduated in Physics from Cambridge University in 1971, and since this has worked on a number of different aspects of cable transmission systems. In 1977 he joined the Cable Group at STL, Now BNR Europe, and worked on design and measurement of optical and electrical cables for a wide range of applications. He is now Manager of the Cable Mechanics and Installation Department.



Mark J. Parry
BNR Europe Ltd
London Road
Harlow
Essex
CM17 9NA
UK

Mark Parry was born in London, England. He joined the Material Science Laboratories of British Telecom in 1978, and received an MSc from the London School of Polymer Technology in 1988. In 1989 he joined the Cables and Materials Applications Department of STL, now BNR Europe Ltd. He is now working on the application of polymeric materials in telecommunications equipment, and the installation of optical cables in the local loop.

Carl J.W. Thomson
NT Integrated Networks
Chester Hall Lane
Basildon
Essex
UK



David F. Harrison
NT Integrated Networks
Chester Hall Lane
Basildon
Essex
UK

Carl J.W. Thomson was born in Grays, Essex, England. He entered a career in communication electronics in 1961, working on several aspects of communication including microwave and HF. In 1989 he joined STC Defence Systems, now Northern Telecom Integrated Networks, as Project Manager on pipeline technology. He is now Engineering Manager for the Project Operation Department.

David Harrison was born in Nottingham in 1966. After receiving his degree in Mathematics with Materials Science from Liverpool University in 1988, he joined STC working in the Cables and Materials Applications Department of STL. He later moved to the Integrated Networks Division of what is now Northern Telecom Europe, where he is involved in pipeline installations.

MASS FUSION SPLICING PARAMETERS FOR OPTICAL FIBER RIBBONS

M.Morooka H.Kawasaki I.Suzuki M.Yoshinuma

Optical System R&D Dpt. Fujikura Ltd.
1440, Mutsuzaki, Sakura-shi, Chiba-ken, 285, JAPAN

ABSTRACT

Mass fusion splicing requires multiple fibers to be joined together in one electrical discharge. This discharge power must be consistent for each fiber pair. A mass fusion splicer has the capability to splice as many as 12 fiber pairs. Because of the various numbers of fiber pairs, from 1 to 12, it is a challenge to maintain the correct discharge power to each fiber pair for different fiber counts.

Large splice losses will occur if the balance between electrical power, the distance between the fibers (end face gap), and the determined amount of travel (Stuffing amount) between each fiber pair is altered or disturbed.

Relationships between splice losses and parameters are clarified. We confirm that ARC TEST is an effective method to measure the discharge power on a fiber pair, and the optimum discharge power is clarified.

1. INTRODUCTION

Fusion splicing has become a common practice for joining optical fibers with low loss. Many papers and journals are concerned with obtaining this low loss. Some of the factors accepted world-wide as determining loss are: core eccentricity, cleaved angle and initial axis offset.^{1) 2)} We have learned in single fiber pair splicing of several key factors that determine splice loss.³⁾ Recently, with the demand and popularity of splicers for multiple fiber pairs, or ribbon fiber, we are forced to identify additional factors that determine splice loss in ribbon fiber.

2. PROBLEMS WITH MASS FUSION SPLICING

Mass fusion splicing requires many fibers to be spliced at the same time in one electrical discharge. There are two characteristic problems that don't exist in single fiber pair splicing. Because these two problems occur at the same time in mass fusion splicing, the analysis is complicated. For that reason, we studied these problems through comparison with single fiber pair splicing.⁴⁾

2.1. Mass heating

In mass fusion splicing, each fiber pair must receive equal and correct discharge power for low splice loss. That condition is achieved by placing the electrodes at higher positions than the fibers, as shown in Fig.1.

A mass fusion splicer has the capability to splice a various number of fiber pairs. It is difficult to maintain the equal and correct discharge power to each fiber pair for different fiber counts. Even with each fiber pair receiving a different discharge power, all fiber pair must be spliced at the same time. The relationship between discharge power and splice loss in mass fusion splicing must be made clear.

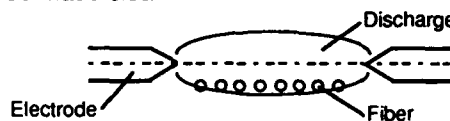


Fig.1 Electrodes position

2.2. End face gap variance

The jacket of fibers is removed and the fibers are cut before splicing, but some fiber end face position variance always exists. This creates a fiber end face gap variance when the fibers are put to the splicer and moved together just before discharge, as shown in Fig.2.(1). The fibers are then stuffed for a certain length that is Gap maximum plus 50 μm during discharge. If the fiber end face gap variance is large, one fiber pair is spliced with a large end face gap, and another fiber pair is spliced with a large overlap. Each fiber pair is spliced with different end face gap and overlap, shown in Fig.2.(2), and sometimes this leads to a large splice loss.

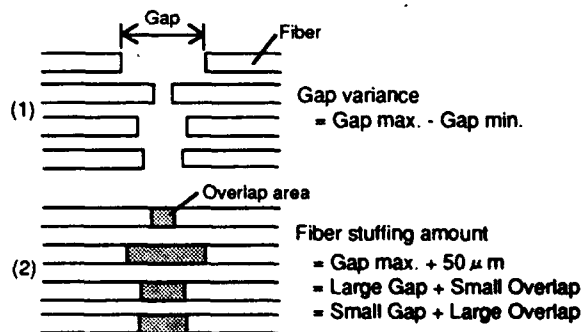


Fig.2 End face gap variance

3. MEASURING DISCHARGE POWER

Fiber end faces are melted for a short time by the discharge before the fibers are stuffed. The fibers are then moved forward and spliced. Melting conditions of the fiber end face depend on the strength of the discharge power, which we consider to be a factor that determines splice loss. But, change of the electrode conditions, such as wear of electrodes and sticking of melting silica, influence the discharge route and discharge power. If the electrode offset or distance is different, the discharge power that the fiber receives is changed. Until now, we have used electric current to compare the discharge power, but this method isn't adequate because it is impossible to measure the power that a fiber receives.

We propose a new method "ARC TEST" to measure the discharge power that a fiber receives. This method involves measuring the melting amount of fibers that are melted by discharge without stuffing movement. This is accomplished by measuring the retreat amount of the fibers, as shown in Fig.3. This procedure is the same as splicing, except no stuffing movement is done.

Fig.4 shows ARC TEST results for a single fiber pair with various electric currents. Melting amount increases and the rate of increase goes down as discharge time increases. Measuring the difference of discharge power for various electric currents is possible.

Fig.5.(1).(2) show ARC TEST results for a single fiber and 12 fibers. The electric current of 12 fibers is larger than that of a single fiber, so that the melting amounts of each are same at 20 second. The increase of melting amount has a large difference, especially also at less than 1 second. There is a flat line before the big increase, and the big increase of 12 fibers is later than for a single fiber.

It is difficult to measure the melting amount correctly after a short time discharge. ARC TEST needs an adequately long discharge time, and we use a 20 second discharge time in this paper.

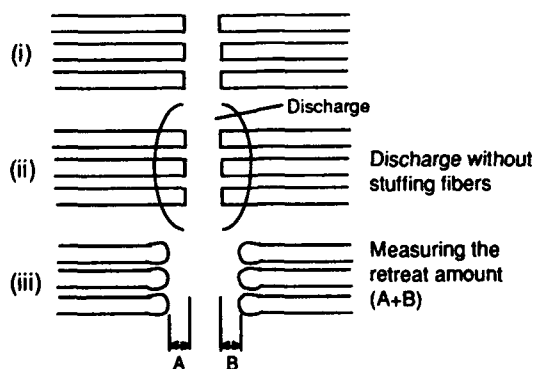


Fig. 3 ARC TEST

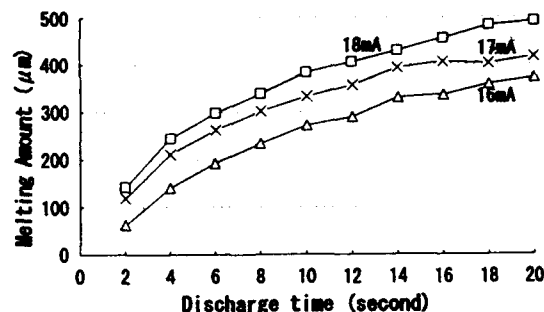


Fig.4 ARC TEST results for a single fiber pair with various electric currents.

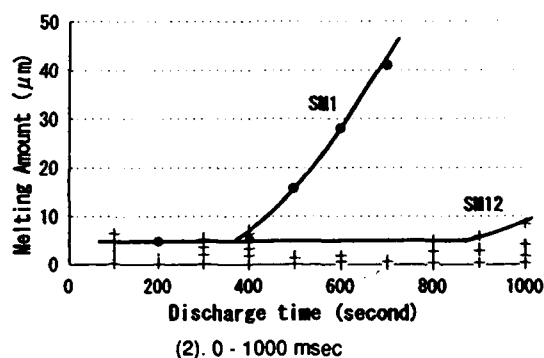
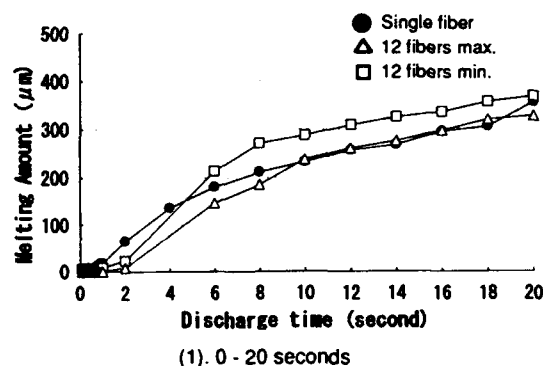


Fig.5 ARC TEST results for a single fiber and 12 fibers.

4. PREFUSION TIME

Fig.6 shows the relationship between prefusion time and splice loss for a single fiber. A short prefusion time (150 msec) is possible to splice at low loss with a wider area of discharge than other prefusion times. Large loss occurs with a long prefusion time (450 msec) as compared with a 150 msec prefusion time. The end face is more heated than necessary with a long prefusion time. The prefusion energy from discharge must be adequate, and is important parameter for a single fiber splicing.

Fig.7.(1).(2) show the relationship between prefusion time and splice loss for 12 fibers. Comparing these graphs there is not big difference. In this experiment, the prefusion times are 150 msec and 450 msec, but there is no difference in melting amount(Fig.5).

There is a difference between 150 msec and 450 msec for single fiber, in spite of melting amounts being the same(Fig.5). We can't ignore this parameter completely, but influence of prefusion time of mass splicing is very small when compared with single fiber splicing.

5. STUFFING SPEED

Fig. 8 shows the relationship between stuffing speed and splice loss for a single fiber. It is possible to splice at any speed, providing various levels of the discharge power. The result at each speed is different. Strong discharge is suitable for high speed and weaker discharge is suitable for slow speed. Time fiber exposed to discharge is expressed as

$$\text{Time} = \text{prefusion} + \text{gap} / \text{speed}$$

Where prefusion time is 150 msec, and gap is normally about 20 μm . The retreat amount of the fibers during prefusion time is so small that it is neglected. The moving time of a fiber for 20 μm is shown in Table.1. If we consider the moving time as prefusion time, this graph coincides with that in Fig.6. We conclude that a change of stuffing speed changes the prefusion time for single fiber splicing. The same reasoning can be applied to mass fusion splicing.

In mass splicing, the end face gap variance leads to differences in moving times. If there is a 30 μm variance, the time difference is 1.5 times of 20 μm moving time in Table.1. But, the influence of prefusion time for mass splicing is very small, leading us to believe that the influence of stuffing speed for mass splicing is also very small.

Table.1 The moving time for 20 μm

Stuffing speed ($\mu\text{m}/\text{second}$)	Moving time for 20 μm (msec)
200	100
450	44
700	29

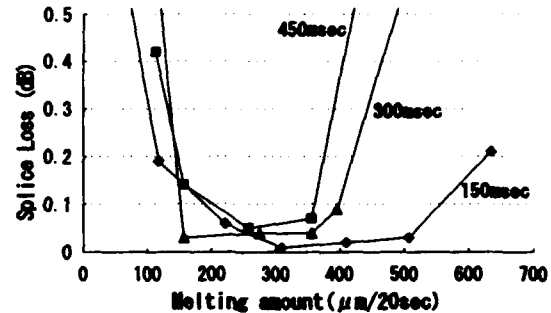
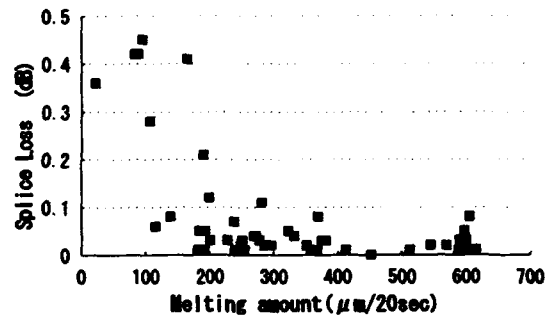
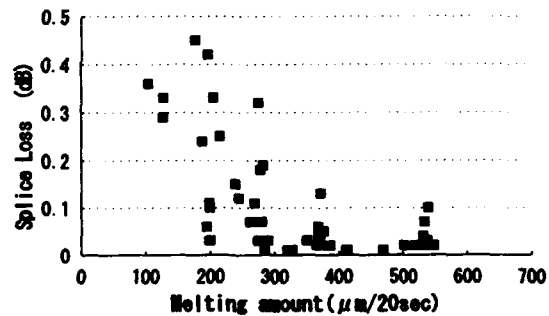


Fig.6 The relationship between prefusion time and splice loss for a single fiber. (Stuffing speed 450 μm)



(1). Prefusion time is 150 msec.



(2). Prefusion time is 450 msec.

Fig.7 The relationship between prefusion time and splice loss for 12 fibers. (Stuffing speed 450 μm)

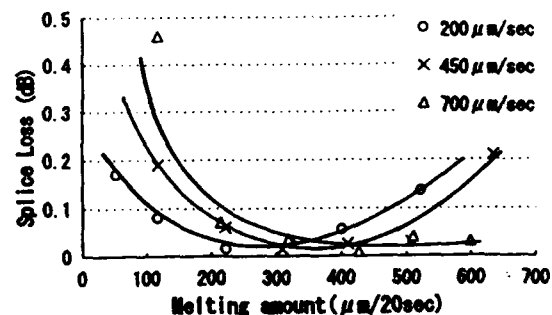


Fig.8 The relationship between stuffing speed and splice loss for a single fiber. (Prefusion time 150msec)

6. END FACE GAP VARIANCE

6.1 Measurement

We use a common 12 ribbon fiber in this study, and measure end face gap variance, as shown in Fig.9. Since the adhesion force of bundled fiber is smaller than that of ribbon fiber, the maximum variance is a little bigger than ribbon fiber. The variance for less than 12 fibers is smaller than 12 fibers. The fiber end face gap variance always exists, and that size is less than $30\text{ }\mu\text{m}$ in normal mass fusion splicing.

6.2 Study

A fusion splicer stuffs the fibers by the gap maximum plus $50\text{ }\mu\text{m}$ during discharge. $50\text{ }\mu\text{m}$ is a constant number for any number of fibers. If there is a $30\text{ }\mu\text{m}$ end face gap variance, the largest gap is $50\text{ }\mu\text{m}$, and the largest overlap is $80\text{ }\mu\text{m}$, as shown in Fig.10. These fibers are spliced at the same time. Further, the discharge power of each fiber in ribbon is different.

Fig.11 shows the relationship between the end face gap and splice loss for a single fiber. It is possible to consider a large gap as an increase of pre-fusion, and the fiber of a large gap as being more heated than the fiber of a small gap.

Fig.12 shows the relationship between overlap and splice loss for a single fiber. For the case of excessive overlap, the fibers are not melted enough and hit each other in solid state. This requires a strong discharge to splice for a large overlap than for a normal overlap. If we apply these results directly to mass fusion splicing, with a large end face gap variance, the range of suitable discharge power is very small.

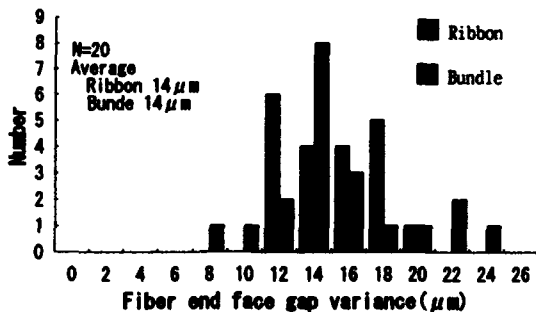


Fig.9 Histogram of the end face gap variance for 12 fibers.

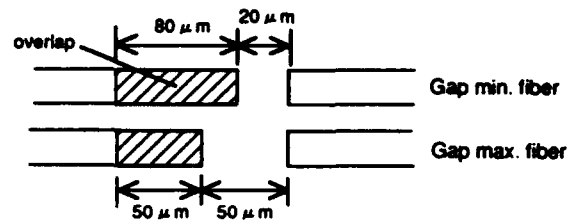


Fig.10 Gap and overlap of the fibers with $30\text{ }\mu\text{m}$ variance.

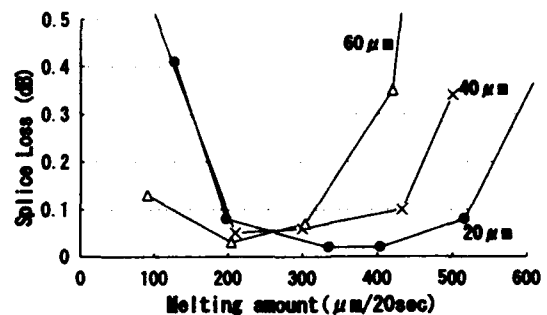


Fig.11 The relationship between the end face gap and splice loss for a single fiber.

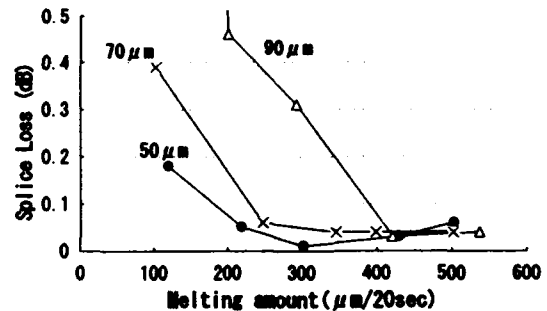


Fig.12 The relationship between overlap and splice loss for a single fiber.

Fig.13.(1) shows the splice loss for a large gap variance (more than $40\text{ }\mu\text{m}$) for 12 fibers at 150 msec prefusion. Prefusion time is the same as for the single fiber experiment. The difference between the gap minimum and gap of each fiber is shown. 0-20 μm is considered to be a large overlap state and 40- μm is a large gap state when fibers are spliced. Even if the gap is large, splice loss for a strong discharge is very low, because prefusion time doesn't significantly influence the splice loss in mass fusion splicing. Conversely, for a weak discharge, there is a correlation to the single fiber case.

Fig.13.(2) shows the splice loss for a large gap variance (more than $40\text{ }\mu\text{m}$) for 12 fibers at 1000 msec prefusion. Large gap fiber has a large loss for strong discharge, and large overlap fiber has a large loss for weak discharge. This is the same as the single fiber case.

End face gap variance is not so much a problem as we first thought. However, melting amount should be 300 - 500 $\mu\text{m}/20\text{sec}$ to obtain a good splice.

7. CONCLUSION

Through research and experimentation, we have found a clear relationship between splice loss and certain parameters in mass fusion splicing. The following conclusions are based on this research:

- 1) It takes a longer discharge time for fibers melted in mass fusion splicing than single fiber. However, the influence of prefusion time is not as large for mass fusion splicing.
- 2) The influence of stuffing speed is small for mass fusion splicing.
- 3) It is possible to perform mass fusion splicing even if there is a large end face gap variance, just the same as the single fiber case.
- 4) ARC TEST is an effective method to measure the discharge power, and optimum discharge power was found to be where the melting amount is 300 - 500 $\mu\text{m}/20\text{sec}$ for mass fusion splicing.

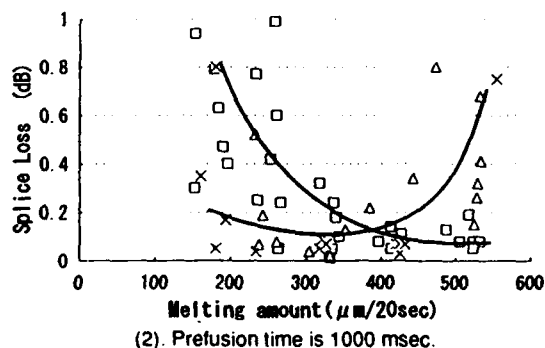
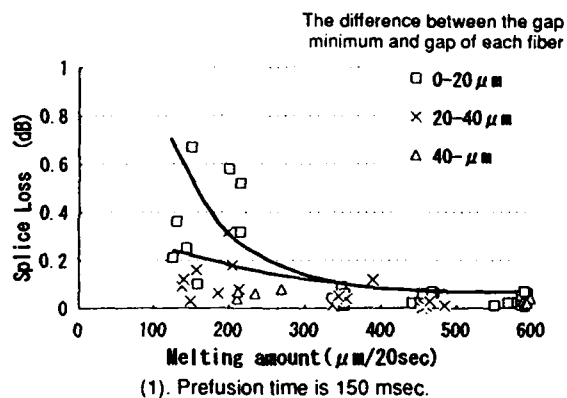


Fig.13 The splice loss for a large gap variance (more than $40\text{ }\mu\text{m}$) for 12 fibers.

REFERENCES

(1) Y.Kato, A.Ishikura, T.Sano and S.Takashima, "Single-Mode Optical Fiber Ribbon Splicer", International Wire & Cable Symposium Proceedings, p.386-391, 1987

(2) K Osawa et al, "Analysis of mass fusion splice loss for optical fiber ribbons", International Wire & Cable Symposium Proceedings, p.205-211, 1989

(3) D.Marcuse, "Loss analysis of single-mode fiber splices", Bell system technical journal Vol.56 No.5 p.703-718, 1977

(4) M.Tachikura and N.Kashima, "Fusion Mass-Splices for Optical Fibers Using High-Frequency Discharge", JOURNAL OF LIGHTWAVE TECHNOLOGY, Vol.LT-2, No.1, 1984



Isao Suzuki

Optical system R&D Dpt.
Fujikura Ltd.

1440, Mutsuzaki, Sakura-
shi, Chiba-ken, 285,
JAPAN

Isao Suzuki was born in 1955. He graduated in mechanical engineering from Tokyo University of Agriculture and Technology in 1978.

He joined the Optical system R&D Dpt. in Fujikura Ltd. in 1984.

He is now an assistant chief of the Precision Instrument Section.



Michio Morooka

Optical system R&D Dpt.
Fujikura Ltd.

1440, Mutsuzaki, Sakura-
shi, Chiba-ken, 285,
JAPAN

Michio Morooka was born in 1965. He received the B.E. degree in mechanical engineering from Chiba University in 1989.

He joined Fujikura Ltd. in 1989 and has been engaged in the research and development of an optical fiber splicer.



Mikio Yoshinuma

Optical system R&D Dpt.
Fujikura Ltd.

1440, Mutsuzaki, Sakura-
shi, Chiba-ken, 285,
JAPAN

Mikio Yoshinuma was born in 1947. He graduated in mechanical engineering from Chiba University in 1971.

After graduation, he joined Fujikura Ltd. and has been engaged in research and development on mechanical equipment and tools for communication wires, cables, and parts.

He is now a manager of the Precision Instrument Section.



Hiroyuki Kawasaki

Optical system R&D Dpt.
Fujikura Ltd.

1440, Mutsuzaki, Sakura-
shi, Chiba-ken, 285,
JAPAN

Hiroyuki Kawasaki was born in 1963. He received the B.E. degree in electrical engineering from Yokohama national University in 1988.

He joined Fujikura Ltd. in 1988 and has been engaged in the research and development of an optical fiber splice machine since 1990.

Mr. Kawasaki is a member of the Institute of Electronics and Communication Engineers of Japan.

PROTECTION AND RELIABILITY OF SINGLE-FIBER AND RIBBON-FIBER FUSION SPLICES

Enrico Serafini

SIRTI S.p.A., Cables and Optical Technologies Division
Via Vida 19, 20127 Milano, Italy

ABSTRACT

The installation of high fiber count cables, mainly used in the local loop, forces the use of high density and high reliability splicing technology. This paper describes a technique to effectively and reliably protect and reinforce fusion splices in the field. The developed splice protection consists in a plastic sleeve filled with an UV curable resin. Such solution allows to keep the protection size very small and is suitable for field installation on single-fiber and multiple-fiber fusion splices. The developed splice protections have been successfully submitted to a complete set of optical, mechanical, environmental and reliability tests. In particular no degradation of splice tensile strength was observed after 2000 hours aging at 80°C and 90% RH, rather a strength increase of about 50% was seen.

1. INTRODUCTION

A recent market survey [1] has established that more than 90% of optical fibers installed worldwide in 1992 have been fusion spliced. Assuming 10 million kilometers of fiber installed and an average cable length of 2÷3 km we get a number of fusion splices and consequently of splice protectors implemented last year (mainly in the transport network) in the range of 3÷4 million.

The improvement of fiber geometrical tolerances like outside diameter and core cladding concentricity has permitted high quality low loss fusion splicing by passively aligning fibers before welding.

The development of low-cost, "V-groove" passively aligning fusion splicers will probably push fusion splicing technology in the distribution network. In this case, the number of fusion splices will strongly increase provided that the reliability of the fusion technology will meet the stringent requirements of the subscriber loop harsh environment.

The reliability of fusion splicing depends on the reliability of the single steps of the splicing procedure such as fiber preparation (coating stripping, fiber cleaning and cleaving), fiber positioning in the splicer, welding process and protection application.

In this paper, a new splice protection technique will be presented and its reliability will be analysed. It is applicable to single-fiber splices or to ribbon-fiber splices.

All the tests reported in this paper have been performed on single-mode fibers made by OVD technology and coated by means of a double layer of acrylate material or ribboned together by means of an additional common extruded coating.

2. FUSION SPLICE PROTECTION

The splice protection makes two basic functions; it increases the splice tensile strength and it seals the bare splice from the external environment in order to assure long-term reliability. Several techniques have been developed to protect fusion splices; one of the most common is based on heat-shrinkable plastic tubes reinforced by metallic or dielectric strength members. These splice protections generally show the following drawbacks:

- a) non symmetric cross-section;
- b) non homogeneous materials employed;
- c) excessive weight and size;
- d) need of a splice holder into the organizer;
- e) low packaging density into the organizer.

While points a) and b) may affect the splice reliability and its thermal behaviour the last three points become crucial when subscriber loop is considered where high fiber count cables are used.

In order to overcome the above drawbacks a new splice protection has been designed and developed with the following characteristics:

- a') no splice loss degradation due to protection application;

- b') high packaging density;
- c') small size (comparable to unspliced fibers) and radial simmetricity;
- d') no need to be fixed to the organizer and full exploitation of the organizer length and width;
- e') good short-term mechanical protection in terms of tensile, crushing, torsion and bending strength;
- f') excellent thermal stability;
- g') high long-term reliability in terms of no strength degradation after aging, high fatigue parameter n, compatibility with cable filling compounds;
- h') easy and fast mounting procedures.

All the above targets have been reached by means of a splice protection consisting in a plastic capillary tube filled with an ultra-violet (UV) curable resin. Such solution allows to keep the size of the protection very small and it is suitable for field installation.

Splice organizers can accomodate several (12 or more) splices protected in this way without necessity of fastening because of their light weight. Thanks to their flexibility, the splices can also be placed along the short side of the organizer. The adhesive used to fill the tube as well as to seal the bare splice from the environment is an UV curable soft acrylate with a low Young's modulus after curing.

The adhesive takes about 30 to 60 seconds to cure. The developed protective sleeves schematically shown in Figure 1 have the following nominal dimensions (mm):

	single-fiber	4-fibers ribbon
length	15÷30 (*)	30
ID	0.38	1.40 x 0.60
OD	0.51	2.15 x 1.20

(*) depending on splicer type

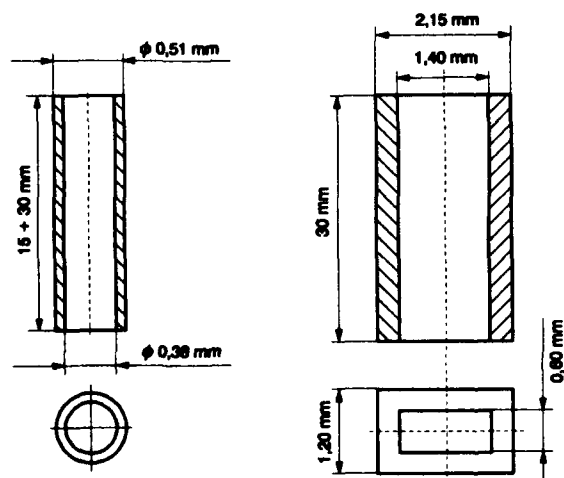


Figure 1 - Schematic of splice protection sleeve

The protective sleeve is easily applied on splices. Before making the splice, the sleeve is inserted on a fiber or a ribbon. After fusion, the sleeve is slid on the bare section of the splice and filled with adhesive.

The adhesive is injected into the sleeve by means of a specific tool consisting in a syringe where the needle has been replaced by 2 small rubber blocks which are pressed against the protective sleeve to be filled thus forcing the adhesive to flow into the sleeve without coming out.

3. TENSILE STRENGTH

In principle the increase of tensile strength due to the protective sleeve is the result of two contributions: a purely elastic effect which depends on size, shape and materials of the protective structure and a fatigue effect.

3.1 Elastic effect

The calculation of splice reinforcement is done by assuming a pure tension stress according to Saint Venant's principle [2]. In Figure 2 the loading configuration is shown for a single-fiber splice.

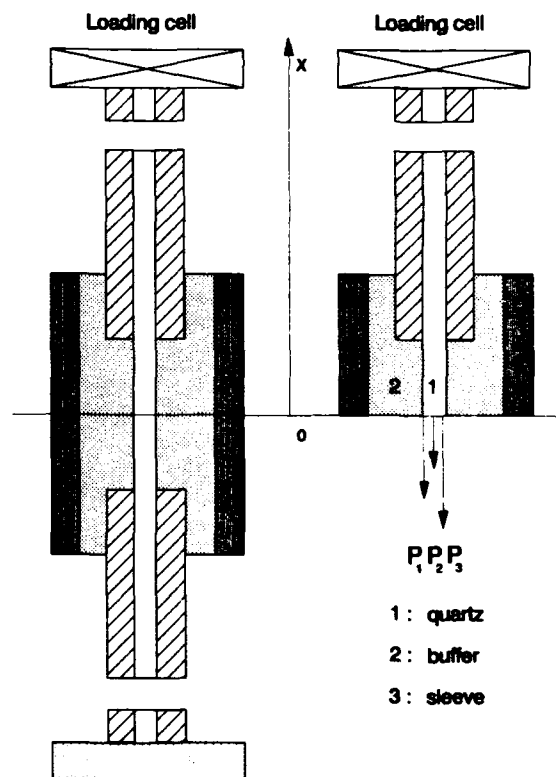


Figure 2 - Schematic of splice loading configuration

The following assumptions have been done:

1. at $x = 0$ pure tension stress state: the load is applied far from the cross-section of our interest and the end effects are not important (the sleeve is sufficiently long);
2. perfect adhesion among the different materials of the protection (no slippage), at least in the range of strains that induce splice failure;
3. multiple-fiber splices are considered failed when the first fiber breaks. Before failure the stress is uniformly distributed among the N fibers.

Equilibrium equation

$$P = P_1 + P_2 + P_3 = \sigma_1 A_1 + \sigma_2 A_2 + \sigma_3 A_3 \quad (1)$$

Compatibility equations

$$\epsilon_1 = \epsilon_2 = \epsilon_3 = \epsilon_0 \quad (2)$$

Hook's law

$$\sigma_1 = E_1 \epsilon_1 \quad (3')$$

$$\sigma_2 = E_2 \epsilon_2 \quad (3'')$$

$$\sigma_3 = E_3 \epsilon_3 \quad (3''')$$

Substituting equations (2) and (3) into (1) we find:

$$\sigma_i = P E_i / (E_1 A_1 + E_2 A_2 + E_3 A_3) \quad i = 1, 2, 3 \quad (4)$$

Let σ_r and P_r the generic splice failure stress and load respectively. In order to calculate the reinforcement we have to compare the bare splice strength to the protected splice strength. In both cases the failure stress is the same while the failure load is different.

Bare splice

$$\sigma_r = \frac{P_r'}{A_1} \quad (5)$$

Protected splice

$$\sigma_r = \sigma_1 = E_1 P_r'' / (E_1 A_1 + E_2 A_2 + E_3 A_3) \quad (6)$$

Thus the reinforcement factor, defined as the ratio between the protected splice breaking load and the bare splice breaking load is:

$$\frac{P_r''}{P_r'} = \frac{E_1 A_1 + E_2 A_2 + E_3 A_3}{E_1 A_1} \quad (7)$$

In Table 1 the typical geometrical and elastic parameters of the 3 zones characterizing the protected splice are reported.

		cross-section mm ²	Young's modulus N/mm ²
Single Fiber Splice	1. Fiber	0,0123	$7,5 \times 10^4$
	2. Adhesive	0,1011	$5,9 \times 10^2$
	3. Sleeve	0,0909	$1,4 \times 10^3$
4-Fiber Ribbon Splice	1. Fiber	0,0491	$7,5 \times 10^4$
	2. Adhesive	0,7909	$5,9 \times 10^2$
	3. Sleeve	1,7400	$1,4 \times 10^3$

Table 1 - Geometrical and elastic constants of the splice materials.

The calculated reinforcement factors for single-fiber and 4-fibers ribbon splices are 1.20 and 1.79 respectively.

3.2 Fatigue effect

The tensile strength of a fusion splice depends on the size of cracks on its surface. When a tensile load is applied to the splice these cracks grow decreasing the inert splice strength. The inert strength is defined as the strength corresponding to the crack distribution before loading, i.e., assuming that flaws do not grow during the tensile test. The presence of the adhesive on the splice allows to decrease the speed of crack growth inducing an improvement of splice strength even ignoring the elastic effect of the protection. The splice strength increase due to the protection can be evaluated as follows.

The splice cumulative percentage of failure is given by equation [3]

$$F(\sigma) = 1 - \exp [- (k/k_0)^b] \quad (8)$$

in which

$$k = \sigma^{n+1} / [(n+1) \dot{\sigma}]$$

$$b = m/(n-2)$$

$$k_0 = [\sigma_0 B^{1/(n-2)}]^{m/b}$$

$$B = 2/[AY^2 (n-2) K_{IC}^{n-2}]$$

σ breaking stress

$\dot{\sigma}$ stress rate

A, n empirical stress-corrosion parameters in the relationship $da/dt = AK_I^n$

K_{IC} critical stress intensity factor

Y factor depending on the shape of the crack

m, σ_0 parameter of the inert strength Weibull distribution

With a little algebra we find:

$$\sigma = \{ (n+1) \sigma_0 \left[\ln \left(\frac{1}{1-F} \right) \right]^{1/b} \}^{1/(n+1)} \quad (9)$$

Knowing A and n in the 2 cases of bare and protected splices and assuming that all the other parameters remain constant we find:

$$\Delta \sigma = \sigma(A_1, n_1) - \sigma(A_2, n_2) \quad (10)$$

3.3 Experimental results

In Figures 3 and 4 the Weibull plots of tensile strength of protected and bare single-fiber and 4-fibers ribbon splices respectively, are shown.

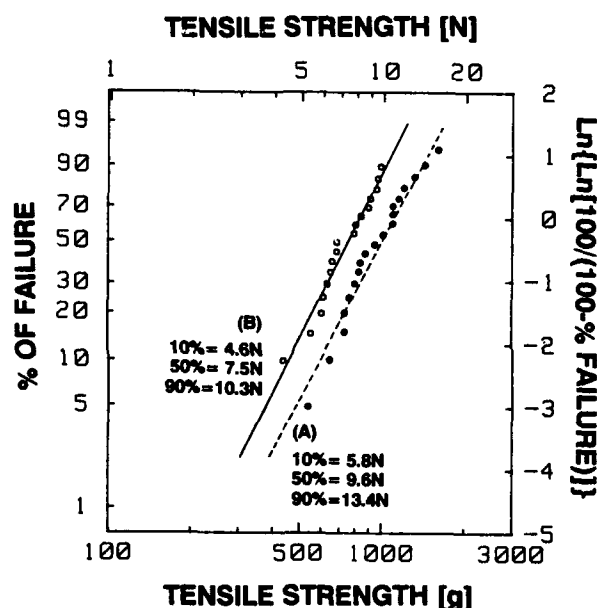


Figure 3 - Weibull plots of tensile strength of:
(A) single-fiber protected splices
(B) bare splices

The optical power has been monitored during the test to know the actual strength of the splice. In fact the maximum strength reached during the test might be higher than the breaking load of the fiber splice.

The median strength increase due to protection, experimentally found has been 28% for single-fiber splices and 100% for ribbon splices. In the former case, as seen in section 3.2, the reinforcement factor due to elastic effect has been calculated to be 20% giving an extra 8% of reinforcement due to fatigue effect. For ribbon splices the same figures are 79% due to elastic effect and 21% due to fatigue effect.

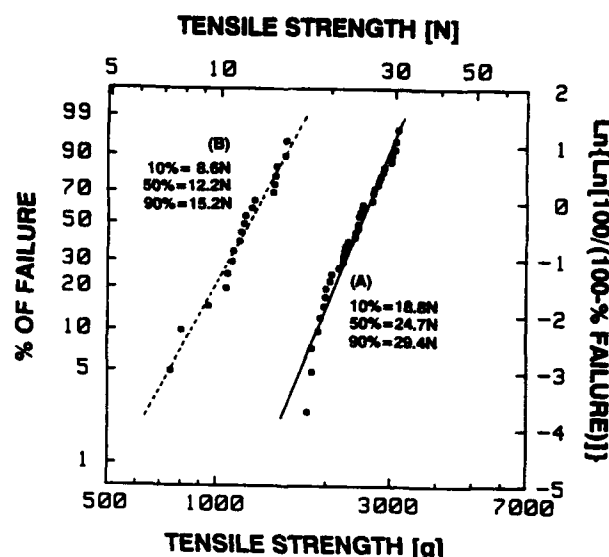


Figure 4 - Weibull plots of tensile strength of:
(A) ribbon-fiber protected splices
(B) ribbon-fiber bare splices

4. CRUSHING STRENGTH

Figure 5 shows the results of the crushing test performed on protected splices. The splices have been crushed for their full length, i.e. 15 mm for single-fiber splices and 30 mm for ribbon splices. Since multiple protections have a rectangular cross-section they have been crushed along the short side and the long side getting similar results.

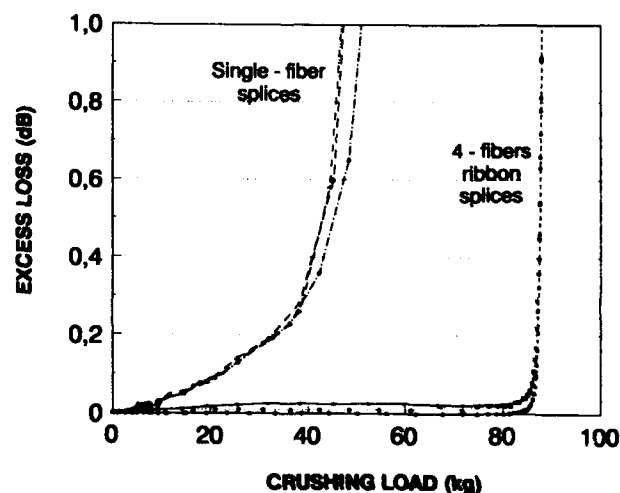


Figure 5 - Crushing strength of protected splices

5. BENDING STRENGTH

One of the design specifications for this new protection was lightness and flexibility in order to entirely exploit the space of the organizer and to avoid handling failures during installation. This test is more critical for multiple protections because of their rectangular cross-section.

Figure 6 reports the results of the bending test on ribbon splices bent in a plane normal to the long side of the cross section. The results are reported in terms of percentage of splices failed at a certain bending radius.

Splices have been considered failed if they showed a permanent loss after the test. Ribbon splices may be bent with a bending radius of 25 mm without failure.

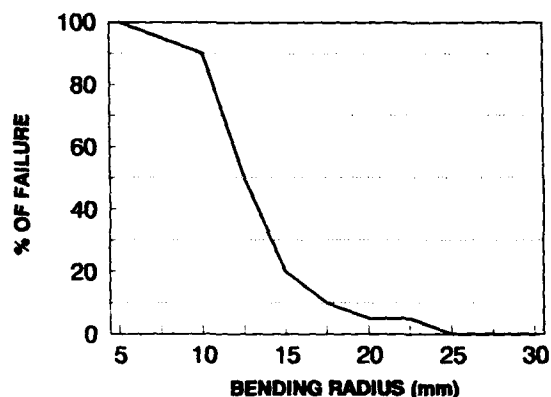


Figure 6 - Bending test on ribbon splices

6. DYNAMIC FATIGUE

From the empirical relationship between the crack growth velocity and the applied stress already mentioned in section 3.2, it is possible to demonstrate that there is a linear relationship between the logarithm of time to failure t and the logarithm of applied static stress σ [4], that is

$$\ln t = -n \ln \sigma + C \quad (11)$$

If the applied stress uniformly increases with time, it can be demonstrated the following relationship between the logarithm of breaking stress σ and the logarithm of stress rate $\dot{\sigma}$ [5]

$$\ln \sigma = \frac{1}{1+n} \ln \dot{\sigma} + D \quad (12)$$

The dynamic fatigue test is preferable to the static one because it is much less time consuming even if many times the two tests give different values of the stress-corrosion parameter n .

In Figure 7 the dynamic fatigue parameter n , calculated from equation (12) is shown as a function of the failure probability for single-fiber splices and ribbon splices respectively.

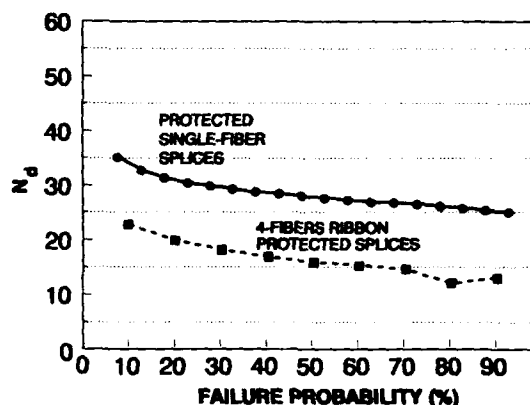


Figure 7 - Stress-corrosion factor of protected splices

7. THERMAL CYCLING

Since the materials surrounding the bare splice have elastic moduli much lower than that of glass they apply a low constraint to the fiber during thermal cycling. The calculated thermal stresses [6] on the splices are reported in Table 3 using the material constants at ambient temperature of Table 2.

	Poisson's ratio	Expansion coefficient °C ⁻¹
1. Fiber	0,17	5,0 · 10 ⁻⁷
2. Adhesive	0,35	9,5 · 10 ⁻⁵
3. Sleeve	0,35	7,0 · 10 ⁻⁵

Table 2 - Material constants of fiber, buffer and sleeve.

	$\sigma_r/\Delta T$ N/mm ² °C	$\sigma_z/\Delta T$ N/mm ² °C
Single-fiber splice	- 0,01	0,98
4-fibers ribbon splice	- 0,01	0,61

Table 3 - Radial and axial stresses on fiber per °C.

If ΔT is 60°C the axial stress σ_z on the fiber for the single-fiber splice becomes 58,8 MPa which can be regarded as a safe value. In fact this figure is conservative considering that Young's moduli of plastic materials decrease as temperature increases lowering the actual axial stress on the glass.

Five cascated single-fiber and ribbon-fiber splices have been thermal cycled from -40°C to +80°C. The insertion loss was monitored and measured every 30 minutes. The variation of the splice loss versus time and temperature is shown in Figure 8. Over the full range of temperatures no excess loss was observed.

8. AGING

An aging test has been performed on protected single-fiber and multiple-fiber splices. The former have been kept for 1000 hours at 80°C and relative humidity of 90%; ribbon splices have been aged for 1000 and 2000 hours at the same temperature and relative humidity. No strength degradation has been observed; rather a progressive strength increase can be observed as shown in Figure 9 which reports the results of the aging test.

It has been demonstrated [7] that aging smooths the rough surface of an intentionally abraded low strength optical fiber. The splicing area, which is a low strength piece of fiber, has probably deep flaws and peaks due to abrasion and fusion process. Aging might round or fill or smooth the bottom of flaws or the top of peaks explaining the strength increase. In order to confirm this trend and to see the limit of strength increase a 3000 hours aging test is in progress.

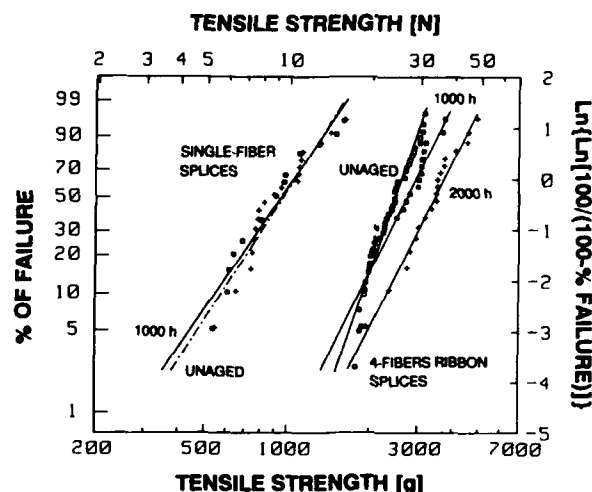


Figure 9 - Weibull plots of tensile strength of aged protected splices

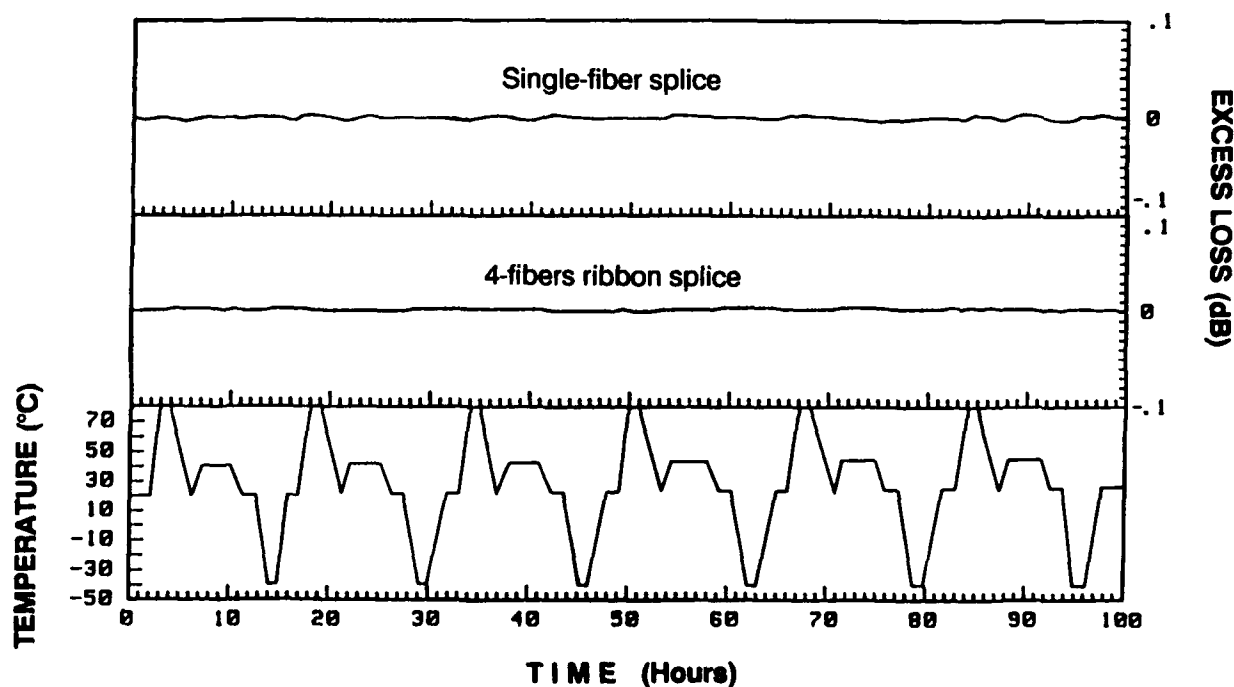


Figure 8 - Thermal cycling of protected splices

9. CONCLUSIONS

A technique to reliably protect and reinforce single-fiber and multiple-fiber fusion splices has been presented. This splice protection technique has the following main merits:

- small size, light weight and high flexibility allowing high packaging density and no need of fixing into the organizer;
- easy and quick to install in the field;
- very high thermal stability;
- adequate mechanical strength;
- no aging degradation of tensile strength.

A complete testing programme has been reported which demonstrated the effectiveness and the reliability of this splice protection method. This technique has been adopted by the Italian operating companies since some years and it has been used on a large scale in the Italian fiber optic telecommunication networks.

REFERENCES

- [1] "Worldwide trends in fiber optic ribbon cable and technologies for fiber splicing", KMI Corp., 1993.
- [2] S.P. Timoshenko, J.N. Goodier, "Theory of elasticity", Mc Graw Hill, 1982.
- [3] Y. Miyajima, "Studies on high-tensile proof tests of optical fibres", IEEE J. Lightwave Technol., Vol. LT-1, No. 2, 1983.
- [4] R. Adams, P.W. McMillan, "Review static fatigue in glass", J. Material Science, 12, pp.643-57, 1977.
- [5] R.W. Davidge, J.R. McLaren, G. Tappin, "Strength-probability-time (SPT) relationships in ceramics", J. Material Science, 8, pp. 1699-1705, 1973.
- [6] S. Stueflotten, "Protection of Optical Fiber Arc Fusion Splices", J. Opt. Commun., 3 (1982) 1, pp.19-25.
- [7] H. Chandan, H.H. Yuce, "Aging and Fatigue Behavior of Low Strength Fibers", to be published in Proc. of EOS/SPIE International Symposium on Fiber Optic Networks, Berlin, April 1993.



Enrico Serafini

Cables and Optical
Technologies Division
SIRTI S.p.A.
Via Vida, 19
20127 Milano - ITALY

Enrico Serafini was born in 1956. He received the Dr. Ing. degree from Politecnico of Milan in 1982. He joined SIRTI in 1984 as research engineer in the field of optical fiber cables measurement and jointing techniques. He is now responsible for Cables and Optical Technologies R&D Division. He is Special Rapporteur for question on passive optical components of COM VI of TSS (former CCITT) and he is member of IEEE.

16-Fiber Optical Connector

Jun Yamakawa, Hiroyuki Yamada, Takashi Shigematsu,
Hiroyuki Yanagase, Ken Kanai

THE FURUKAWA ELECTRIC CO., LTD.
6, YAWATA-KAIGANDORI, ICHIHARA, CHIBA 290 JAPAN

ABSTRACT

For the ISDN era coming, the optical connector, especially multiple-fiber optical connector, is considered one of the key components in the optical fiber networks.

We succeeded in developing the small-size optical connector for 16-fiber ribbon utilizing the high precision plastic molding technique.

We improved the number of fibers per connector by means of reduction the distance between the fiber holes in comparison with that of conventional optical connectors. So the fiber density per unit area ($\sim 1\text{mm}^2$) of newly developed connector is higher than that of conventional connectors. The newly developed high-density optical connector makes it possible to reduce the number of optical connectors and cable-to-cable connecting time.

By investigating the conventional multiple-fiber connector manufacturing process, average connecting loss of 0.2dB for 16-fiber optical connector was achieved.

1. INTRODUCTION

In accordance with diversification of the optical fiber telecommunication networks, the introductions of high-density and high-count optical cables composed of single-mode 16-fiber ribbons are expected. In this case, the important point to note is the increase of cable-to-cable connecting time because of the increase of the number of the fibers. Therefore an easy and collective connecting technique to join optical fiber ribbons is required.

For reasons mentioned above, it is considerably necessary to develop 16-fiber optical connectors with the following properties.

- (1) simple connecting structure
(reconnecting possible)
- (2) small-size
- (3) low-connecting-loss
- (4) long term stability
- (5) low cost

Recently, multiple-fiber optical connectors have been noticed. We have also long been working to develop plastic multiple-fiber connectors such as 4 or 8-fiber optical connectors.

This paper presents a structure of a newly developed 16-fiber optical connector for a 16-fiber ribbon, and its initial characteristics.

2. STRUCTURE OF THE 16-FIBER OPTICAL CONNECTOR

This connector is designed for a 16-fiber ribbon that consists small diameter coated fibers.^{(1) (2)} Figure 1 shows the newly developed 16-fiber optical connector.

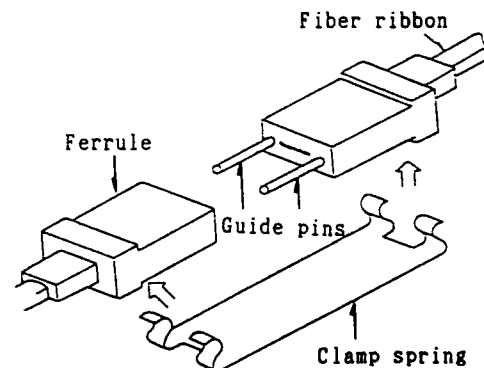


Figure 1 The structure of 16-fiber optical connector

It is similar in structure to that of conventional multiple-fiber connector.^{(3) (4)} It consists of a pair of plastic 16-fiber plugs, two guide pins and a clamp spring to hold the connector closed. As can be seen in Figure 2, the 16-fiber plug consists of a plastic ferrule, a rubber boot

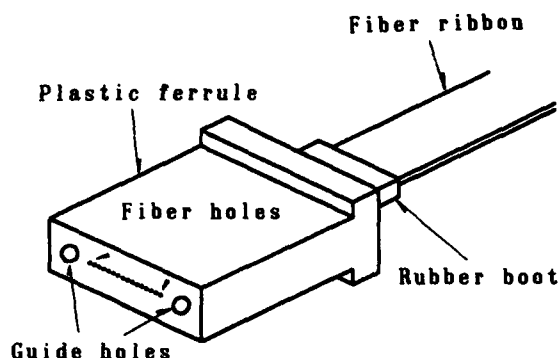


Figure 2 The 16-fiber plug

to protect the fibers, and a 16-fiber ribbon. The plastic ferrule has 16 holes for insertion of the fibers and two holes for the guide pins.

The ferrule is designed as follows. Two guide pin holes are on each side of the fiber holes, positioned symmetrically in relation to their center lines, and the center of the fiber holes is on the same level with the center of the guide pin holes.

This ferrule has the fiber holes in a straight-line at the same pitch as the fiber pitch of the ribbon to attach the fiber ribbon easily and without causing bending stress. In this report, the distance between the fiber holes is shorter than that of conventional connectors (~ 0.25 mm), because of 16-fiber ribbons that consist of coated fibers whose diameter is about 0.2 mm . As the result, the new connector's fiber density per unit area ($\sim 100\%$) is about 3 times against a conventional 4-fiber connector's and about 1.7 times against a conventional 8-fiber connector's respectively. The guide pin pitch is larger only 1 mm than that of conventional 8-fiber connector. Therefore the 16-fiber optical connector is slightly larger than conventional 8-fiber connector. The connector size is about $8(L) \times 11(W) \times 2.5(H)\text{ mm}$.

Besides all this, this 16-fiber optical connector can form the stacked multiple-fiber optical connector using the binding pins. Figure 3 shows the structure of the 80-fiber optical connector (16-fiber optical connector $\times 5$).

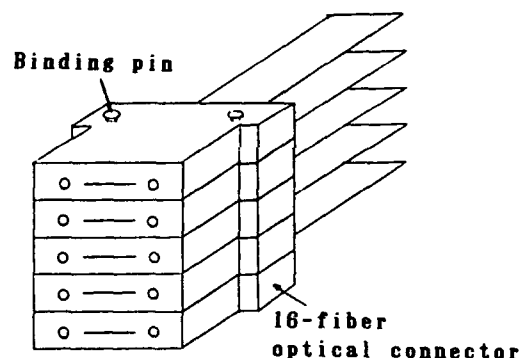


Figure 3 The structure of stacked 80-fiber optical connector

3. MANUFACTURING PROCESS

The manufacturing process of this connector is shown in Figure 4.

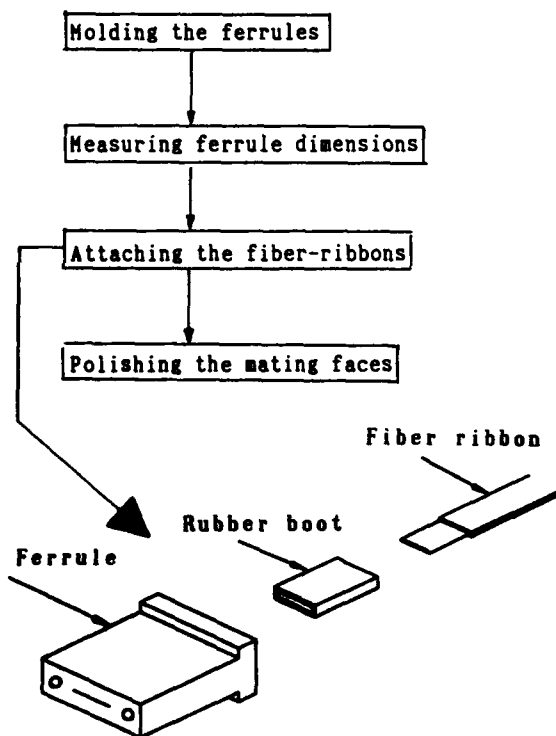


Figure 4 The manufacturing process of 16-fiber optical connector

3-1. Molding the ferrule

The ferrule is manufactured by the high precision transfer molding technique. (We have already studied in detail about this technique in conventional multiple-fiber connector.)

To make the high-precision ferrule, we used the high-precision V-groove in the die, that is to say, a number of high-precision pins of prescribed sizes are fixed in two-large and 16-small V-grooves.

In addition to this, to realize the dimensional accuracy of the submicron order or better in the ferrule, it is important to consider molding materials. We used a thermally cured epoxy resin with very low mold shrinkage suitable for this use.

3-2. Measuring the ferrule dimensions

After molding process, to confirm the quality of the ferrule, the position errors of the fiber holes relative to the guide pin holes on the mating face are measured by means of noncontact multiple edge measurement using a high resolution CCD camera. Its repeatability is $0.1\mu\text{m}$.

3-3. Attaching the fiber-ribbon

The fiber ribbon removed end coatings is inserted in the ferrule through the rubber boot, and fixed with epoxy adhesive.

3-4. Polishing the mating face

Then the mating face of the ferrule is polished to a flat surface and lapped to minimize the return of the light.

4. INITIAL CHARACTERISTICS

4-1. Position errors of the fiber holes

Figure 5 shows the result of the position errors of the fiber holes relative to the guide pin holes. The error is analyzed both X-axis and Y-axis. We obtained the good position errors of the fiber holes, the errors of X-axis and Y-axis are within $\pm 1\mu\text{m}$.

4-2. Connecting loss

The normal and inverse connecting performance with the master plug is shown in Figure 8. The master plug is selected from the same manufacturing lot. The measurement condition is as follows.

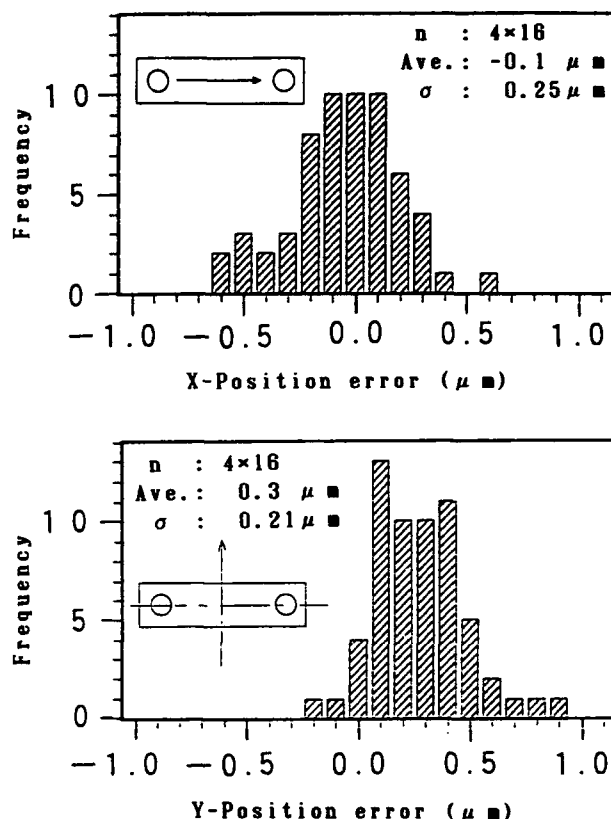


Figure 5 Histogram of the position errors of the fiber holes

- (1) A wavelength is $1.3\mu\text{m}$ (LED).
- (2) A reflective index matching oil is applied to the mating face of the connectors.
- (3) The value is the average of three times reconnection.

The total average value is 0.19dB in normal connection and 0.20dB in inverse connection.

Very low-connecting-loss optical connector comparing with the conventional multiple-fiber connector has been achieved.

4-3. Reconnection

Figure 7 shows the results of the re-connecting test at 100 times.

We obtained the good reconnecting characteristics, the fluctuation compared with the initial connecting loss is within $\pm 0.2\text{dB}$.

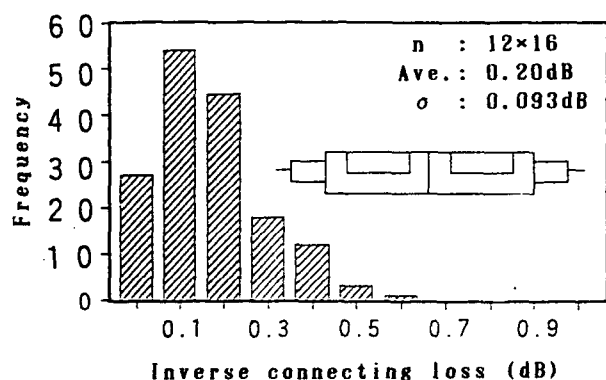
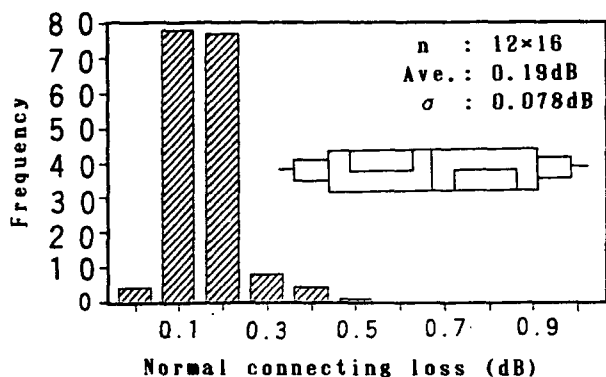


Figure 6 Histogram of the normal and inverse connecting loss with the master plug

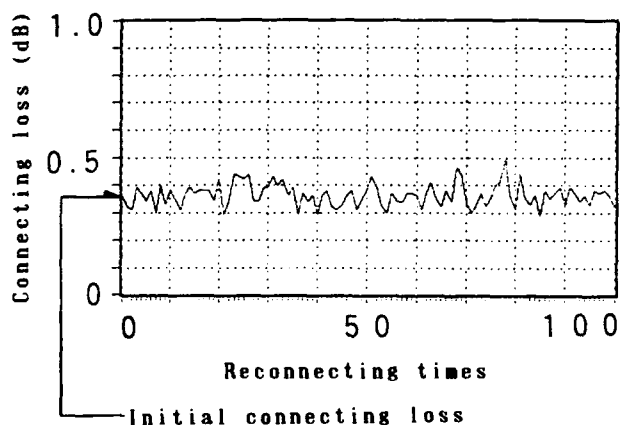


Figure 7 The repeatability of connecting loss during the reconnecting test at 100 times

4-4. Return-loss

Figure 8 shows the results of the return-loss measurement.

We obtained the good return-loss characteristics, with the average value of

reflective attenuation of 48.6dB and minimum value of 36.1dB.

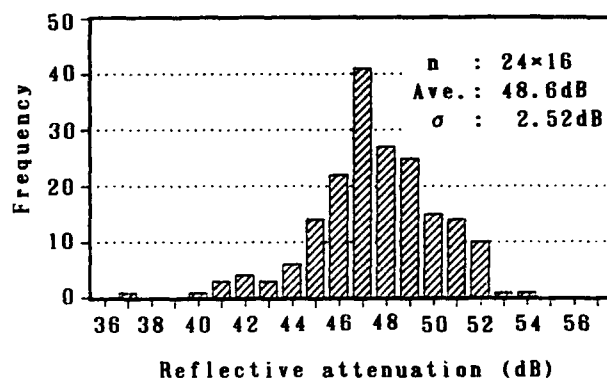


Figure 8 Histogram of the return-loss

4-5. Heat cycle test

Figure 9 shows the result of the heat-cycle test. The test condition is as follows.

- (1) temperature variation : $-40 \sim +70^{\circ}\text{C}$
- (2) term : 7days (4cycles / day)

We obtained the good heat-cycle characteristics, the fluctuation compared with the initial connecting loss is $\pm 0.2\text{dB}$.

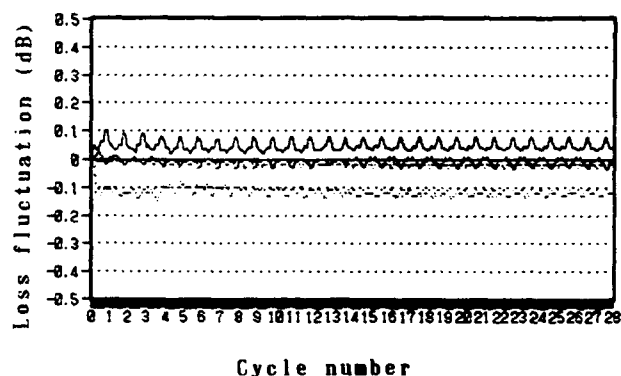


Figure 9 The repeatability of connecting loss during the heat-cycle test

5. CONCLUSION

We succeeded in developing the small-size optical connector for 16-fiber ribbon utilizing the high precision plastic molding technique.

To begin with, the simple connecting structure, high density and small-size optical connector has been achieved. Then, this optical connector proved to have extremely low-connecting-loss characteristics, with the initial connecting loss of about 0.2dB. Finally, this optical connector has superior initial characteristics in reconnecting test and heat-cycle test.

With the optical fiber communication systems to subscriber networks growing, it is necessary to realize still more low-connecting-loss and higher reliability.

We are going to make progress in the development of optical connector to meet those demands.

6. REFERENCE

- [1] S.Tomita, M.Matsumoto, T.Haibara, T.Nakashima, M.Kihara; " Optical Fiber Cable and Connector Technology for FTTH Networks ", IEICE TRANS. COMMUN., VOL. E75-B, No.9, pp.862-870, SEPTEMBER, 1992
- [2] S.Tomita, M.Matsumoto, S.Nagasawa, T.Tanifuji and T.Uenoya; " Preliminary Reserch into High-Count Pre-Connectorized Optical Fiber Cable ", 41st IWCS, pp.5-12, 1992
- [3] S.Nagasawa, F.Ashiya, T.Satake; " Optical Multifiber Connectors ", MICROOPTICS NEWS, VOL.10, No.2, pp.49-55, 26 JUNE 1992
- [4] T.Ohta, Y.Kihara, T.Shigematsu; " High Quality Multiple-Fiber Connector ", FURUKAWA ELECTRIC REVIEW, No.89, pp.9-14, December, 1991
- [5] T.Haibara, S.Tomita, M.Matsumoto and T.Yabuta; " High-Speed, Low-loss Connection Technique for High-Count Pre-Connectorized Cables ", 40th IWCS, pp.296-302, 1991



Jun Yamakawa

The Furukawa Electric Co.,Ltd.

6.Yawata-kaigandori, Ichihara, Chiba, 290, Japan

Jun Yamakawa was born in Hokkaido, Japan, in 1965. He received the B.E. degree in applied electronic engineering from University of Electro Communications, Tokyo, Japan, in 1989. He jointed The Furukawa Electric Company, in 1989. Since then he has been engaged in R&D on optical component. Mr.Yamakawa is a member of The Institute of Electronics, Information and Communication Engineers of Japan.



Hiroyuki Yamada

The Furukawa Electric Co.,Ltd.

6.Yawata-kaigandori, Ichihara, Chiba, 290, Japan

Hiroyuki Yamada was born in Kanagawa, Japan, in 1960. He received the B.E.degree in mechanical engineering from Tokyo Metropolitan University, Tokyo, Japan, in 1983. He jointed The Furukawa Electric Company, in 1983. Since then He has been engaged in R&D on plant and facilities Div.



Takashi Shigematsu

The Furukawa Electric Co.,Ltd.

6.Yawata-kaigandori, Ichihara, Chiba, 290, Japan

Takashi Shigematsu was born in Shizuoka, Japan, in 1963. He received the B.E.degree in precision engineering from Yamagata University, Yamagata, Japan, in 1986. He jointed The Furukawa Electric Company, in 1986. Since then he has been engaged in R&D on plant and facilities Div.



Hiroyuki Yanagase

The Furukawa Electric
Co., Ltd.

8, Yawata-kaigandori,
Ichihara, Chiba, 290,
Japan

Hiroyuki Yanagase was born in Niigata, Japan, in 1968. He received the M.E. degree in electrical engineering from Niigata University, Niigata, Japan, in 1991. He joined The Furukawa Electric Company, in 1991. Since then he has been engaged in R&D on optical component.



Ken Kanai

The Furukawa Electric
Co., Ltd.

8, Yawata-kaigandori,
Ichihara, Chiba, 290,
Japan

Ken Kanai was born in Niigata, Japan, in 1967. He received the M.E. degree in applied chemical engineering from Keio University, Kanagawa, Japan, in 1992. He joined The Furukawa Electric Company, in 1992. Since then he has been engaged in R&D on optical component.

LOW-LOSS MOLDED PLASTIC 16-FIBER SINGLE-MODE CONNECTOR

D. O. Harris, D. L. Dean, Jr., J. R. Merriken, and O. I. Szentesi

SIECOR CORPORATION

489 Siecor Park, Hickory, North Carolina 28603 U.S.A.

ABSTRACT

We have developed a molded plastic 16-fiber single-mode connector for optical ribbons with $180\text{ }\mu\text{m}$ fiber pitch; we have also developed a figure of merit which relates connector ferrule geometry to average insertion loss. Connectors assembled from ferrules with good figures of merit have average insertion loss of 0.19 dB at 1300 nm. Average connector reflectance is -49.0 dB at 1300 nm, while standard deviations of insertion loss change for durability and temperature cycling tests are 0.12 dB and 0.05 dB at 1300 nm, respectively.

INTRODUCTION

Components are currently being developed for the optical subscriber loop in Japan.¹ Realization of this network depends on the development of a 4000-fiber cable which contains 250 16-fiber single-mode ribbons.² In order to allow network reconfiguration and to keep installation time to a minimum, the cable will be pre-connectorized on both ends. We have developed a 16-fiber ribbon connector for this pre-connectorized cable application.

In this paper, we first describe the structure of the 16-fiber connector. Next, we examine connector ferrule geometry, which includes development of a figure of merit that relates ferrule geometry to expected insertion loss. Results of critical geometrical measurements on prototypical ferrules are also presented. Following the discussion of ferrule geometry, we report the results of insertion loss tests on connectors assembled from ferrules with good figures of merit; test results for connector reflectance, durability, and performance during temperature cycling are also reported.

CONNECTOR STRUCTURE

The structure of the 16-fiber ribbon connector is shown in Figure 1; this is an extension of the MT-connector technology^{3,4}. The 16-fiber connector pair consists of two molded plastic ferrules, two guide pins for alignment, and a spring fastener.

The ferrules are rectangular parallelepipeds measuring $6.0\text{ mm} \times 8.0\text{ mm} \times 2.5\text{ mm}$. Each ferrule has 16 fiber holes and two guide pin holes; nominal fiber and guide pin hole diameters are $127\text{ }\mu\text{m}$ and $700\text{ }\mu\text{m}$, respectively. The pitch of the fiber holes must match that of the ribbon, which is $180\text{ }\mu\text{m}$ for the current application. The two guide pin holes lie on the same axis as the fiber holes, equidistant from the nominal center of the fiber hole cluster. Figure 2 summarizes the hole identification scheme and the coordinate axis construction used in determining hole position.

A connector is assembled by fixing the fiber in the holes with epoxy, then polishing the endface to a smooth flat finish that is perpendicular to the fiber axes. Connector pair alignment is achieved by inserting common guide pins into the two guide pin holes; the connection is held in place by the spring

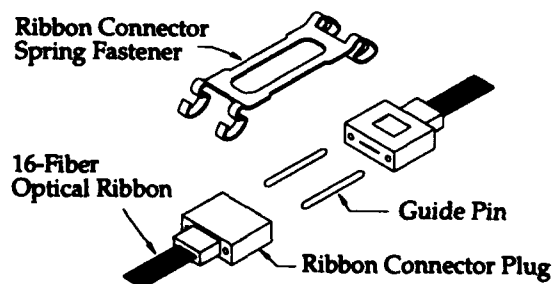


Figure 1. 16-fiber ribbon connector pair.

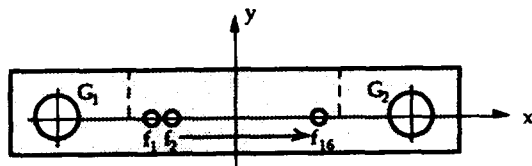


Figure 2. Ribbon connector endface nomenclature.

fastener which applies pressure along the fiber axes. Index matching material is used between the two connectors to reduce reflections.

FERRULE GEOMETRY

Critical elements of ferrule geometry include fiber and guide pin hole diameter, distance between guide pin holes, and fiber hole position.

Since lateral misalignment between fiber pairs can be a dominant cause of insertion loss, guide pin hole diameters must be maintained to approximately one micron of nominal to ensure proper fit between the hole and the pin; if the hole is too large, clearance between the hole wall and pin can introduce excessive variability in the lateral alignment mechanism. Distance between guide pin holes must also be maintained to within a few microns to ensure mateability among the ferrules.

Fiber hole diameter and position both influence lateral fiber alignment. The hole center must typically be located to within a micron of nominal position to enable sufficient fiber pair alignment, and hole diameters must be controlled to within a micron of nominal to maintain reasonably good fiber-to-hole concentricity.

Although all of the geometrical characteristics mentioned above play important roles in lateral fiber alignment, accurate and precise fiber hole position is the most difficult to achieve in practice. The difficulty arises because, in order to meet the hole position requirement, the mold must be machined to submicron tolerances over a distance of several millimeters.

Geometrical Figure of Merit

Insertion loss due to lateral misalignment for a joint between two identical single-mode fibers is given by⁵

$$\text{loss (dB)} = -10 \log_{10} \left\{ \exp \left(\frac{-d^2}{\omega^2} \right) \right\} = 4.343 \frac{d^2}{\omega^2}, \quad (1)$$

where d is lateral offset between the two cores and ω is the mode field radius.

Performance of a ribbon connector is typically quantified by the average insertion loss across all fiber positions for matings to a reference connector. If lateral misalignment is the primary contributor to insertion loss, then the average loss for a given ribbon connector mated to a perfect reference is written as

$$\overline{\text{loss}_R} = \frac{4.343}{\omega^2} \times \frac{1}{16} \sum_{i=1}^{16} x_i^2 + y_i^2, \quad (2)$$

where x_i^2 and y_i^2 are the respective x- and y-axis offsets for the i^{th} fiber core of the connector under test. Equation (2) is identical to equation (1), except the square of lateral offset for a single pair of fiber cores has been replaced with the mean-square offset from nominal position of 16 fiber cores.

Assuming fiber core positions coincide with fiber hole centers, we may let x_i^2 and y_i^2 represent fiber hole offsets. Accordingly, mean-square fiber hole offset can be used as a geometrical figure of merit for selecting ferrules; we write the figure of merit explicitly as

$$M = \frac{1}{16} \sum_{i=1}^{16} x_i^2 + y_i^2. \quad (3)$$

In field applications, average insertion loss is also a common performance indicator; however, connectors are not paired with perfect mates in the field. For normal matings, where f_1 of one connector is paired with f_1 of the other, f_2 with f_2 , etc., the general expression for average loss due to lateral misalignment is

$$\overline{\text{loss}_N} = \frac{4.343}{\omega^2} \times \frac{1}{16} \sum_{i=1}^{16} (x_i^{(1)} - x_i^{(2)})^2 + (y_i^{(1)} - y_i^{(2)})^2, \quad (4a)$$

where the superscripts (1) and (2) refer to the two connectors. Inverse matings, where f_1 is paired with f_{16} , f_2 with f_{15} , etc., are also important in evaluating connector performance, because low inverse losses guarantee good connector symmetry along the x-axis. Average insertion loss for inverse matings is given

by

$$\overline{\text{loss}}_I = \frac{4.343}{\omega^2} \times \frac{1}{16} \sum_{i=1}^{16} (x_i^{(1)} + x_{17-i}^{(2)})^2 + (y_i^{(1)} - y_{17-i}^{(2)})^2 \quad (4b)$$

Note that, for matings against a perfect reference connector, equations (4a) and (4b) are both equivalent to equation (2).

Terms in equations (4a) and (4b) can be expanded to show that, under the assumption fiber core position coincides with fiber hole center, average field loss due to lateral misalignment is represented by

$$\overline{\text{loss}}_N = \frac{4.343}{\omega^2} \times \left\{ M^{(1)} + M^{(2)} + \frac{1}{8} \sum_{i=1}^{16} (y_i^{(1)} y_i^{(2)} - x_i^{(1)} x_i^{(2)}) \right\} \quad (5a)$$

for normal matings and

$$\overline{\text{loss}}_I = \frac{4.343}{\omega^2} \times \left\{ M^{(1)} + M^{(2)} + \frac{1}{8} \sum_{i=1}^{16} (x_i^{(1)} x_{17-i}^{(2)} - y_i^{(1)} y_{17-i}^{(2)}) \right\} \quad (5b)$$

for inverse matings. Equations (5a) and (5b) state that average insertion loss for both normal and inverse matings is proportional to the sum of the figures of merit for the two connectors plus some correction terms.

From equations (5a) and (5b), we find that the average insertion loss of connectors in a population will tend to fluctuate about the line

$$\overline{\text{loss}} = \frac{4.343}{\omega^2} \times \{ M^{(1)} + M^{(2)} \} \quad (6)$$

provided lateral misalignment is dominant, $E\{x_i^2\} \gg E^2\{x_i\}$, and $E\{y_i^2\} \gg E^2\{y_i\}$, where $E\{\cdot\}$ is the expected value operation. This follows the fact that M is dependent on square offset, while the correction terms, although second order, are the products of statistically independent offsets. In effect, the average connector losses are proportional to the sum of the connector figures of merit on average if standard deviations for fiber hole offsets are much greater than the expected absolute offsets for the connector population. In practice, "much greater than" is usually reduced to "on the order of" due the balance

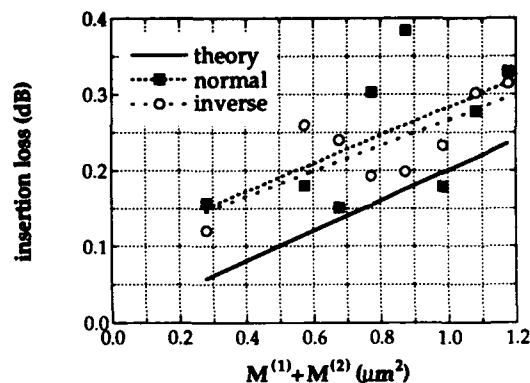


Figure 3. Average insertion loss at 1300 nm versus figure of merit sum.

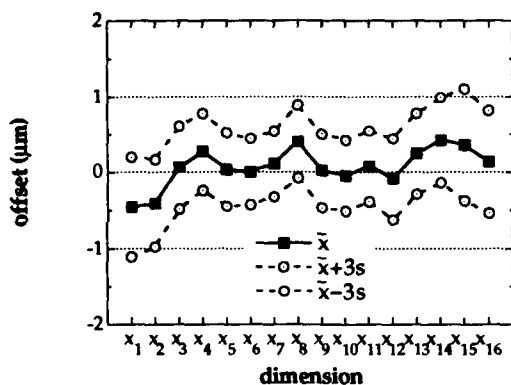
of positive and negative correction terms as well as a typical disparity in M between two mated connectors.

Figure 3 shows results of experimental work comparing figure of merit sums to average connector insertion loss at 1300 nm. In the plot, average insertion loss for normal and inverse matings of eight connector pairs are plotted; each data point represents the average of losses for each of 16 fiber pairs in a connection, which, in turn, are based on averages of three repeated matings. The graph also contains the theoretical insertion loss baseline calculated from equation (6), and least squares fit lines for the actual normal and inverse losses. Both fit lines have approximately the same slope as predicted by theory, demonstrating that insertion loss does, on average, increase linearly according to equation (6). The fit lines, however, are biased by about 0.1 dB with respect to the theoretical line; the observed bias is most likely due to other insertion loss contributors such as angular misalignment and fiber hole-to-core eccentricity.

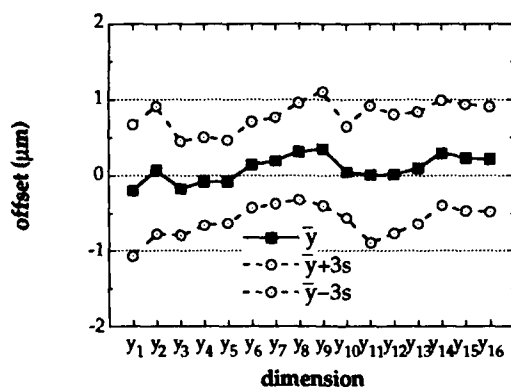
From the fit lines in Figure 3, we estimate that the figure of merit sum for two connectors must be $\leq 0.6 \mu\text{m}^2$ to achieve a target average insertion loss ≤ 0.2 dB. In order to ensure that no pair of field connectors will have figure of merit sums exceeding $0.6 \mu\text{m}^2$, we elect to use only ferrules having $M \leq 0.3 \mu\text{m}^2$.

Fiber Hole Offset

Figures 4 (a) and 4 (b) summarize the respective x- and y-axis offsets versus fiber hole for 306 prototype ferrules with $M \leq 0.3 \mu\text{m}^2$; coordinate axes



(a)



(b)

Figure 4. Fiber hole offset from nominal position along (a) the x-axis and (b) y-axis for 306 ribbon connector ferrules.

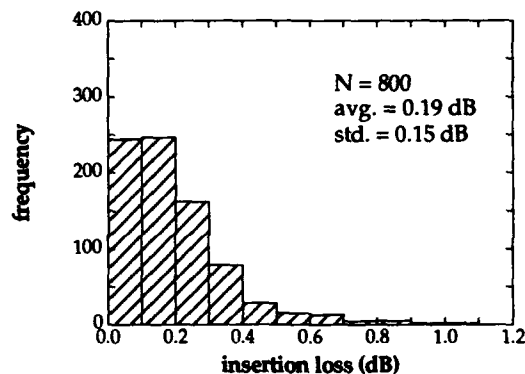
and hole identification conventions follow those of Figure 2. Absolute uniaxial offset averages are less than $0.5 \mu\text{m}$, with "3-sigma" variabilities averaging about $\pm 0.5 \mu\text{m}$ along the x-axis and $\pm 0.7 \mu\text{m}$ along the y-axis.

CONNECTOR PERFORMANCE

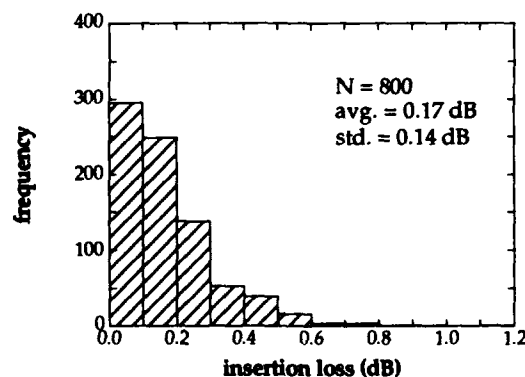
Prototypical connectors assembled from ferrules having $M \leq 0.3 \mu\text{m}^2$ were subjected to various performance tests. These tests include insertion loss and reflectance measurements for matings to a reference connector, and insertion loss change for typical connector pairs in durability and temperature cycling tests. All performance tests were conducted at an optical wavelength of 1300 nm.

Insertion Loss

Given the insertion loss versus geometrical figure of merit data, one would expect low insertion loss from connectors assembled with ferrules having $M \leq 0.3 \mu\text{m}^2$. Figure 5 contains histograms of insertion loss for individual fiber pairs of 50 such connectors mated to a reference connector; here, the reported loss is the average of three matings for each fiber pair. In Figure 5 (a), we see that insertion loss for normal matings averages 0.19 dB, while Figure 5 (b) shows an average loss of 0.17 dB for inverse matings (recall that a normal mating joins f_1 to f_1 , f_2 to f_2 , etc., while an inverse mating joins f_1 to f_{16} , f_2 to f_{15} , etc.). For both normal and inverse matings, the maximum insertion loss is less than 1.2 dB.



(a)



(b)

Figure 5. Insertion loss at 1300 nm for (a) normal and (b) inverse matings.

Reflectance

More and more, reflectance is becoming an important attribute for optical fiber joints, especially for applications like the subscriber loop where video and other high data rate services might be offered. Figure 6 contains a histogram of room temperature reflectance for five 16-fiber connectors mated against the reference connector. Average reflectance is -49.0 dB, with a worst-case less than -46.0 dB. This reflectance will not be maintained over a broad temperature range, however, due to the temperature dependence of the index matching material. Theoretical predictions indicate that the worst-case reflectance over a temperature range of -40°C to 70°C would be about -35 dB, occurring at the temperature extremes.

Durability

Since a primary advantage of connectors is the flexibility to reconfigure optical fiber joints, connector durability over repeated matings is critical. Five connector pairs were selected and tested for durability by mating each pair 100 times and monitoring insertion loss.

Figure 7 contains the histogram of loss change from initial-to-final matings for each of the 80 fiber pairs. Average change was -0.02 dB, with a standard deviation of 0.12 dB; maximum and minimum values were 0.29 dB and -0.30 dB, respectively. Note that about 80% of the insertion loss changes fall within a range of ± 0.15 dB.

A plot detailing insertion loss change for a

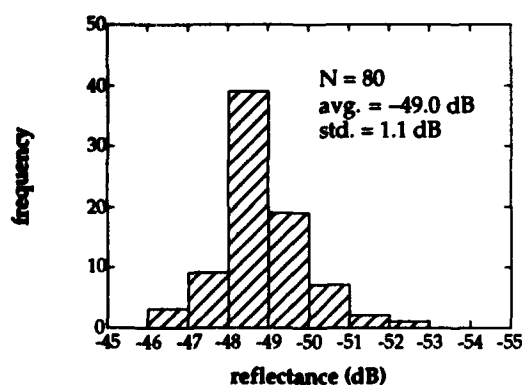


Figure 6. Reflectance at 1300 nm.

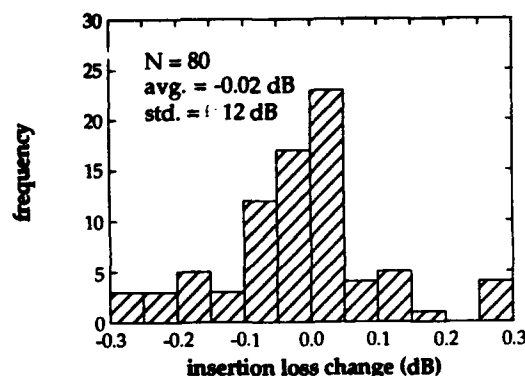


Figure 7. Insertion loss change at 1300 nm after 100 repeated matings.

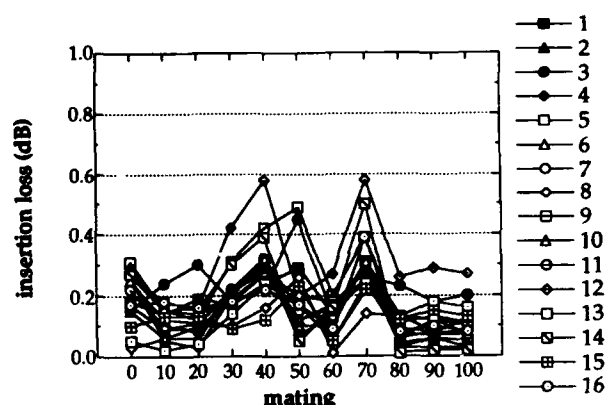


Figure 8. Insertion loss change at 1300 nm for typical connector pair during durability test.

typical connector pair during the durability test is provided in Figure 8. Insertion loss for the initial mating is less than or equal to 0.3 dB for all fiber pairs. For intermediate matings, the insertion losses increase to as high as 0.6 dB in a few instances. The increase in loss is reversible, as is evidenced by losses for the final mating, all of which are again below 0.3 dB. Combining results from Figures 7 and 8 suggests that some of the larger initial-to-final loss changes are due to natural alignment mechanism variability instead of irreversible damage to the connector.

Temperature Cycling

Connectors are often exposed to harsh environments, so good performance over a broad temperature range is important. To test

environmental performance, three prototypical connector pairs were subjected to 10 six-hour temperature cycles, where the temperature ranged from -40°C to $+70^{\circ}\text{C}$. Insertion loss was measured before (initial), during, and after (final) the tests for each of the 48 fiber pairs.

Figure 9 shows the histogram of initial-to-final insertion loss change for the 48 fibers pairs. Average change was $+0.01$ dB with a standard deviation of 0.05 dB; the maximum loss change was 0.14 dB, while the minimum change was only -0.08 dB. Insertion loss change for a typical fiber during the test is shown in Figure 10.

CONCLUSION

We have described a low-loss 16-fiber single-mode ribbon connector and developed a geometrical

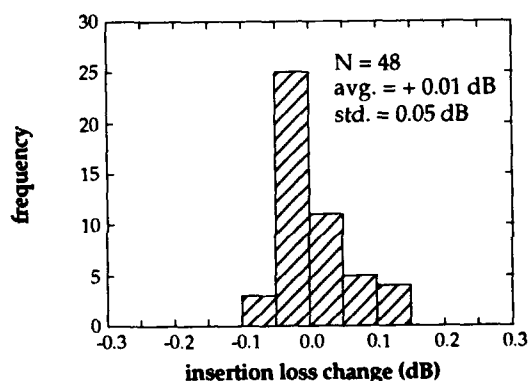


Figure 9. Initial-to-final insertion loss change at 1300 nm for temperature cycle test.

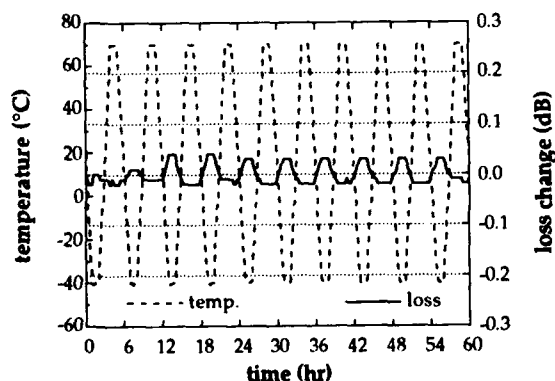


Figure 10. Insertion loss change at 1300 nm for an individual fiber during the temperature cycle test.

figure of merit M which relates connector ferrule geometry to expected insertion loss. Connectors assembled with ferrules having $M \leq 0.3 \mu\text{m}^2$ produced insertion loss averaging 0.19 dB for normal matings and 0.17 dB for inverse matings; average connector reflectance was -49.0 dB. We also observed an average insertion loss change after 100 repeated matings of -0.02 dB with a standard deviation of 0.12 dB, and an average insertion loss change due to temperature cycling of $+0.01$ dB with a standard deviation of 0.05 dB.

Overall, performance of the 16-fiber ribbon connector is excellent. Test results compare favorably with many other single and multiple fiber connector technologies, indicating that this particular connector is suitable for a broad range of fiber-optic communication applications.

ACKNOWLEDGEMENTS

The authors gratefully acknowledge the technical assistance of R. B. Huffman, A. J. Malanowski, and S. L. Stallings of Siecor Corporation. Numerous discussions with S. Nagasawa of NTT are also acknowledged.

REFERENCES

1. N. Kashima, N. Tomita, and M. Matsumoto, "Operating fiber cable in subscriber networks," *IEEE LTS*, vol. 3, no. 4, pp. 20-25, 1992.
2. S. Tomita, M. Matsumoto, S. Nagasawa, T. Tanifuji, and T. Uenoya, "Preliminary research into high-count pre-connectorized optical fiber cable," *IWCS Proc.*, pp. 5-12, 1992.
3. T. Satake, S. Nagasawa, and R. Arioka, "A new type of demountable plastic-molded single-mode multifiber connector," *J. Lightwave Technol.*, vol. 4, pp. 1232-1236, 1986.
4. M. Kawase, T. Fuchigami, M. Matsumoto, S. Nagasawa, S. Tomita, and S. Takashima, "Subscriber single-mode optical fiber ribbon cable technologies suitable for midspan access," *J. Lightwave Technol.*, vol. 7, no. 11, pp. 1675-1681, 1989.
5. D. Marcuse, "Loss analysis of single-mode fiber splices," *Bell Syst. Tech. J.*, vol. 56, pp. 703-718, 1977.



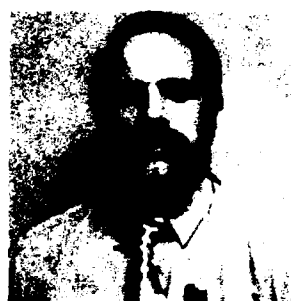
Dan Owen Harris received the B. E. E. degree from the Georgia Institute of Technology in 1981, and the M. S. and Ph. D. degrees in electrical engineering from North Carolina State University in 1987 and 1990, respectively.

He has previously held positions on the engineering staffs of the Georgia Tech Engineering Experiment Station and Siecor Corporation, and has served on the faculty of The University of Alabama in Huntsville. Dr. Harris returned to Siecor in 1991, where he is currently a Staff Engineer in the Hardware and Equipment Technology division, working with fiber-optic jointing technologies. He is also part-time instructor at Lenoir-Rhyne College, and a member of IEEE, OSA, and SPIE.



David L. Dean, Jr. received his B. S. degree in 1983 from North Carolina State University. After receiving his M. S. degree in mechanical engineering from the Massachusetts Institute of Technology in 1985,

he joined Siecor Corporation in Hickory, NC. He is currently employed as a Senior Engineer in the Hardware and Equipment Technology division, working on Siecor's multifiber connector development team. He is author of several technical papers and patents in the area of fiber-optic mechanical splice development. He is also a registered Professional Engineer in the state of North Carolina, and was chosen Siecor's Inventor of the Year in 1990 and Co-Inventor of the Year in 1991.



James R. Merriken graduated from the United States Military Academy at West Point, NY, where he earned a B. S. degree in 1979. He served both stateside and in Europe as an Army Communications Officer. Mr. Merriken

has been employed with Siecor Corporation since 1985, where he was first a Project Engineer and later promoted to Project Supervisor in the Engineering Services Department. In 1987, he was named Project Manager for Siecor's introduction of the multifiber silicon array splice. Once completed, he transferred into Hardware and Equipment Technology where he is presently a Senior Product Development Engineer.



Otto I. Szentesi received a B. S. E. E. from the University of Alberta, Canada in 1966, and a Ph. D. degree from the University of London, England in 1970.

Since 1978, he has been with Siecor Corporation, Hickory, North Carolina, where he was responsible for fiber-optic cable installations, training, project management, and the development and manufacturing of splicing equipment, interconnect hardware, and field test sets. Currently, he is Vice President and Director, Hardware and Equipment Technology responsible for network interface devices, fiber-optic hardware, connectors, splices, splice equipment, and connectorized cables.

Before joining Siecor, Dr. Szentesi was associated with Bell-Northern Research, Ottawa, Ontario, Canada, where his work included acousto-/electro-optics, high power light emitting diode and laser characterization and processing, fiber-optic system design and optimization, and interactive audio/visual/graphic terminal development. He is a registered professional engineer, a senior member of IEEE, and a member of OSA and SPIE.

HIGH FIBER COUNT OPTICAL CONNECTORS

Y. KIKUCHI, Y. NOMURA, H. HIRAO and H. YOKOSUKA

OPTO-ELECTRONICS LABORATORY, FUJIKURA LTD.

1440, MUTSUZAKI, SAKURA-SHI, CHIBA, 285, JAPAN

Abstract

High-fiber-count optical connectors have become important components in subscriber cable networks for FTTH, because they can reduce the connection time for high-count fiber cables.

In this paper, we describe the development of 16-fiber connector with the mean connection loss of less than 0.2 dB using a high precision plastic molding technique. Next, we describe a push-on/pull-off 80-fiber connector composed of five 16-fiber connectors.

1. Introduction

The use of optical fiber cables has quickly broadened into subscriber network. High-fiber-count cables using multi fiber ribbons, mechanically transferable (MT) connectors[1] and techniques for their connection are being used in subscriber networks, in order to shorten the construction period.[2][3] Recently, a 4000-fiber pre-connectorized cable has been studied to construct future FTTH (Fiber To The Home) network.[4] Therefore, a high-count fiber connector with a low connection loss becomes to the key component for the system. In single mode fiber connection, it is necessary for fibers to align within 1 μm to achieve low losses. Thus it is of great important to have a highly accurate production technique for the fabrication of components.

In this paper, we present a 16-fiber connector with low connection loss using a high precision plastic molding technique. Then we present a push-on/pull-off 80-fiber connector composed of five 16-fiber connector.

2. Design criteria

For connectors used to pre-connectorized cables in subscriber network, the following requirements should be taken into account.

- 1) High fiber count and compact design.
- 2) Rapid joining capability.
- 3) Mid span access capability.
- 4) Low insertion loss.
- 5) Low cost

As the reply to above requirements, MT connectors for 4- or 8-fiber ribbon have been already developed and in commercial use. Typical insertion loss of the connector is 0.35 dB on an average. The ferrule of MT connector is produced by using precision plastic molding technique. Thus higher accuracy and lower costs are expected by the progress in the manufacturing technology.

In designing the 16-fiber connector with low connection loss, the following should be insured against increasing fibers.

- 1) Ferrule size should be same as that of MT connector, considering the size of pre-connectorized cable ends.
- 2) Allowable tolerance between fiber and ferrule hole should be insured to facilitate connector assembly
- 3) Reliability should be insured for practically use period.

We have refined existing MT connector manufacturing technology : high-precision plastic ferrule molding technique based on ultra-precision machining and highly accurate measurements for die components. Then we have developed 16-fiber and 80-fiber unit connectors with low connection loss.

3. 16-fiber connector

3.1 Connector Structure

The structure of a 16-fiber connector is shown in Fig. 1. The basic structure of this connector is similar to that of a conventional MT connector. A pair of plugs are aligned by two guide pins and are held by the clamp spring.

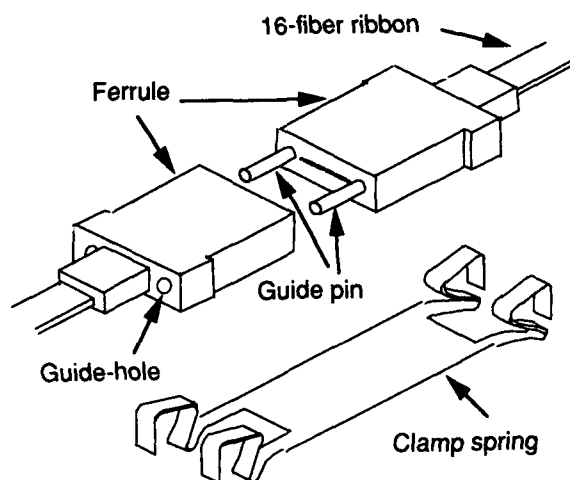


Fig.1 16-fiber connector

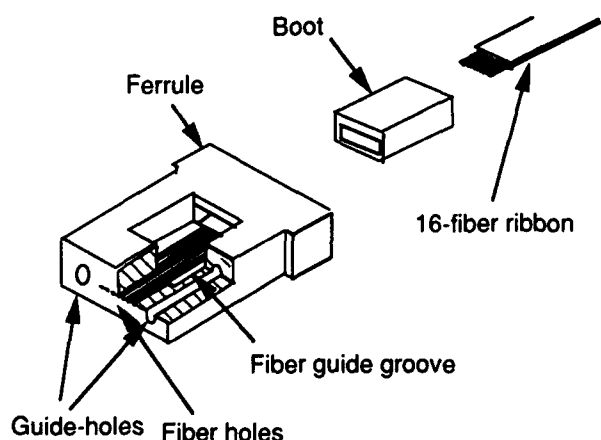


Fig.2 16-fiber connector plug structure

Fig. 2 shows the structure of the 16-fiber connector plug. It is composed of two components: a plastic ferrule designed to position the optical fibers accurately, and a rubber boot designed to relax the bending force applied to the fibers.

To keep compact design as that of MT connector, the fiber hole pitch is made as small as 200 μm or less so as to match the fibers. And the shape of the plug is designed to meet the requirements for a stack type 80-fiber connector.

The fiber assemble process of 16-fiber connector is also similar to that for conventional MT connectors; 125 μm fibers stripped of their coatings are inserted into the fiber holes and fixed with epoxy adhesive. Finally the endface of the ferrules is polished to mirror finish.

3.2 Low-loss connection

One of the most important requirement for optical fiber connectors is low-loss connection. The splicing loss components are transverse offset, angular tilt and end separation.[5] Generally, transverse offset is the most serious factor. However, achieving lower loss of less than 0.2 dB, angular misalignment should be taken into account. The offset causes the loss as[1].

$$L = -10 \log \{ \exp -(d/\omega)^2 \} \quad (1)$$

where L = connection loss (dB)
 d = transverse offset
 ω = mold field radius

For standard single-mode fibers, a transverse offset of 1 or 2 μm causes a connection loss of 0.19 dB or 0.77 dB

In the case of MT connectors, it is known that other deviations than the position deviation of fiber hole center in the ferrule occur at random independently in a limited area and that a centering effect η is to be produced. The mean transverse offset is expressed as[1]

$$d = d_F + \eta (d_o^2 + d_c^2 + d_d^2)^{1/2} \quad (2)$$

where d_F = position deviation of fiber hole center
 d_o = deviation by clearance between fiber and fiber hole
 d_c = core eccentricity in fibers
 d_d = deviation by clearance between guide pin and guide hole.

Namely, to realize low-loss connection using MT connectors, it is most important to minimize the position deviation of fiber hole center. Secondly, it is important to decrease the

deviation by clearance between fiber and fiber hole and that by clearance between guide pin and pin hole.

In order to realize a 16-fiber connector with a mean connection loss of less than 0.2 dB, it is necessary to decrease the position deviation of fiber hole center to less than 1 μm , taking into account the existing tolerance for fiber parameters, and so on. In addition, it is important that the tolerance for the outside diameter of the guide pins be less than 1 μm .

The precision molding technique for ferrules, which is the most important factor in reducing the connection loss of the 16-fiber connector, will be described in the next section.

3.3 Precision molding

The 16-fiber connector is fabricated by transfer molding as shown in Fig. 3. The fiber holes and guide pin holes, whose dimensions are most important in the ferrule, are formed with core pins placed in the V-grooves formed ahead of them as shown in Fig. 4. Therefore, enhancing the machining accuracy of V-grooves is the prerequisite to the fabrication and yield improvement of precision ferrules because the accuracy of the V-groove mold directly affects the dimensional accuracy of the ferrule.

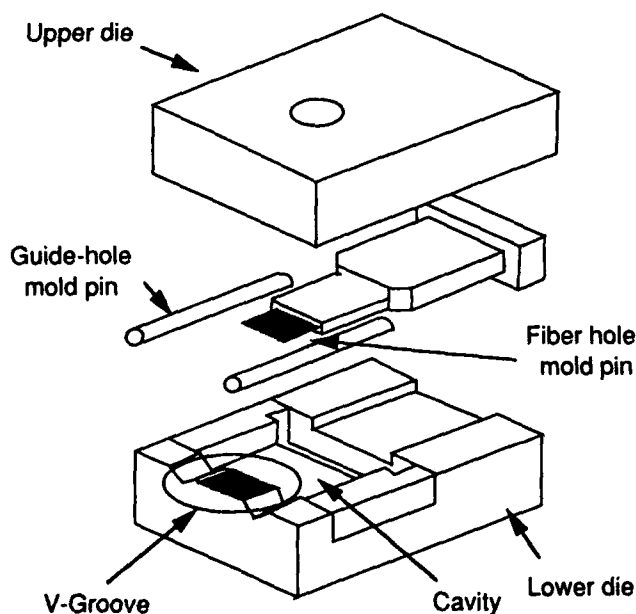
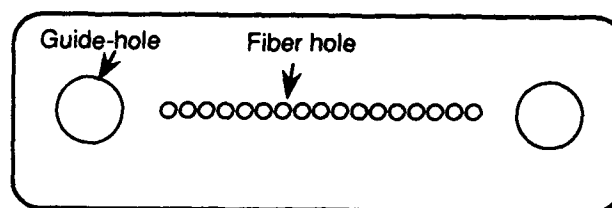
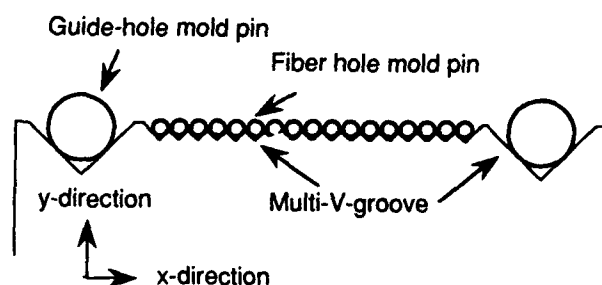


Fig.3. Structure of precision mold



(a) Endface of 16-fiber connector ferrule



(b) Structure of multi-V-grooved mold

Fig.4 Principle of precision mold

To suppress the position deviation of fiber hole center in the ferrule to a mean value of about 0.5 μm , it is necessary that the dimensional accuracy of the V-grooves be higher than that value. To realize this, we optimized the V-groove grinding conditions by use of a high-precision grinding machine and established a precision measuring technique for measuring the shape of V-groove with an accuracy within 0.1 μm . The deviations of molding pin centers from the design value when the fiber hole and guide hole molding pins are placed in the V-grooves are reduced within 0.2 μm .

Fig. 5 shows the measuring set-up for tilt angle of fiber holes. a pair of ferrules inserted the fiber ribbons are set on the stage, then transverse offsets between a pair of fiber ends facing each other are measured. Using this method, we reduce a tilt angle within 0.1° on an average. Outer diameters of the molding pins are evaluated by a contact micrometry technique with a repetitive accuracy of $\pm 0.1 \mu\text{m}$.

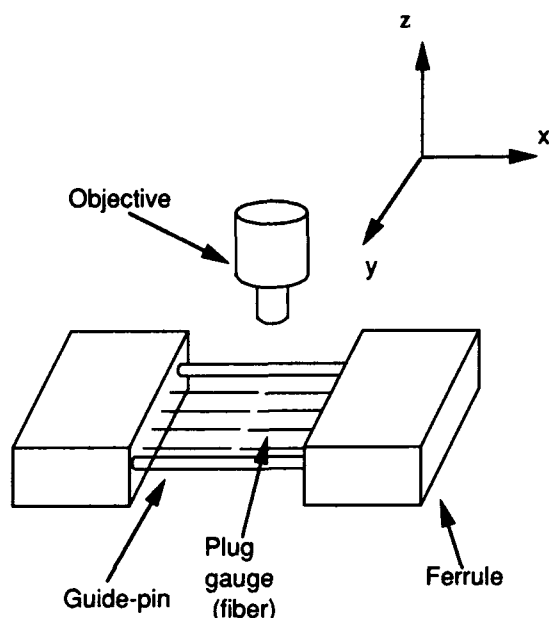


Fig.5 Measuring set-up for tilt angle of fiber hole in MT ferrule

For the molding of MT connectors, it is necessary to use a molding resin having a low shrinkage, dimensional stability under varying environments, high mechanical strength for repetitive connection, and high fluidity enabling low-pressure molding. We succeeded in enhancing the dimensional accuracy of the 16-fiber connector ferrule by using the silica filled thermosetting epoxy resin.

Fig.6 shows the histogram of the eccentricity error of fiber holes in 16-fiber ferrules. The position deviation of fiber hole center in the connectors is about $0.4 \mu\text{m}$ on the average.

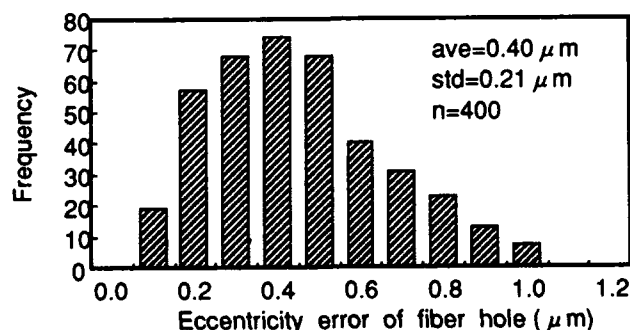


Fig.6 Histogram of eccentricity error of fiber hole

3.4 Characteristics of 16-fiber Connector

A 16-fiber connector was assembled, using a 16-fiber ribbon in which the core eccentricity in a fiber is less than $0.3 \mu\text{m}$ and the clearance between fiber and fiber hole in the ferrule less than $1 \mu\text{m}$. The connection losses of the 16-fiber connector, measured with a master plug, are given in Fig.7. Measurements were taken at a wavelength of $1.3 \mu\text{m}$, with refractive index matching oil. The mean connection loss was 0.19 dB with a standard deviation of 0.13 dB . These are almost half as the value for conventional MT connectors.

Table 1 shows the results of the reliability tests including repeatability test, temperature cycling test, high/low temperature tests. The connector characteristics obtained in all test items were equivalent to those of conventional MT connectors.

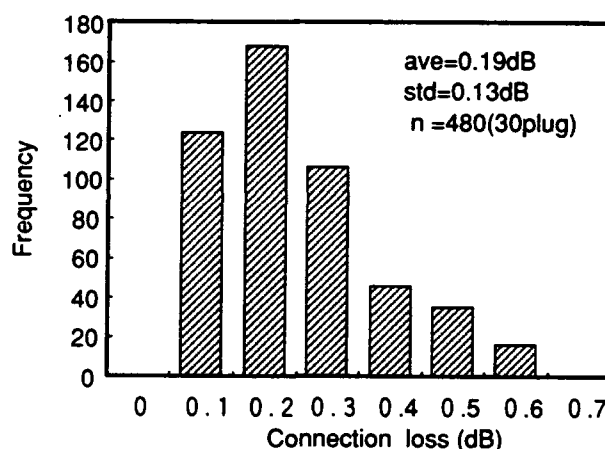


Fig.7 Histogram of connection loss of 16-fiber connector

Table 1 Reliability test results of 16-fiber connector

Testing Item	Condition	Results
Temperature cycling	From -40 to 60°C 4 cycles/day	$<0.2 \text{ dB}$
High temperature	80°C , 100H	$<0.1 \text{ dB}$
Low temperature	-40°C , 100H	$<0.1 \text{ dB}$
Repeatability	100 times	$<0.2 \text{ dB}$

4. 80-fiber unit connector

4.1 Structure

Fig.8 and Fig.9 show the structure of a stack type 80-fiber connector. This connector is designed to be able to be attached and detached by the push-on and pull-off operation, respectively, by means of a housing in which 16-fiber connectors are stacked on one another so that they can be connected as a single block. In addition, to ensure low-loss connection, we elaborated a structural design such that the characteristics of the individual connectors can be exhibited as they are. Specifically, each connector is pressed from behind at a constant pressure by means of a spring and aligned by the guide pins attached to each ferrule.

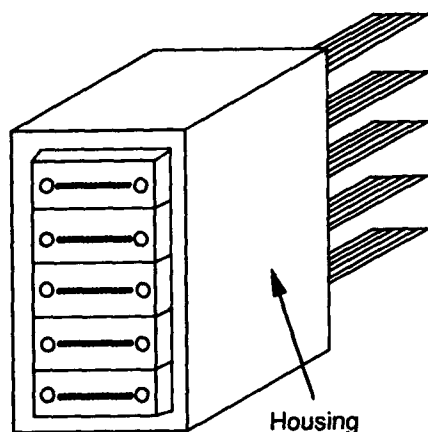


Fig.8 80-fiber unit connector
(16-fiber connector X 5)

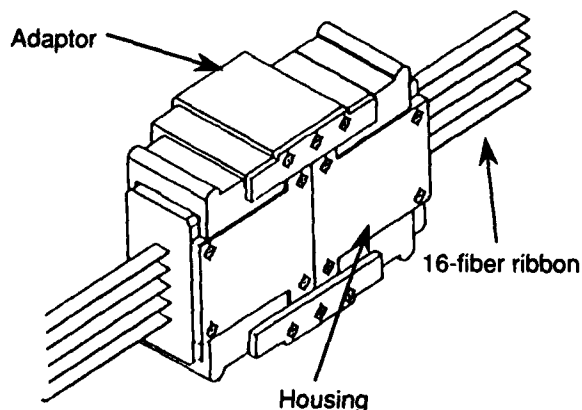


Fig.9 Structure of Housing

4.2 Characteristics

The connection loss histogram of the stack type 80-fiber connector is shown in Fig. 10. The mean connection loss is 0.23 dB and the excess loss by single-block connection less than 0.1 dB. The results from the evaluation of the optical characteristics are summarized in Table 2.

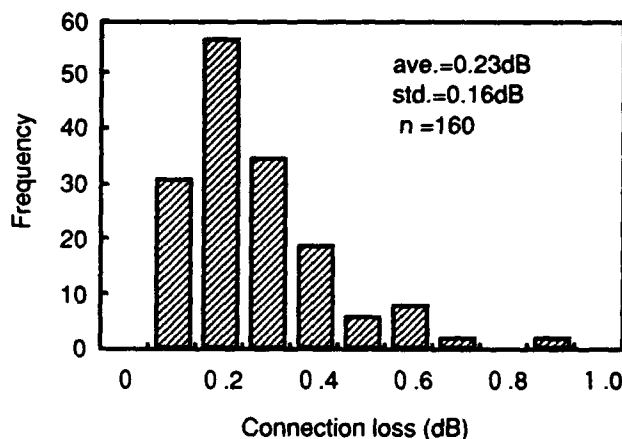


Fig.10 Connection loss of 80-fiber connector

Table 2 Optical properties of developed
80-fiber connector

Item	Result
Connection loss	0.23dB : average
Return loss	>50dB : with index matching gel
Repeatability	<0.2dB : 100 times

5. Conclusion

A high-count fiber connector for 16-fiber ribbons with a fiber pitch less than 200 μm has been developed. The mean connection loss was less than 0.2 dB, so the performance of this new connector is equivalent to that of conventional MT connectors.

Moreover, a push-on, pull-off type 80-fiber connector in which five 16-fiber connectors are stacked on one another has been developed. The connector has the capability of connecting high count fibers in a single motion with a increase in the connection loss of 0.1 dB compared to 16-fiber connector. Therefore, it has become possible to make connections at lower losses and drastically reduce the connection time.

References

- [1] T.Satake, S.Nagasawa and R.Arioka, "A New Type of Demountable Plastic-molded Single-mode Multifiber Connector", J. of Lightwave Technology, Vol.L4, No.8. August, 1986.
- [2] T.Haibara, S.Tomita, M.matsumoto and T.Yabuta, "High-speed low-loss connection techniques for high count pre-connectorized cables", 40th IWCS 1991.
- [3] H.Yokosuka, S.Togo, H.Hirao and H.Hosoya, "Preconnectorized 1000-Fiber cable", 38th IWCS 1989.
- [4] S.Tomita, M.Matsumoto and S.Nagasawa, "Preliminary research into High-Count Pre-Connectorized Optical Fiber Cable", 41th IWCS 1992.
- [5] D.Marcuse, "Loss analysis of single-mode fiber splices", Bell Syst. Tech.J., Vol.56, No.5, 1977.



Yoshio KIKUCHI

Fujikura Ltd.

1440 Mutsuzaki
Sakura, Chiba, 285,
Japan

Yoshio Kikuchi was born in 1955. He joined Fujikura Ltd. after his graduation from Tohoku University with a M.E. degree in 1980. He has been involved in research and development of optical fibers, cables and accessories. He is now an assistant manager in Fiber and Cable Accessory Section within Opto-Electronics Laboratory and a member of the IEICE of Japan.



Yoshikazu NOMURA

Fujikura Ltd.

1440 Mutsuzaki
Sakura, Chiba, 285,
Japan

Nomura was born in 1951. He graduated in mechanical engineering from Shinsyu University. He has been engaged in the research and development of telecommunication cables and accessories. He is presently a manager in the Fiber and Cable Accessory Department within Opto- Electronics Laboratory.



Hideo HIRAO

Fujikura Ltd.

1440, Mutsuzaki
Sakura, Chiba, 285,
Japan.

Hideo Hirao was born in 1951. He received the B.E. degree in agricultural mechanical engineering from Mie University in 1974. He has been engaged in the research and development of telecommunication cables and accessories. He is presently a manager in the Equipment & Component Research & Development Section within telecommunication equipment & Component Division.



Hiroshi YOKOSUKA

Fujikura Ltd.

1440, Mutsuzaki
Sakura, Chiba, 285,
Japan

Hiroshi Yokosuka graduated in mechanical engineering from Tokyo Metropolitan Technical Junior College in 1967. He has been engaged in development of telecommunication cables and accessories. He is now a manager of the Fiber and Cable Accessory Department within Opto-Electronics Laboratory and a member of IEICE of Japan.

DEVELOPMENT OF 16-FIBER CONNECTORS FOR HIGH-SPEED LOW-LOSS CABLE CONNECTION

Tomohiko Ueda, Hidetoshi Ishida, Ichiro Tsuchiya
Toshiaki Kakii and Toru Yamanishi

Sumitomo Electric Industries, Ltd.

Abstract

As a primary step of the development of high-count low-loss optical fiber connector, two types of 16-fiber connectors were successfully manufactured.

One is made of thermoset epoxy resin containing silica filler and the other is composed of V grooved silicon chip covered with thermoset epoxy resin.

Low connector loss of less than 0.2dB has been achieved in both type of the connectors.

We manufactured the proto-type model of the stacked 80-fiber connectors utilizing the developed 16-fiber connectors.

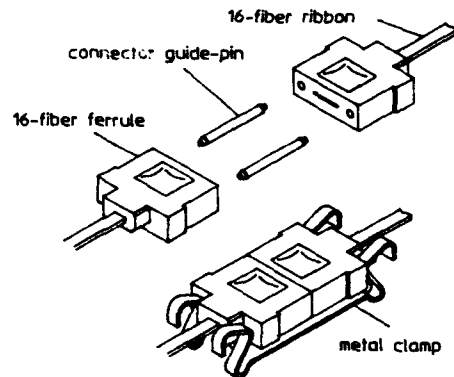


Fig.1 Structure of 16-Fiber Connector

1. Introduction

For construction of optical subscriber cable network, high-speed cable connection techniques for high-count high-density preconnectorized cables is required. It is reported that 100 minutes connection time for 4000 fibers is possible with utilizing 80-fiber connectors, based on the assumption of 2 minutes connection time for each connector [1]. In order to realize a low loss 80-fiber connector, two connector types were considered. One is one body connector with a 80-fiber ferrule and the other is stacked type connector with five 16-fiber connectors. As a primary step for the 80-fiber connector, the development of a 16-fiber connector was conducted.

In this paper, the design concept and the manufacturing process of the low-loss 16-fiber connector and the properties of the proto-type model of stacked 80-fiber connector are discussed.

2. Development of 16-fiber Connector

2.1 Design of 16-Fiber Connector

The design concept of conventional MT connector, 4- or 8-fiber connector, was applied to the 16-fiber connector [2]. As shown in Fig.1, the developed 16-fiber connector consists of a pair of ferrules, two guidepins and a metal clamp. Each ferrule has 16 fiber positioning holes between two pin guiding holes.

The causes of loss generation for fiber connection are classified into three main factors, such as fiber core offset, tilt of fiber axis, and fiber endface separation (Fig.2). For example, the fiber core offset which generates 0.2dB connection loss is $1.0 \mu\text{m}$ theoretically, and 0.8 degree of fiber tilt and $32 \mu\text{m}$ of fiber endface separation are correspond to 0.2dB connection loss individually. As far as MT type connector concerned, it is easy to control the tilt of fiber axis within 0.3° , and there is little fiber endface separation because endfaces of ferrules are pressed against each other. Therefore fiber core offset is dominant factor of connector loss generation.

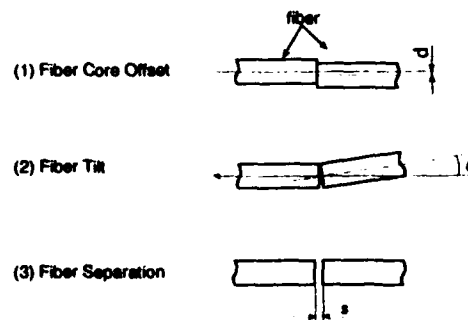


Fig.2 Three Main Causes of Connector loss

Fig.3 shows the definition of the fiber offset for MT type connector. The core eccentricity error, R is defined as the distance between the ideal position and the actual fiber core position in ferrule. As shown in Fig.3, total core eccentricity error is considered as the sum of three offset factors, R_1 , R_2 and R_3 . The distance between the designed position and the actual position for the fiber positioning hole is defined as the ferrule eccentricity error, R_1 . R_2 is the clearance between the fiber and the fiber positioning hole, and R_3 is the difference between the center of the fiber and that of the fiber core. Under the assumption that these all three factors have a normal distribution, we can calculate the core eccentricity error distribution statistically. Using the measured standard deviation of R_2 and R_3 , we calculated the required distribution of R_1 which correspond to average connector loss of 0.2dB. As shown in Fig.4, the required average ferrule eccentricity error to achieve 0.2dB connector loss proved to be within $0.7 \mu m$.

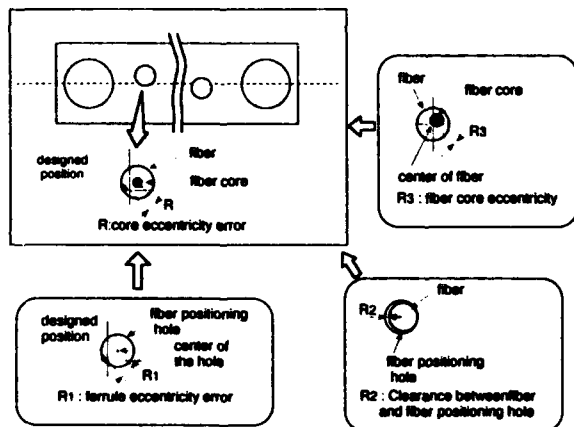


Fig.3 Definition of Eccentricity Error

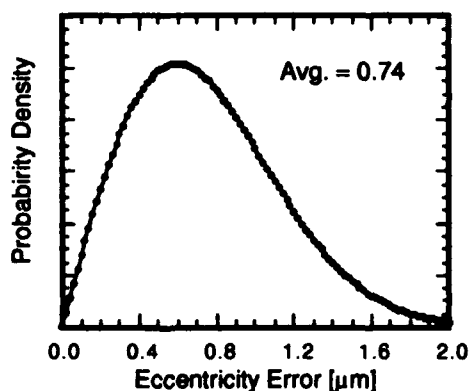
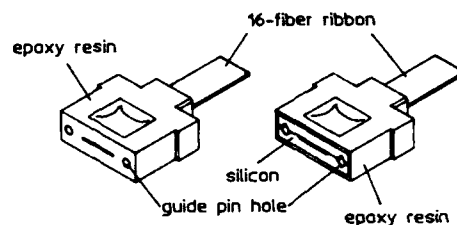


Fig.4 Distribution of ferrule eccentricity error for 0.2dB

In order to achieve this required precision of the 16-fiber connector, we tried to manufacture two different types of connector structure. One is made of thermoset epoxy resin by transfer molding technology (AP-connector, Fig.5(a)), and the other is composed of V-grooved silicon chip covered with thermoset epoxy resin (SiV-connector, Fig.5(b)).



(a) AP-Connector (b) SiV-connector

Fig.5 Two Types of 16-Fiber Connectors

2.2 AP-connector

As the material for the 16-fiber connector, enough mechanical strength for connecting and reconnecting repeatedly is required. Moreover, the dimensional stability of the connector material is essential to guarantee the long time reliability of the connector performances. The thermoset epoxy resin containing silica filler was selected as the candidate of the ferrule material because of its small thermal expansion co-efficiency, enough mechanical strength and good dimensional stability.

As shown in Fig.6, the manufacture process of transfer molding system is very simple. The thermoset epoxy resin is supplied into the metal mold, and cured in several minutes at about $200^\circ C$.

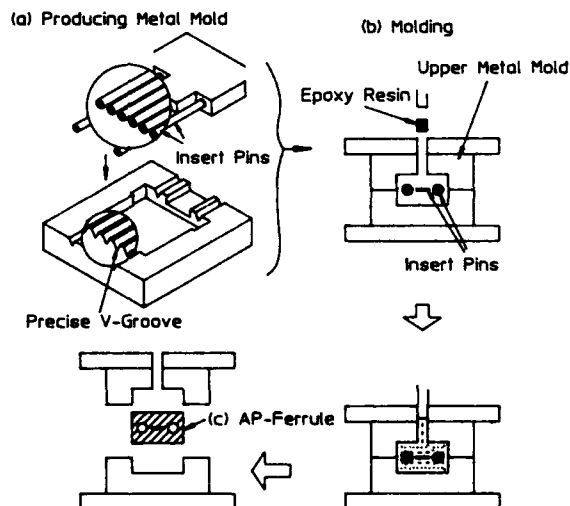


Fig.6 Manufacturing Process of AP-Connector

In order to achieve the $0.7 \mu m$ of the average ferrule eccentricity error for AP-connector, the precision of the V-groove in the metal mold must be within $0.5 \mu m$ in consideration of the dimensional change in molding process, such as shrinkage of material due to the curing. By optimizing the grinding condition, such as temperature control and selection of grinding wheel, we could reduce the average V-grooves' precision to $0.4 \mu m$. Fig.7 shows the typical distribution of the V-grooves offset.

Fig.8 shows the ferrule eccentricity error distribution of AP-connector ferrules molded with this metal mold. The average ferrule eccentricity error of within $0.7 \mu m$ connector ferrule was attained.

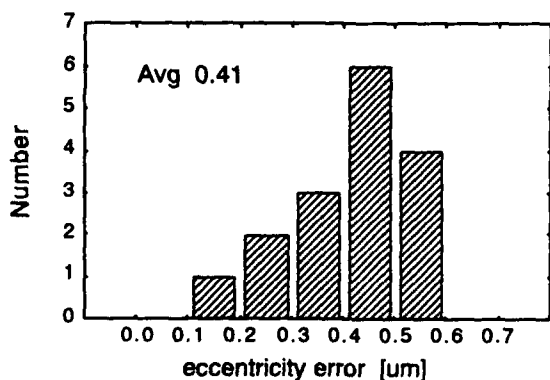


Fig.7 V-grooves offset Distribution for Metal mold

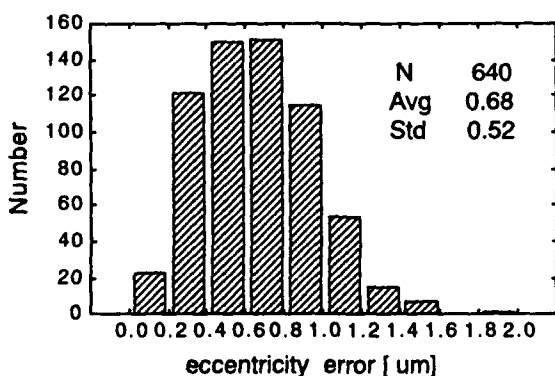


Fig.8 Distribution of AP-Ferrule Eccentricity error

2.3 SiV-connector

Silicon is the material which is comparatively easy to be grinded precisely. We had achieved the precision of within $0.5 \mu m$ in the direction of both pitch and depth at silicon V-grooved connector with utilizing diamond grinding wheel [4]. For the purpose of protecting a brittle silicon V-grooved chip, we came to an idea to cover the silicon with epoxy resin. In order to realize this structure, transfer molding

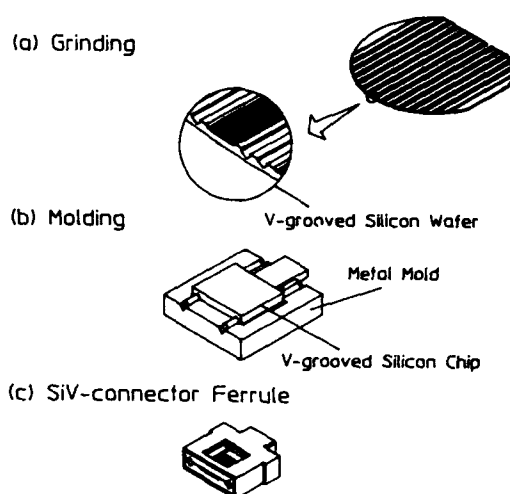


Fig.9 Manufacturing Process of SiV-Connector

technology was also applied. Fig.9 shows the manufacturing process of SiV-connector ferrules. The precisely V-grooved silicon chip (Fig.9a) is inserted into metal mold (Fig.9b), thermoset epoxy resin is supplied around the silicon chip and hardened by curing process. SiV-connector has an advantage that it is not necessary to consider the dimensional change compared with AP-connector. Fig.10 shows the typical eccentricity error distribution of SiV-connector ferrules.

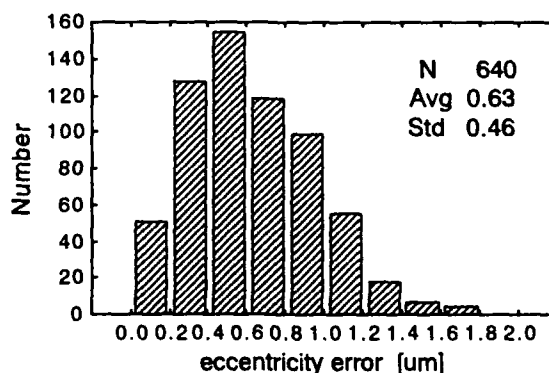


Fig.10 Distribution of SiV-Ferrules' eccentricity error

2.4 Connector Loss of 16-Fiber Connector

We manufactured two types of 16-fiber connectors, AP- and SiV-connector. Fig.11 and Fig.12 show the typical distribution of the connector loss against the master connector for AP-connector and SiV-connector respectively. As a result, an average connector loss of less than 0.2dB was attained for both types of connectors, 0.186dB for AP-connector and 0.175dB for SiV-connector.

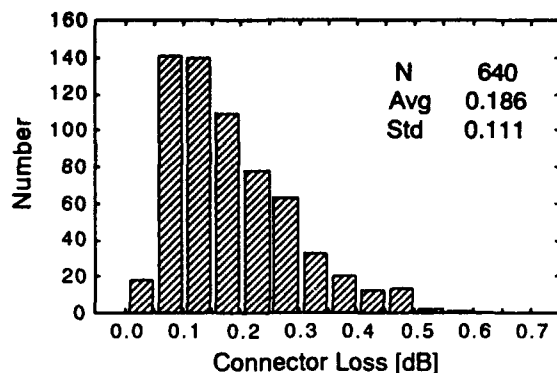


Fig.11 AP-connector loss distribution

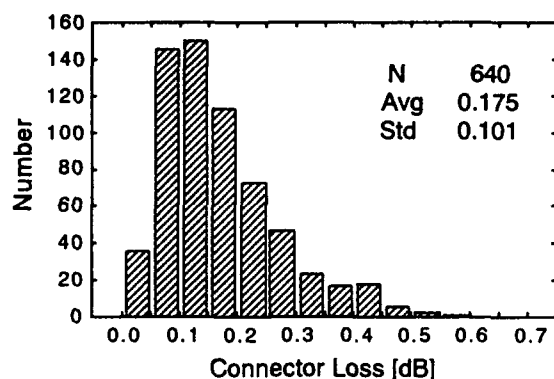


Fig.12 SiV-connector loss distribution

2.5 Measurement of Core Eccentricity Error

As the means of the evaluation of the performance for the 16-fiber connector, we introduced a new measurement method. It is very useful to know the actual fiber position in the connector ferrule so as to understand the relation between the core eccentricity error and connector loss. In the new measurement system, which block diagram is shown in Fig.13, the fiber core is recognized to detect radiated light from connector endface. The measured connector is fixed on the X- and Y-stages, of which positions are measured with the laser interferometer. The radiated light from the core is conducted by fiber itself from the opposite side of the measured connector, and observed by CCD camera through the microscope fixed on the Z-stage. This stage is used for focusing the microscope on the core surface automatically. The fiber core position in the ferrule is calculated by the computer based on the positions of the X- and Y-stages. As the evaluation of this measurement machine, we measured samples of 16-fiber connectors ten times

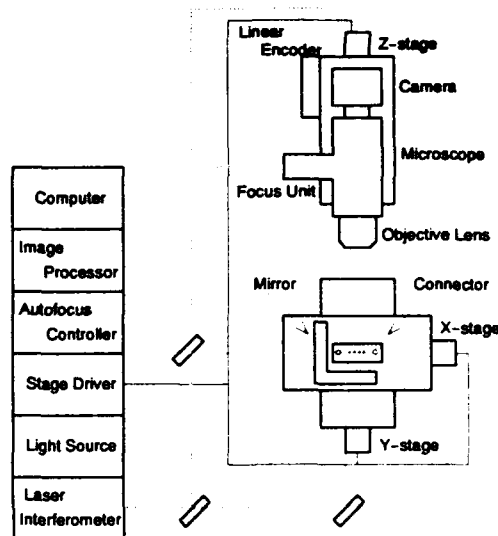


Fig.13 System block diagram of fiber core position measurement system

for each, and the repeatability (standard deviation) of $0.04 \mu m$ was obtained.

With the new core eccentricity error measurement equipment, it is possible to calculate precisely how the core eccentricity error of the ferrule affects to connector loss. Fig.14 shows the relation between the actually measured connector loss and the estimated loss calculated from the measured core eccentricity error, based on the assumption that connector loss is caused by fiber core offset only. The result has so far good correlation in the high connector loss area, but poor correlation in the area where the core eccentricity error is small. The result indicate

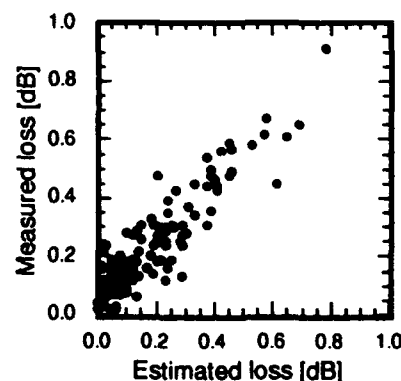


Fig.14 Relation between estimated loss from fiber core eccentricity error and measured loss

that other factors besides fiber core offset are still significant in the low connector loss area. The factors are now under investigation to reduce the connector loss further more.

3. Application to the stacked connector

A trial product of stacked 80-fiber connector using the developed 16-fiber connectors is manufactured (Fig.15). We designed the stacked 80-fiber connector, considering mainly two items, one is housing structure which enable to engage five pairs of 16-fiber connectors by one action, and the other is floating mechanism of the housing so as to be free from any outside force after finishing the connecting action. As the first step of connecting operation, five 16-fiber connectors are packed into the housing which have four pin guiding hole. Then a pair of the housings is combined by four housing guide pins. The combining of the housings makes smooth and automatic engagement of five pairs of 16-fiber connectors. The size of the proto-type model is 13(W) × 20(H) × 30(L) mm³, and cross-section area is only 3.3mm²/fiber.

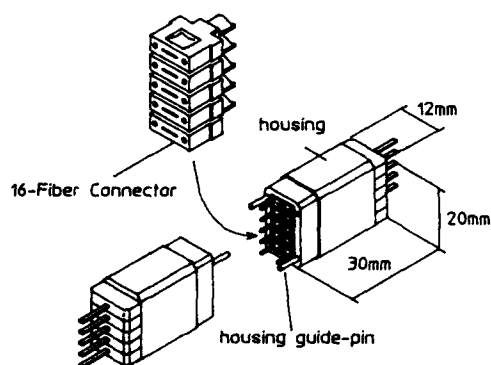


Fig.15 The Stacked Type 16-Fiber Connector

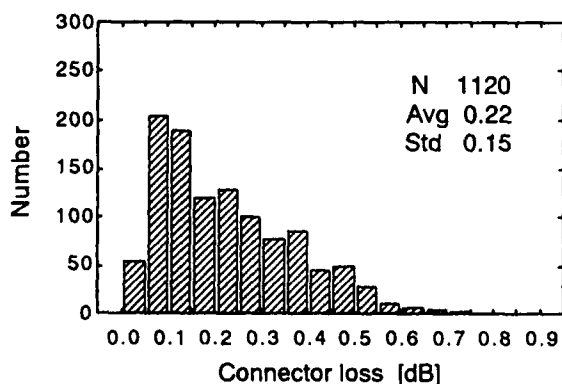


Fig.16 Stacked 80-Fiber connector loss distribution

Fig.16 shows the connector loss distribution of the stacked 80-fiber connectors, which consist of 16-fiber connectors of 0.19dB average connector loss. We could realize the low loss 80-fiber connectors of 0.22dB. Slight loss increase due to stacked process was observed because floating condition had not been optimized yet. Further investigation to reduce the loss increase due to stacked structure is needed.

4. Conclusions

As a primary step to realize a low-loss 80-fiber connector, we have developed two types of low-loss 16-fiber connectors, SiV-connector and AP-connector. The required ferrule eccentricity error for 0.2dB connector loss was calculated at 0.7 μm, and low connector loss less than 0.2dB was attained for both types of the 16-fiber connectors. In order to understand the relation between the dimension of the connector and connector loss, we have developed new measurement method, fiber core position measurement method.

Overmore, using the developed low-loss 16-fiber connectors, we manufactured proto-type model of the stacked type 80-fiber connector with 0.22dB average connector loss.

REFERENCES

- [1] S.Tomita, M.Matsumoto, S.Nagasawa, T.Tanifuji and T.Uenoya, 'Preliminary Research into High-count Pre-connectorized Optical Fiber Cable', 41st IWCS, pp5-12, 1992
- [2] S.Nagasawa, H.Furukawa, M.Makita and H.Murata, 'Mechanically Transferable Single-Mode Multifiber Connectors', IOOC'89, TECHNICAL DIGEST vol.4 of 5, pp48-49
- [3] D.Marcuse, 'Loss Analysis of Single-Mode Fiber Splices', THE BELL SYSTEM TECHNICAL JOURNAL Vol.56, No.5, May-June 1977
- [4] K.Saito, T.Kakil, H.Ishida and S.Suzuki, 'Development of Novel Multiple Single-Mode Fiber Connector Composed of V-grooved Silicon Chip and Guide-pins', 38th IWCS, pp444-449, 1989



Tomohiko Ueda

Sumitomo Electric
Industries, Ltd.

1, Taya-cho, Sakae-ku
Yokohama, Japan

Tomohiko Ueda received a B.E. degree from Tokyo University in 1987. He joined Sumitomo Electric Industries, Ltd. in 1987, and has been engaged in research and development of optical connectors. He is an engineer of Communication R&D Department in Yokohama Research Laboratories.



Toshiaki Kakii

Sumitomo Electric
Industries, Ltd.

1, Taya-cho, Sakae-ku
Yokohama, Japan

Toshiaki Kakii was born in 1955 and received a M.E. degree from Keio University in 1980. He joined Sumitomo Electric Industries, Ltd. in 1980 and has been engaged in research and development of optical fiber jointing technologies. He is a chief research associate of Transmission Media R&D Department in Yokohama Research Laboratories.



Hidetoshi Ishida

Sumitomo Electric
Industries, Ltd.

1, Taya-cho, Sakae-ku
Yokohama, Japan

Hidetoshi Ishida received a M.E. degree from Tohoku University in 1987. He joined Sumitomo Electric Industries, Ltd. in 1987, and has been engaged in research and development of optical connectors. He is an engineer of Transmission Media R&D Department in Yokohama Research Laboratories.



Toru Yamanishi

Sumitomo Electric
Industries, Ltd.

1, Taya-cho, Sakae-ku
Yokohama, Japan

Toru Yamanishi received a B.E. degree from Hokkaido University in 1972. He joined Sumitomo Electric Industries, Ltd. in 1972 and has been engaged in research and development of optical fiber, cable and jointing technologies. He is a chief research associate of Communication R&D Department in Yokohama Research Laboratories.



Ichiro Tsuchiya

Sumitomo Electric
Industries, Ltd.

1, Taya-cho, Sakae-ku
Yokohama, Japan

Ichiro Tsuchiya was born in 1959 and received a M.E. degree from Tokyo University in 1983. He joined Sumitomo Electric Industries, Ltd. in 1983 and has been engaged in research and development of optical fiber manufacturing and jointing technologies. He is a senior engineer of Transmission Media R&D Department in Yokohama Research Laboratories.

Filter-Embedded Optical Connector and Fan-out Cord with High-backreflection

H.Hosoya, K.Asano, M.Akiyama, H.Yokosuka

Opto-Electronics Laboratory, Fujikura Ltd.
1440 Mutsuzaki, Sakura, Chiba, 285 Japan

Optical fiber operations support systems serve to maintain optical fiber lines. One of the most essential functions of the system is to detect an optical fiber line fault by OTDR measurement. Another important function is to distinguish between a line fault and one in the transmission equipment.

We have developed an optical filter that has two functions. One is to separate a transmission signal from a test signal. The other is to confirm that the line is fault free before the filter in front of the transmission equipment since there is higher reflection here than the Fresnel reflection in OTDR light. Initially a filter chip was embedded at a right angle to the optical axis in order to reflect the test signal. However the transmission signal was also reflected because of the small little loss of the filter chip in the transmission wavelength region. Therefore the filter chip was slanted to decrease the reflection.

There are two types of optical filters with high-backreflection; a filter-embedded optical connector and a filter-embedded branch element of a fan-out cord. The filters are easily connected to a single-mode optical fiber. They are very convenient accessories and have been put to practical use.

1. Introduction

Numerous proposals on various systems and forms of fiber optic subscriber networks, aimed at implementing a Fiber-to-the Home (FTTH) system, have been made, contributing to the gradual implementation of the FTTH system. In this respect, the importance of an operations support system, which serves to maintain and operate a huge network efficiently to enhance its reliability, has been pointed out in various fields. Actually, a system intended chiefly for network monitoring and testing^{1), 2)} was lately developed and put to practical application, and started operation. In the optical fiber operations support system, various tests have to be performed with the fiber lines kept in communication service and, therefore, the transmitted light and test light are to be set at different wavelengths. Usually the wavelength of the transmitted light is 1.3 μm and that of the test light 1.55 μm . For the prevention

of interference of these lights, an optical filter, which allows the 1.3 μm light to pass and blocks the 1.55 μm light, is required to be provided just in front of the transmission equipment. Further, it has lately been required to add another function to the optical filter. In order to meet this requirement, a new optical filter has been developed and put to practical application. In this paper, we will introduce the structure and characteristics of this new filter.

2. Optical Filter with Reflection Function

One of the important functions of the optical fiber operations support system is to locate faults. When the fiber line is faulty, this function can be achieved usually by the introduction of OTDR measurement. However, it is important but very difficult to discriminate between the faults of the fiber line and those of the transmission equipment for the following reason. Namely, in the vicinity of the extreme end of the fiber line, short lengths of cable are connected by a number of fusion splices and connectors, so sufficient resolution is impossible to obtain even by highly efficient OTDR measurement and the interface between the fiber line and the transmission equipment cannot be identified.

One method proposed to satisfy the above-mentioned requirement is to provide a reflection point at the line end to ensure fault discrimination by OTDR measurement. 3) This system is shown in Fig. 1. Observing the line end for the presence or absence of the reflection point enables fault discrimination. If the presence of the reflection point is confirmed by this observation, the fiber line is not faulty. If not, the fiber line is faulty.

For distinction from the Fresnel reflection due to a fiber break, a return loss of about 10 dB for the OTDR light is required at the reflection point. On the other hand, for the transmitted light, it is better that there be no harmful reflection at the reflection point. These contradictory functions are attainable by use of an

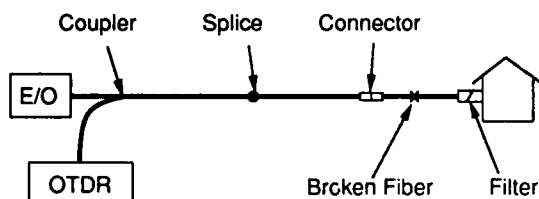
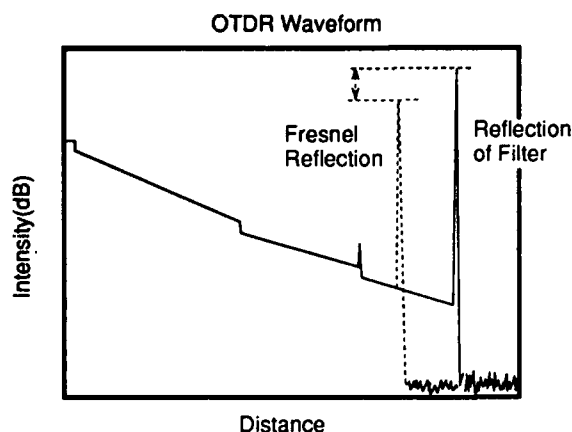


Fig.1 Optical Filter with Reflection Function

optical filter that allows the transmitted light to pass and reflects the OTDR light. In general, multilayer dielectric film type filters have virtually no absorption loss. Therefore, when the transmission loss is high, the quantity of light just equal to that loss is reflected. In case the wavelength of the transmitted light is $1.3 \mu\text{m}$ and that of the OTDR light $1.55 \mu\text{m}$, an optical filter, which allows the $1.3 \mu\text{m}$ light to pass and blocks the $1.55 \mu\text{m}$ light, is to be used.

3. Filter Embedding Method

The idea of the optical filter with reflection function was realized using a fiber type component, taking into account the ease of connection with the optical fiber line. 4) The fiber type component has the advantage of being easy to connect with the optical fiber, or the fiber line, low in insertion loss and small in size. The basic structure of the optical filter is as follows. Namely, a slit is formed in the fiber line, and a thin filter chip is embedded in this slit and fixed with an optical adhesive resin (see Fig. 2). The slit was cut using a high-speed blade with a grinding fluid. The slit width was about $40 \mu\text{m}$ and the thickness of the optical filter chip about $30 \mu\text{m}$. In the case of conventional optical filters, the major characteristic being insertion loss only, the surface

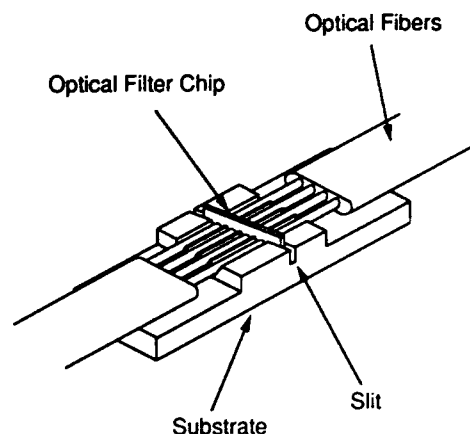


Fig.2 Sutracture of Optical Filter

finish of the end face of the fiber in the slit has not been a particularly important problem. With the optical filter with reflection function, however, the return loss spectrum varies largely if the surface finish in the slit is coarse, therefore, various considerations are needed to prevent this variation. As a result of investigating the grinding conditions, and so on, a very fine mirror finish as shown in Fig. 3 was attained. Consequently, it has become possible to obtain a return loss just equal to the theoretical value.

To realize a high reflection of the OTDR light, it is only required to insert the optical filter chip nearly at right angles to the optical axis of the optical fiber. However, if the filter chip has some loss in the pass region of $1.3 \mu\text{m}$, the wavelength of the transmitted light, it may be assumed that nearly the whole quantity of light equal to that loss is reflected because the absorption loss is virtually equal to zero. For example, a loss of 0.1 dB is equivalent to a return loss of 16 dB . Taking into account the effect of

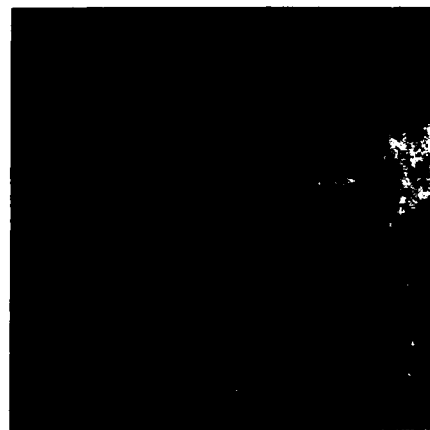


Fig.3 Mirror Finish of end face of Fiber

reflection on the transmission equipment, the return loss has to be reduced to not more than 25 dB for ordinary optical connectors. In order to realize the two contradictory characteristics: attenuation of reflection in this pass region, and addition of the function of high reflection at 1.55 μm , it is necessary that the actual optical filter chip be fixed at a small angle of inclination to the optical axis. To obtain the desired characteristics, the slit is formed at a small angle of 2 to 3° to the plane orthogonal to the optical axis.

4. Structure of Filter Embedded Connector and Fan-out Cord

The extreme ends of the fiber lines are connected by connectors to the transmission equipment in almost all cases. Therefore, the filter with reflection function has to be embedded in the connector. The structure of the filter-embedded connector developed by us is shown in Fig. 4. A fiber holding pipe is incorporated in the rear end of a ferrule. A slit is formed there and an optical filter chip is inserted into the slit. Both the external form and size of this connector are quite the same as those of ordinary connectors. Applicable filter-embedded connectors include various types such as SC, FC and DS.5)

In addition to the filter-embedded connector, a filter-embedded fan-out cord was developed. The structure of this fan-out cord is

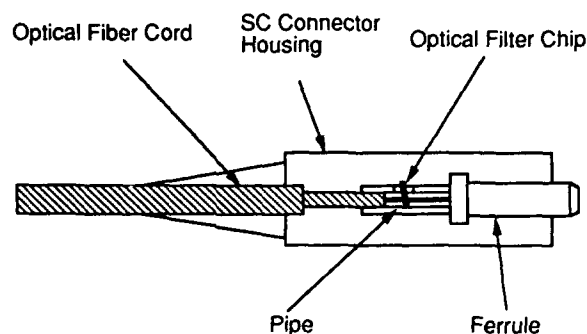


Fig. 4 Structure of Filter-Embedded Optical Connector

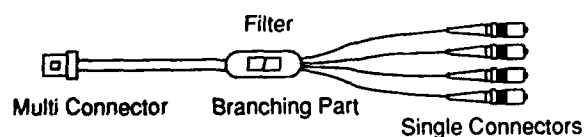


Fig. 5 Structure of Fan-Out Cord with Reflection Function

shown in Fig. 5. The filter chip is installed in the branching part of a fan-out cord. In this case, one each filter is used for high count fiber ribbons. Needless to say, there is no limitation on the type of connectors attached to both ends.

5. Optical Characteristics

This section describes the optical characteristics of the filter-embedded connector. The connector used was the SC type, and the optical filter chip was the so-called SWPF type that allows the 1.3 μm light to pass and blocks the 1.55 μm light. The insertion loss histogram is given in Fig. 6. A pig-tail cord having a connector at one end was measured using the master connector method. The insertion loss at 1.3 μm was within the limits of about 0.4dB to 0.9 dB. The major factors contributing to the variation in insertion loss include the variation in connection loss of the connector, the variation in transmission loss of the optical filter chip and the variation in cutting width of the slit. At 1.55 μm , an insertion loss of more than 55 dB was obtained in all

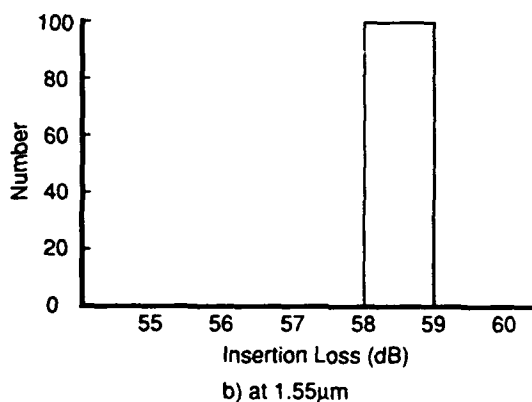
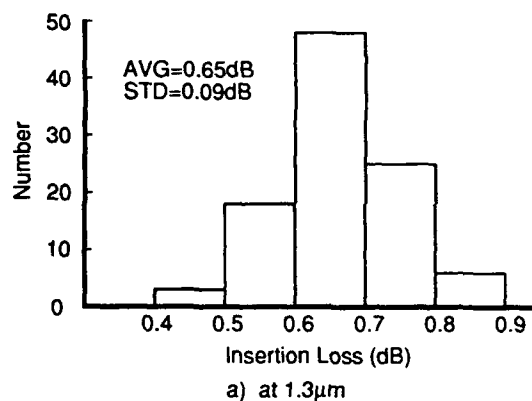


Fig. 6. Insertion Loss Histogram at 1.3 & 1.55 μm

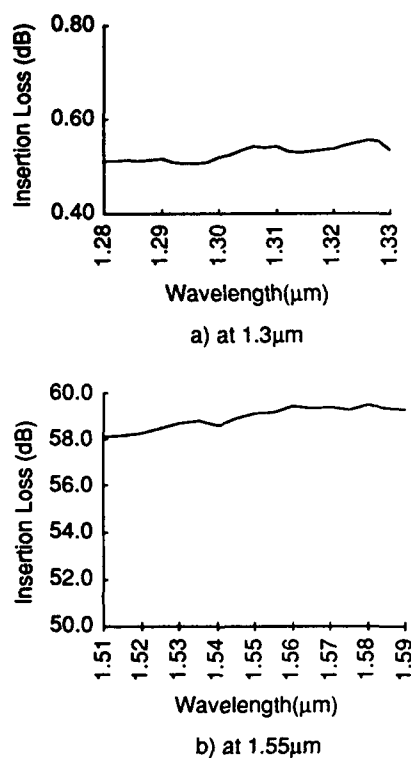


Fig.7 Insertion Loss Spectrum at 1.3 & 1.55μm

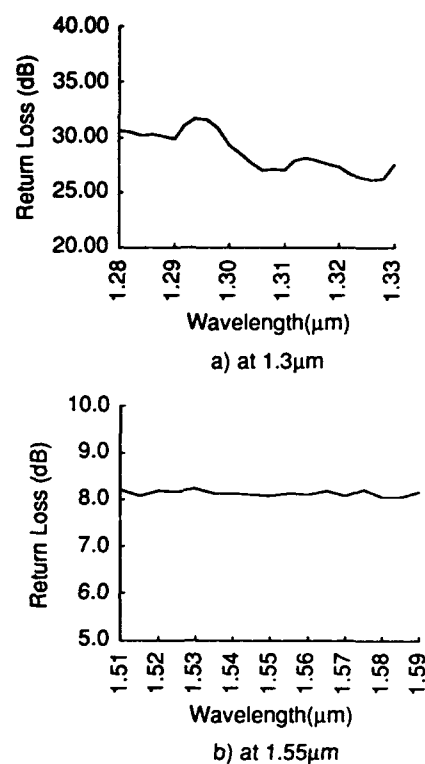


Fig.8 Return Loss Spectrum at 1.3 & 1.55μm

measurements. The insertion loss spectrum is shown in Fig. 7. In the vicinity of 1.3 μm, there is a variation in transmission loss of the optical filter chip, and this variation is exhibited as it is.

An example of the return loss spectrum is given in Fig.8. The measured value includes a return loss of about 30 dB for the SC connector. At 1.3 μm, there is a variation in transmission loss of the optical filter chip, so there is also a corresponding variation in return loss. On the other hand, at 1.55 μm, there is a transmission loss of more than 55 dB, and the reflection at this wavelength is nearly total even if there is some variation in transmission loss. Therefore, the return loss spectrum is nearly flat. The histogram of the minimum return loss $1.31 \pm 20 \mu\text{m}$ and that of the maximum return loss $1.55 \pm 40 \mu\text{m}$ are given in Fig. 9. The major factors contributing to the variation in return loss at 1.3 μm include the variation in transmission loss of the optical filter chip and the variation in reflection of the polished end face the SC connector. The factor contributing to the variation in return loss at 1.55 μm is the angular deviation of the optical filter chip in almost all cases.

Fig. 10 shows how the return losses at 1.3 and 1.55 μm vary when temperature is made to vary. Any of these losses exhibit a very stable value. In addition, the results of various reliability

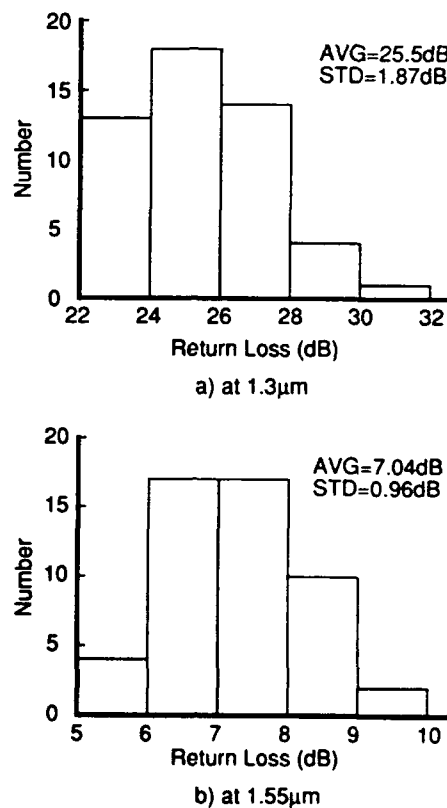


Fig.9 Return Loss Histogram

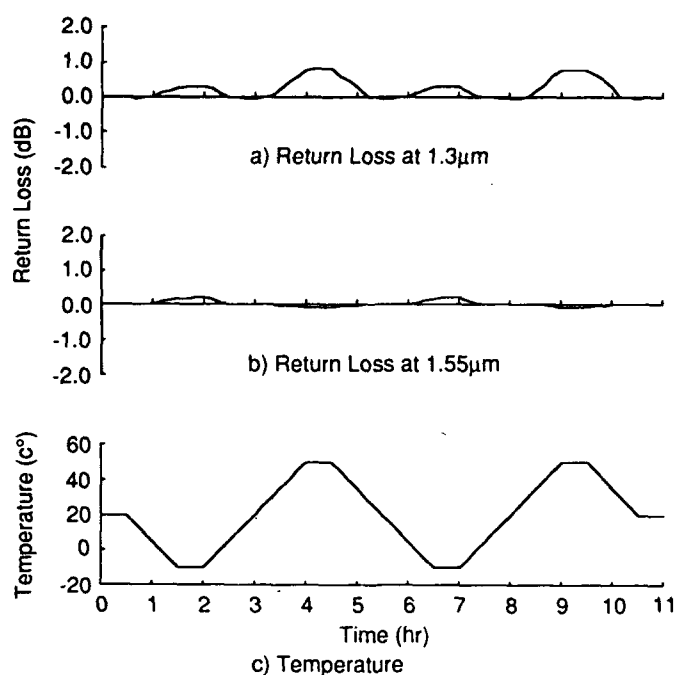


Fig.10 Temperature Cycling Test

Table 1. Reliability Test Results of Filter Embedded Connector

Items	Test Conditions	Results;Residual Loss
Heat Cycling Test	-10 to 50°C 100cycles	less than 0.1dB
Heat and Humidity Test	70°C, 90% RH 100h	less than 0.1dB
High-Temperature Test	70°C,100h	less than 0.1dB
Low-Temperature Test	-20°C,100h	less than 0.1dB
Vibration Test	1.5mm,10-55Hz 3 directions	less than 0.1dB
Impact Test	50G,11ms	less than 0.1dB

Table 2. Example of Optical Characteristics of Filter Embedded Fan-Out Cord

Fiber No.	Insertion Loss at 1.3μm	Insertion Loss at 1.55μm	Return Loss at 1.3μm	Return Loss at 1.55μm
1	1.26dB	58.8dB	27.3dB	8.9dB
2	1.18dB	58.9dB	27.0dB	8.2dB
3	1.33dB	58.5dB	27.0dB	9.0dB
4	1.28dB	58.7dB	30.6dB	8.4dB

tests are given in Table 1.

An example of the characteristics of the filter-embedded fan-out cord is given in Table 2. A 4MT connector is attached to one end of this cord and 2MPO 6 connectors to the other. The optical filter characteristics of this cord are basically the same as those of the SC connector type. The four fibers exhibit nearly the same values of insertion loss and return loss.

6. Conclusion

So far, we have described the structure and characteristics of the optical filters with reflection function which are very useful for the optical fiber operations support system. With the progress in optical fibers, subscriber networks, and so on, further varying functions and forms will be required of such optical assemblies.

References

- 1)H.Takasugi, N.Tomita, T.Uenoya & Y.Yokoo ; IWCS,pp623-629,1990
- 2)H.Matsumoto, Y.Yokoo, K.Sato & T.Uenoya ; IWCS,pp787-792,1991
- 3)N.Tomita, K.Sato & I.Nakamura ; NTT REVIEW,vol.3,No.1,pp97-104,1991
- 4)H.Hosoya, K.Asano, M.Ohsawa & H.Yokosuka ; IWCS,pp1794-1795,1990
- 5)Y.Ando, S.Iwano, R.Nagase, K.Kanayama & E.Sugita ; NTT REVIEW,vol.3,No.3,1991
- 6)S.Nagasawa,Y.Yokoyama,F.Ashiya & T.Satake; ECOC'91,MoB1-7,1991



Hideyuki Hosoya

Opto-Electronics
Laboratory
Fujikura Ltd.

1440,Mutsuzaki,Sakura,
Chiba,285,Japan

Hideyuki Hosoya was born in 1959. He received the M.Sc. degree in Physics from Yamagata University in 1983. He joined Fujikura Ltd. in 1983 and has been engaged in research and development of telecommunication cables and accessories. He is a member of the Institute of Electronics, Information and Communication Engineers of Japan.



Michio Akiyama

Opto-Electronics
Laboratory
Fujikura Ltd.

1440,Mutsuzaki,Sakura,
Chiba,285,Japan

Michio Akiyama was born in 1951. He received the M.E. degree in Electrical Engineering from Yokohama National University in 1975. He joined Fujikura Ltd. in 1975 and has been engaged in research and development of telecommunication cables and accessories. He is now a manager of Fiber & Cable Accessory Section within Opto-Electronics Laboratory and a member of the Institute of Electronics, Information and Communication Engineers of Japan.



Kenichiro Asano

Opto-Electronics
Laboratory
Fujikura Ltd.

1440,Mutsuzaki,Sakura,
Chiba,285,Japan

Kenichiro Asano was born in 1966. He graduated in opto-electronics engineering from Tokyo Kougakuin College of Technology. He joined Fujikura Ltd. in 1989 and has been engaged in research and development of telecommunication cables and accessories. He is a member of the Institute of Electronics, Information and Communication Engineers of Japan.



Hiroshi Yokosuka

Opto-Electronics
Laboratory
Fujikura Ltd.

1440,Mutsuzaki,Sakura,
Chiba,285,Japan

Hiroshi Yokosuka graduated in mechanical engineering from Tokyo Metropolitan Technical Junior College in 1967. He has been engaged in research and development of telecommunication cables and accessories. He is now a manager of Fiber & Cable Accessory Department within Opto-Electronics Laboratory and a member of the Institute of Electronics, Information and Communication Engineers of Japan.

FIBER MOTION IN CERAMIC-FERRULE OPTICAL CONNECTORS

L. A. Reith, R. A. Frantz, L.M. Plitz*, and W. W. Wood

Belcore, Morristown, N.J.

*Belcore, Red Bank, N.J.

ABSTRACT

The ability of fibers in optical connectors to maintain physical contact over their lifetime is critical to achieving low reflectances and thus to connector reliability. Virtually all ceramic-ferrule connectors today have radiussed endfaces to assure good contact. Extreme care is taken to maintain tight tolerances on the protrusion or undercut of the polished fiber relative to the ferrule, as well as on the concentricity of the polished ferrule endface curvature. This ensures that the fibers at the connector endfaces achieve physical contact when mated under typical spring loading forces of approximately two pounds (900 gmf). However, recent work has shown that fibers can permanently withdraw into the ferrule during aging at high temperatures, resulting in loss of physical contact. We are engaged in a test program to identify factors contributing to fiber withdrawal and to determine the amount of withdrawal in hand-assembled and commercially available ceramic-ferrule connectors as functions of load and temperature.

I. INTRODUCTION

A critical factor in optical connector reliability is the ability to maintain low reflectance over the service lifetime. Virtually all ceramic-ferrule connectors on the market today achieve low reflectances by radiussing the ferrule endface and spring-loading the ferrule to ensure good physical contact between the fiber ends. Tight tolerances are placed on the protrusion or undercut of the polished fiber with respect to the ferrule endface and on the concentricity of the polished endface with respect to the fiber position in the ferrule. In conjunction with spring loading forces of approximately two pounds (900 gmf), this ensures that the fibers achieve good physical contact. Recent work, however, has shown that fibers can withdraw permanently into the ceramic ferrule during high temperature aging under load.¹ Fibers subjected to loading forces similar in magnitude to the spring loading forces were pushed back into the ferrule by as much as several microns. Although connector plugs in which such pushback occurs will maintain fiber physical contact as long as they remain in the same mated pairing, reconfigured pairings may not achieve physical contact, leading to unacceptable performance degradation.

Many parameters can affect the motion of fibers in connector

ferrules. We have identified several that are particularly important.

o **Materials Selection.** The choice of the ferrule material is important, but the epoxy is even more significant, since epoxy properties can vary so widely.

o **Dimensional Tolerances.** The relative diameters of the fiber and the clearance hole in the ferrule control the thickness of the epoxy interfacial layer.

o **Assembly Process Controls.** These should assure cleanliness, accommodate the limited pot life of the epoxy, and control of the time and temperature of the epoxy cure cycle.

o **Concentricity.** Good fiber-to-fiber contact requires that the curvature of the polished endface be concentric with the fiber and that both be concentric with the ferrule outer diameter.

o **Fiber Loading Force.** This is applied by the loading springs and shared between the fiber and the surrounding area of the ferrule endface that is in contact.

o **Service Environment.** Temperature and humidity, both of which vary over time, can affect the connector service life.

Table 1 lists some of these parameters, column two shows their expected ranges over the lifetime of a mated connector, and column three shows the test values we used in our experiments.

TABLE 1. Parameters for Preliminary Tests Using Hand-Assembled Ferrules

PARAMETER	SERVICE RANGE	TEST VALUES
TEMPERATURE	-40 TO 75 °C	25 °C; 65 °C
LOADING FORCE	0 TO 2 lbf (907 gmf)	0; 0.5 lbf; 1 lbf; 1.5 lbf
EPOXY	5 KNOWN	2
FERRULE MATERIAL	ZIRCONIA; ALUMINA	ZIRCONIA
FERRULE CLEARANCE	0.5 TO 2 µm	0.5 µm
TIME	YEARS	DAYS

In our experiments, we used commercially available SC connectors (push-pull latching mechanism) with zirconia ferrules from 4 different vendors, as well as hand-assembled zirconia ferrules. Fibers were epoxied into the hand-assembled ferrules using two different epoxies and varying cure schedules. The fibers in both the connectors and ferrules

were then subjected to various known loads and elevated temperatures, and the results were compared. In the case of the hand-assembled ferrules, the amount of fiber motion in the ferrule could be correlated to the curing conditions.

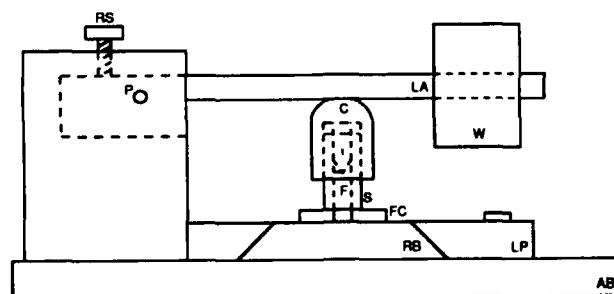
Our work has two goals: (i) to determine the critical parameters that affect fiber motion and thereby define means of minimizing that motion; and (ii) to design a test procedure and criterion for Bellcore's generic requirements that, if passed, will ensure that fiber motion will not result in field failures. We describe the test fixturing and test procedures in Section II. In Section III we show test results, and in Section IV we discuss the results and give our conclusions.

II. EXPERIMENTAL DESIGN AND PROCEDURE

Two types of test arrangements were used. In the first case, either connector plugs or ferrules could be mounted in a removable baseplate and inserted in a fixture designed to place a known, variable load on the fiber alone. The fixture could then be placed in an oven for high temperature aging. The test samples were removed from the chamber at intervals and the change in fiber position with respect to the ceramic ferrule was measured. Fiber position was measured in the connector plugs using an interferometric technique, and in hand-assembled ferrules using a contact scanning profilometer. In the second test arrangement, hand-assembled ferrules were mounted in the contact scanning profilometer using a fixture containing a heater unit. In this case, no load was applied – the temperature of the ferrules was varied and the motion of the fiber measured as a function of temperature.

A. TESTING UNDER LOAD

The test fixture illustrated in Figure 1 is designed to apply known loading forces to the fiber only, in either commercially-available connector plugs or hand-assembled



- KEY:
- F: Fiber/Ferrule Assembly
 - S: Ceramic Sleeve
 - C: Indentor (Conical or Rounded Tip)
 - W: Loading Weight
 - LA: Load Lever Arm
 - P: Lever Arm Pivot Point
 - RS: Lever Arm Release Screw
 - RB: Removable Base
 - FC: Ferrule Clamp (Two Sides)
 - LP: Locking Plate
 - AB: Assembly Base

FIGURE 1 FIBER LOADING TEST FIXTURE

ferrules. A ferrule with a fiber epoxied in place is clamped into the base of the fixture. A ceramic sleeve slips over the ferrule and a zirconia indentor with the same diameter as the ferrule slides into the top half of the sleeve. The sleeve has a clearance of 2–3 μm around the ferrule and the indentor, providing accurate alignment while still giving an easy, nonbinding fit. We used a zirconia indentor with a conical end truncated at a diameter of 85–95 μm . This ensures that the indentor contacts only the surface of the fiber in the ferrule, thereby applying the full loading force to the fiber. The load is applied through a protective cap over the zirconia indentor and is controlled by positioning a known weight at a desired location along a lever arm. The weight can be completely removed by raising the lever arm with a release screw. The section of the base that clamps the ferrule can be removed from the assembly so that ferrules can be measured using either a surface profilometer or an interferometer.

In a typical test procedure, the connectors or the hand-assembled ferrules were measured before going on test. Connector plugs were measured using an interferometric technique that was reproducible to $\pm 0.05 \mu\text{m}$.² Ferrules were measured using a contact scanning profilometer that was accurate to $\pm 0.02 \mu\text{m}$. After the original fiber position was measured, the connector plugs (or ferrules) were placed in the fixture and the load was applied. At various intervals, the fixtures were removed and cooled to room temperature, at which time the weights were removed. Next, the connector plugs (ferrule assemblies) were removed and scanned with the interferometer (profilometer). The fixtures were then re-assembled and placed back into the oven with the weights re-applied to the fibers.

B. TESTING UNDER NO LOAD

Fiber withdrawal can occur also under no-load conditions due to the differing coefficients of thermal expansion (CTEs) of the glass, the ceramic ferrule, and the epoxy. This withdrawal was measured with the contact scanning profilometer using the fixture shown in Figure 2. A fiber is bonded into a ferrule using one of the test epoxies cured under a controlled time-temperature cycle, and the assembly is inserted into the cylindrical aluminum sample holder. A small amount of thermal grease ensures good thermal contact between the holder and the ferrule, while a thermocouple held in contact with the ferrule provides an accurate measurement of the sample temperature. The sample holder also conducts heat to the sample assembly from the circumferential electric wirewound resistance heater, which is powered from a variable-output dc power supply; a voltage-temperature calibration curve was determined to allow the test temperature to be regulated by the power supply setting. The thermal mass of the sample holder helps stabilize the temperature of the sample. An insulating support pad limits the heat flow into the profilometer base, and a draft shield (not shown) around the test fixture interrupts the air currents that would otherwise carry the heat upward into the sensitive electronics of the profilometer mechanism.

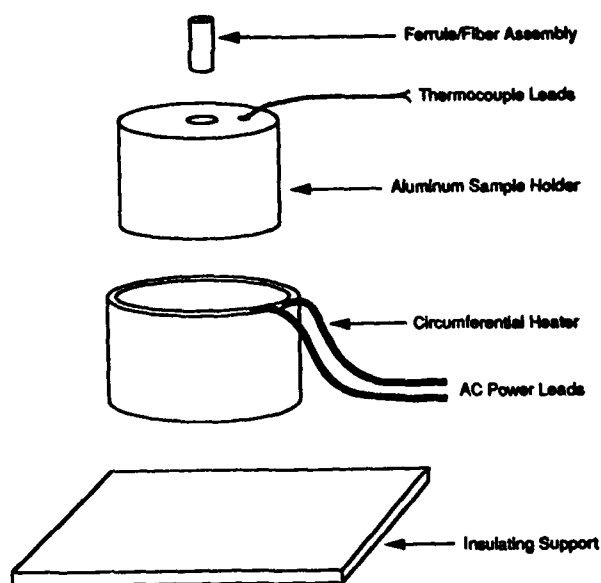


FIGURE 2. THERMAL WITHDRAWAL TEST FIXTURE

The typical test procedure started by inserting the ferrule assembly into the fixture and mounting the fixture in the profilometer. The first scan then measured the initial fiber position at 25°C. The appropriate voltage was applied to the heater to increase the temperature by a 10°C increment as rapidly as possible, after which the fixture/ferrule was allowed to equilibrate for 10 minutes and was scanned again. This procedure was repeated up to 105°C and then back down to 25°C, using the same temperature increments and equilibration times throughout.

III. RESULTS

A. COMMERCIAL CONNECTORS UNDER LOAD

Four single-mode, SC-connectorized jumper cables from each of four different manufacturers were used in this test. One end of each jumper cable was mounted in the test fixture under either 0, 0.5 lbf (227 gmf), 1.0 lbf (454 gmf), or 1.5 lbf (680 gmf) of loading force. The other four ends of the jumper cables were paired and connected using a standard sleeve. The initial part of the experiment was conducted under ambient conditions. After the weights were removed, the mated connector plugs were also disconnected and the fiber positions were remeasured after 12 hr, 20 hr, 36 hr, 66 hr, and 132 hr. After this last measurement, the fixtures were placed in the oven at 65 °C. They were removed from the oven and disassembled and the fiber positions were remeasured after 4 hr, 8 hr, 12 hr, 18 hr, 24 hr, 36 hr, 48 hr, and 72 hr. Figure 3(a) shows the net fiber motion in microns, under known loads, as a function of total test time for the four connector plugs from Supplier 2. Similarly, Figure 3(b) shows the net fiber motion in microns for the mated connector plugs from this supplier. Note the change in scales from (a) to (b). In all cases, most of the fiber motion occurs during the first 24 hr on test. Also note that, although the

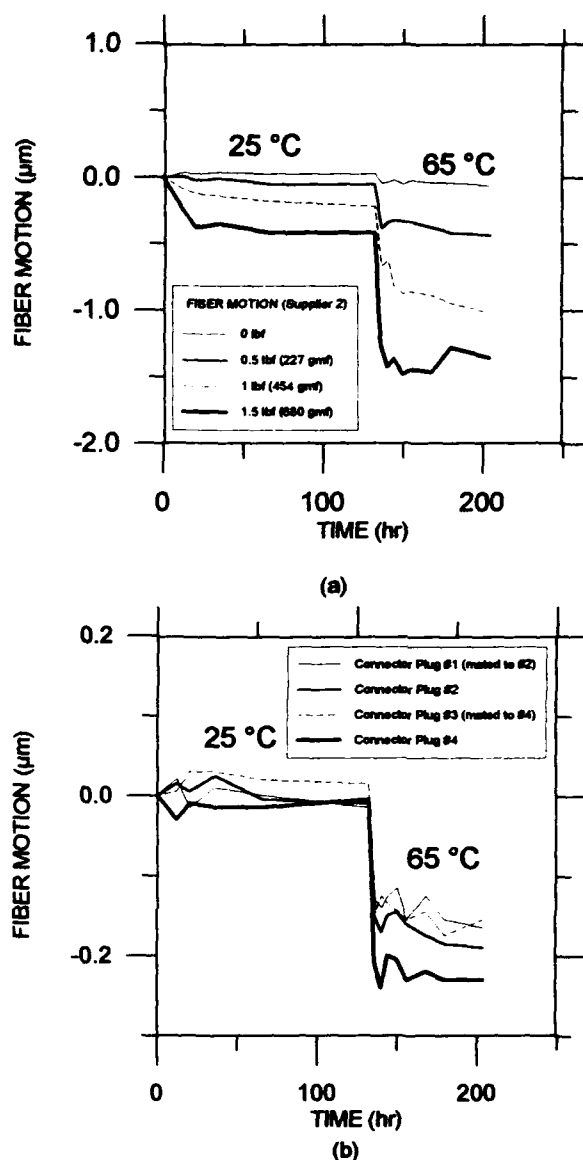


Figure 3. Fiber motion for connector plugs from Supplier #2 as a function of time.

(a) plugs under known loads and (b) mated plugs.

spring-loading force on the connector ferrule is known to be approximately 2 lbf (907 gmf)³, the amount of motion for mated connector plugs implies that the effective loading force a fiber sees in a mated connector is actually less than 0.5 lbf.

This result is more clearly illustrated in Figure 4. In this figure, the total cumulative fiber motion is plotted for each loading force for Supplier 1 and Supplier 2. The data for Suppliers 3 and 4 fall between these extremes. The plotted lines each represent a least-squares linear fit to the data. The crosses represent the motion of the fibers in mated connector sleeves, which have been plotted so as to fall on the fitted line. In no case, for any of the four manufacturers, did the measured motions intersect the lines at loads greater than 0.5 lbf.

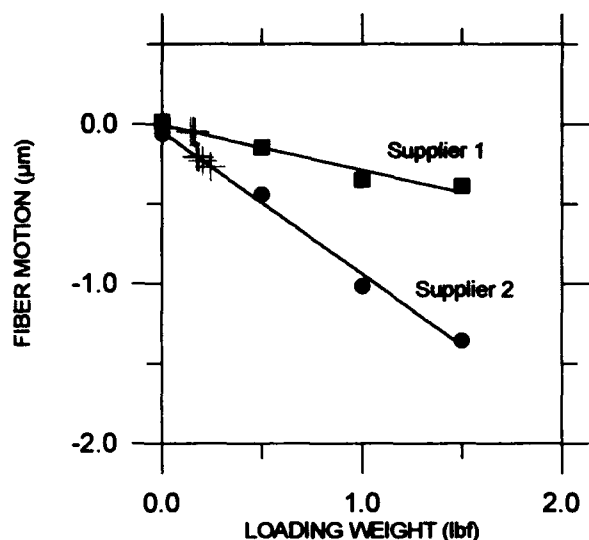


Figure 4. Cumulative fiber motion as a function of loading force for Suppliers 1 and 2, respectively. The + symbols represent the motion of fibers in mated connector plugs under the same environmental conditions.

The loss and reflectance performance of mated connector plugs for each of the four manufacturers was measured both before and after the loading tests using a concatenation technique.⁴ Before the loading tests, all fiber cores made contact, resulting in reflectances less than -40 dB. After the loading tests, those connector plugs loaded in the test fixture had been pushed back into the ferrules so far that they would not always make physical contact. Although the fibers in the mated plugs also had been pushed back into the ferrules, the resulting motions were small enough that no loss of physical contact resulted in any of these cases.

The gap between any pair of fiber cores without spring loading (single-point contact) depends not only on the protrusion/undercut of the two fibers relative to the ceramic, but also on the radius of curvature of the ferrule endfaces and the eccentricity of the endface polish. We assume that the fiber and ferrule are polished to the same radius of curvature. We estimate the gap at the fiber cores due to polishing eccentricity for zero insertion force using the formula,

$$\text{Total Gap} = \Delta_x + \Delta_y, \quad (1)$$

where Δ_x and Δ_y are the contributions to the total gap taken along orthogonal directions in a plane parallel to the ferrule endfaces. Assume we look at each connector endface head-on. We choose the y-direction to be parallel to the key on the connector plug housing; if the connectors are both eccentrically polished in this direction, the eccentricities add to create a larger gap when the connectors are mated. In the x-direction, since the axes are flipped with respect to one another when the connection is made, the gaps due to

eccentric polishing for each plug will compensate and decrease the gap. These contributions to the total gap may be calculated from

$$\Delta_x = x_1^2/(2R_1) + x_2^2/(2R_2) - (x_1 + x_2)^2/[2(R_1 + R_2)], \quad (2)$$

$$\Delta_y = y_1^2/(2R_1) + y_2^2/(2R_2) - (y_1 - y_2)^2/[2(R_1 + R_2)],$$

where R is the radius of curvature of an individual connector plug and the subscripts 1 and 2 identify the respective plugs.

Using this formula we can calculate the gap for different connector pairs for the four different manufacturers. In Figure 5, the measured reflectance after load testing is plotted as a function of the calculated gap. These results bear out earlier data, showing that the spring-loading force must deform each ferrule endface by approximately 0.25 μm to achieve physical

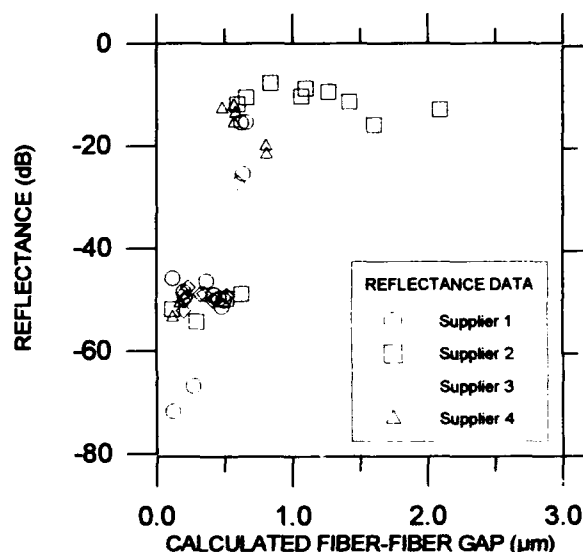


Figure 5. Reflectance performance after aging for connectors from each supplier plotted as a function of the calculated gap, given by Eq. (1).

contact.² This is only a rough measure, but these data show it to be a reasonable rule-of-thumb value.

B. HAND-ASSEMBLED FERRULES UNDER NO LOAD

Ferrules were hand-assembled using two different epoxies, following as carefully as possible the kit instructions for hand-assembled connectors. The epoxies were hand-mixed in bi-packs and were injected into the funneled back ends of the ferrules using a syringe. Short lengths of fiber were stripped and were cleaned with alcohol before being coated with epoxy and inserted into the epoxy-filled ferrules. The epoxies were then cured with varying cure schedules in an attempt to generate complete cures with different glass transition temperatures, T_g .

After the ferrules had cooled, the fibers were cleaved and polished at both ends of the ferrule using a hand-held

polishing tool. Coarse and fine polishing was done to get a smooth finish of the fiber surface. The fibers were flush with the ceramic to within 1 μm on the front surface, and 7 μm on the back surface, but this was not one of our major concerns. After the polishing was completed, a contact profilometer was used to measure the initial protrusion or undercut of the glass relative to the ceramic. The ferrules used had flat endfaces to facilitate this measurement. The profilometer calibration was checked on a weekly basis during the experiment and was found to be repeatable to $\pm 0.02 \mu\text{m}$. The scan width (across the ferrule) was not critical in these experiments, so we elected to ignore a difficult-to-resolve scaling error of about 20%.

When the ferrules were assembled, tiny droplets (roughly 1 mm^3) of the epoxies were put down on Teflon sheets and cured with the ferrules. The cured droplets were then analyzed to determine the T_g and extent of cure. Approximately 2-5 mg of cured droplets were examined on a Perkin Elmer DSC IV Differential Scanning Calorimeter. Each sample was heated at 10 $^\circ\text{C}/\text{min}$ from -50°C to 150°C . All transitions were recorded. The sample was then cooled at 10 $^\circ\text{C}/\text{min}$ and rerun to record a second heating scan. Changes in the T_g and curing peaks (if any) were noted.

We noted during the course of these measurements that predictions of cure level and T_g based on measurements from epoxy films were unreliable. Instead of fully cured samples with varying T_g 's, the samples had varying cure levels, and uniformly higher T_g 's after the first DSC scan. It is likely that, although the small droplets closely simulate the cure in a ferrule, they can still yield different T_g 's and extent of cure, particularly since the amount of exposed surface area is so different for each case. Table 2 describes the results of the analysis for different cure schedules.

TABLE 2. Epoxy Samples Cured for Fiber/Ferrule Movement Study

SAMPLE	T_g ($^\circ\text{C}$)	PEAK TEMP ($^\circ\text{C}$)	ΔH ($\text{cal}/^\circ\text{g}$)	COMMENT
EPOXY 1				
Raw Resin		117	90	
2nd Scan	89			
15 min @100 $^\circ\text{C}$	52	127	5	5% Undercured
2nd Scan	120			
15 min @80 $^\circ\text{C}$				Sample too tacky, not analyzed
45 min @80 $^\circ\text{C}$	60	104	14	16% Undercured
2nd Scan	122			
90 min @65 $^\circ\text{C}$	58	103	18	20% Undercured
2nd Scan	126			
EPOXY 2				
Raw Resin		108	61	
2nd Scan	45			
10 min @100 $^\circ\text{C}$	70			
2nd Scan	79			

As described in Section II, the ferrules were inserted in the heater test fixture under the contact profilometer, and the fiber motion relative to the ceramic ferrule endface was measured as a function of temperature. Figure 6 shows data for a ferrule/fiber assembly using epoxy 1 with the cure schedule recommended by the connector manufacturer (15 min at 100 $^\circ\text{C}$). Figure 6(a) represents the first heating/cooling cycle to 105 $^\circ\text{C}$ and back to 25 $^\circ\text{C}$. The amount of fiber motion relative to the initial position is plotted; the open symbols denote increasing temperature and the filled symbols denote decreasing temperature. Although there is some scatter in the data, it is clear that the fiber

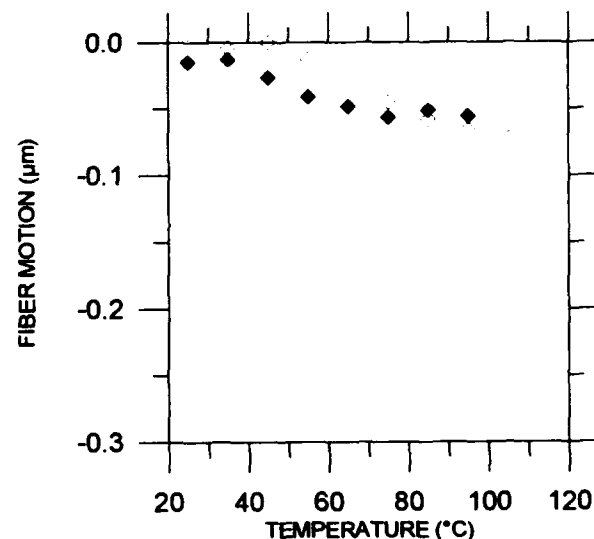
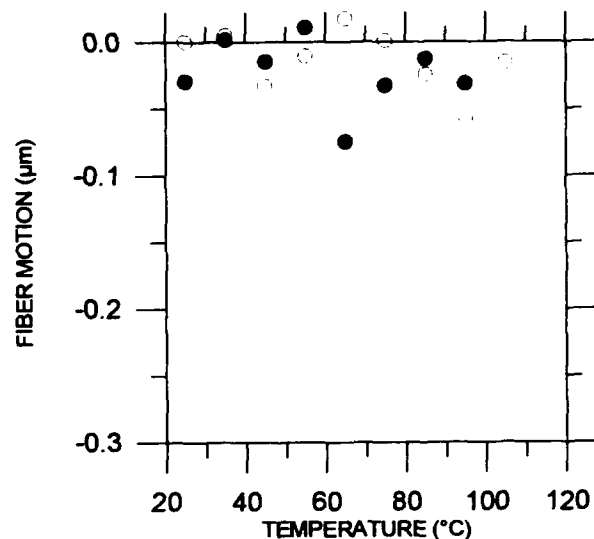


Figure 6. Fiber withdrawal as a function of temperature for epoxy 1 with no load - 100 $^\circ\text{C}$, 15 min cure.
(a) first cycle and (b) second cycle.

withdrawal increases slowly with temperature throughout the temperature range. During cooling, the amount of withdrawal decreases, and the fiber returns to its initial position, within experimental error. Figure 6(b) represents the second heating/cooling cycle, and no further change occurs. The dependence of the fiber withdrawal on temperature is constant.

Although Table 2 indicates that T_g was 52 °C for the first DSC scan, there was no indication of a low T_g in the fiber withdrawal measurement. We believe that the epoxy cured in the ferrule was more completely cured, and therefore had already reached a higher T_g , comparable to the second DSC scan.

Figure 7 again shows data for a ferrule/fiber assembly using epoxy 1, now with a lower temperature cure (15 min at 80 °C). In this instance the epoxy was clearly undercured and noticeably tacky to the touch. Figure 7(a) represents the amount of fiber motion during the first temperature cycle, while Figure 7(b) represents the second cycle. During the first temperature cycle, there is now a large amount of fiber withdrawal, as the epoxy completes its cure; during the second cycle, the amount of fiber motion is comparable to a typical fully cured sample. In this case, the sample could not be analyzed in the DSC.

Figure 8 shows data for a ferrule/fiber assembly using epoxy 1 with an even lower temperature, longer duration cure (90 min at 65 °C). In this case, the DSC measurement suggests that this epoxy was again undercured. The fiber did have a small amount of permanent withdrawal after the first cycle, but this was a small effect. As above, Figure 8(a) represents motion during the first cycle and Figure 8(b) during the second cycle, respectively. Data for an 80 °C, 45 min cure, not shown here, were similar to the data shown in Figure 8.

The data obtained for epoxy 1, as shown in Table 2, indicate that lower temperature, longer duration cures did not result in lower values of T_g , but only in the possibility of undercured samples. In all cases, our first temperature cycle (roughly equivalent to the first DSC scan) resulted in a full cure of the epoxy and a high T_g , above 100 °C. After full cure, and below T_g , the fiber motion was on the order of $1 \times 10^{-4} \mu\text{m}/^\circ\text{C}$.

Figure 9 shows a different behavior for epoxy 2. In this case the epoxy was cured at 100 °C for 10 min. This was recommended by the connector manufacturer in the field-installable kit. DSC analysis of the cured epoxy, shown in Table 2, indicated that it was fully cured but had a lower T_g

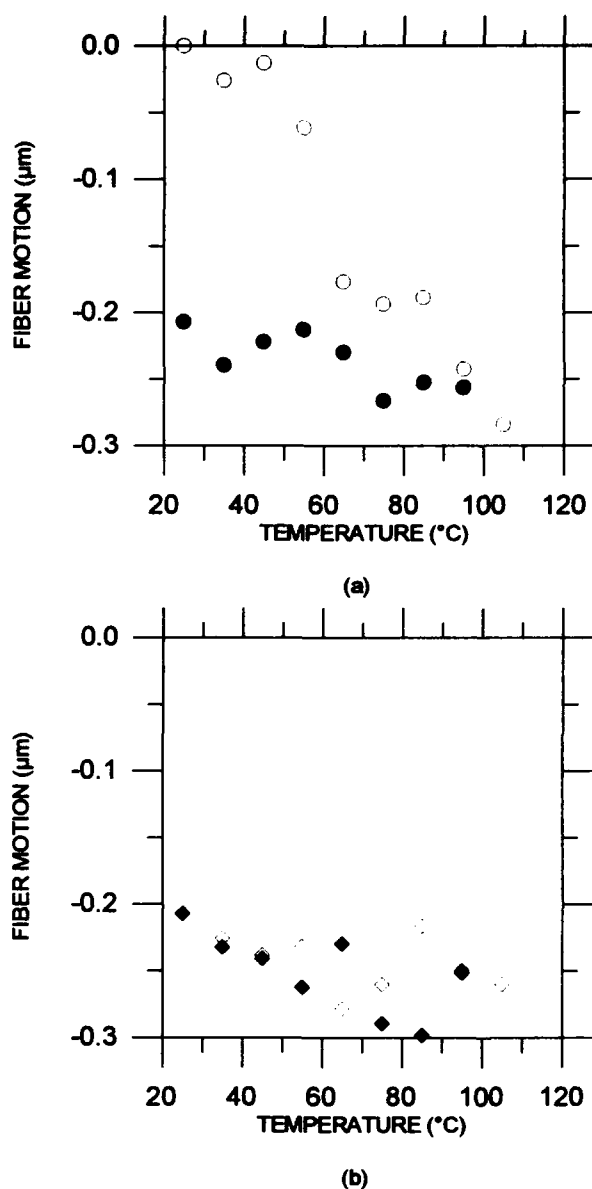
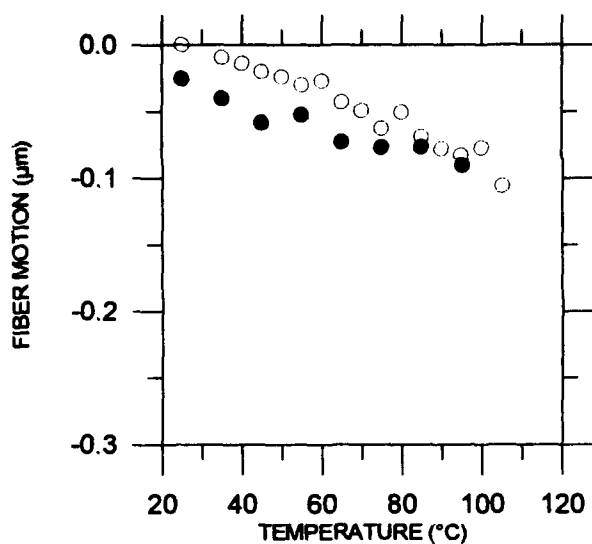
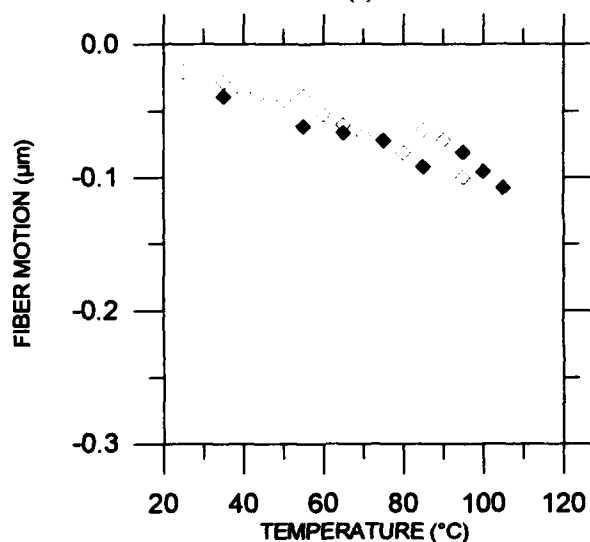


Figure 7. Fiber withdrawal as a function of temperature for epoxy 1 with no load - 80 °C, 15 min cure. (a) first cycle and (b) second cycle.

of about 80 °C. DSC scans of the droplet samples showed that the T_g in this case, unlike the T_g for epoxy 1 cured at 100 °C for 15 min, was stable and did not increase upon a repeat scan. In this case temperature cycling of the ferrule assembly resulted in a small amount of withdrawal, comparable to epoxy 1, out to about 85 °C. At higher



(a)



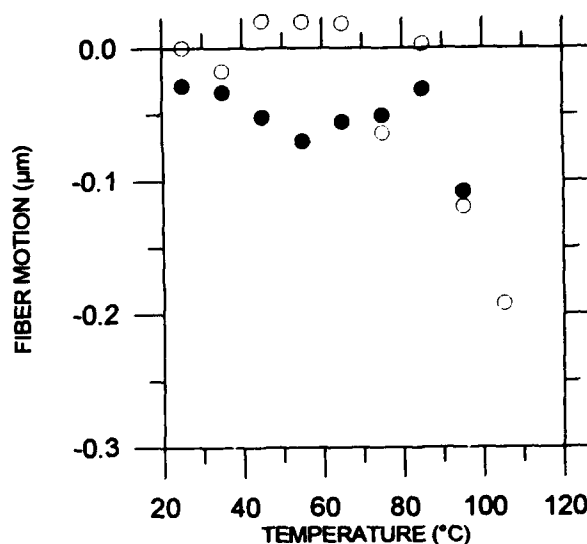
(b)

Figure 8. Fiber withdrawal as a function of temperature for epoxy 1 with no load - 65 °C, 90 min cure. (a) first cycle and (b) second cycle.

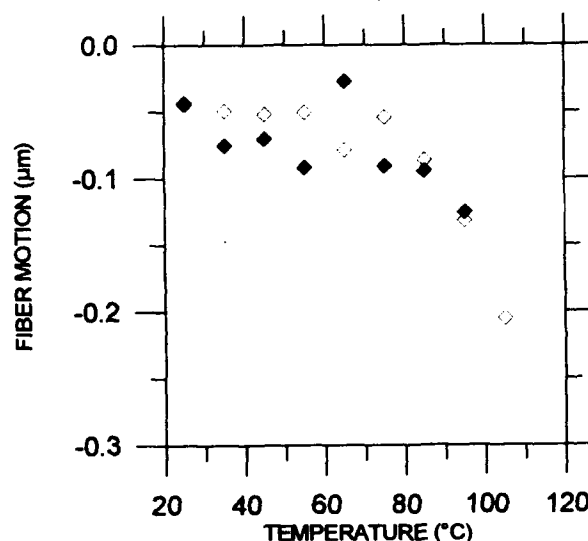
temperatures, commencing just above the T_g , the fiber began to withdraw at a much higher rate. There was also a small amount of permanent fiber withdrawal after the first cycle.

C. HAND-ASSEMBLED FERRULES UNDER LOAD

In our final series of experiments we measured the fiber pushback into hand-assembled fiber/ferrules under 0.5 lbf



(a)



(b)

Figure 9. Fiber withdrawal as a function of temperature for epoxy 2 with no load - 100 °C, 10 min. (a) first cycle and (b) second cycle.

load at ambient and at 65 °C. The ferrules used in this test were part of the same sample batches used in the no-load temperature cycling tests. Figure 10 shows the results of these measurements.

The ferrule samples were first mounted in the test fixture with 0.5 lbf load for 24 hrs. The amount of motion occurring during this time period is shown by the hatched bars. There is no apparent correlation of the amount of fiber pushback to either the epoxy cure schedule or the type of epoxy. Realistically speaking, we would expect to see some

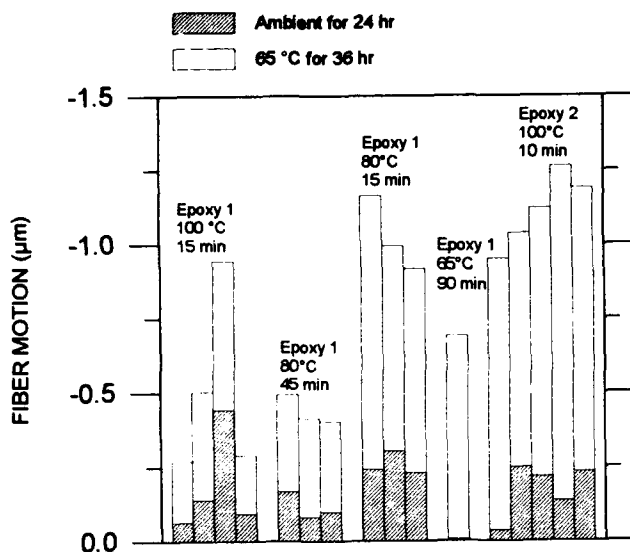


Figure 10. Fiber pushback in ceramic ferrules with 0.5 lbf (227 gmf) load using different epoxies and epoxy cure schedules.

correlation. The fact that we do not implies that other aspects of the assembly process are not under full control.

At higher temperatures, where epoxy creep starts to dominate, we begin to see a trend in the data. In Figure 10, the additional motion of the fiber after approximately 36 hrs at 65 °C is shown by the open bars. In general, we see that epoxy 1 has less motion than epoxy 2, even though epoxy 2 was fully cured. Epoxy 1, when virtually fully cured – 15 min at 100 °C – typically had less fiber pushback than the extremely undercured sample – 80 °C for 15 min – as expected. However, epoxy 1, when cured at 80 °C for 45 min, had a similar level of cure as the 65 °C, 90 min sample, yet the 65 °C cure experienced more fiber pushback. More data and analysis will be required to confirm and understand this phenomenon.

IV. DISCUSSION AND CONCLUSIONS

In this series of experiments we have looked at several different aspects of fiber motion in ceramic ferrules. First, we measured the amount of fiber pushback with respect to the ceramic ferrule in commercially available connector plugs under loads ranging from 0 to 1.5 lbf (680 gmf), under ambient conditions and at 65 °C. The loading forces were chosen based on measurements of spring-loading forces of connector plugs, typically on the order of 2 lbf (900 gmf), and the load was applied to the fiber only. The environmental conditions were picked to be stressful, but yet realistic for actual field situations; we do not consider these to be accelerated tests. We compared the amount of pushback in the artificially loaded plugs to that of connectors that were mated with standard coupling sleeves, and exposed to the same environmental conditions. Although the amount

of fiber motion in artificially loaded connector plugs could be unacceptably large, resulting in later loss of physical contact when the plugs were mated, the amount of fiber motion in connector plugs mated in the standard way was much less. In order to obtain an equivalent amount of motion, a loading force of less than 0.5 lbf (227 gmf) was sufficient in all cases.

We conclude that the ceramic ferrule, by sharing an increasing proportion of the spring loading force as the fiber is pushed into the ferrule, limits the total amount of fiber pushback. Obviously, both the ferrule endface geometry and the epoxy characteristics affect the total fiber motion. In the next stage of our investigations, we plan to consider the effect of ferrule endface geometry both theoretically and experimentally.

Based on the above results, we did a similar series of experiments with hand-assembled fiber/ferrules using two different epoxies and a variety of cure schedules, using only one, more realistic, loading force of 0.5 lbf (227 gmf). As in the earlier tests with connector plugs, the fiber/ferrules were first loaded under ambient conditions, and then the temperature was increased to 65 °C. However, unlike the earlier tests, the fiber was loaded for only approximately 24 hr at ambient and 36 hr at 65 °C. This was based on the results shown in Figure 3, which indicate that virtually all the fiber motion occurs during the first 24 hr of loading.

The results for the hand-assembled fiber/ferrules are shown in Figure 10. Both epoxy 1 and epoxy 2, when cured at 100 °C for 15 or 10 min, respectively, had essentially full cures. However, epoxy 2 had significantly greater fiber motion. Epoxy 2 had a lower T_g than epoxy 1, close to the operating range we were using in these experiments. Hence, it is not surprising that epoxy 2 showed more fiber motion under load at the higher temperature. We are pursuing independent investigations of the physical properties of the epoxies to confirm the cause of the different behavior. Epoxy 2 was also more viscous than epoxy 1, which resulted in more air bubbles being trapped during the mixing process. It was noted for both epoxies that there were occasional bubbles locked into the epoxy at the rear of the ferrule, where there was a wide funnel for the epoxy to fill. However, epoxy 2 had greater numbers of bubbles, sometimes close to the fiber. These could cause high stresses to develop, resulting in fiber fracture.⁵

The other cure schedules for epoxy 1 resulted in incomplete cures, as given in Table 2. Both the 80 °C, 45 min cure and the 65 °C, 90 min cure samples were slightly undercured. This was only apparent by DSC analysis of similarly cured epoxy droplets. Although the 65 °C cure samples showed more motion, with only one data point it is impossible to say whether this is significant. The 80 °C, 15 min cure sample was grossly undercured, and this clearly resulted in more fiber motion. In this case, the epoxy was noticeably tacky during the polishing process.

Our final series of experiments consisted of thermally cycling hand-assembled fiber/ferrules with no load, and measuring fiber withdrawal as a function of temperature. The temperature was cycled twice from room temperature up to 105 °C and back. The results generally correlated to the cure level and T_g of the epoxy. As long as the epoxy was fully cured, there appeared to be no permanent, significant fiber withdrawal, although there was a temporary withdrawal, due to CTE mismatch, over the temperature range. As long as the temperature was below the T_g of the epoxy, this motion was limited to 0.1 μm . However, temporary withdrawal as high as 0.2 μm was possible for an epoxy with a T_g of about 80 °C. The lower the T_g , the larger the expected withdrawal. In the case of a highly undercured epoxy, there was a large amount (0.2 μm) of permanent withdrawal.

Finally, we conclude that the amount of motion for the hand-assembled fiber/ferrules was often unacceptably large. Even in our "controlled" laboratory environment, we have had difficulty reproducing processes reliably, and we are still finding unexpected effects and unanticipated results. This points out the importance and difficulty of controlling assembly process conditions, which would be exacerbated in a field environment. In these experiments, commercially-available factory-assembled product performed satisfactorily when connected in standard mating sleeves. However, failures have been observed in other laboratory experiments, where connectors have been cycled to higher temperatures.⁶ Work will continue in this area.

V. ACKNOWLEDGMENTS

We would like to acknowledge the efforts of C. H. Hasz in the design of the test fixtures and B. Vaning in their fabrication. We also gratefully acknowledge the contributions of D. Dolinoy in the collection of the test data. Finally, we thank O. Gebizlioglu for useful conversations.

VI. REFERENCES

1. R. Ziebol, H. Roberts, and B. Daniel, "Permanent Fiber Withdrawal in Fiber Optic Connectors," Proc. 8th Annual NFOEC, Washington, DC, 1992, Vol. I, April, pp. 211-230.
2. L.A. Reith, R.M. Fagerstrom, G.D. Kiss, E.M. Vogel, W.W. Wood, and H.H. Yuce, "Performance of Ceramic-Ferrule Optical Connectors", Proc. 41st International Wire and Cable Symposium, Reno, NV, Nov. 16-19, 1992, pp. 792-800.
3. T. Shintaku, E. Sugita, and R. Nagase, "Highly Stable Physical-Contact Optical Fiber Connectors with Spherical Convex Ends", *J. Lightwave Tech.*, Vol. 11, February, 1993, pp. 241-248.
4. W.W. Wood and G.D. Kiss, "Procedures for Measuring Optical Performance of Fiber Optic Connectors", Proc. 8th Annual NFOEC, Washington, D.C., Vol. I, April, 1992, pp. 383-394.
5. M. Kinney, "Optical Fiber Stress in a Biconic Connector", Proc. 7th Biennial Conf. on Failure Prevention and Reliability, Boston, MA, DE-Vol. 9, Sept., 1987, pp. 75-79.
6. W.W. Wood, G.D. Kiss, L.A. Reith, E.M. Vogel, and H.H. Yuce, "Reliability of Interconnection Devices", Proc. 9th Annual NFOEC, San Antonio, TX, Book 3, June, 1993, pp. 209-221.

Leslie A. Reith received a B.A. degree from New York University in 1975, the M.Phil. degree from the City University of New York in 1979, and the Ph.D. degree from The University of Texas at Austin in 1981, all in physics. In 1981 she joined AT&T Bell Laboratories as a Member of Technical Staff. In 1984 she subsequently joined Bellcore, where she is presently a member of the Fiber Distribution and Reliability Research group in Morristown, N.J. Her research at Bellcore currently includes reliability issues related to optical splices and connectors.



Rolf A. Frantz is a Distinguished Member of Technical Staff in the Fiber Distribution and Reliability Research Group at Bellcore. He holds BS and MEng degrees from Cornell University and received his PhD at Brown University. He spent eleven years at Bell Laboratories, working principally on applications problems of dielectric materials, and he continued working in this area when he came to Bellcore in 1983. Since 1988, he has been concerned with the applications and reliability problems of fiber coatings adhesives, coloring inks, gels, and related materials used in manufacturing optical fibers, cables, connectors and splices.



Irene M. Piltz is a Member of Technical Staff in Bellcore's Plastics and Rubber Research Group. She graduated from Morgan State University in 1970 with a BS in chemistry and then joined AT&T Bell Laboratories. Since becoming part of Bellcore in 1983, Irene's interests have centered around the degradation, characterization, and reliability of polymeric materials used in the telecommunications industry.



William Wood is a Member of Technical Staff at Bellcore, Morristown, NJ. His current responsibilities include the analysis of fiber optic splices and connectors. Mr. Wood received a Bachelor of Science degree in Mechanical Engineering from Newark College of Engineering in 1955, and a Master of Science Degree in Engineering Mechanics from Columbia University in 1960. He joined Bell Telephone Laboratories in 1957 where he worked on the development of tools and equipment for use in the telephone system. He joined Bellcore in 1984.

Development of a Non-Blocking Opto-Mechanical Switch

Y.Hayashi H.Naidu Y.Nomura H.Yokosuka

Fujikura Ltd. Opto-Electronics Lab.
Chiba Japan

Abstract

A non-blocking opto-mechanical switch has been developed. This switch is assembled using cassettes which can be increased or decreased when necessary. Each cassette has a built-in ferrule moving mechanism. In this switch, any free input side ferrule can be automatically connected or disconnected to any output side ferrule without having to break other connections in the process. The switch was designed such that it is possible to change the matrix size by increasing or decreasing cassettes. The maximum matrix size is 100×100 . An average insertion loss of 0.64 dB was obtained.

1. Introduction

The use of optical fibers in subscriber networks has increased tremendously these past few years. It has become necessary to find efficient ways of installing and maintaining these networks. In particular, efforts at reducing the workload of construction require automatic switching capability.

Generally, an optical fiber switch should exhibit low losses, environmental stability, self latching and a fast switching time. An opto-mechanical switch can satisfy all of these stated conditions except that of a fast switching time. At present, it is advantageous to pursue a mechanical switching approach for practical use in subscriber networks.

In Japan, an operations system aimed at maintaining optical fiber networks and switching of lines has been introduced.

The opto-mechanical switch is being used in this system⁽¹⁾. However, as this switch is being used for selecting certain fibers only, it is not necessary for it to be completely non-blocking. In subscriber networks, since it is necessary to be able to connect any given input fiber to any output fiber, a completely non-blocking switch

exhibiting a large matrix in a compact size is required. Also, as far as the cost factor is concerned, a switch that is flexible enough to meet the changing number of fibers is desirable. For these requirements, various non-blocking mechanical switches have been developed on previously^{(2) (3)}.

In this paper, a completely non-blocking fully automatic switch using a cassette type unit that can be increased according to demand is described.

2. Design of the switch

2.1 Principle of switching

Figure 1 shows a principle of the non-blocking switching configuration. Each ferrule on the A-side can move in the x-direction of the matrix and those on the B-side in the y-direction. Non-blocking switching is accomplished by connecting the ferrules on each side at a unique matrix position for each ferrule combination.

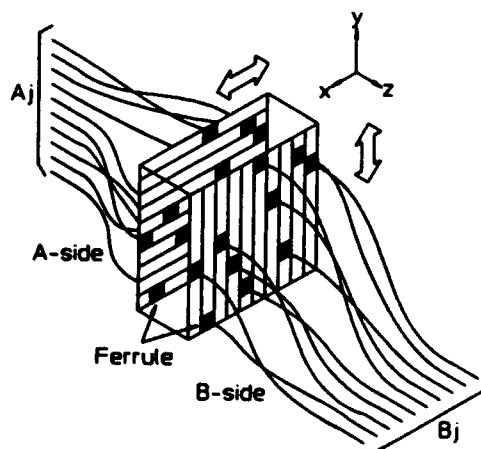


Figure 1 Principle of switching

2.2 Structure

2.2.1 Basic configuration

Figure 2 shows the basic configuration of the non-blocking switch. This non-blocking switch consists of two groups of cassette arrays and actuators. The groups are arranged to face each other at right angles. Each cassette has a ferrule terminated fiber. A ferrule can be moved in the longitudinal direction of the cassette. The actuator selects a cassette, moves the ferrule on the A-side in the x-direction and on the B-side in the y-direction, and joins the ferrules at a crosspoint. The movement range of the fiber terminated ferrule is within the cassette such that switching is accomplished without interference between the fiber and another fiber. It is possible to install or remove a cassette because a cassette forms a unit which includes a ferrule, a fiber and the movement mechanism. This means that, it is possible to change the matrix size.

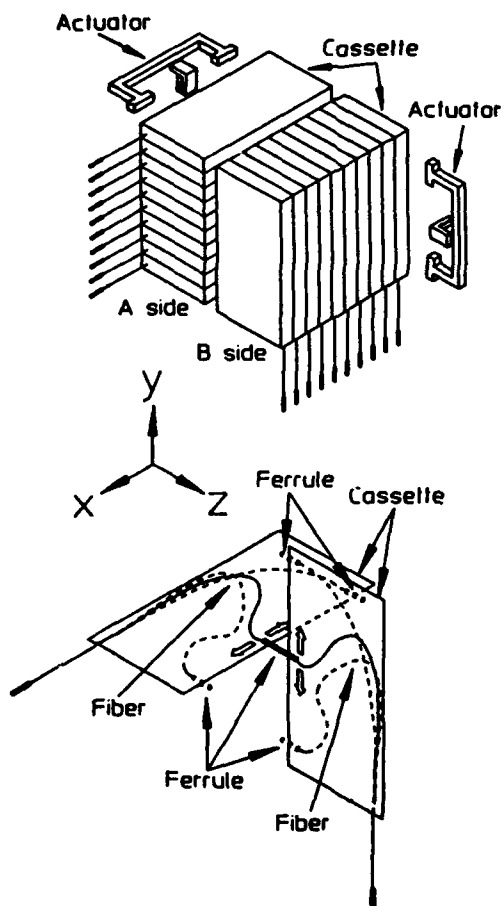


Figure 2 Basic configuration of the switch

2.2.2 Cassette structure

Figure 3 shows the structure of the cassette. A cassette consists of a switch-plate and a container. The switch-plate is composed of a slider in which a ferrule and a fiber are built, a rail which guides the movement of the slider, a wire which is attached to the slider, four pulleys which guide the wire and give tension to the wire, a hook shaped part, and finally a fiber terminated ferrule. The container consists of a base part and a cover. The switch-plate is located between the base and the cover and can be moved in the z-direction by a guide of the container. Each container is fixed to the machine frame.

The switch-plate is pulled in the z-direction by tension springs suspended between a container and a switch-plate. The switch machine frame has grooves for a cassette, so that the cassette can be easily installed and positioned precisely.

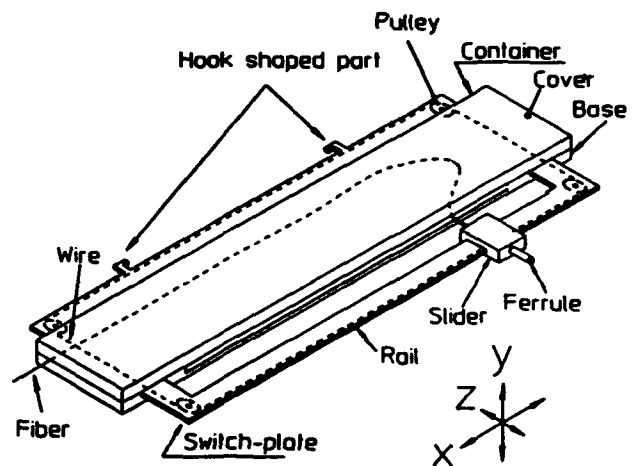


Figure 3 Cassette structure

Figure 4 shows the structure of the slider. A zirconia ceramic ferrule with a diameter of 1.25 mm is built in the slider. An alignment sleeve is fixed to a ferrule on one side (to a ferrule on the B-side in Figure 4). Through this alignment sleeve, precise connection is achieved. The slider which has the ferrule with the alignment sleeve has a taper. The ferrules also have a taper. These tapers help to connect the ferrules even if the sliders have a positioning error of 0.5 mm. The connection force is provided by a compression spring located between the slider and the ferrule.

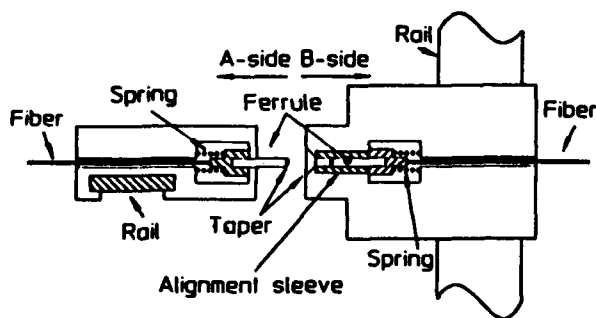


Figure 4 Slider structure

2.2.3 Actuator structure

Figure 5 shows the structure of the actuator. The actuator consists of a wire-hand and a switch-plate-hand. The wire-hand is composed of a wire gripping mechanism and a wire pulling mechanism. The switch-plate-hand selects a cassette by moving in the y-direction on the A-side and in the x-direction on the B-side and pulls the switch-plate in the z-direction outward from the container by hooking the hook shaped part. The wire-hand grips a wire on the opposite side of the cassette rail. The wire-hand pulls and moves the wire in the x-direction on the A-side, and then the slider is moved in the opposite direction of the wire-hand.

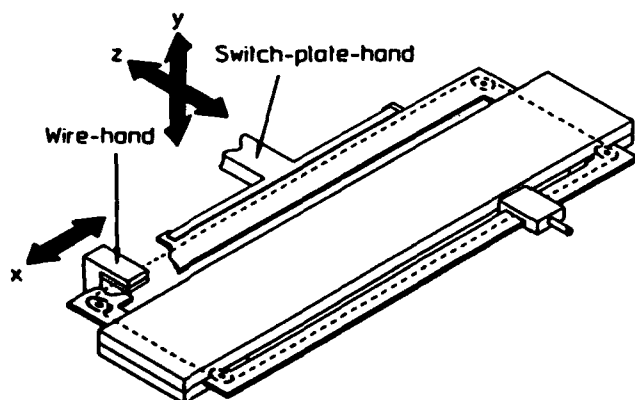


Figure 5 Actuator structure

2.3 Switching procedure

The switching of the A-side and the B-side is automatically performed at the same time and by the same procedure except for the distance moved by the actuator and the slider. The switching procedure in the A-side is described by the following.

- (1) The switch-plate-hand selects a cassette by moving in the y-direction. The switch-plate-hand pulls the switch-plate in the z-direction, releasing the existing ferrule connection.
- (2) The wire-hand grips the wire and moves the wire in the x-direction, so that the slider to which the wire is attached is moved in the opposite direction of the wire-hand. The slider is stopped at the end of the rail by a protrusion. Subsequently the wire-hand senses the increase in the wire tension and stops. Thus, the origin of the slider is determined.
- (3) The wire-hand moves the slider to the position, where the B-side cassette is located, and releases the wire.
- (4) The switch-plate-hand moves in the z-direction. The switch-plate is pulled into the container by tension springs suspended between the switch-plate and the container.

The same procedure as the A-side is carried out on the B-side. Thus the ferrules are connected.

3. Performance

3.1 Features of the developed switch

Actually, 10 cassettes are installed in the center of the each side. A small 10x10 matrix was fabricated in the center of a 100 × 100 matrix. Table 1 shows the size of the switch. The switch size is 650^w × 450^d × 460^h. The ferrule-pitch is 3 mm. The cassette is thin because no actuators or sensors are contained within the cassette.

3.2 Positioning error

The allowable slider positioning error in the movement direction is estimated to be 0.5 mm of the mechanical clearance and taper of the sliders and the ferrule-ends. The fluctuation magnitude of stationary positions on the sliders was measured 5 times for 10 combinations of cassettes with a digital vernier scale. The results are shown in Table 2. The maximum fluctuation was 0.07 mm. The average fluctuation was 0.04 mm.

3.3 Switching speed

The switching speed is dependent on the initial position of the switch and the required cassette position. The switching time was measured with the machine starting from the origin, finishing the switching and returning to the origin. Table 3 shows the switching time. The shortest switching time was 52 seconds for the cassettes which were nearest to the origin. The longest switching time was 88 seconds for the cassettes which were furthest from the origin. The switching time for the cassettes in the center of the matrix was 72 seconds.

3.4 Insertion loss

This switch has three connections at the input and output sides and the ferrules for switching. Therefore, the insertion loss of this switch is the sum of the losses of these three connections.

Conventional zirconia ferrules are used for the input and output sides of the switch. 10/125 μm single mode fiber was used in this switch. Figure 7 shows the insertion loss measurement setup. A 1.3 μm wavelength LED light source was used. The histogram of insertion losses of 100 combinations of cassettes for a 10×10 matrix is shown in Figure 8. The average insertion loss was 0.64 dB.

3.5 Loss fluctuation

Table 4 shows the loss fluctuation of five repeated switchings. A maximum loss fluctuation of 0.12 dB was obtained. The average loss fluctuation was 0.02 dB.

Table 4 Loss fluctuation

Maximum	0.12 dB
Average	0.02 dB

4. Conclusions

A non-blocking opto-mechanical switch has been developed. The switch is assembled using cassettes which can be increased or decreased when necessary. The maximum matrix size is 100×100 where 100 cassettes each are used for both input and output sides. The ferrule-pitch was 3 mm. The average insertion loss was 0.64 dB.

Table 1 Size of the switch

Matrix size	100×100
Dimensions	$650^{\circ} \times 450^{\circ} \times 460^{\circ}$ mm
Ferrule-pitch	3 mm

Table 2 Positioning error

Maximum	0.07 mm
Average	0.04 mm

Table 3 Switching time

Minimum	52 seconds
Maximum	88 seconds
For the center cassettes	72 seconds

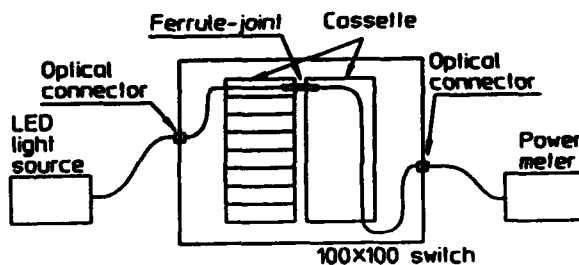


Figure 7 Loss measurement setup

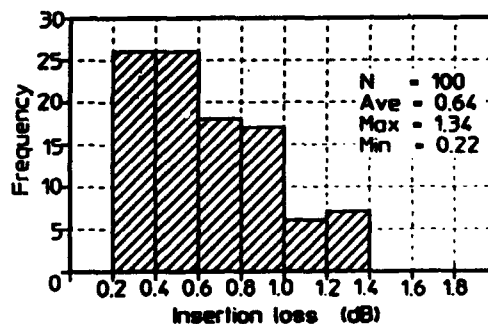


Figure-8 Insertion Loss

References

- (1) Y.Tamaki, et al., "MT-type Fiber Selector for Optical Fiber Monitoring System", 41st IWCS, pp.820-825, 1992.
- (2) T.Katagiri, et al., "NONBLOCKING 100 × 100 OPTOMECHANICAL MATRIX SWITCH FOR SUBSCRIBER NETWORKS", 40th IWCS, pp.285-290, 1991.
- (3) T.Katagiri, et al., "Cassette-Type Non-blocking 100 × 100 Optomechanical Matrix Switch", IEICE Trans. Commun., Vol.E75-B, No.12 December 1992, pp.1373-1375.



Yukio Hayashi
FUJIKURA LTD.
Opto-Electronics Lab.
1440 Mutuzaki
Sakura City, Chiba
Japan

Yukio Hayashi was born in 1963. He received the M.E. degree in mechanical engineering from Chiba University in 1988.

He joined Fujikura and has been engaged in research and development in the Fiber and Cable Accessory Section.

Mr. Hayashi is a member of the IEICE of Japan.



Yoshikazu Nomura
FUJIKURA LTD.
Opto-Electronics Lab.
1440 Mutuzaki
Sakura City, Chiba
Japan

Yoshikazu Nomura was born in 1951. He graduated in mechanical engineering from Shinshu University. He has been engaged in the research and development of the telecommunication cables and accessories. He is presently a manager in the Fiber and Cable Accessory Department.



Hariharan Naidu
FUJIKURA LTD.
Opto-Electronics Lab.
1440 Mutuzaki
Sakura City, Chiba
Japan

Hariharan Naidu was born in Perak, Malaysia. He graduated from the National University of Singapore with a degree in mechanical engineering in 1990. He joined Fujikura in the same year and has since been involved in the research and development of telecommunication switching devices and connections.

Mr. Naidu is a member of the Institution of Mechanical Engineers U.K.



Hiroshi Yokosuka
FUJIKURA LTD.
Opto-Electronics Lab.
1440 Mutuzaki
Sakura City, Chiba
Japan

Hiroshi Yokosuka graduated in mechanical engineering from the Tokyo Metropolitan Technical Junior College in 1967. He has been engaged in the development of telecommunication cables and accessories. He is presently the general manager of the Fiber and Cable accessory Department.

Mr. Yokosuka is a member of the IEICE of Japan.

PERFORMANCE OF CURRENT LOCAL CABLE DESIGNS IN HIGH BIT RATE APPLICATIONS

G. D. Maltz, Ch. Chojetzki, J. Schulte, G. Verdenhalven, K. Verlande

Kabelmetal Electro GmbH
Postfach 260
30002 Hannover, Germany

Summary

Copper cables from current production and deployed in different countries for local telephone applications are also widely used for high bit rate transmission. Future use may include bit rates in excess of 2 Mbit/s. Cable performance varies significantly with cable design and manufacturing techniques practiced in different countries. Measurement results are supplied on a wide range of cable designs using either twisted pair or quad construction. Different national cable specifications and standards are reviewed. Evaluation methods of automated cable measurements are compared to the practical needs in the planning and operation of public local networks. It is shown that a number of different aspects of design and manufacturing processes are influencing the high-frequency crosstalk performance of conventional distribution cables.

Background.

Fiber optic cables are without doubt the best solution for very high bit rate and long-distance transmission. However, expensive optoelectronic components as well as the already existing copper cable plant hinder the rapid deployment of fiber optic technology in local short-distance applications. New approaches in FITL (Fiber in the Loop) installations also make use of copper distribution cables. Advances in digital technology have opened doors for the transmission of high bit rates "in the last mile" over existing copper twisted pair or quad cables if HDSL techniques, like CAP or 2B1Q are used to reduce noise problems, such as crosstalk. In some cases specially-designed symmetrical or coaxial copper cables must be installed in-house. Nevertheless, the knowledge of crosstalk-generating mechanisms in symmetrical copper cables is an important factor in transmission system evaluation.

History of Pairs and Quads.

The development of telephone cables in the world has gone into two different directions in the last 100 years. While the U.S.A. has adopted the pair as the predominantly used cable element, many European countries use the star quad as the smallest cable component. The debate of the relative advantages and disadvantages of both technologies is almost as old as the telephone cable itself. The overhead line of one single conductor with return ground gave way to paired symmetrical circuits for overhead line installations as well as for buried or aerial cable applications (Fig.1). The Pupin loading of cables called for an additional telephone line which rendered possible the phantom circuit. This signaled the introduction of the Dieselhorst-Martin quad (DM quad). The DM quad is a two-pair stranded element, of which each pair has a different lay length.^{1,2} This construction offered particular advantages during loading of the phantom circuit. It was not until the 1920s, when carrier frequency utilization of the cables became possible and Pupin loading was abandoned, that the star quad gained acceptance. The star quad offered distinctive commercial advantages.^{1,3,14}

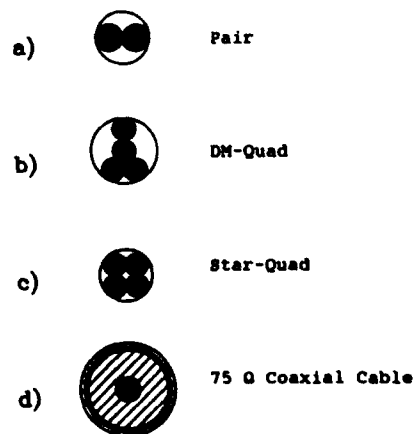


Fig. 1 Stranding elements

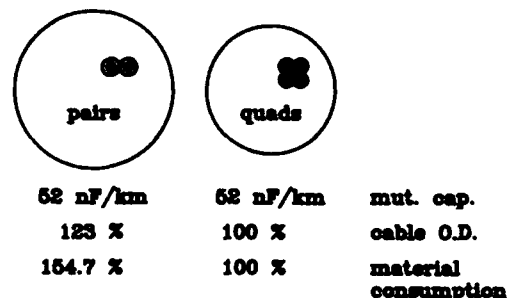
A simple calculation confirms that under given conditions of conductor number, size and mutual capacitance (i.e.: same attenuation and range) in the local network the paired cable has a 23% larger diameter and its material consumption is 54.7% higher than that of a quad cable (Fig. 2a). Under the given conditions of same cable diameter, the mutual capacitance of the quadded cable is 14.4% lower. Its attenuation in the voice frequency range is therefore 8% lower than that of its paired equivalent. Only in the 1 MHz range is the attenuation nearly the same due to the proximity effect of eddy currents (Figs. 2b and 3).*

Theoretically, the star quad offers total decoupling of both circuits of the quad with respect to each other because the electro-magnetic fields, as a result of geometry, are orthogonally oriented. However, practice quickly revealed considerable side-to-side capacitance unbalances caused by geometrical or electrical imperfections. However, it did not take long for the cablemakers to master the side-to-side coupling. As a result, the star quad found wide acceptance in long-distance networks for operation up to 552 kHz, especially in Germany.

One of our in-plant investigations more than 20 years ago confirmed that analog carrier frequency operation with system V 300, i.e. up to 1.3 MHz, is possible with these cables. However, this called for special balancing of the residual coupling of the line. In order to compensate for the effect of the side-to-side far-end crosstalk in the quad it was necessary to introduce additional systematic splice crossings between the circuits of the quad.^{9,12} Fig. 4 illustrates the relationship of these complex interactions. It is remarkable, that the invention of the S2 stranding technique in the late 1960s theoretically renders unnecessary these splice crossings because the continuous change of the direction of lay has the same effect.

The introduction of star quad cabling in Germany called for the adaptation of the cable machinery to this new situation. During the following 70 years the technology was improved to the point where we now dispose of high-precision, highly efficient machines. In spite of widespread diverging opinions the electrical characteristics of local star quad cables fabricated with this machinery are matching or exceeding those of paired cables in nearly all voice and high frequency applications, as we shall demonstrate below.

a) for the same mutual capacitance:



b) for the same cable diameter:

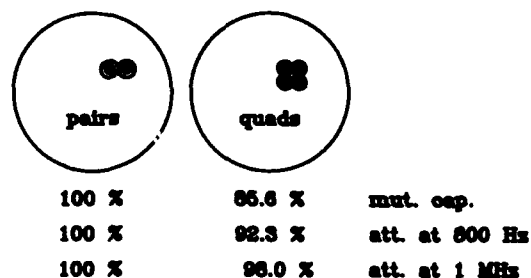


Fig. 2 Comparison between pairs and quads

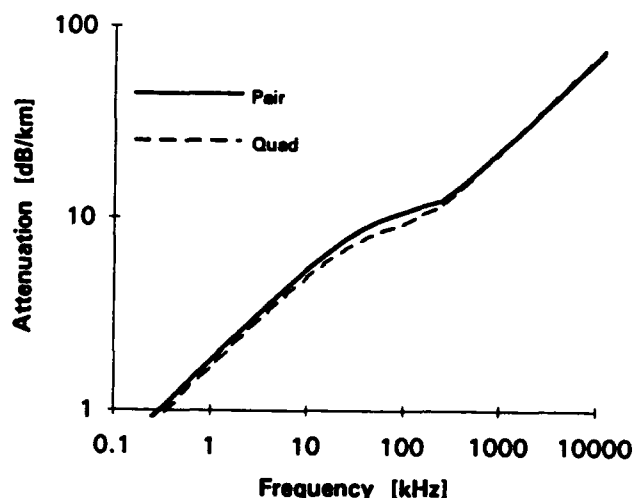


Fig. 3a Attenuation of pairs and quads (for a given cable diameter)

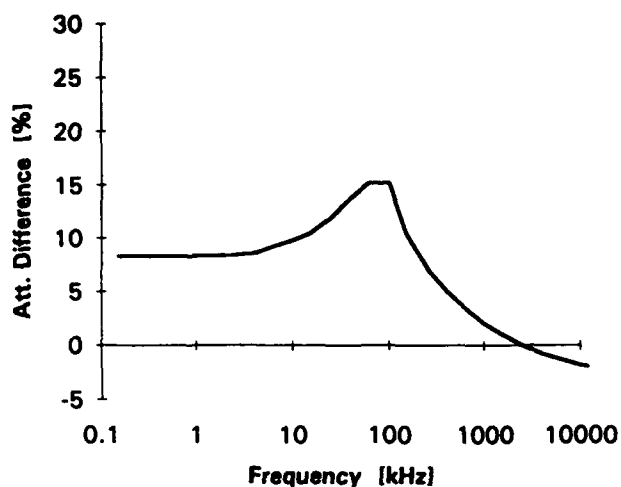


Fig. 3b Difference of attenuation between pairs and quads for a given cable O.D. (referenced to attenuation of quads)

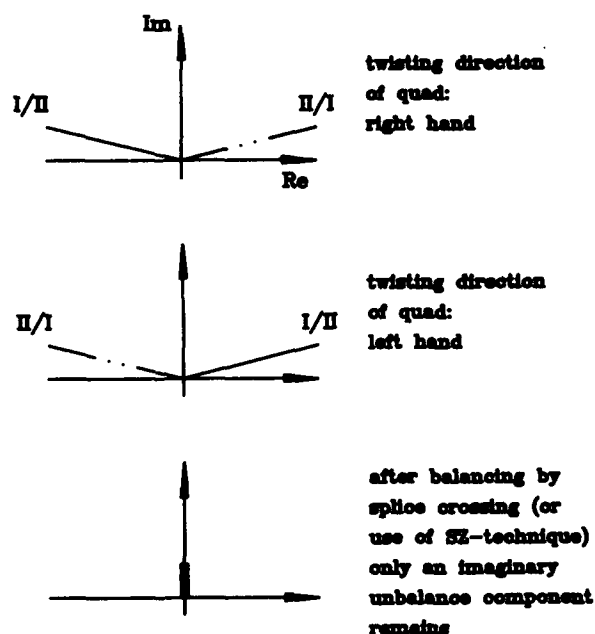


Fig. 4 Side-to-side changing effect of far-end crosstalk (FEXT)

Economical Impact of Local Networks.

Fig. 5 shows the density of the telephone networks (main lines, called "access lines" in the U.S.A.) per 100 inhabitants in different countries since the start of this century.⁶ Both world wars and the economic crisis of 1930 are noticeable in the curves. For example, the average annual growth over the past ten years was 20.1% in Turkey, 3.8% in Germany, 2.7% in the U.S.A. and only 2.0% in Sweden. This shows that the industrial countries are nearly - but not entirely - saturated.¹⁷

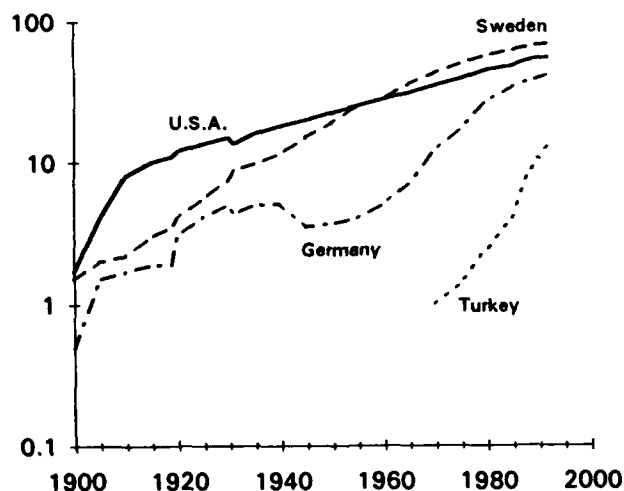


Fig. 5 Access lines per 100 inhabitants

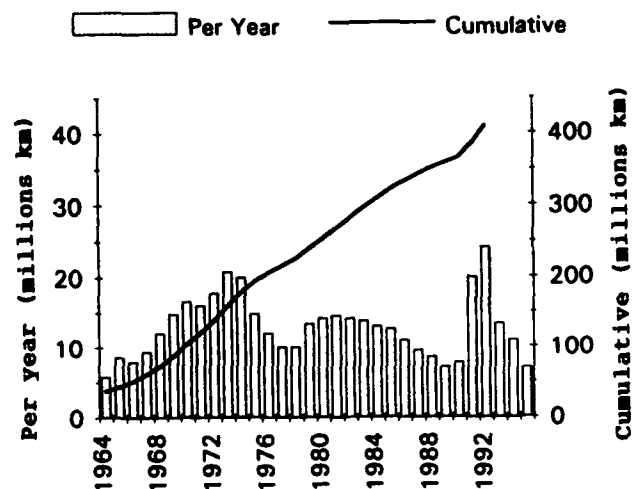


Fig. 6 Shipments (millions km) of local copper cable in Germany (Telekom)

If we add up the yearly order quantities of the German PTT (Fig. 6) it becomes possible to estimate that the installed local telephone network in Germany covers about 320 million conductor-kilometers. Of particular interest is the rapid rise of order quantities in 1991/92 resulting from the retrofitting requirements in the reunited Eastern Germany. The fixed value of the worldwide installed copper cable telephone network is estimated at several hundred billion Dollars.

Little is known about the estimated life time of the telephone network in other countries. As to Germany, the introduction of the plastic-insulated cable technology in the 1960s with its related high quality requirements enables us to forecast an expected life time for these cables much in excess of 30 years.

It is now clear that it is possible to upgrade cable networks that have been installed more than 20 years ago through the use of improved digital electronics at 2 Mbit/s rate, for example, without any problem. This shows that high frequency crosstalk limitation via new cable specifications is generally an additional, although not always, mandatory requirement for new copper cable installations. It is of course possible to find different situations depending on the condition of the network and the line technique implemented by different countries.¹² Whatever the case may be, the existing copper network is a worldwide economic factor that cannot be ignored and which must be utilized, maintained and also extended in the future by the cost-conscious network operator.

Cable construction.

As previously mentioned, the 1960s saw the rapid transformation of the concentric layer-stranded, paper-insulated cable construction into polyethylene-insulated, unit-stranded cables. This evolution was almost worldwide, whereby it is insignificant whether or not it was started from paper-pulp insulated or paper-tape wrapped conductors. Solid polyethylene insulation for 0.4 mm (No. 26 AWG) conductors was replaced by foam- and foam-skin insulation, especially for heavier conductors. It is to be noted that pair stranding exhibits higher mutual capacitance in the cable than the star quad. This results in increased attenuation for paired cables.¹ As to the material, the attenuation of paper-insulated cables shows a steep increase at higher frequencies. Therefore, the use of this type of cable in the MHz-range is not recommended.

High conductor counts in the cable, manufacture and installation needs, made necessary the replacement of the concentric stranding by unit construction.

The dimension of the bundle units is not uniform throughout the world. In Germany 5 quads (i.e.: 20 conductors) make up a unit, whereas in some countries 10 pairs are stranded into a unit. In the U.S.A. 12, 13 or 25 pairs make up a unit. Based on optimum stranding geometry, the French use 1+6 or 4+10 stranding elements in 2 layers as units, whereby 7 or 14 quads are operational (Fig. 7). We do not know of any units in excess of 28 pairs. They would cause problems with respect to color identification of the single conductors. In Germany, as a derivative of the previously mentioned paper cabling technique using imprinted paper with bandmark identification, the four insulated conductors of a quad are individually ring-marked according to VDE specifications. The five quads of the basic unit are identified by the five basic colors: red, green, grey, yellow and white. This permits easy identification of individual conductors in a unit even after all conductors of a unit are mixed during the installation.

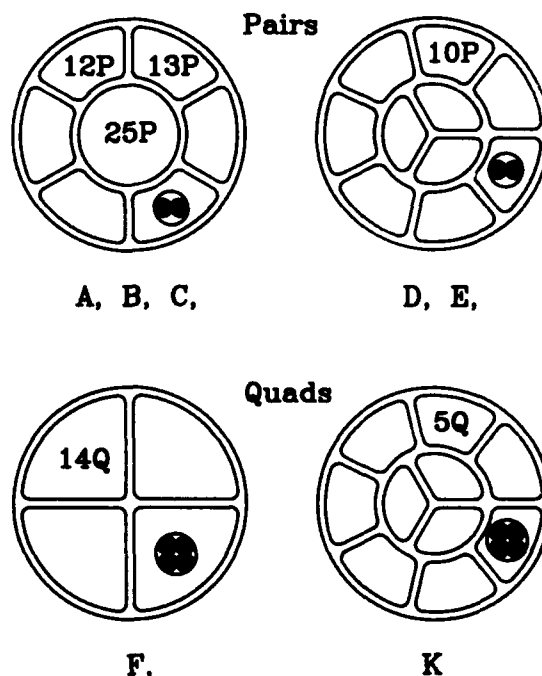


Fig. 7 Different designs of tested cables

Stranding Techniques. Length of Lay Design.

Stranding Element. Pairs are manufactured on a pair twister, in double twisting machines without back twisting or with the SZ strander. Star quads can also be fabricated on double-lay machines with or without back twisting, on conventional quad stranders or with the economical SZ stranding technique.

Unit Bundle. Stranding elements form the unit bundle by being stranded into one or two layers using conventional techniques or with different SZ stranding methods.

Main Bundle. Several unit bundles or parts thereof are stranded into a main bundle. In 100-pair cables the main bundle also serves as the cable core. This is the cable type on which we based our comparative measurements for this paper.

It is possible to combine two or three stranding operations. In modern SZ stranding this applies to the stranding element and the unit bundle (Fig. 8).²⁰ Other modern stranding techniques also combine some operations. It is therefore possible to achieve a controllable, high and uniform quality standard in continuous production without manual intervention or disruptive steps. In addition, the man/machine relationship (i.e.: number of operators per machine or combined operation) is a significant factor in countries where wages are high. Some aspects of SZ cabling gained from our experience with the process are listed in Table 1. The SZ strander is illustrated in Fig. 9.

Finally, the quality and efficiency of the stranding process also depends on the lay length design which, in turn, basically affects the crosstalk. As a rule-of-thumb we assume that a lay length reduction by one-half improves the crosstalk by about 6db. 2,4,10,11,16

Cable Parameters.

The following parameters are measured in paired cables: conductor resistance, resistance unbalance, capacitance, capacitance unbalance between pairs and to ground, crosstalk attenuation, dielectric strength, insulation and mechanical properties. In addition, in quad cables it is necessary to distinguish crosstalk within the quad and between quads.

- Continuous production
- Large core reels (630 mm flange diameter)
- Material savings (3...4 %, no core-remains)
- Combined conductor and unit stranding process
- Very high number of twists per minute
- High production speed (max. 200 m/min.)
- Very large unit production lengths (up to 50 km)
- Reduced manpower (50 %)
- Up to 25 stranding elements, pairs or quads.

Table 1 Features and advantages of SZ cabling

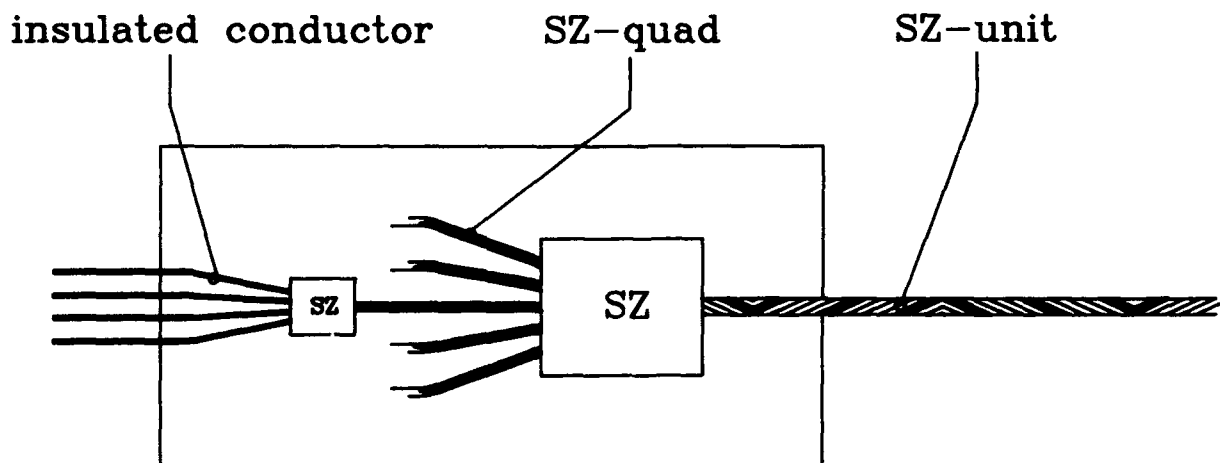


Fig. 8 Combined SZ-stranding

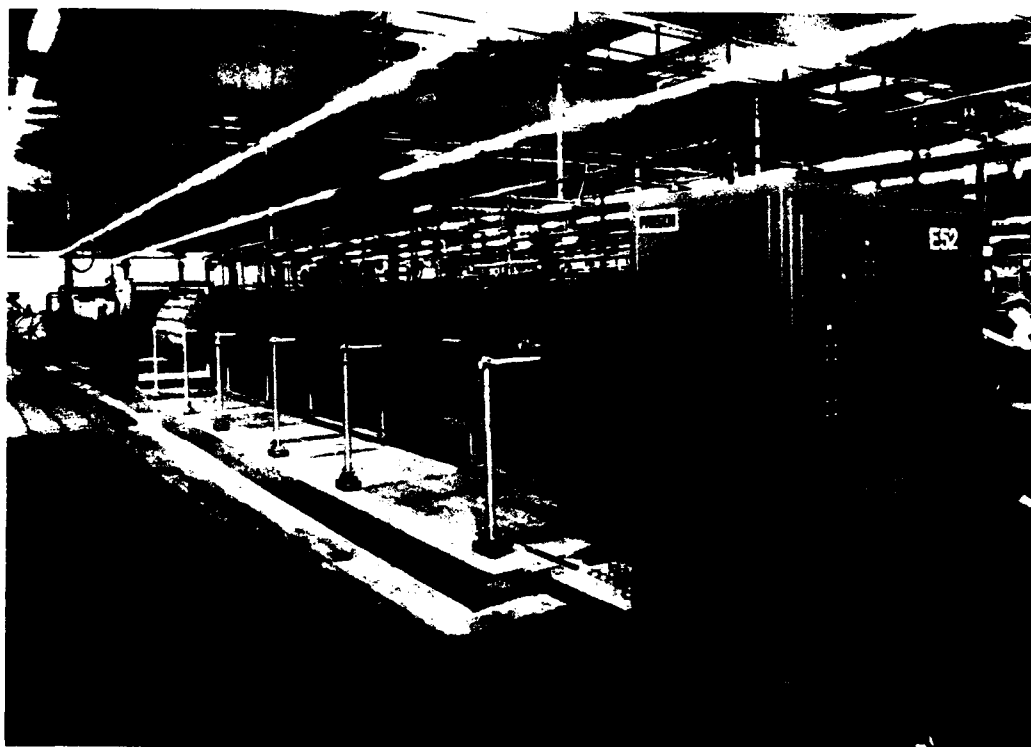


Fig. 9 SZ Strander in Kabelmetal's Stadthagen plant

Crosstalk attenuation values between two quads are identified by a_9 through a_{12} , whereby a_9 represents the crosstalk between circuit 1 of quad 1 and circuit 1 of quad 2, etc. up to a_{12} which relates to crosstalk between circuit 2 of quad 1 and circuit 2 of quad 2. For the capacitance unbalance to ground we distinguish $E_1 \dots E_3$, or unbalance to shield $E_{a1} \dots E_{a3}$.

For high-frequency applications, the crosstalk attenuation near-end (NEXT) and far-end (FEXT) measurements which are defined in Fig. 10, are important.² Other significant factors are: the characteristic impedance and its longitudinal uniformity over the length of the cable and the attenuation unbalance, i.e.: the ratio in db of the balanced voltage to the voltage between center tap and ground. There is also the attenuation constant which is determined by the geometry as well as by the material properties of the cable. The distribution of the crosstalk over the length of the cable can be determined, if required, with pulsed crosstalk test equipment in the time domain.¹⁹

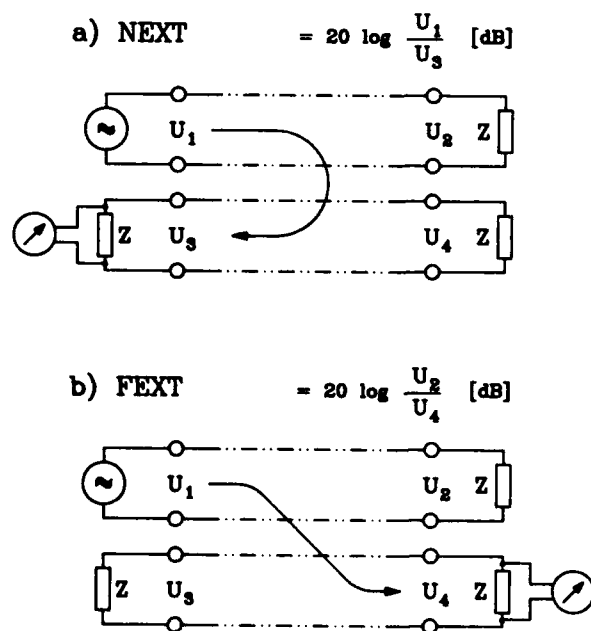


Fig. 10 Definition of crosstalk

PCM Applications.

The carrier frequency technique previously mentioned is controlled by systems which transmit up to 120 or even 300 voice channels over a symmetrical 4-wire circuit. This analog technique requires about 60 dB signal-to-noise ratio. This is a significant, distinct difference from the PCM technique which can be satisfied with signal-to-noise ratios of less than 6 dB, depending on the coding and the particular system. On the other hand, the PCM technique has the singular disadvantage in that it requires a relatively large frequency range to accommodate the PCM signal. The conventional PCM technique requires 8 MHz bandwidth for the transmission of 120 voice channels. In general, symmetrical cables are used only up to 2 MHz, that is for PCM 30, resp. 1.5 MHz for 24 channels of the T1 system. Multiple step codes which serve to limit the required bandwidth have been implemented more recently. Another technique consists of subdividing the required frequency band, after filtering, into several circuits. All of these measures result in a substantial reduction of the required bandwidth and serve to improve the signal-to-noise ratio which is particularly critical at high frequencies, because crosstalk attenuation of a multicore cable decreases with frequency.^{5,7,10,21}

The examination of crosstalk is an important measure in determining the suitability of a cable in a PCM system. In the course of our comparative measurements on local cables we took it for granted that far-end crosstalk is not critical in most applications. Instead, we concentrated our efforts to the measurement of near-end crosstalk (NEXT). Furthermore, we conducted our measurements using five discrete sine wave frequencies instead of PCM-pulses, well understanding that the noise power within the full frequency range of the digital signal is the deciding factor for PCM applications. This power is mainly responsible for the bit error rate (BER) in the discriminator stage of the PCM receiver. In random sampling we swept the NEXT over the 20 kHz to 15 MHz frequency range. These curves of NEXT vs. frequency show many maxima and minima. However, our measurements on five discrete frequencies are sufficiently representative of the noise power of the full range. The crosstalk attenuation measurement corresponding to the individual sinewave frequency was thus evaluated according to particular models. Specifications strictly used in this connection were: REA PE-89, 7CFR1755.890 and ICEA Publication S-84-608-1988.

In the course of our 100% testing we evaluated the following parameters for the unit bundle, for other selected groups of conductors and for the complete cable:

maximum value	max
minimum value	min
arithmetical average	\bar{x} (or mean)
standard deviation	s
difference	$\bar{x} - s$
individual power sum	IPS
worst power sum	WPS
mean power sum	MPS
root mean square	rms

We learned that the mean power sum and worst pair power sum are the most important values. The arithmetical mean of crosstalk attenuation, for example, depends strongly on the performance of the measuring equipment: the better the equipment the higher this value! In our investigations we measured different cables with the same equipment. Therefore, the results of the arithmetical mean value \bar{x} are well suited for a comparison of our different cable designs and manufacturing processes employed.

According to our observations, the above-mentioned REA- and ICEA-Specifications are the most stringent specifications known for local cables. Until now some PTTs do not specify high-frequency requirements for local cables. In PCM applications they select a small number of circuits out of the cross-section of the cable. Therefore, 100% connection to PCM systems of all conductors in the cable is not planned in the network. Our own experience gained from turnkey projects conducted in recently acquired areas of the former East Germany, as well as with the OPAL and FITL programs confirmed that, as a rule, there is no local subscriber area requiring 100% service at 2 Mbit/s. Normally not more than 10% of conductors of a cable are needed for high frequency applications. It may well be that this figure will slightly increase in the future.

Measurement Technique.

In our experiments we used an automated test equipment capable of covering the voice and high frequency ranges up to 10 MHz. A recent improvement of the equipment enabled us to connect 2x200 conductors in one operation.

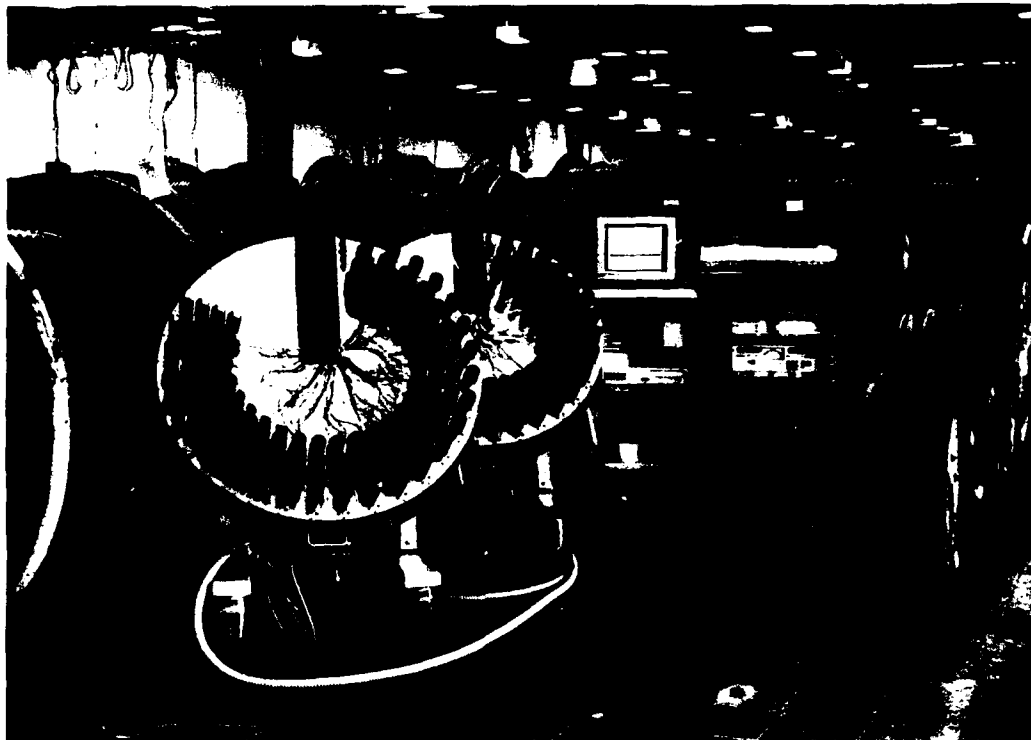


Fig. 11 Automatic cable test equipment type REKAMAT IV in Kabelmetal's Stadthagen plant

Frequency range:	NEXT, FEXT, Meas. range:	Accuracy:
1 kHz to 1 MHz	1... 87 dB	± 0.3 dB
	87...107 dB	± 0.8 dB
	107...120 dB	± 2 dB
1 MHz to 3.15 MHz	1... 87 dB	± 0.3 dB
	87...107 dB	± 0.8 dB
	107...110 dB	± 2 dB
3.15 MHz...10 MHz with shielded characteristic impedance termination:		
NEXT between different segments	to 6.3 MHz	> 110 dB
	to 10 MHz	> 100 dB
NEXT within same segment	to 6.3 MHz	> 105 dB
	to 10 MHz	> 100 dB

Table 2: Attenuation and crosstalk measurements using Automatic Cable Test Equipment type REKAMAT IV

Cables with 100 Pairs, conductor size 0.4 mm (# 26 AWG)					
cable type	twisting of cores	stranding of pairs	unit	stranding of units	cable
A	cont.	with oscillator	25 p/unit; 12 p/subu., 13 p/subu.	cont.	1x25 p-unit +6 subunits
B					
C	SZ comb.	SZ comb.			
D	cont.	random stranding	10 Pairs	cont.	3 + 7 units
E					

Table 3: Design and Processing of Measured Pair-Cables

Cables with quads, conductor size 0.4 mm (#26 AWG)					
cable type	stranding of cores	stranding of quads	unit	stranding of units	cable
F	cont.	cont.	4+10 quads	cont.	4 units
K	SZ comb.	SZ comb.	5 quads	cont.	3+7 units
(designed for voice frequency applications mainly)					

Table 4: Design and Processing of Measured Quad-Cables

This size of the connection frame enabled us to conduct evaluations which we could not accomplish through multiple connections with smaller frames. Since a full description of the properties of a cable design or cable manufacturing techniques can be gathered only through a large series of individual measurements, we conducted 100% testing. The measuring accuracy of the equipment is very high. Some information is given in Table 2. For voice frequencies a measurement resolution of 1 pF is provided with an accuracy of 0.5% of RDG +2 pF for mutual capacitance and 2% of RDG +2 pF for capacitance unbalance. Measurement frequencies of 800 or 1000 Hz or 127 Hz are provided. Measurement procedure, print-out of protocols and evaluation of results can be programmed to special requirements and called up by the operator. A photograph of the equipment is shown in Fig. 11.

Measurements.

We used a total of ten 100-pair cables for our measurements. Most cables were pulled from current production in different countries. Some were experimental cables with optimized properties. Others were designed especially for high-frequency applications. The paired cables under consideration are listed in Table 3 and some of the quad cables in Table 4. Each of these cables features 4,950 crosstalk combinations, as all symmetrical circuits are measured against each other. Considering that there are ten cables and five frequencies we arrive at 247,500 individual NEXT-measurements that had to be conducted for this paper. In addition, we also measured the cables at voice frequencies. The equipment used enabled us to perform this in one single frame connection. Altogether we gathered about one-half million individual test data.

Results and Conclusions.

The large volume of test data was evaluated and reduced for presentation in Figs. 12 through 15. The main results are:

1. The theoretical considerations (Fig. 3) have been confirmed through our measurements (Figs. 12 and 13). Paired cables show significantly higher mutual capacitance than quad cables. In addition, some customer specifications for paired cables (cable A) call for even higher values than we measured on cable C. Cable C was manufactured from cores of the same diameter as are used in quad cable K. Therefore, the attenuation differences between paired cables and quad cables are significantly high (Fig. 13).

This holds especially true for the frequency range up to 200 kHz which corresponds to the frequencies used in the ISDN basic line transmission. This is of major importance for local copper distribution networks.

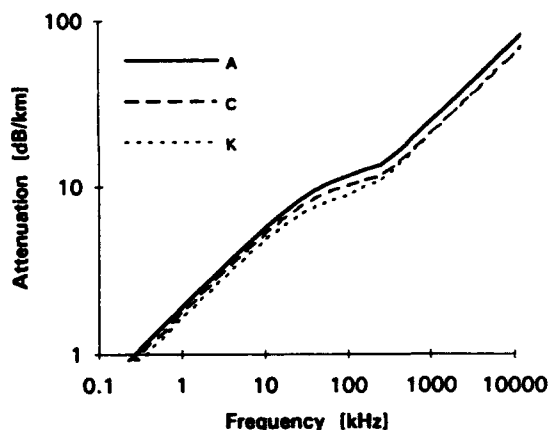


Fig. 12 Attenuation of cables A, C and K

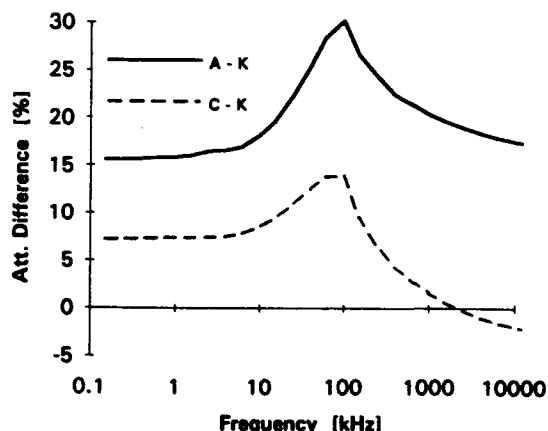


Fig. 13 Attenuation difference: A-K, C-K

2. The insulation thickness of the conductors in cable A is so small that the technological limits of foamed polyethylene extrusion may be reached. If a further reduction of the wall thickness will be demanded, the risk of short-circuits during installation may dramatically increase. In some countries only solid polyethylene insulation is specified.

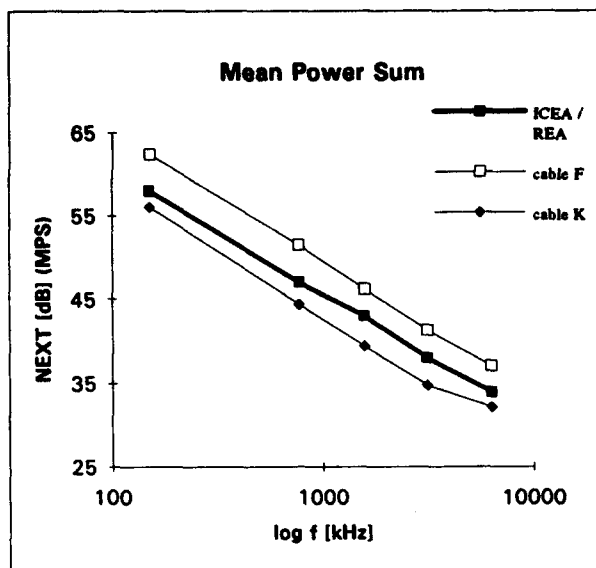


Fig. 14a Crosstalk of cables with quads (mean power sum)

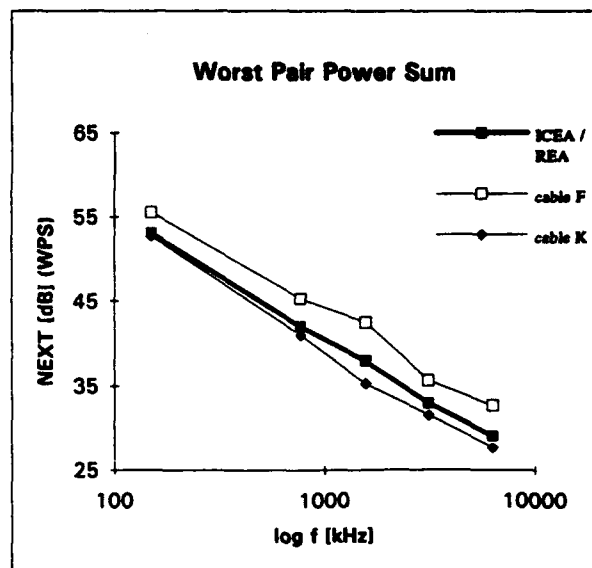


Fig. 14b Crosstalk of cables with quads (worst pair power sum)

3. The crosstalk behavior of the quad cables is shown in Fig. 14. Cable K is designed and manufactured for low frequency applications and does not completely meet the REA and ICEA specifications for MPS and WPS. Separate evaluations, excluding some crosstalk combinations, e.g.: side-to-side combinations of the same quad, showed sufficiently improved results. This approach is intended to simulate less than 100% utilization of the cable for PCM.

From our experience we conclude that general improvements are possible. These will be nearly independent of the type of manufacturing machinery used. Cable F is specifically designed and manufactured to high frequency crosstalk specifications. The REA and ICEA specifications are fully met, including the side-to-side in-quad combinations! This confirms that star quads can be equal or superior in performance to pairs through the use of care in design and manufacture.

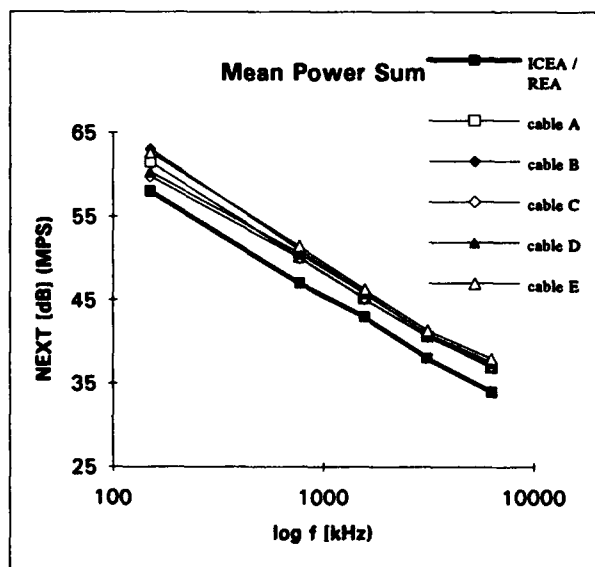


Fig. 15a Crosstalk of cables with pairs (mean power sum)

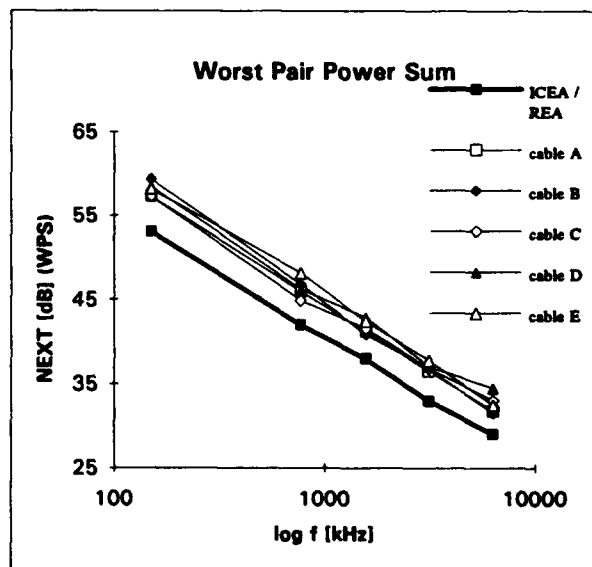


Fig. 15b Crosstalk of cables with pairs (worst pair power sum)

Acknowledgments.

The authors gratefully acknowledge the cooperation of Messrs. Dimitri Stein and Henry Hofheimer of Cable Consultants Corp., Larchmont NY in the review and editing of this paper. They also express their sincere appreciation to Mr. Dieter Vogelsberg, consultant to Kabelmetal's subsidiary Frisch, for several fruitful and stimulating discussions.

References.

1. Abadia, V.: "Study Comparing Pairs and Quads", IWCS 1977, p 329.
2. Chatter, L.M.: "Computerized Automatic Measurement of Telephone Cables", Pacific Coast Meeting, Wire Assn. Intl., Los Angeles CA, Febr. 5, 1979.
3. Deuringer, J.: "Eliminierung von Kopplungen durch Cross-Stranding", Fernmelde-Praxis 9-10/1988, pp.358-368.
4. Geiger, W.: "Systematik der Nebensprechfreiheit zwischen den Paaren verschiedener Sternvierer einer Verseillage", Arch. Elektrotechn. 46 (1962) H.6, pp.345-390.
5. Guba, W.; Mohr, W.: "Hochratige Datenübertragung auf Leitungen", Universität Hannover, Inst. f. HF-Technik, Final Rep. Oct. 1, 1986 -Sept. 10, 1987
6. Herz, K.: "Zur Ausbreitung des Fernsprechers im Gebiet der Deutschen Bundespost", Jahrbuch des elektrischen Fernmeldewesens 1952.
7. Heuser, S.: "Comparison of different methods of 2.048 Mbit/s digital transmission on multi-pair symmetrical cables", Techn. Bericht Nr. 442 TB 76 des Forschungsinstituts der DBP beim FTZ, Oktober 1990.
8. Kaden, H.: "Wirbelströme und Schirmung in der Nachrichtentechnik", Springer-Verlag, Berlin 1959.
9. Klein, W.: "Die Theorie des Nebensprechens auf Leitungen", Springer-Verlag 1955.
10. Kämpfmüller, K.: "Über das Nebensprechen in mehrfachen Fernsprechkabeln und seine Verminderung", Arch. Elektrot. 12 (1923); pp. 160-203.
11. Lau, H.: "Magnetische Kopplung zwischen den Stämmen zweier Sternvierer", (Hackethal-Draht-und Kabel-Werke, Hannover), Arch.Elektrotechn. 44 (1959) Nr.6, pp.331-354.
12. Martin, H.: "Entstehungsmechanismus des Nebensprechens in symmetrischen Kabelanlagen", Ph.D.Th., TH Hannover, 1960.
13. Meinke, H.H.: "Untersuchungen über die Kapazitätsverhältnisse von Paaren und Sternvierern in Fernmeldekabeln", (Hackethal-Draht-und Kabel-Werke, Hannover), Mitt. Forsch.Anst.GHH, Vol. 8, No. 3, pp. 60-70, April 1940.
14. Meinke/Gundlach: "Taschenbuch der Hochfrequenztechnik", Springer, 5th Ed., 1992.
15. Sakaguchi, T. et al.: "Restructuring of Metallic Subscriber Cable Networks for Digital Service", NTT Rev. Vol.4 Nr.3, May 1992.
16. Sieber, K., K.Schlump: "Beitrag zur Theorie des Aufbaues störungsarmer Fernsprechkabel", Neumeyer A.G., Nürnberg, ENT Vol. 11 (1934), No. 4, pp.119-140.
17. Siemens AG: "Internationale Fernmeldestatistik 1993", ON ÖV Marketing, München.
18. Söder, G., K.Tröndle: "Digitale Übertragungssysteme", Springer-Verlag, 1987.
19. Stöckel, H.: "Verfahren zum Orten und Messen von Nebensprechkopplungen mit Hilfe von Impulsen", Howaldtswerke AG, Kiel, 1958.
20. Vogelsberg, D.: "Kopplungseigenschaften SZ-verseilter Ortskabel", Draht und Kabel Panorama, No.2/1990, pp.94-97.
21. Wellhausen, H.-W.: "Eigenschaften symmetrischer Kabel der Ortsnetze und generelle Übertragungsmöglichkeiten", Der Fernmeldeingenieur 43 (1989) No. 10/11.
22. Wuckel, G.: "Neuere Entwicklungen in der Herstellung von Fernsprechkabeln auf physikalischer Grundlage", EFD 36 (1934), pp. 157-169.



Christoph Chojetzki
Kabelmetal Electro GmbH
Gubener Strasse 1
31644 Stadthagen
Germany

Christoph Chojetzki was born in 1963. He graduated in 1988 with a degree in electrical engineering (Dipl.-Ing.) from the Friedrich-Schiller-University in Jena. He joined Kabelmetal Electro in 1991, where he is currently engaged in the engineering of telecommunications cables.



Georg Maltz
Kabelmetal Electro GmbH
Postfach 260
30002 Hannover
Germany

Georg Maltz received his degree in communications engineering from the Technical University Hannover in 1958. During the same year he joined Kabelmetal Electro GmbH. Since 1965 he is responsible for research and development of telephone and carrier frequency cables and, since 1978, also in R & D of fiber optic cables.



Johann Schulte
Kabelmetal Electro GmbH
Gubener Strasse 1
31644 Stadthagen
Germany

Johann Schulte received his physics degree in quantum optics in 1981 and his Ph.D. in engineering in 1986 from the Technical University Hannover. After a research fellowship at IBM, Yorktown Heights, he joined Kabelmetal Electro in 1987, where he is currently in charge of cable engineering.



Gerd Verdenhalven
Kabelmetal Electro GmbH
Gubener Strasse 1
31644 Stadthagen
Germany

Gerd Verdenhalven, joined Kabelmetal Electro in 1969 after completing his studies in communication engineering at the Technical University Hannover. He was active in R & D of telecommunications cables and measuring techniques both in the carrier frequency and digital range. In the 1980s he became responsible for the design and testing of fiber optic cables and, since 1985, he is head of the group for design of telecommunications cables in the Stadthagen plant.



Kurt Verlande
Kabelmetal Electro GmbH
Gubener Strasse 1
31644 Stadthagen
Germany

Kurt Verlande was born in 1933. He graduated in 1958 with a degree in electrical engineering from the Staatliche Ingenieurschule Duisburg. He joined Kabelmetal Electro in 1958. As a senior engineer he currently manages the quality control of telecommunications cables in the Stadthagen plant.

TRANSMISSION PERFORMANCE OF QUADDED WIRE AND CABLE FOR T1 AND HIGH SPEED DATA SERVICES

J.- H. Walling*, P.S.V. Maddali**, P. Kish* and D. Mercier*

* Northern Telecom Canada Limited
Transmission and Components
Cable Group Technology

** Telesector Resources Group
of NYNEX
Outside Plant Technology
Selection

Abstract

The maximum reach of five different quadded cable types has been determined for T1 (primary rate ISDN), 10BASE-T Ethernet and 4 & 16 Mbits/sec Token Ring applications.

The quads were made using three different manufacturing processes. The results indicate that :

- suitably designed quads are equivalent to twisted pairs.
- crosstalk problems with quads are due to design and manufacturing deficiencies.
- not all quads are created equal.
- better performance is feasible.
- performance assessments based upon single point crosstalk measurements are not sufficient and can suggest misleading conclusions. Swept frequency measurements in the bandwidth of interest should be given preference.

Introduction

Quadded cables have a long history and are widely used for telecommunications throughout the world. Quadded cables are smaller and tend to be more cost attractive than comparable twisted-pair cables. In the early years of telephony, quadded cables provided a means to enhance capacity by 50% through the use of phantom circuits. In today's world of high speed communications, the manufacturing of quadded cables has evolved to a high level of sophistication in some countries. In fact, performances similar to data grade twisted pairs can be achieved, and may even be exceeded. For example, data grade quadded cables are manufactured in France that meet or exceed EIA/TIA Category 5 transmission requirements.

In North America, the use of outside plant quadded exchange cables was phased out approximately 45 years ago. Today they are principally used for residential drop and station wiring applications.

PERCEPTION ... Quadded cables are perceived as inferior to twisted pair cables in transmission performance.

This perception, although generally untrue, persists in North America and may be attributed to some bad experiences following divestiture when some inferior designed quadded cables appeared on the market.

REALITY ... Quads have inherently a high crosstalk isolation.

In a symmetrical quad both pairs are geometrically perpendicular to each other. The electromagnetic fields emanating from the disturbing pair relative to the disturbed pair are orthogonal to each other. This yields an effective crosstalk isolation.

The lack of proper controls in the design and manufacturing processes can lead to pair to pair unbalance due to asymmetry of the quad structure. Unbalance is, for the most part, a distributed parameter. For stranded and parallel quads, the unbalance may add up uniformly over the length of the wire and can lead to crosstalk problems accumulating with distance.

Northern Telecom uses a patented oscillating process in the manufacture of quads to ensure that the unbalance changes in sign and is, therefore, randomly distributed over the length of the wire. Thus the accumulated unbalance is minimized.

Within the industry, the idea has been promoted that higher capacitance unbalance pair to pair values impair high speed data transmission, or certain digital access applications.

It has been postulated that when quads are used for Digital Subscriber Loop (DSL), High Speed Digital Subscriber Loop (HDSL) and Integrated Services Digital Network (ISDN) primary rate applications, then substantially shorter service lengths will be required or one pair within the quad has to

be left idle because of crosstalk due to high pair to pair capacitance unbalance - a measurement which is applicable at voice frequencies.

Within the performance specification for the outside plant cables, we could not establish any correlation between crosstalk (NEXT @ 772 kHz) and the capacitance unbalance pair to pair at 1 kHz for quadded cables that were manufactured using Northern Telecom's oscillating process. This is shown for 675 tested wires convincingly in Fig. 1. These results provide further evidence to support the random addition of unbalance for these cables.

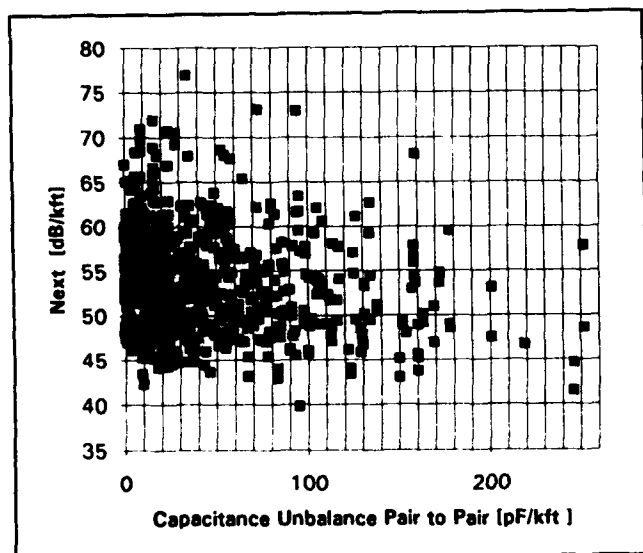


Fig. 1 : Capacitance unbalance pair to pair as a function of NEXT for quads (Aerial Service Wire)

Nevertheless, measurement of capacitance unbalance pair to pair still serves as a powerful control tool for monitoring the performance and the consistency of manufacturing processes.

Subsequent results will also show that it is not possible to rationalize the reach attainable for high speed data applications based solely on unbalance and/or single frequency crosstalk measurements. Crosstalk measurements need to be performed over a range of frequencies in the bandwidth of interest in order to make an accurate assessment.

Rationale

The objective of this paper is to demonstrate that the performance of correctly designed and manufactured quads is fully equivalent to twisted pairs.

To demonstrate this, we selected five quadded cable designs which were produced using three distinctly different manufacturing processes.

These quads were extensively tested using different configurations, to establish the degree of their suitability for high grade data transmission.

We established, furthermore, the maximum attainable reach for T1, and also for different LAN frequencies, and subsequently tried to link these results to the basic electrical characteristics of the population of wires investigated.

The performance achieved for the different designs were investigated with respect to the basic design parameters like insulation material, insulation wall thickness, flammability rating, etc.

Description of the Wire Designs Investigated

With one exception, all the selected quads have 22 AWG conductors.

The description of the wire designs are given in Table I. The flammability listings are also shown, as they have a major impact upon the electrical performance.

Wire	Jacket Dia. (mil)	Insul. Wall (mil)	Insul. - Mat.	UL
1	-	10.0	HDPE	CMX
2	132	7.0	FRPP	MPR
3	114	6.5	FRPP	MPR
4	143	9.5	FRPE	CM
5	126	7.5	PP	CMX

Table I : Construction of wires investigated

The quads # 1; #2 and # 3 were made using Northern Telecom's patented process. Wire # 1 is Northern Telecom's NT-2ADW Aerial Service Wire.

Wires # 2 and # 3 are Northern Telecom's NT-C3 Station Wires. They have a dual UL-listing, i.e. CMX-Outdoor/MPR, and are only differentiated by their gauge size. The wire # 3 is the only wire that has 24 AWG conductors.

Incidentally, these wires are also UL - classified to Level III.

Wires # 4 and # 5 were purchased. These wires are also station wires. Wire # 4 is a stranded quad with 3.8 inch lay. Wire # 5 is a parallel quad, i.e. the conductors are not stranded, but laid up parallel.

Hence forward only the wire numbers are used to refer to these quads.

Measurements and Methodology

Electrical Performance Characterization

Table II summarizes wire resistance, resistance unbalance, mutual capacitance and capacitance unbalance pair to pair for the different wires. Reported are averages, minimum and maximum values of each lot of wires. These measurements were made on a DCM test set.

	CR	CRU	Mut.Cap	CUPP
Wire	[Ohm/mi]	[%]	[nF/mile]	[pF/kft]
1	82.71	.17	81.02	6.0
	82.82	.26	81.80	19.5
	82.99	.46	82.68	37.0
2	83.60	.25	98.60	1.0
	84.36	.34	99.45	23.6
	84.97	.41	99.73	52.0
3	135.0	.02	91.40	4.0
	136.6	.08	92.28	20.3
	138.6	.10	93.55	55.0
4	84.32	.09	79.79	79
	84.75	.36	83.52	200
	85.08	.95	85.89	492
5	87.59	.18	82.47	11.0
	87.82	.39	82.98	67.7
	88.20	.65	83.77	201

Table II : Conductor resistance, mutual capacitance and capacitive unbalance

The frequency domain measurements, i.e. the characterization of the wires subject to sinusoidal signals, was carried out with an HP-network analyzer, in conjunction with an S-parameter test set. All these measurements were made in the frequency range from .1 to 20 MHz. For each scan 401 points were recorded. For the crosstalk measurements, a linear regression has been calculated over the entire population of measurements after a log-frequency transformation. The line obtained has then to be shifted parallel into the lowest point of all measurements, thus yielding the lower envelope of the measurements. The regression line obtained has also been used to calculate the attenuation to crosstalk ratio (ACR) for each wire. The Category 3 requirements according to draft EIA/TIA SP-2840 (ANSI/EIA/TIA-568A revision) [1] for Near End Crosstalk and Attenuation have been also plotted (marked with an arrow).

The results are compiled in Fig. 2 to Fig.16 for the five wires.

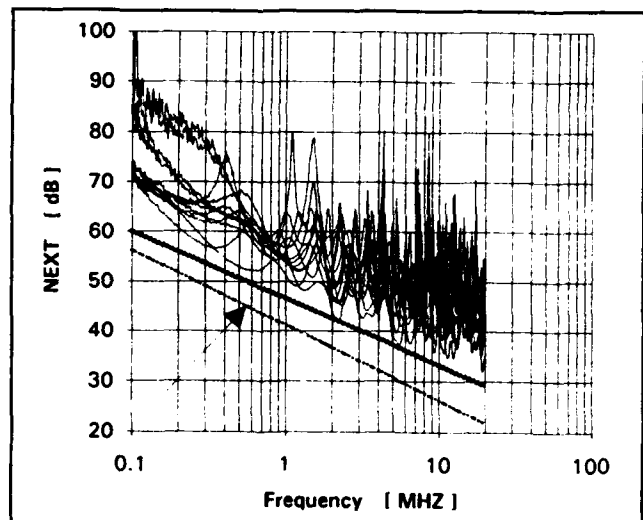


Fig. 2 : NEXT versus frequency for wire # 1

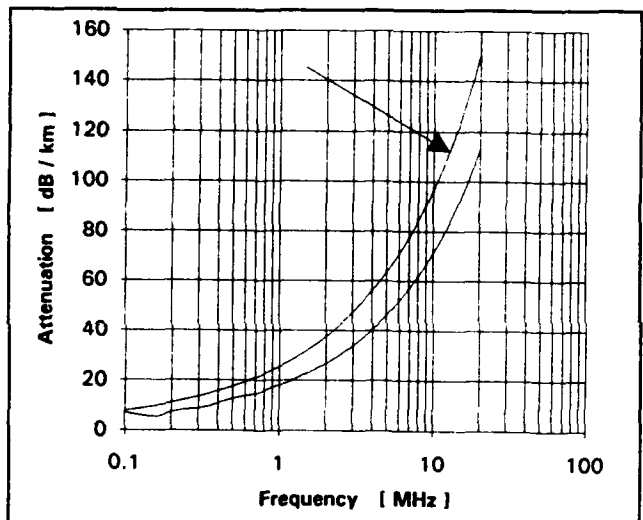


Fig. 3 : Attenuation versus frequency for wire # 1

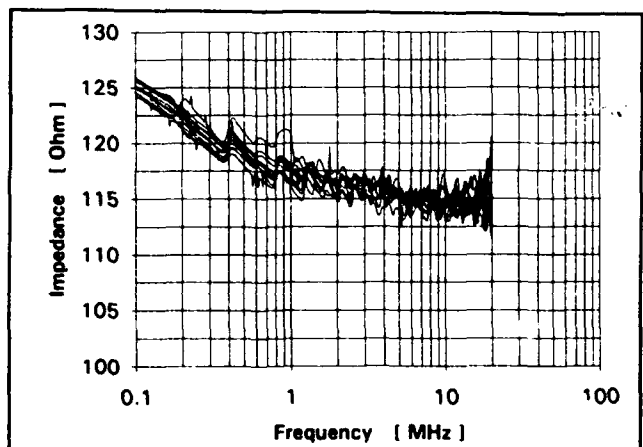


Fig. 4 : Impedance versus frequency for wire # 1

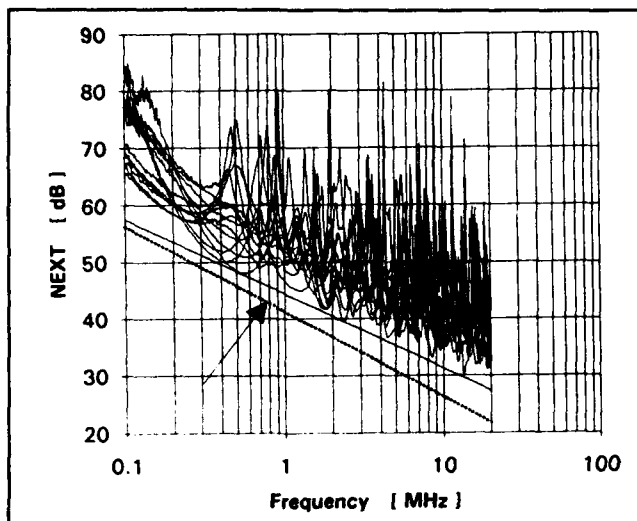


Fig. 5 : NEXT versus frequency for wire # 2

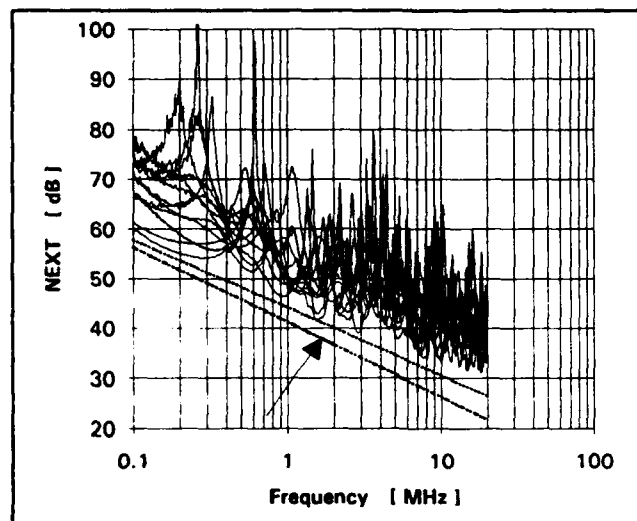


Fig. 8 : NEXT versus frequency for wire # 3

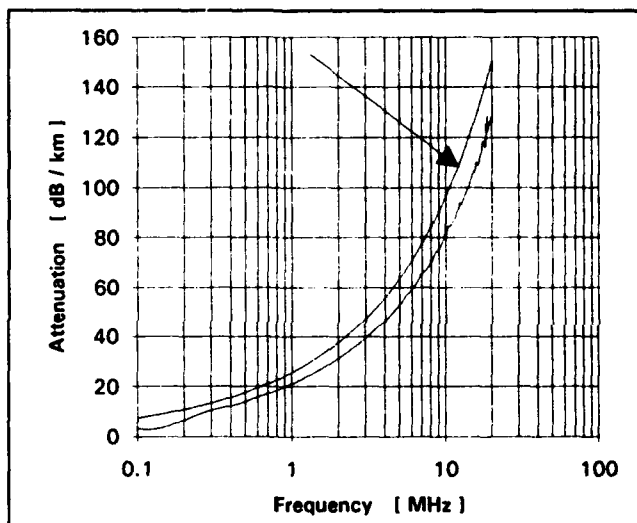


Fig. 6 : Attenuation versus frequency for wire # 2

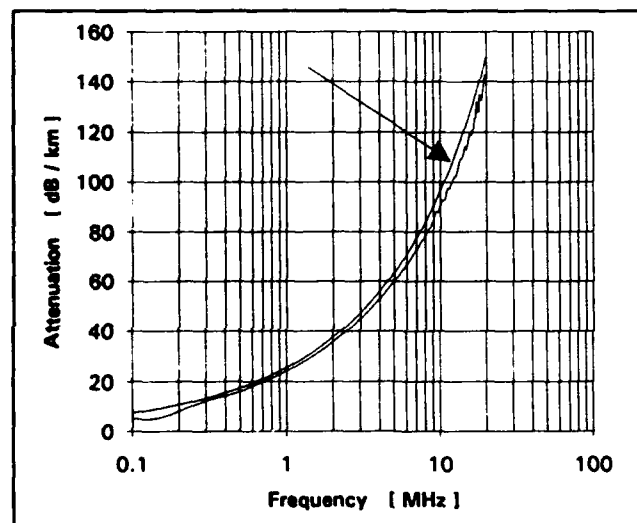


Fig. 9 : Attenuation versus frequency for wire # 3

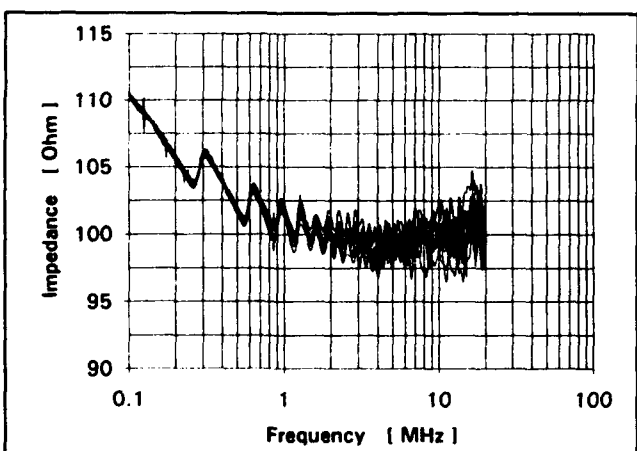


Fig. 7 : Impedance versus frequency for wire # 2

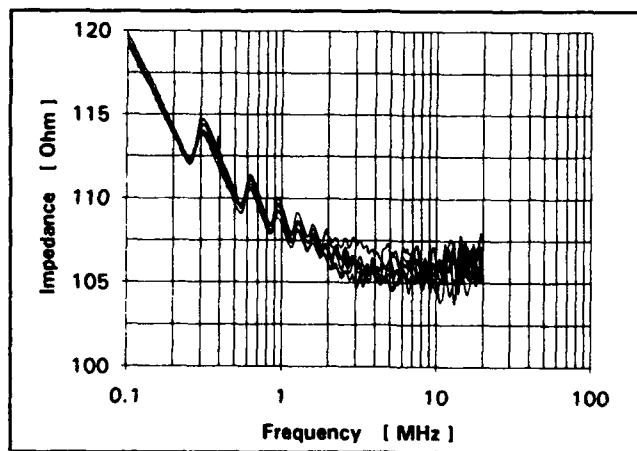


Fig. 10 : Impedance versus frequency for wire # 3

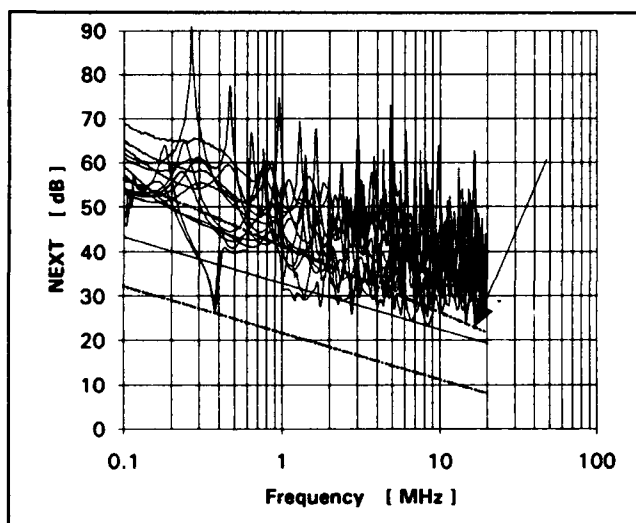


Fig.11 : NEXT versus frequency for wire # 4

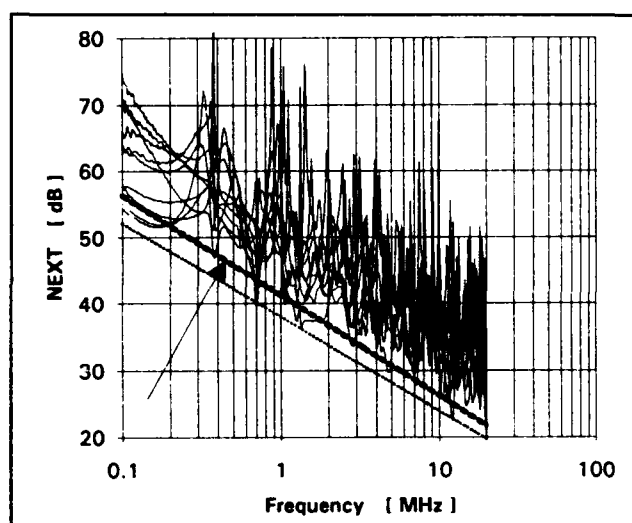


Fig.14 : NEXT versus frequency for wire # 5

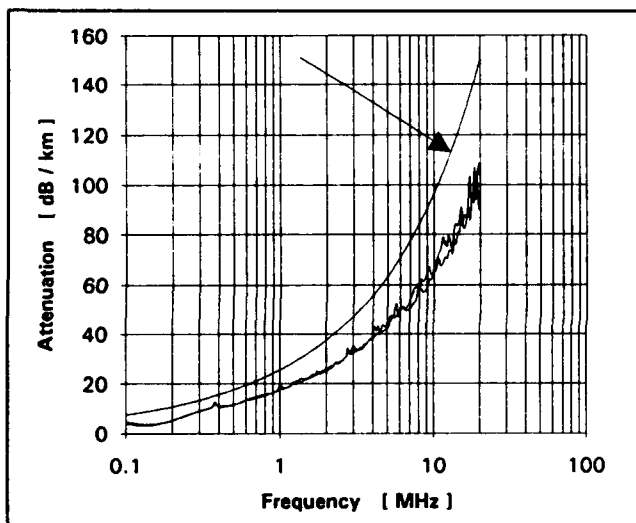


Fig.12 : Attenuation versus frequency for wire # 4

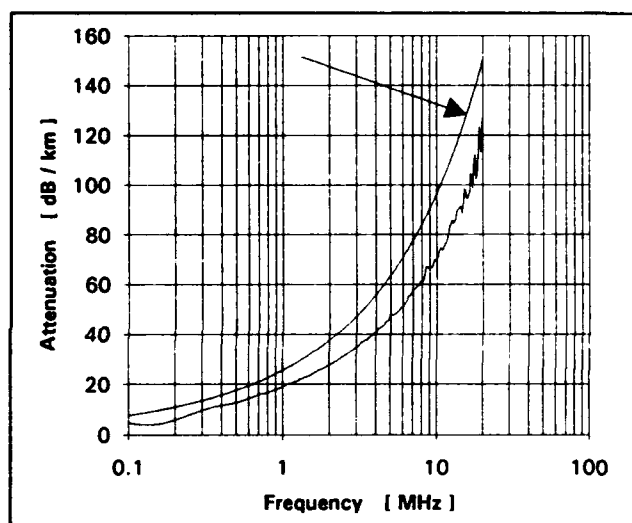


Fig.15 : Attenuation versus frequency for wire # 5

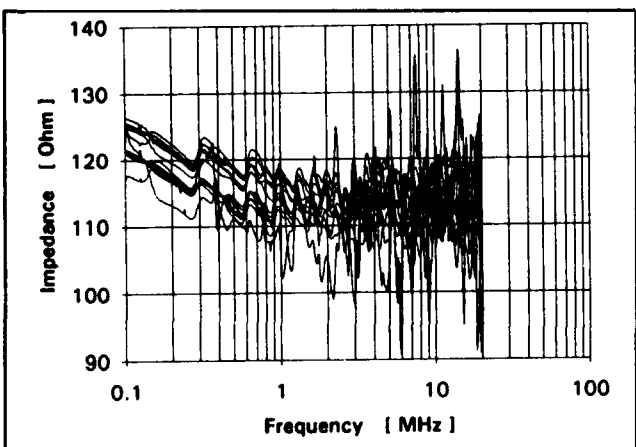


Fig.13 : Impedance versus frequency for wire # 4

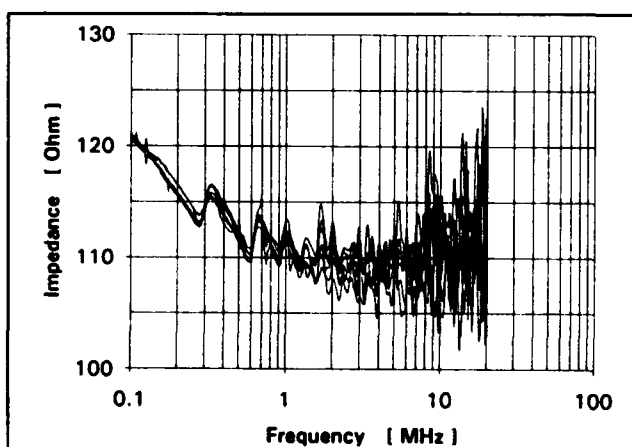


Fig.16 : Impedance versus frequency for wire # 5

T1 - Carrier Reach Measurements

Method

To measure the reach for T1 signals subject to a near end disturber, the wires of several cartons were connected in series such that the entire wire formed a ring. (see Fig. 17)

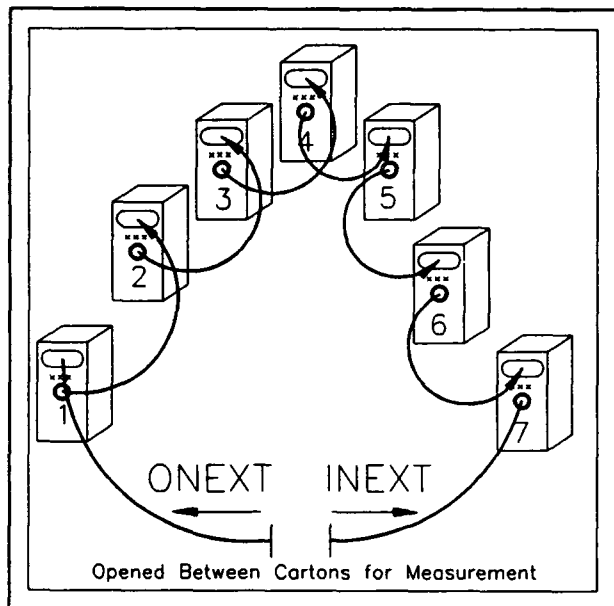


Fig. 17 Schematic setup for measuring the reach at T1 carrier frequency.

The station was connected at each splice point and the bipolar violation rate was measured (BPV). This was done in both directions, so that for each wire the BPV rate for the inside and outside end was determined. This takes into account the difference of measured NEXT, i.e. INEXT and ONEXT and their respective impacts upon the available attenuation to crosstalk margin (ACR).

The reach for T1 signals is based upon the occurring bit error rate (BER) performance. However, to accelerate the measurements, by using readily available equipment, the BPV rate has been used instead.

There is a very good correlation between BER and BPV when the latter is in the order of 10^{-2} or less. However, below this limit a frequent cancellation of BPV's occurs, which yields too favourable BER values. To avoid this, the measurements below a BPV rate of 10^{-2} have been ignored for the reach regression.

The wire of at least two cartons was used as an 'attenuator', i.e. it was placed in the centre of the measured loop. This wire was gradually shortened to progressively decrease the BPV rate.

Each measurement was carried out at slightly over 10^{15} Bits. At a bit rate of 1.544 Mbits/sec this corresponds to a monitoring time of 11 minutes per measured point.

The BPV rate is dependent upon the pulse pattern used. Therefore, seven different pulse patterns were used consecutively. The BPV rate for each one was determined as well. Their average has been used for the reach assessment. Thus the total number of bits transmitted was in excess of $7 \cdot 10^{15}$.

The pulse patterns used for this purpose were 1:1 ; 1:7 , 3:24 ; a quasi-random signal source and three different random signal sources with $(2^{15} - 1)$; $(2^{20} - 1)$ and $(2^{25} - 1)$ repetitive bit patterns.

The BPV also depends upon the power input at the disturber side. The disturbing power input has been, therefore, kept constant for all measurements.

The logarithm of the BPV rate is inversely proportional to the power of the signal. We have, therefore, a linear relationship between the logarithm of the BPV and the inverse of the wire length.

This hyperbolic dependency is shown for one set of measurements in Fig. 18.

This relationship has been used to determine the acceptance limit of

$$BPV \approx BER \approx 10^{-7}$$

for a T1 system out of a transformed linear regression.

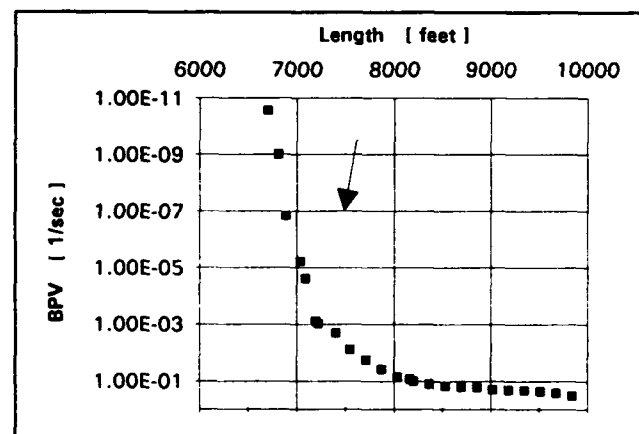


Fig.18 : Bipolar violation rate as a function of the wire length (wire # 2)

Table III shows the results which correspond to the graph in Fig. 18.

No.	Length [ft]	B P V [1/sec]	Att. [dB]
1	6700	2.81 e-11	27.59
2	6815	9.81 e-10	27.82
3	6890	1.46 e-07	28.28
4	7034	6.21 e-06	28.48
5	7084	2.49 e-05	28.51
6	7192	7.93 e-04	28.86
7	7220	9.61 e-04	29.25
8	7400	2.07 e-03	29.75
9	7546	7.73 e-03	30.26
10	7715	1.78 e-02	30.81
11	7874	3.81 e-02	31.16
12	8038	7.21 e-02	31.63
13	8167	8.63 e-02	31.84
14	8202	1.00 e-01	32.02
15	8366	1.31 e-01	32.35
16	8530	1.51 e-01	32.74
17	8694	1.61 e-01	32.64
18	8858	1.70 e-01	33.20
19	9022	1.99 e-01	33.68
20	9186	2.11 e-01	34.14
21	9350	2.16 e-01	34.39
22	9514	2.35 e-01	34.81
23	9678	2.59 e-01	35.14
24	9843	3.36 e-01	35.55

Table III : BPV as a function of the length of the wire. (wire # 2)

Additionally, each carton used, has been measured for the basic electrical parameters and also for the NEXT at the Nyquist frequency and its first three harmonics. It was thought that these measurements might be correlated to the reach as suggested in [2] based upon the assumption of a "smooth" crosstalk model.

Results

The final results are compiled in Table IV. As the amount of individual measurements was massive, only the final calculated results are reported.

Furthermore, only the lowest reach values of each wire are listed. In this table the single point 772 kHz crosstalk values and the reach corresponding signal attenuation are also compiled.

Wire No.	Reach [ft]	NEXT [dB]	Atten. at Reach [dB]
1	8177	53.2	36.96
2	6317	49.2	34.93
3	6166	55.6	28.55
4	4869	46.6	22.54
5	7024	46.0	34.56

Table IV : Reach for T1 carrier, NEXT and signal attenuation at reach

The single point NEXT measurements at the power frequency of the T1 carrier and its first three harmonics yielded for wire # 1 the scatter of results in Fig. 19. It shows that the use of point measurements for crosstalk assessment and its impact on transmission properties is not necessarily adequate, if the minimum performance requirements of the wire are met or exceeded. The reporting of the crosstalk results at the harmonics of the Nyquist frequency is, therefore, omitted here.

The above illustrates the questionable use of such measurements and the drawback to this method versus swept frequency crosstalk measurements described above.

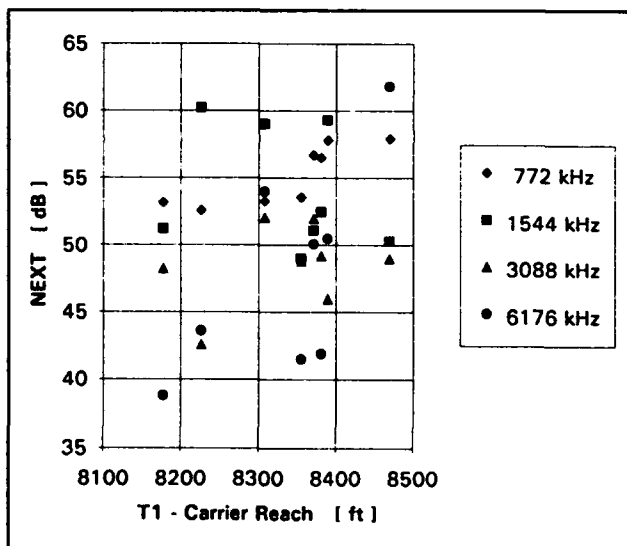


Fig. 19 : NEXT vs T1 - carrier reach for different frequencies

Each of the cartons used, was measured on the HP-network analyzer, in conjunction with an S-parameter test set, to determine its NEXT, input impedance and attenuation. These measurements allow a comprehensive interpretation of the results obtained.

Pulse Mask Measurements

Method

Pulse mask testing was performed using a T-BERD-209. All the measurements carried out used DS1 (1.544 Mbit/sec) only.

Pulse mask failures occur with either very short or too long wires.

Only an upper limit requirement for the length is specified. The reference length for the pulse mask test is 655 feet (200 m) for 22 AWG wire and 450 feet (137 m) for 24 AWG wires. These length are normally required in the central offices for cross-connect wires.

No minimum length requirements are specified.

However, the interest here was only to determine the upper limit of the wire length, passing the pulse mask test.

This seems to become more and more important, as inside wires are increasingly used also for multiplexer interconnections.

The pulse mask test were carried out with two different pulse patterns, a 1 out of seven and a 3 out of 24 pattern. Both patterns yielded essentially the same results.

The measurements started at a length 10 % higher than the specified length. The pulse mask testing was performed, and upon failure the wire has been shortened gradually. The rate of length reduction was arbitrary judged by the apparent degree of pulse mask failure.

Care has been given to ensure that the worst pair and also the signal direction, yielding the worst result, was monitored.

The pulse mask testing time for each result has been limited to 5 minutes. In case of a pass, the second wire pair was tested as well. Then both pairs have been tested in reversed direction before accepting a pulse mask reach value.

Wire No.	T1 - Pulse Mask Reach [m] (ft)	% of ANSI Requirement
1	205 (672)	102.60
2	189 (620)	94.66
3	130 (427)	94.89
4	178 (584)	89.16
5	192 (630)	96.18

Table V : T1 pulse mask compliant reach. The percentage of ANSI requirement for cross-connect wire is also indicated.

Results

Only the shorter reach of the wire tested with both pulse patterns is reported in the result table. (see Table V)

As an indication, in Fig. 20 a pulse mask failure is shown which necessitated a reduction of the length of approximately 12% in order to obtain a pass.

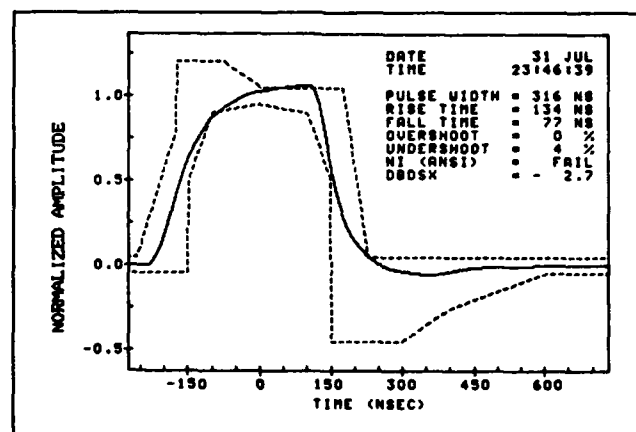


Fig.20 : Failing AINSI pulse mask test due to too long wire

For the same wire the passing pulse mask is shown in Fig. 21.

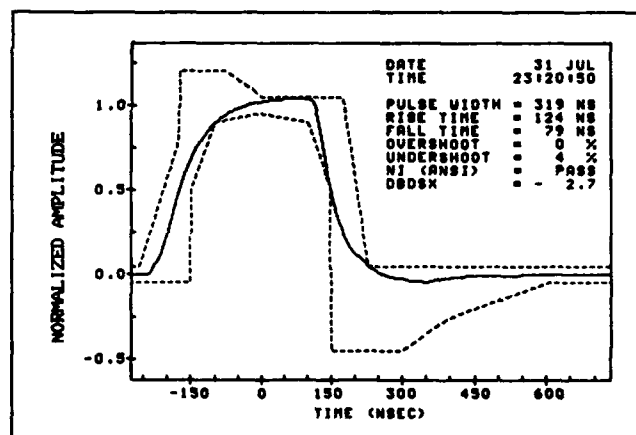


Fig.21 : Pulse mask test at maximum reach

The Reach at LAN Frequencies

Method

To measure the reach at LAN frequencies, i.e. at the bit rates of 4 Mbits/s; 10 Mbits/s and 16 Mbits/s, a LAN was set up with both Ethernet and IBM-Token Ring cards installed. An active hub was used as a concentrator. To determine the reach for the different wires, the traffic between hub and server was sent over the wire under investigation (see Fig. 22)

This effect was used to determine the reach of the wires. A large file of randomly assembled information was loaded into the buffer of the LAN - server. The file has

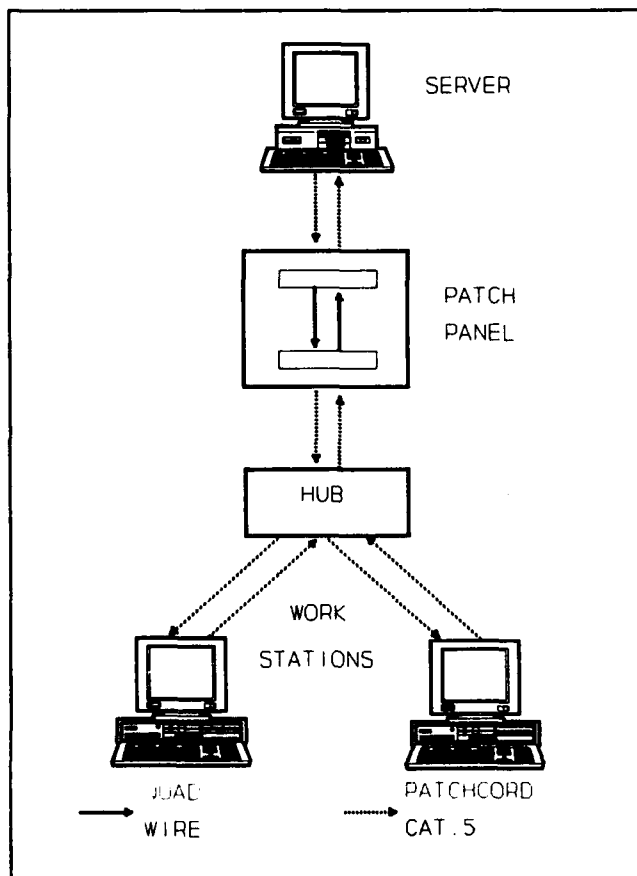


Fig.22 : Schematics of the LAN with the patch panel to connect the wire under test.

then been read several times over by the LAN station. The time to read out the file for a predetermined number of cycles was clocked within the LAN station. Care was taken to ensure that the entire information transferred was stored in the buffer. As a zero reference transfer time the time, consumed by the shortest jumper possible between LAN server and active hub was used.

Acceptable is a link over a certain reach only, if the transmission time is very close to the reference time using the jumper.

The information transmission time increases with the error occurrence. To monitor this, a 'LAN-Manager' software package was additionally used.

Only if token and framing error occurrence were zero was the reach declared acceptable.

Incidentally, for these measurements, a

comparison between the utilization of an active hub versus a passive hub was made. As the results were very close, the active hub was given preference. This avoided the need to change the patchcords during the switch from Ethernet to Token Ring.

The IBM-Token Ring uses a card-internal assessment of the token error rate. If the line is too long, i.e. if the token errors in the loop are too high, the card design does not recognize the existence of a valid link. This is best described by a step function, i.e. below a critical length the link is recognized, beyond this length the token ring card does not acknowledge the link.

However, this is not a sharp edged step function, but it is more an S-shaped function, in which the token error rate increases with increasing wire length. This results in increasing transmission times for a given amount of tokens.

The 10 Mbit/sec Ethernet system is more forgiving to errors, however, only at the expense of a substantial increase of transmission time. The transmission time over the wire length for the Ethernet shows a flatter S-shape than for the token ring. The procedure to evaluate the reach was, however, equivalent to the one used for the IBM token ring.

Both, the Ethernet and the IBM token ring use Manchester or differential Manchester coding respectively on a bi-directional link.

To evaluate the worst case crosstalk condition, the data traffic of the lines of the LAN station to the hub and the server to the hub were crossed in opposing directions to obtain worst case near end crosstalk conditions.

However, very similar values resulted from the measurement of data transfer times and error occurrences than those obtained by using the wire for only the bi-directional link, where the 'Transmit-' and 'Receive-' lines are naturally affecting each other as mutual near end crosstalk disturbers.

Therefore the reach measurements were limited to a bi-directional link only.

Results

The results are reported in Table VI . Indicated is also the NEXT value of the wire which has been used - connected at the corresponding end - to determine the reach. The wires in this case were removed from the Reellex cartons, but were freely suspended in air with a wire to wire distance of approximately 1 inch. The attenuation which corresponds to the reach is indicated and

the corresponding ACR value is derived.

Wire No.	Reach [m]	NEXT [dB]	Att. [dB]	ACR [dB]
Token Ring at 4 Mbits/sec				
1	422	44.9	17.0	27.9
2	372	46.4	17.3	29.1
3	313	43.0	16.4	26.6
4	419	32.9	16.1	16.8
5	416	35.0	17.0	18.0
Ethernet at 10 Mbits/sec				
1	224	53.7	15.9	37.8
2	200	40.9	16.3	24.6
3	181	45.1	16.4	28.7
4	233	33.8	15.4	18.4
5	248	31.4	17.4	14
Token Ring at 16 Mbits/sec				
1	204	57.5	20.5	37.0
2	187	35.7	20.3	15.4
3	168	35.8	20.0	15.8
4	187	30.7	17.7	13.0
5	189	33.3	19.7	13.6

Table VI : Reach for Ethernet and Token Ring, including NEXT, attenuation over the reach and ACR.

Incidentally, these results compare very favourable to those obtained by M. Plasse et al [3]

Discussion of Results

T1-Carrier Reach and Pulse Mask

Table I lists the basic design dimensions. All wires have been crush-extruded. The insulating material of wire # 1 and wire # 4 are basically the same except that wire # 4 contains some flame retardant, in order to pass the CM requirement.

This should, however, have only a minor impact on the resulting SIC and, therefore, also on the electrical performances of these wires. In fact the performances should be comparable to wire # 1, as the insulation thickness is nearly the same. However, the T1 carrier reach for wire # 4 is only slightly over half that of the wire # 1.

The repeater distance for T1 is 6000 feet for exchange cables. This length, obtainable with equalizing and regenerative repeaters, has, therefore, been used as a minimum performance requirement for the wires. Therefore, wire # 4 is not acceptable.

Several reasons for this failure were identified :

- very poor crosstalk performance close to the required frequency range (see Fig. 2 versus Fig.11).

- Note:** This demonstrates the inconclusiveness of single point crosstalk measurements !
- a very 'rough' attenuation trace (see Fig. 3 and Fig.12 for both pairs), yielding serious signal reflection problems.
 - an unacceptable impedance characteristic (Fig.4 versus Fig.13).
 - widely spread mutual capacitance variation (see Table II).

The crosstalk regression over the entire population of wire # 4 was redone, omitting the two series of measurements yielding the very low crosstalk values. This resulted in two lower envelopes which are nearly parallel. It should be mentioned, however, that for acceptance testing purposes the lower of both curves should prevail.

The Table I indicates that wire # 5, having a slightly heavier polypropylene insulation, would be expected to have a lower attenuation. This shows up in the T1 carrier reach comparison (see Table IV). However, the absolute difference of attenuation and also in reach is smaller than expected. This can be attributed to poor crosstalk performance only. The asymptotic value of the impedance at high frequencies of wire #5 over wire # 2 is expected. (see Fig. 7 versus Fig. 16)

The pulse mask reach measurement, indicates that the attenuation is predominant for the pulse mask performance. But the impedance regularity is also important.

The very rough and irregular traces of the impedance for wire # 4 and wire # 5 yield evidently transmission problems (see Fig. 13 and Fig.16).

Wire # 3 is an example of a balanced design, which is well positioned versus its 22 AWG counterpart (wire # 2). It can be seen that wires # 2 & # 3 comfortably meet the UL-level III requirements.

From this comparison it follows that suitably designed quads combined with a controlled manufacturing process, may, in fact, exhibit a performance that matches very well the transmission characteristics of outside plant exchange cables.

Our study, furthermore, indicates very clearly that point measured crosstalk is, at least for quads, insufficient, and that the frequency domain measurement should be given preference.

Reach at LAN Frequencies

Table VI shows reach values for the different wire length at LAN frequencies. Only one carton could be measured for the reach determination. The crosstalk,

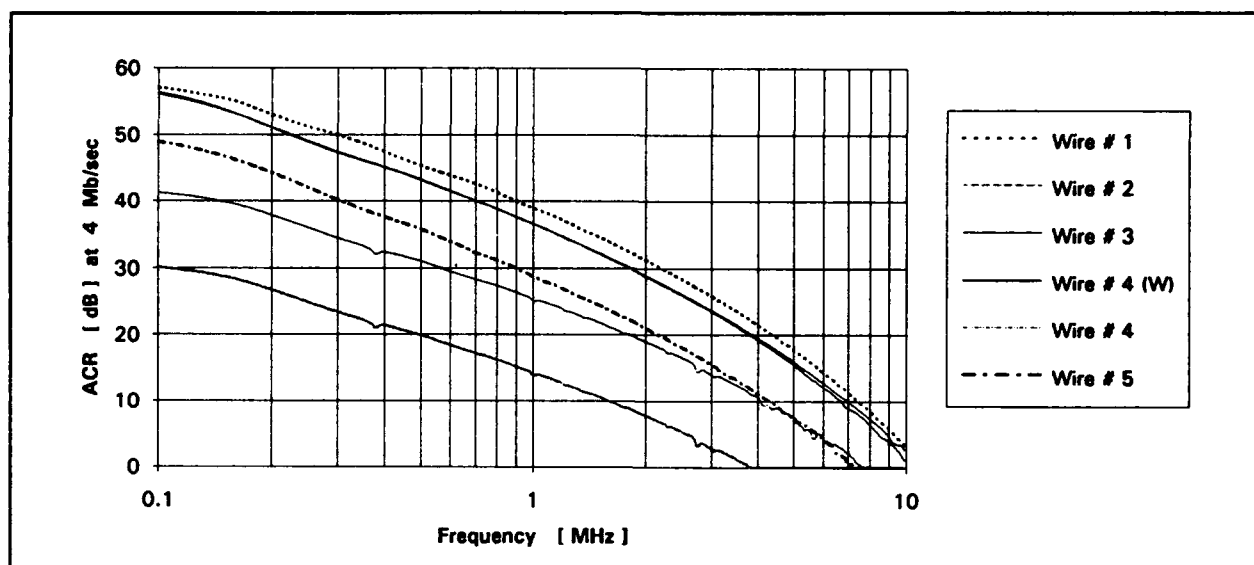


Fig. 22 : Attenuation to Crosstalk Ratio at 4 Mbits/sec

attenuation and ACR values have been interpolated from the values for the specific carton tested. These values are referred to in the Table VI. However, they give an incomplete picture, as they do not cover the behaviour expected in the worst case for a statistical population of wires.

This was the reason for determining the lower envelopes for crosstalk and for calculating the attenuation for the maximum reach (see Table VI). From these values the attenuation to crosstalk ratio (ACR) for the reach length can be derived. These values are plotted, for the LAN frequencies used,

in Fig. 22; Fig. 23 and Fig. 24. These graphs show that the required attenuation to crosstalk ratios (ACR) for the corresponding frequencies would probably not be met in the worst case by those wires which have either a stranded or a parallel quad construction. This is consistent with the fact that they do not meet the Category 3 requirements, and this by a relatively large margin.

Quads manufactured using the oscillating process as exhibited by designs # 2 and # 3, have nearly identical ACR values over the entire frequency range under worst case condition.

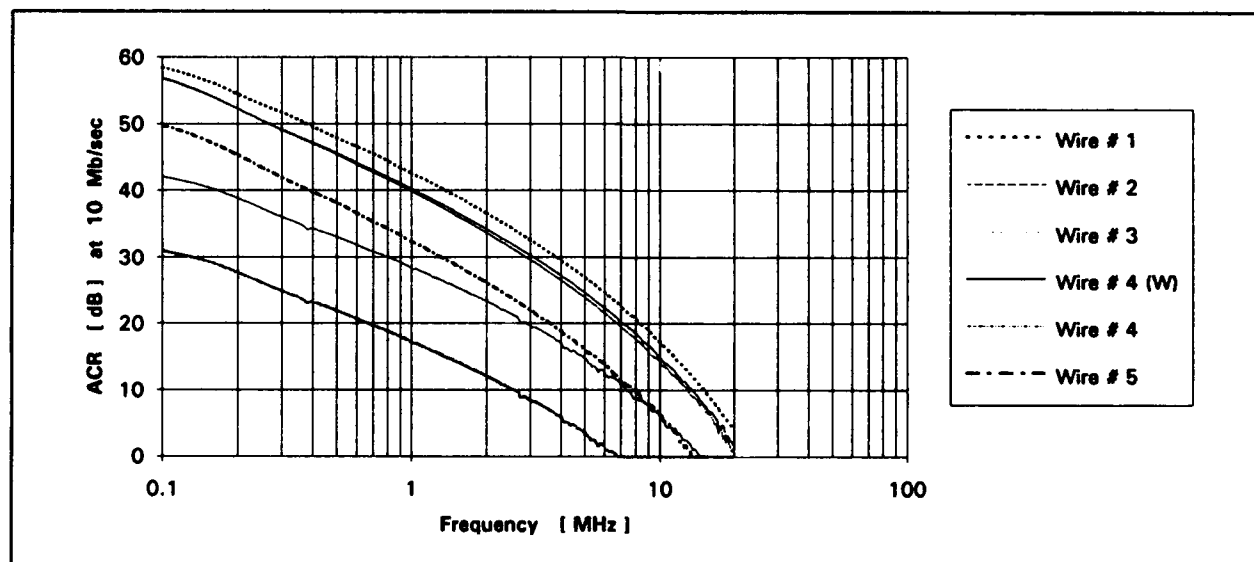


Fig. 23 : Attenuation to Crosstalk Ratio at 10 Mbits/sec

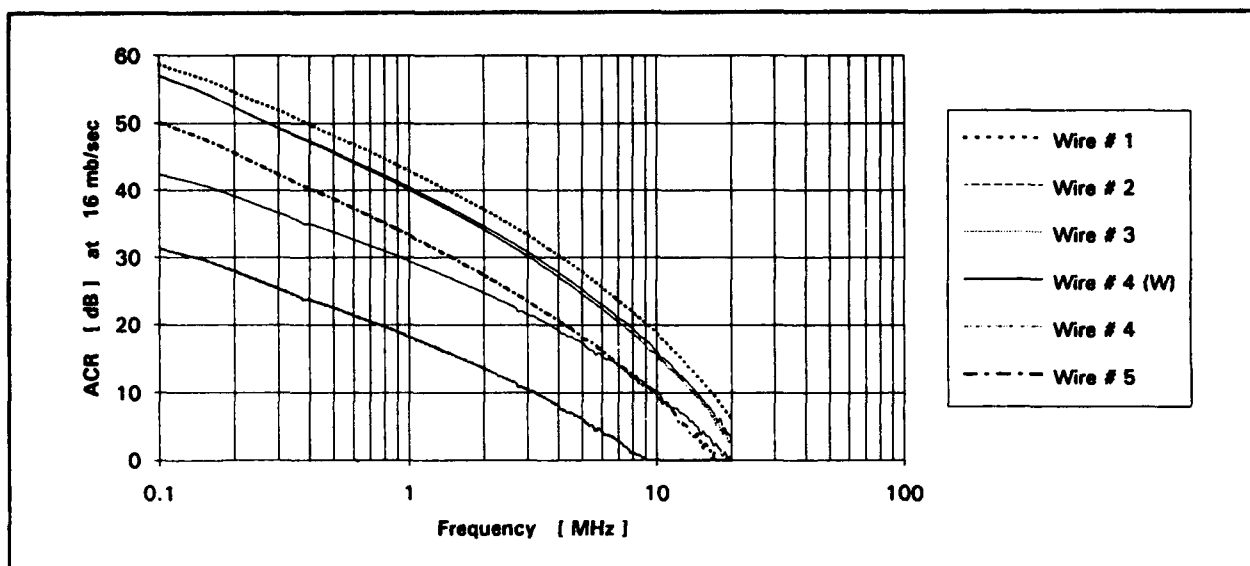


Fig. 24 : Attenuation to Crosstalk Ratio at 16 Mbits/sec

Summary and Conclusion

Our results show that quads can be designed and consistently manufactured to meet not only the requirements for the outside plant exchange loop, but also at more demanding data grade transmission rates.

A correlation between capacitance unbalance pair to pair at 1 kHz and NEXT at the Nyquist frequency of the T1 carrier, i.e. 772 kHz, could not be confirmed, if the basic performance requirements are met.

The reach results indicate, that length limitations for Digital Subscriber Loop (DSL); High Speed Digital Subscriber Loop (HDSL) and Integrated Services Digital Network (ISDN) primary rate applications are unfounded when using suitable quads. In fact, the service length can be extended to the full repeater distance of 6000 feet, and in some cases even beyond this length.

Our results clearly demonstrate that single frequency measurements of crosstalk are not suitable and should be replaced with swept frequency measurements within the corresponding bandwidth of interest.

Quadded designs have been shown to be fully equivalent to twisted pair designs.

Our results indicate, furthermore, that higher performances are also achievable.

References

- [1] EIA/TIA SP-2840 Draft. Commercial Building Telecommunications Standard.
- [2] M.R. Aaron : PCM Transmission in the Exchange Plant. BSTJ 41(1962)Jan. p. 109-151
- [3] Plasse, M. et al : High Performance Twisted-Pair Cable for LAN Systems. IWCS Proceedings 38(1989), p.27-35

Appendix

Measuring Equipment Used

1. DCM - Test - Set and Fanning Fixtures
2. HP - 3577A Network Analyzer
3. HP - 35677A S-Parameter Test Set
4. Compaq 486-SX used as Server
5. IBM Token Ring Adapter Cards
6. Ethernet Adapter Cards
7. Compaq 286 as Lan Stations
8. Cabletron Systems Active Hub (equipped both for Ethernet and Token Ring, i.e. TR-MIM24A and TT-MIM 24)
9. Northern Telecom Passive Hub
10. Telecommunications Corporation's (TCC) T-BERD 209 T1 Transmission Analyzer
11. Cross-Connect Patch Panel

Jörg-Hein (Jo) Walling received his diploma in Mechanical Engineering, Materials Technology in 1966 at the Technical University of Berlin. In 1974 he obtained a Doctor's Degree (Dr.-Ing.) in Engineering, Material Science, at the same University. At the end of 1974 he



joined Northern Telecom Canada Ltd. in the Research and Development Department of the Communication Cable Division. Since 1976 he has been senior engineer at the Lachine Cable Plant. He is responsible for the design of Outside Plant and Data Grade Wires and Cables.

Prasad Vic Maddali is an Associate Director in Outside Plant Technology Selection Department at Telesector Resources Group of NYNEX. He is in charge of technical aspects of metallic cable and wire products. Vic joined Bell Labs in 1969 as a Member of Technical Staff in the Cable Terminating Apparatus



Department in Baltimore and moved to Whippany, N.J. when Baltimore Labs were closed. He became involved in the design, development and engineering control of various cable apparatus such as Connecting, Protector and Terminal Blocks. He was also involved in testing and statistical analysis of various cables, wires and materials' compatibility with these products. At divestiture, he joined Bellcore as a Member of Technical Staff, in the Outside Plant Lab at Morristown, N.J. He wrote the TA on "Feeder Distribution Cabinets with Quick-Connect Terminals". He then joined Bellcore Fibre Optic Cable group and established some of the chemical, material and mechanical requirements of fibre cables. In addition, he conducted experimental work on the intermatability of fibre optic connectors,

such as biconic connectors.

He joined NYNEX in April 1988 and was involved in the selection and technical evaluation of metallic cable and wire products.

Vic hold a Master's degree in Physics from the University of Jabalpur in India. He is a member of the New York Academy of Sciences. He represents NYNEX in "Telecommunications Wire and Cable Standards Technical Advisory Committee and served consecutively as the Vice-Chairperson and Chairperson.

Paul Kish received an M.A.Sc. degree in Electrical Engineering from the University of Waterloo in 1972. He has 20 years experience with Northern Telecom in the design and development of telecommunications cables. He is currently Product Manager, Copper Cables for the Cable Group of Northern Telecom. Mr. Kish has published a number of technical papers in the field of cable design and performance evaluation. He is the chairman of TIA TR-41.8.1 working committee for Commercial Building Wiring Standards and participates on BICISI, IEEE, and CSA committees on wiring standards.



Daniel Mercier received his B.A.Sc degree in 1988 at Ecole Polytechnique of Montréal, Qué., Canada. In 1987 he joined Telecom Canada Ltd. as a member in the industrial engineering department. Since 1989 he has been a project engineer in manufacturing at Northern Telecom's Lachine Cable Plant.



TMP IMPLEMENTATION: CAN THE PROGRAM SURVIVE COST CUTTING AND DOWN SIZING?

D. W. HOLLEY

AT&T Network Cable Systems
Phoenix, Arizona

ABSTRACT

Our maintenance department had historically been a highly reactive breakdown maintenance organization. Little or no attention was paid to planned maintenance. However, with increased competition and the understanding that every dollar saved in maintenance cost would go to the bottom line, the maintenance department made the decision to implement a Total Productive Maintenance (TPM) program.

This paper presents a look at how a maintenance department struggling with budget cuts, layoffs and a breakdown maintenance philosophy managed to implement a successful TPM program. This paper will explain how a seven-step strategy has (at the two and a half year point of a five-year TPM program) increased the effectiveness of equipment and tradespeople, while helping the company's bottom line. Results such as effectiveness of tradespeople and level of planned work will be presented together with other significant measurements.

INTRODUCTION

In the late 1980's the Phoenix Works began to feel competitive pressures from other telephone cable manufacturers. It was apparent that reductions in operating expenses would have to be made in order to stay competitive. The maintenance department was faced with all the problems associated with doing more work with less people. A department that was essentially operating in a 95% breakdown mode suddenly had to find a way of not only maintaining equipment in a predictive manner, but also at a much lower cost.

In late 1989, an intensive study of the concepts of TPM was done to see if this type of program could help our maintenance department. What we found was that TPM is a plantwide process that includes all employees from top management to workers on the shop floor. TPM seeks to maximize overall equipment effectiveness, involve operators in daily maintenance and promotes team work at all levels of the organization. We also discovered in our

investigation of TPM, that TPM is based on five pillars, which are as follows:

1. Improving equipment performance
2. Involving operators in maintenance tasks
3. Improving maintenance efficiency and effectiveness
4. Provide training to increase skill levels
5. And initiating a system of maintenance prevention and early equipment management

Based on our research and a customer focused strategy which demanded proactive initiatives rather than reactive responses to equipment failures the decision was made to implement a TPM program.

Expert opinion states that TPM is not just a maintenance department program but a company wide approach to improving manufacturing effectiveness. Going into the program the TPM team found that most of the problems that stood in the way of a successful program were in maintenance. Some of the problems the TPM team had to overcome are listed below:

- an aging work force
- layoffs
- resistance to change
- too many area specialists in a declining work force
- union resistance
- tight budgets
- no computerized maintenance management system
- little or no planned maintenance
- no maintenance planners
- a disorganized and costly maintenance parts storeroom.

Based on this knowledge the decision was made to focus the TPM efforts mainly on the maintenance department for the first two and a half years of the program. The reason for this departure from the standard TPM implementation process was that the TPM team believed the maintenance department was the best place to use our limited resources.

After identifying the problem, the TPM team put together a TPM strategy to address these problems. Shown in figure 1 are the seven elements of the TPM strategy that were developed.

CENTRALIZED MAINTENANCE

Traditionally the maintenance department had been organized into an "area" maintenance configuration. This organizational structure consisted of eighteen maintenance shops spread around the facility. This type of organizational structure could only succeed with large numbers of area specialists. However, with mandated reductions in the maintenance budget and a dramatic reduction in maintenance personnel and supervisors, as shown in figure 2, some other way of providing service needed to be found. The TPM team solution was to reduce the number of shops from eighteen to two centrally located maintenance shops. After some study the TPM team found that the facility benefited in five ways with this type of organizational structure.

Consolidation of Resources

By consolidating both the tradespeople, maintenance parts and the maintenance repair equipment in just two locations, rather than eighteen small shops, the reduced number of maintenance supervisors could manage their expanded maintenance responsibilities more efficiently. Also this meant that even with a 30% reduction in manpower, due to layoffs, the mainten-

ance department was able to maintain previous service levels and even improve service in some areas. Figure 3 shows a steady increase in planned work and trades effectiveness from 1990 to the middle of 1993.

Better Craft Communications

The second benefit was to promote direct communication between the tradespeople, rather than the supervisors trying to collect equipment information and pass it on to the next shift's supervisor. In area maintenance the tradespeople were left out of the communication loop. The centralized shops located the tradespeople together which brought them back into the communications loop. This resulted in a much smoother and more efficient transfer of vital equipment information. A side note to this was that, the tradespeople had been out of the communication loop for so long that training in communication techniques was needed to help them communicate responsibly with each other.

Faster Response Time

When the maintenance department moved from area maintenance to centralized maintenance, the TPM team was initially afraid that this would increase response times. But what they found was that in the old area maintenance structure, once the first or second maintenance call in an area was answered, the preceding calls had to wait until there was a tradesperson available. Tradespeople from other area shops were

TPM STRATEGY

- **CENTRALIZED MAINTENANCE**
- **MAINTENANCE MANAGEMENT SYSTEM**
- **MATERIAL MANAGEMENT**
- **PROJECT PLANNERS**
- **TRAINING**
- **OPERATOR BASED MAINTENANCE**
- **MAINTENANCE MEASUREMENTS**

FIGURE 1

PHOENIX WORKS MAINTENANCE REDUCTION IN TRADES AND BUDGET

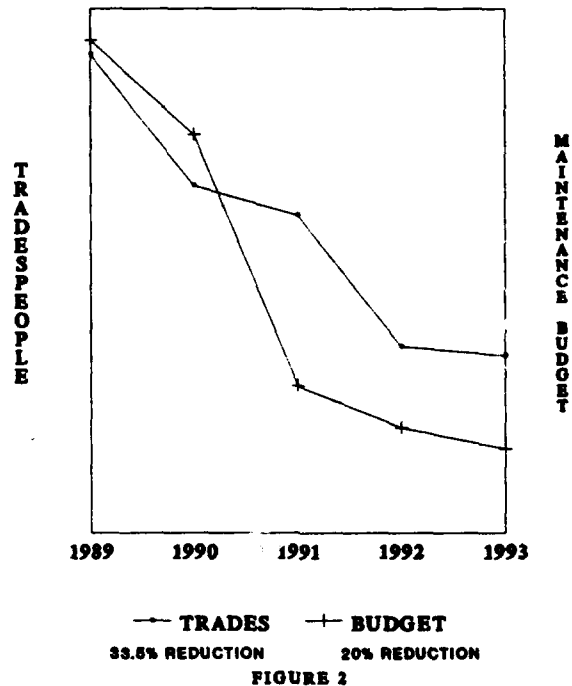


FIGURE 2

PLANNED WORK and TRADES EFFECTIVENESS

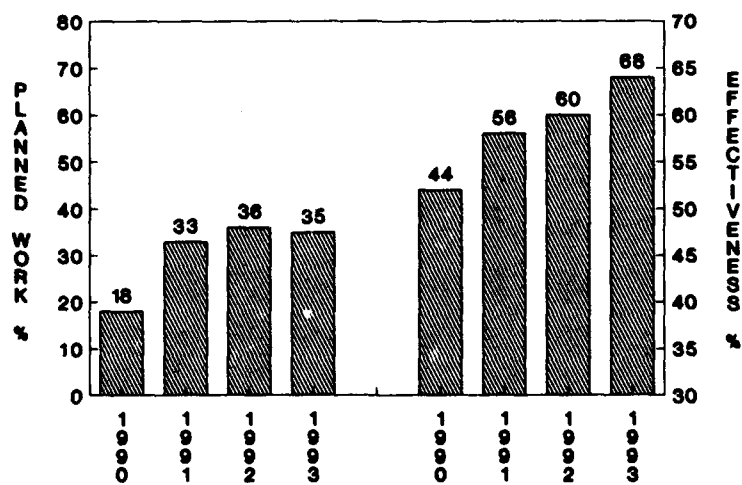


FIGURE 3

not able to help because of lack of knowledge and training in the area that needed the extra help. In fact, when supervisors got desperate and moved tradespeople to areas with numerous calls the tradespeople resented having to leave their own areas to help in another area. In the central shop structure that third and fourth call could now be answered. Tradespeople were trained to work not in just one area but in several areas. What we lost in area trades specialist expertise we more than made up for in faster response times and less overall downtime.

Reduced Floor Parts Inventory

As all the area shops were emptied of their parts it was found that there were many duplications of machine parts in the area shops. In fact after the central shops were stocked with high use items from the area shops, over \$900,000.00 worth of other parts were returned to the maintenance parts storeroom in the first year of the TPM program.

Replaces Idle Time with Planned Work

The TPM team found that the old maintenance structure had created what the TPM team came to call "Institutional Idle Time". With eighteen area shops the supervisors had a very difficult time keeping the tradespeople busy when they did not have any calls. The tradespeople would only be busy when they were on a call and idle when they were not on a call. This had gone on for so many years that this wasteful practice had, to the horror of the TPM team, become institutionalized in the minds of the tradespeople.

The TPM team chose to address this problem in two ways. The first was to move the tradespeople into the central shops and provide them with meaningful planned work and not just fill in work. The second was to communicate openly with the tradespeople that their operating customers could not produce quality products efficiently on poorly maintained equipment and that the old maintenance structure could not meet the goal of increasing equipment performance. Furthermore, if their customers' needs were not met the result of this would be lost business and more layoffs. The important outcome of this is that tradespeople are busy with planned work when not answering calls. This has had a positive effect on response time, equipment performance, repair times and downtime.

COMPUTERIZED MAINTENANCE MANAGEMENT SYSTEM

The TPM team realized early on that the maintenance department would need some way to collect, track and use data to their advantage. The TPM team found that the only practical way of doing this was with a computerized maintenance management system (CMMS). After researching over thirty programs, a UNIX based program was selected for the job. After the program was installed the TPM team made one of the toughest decisions that any TPM team would ever have to make. It was decided that the system would not be reserved just for a few planners, supervisors, or engineers but for everyone who could benefit from the system. This meant that over six hundred people would have to be trained. The TPM's teams rationale behind this was that TPM is not just a maintenance program but a plantwide program of improvements and that a maintenance management system would be a good way to get everyone involved. Some of the benefits of this strategy are as follows:

Operator/Tradespeople Driven Data

The CMMS has proved to be very helpful to the machine operators. Instead of writing a call on a call sheet and turning a light on, they can now write a work order and input several levels of data on the work order. They can contribute their years of experience and knowledge about equipment problems by using CMMS failure causes codes that they helped create. They also were able to explain their problems in more detail by using the additional description option included in the CMMS package. These features gave them a sense of control and ownership they had never had before. This had the added benefit of encouraging the operators to learn more about their equipment.

The tradespeople could also contribute their knowledge and expertise to the CMMS data base. At the shop level they could get printed work orders, log on and off work orders, transfer work orders to other trades, carryover work orders, input repair data, input labor hours, add additional descriptions, check equipment history, and extract parts information.

Real Time History

Now for the first time the operators and the maintenance people could get real time machine history. With a little training, an operator or maintenance person could go to the nearest terminal and find out maintenance history on a particular

machine with just a few key strokes. An operator could check history before writing a work order to see what work had been done on his or her machine. This information helped the operator decide what information to include on their work orders. The tradesperson could, by checking history, get a good idea of what parts and tools to take to the job. And if the operator's information was thorough enough have a reasonable idea of what might be wrong with the machine before he leaves the shop.

Component Level

One of the goals of the TPM team was to make it easy for the operators to input data, down to component level. The TPM team realized, that since we already knew the run times of machines from hour meters on the machines, the next logical step was getting the operators and the tradespeople to input component data. The TPM team was able to do this by creating a set of windows inside the CMMS. Once the operator chooses a component from the window he or she is given another window with all the possible failures for that particular component. After the operator makes the choices the work order is sent to the correct trade. The trades part in this is to correct the operator's component data, if necessary. The windows feature dramatically increased the amount of data for failure analysis and gave the maintenance department a much clearer picture of equipment failures. Some of the benefits of using the CMMS to gather component data are listed below:

- involves the operators in the repair of their equipment
- gives the operators a sense of ownership of their equipment
- helps the operators learn diagnostic skills
- makes it possible to identify and prevent recurring equipment failures
- makes it possible to create pm routines to extend the useful life of equipment
- makes it possible to create predictive maintenance routines that anticipate failures
- helps production and trades teams develop permanent fixes rather than band-aid approaches

Data is Available to Everyone

Before the TPM program there was little or no equipment data available. Now equipment and maintenance data is available to anyone who wants it. Operators, tradespeople, engineers, quality of work life teams, quality improvement teams, and yield improvement teams can retrieve data easily and quickly. With the data the different teams are able to identify

recurring problems and search out solutions. The CMMS system gave everyone a chance at participating in activities that improved equipment performance, reliability and maintainability.

An example of people using data to identify and correct a problem happened in our poly jacketing area. A poly jacketing team identified a particular troublesome problem with corrugators that were causing considerable downtime and scrap. A maintenance team took up the challenge of solving the corrugator problem. By using the CMMS data they were able to identify which components in the corrugator were failing and how often. This then lead the maintenance team to a practical solution. The solution to this problem is now saving over \$100,000.00 a year in parts, labor, and scrap. This is only one of many examples of the CMMS data being used to correct equipment problems.

Preventive and Predictive Maintenance Routines

The CMMS has helped the maintenance department go from almost no preventive maintenance (pm) routines to over three thousand routines in the CMMS system. The system is able to print pm routines based on the amount of time a piece of equipment runs or on a calendar basis, weeks, months, etc. The CMMS system is also able to track the progress of the pm's and report what percent of pm work is backlogged.

Predictive maintenance routines have been added to the CMMS system which include oil analysis, thermal scanning of electrical connections and the use of special instruments to detect air leaks. This combination of preventive and predictive maintenance has helped us to reverse the deterioration of equipment and extend its useful life.

MATERIAL MANAGEMENT

The third strategy the TPM team undertook was to replace the old and out dated maintenance parts storeroom manual records system. This sytem produced many mistakes and was slow to respond to maintenance requests for timely ordering, stocking and delivery of parts.

On Line with CMMS

Once the CMMS was loaded with the store-room information we were able to improve the storeroom operation almost immediately. Instead of taking nine days to order a part, from the time it got down to minimum levels with the old system, we now get an order out the same day the part

reaches its minimum level. The system also has helped us identify thousands of dollars worth of obsolete and duplicate parts.

Parts Usage Tracking and Vendor Partnerships

We can now track the parts usage data so well, that we have been able to lower the maximum levels on over fifty percent of the parts in the maintenance parts storeroom. With the CMMS we could now track parts usage by business unit all the way to component level on the equipment. This allowed us to see where the shop floor was being hurt the most in terms of parts usage and unexpected breakdowns. With this information the project planners or one of the teams could investigate why there was a high use rate. Once the reason was known a plan of action could be formulated to solve the problem. Some of the problems found by analyzing parts usage data are listed below:

- improper installation
- poor quality parts
- improper set up procedure
- machine speed exceeding parts tolerance
- improper lubrication or no lubrication
- improper adjustments of parts

The TPM team set up vendor partnerships with local suppliers; whereby, the vendors stock machine parts in their storerooms which allows us to lower the inventory in our maintenance parts storeroom. These items have proved to be a great help in lowering our machine parts storeroom investment as seen in figure 4.

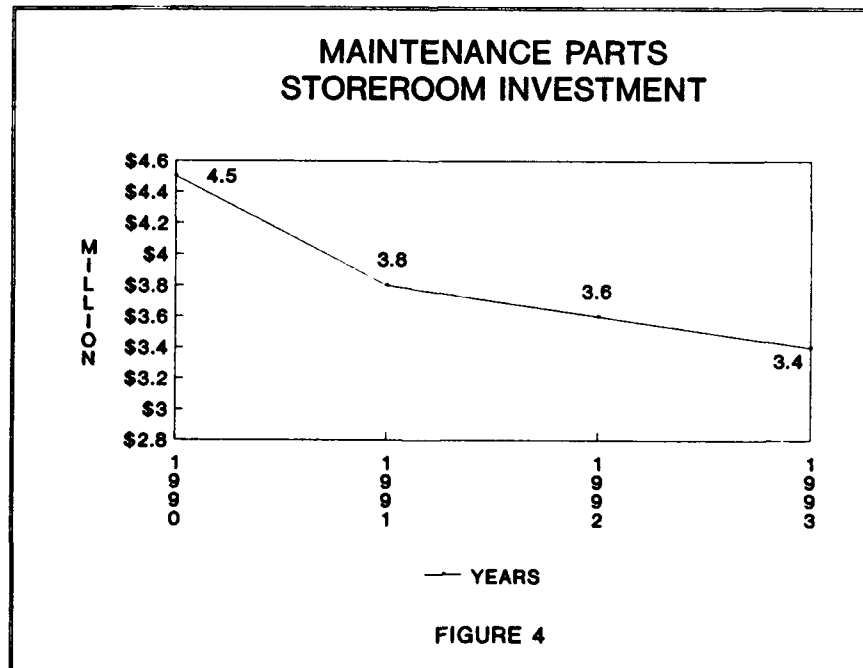
Remote Service and Parts Searches from Remote Locations

The TPM team recognized that to have the tradesperson leave the job site to go to the storeroom to get parts only increased repair times. So the team set up a system whereby the tradesperson called in the order for parts and they were then delivered to the job site by the storeroom attendant. The attendant is also required to wear a pager so that he or she is available at all times to answer parts requests. Another benefit of the CMMS was that instead of the tradespeople coming all the way to the storeroom to get parts information, they can now access parts information from terminals in their shops or terminals on the shop floor, thus eliminating unnecessary trips away from the job.

PROJECT PLANNERS

Before the TPM program there was little or no job planning. What planning was done was done by maintenance supervisors. But due to the demands on their time planning was not done very well. It was decided by the TPM team to create a job description of project planner. This was completed and five maintenance people were chosen as project planners. These five planners were initially given one hundred and twenty hours of training. Some of the areas they received training in were as follows:

- planning projects
- failure analysis
- communications



- technical writing
- word processing
- using the CMMS
- presentation skills
- time management

The planners have proved to be very good at planning both small and large projects. They have been able to save considerable time and money. Large jobs that took four or more weeks to complete, have now been cut to as little as five days or less. The planner's ability to use the CMMS data to identify where the real equipment problems are, plan the jobs and put them into our schedule has helped the maintenance organization to do more work with less resources than ever before.

TRAINING

The TPM team put a high priority on training from the beginning of the TPM program. Some of the areas of training offered by the maintenance department in conjunction with the resident training organization are listed below:

- CMMS training
- team building skills
- technical training on electronic drive systems
- communication skills training
- understanding TPM and the TPM strategy
- cross training
- learning how to document successful equipment improvements
- failure analysis training

The training is an ongoing everyday process and has proven worth the expense and effort.

OPERATOR BASED MAINTENANCE

The TPM team felt from the start that operator based maintenance was the one strategy that would produce the most results. But due to the pressing need to get the maintenance organization to a higher level of performance, it was decided to put aside this part of the TPM strategy until the TPM team could devote more of its time and resources to it. The TPM team believes that some of the advantages of implementing a program of operator based maintenance in our facility are as follows:

- 20% less downtime
- 30% reduction in routine maintenance calls
- faster repair times
- elimination of sources of contamination
- less backlogged pm work
- a greater sense of ownership by the operators
- makes it possible to accelerate machine conditioning programs

- more reliable equipment producing less downtime and scrap

At the two and a half year point of the TPM program the TPM team is now shifting its focus to operator based maintenance. A representative from the company and union have been chosen to head up the team that will implement this part of the TPM program. The team has chosen the pilot area, and has scheduled initial cleaning of the equipment. Identification of tasks to be transferred to operator has begun. A maintenance skills training program for operators is being developed. The operator based maintenance part of the TPM is projected to take two and a half years to implement throughout the facility.

MAINTENANCE MEASUREMENTS

The TPM team knew that for the TPM program to be successful it was important to find meaningful ways to measure the program, besides the usual financial metrics of labor and material costs.

Planned to Unplanned Work

The first metric they chose was planned to unplanned maintenance. Planned work is classified as work that is planned by a project planner. Planned work can be preventive or predictive maintenance, scheduled repair or shop work. Scheduled repair work is planned work that is done on the shop floor. Our machine condition program is an example of this type of work. Shop work is planned work that is done in one of the two maintenance shops and is usually refurbishing of parts and spare equipment. Unplanned work is simply any work originating from the operator of a machine that is scheduled to run on that day and is down because of a maintenance problem.

Maintenance Effectiveness

Maintenance effectiveness is simply a calculation of trades hours in the facility minus training, personal time or safety instructions divided into the amount of time the tradesperson spends on either planned or unplanned work. A figure of 75% is considered excellent.

Maintenance Downtime

Maintenance downtime is the time that the machine was available minus the amount of time the machine was down for unplanned maintenance. Before TPM, figures of well above 10% downtime were not uncommon, but since TPM most downtime figures are well below 10%.

Maintenance Response Time

Maintenance response time is the result of operating departments wanting some type of measurement of how fast maintenance was able to respond to their equipment breakdowns. Maintenance response time is the amount of time between when the work order is written by the operator and sent to the maintenance shop and the time it takes the tradesperson to log on to the work order. This metric is reported to the operating departments monthly.

Parts Usage

Parts usage is tracked monthly by department and individual machine. Any sudden rise in parts usage is investigated by the project planners and storeroom personnel with recommendations being sent to the maintenance supervisors for action.

Repair Time

Repair time is tracked by job type, trade type and machine type. Planners use this information to estimate time and cost of future planned work.

CONCLUSIONS

The results of our TPM program at the AT&T Phoenix Works cable manufacturing facility have been very encouraging. The TPM program has made it possible for the tradespeople to learn team building skills, improve communication skills and learn failure analysis skills. In the first two and a half years of a five year TPM program, the maintenance department has increased preventive and predictive maintenance (planned work) from 5% in 1989 to 35% in 1993. Equipment that has been included in the TPM program has had increases of 20% to 30% in efficiency. The effectiveness of the tradespeople has increased from 36% in 1989 to 68% in 1993. These improvements were obtained at the same time the maintenance budget was substantially cut and with a corresponding 35% reduction in tradespeople and a 50% reduction in maintenance supervisors.

The TPM team has concluded the planned work figure is as high as it will get with our present resources. To increase the planned work number any higher will depend on the success of the operator based maintenance program. Given how much is riding on this one strategy, the TPM team is spending a lot of time and energy on this part of the TPM project.

What should be obvious to anyone who is familiar to TPM is that we did not implement our TPM program by the book. The question has to be asked, "Were we correct

in the way we implemented our TPM program?" Given the resources available and the results to this point in the program, our answer to that question would have to be yes. Have there been any disappointments in our program? Yes, we have had to delay activation of some of our pm's and we have had to delay some very important machine conditioning work. Both of these items are vital to the success of this facility but are delayed due to a lack of available maintenance resources (labor and material). Has this caused the TPM team and the maintenance department to give up and say, "this is the best we can do"? No, we are continuing to work hard with the resources we have to reach our goals.

There are some lessons to be learned from our experiences with TPM. The first is, always remember that the most important goal of TPM is to increase equipment performance. The second lesson is, maintenance cannot afford to isolate itself from production. The "go it alone" approach of the past has no place in a TPM program. And from our view point, the most important lesson is, if you wait until you have the resources and everyone's support, you will probably never get a TPM program off the ground. Our advice is, don't wait, get started now with the resources you have.

REFERENCES

Nakajima, Seiichi (ed.). Introduction to Total Productive Maintenance (1988). Productivity Press, Cambridge, Mass.

Wireman, Terry, (1991). Total Productive Maintenance: an American Approach. New York: Industrial Press, Inc.

DAVID W. HOLLEY
AT&T Network Cable
Systems
Phoenix, AZ



David W. Holley is a Maintenance Supervisor at the AT&T Phoenix Works Cable facility in Phoenix, AZ. Mr. Holley has degrees in Electronic Technology and Business. He also has a Masters degree in Management. He has been with AT&T for twenty three years. His present assignment is TPM supervisor.

ASSURING THE OVERALL PERFORMANCE OF COPPER CABLING SYSTEMS

Ned A. Sigmon

AMP Incorporated
Winston-Salem, N. C.

ABSTRACT

While a great deal of emphasis has been placed in recent years on improving the transmission characteristics of communications cabling components (cables and connecting hardware), the bottom line is the overall or end-to-end performance of install runs. Networking standards, for example, will typically specify minimum channel performance where most if not all of the channel is the cabling link between a transmitter and receiver.

This paper examines the alternative of cabling system or link performance, the relationships between link performance and component specifications, and the current status of link performance specifications.

INTRODUCTION

The Continuing Evolution of Communications Wiring

Communications wiring has changed a great deal over the past eight to 10 years, evolving from an environment of separate telephone and data wiring systems and proprietary data wiring configurations to generic, structured cabling systems that integrate telephone, data, and potentially even other building communications such as control, safety, etc. A major factor in this evolution has been the development of the EIA/TIA 568 Standard for Commercial Building Telecommunications Wiring¹ and a migration toward international standardization of communications cabling.

During this same period, the data communications needs to the desktop have jumped from a few kilobits per second to over a hundred megabits per second, with no end yet in sight. To meet the needs of these higher speed applications, the manufacturers of copper cabling have developed new cables and connecting hardware of increasingly higher transmission performance capabilities. The EIA/TIA working group has responded by

incorporating new specifications for these higher performance components, and networking standards committees have adopted the new specifications as a basis for higher speed networks.

The latest development in the evolutionary process is a shift in emphasis from component specifications to overall or end-to-end performance specifications for complete cabling systems. A draft revision of the EIA/TIA 568 Standard² contains guidelines for estimating the attenuation and year end crosstalk of a horizontal cabling link. A proposed ISO/IEC cabling standard³ takes the bolder step of actually specifying end-to-end performance for both the horizontal and backbone links.

THE ISSUE OF LINK PERFORMANCE

Why Do We Need Link Performance?

The arguments for link performance can be boiled down to two:

1. Local area network standards require it.
2. Customers are demanding it.

Local area networks have been the driving force behind the development of higher performance copper cabling. The 10BASE-T standard was the first to define the characteristics for what is now known as Category 3 unshielded twisted pair (UTP). IEEE 802.5 created the need for Category 4 to support 16 Mbps Token Ring, and 100 Mbps TP-PMD (FDDI over copper) requirements led to Category 5.

In all of these applications, the transmitter-to-receiver channel has been defined in terms of maintaining a certain minimum signal-to-noise ratio. The cabling system equivalent to the signal-to-noise ratio is the combination of attenuation and near end crosstalk (NEXT) that, depending on which standard you read, is called the attenuation-to-crosstalk ratio (ACR), or the NEXT-to-insertion loss ratio (NIR). Return loss and balance are other cabling system parameters that can affect signal and noise levels, but up to now,

these have been assumed to have less impact on network performance than the ACT/NIR.

As high performance copper cabling becomes more prevalent, there is a growing realization that component specifications alone will not necessarily assure an adequate level of link performance. The care and techniques used in installing the cabling system are equally important. Run lengths, connector terminations, and cable management are but a few of the factors that can affect installed performance. A poorly controlled installation can negate the advantages of using higher performance components.

The purchasers of high performance systems currently have no reference for what to expect from a properly installed system, and, until recently, no way to accurately measure installed performance to the levels and bandwidths needed to verify the system. In effect, they are at the mercy of the cabling system designers and installers.

To make the situation worse, most of the high performance cabling being installed today is not actually being used for the higher data rate applications. It may be years before users upgrade their networks and learn that they have a problem. Purchasers are therefore beginning to demand guarantees that the installed system will provide the performance to support future needs and will maintain that performance over the expected life of the cabling system.

The Status of Link Performance Specifications

The next revision of the EIA/TIA 568 Standard, estimated to be available around mid-1994, will include guidelines for estimating the attenuation and NEXT loss for Category 3, 4, and 5 UTP links using the component specifications. As currently proposed, these guidelines will be in an informative annex that is technically not part of the standard, although customers may miss that distinction in applying the specifications.

The EIA/TIA guidelines provide an example calculation using the link model shown in Figure 1. The worst-case ACR or NIR values predicted from this model are shown in Figures 2 and 3, which show slightly different values between the outlet and wiring closet ends of the system. This results from the different numbers of connecting hardware components at each end and the assumptions used in calculating NEXT loss.

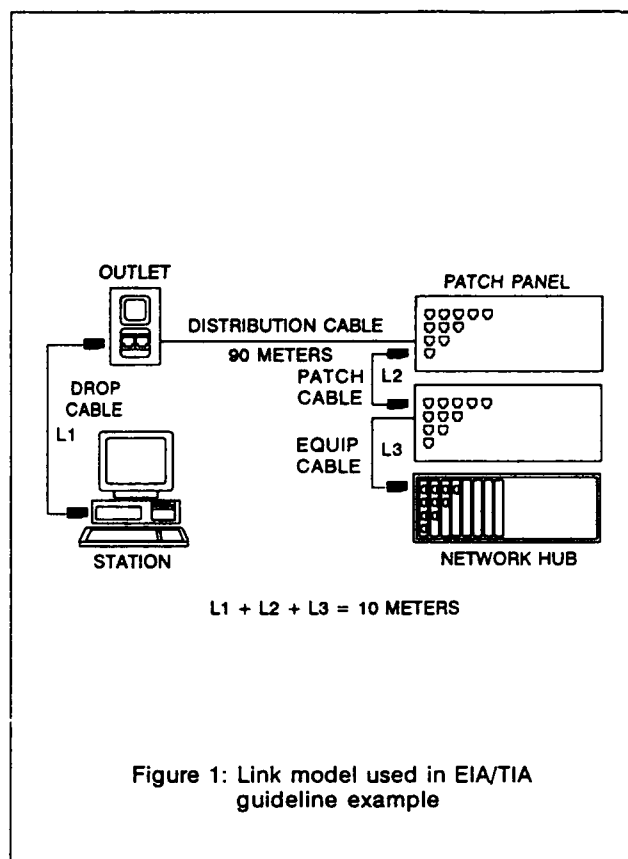


Figure 1: Link model used in EIA/TIA guideline example

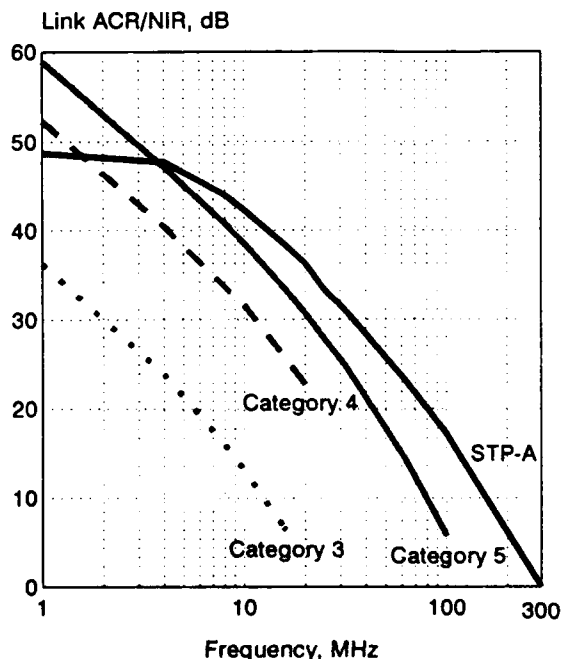


Figure 2: ACR/NIR at the *work station* end of a horizontal cabling link, as predicted by EIA/TIA guidelines

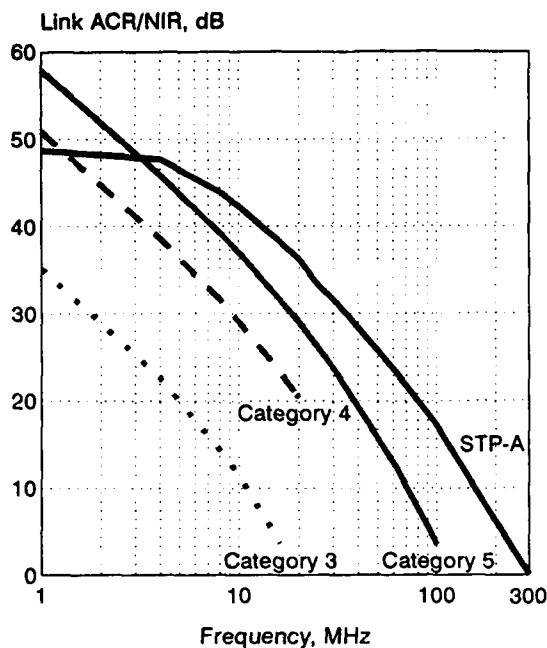


Figure 3: ACR/NIR at the *wiring closet* end of a horizontal cabling link, as predicted by EIA/TIA guidelines

Overall attenuation can readily be calculated by summing the component attenuations, but NEXT loss is more difficult due to phase shifts between component contributions and the effects of cable lengths. The link NEXT in the EIA/TIA guidelines is based on two key assumptions:

1. Unless the link is very short, only the NEXT from components near the end of interest will be significant.
2. In the worst case, the NEXT contributions of these components will be in phase with each other and can be combined as a voltage summation.

Logically, the second assumption may seem overly conservative since one would not expect the NEXTs to be in phase. However, the initial data available to the EIA/TIA working group has been more closely approximated by voltage summation than by less conservative models. Voltage summation produces the following formula:

$$\text{Total NEXT Loss (dB)} = -20 \log_{10} (10^{-N1/20} + 10^{-N2/20} + \dots)$$

where $N1$, $N2$, etc. are the NEXT losses in dB of the cable and connecting hardware.

The 568 revision provides no guidelines

for 150 ohm STP cabling (upgraded in performance to STP-A), but presumably the same criteria would apply. The resulting ACR/NIR values for STP links are also shown in Figures 2 and 3.

A proposed ISO/IEC standard divides the horizontal links into four classes designated A through D, specifying maximum attenuation and minimum NEXT loss for each. For Class D, the ISO/IEC standard additionally specifies ACR values that override the individual attenuation or NEXT loss specifications with a more demanding requirement. The purpose is to provide the engineering option of using shorter links of lower performance components.

The link model used by the ISO/IEC standard is shown in Figure 4. The ACR/NIR specifications for Class C and D links are shown in Figure 5.

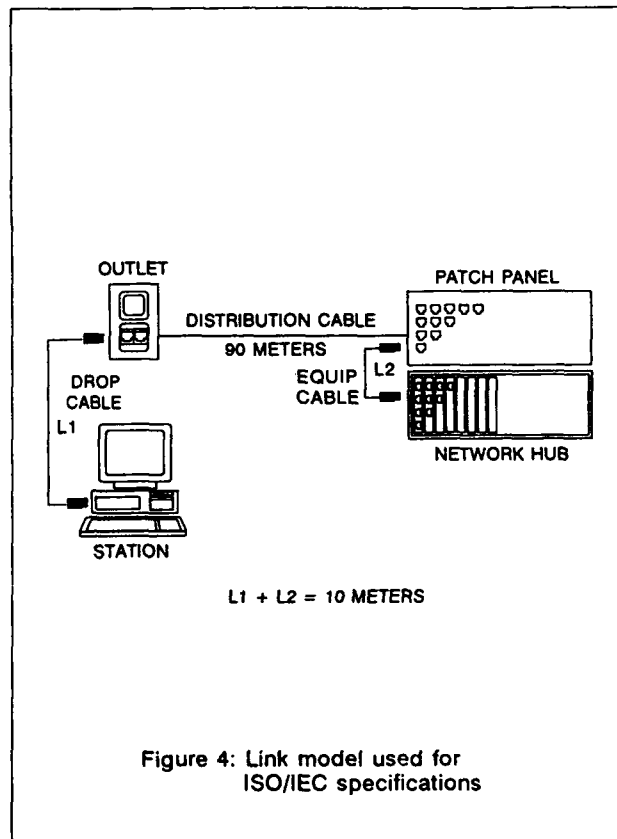


Figure 4: Link model used for ISO/IEC specifications

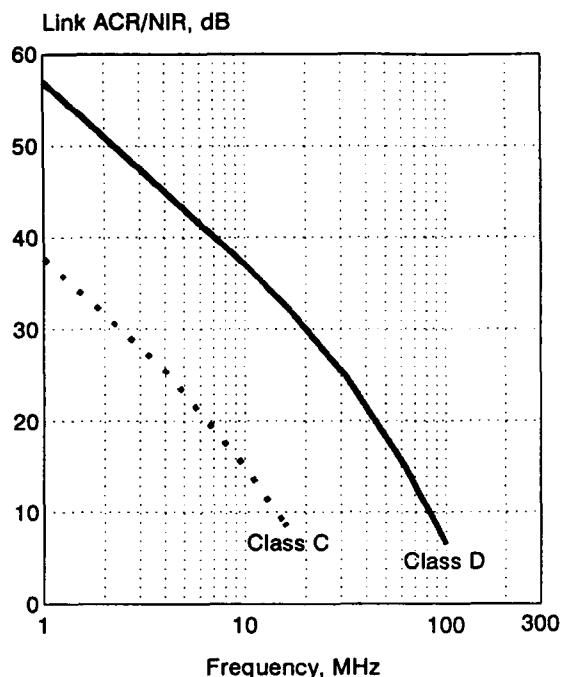


Figure 5: ISO/IEC specifications for link ACR/NIR

The ISO/IEC model differs from the example model in the EIA/TIA guidelines in that drop or equipment cables are not included and only half of the cross-connect in the wiring closet is considered as part of the link. This theoretically should produce better results than the EIA/TIA example, but in comparing the two, that does not seem to be the case.

Since the link Classes can apply to 120 and 150 ohm cabling, as well as 100 ohm UTP, the ISO/IEC standard avoids a correlation between link Class and component Category. However, Classes C and D roughly correspond to the EIA/TIA Category 3 and 5 systems as a comparison of Figures 2 and 4 will indicate.

Comparing the Proposed Specifications to Network Requirements

Since the main purpose of link performance is to assure conformance to network standards, the proposed guidelines or specifications should at least provide an adequate margin to the requirements of known standards. Figure 6 shows the NIR requirements of a 16 Mbps token ring using a passive concentrator, as defined in the draft IEEE 802.5 standard.⁴ These requirements are compared to the NIRs computed from EIA/TIA guidelines or ISO/IEC link specifications. Although the NIR would also include other factors such as concentrator attenuation, a Category 5 or Class D link specification should leave plenty of margin.

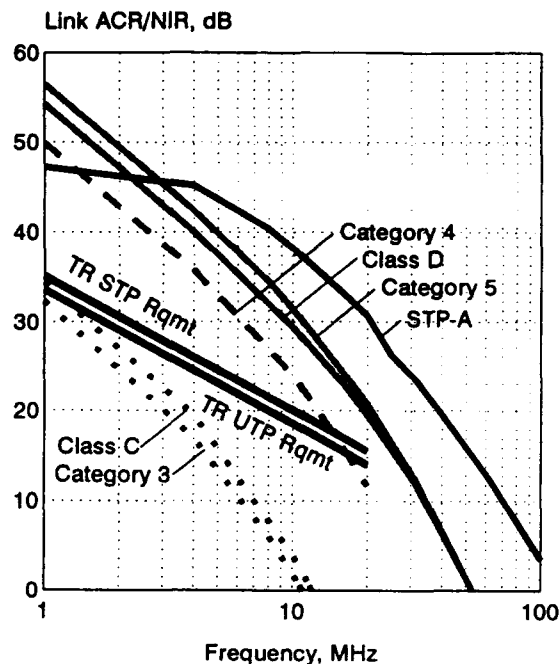


Figure 6: Comparing EIA/TIA guidelines and ISO/IEC specifications to 16 Mbps token ring/passive hub requirements

Figure 7 compares the ACR requirements of the proposed X3T9.5 standard for 100 Mbps TP-PMD to the EIA/TIA guidelines and the ISO/IEC link specifications.

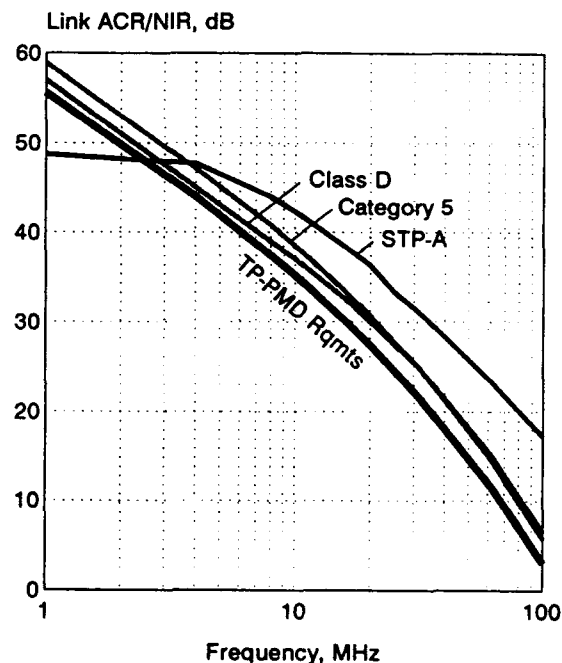


Figure 7: Comparing EIA/TIA Guidelines and ISO/IEC Specifications to 100 Mbps TP-PMD Requirements

The TP-PMD requirements fall very close to the Category 5 or Class D expectations, which is not totally unexpected since the TP-PMD requirements have been based on the expectations of the EIA/TIA UTP guidelines. However, the margins allowed by the TP-PMD requirements are only a few dB.

Comparing the Proposed Link Specifications to Current Capabilities

If network standards and network hardware are being designed around proposed guidelines or specifications with minimal margins, then it is vital that the specifications conservatively represent the capabilities of actual installations. NEXT voltage summation was assumed to be an adequately, if not overly, conservative approach, but more recent data casts doubt on this assumption. To illustrate, Figure 8 shows the NEXT of a system constructed to the model of the EIA/TIA guideline example, using commercially available Category 5 cables and connecting hardware and measured from the outlet end. The data demonstrates the peaks and nulls that are typical of such measurements and that make accurate interpretation somewhat difficult. Taking the peaks as the worst-case NEXT, the system performance passes the EIA/TIA guideline estimates, but only barely.

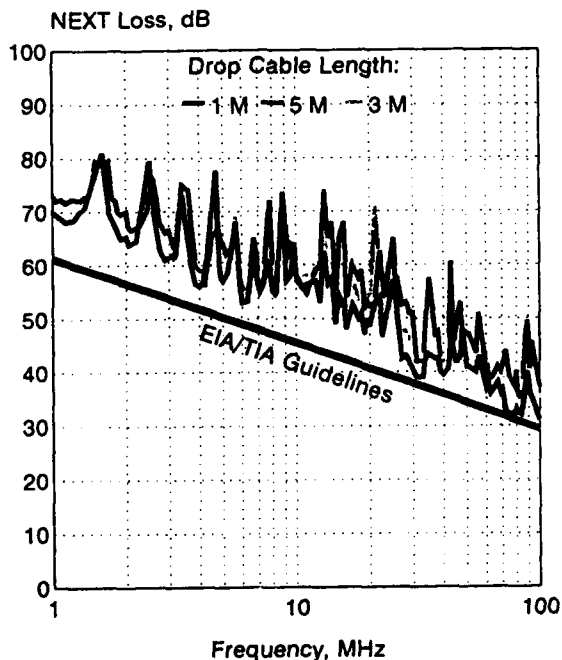


Figure 8: NEXT loss of a typical Category 5 cabling link, measured from the outlet end

Looking at the same system from the closet end, Figure 9 shows that some of the NEXT peaks actually exceed the guideline estimates. Per this interpretation of the data, the guidelines are not conservative. The ACR/NIR may still meet the requirements of the network standards, but only if attenuation is less than maximum.

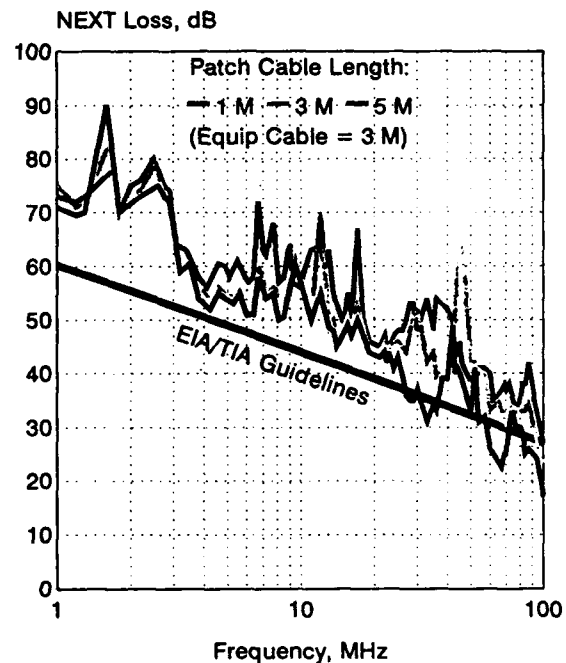


Figure 9: NEXT loss of a typical Category 5 cabling link, measured from the wiring closet end

These measurements were made under relatively controlled laboratory conditions using precision network analyzers. In reality, link performance will be judged against field measurements made under less controlled conditions using less precise instrumentation. This will undoubtedly introduce additional variability.

Where Do We Go From Here?

Link performance is a complex issue that, as this is being written, needs further study before firm specifications can be defined. In recognition of this need, a TIA task group has been formed to reevaluate the current guidelines, as well as the test procedures and the test instrument specifications for verifying link performance.

In the meantime, link performance is here to stay whether we like it or not. If improved field instruments and link

performance guidelines are available, customers will use them to evaluate their installations and will demand guarantees of link performance or capabilities. In response, the manufacturers of communications cabling must start to "think link," looking at component design from the standpoint of maximizing installed performance and minimizing installation variables.

REFERENCES

1. ANSI/EIA/TIA-568-1991: "Commercial Building Telecommunications Wiring Standard," July 9, 1991
2. Standards Proposal No. 2840, Proposed Revision of EIA/TIA-568: "Commercial Building Telecommunications Wiring Standard," Telecommunications Industries Association, July 28, 1993
3. ISO/IEC JTC 1/SC 25 N303, the July, 1993, Draft of a Proposed International Standard for Generic Communications Cabling
4. IEEE Draft Standard 802.5q/D4 (Proposed Revision to 802.5): "Information technology - Local and metropolitan area networks - Part 5: Token ring access method and physical layer specifications," July 23, 1993
5. X3T9/92-X3T9.5/92-TP-PMD/248, Rev. 1.0, Working Draft of a Proposed American National Standard: FDDI Twisted Pair Physical Layer Medium Dependent (TP-PMD), June 23, 1993

Ned Sigmon is Technical Marketing Manager for the Communication Products Division of AMP Inc., located in Winston-Salem, North Carolina. AMP's Communication Products Division manufactures cabling systems for building communications and power, as well as I/O connectors for communications equipment.

In his current position, Ned is responsible for the technical performance of premise wiring products and the technical support of sales engineering and customer applications. Prior to this position, he was responsible for development of new premise wiring products.

Ned is a member of the EIA/TIA TR 41.8.1 Working Group, the ANSI X3T9.5 TP-PMD Working Group, and the IEEE 802.5 PHY Working Group. He holds a Master's Degree in Mechanical Engineering from the University of New Mexico, as well as a Bachelor's Degree from North Carolina State University.

**TOTAL QUALITY MANAGEMENT - A PRACTICAL APPROACH TOWARDS
IMPLEMENTATION OF A CIM BASED QUALITY PROGRAMS IN A
MODERN TELECOMMUNICATION CABLE PLANT**

M. J. Khan

**Saudi Cable Company
Tele-Cable Division, Jeddah, Saudi Arabia**

ABSTRACT

This paper describes a practical approach towards implementation of a CIM based quality system from the time an enquiry is received from the customer till the cables are manufactured and shipped. A customized software developed and implemented on a PC based LAN integrates the various shopfloor activities and provides a common data base for key personnel in the Sales/Marketing, Technical, Research & Development, Material planning and logistic control, Production shopfloor and Quality Control departments besides providing direct access to Management and Corporate Quality Auditor (Quality Assurance department). The system provides instant traceability of finished cable measurements (final inspection) with the in-process measurements on it's sub-components and hence provides the basis to employ statistical tools in order to determine process capability and performance to improve product design criteria. All efforts have been directed to improve the processes involved in the manufacture of the product rather to concentrate alone on the quality improvement of the product. Thus the objective of Quality at its best has been greatly achieved in the form of optimized production and material consumption and reduced scrap etc.

INTRODUCTION

The present race among the manufacturers to have early accreditation to the International Standard Organization (ISO 9000 series or equivalent) has necessitated to allocate enormous resources in order to achieve this objective. ISO certification has virtually become a requirement for doing

business in the European community. It is a quality system whose fundamental requirement is to document every action, process and operation of a company's manufacturing operations and make changes in the documents as required for quality improvement purposes etc. thru documented control forms developed for the purpose. The ISO certification provides a certain degree of confidence in the customer's minds that the company (supplier) has adopted a well documented quality system in it's operation and the products are expected to be of high quality. However, it does not necessarily mean that an ISO certified supplier would always supply a guaranteed quality product. Infact it is no more sufficient for a manufacturer in this competitive world market that it's products pass the final acceptance tests but the whole organization involved in the manufacturing must assure that all production processes are under strict control, the ultimate goal to be met, being the optimized production and material consumption, reduced scrap and just-in time delivery concept. In this paper efforts have been made to achieve this goal and objective by developing and implementing a customized software which provides information on measurements at various production stages to key personnel directly involved with the production processes. The semi-finished product manufacturing at sensitive machines and processes which directly influence the quality of the finished cable are monitored thru vigorous measurement of physical dimensions as well as using computerized test sets to measure electrical parameters. These information are entered in the PCs located at the work stations on the production shop floor and connected to the plant manufacturing system in a local

area network. Thus a complete traceability of an accepted (or rejected) finished product to the in-process measurements on its components at various production stages is instantly available. The well traceable data of measurements at WIP stages and final inspection provides on one hand the necessary input to the statistical tools employed in order to determine process capability and performance where as on the other hand, it provides early detection of defect(s) to be prevented from further processing. The production shop floor feed back information and statistical analyses carried out by the system software, enhanced the capability of the production environment to achieve better performance of the manufacturing processes resulting in quality products, optimal cable design, material consumption and reduced scrap.

TOTAL QUALITY MANAGEMENT (TQM) CONCEPTS

The term, TQM was first introduced by the U.S. Naval Air Systems Command to describe its Japanese - style management approach to quality improvement [1]. Since then, Total Quality Management has taken on many meanings. It is a multi-dimensional product attribute relating all the processes and a series of systematic documented actions by virtue of which the product was produced to the best of customer's satisfaction. It is a management approach to long-term success through customer's satisfaction based on the participation of all members of an organization in improving processes, products, services and above all, the culture they work in. Under the new understanding of quality culture, the survival of companies over the long term period depend only on strategic planning in quality. The management must expect user acceptable quality from every employee of the organization. Customer's satisfaction is what need to be addressed as over all goal for each employee of a company i.e. accountant, financial analysts, production, engineering, sales and marketing and of course the vendors. The only way to make consistently user acceptable quality product is to build quality at every stage / line of the production process and at the support departments giving the necessary information for producing the product. One has to study each part, every

procedure and set statistical controls to prevent variation in quality and prevent re-occurrence of non-conformance.

Companies and businesses of the remaining decade and 21st Century are going to be competitive. The challenge of the present day is to respond faster to market demands, most competitively with high degree of reliable products which are consistent in quality every time. This sets a rigid frame work for the management of a manufacturing unit to optimize product design, apply stringent process and quality controls based on quick and accurate production feedback system using an efficient information data base and thus reduce waste, increase operational efficiencies and produce the product repetitively with the same degree of quality at reduced costs.

The concept of Total Quality Management, quality circle, quality control and product improvement is to satisfy the changing needs and requirements of the customer. Application of productivity improvements techniques are essential, however, not at the cost of sacrificing quality. As the proverbial quote - quality is produced not inspected; each employee and vendor at its own level must be trained to give only quality output (product). Total productivity and efficiency should therefore be determined on the basis of "Quality Production" in qualitative forms and must not be weighed against the quantity produced. As the Japanese manufacturers call it KAIZEN, no product is ever perfect or good enough. One has to continually strive for perfecting / improving the product in terms of quality. New ideas should be given chance even if they fail to achieve objectives sometimes. Motivation of staff members is essential so they feel part of the total quality concept being introduced and implemented in the company. Regular communication and timely announcement will keep every employee of the organization aware of the plans and operations and keep them motivated on the achievement to target objectives and long terms plans. TQM concepts benefit all organization members and society. The methods for implementing this approach are found in the teachings of such quality leaders as W. Edwards Deming, Philip B. Crosby, Kaoru Ishikawa and J.M. Juran.

AN EFFICIENT SYSTEM

A customer's desire would be to promptly receive manufacturer's response with respect to the key questions of his enquiry. These are ;

- o Full compliance with specs. (Quality)
- o Delivery (Commitment)
- o Price (Competitive)

A cable manufacturer's desire would be to respond to customer at it's earliest, quoting best price, minimum delivery period and full compliance with the specification requirements. Upon receipt of an enquiry, the first decision is to determine if the product(s) can be quoted. In the process, sales, technical/design engineering and planning departments are involved to prepare technical offer / compliance, prices and delivery schedule of the cables requested. In case an order is placed, the cables have to be manufactured according to the agreed (contract) technical specification / design and quality test requirements. These actions are carried out starting from the design engineering to planning, process engineering, production, quality control, raw material as well as in-process and finished goods inspection until the cables are transferred to shipping department or customer. Various information and documents are thus needed to complete the customer order.

Fig. 1 summarizes the above activities and terms it an efficient system if an enquiry is responded within the stipulated time frame requested by a customer where as for the ordered cables, the traceability of manufacturing data and documents is maintained and retrievable at any stage and time. Such an efficient system has implicitly built-in quality system, which are translated into a Total Quality Manufacturing Program as shown in Fig. 2. In this program, customer's specification requirements are defined, production / machine capabilities are determined, cable design / construction is made and translated into a manufacturing document, process methods and machine routing etc. are defined and finally a production schedule is chalked out. On the other hand, the customer's test requirements, test frequencies, values, limits are specified and merged into the total quality manufacturing program.

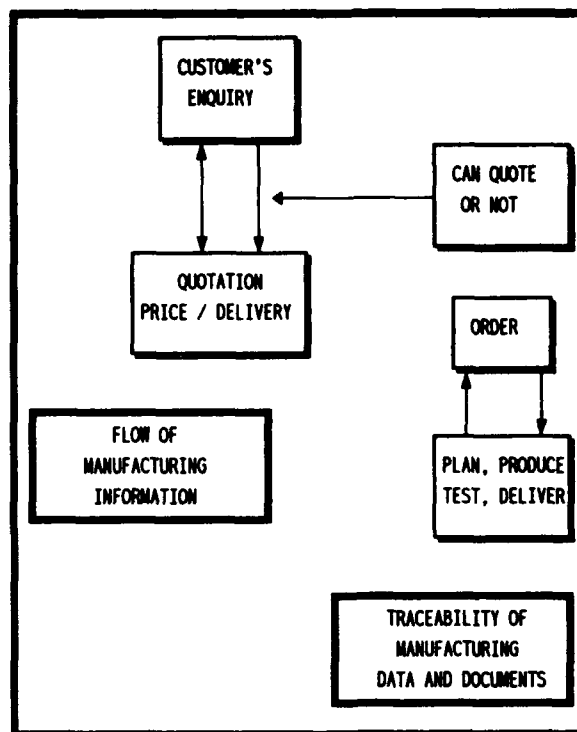


Fig. 1 An Efficient System

THE TQM SYSTEM

Actions are generated in a cable manufacturing industry after either receiving customer's enquiry (tender) asking for prices, delivery period and technical compliance to specifications or an order whereby the cables are to be manufactured according to the agreed technical specifications. The TQM software developed, integrates all the actions generated by the departments involved from customer's initial contact to customer's receiving the cables after placing the order. Fig. 3 shows TQM software implemented in a multi-user environment on PC based Novell local area network accessible by various departments of a typical telephone cable manufacturing plant. It consists of a main module which generates the cable design (including materials weights, dimensional data of each component and machine routing etc.) and a number of sub-modules pertaining to each department. The basic elements of the entire system and it's function have been described in reference [2]. It is a product code and menu driven system offering multiple options and features to select from.

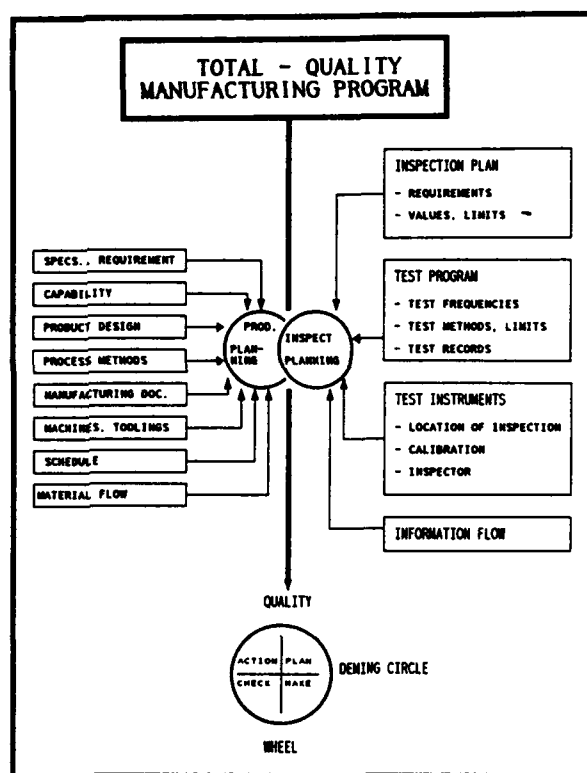


FIG. 2. Total Quality Manufacturing Program

Fig. 4 shows the TQM software department wise menu of some key reports. Master enquiry and product lists can be seen on each PC by all departments. The master enquiry list which gives the latest update on the customer's enquiry e.g. cable types, quantity per type and size and status (whether pending or responded) can be instantly retrieved. Similarly Master Product file gives the listing of total products of the company and is up-dated as new cable types and sizes are offered to different customer's specifications. Any information related to the product (Price, material weights, material costs, to which orders (customers) it was produced, production and quality data etc.) can be retrieved by simply pushing few buttons (menu driven actions) on the key board. It is interesting to note that the information can be tracked backwards from the finished delivered product to cable final inspection, in-process inspections, various stages of production, customer's order, quotation and enquiry stage or vice versa. Thus full traceability of manufacturing data and cross-reference of various information / documents is maintained. It is therefore may not be necessary to keep hard copies of these information / reports since they are readily available and retrievable from the system.

THE PRACTICAL APPROACH

The conventional methods of implementing TQM concepts as briefly described above have been vigorously pursued by majority of companies. The interpretation of the term "TOTAL QUALITY" beyond the quality of the product alone has been well understood by the industry. ISO 9000 has provided adequate basis for actions taken in the manufacture of a product and requires that such actions should be taken under written and approved procedures. Thus massive documentation and control procedures are required to be written for each action in order to apply for ISO (or equivalent) certification. These quality documentation are basically divided into three levels. The Level 1 explains the supplier's management policy to clearly define and document its objectives for, and commitment to, quality. The Level 2 documentation describes the procedures and in the Level 3, work instructions and test methods etc. are written. In the changing environment of global competition in the market place on the basis of quality and cost competitiveness, the management's quality policy of a company in one continent may not be different than the other in another continent. Similarly the various procedures, operator's manuals, work instructions, raw material specifications, test methods, inspection plans etc. may also exist in one form (format) or the other. However, concerted efforts are needed to implement these procedures and methods on the production floor, keep traceability and cross-reference of various information, instructions and documents.

With the availability of present day enhanced capability computers and softwares, it is possible to computerize each action a person takes in a manufacturing company. Even the Quality manuals, operator's manuals which are text information can be stored in the computer, the selected parts and sections of which can be retrieved as required by a user using easy access keys. In other words, once the basic structure of the system is built and the database developed, one may get all the information from the PC next to his/her desk by a simple push of button(s) on the key board. One may not refer to files (hard copies of reports) to find the status of cable rejects on a certain order or any other information related to a product from the stage of receiving an enquiry, then order and until it is shipped to the customer. This means that it is possible to

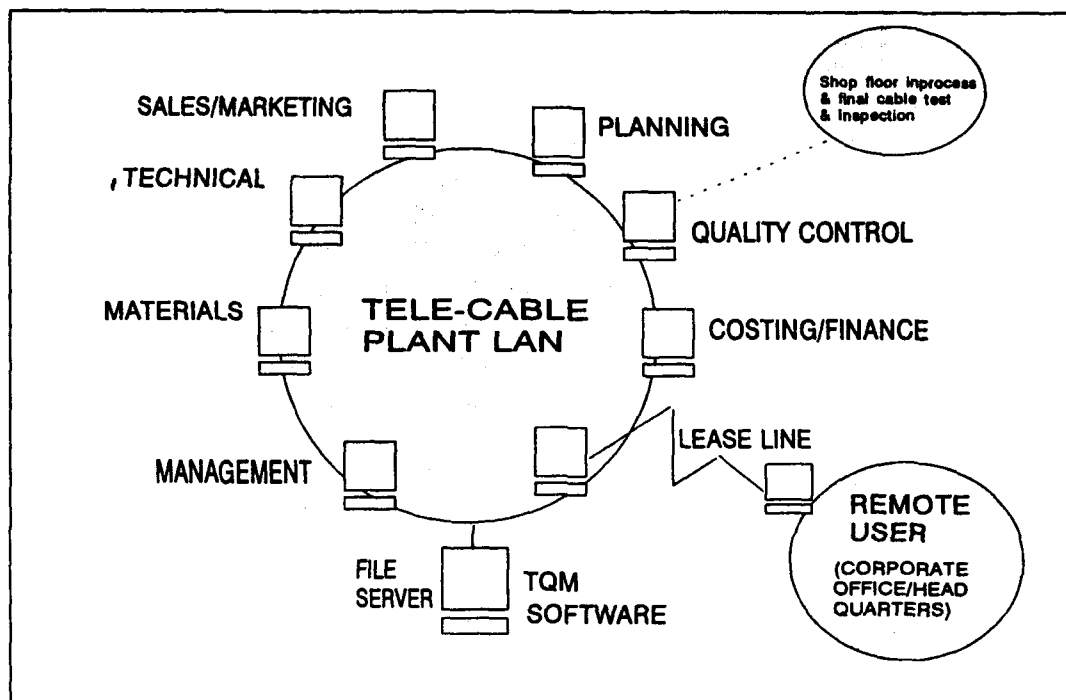


Fig. 3 Local Area Network

avoid writing procedures and instructions for each action and keep record of these actions each time they are executed in addition to track (manually) any changes / variations resulting out of these actions which may become cumbersome to maintain as the time passes. The whole operations of the manufacturing plant can rather be expressed in a couple of flow charts and for each function of the flow chart, a versatile software can be written in a modular plug-in modules to make available the desired information on finger tips. Fig. 5 shows a typical flow chart of important operations in a telephone cable plant.

The system developed and implemented on a PC based LAN provides a common data base for key personnel involved in the manufacturing process. The system generates all the needed manufacturing documents, keep traceability of production data and quality measurements, uses the feed back information to improve on the cable design criteria and thus provides a perfect and practical environment for Total Quality Management.

IMPLEMENTATION OF QUALITY PROGRAMS

The raw materials used in the telecommunication cables and it's production at various manufacturing stages

undergo a severe quality control and inspection. The raw materials are inspected and tested according to the well established standards (ASTM, BS, IEC etc.) the reference of which are generally given in the raw material specifications which are also the basis of buying the raw materials from the suppliers. The in-process tests and inspections on the semi-finished products at various production stages are extremely important to;

- i) detect non-conformance/defects at an early stage of production.
- ii) ensure compliance, that the product would meet customer's specification requirements when finished.
- iii) maintain statistics of quality measurements to ensure consistence in the process parameters and detect abnormalities in the production processes.
- iv) improve product design, reduce raw materials consumption

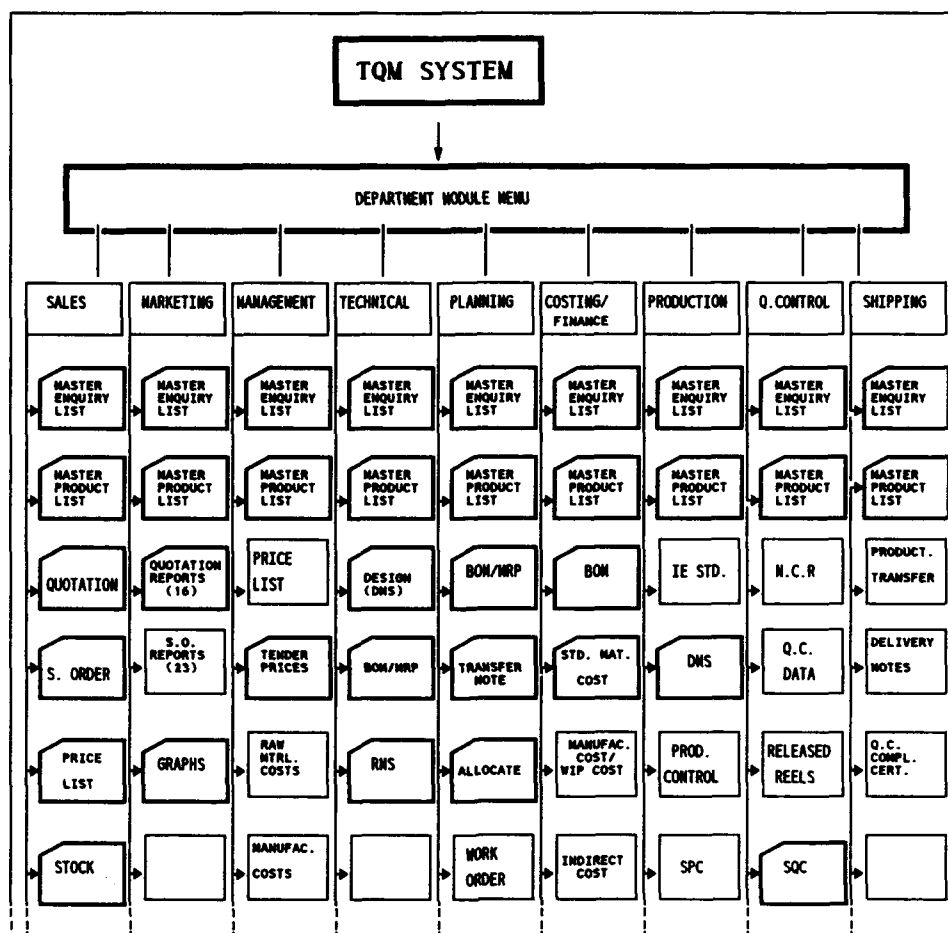


Fig.4 TQM Department-Wise Menu System

To achieve these objectives, data entry/retrieval stations (P.C.s) have been connected in the Tele-Cable LAN and placed at work centres (tandem wire drawing and insulation, group twinning, unit/assembly lines and final inspection / acceptance tests area). The automatic test equipment with 25 pairs connecting frame at group twinning stage, 100 pairs frame at unit making line (drum twisters) and a number of connecting frames and test systems for LF/HF tests as well as HV and insulation resistance measurements in the final inspection area, all are connected in the LAN as shown in Fig. 6. Production data and Q.C. measurements are entered in the PCs at each stage as the production of cables continues. The TQM software implemented on the production shop floor is extremely user friendly and integrated into the total system from customer's enquiry to shipment of the finished cables. Thus if quality data/statistics on any product is desired, simply select it from the master

product list with the characteristic for which the statistics is desired. A list of production work orders along with measured values will appear against which the product was produced at different times during the year (the system is set to display only last six months data). This is shown in Fig. 7 where product no. 10008 (2400 x 2 x 0.4) has been selected. This product was produced in 20 work orders during a six months period. Each work order represent a production batch of a certain number of reels for the same size and cable type, however the number of reels in a batch depends upon the customer's order. The TQM softwares then offer multiple choices to select the sample size (data of certain no. of reels) in each work order and the total no. of work orders to carry out the statistical analyses on the selected quality parameters / characteristics. In addition, the system offers complete traceability of a finished cable parameter to the single insulated wire produced on a certain tandem insulation

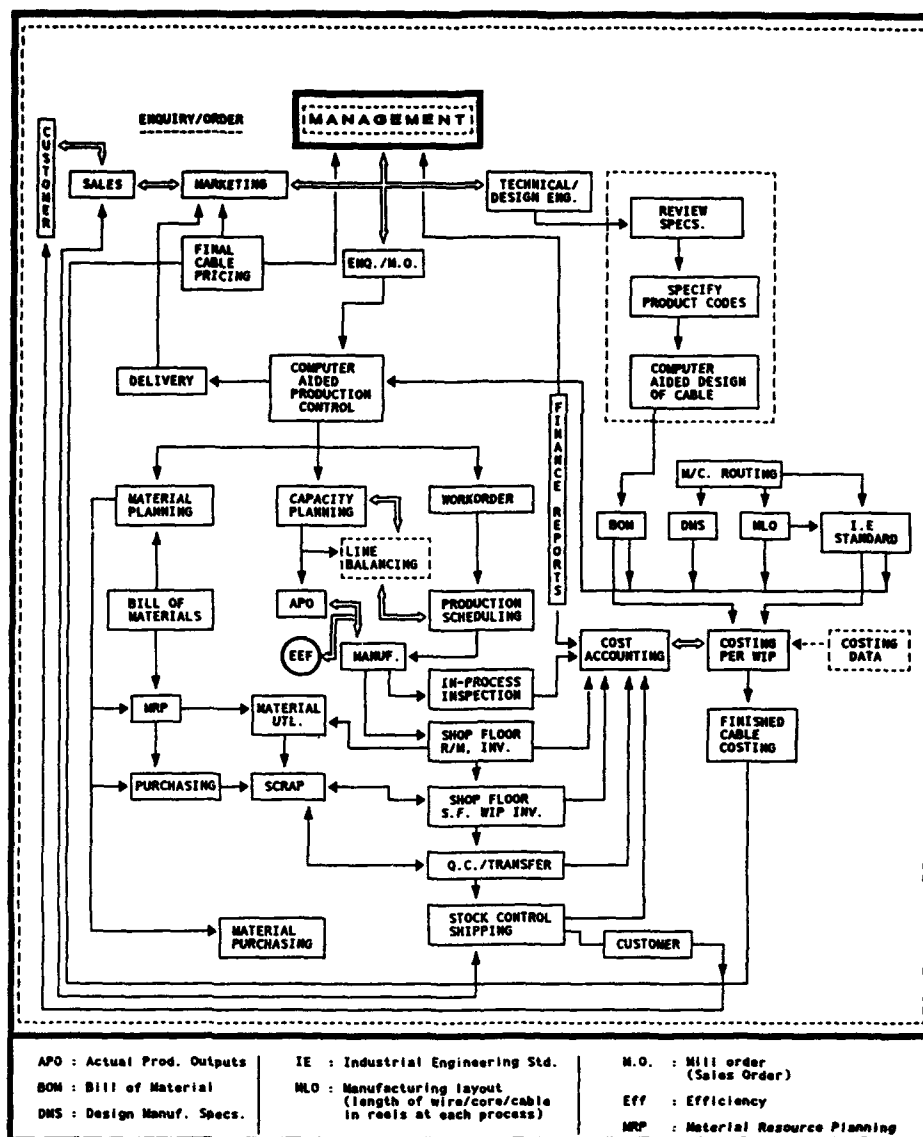


Fig. 5 Flow Chart of typical Manufacturing actions after receipt of customer enquiry/order.

line showing the test results (summary of key data) besides, the information on raw materials (material grade & it's supplier's name and physical laboratory test results). For example, the average mutual capacitance of a finished cable can be traced to the conductor and insulated wire diameter used in that cable. The information are of vital importance to know if the measured average mutual capacitance of the cable in the final inspection exceeds the specification requirement.

The system also generates Non-Conformance and Hold tags. For this purpose, all probable defects expected in telephone cable manufacturing have been codified. In total

97 types of defects are envisaged as listed in table 1. Again select a defect code from the TQM menu and it will list all the reel nos., W.O. nos. and the cable types / sizes which had this defect. The data can be plotted in different graphical presentations for quick analyses of the problem.

SPC / SOC APPLICATION

The complete quality inspection of each and every product and its sub-components in any industry is not possible. In the telecommunication cable industry, there are several manufacturing and process variables which must be monitored continuously and controlled in order to result in

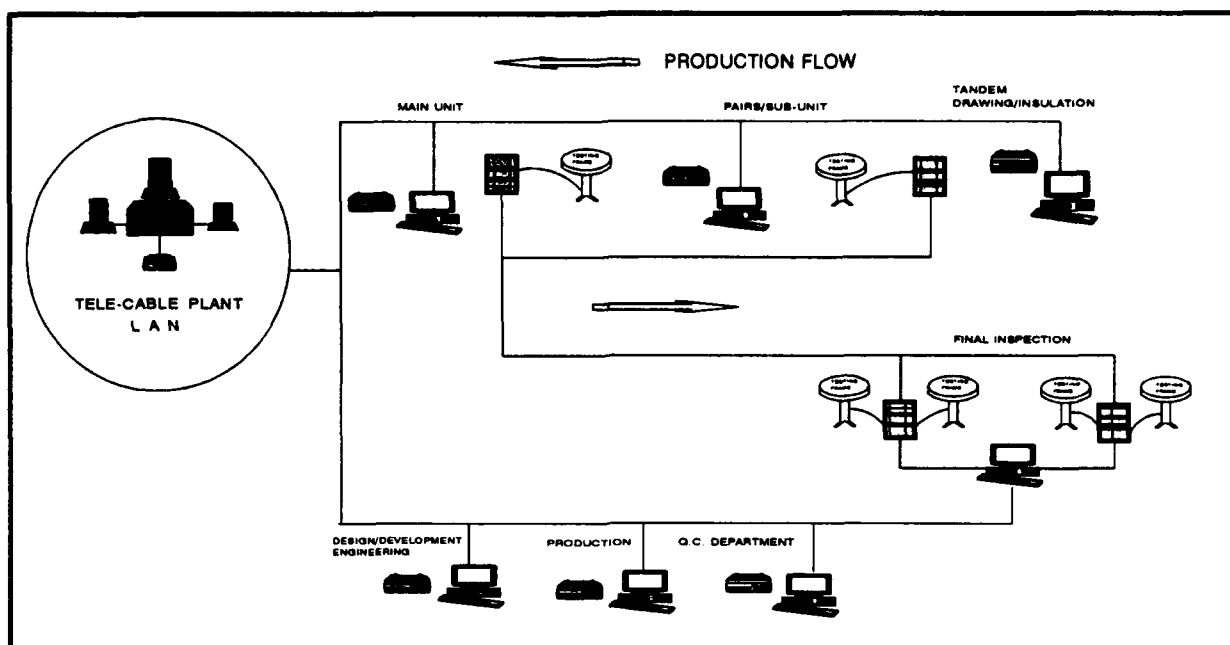


Fig. 6: Production / Q.C. measurements / Data entry stations

the finished cable product that guarantees the stipulated design and meet or exceed the specification requirements. Among these, tandem wire drawing - insulation and pairing / group - twinning are highly sensitive processes. The key manufacturing variables which influence directly the finished cable electrical characteristics are conductor and insulated wire diameters, eccentricity and insulation defects (pin-holes) in the insulation extrusion process affecting the d.c. resistance, resistance/capacitance unbalances, attenuation and average mutual capacitance. In the pairing / group twinning process, the twist lay, consistent similarity of lays, un-even tension on wires, inter-axial spacing have bearing on the resistance / capacitance un-balances. The statistical analyses of the key parameters are therefore essential to evaluate the quality of a measured characteristic and determine process capability and stability. The statistical tools used for evaluating the quality of a measured parameter is \bar{X} -R control chart. The \bar{X} -R control chart shows both the mean value \bar{X} , and the range R, usually drawn on the same sheet (paper) with \bar{X} chart at the top and R chart at the bottom. The \bar{X} control chart mainly shows any changes in the mean value of the process while the R portion of the chart shows the dispersion of the process. The \bar{X} -R

control chart is very useful in examining the abnormalities in the process since it shows changes in the mean value and dispersion of the process at the same time.

The TQM software application of the \bar{X} -R control chart to the "Average Mutual Capacitance" of the finished cable (product no. 100008, 2400 x 2 x 0.4) is shown in Fig. 8. The measured capacitance values of a sample size 5 (5 reels in each work order taken from 20 samples) executed in different times is shown in Fig. 7. The mutual capacitance of 100 pairs (one unit) in each layer of the 2400 pair cable is measured and the selection of the units is made so, that all the units are tested in turn for the reels in a production batch comprising a work order. From Fig. 8, it can be seen that although the production is controlled, \bar{X} & R charts do show some fluctuation but are within the control limits. Generally, a change in the mean for the production process will result in an abnormality appearing on the \bar{X} control chart. However, a change in the dispersion of the production process would result in abnormality appearing on both the \bar{X} and R control charts. As the dispersion of the production processes increases, the points on the R control chart will also increase with \bar{X} control chart showing greater spread.

D. Code	Description of Defects
ANN. CU. Wire	
001	CU Wire Dia. < Specs.
002	CU Wire Elong. < Specs.
003	CU Wire Tensile < Specs.
004	CU Wire Surface Oxidized/Tarnished.
005	CU Wire Resistance > Specs.
POLYETHYLENE	
006	Ins. Wire Dia. < Required.
007	Ins. Shrinkage > Min. Required.
008	M. F. I. Not to specs.
009	PE Ins. Comp. With PJ Failure
010	PE Density not to specs.
011	PE Elong. < Specs.
012	PE Carbon Cont. not to specs.
013	PE JKT Elong. < Specs.
014	PE JKT T. Strength < Specs.
015	Ins. R.T. < Min. Required.
016	Ins. T. Strength < Specs.
017	Ins. Adhesion to Cond. failure.
018	Ins. Res. to Compression failure.
019	Ins. Eccentricity > Specs.
020	Ins. Elong. < Specs.
021	Tub. Ins. Phy. Tst/ Fail. after aging.
022	Capillary between Ins. & Conductor.
023	Co-Axial Cap. > Specs.
BINDER AND ID TAPES	
024	Bin Tape Phy. Tst. failure.
025	I. D. Tape Phy. Test failure.
FILLING COMPOUNDS	
026	P. Jelly TOT. Acid Val. > Max.
027	P. Jelly Drop Point < Min. Required.
028	P. Jelly Flash Point < Min. Required.
029	P. Jelly Integrity Test failure.
030	P. Jelly D.F. > Specs.
031	P. Jelly DI. Elec. constant > Specs.
032	P. Jelly Volume Resistivity < Specs.
033	P. Jelly Corrv. Components failure.
034	Wrapping Tape T. Strength < Specs.
035	Wrapping Tape Elongation < Min. Specs.
036	Wrapping Tape Thickness < Specs.
AL. FOIL (APL)	
037	APL Thickness < Specs.
038	APL - PE Coating < Specs.
039	APL Over Lap < Specs.
040	APL Elongation < Min. Required.
041	APL T. Strength < Specs.
042	APL Peel Strength with PE JKT < Min.
043	APL Over Lap Seal Strength < Required.
044	PE Adhesion to APL < Min. Required.
045	APL Resistance > Spec.
STEEL TAPE	
046	Steel Tape Elongation < Min. Required.
047	Steel Tape Tensile Strength < Min. Required.
048	Steel Tape Zince Coating WT. < Min. Specs.
049	Steel Tape Zince Coating not uniform.

D. Code	Description of Defects
R. L. W. P.	
050	Water Seepage Through Insulation.
051	Water Seepage Through Core.
052	Water Seepage under Mylar.
053	Water Seepage under APL.
SWELLABLE TAPE	
054	Swellable Tape Swellability < Specs.
ELECTRICAL PARAMETERS	
055	Resistance U/B > Max. Spcified.
056	Mutual Cap. Ave. > Specs.
057	Mutual Cap. IND. > Specs.
058	Pair to Pair Cap. U/B between Adj/Units > Spec.
059	Pair to Earth Cap. U/B > Specs.
060	Pair to Pair Cap. U/B. within S/Unit > Specs.
061	HVT Failure Cond. to Cond.
062	HVT Failure Cond. to Shield.
063	Open Wire.
064	Short between Conductors.
065	Attenuation > Specs.
066	X-Talk Power sums El-Fext < Specs.
067	X-Talk IND. P/S Next < Specs.
068	X-Talk 1% Worst pair Next < Specs.
MISCELLANEOUS	
069	Bad Lagging of Reel.
070	Bad winding.
071	Over filled Reel.
072	Improper Reel size.
073	Weak Reel.
074	Non Stantard Length.
075	Cable O. D > Specs.
076	Min. /Max. Cable Dia. Ratiao > Specs.
077	Missing Print of Outer Jacket.
078	Outer Jacket R.T. > Specs.
079	Inner Jacket R.T. > Specs.
080	Mix-up Wire of diff. Types.
081	Mix-up Wire of diff. Sizes.
082	LDPE used instead of HDPE.
083	HDPE used instead of LDPE.
084	Length Not Accor. to W.O.
085	See NCR.
086	Non Standard Insulation Colour.
087	Open PE Jacket.
088	Without ID. Tape.
089	Core Dia. < Nom. Specified.
090	Deformed Insulation in cable core.
091	Spark Tes Failure.
092	Steel Tape. Gap > Specs.
093	PE Jacket Surface defects (Lumps, Ridges, Loose).
094	Wrong Binders Sequence / Colours.
095	Wrong Sequence of S/Units.
096	Wrong Sequence of Unit in Cable Core.
097	Cable Over All Diameter > 90mm.

Table 1. Cable Defect Codes.

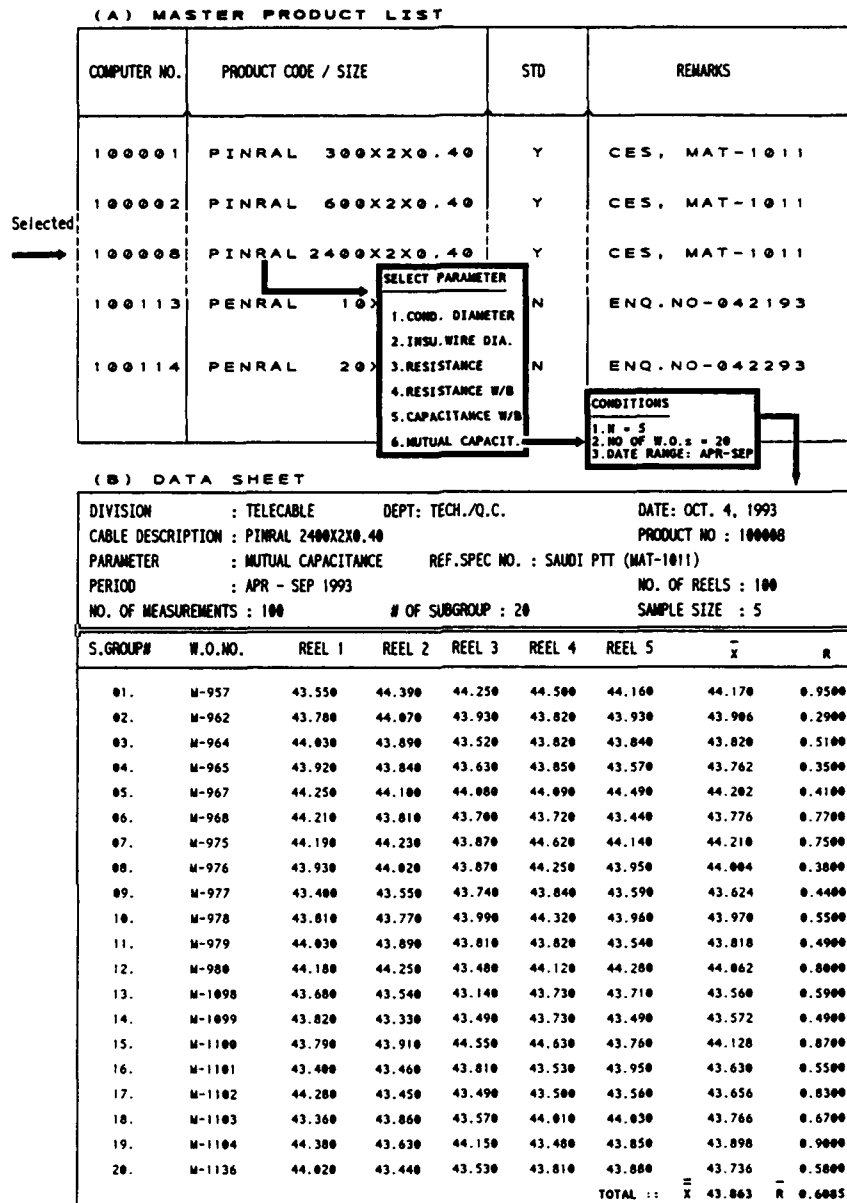


FIG. 7. Selection of a Product for Statistical Analyses.

The \bar{X} & R control charts are very useful to indicate the process mean and process variability. This example shows that the output of the production process mean and standard deviation are in control. Since the specification limits are outside the upper and lower natural tolerance (6σ) as a result, there will be virtually no non-conforming length produced. The process will therefore be termed as capable of producing 100% of the product meeting the specification requirement. In statistical language, this is

defined as process capability index (C_p) or process capability ratio (PRC).

$$C_p = \frac{\text{Permissible Process Spread}}{\text{Measured Process Spread}} = \frac{USL - LSL}{6\sigma} \geq 1.0$$

where

- USL = Upper specification limit
- LSL = Lower specification limit
- σ = Standard deviation

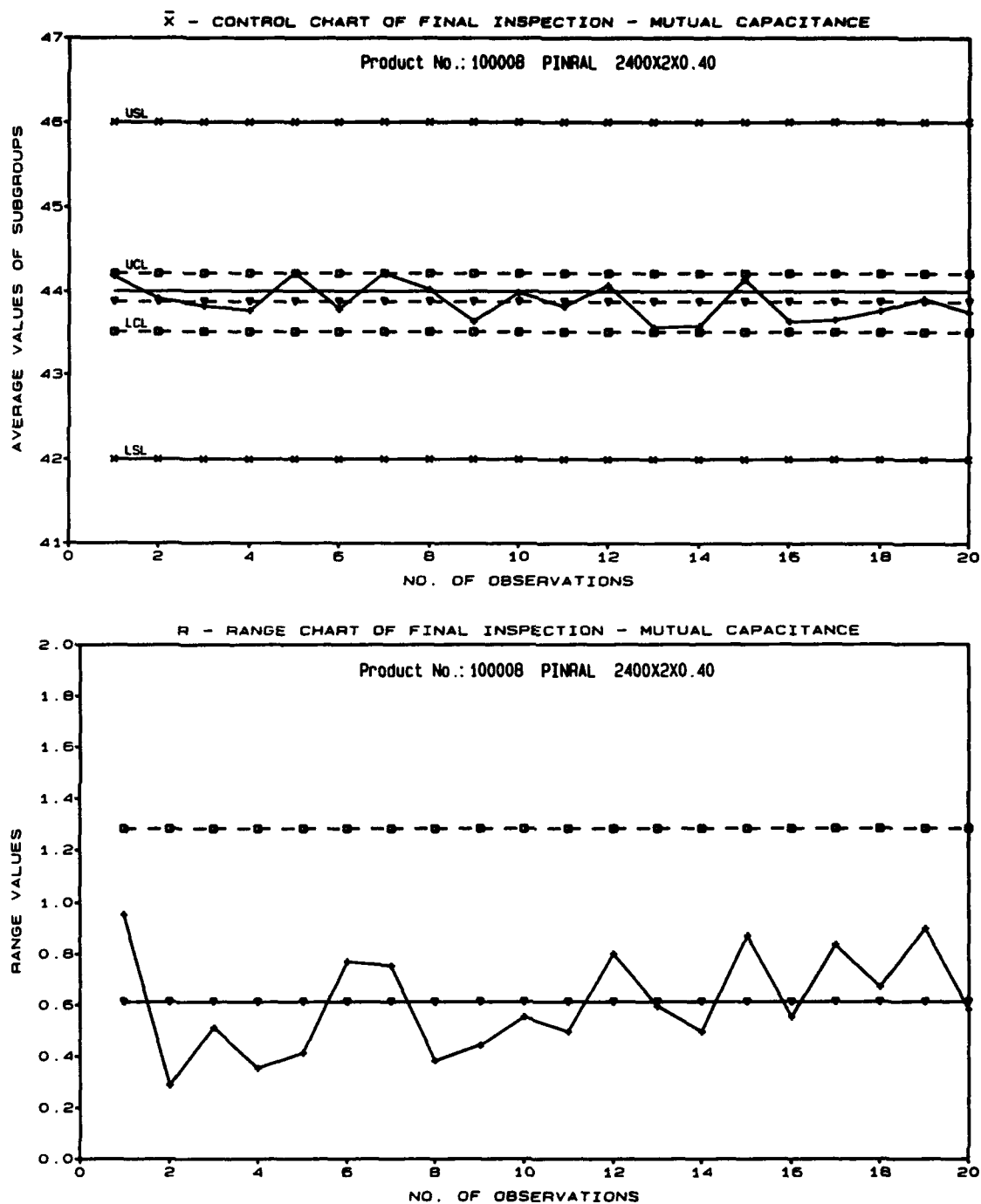


Fig. 8. \bar{X} -R Control Chart for Mutual Capacitance

The value of 1.0 for C_p indicates that the process is just capable, however in order that a characteristic meets the specification requirements with virtually no rejects, the C_p value should be equal to or greater than 1.33. The process capability index C_p relates the actual process

spread with the specification allowance (in the example of 2400 x 2 x 0.4 cable, $USL = 46$ & $LSL = 42$). However, the attribute on process mean is not considered which represents the process stability and performance. Therefore, another indicator C_{pk} is defined as a measure

of process performance ;

$$C_{pk} = C_p (1-K) \text{ where } K = \frac{2 (M_s - \bar{X})}{USL - LSL}$$

K represents the deviation of the process mean from mid point (Ms) of the specification limits.

The Cp and Cpk values for the mutual capacitance parameter of 2400 x 2 x 0.4 cable are computed as follows ;

$$C_p = \frac{USL - LSL}{6 \sigma}$$

Where

$$USL = 46.0$$

$$LSL = 42.0$$

$$d_2 = 2.326 \text{ for sub-group sample size(5) as per table 2.}$$

$$R = 0.6085 \text{ as per Fig. 7}$$

$$\sigma = \frac{R}{d_2} = \frac{0.6085}{2.3260} = 0.2616$$

$$C_p = \frac{46 - 42}{6 \times 0.2616} = 2.55$$

$$C_{pk} = C_p(1-k); K = \frac{2(M_s - \bar{X})}{USL - LSL}$$

$$k = \frac{2 (44 - 43.863)}{46 - 42} = 0.0685$$

$$C_{pk} = 2.55 (1-0.0685) = 2.38$$

Sample Size n	A ₂	D ₃	D ₄	d ₂
2	1.880	.0	3.268	1.128
3	1.023	.0	2.574	1.693
4	.729	.0	2.282	2.059
5	.577	.0	2.115	2.326
6	.483	.0	2.004	2.534
7	.419	.076	1.924	2.704
-	---	---	---	---
-	---	---	---	---
-	---	---	---	---
-	---	---	---	---
Formulae for computing control limits.				
For Averages			For Ranges	
X UCL = $\bar{\bar{X}} + (A_2 \times \bar{R})$			R UCL = $D_4 \bar{R}$	
X LCL = $\bar{\bar{X}} - (A_2 \times \bar{R})$			R LCL = $D_3 \bar{R}$	

Table - 2. Factors for Computing Control Limits. [4]

Both values of Cp & Cpk are greater than 1.33 showing excellent performance and stability of the production processes. If several production lots for key product parameters (conductor diameter, insulated wire diameter and finished cable average mutual capacitance) displayed such good values of Cp & Cpk, one can confidently improve the product design to reduce material consumption.

This is demonstrated in Fig. 9 where the cable is re-designed for nominal average mutual capacitance of 45 nF/Km. The process variability should remain within the control limits where as the process mean value is expected to fall below the nominal average value (45 nF/Km) of the specification. This means shifting both specification and process mean values closer to the upper specification limit (USL) thereby reducing the insulation wall thicknesses and hence the consumption of rest of the materials.

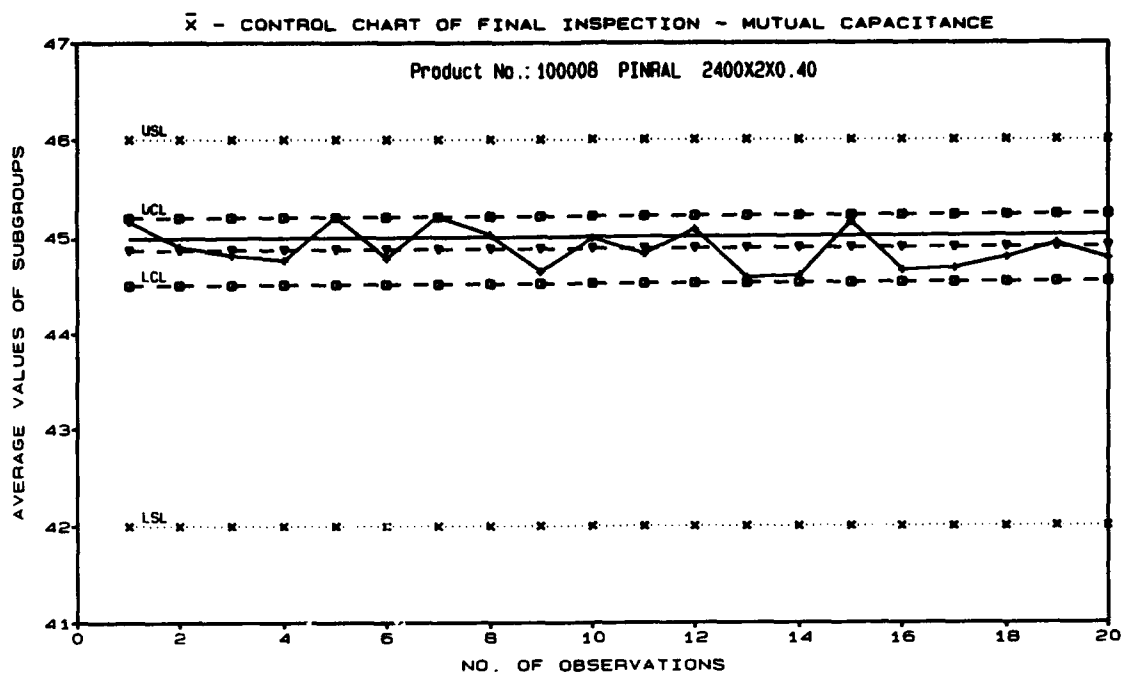


Fig. 9. \bar{X} Control Chart for Mutual Capacitance of re-designed cable.

CONCLUSION

In order to achieve the objectives of Total Quality Management, a practical approach has been described by developing a complete TQM software. This approach, which has been implemented on a PC based LAN, computerizes each and every action a person takes to manufacture a product from the stage of receiving an enquiry till it is produced and shipped to the customer. The system has reduced the number of procedures, generates several manufacturing documents, keep traceability of production data and quality measurements, uses statistical tools to improve on the cable design, production operations and thus provides a perfect environment for Total Quality Management.

REFERENCES

- [1] "The Quality Glossary"
Quality Progress, February 1992.
- [2] "Interactive Manufacturing & Costing System (I_MACS) for Multi-pair Telecommunication cables"
M.J. Khan, 41st IWCS, Reno, Nevada 1992.
- [3] "A new Approach to Total Quality Assurance in Telephone Cable Plants"
E. Esposito, G. More, 39th IWCS, Reno, Nevada 1990
- [4] "Guide to Quality Control"
K. Ishikawa, 1988

M. Javed Khan received his BS degree from the University of Pehawar, Pakistan in 1974 and M.A.Sc. degree from the University of Windsor, Ontario, Canada in 1980, both in electrical engineering.

He worked with Phillips Cables (Brockville, Ontario) as Cable Design Engineer before joining Saudi Cable Company late in 1982. He is presently responsible for Design Engineering and Quality Control Departments of Telecommunication (Metallic and Optical Fibre) Cable Plants at Saudi Cable Company.

ADVANCED TWISTED PAIR CABLE DESIGNS: FIELD TRIAL VALIDATIONS

William Reichert & Kevin St. Cyr - Champlain Cable Corp., Colchester, VT

Champlain Cable Corporation, Colchester, Vermont

Abstract

Reliability and performance of advanced twisted pair cable systems is critical for their ultimate use in local area networks (LANs). Although most cable manufacturers supply product performance data, the end-user needs to be satisfied that the cable system will actually support the current and future network requirements. Typically, four unshielded twisted pair (UTP) cables are used to connect users through a common wire closet. Each of the major LAN protocols requires a different category of cable. With a variety of LAN protocols, combined with a diverse copper twisted pair product offering, it is important to understand actual field performance. This paper will discuss the findings of independent field trials in which various cable designs were validated in the major LANs. The analysis will include 4-25 pair designs tested at The University of New Hampshire, Synoptics' Token Ring Interoperability Lab, Chipcom, and Ungermann-Bass.

The emergence of the Anixter "level" program significantly and successfully defined twisted pair cable designs. This structured wiring solution established a listing of cabling options for each LAN topology. Concurrent with this is the standardization currently underway with the EIA/TIA 568 standard. This "categorization" of cables will further differentiate twisted pair designs as network cables of choice.

High speed local area networks are typically rated by the network protocol and respective data rate, as shown in Table 1.

TABLE 1

LAN PROTOCOL	CABLE CATEGORY	SPEED
Ethernet	3	10 Mbits/sec
Token Ring	4	16 Mbits/sec
FDDI/ATM	5	100+ Mbits/sec

Standards

EIA/TIA

The EIA/TIA 568 standard for "Commercial Building Telecommunications Wiring" is one of the primary sources of premise cable performance criteria. This standard defines a telecommunications wiring system for commercial buildings that will support a multi product, multi vendor environment. The standard meets most current and future network requirements and its goal is to define cabling independent of applications. The EIA activity will actually serve to eliminate future building rewiring costs since a structured wiring plan will be designed and installed in the economically favorable building design and construction phase. Even though the standard defines both "inter" and "intra" building wiring, this discussion will center around the "intra" building environment. Therefore, the twisted pair cabling types considered will be:

Introduction

Advanced copper twisted pair cable designs for data applications have been a major deterrent to "fiber to the desk". Although the electrical performance supplied by cable manufacturers is important, actual verification trials at OEM's and Interoperability Labs, for example, can provide final validation for these products. As LAN speed requirements increase to and beyond 100 Mbits/sec, twisted pair cable designs will require further application testing in order to validate performance.

The LAN segment is one of the fastest growing in the communications market. This is primarily due to the necessary networking of information processing taking place in many industries. At the same time, the number of cabling options has increased, adding confusion to an already tough decision. Several "industry" standards have emerged which have differentiated the performance of some of these choices.¹

Horizontal Wiring: connecting work area outlets to the telecommunications or wiring closet. Typically this is 24 AWG, 4 UTP cable.

Backbone Wiring: connecting wiring closets in same building, from floor to floor or closet to closet. Typically bundled 4 UTP cables, or 25 UTP cables.

UL LAN Cable Verification Program

This program was established to address the important issue of independent validation of cable performance. It is intended to assist specifiers with cabling decisions. Among the features are: a four level 100 ohm cable performance program; independent cable level performance identification; recognition of the EIA/TIA 568 standard; follow-up services and quality support to monitor performance; and, actual data validation.²

Design and Applications

Design

The typical cable used in network applications is an unshielded twisted pair, 100 ohm, 4 pair cable design. Figure 1 illustrates a typical twisted pair cable design. The design considers the three main electrical requirements of: characteristic impedance, attenuation, and near end crosstalk (NEXT). Each of these requirements is defined by the categories which they address. (Appendix 1 lists the electrical requirements for Category 3, 4, and 5 cable.) The intent is to design cables which will operate over the frequency range to be utilized in the network application.

Figure 1



Network Decisions

Today's network requirements are concerned with the "Big Three" electricals³:

- ▶ Near End Crosstalk, worst pair
- ▶ Attenuation
- ▶ Impedance

Other electrical considerations, such as Structured Return Loss (SRL) and Jitter are generally satisfied if the "Big Three" are satisfied. Appendix 1 lists a cross comparison of Category 3 through 5 cable properties. These three categories account for the majority of work stations up to 100 meters.

Many decisions need to be made when considering network transmission media. Perhaps the most important are which cable category to select, and how to manage the cable plant. As shown in Appendix 1, the three more common protocols each require a distinct cabling system. Management of the cable plant requires decisions and considerations of some or all of the following:

- ▶ Network Type
- ▶ Space
- ▶ Frequency At Which The Network Operates
- ▶ Length of Nodes
- ▶ Number of Nodes
- ▶ Connecting Devices
- ▶ Future Needs
- ▶ Shielding Requirements
- ▶ Industry Standards
- ▶ Systems Life Cycle

While it is not necessary to get into a long discussion on each of these issues, it is important to understand the interactions of these variables so as to maximize the cabling system chosen and obtain successful electrical performance.

Applications

The applications to follow are from actual field evaluations. They were selected due to their applicability of UTP designs, as well as the unique performance results which were obtained.

Category 3: A 4 pair UTP was trialed and tested in the Token Ring Interoperability Lab at Synoptics, Sunnyvale, CA. The cable was installed to support 144 stations, at each of six discrete cable lengths. Each run was characterized for NEXT, attenuation,

and impedance in accordance with ASTM D 4566-90 methodology over the frequency range of 1 KHz - 20.5 MHz, which is the range of frequency excitation in 16 MB/sec Token Ring. EIA/TIA Category 4 connectivity was used. Following is a brief summary of Synoptics' findings at 16 MHz:

Cable:	CHAMPLAIN CMP3-24-4 pair	
Cable runs:	50 ft.	310 ft.
Impedance:	100 ohms +/- 1 ohms	100 ohms +/- 1 ohm
Average NEXT:	34.20 dB	31.56 dB
Average Attenuation:	3.38 dB/100 ft.	3.24 dB/100 ft.

In all cases, the recorded characteristics exceed the manufacturer's published numbers. Even though the NEXT data is below Category 4 specifications, it is shown that this high performance Category 3 cable exceeds its design parameters and does support a passive 16 MB Token Ring environment.

Category 4: At Chipcom Corporation, Southborough, MA, a new facility was being wired for a 10BaseT and future Token Ring network installation. One Category 4 cable and one Category 5 cable was pulled and terminated at each workstation. Approximately 370 workstations were connected using Category 4 connectivity hardware. A variety of Category 4 patch cords and drop cables were also used. The maximum system length was not more than 85 meters (80 meters+3 meter office+2 meter patch). Initially, there were no problems as the system was up on a 10BaseT network. As Token Ring nodes were connected, certain stations failed to go "in ring." Further investigation indicated that these issues were connectivity related, and not due to the cable. This is mentioned since a valuable lesson of termination was learned through this installation. It is extremely important to maintain the twisting of the pairs up to the termination jack. Crosstalk problems will occur if this is not properly done. In fact, the testing indicated that at 16 MHz one isolated drop performed at 4.5 dB below expected results. Out of 6 to 8 drops tested, a NEXT range of 33 dB to 39 dB was experienced at 16 MHz, well under the Category 4 (38 dB) and Category 5 (44dB) specifications.

To assist in the problem isolation, a controlled Category 5 cable test was performed utilizing the same Category 4 connectivity hardware. Based on these results it was determined to be a hardware problem. Further, the problem was caused by the termination technique to the jack. There was found to be a substantial difference in NEXT based on termination technique.

INITIAL TERMINATION TESTING

Cable:	CHAMPLAIN CMP4-24-4 pair	CHAMPLAIN CMP5-24-4 pair
Connectivity:	Category 4	Category 4
Cable Runs:	62.5 meters	61.9 meters
Attenuation: (16 MHz)	5.7 dB/100 meters	5.2 dB/100 meters
NEXT:		
16 MHz (cond. 1236)	>45 dB	>45 dB
(cond. 3645)	41.5 dB	44.9 dB
10 MHz (cond. 1236)	>45 dB	>45 dB
(cond. 3645)	41.9 dB	43 dB

RETERMINATION TESTING

Cable:	CHAMPLAIN CMP4-24-4 pair	CHAMPLAIN CMP5-24-4 pair
Connectivity:	Category 4	Category 5
Cable Runs:	61.9 meters	61.9 meters
Attenuation: (16 MHz)	5.6 dB/100 meters	5.1 dB/100 meters
NEXT:		
16 MHz (cond. 1236)	>45 dB	>45 dB
(cond. 3645)	43.3 dB	>45 dB
10 MHz (cond. 1236)	>45 dB	>45 dB
(cond. 3645)	42.5 dB	>45 dB

Conclusions drawn from Chipcom testing on Champlain cabling indicate that their Token Ring product is stable on a good Category 4 cable plant. Even so, the results they achieved convinced them to utilize Category 5 UTP for future cabling needs to avoid network issues and increase the future upgradability.

Category 3 & 5: A third validation was performed at the University of New Hampshire Interoperability Lab. The objective was to determine interoperability of six different "hubs" with four different adapter "cards" in a 16 MB Token Ring environment. The following table summarizes the findings.

CHAMPLAIN
Category 3, 100 meters

CHAMPLAIN
Category 5, 100 meters

Hub	CARD				CARD			
	1	2	3	4	1	2	3	4
A	P	P	P	P	P	P	P	P
B	F	F	P	F	P	P	P	P
C	P	F	P	F	P	P	P	P
D	F	F	P	F	P	P	P	P
E	F	P	P	F	P	P	P	P
F	P	F	P	P	P	P	P	P

F=Fail P=Pass

Results on Category 3 (minimum specification) cabling were not surprising. Hub "A" was interoperable with all cards. Card "3" was interoperable with all hubs. However, several failures are an indication of the risk in running baseline Category 3 cable in a 16 MB Token Ring Network.

Not surprisingly, however, was the fact that all "hub" and "card" combinations passed interoperability trials using Category 5 UTP cable.

Category 5, 25 Pair

High performance 25 pair cables have been used in network applications as

- file server to concentrator connections
- wire closet to modular furniture
- wire closet to wire closet (backbone)

Ungermann-Bass has worked closely with cable and connector manufacturers to develop a Category 5 compliant cable system per EIA 568. This includes complying with the latest near end crosstalk specification, Power Sum NEXT. This is a more demanding method of measuring crosstalk in multiple pair cables than the Worst Pair NEXT method. "With this tighter tolerance measurement, the effects of higher frequency signals and uncorrelated disturbing energies, which could interfere with neighboring pairs using the backbone,

should not effect the other pairs in the cable". Ungermann-Bass' work, in conjunction with Category 5, 25 pair cable and connector manufacturers, was aimed at maximizing crosstalk performance of the cable/connector system. Through modifications of "pin-outs" in 50 pin connectors, they were able to maximize crosstalk performance by:

- Maintaining pairs' twists all the way to the connectors' contacts;
- Displacing transmitters and receivers at opposite ends of the connector.

Both A and B have resulted in a better 25-pair system with greatly improved crosstalk. Finally, the Ungermann-Bass developments are compliant with EIA/TIA 568-A draft proposal as of this writing.

Conclusions

High performance unshielded twisted pair cables, which meet various electrical performance "categories", successfully support the network applications for which they were designed.

Further validations by OEMs, Interoperability Labs, and end users has also proven the following:

- High performance Category 3 (3+) cable, with improved crosstalk, supports passive 16 MB Token Ring LANs.
- Maintaining pair "twists" is critical in termination of UTP cable systems in order to avoid excessive crosstalk.
- Interoperability of hubs and adapter cards was "universal" in a trial using Category 5 UTP cable in a 16 MB Token Ring LAN.
- A 25 pair Category 5 cable system has been proven for backbone applications utilizing high performance cable, a redesigned connector and "tight" pair twists to the connector which meets Power Sum Near End Crosstalk requirements.

Acknowledgments

The authors would like to thank the following people and organizations for their valuable assistance in developing and preparing this paper.

Carol Weinreich, Manager-Token Ring Interoperability Lab, Synoptics Communications, Sunnyvale, CA.

Doug Ruby, Systems Manager, Chipcom Corporation, Southborough, MA. Also to Comlink, Chipcom's VAR, for their support through this experience. Special thanks to Rich Sanborn for doing the work and to Jeff Lavin for being committed to customer satisfaction.

Barry Reinhold, University of New Hampshire, Durham, NH.

Dan Jaffe, Support Engineer, Ungermann-Bass, Andover, MA. In addition, Dick Lena, Sharam Hakimi and Mike Rogers, also of Ungermann-Bass, for their efforts.

References

¹Gantz, John, "The Networking Voyage: Looking Back, Looking Ahead, *Networking Management*, 6/93.

²UL's LAN Cable Certification, Program, 3/92

³Daquino, Tony, "Designing, Manufacturing, and Marketing "Level Program" Wire & Cable In Today's Plenum Environment."

⁴Jaffe, Dan, "The New Enhanced Main Distribution Frame Cabling Structure," 9/93

Bibliography

William Reichert

Bill Reichert is the LAN Market Manager at Champlain Cable Corporation in Colchester, Vermont. He has been in the wire and cable industry for 9 years, 5 of which have been in various operations and sales/marketing assignments with Champlain Cable. He was also instrumental in Champlain's ISO-9001 quality system registration. He received his Bachelor of Science degree in Chemistry in 1983, and his MBA in 1993, both from the University of Vermont.

Kevin St. Cyr

Kevin is Vice President, Business Manager for Champlain Cable. He has been with Champlain for 4 years, and prior to that he spent ten years in various sales, technical, and marketing assignments with General Electric. He holds a Bachelor of Science degree in Plastics Engineering from the University of Lowell.

APPENDIX 1

	<u>Category 3</u>	<u>Category 4</u>	<u>Category 5</u>
Frequency (maximum)	16 MHz	20 MHz	100 MHz
Impedance	100 ohms	100 ohms	100 ohms
Near End Crosstalk, Worst Pair			
1 MHz	41 dB	56 dB	62 dB
16 MHz	23 dB	38 dB	44 dB
100 MHz	-----	-----	32 dB
Attenuation			
1 MHz	2.6 dB/100M	2.1 dB/100M	2.1 dB/100M
16 MHz	13.1 dB/100M	8.9 dB/100M	8.2 dB/100M
100 MHz	-----	-----	22 dB/100M
Cable Design			
# of Pairs	2 - 25	2 - 25	2 - 25
AWG	24	24	24
O.D. (4 Pair)	0.145"	0.145"	0.150"
System Flexibility	Moderate	High	High
Network Support	Ethernet	Token Ring	FDDI

KD1WC3.02

LOCAL LOOP EVOLUTION - EMERGING TECHNOLOGIES

Gary L. Sparks

GTE Telephone Operations, Irving, Texas

The following text links and provides narrative explanation of the following presentation material. The text format relates to individual presentation subjects as denoted in their headers.

ABSTRACT

The intent of this analysis is to assess the impact of emerging technologies on existing local loop deployment plans with respect to potential reductions in copper twisted pair deployment. The analysis assesses deployment rates based on the on-going provisioning of basic telephony services.

DIRECTION: The Direction section:

- presents GTE's perspective relative to continued copper deployment.
- defines technology substitution and electronic augmentation procedures as means of curtailing continued copper twisted pair deployment.
- identifies 4 Emerging Technologies for assessment of their potential impact to reduce copper deployment.

ASSESSMENT ASSUMPTIONS: The Assessment Assumptions section

describes the analysis as being based upon POTS provisioning, GTE's expected 5 Year capital expenditure levels, distinction between feeder and distribution facilities, and expected cost parity between copper twisted pair deployment with Fiber-To-The-Curb (FTTC) and Rural-Fiber-In-The-Loop (RFITL).

Presented are two graphs depicting (life cycle (Net Present Value/NPV) and first cost) expected cost trends for copper twisted pair extended from a Digital Loop Carrier (DLC) and FTTC. Three FTTC trends lines are presented, most likely (the middle), optimistic (the lower), and pessimistic (the top). These represent a range based upon learning curve levels and economies of scale efficiency expectations.

EMERGING TECHNOLOGIES - FIBER-TO-MAJOR-BUSINESSES (FTMB): This

presents the first Emerging Technology as a means of reducing copper deployment by extending fiber (up to 1 miles) to major business (over 500 customers at a site). Although this had minimal impact on copper deployment, it was felt to be strategically important to increase the Quality, Functionality, & Timeliness of service to major businesses.

EMERGING TECHNOLOGIES - DIGITAL SUBSCRIBER CARRIER (DSC): DSC

overlays existing copper twisted pairs to provide additional voice grade services. Its primary application is for 2nd line services, however it can be used for adjacent property services. DSC relieves existing copper facilities, negates additional copper cable reinforcement, does so cost effectively. It results in capital savings and reduced copper deployment.

EMERGING TECHNOLOGIES - DIGITAL SUBSCRIBER CARRIER (DSC): DSC

overlays existing copper twisted pairs to provide additional voice grade services. Its primary application is for 2nd line services, however it can be used for adjacent property services. DSC relieves existing copper facilities, negates additional copper cable reinforcement, does so cost effectively. It results in capital savings and reduced copper deployment.

EMERGING TECHNOLOGIES - FIBER-TO-THE-CURB (FTTC): As FTTC

achieves cost parity with traditional copper paired cable, its deployment will become the norm. Full 100% deployment of FTTC will take several years as many housing developments have already been set up for copper cabling. FTTC will start with new housing developments or in distribution rehabilitation projects.

EMERGING TECHNOLOGIES - RURAL-FIBER-IN-THE-LOOP (RFITL): RFITL

is basically FTTC technology adapted to rural applications by extending the operating distances. RFITL can provide a cost effective means of providing Upgrades, Analog Carrier Replacement, or means of providing isolated growth in rural environments where cabling requirements are extensive.

ANALYSIS OF RESULTS - COPPER CABLE ASSESSMENT: This set of

graphs defines the expected reductions in copper deployment for each of the Emerging Technology applications (from original budget levels) in terms of Capital Dollars, Pair Miles, and Sheath Miles.

ANALYSIS OF RESULTS - FIBER CABLE ASSESSMENT: This set of graphs

depicts the expected increases in fiber deployment over current expected levels for InterOffice trunking (IOF) and Customer Access Facilities (CAF - local loop). The analysis defines the increases in terms of Capital Dollars, Fiber Miles, and Fiber Sheath Miles.

ANALYSIS OF RESULTS - BUDGETARY IMPACT: The Copper reductions

and the Fiber increases only illustrate the facility medium changes. This bar chart illustrates the overall budgetary impact of the assessment. The left bar (for a given year) represents the expected expenditures for copper cable, support structures, and fiber cable. The right bar represents the potential incremental changes in expenditures levels from the assessment of the Emerging Technologies.

As illustrated in the bar chart, the overall expenditure levels remain relatively constant. However, by 1997 there exist a significant potential for shifts in "what" is deployed, copper can be reduced significantly, support structures reduced a little, fiber increased significantly, and significant electronics added for DSC, FTTC, & RFITL.

CONCLUSIONS: The conclusion of this analysis is that Copper Twisted Pair deployment can be significantly reduced over the next 5 years by deploying fiber based solution and electronically augmenting existing copper twisted pairs.

DIRECTION

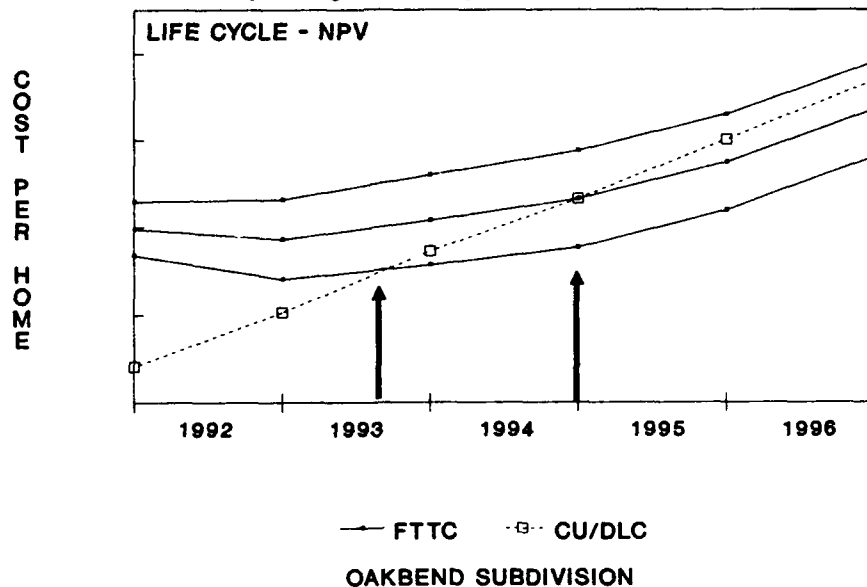
- **COPPER (twisted pair) TECHNOLOGY DOES NOT OFFER THE LONG TERM INFRASTRUCTURE TO MEET EXPANDING CUSTOMER REQUIREMENTS IN A TIMELY COST EFFECTIVE MANNER.**
- **EMERGING TECHNOLOGY APPLICATION IN THE LOCAL LOOP WILL ALLOW:**
 - **SUBSTITUTION OF FIBER & ELECTRONICS FOR COPPER.**
 - **DEFERRAL OF COPPER RELIEF AUGMENTATION.**
- **EMERGING TECHNOLOGIES EVALUATED:**
 - **Fiber-To-Major-Businesses (FTMB)**
 - **Digital Subscriber Carrier (DSC)**
 - **Fiber-To-The-Curb (FTTC)**
 - **Rural-Fiber-In-The-Loop (RFITL)**

ASSESSMENT ASSUMPTIONS

- **BASED ON POTS PROVISIONING**
- **BASED ON CURRENT 5 YEAR STRATEGIC PLAN WITH COPPER DEPLOYMENT**
- **FEEDER & DISTRIBUTION ANALYZED SEPARATELY**
- **BASED ON FIBER-TO-THE-CURB ECONOMIC ANALYSIS**
 - **Economic (Life Cycle & First Cost) Parity With Copper Starting in 1993/94**
- **RURAL-FIBER-IN-THE-LOOP ASSUMED COST PARITY**
 - **Subsequent Analysis Indicates Potential RFITL Cost Advantages**

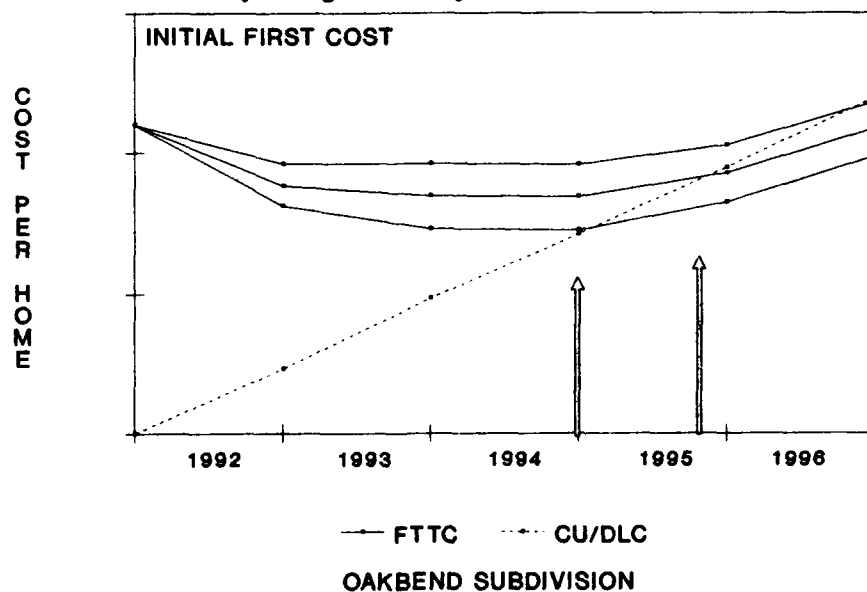
ASSESSMENT ASSUMPTIONS

Economic Study/Single-Family Results



ASSESSMENT ASSUMPTIONS

Economic Study/Single Family Results



EMERGING TECHNOLOGIES

FIBER-TO-MAJOR-BUSINESSES (FTMB)

DESCRIPTION:

EXTEND FIBER TO MAJOR BUSINESS CUSTOMERS IN
CABLE ROUTES WHERE FIBER EXISTS AND TRANSFER
SERVICES TO FIBER BASED DLC.

APPLICATION:

- START EXTENSIONS IN 1992 (Existing Fiber Routes)
- FREES UP EXISTING COPPER PAIRS FOR REALLOCATION
- QUALITY EFFECTS
 - Increased bandwidth and functionality
 - Increased flexibility for capacity
 - Improved quality and reliability
 - Improved response time to customer needs
- STRATEGIC IN NATURE; OVERALL IMPACT ON COPPER
DEPLOYMENT IS MINIMAL.

EMERGING TECHNOLOGIES

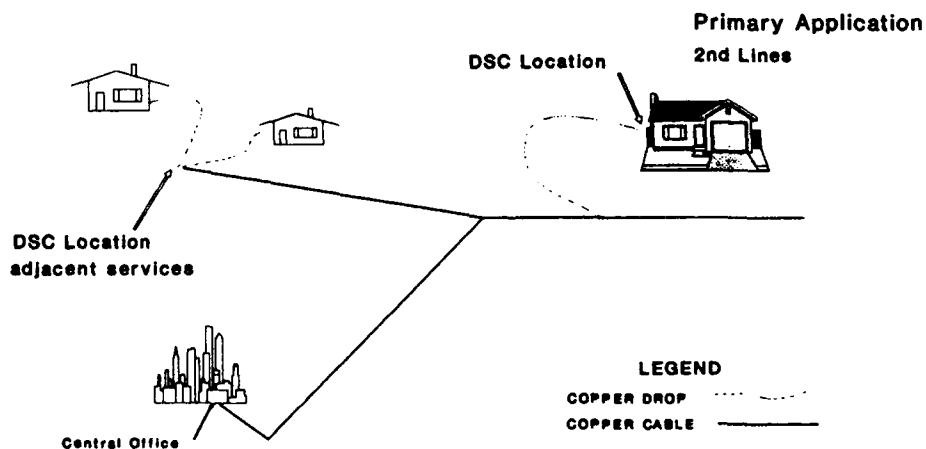
DIGITAL SUBSCRIBER CARRIER (DSC)

Electronically derived second line (on existing copper pair)

HOLDING STRATEGY

- relieve/augment existing facilities
- avoid additional copper placement
awaiting Fiber based replacement

RANGE: 14-18 Kft.
ISDN format (quality & reliability)
No Analog Cxr.
No Single BridgeTap > 2Kft.

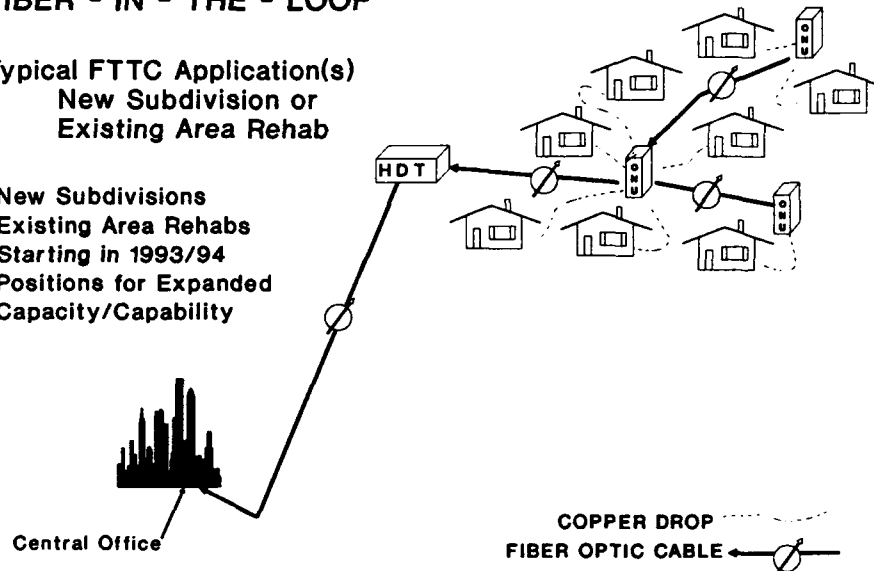


EMERGING TECHNOLOGIES

FIBER - IN - THE - LOOP

Typical FTTC Application(s)
New Subdivision or
Existing Area Rehab

- New Subdivisions
- Existing Area Rehabs
- Starting in 1993/94
- Positions for Expanded Capacity/Capability

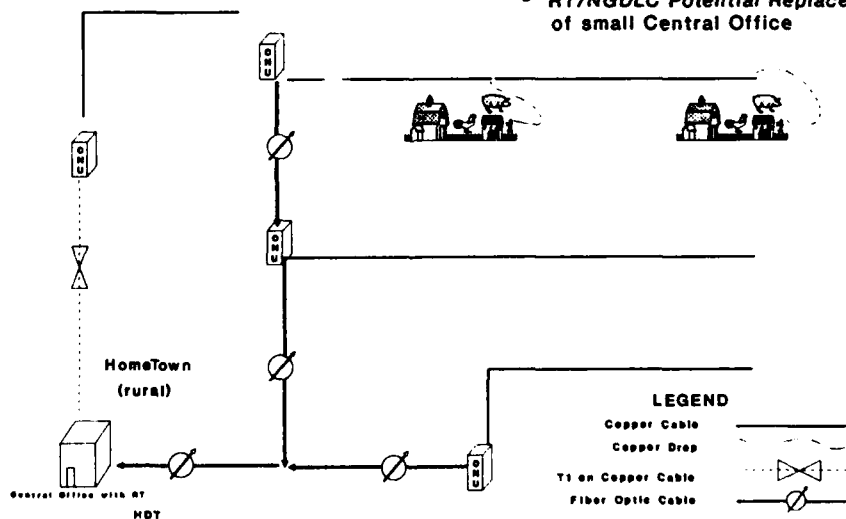


EMERGING TECHNOLOGIES

RURAL - FIBER - IN - THE - LOOP (RFITL)

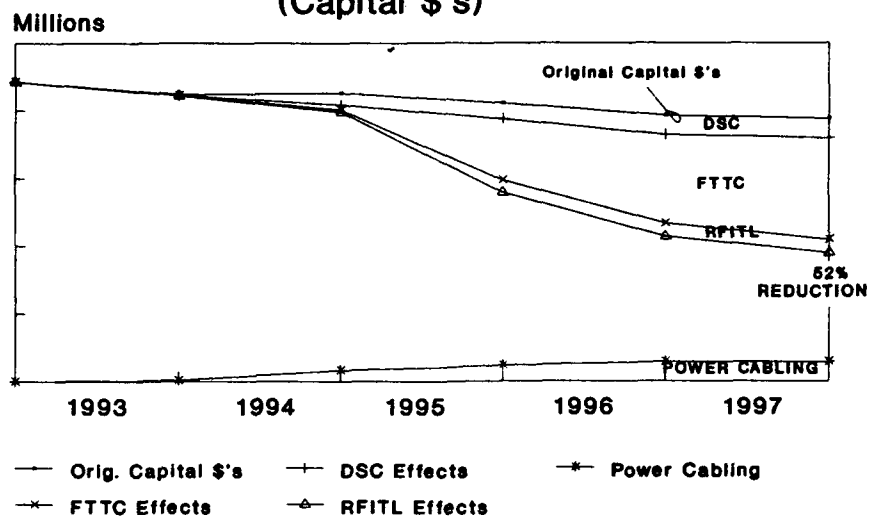
FTTC Adapted for Rural Applications
(distances extended)
Fiber Extended Out Into The Network
Integrated Feeder & Distribution Plan/Prov.

- provide Upgrades
- repl. analog CXR
- isolated growth
- RT/NGDLC Potential Replacement of small Central Office



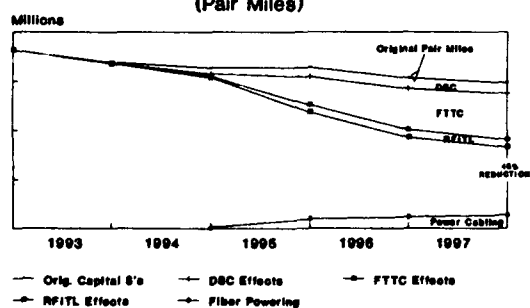
ANALYSIS AND RESULTS

COPPER CABLE ASSESSMENT (Capital \$'s)



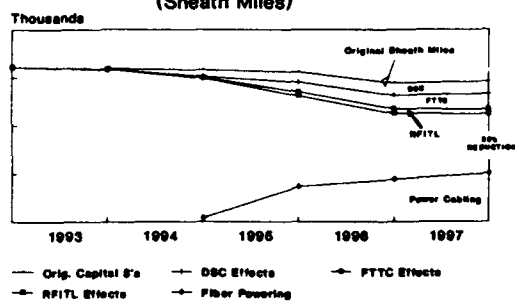
ANALYSIS AND RESULTS

COPPER CABLE ASSESSMENT (Pair Miles)



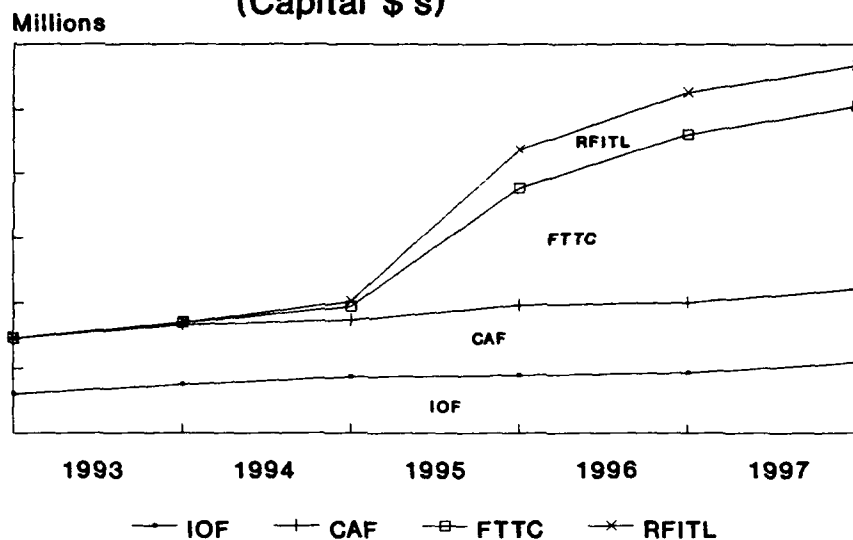
ANALYSIS AND RESULTS

COPPER CABLE ASSESSMENT (Sheath Miles)



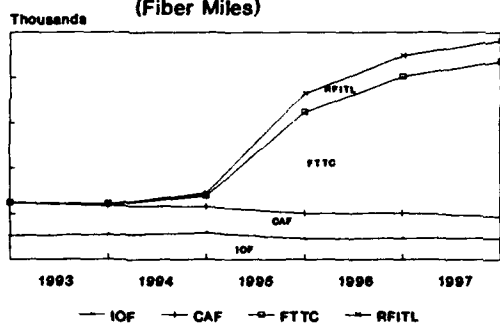
ANALYSIS AND RESULTS

FIBER CABLE ASSESSMENT (Capital \$'s)



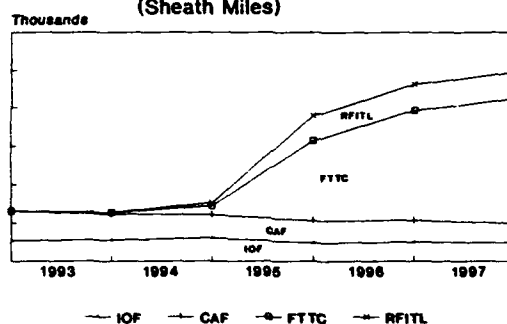
ANALYSIS AND RESULTS

FIBER CABLE ASSESSMENT (Fiber Miles)



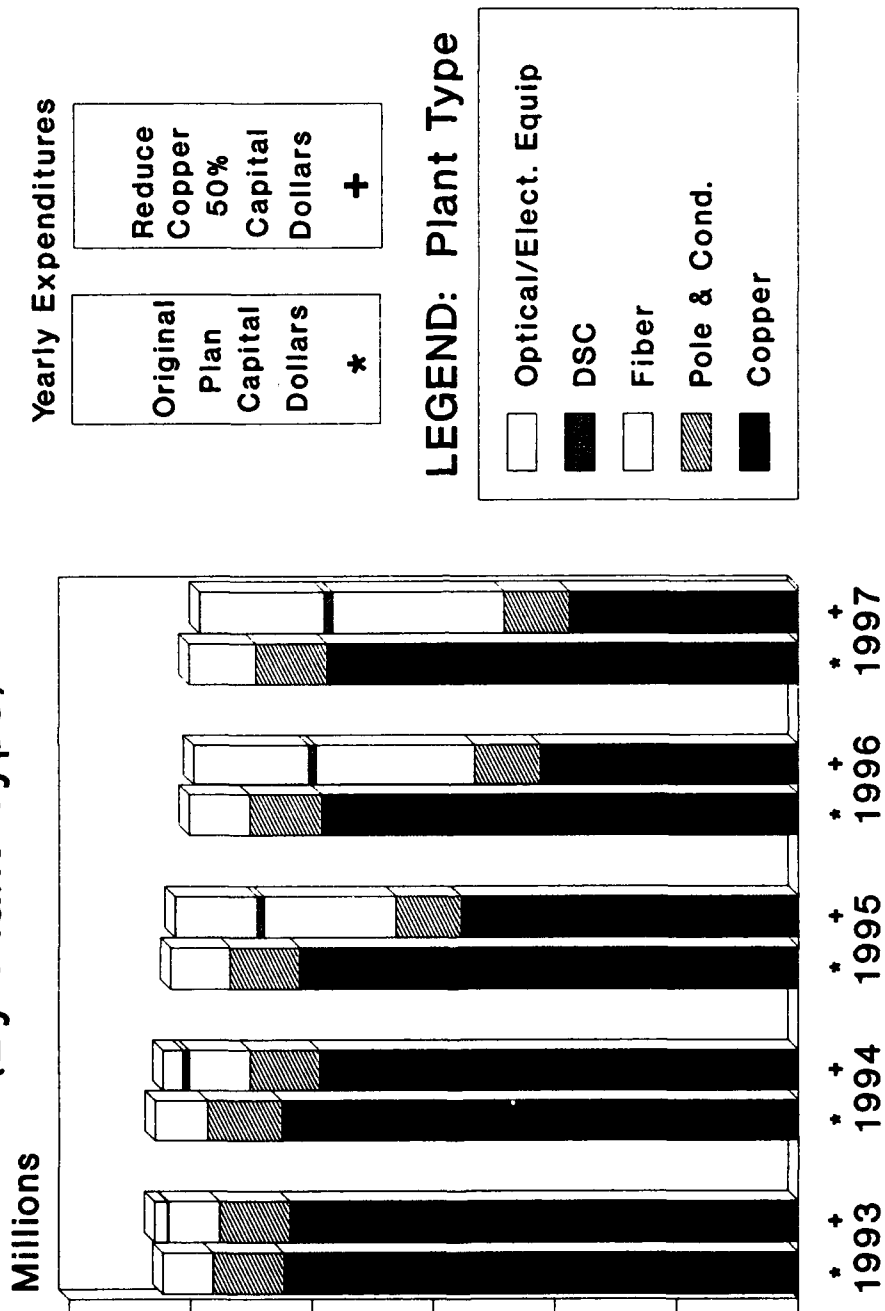
ANALYSIS AND RESULTS

FIBER CABLE ASSESSMENT (Sheath Miles)



ANALYSIS AND RESULTS

BUDGETARY IMPACT (By Plant Type)



CONCLUSIONS

- THE CURRENT STRATEGIC PLAN HAS A DECLINING RATE OF COPPER DEPLOYMENT.
- THE COPPER DEPLOYMENT RATE CAN BE DRAMATICALLY REDUCED BY:
 - 45% IN TERMS OF PAIR MILES
 - 33% IN TERMS OF SHEATH MILES
 - 52% IN TERMS OF GROSS ADDITIONS FOR COPPERWITH NO SIGNIFICANT CHANGE TO TOTAL CAPITAL.
- EXPENDITURES WILL SHIFT FROM COPPER TO FIBER AND ASSOCIATED ELECTRONICS.
- FUNDAMENTAL STRATEGY TO AGGRESSIVELY REDUCE COPPER DEPLOYMENT
- CONTINUE WORK ON OAM&P ISSUES FOR EFFECTIVE OPERATIONS.
 - OSS
 - WORKFORCE
 - TRAINING
 - TOOLS
- REEVALUATE CURRENT POLICIES AND PROCEDURES DRIVING NEAR TERM COPPER INTENSIVE EXPENDITURES. THESE NEED TO BE REVIEWED FROM A FIBER-BASED TECHNOLOGY SUBSTITUTION PERSPECTIVE.

Gary L. Sparks, Staff Manager

Network Planning

GTE Telephone Operations

Irving, Texas

Gary has 21 years of experience in Outside Plant Engineering

- Construction and Network Planning; working in GTE's Indiana, California, and Texas operations in both Staff and Line positions; graduate of Purdue University - BSIM.

To Make The Economical Deployment of Subscriber Networks

Takuya Nakayama, Hiroaki Okabayashi, Eiji Kondo*, and Satoshi Matsushashi

NTT Telecommunication Field Systems R&D Center

Tsukuba, Ibaraki, 305, Japan

***NTT Customer Systems Development Department**

Chiba, Chiba, 261, Japan

Abstract

To deploy optical fiber subscriber networks more economically, particularly for distant, isolated individual subscribers who need very few fibers, we have developed a new type of small, lightweight cable and closure. To facilitate the integration of this cable into existing systems, we needed an efficient way to branch off a new cable from an established optical fiber cable. Thus, we also developed an improved splicing technique. This paper describes the new cable, closure and related technologies.

1. Introduction

NTT is making progress toward a fully digital network by installing optical fiber loops to serve subscribers in large cities. These loops consist of cables containing up to 1000 fibers. As the ISDN service area expands, however, there are an increasing number of subscribers in rural areas who require only a few fibers. Coping with these two opposite types of demand efficiently requires minimizing the financial outlay for materials and construction. Naturally, too, to accommodate subscribers quickly, it is necessary to simplify the installation procedures for easier, quicker deployment. To meet those requirements, we have designed a new outdoor system to provide optical services in rural areas where only a few fibers are required, and have developed the materials necessary to produce it.

This system consists of a new underground cable, aerial self-supporting cable, underground closure to

splice underground cable, and aerial splicing closures.

Both underground and aerial cables are low-count optical fiber cable with small diameter, containing only 4 or 8 fibers. We have also developed a splicing technique for branching off several cables from an established high-count subscriber optical fiber cable.

2. Underground System

2.1 Low-Count Optical Fiber Cable with Small Diameter

The existing optical fiber cable with water blocking (WB) has the same structure for 8 fibers or 100 fibers, making it cost-efficient and suitable for long-distance applications. However, we have examined a new optical fiber cable containing only 4 or 8 fibers for low-density long-distance applications, since demand has been increasing in rural areas. Our new cable is smaller in diameter and lighter than existing cable, and it can be laid through the conduit using only one-eighth the tractive force necessary previously. This reduction in the pulling force means that the connector-equipped end of the cable be miniaturized so that it can be laid through the conduit. We have now made and tested cable that is pre-connectorized at both ends. This new cable is economical in terms of both material and network construction costs.

2.1.1 Cable Structure

The physical features of the new cable are compared with those of the conventional cable in Fig. 1 and Table 1. The new cable has 57% the diameter and 29% the weight of the conventional cable.

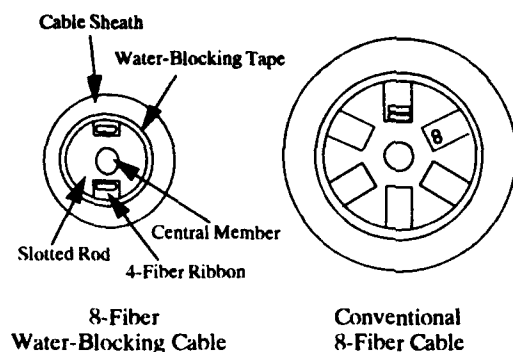


Fig. 1 Cross-Sectional Structures of New and Conventional Cables

Table 1 Features of and Old Cables

Characteristic	New Cable	Old Cable
Outer Diameter (mm)	8.6	15
Weight (g/m)	0.06	0.21
Number of 4-Fiber Ribbons	4, 8	8 ~ 100

2.1.2 Characteristics of New Cable

Table 2 shows the characteristics of the low-count, small-diameter optical fiber cable. Heat cycle testing from -30 to $+60^{\circ}\text{C}$ indicates that the new cable has almost the same properties as the conventional cable. The optical loss due to mechanical stress (crush, repeated bending, tensile, dynamic squeezing) is also the same, and the strain under tensile and dynamic squeezing is confirmed to be the same as well. Trial laying of the new cable shows good optical loss properties and operating efficiency.

2.1.3 Structure of Pulling End with pre-connectorized Fiber

For long-distance installation, the current standard cable has been designed to withstand about 2×10^3 N tractive force. So we cannot affix connectors to the fibers at the pulling end, because the pulling end is bigger than the conduits when it is pre-connectorized

Table 2 New Cable Test Results

Test	New Cable
Heat Cycle: $-30 \sim +60^{\circ}\text{C}$	Change in loss < 0.1 (dB/km)
Crush (Pressure: 1960N/10cm)	Change in loss < 0.1 (dB/km)
Repeated Bending (Bend Radius: 86 mm) (Bend Number of Times: 10)	Change in loss < 0.1 (dB/km)
Tensile (Pulling Force: 245 N)	Change in loss < 0.1 (dB/km) Change in Strain < 0.2 (%)
Dynamic Squeezing (Pulling Force: 245 N)	Change in loss < 0.1 (dB/km) Change in Strain < 0.2 (%)

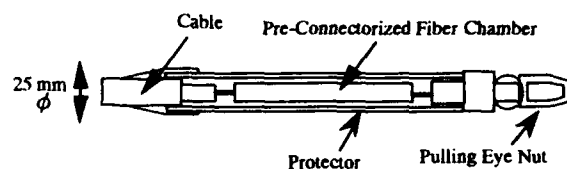


Fig. 2 Structure of Pulling End

and protected against the 2×10^3 N tensile. Thus, we have designed the new cable with small diameter and light weight, thereby reducing the tensile to about 2.5×10^2 N. Because it requires less protection, the pre-connectorized pulling end can be miniaturized. Consequently, we were able to produce a cable that is pre-connectorized at both ends and can be installed through the conduits. Figure 2 shows the structure of the pulling end.

2.2 Subscriber Optical Fiber Cable Closure

We have developed a new optical fiber cable closure to accommodate the new cable. At present, the same closure is used to splice 8 fibers or 200 fibers. We developed a smaller, lighter one tailored to accommodate only 4- or 8-fiber WB cables.

2.2.1 Closure Structure

A photograph of the new optical fiber closure is

shown in Fig. 3. This closure consists of a water-proof case, the frame in the case, and the trays to store the fibers. A conventional closure can be installed with six cables for a capacity of 200 fibers. The new closure is simpler and cheaper for direct connections. The tray is the same as in the conventional closure and can store and protect up to 5 4-fiber ribbons.

2.2.2 Characteristics of The New Closure

As seen from Table 3, which compares the conventional and the new closures, the new closure has 67% the weight and 51% the volume of the conventional closure.



Fig. 3 New Closure

Table 3 Comparison Between New and Old Closure

Characteristic		New Closure	Old Closure
Closure case	Outer Diameter (mm)	150	210
	Weight (kg)	6.6	10
	Length (mm)	685	685
Closure Frame	Height (mm)	28	90
	Width (mm)	90	180
	Length (mm)	570	570

2.3 Branch Splicing Technique

To deploy the new cable, we have to branch off a new cable from an established one, in a procedure called mid-span entry. However, the splicing span is relatively

long, about 1 km, so mid-span entry into an established cable that has no closure is becoming more common. Obviously, with in-service fibers in these established cables, the bending loss arising from mid-span entry must be low enough that it does not interrupt signals. We have therefore developed an improved splicing technique for these cables.

In the near future, as subscriber number multiply, many new cables will have to be installed in one closure. But the existing closure can accommodate only 4 branch cables. So we have developed a new closure with triple the branch cable capacity of the old one.

2.3.1 A Mid-Span-Entry

A photograph of the splicing of the mid-span-entry is shown in Fig. 4. There are three special items for the closure used in mid-span entry. The first is a fiber storage sheet which can store and protect up to 40 fibers. Inside, it has a sheet of polyethylene bubbles to protect the fibers from outside pressure. The second item is a slotted rod cap which protect fibers from the slotted rod's cutting section. Finally, the fiber protector protects fibers from being damaged by the closure itself or from bending during assembly or disassembly of a closure.

2.3.2 Mid-Span Entry Procedure and Resulting Optical Loss

The steps of the mid-span entry procedure are shown in Table 4, and the optical bending loss arising from each operation is shown Fig. 5. These results indicate no practical problem for less than 1 dB.



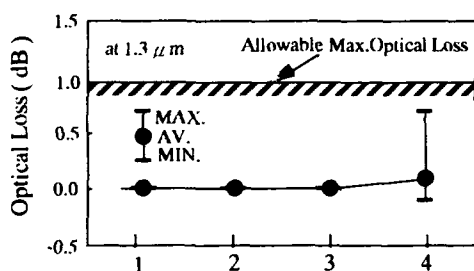
Fig. 4 Splicing of Mid-Span-Entry

2.3.3 Multiple Branch Splicing Technique

We have developed an adapter which is installed in an existing closure to make it possible to deploy up to 12 new cables (see Fig. 7). The adapter (see Fig. 8) consists simply of an airtight seal and a clamp for fixing the cables.

Table 4 Mid-Span Entry Operation

Process
(1) Peel the cable sheath from established cable.
(2) Cut and fix the central member.
(3) Wrap the fibers in storage sheet. (see Fig. 6)
(4) Cut the slotted rod.
(5) Put on the slotted rod cap.
(6) Splice the established fibers and the new branch fibers.
(7) Store the fibers and put on the fiber protector.
(8) Assemble the closure.



1. Peel the cable sheath from established cable
2. Cut and fix the central member.
3. Wrap the fibers in storage sheet
4. Cut the slotted rod

Fig. 5 Optical Loss



Fig. 6 Wrapping the Fibers in Storage Sheet

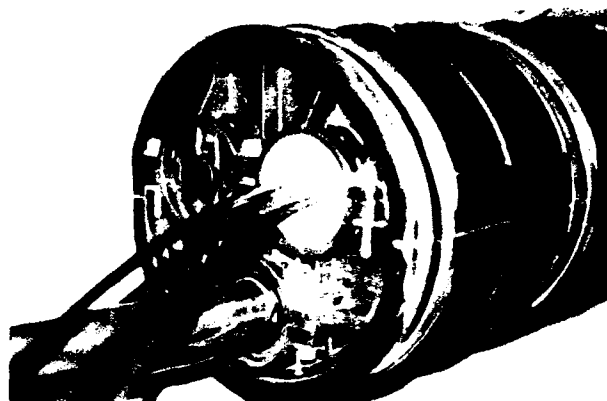


Fig. 7 Adapter on Closure and Branched New Cable

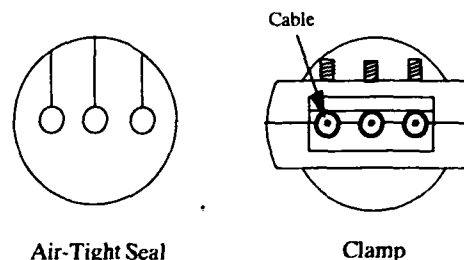


Fig. 8 Adapter

3. Above-Ground System

As with the underground cable, the new type of aerial cable is also narrower and lighter than conventional cable, and is more efficient to install. This new cable also has only 4 or 8 fibers.

3.1 Low-Count Optical Fiber Cable with Small Diameter

Figure 9 and Table 5 show the structures of the new cable and the conventional cable. The new cable has 13% the weight of the conventional cable, and involves lower material and installation costs.

Table 6 shows the characteristics of new cable. In terms of the properties listed, the new cable is nearly identical to the conventional cable. Laying tests with the new cable reveal good optical loss and operating efficiency.

3.2 Aerial Optical Fiber Closure

A new aerial closure was needed to accommodate the new cable; hence we have developed the aerial closure, in 2 types (I, II) to adjust to different cases. Both are small, lightweight, easy to assemble, and cost-efficient. Table 7 shows their characteristics in comparison with those of the conventional aerial closure.

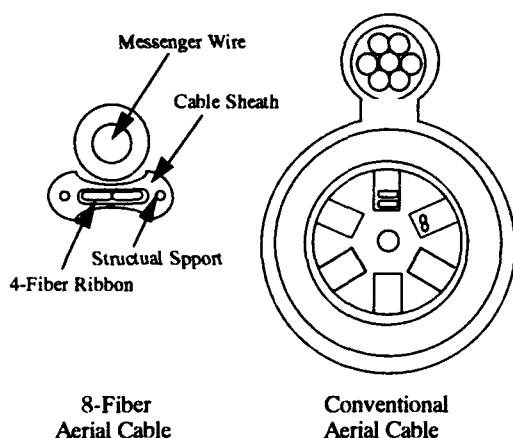


Fig. 9 Cross-Sectional Structures of New Cable and Conventional Cable

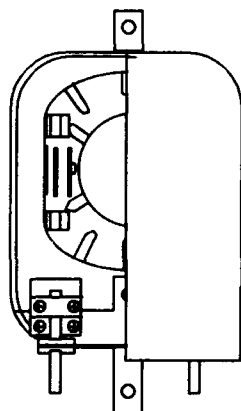


Fig. 10 New Aerial Closure Type I

3.2.1 Aerial Closure I

Aerial closure I's structure is shown in Fig. 10. This closure can store 8 fibers and be fixed on a pole. It is used mainly for underground cable and aerial cable splicings.

Table 5 New and Old Aerial Cable Features

Characteristic	New Cable	Old Cable
Outer Diameter (mm)	7 × 4	15
(g/m)	0.07	0.55
Number of 4-Fiber Ribbons	4, 8	8 ~ 100

Table 6 New Aerial Cable Test Results

Test	New Cable
Heat Cycle: -30 ~ +60°C	Change in loss < 0.1 (dB/km)
Crush (Pressure: 1960N/10cm)	Change in loss < 0.1 (dB/km)
Repeated Bending (Bend Radius: 86 mm) (Bend Number of Times: 10)	Change in loss < 0.1 (dB/km)
Tensile (Pulling Force: 1900 N)	Change in loss < 0.1 (dB/km)
	Change in Strain < 0.2 (%)
Dynamic Squeezing (Pulling Force: 490 N)	Change in loss < 0.1 (dB/km)
	Change in Strain < 0.2 (%)

Table 7 Features of New and Old Aerial Closures

Characteristic	New Closure I	New Closure II	Old Closure
Length (mm)	140	160	690
Width (mm)	40	40	110
Height (mm)	210	120	160
Weight (kg)	0.37	0.4	1.7
Max. Number of 4-Fiber Ribbons	8	8	100

3.2.2 Aerial Closure II

Subscriber networks mainly employ aerial optical fiber cable which is pre-connectorized at both ends, but the rest of the cable is coiled where the messenger wire is hung. (see Fig. 11) So we have developed a second type of aerial type II to solve the problem of this extra cable, to use the cable effectively, and to improve the installation procedure. It can also store 8 fibers, be hung on messenger wire between poles, and be used to directly connect new aerial cables. The structure of aerial closure II's is shown in Fig. 12, and it is shown hung on the messenger wire in Fig. 13. This configuration, with the closure on the messenger wire rather than fixed to a pole, means that the wind will have a stronger effect on the system, we therefore conducted vibration tests (see Table 8), and determined that the new setup will not adversely affect service.

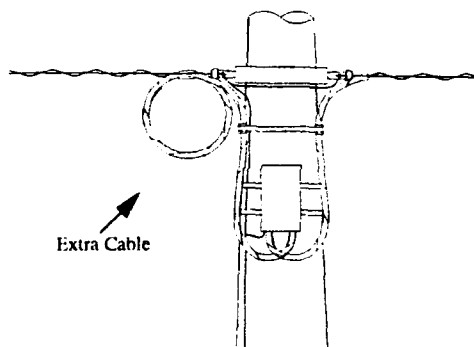


Fig. 11 Extra Cable Position

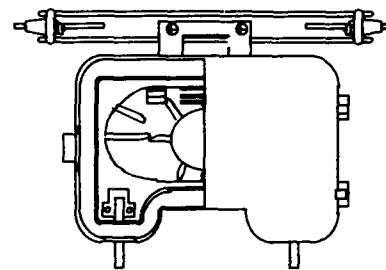


Fig. 12 New Aerial Closure Type II

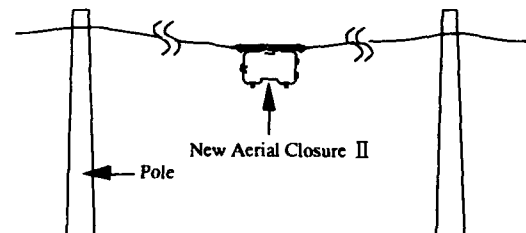


Fig. 13 New Closure II, Hanging

Table 8 Vibration Test Results

Position on Messenger Wire	Oscillation	Change in Strain (%)		Change in Loss (dB)		Damage to Messenger Wire, Closure, etc	Fiber Condition
		Max.	Residue	Max.	Residue		
Midway between Poles	2.95 Hz ± 20 mm	0	0	< 0.1	0	No	Good
	5.0 Hz ± 21 mm	0	0	< 0.1	0	No	Good
1/4 of pole-to-pole distance	2.3 Hz ± 45 mm	0	0	< 0.1	0	No	Good

4. Conclusions

We have developed new ways to make the deployment of optical networks more economical: a low-count optical fiber cable with small diameter, the optical closures to accommodate the cable, and a branch-splicing technique. Thanks to these, we have streamlined the installation procedure and reduced the associated costs and time required to deploy optical subscriber networks. We also introduced simpler branch splicing and multiple branch splicing to cope with the increasing number of subscribers.

Acknowledgment

The authors thank Akiyoshi. Sekiguchi, Takaharu. Yoshitomi, Kiminori. Sato, Minoru. Nakamura, and Akira Hirooka for their helpful discussion and suggestions.

References

- [1] E. Kondo, M. Uesugi, N. Ohno, and T. Sano, "Characteristics of Low Count Optical Fiber Cable with Small Diameter" The Institute of Electronics, Information and Communication Engineers, B-874, 1993.
- [2] E. Kondo, H. Matsumoto, K. Sato, "A Study on The Structure of OpticalFiber Cable" The Institute of Electronics, Information and Communication Engineers, B-630, 1992.
- [3] Y. Mitsunaga et al. The Institute of Electronics, Information and Communication Engineers, Technical Report, communication Systems, Vol. 78-213, 1979.



Hiroaki Okabayashi

NTT Telecommunication
Field Systems R&D Center
Tsukuba, Ibaraki, 305,
JAPAN

Hiroaki Okabayashi graduated from Sakai technical high school. He joined NTT in 1983. He is an engineer in the Outside Plant Engineering Systems Development Project Group in NTT Telecommunication Field Systems R&D Center.



Kondo Eiji

NTT Customer Systems
development Department
Chiba, Chiba, 305, JAPAN

Kondo Eiji received B.S. and M.E. degree in electrical engineering from Tokyo University in 1989, and 1991, respectively. He joined NTT in 1991. He is an engineer in the Telecommunications Cable Systems & Outside Plant Group in NTT Customer Systems Development Department.



Takuya Nakayama

NTT Telecommunication
Field Systems R&D Center
Tsukuba, Ibaraki, 305,
JAPAN

Takuya Nakayama received B.S. degree in electrical engineering from Ibaraki University, Ibaraki, Japan, in 1988. He joined NTT in 1988. He is an engineer in the Outside Plant Engineering Systems Development Project Group in NTT Telecommunication Field Systems R&D Center.



Satoshi Matsushashi

NTT Telecommunication
Field Systems R&D Center
Tsukuba, Ibaraki, 305,
JAPAN

Satoshi Matsushashi received B.S. degree in electrical engineering from Hokkaido University, Japan, in 1981. He joined NTT in 1981. He is a senior engineer in the Outside Plant Engineering Systems Development Project Group in NTT Telecommunication Field Systems R&D Center.

NETWORK COMPONENTS AND CABLES FOR EFFECTIVE FIBER HANDLING OF STAR TOPOLOGY IN FTTH FIELD TRIAL IN BALLERUP, COPENHAGEN

Hans Olofsson, Johan Meyer*

Telecom Cables Division, Ericsson Cables AB, Hudiksvall, Sweden
*Application Lab Fiber Access, Ericsson Telecom AB, Stockholm, Sweden

ABSTRACT

When building a Fiber-To-The-Home, FTTH, system using a fiber rich topology such as a full star, it is essential to use network components capable of handling a large number of fibers. An all ribbon concept has a great potential to solve some of the fiber handling problems related to fiber rich topologies. It is important to keep the ribbon format as extensively as possible. In the field trial, ribbon is used from circuit boards to the customers premises. Termination of cable and fiber should be prefabricated to a great extent, cutting cost for installation and yet ensuring high transmission performance. Connectors with a push-pull mechanism are used consistently for easy handling and compact design. There is one flexible point in the network, the optical distribution frame, ODF, where all individual fibers can be accessed for measuring purposes, adding, deleting or upgrading services etc.

INTRODUCTION

This paper describes the system aspects and the technical realization of the Ericsson part of a Fiber-To-The-Home field trial in Ballerup, Copenhagen, Denmark. The field trial is managed by the telecommunications administration of Copenhagen, KTAS. Ericsson delivers equipment which will serve 50 customers in two phases; the first to be finished in autumn 1993 and

the second in summer 1994. Each phase involves approximately 25 subscribers.

General

The network topology is based on a full star concept. There are two services provided in the field trial, interactive services delivered on a 2 Mb/s basis and distributive service i.e. analog CATV.

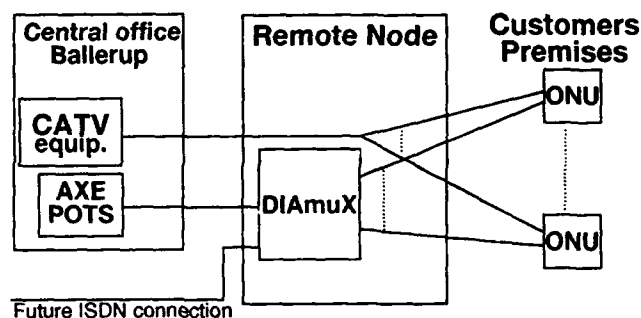


Figure 1: Survey of the field trial

Interactive Services

The interactive system uses a remote multiplexer, a DIAMuX, located in a Remote Node (RN). The DIAMuX is connected to existing Ericsson AXE PSTN switching equipment which provide all the subscribers with POTS, (Plain Old Telephony Service). ISDN-BA will be provided later on. Other accesses are also possible such as computer interfaces etc. within the system concept as long as the accumulated bitrate to each ONU is less than 2 Mb/s.

The DIAMuX concept is designed as an open system using 2 Mb/s PCM highways towards its internal switch. This makes the system very flexible.

The optical framework is a bidirectional point-to-point link.

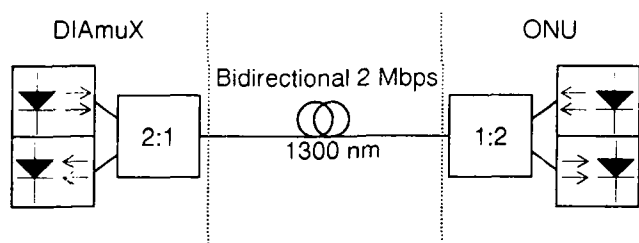


Figure 2: Telephony, optical framework

CATV

The CATV-system will receive its signals from the Danish national CATV-system, DOCAT, in an electrical AM-VSB-format. The electrical signal, with a bandwidth of 47 - 862 MHz, will modulate three highly linear lasers in the 1300 nm window. The laser transmitters are located in the Ballerup Central Office, 3 km from RN. Each laser will feed an 1:16 splitter. The splitters are placed in ODF-boxes at the same remote node as the DIAMuX. The CATV-system is designed to have a potential to feed 64 subscribers.

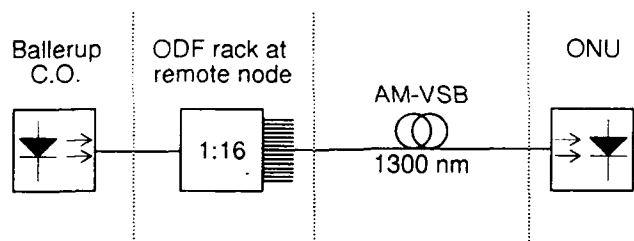


Figure 3: CATV, optical framework

Optical Network Unit

At the customer's premises there is an Optical Network Unit (ONU) containing optical transceivers for 2 Mb/s and O/E converters for CATV along with local powering and backup batteries. The batteries are dimensioned for

more than 5 hours stand-by including one half hour active use of POTS.

Up to eight circuit boards of different access types can be installed of which at least one is used for a 2 Mb/s connection to the switch. The boards used in this trial are for optical 2 Mb/s interfacing, POTS (and later on ISDN-BA) and CATV. The ONU contains a fiber organizer for fanout and termination of fiber ribbon it also houses couplers etc.

Operation & Maintenance

A full star network configuration offers a straightforward operation & maintenance, O&M, system. The system uses the standard O&M for DIAMuX, DIAx OM. However there are several additions for handling the optical system.

The O&M system for interactive and CATV services is integrated. Laser power down e.g. is one of the additions which handles the output power level from the CATV transmitter. In case of cable break there will be an immediate decrease of output power to an inherent secure optical output power level.

NETWORK COMPONENTS

Ribbon cables and mass splicing techniques will help cutting costs and minimizing size. The use of preassembled fiber and cable terminating components that simplify use of ribbon technology are evaluated. The aim has been to prove the feasibility of an all ribbon concept from circuit boards all the way to the customers premises with one flexible point at the RN where physical access to single fibers is possible. The network configuration is shown in figure 4. Two copper pairs for each subscriber is provided by KTAS and they are spliced to the subscriber cable at the DP. One pair can be used for POTS in case of failure of the FTTH system.

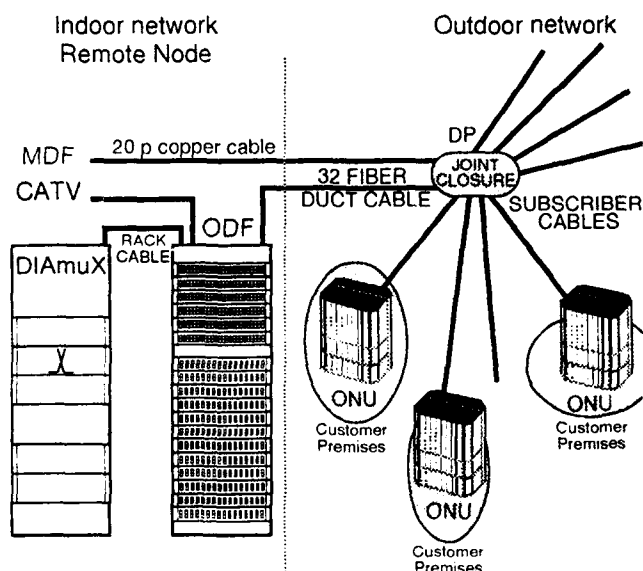


Figure 4: Network configuration

Fiber Optic Cabinet Interconnect

Quad Optical Transceiver. The main part of the field trial is built using quad optical transceiver cards, i.e. a circuit board with four bidirectional 2 Mb/s systems. The board is equipped with a fiber organizer, 140 x 90 mm, where four 2:1 couplers and all fibersplicing is organized. Each coupler is fusion spliced to a laser and a PIN diode. The fusion splices are protected by means of recoating. The recoating is made with an Ericsson EFR 1000. The fusion splice is put in a mould filled with an UV curable polymer. The polymer is cured with the built in UV lamp, now the splice is coated with a layer of cured polymer having the same diameter as the primary coated fibers. Using recoating means that fiber looping in the cassette will be simplified since there is basically no limitation on the number of splices that can be handled and no restriction on where splices can be put. This makes fiber storage and handling on circuit boards more efficient compared to using protection sleeves.

The output from the board is made by splicing the four couplers to a 4-fiber ribbon fitted with an MPO connector. The MPO connector is basi-

cally an angle polish MT connector with a push-pull mechanism and a special housing. The housing is fixed to the edge of the board allowing for easy access. The layout of the circuit board can be seen in the photograph in figure 5.

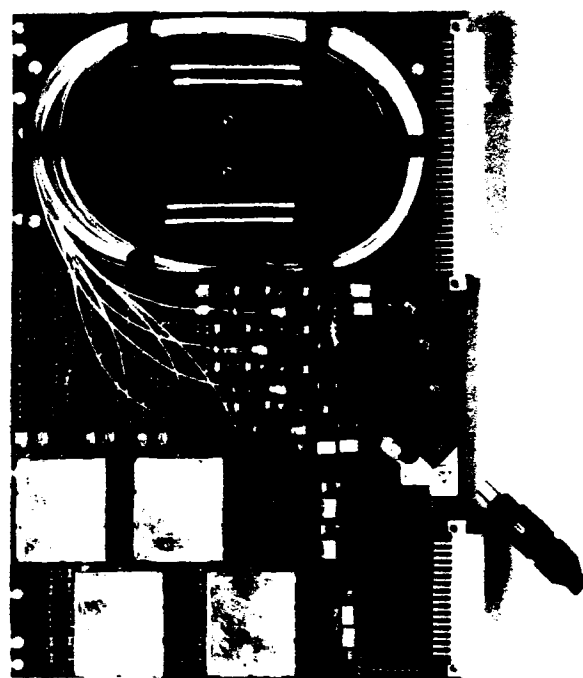


Figure 5: Quad Optical Transceiver

The active full star topology gives us a high power budget, which allows us to have generous system margin for couplers and insertion losses from connectors etc., i.e. loss is no major design problem. Due to the use of couplers the return loss should be higher than 25 dB. When using standard MT-connectors a high return loss is achieved by means of index matching gel. We want to avoid using index matching gel in combination with electronic equipment since the gel often contains silicone and the silicone can contaminate electric connectors and relays and thus causing malfunction. Since the MPO connector is angle-polished, very high return loss is achieved without gel, higher than 50 dB, making the total design very robust.

Rack Cable. The rack cable from the DIA-muX cabinet is a slotted core ribbon cable, basically the same construction as the ribbon cable in figure 8 except for the copper pair. The cable is terminated from factory in an ODF box with SC connectors. In the cabinet the cable is terminated with a cable fanout shown in figure 9.

An alternative method used in the first part of the field trial is to terminate the rack cable in fiber organizer cassettes. The cassettes are mounted directly on the cabinet wall with a special fixture including a cable stranding facility. Since the termination is protected by the cabinet no extra protection is needed. This is a low cost termination which can be assembled at factory with tailored lengths on rack cable and pigtails or appropriate pigtails can be spliced to the rack cable on site.

Optical Distribution Frame

In the network there is a need for a flexible point where single fibers can be accessed for monitoring and where services can be added, deleted or upgraded. At this point fibers from the outside plant are terminated and here cross connection is possible. The solution is an Optical Distribution Frame, ODF.

The basic building block is a box which takes care of ribbon fan-out and cable termination. The box is designed for 19 inch rack mount. The front is exchangeable allowing for different types and number of connectors. It has a tray for fiber and splice organization, underneath the tray there is room for fiber or ribbon storage. If a couple of meters of fiber or ribbon is stored in the ODF box, the tray can be pulled out of the guides and put in a more convenient position when working.

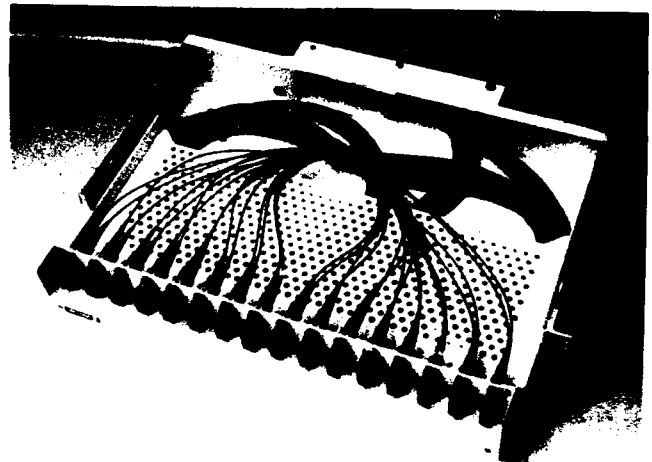


Figure 6: The ODF Box

In the trial all connectors are SC type which is a single fiber connector with push-pull mechanism which allows more compact ODF design than traditional FC/PC connectors. Insertion loss for the connector is less than 0.5 dB (typically less than 0.2 dB) and minimum return loss is 40 dB. These values are stipulated by the analogue CATV system

The box can also be used for housing passive components, like done in the field trial, where three 1:16 splitters are put in one ODF box giving us 48 outputs on 1.5 u height, as shown in figure 7.

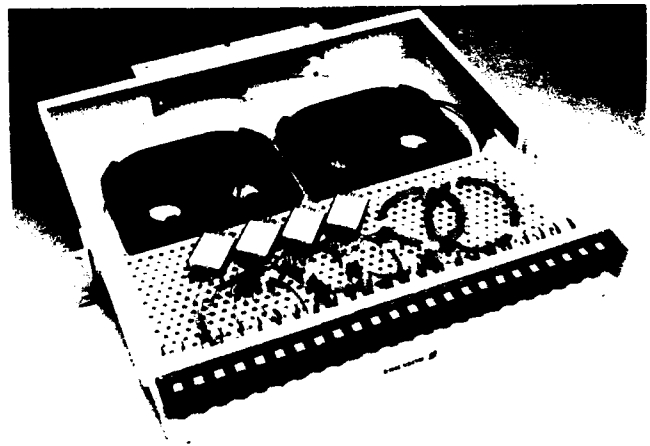


Figure 7: The CATV Splitter Unit

This is the maximum number of standard SC connectors that can be handled in one ODF box. The splitters are protected by fiber organizer cassettes put on the bottom of the box and there is room for yet another splitter in the box resulting in a total of 64 outputs. To handle 64 outputs in one ODF box we have to change connector type. The easiest way would be to remove the push-pull mechanism from the SC connector, making connector access possible only with a special tool. If this is not regarded as a big disadvantage, connector density could be doubled.

The cables from the outside plant are terminated in separate ODF boxes for most convenient management. It could be built more compact allowing termination of two cables in each box, again this means that we would need different types of connectors.

Outside Plant

Primary Cable. The network is built using 32 fiber cables (eight 4-fiber ribbons) as primary network. It is a slotted core design, which is well documented and already installed in many networks. It has a water swelling tape for water blocking and a non halogen flame-retardant polyethylene sheath which makes the cable suitable for outdoor as well as indoor installations.

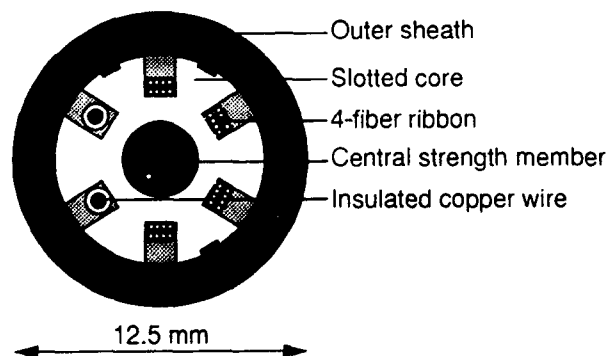


Figure 8: Cross section of the 32 fiber slotted core cable

The cable is fitted with a factory made fanout which contains no splices and thus will not contribute to any loss. The individual pigtailed are fit-

ted with SC-connectors to allow compact ODF construction. High performance termination is guaranteed through factory prefabrication and control.

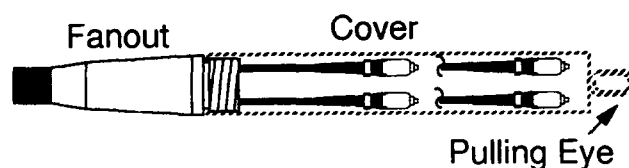


Figure 9: Cable fanout

The cable is drawn in buried plastic pipes to the distribution point, DP. The cable fan-out is fitted to the ODF, where it, like in the field trial, can be put into an ODF-box or it may be mounted directly in the rack.

Distribution Point. At the distribution point, close to the customers premises, one 4-fiber ribbon and two copper pairs are spliced to each subscriber. The joint closure has been modified to handle both fiber and copper splices for eight customers.



Figure 10: Joint Closure

The ribbons are fusion spliced with a ribbon splicer in order to optimize installation time and fiber handling. The splices are protected and the ribbons are put into a fiber organizer. The organizer is designed to store all kinds of fibers including ribbons with up to 12 fibers. In the field trial only one organizer is needed since it can handle the eight splices made at each DP.

The standard configured closure can house eight organizers and it can be fitted with different types of cable inlets, for cables with various diameters, thus forming a modular system for cable termination and distribution. The joint closure, made of stainless steel, is watertight and pressure resistant which makes it suitable for a buried installation such as in Ballerup.

Subscriber cable. The subscriber cable contains one tube with a loose 4-fiber ribbon, two copper pairs and a small amount of aramid yarn to increase tensile strength. It is water blocked and has a non halogen, flame retardant sheath which allows for an uninterrupted installation from the DP to ONU.

The main issues when constructing the subscriber cable was to make it flexible, lightweight and thin. The intention is to use it for very short drops only, therefore a low pulling force can be accepted. In the field trial a length of approximately 100 meters has been successfully installed. Tensile tests show no increased attenuation for cable loads up to 600 N.

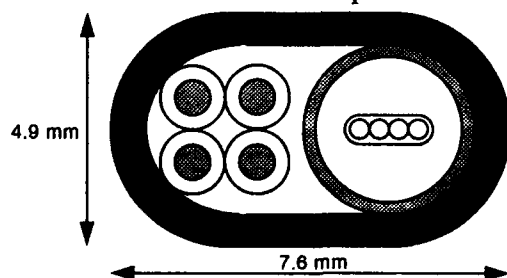


Figure 11: Subscriber cable

Crush tests using plates of 100 mm diameter and a rod of 25 mm diameter show no increased attenuation for loads up to 5 kN.

Subscriber Termination

The cable is stripped, the ribbon tube is cut and anchored to the fiber organizer in the ONU and a couple of meters of ribbon is split to get access to the individual primary coated fibers. The termination is made by fusion splicing pigtails and preconnected 2:1 couplers to individual fibers. Fibers not used are stored in the organizer for possible future use. The organizer is the same type used in the joint closure.

CONCLUSION

The presented network components in this field trial supports an active full star deployment built with ribbon cables from the circuit boards to the customers premises. This strategy allows for a future unlimited upgradeability.

Fiber ribbon cable technology will be tried out both as rack cable and subscriber cable. The fiber ribbon cable has a high potential to solve some of the fiber handling problems accompanying a full star deployment. Using dedicated components and prefabricated terminations gives opportunities to build compact systems with reduced installation costs.

The concept of the field trial could be seen as an important step towards integration between telephony and CATV in the subscriber loop. Access to point-to-point links entail possible upgradeability to bidirectional, dual-wavelength high-speed links for B-ISDN and related services.

REFERENCES

Frohm, Hansen & Madero: *The DIAMuX System Series - Flexibility in the Network*. Ericsson Review 70 (1993):1, pp. 30 - 40.



Hans Olofsson
Telecom Cables Division
Ericsson Cables AB
S-824 82 Hudiksvall,
Sweden

Hans Olofsson was born in Delsbo, Sweden. He graduated from Chalmers' University of Technology, Gothenburg, Sweden with a Master of Science in electronics engineering 1983. He joined Ericsson Cables AB in 1984 where he worked at the transmission laboratory until 1991 when he was engaged in the Ericsson Application Lab Fiber Access.



Johan Meyer
Application Lab Fiber
Access
Ericsson Telecom AB
S-126 25 Stockholm,
Sweden

Johan Meyer joined Ellemtel Telecommunication Laboratories, Stockholm, in 1982 after he had received the Master of Science degree in electronics engineering from the Royal Institute of Technology, Stockholm, Sweden. Here he was involved in developing analogue line circuits. Since 1986 he has been with Ericsson Telecom AB where he has been working on algorithms and signal processor architecture for analog subscriber lines. In 1990 he was engaged in the Ericsson Application Lab Fiber Access where he has been studying FITL-issues.

FIRST LARGE SCALE FITL INSTALLATION: EXPERIENCE FROM OPAL '93

W. Wenski, H. Dominik, W. Liese, H. Schönfeld

Kabelmetal Electro GmbH
Postfach 260
30002 Hannover, Germany

Summary.

The described FITL (Fiber in the Loop) networks which are installed within the scope of the OPAL '93 program of the German Telekom, are already now cost-competitive with copper networks. We have developed a novel modular network concept using passive optical networks (PON) for distributive services (DS), such as TV, and an active optical network (AON) structure for interactive services (IS), such as POTS and ISDN. This concept provides flexibility and economics and meets the specific demands of all areas considered. The execution of the project on a turnkey basis reduced the time from contract signing to commissioning of networks for 24,000 lines in December 1993 to less than one year.

FITL in Germany: The OPAL Program.

Fiber optic networks in Germany started in 1978 with the first pilot and operating trials. Today the long distance traffic runs on a fiber optic backbone. Local area networks (LANs) in business centers are nearly exclusively based on fiber technology. There is now only one link missing for an all-fiber network: the last mile of the access loop from the Central Office (CO) to the customer.

German Telekom addressed the future services in this last mile in the BIGFON program (1983 - 1986) using analog transmission technology.¹

A new approach was taken by the OPAL program starting in 1990, with selected pilot projects totalling a few thousand subscribers. The ultimate goal of OPAL (Optical Access Line) is FTTH, fiber to the home, where the terminal of each customer is reached by an individual fiber.^{2,3}

More programs have been announced worldwide with different services. In the U.S.A. alone some 300 CATV projects, involving fiber, are known.⁴

The German re-unification and the requirement to rebuild the complete telecom network of the former East Germany from 700,000 to 7 million access lines in only 7 years, also made it necessary to redirect and speed up the OPAL program. Development of optical access lines thus became a part of the restructuring program. However, FITL costs had to meet the cost of copper in all proposed networks before planning could begin.

This new OPAL program started with the announcement by DBPT Telekom to provide, as the first operator in the world, integrated interactive and distributive services in an optical access network. This network will cover up to 1.2 million subscribers by 1995, 200,000 of which will be connected in OPAL'93.^{5,6} The large scale of this program has stimulated mass production of components to a point where the construction of networks can now be achieved economically, at prices equivalent to the cost of copper, as we shall show further below.

Alcatel Kabelmetal and Alcatel SEL were awarded a share of 24,000 subscribers of the OPAL'93 program on a turnkey basis. The following describes the experience gained from the construction and commissioning of these first FITL networks, which have been installed. (Fig. 1).



Fig.1: Start of FITL in Germany: Installation of the first combined flexpoint / curb in Quedlinburg (June 1993).

Targets of OPAL'93.

The network is to be constructed with a full set of options for future services and possible conversion to a later PON - FTTH structure, recognizing that FTTH in today's technology is not economically feasible.⁷ Strategies for cost reduction include fiber sharing and equipment sharing. This leads to transmission networks, where data are multiplexed for the transport on one common optical fiber. The data are delivered to a point close to the customer's terminal, ending either at the curb (FTTC), a maximum of 200 m from the customer or at the building / block (FTTB) where they are demuxed. The final leg from the curb or basement to the subscriber's terminal utilizes conventional copper installations.

The networks for IS (POTS, ISDN and leased lines > 2 Mbit/s) and DS (CATV) are operated separately but use the same infrastructure, e.g. the CO and the cable plant. They use different fibers in the same cable.

The networks are planned for a potential radius of 10 to 20 km around one Central Office.

Demands in Selected Regions.

Network costs, component availability and the mandate to provide services to average, not hand-picked urban, residential and rural areas required a network solution with far higher flexibility than pure-breed passive optical networks with FTTH, FTTB or FTTC solutions. The electronic equipment in remote branches of the distribution network and not the relatively low cost of the cable, presents the challenge for developing low-cost networks. This becomes evident if we review networks in the different area types.

Three regions encompassing a total of 9,300 lines from regions designated as urban, residential and rural are reviewed below. They illustrate the differences in demand to be covered by our network concept.

Area 1: Urban (Berlin): The surveyed section of Berlin is characterized by buildings with 4 to 5 stories, containing up to 20 apartments. The backyards of the city blocks carry a high proportion of small industry. Public services and some larger industrial units generate high demand for business lines.

The relative low density of building and dwelling units in area 1 (Table 1) is due to the presence of industrial zones using PABXs. This is typical for an urban setting containing a mixture of residential and business zones. In addition, a larger area is reserved here for the Olympic Games 2000 for which the demand is not yet specified.

Area 2: Residential (Quedlinburg): This surveyed area is characterized by large prefabricated concrete buildings, each with up to 60 apartments. Business subscribers are lacking here.

Area 3: Rural (Limbach-Oberfrohna): The area of Limbach - Oberfrohna can be subdivided into two parts, each consisting of a rather dispersed mixture of small, owner-occupied houses or buildings with up to 5 apartments. The demand for business lines is generated by small industry and a single industrial zone.

Intuitively, it is felt that the number of dwelling units per square kilometer should be highest in urban regions, followed by residential and rural areas.

	area 1 urban	area 2 residential	area 3 rural
buildings per sq. km	210	815	413
dwelling units per sq. km	2000	10400	1038
dwelling units per bldg.	10	39	3
residential lines	2173	1975	3188
business lines	1015	76	904
ratio: resid./bus. lines	2.1	26	3.5

Table 1 Main characteristics of the surveyed urban, residential and rural areas.

This survey demonstrates that administrative boundaries, such as city limits or zoning regions, are not sufficient to indicate -even roughly- the character of an area. It is clear from Table 1, that the demand for business, residential lines and the structure expressed in dwelling units per square kilometer vary widely with the regions considered: the variations are, in fact, exceeding a factor of ten! Similarly, the demand within a given area also shows large variations. This requires close adaptation of the network modules (flexpoints, curbs, ONUs etc.) to the local requirements of a region.

FTTF: A New Modular Network Concept.

As a result of our findings, our solution is therefore based on a few network modules using modular components. These are implemented throughout the combined passive/active optical network with FTTC and FTTB elements at the customer's end. Modularity and network architecture permit growth into B-ISDN and FTTH solutions in accordance with demand.

Distributive services are transmitted as optical analog signals in the frequency range from 47 to 606 MHz at 1550 nm using optical amplifiers at the CO. The signals leave the CO from the optical distribution frame (ODF). Fiber optic splitters in the distribution points with splitting ratios 1:8 to 1:32 distribute the signal to optical network units (ONU) in curbs (FTTC) or in the buildings (FTTB) (Fig.2). For the curb solution a miniature local coaxial distribution network serves neighboring subscribers through HF splitters. For FTTB, a standard interface for intra-building distribution is provided.

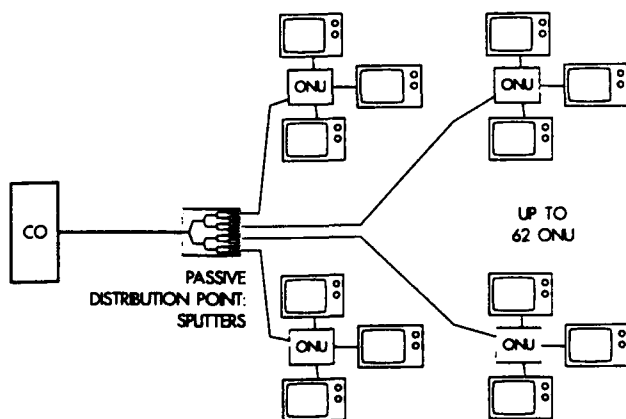


Fig. 2: Passive optical network (PON) for distributive services

Interactive services are transmitted at 147 Mbit/s. The data enter the distribution point via fiber in the main cable. Here the OLU (optical line unit), an active electronic unit, performs mux/demux operations and electro-optical conversions. It transmits the digital signals as optical 2x2 Mbit/s data streams on a single fiber to one dedicated "dumb" ONU close to the customer (Fig. 3). We call this active distribution point the "flexpoint", for it provides enhanced flexibility in network planning.

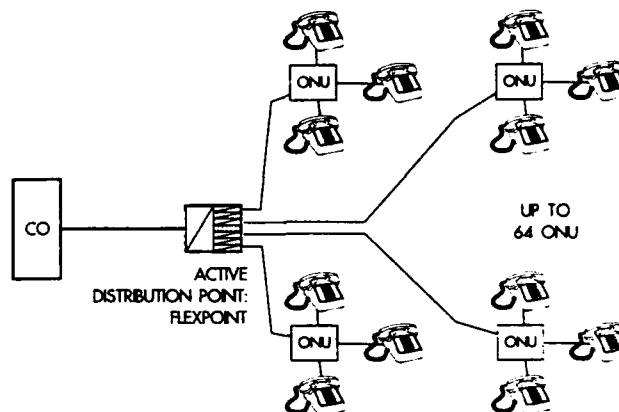


Fig.3: FTTF: Active optical network structure (AON) for interactive services (IS)

It is appropriate to name this solution FTTF, fiber to the flexpoint, since the mux/demux electronics at the customers' end are concentrated here instead of in curbs (FTTC) or in buildings (FTTB). This interpretation is consistent with the previously introduced acronyms.

What seems technically complicated performs a miracle of flexibility in practical network planning. Four OLU's in a flexpoint can serve a maximum of 64 ONUs in buildings or curbs. With a maximum capacity of 64 POTS per ONU up to 4,096 dwelling units can be reached from a single flexpoint.

The ONU capacity for FTTC and FTTB is identical. Two ONU sizes providing 32 or 64 POTS (corresponding to 16 or 32 ISDN 64-kbit ports) offer a modular selection for improved equipment utilization. All ONUs permit a mixture of digital and analog services.

Planning Rules.

The selection of FTTB or FTTC depends on the local density of buildings and dwelling units in the areas considered. Buildings with less than 10 dwelling units are served from a Curb-ONU. Buildings with more than 10 dwellings are served from a FTTB-ONU. For high dwelling counts in one building two ONUs are placed back to back.

For the cable plant design the loss budget, the dispersion and the number of lines served (including a safety factor of 1.2 for future expansion) as well as the list of approved cables and equipment are key design elements. Highlights of the planning rules are summarized in Table 2.

distribution point, half size											
main cable 20..100 fibers 10 fibers/tube			distribution point		distribution cable 20..100 fibers 10 fibers/tube				max. ONUs connected to distrib. point		
fibers for			active:	passive:	fibers for				IS	DS	
IS	DS	spare	IS-OLU	splitter	IS	DS	spare	dark			
4	2	2	2	1 * 1:32	1	1	2	1	32	31	
2	4	2	2	2 * 1:16	1	1	2	1	32	30	

distribution point, full size										
main cable 20..100 fibers 10 fibers/tube			distribution point		distribution cable 20..100 fibers 10 fibers/tube				max. ONUs connected to distrib. point	
fibers for			active:	passive:	fibers for				IS	DS
IS	DS	spare	IS-OLU	splitter	IS	DS	spare	dark		
8	4	2	4	2 * 1:32	1	1	2	1	64	62
8	8	2	4	4 * 1:16	1	1	2	1	64	60

ONU Type	drop cable 4 or 6 fibers 2 fibers/tube				max. lines (POTs)*
single ONU	fibers for				64
	IS	DS	spare	dark	
	1	1	2	0	
double ONU	fibers for				128
	IS	DS	spare	dark	
	2	1	2	1	

* one ISDN-line uses the capacity of two analog POTs

Table 2 Sizing of the network by design rules: Fiber count in main and distribution network and capacity of the distribution points and ONUs.

Powering Concept.

Since there are only few flexpoints in the network they are treated as part of the curb powering concept. Each flexpoint requires 200 W, each curb 100 W and the transmission loss is budgeted as 100 W. Curbs and flexpoints are remotely powered from a central master curb with 115 VDC in separate power cables. Trenches or ducts are shared with the FO telecom cables. Only in exceptional circumstances are the flexpoints powered directly from the 220 VAC grid. Fig. 4 illustrates the powering of a flexpoint and four curbs from one master curb. Compared to direct powering from 220 VAC our concept reduces the costs for power installations by 10 to 20 %. All active points include a four-hour battery back-up.

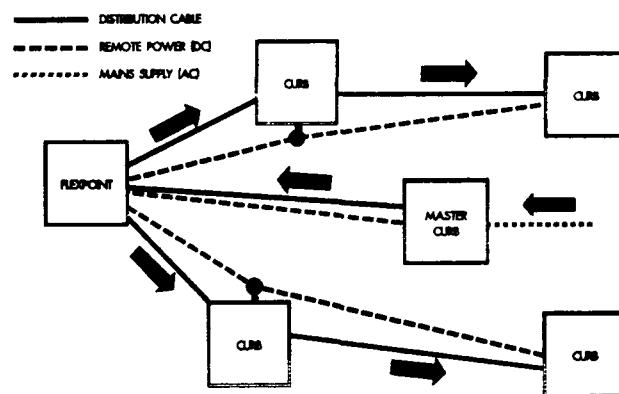


Fig. 4 Powering concept

Cable Plant.

The principal technical data for the networks of Table 1 are summarized in Tables 3 and 4.

	area 1 urban	area 2 resident.	area 3 rural
total lines:	3188	2051	4092
flexpoints:	7	2	3
FTTC-ONU (curbs):	55	2	89
FTTB-ONUs:	119	57	35
ONUs per flexpoint:	25	30	41
lines per FTTC-ONU:	24	12	36
lines per FTTB-ONU:	18	38	16

Table 3 Principal network characteristics: number of network modules (flexpoints, FTTC-ONUs (curbs), FTTB-ONUs) and their average utilization.

cable type	area 1	area 2	area 3
FO main & distrib. cables	58	17	124
FO drop cables	13	3	12
total fiber	655	204	1320
copper pairs	130	3	928
remote power feed cable	6	1	12
total FO/line	0.205	0.100	0.325
total copper/line	0.040	0.001	0.230
total power cable/line	0.002	0.001	0.003

Table 4 Total cable, fiber and copper pair lengths installed and ratios per subscriber line (in km).

The load of the flexpoints, and ONUs reflects the local structure of the area and is a measure for the efficiency of equipment sharing. Reviewing the equipment capacities, Table 2 shows, that the utilization degree for ONUs is above 60% and that of the flexpoints between 60 and 70%. A required reserve of 20% for future expansion has been included in these numbers.

In the flexpoints the sharing of some expensive components is greater by a factor of ten when compared to standard ONUs. This reduces the cost. Furthermore, FTTF permits a cost trade-off between the electronics and the cable plant. Table 4 summarizes the cable content of the networks.

Table 5 shows a comparison of the average distances between CO, distribution point and the ONUs close to the subscribers.

If we compare the fiber volume and copper-pair volume required per subscriber in Table 4 with the length of the cable plant, Table 5, it becomes obvious that the concept of cable and equipment sharing has reduced the installed cable lengths to a bare minimum with FTTF.

FTTF-Network Components.

The FITL installations on the subscriber premises for FTTB are illustrated in Figs. 5a and b. Installations for the curb area with FTTC are shown in Figs. 6a and b.

average length	area 1	area 2	area 3
CO to distrib. point main cable	1.320	1.435	1.710
flexpt. to FTTB-ONU distrib. cable	0.340	0.275	0.785
flexpt. to FTTC-ONU (curb) distrib. cable	0.460	0.325	0.790

Table 5: Average cable lengths in the three project areas (in km)

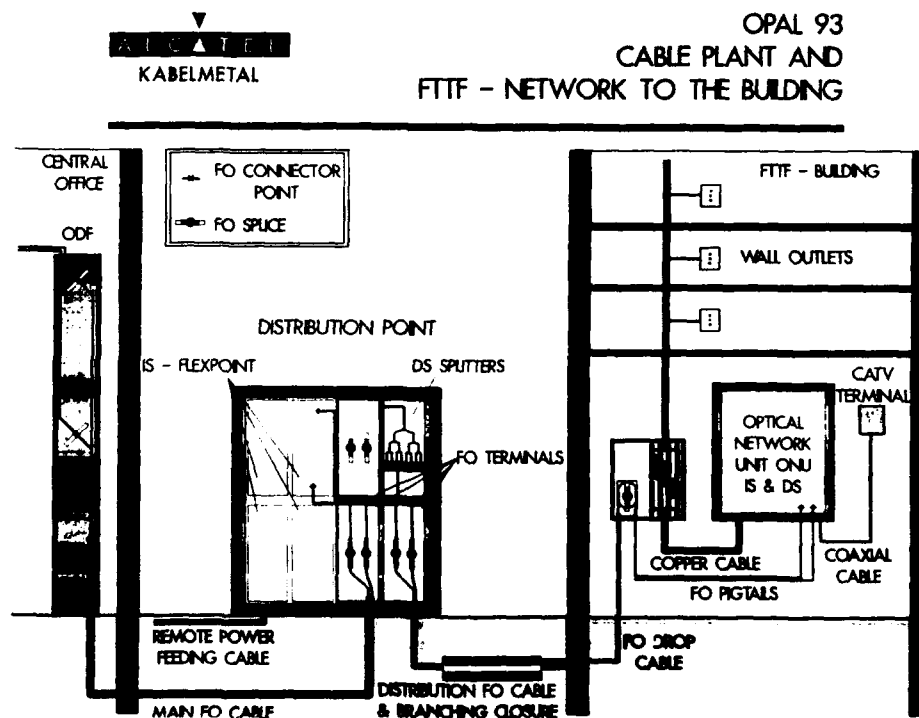


Fig. 5a Cable plant and active components for a FTTF-network to the building (FTTB)

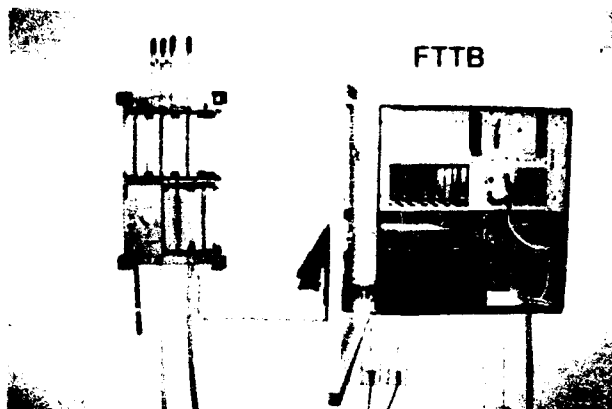


Fig. 5b Installation in the building: OF and copper inside, outside cable termination and FTTB-ONU.

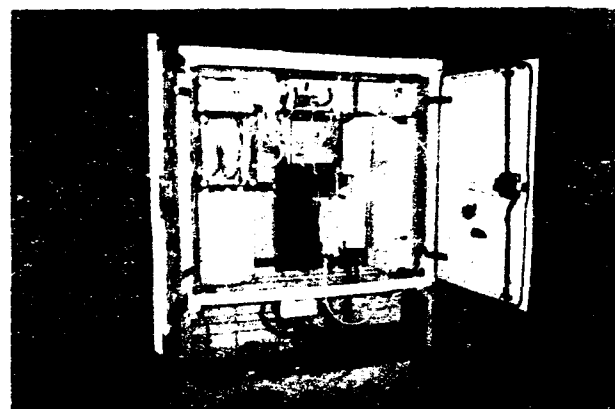


Fig. 6b Installation in a curb (FTTC-ONU) with power base for back-up power.

▼
ALCATEL
 KABELMETAL

OPAL 93 FTTF - NETWORK TO THE CURB

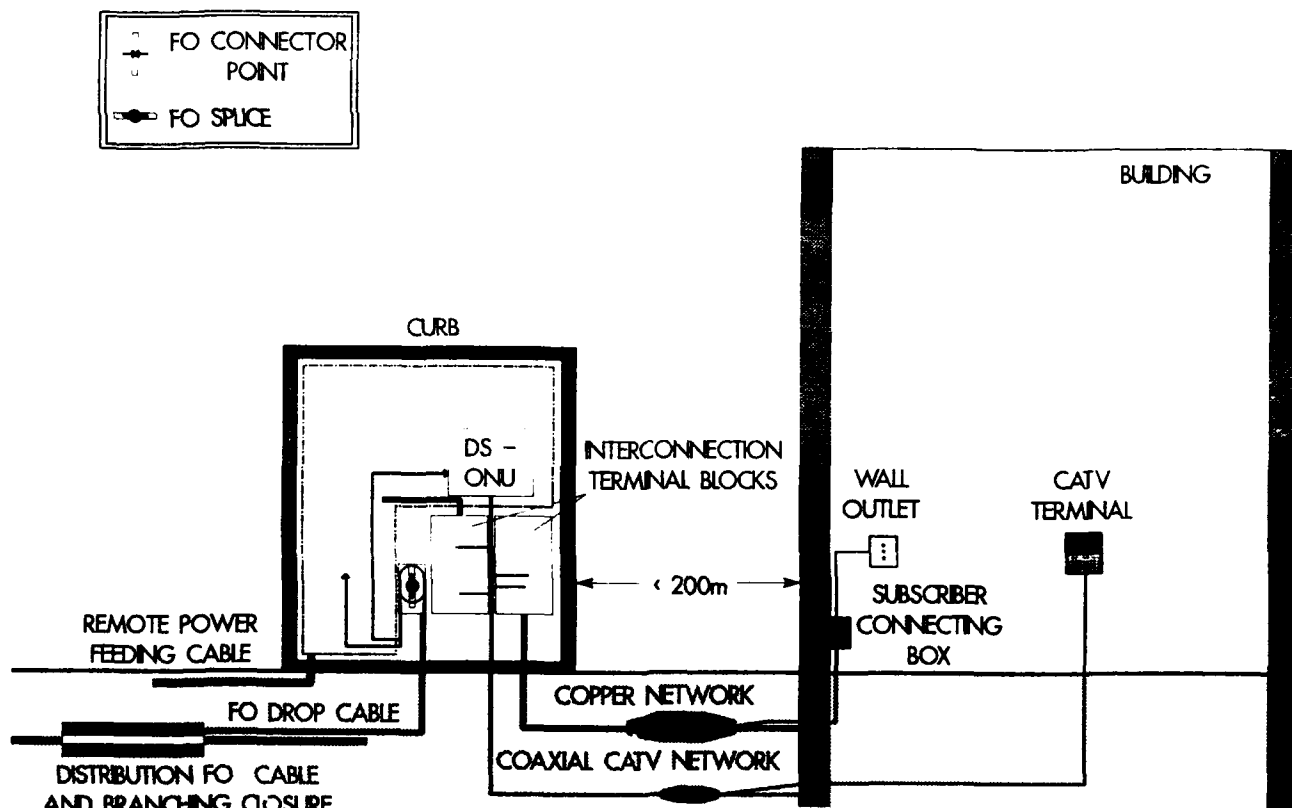


Fig. 6a Cable Plant and active components for FTTF-network to the curb (FTTC).

Cables. Main and distribution FO cables of stranded loose tube design range in fiber count from 20 to 100 fibers. Tubes with 10 fibers each form the base unit of these cables.

Drop cables with a fiber count of 4 to 10 fibers use tubes with 2 fibers. All cables are manufactured according to the specs of DBPT.

The distribution copper network in curb areas consists of conventional quad stranded cable with 0.4 mm PE-insulated conductors (#26 AWG) and up to 50 pairs. The TV distribution in curb areas employs conventional coaxial cables, type 1 nKx (2.2/8.3).

For FTTC/FTTB networks, stranded loose tube cables have proven to be a good choice. Ribbon cables will be advantageous only if much higher fiber counts are needed and if substantially more fiber needs to be spliced, such as in pure FTTN networks.

The modular arrangement of current standard cables is based on tubes with 10 or 2 fibers. Since ONUs will require 4 fibers each this is rather inflexible and leads to some dark or even superfluous fibers in the network. Cables based on tubes with 4 and 12 fibers will provide a better fit.

Main cables are laid in ducts and branched if more than one flexpoint or splitter point is to be served. Distribution cables are direct-buried. They feed several branching closures that are linked together alongside the cable route. Up to 4 drop cables with 4 or 6 fibers from each branching point serve one or two ONUs.

Power requirements for curbs and flexpoints at the customers' end will call for hybrid power/FO cables in the future. In curb areas, to avoid later civil works, it makes sense to supply copper pairs with dark fibers in a hybrid telecom copper/fiber cable now. These composite cables will become more important in future FITL applications.

Since the cable cost represents a small part (approximately 5%) of the total network cost, including the complete network transmission electronics, when compared to the civil works costs (approximately 35 %) and the labor-intensive installation, future cable plant optimization must focus on improving these relatively large cost elements.

Optical Splitters. The splitters are needed in the CO in conjunction with the optical amplifiers and in the distribution points of the DS network. Modules from biconically-tapered fused fiber couplers and integrated planar monolithic couplers have both been installed to compare their performance. Fused couplers developed and manufactured by us show very good loss performance. The integrated couplers have some appeal due to their wavelength-independent transmission properties. Pig-tailed splitter modules are arranged in a stack of modified splice trays. A maximum of 5 trays is required for a 32- port coupler module. These rugged modules can be accommodated in standard hardware and need no special handling. Starting in 1994 the use of integrated coupler modules will increase in installations calling for a high splitting ratio.

Cable splices. Standard thermoplastic closures are used for all FO cables. Future FO splices may also benefit from heat-shrinkable closures. Copper splices use standard heat-shrinkable and thermoplastic closures.

Fiber Optic Connectors. The operation of the DS analog transmission system with fiber optic amplifiers requires high return loss (> 50 dB) at the connectors and at the dead coupler output ports. A connector type was selected which is compatible with the already introduced DIN connector. Mated and unmated it exceeds the very high return loss specifications.

For future applications new connectors with improved material and processing costs are envisioned. Higher packing density and push-pull mating are useful features.

Distribution Frame. In the CO, standard type 7R fiber optic distribution frames, (ODF) accommodating up to 60 connectors, are used. Wherever possible, the PE-jacketed outdoor cables are terminated directly in the ODF. Alternately, the cables are terminated in a distribution closure, from where the ODF is connected through installation cables. Future connector technology should lead to improved distribution frames with higher packing densities.

Cabinets. Cabinets for distribution points (flexpoints and splitters) and curbs are identical and - when needed - equipped with an additional power base. The cabinet is the well-proven type KVz 83 MXs which is currently used for coaxial TV distribution in Germany.

Panel on Subscribers' Premises. On the subscribers' premises the cable is terminated inside of modified paneled cabinets. The terminating hardware provides for the interconnection between ONU and building wiring as well as for a termination point for the FO cable and connectorized pigtails. In curb-served areas the subscriber connection is built using conventional copper technology.

Cable Plant Costs.

Meaningful comparisons between copper and FO network costs require a well-defined common base.⁹ For our purposes the comparison takes only current services into account, that is: TV, POTS and ISDN. It does not include future potential services. Cost elements of the cable plant included in this review are: civil works, material, installation, documentation, startup, project management and, in addition for FITL: active equipment and training.

The total cost of the installed FITL cable plant, excluding the electronics, is affected by a few cost elements, of which the civil works portion by itself contributes 25 - 70 % to the total cost in the surveyed three regions. This is a very significant portion (Fig. 7).

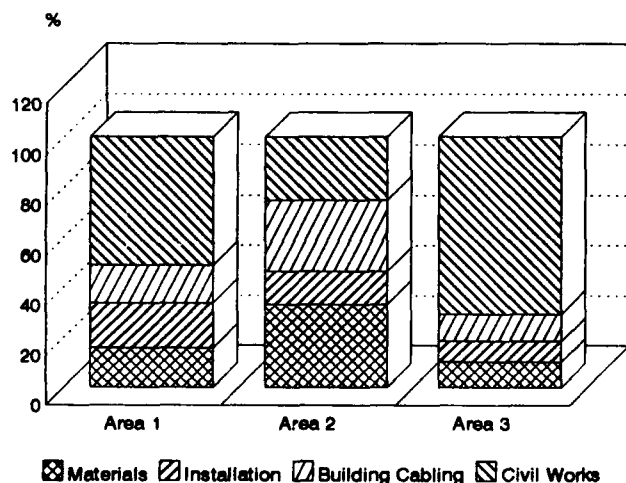


Fig. 7 Relative cost comparison in the three selected areas. Cost of cable plant (excluding electronics).

The large variations in the cost contributions between the three regions are reduced if civil works are excluded (Table 6). This emphasizes the key position of civil works for further cost planning.

	area 1	area 2	area 3
materials	32 %	44 %	35 %
installation	37 %	18 %	28 %
bldg. cabling	31 %	38 %	37 %

Table 6 Cost distribution in FITL networks in three selected regions, excluding civil works.

Network costs from urban, residential and rural settings were averaged to yield one figure for the average cost per subscriber.

Data for copper networks are taken from our projects within the Turnkey '91 - '93 program. These also served to build up the telecom infrastructure in comparable regions in the Eastern parts of Germany.

Table 7 compiles the cost of copper and FITL networks in Eastern Germany for 1993 (converted to U.S. \$ at the 1.7 DM = \$ 1.00 exchange rate). The important result is that FITL meets copper costs!

The larger cost variation for randomly chosen copper networks is influenced by the fact, that a) the optical networks were pre-selected for their suitability to optical conversion, b) the copper base comprises a more than tenfold larger number of subscribers and c) there is no trade-off possible between cable plant and electronics in copper networks.

Cost per connected dwelling unit (\$ US / unit)			
network:	min:	avg.:	max.:
copper	880 (50 %)	1690 (100 %)	2590 (150 %)
fiber optic	1680 (100 %)	1780 (105 %)	1920 (115 %)

Table 7 Cost of copper and FITL networks based on our FTTF concept in Eastern Germany in 1993.

Copper and FTTH - FITL networks are planned on a one customer-one line basis. This does not hold for any other FITL concept, including our FTTF. In addition, a critical success factor for cost in these concepts is the degree of equipment and fiber sharing.

Network line demand has to be matched with the capacities of network modules, such as cables, flex-points or ONUs. High modularity of cable plant and electronic components provide the flexibility for high utilization of the components. Thus, matching becomes more critical in FITL networks than in copper networks. Therefore, FITL networks currently require more precise engineering.

As shown, FITL networks can now compete with copper on a cost basis while, in addition, offering the supplementary benefits of FO networks:

- a) potential extension of the served area around the CO to approximately 20 km radius and more;
- b) higher capacity for IS;
- c) 2 Mbit/s leased lines;
- d) more DS channels, higher quality and larger range to be served without amplifiers in the field;
- e) better O&M features.

The positive results of our FTF concept encourages further introduction of modified AON electronics for even higher flexibility and extended range. These features are important, if FITL is placed into an environment with existing, still operating copper networks during the introductory phase of FITL. It will also enable introduction of FITL in widely dispersed residences, such as in rural settings.

Conclusions.

We have developed a new concept for a cost-optimized approach to FITL networks. Our concept provides for greater planning flexibility with a targeted equipment utilization of 80% which also reduces the cost for rural areas. All necessary equipment has been developed and the system is now installed in the field. These FITL networks can already today compete with copper on an installed network cost basis.

Several key factors were instrumental in the success of this project. Previous OPAL pilot projects resulted in initial concepts and pre-specification equipment. Mass production of the components and the need to restructure the telecommunications network of the re-united Germany made it possible for these components to be available today. The necessity to fit network technology closely not only to the regional, but also to local requirements (e. g. the size of city blocks) led to FTTB, FTTC and FTTF as network modules and to a concept that deviates from PON. In addition, an economical solution for powering of the network has been developed.

Finally, the increased demand of these FITL networks on engineering during the planning and execution phases has benefitted from our experience in several large-scale turnkey projects in Germany and overseas.

Further improvements can be achieved by introducing cables based on tubes with 4 and 12 fibers, by adopting the planar technology for couplers with a large number of gates, by a further expansion of the AON - FTF concept, by larger selection of ONU-capacities and by intelligent planning leading to a reduction of civil works.

Since we demonstrated that today's FTTF access network is already economical, further cost advantage over copper will result from larger areas to be served from one CO.

Acknowledgements.

The authors wish to express their gratitude to Mr. D. Stein and Mr. H. Hofheimer of Cable Consultants Corporation, Larchmont NY, for their comments and valuable assistance in the preparation of this paper. We also like to thank Dr. Chahabadi from KE Communications Elektronik, Hannover, for numerous stimulating discussions. Last but not least we like to thank our partners at Deutsche Bundespost Telekom for their close cooperation in this challenging project.

List of Acronyms used in this Paper.

AON	= Active Optical Network
CO	= Central Office
DBPT	= Deutsche Bundespost Telekom (German telecom carrier)
DS	= Distribution Service
FO	= Fiber Optic
FITL	= Fiber in the Loop
FTTB	= Fiber to the Building
FTTC	= Fiber to the Curb
FTTH	= Fiber to the Home
FTTF	= Fiber to the Flexpoint
Flexpoint	= Distribution Point with Active IS-Components
IS	= Interactive Service
ISDN	= Integrated Services Digital Network
LAN	= Local Area Network
ODF	= Optical Distribution Frame
O & M	= Operation and Management
OLU	= Optical Line Unit (in flexpoint)
ONU	= Optical Network Unit (in curb/building)
OPAL	= Optical Access Line
PABX	= Private Access Branch Exchange
PON	= Passive Optical Network
POTS	= Plain Old Telephone Service
OLT	= Optical Line Termination(in CO)

References.

1. "Fibre to the Home: Introduction of Optical Fibre in the Subscriber Loop"; Gerd Tenzer, R.v.Decker's Verlag. G. Schenck, Heidelberg; 1991

2. "Fiber in the Loop Architectures and Radio and Copper Access Technologies"; A. Tellado, J. Rueda; Conference Proceedings: Optimizing Fiber Optics, Cable and Radio in the Local Loop, IIR Seminar; London; January 28-29, 1993.

3. "Fiber to the Home - no more a Trial an Operational Reality!" J.P. Boinet, M. de Vecchis, J. De Vitry; Proceedings of International Symposium of Subscriber Loops and Services, Amsterdam, April 22 - 26, 1991, p 218.

4. "Bringing Fiber Optics to America: The Cable Television Experience"; Donald P. Dulchinos, Fiber and Integrated Optics, vol. 11, pp 177-188.

5. "Telekom answers a Call for 1.2 Million New Lines"; Optics & Laser Europe, May 93, pp 25-29

6. "Glasfasernetze im Teilnehmeranschlussbereich"; W. Weippert, W. Rosenau; in Telekommunikation, 9th supplement 1992; Franz Arnold (ed.), Deutscher Wirtschaftsdienst

7. "Optische Übertragungstechnik für Flächendeckende Teilnehmeranschlüsse" Teil 1-3; in: "Der Fernmeldeingenieur", Verlag für Wissenschaft und Leben, Georg Heidegger GmbH, Erlangen, Vol. 4, 5, 10; 1992 .See also: "Local Nets Drive Asian Fiber Market", T. Sweeney; Comm. Week Internatl.; July 19, 1993.

8. "Parametric Methodology for Analyzing Implementation Strategies of Residential Broadband Networks: The incremental cost of integrated access"; R. Diaz de la Iglesia, IEE Journal on Selected Areas in Communications, vol. 10, no. 9, Dec. 1992.



Hans Dominik
Kabelmetal Electro GmbH
P.O. Box 260
30002 Hannover
Germany

Hans Dominik received his electrical engineering degree from the Technical University Braunschweig in 1986 and his Ph.D. in 1991. He then joined the R & D department of Kabelmetal where he was in charge of several European development projects for passive optical components (RACE, ASSYSTO). Currently, as project manager for FITL he is responsible for Kabelmetal's part of the OPAL'93 Project.



Wolfgang Liese
Kabelmetal Electro GmbH
P.O. Box 260
30002 Hannover
Germany

Wolfgang Liese received his Ph.D. degree in physics from the University of Hannover in 1977. Thereafter he concentrated his activities to the commercialization of technology. From 1978 to 1991 he occupied technical positions in Canada, including head of the optics group at Seastar Optics, Sidney BC and manager of the fiber research group at Northern Telecom. Upon returning to Germany he joined Kabelmetal where he is manager of marketing in the Telecommunications Division.



Hans Schönfeld
Kabelmetal Electro GmbH
P.O. Box 260
30002 Hannover
Germany

Hans Schönfeld was born in 1941. After graduating from the Ohm Polytechnikum in Nürnberg he joined Kabelmetal in 1966, where he has been engaged in the field of telecommunications cables development and marketing. Currently he assumes the position of senior engineer for telecom cable plant installations. As member of the Alcatel Kabelmetal FITL team he is currently working on the OPAL'93 Project.



Wolfgang Wenski
Kabelmetal Electro GmbH
P.O. Box 260
30002 Hannover
Germany

Wolfgang Wenski received his electrical engineering degree from the University of Braunschweig in 1984. After developing electronic circuits for laser and LED modules he joined Kabelmetal in 1986. As a group leader he was responsible for the development of telecommunications cables and, especially, for fiber optic cables. In 1990-91 he was general manager of a cable plant before taking on management responsibilities in the domestic sales group for the public market. In this position he manages the FITL program and the OPAL'93 Project for Kabelmetal.

Wireless LANs Complement Wired LANs With Flexible, Mobile Network Solutions

Alex Alavi

Altair Product Operations
Wireless Data Group
Motorola, Inc.
Schaumburg, Illinois

Abstract

Wireless LANs are new, fast-growing technologies that complement or extend the capabilities of wired LANs. The two major forces driving the growth of wireless LANs are the increasing need for greater worker mobility and networking flexibility. Other reasons for installing wireless LANs include overcoming physical architectural impediments, temporary installations, and disaster recovery. Motorola produces wireless LANs that are uniquely based on the 18 GHz technology. Other transmission approaches include spread spectrum radio frequencies and infrared. Wireless LAN technology provides the wire and cable industry with a growing opportunity to better serve changing user needs.

Introduction

Wireless data communications is emerging as one of the most important strategic technologies of the 1990's. Virtually every major computer manufacturer is exploring ways to apply the capabilities and promise of this technology to their product lines in the hope of seizing a substantial user base. Recognizing the explosive growth of portable computers, which are largely responsible for wireless computing's potential, the computer industry is poised for the next wave of mobile computing. In the words of Motorola Chairman and CEO, George Fisher, the stage is set for "the wireless decade - where you'll have access to all the information you need any time, anywhere, in the palm of your hand."

The world is entering a new era of mass wireless data communications. One reason, in the U.S., is that the workforce is increasingly on the move. According to studies by *McLaughlin and*

Associates Inc., roughly 40 percent of workers - 48 million people - do part of their job away from the office. Their need to perform functions such as accessing information, sending electronic mail, and updating calendars has made portable computers the fastest-growing segment in the industry. According to Dataquest, the market for notebook computers alone will grow to six million units by 1994. Connected to a wireless modem, these notebook computers become powerful tools for receiving E-mail or accessing corporate information resources on the move.

Today, according to a *McLaughlin and Associates* studies, there are about 200,000 users of two-way wireless data systems. These studies forecasts explosive growth for this market with the number of users of one and two-way wireless data mushrooming to 20 to 26 million worldwide by the end of the decade. *BIS Strategic Decisions* expects the wireless data market to reach \$12 billion by 2000.

According to *BYTE Magazine*, within three years wireless data communications will be as commonplace as wired data communications are today. *The Yankee Group* is equally optimistic about the increased demand for untethered communications, stating that "the wireless data user market will quadruple over the next five years, driven by the demands of a new generation of mobile professionals and the availability of better tools for migrating current applications to the wireless/mobile environment. Hence, industry observers predict that sales of wireless LANs will grow from ten million dollars in 1990 to total revenues ranging from \$150 to \$600 million by 1995. These estimates vary widely, but all of them indicate that there will be significant growth in sales of wireless LANs in

coming years.

One of the major forces driving the growth of wireless LANs is the need for mobile workers to access information while on the move. Another significant force fueling this growth is the need for network flexibility to facilitate the concept of "LAN-on-demand" -- the ability to quickly and easily set up and relocate LANs to support emerging virtual workgroups. This paper examines these forces in more depth, discusses other factors spurring the development of wireless LANs, and analyzes important wireless LAN user issues.

Forces Driving Wireless LAN Growth

Workforce Mobility

Although the wireless data applications are at their early stage of development, the emergence of compact and portable computers such as laptop, notebook, palmtop, pen based, Personal Intelligent Communicators (PICs) and Personal Digital Assistants (PDAs), along with the wireless connectivity as the enabling technology, is giving rise to a new breed of wireless mobile applications. When wireless connectivity is added to portable computers, it offers executives and professionals a powerful tool to access information resources any time and anywhere.

Many leading PC manufacturers have announced plans to develop portable computers with a PCMCIA compatible card slot that enables memory and peripheral devices developed to this standard to be added to their computers. The PCMCIA (Personal Computer Memory Card International Association), is a group of over 300 companies who have developed standards for memory cards and peripherals such as modems and adapters for portable computers. Motorola and other vendors in concert with computer manufacturers are developing one-way and two-way PCMCIA wireless modem cards for use in both in-building and out-of-building applications.

It is estimated that more than 70 percent of the 11 million portable computers projected for the marketplace by 1996 will have slots for PCMCIA cards with wireless communications capabilities. These wireless enabled computers will be used for a wide range of mobile applications to optimize time spent out of office and increase workers' productivity. Many of these applications are now in the process of being developed and include:

- Sending and receiving E-mail and messages anywhere any time
- Groupware and informal meetings at which workgroups create, share and distribute results
- Distribution, retrieval and printing of files
- Accessing information and database services
- Sharing printers and other peripherals

Users of these wireless mobile applications include executives and managers in business and industry, and professionals such as consultants, accountants, lawyers, real estate brokers, financial planners, and hospital and medical personnel.

Handheld computers equipped with bar code readers and radio frequency data collection systems have also been deployed in businesses and industries such as retail, wholesale distribution, transportation, utilities, and manufacturing for several years. These devices are typically used in distribution centers and warehouses for receiving, shipping, just-in-time inventory control, and storage and retrieval of goods. They are also used for fleet management in the airline, car rental, trucking and railroad industries. These systems were initially designed to handle a single application and hence interfaced to a specific host computer over the radio network. In recent years, vendors targeting this market segment have developed new LAN-based products to enable the workers to access a broader range of information residing on servers and host computers connected to the LAN-based enterprise network.

Network Flexibility

Networking has become the centerpiece of information systems strategy as companies look for ways to become more competitive, improve productivity and increase efficiency to maximize return on investment. A recent *Gallop* interview of 250 executives from *Fortune 1000* companies indicated that networking is the most challenging issue facing these managers in the 90's.

In the last few years, LAN technologies and emerging WAN (Wide Area Network) technologies have become the most important part of enterprise networking strategies. The *Network World 500* study conducted in 1993 by IDC, based on interviews with 500 networking executives from some of the largest companies in the U.S., revealed that 95% of the respondents expected that LANs would be critical to enterprise networking strategies by 1996. Another study by the *Yankee Group* in 1992, called *Managing the Enterprise LAN*, reported that

companies in the *Fortune 1000* with annual revenues greater than \$1 billion planned to more than double their mean number of LANs by 1997, while firms with annual revenues of less than \$1 billion had the even more ambitious plan of tripling their LANs in the same time period.

Meanwhile, the number of business PCs installed worldwide will nearly double from 45 million in 1991 to 90 million in 1995, according to *IDC*. During this same time, the number of PCs connected to LANs will triple from 15 million to 45 million. In the U.S., *Network World 500* respondents estimated that in 1990 only 28.1% of their installed PCs were connected to LANs. By 1992, the percent of LAN-connected PCs increased to 63.2%, and by 1996 *Network World 500* managers expect that nearly 90% of PCs will connect to a LAN. These estimates of PC LAN connectivity are generally higher than overall industry averages, reflecting the leading-edge nature of these organizations. *IDC* estimates that by year end 1996 about 69% of business PCs in the U.S. will be network-connected, up from 28% in 1991.

Furthermore, the number of portable computers will nearly triple from about 4 million in 1993 to 11 million in 1996, according to *Dream IT*. *Dataquest* forecasts that 57 percent of the PCs shipped will be portable by 1995, with handheld and pen-based systems alone accounting for 31.7 percent of the market. Although portables will dominate the PC market in 1995 in terms of growth, they are not expected to dominate from the standpoint of LAN connectivity. *Dataquest* projects that only 43 percent of portable computers will be connected via a LAN by 1995, as opposed to 75% of the desktop and deskside installed base.

A recent *Yankee Group* research revealed the following facts about the state of traditional wired LANs:

- An average of three weeks is required to plan and execute a 30-node wired LAN move
- Over 70% of problems in twisted-pair LANs are attributable to the wiring before the implementation of hubs and structured wiring, 35% afterwards
- It costs \$500 or more per node to move an Ethernet Unshielded Twisted Pair (UTP) LAN – much higher in metropolitan areas with high labor rates and for fiber-based LANs

- More than 60 percent of the cost of moving a wired LAN is in the labor

As a result of these compelling reasons, industry experts project a significant growth for wireless LANs, ranging from \$150 to \$600 million within the next few years. This growth is primarily fueled by increasing demand for LAN connectivity and flexibility of wireless technology offering LAN-on-demand for easy and rapid installation, as well as relocation of the network. Another major factor contributing to this growth is the emerging mobile computing applications driven by portable computers and enabling wireless technology.

The *Yankee Group* recently polled more than 200 communications managers of Fortune 1000 corporations. Nearly half of the 102 respondents, which represented all major industries and ranged in annual revenues from \$500 million to more than \$10 billion, said they planned to implement wireless LANs over the next five years with 33 percent planning to install them within the next two years. One of the predominant reasons that the managers were making these wireless LAN plans was the costs of installations, moves, adds and changes associated with wired LANs.

Installations, moves, adds, changes

According to a study by *Frost and Sullivan*, \$5 billion of America's LAN budget of \$12.2 billion in 1990 was spent on installations, moves, adds and changes. Labor and material costs for installation of a LAN node can range from \$200 to \$1,000 for copper wire. Installation costs are even higher for coax and optical fiber.

Moves, adds and changes cost about \$500 or more per LAN node, according to the *Yankee Group*. These costs can rise substantially in metropolitan areas and based on building construction, insulation and age. Moreover, a study by *Forrester Research* found that 20 percent of firms have to trash half of all their horizontal wiring every three years due to moves, adds and changes. Some firms attempt to minimize this waste of wire by deploying structured distribution or wiring systems. But *Forrester* adds that this does not solve the problem because moves, adds and changes regularly wipe out the best-laid structured wiring plans.

Costs due to moves, adds and changes mount rapidly because of the great mobility of today's information workers. According to the *Yankee Group*, the average company moves 20% of its

employees annually; *KPMG Peat Marwick* places this percentage even higher at about 50 percent.

But these hard costs due to moves, adds and changes are not the end of the story. There are additional soft costs due to lost time. The Yankee Group points out that it requires an average of three weeks to plan and execute a 30-node LAN move. The group estimates that loss productivity resulting from 2% network down time, caused by changes to the network during moves and changes, is costing *Fortune 1000* companies about \$1,000 to \$1,500 per employee annually.

On the other hand, wireless LANs significantly reduce the high cost and lost time resulting from installations, moves, adds and changes associated with wired LANs. For instance, a few live examples of wireless applications include:

- The City of Mission Viejo, California installed a Motorola Altair® wireless LAN taking less than five minutes per node. According to Joe Potocny, information system specialist, the Altair system saved the city \$12,000 to \$14,000 of down time expenses in just two months.
- Germany's Deutsche Messe Gesellschaft AG took less than half an hour per floor to equip an eight-story building with an Altair wireless LAN system. A comparable wired LAN would have taken a week to a week-and-a-half to install per floor.
- John Brown Company, a large engineering firm, closed a remote Chicago suburban office on a Friday afternoon and moved to their downtown offices. Their Altair network was up and running on Monday morning at 8:00 am. The total effort to disassemble, move, and reinstall a thirty-five node Altair wireless network took about six hours.

Hard and soft costs due to installations and future moves, adds and changes are usually not considered in LAN acquisitions because they are either treated as routine monthly expenses or not even quantified. Yet these life cycle costs can often times exceed the costs of LAN acquisitions. As life cycle costing is increasingly used to determine the true costs of LANs, it is anticipated that wireless LANs will demonstrate paybacks justifying their installation in more and more applications.

Other Reasons For Wireless LANs

In addition to worker mobility and networking flexibility, there are a number of other reasons why wireless LANs are installed.

Physical Building Problems

Wireless LANs are particularly suitable to overcome physical building problems which make the installation of wired LANs uneconomical or even impractical. This may be the case, for example, in older or historic buildings which are not prewired or up to current building codes, or in those buildings with asbestos. In other cases, buildings may simply have run out of duct space or have full cable troughs. Physical building problems can be expected to become more and more prevalent as facilities that are adaptable to wired LANs are increasingly used up with continuing LAN growth.

Industrial Environment

The wireless LANs are ideal solutions for industrial and factory sites with high ceilings and concrete floors where cabling creates safety hazards and where the operations need more flexibility to respond to changes in the business conditions.

The Altair wireless LAN from Motorola is particularly suitable for factory applications since its 18 GHz frequency operates far above factory generated electromagnetic interference.

Temporary Installations

Wireless LANs are often used in temporary installations where permanent wiring would be time consuming and expensive. For example, wireless LANs can be used to support temporary work groups at a training session or exhibits at trade shows, conventions and other events. Wireless LANs can also be used on a temporary basis while wired LANs are being installed or changed, or wired LAN problems are being resolved. Other uses are in facilities with short-term leases or in dynamic organizations.

Disaster Recovery

Disaster recovery is another very important reason for using wireless LANs. One way to provide disaster recovery capabilities is to maintain on-site, redundant wireless LANs or bridges which can be quickly brought up in place of wired LANs to support mission-critical applications that cannot afford network downtime. Another way is to

speedily install wireless LANs at an off-site facility for relocated workgroups and organizations, in response to disasters that render wired LANs inoperative. The speed and flexibility with which wireless LANs can be implemented make them an ideal solution for disaster recovery applications.

Key Issues For Wireless LAN Technologies

Motorola is one of a number of manufacturers which have introduced wireless LAN technologies. Others include California Microwave, InfraLAN, NCR, O'Neill Communications, Photonics, Proxim, Telesystems and Windata. There are three major wireless LAN technologies: 18 GHz radio frequency used by the Motorola's Altair products, spread spectrum radio, and infrared light wave. Spread spectrum radio products use 902 to 928 MHz, 2.445 to 2.485 GHz and 5.725 to 5.85 GHz. The infrared based products operate at wavelengths of approximately 870 nanometers.

Following is a discussion of the key issues and typical user concerns related to wireless LAN technologies.

Performance

Performance is one of the key criteria in purchase decision for wireless LANs. Although there are many business applications that can sustain low speeds, the multi-platform nature of LAN applications demand throughputs comparable to traditional wired LANs. This is particularly important to maintain transparency among a multitude of network applications regardless of the medium. The *Yankee Group's* recent study revealed that almost 90% of the respondents believe that wireless LANs need to perform at the traditional LAN speeds of more than 2.0 Mbps.

The Altair Plus II wireless LAN from Motorola provides maximum throughput of 5.7 Mbps per microcell through the unique use of the 18-GHz microwave portion of the electromagnetic spectrum. Each microcell can use any one of ten potential frequencies in the U.S. and six to 20 frequencies in other countries.

By deploying multiple microcells operating at non-overlapping frequencies (figure 1), network managers can increase the performance of an Altair wireless network in increments of 5.7 Mbps per microcell, and build virtually unlimited coverage area without sacrificing performance. Although the

signals at 18 GHz easily pass through drywall and other types of office separators, they drop off sharply beyond the coverage area due to the low power (25 mW nominal peak) used by the Altair modules. This makes it possible to reuse frequencies and serve an unlimited number of devices simply by installing additional microcells in other coverage areas.

Most spread spectrum wireless LANs provide a maximum throughput of only 1 Mbps or less. Exceptions are NCR WaveLAN which specifies 2 Mbps and Windata which reports throughput of 5.7 Mbps. Spread spectrum technology typically employs either direct-sequencing or frequency-hopping communications methods. Frequencies can be reused outside of coverage areas to support additional devices. However, performance within coverage areas, which range from 200 to 800 ft., is limited to the throughputs mentioned above, regardless of which communications method is used. This is primarily due to the modulation technique used to make radio communications more secure. In spread spectrum, the radio signals are typically spread over the entire available frequency to reduce potential interference and make unauthorized access more difficult.

As a result, spread spectrum technology may be more appropriate for peer-to-peer applications involving portable devices, low-density applications, or in warehousing and retail applications that may use low-speed terminals spread over a large area.

Infrared products employ diffused or line-of-sight transmission methods. The diffused method of transmission allows transmitters and receivers to aim at a common point, usually the ceiling in a room, for communication. Products based on this method are being added to some portable computers for peer-to-peer applications at 230 Kbps or less. Products using line-of-sight transmission are capable of delivering higher speeds. In this method, a cluster of nearby terminals, usually less than eight, are wired to an Infrared transceiver which sends and receives data in the form of an infrared beam to and from another transceiver which supports a few more terminals. The distance between these transceivers is typically limited to 80 feet. Additional workgroup or terminals must be wired to these networks making this approach limited to smaller groups.

Reliability

Wireless LANs, by definition, substantially reduce the LAN cable and provide fewer connections to the backbone. This in turn can contribute to lower

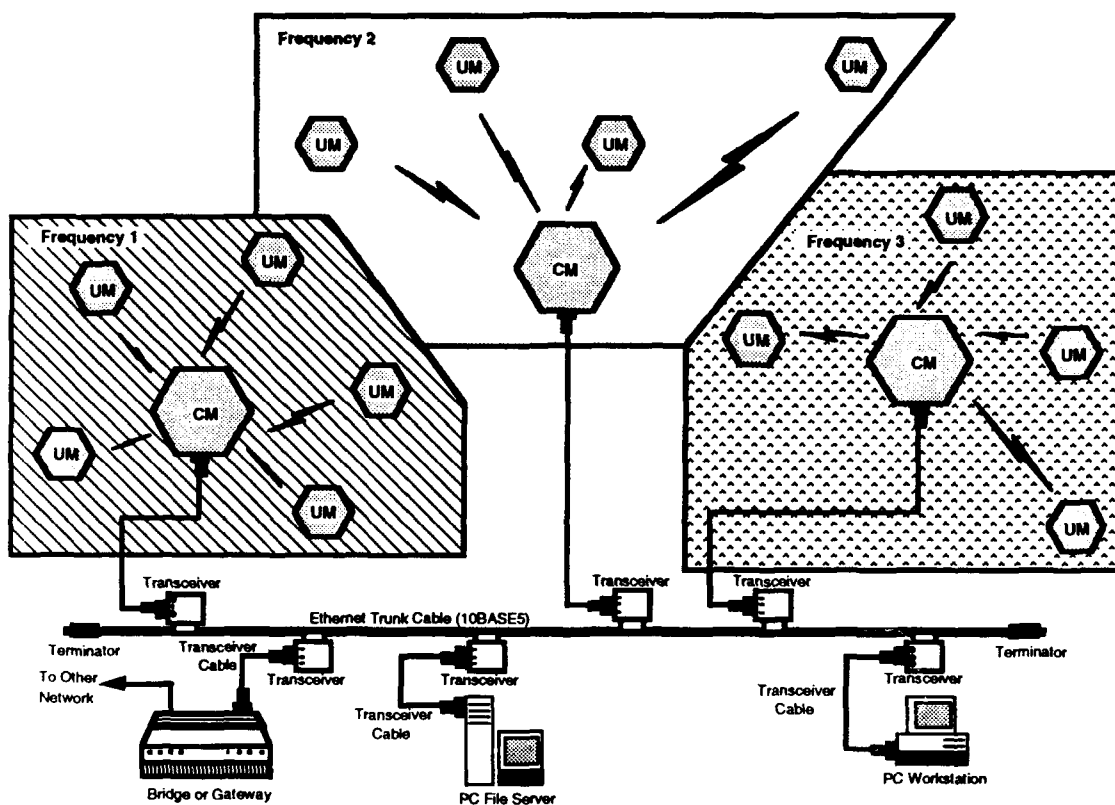


Figure 1: Multiple Microcell Deployment

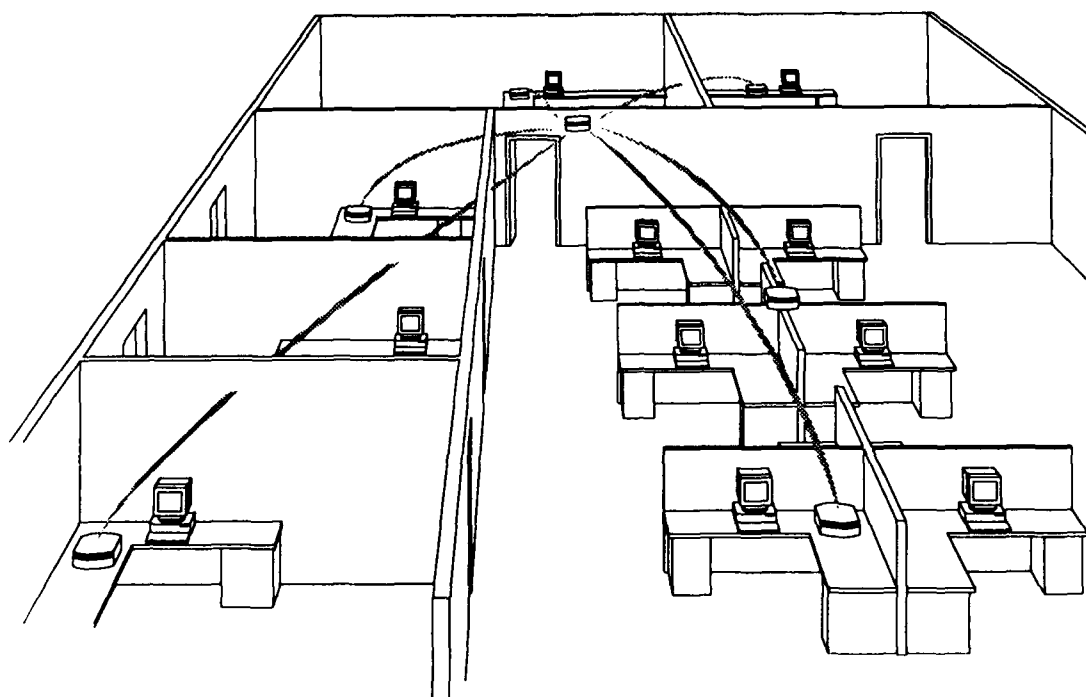


Figure 2: Typical Microcell Configuration

network failure and offer higher availability. As depicted in figure 2, the Altair wireless LAN, for example, has only one point of contact with the backbone for up to 50 users per microcell or workgroup, versus multiple connections for a wired LAN with a bus topology. According to a study by the *Yankee Group*, more than 70 percent of the problems in twisted-pair LANs are attributable to wiring before the implementation of hubs and structured wiring and 35 percent after the implementation.

Interference-Free Communications

There are two primary causes of interference for wireless networks. The first is other radio devices operating on the same frequency or frequencies. The other is electromagnetic noise generated by such things as motors and equipment used in manufacturing environments.

The FCC allocated bandwidth at 18 GHz in 1990 specifically for low power wireless LANs. The Altair Plus II wireless LAN uses the 18 GHz portion of the electromagnetic spectrum which is licensed by the FCC. Users don't need to deal directly with the government or wait for government approval to install a wireless LAN since Motorola has acquired licenses throughout the U.S. Altair products are shipped and delivered ready for immediate installation typically in less than a week. Most importantly, FCC licensing provides users with a legal right to interference-free wireless LAN communications. This unique characteristic of the 18 GHz makes Altair systems ideal for achieving interference-free communications in factory applications where machine-generated noise can reach 4 GHz.

Spread spectrum wireless LANs provide reliable communications as long as there are no other licensed radio frequency products or spread spectrum systems that operate within their coverage area and in the same frequency range.

Infrared technology is not susceptible to electromagnetic interference, and hence, if installed properly, it will deliver interference free communications.

Security

The Altair products provide several levels of security. Operation at 18 GHz eliminates susceptibility to monitoring by conventional radio receivers and scanners which operate around 2 GHz

and below. Racks of very expensive equipment, and a large conspicuous dish antenna would probably be required. The Altair products employ an intelligent six sector antenna to deal with the multipath aspects of the radio waves. This antenna system consists of six 60-degree directional antennas and related circuitry used for both data transmission and reception. As a result, there are up to 36 possible antenna and data path combinations that can be used by transmitting and receiving modules at any one time. During normal operation, the system automatically scans through all of the potential paths dozens of times per second, to identify which combination provides the best signal in terms of quality and strength.

Because of this dynamic antenna selection scheme unique to the Altair products, only bits and pieces of the entire data transmission would likely be received at any given location. The system can continually change transmission paths, making it necessary to change positions several times per second to intercept a complete data transmission. Furthermore, any bits and pieces that are intercepted would be meaningless because the data is scrambled within a unique frame structure. In addition, restrictions may be programmed into Control Modules to limit access to selected User Modules and their connected devices.

An inherent limitation of Infrared systems is that the signals are normally confined to a room. This limitation is an advantage for applications that require a high level of security. The spread spectrum technology enables vendors to develop products with a high level of immunity to eavesdropping. While commercially available encryption software can be used over the Altair network, some vendors of spread spectrum products offer encryption as an option.

Ease of Installation and Use

Most wireless LANs are relatively easy to install and configure. Systems with built-in PC boards provide an additional advantage by eliminating the need for external module or docking station. However, this approach limits users to a specific platform and requires that additional software drivers be installed in the host machine to support various operating systems and protocols.

The Altair system is designed to be "plug-and-play". The User Module connects directly to the Ethernet port of one to eight PCs, workstations and peripherals, using Ethernet cabling or twisted pair,

eliminating the need for user programming to install or move modules to new locations. The Control Module connects directly to an Ethernet port of a server or the network backbone.

Compatibility

The LAN environment typically consists of multi-protocol and multi-vendor products that must be supported by wireless systems. Altair Plus II and Altair VistaPoint™ wireless networking products are fully compatible with the IEEE 802.3 standard Ethernet-connected devices. This means that protocols or network operating systems that run over Ethernet can also run over Altair, including protocols such as TCP/IP and network operating systems such as Novell Netware, Microsoft LAN Manager and Banyan VINES. In addition, Altair directly supports multiple LAN cabling schemes such as 10BASE2, 10BASE5 and 10BASE-T.

Standards

The IEEE is currently working on the development of standards for wireless LANs through its 802.11 Standards Committee. The preliminary specifications are reportedly scheduled for release later this year. When these standards eventually become final, they will help to further spur the growth of wireless LANs.

These standards are critical to the success of mobile applications where portable computers with wireless connectivity from different vendors may be used for peer-to-peer and ad hoc communications. On the other hand, Ethernet is the predominant standard for wired LAN communications. So, for those applications where wireless LANs are used to complement or extend wired LANs, the wireless systems must comply with the wired standards as they establish the common denominator for communications and interoperability among wire and wireless systems.

Safety

Extensive research over the last 40 years shows that the low-power electromagnetic energy to which users of the Altair Plus II wireless LAN are exposed is far below exposure levels specified as safe by the Institute of Electrical and Electronics Engineers (IEEE) and the American National Standards Institute (ANSI). The basis of the current standard of the IEEE, which was subsequently adopted by ANSI, was established after evaluating more than 10,000 studies, articles and reports over seven years of work by more than 100 scientists,

physicians, and engineers from academia and government agencies, as well as 12 scientists from industry. The IEEE/ANSI safety standard specifies a power density limit in the 18 GHz band of 10 mW/cm². The nominal average power density of Altair Plus II wireless LAN modules is less than 0.002 mW/cm² or 5,000 times less than the limit established by the IEEE/ANSI safety standard.

Network Management

It is critical for wireless LANs to be managed in the same way as wired LANs to assure reliable operations. All Altair Plus II modules, for example, are equipped with Simple Network Management Protocol (SNMP) standard MIB II agent software. The modules also include MIB extensions which make it possible to monitor and control the Altair wireless network, as well as wired LANs using a single management station.

Wireless Bridges

Several vendors offer wireless bridges for interconnecting LANs. Altair VistaPoint, for example, provides a high-speed reliable system for interconnecting Ethernet LANs between and within buildings at distances up to 3,900 ft. (1.2 km) in the U.S. and 6,900 ft. (2.1 km) in most other countries. Based on Altair wireless LAN technology, the Altair VistaPoint system consists of a Main and a Remote Module which communicate with each other via line-of-sight at a maximum throughput of 5.3 Mbps using secure, interference-free 18 GHz licensed frequencies. The Altair VistaPoint system is designed for quick and easy installation. The system provides a cost-effective way to:

- Interconnect LANs between buildings separated by rights-of-way such as highways and railroads or natural obstacles such as rivers
- Avoid the costs and delays of digging trenches and installing cables
- Establish a back-up link in case of disaster
- Tie LANs on separate floors together in a leased building
- Eliminate recurring monthly charges associated with telephone facilities or the delays involved in obtaining licenses for conventional microwave communications

Conclusion

While wire remains the dominant medium for LAN connectivity, wireless LANs are emerging as an integral part of the information systems networking strategy. They are being deployed in a broad range of applications from tactical to strategic. This is primarily being fueled by the growing demand for LAN connectivity, diversity of applications and architectural environments, and the growing user demand for greater workforce mobility and networking flexibility.

For instance, wireless LANs and bridges are being deployed in many companies as a redundant connectivity solution, or for rapid relocation of workforces and networks for disaster recovery. They are also being deployed in industrial and manufacturing plants to automate operations and integrate isolated islands of machinery and resources with corporate information resources to implement "Just-In-Time" operations, and hence improve productivity and efficiency. Wireless LANs are also offering significant flexibility to dynamic organizations that need greater worker and mission mobility. In addition, intelligent buildings are being planned with wireless connectivity in mind.

Wireless LANs today complement and extend the capabilities of wired networks to offer optimum networking flexibility to users in networking. The wire and cable industry is in a position to benefit from this technology, as it has from the propagation of other technologies, to expand its services and better serve changing customer requirements.

###

Motorola, Altair, Altair Plus II and Altair VistaPoint are trademarks of Motorola, Inc.



Alex Alavi is responsible for directing worldwide product and marketing plans, market research, as well as public relations and advertising for the Altair wireless in-building network products.

Prior to joining Motorola, Alavi held positions in product development, marketing, and management of voice and data communication products. He was a product manager for Central Office and PABX systems at GTE Communication Systems Corporation, and a senior marketing manager at Itron, a mobile computer equipment manufacturer.

Alavi earned a B.S. in Electrical Engineering from Marquette University in Milwaukee, Wisconsin.

Characteristics of Carbon-Coated Optical Fibers and Structural Analysis of the Carbon Film

Haruhiko AIKAWA, Motonori NAKAMURA, Hiroki ISHIKAWA,
Isamu FUJITA and Toshio DANZUKA

Sumitomo Electric Industries, Ltd.
1, Taya-cho, Sakae-ku, Yokohama 244, Japan

1. ABSTRACT

In order to study the hermetic characteristics of carbon-coated optical fibers, several types of experimental carbon-coated fibers were manufactured and their hermeticity against hydrogen were investigated. Their characteristic constants with hydrogen permeation in the carbon layer were obtained by using accelerated hydrogen testing methods. Using the experimental results, hydrogen-induced loss increases were predicted after a long-term. To investigate the causes of different characteristics against hydrogen, structural analyses were performed by using SEM, AFM and AES. As a result, variations regarding the surface morphology and the chemical state were observed.

2. Introduction

The appearance of hermetically coated optical fibers have enabled silica-based optical fibers to greatly improve their long-term reliability. It is known that the adsorption of moisture onto the surface of the silica glass promotes mechanical fatigue of the glass and that the entrance of hydrogen into the fiber core region increases the transmission loss. Since the hermetic coating layer on an optical fiber can effectively prevent the diffusion of water and hydrogen to glass, it gives silica optical fibers the ability to withstand severe environments such as at the bottom of the sea. Hermetic coating films consist of metals, ceramics, carbon or similar materials, and are coated onto the surface of glass fibers. Of the sheathed fibers, carbon-coated optical fibers have been widely noticed and studied mainly because they have significant advantages, such as excellent hermeticity,

high failure strength and relatively simplified manufacturing methods.^{1),2),3)} Carbon-coated optical fibers, which have excellent hermeticity, can prevent strength degradation caused by the presence of H₂O on the fiber surface and can also prevent loss increases caused by hydrogen diffusion into the fiber. The study of the hydrogen permeability in the carbon coating film is important when discussing the coating's hermeticity, primarily because the size of a H₂ molecule is smaller than that of a H₂O molecule. The property of hermetic coatings is expected to be dependent on the coating materials and the structure of the coating film. Thus, it is important to pay attention to the actual structure of the carbon film.

In this study, we manufactured several carbon-coated optical fibers which have varying characteristics regarding hydrogen resistance, and studied the hydrogen permeability with each of them. Additionally, we analyzed microstructure of the coating layer which would cause characteristic differences. In this paper, we describe the details of these experimental results.

3. Experimental

Germanium-doped silica core single mode fibers were used in this study. They were coated with a thin film of pyrolytic carbon by the chemical vapor deposition (CVD) method during the drawing process. Figure 1 shows a schematic diagram of the carbon coating equipment. The reactor for coating the carbon is situated beneath the drawing furnace, and the raw material gas such as hydrocarbon is introduced here. The silica fiber which is heated in the furnace and drawn to a diameter of 125 μ m is then

immediately fed into the reactor and coated with a carbon film measuring approximately 0.03 to 0.05 μm in thickness. Following that, the fiber is also coated with a UV-cured acrylate resin, obtaining a finished diameter of 250 μm . A typical cross-sectional view of a carbon-coated fiber is shown in Figure 2.

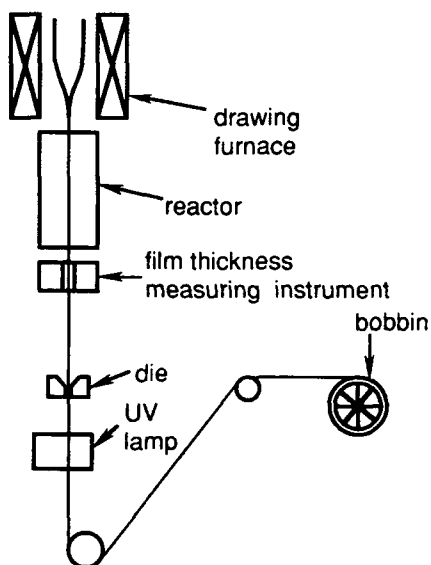


Fig. 1 Optical fiber carbon coating equipment

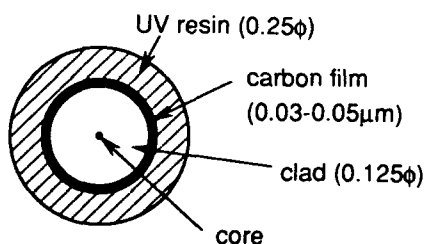


Fig.2 Typical structure of a carbon-coated optical fiber

By alternating the manufacturing conditions, four kinds of carbon-coated optical fibers(A, B, C and D) were obtained. In order to investigate their hydrogen permeability, accelerated

hydrogen testing methods were utilized. The tests were performed using hydrogen at a pressure of 10atm. The test temperature was alternated between 100 $^{\circ}\text{C}$ and 140 $^{\circ}\text{C}$. After the hydrogen treatment, attenuation spectra and absorption losses at 1.24 μm caused by hydrogen molecules were measured.

Additionally, we attempted to observe and analyze the structure of the carbon film using SEM(Scanning Electron Microscope), AFM(Atomic Force Microscope) and AES(Auger Electron Spectroscopy).

4. Results and Discussion

4-1. Hydrogen Permeability in the Carbon Layer

Table 1 shows loss increases at 1.24 μm after hydrogen treatment ($\Delta\alpha_{1.24}$) which was performed using a hydrogen partial pressure of 10atm and a temperature of 100 $^{\circ}\text{C}$ for 50 hours with fibers A, B, C and D. These results are expressed as values divided by saturated loss increases($\Delta\alpha_{\infty}$). Fiber D exhibited an excellent stability against hydrogen diffusion, while fiber A had minimal hydrogen resistance. However, the fatigue parameter(n-value) which was obtained by the dynamic fatigue tests was more than 100 in all of the fibers.

To investigate and compare the fibers' properties in more detail, we tried to predict the long-term loss increases at 1.24 μm with fiber B,C and D. If an optical fiber is exposed to hydrogen using a hydrogen partial pressure of P_{H_2} [atm], a temperature of T [K] and a time of t [hours], the loss increases ($\Delta\alpha_{1.24}$) can be expressed by equation(1), as described by Lemaire et al.^{4),5)}

$$\Delta\alpha_{1.24}(t,T) = \left[1 - \exp\left\{ -\frac{t - \tau_i}{\tau_f} \right\} \right] \cdot \Delta\alpha_{\infty}(T) \cdot P_{H_2}$$

$$\frac{\Delta\alpha_{1.24}(t,T)}{\Delta\alpha_{\infty}(T) \cdot P_{H_2}} \cong \frac{1}{\tau_f} \quad \dots \quad (1)$$

Table 1 Loss increases at 1.24 μm after hydrogen treatment

	Fiber A	Fiber B	Fiber C	Fiber D
$\Delta\alpha_{1.24}/(\Delta\alpha_{\infty} \cdot P_{H_2})^{*1}$	1	3.4×10^{-2}	3.1×10^{-3}	6.3×10^{-4}
n-value ^{*2}	>100			

* 1 After H₂ 100%, 10atm, 100 $^{\circ}\text{C}$, 50hrs treatment

* 2 Obtained by dynamic fatigue tests

where τ_f is the characteristics time constant and τ_i is the lag-time. τ_f is a function of temperature and given by equation(2).

$$\tau_f = A \cdot \exp\left(\frac{\Delta E}{RT}\right) \quad \dots \quad (2)$$

where ΔE is an activation energy, A is a frequency factor and R is the gas constant.

We applied this model to our carbon-coated fibers. The dependence of loss increases at $1.24\mu\text{m}$ upon time and temperature was investigated to obtain the characteristic constants with each of fibers B, C and D.

Figure 3 shows the loss increases at $1.24\mu\text{m}$ for each fiber after hydrogen treatment. The horizontal axis represents the elapsed time while the vertical axis represents the left side of the equation(1). Figure 4 shows the Arrhenius plots of τ_f which was calculated from a reciprocal of the slope shown in Figure 3. By calculating A and ΔE in eq.(2) from these results, we can estimate the hydrogen loss increases at various temperatures and time periods. Table 2 shows the characteristic constants of each fiber. The fibers, which exhibited strong resistance to hydrogen permeation, tended to have a high activation energy. The prediction of loss increases at $1.24\mu\text{m}$ after 20 years in the various conditions for fibers C

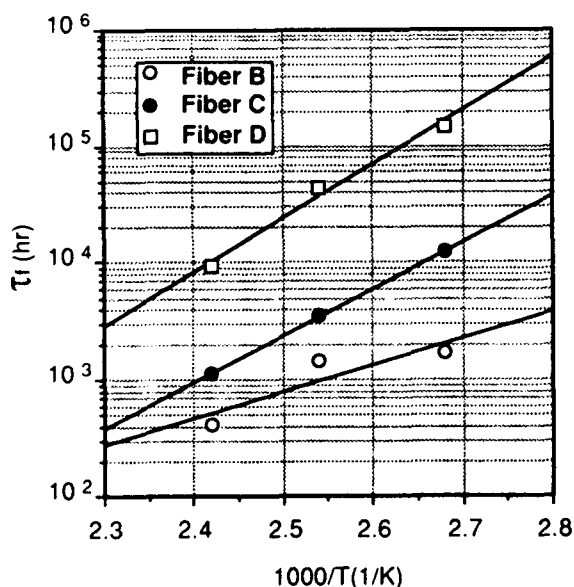


Fig.4 Permeation time constants for hydrogen in carbon against inverse temperature

and D are shown in Figure 5. If the fibers are exposed to hydrogen of 1atm at 10°C for 20 years, $\Delta\alpha_{1.24}$ of fiber C and D are estimated to be 0.065dB/km and 0.0015dB/km, respectively.

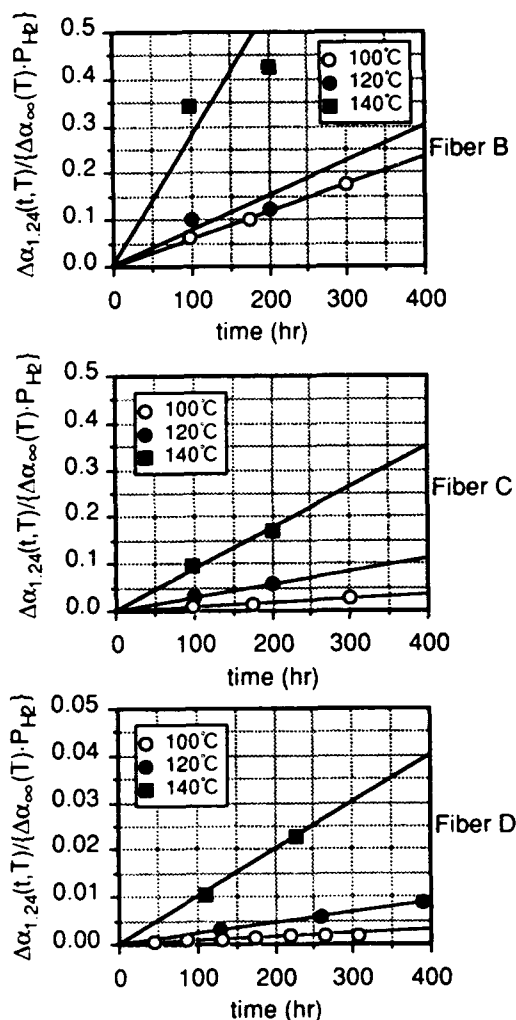


Fig.3 Hydrogen peak height at $1.24\mu\text{m}$ divided by equilibrium value against time

Table 2 Characteristic constants for prepared carbon-coated fibers

	Fiber B	Fiber C	Fiber D
ΔE (kcal/mol)	10.5	18.3	21.1
A (hrs)	1.4×10^{-3}	2.4×10^{-7}	7.4×10^{-8}

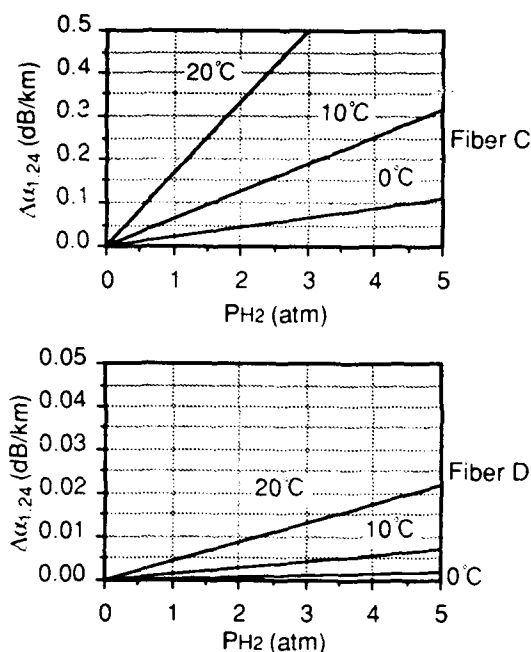


Fig.5 Estimation of hydrogen loss increases at 1.24 μ m after 20years

4-2. Structural analysis of the carbon film

When discussing the reliability of carbon-coated fibers, it is important to clear what differences in such characteristics depend on. Since the hydrogen permeability is expected to be greatly dependent on the coating's thickness, the carbon film thickness was first examined by SEM.

Figure 6 shows the SEM images of the cross-section for fibers B and D. However, no variations were observed regarding the film thickness. Thus, the hydrogen diffusion in the carbon layer would be controlled by the structure of the carbon film itself. Thereupon, we tried analyzing the microstructure of the carbon layer.

The surface of the carbon layer was so smooth that variations in the surface morphology could not be discovered by SEM observations. We then attempted to observe the surfaces using AFM. Figure 7 shows the AFM images of the carbon surfaces. The observation area selected was 500nm square.

The surface of fiber A, which had no hydrogen hermeticity, exhibited a steep and rugged morphology. In comparison with this, the surface of fiber C was flatter and smoother. The average height and size of the roughness estimated by AFM are shown in Table 3.

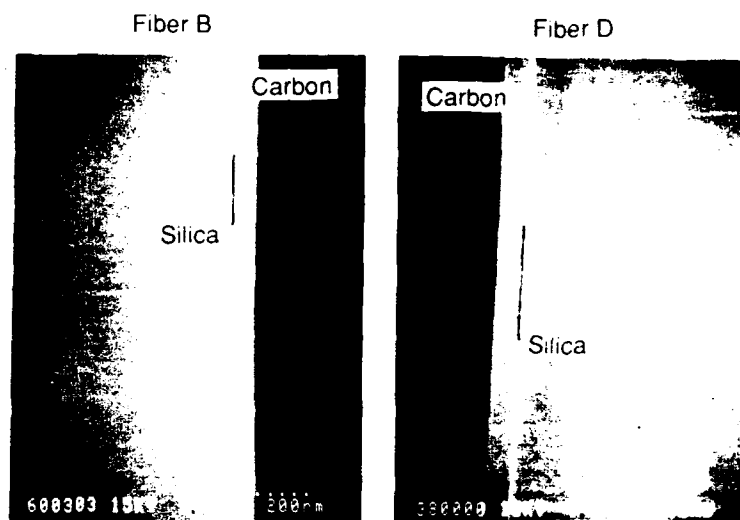


Fig.6 SEM cross-sectional photographs of carbon-coated fibers

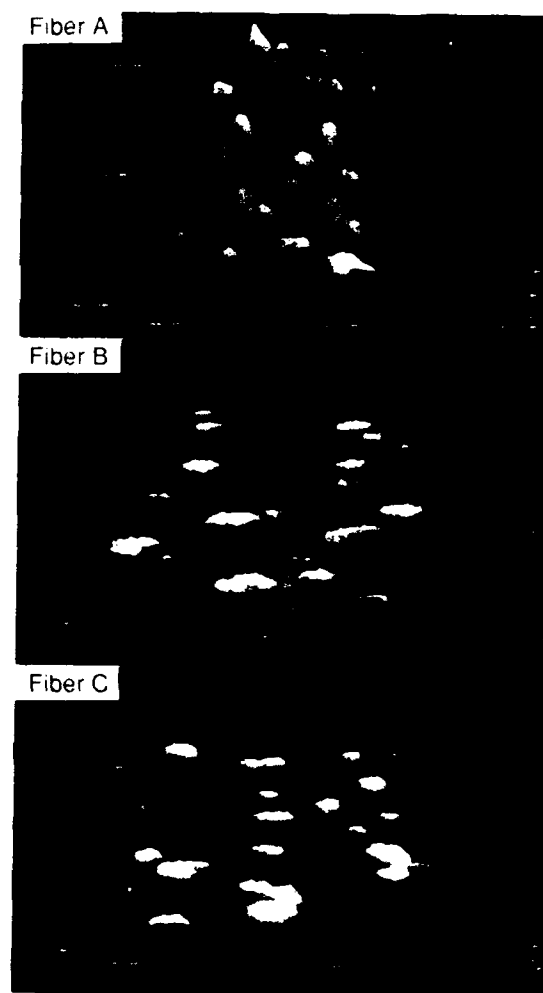


Fig.7 AFM images of the carbon surface

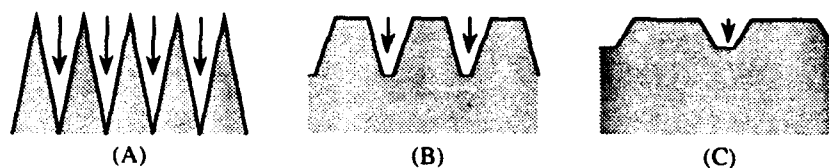


Fig.8 Schematic diagram of a model explaining H₂ permeating

Table 3 The average size of the roughness obtained by AFM observations

	Fiber A	Fiber B	Fiber C
Height	~5nm	~3nm	~2nm
Diameter	~50nm	~80nm	~100nm

The results could be explained in the following. We show a schematic diagram of a model to explain H₂ permeation in figure 8. Concerning diffusion in solids, the boundary diffusion rate is generally higher than the volume diffusion rate. Therefore, if the boundary area is large, hydrogen diffusion will be induced because of diffusion channel increases. And it is expected that molecules will easily diffuse when a lot of valleys between grains constructing the structure of a coating layer are deep. Accordingly, it can be thought that if the surfaces are rough such as fiber A, hydrogen can easily diffuse in the direction of the film thickness, but the smooth surfaces such as fiber C, are hard to permeate. However, a great deal more information regarding inner morphology is furthermore needed to conclude these views.

Then we studied the inner structure of the carbon layer. In the AES analysis, the chemical state of carbon film was investigated in the direction of the film thickness.

The detected intensity profiles of C(carbon) and Si(silicon) for fibers B and C are shown in Figure 9. The horizontal axis represents the value corresponding to a distance from the surface. In comparison with both figures, minor variation can be observed regarding a composition change near the interface. It can be observed that the composition near the interface of fiber C gradually changes as compared with that of fiber B. This result could suggest that fiber B had a relatively clear interface and fiber C had a boundary layer formed by interdiffusion between the carbon and silica layer. Thereupon, we investigated the state of a carbon-atomic kinetic energy both at the surface and the interface. Figure 10

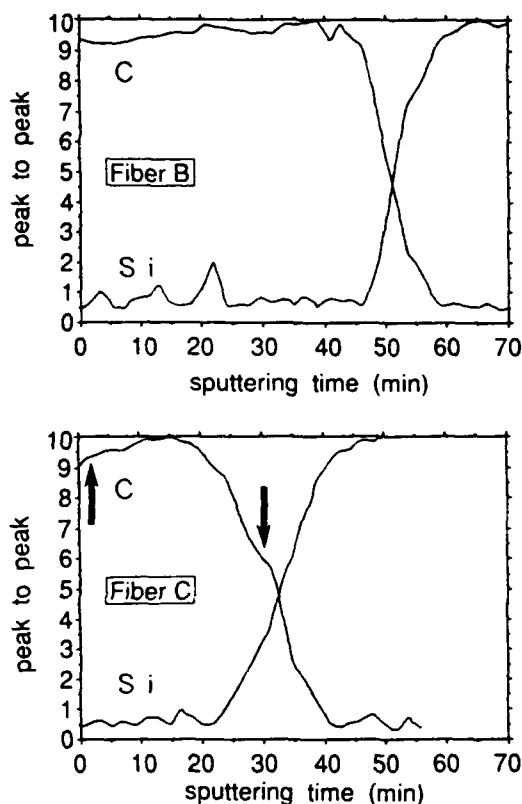


Fig.9 Peak intensity distribution of carbon and silicon in the direction of the thickness of the carbon layer by AES

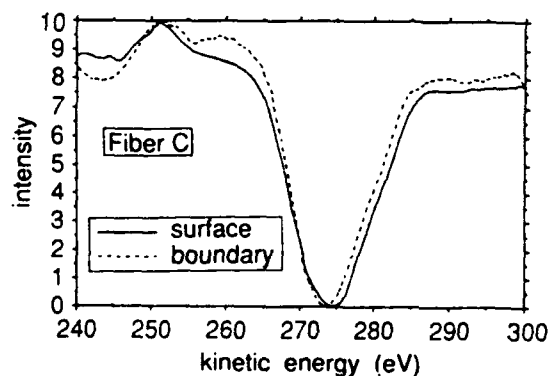


Fig.10 AES spectra of the carbon layer of Fiber C

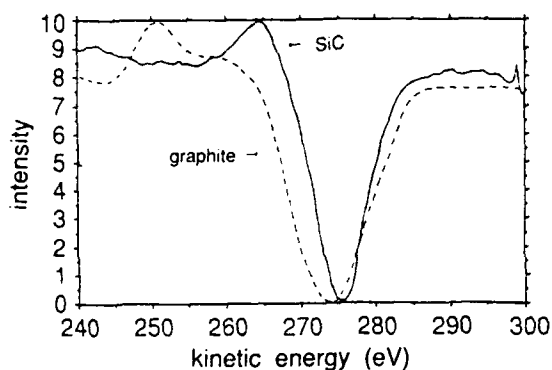


Fig.11 AES spectra of standard samples (C,SiC)

shows the AES spectra for the carbon-atom in the carbon layer of fiber C. The solid line and the broken line represent a spectrum in the surface region and the boundary region, respectively. As shown in this figure, a spectrum like Si-C bonding peak was observed in the boundary region. Figure 11 shows the AES spectra of an SiC and a graphite standard sample. From these results, it can be thought that the carbon layer and the silica layer would interact near the interface, and a boundary layer partially including Si-C bonding could be formed. As for fiber B, the peak intensity was smaller than that of fiber C. Although we have not made clear how the existence of such an interaction layer contributes to the hermeticity, we're going to study the mechanism of a hydrogen diffusion process continuously in the future.

5. Conclusion

Four types of experimental carbon-coated optical fibers which had different characteristics were manufactured. Their characteristic constants with regard to hydrogen diffusion in the carbon layer were obtained using accelerated hydrogen testing methods. The results indicate that the fiber which exhibited strong resistance to hydrogen permeation tended to have a high activation energy and a smooth surface of carbon film. And the possibility of a boundary layer formed by interdiffusion is also suggested.

References

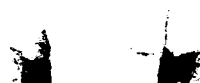
- 1) R.G. Huff, F.V. Dimarcello and A.C. Hart, "Amorphous Carbon Hermetically Coated Optical Fibers", Technical Digest for OFC, TUG-2, 1988.
- 2) K.E. Lu, M.T. Lee, D.R. Powers and G.S. Glacemann, "Hermetically Coated Optical Fibers", Technical Digest for OFC, PD1-1, 1988.
- 3) N. Yoshizawa and Y. Katsuyama, "High-Strength Carbon-Coated Optical Fibers", Electron. Lett., 25, No.21, 1429-1431, 1989.
- 4) P.J. Lemaire, K.S. Kranz, K.L. Walker, R.G. Huff and F.V. Dimarcello, "Hydrogen Permeation in Optical Fibers with Hermetic Carbon Coatings", Electron. Lett., 24, No.21, 1323-1324, 1988.
- 5) P.J. Lemaire, "Reliability of Optical Fibers Exposed to Hydrogen: Prediction of long-term loss increase", Opt. Eng., 30, No.6, 1991.



Haruhiko Aikawa

Sumitomo Electric Industries, Ltd.

1, Taya-cho, Sakae-ku
Yokohama, Japan



Haruhiko Aikawa was born in 1964 and received his M.S. degree in metallurgical engineering from Tohoku University in 1989. He joined Sumitomo Electric Industries, Ltd. the same year and has been engaged in the research and development of industrial technology for optical fibers. He is an engineer of Transmission Media R&D Dept. in Yokohama Research Labs.



Motonori Nakamura

Sumitomo Electric
Industries, Ltd.

1, Taya-cho, Sakae-ku
Yokohama, Japan

Motonori Nakamura was born in 1968 and received his M.S. degree in physical chemistry from Osaka University in 1992. He joined Sumitomo Electric Industries, Ltd. the same year and has been engaged in the research and development of industrial technology for optical fibers. He is an engineer of Transmission Media R&D Dept. in Yokohama Research Labs.



Isamu Fujita

Sumitomo Electric
Industries, Ltd.

1, Taya-cho, Sakae-ku
Yokohama, Japan

Isamu Fujita was born in 1965 and received his M.S. degree in mechanical engineering from Tokyo University in 1990. He joined Sumitomo Electric Industries, Ltd. the same year and has been engaged in the research and development of fusion splicing technology for optical fibers. He is an engineer of Optomechatronics Systems R&D Dept. in Yokohama Research Labs.



Hiroki Ishikawa

Sumitomo Electric
Industries, Ltd.

1, Taya-cho, Sakae-ku
Yokohama, Japan

Hiroki Ishikawa was born in 1965 and received his M.S. degree in applied physics from Tohoku University in 1990. He joined Sumitomo Electric Industries, Ltd. the same year and has been engaged in the research and development of fiber-optic cables. He is an engineer of Communication R&D Dept. in Yokohama Research Labs.



Toshio Danzuka

Sumitomo Electric
Industries, Ltd.

1, Taya-cho, Sakae-ku
Yokohama, Japan

Toshio Danzuka was born in 1956 and received his M.S. degree in mechanical engineering science from Tokyo Institute of Technology in 1982. He joined Sumitomo Electric Industries, Ltd. the same year and has been engaged in the research and development of industrial technology for optical fibers. He is a senior engineer of Transmission Media R&D Dept. in Yokohama Research Labs. and a member of the Institute of Electronics, Information and Communication Engineers of Japan.

Hermetic Product Performance: Ensuring the Uniformity of the Carbon Layer

M.R. Tuzzolo, A.E. Allegretto, E.H. Urruti

Corning Incorporated Wilmington, NC and Corning, NY

ABSTRACT

Carbon coated hermetic fiber developed by Corning for applications in adverse environments such as submarine optical cable systems, possesses critical attributes of fatigue and hydrogen resistance. The enhanced fatigue performance ($n > 100$) is achieved through water exclusion by the carbon layer. Since the molecular diameter of water ($\approx 3 \text{ \AA}$) is greater than that of hydrogen (0.74 \AA), product evaluation focused on hydrogen resistance. This approach represents a more stringent test of the hermetic layer's effectiveness. A relationship between carbon layer thickness, hydrogen resistance and fatigue susceptibility will be shown for Corning's hermetic fiber using a variety of on-line and off-line surrogate measurement techniques.

Additionally, a direct correlation between carbon layer thickness and hydrogen induced attenuation after exposure to accelerated aging conditions of 21 days at 11 atmospheres pure hydrogen and 85°C . Results under these test conditions for over 500 samples, from more than 2 years of manufacturing experience, have shown an average 1240 nm (the first harmonic of the fundamental hydrogen vibration) induced attenuation increase of 0.00 dB/km and a standard deviation of 0.01 dB/km. This corresponds to a predicted 0.00 dB/km induced attenuation in the 1310 and 1550 nm operating windows over an expected 30-year life cycle.

BACKGROUND

With the increased deployment of optical fiber transmission systems optical cable is being installed in areas of harsh environmental conditions, such as submarine

optical cable systems. Standard polymer coatings are incapable of preventing optical loss due to hydrogen ingress and cannot totally prevent long term strength degradation, due to water, both of which are present in these environments. Therefore, an additional hermetic barrier, such as amorphous carbon, is needed. Amorphous carbon coating is typically deposited via chemical vapor deposition (CVD) during the fiber draw process. Since it is necessary to guarantee consistent layer deposition throughout the fiber length, to provide sufficient resistance to permeation of both water and hydrogen an on-line method of ensuring carbon layer integrity is needed during manufacture.

Research indicates that a "ribbon" model is an appropriate representation of amorphous carbon. The intertwining of ribbon layers gives the structure narrow interstices and provide a "maze-like" path for molecular diffusion. No optical technique can detect a tortuous path diffusional mechanism. Therefore, functional testing must consist of actual hydrogen permeation resistance measurement, which is a destructive test. To ensure consistent performance of the hermetic layer, hydrogen performance must be correlated, through exhaustive testing, to a parameter that can be measured "on-line" during manufacturing.

Typically, the layer thickness is used as a measure of the hermetic coating's hydrogen and fatigue resistance. A number of methods for measuring the thickness of the hermetic coating exist. Devices that utilize the electrical and optical techniques have previously been described. Evidence of the correlation of these measurements to functional performance is needed.

For hermetic fiber manufactured by Corning Incorporated, a direct relationship has been shown between carbon layer thickness and fiber linear electrical resistance

(Ω/cm). In addition, fiber resistance has been correlated to both hydrogen and fatigue performance. Electrical resistance has been measured using an on-line, non-contact electrical device and verified with a contact electrical resistance measurement. Both techniques measure overall carbon content. An optical device, which measures thickness at points of transmission, has shown excellent correlation with the electrical measurement.

This paper will demonstrate the overall consistency of Corning's hermetic layer, using both total carbon detection and point measurements, each of which have been verified with extensive hydrogen test data. The consistent carbon layer ensures the critical attribute performance of Corning's hermetic fiber product.

Carbon Layer Measurement

The electrical properties of amorphous carbon allow a direct resistance measurement via metallic contact to the carbon and an ohm-meter. Transmission Electron Microscopy (TEM) has been used to define a relationship between coating thickness and linear fiber resistance. Figure 1 is a graph showing the inverse proportionality of resistance with measured layer thickness.

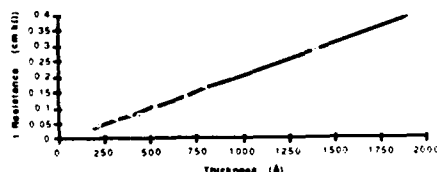


Figure 1 - Inverse resistance versus thickness.

Equation 1 defines the empirical relationship of resistance to carbon coating thickness.

$$R = \frac{\rho}{\pi \cdot D \cdot T} \quad (1)$$

where R = fiber resistance ($\text{k}\Omega/\text{cm}$)
 ρ = carbon layer resistivity ($\Omega \cdot \text{cm}$)
 D = fiber diameter (μ)
 T = carbon layer thickness (\AA)

To relate resistance to hydrogen and fatigue performance, fiber was drawn at various nominal linear resistances. The fiber was subsequently tested for both hydrogen permeation and fatigue resistance. Based on work previously reported¹, hydrogen permeation resistance is determined by exposure to 11 atmospheres of 100% hydrogen, at 85°C for 21 days, and measuring the attenuation increase at 1240 nm. Dynamic fatigue resistance was determined using FOTP-76 (0.5m gauge length, 0.025, 0.25, 2.5, & 25.0%/min. strain rates, 100% relative humidity). Values in excess of 200 were assigned a value of 200. Figure 2 is a plot of linear resistance versus both attenuation increase at 1240 nm due to hydrogen permeation and the fatigue constant (n). For Corning hermetic fiber, attenuation increase due to hydrogen is essentially zero until fiber resistance reaches approximately 21.9 $\text{k}\Omega/\text{cm}$ (at an approximate layer thickness of 250 \AA). Fatigue resistance is maintained until the linear resistance is 25 $\text{k}\Omega/\text{cm}$ ($\approx 200 \text{\AA}$). Corning controls the fiber resistance to ensure specified performance.

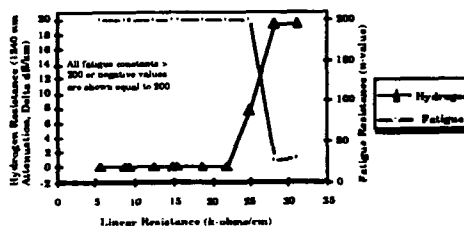


Figure 2 - Correlation of Hydrogen and Fatigue Resistance vs. Linear Resistance for Corning Hermetic Fiber

A disadvantage of the contact electrical measurement is that it penetrates the acrylate coating to reach the carbon layer and hence, is destructive. A method of verifying that the proper carbon thickness is deposited during fiber manufacture has been developed, which uses a non-contact device for on-line measurement of coating electrical properties. An electrical parameter (" Q ") of an energized inductive coil is measured as the carbon coated fiber is drawn through it. " Q " is a figure of merit used to describe an RLC circuit at resonance. The electrically conductive layer causes loading of the inductive coil and results in changes in Q . Dynamic fluctuations in the hermetic coating thickness will change the Q of the coil.

Values of Q have been correlated to fiber with carbon coatings of known linear resistance (i.e., thickness). Additional product quality assurance is obtained by verifying the on-line measurement using the contact electrical device.

Both the contact and non-contact electrical devices described above measure the total carbon deposited on the fiber. An on-line optical technique has also been developed that uses point transmission measurements. A laser impinges on the fiber and results in a reflected and refracted light ray producing a fine structure (fringes) that is analyzed in the spatial frequency domain. The refracted beam penetrates through the hermetic layer and is attenuated, changing the contrast, or signal strength of the fine structure. By monitoring the signal strength, the hermetic layer thickness is measured. In order to account for laser power drift and spatial power fluctuations, a ratio of the signal strength to the DC component of the laser power, both linearly related to the intensity of the laser radiation, is obtained. Equation 2 describes the relationship of the measured ratio to carbon layer thickness.

$$\text{Ratio} = \frac{\text{signal strength}}{\text{DC power}} = k_{\text{eff}} e^{-2AT} \quad (2)$$

where T = hermetic layer thickness (Å)
A = attenuation factor for the hermetic layer (Å⁻¹)
k_{eff} = proportionality constant relating attenuation to Ratio

To ensure equivalent response to fluctuations in layer thickness, the optical technique was compared to the non-contact electrical technique using both devices on the draw tower at the same time. Figure 3 is a plot of both types of measurements taken during an experimental draw run when the hermetic layer was allowed to vary over a broad range of thicknesses. The two devices show excellent correlation over the entire range.

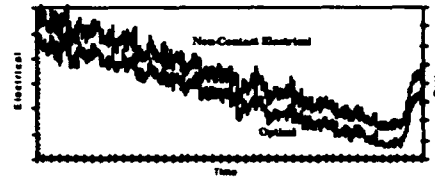


Figure 3 - Correlation of the non-contact electrical device to the optical device.

The optical device has an additional advantage. It has a 2 view system that can detect azimuthal thickness differences. The device has also been used to relate fiber xy position in the CVD reaction vessel to uniformity of coating deposition. Figure 4 is a plot of the ratio of the two views during fiber draw where the fiber position was purposely misaligned and then realigned. Misalignment causes circumferential thickness differences in carbon deposition. The total amount of carbon deposited, as measured by electrical techniques, may have a layer of sufficient thickness. A misaligned fiber, however, may have a sufficient barrier on one side of the fiber, while being deficient in carbon on another side of the fiber. Corning's hermetic fiber radial thickness uniformity is assured using this technique to ensure the necessary fiber alignment.

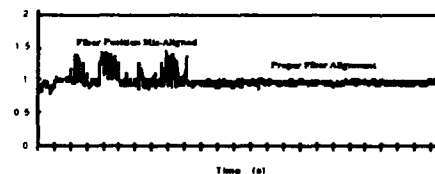


Figure 4 - Optical device, ratio of two views: effect of fiber position on coating radial thickness uniformity.

Additional analysis of the carbon layer was conducted using Scanning Tunneling Microscopy (STM). Figure 5 shows a typical STM generated surface plot. The average surface roughness measured is 0.92 nm. The measurement provides added evidence that no severe oscillations in hermetic coating thickness exist, which could create localized regions for hydrogen and/or water permeation.

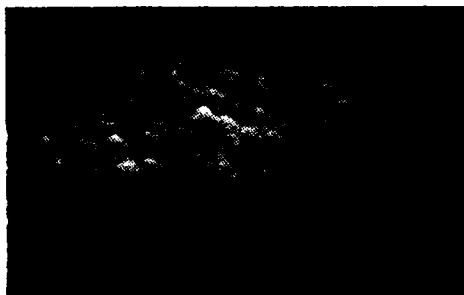


Figure 5 - STM micrograph of amorphous carbon layer.

As stated before, both linear resistance (electrical) and optically attenuated signal measurements are only surrogate measures for the hydrogen performance of hermetic fiber. True performance is measured by the lack of attenuation increase that would otherwise occur due to the presence of hydrogen in the fiber. For over 500 measurements and 2 years of manufacture, the average increase in attenuation at 1240 nm is 0.00 with a standard deviation of 0.01.

Summary

For Corning hermetic fiber, surrogate testing for assurance of product critical attribute performance has been developed through correlation to hydrogen test results. Consistency of the carbon layer has been shown by correlating electrical (total carbon) measurement to optical (point) measurements. Additional assurance for circumferential uniformity of the coating is obtained by maintaining proper fiber position during hermetic layer deposition. STM measurements show that surface roughness is minimal and indicates no oscillations of layer thickness that might allow areas for hydrogen and/or water penetration. Finally, extensive hydrogen testing has proven the performance of Corning hermetic fiber with an average attenuation increase at 1240 nm of 0.0 dB/km at accelerated aging conditions, corresponding to a predicted 0.00 dB/km induced attenuation in the 1310 nm and 1550 nm operating windows over an expected 30 year lifetime.

¹ Lee, K.F., Glaeserman, G.S., Lee, M.T., Powers, D.R., Abbott, J.G., "Mechanical and Hydrogen Characteristics of Hermetically Coated Optical Fibre", Optical and Quantum Electronics, 22, 221-237, 1990.

² Bonfiori, J.Y., Brehm, C., Rousseau, J.C., Augrain, J.M., Roussy, G., Ayache, J., "New Characterization Techniques for Hermetic Carbon Coated Fibers", IOOC-ECOC '91, 17th European Conference on Optical Communication ECOC '91, 8th International Conference on Integrated Optics and Optical Fibre Communication IOOC '91, pp. 37-40, Vol. 1, 1991.

³ Bonfiori, J.Y., Brehm, C., Rousseau, J.C., Augrain, J.M., Roussy, G., Ayache, J., "New Characterization Techniques for Hermetic Carbon Coated Fibers", IOOC-ECOC '91, 17th European Conference on Optical Communication ECOC '91, 8th International Conference on Integrated Optics and Optical Fibre Communication IOOC '91, pp. 37-40, Vol. 1, 1991.

⁴ DeVita, S., US Patent No. 4, 929, 837, May 29, 1990.

⁵ Shreve, D.W., Orzel, G., "A Method to Inspect Hermetic Coatings on Optical Fibers", Army MICOM EOC-M Symposium, pp. 111-10 - 111-21, May, 1992.

⁶ Bravce, R.E., Sitigali, D.R., US Patent No. 4, 943, 343, Nov. 20, 1990.

⁷ Kingsbury, P.L., US Patent No. 5, 142, 228, Aug. 25, 1992.



Michelle Tuzzolo received a B.S. in Ceramic Engineering in 1989 and an M.S. in Glass Science in 1990 from Alfred University. During this time, she had

internships at IBM Corporation (1987) and Galileo Electro-Optics Corporation (1989). Michelle began her employment with Corning, Inc. in 1991 as a Development Engineer where she works to develop new products and processes in optical fiber and is currently leading hermetic coating development.

1989, Eric joined the development group in Corning's Wilmington, North Carolina fiber production facility working on hermetic coatings. In 1993, Eric returned to Corning, New York where he is a Project Manager for new coating development.



Allen Allegretto received a B.S. in Electrical Engineering from Penn State University in 1983. Allen served in the U.S. Naval Nuclear Submarine Force until 1990. Allen

began his employment with Corning, Inc. at the Wilmington, North Carolina fiber production facility as a Senior Engineer in the fiber Draw process area where he is involved in manufacturing systems, controls and instrumentation.



Eric Urruti received his B.S. degree in Chemistry from Indiana University in 1981 and his Ph.D. in Polymers and Coatings from North Dakota State University in

1986. He joined Corning, Inc. in 1986 in Corporate R&D in Corning, New York working on fiber optic coatings. In

STUDY OF MICROBENDING LOSS IN THIN COATED FIBERS AND FIBER RIBBONS

K.Kobayashi, J.Baldauf, N.Okada, K.Ishida,
S.Araki, and M.Miyamoto

Opto-Electronics Laboratory Fujikura Ltd.
1440 Mutsuzaki, Sakura-shi, Chiba-ken 285 Japan

Abstract

We investigated the microbending loss of thin coated fibers and fiber ribbons. First, we determined a relationship between the induced fiber bending spectrum by the fiber environment and the mechanical characteristics of dual coated fibers. From this relationship, a coating design parameter which is proportional to the microbending loss was determined. Then, we measured the microbending loss induced by drum-winding of prototype thin coated fibers with diameters from 160 μ m to 200 μ m and fiber ribbons.

We verified that the measured microbending loss and our theoretically determined coating design parameter have a linear relationship. From this, we have concluded that the mechanical design parameter can be used to design low microbending loss fibers.

1. Introduction

To realize FTTH on a full scale, cables which contain several thousand fibers would be required [1]. Reducing the coating diameter of the optical fibers and the size of the fiber ribbons is the most effective method for realizing small diameter cables with such high fiber density. However, reducing the coating diameter worsens the fiber's resistance to microbending caused by lateral forces. Therefore, clarifying the microbending performance of thin coated fibers and ribbons has become of great interest for designing high fiber density optical cables.

In this paper, we studied the microbending loss of thin coated fibers and fiber ribbons. We calculated a relationship between the induced

fiber bending spectrum by the fiber environment and the mechanical characteristics of dual coated fibers. We then measured the microbending loss induced by drum-winding of prototype thin coated fibers with a diameter from 160 μ m to 250 μ m and fiber ribbons to determine whether the theoretically determined mechanical parameter can be used to design low microbending loss thin coated fibers.

2. Microbending theory

2-1. Induced optical fiber power bending spectrum by the fiber Environment

For dual coated fiber systems, the bending of the fiber due to external forces is governed by two differential equations [2].

$$H_f \frac{\partial^4 \phi(z)}{\partial z^4} + \kappa_s(\phi(z) - w(z)) = 0 \quad (1)$$

$$H_0 \frac{\partial^4 w'(z)}{\partial z^4} + D_0(w'(z) - v(z)) = 0 \quad (2)$$

Where $\phi(z)$ is the deformation of the fiber axis, H_f is the stiffness of the glass fiber, κ_s is the buffer spring constant, $w(z)$ is the deformation of the secondary coating inner surface, H_0 is the stiffness of the secondary coating, D_0 is the lateral rigidity of the secondary coating, $w'(z)$ is the deformation of the secondary coating axis, and $v(z)$ is the deformation of the fiber environment.

Using equations (1) and (2) and modifying Gloge's analysis [2], [3], the relationship between the fiber bending spectrum, $\Phi_{\text{bend}}(k)$, and the mechanical characteristics of the coating can be expressed as a mechanical parameter, C_{mech} [2].

$$\Phi_{\text{bend}}(k) \sim C_{\text{mech}} \frac{f_0 \sigma}{H_f^2},$$

$$C_{\text{mech}} \sim \frac{\kappa_s^2}{D_0^{1.125-0.25\mu} H_0^{\frac{2\mu-1}{8}}} \quad (3)$$

Where σ , μ are parameters dependent on the drum surface, and f_0 is the lateral pressure on the fiber. The value $\mu = 3$ is adopted as a typical value of μ [2], [3], [4]. Therefore, the mechanical parameter is given as (4).

$$C_{\text{mech}} \sim \frac{\kappa_s^2}{D_0^{0.375} H_0^{0.625}} \quad (4)$$

Using this formula, optimum mechanical designs for dual coated fibers can be determined.

2-2. Optical loss due to fiber axis bending

The microbending loss in a single mode fiber has been theoretically determined by Petermann [5].

$$\alpha = \frac{1}{4} (k_0 n_1 \omega_{02})^2 \Phi_{\text{bend}}(k_c)$$

$$k_c = \frac{2}{k_0 n_1 \omega_{01}^2} \quad (5)$$

Where α is the microbending loss, k_c is the coupling wavenumber between the LP₀₁ and LP₁₁ modes, ω_{01} and ω_{02} are the first and second Petermann modified spot sizes, Φ_{bend} is the power bending spectrum of the fiber, k_0 is the free space wavenumber of the light, and n_1 is the refractive index of the core. Therefore, the bending spectrum of the glass fiber axis can be determined from the measured microbending loss by (6).

$$\Phi_{\text{bend}}(k_c(\lambda_0)) = \frac{\alpha(\lambda_0)}{\frac{1}{4} (k_0 n_1 \omega_{02})^2} \quad (6)$$

3. Experiment

To estimate the microbending characteristics, we adopted the drum winding test shown in Fig.1. The microbending loss of the tested fibers was determined by winding each

optical fiber on the drum under constant backtension. The drum diameter is 380mm ϕ and its surface was wrapped with sand paper. The same drum is used for all tests. The lateral pressure induced on the fiber is given by (7).

$$f_0 = \frac{\text{Tension}}{\text{Drum Radius}} \quad (7)$$

The optical loss of the fiber is then measured over the range of 1.3 μm to 1.6 μm . The loss of the fiber in a loose coil is also measured. The microbending loss is the difference in loss between the fiber wound on the drum and the loosely coiled fiber. (8)

$$\alpha_{\text{microbend}}(\text{dB/km}) = \alpha_{\text{drum}}(\text{dB/km}) - \alpha_{\text{free}}(\text{dB/km}) \quad (8)$$

Fig.2 shows the typical measured loss spectrum of a thin coated fiber. The open circles indicate the loss when wound on the drum and solid ones indicate the loss of the loose coil.

3-1. Thin coated fibers

3-1-1. Samples

We made prototype thin dual coated fibers with diameters from 160 μm to 200 μm . These fibers are made with various dimensions which result in different mechanical parameters (C_{mech}). Table 1 shows the dimensions of the optical fibers. To determine the mechanical parameter of the coating, we calculated the κ_s and D_0 using the FEM with a model as shown in Fig.3, and H_0 from Formula (9).

$$H_0 = \frac{\pi E_2 (r_2^4 - r_1^4)}{4} \quad (9)$$

3-1-2. Results

Fig.4,5,6 show the relationship between the normalized measured loss and the diameter of the secondary coating, diameter of the primary coating under fixed secondary diameter, Young's modulus of the primary and secondary coating, respectively. From these figures, it is apparent that a smaller diameter of the secondary coating, a higher Young's modulus of the primary coating, and a lower Young's modulus of the secondary coating result in a larger loss increase.

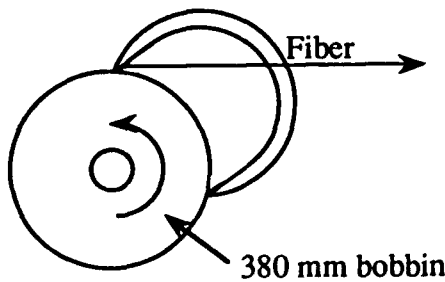


Fig.1 Illustration of the bobbin winding test

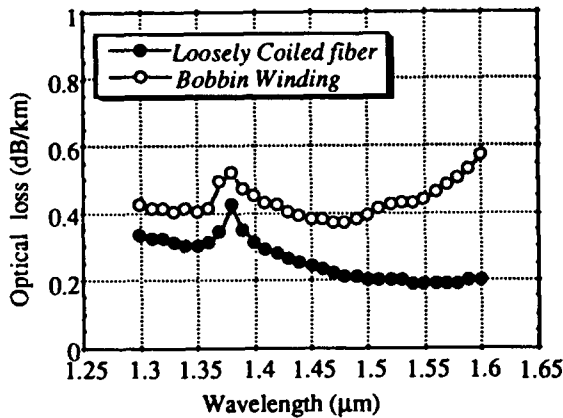


Fig.2 Typical measured loss spectrum of thin coated fiber

Table 1 Coating structure of the thin coated fibers

S.No	Secondary diameter (μm)	Primary diameter (μm)	Secondary Ym (relative value)	Primary Ym (relative value)
1	160	145	2	1
2	180	160	2	1
3	200	170	2	1
4	180	150	2	1
5	180	160	2	1
6	180	170	2	1
7	180	160	2	0.4
8	180	160	2	1
9	180	160	2	2
10	180	160	3	1

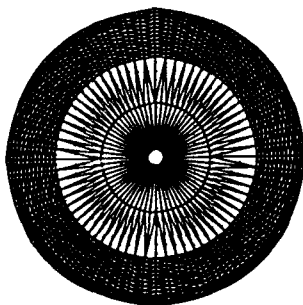


Fig.3 Dual coated fiber model for FEM analysis

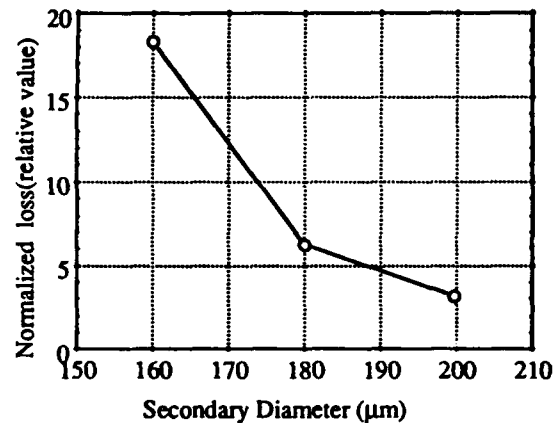


Fig.4 Measured excess loss at 1.55μm of the thin coated fibers as a function of the secondary diameter

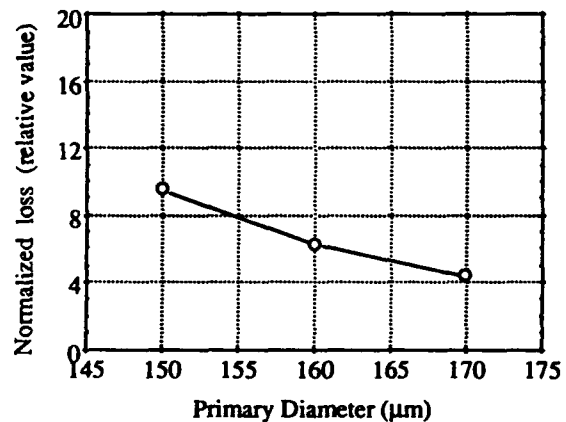


Fig.5 Measured excess loss at 1.55μm of the 180μm thin coated fibers as a function of the primary diameter

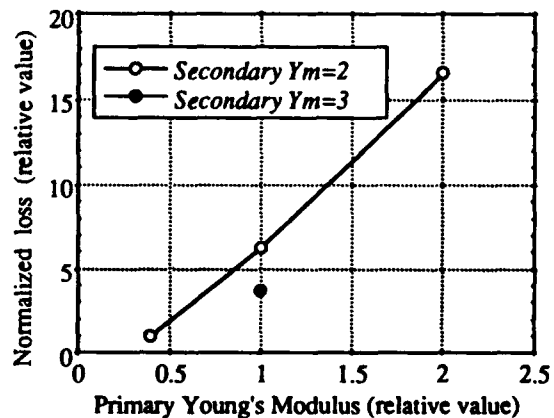


Fig.6 Measured excess loss at 1.55μm of the 180μm thin coated fibers as a function of the primary Young's modulus

Fig.7 shows the relationship between the fiber bending spectrum calculated from formula (6) and the mechanical parameter, C_{mech} . Since the relationship between them is linear, it is apparent that the mechanical parameter, C_{mech} , can be used to design low microbending loss thin coated fiber.

3-2. Thin coated fiber ribbons

3-2-1. Samples

We then tried to estimate microbending characteristics of fiber ribbon. We made prototype thin coated fiber ribbons with the thin coated fibers. To achieve a single layer ribbon winding on the drum and simplify the models for this experiment, four fiber ribbons were used. We calculated the κ_s and D_0 from the FEM with a model as shown in Fig.8. Table 2 shows the dimensions of the ribbon fibers.

3-2-2. Results

The measured microbending loss of the fiber ribbons are shown in Fig.9, 10 and 11. In these figures, the vertical line indicates an average normalized microbending loss of the four fibers in a ribbon.

From these figures, it is apparent that a smaller diameter of the secondary coating in the ribbon, a higher Young's modulus of the primary coating in the ribbon and a thinner ribbon result in a larger loss increase.

Fig.12 shows the relationship between the fiber bending spectrum calculated from formula (6) and the mechanical parameter, C_{mech} . Fig.12 shows a linear relationship between them just as for the thin coated fibers. Therefore, it is shown that the mechanical parameter, C_{mech} , can also be used to design low microbending loss thin coated fiber ribbon.

As described above, reduction of microbending loss in fiber ribbon will be obtained by having a small C_{mech} ; that is large D and H , and small κ_s . In order to achieve a small C_{mech} with a fixed size of fiber ribbon, newly developed high Young's modulus

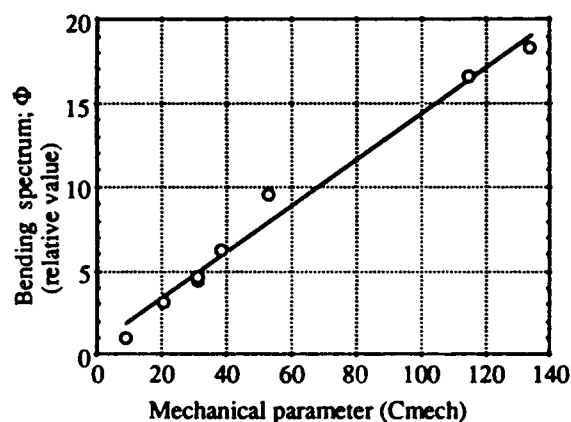


Fig.7 Measured excess loss at $1.55\mu\text{m}$ of the thin coated fibers as the function of a mechanical parameter, C_{mech}

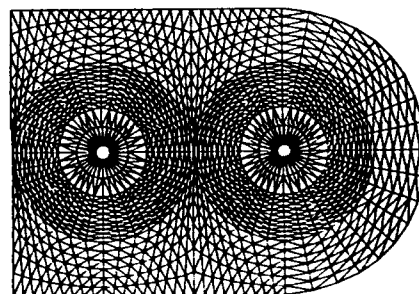


Fig.8 Fiber ribbon model for FEM analysis

Table 2 Coating structure of the thin coated 4 - fiber ribbons

S.No	Secondary diameter (μm)	Primary diameter (μm)	Ribbon thickness (mm)	Secondary YM (relative value)	Primary YM (relative value)
1	160	145	0.20	2	1
2	180	160	0.22	2	1
3	200	170	0.25	2	1
4	180	160	0.25	2	1
5	180	160	0.30	2	1
6	180	160	0.22	2	0.4
7	180	160	0.22	2	2

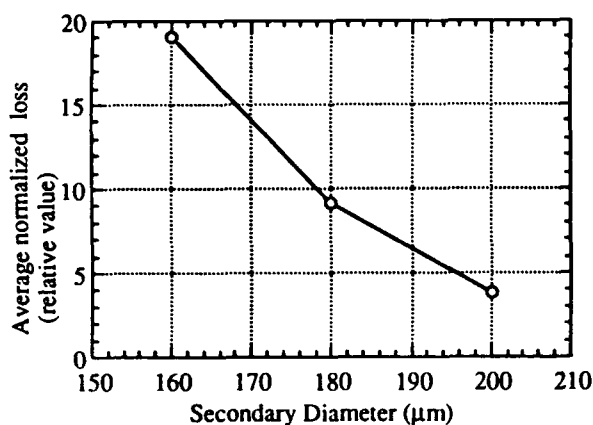


Fig.9 Measured excess loss at 1.55μm of the 4-fiber ribbons with thin coated fibers as a function of the secondary diameter

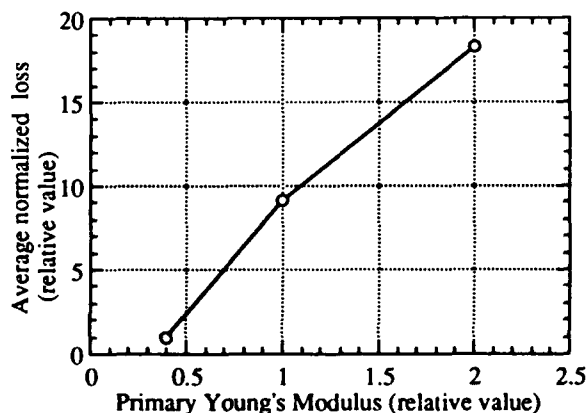


Fig.10 Measured excess loss at 1.55μm of the 4-fiber ribbons with thin coated fibers as a function of the primary Young's modulus

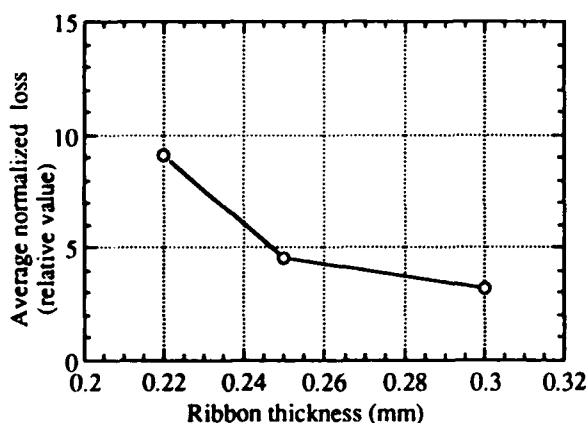


Fig.11 Measured excess loss at 1.55μm of the 4-fiber ribbons with 180μm thin coated fibers as a function of the ribbon thickness

secondary and low Young's modulus primary should be used and the primary diameter should be made thicker. However, these items can cause degradation in mechanical strength and loss characteristics, so the design of structure of the fiber should be done with care.

4. Other general characteristics of 16-fiber ribbons

We then made prototype 16-fiber ribbons with thin coated fibers with low Young's modulus primary 'a' or 'b' and high Young's modulus secondary 'c' or 'd' and investigated the general characteristics. The coating materials and dimensions of the ribbon structure which is shown in Fig.13 are given in the table 3.

First, we performed a metal plate lateral pressure test. Fig.14 shows an illustration of the test. It can be seen from the lateral pressure test results in Fig.15 that loss increases at 100kg were scarcely observed in either of the ribbons.

Next we investigated the loss stability of the fiber ribbons at high and low temperatures. The fiber ribbons were 500m long in a loose coil. The temperature was changed cyclically in the range of -40°C to +60°C. Fig. 16 shows that the loss changes in all fibers of ribbon A were less than 0.02dB/km from -40°C to +60°C, while in ribbon B, a loss increase of about 0.2dB/km at low temperature was observed. These results indicate that the coating materials b and d can be a bad influence on the loss stability of fiber ribbon. Therefore, the selection of coatings for thin coated fiber ribbons requires careful consideration.

5. Conclusion

We studied the microbending loss of thin coated fibers and fiber ribbons. We verified that the measured microbending loss and the theoretically determined mechanical design parameter have a linear relationship. Therefore, this parameter can be used to design low microbending loss fibers and fiber ribbons.

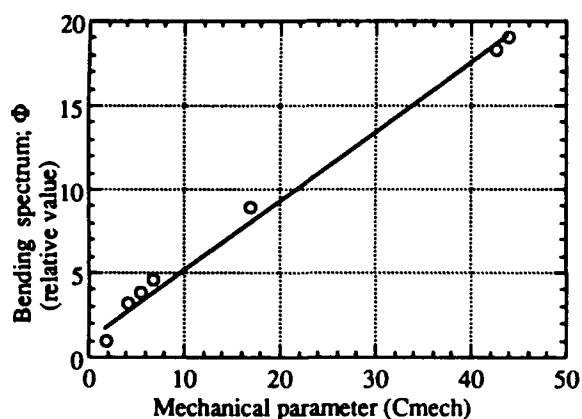


Fig.12 Measured excess loss at 1.55 μ m of the 4-fiber ribbons as a function of the mechanical parameter, Cmech

Table 3 Coating structure of the prototype 16 - fiber ribbons

		Ribbon	
		A	B
Primary	Material	a	b
	YM(relative value)	0.4	0.4
	diameter(μ m)	160	160
Secondary	Material	c	d
	YM(relative value)	3	3
	diameter(μ m)	180	180
Ribbon Thickness(mm)		0.22	0.22

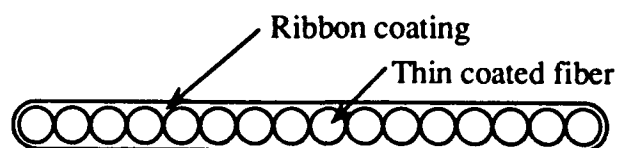


Fig.13 16-fiber ribbon

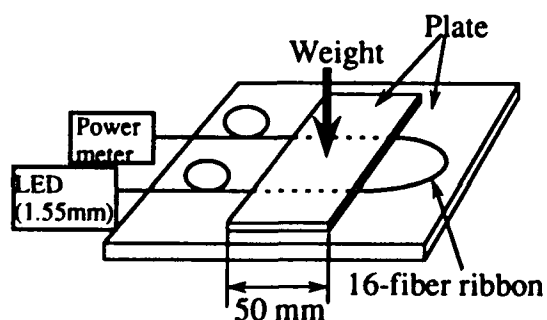


Fig.14 Illustration of the metal plate test

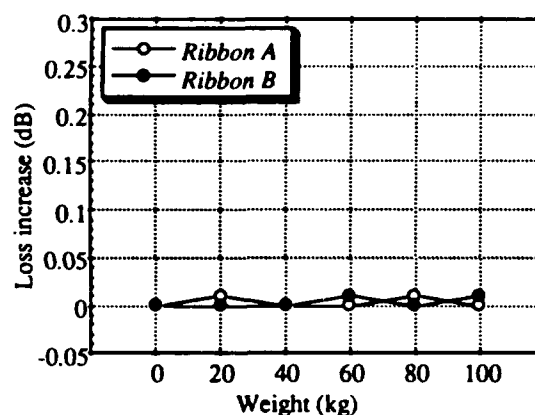


Fig.15 The loss increase of the fiber ribbons due to the metal plate test

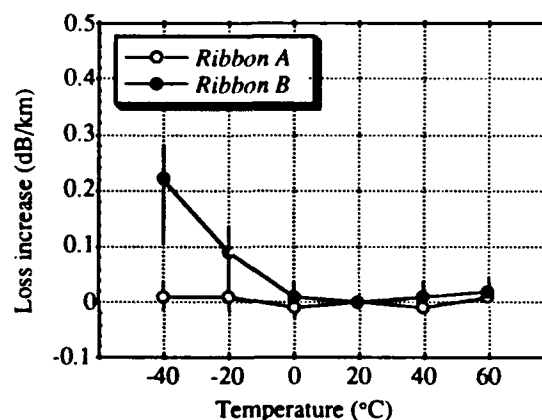


Fig.16 The loss stability of the fiber ribbons at high and low temperature

References

- [1] S.Tomita *et al*, "Preliminary research into ultra high density and high count optical fiber cables," *IWCS Symposium Proceedings*, 1991, pp.8-15.
- [2] J. Baldauf, N. Okada, and M. Miyamoto, "Relationship of mechanical characteristics of dual coated single mode optical fibers and microbending loss," *IEICE Trans. Commun.*, vol. E76-B, no. 4, April 1993, pp. 352-357.
- [3] D.Gloge, "Optical-fiber packaging and its influence on fiber straightness and loss," *The Bell System Technical Journal*, February 1975, pp.245-262.
- [4] W.B.Gardner, "Microbending loss in Optical fibers," *The Bell System Technical Journal*, February 1975, pp.457-465.
- [5] K.Petermann, "Fundamental mode microbending loss in graded-index and w fibers," *Optical and Quantum Electronics*, 1977, pp.167-175.



Kazunaga Kobayashi

Opto-Electronics
Laboratory
Fujikura LTD.

1440 Mutsuzaki,
Sakura-shi, Chiba-ken
285 Japan

Mr. Kobayashi was born in 1961. He joined Fujikura LTD. after his graduation from Gunma University with a M.E. Degree in 1985 and has been engaged in research and development of optical fibers. He is now an engineer in the Telecommunication Cable Material Section and a member of the IEICE of Japan.



Katsuyoshi Ishida

Opto-Electronics
Laboratory
Fujikura LTD.

1440 Mutsuzaki,
Sakura-shi, Chiba-ken
285 Japan

Mr. Ishida was born in 1967. He joined Fujikura LTD. after his graduation from Gunma University with a B.E. Degree in 1991 and has been engaged in research and development of optical fibers. He is now an engineer in the Telecommunication Cable Material Section and a member of the IEICE of Japan.



John Baldauf

Opto-Electronics
Laboratory
Fujikura LTD.

1440 Mutsuzaki,
Sakura-shi, Chiba-ken
285 Japan

Mr. Baldauf was born in Tennessee in 1965. He joined Fujikura LTD. after receiving his Ph.D. Degree from the University of Illinois in 1991 and has been engaged in the research and development of optical fiber cables. He is now an engineer in the Telecommunication Cable Section and a member of the IEICE of Japan and the IEEE.



Shinji Araki

Opto-Electronics
Laboratory
Fujikura LTD.

1440 Mutsuzaki,
Sakura-shi, Chiba-ken
285 Japan

Mr. Araki was born in 1950. He joined Fujikura LTD. after his graduation from Tokyo Metropolitan University with a B.E. Degree in 1974 and has been engaged in design and research of optical fibers. He is now a section chief of the Telecommunication Cable Material Section and a member of the IEICE of Japan.



Naoki Okada

Opto-Electronics
Laboratory
Fujikura LTD.

1440 Mutsuzaki,
Sakura-shi, Chiba-ken
285 Japan

Mr. Okada was born in 1964. He joined Fujikura LTD. after his graduation from Chiba University with a B.E. Degree in 1986 and has been engaged in research and development of optical fiber cables. He is now an engineer in the Telecommunication Cable Section and a member of the IEICE of Japan.



Matsuhiro Miyamoto

Opto-Electronics
Laboratory
Fujikura LTD.

1440 Mutsuzaki,
Sakura-shi, Chiba-ken
285 Japan

Mr. Miyamoto was born in 1953. He joined Fujikura LTD. after his graduation from Tokyo Institute of Technology with a M.S. Degree in 1978 and has been engaged in design and research of optical cables. He is now a section chief of the Telecommunication Cable Section and a member of the IEICE of Japan.

A ZERO-STRESS AGING RELATIONSHIP FOR OPTICAL FIBER

James J. Carr

Corning Incorporated
Center for Fiber-Optic Testing
103 Canada Road
Painted Post, New York 14870

Abstract

Recent experimental studies at Corning's Center for Fiber-Optic Testing have demonstrated and characterized the zero-stress aging effect on commercially available acrylate-coated optical fiber. This work has led to the discovery of an analytical, exponential decay function that relates fiber strength to aging time for a given set of conditions. Data collected thus far on fiber aged in water at 85°C, 65°C, and 45°C indicate a strong dependence on temperature. The exponential relationship and sensitivity to temperature imply that fibers directly exposed to water, at temperatures expected under normal conditions of use, retain a high percentage of strength even after long periods of time.

Introduction

In the general sense aging (or ageing) is any change over time; more specifically a gradual change of observed or measured qualities within a defined interval of time. Zero-stress or stress-free aging of optical fiber refers to a measured strength change over time in a mechanically stress-free deployment. It was the absence of stress that had distinguished aging from fatigue. More recently however, surface roughening or pitting has been advanced as a convincing cause for zero-stress aging. Most investigators to date have exposed optical fiber samples to temperature controlled humidity or water bath environments. As a consequence of particular environments, glass compositions and test techniques, aged specimens exhibit varying rates of strength changes as a function of exposure times. Strength changes are usually defined relative to an initial or day-zero measurement for a sample not in the aging environment. Qualitatively, environments drier and cooler than the initial conditions lead to increases in measured strength, whereas wetter, warmer conditions result in strength losses with time.

Experimental

Test Sample

A single optical fiber product type was chosen for testing; one sample of commercially available SMF-28™ fiber. It is a 125-micrometer diameter pure silica clad glass, with a 250-micrometer dual-layer, acrylate coating. This fiber type has historically demonstrated very consistent overall performance in laboratory mechanical tests and in a broad range of in-service field deployment conditions.

Sample Preparation

Continuous lengths of fiber, sufficient to conduct an individual strength test were each wrapped on (low expansion Pyrex) glass spools. Nominal combined stresses due to wrap tension and bending were estimated at 5 to 7 kpsi. One spool of fiber designated as the control or day-0 specimen from the group was maintained at room temperature and humidity.

Aging Conditions

A large stainless steel container filled with deionized water was used for each test set of samples. Bath temperatures were allowed to stabilize before sample immersions and subsequently controlled to $\pm 2^\circ\text{C}$. Sample spools were actually immersed in a reverse time sequence to allow retrieval of all samples for testing at the same time. Bath pH was not controlled nor was any form of water agitation or stirring used. Except for occasional replenishment of evaporated water, the bath remained undisturbed throughout the aging period.

Aging temperatures at 85°C, 65°C, 45°C and 25°C (data unavailable for this report) were arbitrarily selected but intended to clearly portray temperature dependence. Aging times were limited to five predetermined intervals, (including day-0) different for each temperature and meant to capture salient features of trend.

Strength Tests

Aged samples for a specific temperature were retrieved simultaneously and, with the control, immediately placed in a stabilized preconditioning chamber at room temperature, 100% relative humidity for 12 to 15 hours.

A sixteen-station rotating capstan tensile test device was employed for all post aging strength measurements. Testing was performed in accordance with TIA Fiber Optic Test Procedure 28 (FOTP-28).

Results

Measurements Data

Measurement results, shown below for 85°C, 65°C and 45°C are graphed in figures 1, 2, and 3 respectively. Observe that variability increases as temperature decreases. This is presumably due to weakening effects of the aging mechanism and a need to have extended measurement intervals, particularly at the 45°C temperature.

Aging Data at 85°C

Aging Time (days)	Strength (%)
0	100
0.25	96
1.0	91
4.0	83
16.0	69

Aging Data at 65°C

0	100
1.0	98
9.0	86
25.0	82
49.0	72

Aging Data at 45°C

0	100
36.0	99
100.0	92
144.0	93
324.0	95

Data Analysis

The smooth data trends in figures 1 and 2 suggested an exponential decay. And in fact, the data conform exceedingly well to an exponential function of the form,

$$S(t) = S_0 e^{-\alpha t^{1/2}} \quad (1)$$

$S(t)$ → aged strength

S_0 → initial strength

α → aging parameter

t → aging time

Taking the logarithm of equation (1), one obtains a linear relation for logarithm strength versus square root time, equation (2). Then the slope of a linear regression on the transformed data is the aging parameter α . Magnitudes of the aging parameters for 85°C, 65°C and 45°C data are 0.093, 0.047 and 0.004.

$$\ln S = -\alpha t^{1/2} + \ln S_0 \quad (2)$$

Figures 4, 5 and 6 are graphs of data from figures 1, 2 and 3, plotted as logarithm (percent) strength versus square root time. The strong linearity, in figures 4 and 5 especially, implies the validity of equation (1) as an analytic relationship describing zero-stress aging behavior.

Further Analysis

The opportunity was taken to explore a substantiation of the proposed zero-stress aging model expressed in equation (1), with data from four previously published studies. In all cases α , the aging parameter for a specific data set, is the magnitude of the slope of a linear regression on log strength as a function of square root time. And r is the associated regression correlation coefficient.

Case 1

In a 1988 paper by Matthewson and Kurkjian¹ entitled "Environmental Effects on the Static Fatigue of Silica Optical Fiber," one section of the discussion described results of a zero-stress aging test. The sample was "a UV-curable epoxy acrylate coated silica fiber, immersed in 100°C distilled water under zero stress." Data interpolated from their graph is given below; α equals 0.176 with an r of 1.00.

Aging Time (days)	Strength (%)
0.7	88
3.5	74
11.6	56

Case 2

Haslov et. al.² reported aging results in the 1992 International Wire & Cable Symposium Proceedings for their dual UV-acrylate fiber samples stored in "glass vessels filled with deionized water buffered to a pH value of 7." Although no aging (strength degradation) had yet occurred at 65°C, data interpolated from their graphs for 95°C and 80°C are tabulated below. Aging parameters (α 's) equal 0.119 and 0.039 with r-values of 0.97 and 0.98 respectively.

95°C

Aging Time (days)	Strength (%)
0	100
9	73
44	42
175	32
210	17
290	11

80°C

0	100
9	96
44	82
90	77
175	59
290	54

Case 3

Willem Griffioen³ also presented stress-free aging graphs in the 1992 International Wire & Cable Symposium Proceedings for what was described as "standard fiber A" at 20°C, 30°C, 40°C, 50°C and 60°C. Samples "were placed in water...[with] a pH-value of about 7." Data interpolated from the 60°C, 40°C and 20°C graphs are shown below with respective α -values of 0.068, 0.027 and 0.009 and correlation coefficients of 0.99, 0.98 and 0.98.

60°C

Aging Time (days)	Strength (% strain)
30	3.7
60	3.0
120	2.4
210	2.0

40°C

30	4.9
60	4.4
120	4.1
210	3.8

20°C

210	5.7
285	5.5
480	5.3

Case 4

At the 1990 Optical Fiber Communication Conference (OFC) a postdeadline paper, prepared by three Bellcore researchers,⁴ described results from a fiber aging study. Samples were aged in 80°C deionized water, then removed at intervals of 1 day, 1 week and 3 months. Sample surfaces were examined with a Scanning Tunneling Microscope (STM) and inert strength measurements were conducted using a two-point bending apparatus. STM photographs displayed a roughening of fiber surfaces with increased aging time. Furthermore, increased median roughness depths, a , were consistent with decreased median strengths, S , in keeping with the Griffith relationship. That is, the product of break stress and square root flaw depth is a constant, C .

$$C = S \sqrt{a} \quad (3)$$

$0 < S < \text{theoretical strength}$
 $0 < a < \text{fiber diameter}$

The thrust of the Bellcore work was to establish direct evidence for a cause-and-effect relationship between aging induced strength loss in optical fiber and surface roughening. But relationships of strength loss or roughening depth to aging time were not examined. A later publication by Robinson and Yuce⁵ included 9-month measurements; the table below is actual data as published.

Aging Time (days)	Strength (GPa)	Flaw Depth (nm)	C (MPa·√m)
0	14.2	5.4	1.04
1	11.7	6.6	0.95
7	10.3	8.0	0.93
91	6.7	19.0	0.93
274	4.3	50.4	0.96

Again, the Bellcore aging data is very well described by equation (1) with an aging parameter (α) equal to 0.068 ($r = 0.99$). Perhaps as important as the zero-stress aging data is an apparent confirmation of the Griffith relationship on the nanometer scale of roughness or pit depth. Because C is (nearly) constant, equation (3) can be substituted into equation (1) and solved for pit depth as a function of aging time.

$$a = a_0 e^{2\alpha t^{1/2}} \quad (4)$$

The slope of logarithm pit depth versus square root aging time is now positive and equal to twice the magnitude of the aging parameter (2α). The regression yields a value of 0.132 (almost twice 0.068) with a nearly perfect correlation coefficient (0.999).

Summary and Conclusions

Recent data obtained at Corning's Center for Fiber-Optic Testing, and from several other previous publications on the zero-stress aging phenomenon in water appear to obey an analytical relationship between long term strength and time, defined in equation (1). This equation models optical fiber aging with an exponential strength decay as a function of time and an aging parameter α , associated with fiber type and environmental conditions.

Aging parameters display a strong dependence on temperature, decreasing nearly an order of magnitude between water soak temperatures at or above 85°C and those at or below 45°C. The implication for reliability therefore, is that fiber exposed to water at temperatures expected in typical deployment conditions retain a large percentage of initial strength, despite prolonged periods of time.

Although the model predicts no minimum aging strength, the possibility exists for lower limits which might depend upon such specifics as (fiber) glass/coating product type or water pH. There are

also possibilities of threshold conditions, for example a temperature below which the aging mechanism would not occur. And some very preliminary test measurements have suggested strength losses associated with aging could be delayed for various lengths of time.

When surface roughness or pit depth is used to express flaw depth in the Griffith relationship, a substitution into the aging equation yields pit depth as a function of time, in equation (4). This formulation may offer a theoretical direction to pursue for modeling the aging mechanism itself.

Acknowledgments

The author wishes to acknowledge Dan Hill for his diligent and resourceful testing efforts, as well as Lori O'Dell and Jeff Smith for data analysis and graphs.

References

1. Matthewson, M. John and Charles R. Kurkjian. 1988. Environmental Effects on the Static Fatigue of Silica Optical Fiber. Journal of the American Ceramics Society 71: 177-183.
2. Halsov, Peter, Knud Bundgaard Jensen and Niels H. Skovgaard. 1992. Degradation Study for Stressed Optical Fibres in Water: New Worst Case Life Time Estimation Model. 41st International Wire & Cable Symposium Proceedings: 423-427.
3. Griffioen, W. 1992. Ageing of Optical Fibres in Water. 41st International Wire & Cable Symposium Proceedings: 622-628.
4. Yuce, H.H., R. S. Robinson and P.L. Key. 1990. A Scanning Tunneling Microscope Study of Optical Fiber Corrosion. Optical Fiber Communication Conference Postdeadline Papers PD14: PD14 1-4.
5. Robinson, R.S. and H. H. Yuce. 1991. Scanning Tunneling Microscopy of Optical Fiber Corrosion: Surface Roughness Contribution to Zero-Stress Aging. Journal of the American Ceramics Society 74: 814-818.

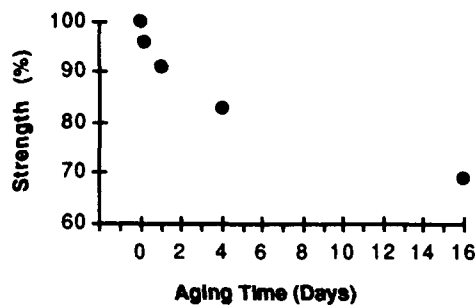


Figure 1 Percent strength retained versus aging time at 85°C.

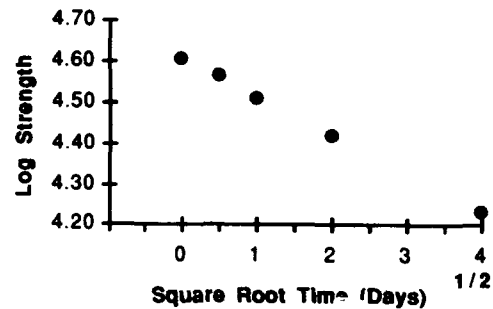


Figure 4 Aging data at 85°C on logarithm strength versus square root time axes.

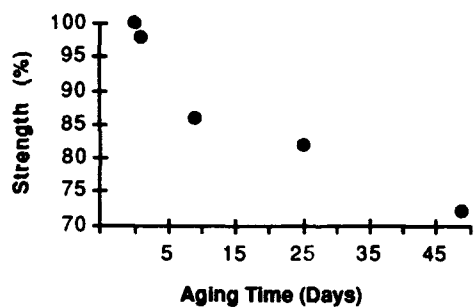


Figure 2 Percent strength retained versus aging time at 65°C.

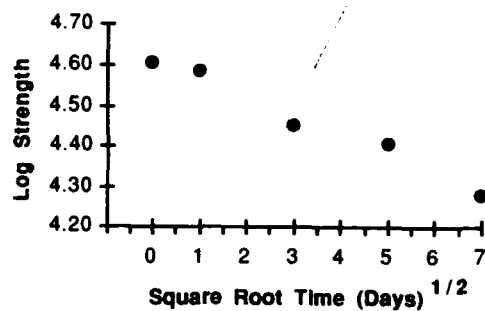


Figure 5 Aging data at 65°C on logarithm strength versus square root time axes.

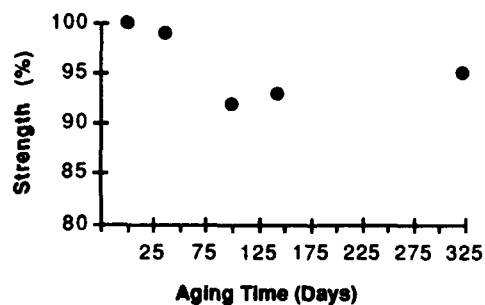


Figure 3 Percent strength retained versus Aging Time at 45°C.

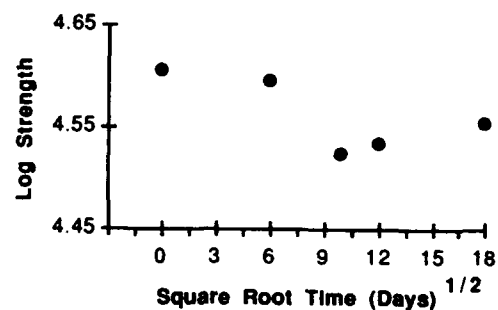


Figure 6 Aging data at 45°C on logarithm strength versus square root time axes.

Biography



Jim Carr received his B.S. and M.A. degrees in physics from the State University of New York in 1976 and 1979. He joined Corning Incorporated in 1985 and is presently a Senior Mechanical Engineer at the Center for Fiber-Optic Testing. His responsibilities include development, coordination, and evaluation of mechanical reliability testing of optical fiber.

REDUCED CORROSIVE AND LOWER SMOKE FLAME RETARDANT W&C FORMULATIONS

Dr. Ronald L. Markezich and Mr. David G. Achbacher

Occidental Chemical Corporation, Grand Island, New York

ABSTRACT

Flame retardant wire and cable formulations with greatly reduced smoke and corrosivity properties have been developed. This has been accomplished using traditional halogenated flame retardants with a unique combination of filler and inorganic salts. Smoke levels on combustion are greatly reduced and less acid gases are produced. The physical and other properties of these materials are maintained when compared to traditional flame retardant systems.

Using mixtures of a thermally stable chlorinated flame retardant with inorganic salts, such as, magnesium hydroxide allows the antimony oxide level to be reduced and yet still maintain high oxygen indexes and physical properties. The FR-EVA wire and cable formulations using this combination of flame retardants give less smoke when burned in the NBS smoke chamber and produces less acid gases.

INTRODUCTION

Millions of pounds of polyolefins and polyolefin copolymers containing halogenated additives have been produced over a number of years to meet the high standards of the wire and cable industry. Formulators are now faced with the additional task of how to provide the same critical performance in combustion properties while providing reduced smoke and corrosivity during combustion.

Progress is continually being made to introduce compositions with reduced smoke generation by methods, such as substituting aluminum trihydrate for halogen additives⁽¹⁾. Technology has also been developed which allows the continued use of the traditionally accepted halogenated additives and achieve lower smoke^(2,3). While this technology lowers the smoke during combustion, the corrosivity of the gases is probably effected very little.

We have now developed a method by using a combination of a halogenated flame retardant and magnesium hydroxide to flame retard wire and cable material which results in lower smoke and also lower corrosivity.

MATERIALS AND PROCEDURES

Materials

The ethylene vinyl acetate copolymer (EVA) used in these evaluations was obtained from commercial sources and contained 9% vinyl acetate and had a melt index of 3.2. The chlorinated flame (CFR) used in this work is available from Occidental Chemical. It is the Diel-Alder diaduct of hexachlorocyclopentadiene and 1,5-cyclooctadiene. The magnesium hydroxide used was from the Solem Division of J.M. Huber Corporation and has been modified for ease of dispersion. The talc used was from Cyprus Industrial Minerals and is zinc stearate treated.

The experimental samples were mixed on a two roll mill to obtain homogeneous samples. Compounded samples were sheeted and granulated prior to molding. Molding was accomplished by standard techniques.

Testing

Oxygen Index: The test employs is the ASTM D-2863. The minimum concentration of oxygen, expressed as volume percent, in a mixture of oxygen and nitrogen that will just support flaming combustion.

Smoke Generation: Testing was performed in a NBS Smoke chamber according to ASTM E-662. The samples, 3 by 3 inch by 0.085 inch thick were exposed to radiant heat plus propane microburners (flaming combustion). Smoke evolution was continually recorded during the test period. Results are reported as specific optical density, Ds.

Cone Calorimeter: Testing of materials was conducted by Underwriters Laboratories Inc®, Northbrook, Illinois, in general accordance with the procedure specified in the proposed ASTM D0.21.4. The sample size was 6 inch by 6 inch by 1/4 inch thick. The tests were conducted in the horizontal orientation and the radiant flux of the cone heater was set at 50 kW/m. The initial exhaust mass flow was 30 g/s.

kW/m. The initial exhaust mass flow was 30 g/s.

Corrosivity: The gases from the cone calorimeter were tested for corrosivity using a corrosion target Model No. 030788-SO.35-8061 (nominal 45,000 angstrom span) from Rohrback Cosasco. A CK-3 corrosometer from Rohrback Cosasco was employed to measure the corrosion of the probes.

RESULTS

Table 1 gives some typical talc filled FR-W&C formulations using CFR as the flame retardant in combination with magnesium hydroxide. The total flame retardant level is constant at 25% with 5% Sb_2O_3 . Figure 1 shows a graph of the % MgOH versus oxygen index. There is a synergistic effect between the chlorinated flame retardant and magnesium hydroxide which gives the highest O.I. with 20% CFR and 5% MgOH.

Some additional FR-EVA W&C formulations are shown in Table 2 in which 0.1% ferric oxide has been added. Ferric oxide when used in combination with CFR and zinc stearate treated talc has been shown to increase the oxygen index 1 to 1.5% and also lower the NBS smoke values⁽⁴⁾. Figure 2 shows a graph of formulation 3 where the CFR is decreased from 25 to 5% and the MgOH is increased from 0 to 20%. There also appears to be a synergistic effect with the max O.I. with 8% MgOH and 17% CFR.

The use of alumina trihydrate, instead of magnesium hydroxide, in these talc filled EVA W&C formulations does not show the same synergist effect as MgOH does (shown in Figure 3).

Table 3 shows FR-EVA formulations that have been tested that do not contain talc. The oxygen indexes of these formulations are shown in Figure 4. There is a maximum oxygen index when the mixture contains 5 to 10% MgOH with 5% Sb_2O_3 .

The NBS smoke generation data for some of the FR-EVA formulation is shown in Table 4. As can be seen the mixed CFR/MgOH (15:10) formulation gives the lowest smoke values.

Table 5 lists the formulations that were tested in the cone calorimeter, and the results are listed in Table 6. The corrosion values of Samples 2 to 4 are listed in Table 7. The use of the mixed CFR/MgOH gives a four to five fold decrease in corrosion values.

Table 1
FR-EVA W&C FORMULATIONS

Weight %	1	2	3	4	5
EVA	47.9	47.9	47.9	47.9	47.9
CFR	25	20	15	10	5
Sb_2O_3	5	5	5	5	5
MgOH	0	5	10	15	20
Talc	20	20	20	20	20
Agerite Resin D	1.4	1.4	1.4	1.4	1.4
Luperox 500R	0.7	0.7	0.7	0.7	0.7
Results					
O.I. (%)	28.1	28.75	28.41	27.42	27.25
Tensile % Elongation	350	320	300	190	140

Table 2
FR-EVA W&C FORMULATION

Weight %	1	2	3
EVA	47.8	51.8	52.8
CFR	25 to 5	25 to 5	25 to 5
Sb_2O_3	5	1	0
MgOH	0 to 20	0 to 20	0 to 20
Talc	20	20	20
Ferric Oxide	0.1	0.1	0.1
Agerite Resin D	1.4	1.4	1.4
Luperox 500R	0.7	0.7	0.7

Table 3
FR-EVA W&C FORMULATION
(No Talc)

Weight 1%	1	2
EVA	67.9	62.9
CFR	30 to 5	30 to 5
Sb_2O_3	0	5
MgOH	0 to 25	0 to 25
Agerite Resin D	1.4	1.4
Luperox 500R	0.7	0.7

Table 4
SMOKE GENERATION OF
FR-EVA 20% TALC FILLED FORMATIONS
(E-662) (Flaming Mode)

	1	2	3
CFR	25	15	15
Sb ₂ O ₃	5	5	0
MgOH	-	10	10
Results			
	Dm		
1.5 Min	4	1	7
4 Min	247	108	213
Max	416	276	301
Time to Max (Min)	9.8	10.2	8.8

Table 5
FORMULATIONS TESTED IN THE CONE CALORIMETER
(Weight %)

	1	2	3	4
EVA	42.3	47.8	47.8	51.8
CFR	---	25	15	15
Sb ₂ O ₃	---	5	5	1
Talc	---	20	20	20
MgOH	54	---	10	10
Luperox 500R	1.5	1.4	1.4	1.4
Agerite Resin D	---	0.7	0.7	0.7
Ferric Oxide	---	0.1	0.1	0.1
Ca Stearate	0.9	---	---	---
Vinyl Silane	1.3	---	---	---

Table 6
RESULTS OF THE CONE CALORIMETER
(Heat Flux 50 kw/m²)

	1	2	3	4
Time to Ignition (Sec)	122	87	99	95
Max Heat Release Rate (kw/m ²)	308	130	180	120
HRR Ave. 180 Sec After Ignition (kw/m ²)	246	117	145	160
Total Heat Released (Kj)	1523	1178	1284	1282
Wt. Loss (%)	50.6	54.4	47.2	44.4
Average Heat of Combustion (Kj/g)	30.1	21.7	27.2	28.8
Average Specific Extn. Coefficient (M ² /g)	0.376	0.755	0.705	0.789

Table 7
CORROSION VALUES W&C FORMULATIONS

	2	3	4
Metal Loss End of 60 Min Exp. (angs)	6577	1733	1673
Metal Loss 24 Hour Exposure (angs)	9840	2077	2235

Figure 1
Oxygen Index of FR-EVA/20% Talc/5% Sb₂O₃
25% CFR Minus % MgOH

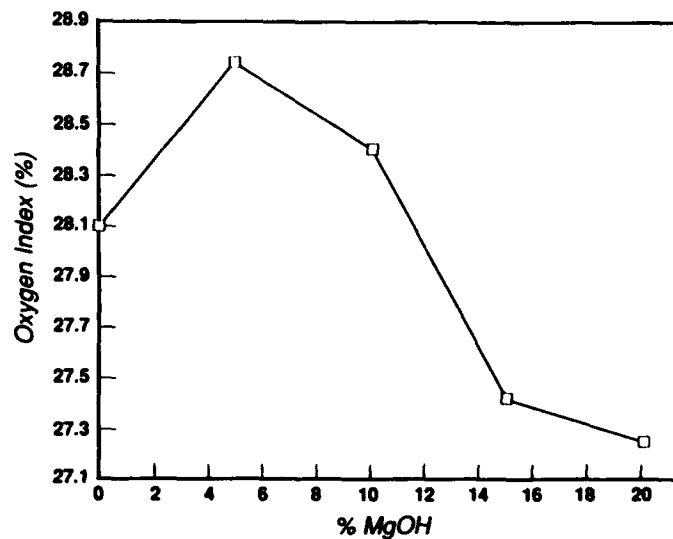


Figure 2
Oxygen Index of FR-EVA/20% Talc/0.1% Fe₂O₃
25% CFR Minus % MgOH

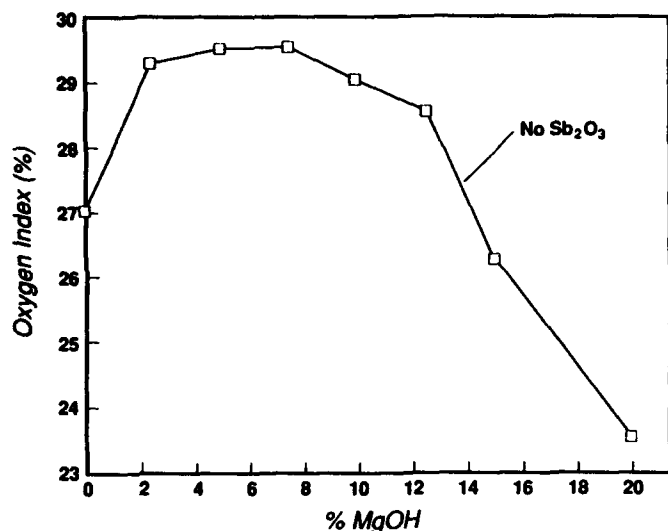
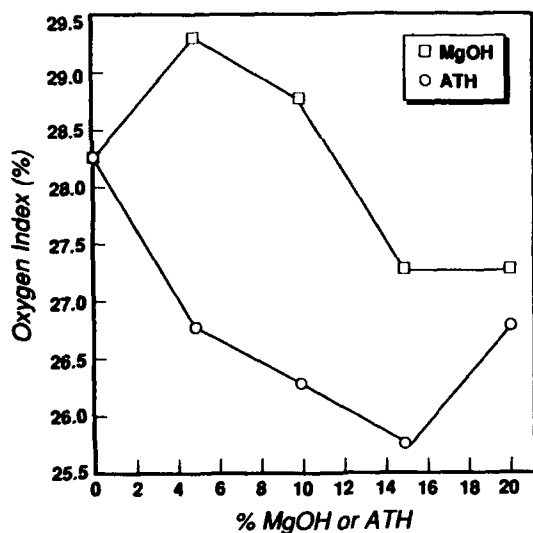


Figure 3
Oxygen Index of FR-EVA/20% Talc/5% Sb₂O₃
25% CFR Minus % ATH or MgOH

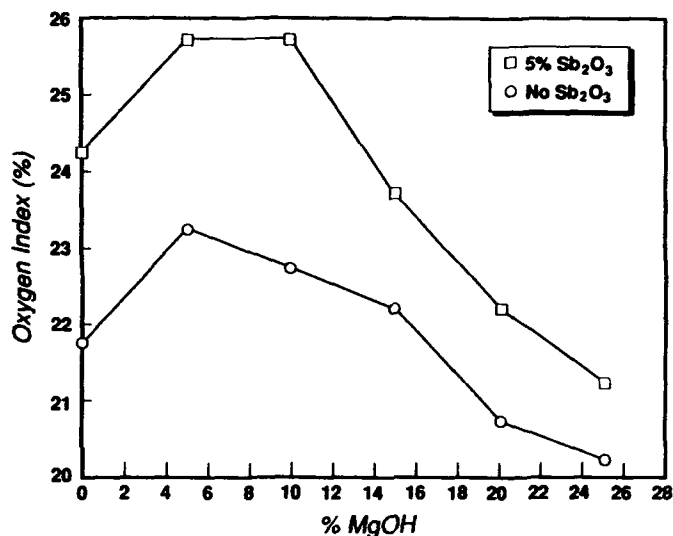


R.L. Markezich



D.G. Aschbacher

Figure 4
Oxygen Index of FR-EVA
30% CFR Minus % MgOH



REFERENCES

1. J.R. Pedersen. et.al., "Low-Smoke, Halogen Free Ship-Off Shore/On Shore Cables with Improved Flame Retardance and Fire Resistance", IWCA, Cherry Hill, November 1993.
2. J.D. Duffy and C.S. Ilardo, "New Reduced Smoke, Flame Retardant Wire and Cable Formulations Containing Halogenated Additives", IWCA, Reno, November 1994.
3. C.S. Ilardo and R.L. Markezich, "Reduced Smoke Flame Retardant Formulations for High Performance Applications", Wire Association International Conference, Atlanta, May 1988.
4. C.S. Ilardo, "Flame Retardant Polyolefins Compositions", U.S. Patent 4,567,214 (1986).

BIOGRAPHY

Ronald L. Markezich is Technical Manager/Flame Retardants at Occidental Chemical Corporation, Technology Center, Grand Island, New York. He holds a B.A. degree in Chemistry from Knox College and a Ph.D. in Organic Chemicals from the University of Wisconsin at Madison. He spent seven years at General Electric Company and the last thirteen years at Occidental Chemical. He has sixteen U.S. Patents and over twenty publications.

David G. Aschbacher is a Staff Technician at Occidental Chemical. He has been involved in development of flame retardant formulation for the past fifteen years.

TESTING OF CORROSIVITY OF SMOKE FROM CABLE PYROLYSIS

Göran Mälhammar * and Carl-Gustaf Ekroth **

* Ericsson Telecom AB, S-126 25 Stockholm

** Ericsson Cables AB, S-824 82 Hudiksvall

ABSTRACT

Measurements of pH and conductivity are sometimes used to set limits for the corrosive properties of gases from cable fires. In this work such measurements (DIN 57472-813) are compared to more direct corrosion measurements of pyrolysis gases on copper. Four telecom cables and the insulation materials in them were investigated separately and the materials were also measured together with the metals aluminium and tinned copper. The results show, that pH, conductivity and corrosion of copper were affected by the presence of aluminium in the case of PVC and of PA12. For PVC the corrosion decreased and for PA12 the corrosion increased in the presence of aluminium. An important conclusion to be drawn from this work is, that product tests rather than material tests should be used to predict the corrosive properties of cables.

INTRODUCTION

Some customers demand cables with minimized production of corrosive gases by a possible fire. As a measure of the degree of corrosivity they specify certain limits according to IEC 754-2 or DIN 57472-813. In those standards measurements of pH value and conductivity of pyrolysis gases of polymeric materials are described. Those values give only an indirect measure of the corrosivity of the polymeric materials used in the cables so the following questions are raised.

Is there any correlation between results from measurements according to IEC 754-2 or DIN 57472-813 and corrosivity measured by a more direct method?

Should the measurements be made on the polymeric materials separately as is stated in the standards or on pieces of a cable? The last question is raised because it is known from literature, that the presence of metal can influence the smoke production by fire¹.

To investigate further, some cables from our production were chosen and their polymeric materials with and without the presence of different metals in the cable were investigated with one of the above mentioned methods and also with a direct method of resistance measurement of a copper conductor exposed to pyrolysis gases.

EXPERIMENTAL

pH and conductivity measurements

Those measurements were made according to DIN 57472-813. Figure 1 gives an idea of the principle. The values used for the most important parameters were:

Temperature in oven: 800°C
Air stream: 10 l/h
Volume of deionized water: 170 ml

It must be noticed that results of DIN 57472-813 can not be compared with results from IEC 754-2, mainly depending on the fact that the latter uses a volume of 1 liter deionized water instead of 0.17 liter.

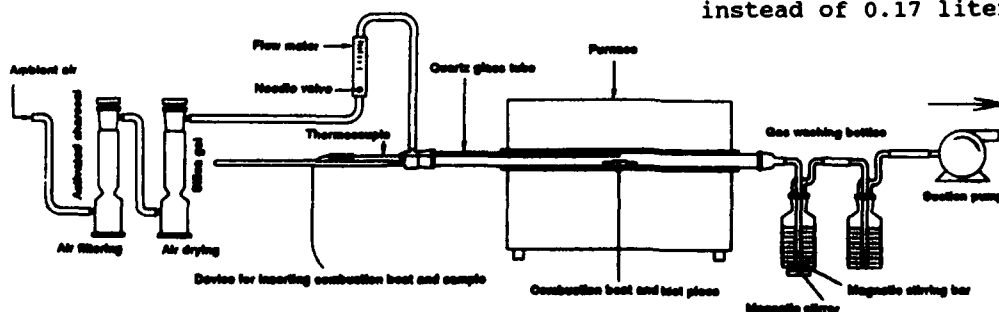


Fig.1. IEC 754-2

Direct corrosion measurements

The direct corrosion measurements were made in a 6 dm³ glass vessel equipped with a 20 mm sealed silica tube which could be heated in a high temperature oven (see figure 2). 1 gram of polymeric material was pyrolyzed at each time at 950°C for 15 minutes. That amount of polymer yields much more water than corresponding to 100 % humidity. The temperature in the glass vessel, which was found to be about 23°C, and the humidity were measured continuously. The measuring object was placed at the bottom of the glass vessel and connected to a data logger with wires through a rubber bung. In some runs a fan was placed in the glass vessel to agitate the smoke and the gases evolved in order to distribute them evenly.

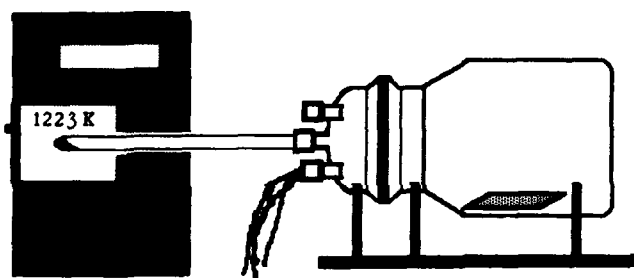


Fig.2. Device for direct corrosion measurements.

The corrosion measurements were made by following the change in resistance of a copper pattern on a printed circuit board for about three hours after the 15 minutes pyrolysis. Two different circuit boards were used. In one design (type 1) a "triple track pattern" was made with three parallel patterns, each 300 μ m broad and with an insulation distance of 300 μ m. The height of the pattern was 5 μ m. The design can be seen in figure 3.

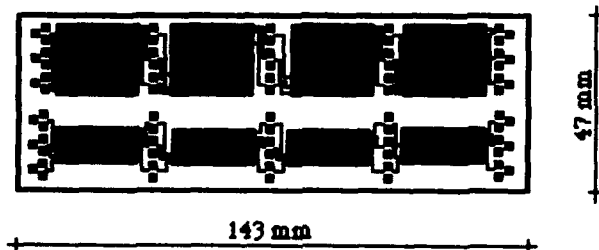


Fig.3. Design of a printed circuit board for direct corrosion measurements.

The other design (type 2) was made with a sputtering technique and was only 0.5 μ m (5000 Å) high and with a width and an insulation distance of 75 μ m. The main difference in use is the sensitivity. In type 1 we have around 2000 Å corrosion for every ohm change in resistance. The corresponding figure for type 2 is around 4 Å. Probes of that type are now commercially available and their use is described in the literature^{2,3,4}. By calculating the amount of corrosion it was assumed that it was evenly distributed over the surface of the copper pattern.

Materials used

Cables Four cables used in telephone exchanges were chosen for the investigation.

ENOX-FR A halogen free flame retardant cable meeting a flame propagation test in accordance with IEC 332-3, category C and with weakly acidic gases in accordance with IEC 754-2 (pH \geq 3.5 and conductivity \leq 100 μ S/cm).

Conductor: Tinned solid copper wire, diameter=0.4 mm.

Insulation: Polyamide 12, flame retardant (PA12 FR), free from halogen and phosphorous, oxygen index \geq 30 (ASTM D2863), wall thickness=0.1 mm.

Sheath: A halogen free, flame retardant ethylene plastic compound (E/VAC), oxygen index \geq 35.

ENAF0-FR A halogen free flame retardant, screened cable meeting a flame propagation test in accordance with IEC 332-3, category A and C and with weakly acidic gases in accordance with IEC 754-2 (pH \geq 3.5 and conductivity \leq 100 μ S/cm).

Conductor: Tinned solid copper wire, diameter=0.4 mm.

Insulation: Polyamide 12, flame retardant (PA12 FR), free from halogen and phosphorous, oxygen index \geq 30 (ASTM D2863), wall thickness=0.1 mm.

Wrapping: PET-foil.

Screen: The HF screen consists of a laminated aluminium foil with aluminium on both sides, longitudinally applied. The LF screen consists of a braid of tinned copper wires, optical coverage more than 60 %.

Sheath: A halogen free, flame retardant ethylene plastic compound (E/VAC), oxygen index \geq 35.

ENKX A switch board cable meeting flame propagating test in accordance with IEC 332-1.

Conductor: Tinned solid copper wire, diameter=0.4 mm.

Insulation: Polyamide 12 (PA12).

Sheath: Plasticized polyvinylchloride compound (PVC) with a Cl content of about 25 % and with flame retardant additive (Sb_2O_3), oxygen index > 28 (ASTM 2863).

ENAFK A screened, switchboard cable meeting at least flame propagation test IEC 332-1.

Conductor: Tinned solid copper wire, diameter=0.4 mm.

Insulation: Polyamide 12 (PA12).

Screen: The HF screen consists of a laminated aluminium foil with aluminium on both sides, longitudinally applied. The LF screen consists of a braid of tinned copper wires, optical coverage more than 60 %.

Sheath: A plasticized PVC with Cl content of about 25 % and with flame retardant additive (Sb_2O_3), oxygen index > 28 (ASTM 2863).

Polymers 1 gram of each of the following polymeric materials were used in the investigation.

PVC
PA12
PA12 FR (flame retarded PA12)
E/VAC no 1 (E/VAC copolymer with flame retardant)
E/VAC no 2 (E/VAC copolymer with flame retardant)

In addition to these materials they were further investigated together with tinned copper and with aluminium foil (the amount of metal was calculated from the cable design).

RESULTS AND DISCUSSIONS

pH and conductivity

Figure 4 shows the results of pH measurements according to DIN 57472-813. As expected the PVC materials with and without the presence of metal as well as the cables containing PVC give very low pH values. The E/VAC materials are slightly acidic and the PA12 materials as well as the cables without PVC (but with PA12) are slightly basic.

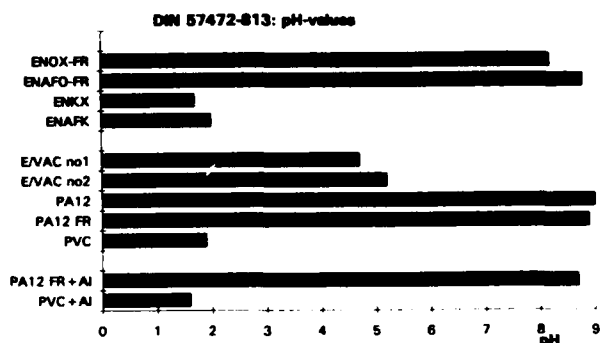


Fig.4. PH values according to DIN 57472-813 for different cable and material combinations.

The conductivity values are very low for E/VAC materials and also for the cables without PVC. The PA12 materials give medium values and the PVC materials including the cables with PVC show very high values (figure 5).

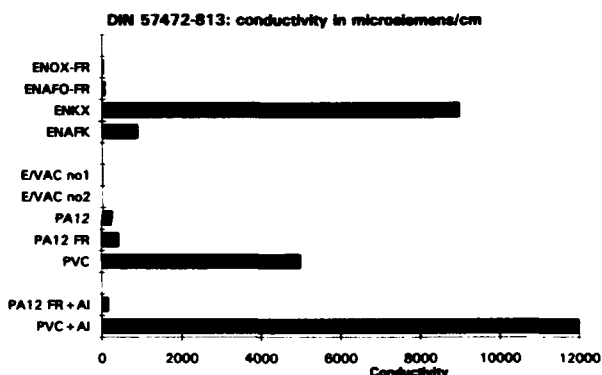


Fig.5. Conductivity values (in $\mu S/cm$) according to DIN 57472-813 for different cable and material combinations.

Corrosion measurements

The change of resistance (for type 1 probe) as a function of time after 15 minutes of pyrolysis was followed over 24 hours for three PVC samples. The result is shown in figure 6. 80 % of the change occurred in the first 3 hours, hence that time, measured from the start of the pyrolysis, is used in this report to get the increase in resistance from which the thickness of the corrosion (in Å) is calculated.

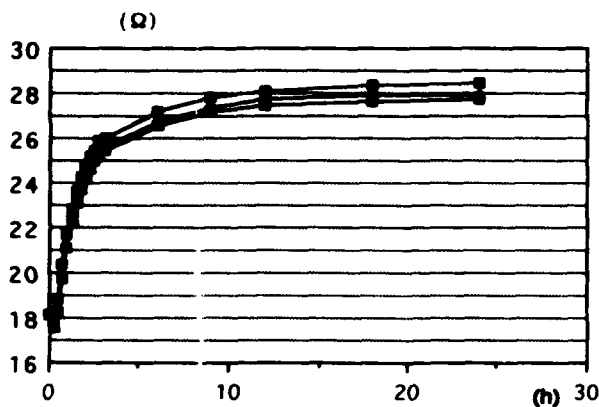


Fig. 6. Resistance (probe of type 1) as a function of time for three PVC samples.

Fig 7 gives the corrosion results (probe of type 1) for the polymeric materials and two of them include aluminium. With tinned copper present the results were practically the same as without tinned copper for all polymers. With aluminium present together with the E/VAC polymers there was a very small change in resistance compared to the polymer alone. By pyrolysing pieces of cables no reliable results could be reached for the PVC containing cables. It was observed that soot particles were formed which were deposited on the circuit board giving spot corrosion and in some cases even caused breakage of the copper pattern. Moreover, it could be seen by observation, that substantial corrosion had occurred. A lesson from this is that the gases from pyrolysis should be filtered before reaching the measuring probe. The cables not containing PVC gave very little corrosion.

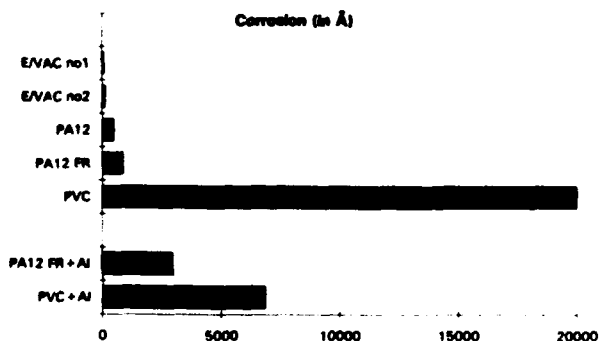


Fig. 7. Corrosion (in Å) for different materials.

Only a few measurements were made with probes of type 2 because of difficulties in manufacturing them but those few results supporting those from type 1. Consequently in most cases in this report results from type 1 probes are given.

By stirring the gases with a fan a much lower value of corrosion was achieved. The method was tried on PVC with and without the presence of aluminium. The relative magnitude between the two different samples was kept constant. The results indicate that rather heavy corrosive gases are evolved, which usually flow to the low position of the probe in the vessel. With a fan the corrosion level will be lower for all samples but by using probes of type 2 that will probably not be a problem because of the much higher sensitivity of that probe.

The most interesting result from this investigation is the fact that the presence of a metal can change the corrosion dramatically (by a factor of more than 3) as shown in figure 8. One can speculate about the underlying chemistry. In the case of PVC and aluminium the HCl is probably partly consumed by reacting with aluminium forming chlorides but no analysis is made to try to confirm that and the results of the conductivity measurements gave a slightly lower pH value for PVC with aluminium compared to that without. In the case of PA12 it is more difficult to find a possible chemical reactions which give more corrosive products with aluminium present. A GC-MS investigation were made to analyse the organic products formed by pyrolysing PA12-FR with and without the presence of aluminium (compare with ref. 1). Small differences were found but the investigation must be made more comprehensive before any conclusions can be drawn.

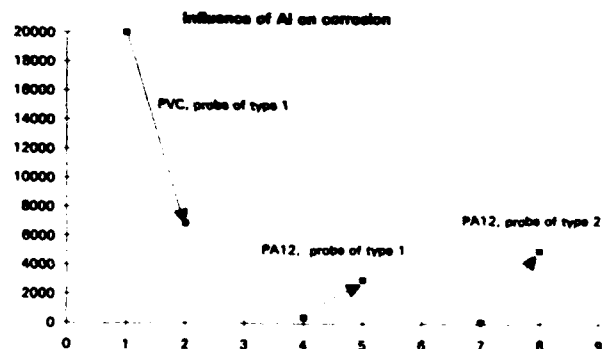


Fig. 8. Influence of aluminium on the corrosion (in Å).

The question raised in the beginning of the paper, if there is any correlation between measurements of pH or conductivity and direct corrosivity measurements can now be addressed. In figure 9 the corrosion is plotted as a function of the deviation of pH from 7. That type of plotting is more relevant than to plot it directly against pH which can also be seen from the literature⁵. The presence of aluminium gives small changes in pH in an unpredicted direction. In the PVC case the addition of aluminium gives an increase in the deviation from pH 7 at the same time as the corrosivity is diminishing. In the PA12 case there is a decrease in the deviation from pH 7 at the same time as the corrosion is increasing. There seem to be no logical connection between pH of a water solution of the pyrolysis gases and the corrosion with the presence of aluminium.

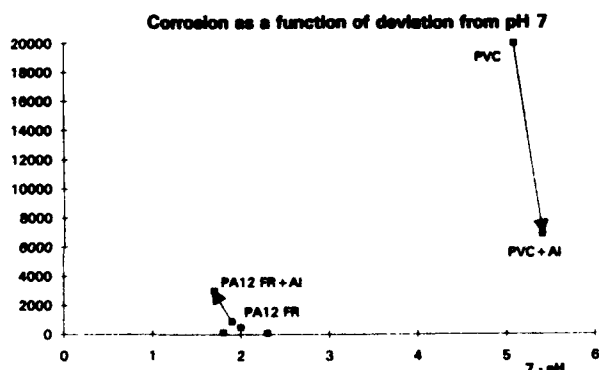


Fig.9. Corrosion (in Å) as a function of deviation from pH 7.

In figure 10 the corrosion is plotted against the conductivity. Neglecting the results with aluminium present there is an increase in conductivity with an increasing corrosion. But again looking at the results in the two cases with aluminium present there is an increase in conductivity with a decrease in corrosivity, quite opposite to what could be expected.

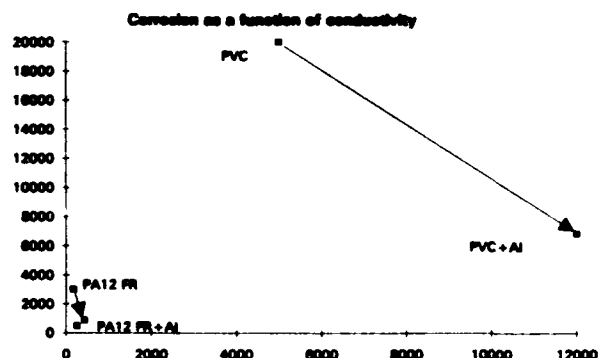


Fig.10. Corrosion (in Å) as a function of conductivity (in µS/cm).

CONCLUSIONS

The following conclusions can be drawn from this paper.

Measurements according to IEC 754-2 or DIN 57472-813 do not give any reliable conclusion about corrosion of pyrolysis gases from cables.

The presence of aluminium together with PVC and PA12 affects the corrosion from the pyrolysis gases.

Corrosion measurements of pyrolysis gases from polymers in a cable give no reliable results when aluminium is included in the cable design. Preferably product tests should be used.

ACKNOWLEDGEMENTS

Many thanks to Magnus Jahnsson who made the measurements on DIN 57472-813 and the corrosion measurements.

REFERENCES

1. Nelson, G. L. and Chan E. K., "Synergistic Fire Performance between Zinc Coating and a Modified Polyphenyleneoxide Substrate", Fire and Polymers, ACS Symp. Ser. 425, Chapter 21, 1990.
2. Chu, Fun L., "Techniques to Characterize the Corrosivity of Cable Fire-Products", IWCS Proceedings, page 545-547, 1992.
3. Technical Committee No 89, "New Work Item Proposal", IEC, Nov. 1991.
4. Gibbons, J. A. M. and Stevens, G. C., "Limiting the Corrosion Hazard from Electrical Cables Involved in Fires", Fire Safety Journal, No 2, 1989.
5. Hirschler, Marcelo M., "Update on Smoke Corrosivity", IWCS Proceedings, page 661-672, 1990.



Dr. Göran Mälhammar
Ericsson Telecom AB
S-126 25 Stockholm

Dr. Mälhammar has a M.Sc. degree from the Technical University of Stockholm and a Ph. D. (Dr. Ing.) from the Technical University of Darmstadt, Germany. He has worked in the industry with plastic coated textiles (Galon AB) and with plastic and rubber problems in the car industry (AB Volvo) and from 1978 in the Swedish Plastics and Rubber Institute. Since 1990 he is working with Ericsson Telecom on fire safety problems and with polymeric applications in telecom equipment.



B.Sc. Carl-Gustaf Ekroth
Ericsson Cables AB
S-824 82 Hudiksvall

Mr. Carl-Gustaf Ekroth received the B.Sc. (Eng.) in chemical technology from the Swedish Institute of Technology, Helsinki, Finland in 1969. He joined Ericsson Cables, Telecom Cables Division, Sweden 1969. He has worked as Development Engineer, Manufacturing Manager, Quality Control Manager and Manager of Material Technology. Since 1991 he has been Assistant Technical Manager, responsible for Copper Cables and Material Technology.

ULTRAVIOLET AND OXIDATIVE THERMAL DEGRADATION STUDIES ON FLAME RETARDANT CABLE SHEATHING COMPOUNDS

Sitaram Rampalli

Andrew Corporation, Orland Park, Illinois, USA.

ABSTRACT

This paper describes in detail, the effects of ultraviolet and oxidative thermal aging on flame retardant cable sheathing compounds. Experimental work on five different commercially available compounds was carried out. The course of ultraviolet and thermal degradation was followed by DSC, HPOIT, and Tensile Property measurements. In all the cases it was found that the flame retardant compounds are highly susceptible to oxidation caused by UV and heat aging. Arrhenius models were developed to extrapolate the stability of these materials to room temperature. A specially formulated additive package consisting of a combination of light stabilizers was found to provide adequate UV and Oxidative Thermal stability.

INTRODUCTION

Demand for flame retardant polymers is on the rise during the past 10-15 years. This increase in the usage has been the result of various catastrophic fires and the resulting loss of human life and property damage. During 1970s and 1980s, Polyvinyl Chloride, Chlorinated Polyethylene, Chloroprene were used extensively on cables for sheathing applications. Even though, all these materials provide adequate fire retardancy to the cables, they also generate large quantities of smoke, and toxic fumes in the event of a fire. Further, it was also observed that the presence of halogens increases the corrosivity of the fire gases, thereby causing extensive damage to the expensive electronic equipment in the vicinity of the cables. To combat this problem several polymeric compositions commonly known as "nonhalogenated", "halogen free", or "zero halogen" flame retardant compounds came into existence. Many of these compounds are now commercially available to the cable manufacturer.

Majority of halogen-free cable sheathing materials exhibit excellent fire resistance, very low levels of smoke, toxicity, and corrosivity. However, the long-term performance of these materials under a variety of service conditions is not very well documented. There are several reasons for this lack of information on the long term behavior of non-halogenated materials. One of the main reasons for this lack of information is that, the chemistry of nonhalogenated flame retardant polymers is a new phenomenon. The technology utilizes various hydrated metal oxides such as aluminum trihydrate, magnesium hydroxide, either singly or in combination, elemental phosphorous, phosphates, boron and nitrogen compounds, metal complexes and various other organometallic compounds¹ to transform the ordinary polymers into non-halogenated or zerohalogen flame retardant polymers. Because of several such possible combinations to achieve the desired flame retardancy, low smoke, and low toxicity, these materials behave very much differently under actual service conditions when compared to unfilled neat polymers.

It is a common belief that flame retardant cables are intended for indoor use only and hence it is sufficient for the sheathing compounds to exhibit adequate fire, smoke, and toxicity without much regard for other performance characteristics. However, in reality this is not true. Even though, almost all the cables are for indoor use, there are several situations wherein the cable is installed in a hostile environment. One type of cable known as leaky or radiating coaxial cable, in particular, is very often installed in subway tunnels, high rise buildings and mines² for two-way radio communications. For cables installed in such locations, there is a strong possibility that they can be periodically exposed to an intense electric arc, which is a powerful source of heat and ultraviolet radiation. Often times the leaky coaxial cables are extended from inside of the buildings and tunnels and are connected to another point source an-

tenna for voice or data communications. Sometimes, cables may encounter hot hydrocarbon exhaust gases from the passing vehicles in the tunnels. Other possible sources of sheathing degradation are: thermal, thermooxidative, reactions with fuel oils and other chemicals on cables installed in the engine rooms of ships, ultraviolet degradation during the storage of the cables to name a few.

Polymer degradation can occur in several ways³⁻⁶. The four most important categories of polymer stability that one should consider while estimating the lifetime of a sheathing compound are:

1. Ultraviolet Light Stability
2. Oxidative Thermal Stability
3. Chemical Resistance
4. Environmental Stress Crack Resistance

The present work addresses the first two aspects, namely, the ultraviolet light stability and oxidative thermal stability of some important commercially available flame retardant cable sheathing compounds. Systematic aging studies on the materials under a variety of exposure conditions were carried out. The course of polymer degradation was followed by a detailed examination of their thermal profiles generated by differential scanning calorimetry (DSC), by measuring residual high pressure oxidative induction times, and by tensile property measurements.

EXPERIMENTAL

MATERIALS

A generic description of the materials selected for the current study is given in Table I. All the materials used in this study are commercially available from various manufacturers. Due to the proprietary nature of these formulations, the materials were assigned code names such as Material A, Material B etc., Typical properties of the materials investigated are listed in the Table II. All the information given in the Table II was taken directly from the data supplied by the manufacturers. The natural grade resins were compounded with 2.5 phr of carbon black on a laboratory two roll mill. The only compound that was used in its natural form is the one designated as 'Material G'. After milling, the stock was molded into 9" x 9" x 0.05" plaques on a Wabash compression molding press. The plaques were

TABLE I
DESCRIPTION OF THE MATERIALS USED IN THIS STUDY

<u>MATERIAL</u>	<u>DESCRIPTION</u>
A	Low Density Polyethylene Copolymer.
B	Non-Halogenated FR Polyethylene Copolymer with Aluminum Salts.
C	Non-Halogenated FR Polyethylene Copolymer with Magnesium Salts.
D	Halogenated LDPE with organic bromine and metal oxides.
E	FR Polyether not based on hydrated metal oxides.
F	Similar to material B, plus UV stabilizer.
G	Same as material F, with 2.5 phr of carbon black.

then cut into dumbbell shapes according to the procedure described in ASTM D 638⁶.

METHODS

Aging Studies

Ultraviolet Aging: Ultraviolet aging on the materials was carried out in a QUV test apparatus according to the procedure described in the ASTM G 53 standard⁷. The equipment was manufactured by Q-Panel Co., Cleveland, Ohio. UV-B fluorescent lamps were used throughout this work. UV-B lamps have a ultraviolet radiation in wavelengths between 280 nm and 315 nm. The UV exposure

TABLE II

PROPERTIES OF VARIOUS FLAME RETARDANT COMPOUNDS¹

PROPERTY	MATERIALS					
	A ²	B	C	D	E	F/G
Elongation, %	700	150	180	200	475	200
Tensile Strength (psi)	2,100	2,175	2,200	1,300	2,200	1,670
LOI, %	17	35	39	26	31	33
Smoke Index	NA	50	11	NA	NA	NA
Temperature Index, °C	NA	270	350	NA	NA	255
Toxicity Index	NA	1.5	1.5	NA	1.2	NA
Flame Spread VW-1 / IEC 332-1	Fail	Pass	Pass	Pass	Pass	Pass
Flame Spread IEEE 383 / IEC 332-3	Fail	Pass	Pass	Fail	NA	NA

1) Information as supplied by the manufacturer.

2) This is a non-flame retardant compound

NA Information is Not Available.

studies were performed at 50°C, 60°C, and 70°C temperatures. The condensation temperature was kept at 50°C in all the experiments. The typical experimental cycle is as follows: 6 h of UV followed by 4 h of condensation. Samples were withdrawn from the UV chamber at preset time intervals, bolted dry with a tissue and sealed in clean plastic bags until they are ready for further analysis. UV aging experiments were terminated at the end of six weeks (1008 h).

Oven Aging: Air oven aging experiments were conducted in standard laboratory ovens manufactured by Blue M. A constant air flow of 100 ml/min into the ovens was maintained through out the aging experiments. Thermocouples were placed at different locations in each of the ovens used to record accurately the inside temperature. Dumbbell shaped specimens were suspended in the ovens from one end by using a thin stainless steel wire. The aging studies were carried out at 70°C, 90°C, and 105°C and

sample specimens were withdrawn from the oven at preset time intervals, cooled in a desiccator and stored in clean plastic bags.

ANALYSIS AND CHARACTERIZATION

The course and extent of degradation resulting from the ultraviolet and oven aging were followed by measuring the changes in the thermal and tensile properties of the materials.

Differential Scanning Calorimetry (DSC): Thermal Analyst 2000 equipped with 2910 DSC Module manufactured by TA Instruments was used for performing the thermal analysis. Differential Scanning Calorimetry was used to follow the changes in the material during the aging experiments. Nitrogen purge gas at the rate of 50 ml/min was used for running all the DSC experiments.

Oxidative Induction Time Evaluation: Oxidative Induction times for all the materials under study before and after aging experiments were evaluated by using differential scanning calorimetry. The normal practice for the determination of OIT is according to the procedure described in the ASTM⁸. However, in the recent times another technique known as High Pressure Differential Scanning Calorimetry (HPDSC) is gaining more popularity for the determination of oxidative induction time of polymeric materials⁹⁻¹⁴. It was argued that, in the conventional method the volatilization of the stabilizers and other additives in the polymer complicates the thermal and chemical reaction rates, due to the high temperatures that are used during the test. It was also found that there has been a lack of correlation between the OIT values determined by using the standard technique and the aging experiments which are typically performed at much lower temperatures. Further, it was found out that the thermal stability of a given material in the real life can not be predicted based on the OIT information obtained from the standard technique¹⁵.

One of the ways to overcome the limitations of the conventional OIT test method is to run the test by using a combination of pressure and temperature. There are two distinct advantages in using very high pressures in oxidation experiments:

1. The high pressure reduces the volatility of the various additives by elevating their boiling point.
2. The high pressure increases the concentration of the reacting oxidizing gas. This makes it possible to employ lower test temperatures or provides significantly shorter test times at equivalent temperature.

To run the experiments under the modified conditions of pressure and temperature, a high pressure DSC cell made by TA Instruments was used. It is basically a standard DSC cell surrounded by a canister rated for high pressure work (upto 1000 psi). The usual range of pressures used in PDSC work is between 3.45-5.51 MPa (500-800 psi). There are three modes of operation one can use to conduct OIT experiments under high pressures¹⁶.

1. Constant Volume
2. Static Constant Pressure
3. Dynamic Constant Pressure

Constant volume technique involves setting the pressure, closing the cell at ambient temperature and starting the experiment. The pressure may rise during the experiment as the temperature increases. Because of this, the exact pressure may be unknown.

Static constant pressure involves setting the target pressure with an auxiliary regulator and allowing the excess pressure created during heating to vent. This technique ensures that the system is at constant pressure during the course of the entire experiment.

Dynamic constant pressure involves a gas flow under pressure through the cell during the experiment. This is a preferred method if there are off-gas products formed during the experiment.

Static constant pressure technique was used in all the High Pressure Oxidative Induction (HPOIT) work described in this paper. Ultra high purity, extra dry grade oxygen at 5.17 MPa (750 psi) was used for the evaluation of HPOIT.

Tensile Property Measurements: Tensile elongation and tensile strength measurements on the UV and oven aged dumbbell specimens were performed according to the procedure described in the ASTM D 638. Instron Model 4206 Universal Testing Machine with Automated Series IX Data Acquisition Control and Analysis software was used for evaluating the tensile elongation and tensile strength.

RESULTS AND DISCUSSION

ULTRA VIOLET AGING STUDIES

Differential Scanning Calorimetry: The change in the DSC profiles for nearly all the materials undergoing ultraviolet exposure at various temperatures are presented in Figures 1 through 7. For Material A, which is a standard low density polyethylene (Fig. 1), the shape of the DSC curves is more or less well defined and in agreement

with the work done by several other researchers in the field⁴. At 50°C, for 6 weeks under UV exposure, there is virtually no difference in the DSC profiles, thus indicating no significant changes in the material. However, at 70°C, there is a well defined shoulder around 95°C but the melting temperature remained steady and did not show any shift. The broad shoulder was found to be due to secondary crystallization that is taking place in the material¹⁷. This secondary crystallization was the result of carbonyl group formation during the degradation process^{18,19}.

The situation is totally different with the other materials tested. The DSC profiles are much more complex and complicated. Figure 2 shows the DSC profiles of the Material B, which is a non-halogenated flame retardant compound based on ATH technology. This material showed very significant changes at the end of 6 weeks of aging at 50°C. At 60°C, (curve 3) after 1 week of aging, the profile looked very similar to the one at 50°C for 6 weeks. However, at 70°C (curve 4) the melting curve has shifted towards higher temperature. It is quite possible that there must be a reasonable amount of carbonyl group formation due to degradation at 50°C. As the UV exposure temperature is increased to 70°C, the melting peak became sharper, and shifted towards the high temperature. It appears that, at

higher temperatures the material must have undergone a significant amount of crosslinking reaction. In fact, the tensile property measurements showed that the tensile strength has increased by almost 18% indicating some type of crosslinking associated with ultraviolet aging.

For Material C (Fig. 3) which is also a halogen-free flame retardant composition based on magnesium salts, the change in DSC profiles at 50°C are less dramatic, suggesting virtually no change is taking place under ultraviolet radiation. At 70°C, the changes are rather complex. Even though, the main melting peak at 120°C did not shift, there were some significant transformations that took place below 120°C. These are reflected in the two characteristic endotherms present at 60°C and at 95°C.

Most of the flame retardant compositions (especially the nonhalogen type) are blended with several polymeric and non-polymeric additives. It is quite possible, during aging, many of the polymeric additives must have undergone a rapid degradation and/or crosslinking reactions producing a variety of low molecular weight species. These species tend to 'reorganize' or 'recrystallize' into distinct phases melting at specific temperature.

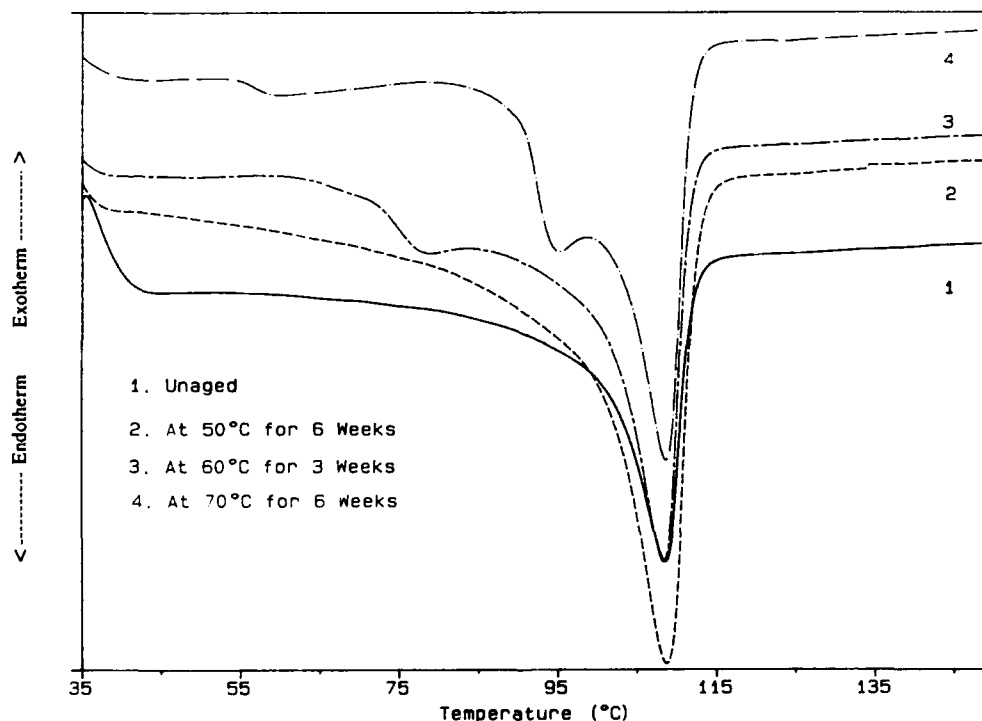


Figure 1. Change in DSC Profiles in UV Aging for Material A

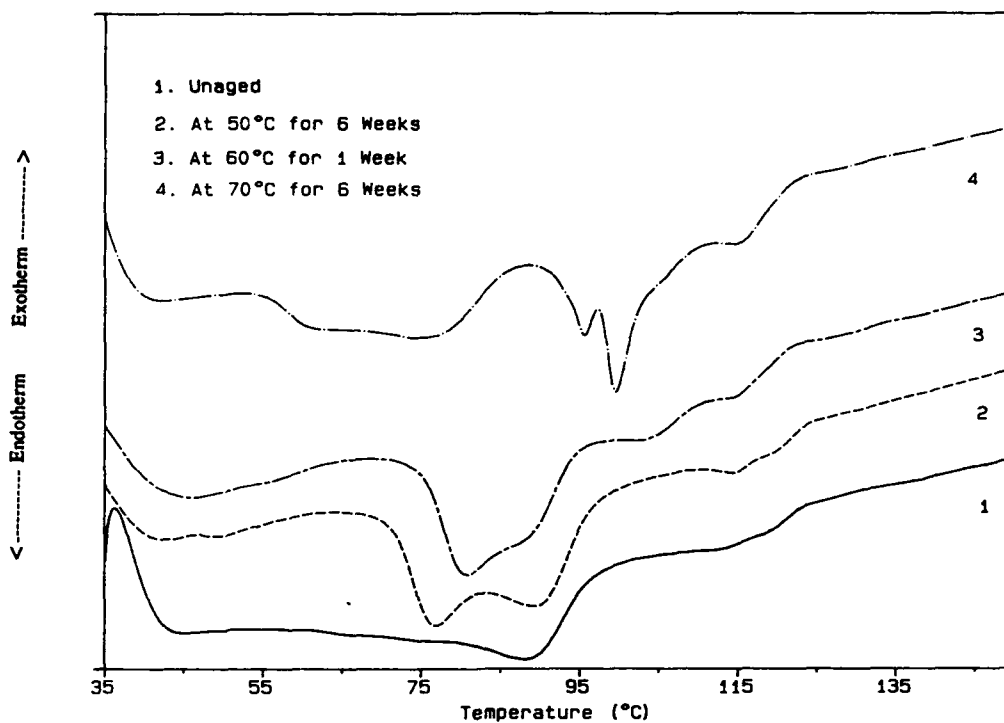


Figure 2. Change in DSC Profiles in UV Aging for Material B

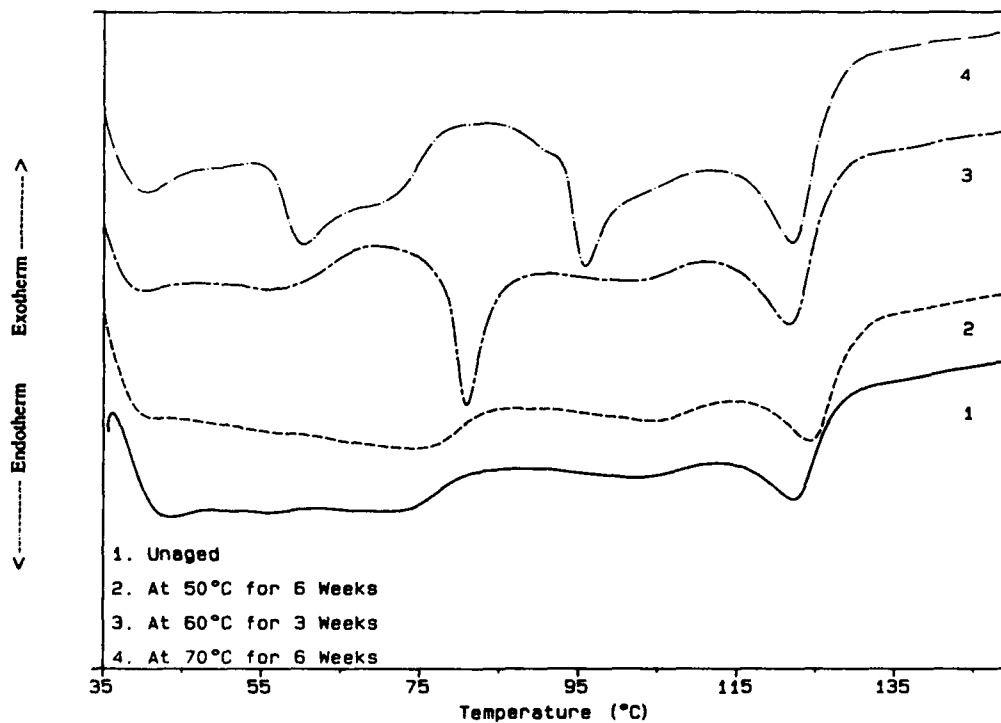


Figure 3. Change in DSC Profiles in UV Aging for Material C

No attempt was made either to study the course of carbonyl group formation using infrared spectroscopy or to isolate the gel fraction by solvent extraction technique.

The amount of useful information one can extract from a thermogram alone depends on the amount of the background information that is available on the material under evaluation. Unfortunately, almost all the flame retardant compositions are regarded as highly proprietary and hence none of the vendors are willing to disclose the composition of the material(s).

For Material D, (Fig 4) the profiles are very similar to Material A, because this is basically a low density polyethylene with brominated additives. Like Material A, in the case of Material D, there is no shift in the melting peak with aging time and temperature. As expected there is a noticeable shoulder at 70°C after 6 weeks of aging time. Comparing this with material A, one would be tempted to conclude that both these materials have identical UV stabilities. However, OIT and tensile studies have indicated that this material is highly susceptible to UV and thermooxidative degradation as discussed in the following sections. Examination of the DSC profile alone will not yield a conclusive evidence about the degradation of a particular material.

Material E, which is a nonhalogenated polyurethane compound the DSC profiles (Fig. 5) showed no significant changes with aging. Only at 70°C after 6 weeks of aging time the material exhibited a shoulder around 98°C. This does not mean that this material did not undergo any degradation under UV radiation. On the contrary, this material exhibited a very rapid and sudden degradation only after about 4 days of exposure in UV at 70°C (see under the discussion on tensile properties). It appears that in the case of Material E, the UV aging did not generate substantial quantities of carbonyl and hydroperoxide groups leading to the secondary crystallization as in the case of polyolefin based compounds.

For materials F and G, (Fig 6 & 7) the effects of UV radiation are rather less severe at 50°C due to the presence of an efficient stabilizer system. Even at 60°C the changes in the material are not significant. However, at 70°C, after one week, there is an appreciable change in the material which is reflected in the endotherm at approximately 100°C.

One important conclusion that can be drawn from the above DSC profiles is that, all the flame retardant compounds are highly susceptible to structural modifications

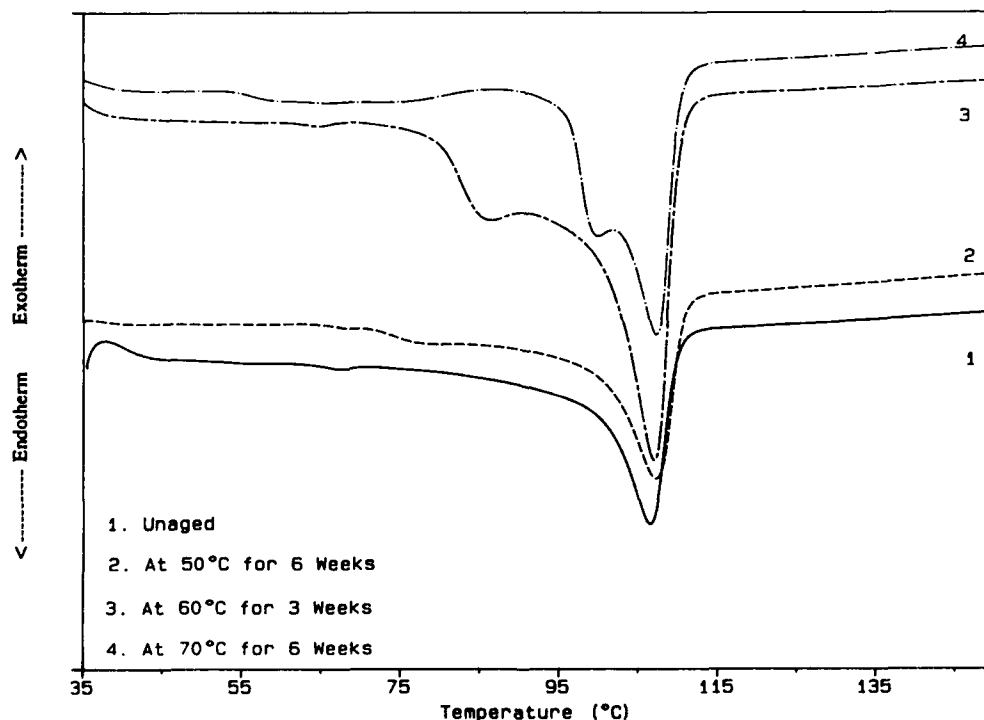


Figure 4. Change in DSC Profiles in UV Aging for Material D

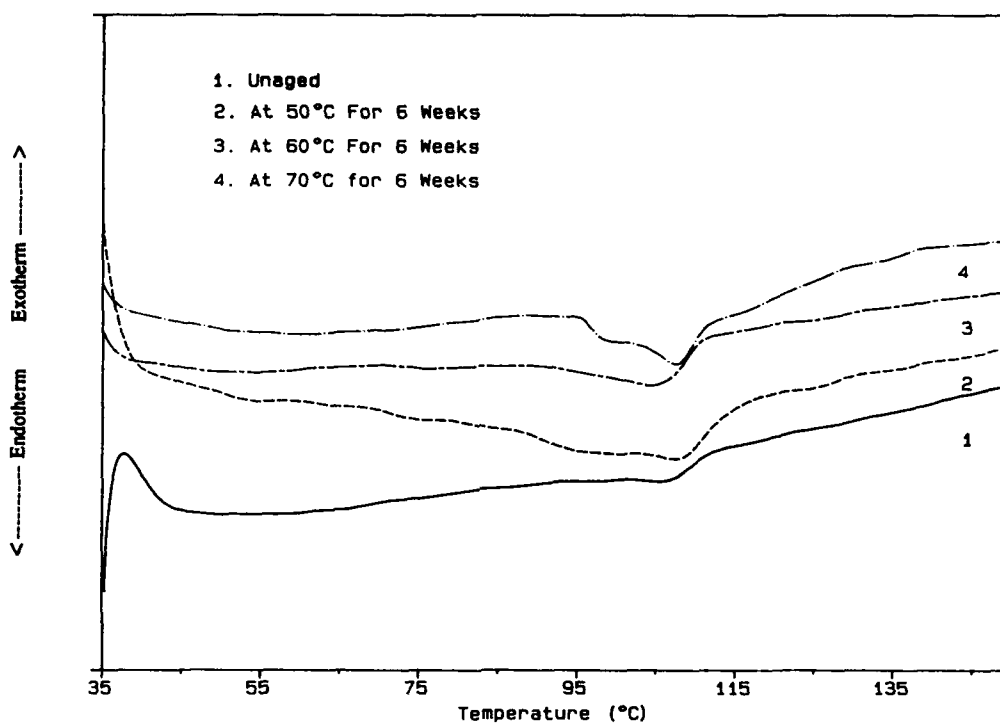


Figure 5. Change in DSC Profiles in UV Aging for Material E

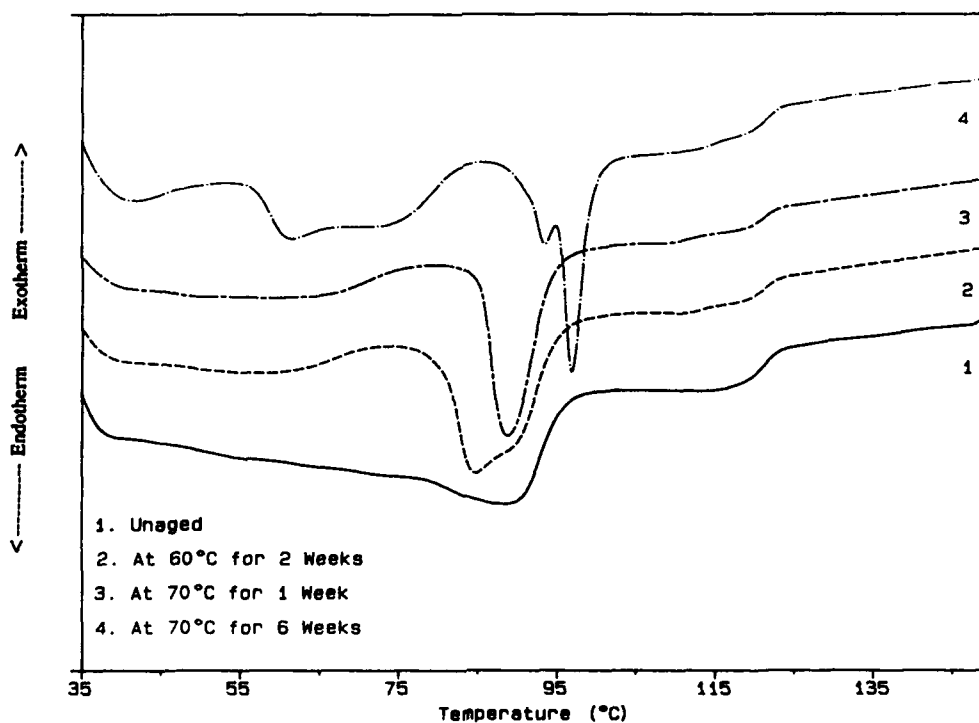


Figure 6. Change in DSC Profiles in UV Aging for Material F

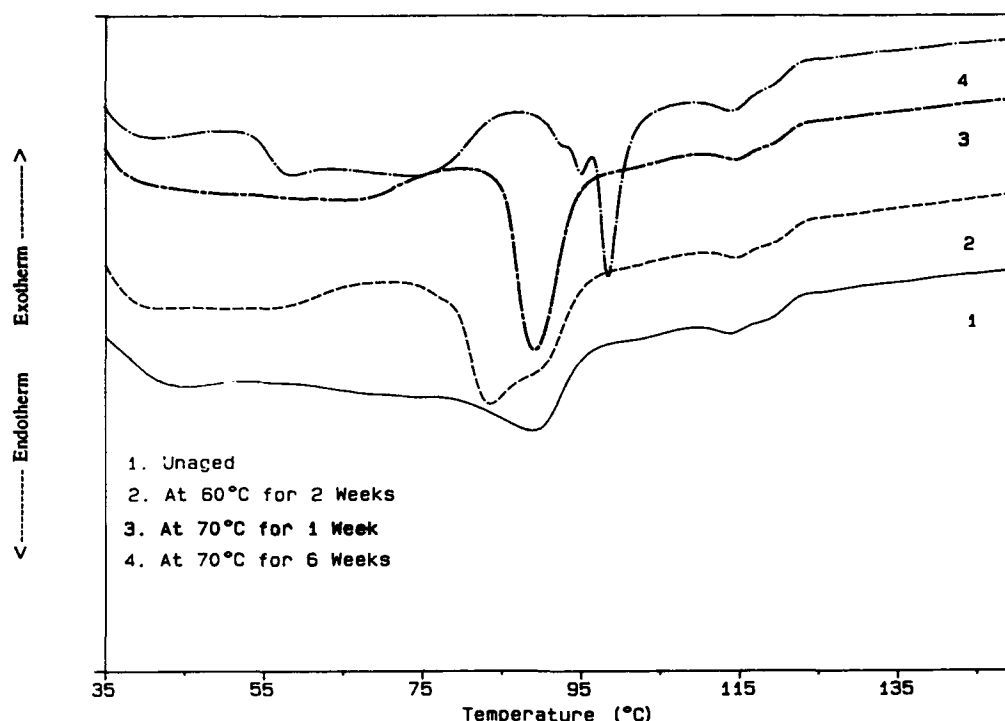


Figure 7. Change in DSC Profiles in UV Aging for Material G

(crosslinking, degradation etc.) within a short duration of UV exposure. These changes in the material behavior are further reflected in their oxidative induction times and tensile properties as discussed below.

High Pressure Oxidative Induction Time: The HPOIT values for all the unaged materials are presented in Table III. Each material has a characteristic OIT value. This is due to the nature, type, and concentration of the stabilizer package that is incorporated into the base material. Based on this information alone, it should not be assumed that Material A is less stable than Material B and so on. A more realistic way to predict the long term stability or durability of the materials is to evaluate the change in the HPOIT as a function of some type of aging or degradation process.

Residual Thermal Stability: Figures 8, 9, & 10 show the percent decrease in the high pressure oxidative induction time plotted against the aging time. The percent decrease in the induction time is defined as follows:

$$\text{Percent Decrease in OIT} = \frac{[\text{OIT}]_i - [\text{OIT}]_t}{[\text{OIT}]_i} \times 100 \dots\dots (1)$$

where: $[\text{OIT}]_i$ and $[\text{OIT}]_t$ are the initial and after an aging time 't' OIT values.

As expected the results showed a continuous decrease in the OIT both with aging time and temperature. However, at 50°C materials A, F and G showed only a minimal reduction in the OIT, whereas the other materials exhibited a fairly large drop in the OIT values. This trend continued as the temperature is increased to 60°C. Finally at 70°C, the drop in OIT is very rapid even for materials A, F, and G.

TABLE III

HIGH PRESSURE OXIDATIVE INDUCTION TIME (HPOIT) FOR VARIOUS MATERIALS

MATERIAL	HPOIT AT 180°C (min)
A	20.76
B	41.21
C	200
D	42.11
E	-
F & G	436.86

For material E the HPOIT is not meaningful.

The slopes of the plots shown in figures 8, 9, & 10 are calculated using the initial straight line regions of the each of the curves. It is assumed that these slopes are nearly equal to the rate constants for the degradation of the materials under study. The calculated rate constants are plotted against the reciprocal of the absolute temperature. Assuming an Arrhenius model:

$$k = A \exp(-E/RT) \quad \text{..... (2)}$$

where A is the frequency factor and R and T are the gas constants and temperature respectively.

Using the above equation one can calculate E, the activation energy for the polymer degradation. Since, most of the materials under investigation are blended with several components, it is rather inaccurate to assign a definite value for the energy of activation for the main chain scission based on the current observation. Instead, the frequency factor (A) was analyzed. Frequency factor is a relative measure of the frequency of reactive collisions in a given system²⁰. The values of A based on the calculations are presented in Table IV. It is evident that the frequency fac-

TABLE IV

FREQUENCY FACTOR OF MATERIALS

MATERIAL	FREQUENCY FACTOR A (min ⁻¹)
A	3.90 x 10 ⁵
B	5.51 x 10 ⁶
C	3.33 x 10 ⁶
D	1.53 x 10 ⁷
F & G	5.15 x 10 ⁵

tor values for materials A, F, & G is much smaller when compared to the rest of the materials. Under ordinary conditions, the rate determining step for the oxidation of the polymer is the initiation step by the radical from the hydroperoxide decomposition. If the reactive collisions are more, it can be assumed that the radical formation is much faster resulting in higher rates of degradation. It is therefore important to counter this by adding adequate amounts

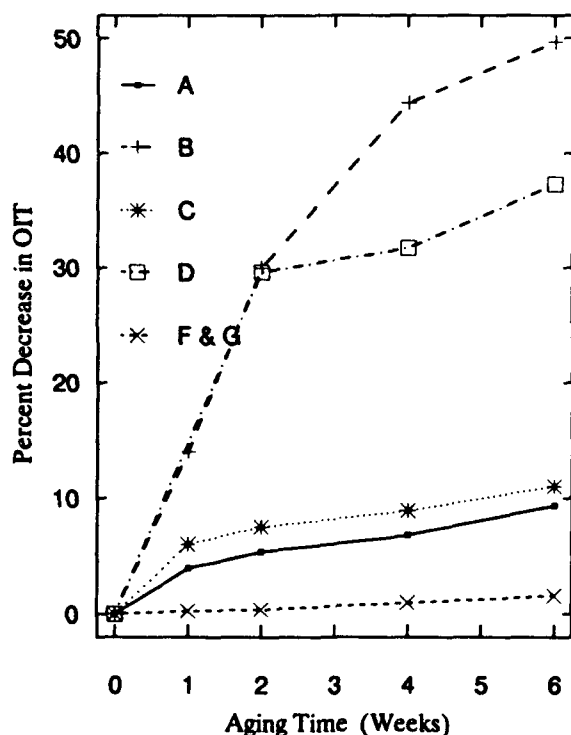


Figure 8. Percent Decrease in OIT vs Aging Time at 50°C

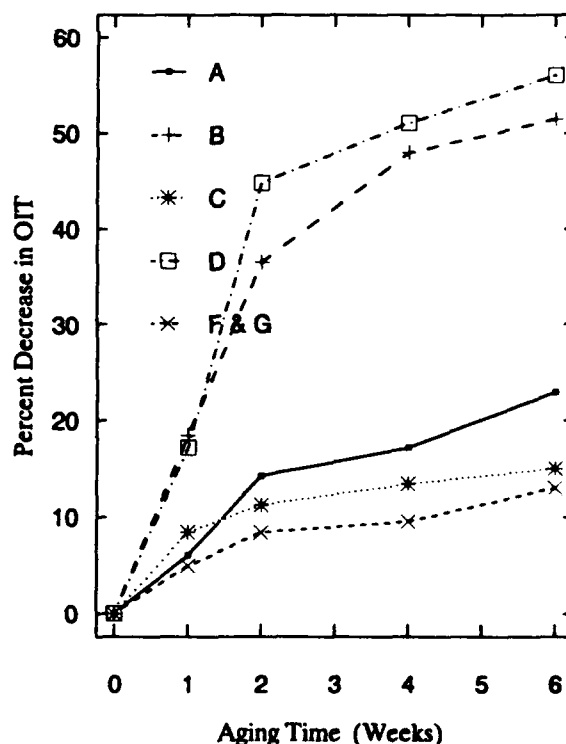


Figure 9. Percent Decrease in OIT vs Aging Time at 60°C

of suitable free radical scavengers and other light stabilizers into the flame retardant compound. Since the flame retardant formulation consists of several components, it is difficult to find a single light stabilizer to provide adequate UV protection. By virtue of its complex composition, a flame retardant compound may need more than one type of UV stabilizer (uv absorbers, quenchers, light screens etc.,) to counter the effects of UV radiation. A detailed study to understand the mechanism of degradation should be the first step towards optimizing a suitable UV package.

Tensile Properties: The elongation and tensile strength on the UV aged specimens are determined at regular intervals of time. The results are tabulated in the form of percent change in elongation and tensile strength from the original unaged values and are shown in Table V. It is clear from the table, with the increase in aging time and temperatures all the materials showed a continuous decrease in elongation. However, the changes in the tensile strength are rather unpredictable. For some materials, the TS first increased, then dropped and increased again. On the other hand, for some materials the TS either increased or decreased continuously. This type of behavior is also reflected in the DSC profiles (figures 1 thru 7) as discussed in the previous section. No elaborate work was done to fully understand the variations in the tensile strength of these materials.

Arrhenius models were developed based on the information on the changes in the elongation properties of the materials under study. For materials B, C, D, & E a drop in the elongation by 50% from the original value and for materials A, F, & G a 10% drop were taken as the end points. The 10% drop in elongation for materials A, F, & G was chosen because of the time constraints on the experimental evaluations, since these materials are much more stable than the rest.

Figures 11 & 12 show the Arrhenius plots for all the materials under study. The end point values are extrapolated to 20°C to determine how these materials behave at this temperature. The results are shown in Table VI. It is clear once again that, materials A, F, & G are far more resistant towards UV radiation when compared to the rest of the materials. However, caution should be exercised in using the extrapolated values, since this information was derived

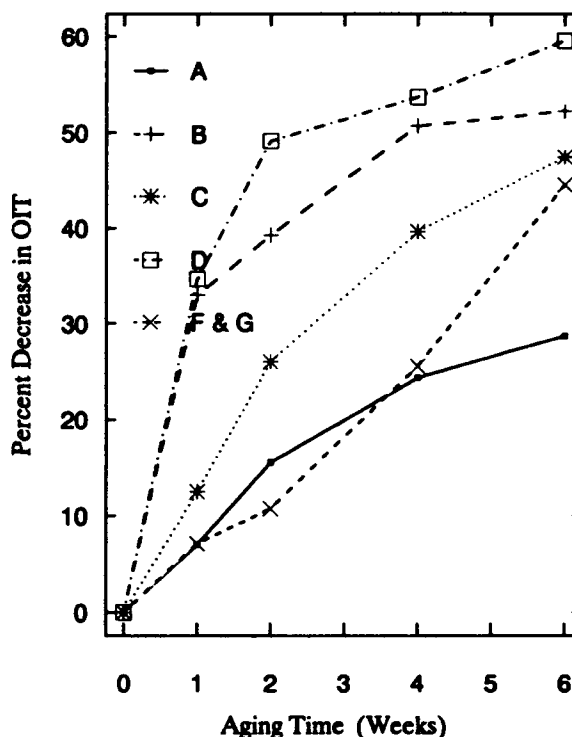


Figure 10. Percent Decrease in OIT vs Aging Time at 70°C

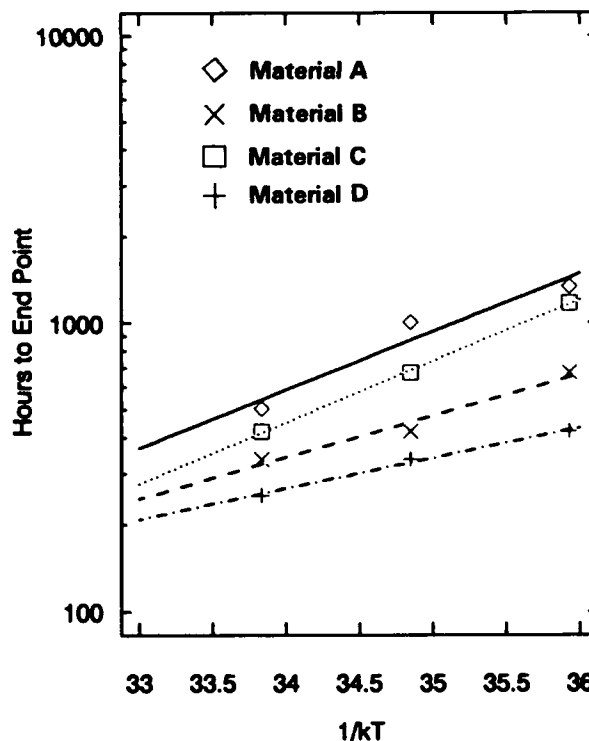


Figure 11. Arrhenius Model for UV Aged Materials

TABLE V
VARIATION OF TENSILE PROPERTIES OF THE MATERIALS DURING
UV AGING

MATERIAL	AGING TIME (WEEKS)	PERCENT CHANGE						COMMENTS
		50°C		60°C		70°C		
		E	TS	E	TS	E	TS	
A	1	0.80	2.30	1.75	2.76	3.60	4.36	TS has increased
	2	2.31	3.12	4.00	3.38	8.30	6.15	
	4	3.50	3.75	7.55	5.15	14.50	7.63	
	6	8.00	4.01	10.30	6.37	18.00	10.23	
B	1	31	2.31	33	2.46	35	11.42	TS at 60° and 70°C has increased first, then dropped.
	2	40	4.33	42	6.00	48.5	3.74	
	4	51	5.32	54	8.50	53.5	10.57	
	6	52	5.41	56	11.50	55.0	17.33	
C	1	1.30	5.00	33.83	1.83	38.52	13.60	TS has increased with aging time & temperature.
	2	8.53	6.33	39.15	7.00	46.70	14.38	
	4	22.72	8.15	48.63	12.90	55.00	15.00	
	6	41.46	9.00	55.00	14.15	67.53	19.02	
D	1	32.70	3.36	40.15	5.00	46.57	16.14	TS has increased at all aging times & temperatures.
	2	48.32	4.20	51.67	7.69	53.75	21.15	
	4	52.00	7.55	55.30	13.60	57.91	26.73	
	6	56.84	9.34	58.40	15.43	59.21	29.67	
E	1	1.23	1.24	2.20	6.00	38.00	45.66	TS decreased at all aging conditions.
	2	12.00	28.18	19.60	30.60	93.10	50.51	
	4	20.35	33.50	35.47	35.90	93.35	53.10	
	6	25.00	35.11	42.26	45.66	93.66	57.61	
F	1	0.50	1.67	1.45	2.35	3.31	3.87	TS first decreased and then showed an increase.
	2	1.34	2.45	3.77	2.55	8.00	5.50	
	4	3.45	3.50	10.32	3.76	15.17	2.67	
	6	5.50	4.00	15.90	5.10	17.00	6.00	

based on the accelerated testing under controlled conditions. Nevertheless, the information obtained is highly useful in comparing the relative stabilities of different materials.

One important conclusion is that the materials F & G behaved almost identical under UV exposure conditions. The only difference between them is that material F is the natural resin with UV stabilizer package, whereas, material G

contains carbon black in addition to the UV stabilizer package. This proves that, in the case of flame retardant compounds, simple addition of carbon black is not going to enhance their UV stability, unlike non-flame retardant polymers. It is therefore extremely important to incorporate a highly effective stabilizer package into the formulation in order to provide adequate ultraviolet stability to the flame retardant compounds.

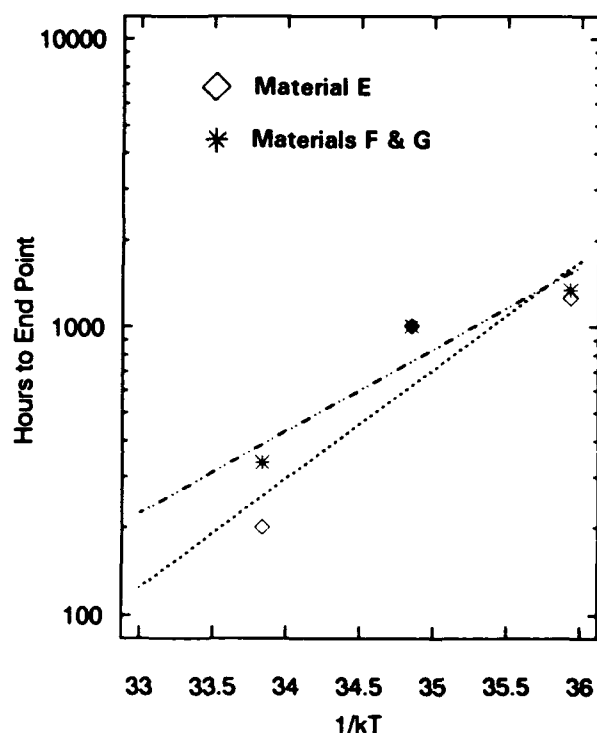


Figure 12. Arrhenius Model
for UV Aged Materials

TABLE VI

EXTRAPOLATION OF THE ARRHENIUS
MODEL

MATERIAL	END POINT CRITERIA (% DROP IN ELONGATION)	TIME TO REACH THE END POINT @ 20°C (hrs)
A	10	7,980
B	50	2,184
C	50	7,056
D	50	1,000
E	50	39,073
F & G	10	9,000

OXIDATIVE THERMAL AGING STUDIES

Differential Scanning Calorimetry: Figure 13 shows the DSC profiles of the oven aged materials in an oxidative atmosphere. The magnitude of changes in oven aging are rather small when compared to the aging in ultra-violet radiation. At 70°C after 12 weeks of aging time, the changes are not very significant (compare with the DSC profiles under UV aging conditions). The oxidation of the materials was also found to be more gradual and less dramatic with aging time when compared to aging under ultra-violet conditions. At 90°C, after 6 weeks, the DSC profiles on the materials started showing signs of rapid changes as reflected in their the endothermic peaks, indicating crystallization (Figure 14), degradation, and perhaps some degree of crosslinking. These changes became more and more significant as the aging time is increased to 12 weeks (Figure 15). Finally it can be seen that after 12 weeks of aging at 105°C (Figure 16), the materials exhibited more and more profound changes.

Comparison of the DSC profiles from the UV and oven aged samples has revealed that the specific temperatures where the endothermic peaks appear are different for the same material, even though, the general trend remained the same. In all the cases the endotherms have shifted toward the higher temperature. The area of the endothermic peaks formed after the oxidation is larger than the peaks in the unaged samples suggesting enhanced crystallinity with the increase in oxidation temperature and time. Table VII shows the percent change in crystallinity of the materials after 12 weeks of oven aging at various temperatures. It appears that the crystallinity has increased initially for all the materials after 12 weeks of exposure at 70°C. It then dropped as the temperature is increased to 90°C and to 105°C. This is attributed to the breaking of the chains in the amorphous phase and subsequent recrystallization by an annealing process. As the autooxidation proceeds during the aging, this process is disrupted and the crystallinity decreases. All the flame retardant compounds in the present study have very low levels of crystallinity. This is due to the high filler loading and the use of copolymers as the base materials. This makes them more susceptible to oxidative degradation when compared to the unfilled polymers. Further, a vast majority of these fillers are either inorganic salts or organometallic compounds. Consequently,

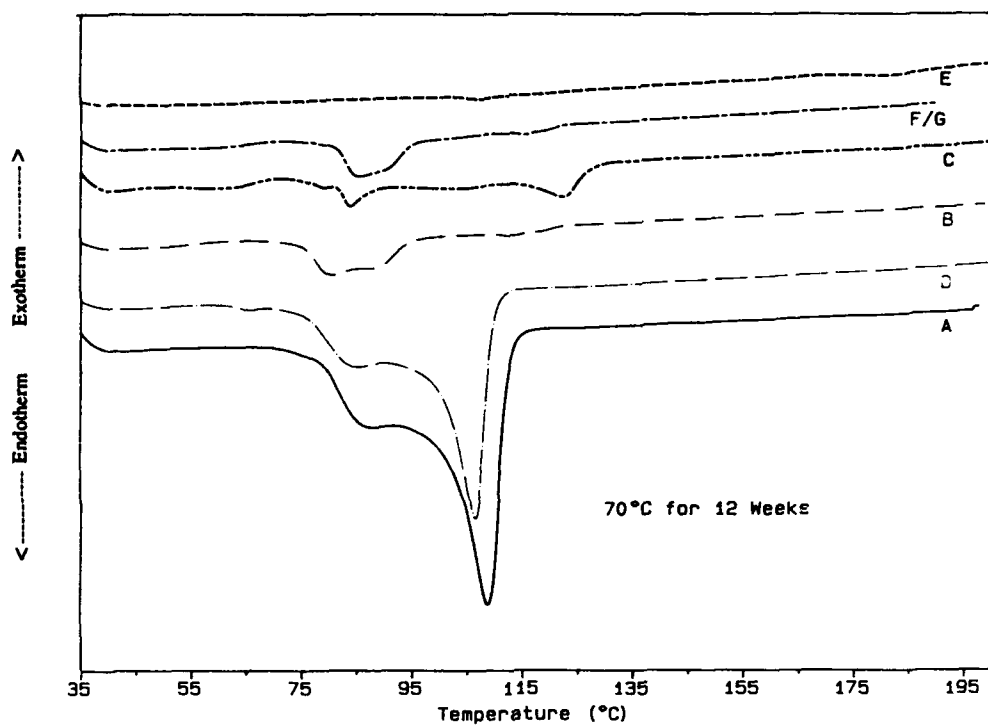


Figure 13. Change in the DSC Profiles for Oven Aged Materials

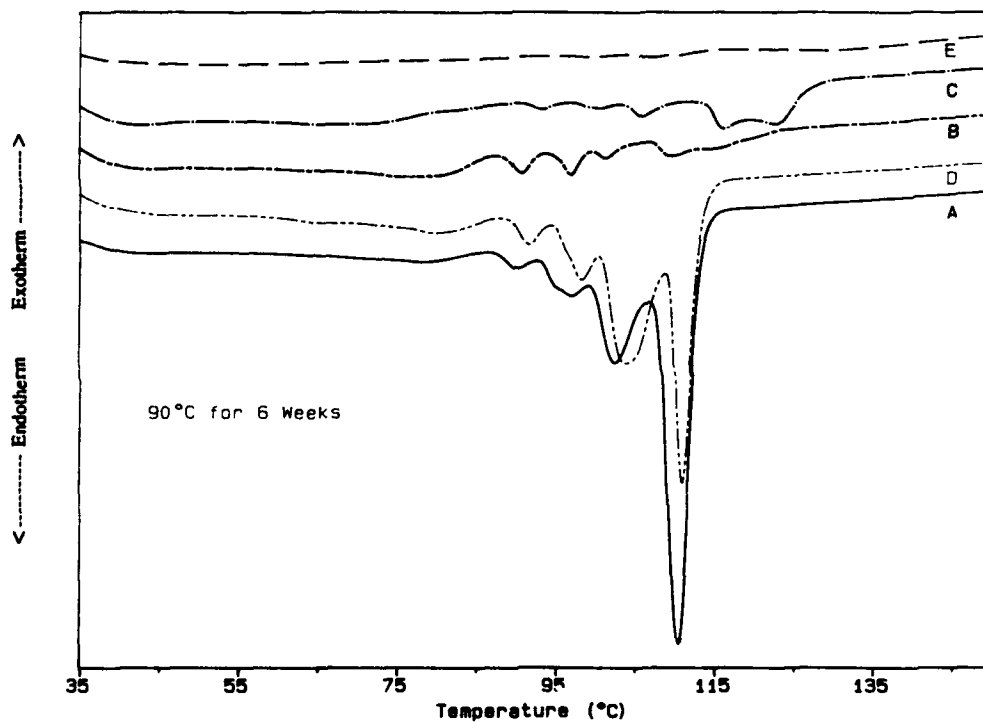


Figure 14. Change in the DSC Profiles for Oven Aged Materials

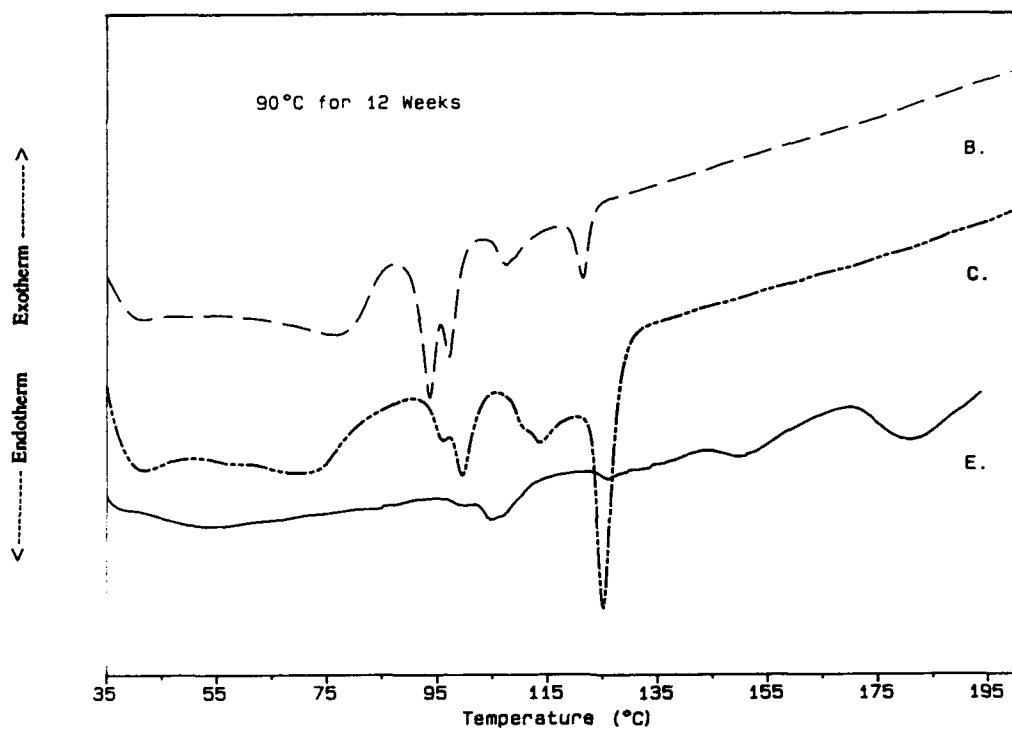


Figure 15. Change in the DSC Profiles for Oven Aged Materials

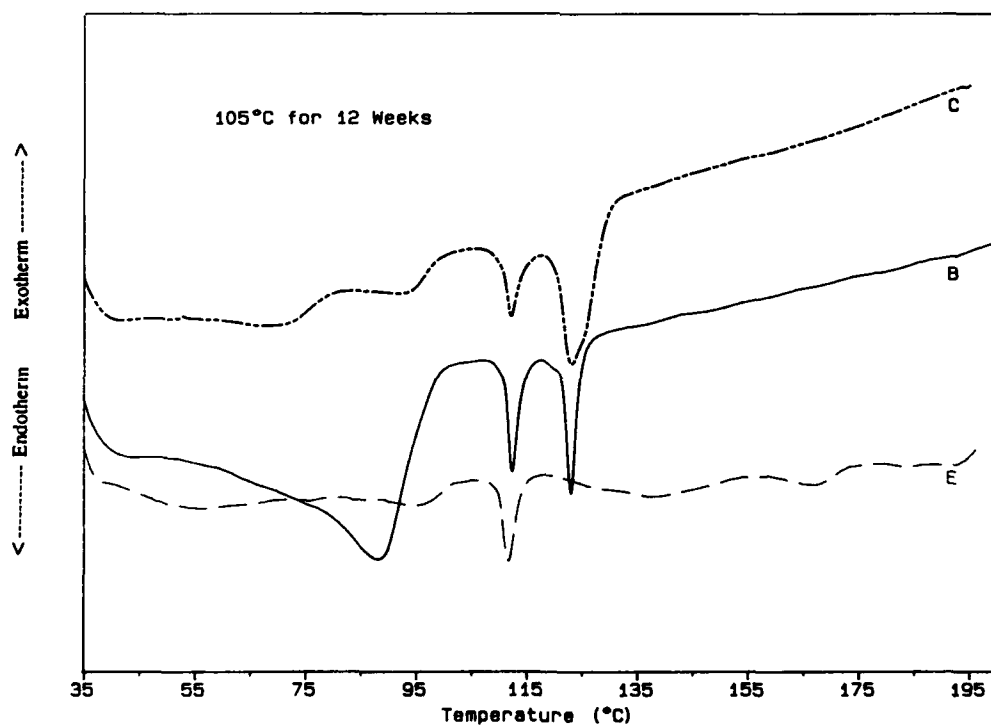
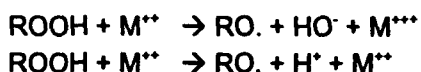


Figure 16. Change in the DSC Profiles for Oven Aged Materials

TABLE VII
CHANGE IN CRYSTALLINITY DURING OVEN AGING FOR VARIOUS MATERIALS

TEMPERATURE (°C)		70	90	105
TIME (HOURS)		2000	2000	2000
CHANGE IN CRYSTALLINITY (%)	A	27.58 → 34.61	SAMPLE MELTED	SAMPLE MELTED
	B	4.79 → 7.57	4.79 → 3.16	4.79 → 6.26
	C	2.59 → 6.02	2.59 → 4.00	2.59 → 3.04
	D	16.56 → 23.17	SAMPLE MELTED	SAMPLE MELTED
	E	1.77 → 2.38	1.77 → 3.26	1.77 → 0.62
	F & G	4.88 → 3.96	4.88 → 2.55	4.88 → 4.25

these fillers exert a strong catalytic effect on the oxidation of the polymer matrix. The fundamental chemical reaction involving the free radical formation is the reaction between the metal ion and the hydroperoxides to produce the free radicals⁴ thus:



The overall reaction of these two consecutive reactions is the bimolecular decomposition of hydroperoxide as shown below:



The above reactions clearly demonstrate the role of metal ions in the formation of free radicals and subsequent degradation of the polymer molecule. A similar type of reaction can be envisioned with trivalent metal ions such as aluminum or chromium. In addition to the metallic salts, processing aids can also enhance the degradation of polymers.

The effect of oven aging on the flame retardant compounds was further studied by analyzing their residual oxidative induction time as discussed in the next section.

Residual Thermal Stability: The residual thermal stability of the different materials was evaluated in terms of their oxidative induction time as outlined in the section under ultraviolet aging studies.

Table VIII shows the percent drop in the oxidative induction time values for various materials after six weeks of oven aging in an oxidative atmosphere. These values were calculated using the equation (1). It is clear from the data, that there is no dramatic drop in the thermal stability of the materials during the first six weeks of oven aging. Further, the drop in OIT is not very much noticeable when the temperature was increased from 70°C to 90°C. However, at 105°C, all the materials started showing significant drop in the induction time. This is a contrast to the OIT values obtained under ultraviolet exposure conditions, where the drop was much more rapid with temperature. In the case of thermal oxidation, the overall oxygen absorption and the formation of the end products are more or less autocatalytic. In the case of the materials in the present study, it appears that the hydroperoxide formation and the subsequent generation of free radicals for the initiation of the chain scission is taking place after 6 weeks of aging at 90°C.

TABLE VIII

**CHANGE IN THE OXIDATION INDUCTION TIME OF THE MATERIALS
AFTER OVEN AGING FOR 6 WEEKS**

MATERIAL	AGING TEMPERATURE (°C)	DECREASE IN OIT (%)
A	70	2.93
	90	6.40
	105	Sample Melted
B	70	0.50
	90	1.65
	105	22.54
C	70	1.00
	90	1.57
	105	10.00
D	70	0.95
	90	11.25
	105	Sample Melted
E	-	***
F & G	70	0.35
	90	1.40
	105	12.67

*** For Material E the OIT values are not meaningful.

The oven aging was continued upto a maximum of 16 weeks. However, after 8 weeks the induction time dropped very rapidly. Materials A and D softened and deformed after 8 weeks at 90°C and within a couple of weeks of exposure at 105°C.

Tensile Properties: The elongation and the tensile strengths of the materials were measured at various time intervals during the oven aging. These values are tabulated in Table IX. It is evident from the table that the tensile properties of the materials (except for Material D) did not show a dramatic drop during the 6 weeks of aging at 70°C. As the temperature is raised to 90°C, materials B, C, and D started showing noticeable degradation in tensile elongation. Materials E, F, and G did not show very significant change in tensile properties. At 105°C, after 6 weeks of aging time all the materials exhibited substantial change in the tensile elongation. The tensile strength of the oven

aged materials showed more gradual decrease than the UV aged samples.

In studies involving the oxidation of single, unfilled polymer systems, it is possible to derive a correlation between the oxidative induction time and the tensile properties. However, when dealing with the flame retardant compositions involving a combination of several additives, it is extremely difficult to find such a correlation. In spite of this limitation, the present study indicated some correlation between oxidative induction time and tensile properties.

The present study has revealed several important aspects of ultraviolet and oxidative thermal degradation involving the flame retardant cable sheathing compounds. However, further work is needed to understand more about the mechanistic aspects of the degradation involving the flame retardant compounds. One study that warrants immediate attention is the determination of molecular weight and mo-

molecular weight distribution of the oxidized polymer. It has been established that the molecular weight measurements on the aged samples is the most sensitive indicator of oxidative degradation, especially during the induction time²¹.

As mentioned previously, all these materials are highly proprietary in nature and hence the nature of the base polymer(s) (homopolymer, copolymer, block polymer, or a blend of several polymers etc.,) as well as the amount and the type of the stabilizer(s) in these materials is unknown. It is highly probable that the presence of stabilizers and fillers in the polymer matrix influences the induction time and hence the course of thermooxidative and ultraviolet degradation. It is therefore very important to select suitable stabilizers and other additives while formulating a flame retardant compound for a high level of ultraviolet and oxidative thermal stability.

CONCLUSIONS

The following important conclusions can be drawn from the above study on the ultraviolet and oxidative thermal degradation of flame retardant cable sheathing compounds:

1. All the flame retardant compounds selected for this study showed a high degree of degradation under ultraviolet exposure conditions than in oxidative oven aging.
2. Degradation was found to be a linear function of temperature and time of exposure in the initial stages both under UV and thermooxidative conditions of aging.

TABLE IX
CHANGE IN THE TENSILE PROPERTIES OF THE MATERIALS AFTER
OVEN AGING FOR 6 WEEKS

MATERIAL	TEMPERATURE (°C)	ELONGATION (%)		TENSILE STRENGTH PSI	
		INITIAL	FINAL	INITIAL	FINAL
A	70	695	663	2316	2248
	90	695	546	2316	2057
	105***	-	-	-	-
B	70	130	120	2030	1957
	90	130	93	2030	2245
	105	130	70	2030	2005
C	70	154	123	1582	1985
	90	154	90	1582	1868
	105	154	62	1582	1809
D	70	143	65.5	1412	1629
	90	143	39.0	1412	1803
	105***	-	-	-	-
E	70	730	476	2019	1284
	90	730	450	2019	1249
	105	730	50	2019	807
F & G	70	224	181	1797	1825
	90	224	150	1797	1860
	105	224	120	1797	1780

*** Sample softened and deformed at 105°C

3. The DSC profiles have indicated that the degree of crystallinity first showed an increase, then a drop as the aging temperature is increased.
4. Under ultraviolet aging conditions, there is a good correlation between the high pressure oxidative induction time analysis and the tensile properties. Data on the frequency factor is a valuable measure of the degree of polymer degradation.
5. The tensile properties of the materials exhibited a gradual decay with aging. Tensile elongation decreased both the aging time and temperature. The tensile strength was more erratic with aging. This may be due to the complex crystallization reactions and rearrangements within the materials.
6. The presence of carbon black in the flame retardant compounds (halogenated and nonhalogenated) did not enhance their ultraviolet stability, like in the case of non-flame retardant black jacket compound. It is therefore absolutely necessary to add a suitable UV stabilizer package to the flame retardant compound.
7. Further addition of carbon black into the UV stabilized flame retardant compound did not show any significant enhancement in UV stability.
8. It was hypothesized that the metallic salts used as flame retardant additives in the compound are primarily responsible for catalyzing the polymer degradation reactions.

REFERENCES

1. Harry S. Katz and John V. Milewski
Handbook of Fillers for Plastics
Van Nostrand Reinhold Company,
New York, 1987., pp. 277-385.
2. S. Rampalli and H. R. Nudd
Proc. 40th Intl. Wire & Cable Symposium,
St. Louis, Missouri, USA., November 1991,
pp. 66-76.
3. Tibor Kelen
Polymer Degradation
Van Nostrand Reinhold Company,
New York, 1983.
4. Norman S. Allen
Degradation and Stabilization of Polyolefins.
Applied Science Publishers, London, 1983.
5. H. H. G. Jellinek
Degradation and Stabilization of Polymers
Elsevier Publishing Company, Amsterdam,
Netherlands, 1983.
6. ASTM D 638
Tensile Properties of Plastics
American Society for Testing and Materials,
Philadelphia, PA, USA., 1992.
7. ASTM G 53
Operating Light-and Water-Exposure Apparatus(Fluorescent UV-Condensation Type) for Exposure of Nonmetallic Materials.
American Society for Testing and Materials,
Philadelphia, PA, USA., 1992.
8. ASTM D 3895
Copper-Induced Oxidative Induction Time of Polyolefins by Thermal Analysis.
American Society for Testing and Materials,
Philadelphia, PA, USA., 1992.
9. M. W. Cadwallader and P. Metzger
Proc. of the 42nd Purdue Industrial Waste Conference, West Lafayette, Indiana. 1987.
10. M. W. Cadwallader
Proc. of the 4th Intl. Conf. on Geotextiles, Geomembranes and Related Products,
The Hague, Netherlands, 1991.
11. G. Dugan and J. D. McCarty
Proc. 13th North American Thermal Analysis Society Conference, Philadelphia, PA, 1984.

12. I. Rhee
Proc. of the 57th Annual Meeting of the National Lubricating Grease Institute, Denver, Colorado, 1990
13. R. W. Thomas and C. R. Ancelet
Geotechnical Fabrics Report, Vol. 10, No. 5, pp. 12-13, 1992.
14. R. W. Thomas, C. R. Ancelet, and J. E. Brzuskiwicz
Proc. of the Annual Technical Conference of the Society of Plastics Engineers (ANTEC) New Orleans, LA, 1993.
15. T. Tikuisis, P. Lam and M. Cossar
Proc. of the 6th Geosynthetic Research Institute, Philadelphia, PA, USA., 1992.
16. TA Instruments Manual on 2910 DSC Module.
17. S. H. Hamid, F. S. Qureshi, M. B. Amin, and A. G. Maadah
Polym. Plast. Technol. Eng., 28, 475-492 (1989)
18. N. C. Billingham, P. Prentice, and T. J. Walker
Polym. Sci. Symp., 57, 287-297 (1976)
19. M. Sebaa, C. Servens, and J. Pouyet
J. Appl. Polym. Sci., 45, 1049-1053 (1992)
20. A. K. Bhowmick, S. Rampalli, and D. McIntyre
J. Appl. Polym. Sci., 30, 2367-2388 (1985)
21. A. Holmstrom and E. M. Sorvik
J. Polym. Sci., Polym. Chem. Edition, 16, 2555-2586 (1978)

ACKNOWLEDGEMENTS

I would like to extend my sincere appreciation to several of my colleagues who either directly or indirectly helped me during this work. Special thanks to Mr. John Gizowski for his excellent and meticulous laboratory work on thermo-analytical and tensile measurements. I would like to ex-

tend my sincere appreciation to Mr. John DeSana, Cable Business Unit Manager, and to Mr. Rick Guipe, Vice President, HELIAX® Products, for their support and encouragement.

Finally, I am grateful to the management of Andrew Corporation for granting me the permission to communicate this paper.



Sitar Ram Rampalli is a Materials Engineer, associated with the HELIAX® Products Group, Andrew Corporation, Orland Park, Illinois. He received his Ph. D. Degree in Chemistry from the Indian Institute of Technology, Bombay, India, and a Master's Degree in Polymer Science from the University of Akron, Akron, Ohio. He is currently responsible for the selection, evaluation, and recommendation of various polymeric materials for wire and cable applications. He holds five patents and several publications in scientific and technical journals.

Dr. Rampalli is a Senior Member in the Society of Plastics Engineers, and a member in the American Chemical Society. He is a part-time instructor at the Illinois Institute of Technology, and at DePaul University, in Chicago, Illinois, and teaches graduate level courses in polymer characterization and analysis.

Dr. Rampalli's research interests are in the application of polymer characterization techniques for wire and cable materials, polymer degradation and structure-property relationship studies.

A Study on Fire-retardant Optical Cable, II

H. Kanzaki S. Shimizu A. Otake

The Furukawa Electric Co., Ltd.
6, Yawata-kaigandori, Ichihara, Chiba, Japan

ABSTRACT

The characteristics of fire retardant optical cable were investigated.

While keeping the cable core temperature approximately below 400°C under the heat condition that the temperature reaches to 840°C for 30 minutes, on the basis of the concept of suppressing temperature rise of the cable core by making use of heat insulation and heat absorption action, the cable structures of using heat insulating materials such as ceramic fiber yarn and flame-retardant plastic tape were tested.

It has proved that a practical fire retardant optical cable with outer diameter of 31 mm can be realized by using flame retardant tape as insulator.

1. Introduction

The fire retardant cable used in a safety and security facility is required to maintain its function for a certain time after beginning of a fire.

Previously it was reported that the characteristics of fire retardant optical cable on the basis of the concept of suppressing temperature rise of the cable core by making use of heat insulation and heat absorption action¹⁾. Some kinds of paper excellent in heat resistance were used as insulator, and during heating test that temperature reached to 840°C for 30 minutes, the cable core temperature was kept under 420°C. Paper, however, releases smoke and flammable gas along with the progress of decomposition by heat. Accordingly, steel corrugated tube was provided to suppress combustion of paper and gas was entrapped at the same time. This structure was considerably large in the outside diameter as compared with an ordinary cable for the extra provisions of heat absorption layer and heat insulation layer, and the outside

diameter was 43 mm.

In this study, while keeping the cable core temperature approximately below 400°C, on the basis of the same concept, 1) the structure of using non-flammable heat insulating material that hardly generates gas even at high temperature, and, 2) the structure of smaller cable diameter were studied.

2. Cable design

Cross sectional structure of cable is shown in Fig.1.

2.1 Cable core

As the optical fiber, the 50/125 graded-index optical fiber was used because it is advantageous for short distance communication.

The optical unit was in heat resisting coated structure that three silicon resin coated fibers were stranded and jacketed with PFA (poly tetrafluoroethylene-perfluoroalkylvinyl ether copolymer).

To protect the optical fiber from mechanical stress of cable constituent material, an optical unit was inserted into the slotted core made of aluminum alloy, and the structure was covered with aluminum alloy tube with outer diameter of 6 mm. The aluminum alloy resists up to 400°C.

2.2 heat absorption layer

As the heat absorbing material, polyethylene (PE) containing 83 wt.% of magnesium hydroxide (Mg(OH)₂) was used, considering onset of endothermic reaction relatively at low temperature, low price, and ease of processing, and it was extruded to cover the cable core to outer diameter of 13 mm.

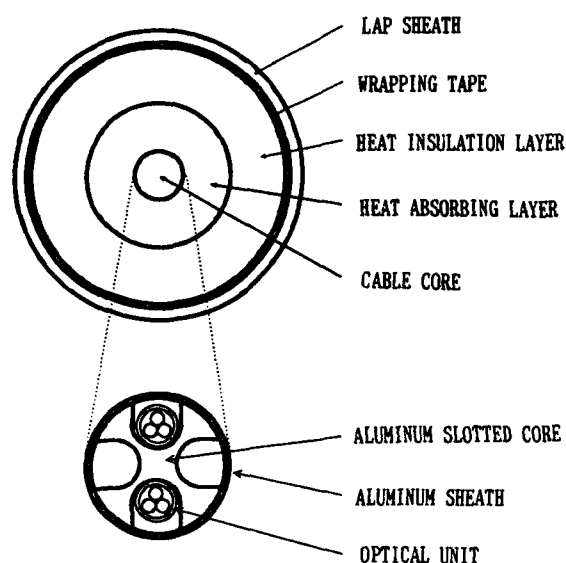


Fig.1 Structure of fire retardant optical cable

2.3 Heat insulation layer

Cables were compared by winding alumina-silica ceramic fiber yarn, or special flame retardant plastic tape, on the heat absorption layer.

Ceramics are heat insulating materials with an excellent heat resistance, but are not flexible in bulk state. To endow with flexibility, accordingly, they were formed into fibers and a multiplicity of yarns were wound for the convenience of fabricating the cable.

However, it is easy to fabricating cable because the thick insulating layer can be easily formed by wrapping the thick flame retardant plastic tape. It was made by mixing EVA (Ethylene vinyl alcohol) and EP rubber and endothermic reaction material.

2.4 Cable sheath

The cable sheath was a LAP (laminated aluminum polyethylene) sheath in order to reduce the cable weight and outer diameter.

Table 1 Heating test condition and results

Item	Value
1) Test sample	
Sample cable Length	1.3 m
weight load	2 times own weight of sample cable
2) Optical transmission test	
Optical fiber	50/125 graded-index fiber
	3-core loop
Measuring wavelength	1.3 μm

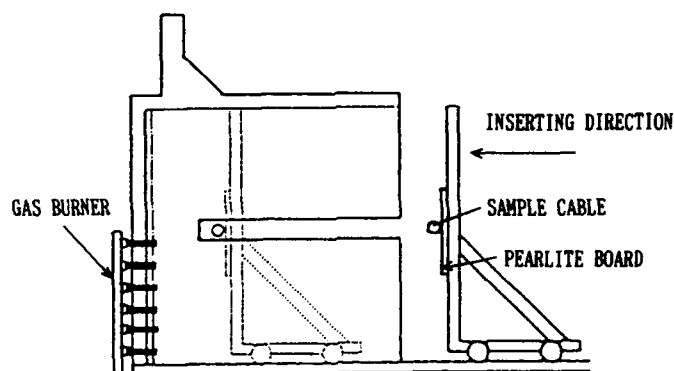


Fig.2 Heating test method

In the test sample, ordinary polyethylene was used in order to evaluate the effect of internal structure, but it is thought that the fire retardation will be much enhanced by using flame retardant polyethylene.

3. Test method

3.1 Cable structure

Two optical units were mounted, and thermocouples were put in two slots of the aluminum slotted core in order to measure the cable center temperature.

Two types of cables differing in insulating layer were tested.

The insulating layer thickness of type A was 11 mm by determining the optimum thickness by numerical calculation from the thermal conductivity and other properties of the ceramic yarn. The cable outside diameter was 43mm.

In type B, since numerical calculation of the insulating effect of the flame retardant tape was difficult, the insulating layer was tested in three thickness types, b-1: 6 mm, b-2: 7.5 mm and b-3: 12 mm, and the optimum thickness was determined. The cable outside diameter was respectively 31, 33 and 43 mm.

3.2 Test apparatus and test conditions

The test conditions are summarized in Table 1 and the test apparatus is shown in Fig.2. A cable sample of 1.3 m in length was horizontally and straightly fixed on a vertical perlite plate. A weight two times the own weight of cable sample was suspended in the middle part of the sample.

As shown in Fig.3, loss change were measured at wavelength of 1.3 μm by jointing three fibers in one optical unit in a loop.

The samples were heated for 30 minutes according to the heating curves shown in Fig.4 and 5. In 30 minutes after starting heating, the temperature in the heating furnace reaches 840°C.

4. Test results and discussion

Cable core temperature and optical loss change are shown in Fig.4 and Fig.5.

4.1 Temperature in cable core

1) Cable type A

The temperature first rose up slowly, and then sharply from 10 minutes after start of heating. In about 19 minutes to 30 minutes, the temperature was maintained around 400°C by endothermic reaction of magnesium hydroxide.

The maximum temperature during the test was 406°C. It was thought that the soundness of the cable core be maintained because the cable core temperature was maintained almost at the resisting temperature (400°) of aluminum alloy.

2) Cable type B

The temperature rise pattern was similar to that in Fig.4, expect that the temperature rise speed was dull around 200°C. This is because of the endothermic material contained in the flame retardant tape.

In the case of sample b-1, the endothermic reaction of magnesium hydroxide terminated about 4 minutes before end of combustion test, and the temperature began to rise gradually and reached to 461°C at the end of test.

In sample b-2, the test finished before the end of endothermic reaction of magnesium hydroxide, and in sample b-3, the initiating temperature of endothermic reaction of magnesium hydroxide was reached only at the end of test.

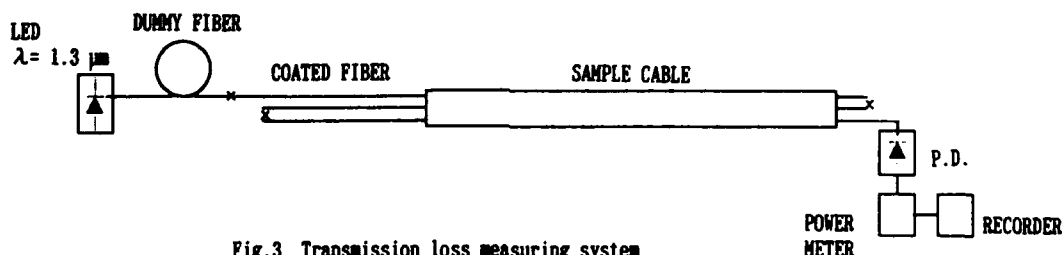


Fig.3 Transmission loss measuring system

The test ending temperatures were 393 and 374°C, respectively.

Sample b-1 presented a temperature profile similar to that of cable type A, which suggests the heat insulating effect is similar.

4.2 Optical fiber loss

As shown in Fig.4 and Fig.5, no optical fiber breakage was found regardless of the type or thickness of insulating layer. The loss changes were within 0.02 dB per an optical unit.

4.3 Appearance changes

The LAP sheath was burnt in about 15 minutes after start of test.

After the combustion test, cable type A retained almost a straight shape, while cable type B was bent 10 to 29 mm

due to effects of the weight and heat.

As a result of disassembly and investigation of cables, the following findings were obtained.

- In cable type A, there was no change in appearance in the ceramic fiber yarn of insulating material.
- In cable type B, the flame retardant tape was partly burnt and the inside was carbonized.
- The heat absorbing material was dehydrated, and was calcined.
- No abnormality was noted in the appearance of the aluminum alloy of cable core.
- The PFA jacket of optical unit was melted, but the silicon coating was not changed in appearance and presented a sound look.

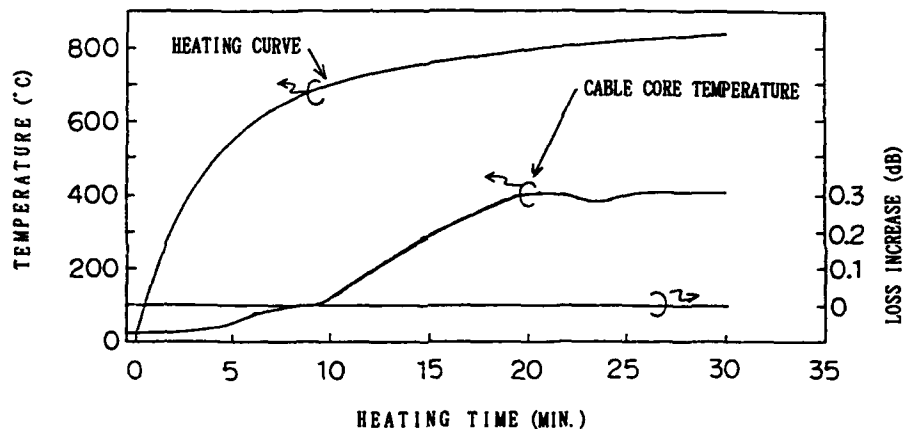


Fig.4 Test results of type A

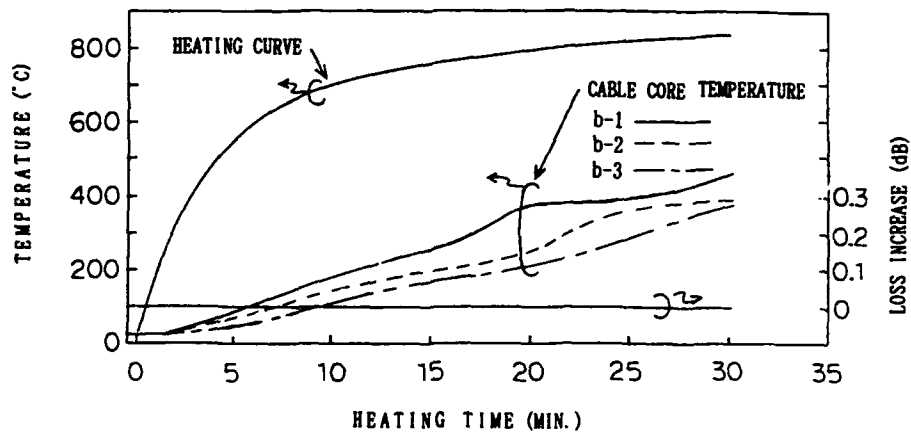


Fig.5 Test results of type B

5. Conclusion

Above results were summarized as following:

- 1) The silicon coated optical fiber was found to retain the soundness in appearance by suppressing the cable core temperature around 400°C in the fire resisting test condition.
- 2) The slotted core was kept nearly at the same heat resisting temperature (400°C) as the aluminum alloy, and the soundness is regarded to be maintained.
- 3) The flame retardant tape used in the test exhibits an equal heat resisting effect by a smaller thickness than the ceramic fiber yarn, so that it is effective for reducing the cable diameter.
- 4) In both types, in the heating test up to 840°C in 30 minutes, loss changes of optical fibers were hardly observed.

Thus, excellent results were exhibited. In particular, in the cable using flame retardant tape as insulator, when the thickness of the flame retardant tape layer is 6 mm, the cable outside diameter is 31 mm, and the diameter could be reduced without deterioration of fire retardant properties.

It was concluded that a practical fire retardant optical cable can be realized by the designed based on the concept of making use of heat resisting and absorbing actions.

Reference

- 1) S. Shimizu, K. Nakata, S. Ikegami, K. Omae and S. Sentsui
A study on fire-retardant optical cable.
IWCS, 1990



Hideaki KANZAKI

The Furukawa Electric
Co., Ltd.
6, Yawata-kaigandori,
Ichihara, Chiba, 290, Japan

Mr. Kanzaki graduated from Kurayoshi Technical school and joined The Furukawa Electric Co., Ltd. in 1969. He has been

engaged in development of optical cables.

He is now a staff engineer of optical fiber transmission research section, and is a member of The Institute of Electronics, Information and Communication Engineers of Japan.



Shigeo SHIMIZU

The Furukawa Electric
Co., Ltd.
6-1,2-chome, Marunouchi,
Chiyoda-ku, Tokyo, 100,
Japan

Mr. Shimizu has received the B.S. degree in engineering from Nagoya University in 1980. He joined The Furukawa Electric Co., Ltd. in 1981 and has been engaged in development of optical fibers and cables.

He is now a staff engineer of optical fiber transmission research section, and is a member of The Institute of Electronics, Information and Communication Engineers of Japan.



Akihiro OTAKE

The Furukawa Electric
Co., Ltd.
6, Yawata-kaigandori,
Ichihara, Chiba, 290, Japan

Mr. Otake graduated from Tohoku University and joined The Furukawa Electric Co., Ltd. in 1974. He has been engaged in research and development of optical fiber cables and those accessories.

He is now a manager of optical fiber transmission research section.

HALOGEN VERSUS NON-HALOGEN MATERIALS FOR TELECOMMUNICATIONS WIRE & CABLE. . . WHAT ARE THE PROS AND CONS?

Charles A. Glew

Gary Corp.
Leominster, Massachusetts

Abstract

"If you can measure it, you can tell something about it". . . Lord Kelvin.

Herein lies the dilemma of the debate over the use of halogen versus non-halogen materials in cables. This paper addresses the impact of the debate on twisted pair cables used for premise wiring for local area network cables. To assume the use of non-halogenated materials in cables is better versus halogen or vice versa should not be the issue. . . rather the debate should be waged over performance specifications that measure the pros and cons of each material. This paper attempts to objectively balance the issue with a review of fire hazard assessment, physical performance, processability and electrical performance.

Groups such as the Polyolefins Fire Performance Council, a unit of the Society of Plastics Industry, Inc. has undertaken broad ranging studies on corrosivity and round robin testing on a range of halogenated materials versus non-halogenated. These types of studies move toward the goal of developing a performance standard which characterize materials. All interest groups must take part in this debate from the materials suppliers of fluoropolymers to polyvinyl chloride to polyolefins. In addition, the wire and cable industry must also play an active role in this debate so that the issues of physical properties, electrical performance and processability become an integral part of the evolution of materials standards and performance.

Unshielded twisted pair cables (herein after referred to as UTP's) used in telecommunication and data transmission applications are extensively used within commercial buildings as a network for voice and data communications from floor-to-floor within vertical, horizontal and plenum air spaces. The materials used on these cables may act as a medium for flame propagation within a building.

UTP's use a wide range of materials with the predominate thermoplastic materials being polyethylene, polypropylene, fluoropolymers and polyvinyl chloride. The halogenated materials are especially effective when fire retardancy is required, and chlorine, bromine and fluorine are the predominately used materials.

Chart #1

PREDOMINANT HALOGENS USED IN WIRE & CABLE MATERIALS TO ENHANCE FIRE RETARDANCY

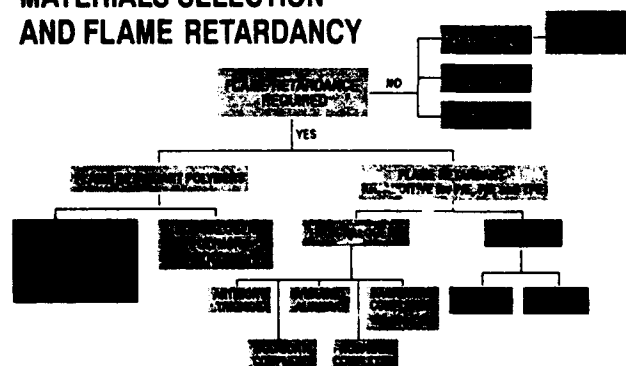
ELEMENT	POLYMER
Chlorine	PVC CPE
Fluorine	ECTFE* FEP PVDF
Bromine	Additive to PE and PP

**Contains both Fluorine and Chlorine*

In today's market, the non-flame retardant materials such as polyethylene, polypropylene and urethane are flame retarded with non-halogenated systems via materials compounding such as antimony trioxides, hydrated alumina, molybdate, magnesium or phosphate complexes or with halogenated systems via chlorine, bromine or fluorine.

Chart #2

MATERIALS SELECTION AND FLAME RETARDANCY



In the U.S. and Canada, a very stringent set of standards exist for flame retardancy for communication and data communications cables. The plenum cable test U.L. 910/CSA FT-6 and riser cable test U.L. 1666 are much more severe than the predominately used International fire test IEC 332-3 which is similar to the IEEE 383/U.L. 1581 test.

Chart #3

U.L. / CSA DESIGNATION	CABLE FIRE TEST	FLAME ENERGY
CMP / MPP	Plenum U.L. 910 CSA FT-6 Horizontal	300,000 BTU/HR
CMR / MPR	Riser U.L. 1666 Vertical	527,000 BTU/HR
CMG / MPG	FT-4 Horizontal	70,000 BTU/HR Burner Angle 20°
CM / MP	IEEE 1581 Horizontal	70,000 BTU/HR Burner Angle 0°

Correspondingly, the efficiency of a materials fire retardancy must be evaluated against this broader definition of flame retardancy.

Chart #4

PARAMETER	IEEE 383 (UL 1581)	FT-4	IEC 332-3
Burner Angle From Horizontal	0°	20°	0°
Cable Spacing	6" Wide on Center --- 1/2 Cable Diameter	6" Wide on Center 1/2 Cable Diameter Bundled if < 1/4 "	Based on Volume
Enclosure Size	Not Specified	Not Specified	1x2x4 Meter
Propagation (Maximum Limit)	2.4 m / 98" From Bottom of Tray	1.5 m / 59" From Burner	2.5 m 98"
Smoke Generation (UL Proposal)	<25 Peak Meters Squared Per Second --- <95 Meters Squared Over 20 minute Test	<40 Peak Meters Squared Per Second --- <150 Meters Squared Over 20 minute Test	None

The most stringent fire and smoke retardancy requirement pertains to plenum cable. Plenum cable materials usage have grown 18% to 20% annually in the last two years with explosive growth from the PVC and polymer alloy type products such as Smokeguard.

Chart #5

PLENUM CABLE RAW MATERIAL USAGES, 1992

COPPER AND FIBER OPTIC CABLES (M LBS.)

PVDF		Smokeguard Type Polymer Alloys		FEP		ECTFE	
Primary Insulation & Buffer	Jacketing	Primary Insulation & Buffer	Jacketing	Primary Insulation & Buffer	Jacketing	Primary Insulation & Buffer	Jacketing
225	5,575	4,330	9,370	10,670	230	1,100	2,280
Total: 5,800		Total: 13,700		Total: 10,900		Total: 3,380	
17%		41%		32%		10%	

Total Lbs.(M) Consumed 1992: 33,780

Data From Survey Prepared by Solvey Polymers

To assess the pros and cons of materials selection for UTP premise cables, the following criteria should be used:

- Fire Hazard Assessment
- Physical Characteristics
- Processability, and
- Electrical Properties

Fire hazard assessment involves four basic principals which requires performance measurement:

- Fire Retardancy and Propagation
- Smoke Generation Characteristics
- Corrosivity
- Toxicity

Chart #6

FIRE HAZARD ASSESSMENT

1. FIRE RETARDANCY	2. SMOKE GENERATION CHARACTERISTICS
<ul style="list-style-type: none"> * Plenum * Riser * FT-4 * U.L. 1581 * VW-1 	<ul style="list-style-type: none"> * Plenum * U.L. 1685
3. CORROSIVITY	4. TOXICITY
<ul style="list-style-type: none"> * Cone Corrosimeter * C-Net 	<ul style="list-style-type: none"> * Univ. of Pittsburg * International and Military Standards

In an effort to compare halogen materials versus non-halogen materials, a review of each area is required.

1. Fire Retardancy and Propagation

A fundamental test for ignitability of materials is the oxygen index test or ASTM D-2863.

The test expresses in percent the minimum concentration of oxygen that will support flaming combustion. The test is a well established method to characterize materials of the same family, but erroneous conclusions can be drawn if varying material i.e. (PVC's or polyolefins) are subjected to full scale flame cable testing.

The following provides a hierarchy of flame retardancy from least to most severe:

Chart #7

SUMMARY OF THE FLAME TEST PROCEDURES

Test	Procedure	Sample Fails Test if
VW-1	816°C Flame is applied for 15 sec. each application with 15 sec. between applications or cessation of burning whichever is longer.	1. Cable supports flame longer than 60 sec. 2. Emits flaming drops which ignites the cotton on the floor
UL 1581	A 70,000 Bru flame is applied for 20 minutes to cables on a vertical tray	1. Cables are blistered and charred at 8 feet level.
UL 1666	A 512,000 Bru flame is applied for 30 minutes to cables in a test chamber	1. Cables must not propagate flame to the top of the 12 foot high compartment.
UL 910	A 300,000 Bru flame is applied for 20 minutes to cables on a horizontal tray inside a tunnel with 240 fpm draft	1. Flame travel exceeds 5.0 ft. 2. Peak smoke optical density exceeds 0.5. 3. Average smoke optical density exceeds 0.15.

The variability of materials versus oxygen index versus the VW1 test is depicted in Chart #8.

COMPARISON OF HALOGEN, LOW HALOGEN, AND NON-HALOGEN MATERIALS

Oxygen Index as a measurement varies dramatically by material: i.e.

MATERIAL	OXYGEN INDEX	VW-1 PASS/FAIL
PVC	>26	Pass
Low Halogen Less than 14%	>30	Pass
Zero Halogen	>35	Variability in Pass/Fail

In the hierarchy of flame test for wire and cable, the results compare PVC, a low halogen with less than 14% halogen content and a zero halogen material.

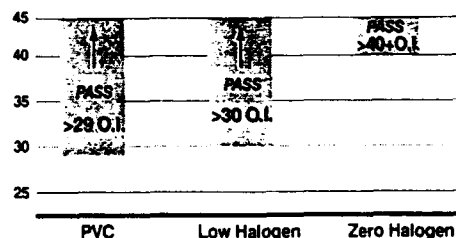
The VW1 test was performed on a 24 awg unjacketed sample with a greater than 26 oxygen index passing with PVC insulation and a greater than 35 oxygen index required to pass with zero halogen materials. These results were demonstrated on each subsequent test which were increasingly severe.

In the 70,000 BTU flame test, the PVC material required a greater than 29 oxygen index while the zero halogen material required an oxygen index of greater than 40.

Chart #9

4 PAIR 24 AWG. JACKET/INSULATION OF SAME MATERIAL

70,000 BTU FLAME TEST U.L. 1581



This test closely approximates the predominate test performed internationally (IEC 332-3) which is used in the European wire and cable market. This fire test methodology would seem to be the highest feasible fire retardancy level for a zero halogen unshielded twisted pair cable based on presently available materials. Noteworthy, this test is the predominate benchmark fire test for zero halogen materials.

The more severe fire tests such as the riser cable test or the plenum cable test, using the same material as insulation and jacket in a four pair cable construction with zero halogen materials performed poorly. All samples failed. The low halogen cable passed the riser test only with an oxygen index of greater than 37. The PVC based products with an oxygen index greater than 32 passed the riser and the PVC polymer alloy types with an oxygen index greater than 48 passed the most severe U.L. 910 plenum cable test.

Chart #10 4 PAIR 24 AWG.
JACKET/INSULATION
527,000 BTU RISER CABLE TEST

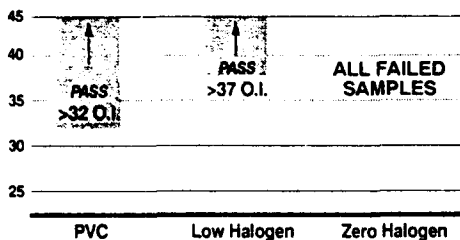
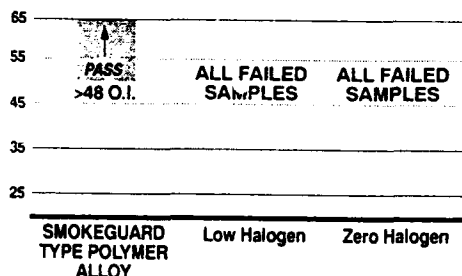


Chart #11 4 PAIR 24 AWG.
JACKET/INSULATION
300,000 BTU PLENUM CABLE TEST



2. Smoke Generation Characteristics

Smoke is the airborne product evolved when materials such as plastics decompose by heat or burning. Smoke as defined here obscures visibility thus impeding the escape of people who may be trapped within a fire situation or inhibit the efforts of fire fighters to rescue and suppress the fire. The predominant test methods evaluate smoke generation and can be broken into two categories: the small scale materials test and the full scale wire and cable tests. Historically, the plenum cable test has measured smoke generation via light obscuration and most recently, Underwriters Laboratories has set up limited smoke test methodologies in conjunction with the riser, FT-4 and U.L. 1581 vertical tray tests. These limited smoke or "LS" tests are a definitive step toward performance standards for smoke generation in assessing materials in an overall fire hazard assessment.

Non-halogen material and the fluoropolymer materials have historically been very low in smoke generation while some of the traditional PVC materials performed poorly. Tremendous strides have been made in PVC materials which have been pushed by the more stringent smoke generation requirements within the wire and cable

market. This exemplifies the need to place performance standards on materials to optimize the development of improved properties.

Chart #12 SMOKE TESTS
SMALL SCALE
MATERIALS SAMPLES

TEST METHOD	NBS SMOKE CHAMBER ASTM 662	CONE CALORIMETER CHAMBER ASTM D0.21.4	ARAPAOE SMOKE TEST ASTM 4100
SAMPLE SIZE	SMALL (3" x 3")	SMALL (3" x 3")	SMALL
AREA EXPOSED	6.6 IN ²	16 IN ²	3/4 IN
THICKNESS	VARIABLE	VARIABLE	1/8 IN
MEASURE METHOD	LIGHT OBSCURATION	OPTICAL	GRAVIMETRIC
FLAME/ HEAT EXPOSURE	RADIANT HEAT FLUX	RADIANT HEAT FLUX	MICRO BUNSEN BURNER

SMOKE TESTS

FULL SCALE WIRE & CABLE

TEST METHOD	U.L. 910 STEDNER/FT-4	U.L. 1666 RISER TEST	U.L. 1581 & FT-4 TESTS VERTICAL TRAY
SAMPLE SIZE	CABLES IN HORIZONTAL TRAY 12" WIDE	CABLES IN VERTICAL TRAY 24" WIDE	CABLES IN VERTICAL TRAY 12" WIDE
MEASURE	LIGHT OBSCURATION	LIGHT OBSCURATION	LIGHT OBSCURATION
FLAME/ HEAT EXPOSURE	300,000 BTU/HR. FLAME WITH 240 FT PER MINUTE DRAFT	512,000 BTU/HR. FLAME TEST	70,000 BTU/HR. FLAME TEST

* U.L. 1685 IS A STANDARD DEVELOPED IN CONJUNCTION WITH THE RISER CABLE. FT-4 AND U.L. 1581 VERTICAL TRAY TESTS THAT MEASURE SMOKE RELEASE RATE AND LIGHT OBSCURATION. "LS" DESIGNATION FOR APPLICABLE PRODUCTS FOR 1993 NEC

The NBS smoke chamber ASTM 662 best characterizes materials in a flaming and non-flaming mode. Chart #13 provides a range of randomly selected materials tested in the NBS chamber from polyethylene to PVC to Douglas Fir.

Chart #13

Typical Values	ASTM 662 NBS Smoke Chamber Non-Flaming	ASTM 662 NBS Smoke Chamber Flaming
Zero Halogen Materials	50 to 100	50 to 100
Low Halogen Materials	100 to 150	100 to 150
Specialty PVC Alloys Smokeguard Type Products	150 to 200	150 to 200
Sampled Polyethylene Range	250 to 750	280 to 390
Sampled PVC Range	170 to 350	280 to 740
Douglas Fir	380 to 438	110 to 156

Today non-halogen materials, low halogen materials and even modified low smoke PVC's perform relatively similar in the NBS smoke chamber test. Full scale fire testing to exceed the "LS" limited smoke test and the U.L. 910 Steiner Tunnel test can be passed by all of these materials.

3. Corrosivity

Increasing attention is being given to the measurement of corrosivity when comparing materials. The numerous test methods characterize the corrosive aspect of gases in fires which in the real world situation would effect the survivability of computer hardware and telecommunications equipment. Many of the corrosivity standards are in the formative stages with emphasis being placed on the test methodologies reproducibility and accuracy to depict corrosion in a full scale fire scenario. Unfortunately, no one test satisfies all criteria. A wealth of comparative material data exists from the CNET test method (Centre National d'Etudes et de Telecommunications) which captures the combustion gases and exposes a 170,000 angstrom printed copper circuit board. The resistance is measured and defined in terms of a percentage corrosivity factor which is the difference between initial and final resistance referenced to a standard board of 8 ohms resistance. This test and all corrosion target tests have a high degree of variability but the chart that follows provides a ranking of materials based on the CNET test results.

Chart #14

CNET Test Results

Halogenated Materials	% of Corrosivity
CPE (Chlorinated Polyethylene)	10.9
Low Halogen (Chlorine Fire Retardant System)	4.5
PVC - Wire and Cable Grade	14.2
PVC - Smoke Suppressed	11.7
PVC - Low Acid Gas Generation	8.8
PVDF	12.9
PTFE	14.1
Non-Halogenated Materials	% of Corrosivity
PE	0.0
Nylon	0.6
EVA/ATH	0.6
LDPE	3.5

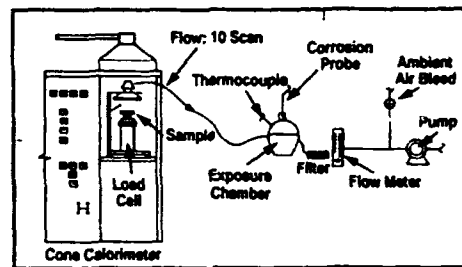
The CNET test should be used as a benchmark only and clearly does not fully correlate to the real fire environment in which the variability of heat, condensed water vapor and oxygen play an important role.

Efforts are underway to employ the cone corrosimeter inconjunction with full scale wire and cable tests.

The cone corrosimeter test uses a combustion chamber and exposes a copper circuit target. For example, a 45,000 angstrom probe can be exposed to a range of heat fluxes up to 100 KW/m². The resistance to change is measured and the corrosion is defined in terms of metal loss in angstroms.

Chart #15

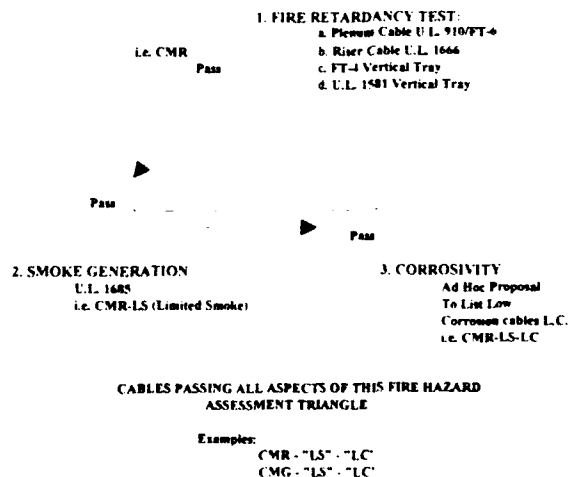
CONE CORROSION TEST GAS SAMPLING SYSTEM



As a part of a more full scale cable test and similar to the work being done on the "LS" limited smoke requirement, U.L. has set up an Ad Hoc Committee to apply the cone corrosimeter test apparatus to the plenum, riser, FT-4 and U.L. 1581 tray cable tests. Initially, the objective would be round robin materials testing on commonly available materials used in cables to include UTP cables. The test would provide a performance benchmark for corrosivity and move the total performance standard forward in its attempt to list "LC" or low corrosion cables. The cone corrosimeter would collect the gases from the plenum, riser, FT-4 or U.L. 1581 test and develop a pass/fail standard for corrosion as well as for flame spread and smoke. This test methodology promotes an overall fire hazard assessment which fosters a performance specification.

Chart #16

UNDERWRITERS LABORATORY AD HOC COMMITTEE USING THE CONE CORROSIMETER FOR CABLE TESTING



4. Toxicity

Biological toxicity provides the final benchmark. The University of Pittsburgh test was utilized by the State of New York Building Code #15/11201 to register all wire and cable materials. The study provides one of the most extensive research projects that ranks materials toxicity. Clearly, the results of the study do little to separate halogen materials from non-halogen materials. To the surprise of many researchers, all materials commonly used in wire and cable grouped relatively close together. In the University of Pittsburgh test, combustion toxicity test animals are exposed to the fumes generated by materials heated in an oven. The LC₅₀ value is the concentration of material which causes 50% mortality of the test animals i.e. (lethal concentration or dose). The unit is LC₅₀ in grams and correspondingly the lower the value, the more toxic the material.

Based upon the NEMA (National Electrical Manufacturers Association) classification groupings, five single material categories were developed with the following results:

	Mean LC ₅₀ Value
Fluoroplastics	8.9 grams
Polyolefins	9.9 grams
PVC	17.6 grams
Hydrocarbon Rubber	18.4 grams
Chlorinated Rubber	22.7 grams

It is important not to take these results out of context. By themselves this data is unsatisfactory for choosing safer cable materials. As long as carbon backbone organic polymers are used, carbon monoxide remains one of the most toxic substances for human biological toxicity whether it be synthetic material such as plastic or naturally found materials such as wood.

This data can be extrapolated to assess the LC₅₀ value in meters which would be most relevant to wire and cable and to a comparison of halogenated cables versus non-halogenated cables relative to toxicity of a four pair UTP cable. In an effort to transform LC₅₀ grams into LC₅₀ values in meters, the following calculation must be made:

1. Insulation Calculation

$$\text{Linear Density (g/m)} = \frac{1500}{\pi} p [(D/2+t)^2 - (D/2)^2]$$

where:

D = Conductor Diameter (mils)
t = Insulation Thickness (mils)
p = Density (g/cm³)

$$\text{LC}_{50} \text{ (meters)} = \frac{\text{LC}_{50} \text{ (grams)}}{\text{Linear Density}}$$

2. For a Four Pair Cable with Jacket

$$\text{Linear density of insulation (g/m)} = 8 \times \text{linear density of single insulated conductor}$$

$$\text{Core diameter over twisted pairs (mils)} = 5(D+t)$$

$$\text{Linear density of jacket (g/m)} = \pi (\text{core diameter}) t_j p$$

$$\text{LC}_{50} \text{ (meters)} = \frac{1500 \text{ LC}_{50} \text{ (grams)}}{(\text{jacket linear density} + \text{insulation linear density})}$$

(Calculations and formula from the paper: "Using Combustion Toxicity Data in Cable Selection" by Stanley Kaufman, Rosalind Anderson, et al, IWCS Proceedings, November, 1988.)

Assuming that the following halogenated cables were produced in a UTP four pair CMR cable or a four pair CMP cable, the following data appearing in Chart #17 would result.

Chart #17 LC₅₀ (METERS) FOUR PAIR CABLES

MATERIAL	SPECIFIC GRAVITY	THICKNESSES		TENSILES		LC ₅₀ METERS MEAN	LC ₅₀ VALUE MEAN
		INS. (MILS)	JKT. (MILS)	INS. (PSI)	JKT. (PSI)		
ALL PVC CMR	1.35 / 1.40	6	20*	3000	2000	1.39	17
ALL FLUOROPLASTIC CMP	1.75 / 2.19	6	8	2500	4000	1.09	8
ZERO HALOGEN CM	1.40 / 1.50	8	30*	1500	1500	1.2	35

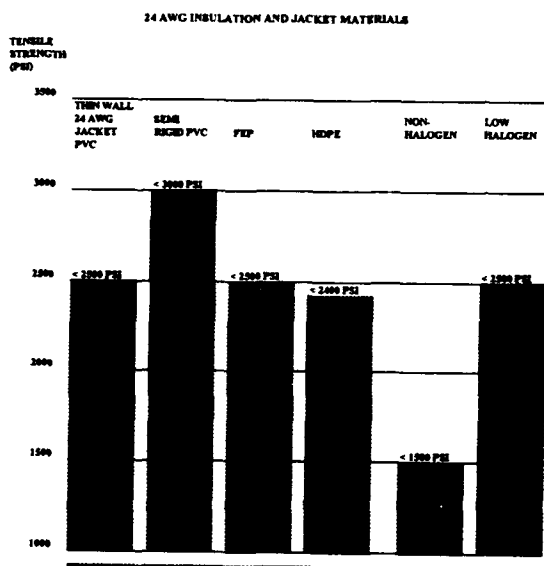
* WALL THICKNESS ADJUSTED BASED ON PHYSICAL PROPERTIES AND THE REQUIREMENTS OF U.L. 444 FOR CABLE WALL THICKNESSES

Therefore, to exceed the LC₅₀ value in meters of a PVC CMR type cable, several factors come into play:

1. The LC₅₀ value in grams, and
2. The physical characteristics of the material which effect the wall thickness per U.L. 444 requirements.

Appropriately, physical properties effect the fire hazard equation. Relative to toxicity, all material group very closely together especially when you calculate the LC₅₀ value in meters based on increased wall thickness required for zero halogen materials. The following chart provides the tensile characteristics for materials used in communications wire.

**Chart #18 HALOGEN vs. NON-HALOGEN
vs. TENSILE STRENGTH**



It is clear that halogenated materials have superior physical characteristics. Correspondingly, a customer would seemingly use less material (thicknesses in mils) both as the insulation and jacket.

As most cable manufacturers know, materials development is half the battle while processability of materials on a range of extrusion equipment is very important. A four pair UTP cable requires a special balance of materials. An insulation grade must process over 24 awg wire in thin wall (6-8 mils) applications at high speeds of 4,000 to 5,000 feet per minute without cone breaks or spark failures. Jacket grades allow for a somewhat wider window and for a four pair UTP cable, jacket processing speeds should be 500 to 600 feet per minute. There are clear differences between halogen, low halogen and zero halogen materials with respect to processing thin wall products as insulations. Commercially available highly filled zero halogen materials are extremely difficult to process in this respect.

Chart #19

**PROCESSING SPEEDS OF VARIOUS MATERIALS
24 AWG INSULATION**

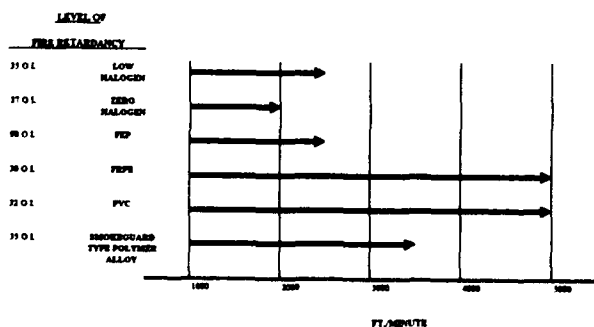
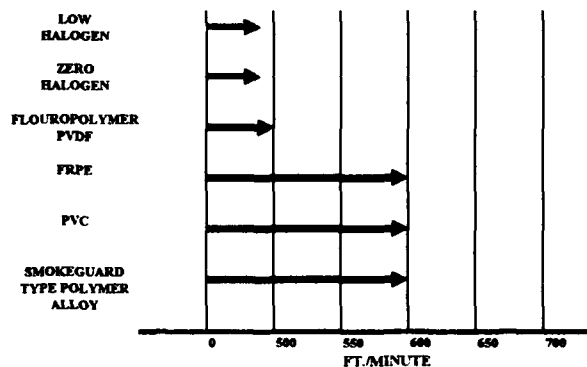


Chart #20

**PROCESSING SPEEDS
4 PAIR JACKETS
RISER OR PLENUM**



Probably the most difficult challenge facing the cable design engineer is the issue of electrical performance of UTP local area network cables. Increasingly demanding specifications have evolved with the advent of the category program.

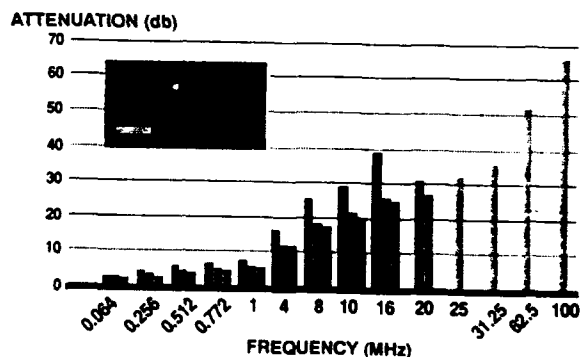
Chart #21

**Twisted Pair
Level Program**

Level	Applicable Standard	Typical Usage
1 Voice	UL 444 ICEA S-80-576	Voice RS232
2 ISDN & Low Speed Data	UL 444 ICEA S-80-576 IBM Type 3 Media Token Ring	IBM 3270 IBM 3X-AS400 RS232
3 LAN & Medium Speed Data	UL 444 ICEA S-80-576 ANSI/EIA/TIA-568 Category 3	10BaseT 4 Mbps Token Ring
4 Extended Distance LAN	UL 444 ICEA S-80-576 TIA TR41 8.1 Category 4 NEMA "Low Loss"	Extended Distance 10BaseT (135 m) 16 Mbps Token Ring
5 High Speed LAN	UL 444 ICEA S-80-576 TIA TR41 8.1 Category 5 NEMA "Low Loss Extended Frequency"	Extended Distance 10BaseT (150 m) 16 Mbps Token Ring COFDM

Chart #22

MAXIMUM ATTENUATION (dB/305 m)



The key material performance requirement necessary to meet the attenuation, impedance and crosstalk requirements of the category program is dielectric constant. In addition, the demands for category 5 cables which run at frequencies from 20 mhz to 100 mhz require low dissipation factors from materials.

Zero halogen materials compounded with flame retardants significantly deteriorate both the dissipation factor as well as the dielectric constant.

Chart #23

FOR CATEGORY 5 CABLE

Dielectric Constant and Dissipation Factor
Are Critical...

	1 mhz	Oxygen Index
FEP	2.1	90
Smokeguard Ins. SRPVC	2.6 - 2.8	35
PE	2.2	19
PP	2.3	19
ECTFE	2.6	60
Smokeguard Jacket	3.3	50
PVDF	9.0	60
FRPE	2.8 - 3.2	28 - 30
Low Halogen	2.4 - 2.8	32 - 35
Zero Halogen	3.3 - 3.6	37 - 39

FEP (fluorinated ethylene propylene) optimally provides the best electrical performance as well as fire retardancy for category 5 four pair UTP cables. Based on the efficiencies of this halogenated material as well as the efficiencies of Smokeguard type polymer alloys and semi-rigid PVC for category 3 cables, it is difficult to find alternate materials that are not halogenated. A non-halogen materials electrical characteristics and fire performance are antagonistic properties. Charts #24 and #25 provides a review of electrical properties expressed in dielectric constant and oxygen index.

Chart #24

HALOGENATED MATERIALS

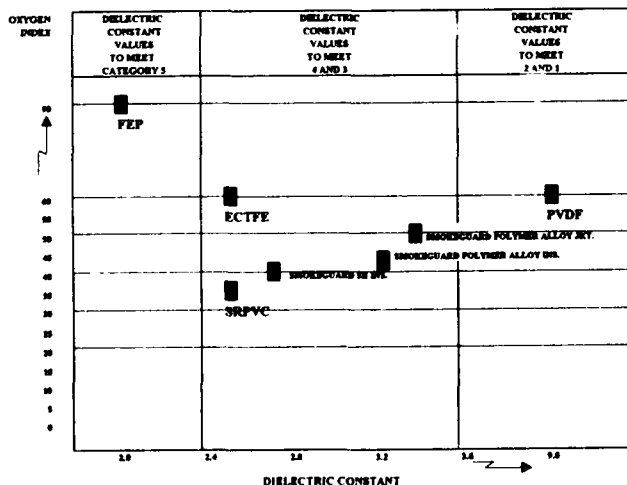
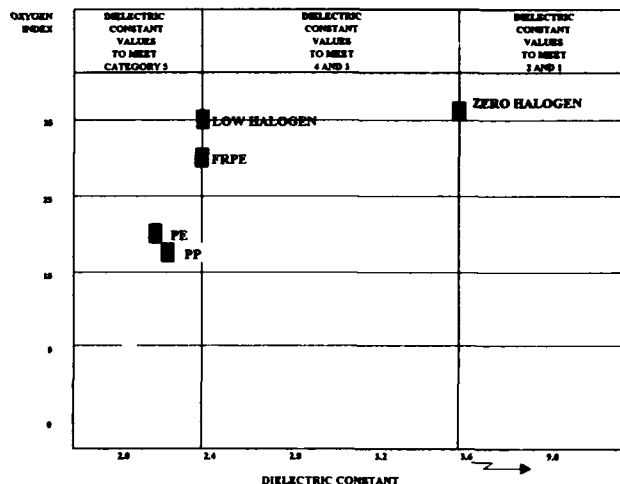


Chart #25

NON-HALOGENATED & LOW HALOGENATED MATERIALS



Conclusion:

Against these performance standards, the objective of zero halogen unshielded twisted pair cables may be unrealistic and more importantly unwarranted. Clearly the objective of both the materials suppliers and the wire and cable industry should be toward safer cables which are tested to performance standards. The ideal UTP local area network cable would be a plenum rated, low smoke, halogen free, category 5 electrical rated product with excellent processability. This remains a noble target, but much can be accomplished by challenging performance standards.

It is clearly debatable whether the issue of corrosivity or toxicity distinguish organic based polymers from one another and secondly whether the test methods which require further validation are in the interest of improved cable performance and public safety.

Recommended Performance Requirements for Low Smoke, Low Corrosivity, Low Toxicity Insulation and Jacket Compounds for Unshielded Twisted Pair Cables Communications Cables

1. Physical Properties

Tensile Strength, psi	1400	U.L. Revision Req'd. to U.L. 444
Elongation (%)	100	U.L. Revision Req'd. to U.L. 444
Air Aging 7 days at 100°C Tensile - Minimum % of Unaged Sample	75	60°C Rated per U.L. 444
Elongation - Minimum % of Unaged Sample	60	60°C Rated per U.L. 444
Cold Bend	-17 ± 2	U.L. 444

II. Fire Hazard Assessment

A. Fire Retardancy

Plenum	CMP	U.L. 910
Riser	CMR	U.L. 1666
General Purpose	CMG	FT-4
IEEE 383	CM	U.L. 1581

B. Smoke Suppressant Characteristics

Plenum	CMP - LS	As per U.L. 910 requirement
Riser	CMR - LS	Apply U.L. 1685 test methodology in conjunction with riser cable test
General Purpose FT-4	CMG - LS	Apply U.L. 1685 test methodology in conjunction with FT-4 test
IEEE 383/ U.L. 1581	CM - LS	Apply U.L. 1685 test methodology in conjunction with IEEE 383 test

C. Corrosivity Test

Plenum	CMP-LS-LC	Perform U.L. 910 test. Capture gases and adapt cone corrosimeter test procedure to determine corrosivity on copper probe*
Riser	CMR-LS-LC	Perform U.L. 1666 test and adapt cone corrosimeter test procedure to determine corrosivity on copper probe*
General Purpose	CMG-LS-LC	Perform CSA FT-4 test and adapt cone corrosimeter test procedure to determine corrosivity on copper probe*
IEEE 383	CM-LS-LC	Perform U.L. 1581 test and adapt cone corrosimeter test procedure to determine corrosivity on copper probe*

* Testing required to determine exact performance requirement.

D. Toxicity Test

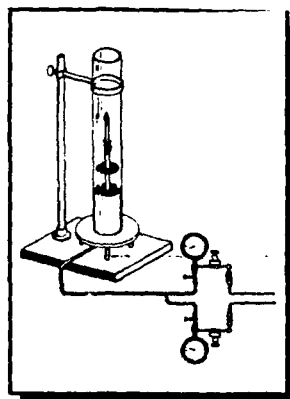
Univ. of Pittsburgh	Pass/Fail	Perform benchmark testing and set materials requirement that no insulation and/or jacket should fall below an LC ₅₀ value of 5 grams or develop LC ₅₀ value in meters, example LC ₅₀ meter >1.0
---------------------	-----------	--

III. Electrical Testing

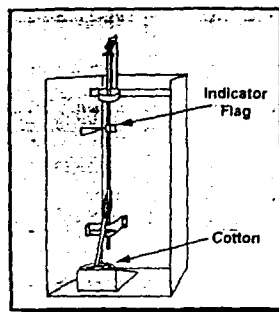
EIA/TIA TSB 36 & 40	Category 5 Values	Performed on UTP cable
EIA/TIA TSB 36 & 40	Category 4 Values	Performed on UTP cable
EIA/TIA TSB 36 & 40	Category 3 Values	Performed on UTP cable

Fire Hazard Assessment Test Methods

OXYGEN INDEX TEST



VW-1 FLAME TEST

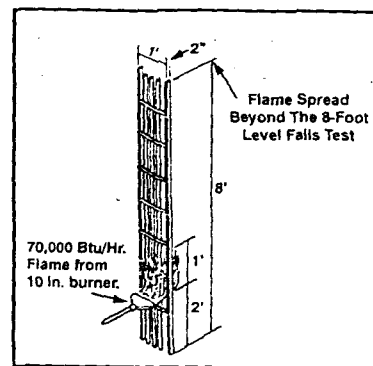


Wire should not convey flame to the flag or burn for more than 1 minute after 5 flame applications of 15 seconds each or the time until flaming ceases (whichever is longer), between applications

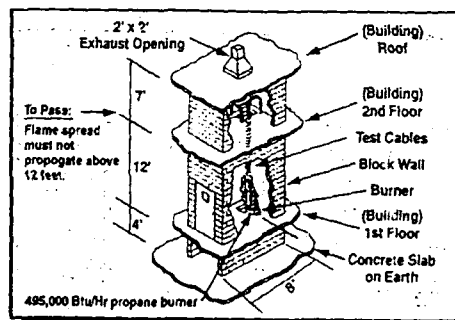
The cotton must NOT ignite

U.L. 1581 VERTICAL FLAME TEST

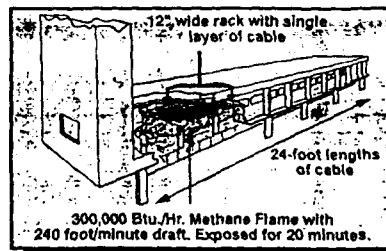
(IEEE - 383 TEST)



U.L. 1666 RISER CABLE TEST

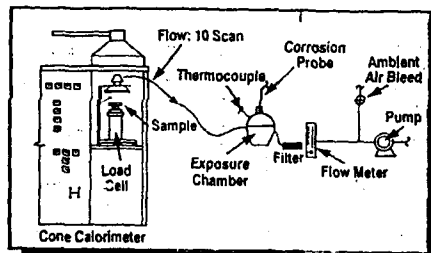


U.L. 910 STEINER TUNNEL TEST



1. Flame spread must not exceed 5 feet beyond end of 4 1/2 foot ignition flame
2. Smoke generation must not exceed peak optical density of .5 (35% light transmission) and average optical density of .15 (70% light transmission)

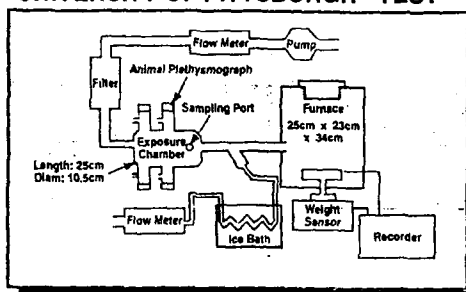
CONE CORROSION TEST GAS SAMPLING SYSTEM



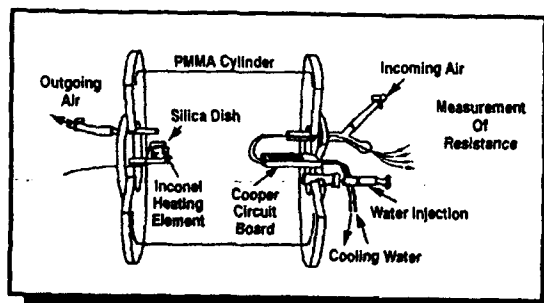
Biography

Charles A. Glew is the Vice President of Specialty Products for Gary Corp. He has a Bachelor of Science Degree in Industrial Technology from Bowling Green University and a Masters Degree in Business Administrations from Bryant College. Charlie has been an active contributor to the National Electrical Manufacturers Association and the Society for Plastics Engineers. He served as co-Chairman of the NEMA Materials Advisory Subcommittee on Toxicity. Previous to Gary Corp., his work experience includes 10 years with ITT Royal Electric and wire and cable marketing experience with Solvay Polymers.

NEW YORK STATE TOXICITY TEST ARTICLE 15 UNIVERSITY OF PITTSBURGH - TEST 15



CNET TEST APPARATUS



Acknowledgements

The author wishes to thank Guerry Grune and Tony Sansone who provided technical support and guidance in preparing this paper. The efforts of Tina Sundstrom for her assistance in preparing the text of the paper and Jay Munsey for his preparation of many of the charts is very much appreciated. Finally, let me thank my wife, Kathie, for her continued support and assistance in this and all my endeavors.

References

1. "The 1990 National Electric Code - Its Impact on the Communications Industry", S. Kaufman, IWCS Proceedings, November, 1989.
2. "Combustion Toxicology: Principles, Methods and Regulations", Steven Packham, IWCS Proceedings, November, 1987.
3. "Flammability Handbook for Plastics", Carlos Hilado, Copyright, 1990, 4th Edition.
4. "Update on Smoke Corrosivity", Marcelo Hirschler, IWCS Proceedings, November, 1990.
5. "Flammability Testing of New Vinyl Compounds with Low Flammability and Low Smoke Release in Cables", A.W. Coaker, M.M. Hirschler et al, IWCS Proceedings, November, 1990.
6. "Acidity and Corrosivity Measurements of Fire Effluent", M.F. Bottin, IWCS Proceedings, November, 1990.
7. "Using Combustion Toxicity Data in Cable Selection", S. Kaufman, J. Refi, R.C. Anderson, IWCS Proceedings, November, 1988.
8. "Combustion Toxicity Evaluation of Polymers for Electrical and Building Applications", H.R. Bratvoid, W.J. Christian, S.P. Woymerowski, IWCS Proceedings, November, 1988.
9. "Registration Categories for Wire and Cable Products: Toxicity Study of the National Electrical Manufacturers Association", R.C. Anderson, IWCS Proceedings, November, 1988.
10. "Wire and Cable Performance as Determined by the Cone Calorimeter", A.F. Breazeale, IWCS Proceedings, November, 1988.
11. "Criteria for Selecting Flame Retardant, Low Smoke, Low Toxicity Coaxial Cables for Radio and Microwave Applications" S. Rampalli, V.K. Chopra, Wire Journal, September, 1990.
12. "Recent Advances in the Designs of Radiating (Leaky) Coaxial Cables", S. Rampalli, H. Nudd, IWCS Proceedings, November, 1998.
13. "The Physiological and Toxicological Aspects of Degradation Products During the Combustion of PVC Polymers in Flammability of Solid Polymer Cable Dielectrics", Einhorn & Grunnet, EPRI Publication TPS 77-738, Palo Alto, CA, November, 1979, pp. 3.1.3-48.
14. "The Acute Inhalation Toxicity in Rats from Pyrolysis Products of Polymeric Materials", R.R. Raje, J.J. Sciarra, L. Greenberg, A & M Schwartz, Combustion Toxicology, 8, pp. 45-51, February, 1981.
15. "Physiological and Toxicology Aspects of Smoke Produced During Combustion of Polymeric Materials", I.N. Einhorn, Environmental Health Perspectives, 11, pp. 163-189, 1975.
16. "Fire and Smoke - Understand the Hazard", Committee on Fire Toxicology National Academy of Sciences, 12-29, 63-77.
17. "Toxicologic and Acute Lethal Hazard Evaluation of Thermal Decomposition Products of Synthetic and Natural Polymers", Y. Alarie, R.C. Anderson, J. Tox. & Appl. Pharmacol. 51, 341, 1979.

CORROSION AND CORROSION CONTROL OF THE COMMUNICATION CABLE PLANT

George Schick

Bell Communications Research
Morristown, NJ

Abstract

The largest part of the telecommunication cable plant is made of cables with copper conductors. Corrosion of the cable plant is primarily caused by man-made dc currents. With the change from lead sheathed to polyethylene jacketed cable, the majority of corrosion problems transferred from the cables to the manholes. In areas where man-made currents don't get on the cable plant, corrosion can be caused by specific corrosive chemicals, galvanic effects, sulfate-reducing bacteria, and stress-corrosion cracking. Corrosion of the telecommunication plant is controlled by: material selection, stress relieving heat treatment, air pressurization or filling compound in the cable core and in closures, jacketing, coating, insulating joints, drainage bonds, and cathodic protection.

Introduction

Telephone companies in the United States invested billions of dollars to establish a far and wide reaching, reliable, and easily accessible telecommunication network. Although the new cable plants use, significant lengths of optical fiber cables; approximately 94 percent of the telecommunication plant still relies on cables with copper conductor pairs. In addition almost half of the newly installed cables are still copper. The cables represent the most extensive part of the telecommunication plant, but engineers in general and corrosion specialists in particular have to take into consideration the various support hardware, closures, grounding, and electrical protection systems. The common aspect of all the above telecommunication plant components is that all of them have metallic components or are made entirely of metals. This article describes the various types of corrosion affecting the telecommunication plant and the various built-in or applied control measures taken to prevent or minimize failures.

Effects of man-made currents and their control

A basic tenet of corrosion is that the rate of metal loss is directly proportional to the current that leaves the corroding metal per unit surface area to enter the surrounding environment (electrolyte). The most common environments where corrosion, due to man-made currents, take place are wet soil and water.

Some of the most basic telecommunication plant designs address concerns about corrosion. Cables and splice closures are constructed to exclude moisture ingress into the cable core. This first line of defense is supplemented with air pressurization (mainly in toll cables) or with filling compounds. Both of these means are capable to keep moisture out of the cable core. However, as a last line of defense against disastrous failure, one member of each wire pair is connected together with the cable shield (ground) to the positive side of the central office (CO) battery (tip), and the other member of each wire pair is connected to the -48 volt side of the battery (ring). The reason for this powering scheme is that if, in spite of all the precautions, water enters the cable core, and small wire insulation defects expose bare copper on oppositely energized wires, small leakage

current will flow. It has been shown statistically that during manufacturing 100 defects are created per 1 million conductor feet⁽¹⁾. If the conductor, connected to the more positive (ground) side of the CO battery, was not also connected to the shield; corrosion due to the small leakage currents would render the conductor discontinuous in a matter of days. By being connected to the shield, the current is distributed on a larger metal surface area (orders of magnitude) than what is exposed by the insulation defect, thus the conductor is preserved.

In the not too distant past the outer sheath of telecommunication cables were made of lead. One of the important properties of lead is its resistance to corrosion in natural environments. Man-made stray dc currents (dc electrified rail transport systems, mining and welding operations, cathodic protection rectifiers of "foreign" plants) caused most of the lead sheathed cable corrosion. The telephone companies protect their plant against these stray dc currents with low resistance drainage bonds (a path that allows the current to return to its origin without causing corrosion), cathodic protection (applied current that counteracts corrosion currents), and insulating joints (gaps in the cable shields limiting the pick-up of dc stray currents).

The newer, polyethylene jacketed, telecommunication cables have either aluminum or aluminum and steel shields under the outer jacket. Most of these shields are further protected against corrosion by a bituminous flooding compound. The polyethylene outer jacket protects against both pick-up and discharge of stray dc currents, thus the cable itself does not corrode. However, manhole hardware in the underground plant, and buried plant support hardware, ground rings around Controlled Environment Vaults (CEVs), and huts, and guy anchors of the aerial plant can pick up stray dc currents. The metallic shield in the cable can transmit these currents to the next manhole, or CEV, or hut, or guy anchor where it can leave the plant and cause corrosion⁽²⁾. This means that corrosion, caused by man-made currents, does not disappear with lead sheathed cables, but transfers to manhole and buried plant hardware, ground rings, and guy anchors. Thus, our efforts concerning corrosion control are transferred from the lead sheathed cable to other bare metallic components of the telecommunication plant. The mitigative measures with insulating joints, low resistance drainage bonds, and cathodic protection are also applicable to these other segments of the plant.

Effects of the environment and their control

The underground plant consists of ducts and manholes. Flooded manholes are the locations where most of the corrosion problems arise in today's telecommunication cable plant. These waters can be contaminated by sea water, deicing salts, industrial effluents, fertilizers, and some microbiological species (e.g., desulfovibrio-desulfuricans). All these environments can cause corrosion of bare metallic hardware in the manhole.

Galvanic corrosion in the manhole

About 20 years ago apparatus cases were made of a galvanized cast iron base and a galvanized sheet steel cover. The cover was painted and secured to the base with a stainless steel clamp. Since galvanized steel is considerably more anodic than stainless steel the cases can form a galvanic corrosion cell. Where the paint on the cover becomes damaged the

galvanic corrosion cell perforates the underlying galvanized steel. A study was conducted in simulated manhole water to evaluate the effect of anode/cathode surface area ratio on the corrosion rate of the galvanized steel. The results of this study are plotted in Figure 1. Considering that 0.001 inch of zinc can be removed by 1.69 micro amp/cm² in one year, and 0.001 inch steel can be removed by 2.19 micro amp/cm² in one year; the low anode/cathode surface area ratios can lead to relatively rapid perforation. The solution to this problem was the removal of the organic coating, and cathodic protection with either 0.020 inch of flame-sprayed zinc or placement of a magnesium anode in the manhole.

side effect of SRB is that the galvanic relationship between copper and steel is reversed, and the copper or tin-coated copper bonding ribbon becomes the corroding anode. Both galvanized steel support hardware and copper or tin-coated copper bonding ribbon can fail in manholes with large SRB colonies (Figure 4). The solution to this problem is a spray application of an oxidizing agent (NaOCl) that temporarily removes the live SRB colonies⁽³⁾.

The buried plant is also exposed to widely varying soil conditions. The corrosivity of the soil depends on its resistivity (low resistivity soils are more corrosive), pH (ranges between 2.3 (acidic) and 9.5 (alkaline) in the

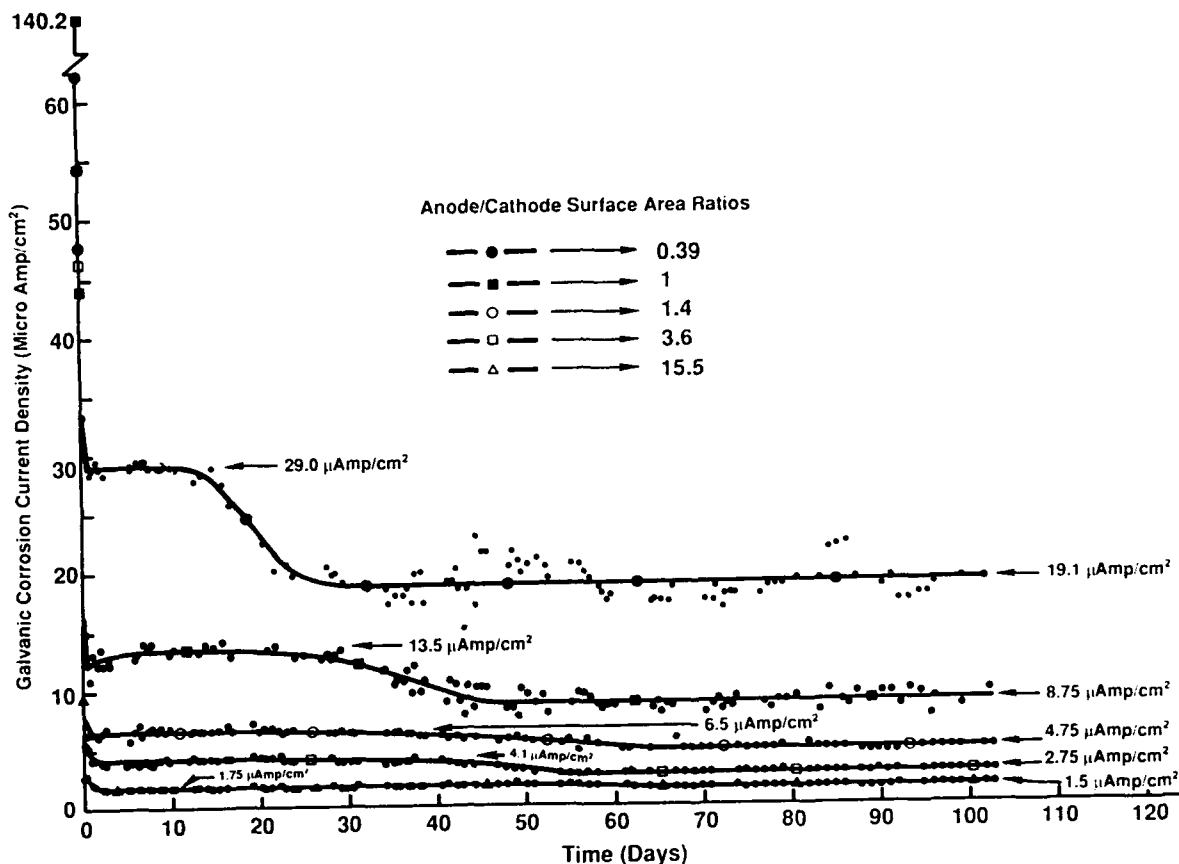


Figure 1 Galvanic Corrosion Between Hot Dip Galvanized Steel and Type 304 Stainless steel in a solution Containing 266 mg/liter Cl⁻ and 70 mg/liter SO₄²⁻

Stress-corrosion cracking in manholes

Ammonium compound from fertilizers seeped into manholes and caused stress-corrosion cracking of coaxial cable terminals made of cartridge brass (70% copper, 30% zinc). The cracked brass terminal is shown in Figure 2. Figure 3 contains two photomicrographs illustrating the stressed and cracked brass structure. The short term solution to this problem was the application of a heat-shrinkable, cross linked, irradiated, adhesive lined, "wrap around" sleeve to isolate the metal from the environment. The long term solution was to use red brass (85% copper, 15% zinc) instead of cartridge brass and a heat treatment (annealing) to relieve the manufacturing stresses.

Microbiologically induced corrosion in manholes

A large number of manholes in various locations in the continental USA contain stagnant water, and the resulting quasi anaerobic conditions promote the proliferation of sulfate-reducing bacteria (SRB). An unusual

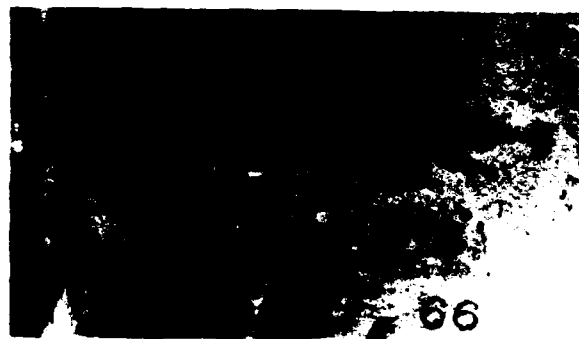


Figure 2 Stress-corrosion cracked cartridge brass coaxial cable terminal

continental United States), and the type of chemical compounds in the soil (chlorides, sulfates, nitrates, ammonium salts, acetates are corrosive to various types of metals). Locally some man-made corrodents can create strongly corrosive environments. Cinders contain carbon that causes galvanic corrosion, and it is also acidic thereby further accelerating corrosion. Deicing salts, industrial effluents, fertilizers, and SRB all contribute to the corrosivity of the soil. Lead sheathed cables, bare galvanized steel mounting posts of pedestal terminals, and grounding electrodes are the bare metallic components that are directly exposed to the soil. Corrosion caused by aggressive environment in the buried plant is most often controlled with coating and cathodic protection.



Figure 3 Photomicrographs of stress-corrosion cracked cartridge brass structure

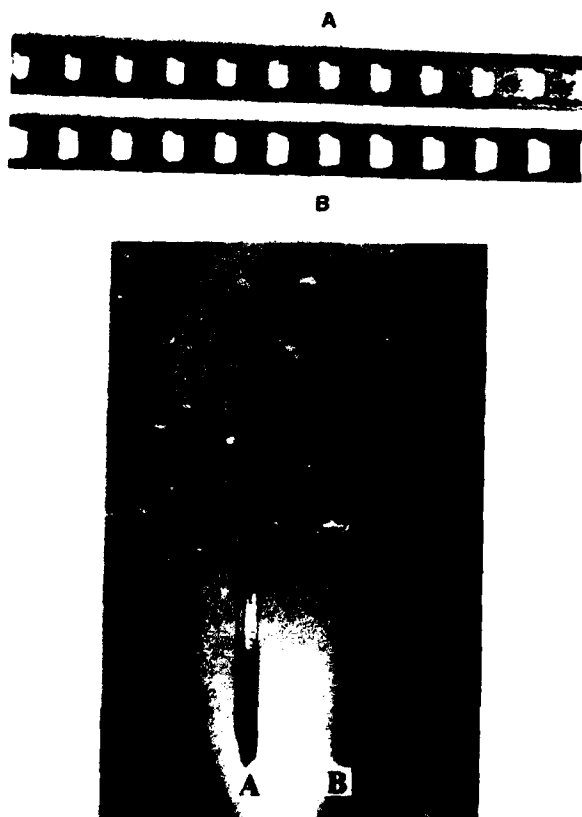


Figure 4 Hardware and bonding ribbon corrosion in a SRB contaminated manhole (A) New, (B) Corroded

The **aerial plant** can be exposed to three distinctly different environments: industrial, marine, and rural. The primary pollutants in an **industrial** atmosphere are carbon dioxide (CO_2) and sulfur dioxide (SO_2). The atmosphere can also contain nitrogen dioxide (NO_2), hydrogen sulfide (H_2S), chlorine (Cl_2), and ammonium compounds. The industrial pollutants generally create acidic environments that readily attack zinc and steel. The industrial environment also contains oxidizing agents (SO_2 , NO_2) which, together with oxygen, can maintain a protective passive film on the surfaces of aluminum and stainless steel. Thus, aluminum, aluminum-clad steel, and stainless steel aerial strands and hardware corrode at a lower rate than galvanized steel in most industrial environments.

An extremely aggressive environment may exist in the vicinity of chemical plants. An example is the manufacturing of chlorine gas by salt brine electrolysis. Small amounts of chlorine may be occasionally released into the atmosphere. The chlorine, in contact with moisture in the air, forms hydrochloric acid (HCl). In the vicinity of such a chemical plant the galvanized steel strand and aluminum cable shields in non-sealed splice closures experience corrosion failures. Figure 5 illustrates galvanized steel strand failure on the premises of a chlorine gas manufacturing chemical plant.



Figure 5 Corroded galvanized steel strand from a chemical plant manufacturing chlorine gas by salt brine electrolysis

The corrosivity of **marine** atmosphere is due to airborne chloride salt solution. Foggy sea coastal areas can further aggravate the corrosive conditions by forming a thin moisture film on the metal surface. Oxygen from the air saturates this moisture film and acts as a cathodic depolarizer. The depolarization process increases the corrosion rate of the metal. Sea coastal areas are generally corrosive for galvanized steel, aluminum, and even for 400-series stainless steel. Corrosion problems of aerial strand in marine environment can be solved by using heavy galvanizing. Another method of controlling aerial strand corrosion in any type of corrosive environment is using figure 8-type cable, where the strand is jacketed and a plastic web connects it to the cable jacket.

The least corrosive environment is the **rural** atmosphere. CO_2 contaminants of condensed moisture usually form a dull haze on galvanized steel, aluminum, and lead. Rural areas affected by acid rain may show corrosion similar to that in industrial atmospheres.

Telecommunication plant components exposed to contaminated air may be subject to other than general corrosion. Figure 6 shows copper tail wires of aerial drop wire clamps that failed by corrosion fatigue at a sea coastal area. Figure 7 is a magnified section near the failure of a copper tail wire showing closely spaced multiple cracks that is characteristic of corrosion fatigue.

Stressed brass components exposed to moist ammonia or ammonium compounds may fail by stress corrosion cracking. Figure 8 illustrates parts of a gas tube protector that was placed in a Bakelite® housing, and

Bakelite is a registered trademark of Union Carbide Corp.

mounted on the side of a house. The tin coated brass cage failed by stress-corrosion cracking. In order to avoid such failures a stress-corrosion cracking study was conducted in Mattsson's solution⁽⁴⁾. Figures 9 and 10 show the test results of coated and non-coated protector cages and caps, respectively. Based on this study, a 24-hour test was established in Mattsson's solution. The tests indicate that yellow brass with or without solder or nickel coating is not acceptable.



Figure 6 Failed copper tail wires of an aerial clamp



Figure 7 Copper tail wire near the failure point (4X)

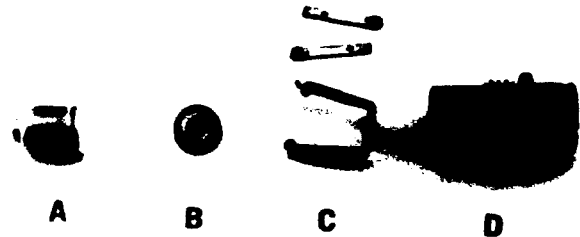


Figure 8 Gas tube protection parts
(A) gas tube, (B) fusible pellet, (C) tins coated brass cage (stress-corrosion cracked), (D) brass cap

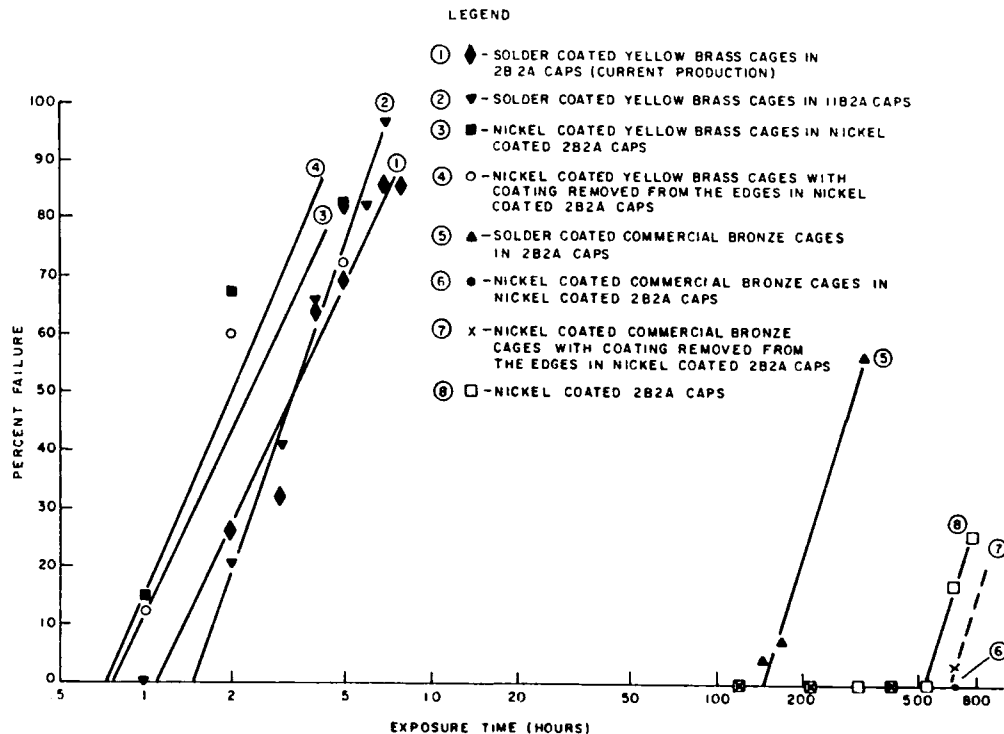


Figure 9 Stress corrosion cracking of coated protector cages and caps in pH = 7.2 Mattsson's solution

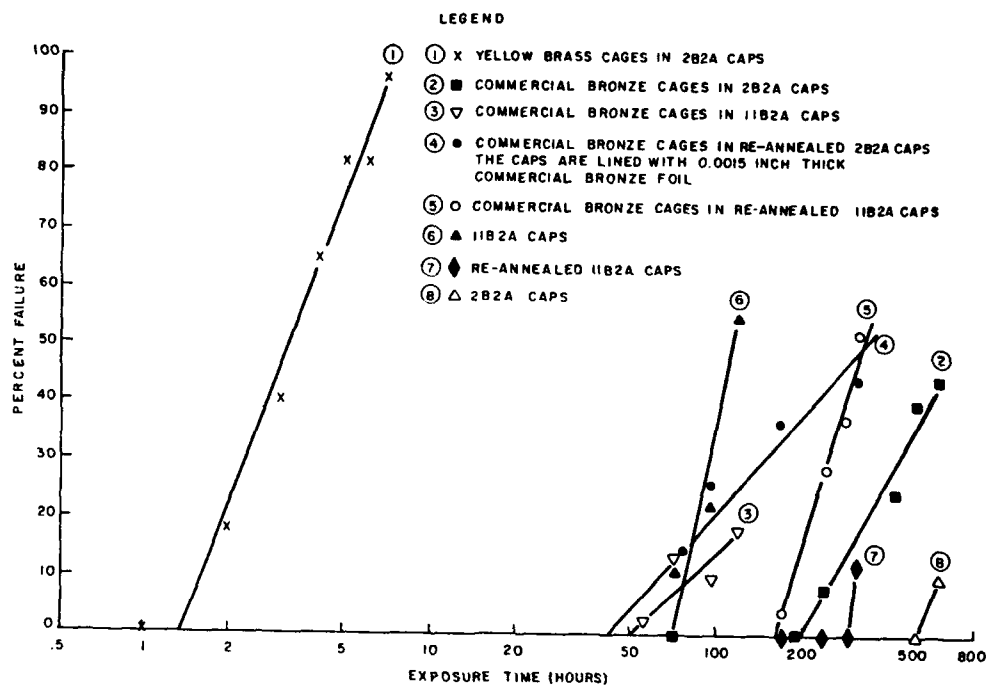


Figure 10 Stress corrosion cracking of non-coated protector cages and caps in pH = 7.2 Mattsson's solution

Summary

The telecommunication plant is made mainly of cables with copper conductors. Man-made dc currents are the main cause of underground and buried plant corrosion. The corrosive nature of the environment also contributes to the corrosion of the telecommunication cable plant. Aggressive salts, such as chlorides, acidic or alkaline soils, industrial effluents, some components of fertilizers, and certain microbiological species are contributors to the corrosion of the underground and buried plants. Corrosion of the aerial plant is caused by atmospheric pollutants, e.g., acid rain, and wind borne salt solution droplets at sea coastal areas.

The control of telecommunication cable plant starts at the manufacturing process by material selection, stress relieving heat treatment, coating and jacketing. The "in place" plant can be protected by insulating joints, low resistance drainage bonds, cathodic protection and chemical additives.

REFERENCES

1. W. M. Hladik, private communication
2. S. A. Potocny, "Telephone Pole Guy Rod Corrosion by Stray Currents", *Materials Performance*, Vol. 18, No. 12, pp. 19-25, 1979.
3. G. Schick, "Freshening Up Manholes", *Telephony*, Vol. 223, No. 13, pp. 34-38, September 28, 1992.
4. Standard Recommended Practice for Use of Mattsson's Solution of pH 7.2 to Evaluate the Stress-Corrosion Cracking Susceptibility of Copper-Zinc Alloys, ASTM G 37, 1990.

AUTHOR



George Schick received a Dipl. Eng. degree in Electrochemistry and Electrometallurgy from the Ecole Nationale Supérieure d'Electrochimie et d'Electrometallurgic de Grenoble, France in 1958, the MS degree in Metallurgy from Massachusetts Institute of Technology in 1961, and the Ph.D. in Metallurgy and Materials Science from New York University in 1972. He worked at Bell Telephone Laboratories from 1961 to 1983 in the area of corrosion. In 1984 he joined Bell Communications Research where he is working on corrosion control and on the effects of the environment on optical fibers. Dr. Schick is a member of the National Association of Corrosion Engineers and the American Society for Testing and Materials.

**LABORATORY TEST AND FIELD TRIAL DATA OF COPPER
CABLE PROTECTED WITH WATER ABSORBENT THIXOTROPIC GEL**

Lawrence E. Davis

WaterGuard Cable Products, Inc.
Houston, Texas

Abstract

A field trial of twisted pair cables filled with the ATG was undertaken to evaluate in-service use of the new technology. Illinois Bell installed ATG filled cable into the Crystal Lake development in the Chicago area. The cables were installed approximately two years ago in a high water table area. The cables and associated ATG filled splices are currently functioning without any reported problems; measurements indicate no change in electrical properties.

Introduction

Absorbent thixotropic gel (ATG) filling compound is a recent innovation in providing a barrier to water penetration and migration into telecommunications cable. Several cable manufacturers have produced and evaluated copper cables containing ATG. All of the cables comply with the electrical specifications and demonstrate the ability to prevent water ingress at significantly higher water head pressure than required in current specifications. Simulated water head pressures of up to 50 feet have been maintained on two feet of cable for over a year. However, there was no field experience which cable users could employ as a cable performance benchmark. Illinois Bell, in conjunction with Essex and Superior Cable, undertook the task of establishing a field trial for cables filled with an ATG which absorbs and encapsulates water attempting to penetrate the cable.

The traditional approach to prevent water ingress into cable is exclusion by mass through the use of a grease or hot melt hydrophobic material. The use of a compound which may attract water, such as ATG, to prevent ingress is at first glance contradictory. The use of hydrophilic material with water blocking properties, however, does have some historic precedence.

Cables formed using paper or pulp insulated wire block water flow by the swelling of the insulation when they are exposed to water. The paper or pulp insulation would block the water flow and localize cable damage until the cable could be dried. However, the cellulose material would wick moisture and continue to wet pulp and paper insulation. Wet pulp and paper insulation are not effective insulation, and they can cause transmission problems.

Powdered absorbent material has also been applied to plastic insulated cores. A distributed powder would swell in contact with water and prevent further water ingress by forming a block. Unfortunately, maintenance of a uniform distribution of powder in the cable core was problematic. Superabsorbent materials impregnated or incased in a fibrous material or tape are also being used to block water flow between cable layers, but tapes or impregnated cords do not block water from the core of a twisted pair cable. The use of superabsorbents with fibrous material may lead to wicking of moisture into the cable.

ATG, used with plastic insulation, prevents the moisture wicking problems observed with tapes. The water absorbent polymer is dispersed in a hydrophobic material and is released from the matrix when water contacts the gel. The superabsorber then gels the water creating a dam which stops water flow. The hydrophobic matrix sets up a barrier to wicking thereby preventing moisture migration.

The Rural Electrification Administration's (REA) water immersion test was conducted by a cable producer on a 25 pair, 24 gauge ATG filled cable and a ETPR filled cable. Three pairs in each cable were monitored for capacitance change. A hole was cut through the sheath to expose the core along every foot of cable, and the cable was placed under a three foot head of water except for the ends. The data in Table I shows that the ATG material does not undergo capacitance change due to absorption of water. The capacitance change observed is within measurement error. If ATG compound wicked moisture into the cable, a significant capacitance change would have been observed.

The field trial is intended to test the validity of the ATG technology and to determine craft sensitivity to the material. As part of the field trial, splices were protected using ATG encapsulant materials. Using ATG materials to fill the cable and to protect the splices ensures compatibility within the system. Compatibility of ETPR and Petrolatum Jelly Polyethylene (PEPJ) compounds with foam skin insulation is a current concern. Several International Wire and Cable Symposium sessions over the last six years have been devoted to the subject.

In 1988 when premature failure of foam skin insulation was recognized, Bellcore published the following statement; "Improved cable formulations may improve these lifetimes by changing the resin, the stabilizers and/or filling compounds. These formulations are complex mixtures and, therefore, compatibility between components needs to be considered early in the design process to avoid deleterious interactions and seek advantageous synergies." (Reference 4). I totally agree with the above statement. The industry has concentrated on increasing stabilizer content to obtain improvement in foam skin life expectancy. While increasing stabilizer content does improve foam skin performance, it does not address the fundamental compatibility issue. It is generally recognized that the most significant reduction of stabilizers in the insulation results from the aging of the insulation in filling compound; this extraction results in the need to increase stabilizer levels. Increased levels of stabilizer tend to mask the fundamental compatibility issue which should be addressed when designing the cable.

In discussing the fundamental compatibility problem between filling compound - insulation interaction, Koksál Tonyali stated that "The sorption-desorption process may generate changes in the polymer morphology and reorganization of the crystalline structure. Such changes may create defects or channels which enhance the stabilizer migration and ultimate cracking of the insulation." He further stated that one solution to prevent cracking in polyolefin insulation is: "The elimination of the aggressive component of the filling compound which swells or plasticize the polymer." (Reference 3, 6, 7).

ATG products have been formulated to address foam skin compatibility issues by having oxidation stability levels above industry specification, by selecting base oil with higher molecular weight than the oil in ETPR and PEPJ, and by cold filling. The type of oil selected also affects compatibility with polyethylene.

Typical oxidative induction time (OIT) criteria for filling compound is (in Bellcore Technical Reference TR-NWT-000421) 10 minutes when tested at 190°C in copper pans. Absorbent Thixotropic Gel OIT is run at 220°C in aluminum pans. Chemical reaction rates such as oxidation are expected to double for every 10°C rise in temperature (OIT reduced by one-half). Therefore, tests conducted at 220°C would be expected to occur eight times faster than tests conducted at 190°C. Typical OIT values for ATG material when run at 220°C are greater than 60 minutes (Table II). Therefore, ATG filler is many times more resistant to oxidative degradation than the criteria requires.

Hot melt materials will immediately begin to degrade polyethylene insulation when they are applied. The hotter the material and longer the core is maintained at an elevated temperature, the greater the polyethylene degradation. Degradation occurs in the form of leaching of antioxidants from the insulation and from the migration of the oil into the insulation which affects the morphology of the insulation. Since ATG material is applied cold, there is less tendency for ATG material to affect the insulation.

The type of oil used to make a filling compound also affects compatibility. A general rule of chemistry is that like materials dissolve like materials. The closer two compounds are in molecular structure the greater the solubility of the combination. Polyethylene is a

saturated straight chain hydrocarbon. The paraffinic oil contained in PEPJ and ETPR compounds is also a saturated straight chain hydrocarbon. Therefore, the free oil in these compounds has an affinity to swell and plasticize the wire insulation. The ATG compound is formulated with a ring structured oil which has less tendency to solvate the polyethylene.

The size of the solvating molecule also affects the ability of the free oil to plasticize the insulation. Viscosity is an indirect measure of molecular weight. The higher the viscosity of the base compound the less migration of oil into the polyethylene. Large oil molecules cannot migrate into the polyethylene as readily as the smaller oil molecules in ETPR.

ATG and 80°C drip ETPR were subjected to the Siecor oil separation procedure at 80°C. (Reference 8). The ATG compound exhibited an oil separation of 4 percent as compared to ETPR performance of 50 percent. Both samples were taken from a quart sample of material. The cooling rate for the ETPR sample may have affected the oil separation characteristics of the hot melt material, but the test illustrates the difference in the ability of the lighter oil in ETPR to migrate.

ATG materials use thixotropic agents to bind oil into a gel matrix, and they do not depend exclusively on synthetic microcrystalline wax and rubber to prevent oil migration. Therefore, as the temperature increases, less oil is free to migrate into insulation. Since the thixotropic property of ATG allows cables to be filled cold, there is no initial heat soak to begin migration of oil into insulation such as occurs with hot melts. The high viscosity, the high molecular weight, and the structure of the oil component in ATG material all reduce migration of oil into insulation. The result of the reduced tendency of ATG to migrate into polyethylene prevents ATG compounds from imparting additional stress to the insulation as opposed to the ETPR class of compounds. Lower stress levels within the insulation mean reduced cracking.

In May 1991, Superior Cable began a pedestal aging test on a sample of ATG filled cable submitted to the Illinois Bell field trial in accordance with the Bellcore TR-NWT-000421 in effect at the beginning of the test. A 70°C two-week preaging was conducted prior to placing the cables in the pedestal. The pedestal test was terminated after 365 days

(preaging not included). There were no cracks exhibited by the foam skin insulation. Compatibility of ATG with foam skin insulation was clearly demonstrated.

Several IWCS papers such as those presented by Witco Corporation, Alvin C. Levy and Associates, and others, have demonstrated deleterious effects on insulation from oil contained in PEPJ and particularly ETPR. The oil caused changes in the polyolefin insulation morphology thereby resulting in reduced strength, swelling, OIT reduction, and mutual capacitance changes between wires. Capacitance change is an easy way to evaluate the degree to which the oil in filling compounds attacks insulation particularly foam skin. Capacitance change measurements show that the ATG material is more compatible with foam skin insulation than ETPR (Reference 13). This again demonstrates increased compatibility of ATG compound with foam skin insulation over ETPR material.

Field Trial

Cables supplied by Essex Group and Superior Cable were installed into the Crystal Lake development in the Chicago area by Illinois Bell. The cable types employed in the field trial were AFMW 100 pair 24 gauge and AFMW 200 pair 24 gauge cables filled with ATG filling compound. Several underground splices were constructed using ATG splicing compound during the installation of the cable. Most of the cable access points, however, were located in pedestals.

The Crystal Lake development is located in what was considered a wetlands area. The installation of the cable began in May 1991, but construction was halted due to concern over proper drainage. After the cable was placed in the ground and cut for termination the courts ordered a halt to construction until the project developer satisfied water drainage concerns. A delay of six months was incurred and the cables were left relatively unprotected during this period. Due to the interruption in construction, Illinois Bell field service personnel expected some pairs to exhibit trouble, but they were pleasantly surprised when the ATG filled cables did not show any signs of water damage as a result of the construction delay.

At the time of installation, the locations of the cables were placed in the maintenance trouble system and flagged so that any problems associated with the ATG cables would be reported. Most recently, WaterGuard requested

Illinois Bell to check the records in August 1993. No service interruptions have occurred. In addition, Essex selected 2 pairs from each of the four binder groups of a 100 pair cable for periodic testing. Pairs 24, 25, 49, 50, 74, 75 and 99 were reserved for testing and pair 100 was used as the return pair required for conductor resistance and shield resistance measurements. The field test measurements were made following the Essex Field Test Procedure EP 201, and temperature corrections were made by measuring the ground temperature at twenty inch depths and the ambient temperature.

The cable Essex selected to monitor was installed in January 1992 and the initial field data was measured March 19, 1992. The test pairs measured were found to be close to expected values for installed cable. The test results are shown in Figure 1. Essex originally planned to measure the test pairs every six months to monitor any change but was unable to do so because of high water in the area each time Essex attempted to remeasure the cable. A second measurement was made August 27, 1993. Pairs 74 and 75 had been placed in service and could not be measured. The data indicated no change in the electrical parameters of the cable. Differences in the reading were attributed to measurement error and temperature effects.

Field personnel found the ATG filled cable easy to work with, and the filling compound was readily removed from hands and tools without the need of solvents. The splicers found the ATG encapsulant as easy to work with as the ATG filling compound, and they had no complaints concerning the use of the encapsulant or the ATG encapsulant splice filling procedure.

CONCLUSION

ATG material is designed to have improved compatibility with polyolefin insulation for hot melt compounds.

ATG filled cables and splices have been in operation in the field trial for over 20 months with no reported problems and no measurable change in electrical properties.

ACKNOWLEDGEMENT

The author wishes to thank the telecommunications product division of Essex Group and Illinois Bell for their work in obtaining field measurements and Superior Cable for providing cable performance test data.

REFERENCES

1. Y. Gau, E. D. Nelson, K. D. Dye, "Evaluation of Antioxidant Uniformity in Polyethylene Insulation." Proceedings of the 41st IWCS, 298-303 (1992)
2. Koksai Tonyali, "Investigation of Factors Affecting Long Term Heat Stability of Polyolefin Insulation Resins." Proceedings of the 41st. IWCS, 304-309 (1992)
3. K. D. Dye, V. J. Kuck, F. C. Schilling, M. G. Chan, L. D. Loan, "Analysis of Stabilizer Concentrations In Polyolefin Cable Materials." Proceedings of the 38th. IWCS, 98-103 (1989)
4. T. N. Bowmer, E. P. Hjorth, R. J. Miner, O. S. Gebizlioglu, "Stability of Polyethylene Insulations in the Field and Laboratory." Proceedings of the 37th. IWCS, 490-499 (1988)
5. G. D. Brown, L. E. Davis, "Evaluation of Material for Improved Life Expectancy of Foam Skin Insulation." Proceedings of the 36th. IWCS, 734-743 (1987)
6. G. D. Brown, "Performance of HDPE Insulation Antioxidants in Filled Telephone Cable Applications." Proceedings of the 36th. IWCS, 337-343 (1987)
7. L. E. Davis, "A Global Test Method for Long Term Stability of Solid and Foam Skin Insulation." Proceedings of the 36th. IWCS, 475-482 (1987)
8. M. C. Light, Jr., "An Oil Separation Test to Predict Elevated Temperature Drip Performance of Optical Cable Buffer Tube Filling Compound." Proceedings of the 37th. IWCS, 459-464 (1988)
9. A. W. Stratton, T. J. Roessing, J. D. Burkhard, "A Comparative Stability Study Related to the Performance of PEPJ And ETPR Filling Compound." Proceedings of the 36th. IWCS, 322-326 (1987)

10. S. G. Foord, "Compatibility Problems in Filled Cellular Polyolefin Insulated Telephone Cables." Proceedings of the 26th. IWCS, 23-29 (1973)
11. C. K. Eoll, "The Aging of Field Cable with Cellular Insulation." Proceedings of the 27th. IWCS, 156-170 (1978)
12. J. P. Garmon, L. E. Davis, "A Comparison of the Properties of Foam and Foam Skin Insulation in Filled Cables." Proceedings of the 28th. IWCS, 232-243 (1979)
- 13) A. C. Levy, S. C. Welch, P. V. Croft, "Properties of Waterabsorbent Gels Formulated for use as Filling Compounds for Copper Telecommunications Cable and As Splice Case Encapsulants." Proceedings of the 40th IWCS, 242-250 (1991)

BIOGRAPHY

Lawrence E. Davis is the Manager of Engineering and Development for WaterGuard Cable Products. He received his B.S. degree in physics from Appalachian State University in 1969 and his M.S. degree in physics from the University of Wisconsin, Milwaukee in 1974. Prior to joining WaterGuard Cable Products Mr. Davis was the Senior Engineer in charge of designing and processing specialty fiber optic cables for Andrew Corporation, Senior Engineer for Materials/Processing for Superior Cable Corporation, Materials Engineering Manager for the Technical Staff of Siecor Corporation, and he was formerly a Materials Engineer for Continental Telephone Laboratories.

TABLE I

CABLE CAPACITANCE STABILITY
WATER IMMERSION AT AMBIENT TEMPERATURE
(25 pair, solid insulation, 24 gauge)
(avg. of 3 pairs)

DAYS	WATER TEMPERATURE (O C)	WATERGUARD FILLED CABLE
		% CHANGE
1	25	0.36
9	27	0.08
17	27	0.16
27	27	0.16
69	24	-0.4
87	21	-0.52
121	16	-0.76
218	14	-1.13
335	25	0.16

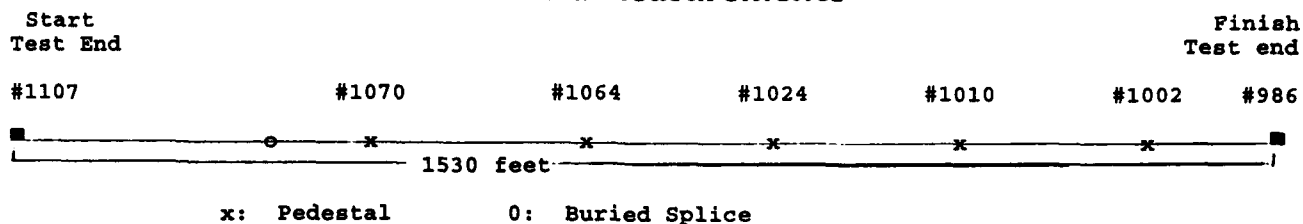
TABLE II
OIT OF ATC

SAMPLE	MINUTES	SAMPLE	MINUTES
1	95	5	65
2	60	6	102
3	71	7	77
4	63	8	117

TEST PARAMETERS: 220°C ALUMINUM PAN**CRITERIA: 10 MINUTES AT 190°C PREOXIDIZED
COPPER PAN**

FIGURE I

**Schematic of Essex's Cable run Selected
For Field Measurements**



Summary of Field Test Results

<u>Test</u>	<u>Requirement</u>	<u>Result</u> 3/19/92	<u>Result</u> 8/25/93
D.C. Resistance (Ohm/Mile)	140 Avg. 144 Max.	142.6 Avg. 143.2 Max.	142.1 Avg. 142.5 Max.
D.C. Resistance Unbalance (% Variance)	5% between any pair Average of all pairs 1.5%	Average 0.4 Max. Individual 0.9	Average 0.6 Max. 0.8
Mutual Capacitance (nF/mile at 1 Khz)	Average 83 ± 4 Max. Individual 92	Average 84.9 Max. 85.7	Average 84.6 Max. 85.5
Pair-to-ground (pF/Kft)	Max. Average 175 Max. Individual 800	Average 42 Max. Individual 76	Average 40 Max. 88
Attenuation (dB/Kft) at 772 Khz	Max. Average 5.6	5.09	5.23
Insulation Resistance (gigohm - mile)	≥ 1.0	Min. Individual 53	Min. Individual 29
Temperature		37°F	73°F

CORROSION TESTS FOR SHIELDING MATERIALS IN COPPER CABLE

Gardner Haynes and Robert Baboian

Texas Instruments Incorporated
Attleboro, MA 02703

The corrosion behavior of shielding materials in buried telephone cables has been studied extensively. A wide range of corrosion tests has been used. This paper reviews the various corrosion tests, discusses the applicability of these tests and highlights the relevance of existing data. Problems and pitfalls with the various techniques are pointed out and a hierarchy of corrosion tests is presented. It is concluded that the more rapid testing techniques provide useful information on corrosion mechanisms and that long term in-situ tests provide the most reliable data.

Introduction

The object of an accelerated test is to cause degradation or failure in a shorter time period than under natural conditions without changing the failure mechanisms. This can be accomplished using electrochemical techniques, simple immersion tests, and simulated soil burial tests. Soil burial tests where the specimens are buried in the actual soil environment are quite valuable. In general, the ability of the test to predict actual service performance increases with the length and complexity of the test. The most reliable predictor of performance is, of course, field service testing and experience.

Often, however, the need to evaluate new materials or constructions dictates that accelerated corrosion tests be used. The most rapid methods for making predictions involve the use of electrochemical techniques.¹ Zero resistance ammeter, polarization resistance, constant potential, potentiodynamic polarization, and AC impedance measurements have been applied to the prediction of corrosion behavior of cable shielding materials. Immersion studies, simulated soil burial in the laboratory and actual soil burial tests have been used when more time is available. Often results from these accelerated tests have been confirmed in field service trials. The purpose of this paper is to critically review these corrosion tests as well as the data generated by them. The benefits and limitations of the techniques are highlighted.

Electrochemical Tests

Although electrochemical measurements can be made in soils, electrochemical techniques have only been used in the laboratory to evaluate materials for copper cable. These techniques require discrete electrodes (so that current flow between them can be measured) and a supporting electrolyte. Ideally, the measurements are made in the actual electrolyte (solution) from the soil, however, synthetic solutions to simulate known soil compositions have also been used.

The zero resistance ammeter technique has been used

to monitor galvanic effects between dissimilar metals. The members of the galvanic couple are maintained at zero potential difference with an operational amplifier and the galvanic current between them is monitored (Figure 1).² This technique provides an instantaneous measurement of the galvanic current in the corroding system. Although it is useful for determining galvanic interactions, results from short term tests may not necessarily predict long term behavior. Often the galvanic current may decrease with increased exposure time due to film buildup, however, in cases where galvanically induced localized corrosion can occur the current may increase with increased exposure time.³ In some cases reversal of the anodic and cathodic members can occur. This test has been used by Schick to demonstrate that inhibitors in petroleum jelly can decrease galvanic corrosion between steel and aluminum in cables but he cautions that leaching of inhibitors over time will affect the results.⁴ This technique has been used to show that steel causes galvanic corrosion of coated (flooded) aluminum in certain environments and that plastic coated aluminum was superior.⁵ However, they compared total galvanic corrosion currents rather than current densities which may give a distorted view of corrosion mechanisms and neglected the long term degradation which can occur with organic coatings (leading to an induction period during which electrochemical methods can give misleading results).

The polarization resistance technique has been used to measure the instantaneous corrosion rate of metals. The current density necessary to polarize the metal a few millivolts from its open circuit potential is measured and converted to a corrosion rate.¹ The technique requires a working electrode (metal of interest), a counter electrode and a reference electrode. Since it measures the instantaneous corrosion rate, it is more useful for in-situ corrosion monitoring rather than long term prediction. It has been widely used for corrosion monitoring in the chemical process industry. This technique has been used for cable shielding materials and predicted that plastic coated aluminum would last 400 years while copper would last only 2.9 years in a sandy loam soil.⁶ Actual NBS-REA soil burial tests, however, have shown that copper is acceptable and that coated aluminum undergoes severe corrosion in this soil. This example illustrates the danger of extrapolating results from short term laboratory tests to long term service performance.

Constant (controlled) potential tests have been used to conduct mechanistic studies for cable shielding materials. The potential of the metal versus a reference electrode is held at a fixed value with a potentiostat.¹ This allows the investigator to control the oxidizing or reducing power of the environment and simulate effects such as stray currents, galvanic couples, aeration, etc.

This technique was used to confirm the potentials at which hydrogen is produced on cable shielding materials (Table I).⁷

Potentiodynamic polarization measurements have been used to evaluate mechanisms of corrosion of cable shielding materials. In this technique the current density of the metal (anodic or cathodic) versus a reference electrode is measured over a wide range of potentials.¹ The resulting curve can be used to predict the mechanisms of corrosion at any particular potentials. Computer controlled instruments are available for making these measurements (Figure 2). The technique is useful for predicting the behavior of passive metals, evaluating galvanic effects, determining the rate of cathodic reactions such as hydrogen reduction and measuring the corrosion rate. Potentiodynamic polarization curves have been used to demonstrate that copper galvanically protects type 430 stainless steel from pitting and crevice corrosion and causes galvanically accelerated corrosion of aluminum in soil water extracts.⁸ In the same study the mechanism of differential aeration corrosion of aluminum was described with measurements in aerated and deaerated soil water extracts. These mechanisms of corrosion have been confirmed in soil burial tests. More recently they have determined that oxygen reduction is the principle cathodic reaction on copper and type 430 stainless steel and hydrogen reduction predominates on aluminum in soils using potentiodynamic polarization.⁷ Anodic polarization measurements have been used to show that copper and type 430 stainless steel were more corrosion resistant than aluminum or steel in synthetic soil solutions.⁹ Although his predictions correlate well with data from soil burial tests they were based solely on the pitting potentials and neglected uniform corrosion. In acid soils or soils with readily reducible species, this methodology may not correctly predict corrosion resistance.

The AC impedance technique has been used to measure corrosion rates in high resistivity electrolytes and degradation of organic coatings. A small AC potential is applied to the test specimen and the resulting AC current is measured as a function of frequency.¹ The instantaneous corrosion rate is then calculated from the polarization resistance at an appropriate frequency in the spectra. This technique also allows the measurement of the impedance and capacitance of organic coatings on metals. This serves as a measure of initial quality of the coating and degradation of the coating in service results in changes in these values. AC impedance requires a three electrode system and computer controlled instrumentation. All of the properties measured by AC impedance are instantaneous values so that the technique is useful for mechanistic studies but should not be used for long term predictions. It has been extensively used in coatings research since it allows the properties of the coating to be followed as a function of exposure time to real world environments. This technique was used to compare electrolytic chrome coated steel to plastic coated steel.⁹ It was concluded that corrosion performance of the coated steel with defects was superior to bare steel and that undercutting of the coating does not occur. These results conflict with those from the NBS-REA soil burial tests where undercutting was observed in certain environments.

Immersion Tests

The corrosion behavior of shielding materials has also been evaluated in laboratory immersion tests. Guidelines for conducting these tests are given in ASTM G31-72, Standard Practice for Laboratory Immersion Corrosion Testing of Metals. A critical factor is selection of an appropriate electrolyte

to represent real world environments. Most of the tests for shielding materials have used actual solutions from soils or synthetic solutions of the electrolyte from NBS-REA test soils.

Simple immersion testing has the drawback that it does not produce some of the corrosion mechanisms that occur on buried cable. The fact that specimens are continuously immersed and have ample access to oxygen in the solution obscures differential aeration effects. Solution mobility also allows reactants or corrosion products to diffuse to or from the specimen surface so that concentration effects which occur in the static soil electrolyte are not reproduced. A modification of this procedure (soil beaker test) consists of burying the specimens in a washed sand in tall beakers and adding solutions with controlled chloride and sulfate concentrations that are equivalent to those found in most soils.¹⁰ Specimens can be retrieved periodically and metallographic analysis can be used to determine the degree of corrosion.

Soil Burial Tests

The National Bureau of Standards (now NIST) and the Rural Electrification Administration (REA) investigated the corrosion resistance of shielding materials through extensive burial tests.¹¹⁻¹⁸ These studies included over 100 different shielding materials and employed electrically isolated lengths of cable which had damage sites (windows and rings to simulate rodent, lighting, or other forms of damage) in the jacket as well as similar lengths of cable which were galvanically coupled to copper strips (Figure 3). The tests were conducted at established NBS test sites whose soil characteristics ranged from relatively benign to very corrosive. Earth resistivity was as low as 55 ohm-centimeters and as high as 30,000 ohm-centimeters while soil pH ranged from 4.0 to 8.8. Specimens were retrieved and evaluated yearly for up to 6 years. These studies provide a valuable source of information on the comparative corrosion resistance of various cable shielding materials. Results have been widely referenced and have often been used to judge the applicability of more rapid test methods.

The NBS-REA studies showed that corrosion behavior is strongly dependent on materials, design, and soil environment. For example bare aluminum and bare steel were severely corroded in most soils while stainless steels were corrosion resistant. Copper was susceptible in acid and sulfide containing soils but corrosion resistant in others. Organic coatings provided increased corrosion resistance when they were not damaged. Copper clad stainless steel had excellent corrosion resistance in all soils while copper clad steel had good corrosion resistance.

Another study evaluated the corrosion of sheet metal panels in burial tests for up to 10 years in four soils.^{19,20} The earth resistivity ranged from 24 to 29000 ohm-cm while the pH ranged from 3.4 to 7.3. The purpose of these tests was to compare the performance of metal panels to actual shields of the same materials in cables. The results, which were in agreement with the NBS-REA studies, showed that aluminum, steel, and copper corrode in one or more of the soils while copper clad steel has good corrosion resistance in all of the soils.

Field Service Tests

Service experience and field service tests are the most reliable predictor of actual performance. They include exposure in the actual environment as well as the effects of operating conditions on the cable. Operation of a cable design for long

periods of time in a particular environment can be used to judge the performance of that design in similar environments.

A major field service test program was conducted jointly by REA, Horry Telephone Cooperative, Dow, and Texas Instruments to determine the effects of alternating current on corrosion of cable shielding materials.²¹⁻²⁴ Five hundred foot lengths of telephone cable with intentional damage sites (windows, rings, and holes) were buried three feet deep and electrically connected in series to each other and in parallel to an existing cable which had a high level of AC. Short lengths of identical cables were buried two feet away from the test cable to serve as isolated controls. Shielding materials included bare aluminum-bare steel (ASP), coated aluminum-bare steel (CASP), coated aluminum-coated steel (CACSP), aluminum clad steel, coated aluminum clad steel and copper clad steel. They reported on techniques for analyzing the chemistry of the soil as well as measuring pH and resistivity.²² The soils in this study were considered mildly corrosive. Results from this study showed that alternating current increased the amount of corrosion of steel except when it was clad with copper which resulted in a decrease in the amount of corrosion of steel.²¹ Overall the performance of the shields was similar to that found in the milder NBS-REA sites.

Summary

Electrochemical, immersion, and soil burial corrosion tests have been used for shielding materials in copper cable. The applicability and limitations of these tests determine the utility of the results. A basic tenant of all corrosion tests is that longer test periods provide more reliable results. Since corrosion is environment sensitive, closely simulating the actual environment is also important. Obviously exposure of the cable in the actual operating environment for its intended life determines its performance.

Electrochemical techniques yield results in comparatively short periods of time. They require a fundamental understanding of electrochemistry in order to correctly interpret results and should be used with care. They are useful for predicting corrosion mechanisms but are limited in their ability to predict actual service life. In general, they can be used to screen a large number of candidate materials systems and eliminate obviously poor performers. They are also useful for predicting the behavior of galvanic couples and the propensity for localized corrosion.

Immersion tests are easy to conduct but require longer exposure periods. They require care in duplicating the cable environment. Electrolyte composition, aeration, diffusion of corrosion products and crevice effects should be considered in an immersion test program. This is particularly true for materials which are susceptible to localized forms of corrosion. Long test periods are necessary to make useful predictions of performance. A laboratory soil beaker test is preferable to a simple immersion test for predicting actual performance in service.

Soil burial studies are costly and require exposure for several years with intermediate retrieval and evaluation of specimens. They are, however, conducted in the actual environment and provide a reliable method for predicting service performance. Factors which have an impact on corrosion in soils include soil resistivity, pH, soluble salts, aeration, and drainage. The extensive NBS-REA soil burial program provides comparative performance data on a wide range of shielding materials in six different soils.

Field service tests and experience are the most reliable methods for determining the performance of cable shielding materials. Successful operation of a cable for many years in an environment insures that the cable will be satisfactory in similar environments.

References

1. Baboian, R., Ed., *Electrochemical Techniques for Corrosion Engineering*, NACE, Houston, TX, 1986.
2. Baboian, R., and Prew, P., *Low-Cost Electronic Devices for Corrosion Measurements*, *Materials Performance*, Vol. 32, No. 7, July, 1993.
3. Baboian, R., *Electrochemical Techniques for Predicting Galvanic Corrosion*, ASTM STP 576, ASTM, Philadelphia, PA, 1981.
4. Schick, G., *Effect of Inhibitors on Aluminum Shield in Telephone Cable Sheaths*, Paper 107, National Association of Corrosion Engineers, St. Louis, MO, March, 1972.
5. Bow, K.E., and Colter, L.G., *Corrosion Studies on Shielding Materials for Underground Telephone Cables*, 25th International Wire and Cable Symposium, Cherry Hill, NJ, November, 1976.
6. Choo, T.S., *Corrosion Studies on Shielding Materials for Underground Telephone Cables*.
7. Haynes, G., and Baboian, R., *Conditions and Mechanisms for the Formation of Damaging Hydrogen in Fiber Optic Cable*, 39th International Wire and Cable Symposium, Reno, NV, November, 1990.
8. Baboian, R., Haynes, G.S., *Corrosion Resistance of Copper Clad Stainless Steel Cable Shielding Materials*, *Materials Performance*, Vol. 14, No. 8, p.16, 1975.
9. Bow, K.E., *Corrosion Performance of Cable Armoring Materials in Direct Burial Applications*, Paper No. 63, NACE Annual Conference, New Orleans, LA, 1989.
10. Schick, G., Tellefson, K.A., Wieczorek, C.J., Kanen, R.M., and Johnson, A.J., *Hydrogen-Caused Signal Attenuation in Buried Optical Fiber Cables*, 41st International Wire and Cable Symposium, Reno, NV, November 1992.
11. Lohsl, G.A., Romanoff, M., *Corrosion Evaluation of Shielding Materials for Direct Burial Telephone Cables*, paper presented at the 17th International Wire and Cable Symposium, Atlantic City, NJ, 1968.
12. Lohsl, G.A., Romanoff, M., *Progress Report on Corrosion Evaluation of Shielding Materials for Direct Burial Telephone Cables*, paper presented at the 18th International Wire and Cable Symposium, Atlantic City, NJ, 1969.
13. Gerhold, W.F., McCann, J.P., *Corrosion Evaluation of Underground Telephone Cable Shielding Materials*, Paper No. 31, presented at the NACE Annual Conference, Houston, TX, 1976.

14. Gerhold, W.F., Fink, J.L., Corrosion Evaluation of Underground Telephone Cable Shielding Materials, NBSIR81-2243. Prepared for the Rural Electrification Administration; National Bureau of Standards; April, 1981.
15. Gerhold, W.F., Escalante, E., and Fink, J.L., Corrosion Evaluation of Underground Telephone Cable Shielding Materials, NBSIR 82-2509. Prepared for the Rural Electrification Administration; National Bureau of Standards; June, 1982.
16. Fink, J.L., and Escalante, E., Corrosion Evaluation of Underground Telephone Cable Shielding Materials, NBSIR83-2702, prepared for the Rural Electrification Administration; National Bureau of Standards; May, 1983
17. Fink, J.L., and Escalante, E., Corrosion Evaluation of Underground Telephone Cable Pedestals in Underground and Atmospheric Environments, NBSIR84-2810. Prepared for the Rural Electrification Administration; National Bureau of Standards; January, 1984.
18. Fink, J.L., Mathews, D., Hessler, G. and Speed, E., Corrosion Evaluation of Underground Telephone Cable Shielding Materials, NBSIR87-3546. Prepared for the Rural Electrification Administration; National Bureau of Standards, January, 1988.
19. Haynes, G.S. and Baboian, R., A Comparative Study of the Corrosion Resistance of Cable Shielding Materials, Materials Performance, Vol. 18, No. 2, p.45, 1979.
20. Baboian, R., Hartley, S.R., and Hyman, E.D., High Strength, Corrosion Resistant Clad Metal Shielding for Telephone Wire and Cable, paper presented at the 23rd International Wire and Cable Symposium, Atlantic City, NJ, 1974.
21. Baboian, R., Hessler, G., Bow, K., and Haynes, G., The Effect of Alternating Current on Corrosion of Cable Shielding Materials in Soils, Proceedings of the 37th International Wire and Cable Symposium, Reno, Nevada, November 15-17, 1988.
22. Haynes, G., Hessler, G., Gerdes, R., Bow, K., and Baboian, R., A Method for Corrosion Testing of Cable-Shielding Materials in Soils, ASTM STP 1013, ASTM, Philadelphia, PA, 1989.
23. Haynes, G., and Baboian, R., Field Corrosion Testing and Performance of Cable Shielding Materials in Soils, Materials Performance, Vol. 28, No. 9, September, 1989.
24. Haynes, G., and Baboian, R., Field Corrosion Testing and Performance of Cable Shielding Materials in Soils, Outside Plant, March, 1991.

Biographies



ROBERT BABOIAN is Head of the Electrochemical and Corrosion Laboratory at Texas Instruments in Attleboro, MA where he has developed corrosion resistant materials, devices, and test methods for over 25 years. He is a TI Principal Fellow, an ASTM Fellow, an SAE Fellow, and a NACE Fellow. He was Chairman of ASTM Committee G-1 on Corrosion, the NACE Research Committee, and the SAE Automotive Corrosion and Prevention Committee. He received the NACE Speller Award in 1988, the ASTM LaQue Award in 1990, the Suga Weathering Technology Foundation (of Japan) Award in 1991, and the W.T. Cavanaugh Award of ASTM in 1992. Baboian has authored over 140 papers and edited 10 books in the field of electrochemistry and corrosion and has 15 US patents. He received his Ph.D. degree in Physical Chemistry for Rensselaer Polytechnic Institute in 1964 and his BS degree in Chemistry from Suffolk University.



GARDNER HAYNES is currently a Senior Member Technical Staff of the Electrochemical and Corrosion Laboratory of Texas Instruments Inc. He received his Bachelor's Degree in Mechanical Engineering Technology from Northeastern University in 1974. He has been active in the field of corrosion for 20 years and has published many papers, edited one book, and holds 7 patents. His professional activities include chairmanship of numerous groups in both the American Society for Testing and Materials and the National Association of Corrosion Engineers.

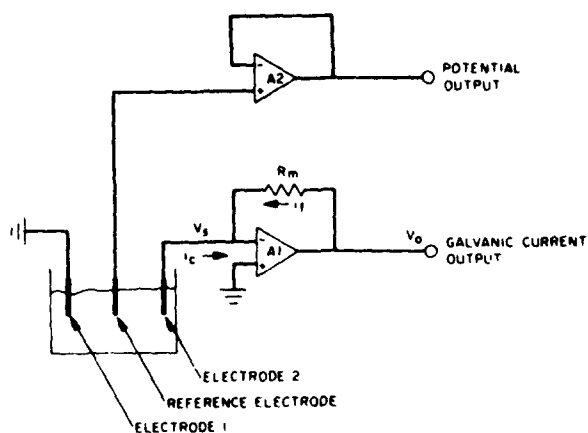


Figure 1 - Schematic Diagram Showing the Use of an Operational Amplifier as a Zero Resistance Ammeter

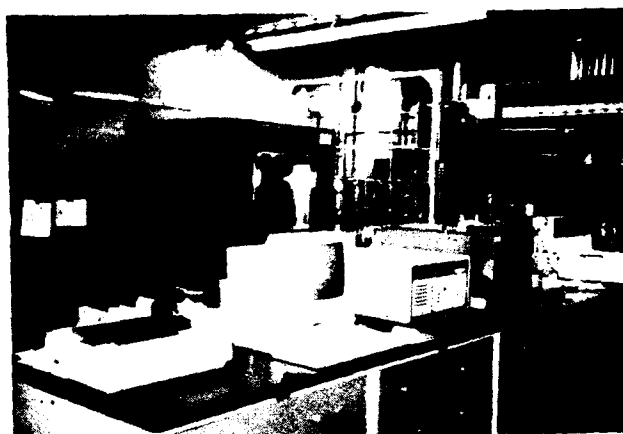


Figure 2 - Computer Controlled Instruments for Making Potentiodynamic Polarization Measurements.

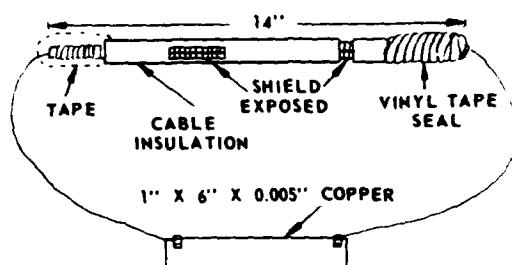


Figure 3 - Schematic Diagram of Cable Specimen with Shielding Coupled to Copper.

Table I
Potential at Which Hydrogen Was
Collected in Constant Potential Tests
(Volts vs. SCE)

Alloy	pH			
	2	4	6	8
Al	-0.65	-1.30	-1.30	-1.30
Steel	-0.70	-1.20	-1.20	-1.20
Cu	-0.70	-1.30	-1.30	-1.30

CORROSION IN SUBMARINE SYSTEMS AND TEST METHODS FOR EVALUATION OF LONG TERM PERFORMANCE

C.J Brown, G.McGurk, F.C Walsh* and B.D. Barker*

STC Submarine Systems Ltd, West Bay Road, Western Docks, Southampton, SO9 4YZ

* Department of Chemistry, University of Portsmouth, White Swan Road, Portsmouth, PO1 2DT.

ABSTRACT

In order to identify cost effective methods for corrosion protection of future submerged cable systems, this paper aims to review the types of corrosion mechanisms and identify suitable strategies for effective protection. The merits of alternative protection systems have been considered together with a description of possible test methods to verify their performance over a 25 year design life. These test methods include full-scale immersion tests in simulated sea water environments together with laboratory tests using standard electrochemical and non-destructive techniques.

1. INTRODUCTION

A corrosion process may be described as the degradation of a metal due to a chemical reaction with its environment. In a marine environment the process is generally electrochemical in nature, where the metal acts as an electrode and the sea water as an electrolyte. The process can be very complex and may involve several chemical reactions; only the basic mechanisms will be discussed in this paper. More detailed information may be obtained from the relevant literature¹⁻³.

1.1 The Corrosion Cell

The process of corrosion can be better understood by considering a corrosion cell shown in Figure 1. This cell represents a specific example of a galvanic cell. Two metals (in this case copper and zinc) are in electrical contact with one another and immersed in an electrolyte. The process involves the corrosion (oxidation) of the zinc electrode which acts as an anode, and the protection of the copper electrode which acts as a cathode. This is an electrochemical reaction in which the transfer of electrons has taken place. The corrosion cell demonstrates the five major components which must be present for a corrosion process to occur:

- an anode site, i.e. the metal
- a cathode site, another metal
- a cathodic (reduction) reaction and cathodic reactant to be reduced at the cathode site
- electronic contact between the electrodes.
- an electrolyte to give ionic contact between the electrodes to complete the cell.

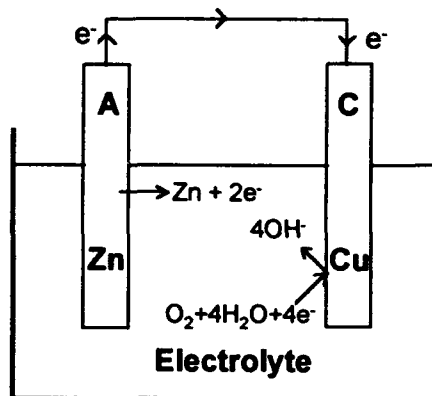


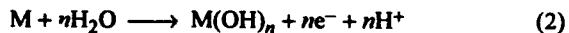
Figure 1. A corrosion cell showing the essential components for a corrosion current to flow, A=Anode, C=Cathode.

1.2. The anode

The anodic process results in the corrosion of the metal. The anodic reaction may involve the loss of electrons to form a cation:



or it may involve the formation of a hydrated metal or oxide layer:



1.3. The Cathode

Anodic metal dissolution will only be possible if a corresponding cathodic reaction is available. In neutral or alkaline solutions such as sea water, the predominant cathodic reaction is the reduction of dissolved oxygen:



However, local conditions may result in the reduction of water:



1.4. The Electrolyte

The ability to conduct electricity is due to the presence of ions in solution. The high salt concentration (35 parts per thousand) of sea water gives it a low resistivity and it is consequently a good electrolyte. There are many factors which influence the corrosive nature of sea water which will be discussed in section 1.6.

1.5. Cell Reactions

The cell reaction involves oxidation at the anode and reduction at the cathode. An electronic contact must exist between the electrodes for the transfer of electrons to occur from the anode, e.g. equation (1), to the cathode where they are consumed, e.g. equation (3).

Although the anodic and cathodic sites may be entirely separate as shown in Figure 1, they generally occur locally on a heterogeneous metal surface (Figure 2). The discrete anodes and cathodes forming individual micro cells can arise from several sources:

- **Differences in structure.** Differences in the metal phase may be present due to local heat treatment such as welding. Orientation and position of grain boundaries and the distribution of a second constituent may produce anodic and cathodic sites.
- **Differences in stress.** Any localised areas that become stressed will tend to be anodic and corrode. The stresses may be internal due to heat treatment or, external as in those introduced by the straining of components.
- **Differences in electrolyte composition.** Variations in local ionic conductivity (salt content) and oxygen content can cause anode and cathode areas to form. Differential aeration can be a major cause of corrosion. An area of metal in a low oxygen content electrolyte will become anodic to an area in a higher oxygen content.
- **Differences in temperature.** The potential exhibited by a metal is dependent on the temperature. Differences in temperature across a structure can result in potential differences and consequently corrosion cells being set up.

These differences may only play a part in the overall corrosion process which involves a very complex reaction sequence. The main corrosion types relevant to the marine environment will be discussed in section 2.

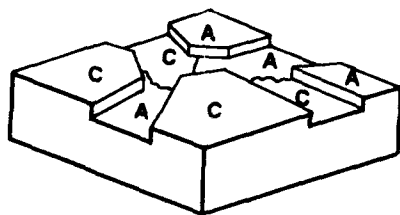


Figure 2 A schematic of a corroding metal. The anodic (A) and cathodic (C) sites are usually macroscopic and arise due to differences in e.g. stress levels, temperature. Imperfections such as grain boundaries and dislocations are usually anodic.

1.6 The Marine Environment

Submerged cable systems experience a range of sea water environments. In one cable system, the marine environment may include a combination of:

- shallow coastal waters
- polluted (industrial, organic) river estuaries
- large tidal zones or bottom currents
- buried/partially buried cable on sea bed
- deep ocean.

Corrosion rates can vary greatly between different environments. The composition of open seas and oceans are fairly constant with regard to their major constituents. The salt content is usually in the range of 33-37 parts per thousand. The parameters affecting the corrosion rates of metals tend to be the concentrations of minor constituents, e.g. dissolved gases and temperature. The effect of depth on the dissolved oxygen (DO) concentration, temperature and salinity (total salt content) for the Pacific Ocean⁴ is shown in Figure 3. The dissolved oxygen concentration is a very important factor in the corrosion of metals. As many corrosion reactions are controlled by the rate of diffusion of oxygen (equation (3)), any change in its concentration will affect the corrosion rate. The variation in dissolved oxygen not only depends on temperature and salinity but also on biological factors and the movement of water. Photosynthesis which occurs only in the upper depths will increase the dissolved oxygen level. At lower depths biological oxidation can reduce the dissolved oxygen level. An increase in water velocity will increase the supply of oxygen for the corrosion process.

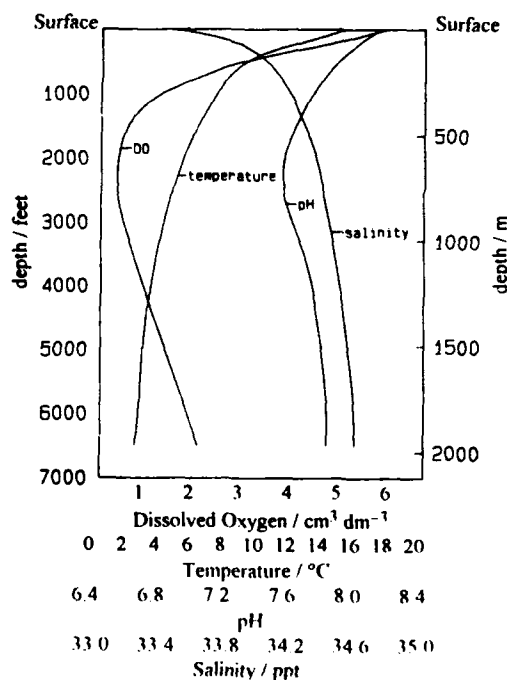


Figure 3 Variation in temperature, dissolved oxygen, salinity and pH for sea water as a function of depth.⁴

The temperature of the oceans can drop from over 20°C at the surface to near freezing point at the deep ocean floor, and from -2°C at the poles to 34°C at the equator. The very low temperatures encountered at the ocean bottom should substantially decrease the corrosion rates of all metals. However, localised 'hot spots' can be present and may be difficult to predict. The ocean water at lower depths cannot be assumed to be still; local and general currents are present and can be comparable to surface tidal currents. Corrosion rates generally decrease with increasing depth due to the decrease in temperature. As a very rough guide, a 10°C drop in temperature will result in a halving of the corrosion rate, however, this does not take into account any change in dissolved oxygen (oxygen concentration increases with a decrease in temperature). Marine fouling and its associated corrosion can also be expected to decrease with increasing depth. The variation in dissolved oxygen can have several effects on the corrosion rates. The effects on long line submerged cables will be discussed in the following section.

2. TYPES OF CORROSION

Corrosion can be divided into two main groups, those associated primarily with the metal and those associated with the environment.

2.1 Corrosion Types Associated With The Metal

2.1.1 General Corrosion

General or uniform corrosion is normally associated with random anode and cathode zones on a 'single' metal surface. When general corrosion rates are very low they do not represent a problem to the integrity of the system.

2.1.2 Localised Corrosion

Of much more concern are situations when corrosion is limited to smaller sites, i.e. it is localised. Figure 4 shows a number of localised corrosion types that can occur in the marine environment:

- **Pitting Corrosion** usually occurs with metals that have an oxide coating. The presence of an aggressive species, e.g. Cl^- , prevents the complete formation of the oxide layer thus enabling pits to develop as the underlying metal will be anodic to the coating. Pitting can occur where there is a weakness in the coating, e.g. at a grain boundary, impurity or second phase.
- **Bimetallic Corrosion** or galvanic corrosion occurs when two dissimilar metals with different potentials are in electrical contact in the same environment. The metal with the most negative corrosion potential will corrode at a faster rate than when it was uncoupled. Conversely, the metal with the most positive corrosion potential will corrode at a slower corrosion rate than in the uncoupled state. In general, large differences in corrosion potentials, high cathode/anode area ratios and highly conducting solutions will result in severe corrosion of the base metal.

- **Stress Corrosion Cracking** is a corrosion phenomenon the mechanism of which is still not fully understood. It will only occur when a continuous tensile load is applied to a surface in a corrosive environment. The load can be the result of internal stress, e.g. resulting from cold working, welding or heat treatment. The combination of stress loading and corrosion causes a crack growth into the bulk metal. Stress corrosion cracking results in the brittle failure of the metal with no plastic deformation occurring before failure. The stresses involved are generally at levels which on their own would not give rise to concern, i.e. below the yield or proof stress.

- **Intergranular Corrosion** can occur at the grain boundaries of a metal. Under certain conditions the grain boundaries can become very reactive resulting in active dissolution of the boundaries which, in severe cases, can result in the complete failure of the metal.

- **Selective Phase Corrosion** can occur in certain alloys. A common example is the graphitization of cast iron where the ferrite becomes anodic and dissolves out leaving the graphite in place.

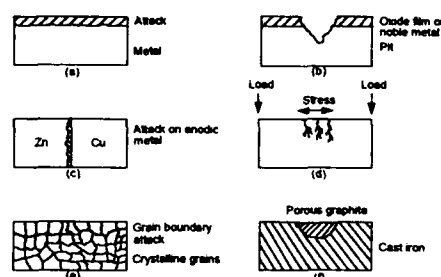


Figure 4. Types of corrosion. (a) General, uniform attack. (b) Pitting. (c) Galvanic corrosion. (d) Stress corrosion cracking. (e) Intergranular corrosion. (f) Selective phase corrosion, e.g. graphitization.

2.2 Corrosion Types Associated With The Environment

Within a submerged cable system, specific environments can be identified which may be detrimental to its corrosion performance. Figure 5 illustrates several of these which are described below.

- **Differential Aeration** of a metal's surface will result in a corrosion cell. The metal surface in a high oxygen concentration environment will be cathodic to an area of metal in a low oxygen environment which will then preferentially corrode. This can occur for example, when a cable is only partially buried. The low concentration of oxygen in the seabed relative to the flowing sea water above it may result in corrosion at the buried interface. It is the size of the concentration difference that is important. A change in oxygen concentration from 1.1 to 1.0 ppm would not cause a problem, whereas a change from 10.0 to 0.2 ppm could cause a failure. As discussed in section 1.6 the oxygen concentration of the open seas varies greatly with depth. This has been the cause of reported 'long line' corrosion effects of deep sea mooring lines, whereby accelerated corrosion has been observed at various depths with less corrosion in between. A differential aeration cell will also be created by differences in water velocity resulting in a different supply of oxygen to each area.

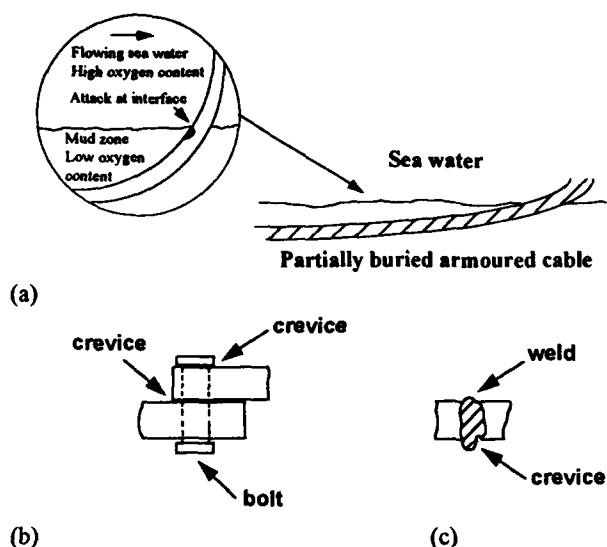


Figure 5. Types of localised corrosion associated with the environment. (a) Differential aeration corrosion. Crevice corrosion at a (b) loose rivet and (c) poorly dressed weld.

- **Crevice Corrosion** can be a severe form of localised corrosion. It can occur, as the name suggests, when a small crevice is introduced at the metal surface such as at a bolt head, washer or lap joint. The mechanism for this type of corrosion is complicated. It initially involves the setting up of a differential aeration cell, whereby the metal within the crevice is in an environment with a low concentration of cathodic reactant i.e. oxygen, and is therefore anodic to the metal outside the crevice. Active dissolution of the metal within the crevice therefore occurs, which results in the build up of positive ions (i.e. Fe^{2+}) within the crevice. The build up of positive ions is balanced by the migration/diffusion of Cl^- ions into the crevice, which results in the formation of metal chlorides. These chlorides are unstable and will undergo hydrolysis to form metal hydroxide and H^+ . It is the presence of a high concentration of hydrogen ions which can cause a rapid increase in the anodic dissolution of the metal within the crevice. The pH of sea water is around 8.1 but in a crevice this can fall to as low as 2.0.

- **Erosion Corrosion** is the combination of corrosion with physical removal of the metal due to mechanical action of the environment, such as flowing sea water with suspended solids. Sand can easily remove loosely adhered oxide films

- **Microbial Corrosion** can be further defined into two types. Fouling in shallow waters by *macro-organisms* such as shellfish, algae and weed can be the indirect cause of corrosion. Their presence can result in increased corrosion due to differential aeration and the prevention of metal oxides from forming complete protective films. *Micro-organisms* such as bacteria can be the direct cause of corrosion. One of the most important bacteria of this type is *Desulfovibrio desulfuricans*, a sulphur reducing bacteria which proliferates in oxygen free environments. The type of environments in which this bacteria may be present and of concern to cable laying operations would be the mud bottom of polluted harbours, inshore and coastal waters. The accepted mechanism of corrosion in the presence

of sulphur reducing bacteria (SRB) is that the bacteria acts as a cathodic depolariser. When no oxygen is present the cathodic reaction is the evolution of hydrogen which is adsorbed on the metal surface and can prevent corrosion. The bacteria remove the cathodically produced hydrogen for use in their metabolic cycle enabling corrosion to continue.

- **Stray Current Corrosion** can occur when a DC electric current passes from a metal to earth. The source of the current can be from the structure itself, i.e. an earth return in a power system. It may also result from induced currents from an external source. In the case of cable systems, location near to other sub-sea structures or installations which have cathodic protection systems (discussed later in section 3.3) in operation may result in stray current corrosion. Of particular importance to long lay cable systems is the effect of *Magnetohydrodynamics* (MHD). A conducting body of fluid moving through the earth's magnetic field will generate a potential perpendicular to the direction of motion. If a cable lies at right angles to the fluid flow, as in a channel, then current loops between the cable and earth points can be set up. This effect has apparently been sufficient to contribute towards the failure of a sub-sea repeater unit in the Straits of Florida⁵. The mechanism for failure was the breakdown of the protective oxide coating due to the potential developed by the stray current, resulting in severe pitting corrosion.

3. CORROSION PREVENTION AND CONTROL

In a medium such as sea water, the complete prevention of corrosion is unlikely. Its effect, however, can be greatly minimised by a combination of careful design, material selection procedures, the application of protective coatings and/or cathodic protection systems.

3.1 Design Considerations

If the Design Engineer is fully aware of the possible consequences of corrosion within the system, then relatively simple but effective measures can be taken to eliminate potential problems. In terms of the geometry of the component(s) to be used in a sea water environment, the main type of corrosion to be aware of is crevice corrosion. Figure 6 gives an example of poor and improved designs with regard to crevice corrosion. Small contact angles, loose fitting bolts/rivets and poorly dressed welds can all create potential areas for crevice corrosion. Crevices can also provide key points for biofouling (microbial corrosion). Other factors which should be considered are the distribution of local stresses and the positioning of earth points in powered systems.

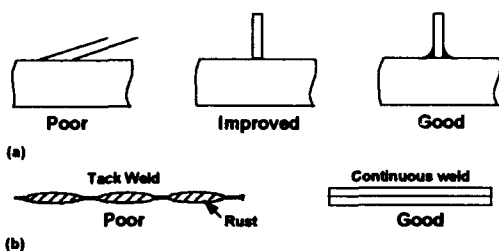


Figure 6. (a) Small or sharp joint angles can create potential areas for crevice corrosion. (b) Tack welds should be avoided.

3.2 Material Selection

The corrosion resistance of a material is only one factor in the overall selection procedure (Figure 7). With the ever increasing number of alloys available, careful selection is essential to avoid a number of corrosion mechanisms.

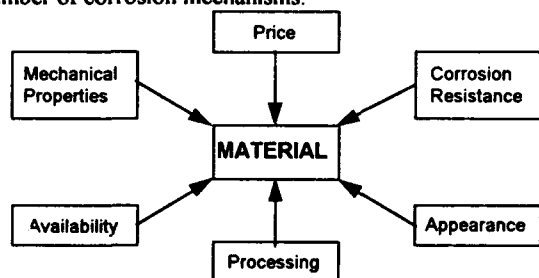


Figure 7. Factors effecting the choice of an engineering material. After Pludek⁷

As discussed in section 2.1.2, bimetallic or galvanic corrosion is possible when two different metals are in electrical contact. The effect of coupling two dissimilar metals can, to some degree, be predicted by consulting a galvanic series (Table 1). The series lists the potentials of the metals/alloys in a given environment, in this case flowing sea water. The further apart the two metals are in the series, the greater the chance of corrosion. However, it is important to realise that a galvanic series does not give any information on the possible rates of corrosion. The series also does not take into account changes in the environment such as flow conditions and temperature. The relative positions of the metals within the series may, therefore, change and its use in predicting corrosion should only form part of a selection and testing procedure. It is rare that a system can be constructed from one material so it is therefore essential that preventative measures are taken to avoid severe galvanic corrosion. Insulation of the metals, i.e. to prevent electronic contact, is the obvious choice, but the insulation must be complete. When bolting two metals together, not only should insulating washers be used, but the thread should also be insulated with a sleeve (Figure 8). It is important that the method of insulation does not compromise the mechanical integrity of the joint since failure of the insulation during service would result in coupling of the metals. It is also not sufficient to rely on protective organic coatings to provide insulation as their integrity over a design lifetime can never be guaranteed. If insulation is not practical then the ratio of cathode/anode area should be as small as possible.

↑	Platinum
Noble or cathodic	Gold
	Graphite
	Titanium
	Silver
	Hastelloy
	18-8 Mo stainless steel (passive)
	18-8 stainless steel (passive)
	Chromium stainless steel 11-3-% Cr (passive)
	Inconel (passive) (80 Ni, 13 Cr, 7 Fe)
	Nickel (passive)
	Monel (70 Ni, 30 Cu)
	Cupronickels (60-90 Cu, 40-10 Ni)
	Bronzes (Cu-Sn)
	Copper
	Brasses
	Inconel (active)
	Nickel (active)
	Tin
	Lead
	Ni-Resist (high Ni cast iron)
	Chromium stainless steel, 13% Cr (active)
	Cast iron
	Steel or iron
	Aluminum (commercially pure)
Active or anodic	Zinc
↓	Magnesium or magnesium alloys

Table 1. Galvanic series of some metals and alloys in sea water.

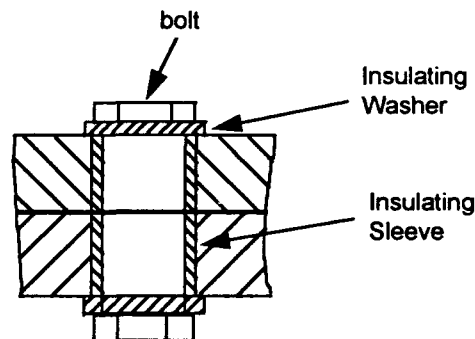


Figure 8. Avoidance of galvanic corrosion by fully insulating the bolted components.

The importance of the environment on material selection cannot be stressed too highly. The application of a material regarded safe in one environment may prove damaging in another. For instance, stainless steels owe their corrosion resistance to their ability to form passive oxide films. However, the application of several types of these alloys, in many marine environments, is limited due to their susceptibility to pitting and crevice corrosion in chloride containing waters. In general, alloys that owe their corrosion resistance to the formation of protective oxide layers, should be selected with care when considered for low oxygen/high chloride environments such as buried sea bed and stagnant waters

3.3 Protective Coatings

The criterion for an effective and economical coating includes:

- greater resistance to the environment than the base material
- compatibility with the base material
- effective application to the geometry of the component.

Protective coatings come under two main categories, metallic or organic/inorganic paint coatings. There are many types of coating which fall into each category whose description is outside the scope of this paper. Only coatings which have seen considerable use in marine environments will be discussed.

3.3.1 Metallic Coatings

Metallic coatings can either be anodic or cathodic to the underlying base metal. Anodic coatings such as zinc and aluminium on iron will protect the base metal at cracks or discontinuities in the coating. Cathodic coatings such as copper on steel should be avoided in marine environments, since any crack in the coating will result in severe pitting corrosion of the base metal. Metallic coatings can be applied to a substrate by a variety of techniques, i.e. hot dipped, spray, diffusion and electrolytic deposition, details of which can be found in the relevant literature⁸⁻¹⁰. Each technique has its own merits (i.e. coating thickness, cost and ease of application) and may be suited to only one component of the system. For example, armour wires for cables are readily galvanised (hot dip zinc coating) to provide a long lasting and effective coating. However, due to the process temperature ($\approx 460^{\circ}\text{C}$) involved, this technique is not suited to components that are sensitive to thermal stresses. Apart from zinc, aluminium is the most widely used metallic coating for steel in marine environments. As with zinc its physical properties allow it to be applied using a number of techniques to suit the substrate requirements. All metallic coatings require specific surface preparations which may include cleaning (solvent or alkali degrease), pickling (removal of mill scale) or blast cleaning. If a metallic coating is to be used then the designer must take both the surface preparation and application techniques into account. For large marine structures, an aluminium-zinc spray coating offers very effective corrosion protection.

3.3.2 Organic/Inorganic Coating Systems

Inorganic coating systems applicable to marine environments include the use of vitreous enamel and metal conversion coatings such as the anodising of aluminium. Organic coatings consist of a primer, undercoat and top coat. Primers can also have a high inorganic content such as zinc primer which will act as an anodic coating to steel. There are a number of organic coating systems which are effective in the marine environment, including epoxy, chlorinated rubbers, polyesters and various polyvinyls. The paint should normally have a resistance in excess of 10^8 ohms for it to offer good protection. Hence the protection provided by the coating is directly related to the coating thickness. As with metallic coatings, the surface preparation prior to coating is of great importance. Inadequate preparation will result in poor adhesion of the coating and its early failure.

For a long design life a combination of a metallic coating and a multilayer paint system will provide the best protection possible. An example of such a system would be the galvanising of a base steel component, followed by an etch primer, then a two pack ($\approx 300\ \mu\text{m}$) epoxy coating, with each layer containing micaceous iron oxide which acts as a good physical barrier.

Cathodic protection is the method by which the potential of a metal is lowered to such an extent that it becomes completely cathodic in nature. The current required for this to occur can be supplied either by a DC power source (an Impressed Current System), or by using sacrificial anodes such as zinc or aluminium. Each system has unique advantages and disadvantages in their applications to submerged cable systems^{1,8}. Sacrificial anodes are simple to install and require no external power source. However, sufficient anode material must be present to avoid costly replacement. For an uninterrupted design life of 25 years they may therefore not be practical. Impressed current systems require a continuous power supply which may not be available. Cathodic protection systems can be used to supply additional protection over that of a paint system which cannot be guaranteed to provide 100% protection. In fact the combination of the two systems will substantially reduce the current requirement for the cathodic protection.

4. CORROSION TESTING

Corrosion testing of materials and assembled components is essential if the quality of the system is not to be compromised with regard to its performance and expected lifetime.

4.1 Corrosion Testing

Corrosion testing can be carried out at several levels depending on such factors as the time and money available, information required and the testing facilities available. As discussed by F.P. Ijsseling¹¹ the corrosion testing may also be classified by the purpose of the test, e.g.:

- tests to obtain data on the corrosion behaviour of systems under practical conditions
- tests aiming to provide insight into the corrosion mechanism of the system
- standardised tests, used to determine whether a material performs within previously agreed conditions
- comparative tests for ranking/screening purposes to assist in material selection.

Classifying testing by the type of facility, one can highlight the experiments that can be carried out and the relevance of the results obtained:

- **Laboratory bench testing** can be used for the screening and initial selection of materials. All standard electrochemical and corrosion techniques (discussed in a later section) can be applied to allow rapid determination and continuous monitoring of free corrosion potentials, possible galvanic couples and corrosion kinetics. Important electrolyte parameters such as temperature, oxygen content and salinity can also be carefully controlled in the laboratory environment, thus providing the

possibility of accelerated testing. The disadvantage of purely laboratory testing is that the test conditions rarely simulate those observed in practice. Small material samples may be different in composition and surface finish giving rise to different results from bulk service materials. However, laboratory testing will provide comparative information and possible insight into the susceptibility of a material to a particular corrosion mechanism.

- **Pilot scale testing** should simulate more closely the corrosion environment expected during service. It should allow the testing of coupon samples of the metal as well as fully assembled components and sections. Although operating on a larger scale, several parameters should be under control, or at least monitored. When using a closed loop test circuit, the electrolyte composition can be controlled as well as the temperature and flow rate. Environmental conditions which can be simulated on a pilot test scale include buried cable sections, the effects of biological activity, and erosion mechanisms. The size of the facility would require greater capital investment and the testing period would obviously be of a longer duration. The results obtained should give an indication of the overall system performance.

- **Field testing** represents the only method by which true corrosion data for the system can be obtained. However, it is seldom¹² undertaken with regard to cable systems due to the expense involved in cable laying/retrieval and the time required for testing (> 6 months). Since remote sensing equipment is also very expensive, continuous monitoring of the system is unlikely, although if used it would represent a powerful tool for the investigation of corrosion.

4.2 Corrosion Measurement Techniques

Measurement techniques used in corrosion studies can be divided into those involving electrochemical, physical or surface analysis methods³.

- **Electrochemical** techniques form the basis of any corrosion study. The measurement of the corrosion potential, E_{COR} , and its variation with time will give an indication to the overall condition of the metal. Galvanic couples are monitored using a zero resistance ammeter (ZRA). This device allows the measurement of the galvanic current flowing between the electrodes without the result being affected by the internal resistance of the meter. Linear polarisation resistance (LPR) measurements (Figure 9) can lead to values for the corrosion current, I_{COR} for a given metal. The techniques mentioned above can all be used in the laboratory and in the field to obtain real corrosion data. Other more sophisticated techniques such as AC impedance, the determination of exchange current densities and transfer coefficients by current vs potential measurements¹³ are based in the laboratory.

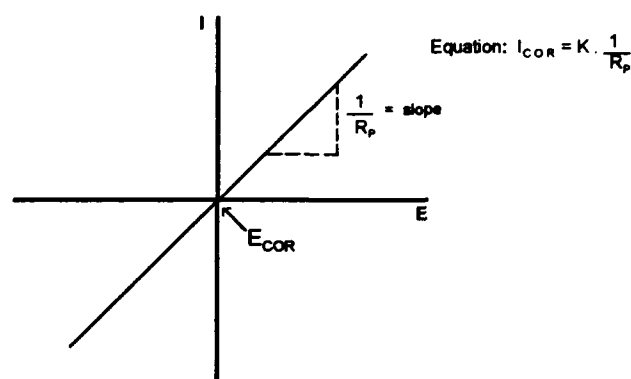


Figure 9. Experimental determination (a plot of current vs potential) of the corrosion current, I_{COR} using the Linear Polarization Resistance technique.

- **Physical** techniques include weight loss measurements which are used to determine corrosion rates of metal samples during pilot and field testing. In laboratory experiments, using closed systems, the analysis of the electrolyte can also give information regarding the active metal dissolution, especially important when dealing with alloys.

- **Surface** techniques include optical and scanning electron microscopy used to determine the surface shape and texture, coating thickness and porosity. Very specialised techniques include X-ray diffraction which looks at phase composition and Energy Dispersive X-ray Spectroscopy which gives a semi-quantitative elemental analysis.

5. CONCLUSION

This paper has reviewed the fundamental aspects and types of corrosion mechanisms involved in the marine environment of submerged cable systems. Protection methods including inorganic/organic coatings, and cathodic protection systems have been considered. For a deep water submerged cable system, the most cost effective protection system would involve a metallic coating with a suitably thick organic coating which would provide additional protection especially during laying operations.

The importance of both material selection and corrosion testing has been discussed. A wide variety of techniques should be used in ascertaining the corrosion performance of materials and components, with the test data being applied in the light of operational experience.

References

1. **Designing For Corrosion Control**, R.J. Landrum, NACE, Texas, 1989.
2. **An Introduction To Corrosion & Protection Of Metals**, G. Wranglen, Chapman & Hall, London, 1985.
3. **Corrosion Engineering**, M.G. Fontana, McGraw-Hill, New York, 1987.
4. **Marine Corrosion**, F.L. LaQue, J. Wiley & Sons, Inc, New York, 1985.
5. E.A. Franke, *IEEE J.of Oceanic Eng.*, 4, 89, July 1979.
6. **Corrosion Engineering**, M.G. Fontana & N.D. Greene, McGraw-Hill, 2nd ed, New York, 1978.
7. **Design & Corrosion Control**, V.R. Pludek, MacMillan Press Ltd, London, 1977.
8. **An Introduction To Metallic Corrosion**, U.R. Evans, Edward Arnold Ltd, London, 1981.
9. **Marine Corrosion**, T.H. Rogers, George Newnes Ltd, London, 1968.
10. **Principles Of Metal Surface Treatment & Protection**, D.R. Gabe, Pergamon Press Ltd, 1972.
11. **General Guidelines For Corrosion Testing Of Materials For Marine Applications**, F.P. Ijsseling, The Institute of Metals, London, 1989.
12. H. Tsunoda, K. Suzuki & H. Hisamatsu, *Review Of The Elec. Comun. Laboratories*, 25, 505, 1977.
13. **Industrial Electrochemistry**, D. Pletcher & F.C. Walsh, 2nd ed, Chapman & Hall, London, 1990.



Craig J. Brown
STC Submarine Systems Ltd
West Bay Road
Western Docks
Southampton
SO9 4YZ
UK

Dr. Craig Brown is a Teaching Company Associate in the New Product Development Group at STC, working with the University of Portsmouth. Since joining STC in July of this year he has been involved with the corrosion testing and design of cable components.

He received a BSc in Applied Chemistry from Portsmouth University in 1989. He then went to the University of Southampton to study Electrochemistry completing his PhD in 1992.



Ged McGurk
STC Submarine Systems Ltd
West Bay Road
Western Docks
Southampton
SO9 4YZ
UK.

Ged McGurk is a Product Development Manager in the New Product Development Group at STC Submarine Systems Ltd, Southampton.

He received a BSc (Eng.) in Metallurgy & Materials Science from Imperial College of Science & Technology, University of London in 1986.

Des Barker
Dept. of Chemistry
University of Portsmouth
White Swan Road
Portsmouth
PO1 2DT
U.K.

Dr. Des Barker obtained a BSc (Eng) in Engineering Metallurgy from London University and subsequently studied for a PhD in Corrosion under the guidance of the late Lionel Shreir. For the last 25 years he has been lecturing in Corrosion & Protection. His research interests include the preservation of marine archaeological artefacts, electroless deposition techniques, marine corrosion and the study of protective coatings. He has been secretary and chairman of the Education Committee of the Institute of Corrosion Science.

Frank Walsh
Dept. of Chemistry
University of Portsmouth
White Swan Road
Portsmouth
PO1 2DT
U.K.

Dr. Frank Walsh is an electrochemical engineer and has 15 years experience of academic and industrial projects in the fields of electrochemical reactor engineering, corrosion protection and electroplating. He holds a BSc in Applied Chemistry from Portsmouth, an MSc in Materials Protection from UMIST/Loughborough and a PhD in Electrochemical engineering from Loughborough. His areas of interest include the mechanism of corrosion inhibition, electrochemical techniques for corrosion monitoring and the evaluation of protective coatings.

MECHANICAL LIFETIME OF OPTICAL FIBERS

W. Griffioen

PTT Research
P.O. Box 421, 2260 AK Leidschendam, The Netherlands

ABSTRACT

A simple lifetime model for optical fibers remained after a COST-218 study of 12 models, based on the power law. It is shown that this law can be used without extrapolation errors. A model is presented for sharp and blunt weak flaws, also in harsh and wet environments, including zero stress aging. Lifetime calculations are compared for different environments using a practical example.

1 INTRODUCTION

Recently there have been huge investments in optical cables installed in trunk networks. In the future the investments are expected to increase dramatically, as optical fiber is introduced into access networks. Optical transmission performance can, largely, be evaluated immediately after installation. Because of the time dependent nature of fiber strength, mechanical performance is difficult to assess at an early stage. Current mechanical lifetime estimations of optical fibers in service are based upon the assumption that stress corrosion is the failure mechanism. This mechanism is often described by the power law.¹ In practice other effects such as crack blunting², zero stress aging³ and fatigue knees³ occur. Detailed understanding of these effects is necessary for manufacturers to optimize optical fibers. Telecom operators are interested more in the extent to which these effects may occur in their (future) installed fibers, without causing premature fracture. In this paper an overview of lifetime models is presented, starting with a framework which remained after a study in the European COST-218 (WG1) project of 12 existing models for ambient environments, and developed further for harsh and wet environments. The different effects are treated worst case.

2 POWER LAW OR EXPONENTIAL LAW

Stress corrosion can be described by the exponential law, based on chemical reaction kinetics, which has a physically reasonable basis:⁴

$$\frac{da}{dt} = v_0 \exp\left(\frac{-E_0 + bK_1}{RT}\right) \quad K_1 = Y\sqrt{a}\sigma \quad (1)$$

with da/dt the speed at which a crack with size a grows, v_0 a scale constant, R the gas constant (8.31 J/K), T the temperature, E_0 the zero-stress activation energy, K_1 the stress intensity factor (catastrophic failure when the critical factor K_{Ic} of 8×10^{-4} GPa $m^{1/2}$ is reached), Y a geometrical factor (1.24 for semi-elliptical cracks), σ the applied stress and b a value, usually assumed constant.⁵

A simpler description, keeping mathematics tractable, is an empirical fit of data with the power law:¹

$$\frac{da}{dt} = AK_1^n \quad (2)$$

with A a scale constant and n the corrosion susceptibility.

Care should be taken when using the power law because it is less conservative for extrapolation to longer (life)times. In Fig. 1 an example is shown where the power law (straight line a)) does not fit the data (COST 218 round robin)⁶. The exponential law (line b)), drawn here in an attempt to fit fatigue knees in water from³, however, fits the round robin even worse (convex instead of concave).

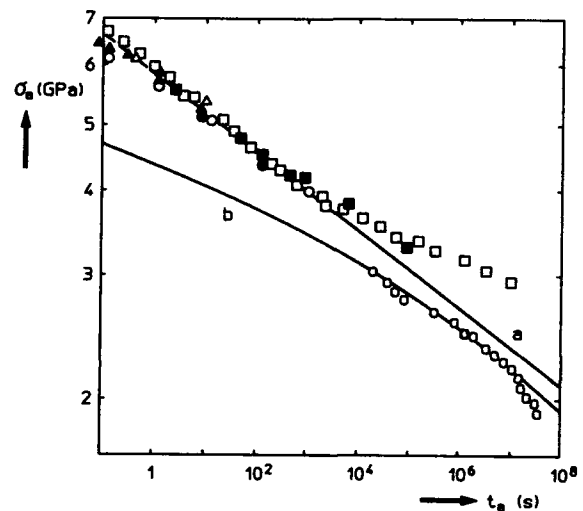


Figure 1 Stress σ_a against time t_a (log-scale) for failure due to stress corrosion. Lines a) (power law) and b) (exponential law) are drawn to fit the COST-218 round robin (different symbols)⁶ at 20°C, 50% RH and double mandrel experiments (circles)³ in water of 30°C respectively.

An increase in n -value for longer measuring times, such as in the COST 218 round robin, is caused by crack blunting according to many investigators.² At low stresses, when crack growth from stress corrosion is small, blunting dominates while for high stresses the opposite is true. When extrapolating measurements to service conditions it should be noted that the important effects occur at the crack tip, i.e. the stress at the crack tip and its related speed of crack growth shall be considered, and not the applied stress or its related time to fracture. In this view it is important to realize that weak flaws that give failure in service are much larger than flaws from the high strength mode. From the power law the following expression for K_1 , which is a measure for the stress at the crack tip and also for the speed of crack growth, can be derived:⁷

$$K_1 = K_{Ic} \left[1 + \frac{\sigma_a^2 t_a}{B} \left(1 - \frac{t_a}{t_f} \right) \right]^{-\frac{1}{n-2}} \quad (3)$$

with B a constant related to A via $B = 2/(AY^2(n-2)K_{1c}^{n-2})$, σ_a the applied stress and t_a the time to failure under this stress. From (3) it is clear that different cracks show equal stress intensity, as a function of the normalized time t/t_a , for equal $\sigma_a^2 t_a$. Hence it follows that, in order to have the same crack tip stress during testing and service, $\sigma_a^2 t_a$ should be the same for different cracks. In service the stress σ_a is much lower (well below the proof test level) than with testing. Hence fatigue testing on intrinsic flaws should be performed in much shorter times (a few weeks) than the service lifetime (30 years) of weak flaws, when the same stress at crack tip and crack speed are required.⁷ In⁷ it is shown that the power law is not necessary to obtain the condition of equal $\sigma_a^2 t_a$.

The following can be concluded. When measurements are performed on the high strength mode, stress corrosion may be distorted by other effects such as crack blunting. Because of that the exponential law may give even worse fits than the empirical power law. Most measurements are performed within a time at which stress corrosion has the same magnitude as for the weak flaws during service. Hence no extrapolation in time is needed for lifetime models and there is no objection to fitting the data with an empirical power law, including effects other than stress corrosion. Hence the power law is a good tool (mathematically tractable) for lifetime models. Short measurements give the lowest n -values and are hence worst case. Care should be taken that n -values are not collected from extremely long measurements. The situation is different in the case of blunt weak flaws (Section 4) where measuring times of a few weeks are also worst case.

3 BLUNT PIT MODEL

In the description of stress corrosion of optical fibers, e.g. by the power law¹, it is assumed that the cracks are sharp. Such a crack is shown schematically in Fig. 2 a). In the case of stress corrosion bond rupture always occurs at the crack tip. The crack growth is hence 1-dimensional (not necessarily a straight path) and the size of the crack tip remains the same as that of a ring in the micro-structure of the fused silica.⁸ When the crack grows slowly, blunting may occur as is illustrated in Fig. 2 b). Blunting is often observed as an increase in n -value for long measuring times (previously discussed) or, sometimes, as an increase in strength after aging in water.⁹ A blunt pit may also grow in pristine fibers under zero stress conditions due to random etching of the environment, a process called zero stress aging.³ When stress corrosion occurs in such a blunt pit, the crack may look like the one in Fig. 2 c), due to the 1-dimensional character of stress corrosion. For stress corrosion, blunting and aging, aggressors are needed to rupture bonds in the fused silica. A small aggressor like water fits easily in sharp cracks, as in Fig. 2 d), and is a major cause of stress corrosion. When cracks are blunt larger aggressors may participate, see Fig. 2 e).

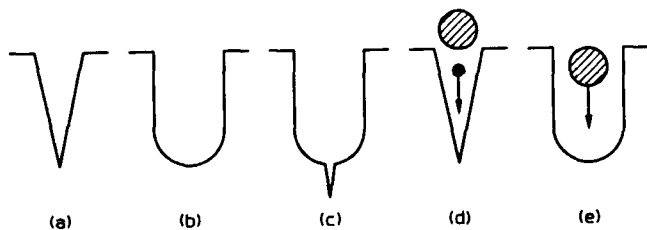


Figure 2 Different crack shapes: a) sharp, b) blunt, c) blunt pit with sharp crack, d) sharp with small aggressor and e) blunt with large aggressor.

The physics of bond rupture, assisted by environmental aggressors, should be the same for stress corrosion, blunting and aging, if only one type of chemical reaction occurs. The effect of stress is simply lowering of the potential well of the bound state of a ring connection in the fused silica. This means that all effects should be described by the same law. The exponential law has a part which describes zero stress aging (the term with E_0). Equation (1) is solved for zero stress conditions and for static loads applied on pristine fibers⁹, bearing in mind that the sharp crack assumption (Griffith)¹⁰ of the calculated stress concentration around a crack (Inglis)¹¹ is no longer valid. From this solution it became clear that zero stress aging and fatigue knees cannot be related using the exponential law. Hence it was concluded that the anomalous effects in water cannot be described by crack growth on a simple sharp crack geometry with only one kind of aggressor that reaches all corners of the crack, as in Fig. 2 d). A blunt pit with a sharp crack was suggested, like in Fig. 2 c).⁹ Here large (and small) aggressors may etch the pit, while only small aggressors (like water), may participate to the stress corrosion in the sharp crack.

In the blunt pit model it is assumed that etching and stress corrosion processes work independently of each other (worst case). Etching (non uniform) causes roughening of the surface (pits), without the occurrence of sharp cracks (this is also how an aged fiber surface looks like under a STM)³. It is assumed that sharp cracks are much smaller than the pits, which is not in conflict with reality¹², and "see" a uniform stress σ_{pit} , which is the concentrated stress at the bottom of the pit. Assume that the pits grow with constant speed. From this a stress amplification factor f_{pit} follows as a function of time t :⁹

$$f_{pit} = C_{pit} \sqrt{t} + 1 \quad (4)$$

with C_{pit} a constant. At the same time a crack grows at the bottom of this tip (Fig 2 c)) under stress corrosion, for which the power law can be used. The exponential law can be used to fit zero stress strength decrease data at different temperatures (here $C_{pit} = Y\sqrt{v_0}/C_p \cdot \exp(-E_0/(2RT))$ with C_p a constant)⁹. With this the zero stress aging data from³ result in an explanation of the knees in static fatigue experiments in⁹. The blunt pit model also helps to understand that abraded fibers can increase in strength when stored in water under zero stress (aging and blunting), while fatigue knees occur under stress (aging and stress corrosion).¹³

4 LIFETIME MODEL

In the recent past 12 lifetime models existed, which were only applicable to ambient service environments. In a COST-218 study these models were condensed to a simple framework of one basic model, with an alternative for on-line proof testing.¹⁴ Later this framework was developed further for harsh (e.g. splice boxes and aerial cables)¹⁵ and wet (e.g. metal free cables)¹² environments. All studied and developed models make use of the empirical power law (2). This is, as discussed previously, a good fit function of the measured results (high strength mode) and does not cause errors when extrapolating to service times (weak flaws). It is assumed that the stress corrosion is the same for the high strength mode (measurements) and the weak flaws (determine service lifetime). This is justified in Section 2 and by experiments on abraded fibers.^{16,17}

The other assumption in the derivation of the presented lifetime model frameworks is a Weibull distribution for the initial inert-strength S_i distribution:

$$LN(S_i) = -\ln(1-F(S_i)) = \frac{L}{L_0} \left(\frac{S_i}{S_0} \right)^m \quad (5)$$

in which N is the cumulative number of flaws per unit of length causing fracture at S_i , F the failure probability for a length L , m the Weibull parameter, representing sharpness of the distribution, and L_0 , S_0 scale constants.

4.1 Basic model

Existing lifetime models all assume sharp weak flaws. The "sharp" basic model, which can be used in ambient and harsh service environment (as long as zero stress aging does not occur), follows from (2) and (5):^{14,15}

$$\sigma_a = \left(\frac{B_a t_p}{B_p t_a} \right)^{\frac{1}{n_a}} \left[\left\{ 1 - \frac{L_0}{L} \ln(1-F) \left(\frac{B_p S_0^{n_p-2}}{\sigma_p^{n_p} t_p} \right)^{\frac{m}{n_p-2}} - 1 \right\}^{\frac{n_p-2}{m}} \right]^{\frac{f}{n_a}} \sigma_p \quad (6)$$

where $f=(n_a-2)/(n_p-2)$, the index p refers to (proof) test and the index a to service. The product $B_p S_0^{n_p-2}$ can be obtained from weak flaw test methods at proof test environment (Section 5.1) and the quotient B_a/B_p from fatigue test at respectively service and proof test environment (Section 5.2). For ambient service environment the indices p and a can be taken equal and (6) takes a simpler form, like the framework that remained after the COST-218 study of existing models.¹⁴

When weak flaws are blunt a slightly different model is found with (2) and (5).¹² Blunt weak flaws are worst case for zero stress aging. With the time dependent stress amplification f_{pit} (4), that was assumed in the blunt pit model, it follows:¹²

$$\sigma_a = \left(\frac{t_p}{G(t_a) t_a} \right)^{\frac{1}{n}} \left[\left\{ 1 - \frac{L_0}{L} \ln(1-F) \left(\frac{B S_0^n}{S_{b0}^2} \frac{1}{\sigma_p^{n_p} t_p} \right)^{\frac{m}{n}} - 1 \right\}^{\frac{n}{m}} \right]^{\frac{1}{n}} \sigma_p \quad (7)$$

$$\text{with: } G = \frac{2}{(f_{pit}-1)^2} \left[\frac{f_{pit}^{n+2}-1}{n+2} - \frac{f_{pit}^{n+1}-1}{n+1} \right]$$

Here S_{b0} is the inert strength at the (pristine) bottom of the weak flaw. With $G=1$ the "blunt" basic model without zero stress aging is obtained. In principle also a model with zero stress aging and stress corrosion parameters that differ from those during (proof) tests can be developed (combination of (6) and (7)).

4.2 Alternative for proof testing on-line

When proof testing is performed on-line the environment is not "seen" by the optical fiber.¹⁴ Therefore the proof test time t_p is not defined in the presented basic models. This problem can be overcome by taking the limit of t_p to zero as a worst case. The basic models then transform into "sharp" respectively "blunt" alternative models:

$$\sigma_a = \left(\frac{B_a}{B_p} \right)^{\frac{1}{n_a}} \left[\left\{ \frac{L_0}{L} \ln(1-F) \right\}^{\frac{m}{n_p-2}} \frac{B_p S_0^{n_p-2}}{t_a^{1/f}} \right]^{\frac{f}{n_a}} \quad (8)$$

$$\sigma_a = \left(\frac{L_0}{L} \ln(1-F) \right)^{\frac{1}{m}} \left(\frac{B S_0^n}{S_{b0}^2} \frac{1}{G(t_a) t_a} \right)^{\frac{1}{n}} \quad (9)$$

Here again the first model (8) can be used for harsh environment without, the second (9) with zero stress aging, and

both for ambient environment when $G=1$ and/or equal corrosion parameters. These models are equivalent to the "dynamic test" model for sharp flaws without aging.¹⁸ When very low failure probability is required during service the alternative models for proof testing on-line give very (too) low allowable surface stress on the fiber.

5 TEST METHODS

5.1 Weak flaw distribution

It is assumed that no zero stress aging occurs during the tests to obtain information about the weak flaw distribution. This assumption is justified because the described test methods can be performed in relatively short times.

Dynamic fatigue testing on long lengths of fiber can be used to bring the weak flaw distribution into picture. During this testing a stress σt is applied to the fiber. With (2) and (5) follows:¹²

$$\frac{B S_0^n}{S_{b0}^2} = \frac{\sigma_{d0}^{n+1}}{(n+1)\sigma} + \sigma_p^{n_p} t_p \quad (10)$$

This is the expression for blunt weak flaws. The expression for sharp weak flaws is obtained by substituting $S_{b0}=S_0$.¹⁴ The term on the left hand side can be substituted directly into the "sharp" respectively "blunt" basic models (6) and (7) and alternative models (8) and (9). The sharp variant of this model is described in^{19,20}.

The values σ_{d0} and m of the weak-flaw distribution, necessary for this model, can be measured by dynamic fatigue testing on long lengths of fiber, with (2) and (5):

$$\ln(1-F(\sigma_d)) = \frac{L}{L_0} \left(\frac{\sigma_d}{\sigma_{d0}} \right)^{m_d} \quad (11)$$

with $m_d=m(n+1)/(n-2)$ for sharp¹⁴ and $m_d=m(n+1)/n$ for blunt¹² weak flaws. The parameters σ_{d0} and m can hence be obtained as the straight part of the (extrinsic part of the) Weibull plot of dynamic-fatigue measurements (see Fig. 3). Note that for high strength levels the intrinsic flaw distribution will come into picture, indicated by the dotted line in Fig. 3. A fit which includes the truncated part of the distribution is also possible.¹⁵

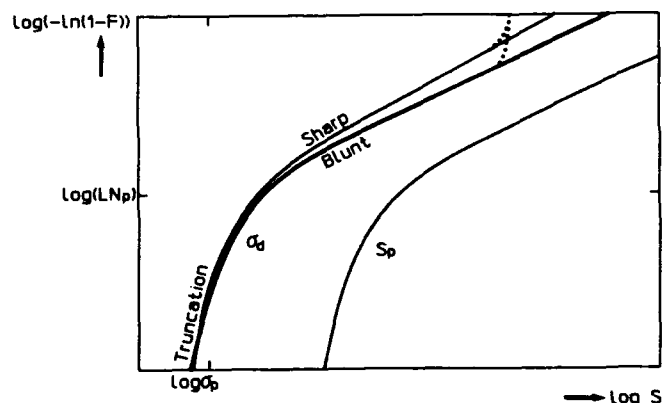


Figure 3 Distribution of dynamic strengths σ_d compared with that of inert strengths S_p , immediately after proof test. The dotted line is the onset of the intrinsic mode.

Repeated screen testing at different levels σ_i during time t_i of long lengths of optical fiber, and measuring the corresponding failure numbers $LN(\sigma_i)$, is another method to

find the weak-flaw distribution. The derivation of the screen-test-based lifetime model is analogous to the dynamic-testing one. With (2) and (5) it follows:

$$\frac{BS_0^n}{S_b^2} = \sigma_{s0}^n t_s + \sigma_p^n t_p \quad (12)$$

with again $S_b = S_0$ for sharp weak flaws. The expression on the left hand side can also be substituted into (6), (7), (8) and (9). The sharp variant of this model is described in²¹.

The straight part of the Weibull plot (not close to the proof test level) of $\log(LN(\sigma_s))$ against $\log(\sigma_s)$ can be expressed as:

$$LN(\sigma_s) = \frac{L}{L_0} \left(\frac{\sigma_s}{\sigma_{s0}} \right)^{m_s} \quad (13)$$

with $m_s = mn/(n-2)$ for sharp¹⁴ and $m_s = m$ for blunt¹² weak flaws. The parameters σ_{s0} and m can hence be obtained. When screen testing is done with the same fiber repeatedly, the failure number $N(\sigma_s)$ should be taken cumulatively. Also here a fit including the truncated part of the distribution can be made.

The proof test can also be used as a testing method. In that case only one point of the Weibull plot of the weak flaw distribution is obtained. The rest of the plot follows with a (worst case) estimation of the m -value (slope in the Weibull plot). The proof test can only be used as input for the basic models¹⁴, which transform to simpler formulas of the Mitsunaga²² type. With (2) and (5) it is found, for sharp and blunt weak flaws respectively:

$$\sigma_s = \left(\frac{B_s t_p}{B_p t_s} \right)^{\frac{1}{n_s}} \left[\left(1 - \frac{\ln(1-F)}{LN_p} \right)^{\frac{n_p-2}{m}} - 1 \right]^{\frac{1}{n_s}} \cdot \sigma_p \quad (14)$$

$$\sigma_s = \left(\frac{t_p}{G(t_s) t_s} \right)^{\frac{1}{n}} \left[\left(1 - \frac{\ln(1-F)}{LN_p} \right)^{\frac{n}{m}} - 1 \right]^{\frac{1}{n}} \cdot \sigma_p \quad (15)$$

5.2 Corrosion parameters

In order to estimate lifetimes for environments during service which differ from those during (proof) tests (e.g. including filling compound, in aerial cables, in splice enclosures or even in water), formulas (6), (8) or (14) must be used in their full form, i.e. including the different B -values. In this Section measurements, to be performed in proof test and service environment, are proposed in order to obtain information about the relation between the different B -values. The measurements need not be performed on the weak flaw distribution. In fact it is proposed to measure the intrinsic distribution, because also n -values must be measured. The tests may be performed in a static or dynamic way. First the unknown term with B -values in the mentioned formulas can be eliminated by writing:¹⁵

$$\frac{B_s}{B_p} = \frac{B_s S_0^{n_s-2}}{(B_p S_0^{n_p-2})^f} \quad (16)$$

with S_0 the Weibull scale constant for the initial inert intrinsic strength distribution. The left and right hand side are exactly the same in this equation (at the right hand side nominator and denominator are multiplied by $S_0^{n_s-2}$). The n -values and the products BS_0^{n-2} , in both environments, can be found with standard techniques.¹⁵

6 NUMERICAL EXAMPLE

The lifetime models will be illustrated with a numerical example like that in¹⁴. A fiber is considered which is proof tested with a level σ_p of 0.5 GPa during a time t_p of 1 s. The weak flaw distribution is characterized with a Weibull parameter m of 2 ($m=4$ as worst case for Mitsunaga²²) and a failure N_p during proof test of 0.02 km⁻¹. The stress corrosion parameters are a B -value of 4×10^{-8} GPa²s and an n -value of 20.³ The intrinsic inert strength S_0 is 16 GPa.³ With this information S_0 -values of 8.43 and 10.9 GPa follow for sharp and blunt weak flaws respectively¹² (these values are not measured but follow among others from the assumption that N_p is 0.02 km⁻¹). The effect of temperature and humidity on corrosion parameters is published in¹⁵. The zero stress aging parameters are a C_p of 5×10^{-5} m^{1/2}, an E_0 of 131.5 kJ and a v_0 of 9.1×10^5 m/s, while the gas constant R is 8.31 J/K (from data of inert strength decrease after aging from³, using⁹). In Table 1 allowable service stresses are shown for different environments, assuming sharp weak flaws (using (6),(8) and (14)) for ambient environment and using the same ratios between allowable stresses as in¹⁵ for the other environments. In Table 2 the allowable stresses are shown for sharp (using (6),(8) and (14)) and blunt (using (7),(9) and (15)) flaws, without and with zero stress aging. For comparison also the results of the Haslöv/Jensen²³ model are shown.¹²

Table 1 Allowable stress σ_s in GPa for required failure probability F of 1 / 0.001 %. Sharp weak flaws are assumed for ambient environment. The allowable stresses for the other environments are obtained assuming the same ratios between allowable stresses as in¹⁵.

Environment	Basic model	Mitsunaga	Alternative
50%RH,20°C	0.21 / 0.14	0.19 / 0.13	0.13 / 0.006
70%RH,20°C	0.20 / 0.13	0.18 / 0.12	0.12 / 0.006
90%RH,20°C	0.19 / 0.13	0.18 / 0.12	0.12 / 0.006
96%RH,20°C	0.19 / 0.13	0.18 / 0.12	0.12 / 0.006
70%RH,40°C	0.18 / 0.12	0.17 / 0.11	0.11 / 0.005

Table 2 Allowable stress σ_s in GPa for required failure probability F of 1 / 0.001 %.

Flaws	Basic Model	Mitsunaga	Alternative
sharp	0.21 / 0.14	0.19 / 0.13	0.13 / 0.006
blunt	0.22 / 0.14	0.20 / 0.13	0.13 / 0.004
blunt + aging	0.10 / 0.06	0.09 / 0.06	0.06 / 0.002
Haslöv/Jensen	0.15 / 0.01	0.13 / 0.008	0.09 / 0.003

It becomes clear that there is not much difference between the basic and Mitsunaga model. The alternative model gives lower allowable stresses, especially for low required failure probability. There is also not much difference for sharp and blunt weak flaws. Humidity and temperature have some effect, but not as large as might be expected at first sight, observing the corrosion measurements.¹⁵ When zero stress aging occurs the allowable stress levels drop by more than a factor 2 in this numerical example.

When the blunt pit model is used, together with the worst case assumption of blunt weak flaws, the situation of Fig. 4 may occur. In¹² it is shown that in the treated numerical example the size of the weak flaw can be of the order of 1 μ m, the "aging pit" at the bottom of the order of 10 nm and the sharp stress corrosion flaw a few nm's. This is a worst case situation that is not proved, but also not in conflict with observations.¹²



Figure 4 Worst case impression of a blunt weak flaw with "aging pits" and sharp flaws.

7 CONCLUSIONS

In a COST-218 study 12 existing lifetime models were condensed to a simple framework of one basic model, with an alternative for on-line proof testing and with a choice of three testing methods for the weak flaw distributions as input. All studied models make use of the empirical power law. It is shown that this is a good fit function of the measured results and does not cause errors when extrapolating to service times. In this paper also a blunt weak flaw variant of the models is given. Furthermore the models are further developed to be used for ambient and harsh service environments, also when zero stress aging occurs. When lifetime calculations are performed without zero stress aging, but assuming blunt weak flaws, allowable stresses during services are found which are almost equal to the estimations with sharp weak flaws. Humidity and temperature have some effect on the model. Zero stress aging results in a decrease of allowable service stresses by a factor 2 for the treated numerical example.

8 ACKNOWLEDGEMENTS

I thank the members of COST-218 WG1, who did a great part of the exhausting job with me, developing the lifetime model framework, in several meetings.

10 REFERENCES

- [1] A.G. Evans, S.M. Wiederhorn, "Proof testing of ceramic materials- an analytical basis for failure prediction", *Int. Journ. of Fracture*, 10 (1974) 379-392.
- [2] C.R. Kurkjian, H. Chandan, D. Inniss, "Current issues in mechanical reliability of optical fibers", *proc. 41th Int. Wire & Cable Symp.* (1992) 599-604.
- [3] W. Griffioen, W. Ahn, A.T. de Boer, G. Segers, "Stress-induced and stress-free ageing of optical fibres in water", *proc. 40th Int. Wire and Cable Symp.* (1991) 673-678 (parameters are updated using²⁴).
- [4] K. Abe, G.S. Glaesemann, S.T. Gulati, T.A. Hanson, "Application of a phenomenological fatigue model to optical fibers", *Optical Engineering*, vol.30, no.6 (1991) 728-736.
- [5] P.C.P. Bouten, "Lifetime of pristine optical fibres", Thesis, Eindhoven (The Netherlands), october 1987.
- [6] A. Breuls, "A COST 218 comparison of n-values obtained with different techniques", to be presented at the *Opt. Fib. Meas. Conf.*, Turin, 21-22 september 1993.
- [7] W. Griffioen, "Effects influencing measurements of optical fibre corrosion susceptibility", to be presented at *Opt. Fib. Meas. Conf.*, Turin, 21-22 september 1993.
- [8] T.A. Michalske, B.C. Bunker, "The fracturing of glass", *Scientific American*, december (1987) 78-85.
- [9] W. Griffioen, "Ageing of optical fibres in water", *proc. 41th Int. Wire and Cable Symp.* (1992) 622-628.
- [10] A.A. Griffith, "The phenomena of rupture and flow in solids", *proc. Roy. Soc. London*, vol. 221a (1920) 163-198.
- [11] C.E. Inglis, "Stresses in a plate due to the presence of cracks and sharp corners", *proc. Inst. Naval Architects*, march (1913) 219-241.
- [12] W. Griffioen, "Mechanical lifetime model for optical fibers in water", to be presented at *SPIE "Fib. Opt. Rel. and Testing: Benign and Adverse Env. II"*, Boston (1993) 2074-01.
- [13] H. Chandan, H.H. Yuce, "Aging and fatigue of low strength fibers", *proc. SPIE "Fib. Opt. Netw., Passive Fib. Opt. Comp. and their Rel."*, Berlin (1993) 1973-21.
- [14] W. Griffioen, T. Breuls, G. Cocito, S. Dodd, G. Ferri, P. Hasloev, L. Oksanen, D. Stockton, T. Svensson, "COST 218 evaluation of optical fibre lifetime models", *proc. SPIE*, vol. 1791 "Fib. Opt. Rel., Benign and Adverse Env. VI", Boston (1992) 190-201.
- [15] W. Griffioen, "Mechanical lifetime model for optical fibres in harsh environments", *proc. SPIE "Fib. Opt. Net., Passive Fib. Opt. Comp. and their Rel."*, Berlin (1993) 1973-22.
- [16] S.P. Craig, W.J. Duncan, P.W. France, J.E. Snodgrass, "The strength and fatigue of large flaws in silica optical fibre", *Eur. Conf. Opt. Comm.* (1982) 205-208.
- [17] G.S. Glaesemann, M.G. Estep, J.D. Helfinstine, J.J. Carr, "Examining the mechanical behavior of intrinsic and extrinsic flaws in optical glass fiber", 94th annual meeting *Am. Ceram. Soc.*, 4-JXVI-92, Minneapolis, april 1992.
- [18] F.P. Kapron, "Theory of stressed fiber lifetime calculations", *proc. SPIE*, vol. 1366 "Fib. Opt. Rel.: Benign and Adverse Env. IV" (1990) 136-143.
- [19] "Strength of Optical Fibres", Document D001, Optical Fibres Deeside, june 1989.
- [20] P.W. France et al., "The Physics of Fiber Optics", ed B. Bendow & S. Mitra (1981) 149-157.
- [21] J. Kurki, L. Storbom, L. Oksanen, T. Räsänen, E. Leino, "Reliability and environmental performance of cabled single-mode optical fibers", *proc. 38th Int. Wire & Cable Symp.* (1989) 380-389.
- [22] Y. Mitsunaga, Y. Katsuyama, Y. Ishida, "Reliability assurance for long-length optical fibre based on proof testing", *Electronics Letters*, vol.7, no.16 (1981) 567-568.
- [23] P. Hasløv, K.B. Jensen, N.H. Skovgaard, "Degradation study for stressed optical fibres in water. new worst case life time estimation model", *proc. 41th Int. Wire and Cable Symp.* (1992) 423-427.
- [24] W. Griffioen, "Effect of nonlinear elasticity on measured fatigue data and lifetime estimations", *J. Am. Ceram. Soc. (USA)* 75 [10] (1992) 2692-2696.

BIOGRAPHY

Willem Griffioen received his M.S. degree in physics and mathematics from Leiden University, Leiden, the Netherlands, in 1980, where he also worked until 1984. In 1984 he joined PTT Research, Box 421, 2260 AK Leidschendam, the Netherlands. Currently his main responsibility is reliability of optical fibers. From September 1991 until March 1992 he worked at Ericsson Cables AB, Hudiksvall, Sweden in the scope of an exchange project.



RELIABILITY TESTING OF FIBER OPTIC LOOSE BUFFER TUBES

JÜRGEN EICKHOLT

Hüls AG, D-45764 Marl, Germany

ABSTRACT

With the more frequent installation of fiber optic cables in environments of higher temperature and humidity conditions, the long term reliability requirements for cable components have become more stringent. Test results must prove that Polybutylene-terephthalate (PBT) used in loose tube fiber optic cables will function adequately for the lifetime of a cable. Reliability testing involves aging the materials under more severe conditions than would be normally encountered in the field, in order to observe a loss of performance in a shorter time. A new test method to determine degradation of thermoplastic polyester loose buffer tubes has been developed. This test method is based on bending by compression and reflects embrittlement much better than the often used tensile test.

INTRODUCTION

Hydrolysis is known as the primary cause of degradation for thermoplastic polyesters at elevated temperature. It is very important to have the knowledge of the degradation mechanism of a material and also which properties one should choose to assess the extent of degradation.

The change of tensile characteristics is often being used in customer specifications. While elongation at break might be suitable as part of process control data, it is not an appropriate method to predict the length of time to a buffer tube failure. In a study on aged loose buffer tubes, the elongation at break ranged from 10% to more than 300%.

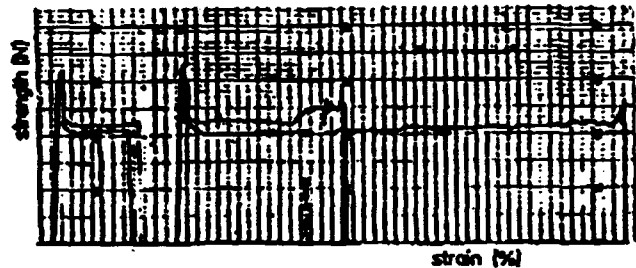


Figure 1: Elongation at break after aging

Because of the extremely high standard deviations, the values of elongation at break are not a reliable indicator of the effect of degradation. Thus, values cannot be used with confidence.

Futhermore an optical fiber can never be exposed to a strain higher than 2% otherwise the fiber will break. There is no benefit in the fact that some fiber optic loose buffer tubes can be stretched to a considerable extent. Fiber optic cables should be designed to accommodate stresses to a degree well below the modulus of elasticity (this is by definition the ratio of the applied stress to the strain in the region in which strain is linearly proportional to stress). Buffer tubes in a cable may only be moved for repair of damage during the service life of a cable or by loadings in aerial cables. In all cases the tubes will be subjected mainly to bending. The outer fiber strain of a bended buffer tube is less than 10% before kinking occurs. Hüls has developed a test method which is based on bending by compression. This test reflects embrittlement more precisely than tensile tests and simulates the actual loadings in the field. This test has the following advantages:

- very simple
- reproducible results
- low standard deviation
- independent of wall thickness

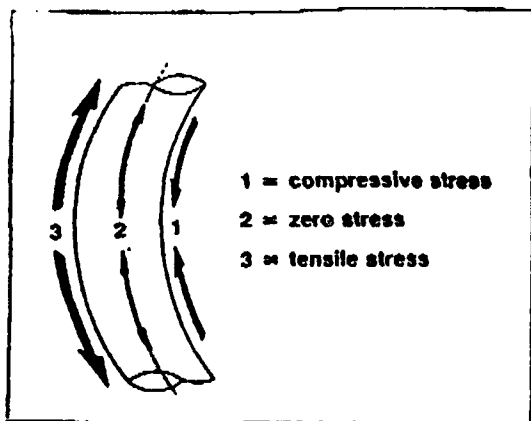


Figure 2: Stresses in a bended fiber optic tube

Several results from this test were used to estimate the correlation between breakage and solution viscosity.

It can be seen, that breakage occurs when the solution viscosity has reached its critical limit of 65 ± 5 cm/g. At this critical solution viscosity the material loses its mechanical integrity. The graph clearly points out the difference between a standard PBTA and a hydrolysis resistant PBTB.

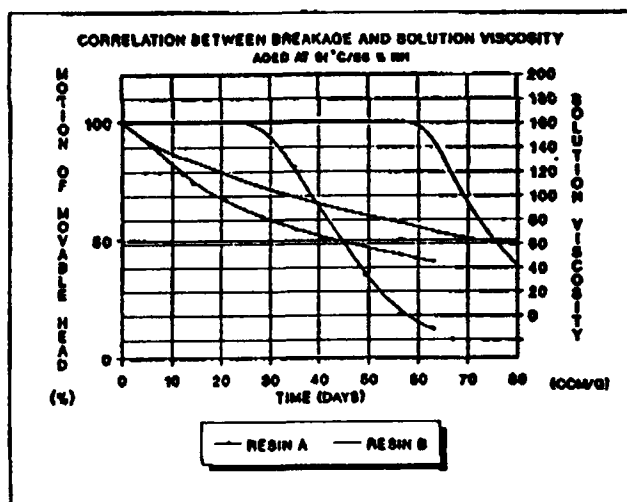


Figure 3

PROCEDURE

Both ends of a buffer tube test sample may be mounted in a tool which is clamped in the jaws of a tensile testing machine which exerts a constant rate of movement. One jaw is fixed and the other is movable. The movable jaw may move at a rate of 50 mm/min towards the fixed jaw (see figure 4).

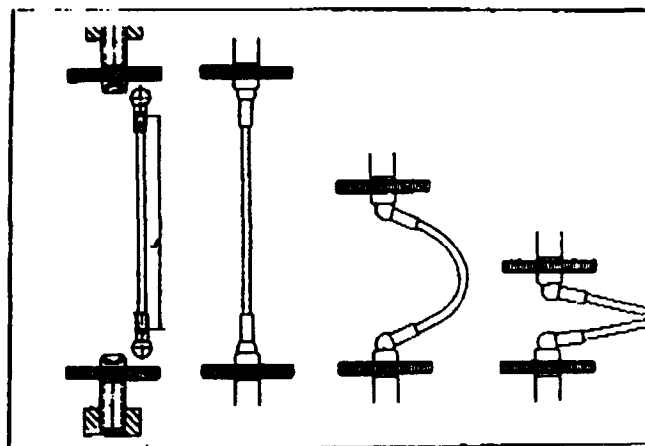


Figure 4: Skeleton sketch

Under load the tube will bend, so that the tube is subject to tensile and compressive stresses as indicated in figure 2. The fixture for holding the test tube should be designed in a manner that the tube might bend in all directions without any further loading. This can be achieved by using a tool as indicated in figure 5.

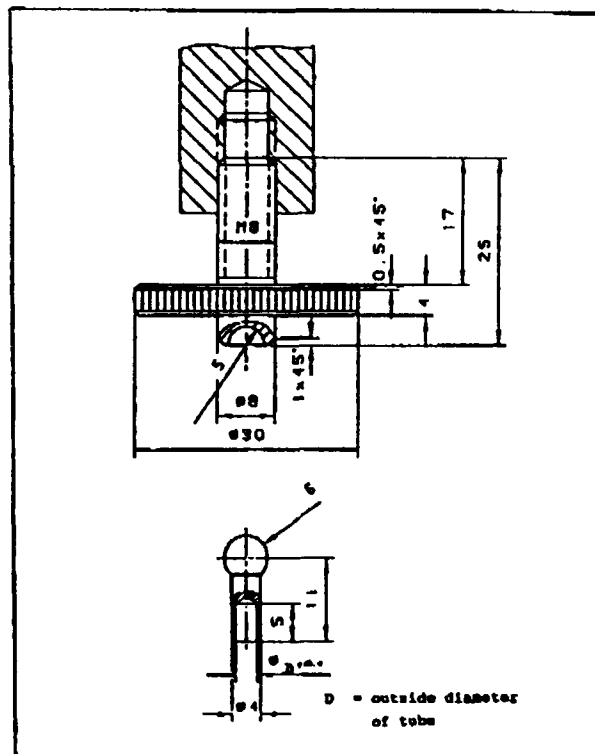


Figure 5: Tool sketch

The minimum length of the test sample depends on the outside diameter of the tube and should be 85 mm for tubes up to 2.5 mm outside diameter. The length of

bigger tubes should be calculated by using the following equation:

$$L_0 > 100 \cdot \sqrt{D^2 + d^2} / 4$$

D = outside diameter of tube

d = inside diameter of tube

L_0 = length of test tube

Example:

Fiber optic tube D = 5 mm, d = 3 mm

$$L_0 > 100 \cdot \sqrt{5^2 + 3^2} / 4 = 100 \cdot \frac{5.83}{4} = 145.8$$

The minimum length of the test tube should be, therefore, 150 mm.

OTHER TEST METHODS

In addition to mechanical tests each resin was examined for its resistance to hydrolysis by an analytical method. Since properties of PBT fiber optic tubes are so dependent on solution viscosity (J) and the carboxylic endgroup concentration (CEC), these are the most important measurements for properly understanding the degradation mechanism of the polymer. These tests require very little sample compared to mechanical tests and can be conducted on granules, as well as on samples taken from finished parts. The sample need not be intact, which is important when actually failed field samples need to be evaluated. Conditioning prior to testing is not necessary.

The melt flow rate (MFR) is not a fundamental property. The rheological characteristics of polymer melts depend on a number of variables. Moisture in PBT not only affects reproducibility of MFR measurement but degradation is accelerated by moisture at the high temperatures used in drying and in testing. It takes a relatively short time to reach the maximum flow of 50 g/10 min., recommended by the ASTM for PBT. Beyond this point, non-newtonian flow is expected and the viscosity-molecular weight relationship becomes non-linear.¹

Besides the above mentioned test methods to determine hydrolytical decomposition of PBT, it is also possible to calculate a lifetime of a buffer tube. As already

mentioned depends the lifetime of a PBT buffer tube mainly on the viscosity number of carboxylic end-groups. Only by knowing these numbers of the virgin material one can calculate a lifetime of a PBT buffer tube at any given temperature and humidity condition.²

CONCLUSION

The new test method reflects embrittlement of PBT fiber optic tubes much better than the often used tensile test. It has been proven that breakage occurs when the solution viscosity has reached its critical limit. Besides analytical test methods, the described test method is the easiest way to determine degradation after aging.



Jürgen Eickholt is a member of the technical service and marketing staff for engineering plastics at Hüls AG, Marl, West Germany. His current responsibilities include the world wide technical service and marketing of materials for fiber optic jacketing and technical support to the research and development group within Hüls AG.

ACKNOWLEDGEMENTS

The author would like to thank Mr. Detlef Argast and Mr. Jürgen Bialluch for their contributions.

REFERENCES

- ¹Neveaux, Jr. P.E., IWCS Proceedings 1991
- Parris, Donald R., IWCS Proceedings 1989
- ²Schüler, R. unpublished Hüls report

PREFORM MANUFACTURING BY FCVD (FURNACE C.V.D.) USING VERY LARGE AND PRECISELY BORED SYNTHETIC SILICA INGOTS

G. LE NOANE - I. HARDY - P. GROSSO - D. LE DROUMAGUET

CNET-LAB/OCM - 22300 LANNION - FRANCE

I - Abstract

The application of optical fiber in the future subscriber cable network requires certainly drastic evolutions of most of the optical components : fibers, cables, passive and active components . So a large technological program is essential to built up the F.T.T.H (fiber to the home) network . In term of preform technologies, fiber manufacturers are under pressure to reduce their costs and to improve some parameters, like geometrical characteristics. As a part of this program, we propose a direct deposition inside very thick and precisely bored silica ingots, using a new manufacturing deposition process and collapsing : the F.C.V.D. (Furnace Chemical Vapor Deposition) . Up to now, results of 120 km preform's capacity with an increased production rate and very precise geometrical characteristics are achieved, and other steps are in progress to get higher preform capacities without major capital investments .

II - Introduction

The application of optical fiber in the future subscriber cable network, F.T.T.H, requires certainly drastic evolutions of most of the optical components : fibers, cables, active and passive components . New technologies and a better adaptation of performances and specifications to the requirements of the local network are probably promising ways to achieve this challenge .

As a part of this program, all synthetic preform manufacturing using very large and precisely bored synthetic silica ingots has very attractive potentialities to achieve low cost fibers and to improve all the geometrical characteristics leading to cheap integrated passive components .

In a first time, we have investigated a two steps manufacturing process composed of a Surface Plasma C.V.D. (SPCVD) for the deposition inside thick tubes and a RF furnace heating for the collapsing of large preforms [1] . Unfortunately we met some difficulties to control essential parameters, as refractive index and geometrical characteristics, along the axis of the preform . Nevertheless, the success of the very efficient collapsing furnace, gives us the way to develop a more efficient process achieving etching and polishing, cladding and core deposition and collapsing in the same machine . The FCVD (Furnace CVD) is a one step process using an horizontal furnace . The high and well-controlled temperature obtained, allows us to use very large and precisely bored ingots .

Considering the above statement, this paper describes the potentialities of very large and precisely bored synthetic silica ingots, and the method of manufacturing large preforms by direct deposition into thick tubes . As an illustration, results of 1.2 meter length, OD×ID : 58×33 mm tube are presented, leading to a single mode preform of about 120 kms with very precise geometrical characteristics and an increased production rate .

III - Techno/economical objectives : the FCVD concept .

The introduction of the fiber in the local cable network needs an evolution of established fiber manufacturing in terms of reduced cost, higher preform capacities and better geometrical characteristics for cheap integrated passive components .

III - 1 Synthetic silica allows reduced deposited part

In the figure 1, the conventional single mode fiber and the all synthetic CVD concept are illustrated . As well known, the major part of the optical signal propagates in a very central part of the fiber [2] . The big problem is the additional OH loss provided by the OH contamination from the substrate tube to the optical part of the fiber . In the conventional CVD process, the substrate tube used is a natural silica tube, with typically 200 ppm OH content, and thus a cladding to core ratio (b/a) of six is commonly required . The use of a synthetic silica tube, typically 1 ppm OH

content, gives the opportunity to reduce the ratio b/a leading to a CVD glass volume fraction of 4% . The result is a reduction of the deposited glass part of the fiber without damaging the high optical quality of the fiber .

Concurrently, recent progress on mass production of high purity low cost synthetic silica for the substrate (volume fraction of 96%), converge to reduce the global cost of the fiber .

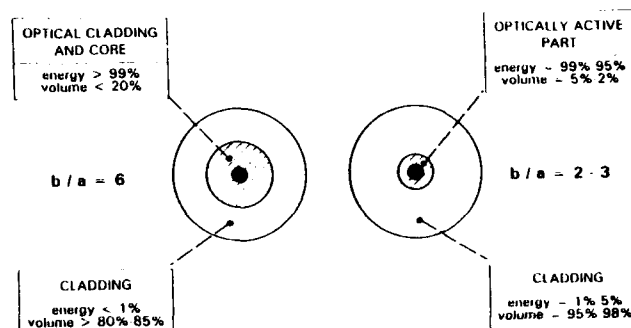


Fig. 1 : Conventional and low b/a SM fiber structures

III - 2 Large C.S.A. tube provides higher preform capacity

With a reduced deposited part, by the use of a synthetic silica tube substrate, the preform capacity is related to the maximal deposited thickness and to the maximal length . By keeping the same deposited section of CVD (or more) as conventional CVD in a natural silica tube, several technologies like hybrid process [3] or overcladding techniques [4] are developed to achieve these large preforms.

The efficiency of FCVD autorizes a direct deposition into thick tubes, and so, the preform capacity is related to the maximum tube thickness and internal diameter . Table 1 illustrates the role of a high CSA tube compared with a

conventional thin tube (ie OD \times ID = 30 \times 25 mm) without or with overcladding techniques . A thick tube is mechanically stable, and combined with a strong and homogeneous heating, larger inner diameter can be used, (up to now > 40mm) providing higher facilities to increase the reactant flow and the total deposit section . In the same way, a thick tube collapses faster and in a more stable way than a thin one [5] [6] and enhances the total rate manufacturing without significant damage on the geometry .

Tube dimensions OD \times ID (mm)	Deposited Section (mm ²)	Preform Capacity km/m
30 \times 25	≈ 9	18
30 \times 25	40,75 *	85
60 \times 30	87,5	180
78 \times 40	145,5	300

* With overcladding technique ; by keeping the same deposited section as conventional CVD in a natural silica tube, $b/a = 6$.

Tab. 1- Role of a high C.S.A tube on the preform capacity

III - 3 Thick tubes lead to more precise geometrical characteristics

At the same time, the use of thick tubes opens the door to a new approach of very precise geometrical characteristics . Even with commercial stretched tubes, the increase of the cross section area, independently of the deposition process, improves the final accuracy of the preform and the fiber (Tab. 2) .

	Outer \times inner diameter tube (mm)	Accuracy on tube diameters (mm)	Resulting accuracy on preform diameter (mm)
Stretched tube	30 \times 25	± 0.5	± 0.1
	60 \times 30	± 0.5	± 0.02
Grinded tube	60 \times 30	± 0.02	$< \pm 0.001$

Tab. 2 - Influence of the substrate tube dimensions and geometry on the final accuracy of the preform and the fiber .

In another way the homogeneous and strong heat transfer of the FCVD process is able to fuse thick layers, (for instance $\approx 100 \mu\text{m}$ thickness) without significant vaporization of the outside of the preform . Likewise, during collapsing, the vaporization of the outside part of the preform is reduced drastically, typically one per cent against thirty to thirty five per cent for a burner collapsing of large CVD preforms (before overcladding step) and so the collapsing preserves in a better way the homogeneity of the final outside diameter .

The following step is to obtain nominal and precise outside and inside diameters and excellent concentricity for the substrate tube . The ability of large ingots or thick tubes to be drilled and / or grinded with an accuracy of plus or minus two hundredth millimeters, represents a basic improvement to achieve very precise and cheap optical fibers, leading to lower connections cost [7] (Tab.2) .

IV - FCVD : principle and apparatus .

The FCVD process is based on the capacity of an horizontal graphite induction furnace, first to heat chemical reactants to the high temperature of CVD inside a rotating thick tube, and then to fuse the deposited material to a transparent glassy film .

The thick walled tube is mounted in a glass lathe (fig. 2) with an horizontal motion .While rotating, the tube traverses through the fixed induction furnace operating within the range 10 - 30 kilohertz . The other equipments, like injection of reactants inside the deposition tube and evacuation of waste powder, are similar to conventional CVD equipments . The stationary hot zone extents axially over six to seven centimeters, depending on the deposition tube dimensions .

For the various steps of the process a good efficiency is obtained by adjusting the translation lathe rate and the furnace temperature . So the successive steps of the process : polishing and cleaning, cladding and core deposition, collapsing, are manufactured continuously on the same apparatus .

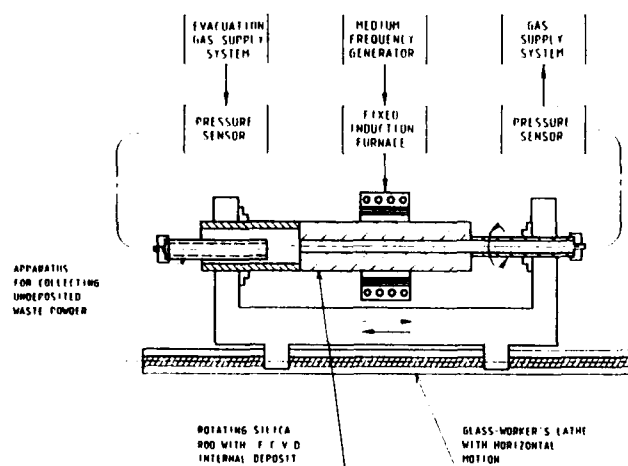


Fig. 2 : Schematic of the furnace deposition and collapsing set-up.

The main feature of the FCVD process is a low, but very homogeneous and strong heat transfer . According to that, tube thickness of twelve to twenty millimeters for instance, can be used, with a moving speed of about three centimeters per minute . This is to be compared to a classical MCVD burner moving speed of twelve centimeters per minute, with two or three millimeters CVD thin tubes . The result for a same deposition rate, is a quarter of layers for the same total deposit section .

V - Main results

Matched-clad single mode preforms with Ge doped core and Ge/F co-doped cladding have been prepared from synthetic silica tubes and with b/a ratio between 2.8 and 3.5 .

Inner diameter tube (mm)	Mean deposition cladding rate (g/mn)	Cladding deposited section (mm ²)
25	0.4	57
33	0.75	71
43	~ 1	134

Tab. 3 - Inner diameter tube influence on deposition rate and deposited section.

It is clear that, in such process, larger inner diameters provide us higher facilities to increase the deposition rate and to fuse thicker deposited layers (Tab. 3) . So we have experimented several tube diameters OD \times ID : 45 \times 25, 48 \times 25, 58 \times 30, 58 \times 33 mm and several lengths: 500, 800 and 1200 mm .

As an example, starting with a substrate tube of 58 \times 33 mm diameters and a 1200 mm length, and after a polishing and cleaning step in-situ, seven layers of co-doped cladding and two layers of core are deposited . The tube is then collapsed to a preform rod of 48 mm diameter . The mean deposition rate is 0.75 g/mn for the cladding and 0.27 g/mn for the core . The collapsing is performed in two passes at 25 g/mn . The total manufacturing time is 13 hours leading, at this stage of the process, to a useful length preform around 800 - 850 mm (120 km) .

Attenuation results are presented in fig. 3 with 0.22 dB/km at 1.55 μ m and 0.41 dB/km at 1.3 μ m . Starting with a precise tube, excellent core and cladding concentricity and circularity are got with an uniform diameter . Fig. 4 shows that we can pull precise fiber with an outside diameter of 125 μ m, with a standart deviation of 0.25 μ m, and a core-cladding concentricity below 0.1 μ m .

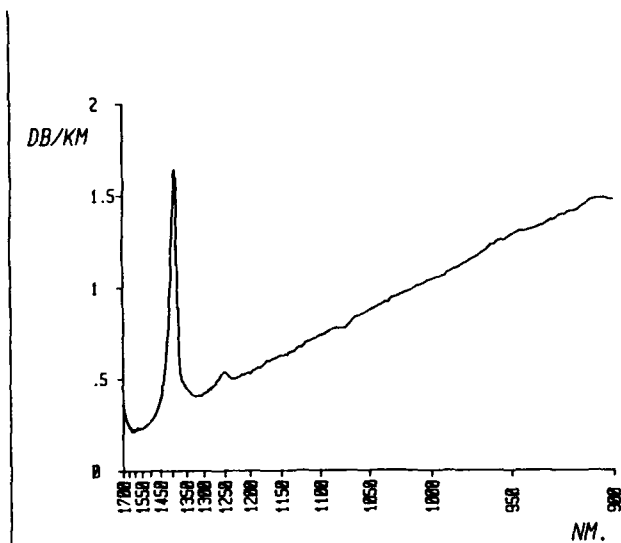


Fig. 3 : Spectral attenuation versus λ^{-4} . MC-SM fiber $b/a = 3.3$, prepared with a synthetic silica tube : OD x ID = 58 x 33 mm and L = 1200 mm

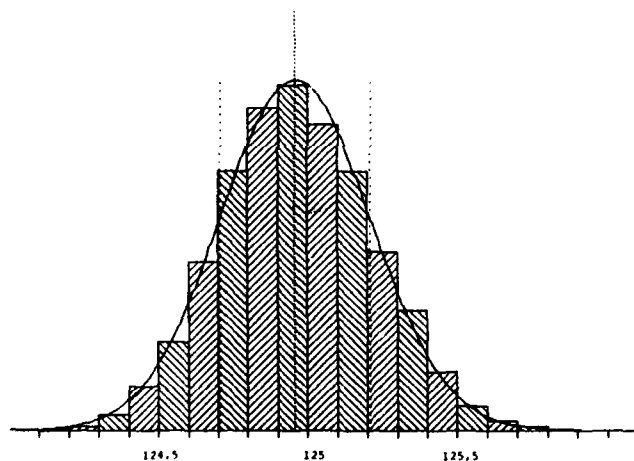


FIG.4 : Fiber pulling diameter distribution
Average : 124.96 μm
 σ : 0.25 μm

In other respects, attenuation results for two different fibers are presented in Fig 5, prepared with the same b/a ratio but two kinds of cladding material . We have observed that attenuation results obtained with a pure silica cladding are slightly higher (factor c of 0.05 dB/km) than co-doped cladding fibers and are difficult to optimize by the fiber drawing conditions (temperature and tension) . So we have demonstrated the heating transfer potentiality of the FCVD process by the deposition of a pure silica cladding but, the low attenuation needs, for such b/a ratio, a Ge/F co-doped cladding deposition (0.22 dB/km at 1.55 μm , 0.36 dB/km at 1.3 μm , $h/a = 3,3$)

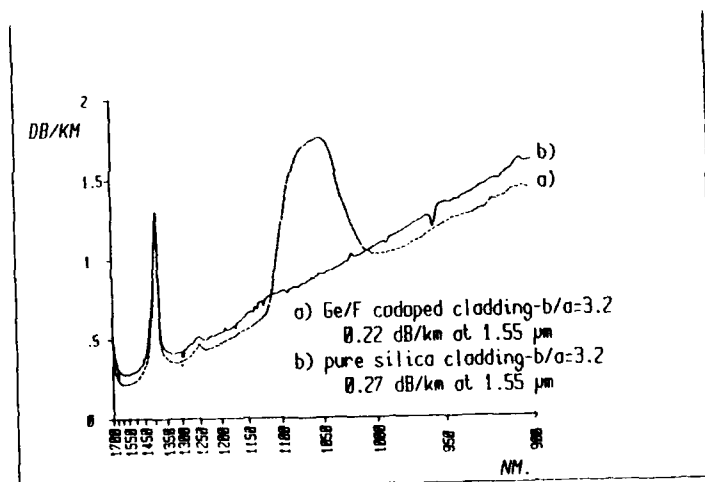


FIG.5 : Spectral attenuation versus λ^{-4}

Fig. 6 gives also some results of attenuation versus the b/a ratio, showing that a very low attenuation can be obtained even with a b/a of 2.8 .

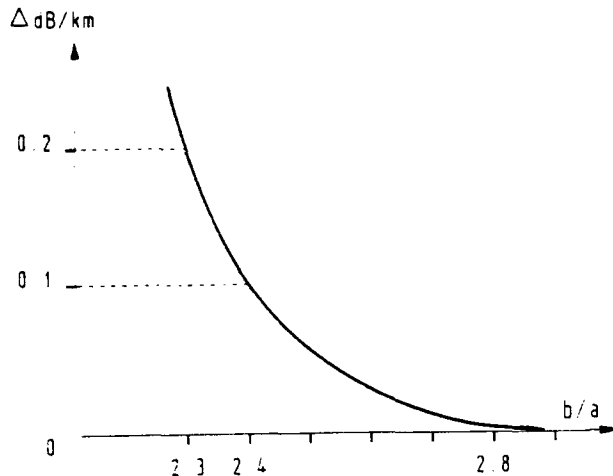


FIG.6 : Additional loss at $1.31 \mu\text{m}$ versus b/a ratio

VI - Conclusion

A new preform manufacturing using very large and precisely bored or stretched synthetic silica tubes has been successfully experimented . The main feature of FCVD is a strong and homogeneous heat transfer, allowing the direct deposition into thick walled tubes . The result is the manufacturing of large preforms with an increased production rate, especially for the collapsing .

Excellent attenuation have been got, even with a cladding to core ratio of three. As we have shown, the use of high precision large ingots, enhances the final fiber geometry in term of cladding to core concentricity and high precision diameter .

Up to now, FCVD should be an attractive process to achieve preform capacities over 300 km/m by increasing the inner diameter tube, and thus reducing the cost of fiber production and connection.

is a strong and homogeneous heat transfer, allowing the direct deposition into thick walled tubes . The result is the manufacturing of large preforms with an increased production rate, especially for the collapsing .

Excellent attenuation have been got, even with a cladding to core ratio of three. As we have shown, the use of high precision large ingots, enhances the final fiber geometry in term of cladding to core concentricity and high precision diameter .

Up to now, FCVD should be an attractive process to achieve preform capacities over 300 km/m by increasing the inner diameter tube, and thus reducing the cost of fiber production and connection.

References

- [1] D. PAVY, C. LE SERGENT and al .
" High potentialities in fiber preform manufacturing using very large and precisely bored silica ingots " . IWCS 91
- [2] L.B. JEUNHOMME . Single mode fiber optics, New-York Dekker (1983) .
- [3] A.H. VAN BERGEN, A.H.E. BREULS . " Large, all synthetic, PCVD preform manufacturing " . EFOC 92
- [4] J.B. Mac CHESNEY and al . Elect. Lett. 23, 19 (1987) pp 1005 - 1007 .

[5] J. KIRCHHOF . " A hydrodynamic theory of the collapsing process for the preparation of optical waveguide preforms " . Phys. Stat. Sol. (a) 60, K127 (1980) .

[6] F.T. GEYLING, K.L. WALKER, R. CSENCISITS . " The viscous collapse of thick walled tubes " . J. Applied Mechanics, 50 (1983) pp 303 - 310 .

[7] G. LE NOANE . Conf. Proc. 9th JNOG, Lannion, (1988) pp 98 - 99 .



Georges LE NOANE
FRANCE TELECOM
CNET/LAB/OCM/FCO
BP. 40 22301 LANNION
FRANCE

Georges LE NOANE, born in 1945, received his engineering degree from the Ecole Nationale Supérieure des Arts et Métiers and joined CNET in 1974 . He began working on optical fiber connector techniques, then switched to cables . Since 1979, he has been responsible for the " Optical Fibers and Cables " Department at the CNET Lannion B Center .



Isabelle HARDY
FRANCE TELECOM
CNET/LAB/OCM/FCO
BP. 40 22301 LANNION
FRANCE

Isabelle HARDY received her engineer diploma from INSA of Rennes in 1981 and her Ingenieur Docteur diploma from University of Toulouse in 1984 . She joined CNET in 1986, where she is in charge of studies on new preform fabrication processes in Department of Optical Fibers and Cables of CNET .



Philippe GROSSO
FRANCE TELECOM
CNET/LAB/OCM/FCO
BP. 40 22301 LANNION
FRANCE

Philippe GROSSO received his optic engineer diploma from CNAM in 1978 . He joined CNET in 1983, where he is in charge of drawing fiber studies in Department of Optical Fibers and Cables of CNET .



Daniel LEDROUMAGUET
FRANCE TELECOM
CNET/LAB/OCM/FCO
BP. 40 22301 LANNION
FRANCE

Daniel LE DROUMAGUET has been working for FRANCE TELECOM since 1974 as technician . He joined CNET Lannion in 1982, where he has been in charged of preforms manufacturing, first by MCVD, and then by new preform fabrication processes (furnace collapsing and FCVD) in Department of Optical Fibers and Cables .

KEYFACTORS TO DETERMINE THE OPTIMUM BALANCE BETWEEN CENTRAL AND PERIPHERAL REINFORCEMENT OF DIELECTRIC OPTICAL FIBER CABLES

Th. Bijker, J.J. Bensink

AKZO ARAMID FIBERS, Arnhem, The Netherlands

ABSTRACT

Optical Fiber Cable producers are more than ever forced to design cables with an optimal mechanical performance and reliability at the lowest possible costs.

A market survey and study have been made into the price/performance of materials that are commonly used as strength member in dielectric Optical Fiber Cables.

In this paper the price/performance of aramid yarn as peripheral strength member is compared with resin impregnated glass rod (FRP) as central strength member for the reinforcement of "loose tube" and "slotted core" cables.

Analysis shows that optimal results can be achieved if small-diameter FRP rods are used in combination with a peripheral reinforcement of aramid yarn.

INTRODUCTION

Loose tube and slotted core constructions of dielectric Optical Fiber Cables are generally reinforced with a central strength member of glass-epoxy, glass-polyester or glass-vinyl-ester rod(FRP). An additional peripheral reinforcement of aramid yarns is often applied.

For cable designers and producers it is important to know the price/performance differences between designs that only contain a central strength member and constructions that use a combination of both central and peripheral reinforcement.

For obvious reasons a rigid central strength member is necessary to provide the cable with sufficient compression strength.

Reinforcement of the cable to resist pulling forces can either be provided by using a thicker central rod or, alternatively, a peripheral layer of aramid yarn in combination with a thin FRP rod.

ARAMID VERSUS FRP AS TENSILE STRENGTH MEMBER.

Twaron aramid yarns are used in various OFC cable designs as protection against linear, radial and flexural loads during production, installation and operation of the Optical Fiber Cable. Twaron aramid is specified, because it combines the following properties:

- High tensile modulus
- Low density
- Good dielectric behaviour
- High breaking strength
- High flexibility
- Good dimensional stability
- Very low creep rate
- Corrosion resistance
- Good chemical resistance and stability
- Good thermal insulating properties
- High heat resistance
- Flame-resistant, self-extinguishing
- Good vibration-damping behaviour

TYPICAL PHYSICAL PROPERTIES:

Glass-epoxy rod (FRP)

Tensile modulus (GPa) : 45 - 55
Specific gravity (g/cm³): 2.1 - 2.3

Para-aramid yarn

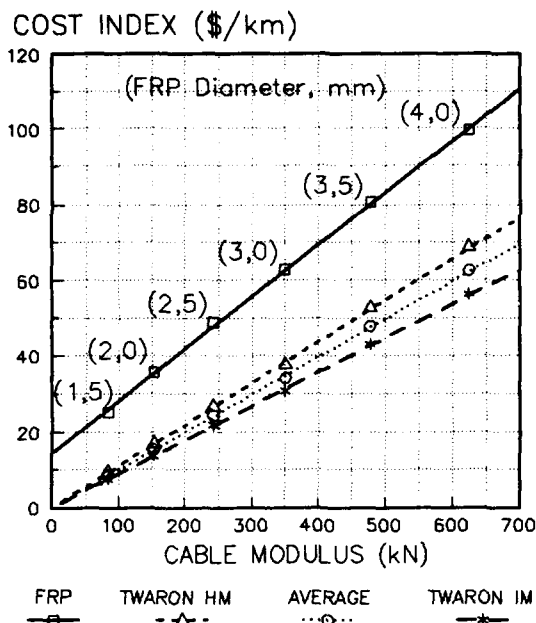
Tensile modulus (GPa) : 85 - 110
Specific gravity (g/cm³): 1.44 - 1.45

Looking at the typical physical properties of FRP and aramid yarns it can be calculated that aramid yarn provides 2 to almost 3.5 times more tensile modulus per unit of weight than FRP.

As far as costs are concerned, a survey of current world market prices shows that aramid yarns offer 2 to 3 times more modulus than FRP rod at the same costs.

In Fig. 1 the (normalized) costs per unit of modulus of both high and intermediate modulus aramid yarn are compared with those of FRP rods of various diameters.

Fig. 4 Relative Costs
Twaron versus FRP as Tensile Strength Member



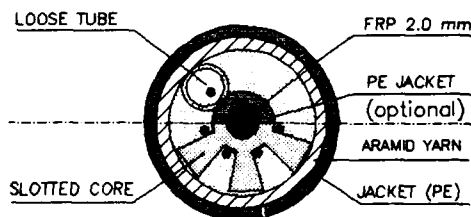
Solution 2; FRP 2.5 mm with peripheral reinforcement

Fig. 2 shows that a 2.5 mm rod has a modulus of approx. 250 kN. The balance of approx. 230 kN can be provided with a peripheral layer of 30,000 dtex high modulus aramid yarn (Twaron HM), resulting in the required total modulus of approx. 480 kN.

From Fig. 3 the weight can be calculated: 3 kg yarn plus 11 kg FRP amounts to 14 kg per km in total.

The cost index follows from Fig. 4: FRP (approx. 50) plus yarn (approx. 25), in total approx. 75.

Solution 3; FRP 2.0 mm with peripheral reinforcement



In the same way as demonstrated above the calculations can be made for 1.5 and 2 mm FRP rods in combination with either high modulus (Twaron HM 1055) or intermediate modulus yarn (Twaron IM 1111).

Fig. 2 shows that a 2.0 mm FRP rod has a modulus of approx. 150 kN. In combination with 45,000 dtex of high modulus yarn (Twaron HM) or, alternatively 55,000 dtex of intermediate modulus yarn (Twaron IM) this will result in a cable with the required modulus of 480 kN.

Accordingly, from Figs. 3 and 4 the total weight and cost index of reinforcement per kilometre of cable are found.

The results can be summarized as follows;

Summary

F.A.S.E. : 0.5% at 2400 N Solutions;	Total weight (kg/km)	Cost index (\$/km)
3.5 mm FRP, no peripheral reinforcement	22	81
2.5 mm FRP, 30,000 dtex Twaron HM 1055	14	75
2.0 mm FRP, 45,000 dtex Twaron HM 1055	11,5	70
2.0 mm FRP, 55,000 dtex Twaron IM 1111	12,5	65
1.5 mm FRP, 65,000 dtex Twaron IM 1111	10	60

ADDITIONAL ADVANTAGES OF PERIPHERAL REINFORCEMENT WITH ARAMID

Besides lower costs and weight, experience in the field has shown that a cable design with a peripheral layer of aramid yarns offers the following additional advantages;

- Protection

The peripheral aramid armour offers the cable better protection against damage during installation, cutting, heat and fire exposure, and is often found to increase the crushing resistance.

Extra protection against water penetration can be provided by using aramid "waterblocking yarns", which may eliminate the need for swelling tapes.

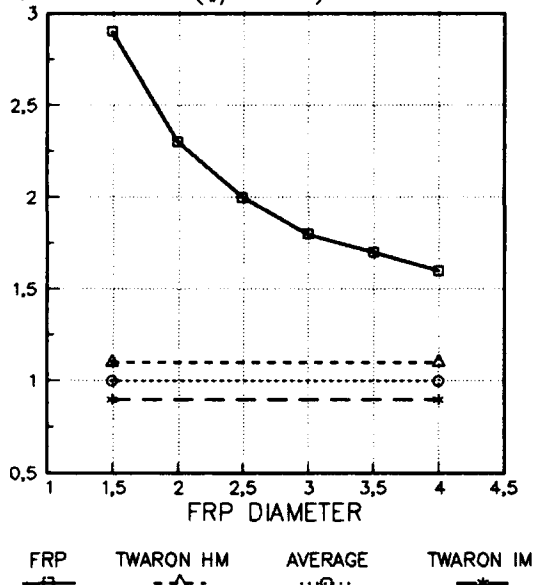
- Reliability

The presence of aramid yarn compensates for weak spots in the central strength member, e.g. at sections where the FRP is spliced or could fail/break during handling.

Fig. 1 Price/Performance

Twaron versus FRP as Tensile Strength Member

COST FACTOR (\$/kN.km)



(Based on Worldmarketprices Q1, 1993)

As shown in Fig. 1, the cost advantage depends on the type of aramid yarn and FRP diameter used.

CABLE CALCULATIONS

On the basis of graphs 2, 3 and 4 quick calculations and comparisons can be made of the costs and weights of cable designs that meet the same "force at specified elongation" (FASE) requirement by using different combinations of FRP, with or without peripheral layers of aramid yarn.

Example:

Cable specification:
maximum cable elongation 0.5% at 2400 N

From this specification it can be calculated that the cable should have a modulus of 480 kN.

Solution 1: FRP 3.5 mm, no peripheral reinforcement

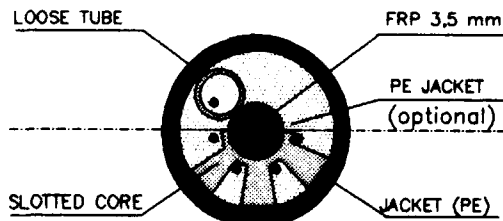


Fig. 2 Modulus

Twaron versus FRP as Tensile Strength Member

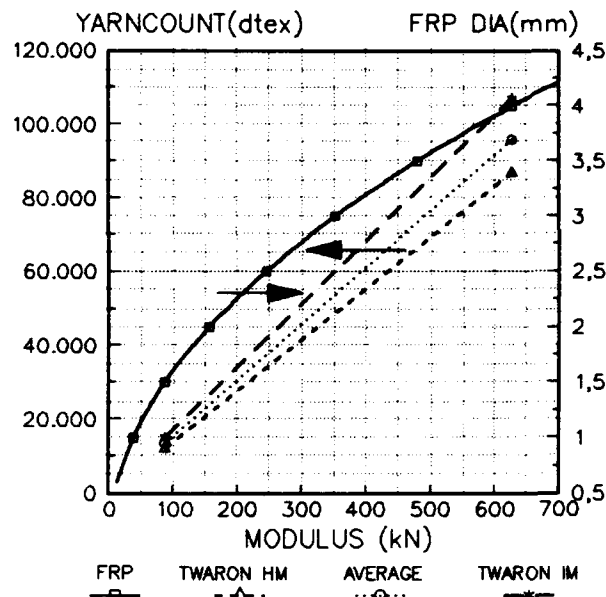
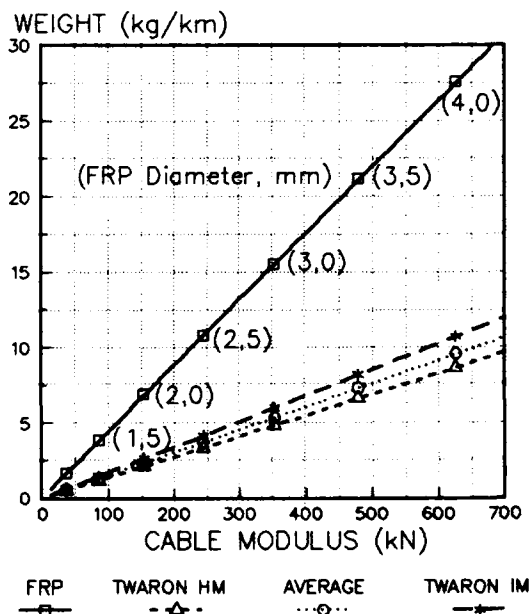


Fig. 2 shows that with a 3.5 mm FRP rod the required modulus of 480 kN can just be obtained, without additional peripheral reinforcement.

From Figs. 3 and Fig. 4 (see next page) the weight (approx. 22 kg) and cost index (approx. 81) per km of reinforcement can be found.

Fig. 3 Weight

Twaron versus FRP as Tensile Strength Member



Experience has shown that during installation in ducts and pulling of a cable with peripheral reinforcement, less failures occur. If the full pulling force is only applied to the central strength member, too high shear forces between jacket and center of the cable may be created, causing damage.

- Installation benefits

Cables that contain thin FRP rods with a peripheral aramid layer have a lower weight (5-10% on total cable weight), smaller diameter and are more flexible, which facilitates installation considerably, especially in narrow ducts and ducts with many curves.

This results in lower pulling forces, while longer pulls can be made with less risk of damage.

- Production benefits

If peripheral reinforcement is present, splices in the central strength member are less critical and can be allowed, which minimizes FRP waste in production.

If aramid yarns are used, the amount of reinforcing material can exactly be tailored to meet the required tensile specifications through the number of yarns, yarn count and yarn modulus chosen.

Furthermore, the size of the FRP rod can be standardized to one diameter which suits the entire range of cables produced.

CONCLUSIONS

From the above analysis it is clear that to minimize the costs and weight of reinforcing materials in both slotted core and loose tube configurations, the diameter of the central strength member should be kept as small as possible and should only be based on the required compression strength.

In practice, an FRP diameter of 1.5 to 2 mm has been found sufficient to meet the general requirements.

In addition, a peripheral layer of aramid yarns can be added to exactly tailor the cable to the required pulling force/FASE specifications.

This concept results in a more flexible and better protected cable compared with designs that use a large-diameter FRP rod without peripheral reinforcement.



Thomas Bijker
AKZO Fibers
P.O. Box 9300
6800 SB Arnhem
The Netherlands

Thomas Bijker was born in 1959 and received his degree in Chemical Engineering at the Institute of Advanced Technology in Amsterdam in 1983. In 1986 he joined AKZO Engineering Plastics as Technical Account Manager. Since 1989 he is working as Sales Manager responsible for the sales of aramid fibers in the field of Optical Fiber Cables and Ropes.



Jack J. Bensink
AKZO Fibers
P.O. Box 9300
6800 SB Arnhem
The Netherlands

Jack J. Bensink was born in 1960 and received his bachelor degree in Mechanical Engineering at the Institute of Technology in Arnhem in 1985. From 1985 to 1992 he worked in several functions at AKZO's Industrial Fibers Institute and the business unit Aramid Fibers in Arnhem. Since June 1992 he has worked as Technical Account Manager for Optical Fiber Cables.

APPLICATION OF SOLVENT TO THE CURE DEGREE MEASUREMENT OF UV CURABLE OPTICAL FIBER COATING

Naoya INOUE, Toshinori SEKI, Takeo SHIONO, Hiroshi MATSUURA

Showa Electric Wire & Cable Co., Ltd.

Abstract

It has become known, when a UV-curable resin for optical fiber coating is immersed in an organic solvent such as methylethyl ketone (MEK), the rate of swelling, or the level of deterioration of stress, in swelling to saturation is affected by the cure degree of the resin. It has also become known that the phenomenon depends also on the kind and temperature of solvent.

When a colored optical fiber is immersed in a solvent, the UV-curable resin coat swells, breaks to pieces and curls as its stress deteriorates to below a certain level, and finally peels from the fiber glass. It is found, in addition, that the time before peeling depends on the amount of ultraviolet light irradiated to the optical fiber.

It has become evident that this phenomenon can be utilized as a means of determining the level of curing of the coating and curing process for UV-curable resin coated optical fibers.

1. Introduction

For ultraviolet (UV)-curable optical fiber coating, it is desirable to develop a method which would allow quick determination of the cure degree of resin after coating and curing. Methods which use expensive instruments such as differential thermal analyzer¹⁾ and infrared spectrometer²⁾ for measurement of double bonds remaining in UV-curable resin have been attempted. Such methods, however, require a high level of skills, and are not yet easy to use, for operators, in the coating and curing process.

We studied physical and chemical characteristics of UV-curable resins in various ways, and found that the cure level of coating can be easily judged by immersing in organic solvent and observing changes in stress which occur in the swelling process. It has also been found that the time required for analysis is adjustable by selecting which solvent to use.

The phenomenon has been utilized in the process of UV-curable optical fiber coating. The method thus developed allows a quick determination of the cure level of coating, and thus will contribute to achieving a stable cure level in the coating and curing process.

2. Basic Studies Using Sheet Samples

2.1 Experimental

UV-curable resins for optical fibers shown in Table 1 were subjected to curing by ultraviolet irradiation and they were made into sheet samples. In curing, 50 to 1000 mJ/cm² of ultraviolet light was irradiated in the air using a 120-W high-pressure mercury lamp.

Sheet samples were immersed in a number of solvents as shown in Table 2 and the degree of swelling, Young's modulus, etc. was measured.

The degree of curing was determined from the weight reduction observed after extraction for 12 hours in MEK at 80°C and vacuum drying.

Table.1 Characteristic of UV resin.

UV resin cured polyurethane acrylates	Young's modulus (N/mm ²)	tensile strength (N/mm ²)	elongation (%)
	890	51	6

Table.2 Characteristic of solvent.

solvent	MW	density (g/cm ³)	boiling point(°C)	vapor pressre (mmHg)	solubility parameter	chemical structure
toluene	92.1	0.87	110.6	22.2	8.9	C ₆ H ₅ CH ₃
MEK	72.1	0.8	79.6	71.2	9.0	CH ₃ COC ₂ H ₅
chloroform	119.4	1.49	61.2	159.6	9.2	CHCl ₃
acetone	58.1	0.79	56.2	184.8	9.7	CH ₃ COCH ₃
n-butanol	74.1	0.81	117.7	4.4	11.4	C ₄ H ₉ OH
ethanol	46.1	0.79	78.3	45.0	12.9	C ₂ H ₅ OH

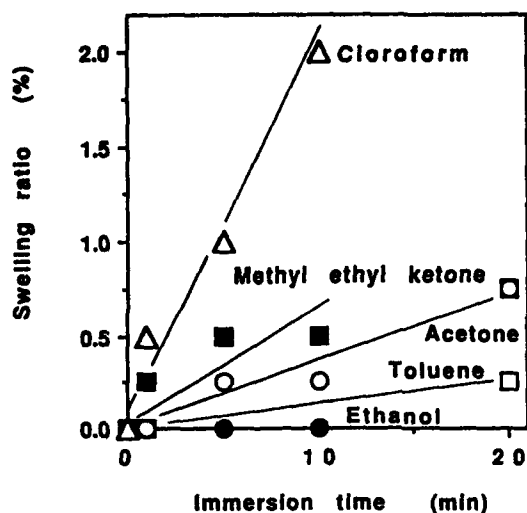


Fig.1(a) Swelling ratio increase with immersion time for different organic solvents at 25°C.

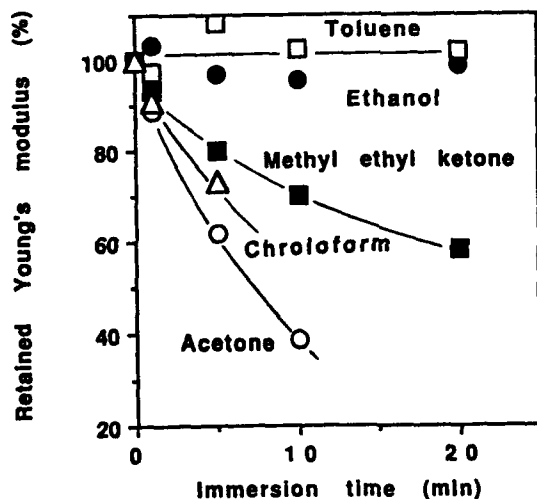


Fig.1(b) Retained Young's modulus decreased with immersion time for different organic solvents at 25 °C.

2.2 Results and Discussion

Effects of solvent

When samples irradiated to 1000 mJ/cm² are immersed in various solvents, the resin coating swells with time as shown in Fig. 1 (a). Young's modulus deteriorates during the time as shown in Fig. 1 (b) indicating an inverse relationship between Young's modulus and swelling.

When the residual Young's modulus after immersion for 5 minutes is checked against the solubility parameter (SP) value of the solvent, Young's modulus deteriorates at the fastest rate at the SP value around 9 to 10 as shown in Fig. 2. Considering that the SP value of the UV-curable resin is in the order of 9 to 10, it can be said that the

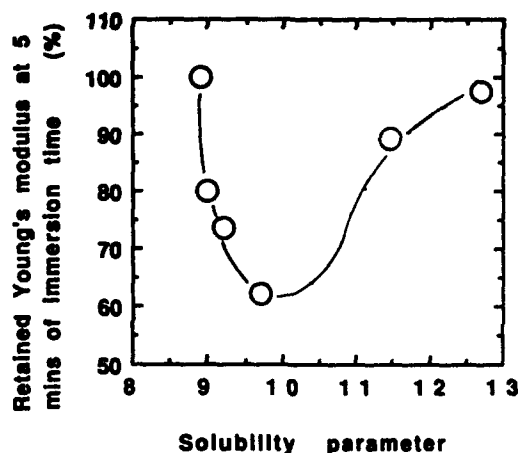


Fig.2 Solubility parameter vs retained Young's modulus after 5 mins immersion.

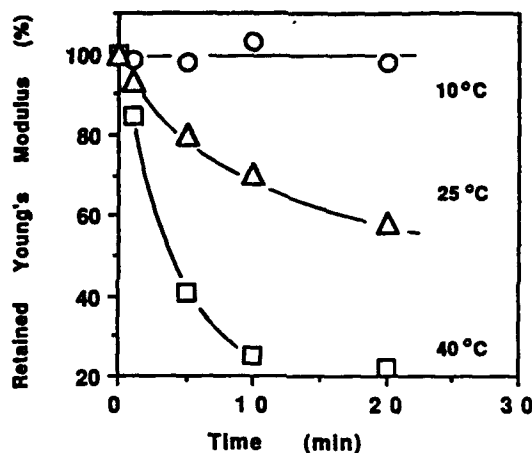


Fig.3 Retained Young's Modulus decrease with immersion time in methyl ethyl ketone at 10, 25, 40 °C.

deterioration in strength which depends on solvent, corresponds to the degree of swelling of UV-curable resin which, also depends on the solvent.

Effects of solvent temperature

When samples irradiated to 1000 mJ/cm² are immersed in MEK at 10, 25 and 45°C, Young's modulus deteriorates at a faster rate when the solvent temperature is higher as shown in Fig. 3.

The sorption rate in Fick-type diffusion sorption is expressed by the following equation:

$$\frac{M(t)}{M(\infty)} = 4 \left(\frac{D_0 t}{l^2} \right)^{1/2} \left\{ \pi^{1/2} + 2 \sum_{n=1}^{\infty} (-1)^n \operatorname{erfc} \frac{n l}{2 \sqrt{D_0 t}} \right\} \quad (1)$$

where $M(t)$ is the sorption of solvent at time t , $M(\infty)$ is the equilibrium sorption, D_0 is the diffusion coefficient and l is the film thickness, and the equation is expressed, for small t , as follows³⁾:

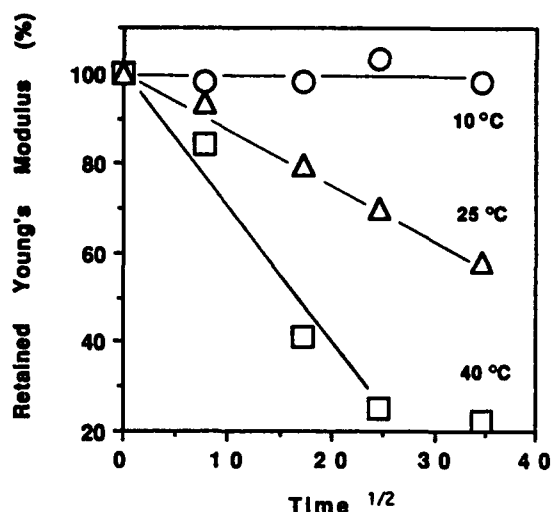


Fig.4 Retained Young's Modulus vs Time $1/2$ plots on methyl ethyl ketone.

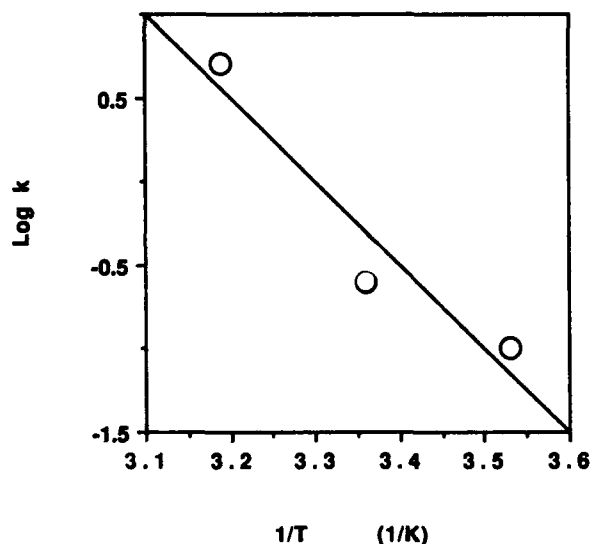


Fig.5 Arrhenius plot of Log k vs $1/T$ on methyl ethyl ketone.

$$\frac{M(t)}{M(\infty)} \propto 4 \left(\frac{D_0}{\pi} \right)^{1/2} \cdot t^{1/2} \quad (2)$$

When the residual Young's modulus obtained from Fig. 3 is plotted against $t^{1/2}$ in reference to Eq. (2), a linear relationship as shown in Fig. 4 is obtained, indicating that deterioration in Young's modulus corresponds to the rate of diffusion and sorption of the solvent in the UV-curable resin.

The temperature dependence of the apparent sorption rate constant (change in residual Young's modulus deterioration), k , given in Eq. (3) exhibits a linear

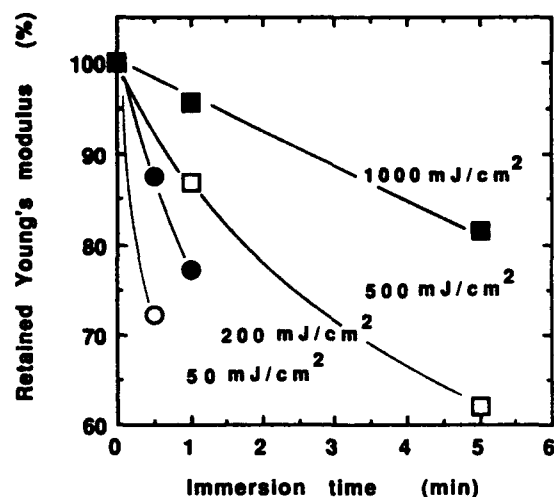


Fig.6 Dependence of the UV dose on retained Young's Modulus.

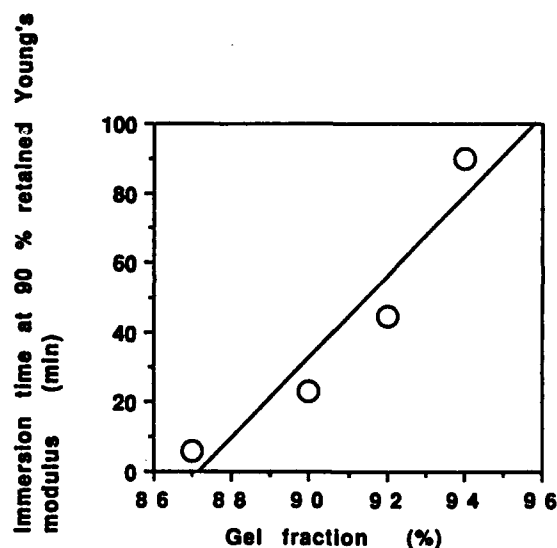


Fig.7 Gel fraction vs Immersion time at 90 % retained Young's modulus.

Table.3 Gel fraction.

UV irradiation (mJ/cm ²)	50	200	1000
Gel fraction (%)	87	90	94

characteristic as shown in Fig. 5.

$$k = 4 \left(\frac{D_0}{\pi} \right)^{1/2} \cdot t \cdot M(\infty) \quad (3)$$

The activation energy of diffusion of MEK into the UV-curable resin obtained from the figure was 22.9 kcal/mol.



a) Before Immersion b) Stress deterioration

Fig.8 Colored fiber with stress deterioration after immersion at 25 °C in MEK.

Effects of gel-fraction

The degrees of curing at irradiation of 50, 200 and 1000 mJ/cm² are as shown in Table 3. When such sheet samples are immersed in MEK, Young's modulus deteriorates faster in less well-cured samples as shown in Fig. 6. A linear relationship shown in Fig. 7 is obtained when the time of immersion in solvent before reaching 90% residual Young's modulus is plotted against the degree of curing. This indicates that the degree of curing of UV-curable resin on sheet can be estimated by immersing in a solvent and checking the deterioration of the Young's modulus.

3. Application to Optical Fiber

The phenomenon observed using sheet samples was applied to optical fibers.

When a white single mode fiber of 10 cm long is immersed in MEK, the solvent diffuses into the resin coating. The resin coating is severed due to stress deterioration and curls, and it peels off from the glass after a certain time as shown in Fig. 8.

The time of peeling of resin coating depends on the SP value of the solvent as shown in Fig. 9, and peeling occurs in a shorter time for fibers with less cured resin coating as shown in Fig. 10.

It is therefore possible, when applying this method to optical fiber fabrication, to simply check the state of curing by immersing the optical fiber in MEK or other solvent and measuring the time to peeling. This method may be useful in process control.

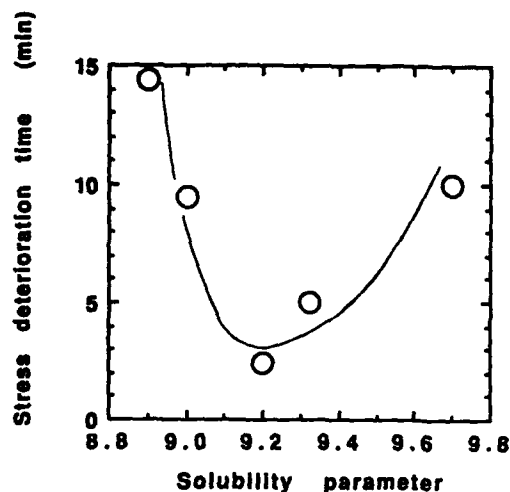


Fig.9 Stress deterioration time of different solvents vs solubility parameter at 25 °C.

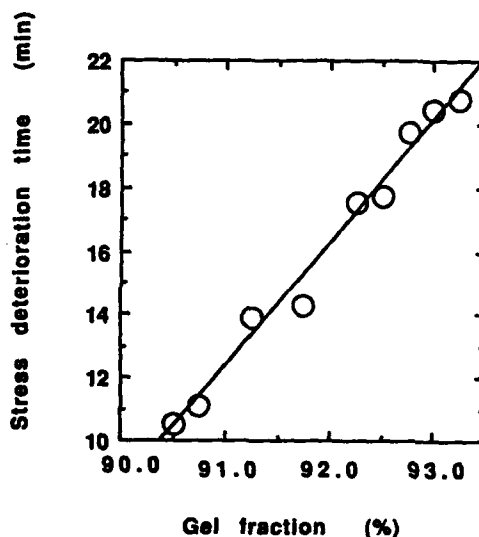


Fig.10 Stress deterioration time on the gel fraction of the UV coat of colored fiber at 25 °C.

4. References

- 1) M. Chiba, T. Hoshino, O. Shimizu, and M. Hanai, Proc. 39th IWCS, 690 (1990).
- 2) A. Mizutani, D. Saito, S. Endo, and N. Yoshida, Proc. 41st IWCS, 249 (1992).
- 3) A. Kishimoto, "Polymer & Water" The Society of Polymer Science, Japan (1972).



Naoya Inoue

Showa Electric Wire & Cable Co., Ltd., 4-1-1 Minamihashimoto, Sagamihara-shi, Kanagawa, 229 Japan.

Naoya Inoue received his M.S. degree from Toyama University in 1985. He joined Showa Electric Wire & Cable Co., Ltd. in 1989. He is a chief engineer of the Material Research Division of Telecommunication R&D Dept.



Hiroshi Matsuura

Showa Electric Wire & Cable Co., Ltd., 4-1-1 Minamihashimoto, Sagamihara-shi, Kanagawa, 229 Japan.

Hiroshi Matsuura received his B.S. degree from Osaka Institute of Technology in 1962. He joined Showa Electric Wire & Cable Co., Ltd. in 1962. He is the director of Telecommunication R&D Dept.



Toshinori Seki

Showa Electric Wire & Cable Co., Ltd., 4-1-1 Minamihashimoto, Sagamihara-shi, Kanagawa, 229 Japan.

Toshinori Seki received his B.S. degree from Science University of Tokyo in 1992. He joined Showa Electric Wire & Cable Co., Ltd. in 1992. He is an engineer of the Material Research Division of Telecommunication R&D Dept.



Takeo Shiono

Showa Electric Wire & Cable Co., Ltd., 4-1-1 Minamihashimoto, Sagamihara-shi, Kanagawa, 229 Japan.

Takeo Shiono received his Ph.D. degree in Chemical Engineering from the University of Tokyo in 1979. He joined Showa Electric Wire & Cable Co., Ltd. in 1979 and works in the development of telecommunication cable's materials. He is the manager of the Material Research Division of Telecommunication R&D Dept.

NEW DIRECTIONS IN FIBER OPTIC SPlice STORAGE

Wesley W. Jones and Gary S. Cobb

AT&T Bell Laboratories Norcross, Georgia

Abstract

The design of a splice organizer module composed of flexible foam and rigid plastic and its advantages for holding many of the common fiber optic splices is described. A formed insert of elastomeric foam is used to hold a multiple number of splices. The geometry of the design in combination with the resiliency and conformability of the foam material allows the insert to accommodate most of the non-polish mechanical splices now available as well as fusion splices having heat shrink sleeves. The foam insert is surrounded by a molded rigid plastic holder to provide containment and prevent the foam from being distorted excessively. The multiple splice modules can be attached to a splice tray to provide a complete system for housing the splices, storing the fiber slack, and controlling the bend radius of the fiber. The use of this new splice storage technology in a number of different applications is described.

Background

Typically when fiber optic splices are housed in splice closures or splicing cabinets, splice trays are used to house the splices and to store the excess fiber slack. These splice trays (sometimes called splice organizers) may be made of metal or plastic and have been constructed in many configurations. The primary purpose of the splice tray is to securely hold the completed fiber splices, i.e. to prevent the splices from moving about as the closure is assembled and placed. Closures are often roughly handled, for instance being dropped into splicing pits or being struck by tools or other objects. Regardless of the external forces on the closure, the splice tray must prevent the splices from moving. For if the splices shift position, the allowable minimum bend radius in the optical fibers may be exceeded which will increase the probability of fiber failure due to static fatigue and may

cause increased splice attenuation. In the most extreme situation, movement of splices within the splice tray may cause fibers to break. The design of the splice tray should also function to insulate the splices from vibration as much as possible. Closures and the splices they contain are exposed to vibration from a number of sources; for example assembly with air wrenches, proximity to heavy vehicular traffic, or exposure to high winds in aerial plant. There is always the possibility with mechanical splices that, if they are not well secured, vibration can adversely affect the optical loss at the splice. Another consideration is, that even though the splices must be securely fastened in position, they must also be held gently, without deforming the splice themselves. Any deformation of the splice devices could also cause increased signal attenuation.

The ways in which splices have been secured in splice trays are very diverse. Magnetic strips have been used to hold sleeved fusion splices. Additionally molded plastic fingers, formed metal tabs, and molded rubber strips have all been used in various ingenious configurations to secure splices in the past. All of these designs and methods had one limiting attribute. They each were designed to function properly with only one or two different splice devices. In the 1980's when the predominant splices in use were the sleeved fusion splice and the rotary/mechanical splice, it was relatively easy for the splice tray designer to accommodate a customer's choice of splicing device. As the number of different fiber optic splices commercially available has increased, it has become more difficult to design new trays (or tray inserts) for each closure to hold each new splice. There have been attempts to design details into splice trays to accommodate more than one type of splice; however the rapid proliferation of different splices has limited the effectiveness of this approach. What was needed was a method of providing a splice tray with more universality or adaptability to different splice geometries.

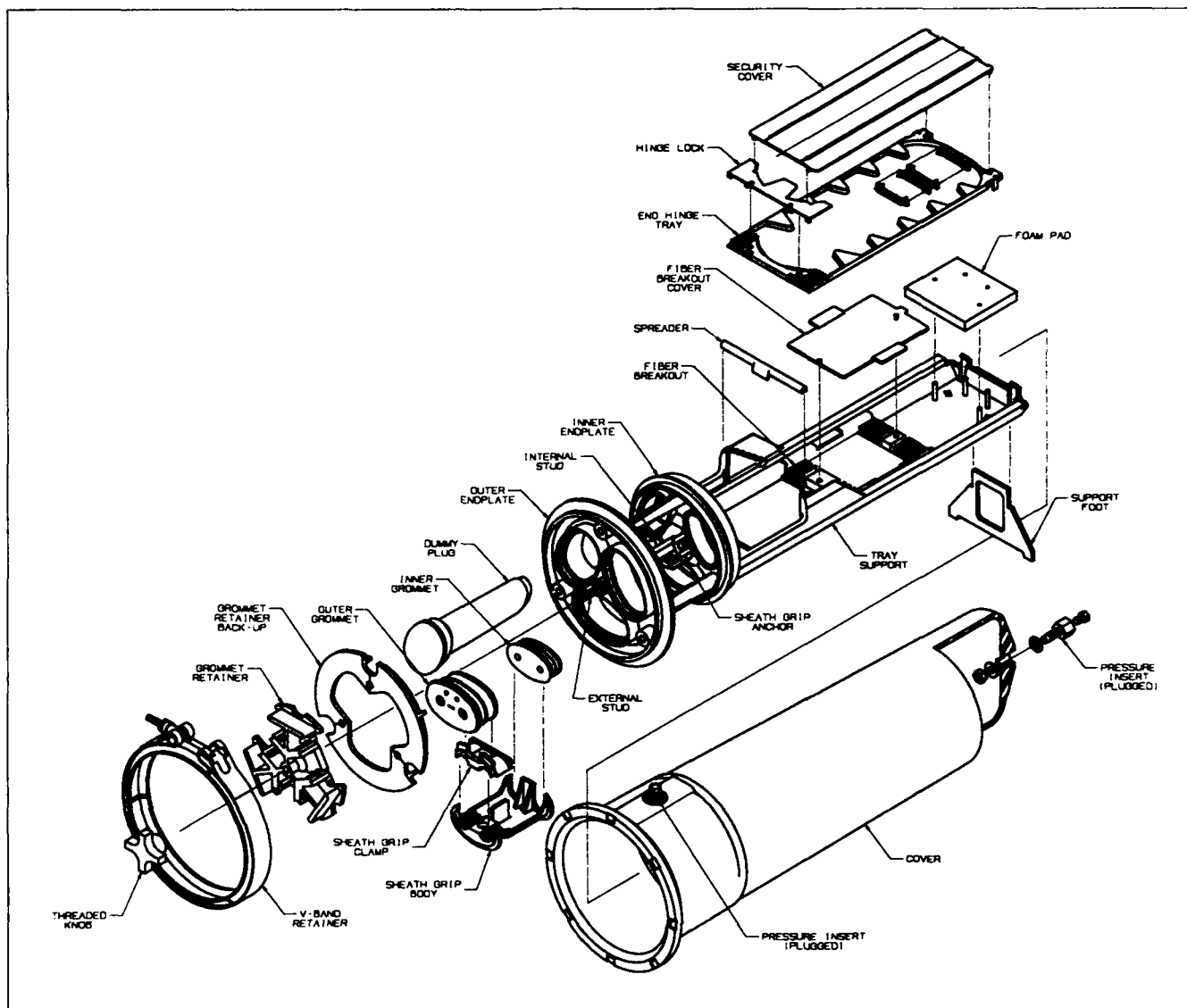


Figure 1. 2600LG/SC1 Closure.

Development Project

In the late summer of 1990, it was decided to increase the splice capacity of the 2600LG/SC1 Fiber Optic Splice Closure. A schematic drawing of the closure is shown in Figure 1. This butt splice closure was capable of holding 6 splice trays each housing 24 individual splices for a total splice capacity of 144 splices. Cable manufacturers at that time were working on increasing the fiber capacities of their cables, so a development project was started to see if the splice capacity of the closure could also be increased. Redesigning the closure cover and end plates would be very expensive and there was no room to add additional splice trays. Therefore,

the redesign efforts were directed at increasing the splice capacity (and splice density) within each tray.

A new splicing technology, the non-polish mechanical splice, was also being employed in cable splicing more and more frequently. Commercial examples of this type of splice are shown in Figure 2. Because the fiber ends do not have to be polished before splicing, these new splicing devices had definite cost and installation time advantages. Obviously any new splice tray design would have to accommodate non-polish mechanical splices.

The following design criteria were established for the splice tray redesign project to increase the splice capacity of the closure. These specific design requirements were



Figure 2. Non-polish Mechanical Splices.

in addition to the normal general requirements for any fiber optic splice tray.

1. Increase the splice capacity of the splice tray from 24 to 36 individual splices. (This would increase the capacity of the closure for individual splices from 144 to 216.)
2. Make no changes in the outside dimensions or shape of the splice tray so that it would be functional with the existing trays.
3. The redesigned splice tray should accommodate fusion splices with heat shrink sleeves and all common non-polish mechanical splices.
4. The redesigned splice tray should allow the different types of splices to be mixed within a tray.
5. The redesigned splice tray should hold the splices securely and withstand vibration per EIA FOTP-11, condition 1.
6. The redesigned splice tray must accommodate loops of fiber of varying diameters in order to dress and store the excess fiber slack.

7. The redesigned splice tray should organize splices in multiples of 6 to conform to the most common cable constructions.

8. The redesigned splice tray should be easy to use.

Design

Examination of the target commercial splices for this application revealed a wide diversity of shapes. However, the non-polish mechanical splices have similar dimensions in length and width. Sleeved fusion splices are typically much smaller in diameter and longer in length. Because of the size similarity of the mechanical splices, an initial design concept was developed to hold them in flexible nests with separate details being utilized to retain the fusion splices. (see figure 3) The splice organizers were designed to hold 6 splices each for modularity. By spacing the 6-splice organizers properly in the splice tray, room would be left for fiber pass-through channels between the organizers. These pass-throughs would be utilized to route fiber and to store loops of fiber slack.

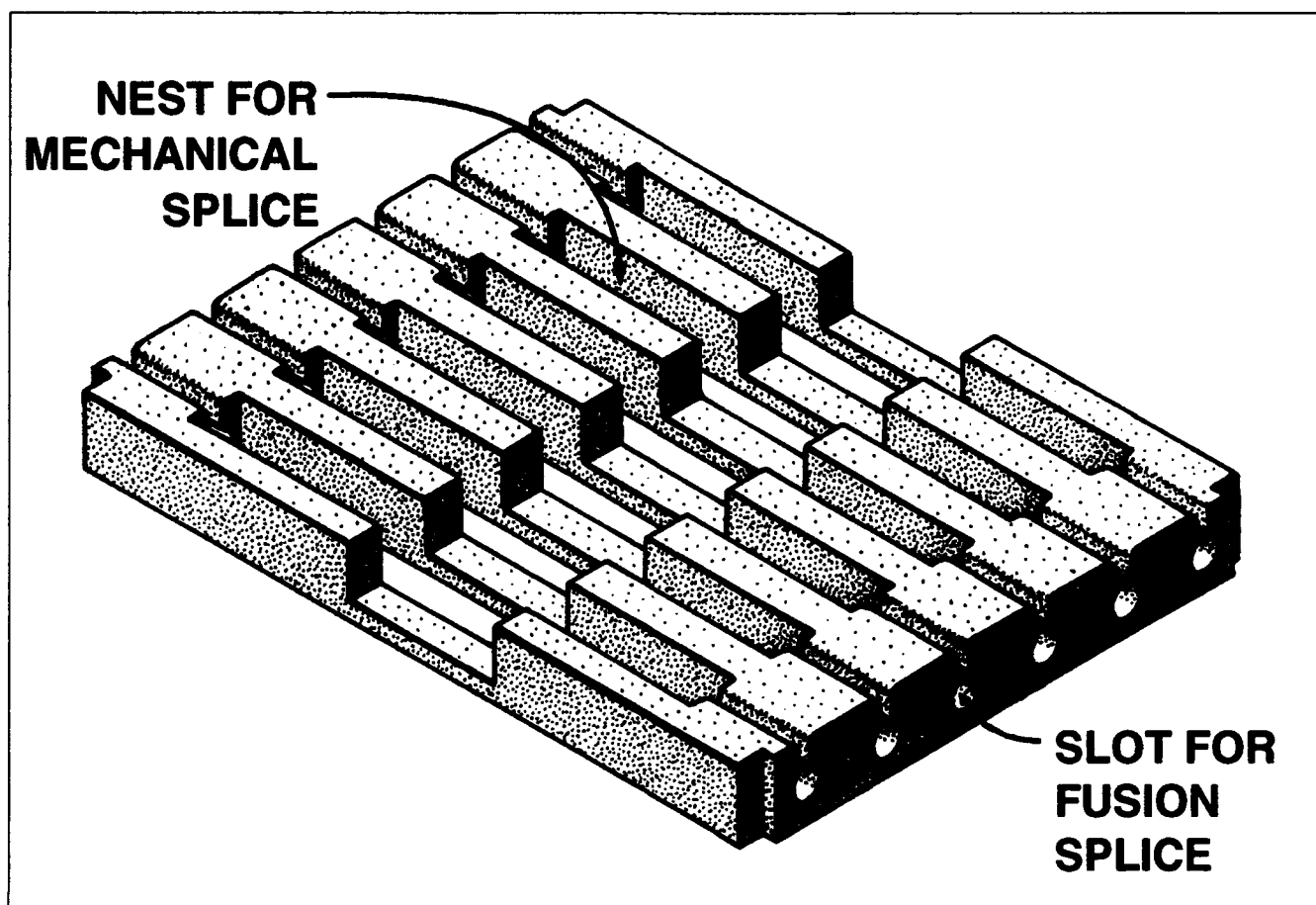


Figure 3. Foam Splice Organizer.

Prototypes

Prototype samples of the 6-splice organizer module were constructed in thermoplastic rubber compounds for evaluation. The samples worked well when the dimensions were adjusted for any particular mechanical splice, but did not satisfactorily meet design requirements #3 and #4. Rubber materials, even when molded with some degree of "foaming", are essentially incompressible. Therefore, when a splice is inserted into its nest, it bulges out the restraining side walls slightly. When the next splice is put in the adjacent nest, it distorts the rubber part more and the effect is cumulative. As additional splices are added, the side walls are bulged out or displaced further. (see figure 4) Careful control of dimensional tolerances can overcome this problem for any given splice, but the dimensional differences of the various splices make rubber an unsuitable material for a universal splice organizer.

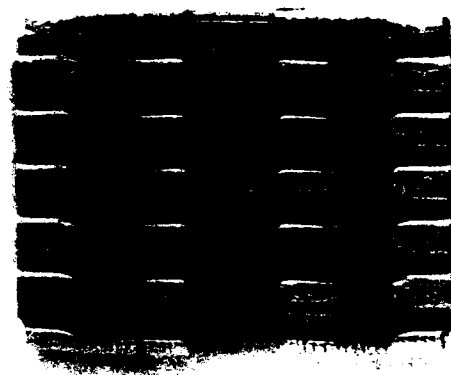


Figure 4. Splice Holder Showing Distorted Side Walls.

What is needed is a material that, in addition to being flexible, is also compressible. It must also be resilient across a wide temperature range, be chemically resistant, and possess low compression set properties. After a period of material development and evaluation, a suitable elastomeric cellular material was chosen.

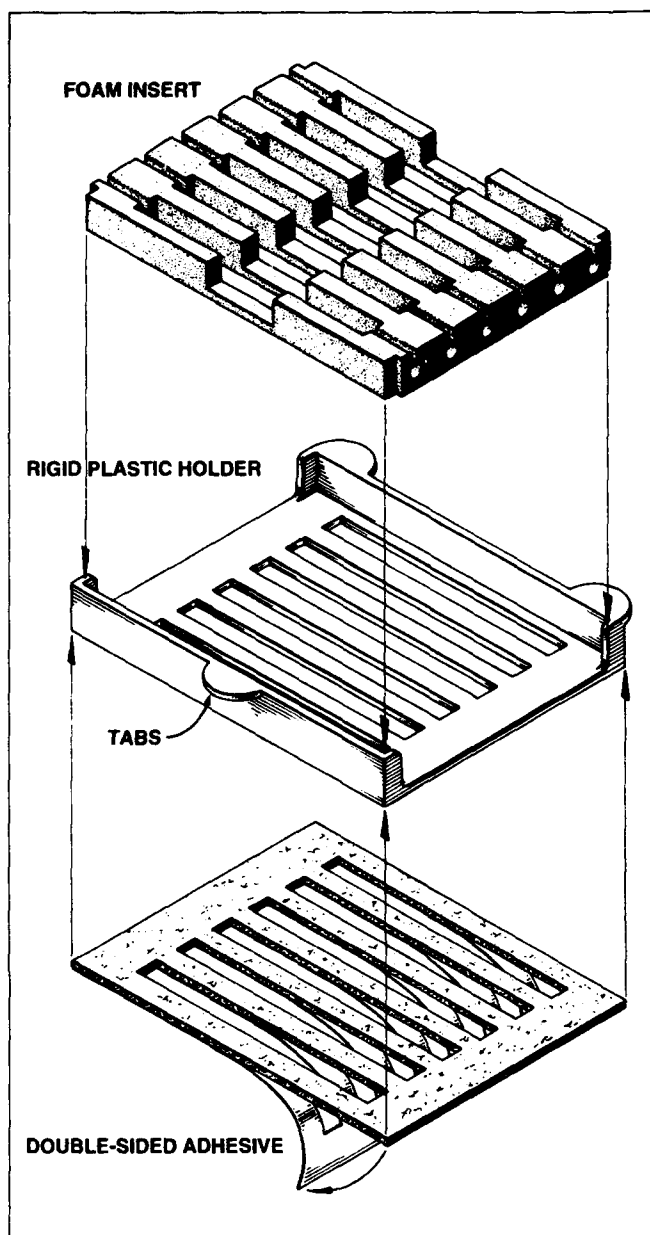


Figure 5. Splice Organizer Components.

Final Design

Testing of prototype organizers made from various foam or cellular materials disclosed one more problem to be solved. The softness and flexibility of the foam which allowed it to conform to the shape and dimensions of various splices also allowed it to distort in an undesirable manner. When loaded with splices, the side walls of two adjacent 6-splice foam organizers would bulge out blocking the pass-through channel between them. To correct this problem, a thin rigid plastic holder was

designed to enclose and contain the foam insert. (see figure 5)

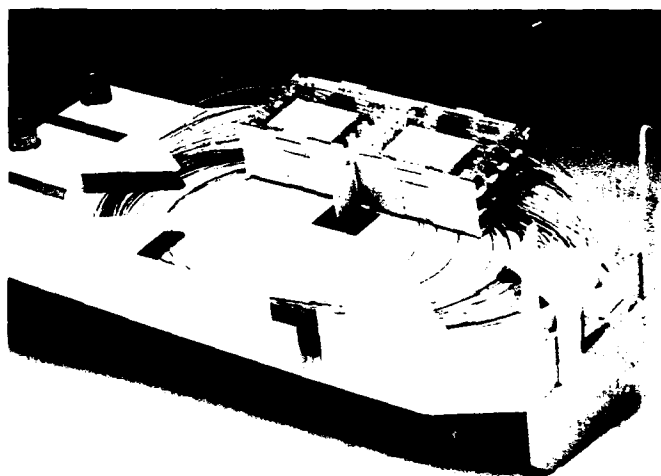
An additional feature of the holder is the inclusion of horizontal fingers or tabs molded to the side walls. When two organizers are located adjacent to one another, these tabs form a serpentine passageway to the fiber pass-through channel under them. The organizers are supplied with double sided adhesive tape on the bottom to facilitate attachment to the splice tray. From 1 to 6 of the organizers can be installed in each 36-splice tray. The design of the organizer/splice tray and the use of a compliant cellular material to hold fiber connecting devices is covered under U. S. Patent No. 5,185,845.

Further Applications

The 6-splice organizers have recently been incorporated into a new splice tray for the 2500LG Fiber Optic Closure. This closure was originally designed as a low fiber count splice or drop closure and was limited to 24 splices. (see figure 6) Because of its popularity due to its compact design and low cost, users requested that its splice capacity be increased. The closure was redesigned with a new splice tray and splice cassettes, each equipped with 3 of the 6-splice foam organizers. (see figure 7) By stacking 2 of the splice cassettes in the splice tray, the splice capacity of the closure has been increased from 24 to 54 splices. Depending on cable type, a third cassette can be added raising the maximum storage capacity to 72 splices.

The foam organizer modules have also been used in modified form in two other applications, a restoration closure for quick repair of cable cuts and an optical

Figure 6. 2500LG Closure Splice Tray.



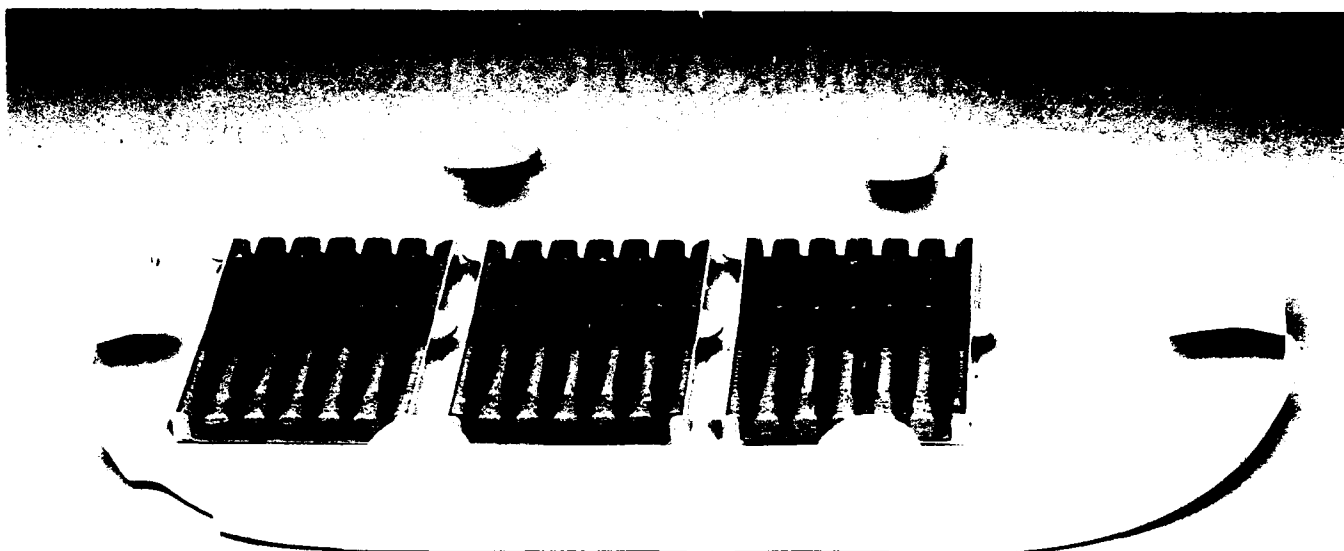


Figure 7. Splice Cassette With Foam Splice Organizer.

network unit for fiber to the curb. Consideration is also being given to molding restraining walls into splice trays to hold the foam splice inserts. These restraining walls would serve the same function as the plastic holder and would simplify assembly of the splice tray.

The modularity and ability of the 6-splice organizers to hold most of the individual fiber optic splices currently in use makes them ideal for many other applications in closures, terminals, cabinets, fiber optic shelves, etc. Because of the versatility of the foam organizer technology, this approach to fiber optic splice storage is expected to see increasing use in the future.



Wesley W. Jones
AT&T Bell Laboratories
Norcross, Georgia

Wesley W. Jones is a Member of Technical Staff in the Fiber Optic Apparatus Development Department at AT&T Bell Laboratories - Norcross, Georgia. Mr. Jones joined Western Electric in 1970 after

receiving a Bachelor of Science in Mechanical Engineering degree from the University of Florida. He has held various engineering positions within AT&T Network Systems, primarily in the area of the design, development, and manufacture of copper and fiber optic splice closures.



Gary S. Cobb
AT&T Bell Laboratories
Norcross, Georgia

Gary S. Cobb is a Distinguished Member of Technical Staff in the Fiber Optic Apparatus Development Department at AT&T Bell Laboratories. Mr. Cobb joined Bell Laboratories in 1963 where he worked in the Ocean Cable and Underwater Sound area for 13 years. For the past 10 years, Mr. Cobb has been active in the design and development of copper and fiber optic splice closures. Mr. Cobb received his BSME degree from Virginia Polytechnic Institute and State University and a MSME degree from the University of Maryland.

A SUBMARINE FIBER OPTIC SPLICE CLOSURE FOR INTERMEDIATE WATER DEPTHS

G.S. Cobb, W.H. Bense, H.O. Lindstrom, P.M. Thomas

AT&T Bell Laboratories 2000 Northeast Expressway Norcross, Georgia 30071

Abstract

A fiber optic splice closure has been designed for use in intermediate water depths. The 2800LG Submarine Closure is constructed using beryllium-copper for its external members. Sealing is provided with redundant O-ring type seals between, a) cable sheath and cable gland, b) between the cable gland and the bottom closure cover. A single O-ring seal is used between cover halves. Reliability is further enhanced by displacing the air within the closure with cable filling compound which in turn is pressurized by the filling compound in the suspended cable. The result is zero pressure differential across the seals. Closure sealing system tests indicate a working depth of 300 meters (1000 feet). Tensile strength across the splice joint is accomplished with a C-Submarine Sled. Single and double externally armored cables having high density polyethylene sheaths can be accommodated. Splice storage capacity is 144 for fusion splices and 108 for tunable mechanical splices. Several actual installations are described.

Introduction

In the late 1980's, several opportunities appeared which indicated the need for a new submarine fiber optic splice closure. First, planning was proceeding for the initial transatlantic fiber optic cable system (TAT-8). A deep water splice closure was designed to join the numerous lengths of unarmored deep water cable both in the factory and on board ship. These closures were extremely reliable, quite complex, can take up to 18 hours to install (including splices) and required specialized injection molding equipment found only on ocean cable laying ships and cable factories. What was not available was a highly reliable, inexpensive, and quickly installable splice closure that could be used to repair the armored cable if there were an accident when landing the shore

end. This scenario would most likely preclude the use of a cable ship due to the relatively shallow water.

A second opportunity or consideration was the increasing cost of acquiring land right-of-way in many parts of the world. Additionally, for many planned routes, the shortest distance was over water. Thus, water crossings and water routes began to receive serious consideration as alternatives to traditional routing.

A further consideration was that transmission systems and fiber designs were evolving that permitted longer lengths of cable without regenerators, thus promoting more water routes. As more cable was placed in more water routes, the greater the chance for cable breaks to occur. There existed only one repair option and that was to replace the entire cable. If a splice closure was available, then an additional option would be to repair the cable depending on the economics of the two options.

It was against this background that the design and development of a submarine fiber optic splice closure was begun. The following sections will discuss the original design criteria, the design details, the closure's development testing results, and field installation experience. To take advantage of an increasing market, testing was later conducted at deeper water depths and these results are discussed. A final section covers future directions of submarine closures.

Initial Design Criteria

Water Depth

Fiber optic splice closures preceding the submarine closure and subsequent to its introduction were typically designed for 3-meter water depths which was the depth of water usually found in manholes. On the other extreme, ocean cable splice closures were designed for water depths exceeding 6000 meters. Thus, "intermediate" falls somewhere between 3 and 6000 meters. Work-

Working Depth	100 meters
Water Environment	Fresh and Salt
Design Life	25 Years
Cable Design	Single or Double Armored, 72 fibers, 10 to 15 mm OD
Splice Type	Fusion and Tunable Mechanical Rotary
Temperature Range	0°C to 30°C
Ass'ly Environment	Work Barge, Cable Ship, Shore
Weight	200kg
Deployment	Sling or by transmission cable
Assembly Time	12 hours maximum
Reenter & Reusable	Yes

Figure 1. Initial Design Requirements

ing with internal and external customers, 100 meters (330 feet) was considered a realistic requirement for the majority of the then envisioned applications.

Water Environment

Both salt and fresh water uses of the closure were considered necessary. In both environments, the closure would be buried most likely by "jetting" so the final resting place would be in bottom material surrounded by either fresh or salt water.

Design Life

Design life was established at 25 years. This was considered reasonable from a materials view and also from a changing technology view. It was also the input from the SL Undersea Cable Development Group.

Cable Design

The closure would be required to accommodate either single or double armored cable having a high density polyethylene jacket with an outer diameter range of 10 mm to 15 mm.

Fiber Count

Fiber counts up to 72 were initially considered. This has subsequently been increased, depending on the splice type to 144 fibers (see Design Enhancements section).

Splice Type

Typically, very low loss splices would be required for these long length systems. Thus fusion and the tunable mechanical rotary splice would be accommodated.

Temperature Range

The applicable working temperature range was established at 0°C to 30°C. This would account for water bottom conditions and expected air temperature extremes during assembly. Storage temperature could range from -20°C to 60°C.

Assembly Environment

Typically the closure would be assembled on a work barge. This would be a worst case situation. Assembly was also envisioned on a cable ship and on shore.

Weight

Total weight would be limited to 200 kg (440 lbs.) to reduce deployment difficulties when working on a barge.

Deployment

A sling or similar rigging would be the preferred method of lowering the closure to the bottom. The closure would not be deployed over sheaves, but could be lowered by the transmission cable especially in deeper water depths, thus exerting a high degree of tensile loading.

Assembly Time

Recognizing the high expense of water operations and the possibility of rapidly changing weather conditions, the maximum closure assembly time was set at 12 hours.

Reentry

The closure must be reenterable and reusable.

Design

Design Concept

In order to fulfill the primary objective of the splice closure, i.e. to protect the exposed fibers and splices from the environment for the expected service life of the cable, a conceptual closure design was first established. The

design concept was to provide a closure system that would function in harmony with the filled cable core of the armored terrestrial cable. By utilizing a filled closure design, the splice compartment would achieve pressure equilibrium with the surrounding water via the filled cable core. In this way a "dual" sealing system is provided for the enclosed splices, an O-ring sealing system between the closure and the cable and a filling compound "seal" between the splices and the closure. Therefore, even under the worst-case condition of an O-ring seal failure, the splice compartment would not be allowed to flood with water. This design concept differed from existing closure designs used in either terrestrial or undersea applications in that the splicing cavity was previously an "air space".

Traditionally, the tensile strength of the splice joint was bridged across the splice by the splice closure members and was typically on the order 50 to 100 kg. Use of externally armored cable creates very large placing loads. The C-Submarine Sled was selected to terminate the external armor and to bridge the splice leaving the "internal" closure to serve simply as a pressure vessel.

Materials Selection

With the conceptual design established, the design effort was focused on the selection of materials for compatibility with the environment and with the enclosed apparatus. Established materials technology in undersea apparatus housings, dating back to the early 1960's with the TAT-3 transoceanic cable installation, was utilized in the selection of the external splice closure housing. Beryllium copper was the material of choice for long term exposure to salt water. There are presently several thousand of these housings in service.

The first choice for a closure filling compound was the compound used in the core of the fiber optic cable. By using the same compound as contained in the cable, compatibility studies with the fibers and cable would not be required. However, there was no experience to draw on concerning the exposure of tunable mechanical splices to filling compound. Therefore, a test program was established to study the effects of filling compound on splice loss at the design temperature and pressure extremes.

The O-ring materials were selected for compatibility with fresh and salt water and filling compounds. Again, existing technology in O-ring sealing systems simplified

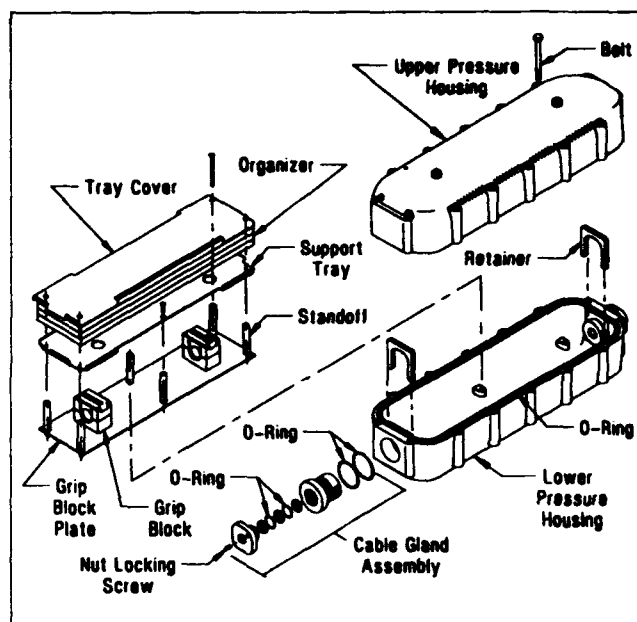


Figure 2. Exploded View of Closure.

the process of selecting materials that would not degrade over time.

Physical Design

In the physical design of the splice closure, attention was given to using existing hardware where possible in order to minimize development cost. Splice trays, cable grips, and bonding hardware from a current production closure were incorporated within the beryllium copper pressure vessel. The C-Submarine Sled was used for armor termination. The sled is a hot-dip galvanized steel structure that was originally designed for termination of the armor wires over lead sheath copper cable used for river crossings.

Since the closure would be expected to operate at pressures up to 10.5 kgf/cm^2 (150 psi) and be re-enterable, an O-ring sealing system was selected. Dual O-ring seals were used between the cable and the pressure vessel to provide an extra level of protection at the most "difficult" sealing surface i.e., the HDPE cable jacket. At the metal-to-metal sealing surfaces, surface finishes and tolerances as recommended by the O-ring manufacturer were used.

The pressure vessel was designed to fit within the C-Submarine Sled with adequate clearance for the installation of plastic spacers between the pressure vessel and sled. In this way, the air space between the two could be filled with an encapsulant that would provide additional me-

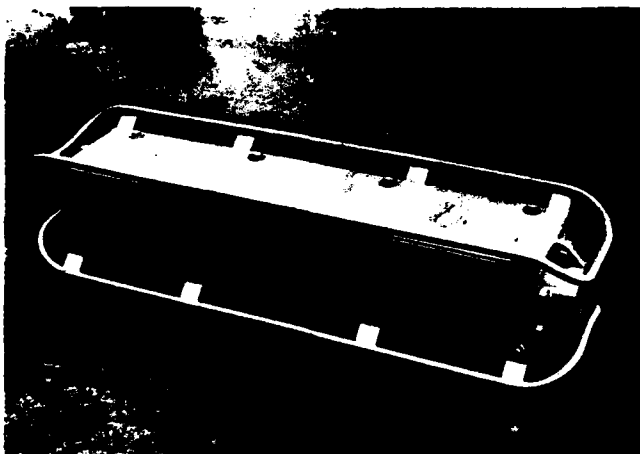


Figure 3. C-Submarine Sled.

chanical shock protection for the splices and protection from possible galvanic action between the dissimilar metals. The completed assembly weighs approximately 200 kg (440 lbs.); 35 kg for the 2800LG, 118 kg for the C-Submarine Sled, 37 kg for encapsulant and 4 kg for cable filling compound.

Development Testing

Test Facilities

As previously discussed, the design working depth was set at 100 m (330 feet). At this depth the water pressure is about 10.5 kgf/cm^2 (150 psi). These pressures were well above what was available in the closure development laboratory. To fill this need, a 17.5 kgf/cm^2 (250 psi) pressure vessel was designed and constructed. The vessel was designed per the ASME Boiler Pressure Vessel Code for a 17.5 kgf/cm^2 (250 psi) facility. This specification would provide very high design margins. The high safety margins coupled with the use of water, not air, as the main medium, provided a very safe test environment.

Test Results

Splice Loss Test A test program was implemented to study the effects of filling compound, under pressure, on the tunable mechanical splice which employs an index matching gel between the fiber ends to minimize insertion loss. Twelve mechanical splices were placed in filling compound within a closure. Two of the twelve splices were assembled using cable filling compound as the index match material while the remaining ten splices

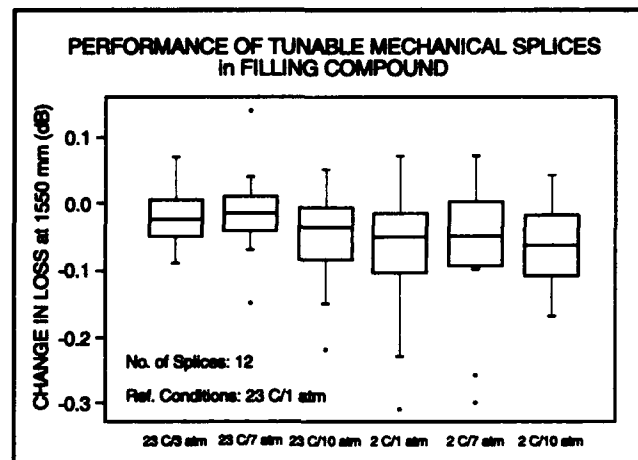


Figure 4. Splice Loss Test Results.

used standard index match material. The closure was then placed in the pressure vessel. The test setup was placed in an environmental chamber and subjected to a range of temperatures and pressures while monitoring the splice loss. Splice loss results are given in Figure 4. No significant change in loss was noted between tests at 1 to 10 kgf/cm^2 (1 to 10 atmospheres) of pressure.

Seal Tests The cable-to-closure seals were tested in conjunction with the splice loss tests. The sealing system design was incorporated into the pressure vessel end-plate. The O-ring seals showed no sign of leakage throughout the splice loss test program.

The beryllium copper pressure vessel was also tested for seal integrity. Seven pressure vessels were tested by installing a continuous length of cable through the closure and applying an internal pressure of 10.3 kgf/cm^2 . None of the seven closures showed any sign of leaks. All O-rings were heat aged before testing to allow the seal material modulus to degrade.

Low Temperature Use of Cable Filling Compound As previously discussed, the submarine closure is post filled with approximately 4 kg of the cable filling compound to provide a pressure balanced sealing system. After completion of fiber splicing and testing, the closure is sealed and the filling compound is injected through one of the two tapped holes in the top of the housing using a conventional grease-type cartridge injection gun. The cable filling compound and injection system must be usable at temperatures near freezing for barge installations.

<u>Temp. & Time</u>	<u>Type A</u>	<u>Type B</u>
27°C after 0 hours	Easy to Pump using ratchet with one hand	Pumpable using two hands on ratchet
10°C after 24 hours	Easy to pump using ratchet with one hand	Extremely difficult to pump with two hands, not practical
-1°C after 5 hours	Easy to pump using ratchet with one hand	-----
-7°C after 5 hours	Can be pumped with minor difficulty	-----

Figure 5. Cold Temperature Performance.

Following the initial closure development, the cable filling compound was changed to reduce excessive oil migration from the cable structure (herein called Type A or B). An injection experiment was performed to ascertain if the new Type B material offered any advantage in cold temperature usage. Test results has shown that the Type A filling compound was usable down to -7°C with the cartridge injection gun. In comparison, the Type B compound was marginal at 10°C. Therefore the Type A filling compound remained the material of choice for this application. Figure 5 summarizes these results.

Design Enhancements

Following the original design and development cycle, customers indicated a need for an increase in splice storage capacity from 72 to 96 tunable mechanical splices and application for water depths greater than 100 meters. This section will focus on these two enhancements along with a study conducted using different filling compounds.

Increased Splice Storage Capacity

The initial submarine closure design was equipped with typical splice organizers that store 18 tunable mechanical or 24 fusion splices per tray and could accommodate four trays for a total splice storage capacity of 72 tunable mechanical splices or 96 fusion splices. The ever increasing need for high capacity transmission routes has caused customers to reevaluate their long range growth

plans and also consider the high cost of future fiber placement in intermediate water depths. These considerations have resulted in an increase in fiber cable counts being placed and therefore the need for a higher splice storage capacity.

To address this need, the submarine closure was modified to accept two additional splice organizers increasing the splice capacity from 72 to 108 tunable mechanical splices and from 96 to 144 fusion splices. These additional two organizers increased the stacked height of the splice organizers by approximately 19 mm. To compensate, the height of the cable gripping hardware and the organizer standoffs (see Figure 2) were reduced proportionally. Any subsequent increases in splice storage capacity beyond the six organizers will require a change to the closure housing components.

Increased Water Depth

The initial design requirement was intended for closure placement in 100 m water depths (9.5 kgf/cm² external pressure). Future installations have been identified that will be in depths to 275 meters (900 feet). To evaluate the submarine closure performance at these greater depths, a test plan was developed and an outside lab, Southwest Research Institute (SRI) was contracted to perform the tests. SRI had available the necessary high pressure test facilities and expertise in hydrostatic pressure testing. This avoided the cost and time delay associated with constructing a new, limited use test facility. Two submarine closures were assembled with two high density polyethylene jacketed fiber optic cables having diameters of 10.6 and 12.7 mm. The closure assemblies (without filling compound) were heat aged for 30 hours at 60°C to allow the O-ring seal material modulus to degrade to that level representative of the material life-time expectancy.

The closures were then placed in a vessel containing water and pressurized to 35 kgf/cm² (500 psi) for 30 days. Water temperature was maintained between 2°C and 4°C. Internal moisture sensors monitored any changes in relative humidity to detect any moisture migration into the closure. After 30 days, no changes in relative humidity occurred and the hydrostatic pressure was increased by approximately 7 kgf/cm²/hr. to determine at what pressure the closure would fail. After 50 minutes at 175 kgf/cm² (2500 psi), the 10.6mm fiber optic cable collapsed and permitted water to pass under the O-rings. The 12.7 mm cable exhibited minor deformation and no water entered the closure.

The combination of accelerated heat aging of the closure sealing system and the sustained external hydrostatic pressure of 35 kgf/cm^2 (500 psi) for 30 days at a low temperature demonstrates a highly reliable sealing system. The failure pressure at 175 kgf/cm^2 (2500 psi) is equivalent to a 1677 meters (5500 feet) water depth indicating a substantial design margin by a factor of five for service to 300 meters.

Testing has not been conducted at this time concerning the effects of this increased pressure on the loss performance of index matching gels. Thus only fusion splicing is recommended when water depths exceed 100 meters.

Field Installation Experience

The submarine fiber optic splice closure has been used in two underwater cable projects. The first occasion was an engineering placement that required more cable than could be manufactured in one length. The second occasion was a "repair" of a planned cable installation. Both situations were located in intermediate depth water.

Long Island Sound Project

The AT&T Long Island Sound Project crossing used the submarine closure to join two pieces of 16.75 km (55,000 feet) of single wire armored fiber optic cable. The route was between Long Island and Connecticut. The cable used in the wire armored cable was a standard terrestrial cable with a sheath construction that contained an inner armor made up of a copper-steel laminated layer and a 14 strand wire layer. The outside armor was constructed of layers of jute and a layer of stainless steel wire coated with high density polyethylene plastic.

The plowing method was selected for the placement of the armored cable in the bottom of Long Island Sound. The cable payout from the ship to the plow required that the cable be held in a drum at the manufacturing location for loading directly into a similar drum on the ship. The armor manufacturer placed the two lengths of the cable in a drum such that the two ends would be accessible outside the drum for splicing. Following splicing, the closure assembly was completed. The assembly of the complete closure combination, submarine closure and C-Submarine Sled, should be considered a two-person operation. The total assembly time, including the fusion splicing, took 20 hours. The assembly time for the closure was well within the 12 hours requirement. After the cable and splice were tested, the complete cable and

splice assembly was loaded onto the vessel for transport to Long Island Sound. The average depth of Long Island Sound is in the range of 27 to 30 meters. The cable was plowed into the Sound up to the location where the closure would enter the water. The closure was supported by a rope as it went into the water even though the tensile strength of the cable was sufficient to hold the 200 kg of the closure and the weight of the suspended cable. A diver was used during the placing of the closure because the chute in the plow was not large enough to pass the complete closure. When the closure reached the plow, the plow was opened, the cable was removed from the plow, the closure placed on the bottom, the cable reinserted into the plow, and the plow was closed. Slack cable was placed at the site so that when the closure was "jetted" into the bottom of the Sound, the cable would not exert tension on the closure.

After the closure was placed and the plowing resumed, the cable was tested to confirm the successful placement of the closure. All fibers tested good.

Santee River Project, South Carolina

The Southern Bell Santee River installation was a repair of an originally engineered wire armored fiber optic cable installation. Before the installation started, however, it was determined that the Santee River had been dredged and the width of the river at the point of placement was now wider than was first anticipated. The armored cable was in position to be placed, but, was now too short for the span. A second cable was ordered and brought to the site for splicing and placing. The splicing was performed at a work-center prior to loading the reel on the placing barge. The two cables were spliced and the completed submarine splice closure was secured to the existing reel with the original cable and the new cable.

The placement of the cable on the bottom of the Santee River involved two steps. The first step was to place the entire length of the cable and then secondly, "jet" the cable into the bottom of the river. The "jetting" process was performed by a diver removing the soil from beneath the cable and closure and allowing the cable and closure to settle into the trench created. The sediment will return to the bottom and cover the cable and closure. The placement was successful again with the lowering of the closure to the floor of the river being partially controlled with a rope.

Future Directions

What began as a repair closure, is now being used for initial installations. As the need for cable right-of-way has risen, the requirements placed on companies asking for the rights-of-way have been changed by the granting authorities. These changes involve the cost, depth-of-plant, position-of-plant, maintenance responsibilities, as well as restrictions on future growth. Therefore, land placement has become increasingly difficult. This leaves communication companies looking for new avenues in obtaining a location for their cable. We now believe splices and thus closures will be designed into future water crossing routes with increasing frequency. The trend will also be to position the splices at ever increasing water depths and as this occurs there will eventually be a need to use the closure on non-armored cable.



Gary S. Cobb is a Distinguished Member of Technical Staff in the Fiber Optic Apparatus Development Department at AT&T Bell Laboratories. Mr. Cobb joined Bell Laboratories in 1963 where he worked in the Ocean Cable and Underwater Sound area for 13 years. For the past 10 years, Mr. Cobb has been

active in the design and development of copper and fiber optic splice closures. Mr. Cobb received his BSME degree from Virginia Polytechnic Institute and State University and a MSME degree from the University of Maryland.



William H. Bensel is a member of the Fiber Optic Apparatus Development Department at AT&T Bell Laboratories in Norcross, Georgia. He joined Bell Laboratories in 1969 after receiving an Associate Degree in Electrical Engineering from Baltimore Junior College. Since 1980, he has been engaged in the development,

testing, and evaluation of fiber optic closure sealing systems.



Phillip M. Thomas is a Member of Technical Staff in the Fiber Optic Cable Design Group at AT&T Bell Laboratories, Norcross, Georgia. He joined AT&T in 1982 after receiving his BMET degree from Southern Technical Institute. He received his BSME degree from the Georgia Institute of Technology and is currently

pursuing a Master's degree. Mr. Thomas is presently involved in the design and development of fiber optic cable for outside plant applications. His past responsibilities included the design and development of fiber optic cable interconnection apparatus, closures, and cable termination hardware.



Harry O. Lindstrom, Jr. is a Distinguished Member of the Technical Staff in the Project Engineering and International Operations Department. Mr. Lindstrom joined Bell Laboratories in 1957 where he worked for 14 years in the design and development of missile guidance systems. For the last 13 years, Mr. Lind-

strom has been active in the areas of Standards development for their installation and protection of fiber optic cable and apparatus, field testing and prove-in of fiber optic cable, consulting on the planning and installation of Outside Plant systems both international and domestic, and quality improvement procedures for cable products. Mr. Lindstrom received his BEE degree from Auburn University and a MSEE degree from Duke University.

MONITORING ACCELERATED AGING OF POLYESTER BUFFER TUBES IN FIBER OPTIC CABLES

Osman S. Gebizlioglu and Irene M. Plitz

Belcore
331 Newman Springs Rd.
Red Bank, New Jersey 07701

ABSTRACT

Poly (Butylene Terephthalate), PBT, the most commonly used buffer tube material, degrades in hot and moist media and becomes brittle. We showed that elongation-at-break, an ultimate tensile property, is very sensitive to tube degradation. For accurate measurement of elongation-at-break, we used a modified version of an ASTM test method, ASTM 348, *Standard Test Method for Rigid Tubes Used for Electrical Insulation*. Based on 10% elongation-at-break as an end-of-life criterion, we estimated a tube lifetime of ten years at 40°C / 60% RH for currently used PBT materials and twenty one years for a new generation of hydrolytically stabilized PBT's entering the telecommunications network.

INTRODUCTION

All three common optical cable designs use plastic tubes to protect optical fibers from the outside environment. In the loose tube design, six to twelve fibers are enclosed in a polyester buffer tube. Six to eighteen buffer tubes may then be arranged around a cable central strength member. In the ribbon and the fiber bundle designs, one or more concentric tubes (core tubes) contain the fiber ribbons and fiber bundles, respectively. For both buffer and core tubes, cable manufacturers commonly use polybutylene terephthalate (PBT) for its favorable processing and mechanical properties. This material, however, is very sensitive to humidity and degrades catastrophically in hot and humid media. The degradation reaction occurs when water molecules attack the ester linkages of the polymer. With recurrent water attack, the

polymer molecular weight drops and the tube fractures into small fragments. The degradation of buffer/core tubes destroys an important environmental barrier for the protection of optical fibers. In this report, we present a method to assess the degradation rate in the tensile mechanical properties of polyester buffer tubes. We use the kinetics of degradation of the mechanical properties to estimate the lifetime of polyester tubes in fiber optic telecommunications cables.

BUFFER TUBE ANALYSIS

Buffer/core tubes must remain robust throughout the entire service life of a fiber optic cable. They must withstand handling and installation stresses, and retain their ductility in the service environment. From a field performance standpoint, a mechanical property test is the most appropriate method of monitoring buffer/core tube degradation. The Belcore document TR-NWT-000020, *Generic Requirements for Optical Fiber and Optical Fiber Cable, Issue 5, December 1992*(1), uses elongation-at-yield to compare buffer/core tubes before and after 30-day aging at 85 °C / 85% RH (Relative Humidity) with a proposal to replace it with elongation-at-break. Hydrolytic degradation results in the reduction of PBT molecular weight. Elongation-at-yield does not correlate with this molecular breakdown(2). We propose that elongation-at-break be used instead of elongation-at-yield to monitor polyester molecular degradation. We could measure this ultimate tensile property by one of three ASTM standard test methods(3-5): 1) ASTM 638(3) is suitable for test bars of rectangular cross section. 2) ASTM 348(4) is applicable to rigid tube samples

having a gauge section of reduced diameter. 3) For rigid, reinforced tubes and pipes, ASTM 2105(5) is an alternative to ASTM 348. We chose ASTM 348 to evaluate the extent of degradation after accelerated aging of buffer tubes. This test method requires tubes with large aspect ratio (sample length-to-width or diameter ratio) to assure homogeneous deformation (uniform strain and stress throughout the test volume). Since 3-mm and 6-mm diameters are more common for loose buffer/core tubes, we adopted a minimum aspect ratio of 25. A key condition of this method is that each test specimen have a central gauge section of reduced wall thickness. The straight mid-portion of this section has one-fifth the specimen length and sixty percent of the nominal wall thickness. At each end of this section, a curved shoulder region joins the gauge section to the outside diameter, schematically shown in Figure 1a. The radius of curvature in the shoulder segment depends on the tube wall thickness(4). For a 1/4-mm thick tube wall, a radius of curvature of about 2 3/4 " (70 mm) gives a smooth transition region. We specified a strain rate (machine cross-head speed divided by gauge section length) of 0.4 min^{-1} ($6.7 \times 10^{-3} \text{ sec}^{-1}$). This rate is higher than the test speed specified in ASTM 348 to reduce the time of testing. However, the test rate should be low enough to produce a broad range of elongation-at-break values for comparing aged samples. Special tensile grip adapters, schematically shown in Figure 1b, are used to hold the tube samples by pneumatic grips.

Sample Aging Procedure

We varied aging temperature from 85°C to 100°C and fractional relative humidity from 0.7 to

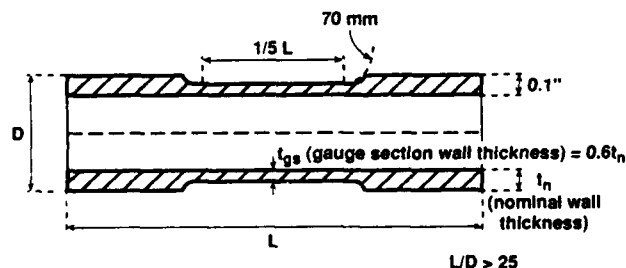


Figure 1a. Machined Tube Cross-Section

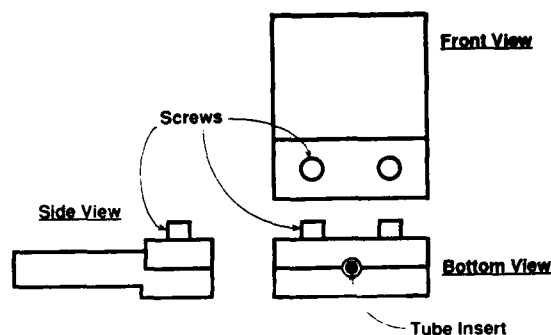
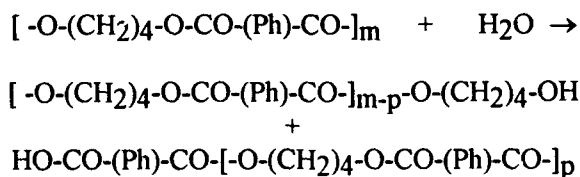


Figure 1b. Grip Adapter for Tube Samples

1.0. Buffer tube samples, either cut to their test length and machined before or after aging, were kept in the aging chamber for up to 90 days.

Buffer Tube Lifetime Estimation

Polyesters, in general, and PBT, in particular, are industrially important materials. Their lifetime, therefore, has attracted considerable attention(6-10). In a humid environment, these materials undergo hydrolysis as shown below for PBT



The subscripts m and p are integer numbers and are called the degree of polymerization. This expression indicates that PBT reacts with a molecule of water and splits into an alcohol (containing the OH group at its end) and an acid (containing -COOH group at the end). As long as water is available, the hydrolysis reaction continues to produce alcohols and acids of decreasing molecular weight.

The rate and conditions of this hydrolysis reaction were studied(6-10) earlier for predicting PBT lifetime. Gardner and Martin(6) used the following empirically developed relationship between half-life (days), temperature T(°K) and relative humidity (RH):

$$\ln t_{1/2} = \frac{A}{T} - B \ln(RH) - C$$

By curve-fitting PBT hydrolysis data to this expression, they estimated a 18-28 Kcal mole⁻¹ activation energy of hydrolysis.

Kelleher, Wentz and Falcone⁽⁷⁾ developed an empirical expression for PBT lifetime, *t* (hours), based on melt flow index (MFR).

$$kt = a (MFR_t^{3.6} - MFR_0^{3.6})$$

This relationship gave an activation energy of 25 Kcal mole⁻¹.

Borman⁽⁸⁾ based his analysis on the reaction kinetics of the PBT hydrolysis and related half-life, *t*_{1/2}, to temperature, *T*(°K), and water vapor partial pressure, *P*_{wv} (mm Hg) as shown in the following equation.

$$\log t_{1/2} = A + \frac{B}{T} - C \log P_{H_2O}$$

This expression, when fitted to hydrolysis data on a broad set of PBT materials, gave an activation energy of 18-20 Kcal mole⁻¹.

Kishore and Sankaralingam⁽⁹⁾ generalized all earlier PBT lifetime prediction attempts in the following equation:

$$\frac{1}{t} = (1 - \alpha) A \exp\left(-\frac{E}{RT}\right) \ln \frac{H_R}{B}$$

In this expression, *E*, *R* and *H_R* refer to the activation energy, universal gas constant and relative humidity, respectively. By curve-fitting this equation to PBT hydrolysis data from the published literature, they obtained an activation energy of 24-29 Kcal mole⁻¹. Finally, Parris⁽¹⁰⁾ used PBT hydrolysis data obtained from buffer tube aging experiments in 60-100°C liquid water to predict PBT lifetime. Since all of these attempts involved PBT materials of different molecular weights and each made specific assumptions such as temperature-independent Henry's law constant⁽⁸⁾, they are not easily applicable to a generalized analysis of PBT lifetime. Moreover, the reported activation energies fall in too broad a range to be useful for PBT lifetime prediction. In the next section, we present a general model of PBT

hydrolysis and use it for PBT lifetime prediction in a typical telecommunications service environment.

For the hydrolysis reaction (a bi-molecular, non-elementary reaction) shown above, we write the following rate expression for PBT depletion:

$$-\frac{d[PBT]}{dt} = k [PBT][H_2O]^n \quad (1)$$

where [PBT], *k*, and [H₂O] refer to PBT concentration at time *t*, reaction rate constant, and water concentration, respectively. The exponent *n* denotes the order of the hydrolysis reaction with respect to water. To determine the amount of PBT left at time *t*, we rearrange this expression as follows:

$$-\frac{d[PBT]}{[PBT]} = k [H_2O]^n dt \quad (2)$$

Integrating over time *t* from 0 to *t_L*(lifetime), we obtain the expression below for *t_L*

$$-\ln \frac{[PBT]_t}{[PBT]_0} = k [H_2O]^n t_L \quad (3)$$

Similarly to Borman's analysis⁽⁸⁾, we use Henry's law⁽¹¹⁾ to replace water vapor concentration, [H₂O], with partial pressure, *P*_{wv}

$$[H_2O] = \frac{P_{wv}}{K} \quad (4)$$

K, Henry's law constant, depends on both pressure and temperature. From the definition of relative humidity, *H_R*,

$$H_R = \frac{P_{wv}}{P^*} \quad (5)$$

where *P*^{*} is the equilibrium vapor pressure of water at temperature *T*. Both Henry's law constant *K* and *P*^{*} are temperature-dependent⁽¹²⁾.

$$\ln K = -\frac{\Delta H}{RT} \quad (6)$$

$$P^* = \exp\left[-\frac{A}{T} + B\right] \quad (7)$$

The constants $A = 5.207 \times 10^3$ and $B = 13.995$ in Eq. 7 were determined by linear regression analysis of P^* (in atmospheres)- T data⁽¹²⁾ for the temperature range from 273°K to 373°K. A third constant for which temperature dependence has to be accounted for is k , the hydrolysis reaction rate constant.

$$k = k_0 \exp\left(-\frac{\Delta E}{RT}\right) \quad (8)$$

Substituting for K , P^* , and k from Equations 6, 7 and 8, respectively, into Eq. 3, we arrive at the following expression for PBT lifetime:

$$\ln t_L = C - 13.995 \times n - n \times \ln H_R + \left[5.207 \times 10^3 n - \frac{(\Delta H \times n - \Delta E)}{R} \right] \frac{1}{T} \quad (9)$$

In this equation, t_L is in hours and T is in °K. In the following section, we evaluate four constants C , n , ΔH , and ΔE by multiple regression analysis of Eq. 9 with t_L - T - H_R data.

RESULTS and DISCUSSION

Figure 2 shows a tensile stress-strain curve of a PBT buffer tube of 2.6 mm (0.1") nominal outer diameter. In this figure, engineering stress

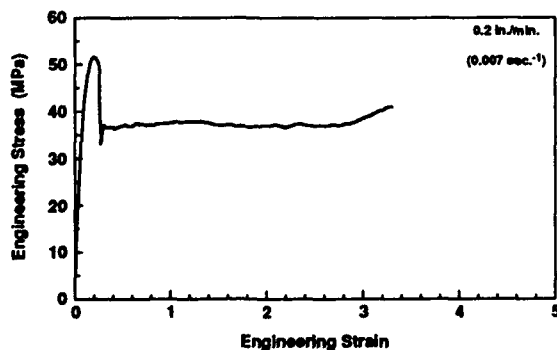


Figure 2. Unaged PBT Buffer Tube in Tension

(load divided by the original sample cross-sectional area in the gauge section) is plotted against engineering strain (change in length divided by initial gauge length). Neither engineering stress nor engineering strain in the elastic deformation region (the initial part of the stress-strain curve where stress is linearly proportional to strain) are corrected for the specimen effective gauge length. Since the actual gauge length is always shorter than the effective gauge length, corrected proportional limit (the end of the elastic deformation region) is smaller than the proportional limit shown in the figure. Thus, the total strain (proportional limit plus plastic strain) shown in the plot is an overestimate of the corrected total strain. The maximum stress, about 52 MPa (MegaPascals) or 7542 psi (lbs in.⁻²) in this figure happens to be the yield stress. Following the yield point, stress drops to a plateau stress also known as drawing stress or flow stress. The flow stress is followed by a narrow region where stress rises with strain (strain-hardening region). This region is terminated when the test sample breaks. The breaking stress for all PBT buffer tubes tested was lower than their yield stress. The tensile stress-strain plot of Figure 2 shows a total strain of about 3.5 or elongation-at-break of 350 percent. This value of elongation-at-break compares well with the elongation-at-break (350-450 percent) of PBT tensile bars tested in accordance with ASTM 638.⁽¹³⁾

Figures 3 and 4 present mean stresses and strains for a set of five PBT buffer tubes aged at 85 °C / 85% RH (Relative Humidity). In Figures 3a and 3b, mean yield stress and mean yield strain exhibit small changes with aging time, respectively. In Figures 4a and 4b, mean breaking stress and breaking strain are plotted against aging time, respectively. The mean breaking stress shows no

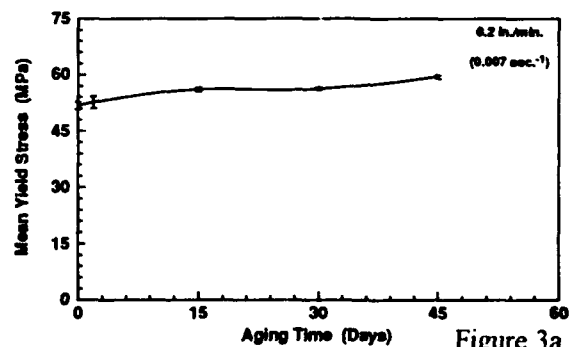


Figure 3a

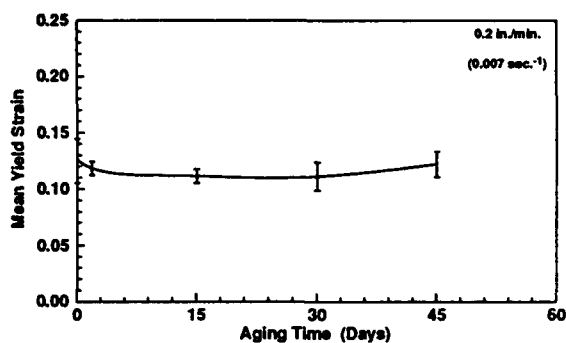


Figure 3b.

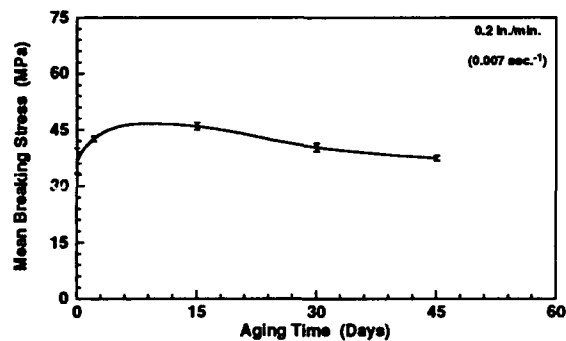


Figure 4a.

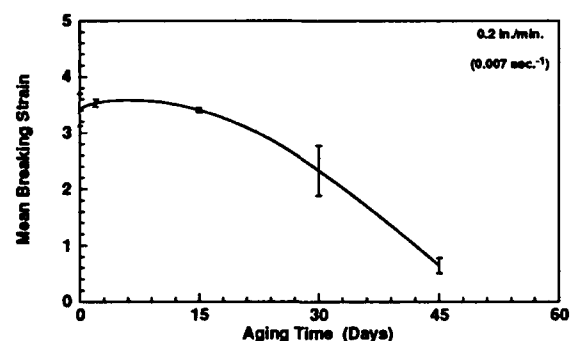


Figure 4b.

significant change in 45-day aging. The mean breaking strain or elongation-at-break, however, exhibits a dramatic drop, after a small initial rise, with aging time. Beyond two-day aging, breaking strain drops from about 3.5 strain units to 0.1 in 48 days. Since a breaking strain of 0.1 (10% elongation-at-break) is comparable to the yield strain shown in Figure 3b, we conclude that the PBT tube samples tested lost their ductility in about 48 days at 85°C / 85% RH aging. For satisfactory field handling and installation performance, buffer tubes must retain some ductility after accelerated aging. Therefore, breaking strain of aged buffer tubes must remain larger than their yield strain. We propose that a breaking strain of 0.1 units, or

10% elongation-at-break, serve as an end-of-life criterion. The plot of Figure 4b shows a mean breaking strain of 2.4 for 30-day aging at 85°C / 85% RH. Taking into account the standard error bar shown in this plot for 30-day aging, we propose that a mean breaking strain lower than 1.2 (120 % elongation-at-break) be considered unacceptable in screening buffer/core tube materials for hydrolytic stability. For 45-day aging, the mean breaking strain drops to about 0.64 (64 % elongation-at-break). In this case, we similarly propose that a mean breaking strain greater than 0.3 (30 % elongation-at-break) be considered acceptable. Thus, the 45-day aging treatment allows us to formulate a less restrictive requirement for including other potentially useful buffer/core tube materials that exhibit lower initial breaking strain than PBT materials tested in this investigation.

Lifetime Estimates

Having developed a method to monitor polyester buffer tube degradation and established an end-of-life criterion of 10% elongation-at-break, we can now estimate tube lifetime by using Eq.9 with the PBT buffer tube aging data. The buffer tube lifetime t_L refers to aging time for which elongation-at-break is about 10%. Tables I and II present t_L -T-HR data for two different sets of PBT buffer tubes.

Table I

Aging Data for PBT Buffer Tube Set I

Temp. (°C)	HR	Time, Days
70	1.0	78
85	1.0	20
100	1.0	5
85	0.7	30
85	0.85	23
85	1.0	20

Table II

Aging Data for PBT Buffer Tube Set II

Temp. (°C)	HR	Time, Days
70	1.0	162
85	1.0	40
100	1.0	11
85	0.7	62
85	0.85	48
85	1.0	40

In Table III, we present a summary of the results of multiple regression analysis of aging data shown in Tables I and II with the expression for buffer tube lifetime t_L given in Eq. 9.

Table III

Set	C	n	ΔH Kcal/gm-mole	ΔE Kcal/gm-mole
I	-10.65	1.14	10.0	22.87
II	-7.94	1.23	10.0	22.37

In this table, n is the order of the hydrolysis reaction with respect to water concentration. The two n values shown suggest that the hydrolysis reaction is first order with respect to water. ΔH accounts for the temperature dependence of K , Henry's law constant. This term is an input⁽¹¹⁾ to the regression analysis. The activation energy of hydrolysis, ΔE , falls in the same range as those of earlier investigations⁽⁵⁻⁹⁾.

By using the parameters of Table III, we computed lifetimes over the temperature range from 25°C to 50°C and relative humidity range from 0.1 to 0.6. Figures 5a and 5b present these results in a 3-D plot of lifetime, t_L , against temperature, T , and fractional relative humidity, H_R . From Figure 5a, one reads a lifetime of about 10.3 years at 40°C and 60% relative humidity ($H_R = 0.6$). For the same conditions, Figure 5b gives a lifetime of 20.5 years for hydrolytically stabilized PBT buffer tube materials. Our lifetime estimates should be considered as underestimates since temperatures shown in these figures are below the glass transition temperature, ($T_g = 55-65^\circ\text{C}$) of PBT.

SUMMARY and CONCLUSIONS

The polyester buffer tubes degrade in warm and moist media, and become brittle. We showed that elongation-at-break, an ultimate tensile property, correlated with the tube degradation. For elongation-at-break measurements, we used a modified version of ASTM 348, *Standard Test Method for Rigid Tubes Used for Electrical Insulation*. The modified test procedure required tube specimens with a gauge section of reduced

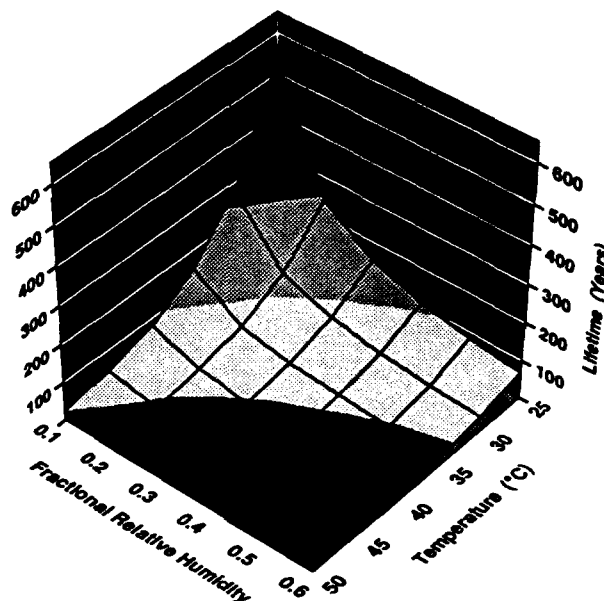


Figure 5a. PBT Buffer Tube Estimated Lifetime

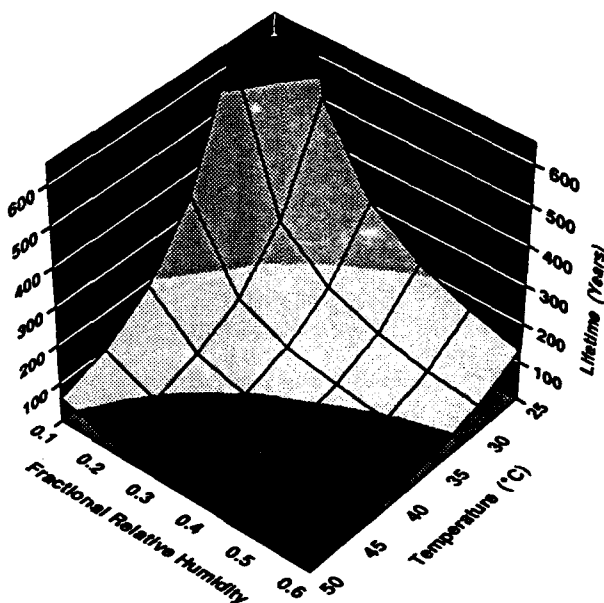


Figure 5b. Hydrolytically Stabilized PBT Lifetime

thickness. From our aging experiments, we defined 10% elongation-at-break as the end-of-useful life of PBT buffer tubes since, at this elongation, they would have lost all their ductility. Based on this definition of end-of-life, we estimated a tube lifetime of ten and a half years at 40°C / 60% RH for PBT buffer tubes currently used in the telecommunications network and about twenty one years for a new generation of hydrolytically stabilized polyester buffer tube materials.

ACKNOWLEDGMENTS

We gratefully acknowledge the invaluable contributions of G.P. Apgar and E.J. Mason of Bellcore in developing tube machining procedures.

REFERENCES

1. Bellcore, Technical Reference, TR-NWT-000020, Generic Requirements for Optical Fiber and Optical Fiber Cable, Issue 5, December 1992.
2. Z. Bin Ahmad and M.F. Ashby, J. Materials Science, 23, 2037-2050 (1988).
3. ASTM 638, Standard Test Method for Tensile Properties of Plastics
Annual Book of ASTM Standards, Vol. 8.01 (1991).
4. ASTM 348, Standard Test Method for Rigid Tubes Used for Electrical Insulation
Annual Book of ASTM Standards, Vol. 10.01, p 84 (1990).
5. ASTM 2105, Standard Test Method for Longitudinal Tensile Props. of Reinforced Resin Pipe / Tube
Annual Book of ASTM Standards, Vol. 8.02, p 85 (1990).
6. R.J. Gardner and J.R. Martin, SPE ANTEC Tech. Papers, 24, 329 (1978) and 25, 831 (1979).
7. P.G. Kelleher, R.P. Wentz and D.R. Falcone, Polymer Eng. & Sci., 22(4), 260 (1982).
8. W.F.H. Borman, Polymer Eng. & Sci., 22(14), 883 (1982).
9. K. Kishore and S. Sankaralingam, Polymer Eng. & Sci., 24(13), 1043 (1984).
10. D.R. Parris, Proc. 38th Int. Wire & Cable Symp., 105 (1989).
11. K. Denbigh, The Principles of Chemical Equilibrium,

Cambridge Univ. Press, Cambridge, 225 (1971).

12. R.H. Perry and C.H. Chilton, Chemical Engineers' Handbook, 5th Ed., McGraw-Hill, New York, p 4-55 (1973).

13. ASM Engineered Materials Reference Book, ASM International, Metals Park, Ohio, p 309 (1989).



Osman S. Gebizlioglu is a Member of the Technical Staff in the Plastics and Rubber Research Group at Bellcore. He holds B.Sc and M.Sc degrees in Chemical Engineering from the Middle East Technical University, Ankara, Turkey. After receiving his Ph.D from Princeton University, Princeton, New Jersey, he did postdoctoral research as a Monsanto Fellow at MIT, Cambridge, Massachusetts. Since he joined Bellcore in 1987, he has conducted research on the mechanical reliability of polymeric materials in fiber optic cables, optical devices and connectors.



Irene M. Plitz is a Member of the Technical Staff in the Plastics and Rubber Research Group at Bellcore. She received her BS in Chemistry from Morgan State University and joined Bell Telephone Laboratories. Since her transfer to Bellcore in 1983, her interests have centered around the degradation, characterization and reliability of polymeric materials used in the telecommunications industry.

STEEL TUBE ARMoured FIBER OPTIC CABLE DESIGN

Dieter Lachmann, Thomas Rödder

NOKIA KABEL GmbH

Piccoloministr. 2

51063 Köln

Federal Republic of Germany

1. Abstract

A new design has been developed for fiber-optic cables. It is economical in production and offers excellent performance. Compared with the plastic loose tubes and moisture barrier sheaths, used normally in cable construction, this new "Steel Tube Armoured Fiber Optic Cable" is extremely compact. It accommodates up to 16 fibers with a diameter of 8.5 mm and weighs 90 kg/km.

By using multiple-function cable elements, the new design allows the packing density to be more than doubled. It also halves the number of different materials used in cable construction and yet gives the same performance as conventionally designed cables.

Tests were conducted to compare the optical, thermal and mechanical characteristics of plastic and steel tube designs. The new cable design produced excellent results, enhanced by the use of longitudinally applied strength members. Aging tests have also been carried out. Standard tools, splice cassettes and cable closures were used to demonstrate the ease and efficiency with which the new cable design can be installed.

2. Introduction

Cables are conventionally designed with a central core tube. They consist i.e. /1/ of a plastic tube enclosed in a swelling tape and an additional moisture barrier sheath. Two unstranded steel tension members are embedded in the cable sheath. Corrugated steel tape is used to ensure a long life span and adequate mechanical behaviour. Our new cable design is based upon a stainless and laser-welded steel tube which is hermetically closed. This makes it possible to eliminate the corrugated steel tape in the cable sheath.

Optical fiber aerial cables using stainless steel tubes have shown excellent resistance against extreme environmental conditions, such as water permeation, mechanical and thermal stresses /2/. With our new design these advantages can also be utilized for buried, duct and indoor applications.

The "Steel Tube Armoured Fiber Optic Cable" design based upon the hermetically sealed, laser-welded central steel tube, contains up to 16 optical fibers. The steel tube is embedded in the cable sheath together with a diametral pair of unstranded steel strength members. Fig. 1 shows the new cable design.

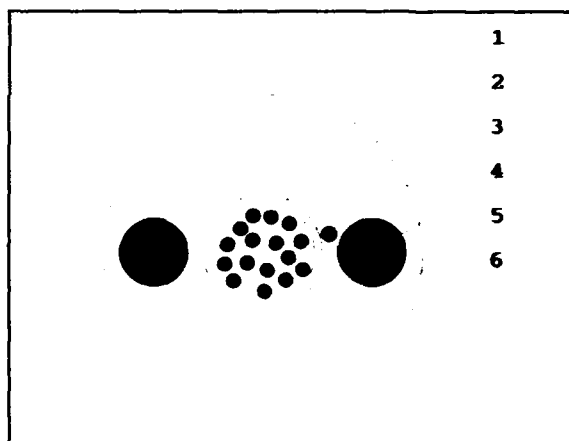


Fig. 1 : Steel Tube Armoured Fiber Optic Cable

- 1: optical fibers
- 2: filling compound
- 3: stainless steel tube
- 4: identification yarn
- 5: pair of steel strength members
- 6: cable sheath

3. Techno/economical objectives

In the past, most development work on fiber optic cable designs has focused on increasingly economical cable structures. The cables have been down-sized, the number of cable materials has been reduced and expensive materials avoided. Because of large quantities of cable required for trunk and overlay networks, development activities tended to concentrate on high and medium fiber count cables.

The emphasis now is switching to low fibre count cables for fiber to the curb (FTTC) or fiber to the home (FTTH) applications. Combining adequate cable performance with a low fiber count in an optimized economic cable design has proved impossible up to now.

If the fiber number exceeds 16, it is useful to have a stranded loose tube design. This design allows clear fiber identification together with suitable and safe handling of the fiber bundles during splicing and laying into closures.

For a lower fiber count, the fibers need not be split off into different bundles. Using a suitable fiber colour code, it is possible to identify up to 16 optical fibers within one central loose tube. Compared with the stranded loose tube design, packing density i.e. number of fibers per cross section increases significantly.

In our new "Steel Tube Armoured Fiber Optic Cable" we have dramatically increased packing density.

Table 1 shows diameter, weight and packing density of three different 12-fiber cable designs for direct buried resp. aerial applications:

Table 1

design	application	OD mm	weight kg / km	fibers mm ²
stranded loose tube	buried / 3 /	14.0	160	0.08
central plastic tube	buried / 1 /	12.4	156	0.10
	aerial / 4 /	10.0	90	0.15
steel tube armoured	buried/ aerial	8.5	90	0.21

To guarantee the functioning of the optical fibers, standard outdoor cables are designed to resist different external influences during and after installation, like :

- longitudinal pulling
- radial compression
- bending, kinking and torsion
- contraction and elongation by temperature
- water penetration and water permeation
- rodent attacks

A few years ago, optical fiber cables were designed with a single function for every cable element i.e. a cable sheath consisted of an aluminium tape against water permeation and additional armouring against rodent attacks or for higher mechanical strength. Nowadays multiple function materials are available, e.g. a corrugated steel tape combines three functions:

- it increases mechanical strength
- prevents water permeation
- protects against rodents

Our new cable design achieves similar effects. The combination of steel tube and steel strength members within the cable sheath eliminates the need for steel tape, melting glue and rovings. Furthermore a separate core wrapping is no longer necessary, because the adhesion between the steel tube and the sheath material leads to mechanical and watertight coupling. A useful additional advantage is the cut-resistance of the tube itself. Adding the number of all different cable elements of the three mentioned designs together shows how the use of materials can be reduced.

Table 2 Consumption of different cable elements

type of material	cable type:		
	stranded tube	central tube	steel tube
coloured fibers	x	x	x
filling compound	x	x	x
loose tubes	x	x	x
central strength member	x		
core filling	x		
core wrapping	x	x	
binding yarns	x		
identification and measuring material	x	x	x
rovings	x		
layer of melting glue	x		
steel tape	x	x	
sheath material	x	x	x
unstranded strength members		x	x
Total	12	8	6

Additionally the cost-intensive stranding process is avoided.

4. Comparative cable testing

A detailed testing program has been carried out to compare the performance of the new "Steel Tube Armoured Fiber Optic Cable" with the above-mentioned standard outdoor cables.

The test conditions comply with those generally considered for direct buried or duct installations.

4.1 Crush test acc. to IEC 794-1-E3

For all three cable designs, negligible mechanical damage occurred up to a load of 5000 N per 100 mm. Attenuation changes are measurable at :

- ≥ 6 kN for stranded loose tube
- ≥ 7 kN for central plastic tube
- ≥ 10 kN for steel tube design

4.2 Impact test acc. to IEC 794-1-E4

All three cable designs withstand an impact energy of 50 Nm with a hammer radius of 300 mm without any attenuation change. The maximum impact energies, at which tolerable mechanical damage occurs, are identical for the different cable designs :

stranded loose tube	20 Nm
central plastic tube	20 Nm
steel tube design	20 Nm

4.3 Repeated bend acc. to IEC 794-1-E6

During the repeated bend test, the cable was bent 30 cycles around a radius of ten times the cable diameter with a load of 10 kg. No attenuation changes occurred and no mechanical damage was observed. The new cable design is competitive with standard cable designs.

4.4 Torsion acc. to IEC 794-1-E7

All three cable designs have been torsioned with 30 cycles ± 180 degrees per meter and a load of 10 kg. No attenuation changes and no mechanical damage occurred.

4.5 Kink test acc. to IEC 794-1-E10

No kinking occurs on any of the three cable designs at a radius of five times the cable diameter. No attenuation changes and no mechanical damage occurred.

5. Cable testing

5.1 Tensile test acc. to IEC 794-1-E1

Fig. 2 shows the relationship between the tensile load, cable elongation and optical fiber elongation for the new cable design.

It can be seen that, up to 2kN, fiber elongation is negligible. At maximum pulling force of 3kN, the fiber elongation does not exceed 0.1%.

Tensile tests on several cables of the same type showed elastic and complete reversible cable behaviour.

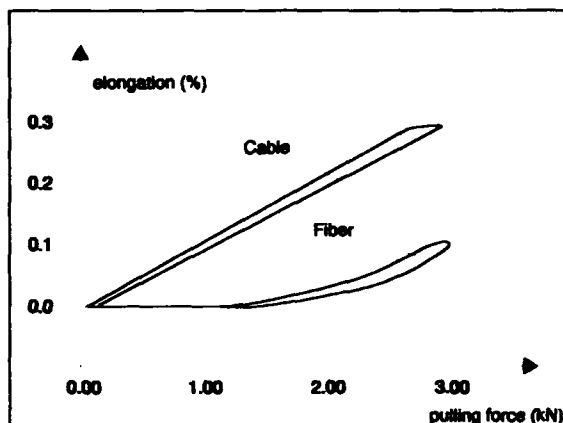


Fig. 2 : Tensile performance

5.2 Temperature cycling acc. IEC 794-1-F1

The steel elements in the new cable construction give the cable a thermal expansion coefficient almost equivalent to that of steel ($10 \cdot 10^{-6}/K$). This is the reason for its excellent attenuation behaviour during temperature cycling. For a 12-fiber steel tube armoured cable, the following test results at 1550 nm are measurable :

- 20 °C to +60 deg. Celsius : ± 0.05 dB/km
- 40 °C to +80 deg. Celsius : ± 0.1 dB/km

All measured attenuation variations were fully reversible.

5.3 Water penetration acc.to IEC 794-1-F5

1m and 3m-samples showed no water penetration after 72 hours.

5.4 Flexing acc. to IEC 794-1-E8

During the flexing test the cable was bent 30 cycles around a radius of ten times the cable diameter with a load of 10 kg. No attenuation changes occurred and no mechanical damage could be observed.

The unstranded strength members had no negative influence on flexing the cable.

5.5 Bending under tension

During the "bending under tension test", the cable is pulled through a 180 degree curvature with a maximum pulling force of 3000 N. No attenuation changes occurred and no mechanical damage could be observed.

5.6 Pulling the cable with socking

The new cable type was pulled to a maximum force of 3000 N for several times with a dwell time of 5 minutes. For coupling the pulling force into the cable, a standard socking without any preparation of the cable ends was used. The excellent friction between the sheath material and the steel elements shows that relative movement between the different cable elements is negligible.

5.7 Electrical resistance in a waterbath

The new cable design withstands a voltage of 20kV/DC for 2 minutes between the contacted steel elements and a surrounding waterbath. The isolation resistance exceeds 50 GOHM at 500V/DC.

5.8 Aging test acc. to Bellcore TR-NWT-000020

This aging test was carried out to investigate the influence of any hydrogen generation of the new cable design on fiber attenuation. The cable was exposed to $85^{\circ}\text{C} \pm 2^{\circ}\text{C}$ temperature for 120 hours after completion of a temperature cycling test. The hermetically welded steel tube showed excellent results and no attenuation changes occurred at the wavelengths 1240 nm, 1300 nm and 1550 nm.

5.9 Drip test acc. to Bellcore TR-NWT-000020

Cable samples were exposed to a temperature of 80°C for 24 hours. No filling compound dripped out of the steel tube armoured fiber optic cable.

6. Splices and closures

Although cables may be constructed with different designs to produce excellent results in all mechanical tests, it is not easy to combine good design with good handling. The main objectives for handling performance are :

- simple and safe installation
- low cost of materials and equipment
- safe handling of fibers
- no duplication

The "Steel Tube Armoured Fiber Optic Cable" design offers additional handling advantages during cable jointing. The worst case for removing the cable sheath will be the use of a simple and low-cost knife. To prevent the central tube resp. fiber from injury by using a knife, cable design should be resistant enough but easy to peel. In this respect, the steel armoured cable shows excellent cut-through resistance. The hot-melt adhesive-free design allows easy removal of the cable sheath. Sheath designs using rip-cords were also successfully tested.

Although it is possible to cut the steel tube by using a file, a special tool shown in figure 3 was designed for this purpose.

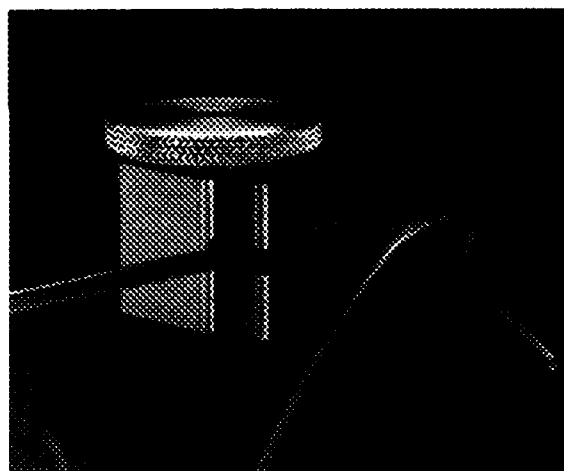


Fig. 3: Cutting tool for removing the steel tube from the fibers

During the investigations on jointing of the new cable design, standard closures and splice cassettes have been used. In the closures, the cables have to be clamped and their metallic elements have to have electrical contact if necessary.

Dielectric insulation of all metallic elements is possible together with heat shrinkable tubing.

With the given adhesion of all cable elements, the steel tube armoured cable ends are safe and easy to fix. In this configuration the pulling force can reach more than 1000N. The reserve fiber loops from cable to cassette are protected in a soft loose buffer tube.

Fig. 4 shows a complete installed cable closure sample.

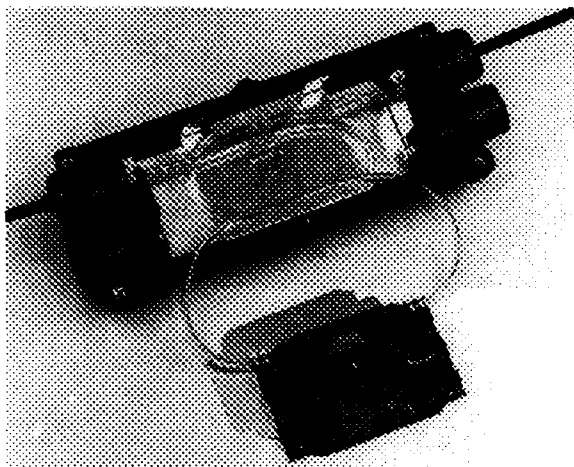


Fig. 4 : Closure for the new cable design

7. Conclusion

A new steel tube fiber optic cable, 8.5 mm in diameter and weighing 90 kg/km, has been designed and tested for up to 16 fibers. Using multiple-function cable elements, the cable consists of a laser-welded central steel tube and a pair of unstranded steel strength members embedded in the cable sheath. Although the number of materials is reduced drastically, the inherent strength of the new design leads to excellent performance in respect of mechanical behaviour and handling.

Several customers have chosen the new cable to acquire practical experience with it in the field. Although intended primarily for duct and buried applications, the cable is also suited for aerial and indoor applications. Further developments will focus on design modifications up to 24 fibers.

References

- /1/ P.D. Patel and M.R. Reynolds, "LXE - a fiber-optic cable sheath family with enhanced fiber access", IWCS, 1988, pp. 72-78.
- /2/ R. Herff, N. Wenzel and G. Znoyck, "LWL-Luftkabel für Energiefreileitungen", etz Bd.112 (1991) H.10, pp.482-488.

/3/ D. Lawrence and P. Bark, "Recent developments in mini-unit cable", IWCS, 1983, pp. 301-305.

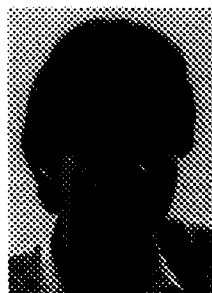
/4/ P.D. Patel and A.J. Panuska, "Lightweight fiber optic cable", IWCS, 1991, pp. 158-165.

Authors' biographies



Dieter Lachmann
NOKIA KABEL GmbH
Dept. NLE2
Piccoloministr. 2
51063 Köln

Dieter Lachmann was born in 1961. He obtained a degree in electrical engineering from the Fachhochschule Köln-Deutz in 1987 on pyrometric fiber optic sensing. In the same year he joined Philips Kommunikations Industrie AG. He specializes in fiber optic cable design.



Thomas Rödder
NOKIA KABEL GmbH
Dept. NVA3
Piccoloministr. 2
51063 Köln

Thomas Rödder was born in 1961. He obtained a degree in electrical engineering from the Gesamthochschule Siegen in 1985 on switched capacitive filter technique. In the same year he joined Philips Kommunikations Industrie AG. He was employed initially on the development of fiber optic cables. He was appointed Product Manager Fiber Optic Cables in 1990. He is now in charge of exports.

(*: since Aug.1st 1993 NOKIA KABEL GmbH)

A Study on Reverse Lay Stranding Loose Tube Cable Containing Ribbon Fibers.

Masayoshi Yamanaka, Naoki Okada
Hiroyuki Sawano, Matsuhiro Miyamoto

FUJIKURA Ltd.
Sakura-shi, Chiba-ken, 285 Japan

ABSTRACT

In order to construct Fiber-to-the-Home (FTTH) lines in the future, it will be necessary to use high-count optical fiber cables. In this study, we attempted to attain shorter fusion splicing time and easier of mid-span access by using a reverse-stranded structure. This is a structure in which loose tubes with encased ribbons are reverse stranded at fixed intervals. The optimum structure of this cable was investigated theoretically to obtain good transmission characteristics. We found that the fiber strain analysis was very important for the reverse-stranded structure, especially when the cable is bent. Based on the analysis, a trial cable was manufactured and tested. By the test results, it is verified that the trial cable shows good performance of mechanical and environmental condition.

INTRODUCTION

In recent years, applications of optical fiber cables are expanding from trunk line to local loop in telecommunication networks. In local networks, cables which are accessible at any point along the cable where a user is located are desirable. Ease of mid-span access is considered to be a key of local cable in FTTH applications.

Another factor in FTTH applications is high-count cables in single-star fiber networks which enable any home user to have broad-band service.

We have developed 432-fiber loose ribbon cable with reverse lay stranding. In this cable, all buffer tubes containing ribbons can be easily taken out without pulling cable because tubes are stranded reversely. Each tube has six ribbons. Using 12-fiber ribbons, the total fiber count amounts to 432 fiber for the case of 6 tubes. The 12-fiber ribbon is adopted to increase fiber count and packing density and is in the form of 12 single fibers each with 250 μ m outer diameter, arranged side by side and cured with a UV resin^[1].

In this paper, loose ribbon cable with SZ stranding is analyzed to find the optimal stranding parameter for having minimum fiber strain due to cable bending. Trial cables were fabricated to confirm the performance of the cables under different of mechanical and environmental conditions.

CABLE STRUCTURE

Ribbon cable structures are divided into two categories. One is the slotted rod structure in which ribbons are stacked tightly. The other is the loose tube structure in which ribbons are stacked and twisted loosely in tubes.

We investigated the loose tube structure as shown in Fig.1. Six loose tubes which have six 12-fiber ribbons are used. The 12-fiber ribbon is suitable for high count and high density cable structure and the reduction of the splicing time.

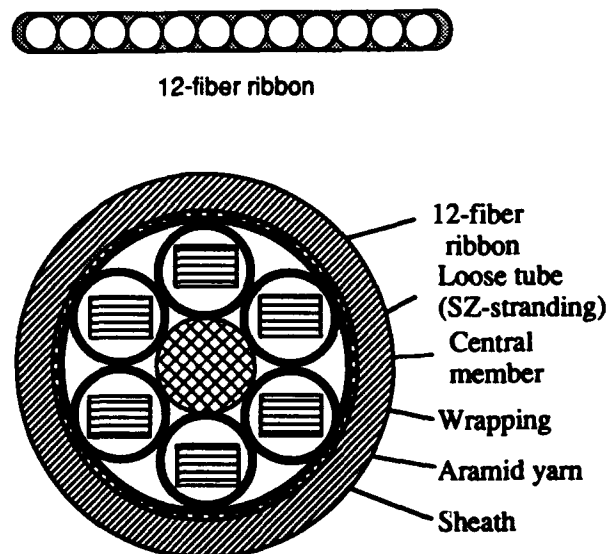


Fig. 1 Cross section of 12-fiber ribbon and the newly developed ribbon loose tube cable

The ribbon fibers are stacked and twisted and then inserted into a tube in one process. Ribbon twisting is needed to reduce the fiber strain due to tube bending or stranding. Each tube is filled with jelly compounds.

Six loose tubes are reversely stranded at fixed intervals around a central member in order to obtain easy mid span access. In mid-span branching using closures, a section of the cable sheath as long as the size of closure is removed. The tubes are easily taken out of the removed span because of its reversely stranded structure.

The interstice among tube units are filled with flooding compounds. The entire circumference of the tube units is wrapped with a tape and aramid yarn as a supplementary tension member.

THEORETICAL CABLE DESIGN

The reverse lay stranding loose tube cable is designed to achieve not only good transmission characteristics but also easy mid span access. The parameters to determine the cable structure are shown in Fig.2. In order to get the easy mid span access, the reverse lay length of the tubes is the most important parameter. Therefore, the twisting pitch of stacked ribbon fibers and the clearance in a tube will be the critical parameters for good transmission characteristics[1], because these factors influence the strain of the ribbon fibers, especially when the cable is bent or wound on a reel.

To mathematically deal with the investigation of these parameters, it is necessary to first define the coordinates for reverse lay stranding. Fig.2 shows

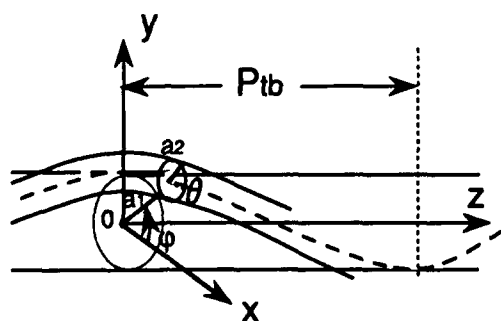


Fig.2 The coordinates for SZ-stranding
 a_1 : the circle radius of tube
 a_2 : the circle radius of twisting lamination ribbons
 θ : the twist angle of tube
 ϕ : the twisting angle of lamination ribbons
 P_{tb} : the reverse lay length

the reverse lay stranding coordinates. The longitudinal direction of the cable is taken as the z-axis and the plane perpendicular to the longitudinal direction as x-y plane. In the figure, a_1 , ϕ and P_{tb} are the pitch circle radius, the stranding angle and the reverse lay length of the tubes. The values, a_2 , θ and P_{rb} are the pitch circle radius, the twisting angle, and the twisting pitch of the stacked ribbon fibers. The value, f , is the reverse angle. Using these parameters, a fiber coordinate (x,y,z) are given as equations (1)[3],[4],[5].

$$\begin{aligned} x &= a_2 \cos \theta + a_1 \cos \phi \\ y &= a_2 \sin \theta + a_1 \sin \phi \\ z &= \frac{P_{rb} \theta}{2\pi} \left\{ 1 + \left(\frac{\pi^2 a_1}{2P_{tb}} \right)^2 \right\}^{-1} \end{aligned} \quad (1)$$

We considered the state of the cable when bent with a bending radius, R , on the plane at an angle of α with x axis as shown in Fig.3. Then, fiber coordinates (x,y,z) are given in equation (2).

$$\begin{aligned} x &= a_2 \cos \theta + a_1 \cos \phi + A \cos \alpha \\ y &= a_2 \sin \theta + a_1 \sin \phi + A \sin \alpha \\ z &= \{ R - a_1 \cos(\alpha - \phi) - a_2 \cos(\alpha - \theta) \} \sin \xi \\ A &= R - \{ R - a_1 \cos(\alpha - \phi) - a_2 \cos(\alpha - \theta) \} \cos \xi \\ &\quad - a_1 \cos(\alpha - \phi) - a_2 \cos(\alpha - \theta) \end{aligned} \quad (2)$$

To derive an amount of fiber strain, we calculated the fiber length at each state. From linear integration of equation (1) and (2), the length of the ribbon in the straight L_s , and bent cable L_b , can be calculated by the equation (3).

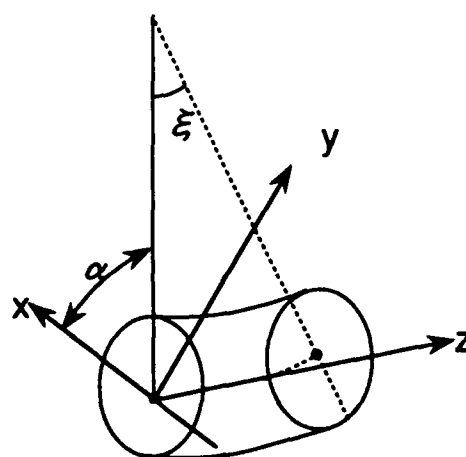


Fig.3 the state of the cable when bent on the plane at an angle of α with x axis

$$L = \int_0^{\theta} \sqrt{\left(\frac{dx}{d\theta}\right)^2 + \left(\frac{dy}{d\theta}\right)^2 + \left(\frac{dz}{d\theta}\right)^2} d\theta \quad (3)$$

The strain of the fibers along the cable when bent was caused by the length difference between fibers when the cable is straight and bent. Therefore, an amount of the strain of the fibers along the cable when bent is derived as the equation (4).

$$\delta(\%) = \frac{L_b - L_s}{L_s} \times 100 \quad (4)$$

The three important parameters mentioned above are determined as follows.

1) Reverse lay length of the tubes

In order to get the easy mid span access anywhere, the reverse lay length of the tubes is expected tube smaller than the size of closure. Considering the length of the closures, we determined that the reverse lay length was 350mm.

2) Twisting pitch of stacked ribbon fibers

The fiber strain when the cable is bent depends on the ratio of the twisting ribbon pitch (P_{rb}) to the reverse lay stranding tube pitch (P_{tb}), as shown in Fig.4. In this calculation, $P_{tb}=350\text{mm}$, $a_1=6\text{mm}$, and $a_2=0.75\text{mm}$ were used.

The strain of the fiber, δ , has a minimum value at $P_{rb}/P_{tb} = 0.6$, and a maximum value at $P_{rb}/P_{tb}=1$. The value of δ increases monotonously when P_{rb}/P_{tb} exceeds 2. Based on these results, P_{rb} was determined to 200mm.

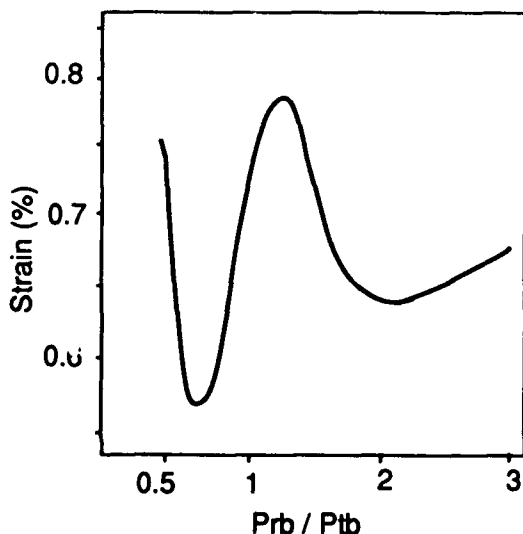


Fig.4 The dependence of the fiber strain on the ratio (P_{rb}/P_{tb}).

3) Clearance in a tube^[1]

From the results in Fig.4, the strain of the ribbon fiber is large. However, the actual strain will be reduced because of its loose structure. Therefore, the clearance in the tubes is a very important parameter, because the fiber moves radially towards the cable center to cancel the fiber strain. The ribbon fiber strain as a function of the clearance in tubes is calculated assuming that only pitch circle radius a_1 changes by the value of clearance to cancel the strain. The results of this calculation are shown in Fig.5. The clearance should be determined taking into account the transmission characteristics and longterm reliability.

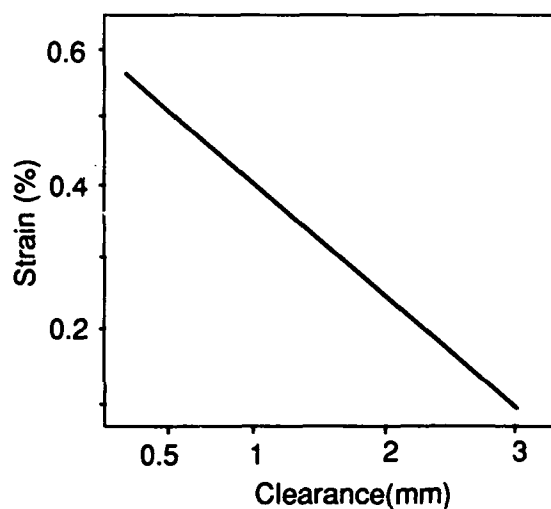


Fig.5 The dependence of the fiber strain on the clearance in a tube

EXPERIMENTS

Twisting pitch effect

First, we fabricated trial cables with different ribbon twisting pitches and investigated cable performance by doing several tests. The parameters of trial cables are shown in table 1.

The cabling process is composed of the ribbon process, tubing process, stranding process, and sheathing process. In the tubing process, ribbons are twisted helically in a tube. A loss change was not observed after the tubing process for all tubes in table 2. In the stranding process, tubes are stranded reversely around a central member and wound on reels with the diameter of 1000mm.

A loss increase was observed in No.2 and No.3 cable when cables were wound on reels. The maximum loss increase of each cable is plotted as a function of the ratio of the ribbon twisting pitch, P_{rb} , and the reverse lay length of the tubes, P_{tb} , and is shown in Fig.6. From Fig.6, it is found that the transmission loss is large when $P_{tb}/P_{rb}=2$ and 3. In the case of the $P_{tb}/P_{rb}=0.6$, no loss increase was observed. This agrees well with the theoretical results discussed above.

These three cables were subjected to bending tests, tensile load tests, and flexing tests. Loss changes were measured during these tests. These cables did not show noticeable loss change under these tests. This seems to indicate that the loose structure absorbs the strain due to bending or tensing by changes of the fiber positions in the tubes.

Table.1 Cable parameters of the trial cables

Cable No.	P_{rb} (mm)	P_{tb} (mm)
1	200	350
2	700	350
3	1000	350

Table.2 The attenuation changes after tubing process

The twisting pitch of ribbon in the tube	The attenuation changes after tubing process
200	$\leq 0.05\text{dB/km}$
700	$\leq 0.05\text{dB/km}$
1000	$\leq 0.05\text{dB/km}$

Performance of trial cable with reverse stranding

Based on the theoretical study and preliminary experimental study, we designed the final cabling parameters and fabricated a trial cable. Dimensional parameters are shown in table 3. The reverse lay length is selected to be 350mm from the viewpoint of the allowable length of removing sheath for closure. The ribbon twisting pitch is designed to be around 200mm considering fiber strain under such conditions as bending, twisting,

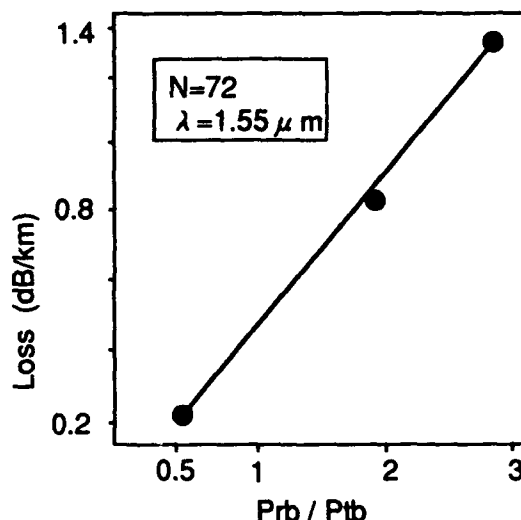


Fig.6 The maximum loss increase of each cable are plotted as a function of P_{rb} / P_{tb} .

temperature cycling. The performance of this cable was investigated under several mechanical test and environmental tests.

a) Optical Attenuation Change in Cable Manufacturing Process

The change in optical attenuation in the cable manufacturing process of the trial cable is given in Fig.7. In the fabrication processes no loss change was observed.

b) Temperature Cycling Test

To predict the long-term reliability of optical attenuation for the cables, we subjected a trial cable to a heat cycle test. The temperature cycle pattern for this test and the obtained results are given in fig.8. During the test, the attenuation change was less than 0.1dB/km at both wavelengths.

c) Mechanical test

The mechanical tests consist of tensile strength of cable, cable twist, cable cyclic flexing, and compressive strength. During these tests, the change of transmission loss was below 0.01dB. The conditions and results of the mechanical tests are summarized and shown in table 4.

In the tensile load test, the load on the cable was increased gradually up to 4400N. During the test, the attenuation increase was below 0.01dB, and there was no evidence of cracking or slitting on the cable after the test.

In the cyclic flexing test, we tested the trial cable changing azimuthal angle from the reversing point of tubes. There was no attenuation increase for the cable in any flexing direction.

In the compression test, the finished cable was subjected to a load of 440N/cm. After the load was removed from the cable, there was no residual attenuation in the cable.

Table.3 Dimensional parameters

Item	Dimension (mm)
Reverse lay length	350
Ribbon twisting pitch	200

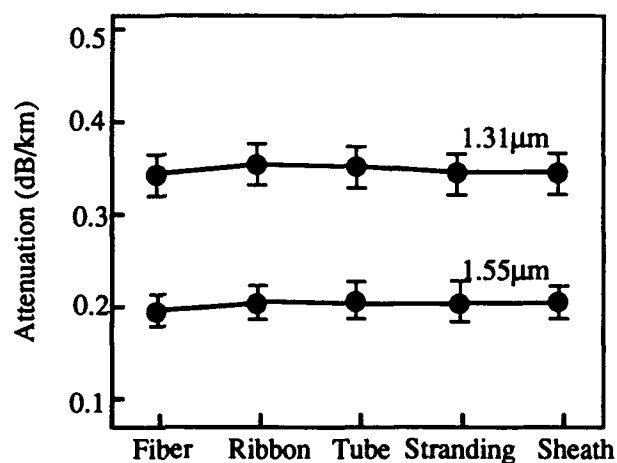


Fig. 7 Attenuation change in Cable Manufacturing Process

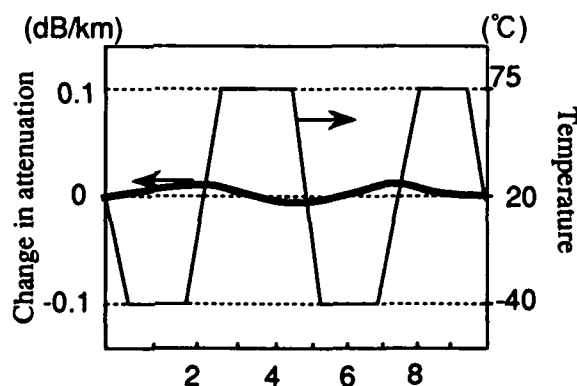


Fig.8 Result of heat cycling test for the trial cable

CONCLUSION

Stranding methods were studied in order to achieve good performance for optical fiber subscriber cable.

Table.4 Mechanical test results

Test item	Condition	Cable Performance
Tensile	Tensile Load : 50m / 3000N	During the test $\leq 0.01\text{dB}$
Twist	10 cycles of $\pm 180^\circ$	During the test $\leq 0.01\text{dB}$
Cyclic Flexing	25 cycles of 180° flexes Sheave Dia. = 600mm	During the test $\leq 0.01\text{dB}$
Compression	440N/cm Compressive load 100mm Compressive Plates	During the test $\leq 0.01\text{dB}$

To cancel the strain on the bent cable, twisted ribbon are generally used. In the case of loose tube ribbon cable with reverse lay stranding of the tubes, the twisting pitch of the ribbons in tubes, the reverse lay length and the clearance in the tube are important factors in achieving stable transmission characteristics.

Considering these factors, 432-fiber ribbon loose cable with reverse-stranding that has the smallest fiber strain when bent was manufactured. Further, the trial cable had stable characteristics in mechanical and environment tests.

REFERENCES

- [1] Y. Kurosawa, H.Sawano, M.Miyamoto, N.Sato, "Development of ribbon loose tube cable for optical subscriber loop", 41st IWCS, 1992.
- [2] T.Fuchigami, Y. Katsuyama, M.Kawase, "Optimum clearance design for a loose optical fiber cable based on suppression of fiber strain", Journal of Lightwave Technology, vol.LT-3, No.1
- [3] T. S.Swiecicki, "Unit core cable structure for optical communication systems" Wire Industry, September 1979.
- [4] Y.Katsuyama, H.Kobayashi, Y.Mitsunaga, K.Harada, Y.Ishida, "Bending property and allowable bending radius for unit-type optical cable", Trans. IEICE Japan, vol.J-66B, no.2,1983.
- [5] R. Yamauchi, K.Inada, H.Ishihara, "Residual stress of fibers in tape-type optical cable and their reduction", Trans .IEICE Japan, vol.63-B, no.8



Masayoshi Yamanaka

Fujikura Ltd.

1440 Mutsuzaki,
Sakura, Chiba, 285,
Japan

Mr. Yamanaka was born in 1966. He joined Fujikura Ltd. after his graduation from Tohoku University with the M.E. degree in 1992 and has been engaged in research and development of optical fiber cables. He is now an engineer of the optical fiber cable section.



Hiroyuki Sawano

Fujikura Ltd.

1440 Mutuzaki,
Sakura, Chiba, 285,
Japan

Mr. Sawano was born in 1955. He joined Fujikura Ltd. after his graduation from Hokkaido University with the M.S. degree in 1983 and has been engaged in research and development of optical fiber cables. He is now an engineer of the optical fiber cable section and a member of IEICE of Japan.



Naoki Okada

Fujikura Ltd.

1440 Mutuzaki,
Sakura, Chiba, 285,
Japan

Mr. Okada was born in 1964. He joined Fujikura Ltd. after his graduation from Chiba University with the B.E. degree in 1986 and has been engaged in research and development of optical fiber cables. He is now an engineer of the optical fiber cable section and a member of IEICE of Japan.



Matsuhiro Miyamoto

Fujikura Ltd.

1440 Mutuzaki,
Sakura, Chiba, 285,
Japan

Mr. Miyamoto was born in 1953. He joined Fujikura Ltd. after his graduation from Tokyo Institute of Technology with the M.S. degree in 1978 and has been engaged in design and research of optical fibers and cables. He is now the manager of the Telecommunication Cable Section and a member of IEICE of Japan.

MICROBEND LOSS OF COLORED OPTICAL FIBERS MEASURED OVER EXTENDED TEMPERATURE RANGE

Zygmunt Pasturczyk & Costas Saravanos

Optical Cable Plant, Northern Telecom Canada Ltd.

Saskatoon, Saskatchewan, CANADA

ABSTRACT

The measurements of microbend loss of colored and uncolored fibers performed over the temperature range of +80°C to -40°C indicated differences in performance which were linked to fiber design as well as specific parameters of fiber coating and coloring ink materials. The thermal stability of these materials was identified as a key parameter. The requirements for coloring and coating materials have been established based on trends observed in the test results.

INTRODUCTION

In modern cable designs, the microbend loss of optical fibers is usually negligible at room temperatures. As the temperature decreases, the fiber attenuation is known to increase. The shrinkage of the cable structure combined with the stiffening of the fiber coating subjects the glass fiber to compound bending resulting in increased attenuation. It is important for the cable manufacturer to know the microbend sensitivity of the optical fiber as a function of temperature in order to be able to predict optical cable performance over the critical low temperature range. Highly over-designed cables can accommodate microbend sensitive fibers, however, it is more economical to minimize the fiber's microbend sensitivity at the fiber level by careful optimization of all its parameters. This paper investigates the effects of different coating and coloring materials and various fiber designs on microbending loss over a wide temperature range.

TEST METHOD

Fiber sensitivity to microbending was measured by a modified basket weave method [1]. A long length of fiber, usually 2.5 km, was wound under tension onto a glass drum. A basket weave winding pitch of 2mm was selected to reflect the worst case fiber arrangement inside the tube. The drum,

resembling a typical fiber reel, was made of pure silica to match the thermal expansion coefficient of the optical fiber. The fiber on the drum was placed inside a temperature chamber and subjected to slow temperature cycling between +80°C and -40°C. This range corresponds to the operating temperature range specified for optical cables. The fiber attenuation was measured by unidirectional OTDR. The OTDR pigtail was spliced to one end of the test fiber, while the other end was cleaved to produce good end reflection. Several fibers on separate drums were tested simultaneously by splicing them together to form a single length. A new OTDR trace was acquired each time the temperature changed by one degree. The traces were processed by a computer to extract the attenuation of all fibers. The temperature in the chamber and the corresponding attenuations were recorded and subsequently plotted.

The repeatability of this test method was verified by comparing plots of attenuation versus temperature measured twice on two different glass drums using the same piece of fiber. It was assumed that the fiber does not undergo any changes between the first and the second tests (e.g. due to thermal aging). To verify this assumption two lengths of fiber, taken from the same reel, were tested in parallel and the results compared. The maximum discrepancy observed was 0.05 dB/km.

TEST RESULTS

Microbend Loss of Uncolored Fiber

The typical response of fiber attenuation to the temperature change is shown in Figure 1. As the temperature increases above room temperature, the attenuation remains constant. To the contrary, as the temperature decreases, the attenuation starts increasing due to microbending. Most coatings protect fiber from microbending very well at room temperature where they remain soft and flexible. Low temperature causes the

coating to harden and transfer external stresses directly to the glass fiber instead of absorbing them through elastic deformation. The thermal stability of the coating material is the most significant parameter directly affecting the fiber microbending performance. The importance of testing microbending performance over the wide temperature range can be realized by comparing the behavior of fibers 1 and 2, as shown in Figure 1.

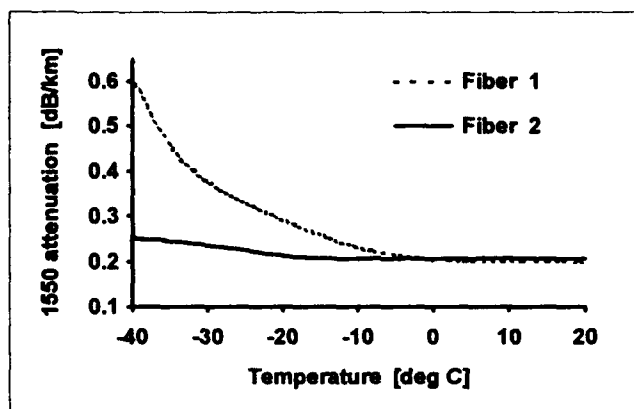


Figure 1. Fiber attenuation at 1550 nm versus temperature.

At room temperature fiber 1 offers slightly better performance than fiber 2. At -40°C , fiber 2 looks much better than fiber 1, making it a better choice for cabling. The direct correspondence between optical fiber loss inside the cable and microbend loss measured on the glass drum has been demonstrated elsewhere [2].

Hysteresis of Microbend Loss

A different aspect of thermal stability of the coating material is shown in Figure 2. The two plots of fiber attenuation versus temperature correspond to the same fiber. The differences between solid curve and dashed curve are due to different cooling/heating rates. The hysteresis loop visible in dashed curve indicates that attenuation changes are lagging temperature changes. Obviously the temperature changes (i.e. $1^{\circ}\text{C}/\text{min}$) were too fast for that particular coating material. The results are difficult to relate to real conditions in the field. The solid curve was produced by slowing down the cooling/heating rate from $60^{\circ}\text{C}/\text{min}$ to $5^{\circ}\text{C}/\text{hour}$. The hysteresis loop was reduced to a single line representing actual microbend performance in the field. All results shown in this paper as a single line were acquired using a sufficiently slow temperature change rate.

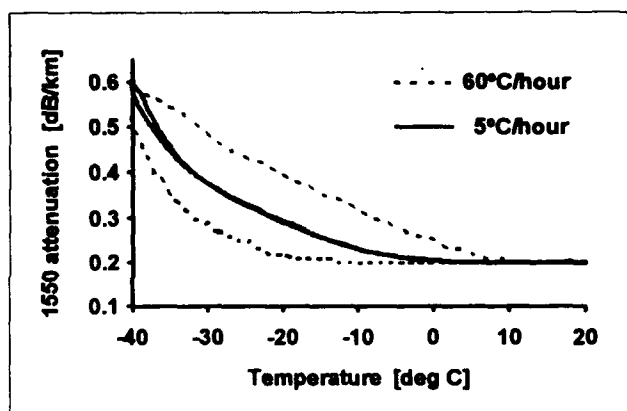


Figure 2. The effect of two different temperature change rates on the test results.

Microbend Loss of Colored Fiber

Several colors were applied to fibers 1 and 2 discussed previously. Both UV and thermally curable inks were used. The key parameters of the coloring process were varied. The results of microbend testing of fibers colored with UV curable inks are summarized in Figure 3.

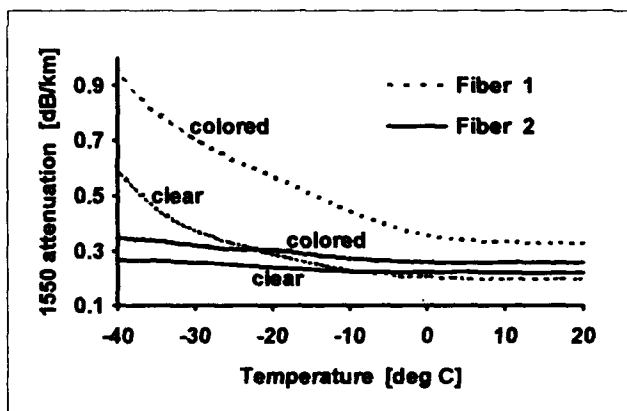


Figure 3. Effect of fiber coloring using UV curable inks on fiber attenuation.

Since no significant differences in performance could be linked to specific colors the results of all colored fibers were averaged. In general the coloring increases the microbend sensitivity of all fibers with fiber 1 being more sensitive to coloring than fiber 2. This can be linked with the high inherent microbend sensitivity of fiber 1 determined prior to coloring.

In addition to a uniform layer of coloring ink discussed in previous section, non uniform coloring was applied to fibers 1 to simulate poor coloring conditions. As shown in Figure 4, irregular coloring further increases the microbend loss. The results indicate that good control of the coloring process will result in superior microbending performance of the fiber.

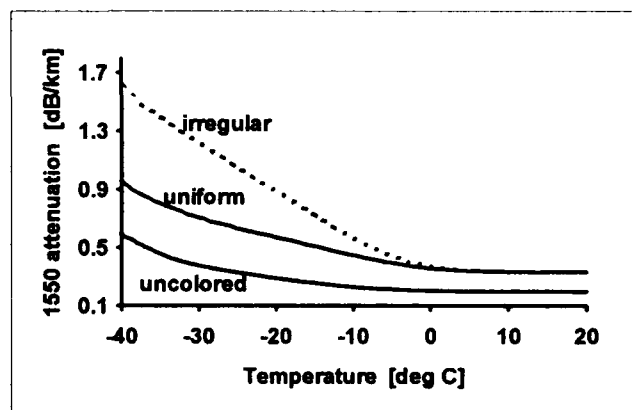


Figure 4. The effect of non uniform layer of UV curable ink on fiber attenuation.

The UV curable inks are compared with thermal inks in Figure 5. Different thermal colors performed similarly and are represented by one line obtained by averaging. As one can see thermal inks increase the fiber's microbending loss to the greater extent comparing with the UV curable inks.

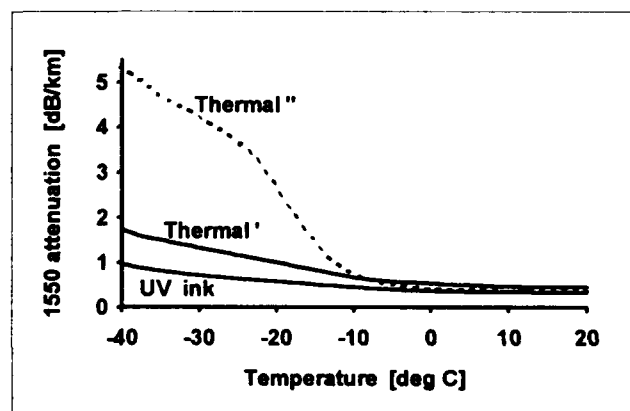


Figure 5. Comparison of UV curable inks with thermal inks. Thermal' and Thermal'' show the dependence before and after +80°C cycle respectively.

In addition the thermal inks demonstrated a dramatic jump in microbending loss after passing them through +80°C temperature cycle. This effect, not observed on UV curable inks, can be explained as follows. At hot temperatures thermal inks soften and bond adjacent fibers together. In the next cold cycle bonded fibers show an increased microbending sensitivity. Fiber bonding by thermal inks has been a well known problem in optical cables over the past years.

CONCLUSIONS

The microbend loss increase observable only at low temperature has been linked to thermal stability of the coating material. The fiber performance tested only at room temperature is insufficient to predict low temperature performance. The microbend loss of colored fibers is higher than that of uncolored ones and its magnitude depends on the coloring process parameters. A uniform layer of ink gives better results than a non uniform one. Fibers colored with UV curable inks result in moderate increase of microbend loss. The increment observed in fibers colored with thermal inks was the most pronounced one, especially after heating the fiber to +80°C.

REFERENCES

- [1] A. Tomita, P.F. Glodis, D. Kalish, P. Kaiser, "Characterization of the bend sensitivity of single-mode fibers using the basket-weave test", *Tech. Digest - Symposium on Optical Fiber Measurements 1982*, Boulder CO, NBS S/P 641, pp. 89-92, 1982.
- [2] Z. Pasturczyk, C. Saravanos, "Fiber microbending test method capable of predicting microbend loss in optical cables", *Tech. Digest - Symposium on Optical Fiber Measurements 1992*, Boulder CO, NIST S/P 839, pp. 37-40, 1992.
- [3] P.A. Sutton, J.L.L. Roberts, A.T. Summers, A. Phoenix, D. Rees, "Development of a non-destructive test for microbend loss mechanisms in cabled fiber", *International Wire & Cable Symposium Proceedings 1989*, Atlanta GA, pp. 450-455, 1989.
- [4] Y. Katsuyama, Y. Mitsunaga, C. Tanaka, T. Waki, Y. Ishida, "Optical loss stability of a fiber cable under lateral force and optimum design of the coated fiber structure", *Appl. Opt.*, vol. 21, pp. 1337-1341, 1982.



Zygmunt Pasturczyk
Northern Telecom
Canada Ltd.
Optical Cable Plant
Saskatoon,
Saskatchewan,
CANADA

Zygmunt Pasturczyk received the M.Sc. degree in physics from the Warsaw Technical University in 1976. In 1977, at the Warsaw Technical University, he was engaged in optical waveguides and integrated optics research. He joined SED Systems in 1982, where he was involved with optical instrumentation for upper atmosphere research. Since 1988 he has been a Research Scientist with Northern Telecom Optical Cable Plant, working initially in development of installation products then moving into the area of fiber drawing and focusing on improvements of fiber coating.



Costas Saravanos
Northern Telecom
Canada Ltd.
Optical Cable Plant
Saskatoon,
Saskatchewan,
CANADA

Costas Saravanos graduated from the University of Athens, Greece, with a B.Sc. degree in Physics in 1973. He received his M.Sc degree in Solid State Physics from the South Dakota School of Mines and Technology and is currently completing his Ph.D. degree in Electrical Engineering from University of Ottawa.

Following a year with the Digital Transmission Division of Northern Telecom, he joined the Optical Systems Division in 1982 where he was engaged in the fiber process optimization. Since 1985 he has been an R&D Manager responsible for the fiber design optimization and the design and development of optical fiberconnectors. In 1991 he became Manager of Northern Telecom's Fiber R&D team.

Effect of Curing Temperature and Thermal History on Mechanical Properties of UV Curable Polyurethane Acrylate for Optical Fiber Coatings

Zen Komiya, Yuji Takasugi, Takashi Ukachi, and George Paternack[†]

Tokyo Research Laboratory, Japan Synthetic Rubber Co. Ltd. and DSM Desotech Inc.[†]

Abstract

Some coatings found to form a higher Young's modulus film when they were cured at higher temperature or higher UV dose. The degrees of cure or crosslink densities measured by gel fraction or E' were found to be comparatively high. The film cured at lower temperatures showed a higher Young's modulus after annealing at appropriate temperature. Photo-differential scanning calorimetry (photo-DSC) was employed to cure samples monitoring temperature and the samples obtained by photo-DSC or conventional curing method were evaluated by thermal mechanical analysis (TMA). The relationship between maximum temperatures during curing and mechanical properties of coatings measured by TMA was established. It is proposed that when the maximum temperature during curing exceeds the glass transition temperature, the changes in the modulus are due to a phase transition taking place during curing.

Introduction

Rapid growth of optical fiber telecommunication networks has prompted intensive research on the materials used to coat and cable optical fibers. Glass optical fibers used in telecommunications require coatings to protect the fiber from physical damage and surface scratches. UV curable polyurethane acrylates are widely used for optical fibers because of their well-balanced mechanical properties and good chemical and weathering resistance. In addition to these features, photocurable resins cure rapidly which enables high productivity of optical fibers.

Conventionally, two layers of coating are applied to glass fibers. One of which is a soft inner (primary) coating and the other is a hard outer (secondary) coating. The hard coating protects the glass fiber from external mechanical damage. On the other hand, the soft coating buffers the fiber from external deformation. It has already been reported that hard coatings having a high Young's modulus provide better microbending protection than hard coatings having a low

modulus¹. Therefore, high modulus hard coatings are of importance to obtain maximum protection for optical fibers.

during the development of hard coatings, we have found several coatings that show a relationship between Young's moduli and curing conditions such as temperature and UV dose. In our previous paper, we presented some of the examples studied on our draw tower². As the draw rate is increased, without changing the cooling distance, the surface temperature of fiber is higher where the coating is applied. For coatings in which the Young's modulus is highly dependent on the temperature of cure, the performance of the resultant optical fiber can vary depending upon the draw rate. We found that the Young's modulus of a particular coating varied from 80 to kg/mm² in the temperature range of 40 to 80°C. therefore, we believe it is desirable to develop new coatings whose properties are less sensitive to the curing conditions.

Experiments

Materials: Three secondary coatings, H-0, H-1, and H-2 were employed for this study. H-1 and H-2 are the same coatings studied in the previous paper².

Preparation of films: Each coatings was drawn down on a clean glass plate using a 250 μ m thickness film applicator. The films were cured by passing the coated glass plate under a metal-halide lamp (80W/cm) in air. The cure dose was varied from 100 mJ/cm² to 1000 mJ/cm² by adjusting the conveyer speed. Cured films were conditioned for 24 hours at 23°C, 50 % RH.

Photo-DSC curing: A photo-DSC system was employed using the DuPont 910 differential scanning calorimeter and the 990 thermal analyzer with an ORC HMW-724S spot UV light source. The cure dose was varied by adjusting exposure time. The intensity of the light was kept at 5.2 mW/cm². Thus, for example, the exposure time for 1000 mJ/cm² dose was controlled to 194 sec. Approximately 30 ~ 40 mg of coatings were placed in the DSC cell and conditioned to the desired

temperature under a nitrogen stream (70 ml/min). The amount of heat generated by polymerization and the temperature change of the sample were monitored by the DSC thermal analyzer.

Evaluation of the samples: Young's moduli of films were measured by a standard method using films of ca. 200 μm thickness. (The moduli were defined by 2.5 %-secant modulus.) Gel fractions were measured by the extractable content of cured films using refluxing (12 hours) methyl ethyl ketone (MEK). Dynamic mechanical response was measured from the same films using TOYO Baldwin's Rheovibron DDV-III-EA in the temperature range of 20 ~ 180 $^{\circ}\text{C}$ at a rate of 2 $^{\circ}\text{C}/\text{min}$ and frequency of 35 Hz. Glass transition temperatures (T_g s) were reported as the maximum of $\tan \delta$. Thermal mechanical analysis (TMA) was carried out using a Rigaku TMA thermoflex in penetration mode. TMA measurements were made by placing cured samples in a quartz cell in contact with a quartz needle having an 1 g load. The sample was heated from 25 $^{\circ}\text{C}$ to 150 $^{\circ}\text{C}$ at a rate of 5 $^{\circ}\text{C}/\text{min}$. The movement of the needle was detected as a function of temperature.

Result and discussion

We determined that the Young's modulus of coating H-0 was highly dependent on the curing conditions, especially the amount of UV dose. When coating H-0 was cured under 100, 300, 500, 1000 mJ/cm^2 of UV dose, the Young's modulus varied dramatically as shown in Table I. The gel fractions of these films showed little variation, and the T_g s determined by $\tan \delta$ maximum were independent of the Young's moduli. a typical pattern of the dynamic mechanical analysis is presented in Figure 1.

Crosslink densities were calculated using E_0 values at 110 $^{\circ}\text{C}$ ($T_g + 40^{\circ}\text{C}$)³. The crosslink density, which is considered to represent the amount of chemical crosslinks per unit volume, was also independent of UV dose. By assuming all of the crosslinkable multifunctional acrylates reacted to

form crosslinks, the crosslink density of H-0 was calculated to be $3.54 \times 10^{20} \text{ cm}^{-3}$. The calculated values were found to be very close to the theoretical value even though using E_0 as a measure of crosslink density is based on rubber chemistry. Crosslinked rubber typically has much lower crosslink densities than those of UV curable optical fiber coatings. The good agreement between the calculated value and theoretical value indicates that the conversion of crosslinkable monomers is very high and most of the crosslinks act effectively to keep the modulus high at elevated temperature. A film cured with 100 mJ/cm^2 of UV light and post heated to 100 $^{\circ}\text{C}$ resulted in the Young's modulus increasing to 164 kg/mm^2 from an initial value of 114 kg/mm^2 . The results are shown in Table II and Figure 2. When the same film was heated at 50 $^{\circ}\text{C}$, the Young's modulus was not affected even after 72 hours of heating. (The temperature dependency post heating effect and independence of the T_g values obtained by $\tan \delta$ maximum peak show that cured film properties are influenced differently when curing takes place.) Since the values of gel fraction and crosslink density indicate that the extent of crosslinking were the same regardless of the amount of UV dose, we believe that the temperature during curing plays an important role in final film modulus. We have already found that the surface temperature to which coatings are applied on an optical fiber draw tower influences the physical properties of resultant cured coating².

To maintain better control of curing conditions, we carried out photo-DSC curing experiments. Temperature change during curing was monitored and the physical properties of the resultant cured samples were evaluated by TMA. The results are summarized in Table III. The amount of heat generated during the polymerization was found to be independent of the temperature during curing. It is interesting to note that the increases in temperature over the starting temperature were essentially the same. The consistency in the temperature increase during curing at different initial temperatures shows the cure rates are not affected by

Table I. Physical properties of H-0 cured by various UV doses.

UV dose (mJ/cm^2)	Young's modulus (kg/mm^2)	Gel (%)	T_g by $\tan \delta$ max ($^{\circ}\text{C}$)	crosslink density ¹⁾ (cm^{-3})
100	110	96	77	3.4×10^{20}
300	106	95		
500	129	96	73	2.5×10^{20}
1000	144	98	73	3.0×10^{20}

1) Calculated from the E_0 values at $T_g + 40^{\circ}\text{C}$ (see text).

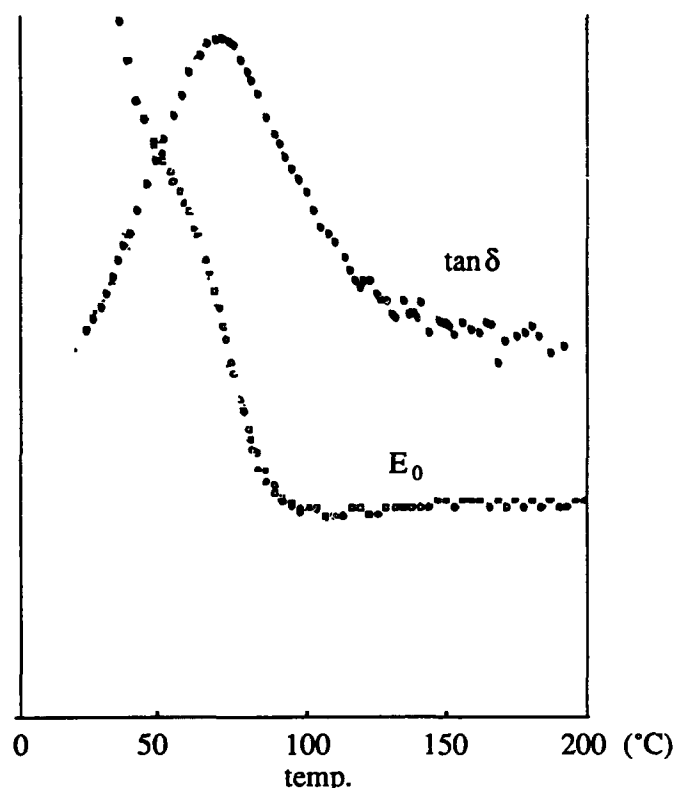


Figure 1. Dynamic mechanical analysis of H-0.

Table II. Change in Young's modulus of the film of H-0 of heatings at 100°C

time (min.)	0	10	30	60	120	240	600
Young's modulus (kg/mm ²)	114	110	115	120	136	149	164

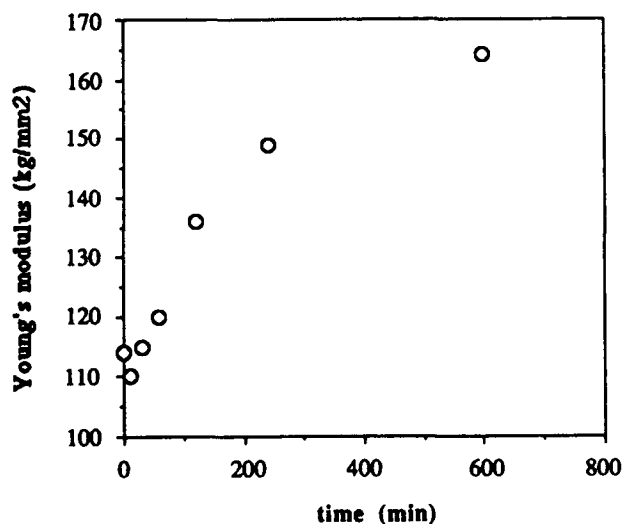


Figure 2. Effect of annealing at 100°C on Young's modulus of cured film of H-0.

temperatures in the range of 30 ~ 80°C. TMA measurements show a dependency on the curing temperature. As mentioned in the experimental section, TMA was carried out in the penetration mode. A schematic description of the TMA instrument is shown in Figure 3, and a typical TMA chart is presented in Figure 4. Upon heating, a sample starts expanding. At the softening point, the quartz needle suddenly penetrates into the sample. the sample resumes expansion as the temperature is continually increased.

The softening points of the samples cured at 30°C are generally lower than other samples cured at 50 or 80°C. Among those samples cured at 30°C, one prepared under the lowest UV dose exhibited the lowest softening temperature have low Young's moduli. Unfortunately, we can't measure the Young's modulus of a film cured in a small DSC cell. However, the film having a low Young's modulus cured at 100 mJ/cm² also showed a lower softening temperature compared to that of the film cured at 1000 mJ/cm² (see Table III). One of the most significant differences between the samples cured at 30°C and those cured above 50°C is the maximum temperature reached during curing. Temperatures of the samples cured at 30°C reached 55°C, which is below the Tg of H-0. Samples cured at 50 and 80°C reached 76°C (Tg of H-0)

Table III. Photo-DSC curing of H-0 and softening point of resultant samples by TMA.

Start temp. (°C)	UV dose (mJ/cm ²)	T _{max} ¹⁾ (°C)	ΔT (°C)	Softening temp. (°C)
30	100	56	26	45
	500	55	25	53
	1000	56	26	51
50	100	76	26	56
	500	77	27	56
	1000	76	26	59
80	100	101	25	58
	500	105	25	56
	1000	105	25	61
film cured by	100	-	-	38
UV conveyer	1000	-	-	43

and as high as 105°C. It is our belief that hydrogen bond formation is facilitated when the maximum temperature during curing exceeds the T_g of the cured film. However, when curing occurs below the T_g, hydrogen bonding (e.g., urethan moieties, acrylate carbonyls and ether oxygen) is restricted because of limited bond mobility. when coatings were cured on a glass plate, the temperature just before the irradiation was

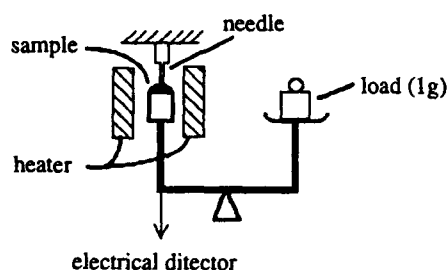


Figure 3. Schematic description of TMA system.

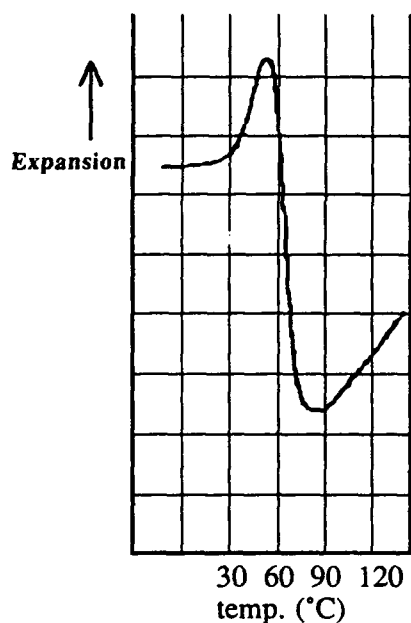


Figure 4. A typical TMA chart. The sample was H-0 cured at 50°C with 100 mJ/cm² dose.

ambient temperature. Compared to photo-DSC equipment, films irradiated on glass plates receive more heat emitted from the more powerful UV lamps used. It is probable that the maximum temperature of the film cured at 1000 mJ/cm² exceeded 77°C resulting in the film having a higher tensile modulus (see Table I). On the other hand, films cast on a glass plate and cured with a lower amount of UV (shorter exposure time) receive less heat. Thus, we can conclude that films having a low Young's modulus must have been cured at temperatures lower than the T_g of the cured film.

Based on the above results, we carried out the same investigation on coatings H-1 and H-2, which we studied in a previous paper using our fiber draw tower². According to the previous results, the Young's modulus of H-1 was highly dependent on the surface temperature to which the coating was applied. coating H-2 was independent of the surface temperature. The results of photo-DSC curing and TMA measurements of the resultant samples are summarized in Table IV. Generally, the maximum temperature H-1 reached, cured at different temperatures, during curing was approximately 10°C lower than that of H-2. this is because the cure rate of H-1 is slower than H-2 as seen from the heat generation patterns obtained by photo-DSC. Since all of the quantities of generated heat are almost the same regardless of curing temperature, the amount of polymerization is estimated to be the same. However, the TMA behavior of H-1 was quite different from H-0 and H-2. the samples of H-1 cured at 30 or 50°C showed dual softening points. On the other hand, H-1 cured at 80°C and all the samples of H-0 and H-2 exhibited a single softening point. Typical TMA charts are depicted in Figure 5.

In a previous paper, we showed that when coating H-1 was applied to a glass fiber surface at a temperature higher than 50°C, the cured coating had a high Young's modulus (200 kg/mm²). When the coating was applied to a glass fiber surface of lower temperature, it exhibited a lower Young's modulus (80 kg/mm²). In sharp contrast, coating H-2 did not

Table IV. Photo-DSC curing of H-1 and H-2 and softening point of resultant samples.

start temp. ¹⁾ (°C)	T _{max} (°C)	H-1			H-2		
		ΔT (°C)	softening temp. (°C)		T _{max} (°C)	ΔT (°C)	softening temp. (°C)
30	50	20	40	73	59	29	61
50	73	23	40	63	82	32	78
80	105	25	-	84	111	31	86

1) UV dose was 300 mJ/cm².

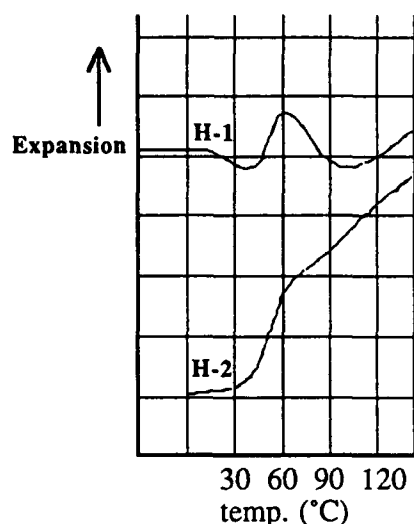


Figure 5. TMA traces of H-1 (cured at 50°C) and H-2 (cured at 30°C).

exhibit sensitivity to glass fiber surface temperature. A Young's modulus value of 200 kg/mm² was obtained in the temperature range of 40 ~ 80°C. We concluded that the tan δ peak at 50°C for H-1 is due to hydrogen bonding and this hydrogen bonding is responsible for the higher Young's modulus achieved when curing takes place at elevated temperatures. In the case of H-1, the temperature of 50°C seems critical to the TMA measured values. In this study, when the maximum temperature during polymerization exceeds the temperature of the second tan δ peak, the cured samples achieve a higher Young's modulus. We suspect that the lower softening point represents phase separation of a soft segment region having a smaller extent of hydrogen bonding. Further investigation is necessary to prove this speculation. In contrast to H-0, when H-1 and H-2 were cured on a UV conveyor with a range of UV doses (100 ~ 1000 mJ/cm²), both films exhibited higher Young's modulus and they were not affected by the amount of UV dose. This is probably due to the lower temperature of H-1 and H-2 compared to H-0 (for H-0, it is 76°C, H-1 50°C, and H-2 50°C). It is likely that in all cases of curing on the UV conveyor, the maximum temperature of the coating exceeded 50°C. This is because of the excessive heat radiated from the high power UV lamps and the less effective removal of heat achievable under photo-DSC curing conditions.

Conclusion

It has been implicated that the temperature during curing would be a very important factor to determine physical

properties of the resultant coatings. We used photo-DSC to cure coatings monitoring temperature and evaluated the resultant samples using TMA. We found that when the maximum temperature reached during curing and the glass transition temperature had close relationship. Namely, when the temperature doesn't exceed the glass transition temperature of the coating, the Young's modulus of coating can be less than that is expected when it is cured at high temperature. We speculate that this phenomena are based on how the hydrogen bonding develops during curing. We pointed out that the curing temperature can be vary dramatically depending on the draw rate of optical fiber and cooling distance. Therefore it is very important to pay attention to the performance of coatings cured at various temperatures.

References

- ¹ Hara, M.; Okagawa, S.; Otake, A. Proceedings of 41st IWCS, 20 (1992).
- ² Ukachi, T.; Aoyama, A.; Naito, Y.; Igarashi, K. Proceedings of 41st IWCS, 261 (1992).
- ³ Maruyama, T.; Bell, J. P. *J. Polym.Sci., A-2*, 8, 437 (1970).



Zen Komiya received his Ph.D. in Organic Chemistry from Hokkaido University, Hokkaido Japan in 1984 and joined Japan Synthetic Rubber Co., Ltd. He was engaged in research on development of new transparent plastics and currently has been engaged in research and development on radiation curable materials.



Yuji Takasugi received his M.S. degree in nuclear engineering from Hokkaido University in 1991. He started work at Japan Synthetic Rubber Co., Ltd. on the development of optical memory disk and now he has been working on the radiation curable materials for optical fiber coating.



Takashi Ukachi received his B.E. degree in biophysics and bioengineering from Osaka University, Osaka, Japan in 1976. He started his professional carrier at Tokyo Research Laboratory of Japan Synthetic Rubber Co. Ltd. where he has been engaged in research on development of optics relating polymeric materials and their applications.

George Pasternack is a technical team leader at DSM Desotech Inc. He has fifteen years experience in the field of UV curable coatings for optical fibers. Dr. Pasternack received his B.S. degree in Chemistry from The City College of New York and his Ph.D. degree in Organic Chemistry from The City University of New York.

A NON-RIGID PRE-TERMINATED CLOSURE SYSTEM FOR FIBER-IN-THE-LOOP (FITL)

Robert G. Sember and James A. Aberson

Raychem Corporation, Telecom Division, Fuquay-Varina, North Carolina

ABSTRACT

A fiber optic splice closure system has been designed for factory pre-termination. To accomplish this, a novel, slack-free fusion splice organizer and an assembly method for taut-sheath cable splices have been developed and enclosed within a proven, durable wrap-around heat-shrinkable sleeve. This combination creates a very small diameter, completely sealed, reelable cable splice closure that can be wound in-line with its interconnected cables onto reels that are 30 inches or more in diameter. The completed closure is less than 1.8 inches in diameter. Also, with its factory pre-termination, this approach eliminates the high costs for equipment, training, and labor; the variable quality encountered in widespread field installation of splices and closures; and the ONU/pedestal exposure of distribution cables.

1.0 BACKGROUND AND INTRODUCTION

This work was undertaken in response to customer needs. First, since current regulatory practices require that Fiber-In-The-Loop (FITL) applications achieve cost parity with alternative copper-based approaches, telecommunications companies are anxious to explore and apply the concepts for fiber optics that have created large cost savings for copper pre-terminated closures. For copper, savings follow directly from being able to limit expensive equipment and trained personnel to a few controlled locations where Raychem's PreTerm™ product and assembly-line techniques [1] can be used to mass produce cable splices that are permanently sealed and wound in-line onto standard reels for field placement in buried and underground locations.

Until now, the PreTerm approach has been denied to fiber applications because storage of fiber slack, unlike copper, requires trays with 3-inch or greater widths to meet minimum-allowable fiber-bending radii. Consequently, the closures needed have been too large to be wound onto reasonably sized cable reels and too large to be installed through 3-inch or smaller ducts.

Second, with traditional ONU/pedestal installations for FITL, every distribution cable is looped entirely through each ONU along its length. With this architecture, damage to any pedestal potentially wipes out the entire network from that point on. However, if distribution cables can be joined to ONUs with factory-installed drops (stubs), looping of downstream fibers is eliminated and destruction of a "pre-terminated" pedestal will affect only the fibers feeding the damaged pedestal.

In this poster paper, a simple innovative way to address these customer issues is disclosed to show that fiber PreTerm [2] is now possible and that it can contribute to making FITL a reality.

2.0 TECHNICAL APPROACH

The approach followed to meet customer needs for cost effective FITL builds on the techniques and materials successfully used in buried-copper installations. Development of analogous closure system for fiber-optic PreTerm applications is discussed and illustrated below.

2.1 Product Concept / Requirements

The customers' major requirements for a finished pre-terminated fiber-optic closure are:

- must be designed for lowest cost
- must connect drop cables with 1 to 4 fibers to the distribution cable
- must be completely sealed for buried and underground installations
- must allow in-line take-up onto and payout from a 36-inch reel
- must retain the axial-pull performance of the cable
- must be capable of being pulled through a 3-inch-diameter duct
- must prevent water intrusion and migration due to damaged cable jacket
- must maintain cable current-carrying capacity

One product which satisfies all these criteria is a heat-shrinkable, non-rigid, taut-sheath, slack-free closure for splicing fiber drop cables to a distribution cable in a factory environment. After installation, this compact closure and its connected cables can be factory-wound in-line onto a standard cable reel for later deployment in field locations. Figure 1 shows a factory assembly line in operation to make reels of preterminated cables. This procedure provides a completely sealed closure system for FITL.

Users of this approach will (1) lower closure costs, (2) reduce labor costs, (3) improve quality (all splices and seals are factory certified prior to shipment), (4) minimize capital (only one multi-fiber fusion-splicing machine and operator are needed for a factory versus multiple machines, crews and vehicles needed for the field) and (5) respond faster to customer service requests.

2.2 Strength Member Reconstruction

For cable types which are deployed by gripping the strength members, the cable's pullout strength is restored at the sheath-entry location by securing the interrupted strength members with heat-shrink sleeves. Figure 2 illustrates the method for preparing, organizing and folding back the cable's strength members prior to the application of the closure sleeve. As the wrap-around sleeve is heat shrunk (Figure 9), its adhesive bonds it to the cable's strength members on both ends and re-establishes the tensile strength of the unopened cable.

2.3 Fiber Guide

The finished PreTerm closure's outer diameter, as shown in Figure 9, is less than 2 inches. This milestone is accomplished by longitudinally removing all fiber slack along the length of the closure rather than keeping it in traditional 3-inch-diameter loops.

To accomplish this, an in-line taut-sheath fiber/splice organizer has been developed that will accommodate either central-core or loose-tube cable designs. This device, whose installation is depicted in figures 3 and 4, covers the fiber-access window cut into the central-core or loose-buffer tube and holds the completed fiber splices.

Using commercial tools, a window is opened in the cable unit and the desired fiber, transmitting a visible light source for added convenience, is located and retrieved with a spudger/dental pick. Sufficient length of window is cut so that 9 inches of fiber is pulled out (Figure 3). With this length, one splice and two re-splice opportunities are possible.

After the distribution fibers are free (Figure 3), the window is wrapped with adhesive-backed foam, the organizer/guide's lower half is snapped over the foam and tie wraps are secured (Figure 4).

The upper half of the guide retains the fusion splices made between the distribution and the drop fibers (see Figure 6). If the drop has multiple fibers, mass fusion splicing is preferred because splicing will be faster and maintaining equal lengths between fibers, which is essential for slackless storage, will be simpler.

The drop cable is kept free so that it can be positioned close to the fusion machine and minimize the amount of fiber needed from the main cable for splicing. The quality of every splice is verifiable with OTDR measurements made along the drop-cable before it is attached to the distribution cable and cut to its final length.

2.4 Slack Removal, Drop-Cable Bonding and Main-Cable Shield Bonding

The drop cable may be electrically connected to the distribution cable by a strap as shown in Figure 5. Typically, this operation occurs after the drop-fiber splices have been made and verified for loss. Then, the drop cable is moved back to the position shown and attached to the distribution cable. In this movement, all slack is taken out of the fibers. Finally, for cables with metallic shields, electrical continuity is restored across the taut-sheath interruption by using a bond wire that connects the main cable's shields as illustrated in Figure 6.

2.5 Heat-Shrink Moisture Block

Figure 7 depicts the two adhesive rings that melt during shrinking of the closure sleeve to form a seal between the cable's core/buffer tube(s) and its jacket. This seal, called a moisture block, prevents water from entering the closure through the cable's core and reaching fibers and splices. Potentially, water can get into the cable core if the outer jacket is pierced and immersed sufficiently deep to force migration.

2.6 SuperSleeve™ Technology

Over 10 million heat-shrunk sleeves utilizing Raychem's SuperSleeve™ material are currently protecting copper splices. SuperSleeve combines proven heat-shrink technology with a durable composite laminate composed of several layers of specially blended polymers and adhesives. The heat-shrink sleeve recovers to a predetermined shape when heated by a torch or oven. Moisture blocking and outer-closure sealing is performed in ONE step by simply shrinking the sleeve and hot melt moisture block simultaneously.

A variable circumference liner, rugged heat-shrink sleeve, and adhesive coating protect the internal components from all water intrusion. The liner illustrated in Figure 8 and the foam dam shown in Figure 7 (adjacent to the adhesive rings) insulate the fibers and splices from the melting adhesives used to seal the closure system. The completed heat-shrink closure, illustrated in Figure 9, provides maximum protection during rigorous field deployment and adverse lifetime-environmental conditions.

2.7 Reeling In and Out

Since the fiber/splice organizer and its surrounding sleeve are small and flexible, the finished closure may be wound onto, stored, shipped and pulled off of 30-inch diameter reels for buried and underground field installations.

2.8 Factory Installation

Factory splicing, testing and torch installation of the sleeve in a quality controlled environment ensures that the assembled cable/closure system meets all requirements before the reel goes to the field.

Factory installation of fiber PreTerm will reduce the high costs associated with equipping all field crews with equivalent field splicing and testing tools and associated vehicles. Multiple PreTerm installations will require the appropriate number of PreTerm closure kits, as well as a one-time investment in the following: (1) mini- or palm-top mass-fusion splice machine (1-4 fibers), (2) appropriate splicing accessories, (3) buffer tube access tool, (4) dental pick, (5) visible light source (optional), (6) OTDR and (7) gas torch. An added step, not used in this work, would be pre-mounting fiber optic connectors onto the ONU ends of the drop cables to eliminate altogether the need for any field splicing.

3.0 PRIMARY CONCLUSION OR RESULT

A fiber optic cable splice closure system has been specifically designed for factory pre-termination. To accomplish this, a novel, slack-free fusion splice fiber organizer and assembly method for taut-sheath cable splices have been developed and enclosed within a proven, durable wrap-around heat-shrinkable sleeve.

This combination creates a very small diameter (less than 1.8 inches), completely sealed, non-rigid cable splice closure that can be wound in-line with connected cables onto reels that are 30 inches or more in diameter and can be pulled through ducts and bores that are 2 inches or more in diameter. Due to its factory pre-termination, this approach eliminates both the high costs for equipment, training, and labor and the variable quality that go with widespread field installation of splices and closures.

Thus, for low investment, a few well-controlled factory, shop, or garage locations can be established where, in assembly-line conditions, fiber distribution and drop cables can be reliably spliced together, ruggedly sealed for direct-buried and underground environments, and finally, compactly reeled together in-line for future field placement. This system brings fiber PreTerm [2] (analogous to copper PreTerm [1]) and its significant cost savings into practice now.

4.0 ACKNOWLEDGMENTS

The authors would like to acknowledge technical contributions to this work by Matt Becker, Carney Claunch, Dan Cockman, Loren Gulak, Tom Holbrook, Terry Hunsinger, John Kizis, Julian Mullaney, Mike Randolph, Craig Ray, Randy Shaw, Amanda Smith, Forrest Yount, and Steve Wald. The figures were developed by Linda Rogosich and the manuscript by Reed Reichardt.

5.0 REFERENCES

[1] XAGA, *PreTerm™ A Guide for Engineering and Administrative Procedures for Pretermination Plants*, Raychem System Practice Section RYCH-65-401, Issue 1, April 1985.

[2] *PreTerm FOSC, -CCT Fiber Optic Splice Closure*, In Press - Installation Instruction Draft Revision 8, July 27, 1993

6.0 BIOGRAPHIES



Robert Sember is a fiber optic product development engineer at Raychem Corporation in Fuquay-Varina, North Carolina. Robert received a B.S.M.E. from Rensselaer Polytechnic Institute, an M.S.M.E. from North Carolina State University and, since 1990, has been a Project Manager for fiber optic cable closures.



Jim Aberson is the manager of Fiber Optic Product Development at Raychem in Fuquay-Varina, North Carolina. He received a Ph.D. from North Carolina State University in Structures and Mechanics, and since 1980, he has worked in research and development of products and methods for making and sealing fiber optic cable splices.

7.0 FIGURES



Figure 1



Figure 2



Figure 3



Figure 4

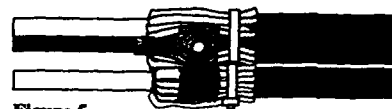


Figure 5



Figure 6

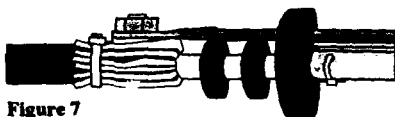


Figure 7



Figure 8

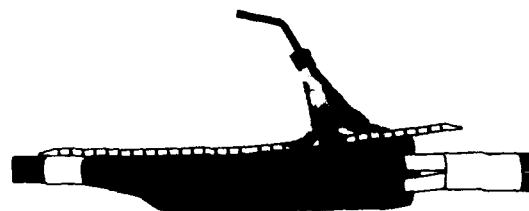


Figure 9

**THE EFFECT OF PROLONGED UV EXPOSURE ON THE PROPERTIES OF
LOW SMOKE, ZERO HALOGEN, FIRE RETARDANT SHERKING COMPOUNDS**

Dr Jack Taylor, Mr Joe Preston, Mr Dudley Sawyer & Miss Lai Ping Cheng

Lindsay & Williams Limited, Columbine Street,
Manchester, M11 2LH England

SUMMARY

As a generic class of materials, the low smoke, zero halogen, fire retardant cable compounds have been available to the wire and cable manufacturing industry for over a decade. Whilst primarily designed for internal use, there are increasing requirements for information regarding the performance of such materials outdoors. This paper presents the first systematic study using an accelerated weathering tester of the performance of a number of commercially available zero halogen, low smoke, fire retardant compounds, and using both UVA and UVB exposure protocols. The paper also presents the results of accelerated weathering on the properties of the commercially available materials which have been specifically stabilised against the effects of UV radiation. The performance of these optimised formulations approach those of the industry standard black LDPE and black PVC materials.

1.0 INTRODUCTION

Since their introduction in the early 1980's, the usage of thermoplastic, low smoke, zero halogen, fire retardant cable compounds has steadily increased as specifiers around the world have sought to improve the performance of cables in fire. Initially, such zero halogen, low smoke, fire retardant cables were used solely for indoor applications, although in recent years there have been increasing enquiries for materials with improved UV stability. The reasons for these enquiries appear to relate to the installation of cables into a given system.

Once a design engineer or specifier has decided to install low smoke, zero halogen, fire retardant cables in an indoor environment, then it is common to find that the services which need to be installed (either power or telecommunication) must be connected to supplies external to the building. The decision must then be taken either to terminate the interior cables outdoors; or bring into the building, cables primarily designed for use outdoors and which

may compromise the low smoke, zero halogen interior cables.

This latter case is clearly undesirable since the properties of the internal wiring should not be compromised, but it is essential that the zero halogen, low smoke cables have sufficient stability to withstand the rigours of external exposure.

2.0 APPARATUS AND METHODS

2.1 Apparatus

The apparatus used in this work was a QUV cabinet¹, using both UVA² and UVB³ tubes.

2.2 Methods

TEST PROTOCOL 1 - UVA Exposure

Exposure Cycle :	lamps on	24 hours per day
	lamps off	0 hours per day
cabinet temperature during		60°C
UVA exposure		
condensation cycle		none
Total exposure time		1008 hours

This exposure protocol was selected since it had been previously reported that it gave good correlation with the French SEPAP apparatus⁹. The spectral distribution of the lamps used in this procedure give a close match to the UV spectrum of natural sunlight⁷.

TEST PROTOCOL 2 - UVB Exposure

Exposure Cycle :	lamps on	8 hours	per 12 hours
	lamps off	4 hours	per 12 hours
cabinet temperature during	60°C		
UVB exposure			
condensation cycle	4 hours	whilst lamps	off
cabinet temperature during	40°C		
condensation cycle			
Total exposure time	1008 hours		

This exposure protocol was selected as one which was in common usage in the industry. The lamps used provide a spectrum with a higher content of shorter wavelength UV radiation than found in

	COLOUR	UV STABILISER
STANDARD GRADE	NATURAL	NONE
STANDARD GRADE	NATURAL	UV1
STANDARD GRADE	NATURAL	UV2
STANDARD GRADE	BLACK	0.8% BLACK(STANDARD)
STANDARD GRADE	BLACK	0.8% BLACK + UV1
STANDARD GRADE	BLACK	2.5% BLACK

Figure 1

SUMMARY OF MATERIAL SELECTION

natural sunlight ⁷. The method is ASTM G53:1989 and the conditions listed above.

2.3 Sample Preparation

The standard commercially available grades ⁸ were used as received without any pretreatment. The experimental compounds were prepared using conventional laboratory mixing and pelletising equipment. For Tensile and Elongation dumbbells, specimens were taken from extruded sheaths. Oxygen Index and Hardness Determination were performed on several plaques.

3.0 RESULTS

The results prior to exposure are presented in Figure 2. For the purposes of this study, the change in properties upon UV irradiation have been evaluated (ie no change=100% retention of properties).

3.1 Changes in Tensile Strength

Figure 3 and Figure 4 show the changes in tensile strength of compound S300 and its various stabilised variants, with exposure to UVA and UVB radiation respectively. Figures 5 and 6 show similar data for LDPE and PVC. The apparently worse results obtained from the UVA exposures are ascribed to the greater intensity and overall UV dose obtained from exposure protocol 1. The standard natural grade provides the poorest results in both exposure protocols, followed by the natural grade stabilised with UV1. The remaining compounds do not provide much discrimination between individual variants. All of the latter materials show excellent retention of tensile strength, similar to those of LDPE and PVC.

The results for compounds S330, S500, and S550 are similar to those obtained for compound S300, and lead to the same conclusions ¹¹, thus demonstrating that the UV1, UV2 and carbon black stabilisation systems provide corresponding

	UV STABILISER	TENSILE STRENGTH MPa	ELONGATION (%)	OXYGEN INDEX	HARDNESS (Shore D)
S300 NATURAL		17.08	140	40	58
S300 NATURAL	UV 1	16.54	162	40	55
S300 NATURAL	UV 2	15.46	178	38	53
S300 BLACK	0.8% BLACK	17.56	140	39	58
S300 BLACK	0.8% BLACK + UV1	14.93	168	41	54
S300 BLACK	2.5% BLACK	16.13	148	38	56
S500 NATURAL		14.02	192	35	54
S500 NATURAL	UV 1	13.41	232	35	52
S500 NATURAL	UV 2	13.36	240	33	51
S500 BLACK	0.8% BLACK	14.96	208	34	54
S500 BLACK	0.8% BLACK + UV1	14.48	208	34	52
S500 BLACK	2.5% BLACK	15.28	194	32	53
S550 NATURAL		15.65	176	39	54
S550 NATURAL	UV 1	14.82	192	39	53
S550 NATURAL	UV 2	14.67	252	37	51
S550 BLACK	0.8% BLACK	15.48	185	39	55
S550 BLACK	0.8% BLACK + UV1	14.52	220	39	53
S550 BLACK	2.5% BLACK	15.04	184	36	55
S330 NATURAL		15.77	144	40	53
S330 NATURAL	UV 1	14.59	172	40	51
S330 NATURAL	UV 2	13.01	236	38	49
S330 BLACK	0.8% BLACK	15.48	164	39	53
S330 BLACK	0.8% BLACK + UV1	15.72	168	40	51
S330 BLACK	2.5% BLACK	16.49	154	37	52
LDPE BLACK	2.5% BLACK	15.67	680	17	47
PVC BLACK		14.96	226	26	39

Figure 2

PROPERTIES PRIOR TO EXPOSURE

protection to all of the products of the same generic class.

3.2 Changes in Elongation

Figures 7,8,9 and 10 present the results of changes in elongation following UVA or UVB exposure of compound S300 and its various stabilised variants along with those of LDPE and PVC. Again the standard natural product displays the poorest results followed by those of the natural compound stabilised with UV1. The standard black compound (ie 0.8%w/w carbon black) gives some improvement and the standard black compound containing UV1 showed almost the same performance, thus demonstrating the ineffectiveness of UV1 in black compounds.

The best results were obtained from compounds containing the higher level of carbon black (ie 2.5%w/w) or from the natural compound stabilised with UV2.

3.3 Changes in Oxygen Index

In all of the experiments conducted in this study, the oxygen index results were virtually unchanged throughout the exposure period. Figure 11 shows a typical result for compound S500 ¹¹.

3.4 Changes in Hardness

Again, in all of the current work, it was found that there was almost no measurable change in

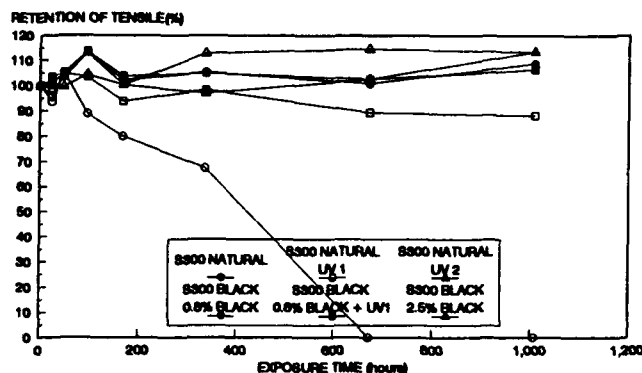


Figure 3 RETENTION OF TENSILE STRENGTH AFTER UVA EXPOSURE

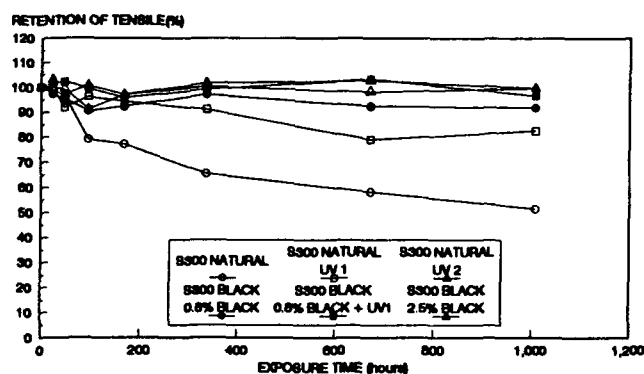


Figure 4 RETENTION OF TENSILE STRENGTH AFTER UVB EXPOSURE

Shore D hardness throughout the exposure period. Figure 12 shows a typical result for compound S550 11.

3.5 Changes in Appearance

3.5.1 Black Compounds

There was no visible change to the surface of the LDPE samples in the above work. The PVC sample however, showed a considerable change leading to a dull matt surface, with no cracks visible to the naked eye. Despite this cosmetic change, the PVC compound showed excellent retention of properties upon exposure.

The black versions of the zero halogen, low smoke, fire retardant compounds showed little visible change to surface appearance throughout the exposure period.

3.5.2 Natural Compounds

The standard compounds without any additional UV stabiliser all showed poor retention of mechanical properties, and these changes were also manifest in the form of surface crazing clearly visible to the naked eye. This surface crazing was accompanied by a bleaching of the surface, which had become dull and matt after

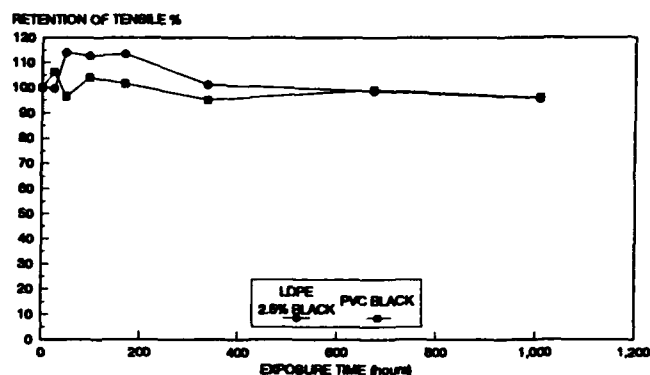


Figure 5 RETENTION OF TENSILE STRENGTH AFTER UVA EXPOSURE

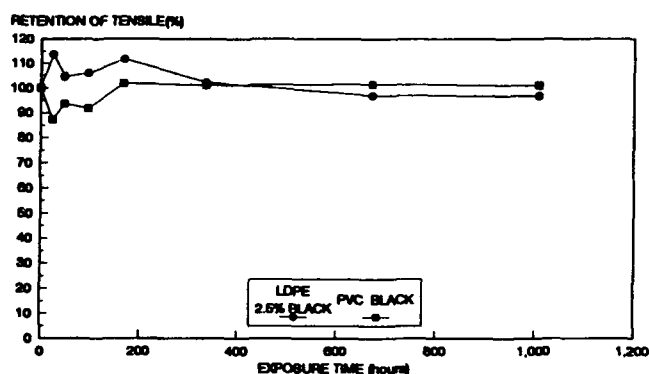


Figure 6 RETENTION OF TENSILE STRENGTH AFTER UVB EXPOSURE

1200 hours exposure.

The natural compounds stabilised with UV1 showed no crazing visible to the naked eye, although after approximately 700 hours exposure the surface started to become matt. This matt effect was worsened after 1200 hours exposure, but there was still no crazing visible to the naked eye.

The natural compounds stabilised with UV2 showed no signs of crazing after 1200 hours exposure, although by this time a very slight yellowing of the surface was observed. Additionally, the surface possessed a very slight matt finish.

4.0 CONCLUSIONS

4.1 Black Compounds

4.1.1

As with other polymer systems, zero halogen, low smoke, fire retardant cable compounds can be stabilised against the effects of UV radiation by the addition of small amounts of carbon black. This conclusion comes as no surprise, but serves to confirm that the highly filled zero halogen, low smoke, fire retardant compounds behave in a similar manner to other polyolefins which have been well documented, and for which there is much experience of use in practice.

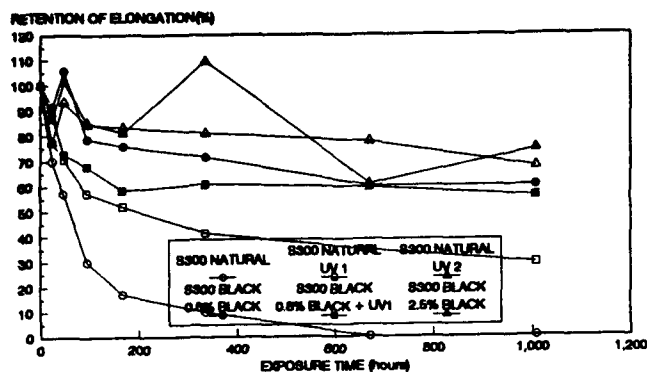


Figure 7 RETENTION OF ELONGATION AFTER UVA EXPOSURE

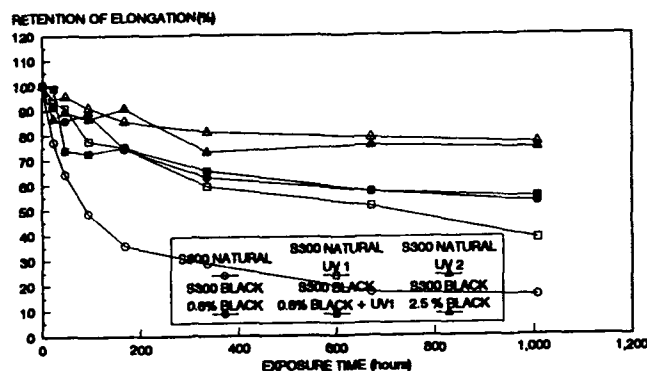


Figure 8 RETENTION OF ELONGATION AFTER UVB EXPOSURE

4.1.2

Increasing the level of carbon black from 0.8% w/w to 2.5% w/w provides additional stabilisation, although in this work, the improvements were relatively small.

4.1.3

The addition of a proprietary non-black UV stabiliser (ie UV1) to a black formulation provides little additional benefit.

4.2 Non-Black Compounds

4.2.1

The natural coloured standard zero halogen, low smoke, fire retardant compounds have been developed primarily for use in indoor or underground applications where UV stability is not particularly important. The retention of mechanical properties and cosmetic appearance is inferior to the equivalent black compounds.

4.2.2

The use of a proprietary UV stabilisation system brought some additional benefits but the resulting compounds were still not as effective as those containing relatively small amounts of carbon black.

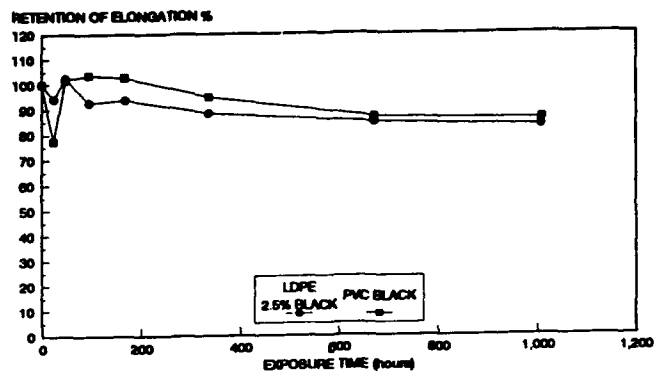


Figure 9 RETENTION OF ELONGATION AFTER UVA EXPOSURE

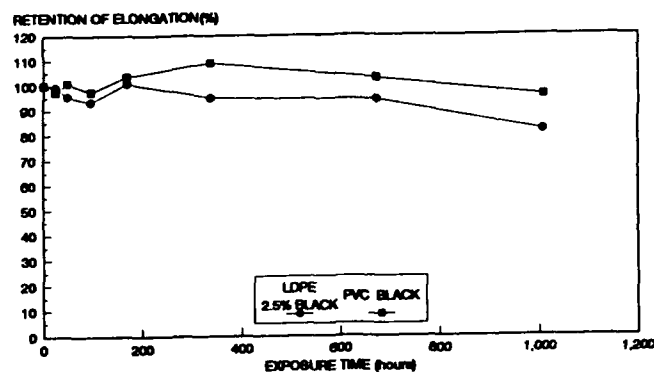


Figure 10 RETENTION OF ELONGATION AFTER UVB EXPOSURE

4.2.3

The addition of a specially developed stabilisation system enables excellent UV stability to be achieved. In this current work, the performance of this new stabiliser system gives similar performance to the corresponding black compounds. Indeed the performance is similar to that of the black LDPE and black PVC materials, which are widely accepted as suitable for use outdoors.

4.2.4

The new optimised UV stabilisation system was effective in all of the compounds tested. The Authors believe that this system will be effective in other compounds of the same generic type.

4.3 General Observations

4.3.1

Despite the differing exposure protocols, the ranking order of stabiliser systems was largely the same in both the UVA and UVB exposure protocols.

4.3.2

The effects on mechanical properties in the UVA exposure protocol appear to be more severe than

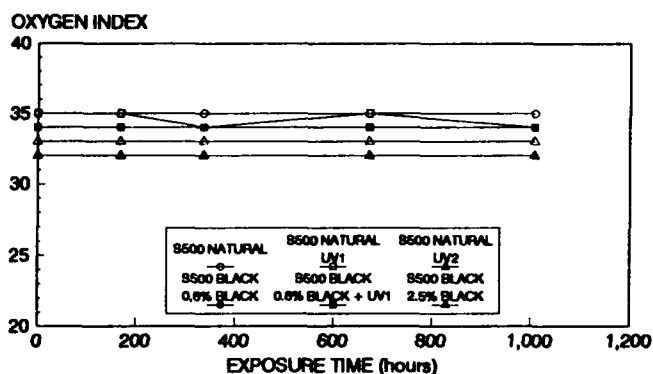


Figure 11 VARIATION OF OXYGEN INDEX AFTER UVB EXPOSURE

that of the UVB protocol. The Authors believe that this is due to the increased intensity and total dose achieved during the UVA exposure.

4.3.3

Neither of the two exposure protocols had any measurable effect on the retention of either oxygen index or Shore D hardness.

5.0 REFERENCES

1. Q.U.V. Accelerated Weathering Tester available from:
The Q-Panel Company
26200 First St
Cleveland
Ohio 44145
USA
Tel : (216) 835 8700
Fax : (216) 835 8738
2. UVA 340 tubes; spectrum 400nm - 315nm; peak emission at 340nm; peak irradiance of 0.75 W/m²/nm at 340nm
3. UVB 313 tubes; spectrum 360nm - 280nm; peak emission at 313nm; peak irradiance of 0.70 W/m²/nm at 313nm
4. Processing Conditions were taken from the published technical data on MEGOLON compounds published by Lindsay and Williams Ltd.
5. BS6469 : 1992 - common test methods for insulating and sheathing materials of electric cables, Part 1, Section 1.1.
6. (i) BS2782 : Part 1, method 141/IV/B : 1986 - methods of testing plastics - determination of flammability by Oxygen Index.
(ii) ASTM D2240-86, standard test method for rubber property - Durometer hardness. Test type D/15.

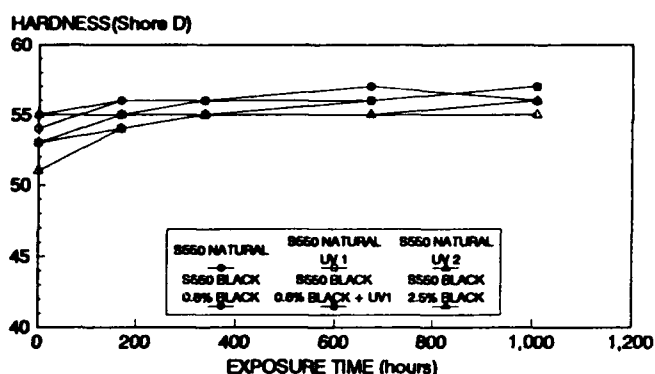


Figure 12 VARIATION OF SHORE D HARDNESS AFTER UVB EXPOSURE

7. Q.U.V. Product Literature, Bulletin L-816, Q-Panel Co. 1
8. Grades S300, S500, S550, and S330 from the MEGOLON range available from Lindsay & Williams Ltd.
9. Wire Industry, January 1993, p35. Developments in fire retardant compounds, J Preston, D N Sawyer, Dr J A Taylor.
10. (i) BS6234 : 1987 - polyethylene insulation and sheath of electric cables.
(ii) BS6746 : 1990 - PVC insulation and sheath of electric cables.
11. In the interest of brevity, not all of the data generated in this study has been reproduced in full detail. The Authors would be pleased to supply full details of all of the data upon request (Contact: Marketing Dept, Lindsay & Williams Ltd, Columbine St., Manchester M11 2LH, UK: tel (+44) 61 320 3636, UK fax (+44) 61 335 0104).



Dudley Sawyer joined Lindsay & Williams Ltd in January 1991 to work on the development of new zero-halogen, flame-retardant extrusion compounds for the electrical cable industry. He gained BSc (Hons) in Chemistry at the University of Manchester and he has extensive experience of the cable industry having previously spent 21 years with BICC Cables from 1969 - 1990, progressing from Assistant Chemist in the Wire and General Cables Division to Senior Materials Technologist.



Lai Ping Cheng studied 'A' levels in both mathematics and chemistry at Central Manchester Colleges prior to joining Lindsay & Williams Ltd in 1990 as a Quality Control Inspector for the Megolon range of compounds. In 1991 she transferred to the development section where she has been instrumental to the development of the latest

Megolon range of low smoke, halogen free, fire retardant compounds. Recently qualified to BTEC ONC in Polymer and Technology she is continuing her studies at Manchester Metropolitan University with a view to attaining BSC(Hons).



Jack Taylor began his working life as a Laboratory Technician examining fibre-reinforced polymers. He gained his BSC (Hons) and PhD degrees in chemistry at the University of Salford, subsequently joining Akzo Chemie UK where he worked on the synthesis of novel halogenated flame-retardants and evaluation of

PVC stabiliser systems. Dr Taylor was Product Manager for the Megolon range of halogen-free, fire-retardant cable compounds until 1988 when he was appointed Sales Manager for all of Lindsay & Williams cable products, which in addition to the Megolon range include semi-conductive cable tapes, insulating cable tapes and an extensive range of self-amalgamating tapes and putty's.



Joe Preston joined Lindsay & Williams Ltd in 1970 as a Laboratory Assistant following 2½ years experience in the Plastics Industry. He studied chemistry at the North Trafford College of Technology. In 1977 he became responsible for the Quality Control function at Lindsay & Williams. He transferred his efforts in

1982 to Development, working on specialised cable tapes, and in more recent years, the Megolon range of low-smoke, halogen-free, fire-retardant compounds. In 1991 he was appointed Technical Manager of Lindsay & Williams, responsible for all development and quality control functions.

Multicomponent Quantitative Determination of Two Antioxidants in ETPR Cable Filling Compound Using Factor Analysis Based on Fourier Transform-Infrared (FTIR) Spectroscopy and the Correlation of Antioxidant Concentrations to the Oxidation Induction Time (OIT).

W. J. Thalman, A. Debska, A. Eckard, J. A. Weaver

Witco Corporation, Petroleum Specialties Group, 100 Bauer Drive, Oakland, NJ 07436

ABSTRACT

An FTIR method has been developed to determine the presence and to quantify the concentration of two antioxidants in Extended Thermoplastic Rubber (ETPR) Cable Filling Compounds. The antioxidants are AO₁ (thiodiethylenebis(3,5-di-tert-butyl-4-hydroxyhydrocinnamate)) and AO₂ (tetrakis(methylene(3,5-di-tert-butyl-4-hydroxyhydrocinnamate))methane). This method will monitor the presence and quantify the individual concentrations of AO₁ and AO₂ individually or as a binary antioxidant system. The method that was developed is based on multicomponent quantitative factor analysis, using a partial least squares (PLS-1) technique. The experiment was designed and the calibration samples prepared according to statistically acceptable methods. FTIR spectra of all calibration samples were collected and a calibration was developed according to the PLS-1 algorithm.

To gain an understanding of the performance of a binary antioxidant system in an ETPR cable filling compound, the oxidative stabilities of prepared samples were measured. Using Differential Scanning Calorimetry (DSC), the Oxidation Induction Time (OIT) was measured and correlated to the two antioxidant concentrations. Surface and contour plots were developed and trends were observed.

INTRODUCTION

A concern to the cable industry is the premature degradation of cable insulation under conditions of accelerated aging in the laboratory. A scenario voiced by the cable industry suggests that the antioxidant contained in the cable insulation migrates out of the insulation and into the cable filler causing insulation failure. A difficulty in testing this hypothesis is that current quantitative methods cannot fully differentiate between the two similar antioxidants (AO₁ and AO₂) that make up this cable insulation/cable filler system. A more precise determination of each of these antioxidants may allow the optimization of Cable Filler performance for this system.

The presence of any migration effects in the cable filler/cable insulation system may be due in part to the

concentration gradient and distribution that exists between antioxidants AO₁ and AO₂ due to their separation in the cable filler/cable insulation system. This effect may be avoided if the concentration gradient is minimized through the use of a binary antioxidant system in the cable filling compound. A quantitative FTIR method which readily determines the presence and concentration of each antioxidant in the cable filling material is proving to be a valuable tool in studying the performance of a cable filling compound containing a binary antioxidant system.

PROCEDURE

FTIR Sample Preparation, Instrument Settings and Analytical Software

Cable filler sample preparation for analysis by FTIR as well as the FTIR instrument settings have already been published¹. The analytical software used for the calculation of the PLS-1 algorithm is a standard, well known scientific applications software package².

OIT Sample Preparation and Instrument Settings

The DSC instrument settings and modified ASTM D3895-80 procedure have previously been published¹.

DISCUSSION AND RESULTS

Theory

The Partial Least Squares (PLS) method for performing quantitative analysis has been applied to spectroscopic data gathered from the FTIR analysis of cable filling compounds containing the two specified antioxidants. PLS is a spectral decomposition technique that creates a simplified representation of the data based on the average spectrum of the calibration spectra. Instead of being limited to a single unknown, a properly calibrated PLS analysis will accurately predict the quantities of multiple components of interest by analyzing an appropriate region of the spectrum of the unknown multicomponent sample. In an analogous fashion, the technique of using linear regression to determine the concentration of a single pure component is done by correlating the area of a single spectroscopic peak to known concentration calibration standards in order to determine an unknown concentration. In PLS this is done by making calibration standards reflect the compositions of all the unknowns and by having them span the same expected range of concentrations and compositions as the unknowns. The spectra of the standards are measured, and a PLS calibration set of equations are generated.

These equations are then used to predict the concentration of the calibrated components in each unknown sample.

Calibration Standards

To produce an adequate set of calibration standards which contain the necessary mixtures that span the range of concentrations and also to avoid any inadvertent calibration mixtures where the concentrations of the components are collinear, an experimental design software applications package was used to aid in the selection of the mixtures for the cable filler calibration standards³.

Spectral Regions Used For PLS Analysis

To simplify the spectral decomposition process, the entire spectrum is normally not selected for PLS analysis. Only selected regions having spectral information corresponding to the components of interest are used. The antioxidants AO₁ and AO₂ both have carbonyl and hydroxyl functional groups, and AO₂ also has the additional feature of having a thio group. FTIR analysis of the pure antioxidants suggested two regions of obvious correlation: 3700 to 3550 cm⁻¹ and 1800 to 1560 cm⁻¹. Both these selected regions were used for the PLS analysis; all other regions were ignored. Part of the second region selected is examined in Figure 1. This figure shows a spectral overlay of the carbonyl region of three samples. The peak at 1747.4 cm⁻¹ is the spectrum of a sample containing 0.6 weight% AO₂ in ETPR cable filler. The peak at 1743.6 cm⁻¹ is the spectrum of a sample containing 0.6 weight% AO₁ in ETPR cable filler. And, the peak at 1744.5 cm⁻¹ is the spectrum of a sample containing both 0.6 weight% AO₁ and 0.6 weight% AO₂ in ETPR cable filler. It can be seen from Figure 1 that the sample containing both antioxidants appears as a single, overlapping peak. The carbonyl functional group from AO₁ and AO₂ both appear in the same region of the spectrum. The same condition of peak overlap can be

found for the hydroxyl functional group for these two antioxidants. This condition of peak overlap disallows the straightforward use of a single peak area to correlate to antioxidant concentration. The Partial Least Squares technique solves this dilemma by associating several regions of the spectrum to the unknown, rather than the area from a single peak.

Accuracy Of The PLS Analysis

To determine the accuracy of the PLS calibration equations produced from analysis of the standards, a series of prepared samples were made. These samples contained various concentrations of either or both antioxidants AO₁ and AO₂ in the range of 0.0 to 1.2 weight% AO₁ and 0.0 to 0.6 weight% AO₂ in Cable Filler base material. These prepared samples were analyzed via the PLS method using two spectral regions for correlation and 5 factors (loading vectors) to model the data. The average difference between the known antioxidant concentrations and the concentrations predicted by this PLS model is 0.012 weight% for predicting AO₁ and 0.006 weight% for predicting AO₂ in the range studied. Statistical analysis of the data gathered from the prepared samples, indicate the predictive powers of this calibration have a correlation coefficient of 0.999. The confidence that a value predicted by this calibration truly corresponds to the actual concentration is given by an F-value close to 13,000. Based on the number of degrees of freedom, there is a greater than 99% probability that the calibration accurately represents the data.

Figure 2 shows the 99% confidence limits bounding the regression line representing the Actual vs Predicted values of the concentration of AO₁ in cable filler base material containing both AO₁ and AO₂. This graph demonstrates how well the PLS calibration predicts the true antioxidant concentrations of an unknown sample. The center line is

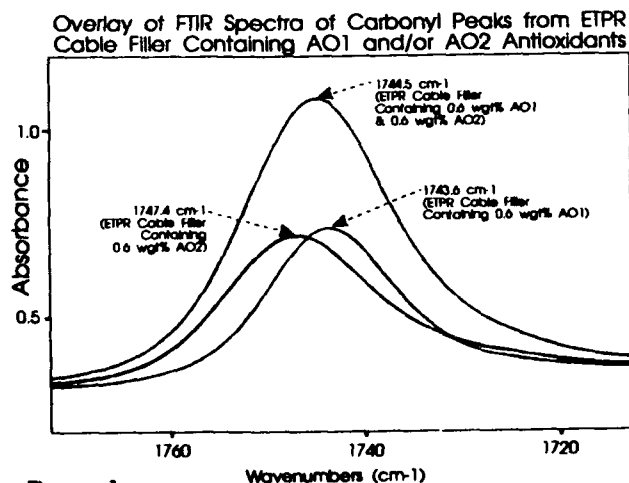


Figure 1

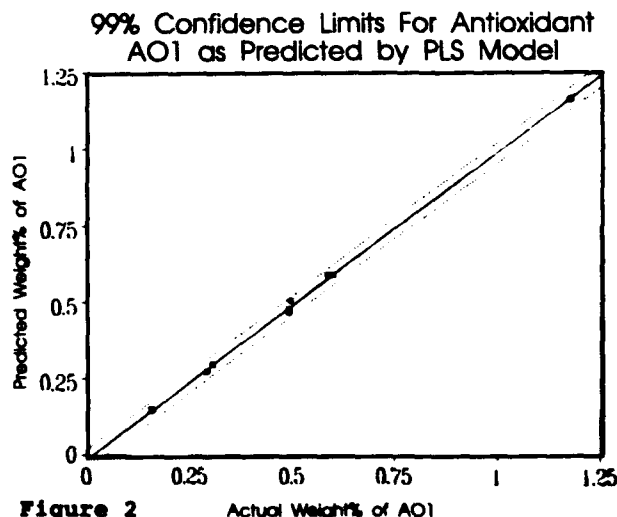


Figure 2

the data regression line, and the two curves bounding that regression line are the confidence limits. Based on this data, there is a 99% assurance that the actual concentration of antioxidant is within the two confidence curves and that the calibration is less than 1% in error for predicting the true value of an unknown. Since the 99% confidence limits for the intercept bound zero, and the 99% confidence limits for the slope bound 1, the PLS calibration does not seem to have any slope or zero-intercept bias. A similar representation was made for AO_2 , with a similar correlation for the actual to predicted values.

Antioxidant Concentrations vs OIT

The optimization of a cable filling compound to minimize the concentration gradients and redistribution of antioxidants in the cable insulation/cable filler system, necessitates the determination of the performance of the binary antioxidant cable filling compound. To this end, a correlation of the two antioxidant concentrations to the performance of the cable filler material, as determined by its oxidation induction time, was developed. From this data, a model was developed that gave predictions of the OIT from the binary antioxidant concentrations, and was comparable to the experimental error of the data. The data was modeled to a quadratic function for mixtures^{3,4}, and had a correlation coefficient of 0.981. The model had an F-ratio of 195 which is a greater than a 99% probability that the model accurately represents the data. The model passed all of the tests for a statistically valid representation of the data³.

Figure 3 is a quadratic surface plot and data points of the two antioxidant concentrations, AO_1 and AO_2 vs. the oxidation induction time. It can be seen that the quadratic surface closely conforms to the data points (the small circles on the surface plot in Figure 3). The surface model

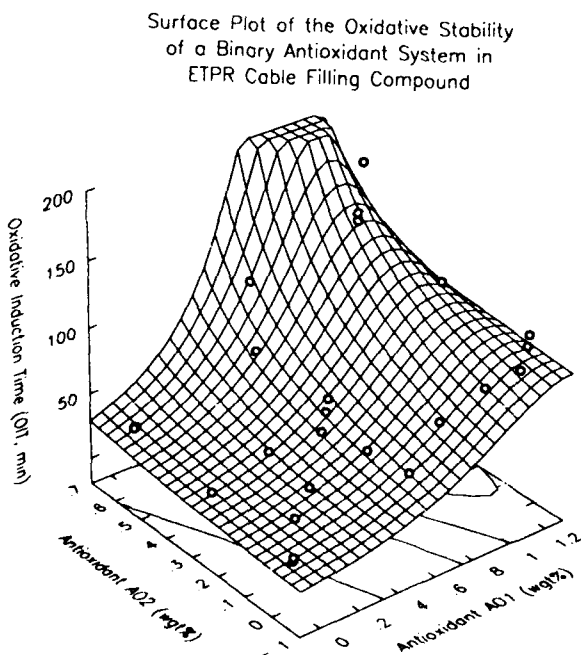


Figure 3

is a better representation than individual data points because it allows conclusions to be more generally applicable since the surface tends to smooth out individual variations of data. The surface displayed in Figure 3 assists in identifying trends in the relationship between the binary antioxidant system and cable filler performance. From this surface model, other more informative plots can be produced. It should be noted that the surface is drawn beyond the data points, so that the area greater than 1.2 weight% AO_1 is beyond the data set and represents an extrapolation of the surface function. The use of data from the extrapolated section of the surface function may not yield valid information. Looking at the surface plot of Figure 3, one can see portions of the contour lines lying under the surface between the two antioxidant axes. A better representation of the contour lines are given in the plot shown in Figure 4. This plot shows the trend for cable filler performance, based on OIT, for a given AO_1 and/or AO_2

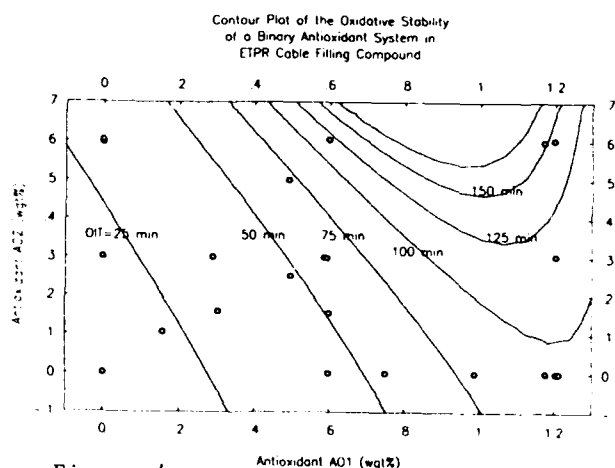


Figure 4

concentration. Please note that the borders of the contour map are not zero. For the contour line corresponding to an OIT of 25 minutes, AO_1 alone, at a concentration of approximately 0.28 weight% in ETPR cable filler gives a performance equivalent to AO_2 alone, at a concentration of approximately 0.42 weight%. Various combinations of the two antioxidants can be determined along the contour lines. This demonstrates that for the same resulting OIT, AO_1 is a more effective antioxidant at concentrations up to approximately 0.7 weight%. A comparison cannot be extended to higher levels because the concentration effects for antioxidant AO_2 were not studied above 0.6 weight%. Analysis of the data at the limits of the study indicate that the effectiveness of the individual antioxidants, AO_1 and AO_2 , in a binary system may vary with concentration and proportion. Further study is warranted.

CONCLUSIONS

An FTIR spectroscopic method has been developed that directly quantifies the individual antioxidant concentrations of a binary antioxidant system in ETPR cable filling compound. This is achieved through the use of a partial least squares technique based on multicomponent quantitative factor analysis.

The repeatability and accuracy of this PLS method is satisfactory for the concentration of AO_1 in the range of 0.0 to 1.2 weight%, and the concentration of AO_2 in the range of 0.0 to 0.6 weight%.

The binary antioxidant concentrations have been correlated to the Oxidation Induction Time (OIT) of the cable filler. From this data, surface and contour plots were developed that compare the effectiveness of the antioxidants AO_1 and AO_2 to the cable filler's performance.

FUTURE WORK

Future work will utilize this PLS-FTIR technique to focus on migration of antioxidants into and out of filling compounds and the effects of various antioxidant combinations on the performance of the cable filling compound as reflected by OIT measurement.

ACKNOWLEDGEMENTS

We would like to thank T. Roessing of our plant facilities for all his help in providing Cable Filler materials, and R. Morawek, T. Roessing, and A. Banaszewski for their suggestions regarding the manuscript.

REFERENCES

- 1.) W.J.Thalman, A.Eckard, A.Debska, "Quantitative Determination of a Thioester Antioxidant in Cable Filling Compounds based on Fourier Transform-Infrared Spectroscopy and Correlation to Oxidation Induction Time," Proceedings of the 41st International Wire And Cable Symposium (IWCS), 548 (1992).
- 2.) Galactic Industries Corp, Spectra Calc Software, PLSplus Chapter, (1991).
- 3.) Stat-Ease Inc., Design Expert Software Ver 3.01, (1992).
- 4.) StatSoft Inc., CSS:Statistica Software , Volumes I, II, & III, (1991)



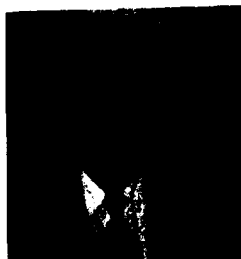
William J. Thalman has received his Masters degree in Chemistry from Montclair State College and is nearing completion of his Ph.D. degree in Physical Chemistry at Rutgers University. Mr. Thalman has been involved in the pilot development of hydrogenation and sulfonation technologies and is currently investigating methods to improve Cable Filler performance. He is employed as a Chemist for the Petroleum Specialties Group of Witco Corporation at their research center in Oakland, NJ.



Dr. Anna Debska-Chwaja has received Masters degrees in Chemical Engineering and Petroleum Technology and a Ph.D. degree in Petroleum Engineering. She was trained and has worked in Poland, Romania, Italy, and France. She is a member of ACS and STLE and is currently employed by the Petroleum Specialties Group of Witco Corporation as a Research Scientist specializing in solid hydrocarbons, lubricants, tribology, and cable fillers. Dr. Debska is the author of 30 publications and 5 patents.



Dr. Alan D. Eckard has received his B.S. degree from Rensselaer Polytechnic Institute and his Ph.D. in Physical Chemistry from the University of Toronto. Dr. Eckard has been involved in development and application of industrial lubricants, coatings and surface treatment chemicals with several international manufacturers of these products for the past 19 years. He is currently Director of Research and Development for the Petroleum Specialties Group of Witco Corporation at their research center in Oakland, NJ.



Joseph A. Weaver, Jr. has received his B.S. degree in Chemistry from Pennsylvania State University in 1972. Mr. Weaver is a member of ASTM and ACS. He has been involved in sulfonation and overbased sulfonates technology and currently formulates soluble cutting oils using statistical experiment designs. He has been employed as a Chemist for the Petroleum Specialties Group of Witco Corporation for 20 years.

EFFECT OF ENVIRONMENTAL AGING ON OPTICAL FIBER COLOR CODINGS

James R. Petisce, Michael D. Kinard, Shahab Siddiqui, and Carl Taylor

AT&T Bell Laboratories Norcross, Georgia 30071

Abstract

Optical fibers are identified from one another in a cabled assembly by the use of a color coding layer on the coated optical fiber. Color codings must conform to color standards listed in the Telecommunications Industry Association (TIA) Standard 598. Today's evolving telecommunications and CATV applications for optical fibers are demanding higher performance in color retention properties of optical fiber color codings. These demands prompted us to develop the use of electronic colorimeters to quantitatively measure changes in color codings after exposure to simulated oxidative and hydrolytic environments expected to be encountered in the above-ground outside plant.

Background

As shown in a Munsell color standard chart from EIA Standard 598 (Figure 1), a color is clearly defined within ranges about a center or centroid value.

The CIELAB tristimulus coordinate system was used to quantitatively characterize the acceptable limits of each color. In this coordinate system, the L value represents the mathematical approximation of the non-linear black-white response of the human eye. A perfect white has an L value of 100, while a perfect black has a value of zero. The quantities "a" and "b", called opponent coordinates, define the degree of yellowness (positive b), redness (positive a), greenness (negative a), and blueness (negative b). The opponent type coordinates are both zero for the neutral colors of white, black, and gray. As the absolute value of the "a" or "b" value rises, the color becomes more intense.

The L, "a", and "b" values for all color chip standards for a specified color were measured using a Macbeth 1500/Plus Color Measuring System. A C illuminant and 2 degree viewing angle were used in all measurements. The colorimeter was calibrated using a Macbeth white reference standard. Centroid ("nominal"), maximum,

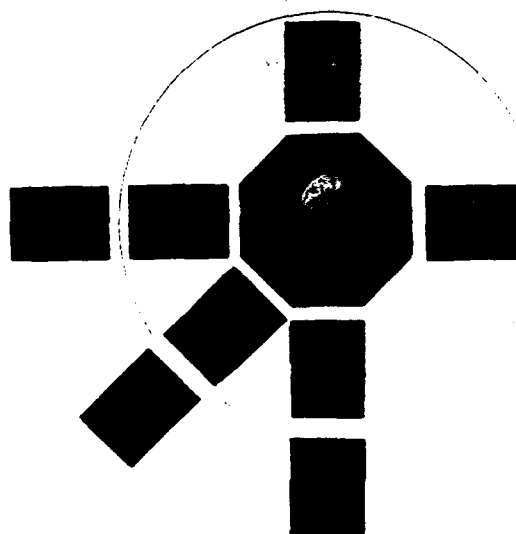


Figure 1.

and minimum values for each color coordinate were obtained.

Experimental

The hydrolytic stability of two color coding systems, #1 and #2, was evaluated by measuring their color on fiber after 35 day exposure to 95°C/95% relative humidity in a controlled environmental chamber. The coating systems on sample fibers under color coding systems #1 and #2 were different. CIELAB color coordinates were measured in-situ using a Minolta CR 241 Chroma Meter. A C illuminant and 2 degree viewing angle were used in all measurements. The colorimeter was calibrated using a Minolta white reference standard. Four measurements, at 90 degree intervals, around the fiber were taken for each color coded fiber. Color coordinates are reported as averages.

The hydrolytic stability of selected colors from develop-

mental color coding system #3 was evaluated on color coded fibers after exposure to 95°C/95% relative humidity for 10, 30, and 40 days. The oxidative stability of selected colors from developmental color coding system #3 was evaluated on color coded fibers after exposure to 125 C in a forced air oven for 10, 30, and 40 days. CIELAB color coordinates were measured on aged and unaged color coded fibers using the Minolta colorimeter as described above.

Evaluation of aqua and rose color coded fibers from color coding systems #1, #2, and #3 was not performed because EIA standards for these colors are currently being redefined.

Results and Discussion

1. Color Coordinates of Aged Fibers

Graphical analysis of color coordinates measured in-situ on aged fibers affords a rapid method to interpret these data for each color. As an example, analysis of the blue color coded fibers is presented.

As shown in Figure 2, the blue color coded fibers from Color Systems #1 and #2 after 35 days at 95°C/95% relative humidity have L values which are within the allowable color space.

In contrast, the Color System #1 blue color coded fiber has an "a" value after aging which is below the minimum allowable value; whereas, the Color System #2 blue color coded fiber has an "a" value after aging which is within allowable color space (Figure 3).

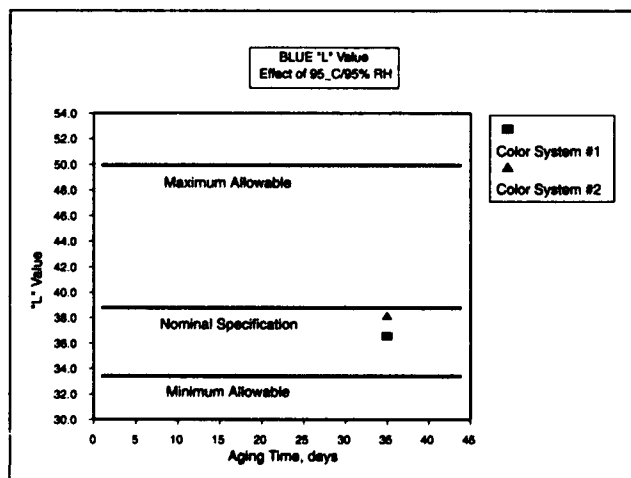


Figure 2.

As shown in Figure 4, the Color System #1 blue color coded fiber has a "b" value after aging which is much greater than the maximum allowable level; whereas, the Color System #2 blue color coded fiber has a "b" value after aging which is slightly above the the maximum allowable value.

These colorimeter data suggest that Color System #1 blue is fading (higher "b" value) and will appear greener (lower "a" value) than Color System #2 blue. Visual examination of these hydrolytically aged blue color coded fibers was consistent with the colorimeter data. (Contribution to color change due to possible fiber coating discoloration is not addressed in this study).² Since the colorimeter data were consistent with visual examination of these fibers, we extended this evaluation to the remaining nine colors (Table I).

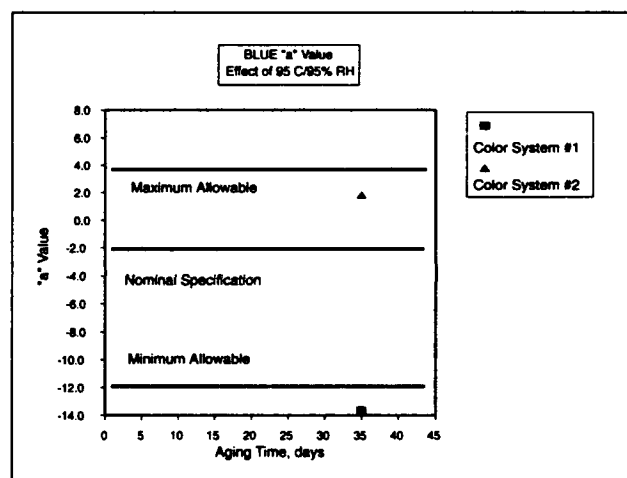


Figure 3.

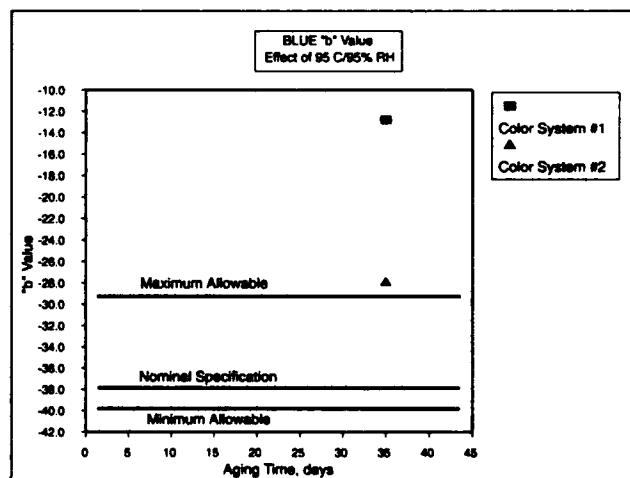


Figure 4.

Table I
Effect of Hydrolytic Aging
35 days 95°C/95%

	L	a	b	Visual Color
Blue #1	ok	low	high	green
Blue #2	ok	ok	high	light blue
Orange #1	ok	low	ok	rust
Orange #2	ok	ok	high	orange
Green #1	ok	ok	high	lime green
Green #2	high	ok	ok	green
Brown #1	ok	ok	high	dark rust
Brown #2	ok	low	ok	brown
Slate #1	low	ok	high	darker
Slate #2	ok	ok	ok	slate
White #1	low	ok	high	hazel
White #2	low	ok	ok	white
Red #1	ok	low	high	red
Red #2	ok	ok	ok	maroon
Black #1	ok	ok	high	black
Black #2	ok	ok	ok	black
Yellow #1	low	ok	ok	mustard
Yellow #2	low	ok	high	yellow
Violet #1	ok	low	high	darker
Violet #2	ok	ok	ok	violet

Presentation of colorimeter data for all ten colors and corresponding aged color coded fiber samples will be included in the poster presentation. This will allow the reader to compare colorimeter data of aged color coded fibers to aged fiber samples. This comparison will demonstrate the utility of colorimetry data in measuring color differences between color coded fibers.

2. Evaluation of Developmental Color Codings

The consistency between colorimeter data and visual examination of aged color coded fibers prompted us to explore the possibility of colorimeter use in color coding development.

Specifically, colorimeter sensitivity to detect minor changes in color coordinates after brief exposure to accelerated aging conditions could be a useful development tool to evaluate the environmental stability of candidate color codings.

The color coordinates of dual coated optical fibers color coded with developmental Color System #3 were measured in-situ with the Minolta colorimeter after 95°C/95% RH exposure. The L and "b" color coordinates of the yellow color coded fiber measured after 10, 30, and 40 day exposure times are presented in Figures 5 and 6, respectively.

The 10 day exposed sample displays lower L and "b" values than the unaged sample which indicates that the yellow color is beginning to darken and become less yellow after hydrolytic exposure. Data on the 30 and 40

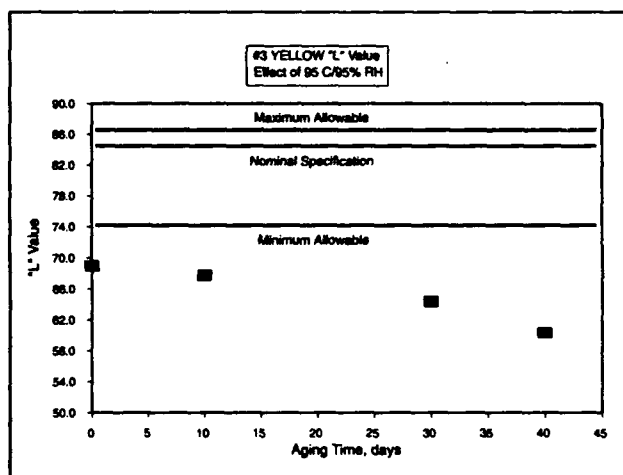


Figure 5.

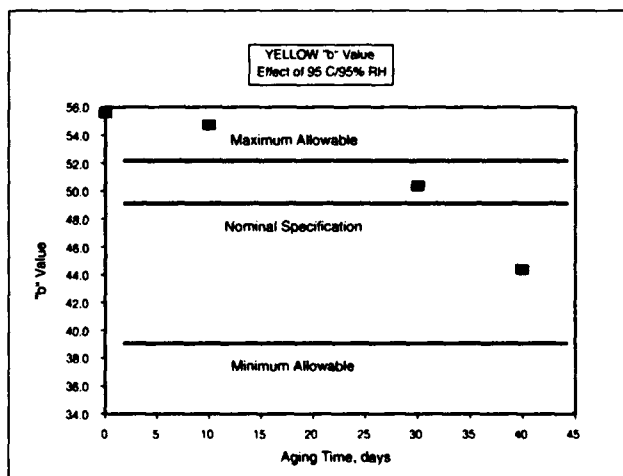


Figure 6.

day exposed samples indicate a continuation of this trend. The "a" value after aging was comparable to the unaged "a" value.

Visual examination of the 10 day aged Color System #3 yellow fiber show very little color change, but changes can be detected in the 30 and 40 day aged samples.

Table II Effect of 95 C/95% RH Aging				
	COLORIMETER		VISUAL	
	10 day	40 day	10 day	40 day
Yellow	darker fade	darker fade	NC	darker fade
Orange	darker	darker	NC	darker
Violet	darker fade	darker fade	fade	darker fade
NC = no change				

Similar analysis of aged violet and orange color coded fibers was performed (Table II).

As shown in Table II, color changes in fibers aged at 95°C/95% RH for 10 days are detectable by colorimetry, but not by visual examination. More importantly, the trends in color change as detected by colorimetry after 10 day aging were observed visually after 40 day aging.

The color coordinates were also measured in-situ after 125°C exposure. The L and "b" color coordinates of the yellow color coded fibers measured after 10, 30, and 40 day exposure times are presented in Figures 7 and 8, respectively.

These data show that after only 10 days at 125°C the yellow coded fibers are beginning to become darker and the yellow color is fading. Visual examination of the 10 day aged sample could not detect this change. Similarly, colorimetric analysis of the violet color coded fiber after 125°C exposure for 10 days detected changes which were not detectable visually.

Presentation of colorimeter data for all aged Color System #3 samples and corresponding aged color coded fiber samples will be included in the poster presentation.

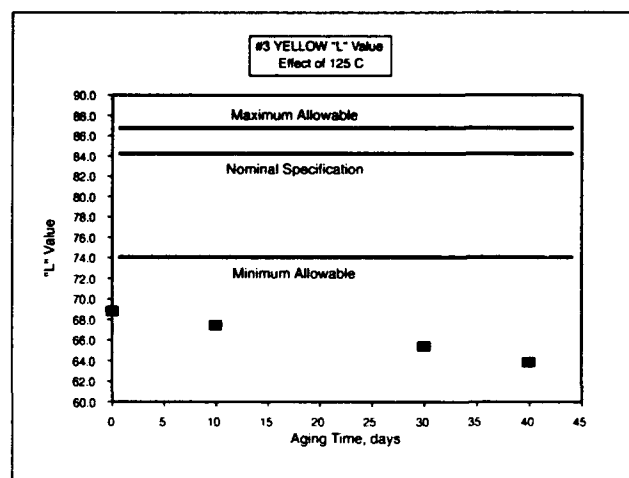


Figure 7.

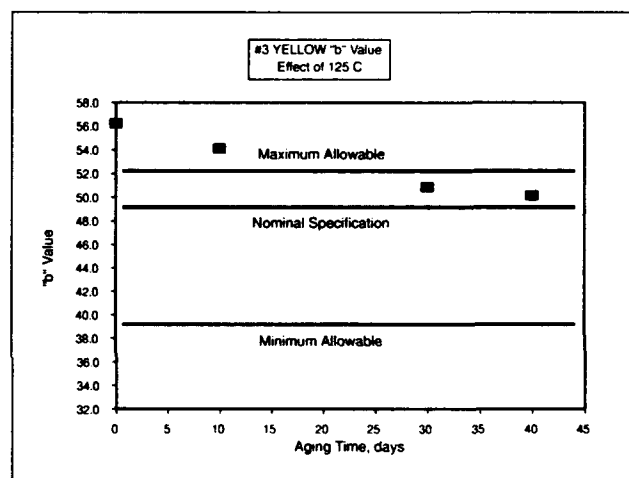


Figure 8.

This will demonstrate the utility of colorimetric measurements in predicting visual color changes after accelerated hydrolytic or oxidative aging conditions.

Conclusions

Visual examination of color coded fibers after environmental aging for short times does not provide sufficient sensitivity to predict gross color changes which do indeed occur after installation in the above-ground, outside plant. Utilization of electronic colorimeters affords sensitivity necessary to detect minor changes in color codings after accelerated aging. Electronic colorimetry used as an analytical tool to measure minor changes in color coordinates of optical fiber color codings has enabled us to predict the color retention capabilities of several color coding formulations after accelerated aging.

Acknowledgements

The authors thank Patsy M. Pruitt, Yvonne Washington, Brian Dritschler, and Andrea Cicilia for colorimeter measurements and Jim True for layout of this manuscript for publication.

References

1. Billmeyer, F.W., Saltzman, M.; "Principles of Color Technology," 2nd Edition, John Wiley, New York, 1981, pp. 28-66.
2. Chandan, H. C., Petisce, J. R., Shea, J. W., Taylor, C. R.; "Fiber Protective Coating Design for Evolving Telecommunication Applications," 41st IWCS, 1992, pp. 239-248.



James R. Petisce is a Member of Technical Staff in the Materials Engineering Department at AT&T Bell Laboratories in Norcross, Georgia. After receiving a BA/MA in Chemistry from Boston University in 1980, he received a Ph.D. in Organic Chemistry from Northwestern University (Evanston, IL.) in 1984. Since joining Bell

Laboratories in 1984, he has worked on the design and development of optical fiber coatings, bonded ribbon matrix materials, UV curable adhesives, index matching compounds, optical fiber color codings, and polyimide optical fiber coating. His present responsibilities include design and development of materials for optical fiber and cable.



Michael D. Kinard holds a BSME from Old Dominion University and an MSME from Georgia Institute of Technology. He joined AT&T in 1979 in Western Electric, working on the development of copper cables. He is now an Member of Technical Staff in AT&T Bell Labo-

ratories, Norcross, GA., involved in fiber optic cable development.



Shahab Siddiqui is a Member of Technical Staff in the Fiber Optics and Materials Development & Engineering Department at AT&T Bell Laboratories in Norcross, GA. After working in many areas of both basic and applied polymer chemistry in Bell Laboratories at Murray Hill, Princeton, and Richmond, he is currently re-

sponsible for the development of color codings for fiber optic applications at Norcross. Mr. Siddiqui received a Ph.D. in Organic Chemistry in 1982 from the University of Kentucky, Lexington and joined AT&T in 1984.



Carl R. Taylor is currently Supervisor of the Materials Technology and Quality Group at AT&T's main Fiber Optic Manufacturing site in Atlanta. The group has responsibility for the design and engineering of materials used in fiber optic cable and apparatus products as well as responsibility for the quality of all incoming materi-

als and components. He has previously been Supervisor of the Plastics Engineering and Characterization Group in Atlanta and Supervisor of the Polymer Materials Research Engineering Group at AT&T Bell Laboratories in Murray Hill, NJ. Prior to joining AT&T Bell Laboratories in 1977, he earned a B.S. in Chemistry from the College of Wooster in Ohio and a Ph.D. in Physical Chemistry from the University of Wisconsin in Madison. His graduate work focused on the physical and viscoelastic properties of polymers.

DEVELOPMENT OF ELECTRONIC WIRE HARNESS WITH LAMINATED FLEXIBLE FLAT CABLE

T.Yamamoto, T.Ohnuma, T.Enami, H.Yoshinaga, H.Komatsuda, C.Tracey

Fujikura Ltd.

ABSTRACT

In order to meet the various requirements for wiring in electronic equipment, such as video tape recorders, we were obliged to carry out wiring using harnesses consisting of individual cables in the past. We have investigated and developed a laminated flat cable that is composed of thin flat conductors and plastic tapes. We have also developed variations of this cable so as to meet our customer's requirements. By investigating these new cable variations, it has been recognized that these types of cables have advantages over conventional wiring harnesses and allow electronic equipment manufacturers to be more innovative in their designs.

INTRODUCTION

Recently, as electronic equipment has rapidly developed, the wiring of such equipment has had to become smaller in size, be capable of greater density, have higher performance and reliability. Furthermore, the cost of wiring systems for such equipment must be reduced because of price competition.

Previously, internal wiring of equipment was carried out using wiring harnesses consisting of individual cables. These harnesses required a significant amount of time to terminate to connectors, as each cable had to be terminated individually. Also, these harnesses were considered to be somewhat difficult to terminate. In such wiring, a few defects occurred which were usually caused by manual wiring. Therefore, the development of a new wiring system which covers all functions of conventional wiring harnesses and also additional functions required to connect automatically without a operator's skill is highly desirable.

In order to meet these requirements and expectations, we have taken the laminated flexible flat cable which was limited to use for jumper wiring and developed variations of it to create a new wiring harness.

CONSTRUCTION

Laminated flexible flat cable is composed of flat conductors and thin plastic tapes. The conductors are tin plated copper wire or phosphor bronze wire. These are laid parallel and laminated with thin plastic tapes. The material of the insulation tape is composed of polyester film with thermoset or thermoplastic adhesive and polyvinyl chloride tape. Electrical and mechanical characteristics of the cables are greatly influenced by the above mentioned combination. So the combination must be chosen according to the condition of the wiring. Fig.1 shows the structure of laminated flexible flat cable.

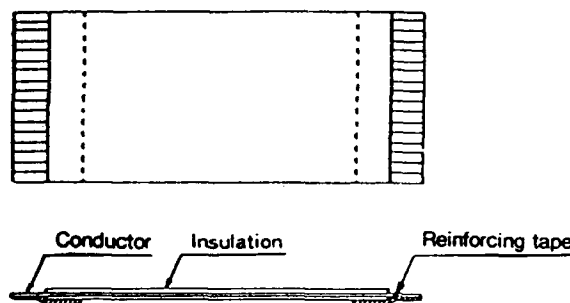


Fig.1 Structure of flexible flat cable

VARIATIONS

High density type

This type of cable has a fine pitch (min.0.5mm space between conductors) which gives a high wire density for application in small sized circuits. This type already has confirmed reliability of termination to connectors and can be used for mass terminations while saving space and weight.

High flexibility type

This type of cable is a combination using 0.02mm (min.) thick conductor with thin special plastic tapes which gives excellent flexibility. It can be applied to a moving and/or bending part such as a printer head.

High rating type

By using special insulation tapes, a higher voltage and temperature type of cable can be constructed.

Shielded type

Fig.2 shows the structure of shielded type cable. It has a $10\mu\text{m}$ thickness shielding metal foil which has a coating layer of special adhesives around the flexible flat cable. The shielding metal foil will be longitudinally connected to a ground conductor/conductors with very low resistance.

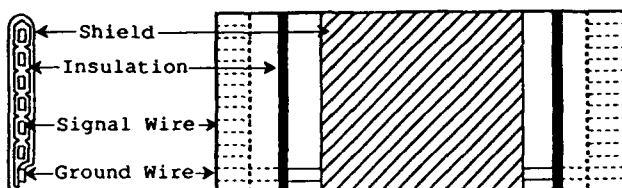


Fig.2 Structure of shielded type

We have studied the relationship between the thickness of shielding metal foil and shielding effectiveness. We adopted the absorbing clamp method test for measuring this relationship. Fig.3 shows a result of this test. It is found that there is no difference in shielding effectiveness for the thickness of the foil if its thickness is more than $10\mu\text{m}$.

Fig.4 shows the shielding effectiveness of shielded flexible flat cable using a $9\mu\text{m}$ copper foil, compared with non-shielded type. It has a good shielding effectiveness for radiation noise in all frequency ranges, especially in the high frequency range.

Fig.5 shows that because of the lower ground impedance and good balance between the signal lines and ground line/lines, the crosstalk characteristic of this type of cable are superior to non-shielded type. Fig.6 shows the test set-up for a measurement of pulse crosstalk.

Although the shielding foil and ground conductor/conductors contact each other with a low impedance, the impedance between the ground conductor/conductors and the earth ground must be low too. The crosstalk depends on the total ground impedance of the shielding system.

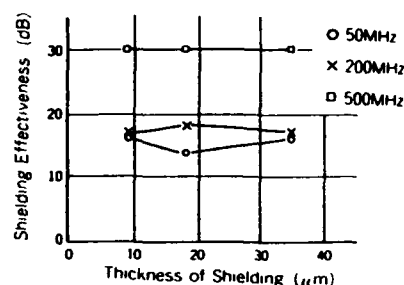


Fig.3 The relation between thickness of copper foil and shielding effectiveness

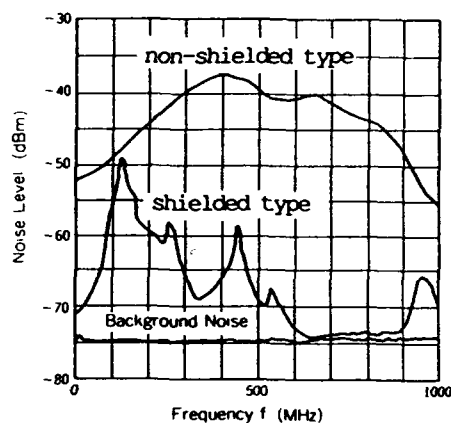


Fig.4 Shielding effectiveness of shielded flexible flat cable using $9\mu\text{m}$ copper shield tape

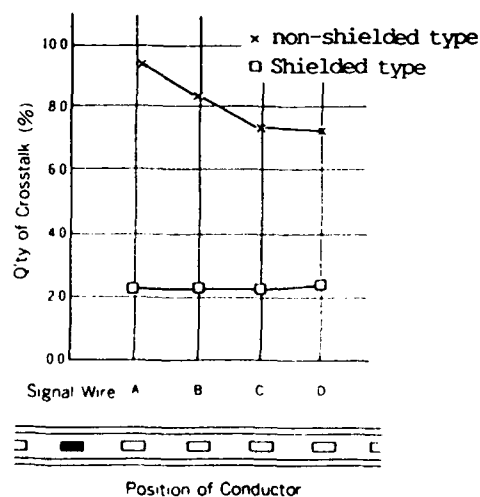
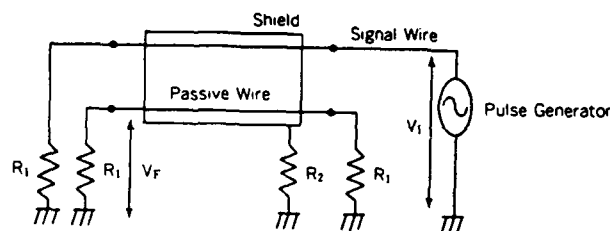


Fig.5 Pulse crosstalk of shielded flexible flat cable

Fig.7 shows the relation between the crosstalk and the ground impedance of shielding foil. The crosstalk increases when the ground impedance increases from 0 to 100 ohm. It can be supposed that there are some cases in which the crosstalk becomes worse because of a lead wire's inductance, such as when the shielding foil is connected to the earth ground by using a lead wire. It is also not be expected that a cable with metal foil without grounding has good crosstalk characteristics. Table 1 shows the method of grounding and the amount of crosstalk.

Through the development of this type of cable, we has solved problems concerning shielding which have caused problem in previous flat type cables. This type of cable can be considered suitable as a shielded multiple cable.



$$Q'ty \text{ of Crosstalk} = \frac{\text{Crosstalk Voltage (V}_F\text{)}}{\text{Input Voltage (V}_1\text{)}} \times 100 (\%)$$

V_F = Voltage of Crosstalk (Far End)

R_1 = Termination Resistance (50 Ω)

R_2 = Ground Impedance

Fig.6 The test set-up for measurement of crosstalk

Branched type

This type of cable consists of two pieces of flexible flat cables, differing in length and number of conductors, which are parallel and combined at one end of cables with a reinforcing tape. This type can reduce the time for insertion and branched wiring. This is a very important property for wiring harnesses.

Mixed conductor type

Different sizes of conductors may be used in a cable. For example, signal wire may be combined with power wire.

Double faced type

This type of cable consists of two pieces of flexible flat cables, facing each other and combined together at one side, which have double faced contacts. By using a special connector, the number of connectors, the time to insert into the connectors, the space may be reduced.

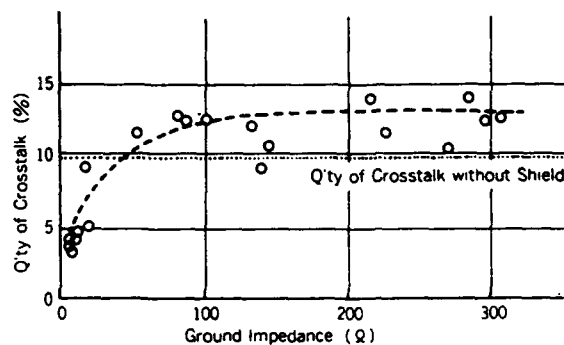


Fig.7 Relation between crosstalk and ground impedance

Ground			
	Non - shield	Connect a shield tape to ground with a 3cm long lead wire	Connect a shielded type to ground with a ground connector
Q'ty of Crosstalk (%)	9.5	4.2	2.3

Table 1 Method of grounding and crosstalk

Fig.8 shows the one of example of complex type cable, which is combined some kinds of above mentioned cable variations.

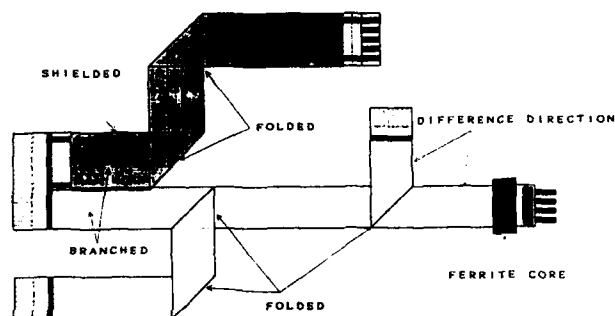


Fig.8 Complex type cable

FEATURES

Dimensions

This cable is about 50% thinner and about 75% lighter than the previous one.

Termination

In combination with the special connectors, it is possible to terminate whole wires in one action with high reliability and productivity.

Bending characteristics

The structure adopting thinner conductors combined with special insulation tapes brings advantageous bending characteristics. This property is important for applications where the cable moves, such as for a printer head. Fig.9 shows the bending characteristics of this cable.

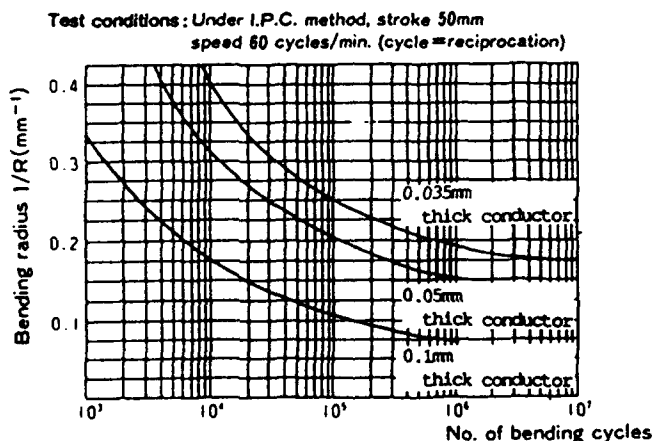


Fig.9 Bending characteristics

Conclusions

By choosing combinations of the above variations to meet customers' requirements, this cable system has been applied not only to a simple application such as a jumper wire, but also to a composite one, such as a wire harness.

This cable can also be inserted into a connector easily. We have developed equipment which performs automatic insertion, eliminating the conventional manual way of wiring and contributing to reducing costs and increasing reliability.

In Japan, one major electronics company has successfully developed automatic wiring for their equipment. It depends on the use of this cable and the development of the insertion machines (robots) for wiring. Apart from the successful application to electronic equipment, the superiority of this cable has also made it feasible for use in cars, where high flexibility and reliability are required.

Reference

- [1] "Electro-magnetic shielding effectiveness of the SHIELD FUJICARD", K.Tanihira et al., 1989
Fujikura Technical review



Tomohiro Yamamoto

Fujikura Ltd.
1440, Mutsuzaki,
Sakura, Chiba, 285
Japan

Tomohiro Yamamoto received the B.E. degree from Kyushu university in 1967. He joined Fujikura Ltd. and has been engaged in engineering and manufacturing of electronic wires and cables. He is a member of Institute of Electrical Engineers of Japan.



Hirofumi Yoshinaga

Fujikura Ltd.
1440, Mutsuzaki,
Sakura, Chiba, 285
Japan

Hirofumi Yoshinaga received the B.E. degree from Meiji university in 1984. He joined Fujikura Ltd. and has been engaged in research and development of electronic wires and cables.



Toshio Onuma

Fujikura Ltd.
1440, Mutsuzaki,
Sakura, Chiba, 285
Japan

Toshio Onuma received the B.E. degree from Tokyo institute of technology in 1972. He joined Fujikura Ltd. and has been engaged in research and development of electronic wires and cables. He is a member of The Institute of Electrical Engineers of Japan and The Textile Machinery Society of Japan.



Hiroaki Komatsuda

Fujikura Ltd.
1440, Mutsuzaki,
Sakura, Chiba, 285
Japan

Hiroaki Komatsuda received the B.E. degree from Ibaraki university in 1988. He joined Fujikura Ltd. and has been engaged in research and development of electronic wires and cables. He is a member of The Institute of Electronics, Information and Communication Engineers of Japan.



Toshiaki Enami

Fujikura Ltd.
1440, Mutsuzaki,
Sakura, Chiba, 285
Japan

Toshiaki Enami received the B.E. degree from Yokohama state university in 1982. He joined Fujikura Ltd. and has been engaged in Research and development of electronic wires and cables.



Colm Tracey

Fujikura America Inc.
1440-100 Galleria
Park way, NW Atlanta,
Georgia 30339 USA

Colm Tracey received the M.S. degree from Queen's university of Belfast in 1990. He joined Fujikura Ltd. and has been engaged in research and development of electronic wires and cables for two years. Now he is working at Fujikura America Inc. as a technical engineer.

NONDESTRUCTIVE EVALUATION AND FAILURE ANALYSIS OF MECHANICAL SPLICES

T. Wei and B.T. Devlin

GTE Laboratories Incorporated, 40 Sylvan Road, Waltham, MA 02254, USA

ABSTRACT

Mechanical splices for optical fiber are being deployed in restoration and fiber-in-the-loop installations. To ensure that mechanical splices are cost-effective, they have to be easy-to-use and reliable. However, understanding reliability of mechanical splices is not an simple task due to the complexity and diversity in different products. Postmortem analysis is effective in providing information about failure mechanisms and essential to understanding the splice reliability.

Failures of mechanical splices during installation were analyzed using nondestructive x-ray imaging and conventional analytical techniques. These complementary techniques allow the identification of failure mechanisms in a number of splice products. Separation between two fiber ends, misplacement of fiber, and breakage of fiber or parts of the splice have been identified as the main causes of failures. These failures are mostly related to deficiencies in the designs or practices of different splice products.

INTRODUCTION

A variety of mechanical splice products have recently entered the market place, aiming at restoration and fiber-in-the-loop (FITL) applications. These new mechanical splices have some common features that make them more appealing to end users: low cost, ease of use, no adhesive, and no need for monitoring. However, because of the diversity and sometimes complexity in their designs, it becomes more difficult to comprehend the reliability issues in each product and assess how mechanical splices will facilitate fiber deployment.

This study investigates failure mechanisms in six mechanical splice products by analyzing splice failures occurred during installation. It offers a unique opportunity to explore if any common failure mechanisms exist among different designs and suggest how they can be eliminated during deployment.

SPLICE ASSEMBLY

Recent studies have shown that the reliability of splices was strongly affected by the assembly process.¹⁻⁷ To understand how mechanical splices could fail during installation, a field trial was set up to prepare a large quantity of specimens and test them individually. All failed splices were then analyzed to elucidate how failures occurred during assembly.

In all, over 360 specimens were assembled from six products and tested in the field trial. These mechanical splices were prepared by a team of six craftsmen to minimize the influence by a single operator. All operators followed the same instructions provided by the vendors. Each splice was individually tested using either an optical time domain reflectometer or a splice-loss test set. Subsequently, specimens that failed to meet the splice-loss specification were subjected to postmortem analyses.

ANALYSIS OF FIELD FAILURES

All failed splices were subjected to nondestructive evaluation (NDE)^{3,5,8,9} and conventional analytical techniques^{3,4,10-12} to identify and understand the common failure mechanisms for mechanical splices during assembly.

NDE was first applied to each failed specimen since it has the advantage of preserving the sample integrity and requires no preparation work. In particular x-ray imaging has been demonstrated to be an effective NDE technique for analyzing mechanical splices because it provides magnified real-time or film images capable of showing internal defects with high resolution.^{5,8,9}

Besides x-ray imaging, optical and scanning electron microscopic (SEM) examinations have also been conducted to verify the cause of failure.^{3,4,10-12} These conventional techniques require, in general, disassembly of each specimen to expose internal parts. Extreme care should be taken to assure the integrity of all parts during dismembering of the specimen. Examinations performed on these parts include fractographic analysis of the fiber fracture surface, inspection of individual parts of the splice, and cleave angle measurement of the fiber end face.

One particularly useful way to determine what had happened to fibers inside each splice is to examine their imprints on the alignment or retention parts. Since silica fiber has a higher hardness than that of the surrounding materials, its imprint can often lead to definitive information about the fiber location before its removal.

FAILURE MECHANISMS

Several common failure mechanisms were identified from x-ray images taken on failed splices that showed a high loss or no transmission. These included separation of two fiber ends, misplacement of fiber, and breakage of fiber or parts of the splice. These observations not only reconfirmed the insertion-loss data from the field trial, but also pointed out some of the deficiencies in the designs, manufacture, and practices of some mechanical splices.

Fiber Separation

The separation of two fiber ends was a common problem for all types of mechanical splices since it is difficult to know if two fiber pieces are in contact. Several factors have contributed to the existence of a gap between two fiber ends: the presence of too much index-matching gel, a bad cleaved end, or the resistance against fiber movement in the alignment parts.

The nondestructive x-ray imaging technique has been demonstrated to be an effective tool for observing the fiber separation.^{5,9} Figure 1 presents three x-ray images of increasing fiber separations for different mechanical splices, shown as "dark color" gaps between "light color" images of fibers. In most cases the index matching gel alleviated the gap problem and allowed low-loss splices to be made (see the top image, Figure 1). Too large a gap however resulted in a high insertion loss (see the middle image, Figure 1) or, even worse, no transmission (see the bottom image, Figure 1).

Another useful technique to verify the fiber locations is to examine the fiber imprints on the alignment parts after removing the fiber pieces from a splice. Figure 2 presents an optical micrograph of the alignment part, showing a gap between the imprints of two pieces of fiber.

Fiber Misplacement

Misguiding of fiber will result in fiber misplacement inside the splice and no transmission. Misplacement of fiber is difficult to detect without a monitoring device since the operator cannot visually locate the fiber during assembly. Verifying the occurrence of fiber misplacement generally requires postmortem analyses based on the x-ray imaging technique or examinations of the fiber imprints. This problem is generally resulted from deficiencies in the designs of mechanical splices.

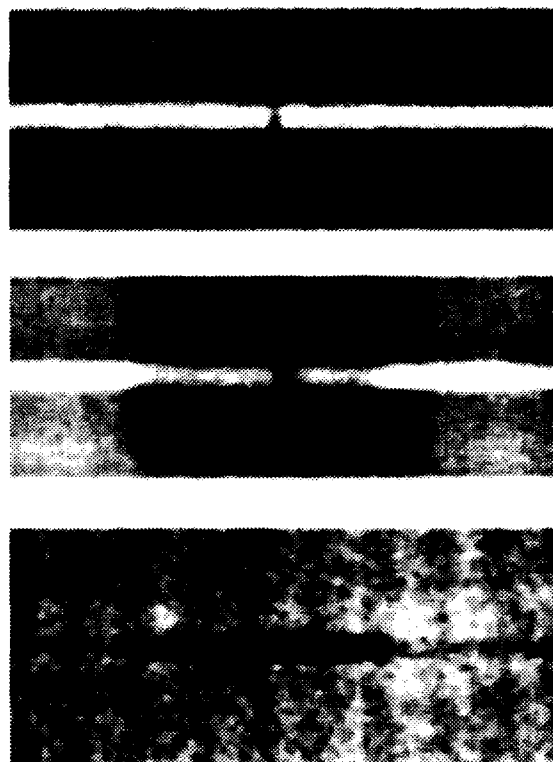


Figure 1. X-ray images of different mechanical splices showing increasing amounts of fiber separation between two fiber ends. Fiber separation is manifested as the "dark color" gap between the "light color" fiber images.



Figure 2. Scanning electron micrograph of an alignment piece showing the gap between two fiber imprints left behind after fiber pieces were removed.

Misplacement of fiber occurred in at least two ways. The first was the result of too much slack between alignment pieces so fiber may not be guided to its proper position during insertion, as illustrated in Figure 3. The x-ray image of a mechanical splice (see the top image, Figure 3) shows that one fiber piece (the "light color" image at the right) was not in the alignment

groove after assembly. The scanning electron micrograph (see the bottom photograph, Figure 3) of an alignment part showing, from the fiber imprint, that one piece of fiber on the left was not in its proper position.

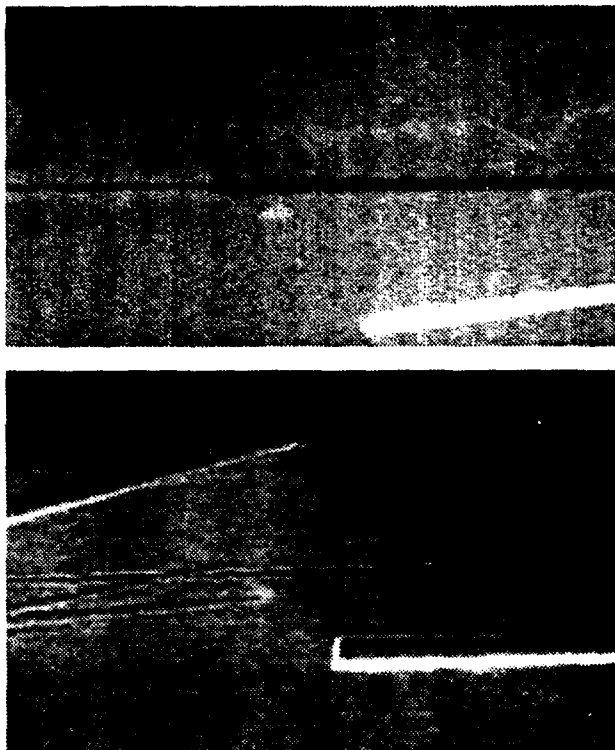


Figure 3. Top: x-ray image of a mechanical splice showing that the right piece of fiber was not in the alignment groove; Bottom: scanning electron micrograph of an alignment part for a different splice showing the misplacement of the left piece of fiber from the fiber imprints.

The second way fiber can be misplaced was related to the irregular finish of the guiding part that interferes with the insertion of fiber during assembly, as illustrated in Figure 4. The x-ray image (see the top image, Figure 4) shows that only one piece of fiber was in the alignment groove and the left piece was missing. Subsequent examination by SEM (see the bottom micrograph, Figure 4) indicated that a piece of fiber could have difficulty climbing up the ledges in the guiding section prior to entering the alignment groove.

Breakage of Fiber or Parts in a Splice

Splice failures also occurred if there was breakage of fiber or splice parts. When pushing a fiber into the alignment parts, excessive abrasion or friction could cause the fiber fracture. This risk was exacerbated by damage to the fiber surface introduced during the fiber

preparation steps prior to splicing. Recent studies have demonstrated that coating stripping and fiber cleaning unavoidably degrade the fiber strength.^{1,2,4} Severe degradation can lead to fiber fractures during installation or service.

Breakage also happened to internal parts of a splice without being detected during assembly. This resulted in the loss of alignment or retention of fiber pieces, and therefore high insertion loss or no transmission.

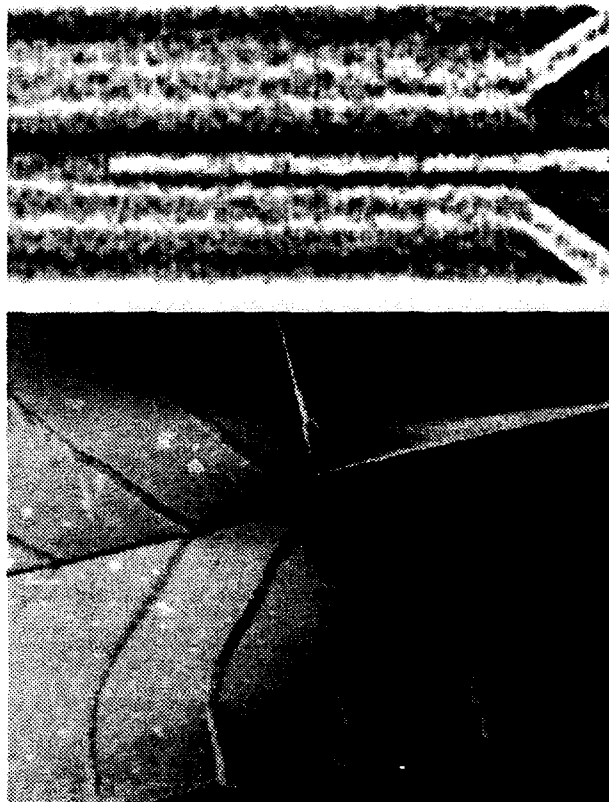


Figure 4. Top: x-ray image of a splice showing the light image of the right piece of fiber and the missing left piece of fiber; Bottom: scanning electron micrograph showing the irregular finish of the guiding section as a fiber piece entering the alignment groove.

CONCLUSION

Both nondestructive x-ray imaging and conventional analytical techniques have been successfully used for postmortem analyses of mechanical splices. These complementary techniques offered valuable information about some common failure mechanisms in a number of splice designs. Improvements of the designs and installation practices should make current mechanical splice products more reliable and cost-effective in FITL and restoration applications.

REFERENCES

1. T. Wei, H.H. Yuce, C.H. Hasz, and P.L. Key, "Degradation of fiber strength during coating stripping," *Proc. 38th Internat. Wire & Cable Symp.*, p. 199 (1989).
2. H.H. Yuce, P.L. Key, and T. Wei, "Mechanical reliability considerations for fusion splices in optical fibers," *Proc. 39th Internat. Wire & Cable Symp.*, p. 400 (1990).
3. T. Wei and H.H. Yuce, "Laboratory testing and failure analysis of fiber interconnections," *Proc. 40th Internat. Wire Cable Symp.*, p. 826 (1991).
4. W.R. Wagner, "Extrinsic fiber damage and its effect on the reliability of optical fiber connectors and splices," *Proc. SPIE*, 1580, 168 (1991).
5. T. Wei, B.T. Devlin and H.H. Yuce, "Analysis of optical fiber splices by the nondestructive x-ray imaging technique," *Proc. SPIE* 1791, 25 (1992).
6. T. Wei, "Product, practice and reliability of optical fiber splices," *LEOS '92 Conf. Proc.*, p. 578 (1992).
7. W.W. Wood, G.D. Kiss, L.A. Reith, E.M. Vogel and H.H. Yuce, "Reliability of interconnection devices," *Proc. 9th Ann. Nat'l Fiber Optic Engineers Conf.*, Book 3, pp. 209-221 (1993).
8. T. Wei, D.J. Cotter, B.T. Devlin and W.D. Koenigsberg, "Nondestructive evaluation of optical fiber splices and connectors," in *Digest of Conf. on Optical Fiber Communication*, 1992 OSA Tech. Digest Series 5, p. 226 (1992).
9. T. Wei, "Nondestructive technique probes connector failures," *Lightwave* 9, No. 10, p. 35 (September 1992).
10. W.R. Wagner, "Failure analysis of fiber optic connectors," *Advances in Ceramics* 22, 389 (1988).
11. H.H. Yuce, A. DeVito, C.J. Wiczorek, W.T. Anderson and J.P. Varachi "Post-mortem failure analysis of optical fiber cables," *Proc. 38th Internat. Wire & Cable Symp.*, p. 611 (1989).
12. H.H. Yuce, J.P. Varachi and P.L. Key, "Post-mortem analysis of optical fibers," *Tech. Digest, Symp. Optical Fiber Measurements*, p. 15 (1990).

T. (Mike) Wei is a principal member of the technical staff in the Network Technologies Laboratories of GTE Laboratories Incorporated, Waltham, MA 02254, where he is responsible for fabrication, characterization, and reliability studies of optical fiber and components. Mike provides technical support to telephone operating companies within GTE on network reliability and fiber optics related issues. He received a Ph.D. degree in physics from the University of Pennsylvania, and has been involved in optical fiber research since 1978.

THERMAL STRIPPABILITY OF 4- AND 12-FIBER RIBBONS

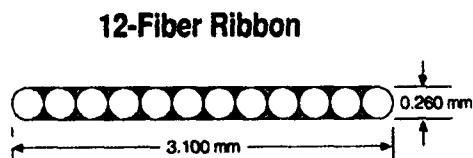
John W. Botelho

Corning Incorporated, Corning, NY 14831

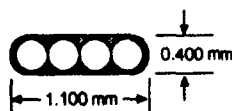
Abstract

The selection of coatings applied to optical fibers contributes significantly in determining the thermal strippability performance of ribbon subunits. This paper details a study that investigated the effect of the outer primary modulus, adhesion to glass of the inner primary, as well as the diameter ratio of the inner to outer primary coatings to thermal strippability. Thermal strippability performance was determined three ways: (1) strip force, the force required to remove all fiber coatings in one pass, (2) post strip fiber cleanliness, a rating of residual debris, and (3) tube-off rating, a measure to the degree which the fiber coatings remain intact (i.e., a tube). Both 4-fiber encapsulated and 12-fiber "edge-bonded" ribbons were studied, with a construction as shown in Figure 1.

Figure 1



4-Fiber Ribbon



Nomenclature

Strip Force: The peak force required to remove all fiber and ribbon coatings from the glass fibers as measured in grams.

Modulus: Young's Modulus. Measured by tensile testing films. Values reported are "Secant Modulus" at 2.5% strain.

Adhesion: Measured by peel testing (180 degree) films of inner primary coatings on a flat glass plate. This test represents a coatings adhesion to glass properties. Testing done at 50% RH.

Cleanliness Rating: A rating scale used to determine the cleanliness of the glass fiber post stripping. Done with the unaided eye (no magnification).

- 5.0 = Incomplete strip, fibers will not wipe clean with an alcohol wipe.
- 4.0 = Heavy Residual Debris. 3+ alcohol wipes required to clean fibers.
- 3.0 = Moderate Residual Debris.
- 2.0 = Slight Residual Debris.
- 1.0 = No Visible Residual Debris.

Tube-Off Rating: A rating done with the unaided eye used to determine the remains of the fiber (& ribbon) coatings after stripping.

- 5.0 = No Tube-Off, Total Disintegration (crumbs)
- 4.0 = Incomplete Tube, Partial Crumbling
- 3.0 = Complete Tube, Moderate Distortion
- 2.0 = Complete Tube, Slight Distortion
- 1.0 = Complete Tube, No Distortion

Data Acquisition Rate: The frequency at which the computer queries the load cell (#/sec).

Introduction

With the potential for the increased use of optical fiber ribbons in high fiber count cables, and to achieve the benefits of mass connectorization, it is important for a fiber manufacturer to understand the fiber coating attributes affecting ribbon performance. One of the most fundamental of all fiber coating requirements is that the coating not only protect the glass from its designed environment, but that it also be removed easily and leave the glass fiber free from any residual debris.

For single fibers, the strip force test method is well defined by industry standard procedures, for example TIA/FOTP-178¹. To date no such procedure exists for fiber ribbons, although one was proposed by Mills². This paper is intended to show how various fiber coating attributes can affect ribbon strip performance, as defined by strip force (peak), fiber cleanliness, and tube-off rating. Also included is a brief section on the affect of data acquisition rate and its effect on reported strip force.

Experimental Setup

Shown in Figure 2 is a schematic representation of the ribbon strip force tester. As reported by Mills², ribbon strip force can be affected by strip speed, strip length, and by strip tool temperature. In an effort to evaluate the effect of fiber coatings, all strip conditions were held constant, as shown in Table 1.

Figure 2
Ribbon Strip Force Tester

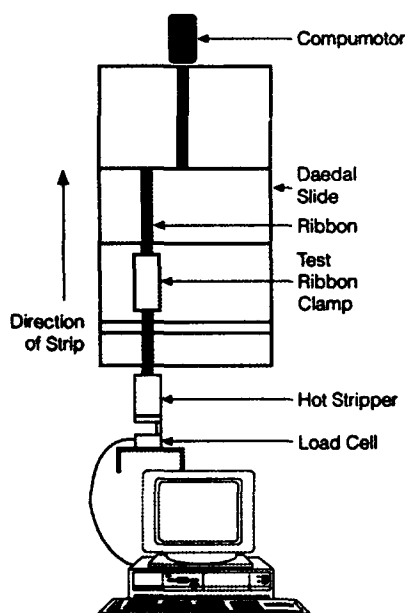


Table 1	
Strip Length	25 mm
Strip Speed	8.5 mm/second
Tool Temperature	100 degrees
Dwell Time	5 seconds
Tool Type	Fujikura Hot Jacket Stripper, Model HJS-01
Blade Gap	150 Microns
Data Acquisition Rate	200 Hz

The same ribbon materials, ink and matrix, as well as the same ribbon making process were used to produce all experimental ribbons. Evaluation of each experimental ribbon was based on a sample of 5 strips.

Results

Figures 3, 4, and 5 show the effect of inner to outer primary coating diameters as studied on 4-fiber ribbons. As the inner primary diameter is reduced with a constant (245 micron) outer primary diameter, ribbon strip cleanliness is improved while neither tube-off rating nor strip force appear grossly affected. In the limited range studied, outer primary modulus appeared to have no effect.

Figure 3

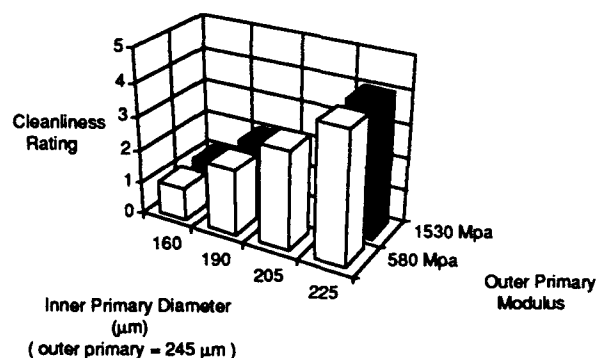


Figure 4

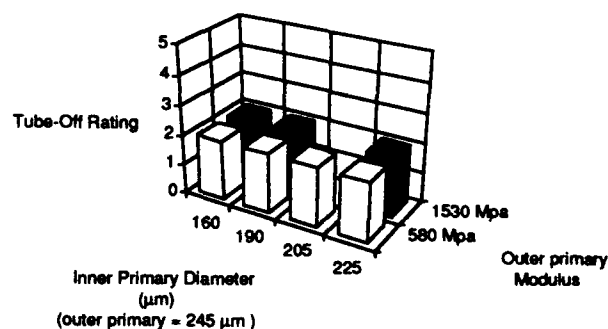
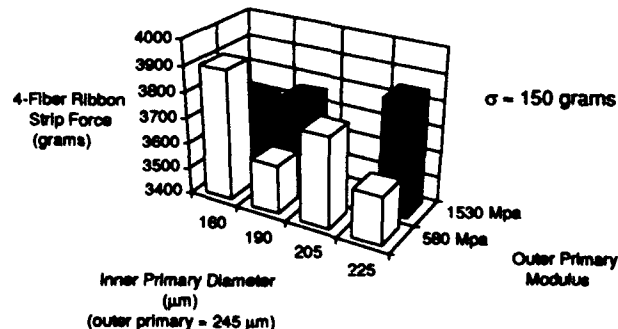


Figure 5



As shown in Figures 6, 7, and 8, adhesion to glass properties of the inner primary play a major role in both 4-fiber and 12-fiber ribbon strip performance. Ribbon strip force appears to increase with the increase in inner primary adhesion for both 4- and 12-fiber ribbons. In the range of adhesions under study, both cleanliness rating and tube-off rating appear unaffected in the 4-fiber ribbon, while in the 12-fiber ribbon incomplete stripping was realized with highest inner primary adhesion.

Figure 6

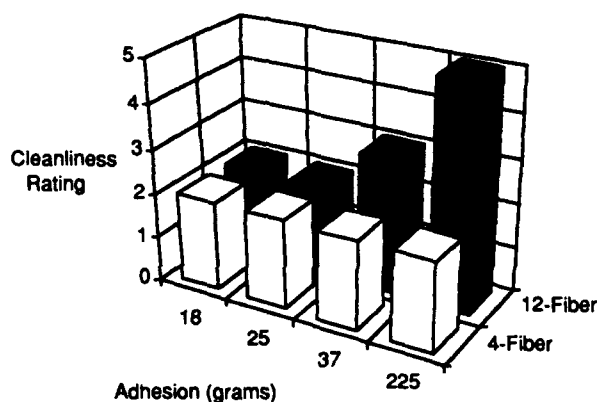


Figure 7

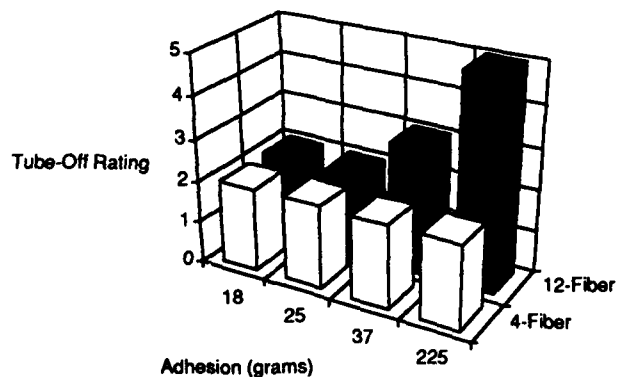
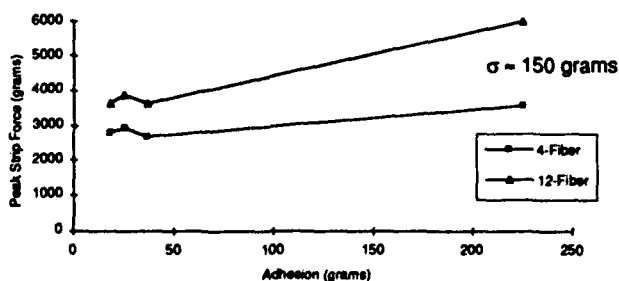


Figure 8



The role of outer primary modulus with a constant adhesion inner primary is shown in Figures 9, 10, and 11. It is clear in 4-fiber ribbons that the outer primary modulus does not affect ribbon strip performance.

Figure 9

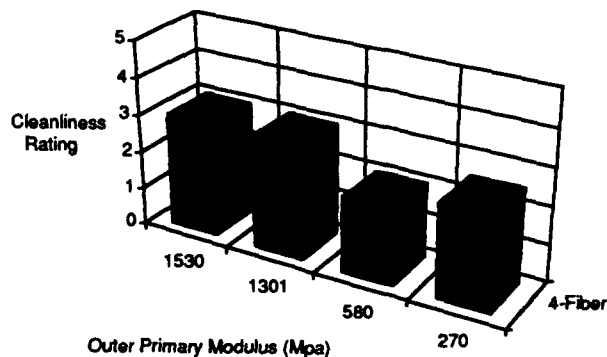


Figure 10

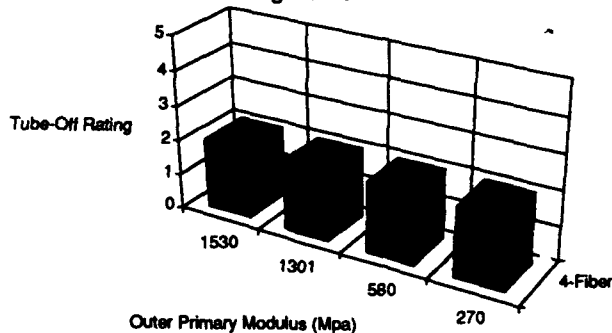
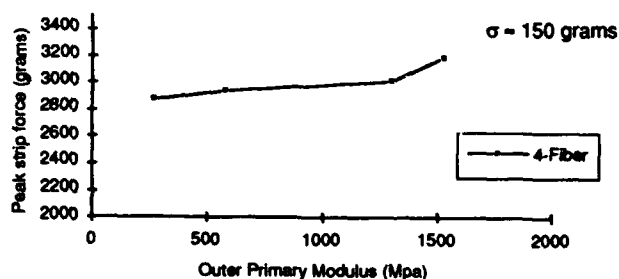


Figure 11



As reported by Mills², the ribbon stripping procedure (length stripped, tool temperature, etc.) will influence the apparent strip results. Figure 12 shows a typical ribbon strip force versus distance trace. Peak strip force is the measure most typically reported. If the data acquisition rate is sufficiently slow, the true peak ribbon strip force will be missed as shown in Figures 13 and 14. It must also be noted that as the ribbon pulling speed (strip

speed) is increased, the data acquisition rate must also be increased.

Figure 12
Typical Strip Force Trace

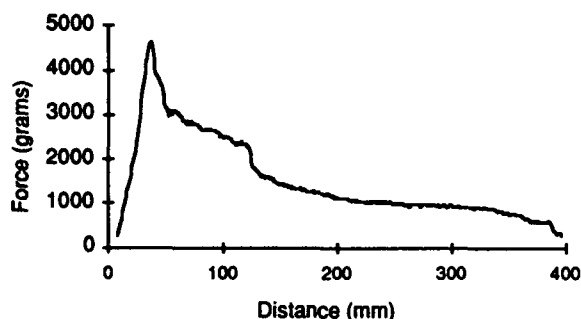


Figure 13
Strip Speed 100 mm/sec
4-Fiber Ribbon

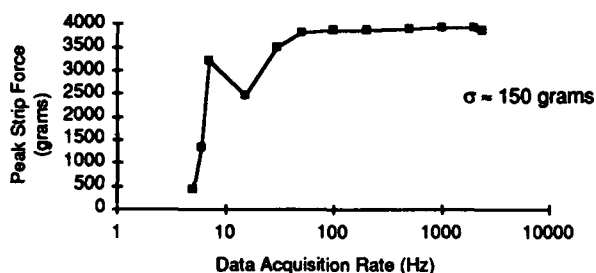
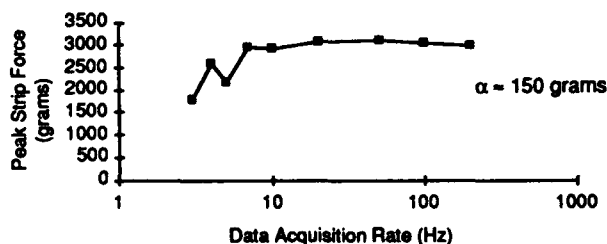


Figure 14
Strip Speed 8.5 mm/sec
4-Fiber Ribbon



Conclusions

For a given ribbon construction, ribbon strip performance is dramatically affected by the selection of inner primary fiber coating as well as the diameter ratio of the inner to outer primary fiber coating. In order to achieve acceptable ribbon strip performance, optical fibers intended for ribbon applications must have an inner primary fiber coating with optimized adhesion properties.

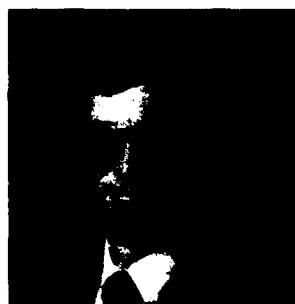
It is important to understand the variables affecting ribbon strip testing and to establish a standardized test and rating system. Ribbon strip force alone does not indicate true product functionality, strip cleanliness and tube-off rating must also be considered. Data acquisition rate used in collecting strip force data is an important test variable, too low and the true peak force will be missed.

Acknowledgements

The author would like to thank H. R. Cole for his diligent work in stripping all experimental ribbons, and for his ability to rate cleanliness and tube-off performance as objectively as possible. The author would also like to thank W. G. Faber for producing all experimental fiber, and J. Gubio for producing all experimental ribbons.

References

- 1 "EIA/TIA Standard FOTP-178, Measurement of Strip Force Required for Mechanically Removing Coatings From Optical Fibers." Published by Electronics Industries Association, Engineering Department, 2001 Pennsylvania Ave., Washington, DC 20006.
- 2 G. A. Mills, "Testing Of 4- And 8-Fiber Ribbon Strippability," Proceedings from the 41st International Wire and Cable Symposium, Page 472, (1992).



John W. Botelho
Corning Incorporated
Corning, NY 14831

Mr. Botelho joined Corning Incorporated in 1981 with a BS Degree in Mechanical Engineering from Southeastern Massachusetts University. He has held a variety of engineering positions in both the Electronic Components Business as well as the Optical Fiber Business. He is currently engaged in Optical Coating Development with focus on emerging ribbon applications.

PERFORMANCE OF IMPROVED AIR BLOWN FIBER SYSTEM

H. Sano, S. Takaoka, S. Tanaka, N. Suzuki, T. Kumakura

Sumitomo Electric Industries, Ltd.
Yokohama, Japan

ABSTRACT

To improve the capability and applicability of blown fiber system, we have developed a new easy and simple blown fiber technique called **transfer blowing technique**, in which a six fiber optical unit is air-blown transferred from a carrier tube to a pre-installed tube without using a conventional sophisticated blowing head. We will discuss the practical advantages and theoretical study of this blowing behavior including the results of a 500 m unit transfer blowing.

As for the conventional blown fiber technology, by improving the blowing equipment, we achieved the **longest one-shot blowing distance of 2000 m** by only one blowing head. We confirmed its temperature dependence of long distance blowing ability in wide temperature range from -20 to 60 °C.

1. INTRODUCTION

The application of optical transmission technology to local and public communication networks is well underway. It is often difficult to predict the future increase in information traffic or expected scale of the optical fiber networks.

The Air Blown Fiber system is a new optical fiber installation technique, that was proposed by British Telecommunications PLC in 1983(ref.1), in which an optical fiber unit is blown into pre-installed empty tube networks by compressed air.

Figure 1 depicts the concept of the Air Blown Fiber system; **Figure 2** shows the cross section of a typical optical fiber unit. The optical fiber unit is blown into the tube (or connected tubes) by blowing head, together with compressed air fed from the compressor, and is drawn through the tube network by blowing force as the viscous drag force of the air.

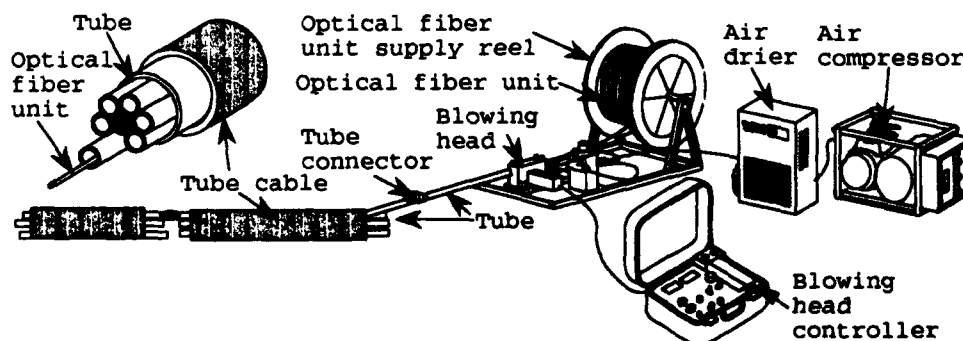


Figure 1. Construction of Air Blown Fiber System

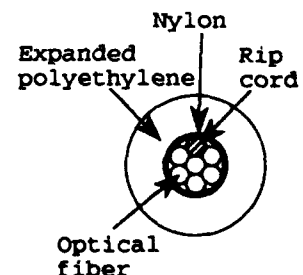


Figure 2. Optical fiber unit

For the installation process, the blown fiber system has the following merits :

- 1) A continuous splice free optical fiber installation dramatically reduces the number of optical fiber splices.
- 2) With adding, re-routing, removing, and replacing optical fiber units, the first investment can be reduced, and the network flexibility is supported.
- 3) Reliable installation is achieved by distributed blowing force over the entire length of the optical fiber unit.

For the merits, Air Blown Fiber system is become to be mainly applied to two fields. One is inter-building local area networks (ref.2), that requires relatively short blowing distance and economical and easy operation. Another is long distance transmission use such as communication networks of rail way companies (ref.3) and so on, that requires much longer blowing length to reduce joints of optical fibers.

The purpose of this study is to improve the Air Blown Fiber technique to extend its applications. For this purpose, we have developed easy and simple blown fiber system, called transfer blowing technique, and have extended blowing distance in various environmental conditions with developed equipment for the conventional Air Blown Fiber system.

2. TRANSFER BLOWING TECHNIQUE

(1) CONCEPT

Air Blown Fiber system is very flexible optical networking system, but optical fiber network demand that lies scattered in time and spaces requires much easier and simpler optical fiber installation system.

Figure 3 shows the system construction of transfer blowing technique. In this system, tube cables are pre-installed and jointed

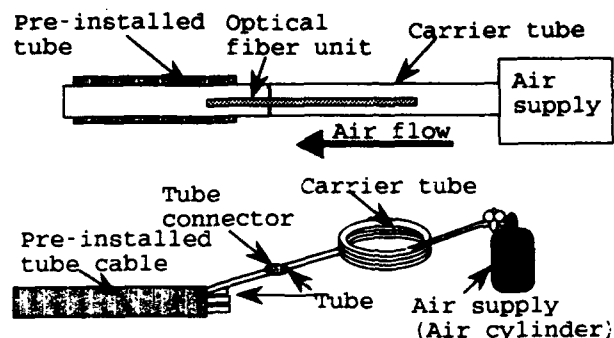


Figure 3. Concept & construction of transfer blowing system

as the conventional Air Blown Fiber system as shown **figure 1**. However, a conventional optical fiber unit is pre-inserted in a carrier tube in a manufacturers' factories, and this carrier tube and a gas supply (such as compressed air cylinder) are transported to the installation field. In the field, one end of the carrier tube is connected with the pre-installed tube cable, another end is connected with the gas supply, then, by the drag force of air, the optical fiber unit is blown from the carrier tube to the pre-installed tube network. In this system, an optical fiber unit is transferred from inside of one tube to another, therefore we call it as transfer blowing technique.

This transfer blowing technique has the following advantages:

- 1) Fast installation and cost reduction for less quantity of equipment in the installation fields.
- 2) High reliability of the field operation, because the optical fiber unit is always protected by tubes, the carrier tube and the pre-installed tubes in transportation and installation.
- 3) Easy and errorless installation because of the easy operation of tube connecting and gas supplying without using the sophisticated blowing head in the Air Blown Fiber system.

(2) BLOWING THEORY

We have reported a theoretical study of blowing fiber process for the conventional Air Blown Fiber system in 1990 (ref.4). By using improved calculation process of previous study, we estimated blowing behavior in transfer blowing with calculating blowing force against position on the optical fiber unit.

The calculation is performed for the blowing model shown in figure 4 by the following process :

- 1) Dividing the route into four portions, of which is the first from the carrier tube inlet to the tail of the optical fiber unit, the second from the tail to the tube connection, the third from the tube connection to the head of the optical fiber unit, and the forth from the head to the pre-installed tube outlet.
- 2) Calculating air pressure at the boundary of the portions under the condition of known pressure at the carrier tube inlet and the pre-installed tube outlet, and known flow resistance of the tubes including the optical fiber unit.
- 3) Calculating pressure drop in the second and the third portions of the route, and blowing force[F] on the optical fiber unit by following equation :

$$F(1) = (\pi \cdot d_1 \cdot d_2 / 4) \cdot (-dP/dl)$$

Where d_1 , d_2 , and dP/dl indicate the tube inner diameter, the optical fiber outer diameter, and pressure drop at the position of the optical fiber unit (ref.1).

- 4) Evaluating the blowing force comparing with insertion resistance caused by friction between the tube and the optical fiber unit at every position of the optical fiber unit.

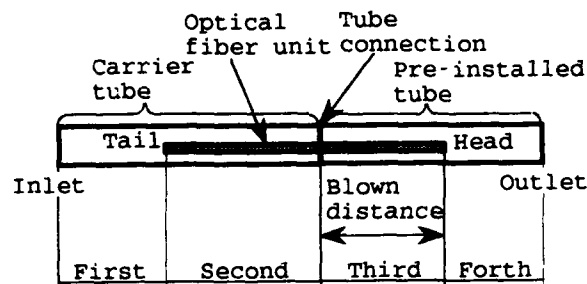
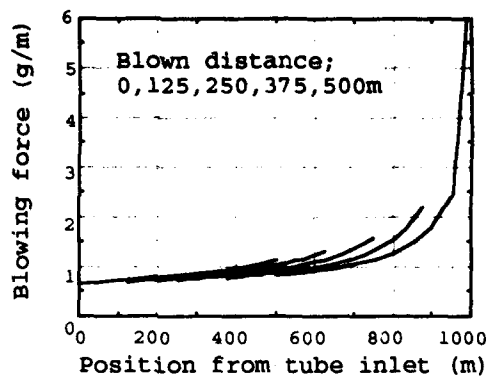


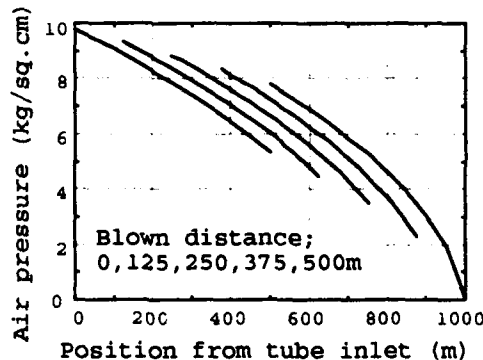
Figure 4. Blowing force calculation model for transfer blowing

CALCULATION RESULT 1 Figure 5(a) shows calculated blowing force distribution in transfer blowing of a simple condition model at blown distance of 0, 125, 250, 375 and 500 m, when both of the carrier tube and the pre-installed tube have the same dimension of 500 m length and 6 mm inner diameter. The optical fiber unit has 500 m length and 2 mm diameter, and air pressure at the carrier tube inlet is 9.8 kg/sq.cm. Figure 5(b) indicates calculated air pressure distribution in this model.

The first characteristic of the calculated results is that the blowing force in figure 5(a) is larger at nearer position from the head of the optical fiber unit, corresponding with the gradient of air pressure shown in figure 5(b). It means the minimum blowing force is located at the tail of the optical fiber unit. This is very similar as the result for the conventional Air Blown Fiber system described in our previous paper (ref.2). The second characteristic is more important one that the blowing force is increasing in the transfer blowing at all position of the optical fiber unit with increasing the blown length. It means that success of the installation can be promised at the beginning.



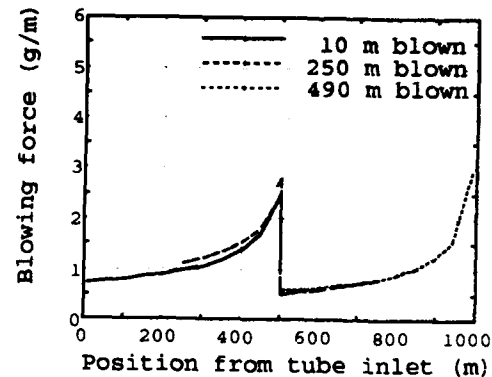
(a) Blowing force distribution



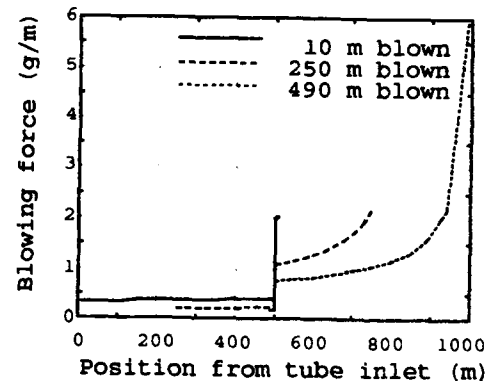
(b) Pressure distribution

Figure 5. Blowing force & pressure distributions in blowing tube in transfer blowing (Air pressure; 9.8kg/sq.cm)

CALCULATION RESULT 2 Figure 6(a) shows calculated blowing force distribution on the optical fiber unit at the blown distance of 10, 250, and 490 m, when the 500 m optical fiber unit transfer from 4.5 mm inner diameter carrier tube to 6.0 mm inner diameter pre-installed tube. On the optical fiber unit in the carrier tube, blowing force is much larger than in the pre-installed tube, because of larger pressure drop brought by air flow resistance in smaller clearance between the tube and the optical fiber unit. This condition enlarges blowing force at the tail of the optical fiber unit, where the blowing force is the minimum in CALCULATION RESULT 1. There is a possibility that supports better blowing performance than transfer blowing between the same inner diameter tubes.



(a) From tube of 4.5mm ID to tube of 6.0mm ID



(b) From tube of 6.0mm ID to tube of 4.5mm ID

Figure 6. Blowing force in transfer blowing between different inner diameter tubes (Air pressure; 9.8kg/sq.cm)

CALCULATION RESULT 3 Figure 6(b) shows the calculation result, when the transfer blowing direction is reversed in the previous calculation 2, from 6.0 mm inner diameter carrier tube to 4.5 mm inner diameter pre-installed tube. The blowing force distribution shown in figure 6(b) is obviously different from the figure 6(a) of CALCULATION RESULT 2. The blowing force is less than 0.5 g/m at the entire optical fiber unit in the carrier tube, and problems such as blowing speed fall can be forecasted.

(3) EXPERIMENTAL RESULTS & DISCUSSION

The experiments were performed in the above calculation conditions. Cross section of tubes and an optical fiber unit used for the experiments are shown in figure 7 and table 1.

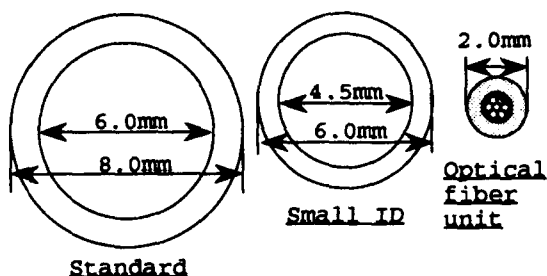


Figure 7. Tubes and optical fiber unit

Table 1. Tubes for experiments

Exp.No.	Carrier	Pre-installed
1	Standard	Standard
2	Small ID	Standard
3	Standard	Small ID

For all experiments, the conventional 6 fiber optical fiber unit was used. In the table 1, "Small ID", and "Standard" mean a tube of small inner diameter of 4.5 mm coiled in 1 m diameter, and a tube of standard inner diameter of 6.0 mm coiled in 1 m diameter, respectively.

EXPERIMENT 1 Transfer blowing between the same inner diameter (6.0 mm) standard tubes of 500 m length was performed with evaluating blown distance against blowing time, and the result is shown in figure 8.

First, we can understand that a 500 m optical fiber unit was able to be installed by transfer blowing in 11 minutes. This blowing distance of 500 m is long enough for applications of inter-building networks, and can cover large part of campus networks.

In this figure, the increment of blowing speed was observed, and this behavior demonstrates the increment of blowing force expressed in the above CALCULATION 1 in transfer blowing between the same inner diameter tubes. In this case, the reliable blowing forecasted was confirmed.

EXPERIMENT 2 The curve (a) in Figure 9 shows transfer blowing results from the small inner diameter tube to the standard one.

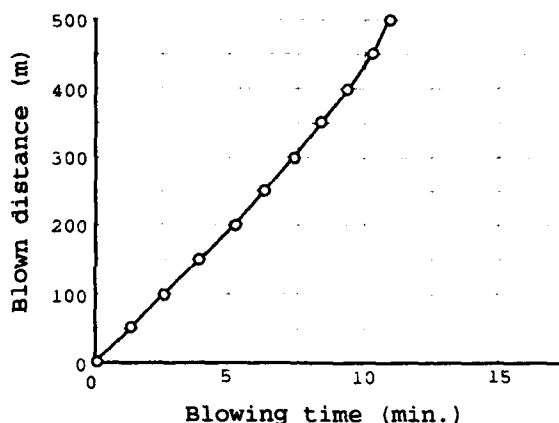


Figure 8. Blowing results in transfer blowing between the same inner diameter tubes (Air pressure, 9.8kg/sq. cm)

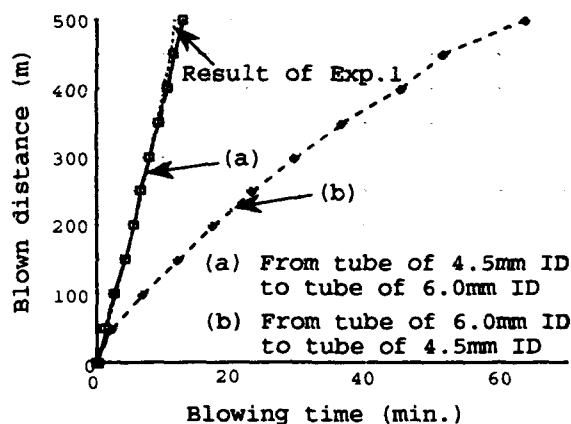


Figure 9. Blowing results in transfer blowing between different inner diameter tubes (Air pressure, 9.8kg/sq. cm)

Blowing speed in this case didn't decrease and it required 12 minutes to install a 500 m optical fiber unit, as similar as EXPERIMENT 1. Smaller clearance between the tube and the optical fiber unit in the carrier tube causes larger friction between them, and it is considered that enlarged blowing force estimated in CALCULATION 1 compensates for the friction force.

This result brought us a smaller package of a carrier tube for practical application with using a smaller diameter tube that has 56 % of cross section of the standard tube.

EXPERIMENT 3 Transfer blowing result from the standard inner diameter tube to the smaller inner diameter tube is shown as curve (b) in figure 9.

As the forecast in CALCULATION 3, blowing speed decreased in transfer blowing, and it took over one hour to install a 500 m optical fiber unit.

From the above discussions and results, we confirmed that the transfer blowing technique has good blowing performance and it can be applicable to practical applications. This easy and simple optical fiber installation method will widely extend the application field of blown fiber system.

3. Long Distance Blowing

(1) CONCEPT

The Air Blown Fiber system is expected to be introduced to the outdoor transmission line such as the railway for the merit of reduced optical splice points, which requires long continuous optical fiber installation. Then, request of the long distance blowing of an optical fiber unit with the minimum operation arises. We have therefore developed the long distance one-shot blowing technique by improving the conventional blowing head.

(2) Blowing Characteristics

This technique was evaluated by using the Air Blown Fiber system shown

in the figure 1. Used tubes were 6 mm of inner diameter and wound with 1000 mm diameter, and total tube length was changed from 1000 m up to 2000 m in testing. Pressure of used compressed airs were 7 kg/sq.cm for 1000 m blowing, and 9 kg/sq.cm for 1500 m and 2000 m blowings.

Figure 10 shows the test result which reveals the blowing distance against accumulated blowing time. A 1000 m and a 1500 m optical fiber unit installations were achieved in 21 minutes and 46 minutes, respectively. We also confirmed to install a continuous 2000 m optical fiber unit successfully in 84 minutes, and the average blowing speed was 23.8 m/minutes. These results are good enough for the practical application.

This technique was realized by improving the blowing head, which gave high torque and stable dragging force to the optical fiber unit.

(2) Temperature Performance

Besides the above, we evaluated the temperature performance of this technique in order to confirm the outdoor field applicability. In following experiments, same equipments were used, but the tube was settled in the temperature chamber of which temperature was changed from -20°C to +60°C.

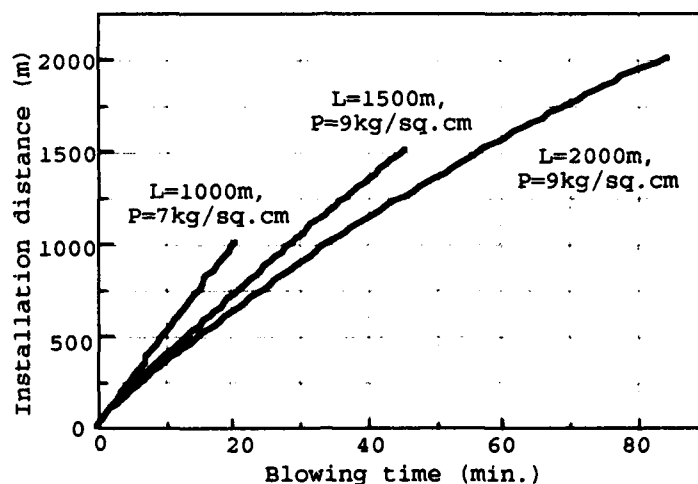


Figure 10. Results of long distance blowing

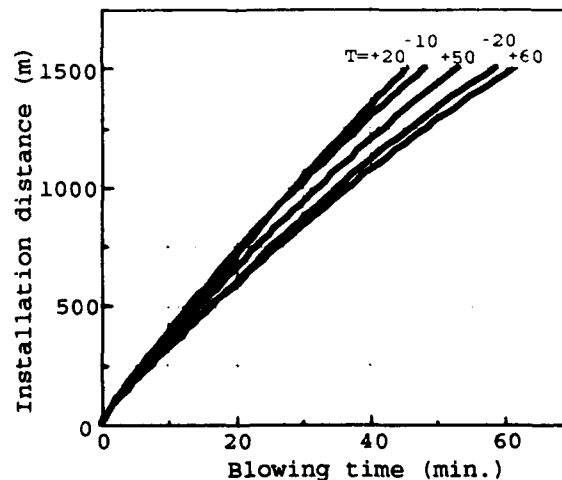


Figure 11. Temperature dependence of 1500 m distance blowing (Air pressure; 9 kg/sq.cm)

Figure 11 shows the temperature stability of blowing performance of a 1500 m optical fiber unit with using air of 9 kg/sq.cm. In this wide temperature range from -20°C to +60°C, blowing installation of 1500 m optical fiber units were successfully accomplished. The lower blowing speed at +60°C was caused by larger friction between the soften surface of the both optical fiber unit and tube. The lower blowing speed at the -20°C was caused by the larger stiffness of the optical fiber unit.

By these results, stable capability of long distance blowing in this wide temperature range was confirmed.

Attenuation changes by the blowing installations in this wide temperature range were measured as shown in table 2. The maximum attenuation change in the installations at the various temperatures was within 0.02 dB/km at both 1310 nm and 1550 nm. These results mean that this long distance blowing technique is very reliable to install the optical fiber unit in wide temperature range.

Figure 12 shows the temperature dependence of attenuation of optical fibers in a 2000 m optical fiber unit installed in a tube. During three temperature cycles between -30 and +70°C, the maximum attenuation deviation was less than 0.03 dB/km at 1310 nm and 1550 nm. Then, the attenuation stability of the installed optical fibers were confirmed.

Table 2. Attenuation change in blowing process in wide temperature range (-20 ~ 60 °C)

Temperature of tube (°C)		Init.	-20	-10	+20	+50	+60
$\lambda = 1310 \text{ nm}$	Avg.	0.36	0.36	0.35	0.35	0.36	0.35
	Max.	0.37	0.37	0.36	0.36	0.37	0.36
$\lambda = 1550 \text{ nm}$	Avg.	0.22	0.22	0.21	0.21	0.22	0.21
	Max.	0.23	0.23	0.22	0.22	0.23	0.22

We have already introduced this technique to the practical field, 1300 m continuous blowing installation in Hokkaido and 1500 m blowing in Tokyo area.

4. CONCLUSION

The concept and good blowing performance of the transfer blowing technique were described. We are preparing to apply the transfer blowing technique to inter-building and campus networks.

The long distance blowing technology was confirmed to have reliable performance in installation process and after installation, and the results demonstrated that the technology is very effective in outdoor optical network construction.

Requirement of optical network is increasing dramatically from small local area networks to large scale transmission infrastructure. We introduced two new generation blown fiber technologies, and are expecting these new effective technologies support wide extension of optical transmission world.

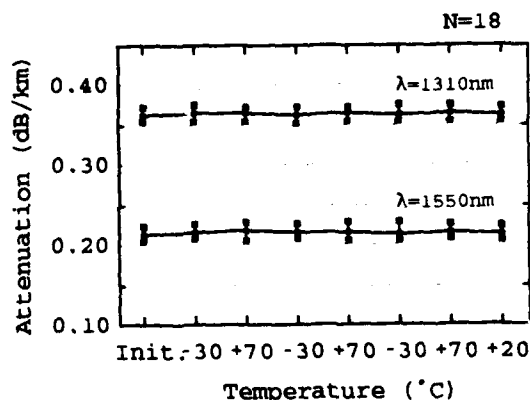


Figure 12. Temperature dependence of attenuation of fibers in a blown unit

REFERENCES

- 1) S.A.Cassidy, M.H.Reeve, IWCS'83 proceedings, pp250-254 (1983)
- 2) H.Sano, Y.Terasawa, et al, IEEE workshop on Local Optical networks '91, 4.4 (1991)
K.W.Cobb, P.D.Jenkins, et al, EFOC '91 proceedings, pp78-82 (1991)
- 3) S.Konnno, et al, IWCS'89 proceedings, pp344-350 (1989)
- 4) Y.Terasawa, H.Sano, et al, IWCS'90 proceedings, pp299-305 (1990)



Hiroaki Sano

Sumitomo Electric Industries, Ltd.
1, Taya-cho, Sakae-ku,
Yokohama, Japan

Hiroaki Sano was born in 1960, and received his M.E. degree in polymer science from Kyoto University in 1984. He joined Sumitomo Electric Ind., Ltd. and has engaged in development of optical fiber manufacturing process and fiber-optic cable design. Mr. Sano is a senior engineer of Communication R&D dept. in Yokohama Research Labs.



Shinya Takaoka

Sumitomo Electric Industries, Ltd.
1, Taya-cho, Sakae-ku,
Yokohama, Japan

Shinya Takaoka received his M.S. degree in electrical engineering from Shizuoka University in 1986. He joined Sumitomo Electric Industries in the same year and has been engaged in the design and development of the fiber-optic cable. He is a member of the Institute of Electronics, Information and Communication Engineers of Japan.

Shigeru Tanaka

Sumitomo Electric Industries, Ltd.
1, Taya-cho, Sakae-ku,
Yokohama, Japan

Shigeru Tanaka was born in 1951 and received the M.E. degree and Ph.D. degree from Tokyo University in 1976 and 1989, respectively. He joined Sumitomo Electric Ind., Ltd. in 1976, and he has been engaged in the characterization and design of optical fibers and fiber-optic cables. Dr. Tanaka is a chief research associate of the Communication R&D Dept. and a member of the Institute of Electronics, Information and Communication Engineers of Japan.



Nobuyuki Suzuki

Sumitomo Electric Industries, Ltd.
1, Taya-cho, Sakae-ku,
Yokohama, Japan

Nobuyuki Suzuki received his B.E. degree in engineering from University of Electro Communication in 1987 and joined Sumitomo Electric Ind., Ltd. He has been engaged in the development and design of fiber-optic cables in the Fiber Optic Division.



Takao Kumakura

Sumitomo Electric Industries, Ltd.
1, Taya-cho, Sakae-ku,
Yokohama, Japan

Takao Kumakura was born in 1950 in Iwate, Japan and graduated in electrical engineering at Tokyo Metropolitan College of Technology in 1972. He joined Sumitomo Electric Ind., Ltd. in 1972 and engaged in production engineering section in Communication Division. He is a assistant manager of Communication Engineering Division.

Effect of waterproofing compound on the performance of optical fiber ribbon

Ting-Chung Chang, Jye-Meei Hsiao, Whei-Jen Chen, Daw-Ming Fann, K-y Chen, Y-c Lin

OSP, Telecommunication Labs, MOC, TAIWAN, ROC

Abstract

The effect of a waterproofing jelly compound on the performance of a optical ribbon is evaluated using the tensile strength, strip force, and macrobending tests. The tensile strength test demonstrates that three types of break can occur among the ribbon. They are (1) simultaneous break; (2) sequential break; (3) defective break. Jelly aging results in more weight of defective breaks and a decrease of the ribbon tensile strength. The strip force test show that two types of stripping mechanisms can appear on the ribbon stripping, which depends on the extent of the adhesion force between the glass and coating and is a way to evaluate the protective ability to the fiber. Jelly aging results in a significant decrease of strip force and adhesion. The macrobending test can examine the individual fiber attenuation of a bended ribbon, and evaluate the relational attenuation when the mother-ribbon is subject to environmental stress. Jelly aging results more additional loss by comparing to the unaged ribbon. At 100°C, the jelly is disastrous to ribbon.

Introduction

To extend the fiber to the subscriber loop, either high-count fibers or high speed transmission is needed to build loop. To meet the high-count loop demand, multifiber linking as a ribbon is implemented into the manufacture of optical cable specially designed for the subscriber loop. In such cables, fibers are physically linked through a matrix coating to form a ribbon which are submerged in a waterproofing jelly compound or wrapped by water-blocking tapes to insulate themselves from the attack of moisture or water[1, 2, 3].

The use of ribbon-type structure has the advantages of compact design, well-fiber-organization, easy assembly into cable, and high counts possibility. However, problems have been complained by the user during field-try-deployment, such as the abnormal high attenuation of certain fiber within a ribbon, geometry distortion of ribbon, difficulty of stripping and separating the adjacent fibers, unexpected breaks of certain fiber within an intact ribbon, and uncontrollable attenuation fluctuated with temperatures and sensitive to the ways of organizing the excess ribbon inside a splice closure. These complains suggest that the performance of the fiber in a ribbon is not as good as that inside the loose tube of a conventional cable even though they are basically the same fibers. Apparently, the characteristics of the individual fiber is strongly related to the status of its mother-ribbon, and the less satisfaction of fiber performance in a ribbon cable maybe results from the abnormal effects that the mother ribbon has experienced. Though the ribbon can be subject to lateral force test, twist test, 90 degree single peel test, and scrubbing test to ensure its mechanical performance[4], we still feel strongly that there is a need for additional test method to address the individual fiber performance and its long term reliability, specially, when the mother-ribbon is subject to environmental stress influence such as the waterproofing jelly immersion effect that has been found disastrous to fiber coating [5]. In this study, we use (1) tensile strength test of ribbon to elucidate the ribbon fracture characteristics, failure strength, and demonstrate that hidden broken fiber can exist inside an intact ribbon, (2) strip force test to examine the property of the ribbon coating, (3) macrobending test to examine the individual fiber attenuation of a bended ribbon, and demonstrate that the same bend may lead

to different extent of induced losses among the constituted fibers. Furthermore, these methods are used to evaluate jelly effect on the change of ribbon performance by looking at the change of break strength, the change of strip force, and the change of induced macrobending losses.

Experimental

Materials :

The fibre ribbon is an edge-bonded type. It is constituted from 12 single mode fibers ($125\ \mu\text{m}$) coated with dual coatings to a diameter of $250\ \mu\text{m}$. The waterproof compound is a thixotropic jelly composed of mineral oil and SiO_2 , and is commercial available.

Aging :

A 12-fiber ribbon was cut to numbers of samples at a length of ca. 1000 m and were loosely wound as circles (diameter =300 mm) that placed in containers with the ends of ribbons leaving outside the containers. The samples were divided into two groups. One group was aged at 50, 70, and 100°C in air, and the other was aged in jelly compound at 50, 70, 100°C . Sample of ribbons were removed from aging at period of time and the change of tensile strength, strip force and bending loss were measured.

Tensile Strength :

Minimum of 20 specimens for each sample were measure in a Universal Testing Machine using a gage length of 500 mm and a strain rate of 20 mm/min under a laboratory ambient environment of 23°C and relative humidity of 60%.

Strip Force :

Minimum of 10 specimens of each sample were measured in a customized stripping tensile testing machine mounted with a commercial 12-fiber stripping tool. The tool was pre-heat for 12 seconds using a DC power supply in a current output of 2.5 ampere to reach the temperature of $105 \pm 5^\circ\text{C}$ before stripping. The gage length is 100mm and stripping length is 15 mm with a stripping rate of 150 mm/min. Strip force were collected through out the stripping process. Each

sample datum was taken from the median of 10 tested specimens.

Macrobending Loss :

The attenuation of each sample (ca. 1000 m) was measured in a commercial spectrum meter scanned from 1000 nm to 1600 nm using cut-back method. First, the ends of a loosely winding sample (diameter=300 mm) was coupled to the input and output of a spectrum meter and the power output (P_0) was measured. Second, taking the middle part of the testing fiber without disturbing the input and output coupling and winding the fiber on the outside of a glass mandrel (diameter=30 mm) for 0 to 40 turns. The power reading was then taken as (P_i) according to each specified mandrel diameter and number of turns. Finally, cut the fiber back to a length of 2 m and reconnect it to the detecting position. Obtain a short-length power (P_f) as the reference. Attenuation (A_i) of each bend condition was then calculated as: $A_i = 10 \log (P_f/P_i)$ $i = 0, 1, 2, \dots$

Result and Discussion

Fracture characteristics of ribbon

The tensile characteristics of ribbons were studied in different strain rates. It appears that the maximum breaking strength is indifferent to the strain rates within the testing range. The maximum break strength of a ribbon usually equal to the sum of the strength of all constituted fibers provided that the matrix coating applies equal stress on all the individual fibers. However, by carefully examining the tensile-stress-strain profile, It was observed that, in some cases, a minor break that corresponding to the break of one particular fiber can occur below the peak breaks (the maximum break) of a ribbon. It was also observed that multiple breaks (corresponding to multiple fiber breaks) following the peak breaks can be distinguished. In short, three types of fracture mode can be characterized : They are (1) simultaneous breaks as shown in Figure 1-a, where all the individual fibers break at the maximum point instantly; (2) sequential

break as shown in Figure 1-b, where, after the maximum break point, the fibers starts breaking in observable sequential manner; (3) defective break as shown in Figure 1-c where a minor break occurs below the maximum break. In the mode-type 3, a defective break that corresponding to the break of certain fiber may have occurred while the ribbon remains showing reasonable strength sufficient to pass the proof test. This may lead to an incorrect ribbon proof test since the ribbon has passed but, actually, a fiber has failed and undetected. We have found that in a typical group of test, it shows that simultaneous breaks occupy a weight of 72 %, accompanied by 20 % of sequential breaks and 8 % of defective break. The truth of the exist of such 8% defective breaks may account why there is always having complain about unexpected breaks of certain fiber within an intact ribbon in ribbon cables. In addition, by apply a load of high stress but below the breaks such as the proof test on a ribbon may cause an unrecoverable geometry distortion of ribbon as shown in Figure 2. Such permanent deterioration will give the constituted fibers differ amount of stress that cause some of the fiber showing an *abnormal attenuation provided that such ribbon have passed the proof test and manufactured into the cables*. As a result, proof test of ribbon has to be done in a careful manner and additional examination of ribbon is required.

Tensile strength of ribbon aged in Jelly

Figure 3 shows the Weibull plot of the tensile strength of fiber ribbon aged in jelly for 5 month at 50, 70, and 100 °C along with the unaged original. The failure strength is defined as the tensile load that corresponding to the first break wherever occurred. In Fig. 3, all three jelly aged ribbon show decreases of strength with a trend of higher aging temperature showing more drop of strength. for example, at 100 °C, the median ribbon strength dropped by 37% of the original strength. This is consistent with a previous study showing improper jelly may have penetrated the coating and causes the deterioration of coating to result in a drop of fiber strength [5]. The drop of strength is not a heat effect or measure condition effect since, as

shown in Figure 4, the heat-aged sample shows a little drop of strength but the jelly aged sample gives more drop. In addition, after 5-month of aging in 100 °C, the ribbon has become sticky and sometime looks swelling. Also, handling and separating become extremely difficulty. During separating, bare fiber instead of the supposed color coded fiber was always obtained since the inner primary coating always comes out and stick with the matrix coating. Apparently, the adhesion of primary coating has completely disappeared and the coating can be peel off sometimes just simply by bare fingers. Finally, a grouping of the break types for this jelly-aged ribbons has shown that simultaneous breaks occupy a weight of 26 %, accompanied by 32 % of sequential breaks and 42 % of defective break. The defective breaks have significantly increased and the ribbon is no longer considered as reliable.

Figure 5 shows the infrared absorptions of matrix coatings that aged at 100 °C for 4 weeks, 2 month, and 4 month. As the aging time increases, the absorption at 805 cm^{-1} decrease. This is an indication of the degradation of coating and the degree of degradation can be followed by monitoring this peak.

Strip Force

Figure 6 shows the strip force profiles of the jelly-aged and unaged ribbons. The unaged and 70 °C-jelly-aged ribbons show similar profiles with a sharp rise of strip force followed by a fluctuation of forces and end suddenly. On the other hand, the 100 °C-jelly-aged ribbon shows a complete different profile with a moderate rise of force followed by smooth and gradual drop of force to the end. The difference of the maximum force and stripping profile shown on Figure 6 that can be grouped into two categories indicates two completely different stripping mechanisms have experienced by the ribbons. In Category (1) as represented by the un-aged ribbon, the stripping start with severing the strip part from the main part by the tool blade, in the meantime, the strip part is squeezed by the tool blade and, due to the strong adhesion, the coating of the strip part begins to buckle, twist, partially crack, and finally rupture to shreds. In such a process, the squeezing and bulking will give a sharp rise of strip

force followed by the cracking and rupture that reflect a drop of the strip force. Since the squeezing-cracking occurs instantly, and actually is progressed alternatively until the strip part is completely stripped off, as a result, the profile of such stripping will show a rise/drop type of fluctuation of forces. More evidences that support this mechanism can be seen when carefully examining the stripped ribbon and the stripped matrix coating debris. As shown in Figure 7, the stripped bare fibers always contain debris of coating and the strip matrix coating is totally broken to pieces. This indicates that strong adhesion between the coating and glass remain effective. In Category (2), as represented by the 100°C-jelly- aged ribbon, the stripping is more like a sliding behavior. Initially, the rise of strip force is proportional to the friction resistance force until the force overcome the maximum static friction force to transcends to dynamic friction forces, and the strip force decreases smoothly and gradually to zero as the matrix coating comes off. More evidences are seen in Figure 8 as the stripped-off matrix coating remains intact without any rupture (just like coming out with whole piece) and the stripped bare fibers are shining clean without any debris on it. The sliding mechanism reflects the adhesion between glass and coating is ineffective and the strip force is lower.

Strip forces of aged ribbons

The strip forces of aged ribbon are listed in table 1. The strip force show no substantial change on those ribbons aged at 50 and 70°C by heat or jelly. But for the ribbon aged at 100 °C , the heat aging gives an progressive increase of forces as the aging time increases while the jelly aging gives initially rise of strip force within 2 month of aging and is followed by a significant drop thereafter. This drop of strip force are consistent with the tensile strength observations and stripping profile discussed above. All the evidences indicate that, under such aging condition, the coating has deteriorated and the adhesion has disappeared to result in ineffective protection on the fiber. Also, the ribbon is difficulty to handle and splicing.

Macrobending Loss

Figure 9 showed the macrobending attenuation spectra of the #1, #6, and #12 fiber in an unaged ribbon. The macrobending is induced by winding the ribbon over a glass mandrel of 3 mm diameter for 0 to 40 turns. More turns results more loss at wavelength beyond 1500 nm and is shown as a typical macrobending loss. Both edge fibers of the ribbon (#1 and #12) show higher losses than the inner fiber (#6) since the edge fiber were endured more stress when the bending is imposed. Also, by placing the #1 fiber in the left hand side or right hand side during winding the ribbon will yield different induced loss. As showing following, left hand side gives more stress.

Placing position	Induced loss at 1550 nm
Left	0.477 dB at 40 turns
Right	0.365 dB at 40 turns

This demonstrates that certain fiber within a ribbon may show an unexpected high attenuation if the ribbon is distorted or bended.

Macrobending loss of aged ribbon

Figure 10 show fibers of #1, #6, and #12 attenuation spectra from the ribbon that jelly-aged at 100°C for 5 mcnth. Effect of jelly, especially under the combination of heat can result more induced losses. All three fibers show additional losses by comparing to the unaged one. This means that, under the same bending condition, the aged ribbon will be more sensitive to bending. the result is consistent with a previous study [?] that the heat and jelly aging fibers become much vulnerable to macrobending because of the thermal aging can induce the post-curing of buffer coating and the entering jelly can soften the dual coating. The result is a compromising effect that always induce an additional loss. The effect is more apparent for ribbons since the jelly effect major softening the primary coating only (cause a drop of strip force) while the secondary and matrix coating ribbon may have been hardened by the heat effect (Figure 8 shows the stripped-off coating is intact). The final effect will be a harder matrix coating

exerting on the fibers and less buffering that result in more induced loss when the bending imposed. The fiber is more restricted by the matrix coating, and is no longer as free as that inside a loose tube in a conventional cable. The matrix coating should be considered as a disadvantage material when the free motion of fiber inside a cable is more important.

Conclusion

The tensile strength test of ribbon can elucidate the ribbon fracture characteristics, failure strength, and uncover the ribbon with hidden low strength fiber. The strip force test can examine the property of the ribbon coatings to evaluate the adhesion and protective ability to the fiber. The macrobending test can examine the individual fiber attenuation of a bended ribbon, and evaluate the relational attenuation when the mother ribbon is subject to environmental stress. Furthermore, these methods are used to evaluate jelly effect on the change of ribbon performance by looking at the change of break strength, the change of strip force, and the change of induced macrobending losses. At 100°C, the jelly is disastrous to ribbon that tested in this study.

Reference

1. T.T.Wang, H.M.Zupko, J.Materials Science, p2241 (1978)
2. W.J. Duncan, P.W. France, and S.P.Craig, " The effect of environment on the strength of optical fiber" in Strength of Inorganic Glass, C.R.Kurkjian, ed,Plenum Press, New York (1985)
3. A.Iino, M.Kuwabara, and K.kokura, J. Lightwave Technol. 8(11),p1675 (1990)
4. K.W.Jackson, P.D.Patel, M.L.Pearsall, J.R.Petisce , Proceed. 38th IWCS, p569 (1989)
5. J.M.Hsiao, S.I.Wang, K.Y.Chen, T.C.Cheng, D.M.Fann, Y-c.Lin, Proceed. 41th IWCS, p453 (1992)

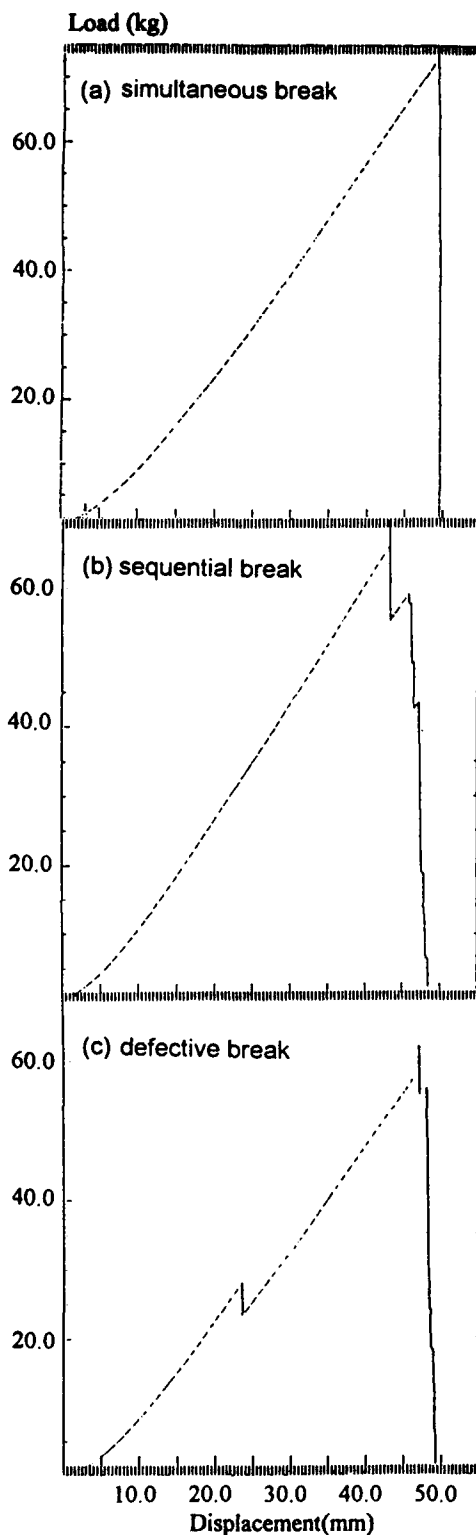


Figure 1. The tensile characteristics of ribbons:
 (a) simultaneous break
 (b) sequential break
 (c) defective break



Figure 2. The geometry distortion of a ribbon

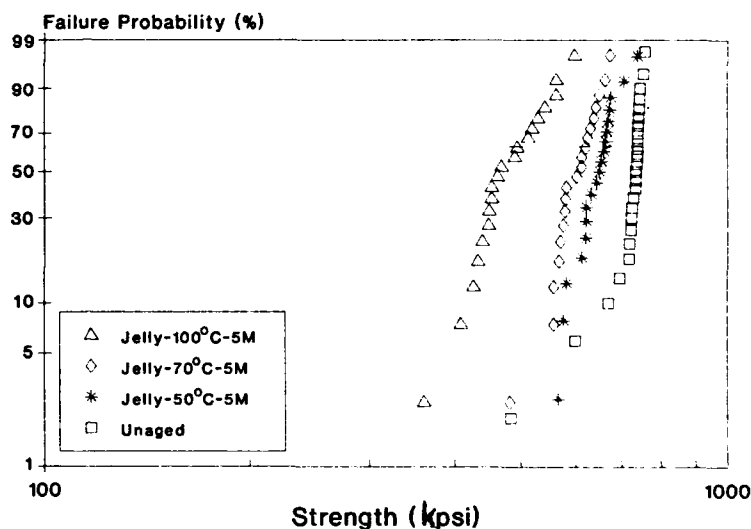


Figure 3. The Weibull plot of the tensile strength of fiber ribbon aged in jelly for 5 month at 50, 70, and 100°C

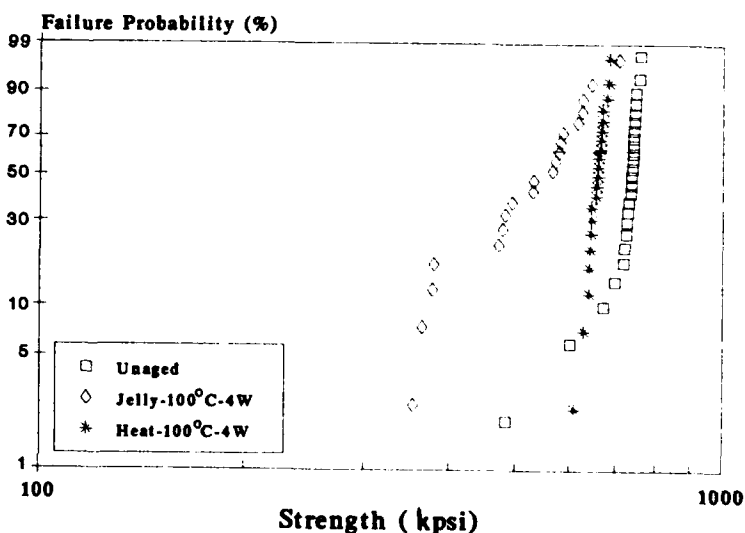


Figure 4. The Weibull plot of the tensile strength of fiber ribbon aged in heat and jelly for 4 weeks at 100°C

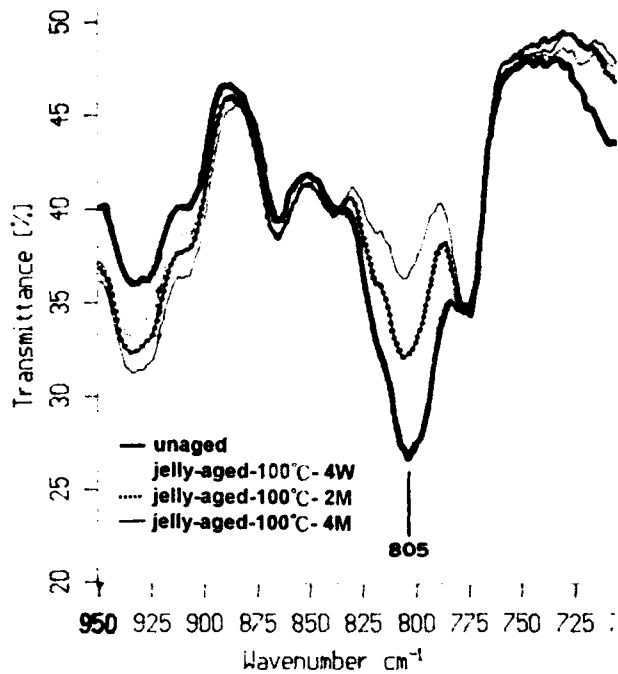


Figure 5. The infrared absorptions of matrix coatings from the ribbons aged at 100°C for 4 weeks, 2 month, and 4 month

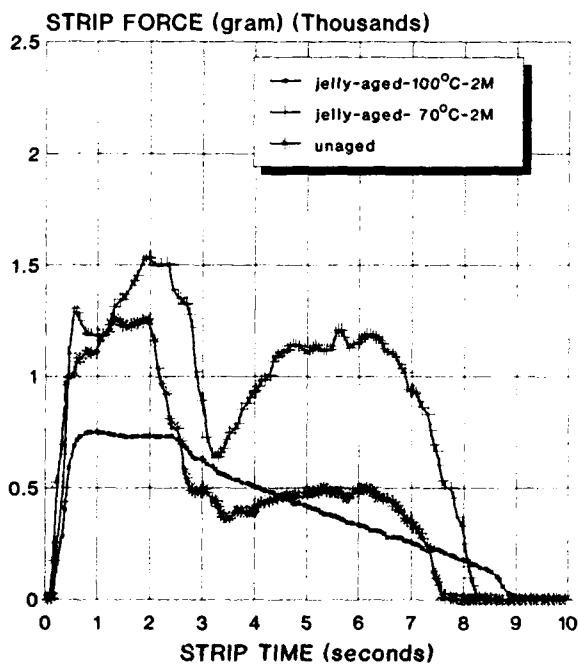


Figure 6. The strip force profiles of jelly-aged and unaged ribbons

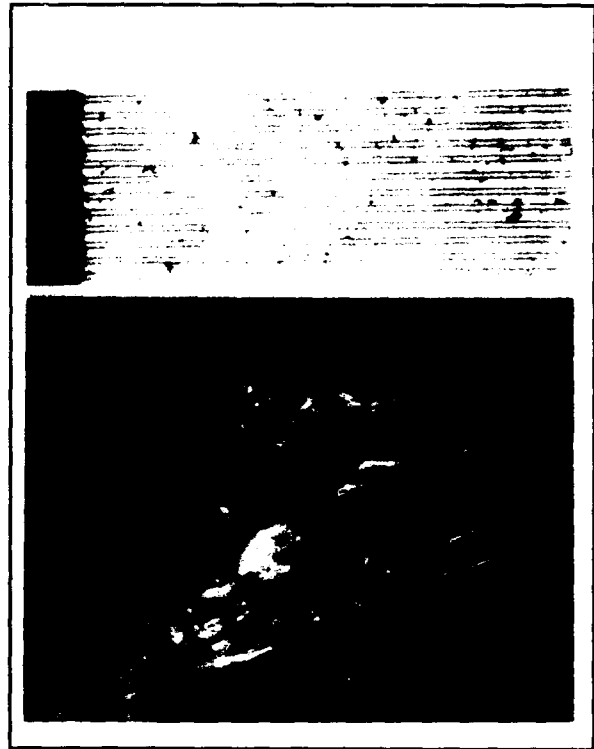


Figure 7. The stripped bare fibers and stripped-off matrix coating from the unaged ribbon.

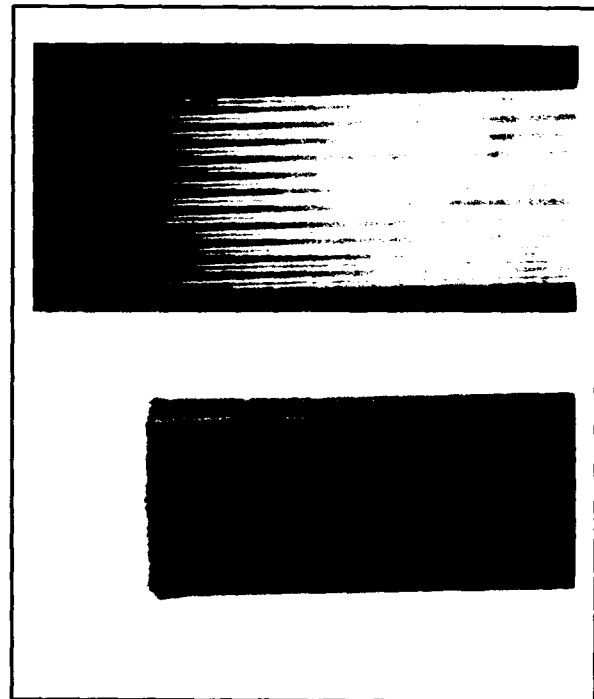


Figure 8. The stripped bare fibers and stripped-off matrix coating from the ribbon aged at 100°C for 2 month

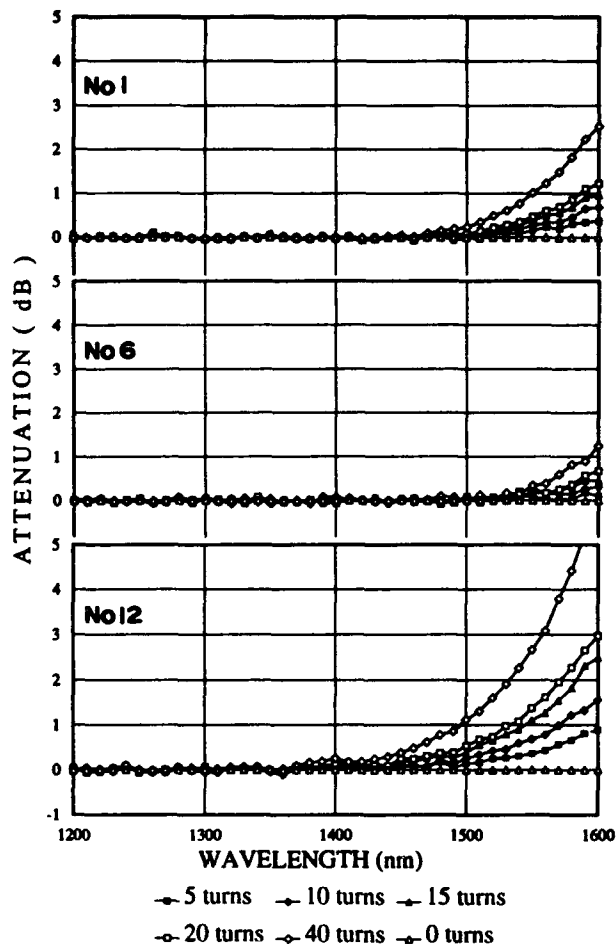


Figure 9. The macrobending attenuation spectra of the #1, #6, and #12 fiber from an unaged ribbon

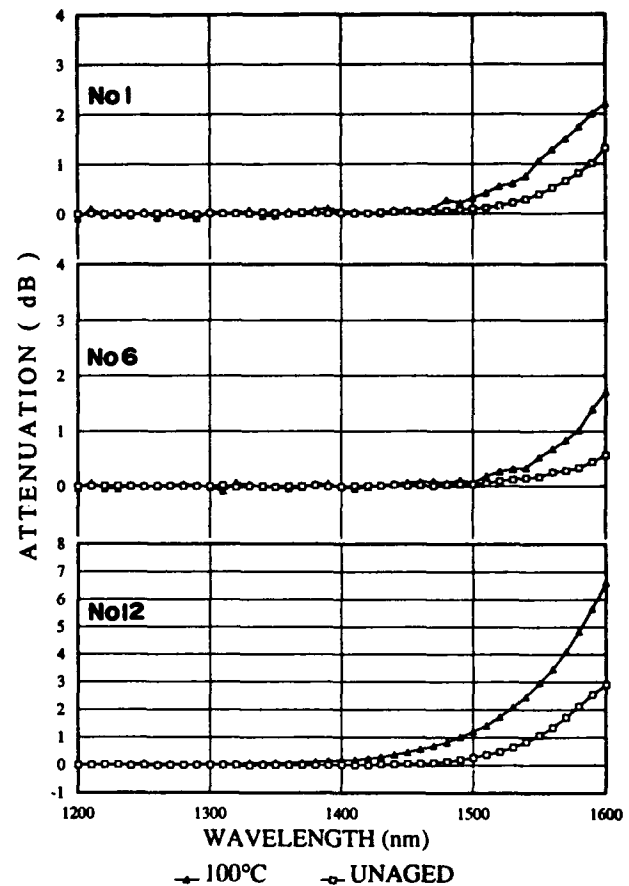


Figure 10. The macrobending attenuation spectra of the #1, #6, and #12 fiber from the ribbon aged in jelly at 100°C for 5 month

TABLE 1 STRIP FORCES OF AGED RIBBONS

aging condition	STRIP FORCE (gram)					
	UNAGED	1 WEEKS	2 WEEKS	4 WEEKS	2 MONTHS	4 MONTHS
50°C-jelly	1250	1152	1224	1327	1436	1180
70°C-jelly	1250	1231	1290	1357	1525	1230
100°C-jelly	1250	1271	1278	1380	743	560
50°C-heat	1250	1156	1213	1318		
70°C-heat	1250	1231	1256	1301		
100°C-heat	1250	1365	1321	1511		

IMPROVED AUTOMATIC OTDR MEASUREMENT OF FIBER-RIBBONS OR FIBER BUNDLES USING RIBBON HANDLING TECHNIQUES.

J. Piffaretti and B. Jenzer

CABLOPTIC S.A., CH - 2016 Cortaillod, Switzerland

Abstract

Fast and reliable automatic OTDR measurements of optical fiber-ribbons or temporarily ribbonized fiber bundles can be performed using an experimental alignment and switching device.

A short description of the apparatus is given. Tentative specifications and test-performances are presented.

1. Introduction

Numerous checks of the optical fiber performances, account for a sizeable part of the cable manufacturing costs. This charge is becoming increasingly heavy as the fiber count in telecom. cables keeps going up.

Something has to be done to compensate the inflation of the fiber count by reducing as much as possible the time spent by operators in fiber-, OTDR - and data-handling.

The amount of fiber handling can be greatly reduced by adopting standard fiber-ribbon preparation techniques, even for fiber-bundles temporarily ribbonized. The OTDR - and data-handling times are best reduced by automating the measurement process by mean of PC connections. The idle periods of the OTDR are also optimally reduced by this means.

This rationalising scheme cannot be achieved without an opto-mechanical interface, remotely operable, used to connect in sequence all fibers in a series of ribbons to the OTDR pig-tail. The principles of the operation we have chosen for these devices, their main features and test-performances are described in this paper.

2. System prerequisites

2.1 Combined alignment and switching functions

Automatic OTDR measurement sequences may be carried out either by means of sealed 1-N fiber-switches with the addition of N manual connection systems, or by some dedicated device combining the functions of switching and alignment (see fig. 1).

In the first case, each fiber to be measured must be manually connected beforehand to a corresponding fiber from the switch. In the other case, the fibers are only loaded onto the multi-functional device where all necessary connections are performed later without additional handling. Less time and manual skill are needed in the latter case.

Other advantages of function-combining systems are: maximum flexibility (any kind of 125 μ m fiber, singlemode or multi-mode, can be measured), low return losses (the use of index-matching fluid is possible), easy recovery from bad connections which can be automatically repeated or pointed out.

Both categories of systems may be equally perturbed by connection problems at the levels of the measured fiber cleaves.

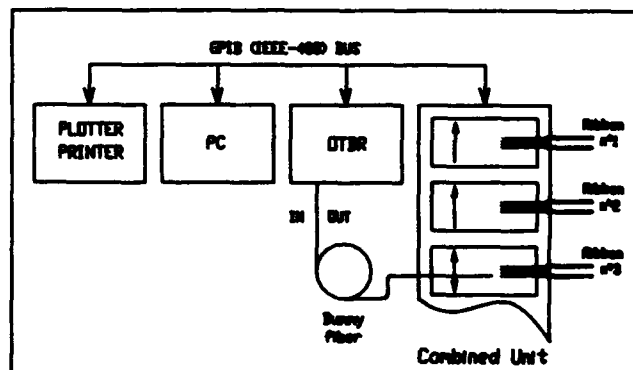


Fig. 1: Automatic measurement set-up with a combined switching and alignment unit.

2.2 Adjustmentless fiber alignment

No core alignment is performed before collectively splicing fiber-ribbons or mounting them into multi-fiber connectors. In both applications, fibers are aligned with respect to their reference-surface (diameter of 125 μm) in V-groove arrays. The connection-losses obtained are nonetheless satisfactory with averages claimed below 0.3 dB. Such results are compatible with the needs of OTDR measurements which are self-referenced anyway.

For the sake of simplicity and economy, V-groove adjustmentless alignment method was chosen for our developments.

2.3 Full compatibility with ribbon-preparation tools and techniques

Stripping and cleaving of fiber-ribbons containing currently up to 12 fibers can be performed as quickly as that of single fibers thanks to standard tools, now widely distributed.

The normal fiber-ribbon preparation time is recalled in fig. 2. Only a short length of the fiber remains after cleaving, which keeps the deformations arising from hot-stripping, electro-static forces or capillary attraction under control.

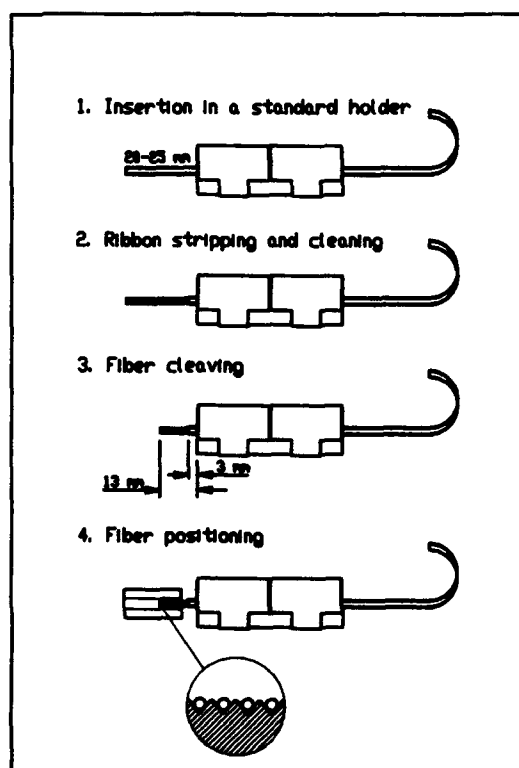


Fig. 2: Ribbon preparation and positioning.

The distance of the fiber cleave from the front face of the ribbon-holder is reproducible within 10 microns for any definite cleaving tool.

A key element in the routine is the standard ribbon-holder where ribbons can be easily but accurately inserted. This holder is used as a handling support throughout the process which saves a lot of handling time.

Full compatibility of our alignment systems with the above routine was considered very important.

3. Realisation of an experimental alignment device

3.1 Basis of realisation

At least one device satisfying all the above prerequisites is currently available [2], [3]. Automatic measurements of single-mode fiber ribbons performed with this apparatus are more than 95% successful (with connection-losses below 1 dB). Most higher losses can be brought back into this acceptance range by mere realignment (automatic) or reloading (manual) without need for a new ribbon preparation. Such an operation-record can be considered very good but it still leaves room for further improvements.

With this goal in mind, experiments were conducted on a standard Multiple Alignment System (see fig. 3) whose superstructure was modified for this purpose. Potential sources of alignment disturbance were investigated and analysed (see section 4.3).

Possible evolutions of the ribbon-loading system and measuring sliding arm are outlined in the next sections.



Fig. 3: Superstructure of a standard Multiple Alignment System.

3.2 Ribbon loading

Fiber-ribbons prepared as shown in fig. 2 / step 3 are next loaded manually onto the alignment system (see fig. 2 / step 4). Two equivalent loading devices have been tested extensively, both making this operation simple and reliable.

In a version already widely in use, the ribbon-holders are mounted on hinged supports which are then swung down introducing all the fibers into the corresponding alignment grooves [2]. In a simpler version, the ribbon-holders are guided down sloped ramps with the same final outcome (see fig. 4).

3.3 Mechanical switching motions

The test-signals from the OTDR pig-tail (or dummy-fiber) are injected by butt-end alignment into any fiber loaded on the system without manual handling. The necessary motions are carried out by a sliding arm supporting the OTDR fiber. The mobile fiber points downward under a fixed angle close to that of the loaded ribbons.

The sliding arm can move sideways to automatically face any alignment groove in the system. It then moves downward until the fiber tip touches the groove and continues until it becomes tangential to it. Finally it is brought forward until optical contact with the opposite fiber is reached. Both vertical and horizontal motions can be combined in a single diagonal motion (see fig. 4).

All motions take place along ball slides by step-motor actuators. The magnitude of each displacement is fixed and does not need frequent adjustments.

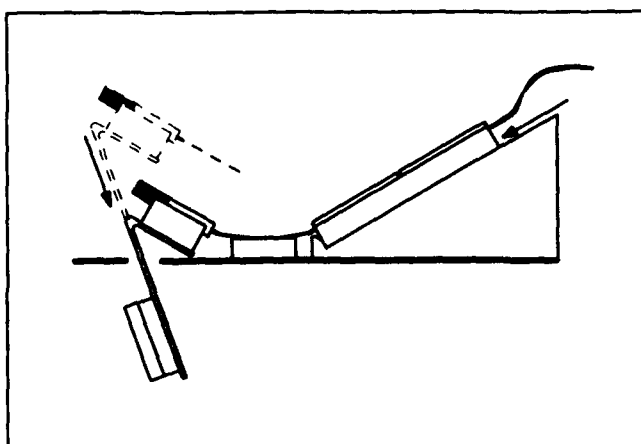


Fig. 4: Alignment layout

3.4 Mastering alignment disturbances

Disturbances of several kinds can bias V-groove alignments. Fortunately, most of them are mastered merely by concentrating the transverse alignment pressures as close as possible to the fiber tips. Extended contacts between fibers and grooves must be avoided.

Dust particles of small diameter, most common in a normal atmosphere [4], may induce misalignments much larger than their own size if they get stuck between fiber and groove. The disturbance can be especially pronounced if the insertion occurs far from the cleaves within an extended contact area between fiber and groove (see fig. 5a). This is however unlikely if the alignment pressure is produced by bending and is located at the fiber tip.

Angled cleaves are occasional sources of misalignment. Fibers abutted, even under moderate axial pressure, may slide aside if one of them has an angled cleave. This bias is induced by the component of the abutting force tangential to the cleave (see fig. 5b). It is cancelled only if the transverse alignment forces are applied on the fiber tips.

If one of the fibers to be aligned is initially angled with respect to the alignment axis and rotates later into alignment by flexing; it was observed that it can act as a lever on the other fiber. Misalignment results from this mechanism but can be prevented by adjusting the point of contact between the levered fiber and the groove at its exact tip (see fig. 5c).

All these troubles are avoided if the alignment layout is optimal.

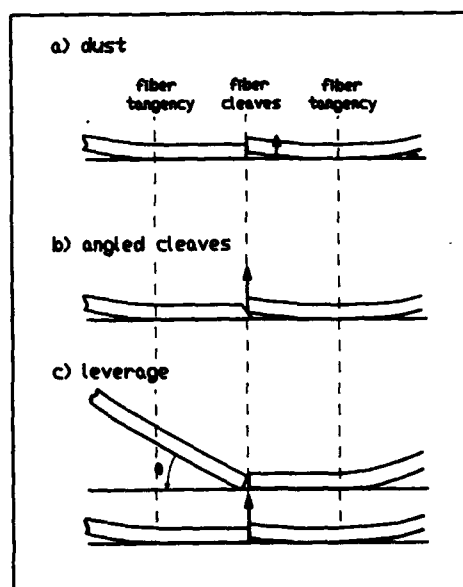


Fig. 5: Sources of alignment disturbance

4. Specifications and Testing of the experimental device

4.1 Technical specifications

The above prerequisites and new notions led to the realisation of an experimental alignment and switching device with the following tentative specifications:

Operation modes: GPIB (IEEE 488) or manual
Alignment: mechanical (see section 3.1)
Types of fibers: singlemodes or multi-modes
Types of ribbons: currently 2-to 12-fiber ribbons
Fiber spacing: currently 0.250 mm
Switching time: 1 second
Alignment losses: see section 4.2.
Reproducibility: see section 4.2.
Stability: better than ± 0.05 dB.

Ribbon-holders for 2, 4, 8, 10 and 12-fiber ribbons (or ribbonized fiber-bundles) are compatible with the same sloped ramp loading system. The 12-groove array is used for all kinds of ribbons of 0.250 mm pitch.

4.2 Test performances

Tests were performed with ribbons containing 4, 8, 10 (ribbonized fiber-bundle) and 12 fibers. Reproducible low-loss alignments were obtained for all kinds of ribbons without having to readjust the alignment layout. The same cleaving tool was used exclusively to keep the fiber-lengths constant.

Alignment appears very robust. Dust induces no noticeable disturbance even after several days without V-groove cleaning. Self-cleaning of the system by fiber-friction along the alignment grooves seems very effective.

Loss-increases due to angled cleaves were never observed, except when large abutting pressures between fibers were produced for test purposes.

As a final test, cyclic measurements were performed on a 12 fiber ribbon at 2 wavelengths for several days. The anti-dust cover of the alignment-system was removed on purpose during this test to increase its significance. A total of 8520 alignments and switchings were performed, without repeating contact in the case of a miss.

The unidirectional splice-losses observed by the OTDR for the 12 fibers are plotted as a time function in fig. 6a (1300 nm) and fig. 6b (1550 nm). One single value only is off-scale. No degradation appears over the measurement period of four days.

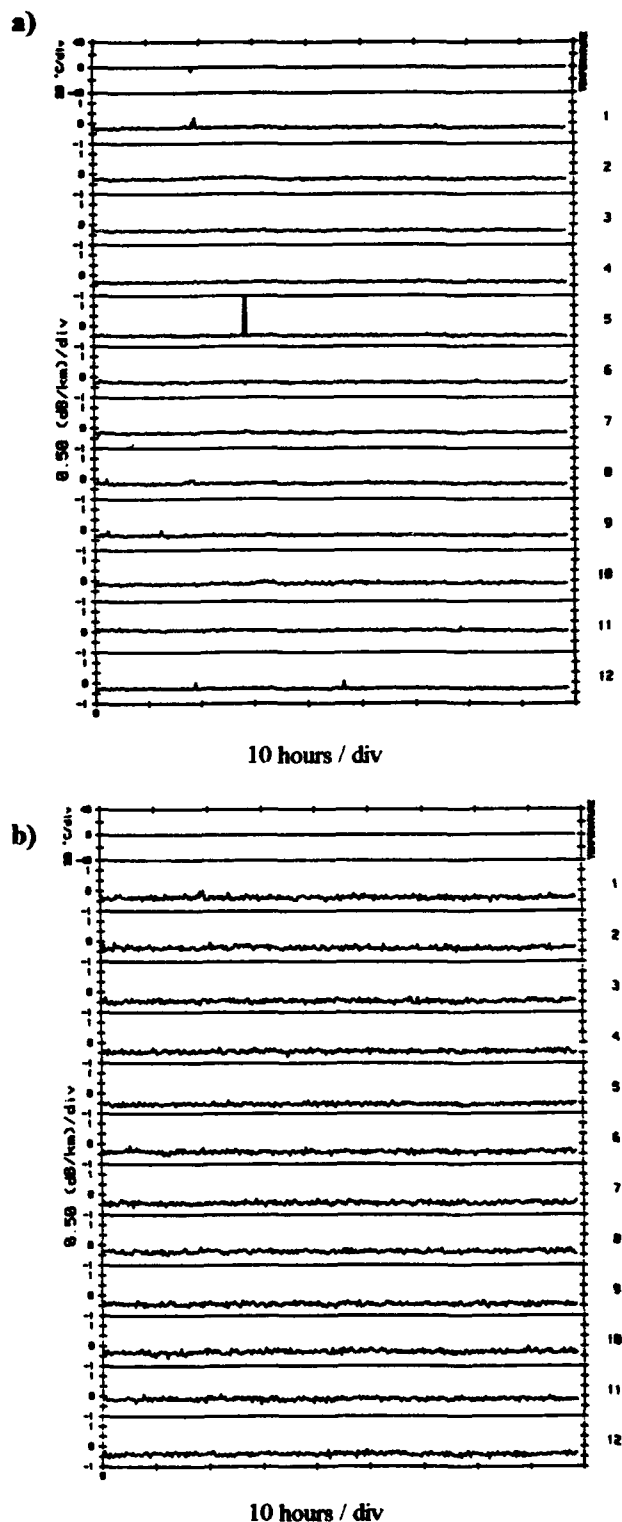


Fig. 6: Reproducibilities of the OTDR splice-losses of a 12 - fiber ribbon at 1300 nm (top) and 1550 nm (bottom). 8520 alignments were performed over a four day period.

Splices-losses histograms of 3 fibers from the same data are superposed in fig. 7 (1300 nm measurements). The standard variation of any of these histograms is close to 0.04 dB.

Negative mean-values of the splice-losses appearing in fig. 7 are explained by spot-size differences between the dummy-fiber and the measured fibers.

5. Conclusions

This development has derived much benefit from years of practical experience gathered in service with different alignment systems.

The confirmed advantages of the experimental device are its high tolerance of dust and its good loss reproducibility, both derived from optimal alignment layout. Less cleaning of the alignment grooves should be required with such a system owing to the robustness of its alignments and to the self cleaning action of its operation.

References:

- [1] J. Piffaretti, M. Pfister, O. Rickli "A new switching device allowing automatic OTDR measurement of series of single-mode fibers", Proceedings EFOC/LAN-88.
- [2] B. Jenzer, J. Piffaretti, O. Rickli "Automatic measurement of optical fiber-ribbons using a new alignment and switching device", Proceeding EFOC/LAN-90.



José Piffaretti
CABLOPTIC S.A
Rue François Borel
CH-2016 Cortaillod
Switzerland

José Piffaretti received his PhD in Physics from Neuchâtel University in 1970. He was engaged in Nuclear and Particle Physics until 1981 and then joined CABLOPTIC where he is involved in the development of optical fiber, cabling elements and measuring systems.

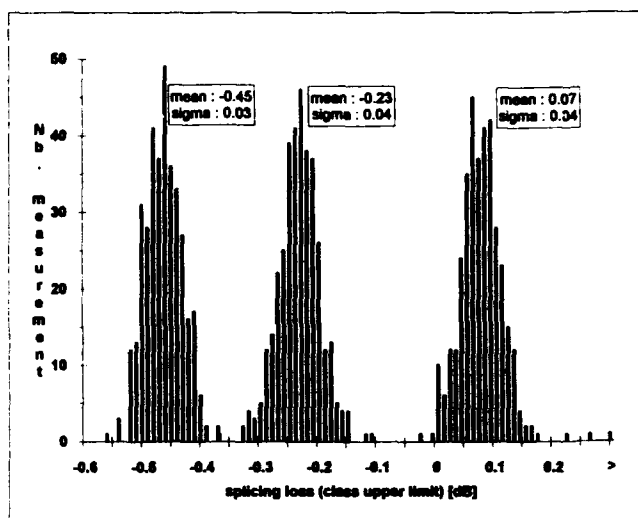
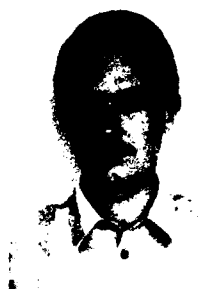


Fig. 7: Splice-loss histograms of 3 fibers, from the same data as Fig. 5 (top), 1300 nm.

- [3] "MAS-900", AESA-Cortaillod, CH-2016 Cortaillod, Switzerland.

- [4] K.E. Noll and M.J. Pilat "Size distribution of atmospheric giant particles", Atmos. Environment 5 (1971) 527-540.



Bernard Jenzer
AESA
Rue de la Fabrique 2
CH-2016 Cortaillod
Switzerland

Bernard Jenzer received a diploma in Microtechnics Engineering in 1989 from the Ecole Technique Supérieure de Yverdon. He joined CABLOPTIC in 1990 and AESA in 1993. He is active in the development of measuring systems and new cabling elements.

HIGH DURABILITY COUPLERS

Satoshi Endo, Takashi Ide, Tomoyuki Hattori, Thomas Morrison, and Toshiyuki Wakinosono

Sumitomo Electric Industries, Ltd.
1, Taya-cho, Sakae-ku, Yokohama, 244, Japan

ABSTRACT

This report describes research and testing methods and computer modeling techniques used for the development of high durability optical fiber couplers with good vibration resistance characteristics and good optical performance stability under adverse thermal conditions. Further, it describes a quality assurance tensile test screening method for elongated optical fibers to assure a minimum 20 year coupler performance lifecycle. First, the fiber tensile test screening method for long term coupler quality assurance is outlined. Next, the computer aided engineering methods and experimentation used to develop couplers with good vibration resistance is outlined. Finally, the experimentation which led to the establishment of design parameters for couplers with good thermal stability is outlined. These methods are general in nature and apply to couplers of all types including: wideband, wavelength division multiplexing, and splitter couplers.

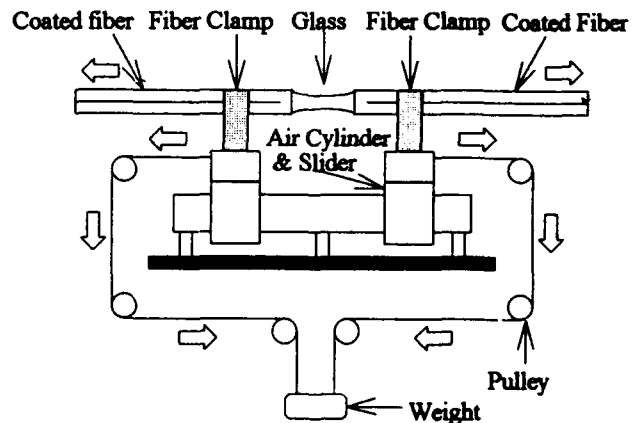
INTRODUCTION

With an increase in the diversity and number of coupler applications and the demand for improved coupler optical performance under adverse conditions comes the need for the development of high durability couplers with good vibration resistance and good thermal stability. Special applications such as the automotive and aerospace industries require couplers to have minimum critical frequencies and maintain minimum insertion loss values and minimum changes in insertion loss values within stringent temperature ranges. Coupler operating environments are different for different applications, but usually within temperature ranges of -20°C to $+60^{\circ}\text{C}$ and are subjected to vibrations below 1000 Hz. This temperature range and minimum critical frequency were used for testing purposes and to establish coupler design criterion.

COUPLER RELIABILITY ASSURANCE

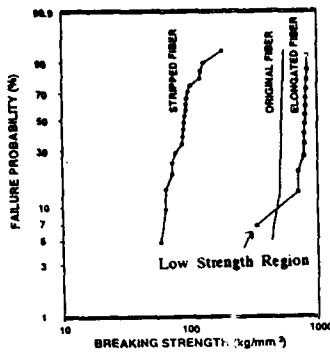
Couplers are made from fused elongated optical fibers. Fiber preparation procedures leading up to fusion and elongation cause crack generation on the glass surface. Most of these cracks disappear after elongation making the elongated fiber breaking strength comparable with that of original coated fiber; however, as shown on the elongated fiber Weibul plot, there is a low strength region. Thus, some cracks remain which may allow for fiber breakage in the presence of stress.

An effective on-line quality assurance screening method (see Fig#1) has been established to assure minimum 20 year endurance life cycles for optical fiber couplers. Coupler fused taper glass regions are subjected to tensile testing. This proof testing is an effective method for eliminating defects¹⁾. From tensile testing results and normalized proof stress calculations, theoretical failure probability calculations²⁾ can be performed to assure minimum established coupler life cycles. The graphs below (see Fig#2 & Fig#3) show Weibul strength curves for stripped, standard coated, and elongated fibers and theoretical failure probability calculations from tensile testing.

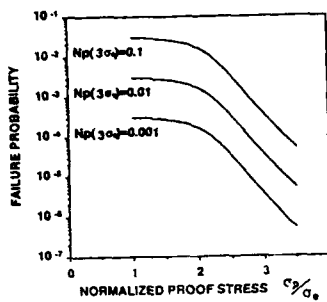


Fig#1 SCREENING METHOD

COUPLER RELIABILITY ASSURANCE (Continued)



Fig#2 WEIBUL PLOT OF BREAKING STRENGTH FOR STRIPPED AND ELONGATED FIBER (gauge length for original and stripped fiber 300mm, elongating length 6 mm)



Fig#3 RELATIONSHIP BETWEEN PROOF STRESS AND FAILURE PROBABILITY ($t_p = 1$ sec)

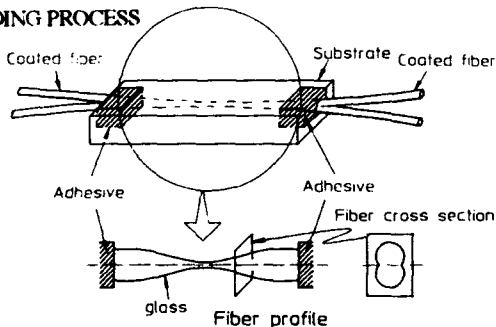
$$F = 1 - \exp \left[-N_p (\sigma_p) \left\{ 1 + \left(\sigma_e / \sigma_p \right)^{2n} \left(t_p / t_p \right)^{m/2} \right\} \right]$$

$N_p (\sigma_p)$ = failure number
 t_p = time to failure
 σ_e = equivalent applied stress
 σ_p = proof stress

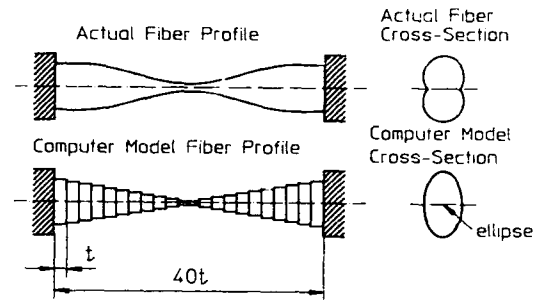
VIBRATION RESISTANT COUPLERS

Computer aided engineering techniques were used to model the first mode of vibration for coupler fused taper glass portions to aid in the optimization of the design of couplers with critical frequencies above 1000 Hz. Diagrams of the actual coupler structure and the representative geometries used for computer modeling are shown in Fig#4 and Fig#5.

MOLDING PROCESS



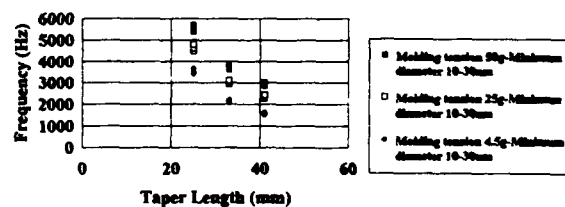
FIG#4 ACTUAL COUPLER STRUCTURE



Fig#5 ACTUAL AND MODEL FIBER GEOMETRIES

Coupler vibration resistance is a function of the fiber tension during and after molding (joining of the fused taper glass portion to substrate) and the fused taper portion length. As shown in the computer model diagram, elliptical cross-sections were used for representative fiber cross-sectional geometries. The necked down fiber geometry was represented by stacking constant thickness elliptical discs of different heights and widths. Longitudinal vibrations are represented by movement of the fiber along the long (major) axis of the ellipse and axial vibrations are represented by movement of the fiber along the short (minor) axis of the ellipse. Computer generated data for both vibration planes showed that, in general, couplers are more sensitive to longitudinal vibrations. Theoretical graphs for coupler minimum critical frequencies as functions of taper lengths and molding tensions were generated for different minimum fused fiber portion cross-sectional diameters (see Fig#6 & Fig#7). These generalized graphs represent the superposition of all worst case data points at different molding conditions. Results showed that coupler vibration resistance is improved by reducing taper lengths and increasing fiber tension during molding. From the computer model data, it was shown that a minimum 25 gram fiber tension during molding is required to assure manufacturing of couplers with minimum 1000 Hz critical frequencies for all taper lengths. Further, it was shown that the minimum fused portion cross-sectional diameter in the range from 10 ~ 30 microns does not greatly influence coupler vibration characteristics.

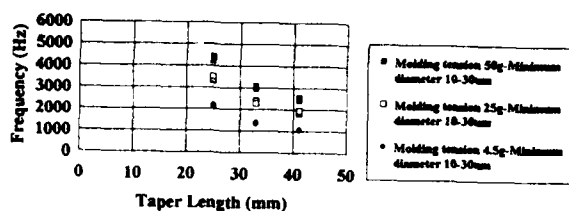
AXIAL VIBRATION



Fig#6 CRITICAL FREQUENCY VERSUS TAPER LENGTH FOR DIFFERENT MINIMUM DIAMETERS AND MOLDING TENSIONS (THEORY)

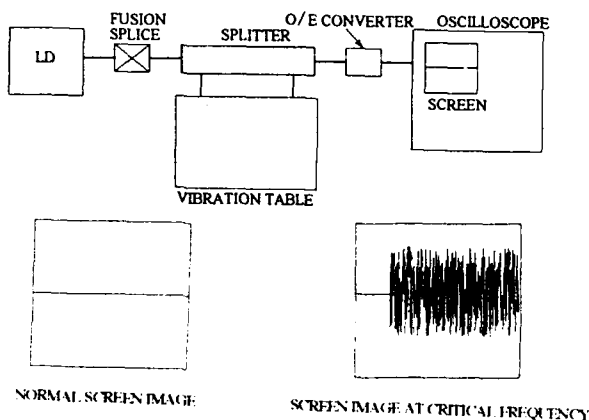
VIBRATION RESISTANT COUPLERS (Continued)

LONGITUDINAL VIBRATION



Fig#7 CRITICAL FREQUENCY VERSUS TAPER LENGTH FOR DIFFERENT MINIMUM DIAMETERS AND MOLDING TENSIONS (THEORY)

EXPERIMENTAL MODEL AND RESULTS



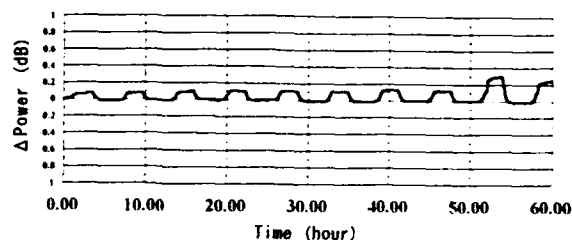
Fig#8 COUPLER VIBRATION TEST

Nine coupler samples were made with different taper lengths and molding tensions and subjected to forced vibrations in order to measure critical frequencies and draw a comparison between theoretical and actual data. As shown above (see Fig#8), coupler stability is represented by a straight line oscilloscope screen image. Critical frequencies are easily determined by determining which frequencies cause wavy screen images. Theoretical and experimental data points showed good correlation. Data differences may have resulted from the difference in actual and model geometries.

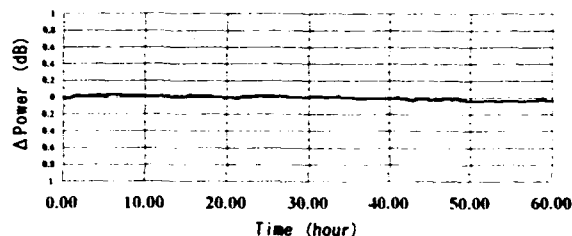
THERMALLY STABLE COUPLER DEVELOPMENT

Couplers are assembled using components made from several different materials having different thermal expansion coefficients. The inherent thermal expansion coefficient of the fused taper glass portion is lower than the coefficient of the adhesive used to secure the fiber to a substrate to form the coupler assembly. This thermal expansion difference induces stresses in the fiber during temperature cycling causing fiber tension changes which lead to optical performance instability.

Since these inherent material thermal expansion differences cannot be avoided, it is necessary to select the fiber tension during molding (see molding process diagram Fig#4) which forms couplers least affected by material thermal expansion differences in order to optimize coupler optical performance thermal stability. Research data shows that standard coupler samples made with low molding fiber tensions experience much higher insertion loss fluctuations during temperature cycling than couplers manufactured with higher molding fiber tensions. The graphs below (see Fig#9 & Fig#10) show the coupler optical power (LED) thermal stability for samples made at 3 gram molding fiber tensions and samples at 25 gram molding fiber tensions when subjected to $-20^{\circ}\text{C} \sim +60^{\circ}\text{C}$ temperature cycling.



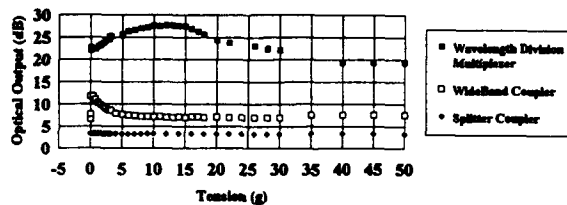
Fig#9 CHANGE IN POWER VERSUS TIME DURING HEAT CYCLING ($-20^{\circ}\text{C} \sim +60^{\circ}\text{C}$) FOR SAMPLE MOLDED AT 3 GRAM FIBER TENSION



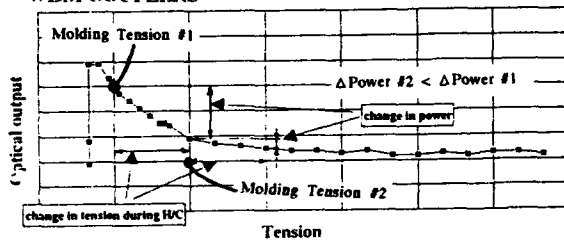
Fig#10 CHANGE IN POWER VERSUS TIME DURING HEAT CYCLING ($-20^{\circ}\text{C} \sim +60^{\circ}\text{C}$) FOR SAMPLE MOLDED AT 25 GRAM FIBER TENSION

It can be seen from the graphs that the fiber tension at which the coupler is molded affects the amount of power change for the same amount of change due to inherent induced fiber tension change during temperature cycling. These graphs show that in changing the fiber molding tensions for wideband coupler samples from 3 grams to 25 grams, the power fluctuation was reduced from 0.32 dB to 0.06 dB for heat cycling conditions from $-20^{\circ}\text{C} \sim +60^{\circ}\text{C}$. This concept applies to different coupler types (Fig#11) but is most clearly represented by the graphs constructed for wideband couplers (Fig#12).

THERMALLY STABLE COUPLERS (Continued)



Fig#11 RELATIONSHIP BETWEEN MOLDING TENSION AND OPTICAL OUTPUT FOR WIDEBAND, SPLITTER, AND WDM COUPLERS



Fig#12 RELATIONSHIP BETWEEN MOLDING TENSION AND CHANGE IN POWER DURING TEMPERATURE CYCLING (-20°C ~ +60°C) FOR WIDEBAND COUPLER

CONCLUSION

Through research and development and computer aided engineering, used to model the coupler molding stage, optical fiber coupler manufacturing methods and design parameters were established which allow for the production of couplers with good vibration resistance characteristics, good optical performance thermal stability, and good long term reliability assurance. It was found that by increasing fiber tension during the coupler molding stage, coupler vibration resistance and thermal stability were greatly improved. Also, it was found that tensile testing of fibers after elongation is an effective method for long term optical performance reliability assurance.

REFERENCES

- 1) H. Suganuma, H. Honjo, et al., "Long Term Reliability of optical fiber coupler," 1990 Spring National Convention Record. The Institute of Electronics, Information and Communication Engineers, Part.4 C-282 (1990)
- 2) Y. Mitsunaga, Y. Katsuyama, H. Kobayashi, and Y. Ishida, "Failure Prediction for Long Length Optical Fiber based on Proof Testing," J. Appl. Phys. 53(7), 4847-4853, (1982).

BIBLIOGRAPHY



Satoshi Endo

Sumitomo Electric Industries, Ltd.

1, Taya-cho, Sakae-ku
Yokohama, Japan

Satoshi Endo graduated from Tohoku University in 1985. He joined Sumitomo Electric Industries, Ltd in 1985 and has been engaged in optical fiber component design. Mr. Endo is a member of the Communication Cable Apparatus Engineering Section.



Tomoyuki Hattori

Sumitomo Electric Industries, Ltd.

1, Taya-cho, Sakae-ku
Yokohama, Japan

Tomoyuki Hattori received a M. S. degree in chemistry from Kyoto University in 1987. He joined Sumitomo Electric Industries, Ltd in 1987, and has been engaged in research and development of optical fiber cable, optical device, and the reliability of optical fibers. He is a member of the Transmission Media R & D Department in Yokohama Research Laboratories.



Takashi Ide

Sumitomo Electric Industries, Ltd.

1, Taya-cho, Sakae-ku
Yokohama, Japan

Takashi Ide received a B. S. Degree in Mechanical Engineering from Waseda University in 1983. he joined Sumitomo Electric Industries, Ltd. the same year. he has been involved in the development of optical fiber jointing and switching technologies. He is a member of the Cable Apparatus & Systems Manufacturing Department in the Communications Division.



Thomas Morrison
Sumitomo Electric
Industries, Ltd.

1, Taya-cho, Sakae-ku
Yokohama, Japan

Thomas Morrison received a B. S. Degree in Mechanical Engineering from North Carolina State University in 1991. He joined the Connection Systems Group at Sumitomo Electric Fiber Optics Corporation in Research Triangle Park, North Carolina in 1992. He is currently involved in a two year training position in the Connection Systems Engineering Section in the Communication Division at Sumitomo Electric Industries, Ltd. in Yokohama, Japan.



Toshiyuki Wakinosono

Sumitomo Electric
Industries, Ltd.

1, Taya-cho, Sakae-ku
Yokohama, Japan

Toshiyuki Wakinosono received a B. S. Degree in Mechanical Engineering from Chiba University in 1991. he joined Sumitomo Electric Industries, Ltd. the same year. he has been engaged in optical fiber component manufacturing and mechine design. He is a member of the Cable Apparatus & Systems Manufacturing Department in the Communications Division.

NEW WIDE BANDWIDTH MICROWAVE LEAKY COAXIAL CABLES

K. Watanabe, J. Baldauf, M. Miyamoto, Y. Suzuki, and K. Ogawa

Opto-Electronics Laboratory, Fujikura, Ltd.
1440 Mutsuzaki, Sakura-shi, Chiba-ken 285 Japan

Abstract

Personal communications services and mobile communications are experiencing rapid growth. In order to realize universal broadcast coverage for these services, transmitting inside of buildings, tunnels, and other structures which block standard broadcast waves is necessary. The growth of new communication services will also increase the number of frequency bands in use and lead to a need for wider frequency band communications capability. To insure affordable and universal coverage of these services, wide bandwidth LCX cables which can be used at microwave frequencies will be needed. In this report, the design and testing of wide bandwidth microwave LCX cables which meet the design requirements of future communications systems are discussed. Test results will show that system requirements have been met.

I. Introduction

Personal communications services and mobile communications are experiencing rapid growth. In order to realize universal broadcast coverage for these services, transmitting inside of buildings, tunnels, and other structures which block standard broadcast waves is necessary. There are various ways to broadcast inside these structures. One method, which has been used for transmitting inside tunnels, is to send and receive signals with leaky coaxial (LCX) cables. LCX cables are coaxial cables which have holes or slots cut into the outer conductor (Figure 1).

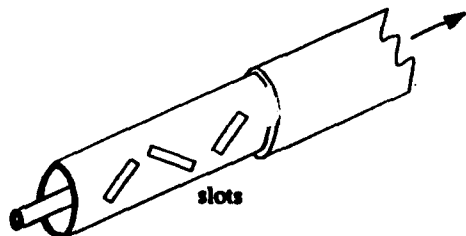


Figure 1. LCX cable: Coaxial cable body with periodic slots in the outer conductor which radiate power.

These holes or slots allow power from a signal which is travelling inside the cable to leak or radiate to a receiving antenna. These cables can be installed in tunnels or buildings and parking garages to provide broadcast coverage which conventional antenna transmissions cannot

provide and are useful where a received electric field with little variation is desired.

The growth of new communication services will increase the number of frequency bands in use and lead to a need for wider frequency band communications capability. To insure affordable and universal coverage of these services, wide bandwidth LCX cables which can be used at microwave frequencies will be needed. In addition to meeting the electrical and radiating system design requirements, these cables must also have good mechanical characteristics such as durability in a high vibration environment.

In this report, the design and testing of wide bandwidth microwave LCX cables is discussed. We will discuss the system requirements, how an LCX cable functions, and the design and testing of the cables. The test results show that system requirements have been met.

II. System Requirements

A. Cable electrical characteristics

LCX cables are usually installed along the wall of a tunnel or along a roadway. As the signal travels down the cable, the leakage of power and ohmic losses in the cable reduce the power of the signal. The power received by a standard dipole antenna properly aligned and 1.5 meters from the cable is given by (1).

$$P_r(\text{dBm}) = P_t(\text{dBm}) - L_c(\text{dB}) - \alpha(\text{dB/m}) \cdot l(\text{m}) \quad (1)$$

Where P_r is the received power, P_t is the transmitted power, L_c is the coupling loss, α is the cable attenuation, and l is the length of cable from the transmitter to the receiving antenna. From (1), it is apparent that as the distance from the transmitter becomes larger, the received power can be maintained at a constant level by decreasing the coupling loss of the cable. Therefore, we designed cables with coupling losses of 80 dB, 70 dB, and 60 dB which can be cascaded in decreasing order of coupling loss to maintain a relatively stable received power level.

In order to ensure reliable coverage using LCX cables for tunnel communications, the cables must satisfy certain electrical and mechanical requirements. The cables are designed to transmit at four frequency bands: 250 MHz, 450 MHz, 900 MHz, and 1500 MHz as shown in Table 1.

frequency Band	f (MHz)
Band 1	250 - 285
Band 2	330 - 470
Band 3	800 - 970
Band 4	1420 - 1530

Table 1. Broadcasts bands for LCX cable.

To function well in all four bands, the radiation characteristics of the cables should meet system requirements from 250 - 1530 MHz. The coupling loss of the cable should have low variation along the length of the cable over the entire frequency range. The characteristic impedance of the cables should be 50 ohms, and the voltage standing wave ratio (VSWR) of the cables should be less than 1.5 within the four frequency bands given in Table 1.

B. Cable mechanical characteristics

Since the cables will be installed in tunnels and other harsh environments, the mechanical characteristics of the cables are very important. The cables should be able to withstand strong vibrations and should bend to a 1.2 meter radius without the cable materials cracking, breaking or being otherwise adversely affected. Two tests are performed on the cables to determine its mechanical characteristics: a bending test and a vibration test. The test conditions are given in Table 2.

Test	Test conditions
Bending Test	Cable length used: 5 meters Bending diameter: 1.2 meters Repetitions of bending: 2 Bending angle: 180°
Vibration Test	Vibration Amplitude: ± 2.5 mm Vibration Frequency: 30 Hz Cable length: 1 meter section with fixed ends

Table 2. Conditions for the mechanical tests.

III. Basic LCX theory and design

A. Basic cable structure

The basic structure of the LCX cable is essentially the same as a coaxial cable as shown in Figure 2.

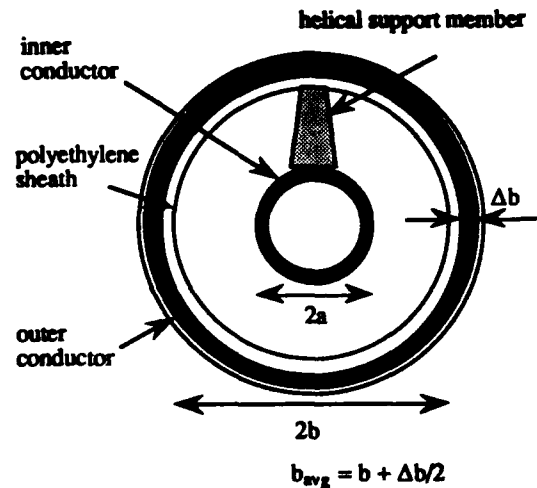


Figure 2. Basic structure of the LCX cable.

The inner conductor and the outer conductor are separated by a helical support member which also strengthens the cable against lateral pressure. The outer conductor of the cable is aluminum, and the inner conductor is copper, which reduces the ohmic losses in the cable. The characteristic impedance of the cable is given by (2).

$$Z_0 = \sqrt{\frac{L}{C}} \quad (2)$$

Where L is the inductance per length and C is the capacitance per length of the cable. The inductance of the cable can be calculated by (3) [1].

$$L = \frac{\mu_0}{2\pi} \left[\ln(b_{avg}/a) + \frac{1}{a\sqrt{4\pi f\sigma_{in}}} + \frac{q}{b_{avg}\sqrt{4\pi f\sigma_{out}}} \right] \quad (3)$$

Where μ_0 is the magnetic permeability, b_{avg} is the average outer conductor radius, a is the inner conductor radius, f is the frequency, σ_{in} is the conductivity of the inner conductor, σ_{out} is the conductivity of the outer conductor, and q is a factor related to the corrugation of the outer conductor.

The capacitance is calculated by (4).

$$C = \frac{2\pi\epsilon_{eq}}{\ln(b_{avg}/a)} \quad (4)$$

Where ϵ_{eq} is the equivalent dielectric constant of the space between the inner and outer conductors, including the effect of the support member, inner sheath, and the corrugation of the outer conductor.

By properly choosing the radii of the inner and outer conductors while taking into account the effect of the support member and sheath inside the outer conductor, an impedance of 50 ohms can be achieved.

B. Radiating slot pattern

The radiation of the leaky coaxial cable comes from the holes in the outer conductor of the cable which are cut

in a periodic pattern. These holes act like antennas in an antenna array. Since the cable is very long, the antenna array is considered to be infinite to simplify the analysis of the cable. The radiation from the LCX cable can be considered as the vector sum of the contributions from all of the slots in the cable. The relative phase of the contribution from each slot is affected by both the angle of radiation and the position of the slot on the cable. The dependence of phase on the slot position is due to the change in phase of the signal as it propagates down the cable (Figure 3).

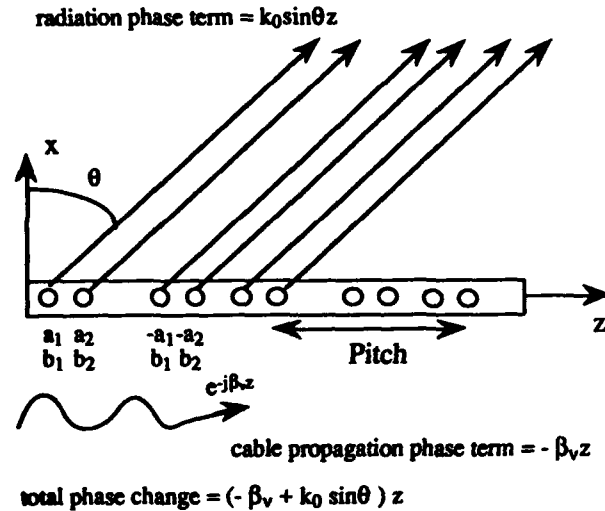


Figure 3. Radiation from the slots in an LCX cable. The radiated fields are the vector sum of the contributions of all of the slots. Since an alternating slot pattern like that shown in Figure 1 is used, the E_ϕ coefficients, a_m , alternate as $a_1, -a_1, a_1, \dots$

The sum of the slot contributions for the two principle radiating polarizations is given by (5).

$$E_\phi = \left(\sum_{m=0}^{M-1} a_m e^{jmx} (-\beta_v + k_0 \sin \theta) \right) (1 - e^{j\frac{P}{2}(-\beta_v + k_0 \sin \theta)} + e^{jP(-\beta_v + k_0 \sin \theta)} - \dots) = \left(\sum_{m=0}^{M-1} a_m e^{jmx} (-\beta_v + k_0 \sin \theta) \right) \left(\frac{1}{1 - e^{j\frac{P}{2}(-\beta_v + k_0 \sin \theta)} - j\pi} \right) \quad (5a)$$

$$E_z = \left(\sum_{m=0}^{M-1} b_m e^{jmx} (-\beta_v + k_0 \sin \theta) \right) \left(\frac{1}{1 - e^{j\frac{P}{2}(-\beta_v + k_0 \sin \theta)}} \right) \quad (5b)$$

Where P is the pitch of the slots, x is the subpitch, k_0 is the free space wave number of the radiation, and θ is the radiation angle as defined in Figure 3. The contributions of (5) are relatively small unless the denominator of the second term is zero. This results in the propagating conditions for the E_ϕ directed and E_z directed modes (6).

$$E_\phi: \frac{P}{2} (-\beta_v + k_0 \sin \theta) = \pi(2n+1) = m\pi \quad (6a)$$

$$E_z: \frac{P}{2} (-\beta_v + k_0 \sin \theta) = 2n\pi = m\pi \quad (6b)$$

For the systems being considered, only the E_ϕ directed radiation will be considered. The E_z modes ($m=-2, -4, -6, \dots$) will affect the VSWR of the cable, but will only slightly affect the radiated power so long as the slot angles are relatively small. By properly choosing the strength of the radiation of the slots (varying a_m) and the subpitch of the slot pattern, x , some of the higher modes ($m=-3, -5, -7, -9, \dots$) can be eliminated. The cable design eliminates modes such that among the E_ϕ modes, only the first ($m=-1$) radiates over the system bandwidth. This ensures that the variation of the radiation along the length of the cable is low.

In order for the cable to only radiate the ($m=-1$) mode over the range of 250 - 1530 MHz, it can be seen that at least two modes ($m=-3, -5$) must be eliminated. Actually, due to the VSWR system requirements, at least three modes ($m=-3, -5, -7$) must be eliminated for the cable to function well.

C. Slot design

The power which is radiated by the cable is related to the size of the slots and their angle with respect to the axis of the cable. Studies have shown that the relative strength of the radiated electric field from a slot is given by (7) [1].

$$E_\phi \sim l^2 \sin(2\gamma) \quad (7)$$

Where l is the length of the slot, and γ is the tilt angle of the slot. By varying the length and the angle of the slots, the coupling loss can be controlled. Also, to achieve the different coefficients in (5), slots with different angles are used in each pitch length.

D. VSWR design

In order to ensure that the VSWR is small over the broadcast bands, care must be taken to design the radiation mode resonances of the cable to fall outside of these bands. For the E_ϕ modes, this has already been achieved by designing the slot pattern such that only the $m=-1$ mode propagates over the utilized bandwidth. The E_z modes, however, produce VSWR peaks for the $m=-2, -4, -6, \dots$ modes. These VSWR peaks occur at the frequencies where the modes change from leaky (exponential decay in the radial direction) to propagating (8).

$$f_m = \frac{|m| 300 \text{ MHz}}{P(\text{meters}) (1 + \sqrt{\epsilon_{eq}})} \quad (8)$$

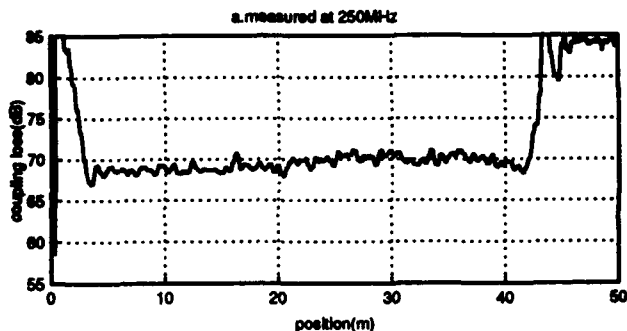
The pitch of the slots should be chosen such that f_m does not fall inside of the broadcast bands for $m=-2, -4$, etc.

IV. Cable Testing

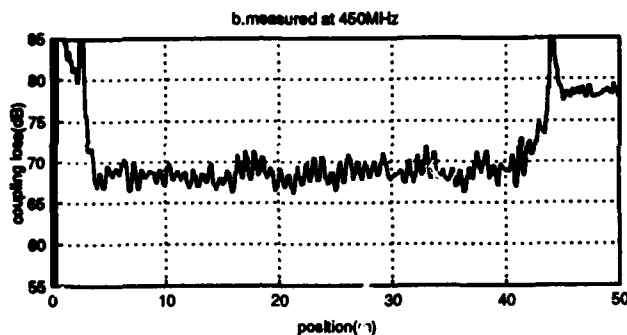
The radiation characteristics of the cable were tested by measuring the power radiated from the cable along a line 1.5 meters above the cable while it is lying in a straight line on a concrete platform. This power measurement was performed using a wire pulled cart on a rail upon which was mounted a dipole antenna. The dipole was connected to a receiver tuned to the test frequency. A 50 meter long section of cable was connected to a signal generator at the test frequency, and the cart with the dipole antenna travelled 1.5 meters above the cable, measuring the radiated power.

This measured power was compared to the power measured at the input of the cable to obtain the variation of the coupling loss along the cable.

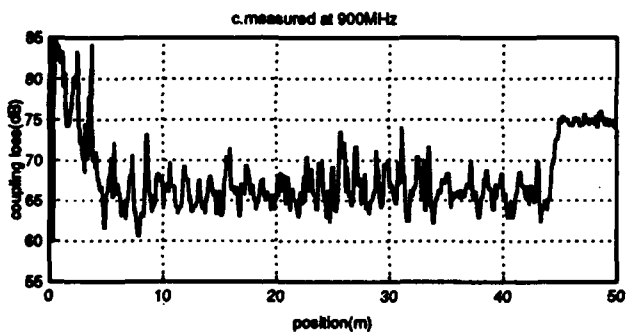
The coupling loss is measured at 250 MHz, 450 MHz, 900 MHz, and 1500 MHz. These frequencies correspond to the four frequency bands given in Table 1. Figure 6 shows an example of the measured coupling loss at these frequency bands. From this figure, it can be seen that the variation of the coupling loss along the length of the cable is 10 dB or less in these four frequency bands.



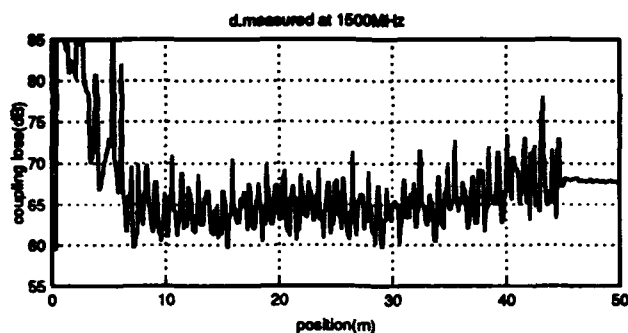
(a)



(b)



(c)



(d)

Figure 6. Variation of the measured coupling loss as a function of the distance along the cable: the frequencies are, (a) 250 MHz, (b) 450 MHz, (c) 900 MHz, (d) 1500 MHz.

As the frequency changes, so does the coupling loss. Figure 7 shows the average measured coupling loss for a cable as a function of frequency.

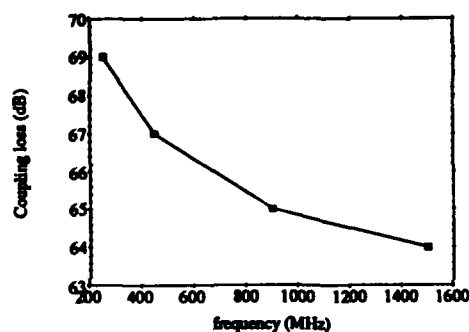


Figure 7. The measured average coupling loss as a function of the frequency.

The VSWR of the cable is measured using a network analyzer over the frequency range of 200 - 2000 MHz. Figure 8 shows the maximum VSWR in the four frequency bands given in Table 1.

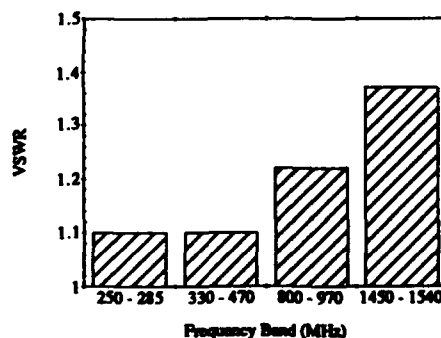


Figure 8. Maximum VSWR in the four frequency bands given in Table 1.

The mechanical tests on the cable showed that the cable can withstand vibrations well, and that when bent to a 1.2 meter radius, the mechanical characteristics of the cable do not change significantly. This indicates that the cable meets the system's mechanical requirements.

V. Conclusions

Wide band LCX cables which function well up to microwave frequencies have been successfully designed and tested. These cables are well suited for ensuring reliable coverage for future communications services in tunnels and other structures which block conventional broadcasts. The system requirements of a low variation of coupling loss, a VSWR of 1.5 or less over the operating frequencies, and a sufficiently low coupling loss over the range of 250 - 1530 MHz have been met. These requirements have been met by carefully choosing the pattern of slots from which the cable power radiates. In addition, the mechanical tests showed that the cables are suitable for high vibration environments and meets the bending radius requirements.

VI. References

- [1] T. Iwamoto, N. Sasaki, *LCX Communication Systems*, IECE press, Tokyo, 1982 (in Japanese).



John Baldauf was born in Tennessee in 1965. He received a B.S. degree in electrical engineering from Virginia Polytechnic Institute in 1987. He received M.S. and Ph.D. degrees in electrical engineering from the University of Illinois at Urbana-Champaign in 1989 and 1991. Since joining Fujikura, Ltd. in 1991, he has worked on the development of optical fiber cables and leaky coaxial cables. He is currently employed in the Telecommunications Cable Section of the Opto-electronics laboratory.



Matsuhiro Miyamoto was born in 1953. He graduated from Nagoya Institute of Technology with a B.E. degree of electrical engineering. He joined Fujikura Ltd. after his graduation from Tokyo Institute of Technology with a M.S. degree in 1978 and has been engaged in research and development of optical fiber and optical fiber cables. He is now a manager of the optical fiber cable section.



Kohichiro Watanabe was born in 1959. He received a B.S. degree in electrical engineering from Tohoku University in 1982. Since joining Fujikura, Ltd. in 1988, he has worked on the development of optical fiber cables and leaky coaxial cables. He is currently employed in the Telecommunications Cable Section of the Opto-electronics laboratory.

"A device for making connection to MDF terminating blocks and pair identification system without interrupting data services on copper cables"

Shuji Asakawa, Koji Ishikawa, Takafumi Sakaguchi*, Satoshi Matsushashi

**NTT Telecommunication Field Systems R&D Center
*NTT Customer Systems Development Department**

Abstract

An accessing device that connects hundreds of pairs at once at the MDF (main distribution frame) is described. This accessing device and a pair identification system that does not interrupt data services, such as the ISDN 2B+D service, are developed for copper cables. The system adopts as a remote control to reduce the cost of operation.

1. Introduction

How would you deal with the following situation? During very important data transmission from Japan and suddenly your data transmission is interrupted by the telephone company performing pair identification on the copper cable carrying your data communication. Normally, pair identification interferes with data services and can generate many communication errors. Most of the many data communication lines that now exist are used in business as productive lines. Telephone companies understand that they should not cause any data errors through pair identification on copper cables, and provide better service 24 hours a day. Users expect continuous error free data telecommunication, so pair identification should be done without any interruption of data services. To meet this demand, the CATS System (Cable Transfer Splicing System) was developed^{(1),(2)}. This system identifies pairs in a cable without interrupting any data service on copper cables. This system is thus very important for both telephone company and user in assuring high reliability and quality in data telecommunication services.

It is also essential that accessing to telephone and data circuits, needed for sending pair identification tone signals, be performed with no interruption to data services. To accomplish this, new accessing and scanning device for hundreds of telecommunication lines at terminating blocks at the MDF were developed. They are designed not to generate any communication errors in data services. Moreover, for high efficiency and lower operation cost, the system OUs (office units) are modified so that they can be controlled remotely field sites where the pair identification is done. This new remote controlled

CATS with the accessing device is very practical, reducing the man power needed to operate the CATS System by two-thirds.

2. Accessing Device

2.1 Accessing Data Circuits in use

Pairs of conductors in copper cables are connected to switches or exchanges at terminating blocks at the MDF. Tone signals for pair identification are sent through these blocks during the pair identification done prior to cable transfer splicing. Here connecting the OU of the pair identification system must be connected to the pairs to accessing the services. The accessing is not a problem when the lines are not in use. When data communication in progress on these lines, they should be handled carefully. When data circuits are accessed to send tone signals with a probe of the OU of the pair identification system, data errors may occur. The electrical capacitance of a probe should be such that there is no effect on data communication. The capacitance also the contact method is considered. For example, the clips used to connect to terminals from the OU at the MDF usually generate some noise, which produces data errors. Inserting probes into the test slits of terminal blocks is another method, but it unavoidably produces communication errors in data circuits. Moreover, the devices for connection to the terminal blocks must be connected to terminals one by one, which is very inefficient.

Photo 1 shows a typical terminal block used in Japan. Although a new type of terminal block was introduced years ago, this type of terminal blocks is still common at MDFs all over Japan. Thus, access to data circuits through these old types of blocks must be managed without any problem. Figure 1 shows an example of disconnection caused when a probe for sending tone signals is inserted to a test slit of the terminal block to access a circuit. The disconnection time is only about 1 millisecond, but it is enough to cause errors in data communication. This accessing method cannot be used for reliable pair identification.

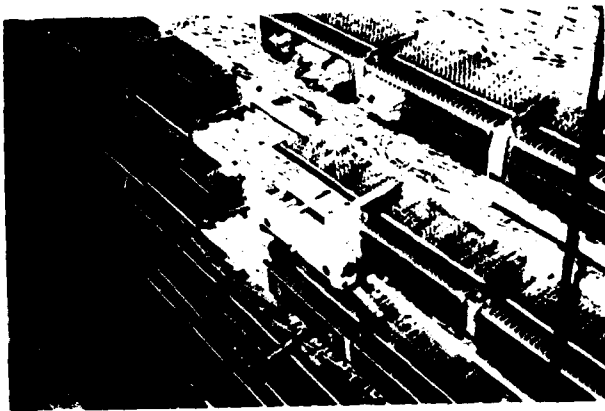


Photo 1 Typical terminal block

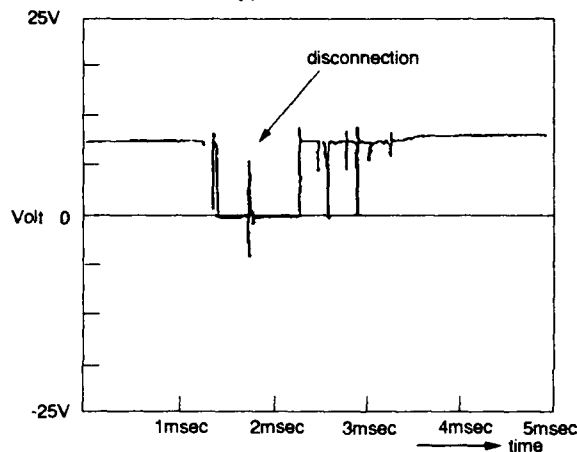


Fig. 1 Disconnection in a terminal block

2.2 Accessing Device for Data Circuits

There are two essential points for an accessing device to prevent introduction of noise to data communication services.

- good electrical characteristics of the connection between terminal and probe (mainly contact resistance)
- electrical capacitance of the cord between the probe and the pair identification OU

The new type of accessing device has two features. First, the device was the probe shown in figure 2 for very stable contact with the terminals.

The probe has a spring inside to press the probe to the terminal with a certain force. When the force is chosen properly, the contact resistance at the terminals is low. The head of the probe is also important here, and its shape is one of the keys in reducing the contact resistance. The second feature is that, the capacitance of the cord is as low as possible so that effects of bridge tapped circuits on the data circuit are minimum so as to allow the accessing of data services in use. Transmission error caused by making contact is eliminated by these two techniques. Table 1 shows the result of access with this probe. Not only in analog data transmission, but also in digital data transmission including ISDN 2B+D on copper cables, the probe can access without causing errors.

Table 1 Accessing result

Circuits	accessing result (errors)
telephone	no noise
9600b/s analog data (QAM)	no error
3.2k - 64kb/s digital data	no error
ISDN 2B+D data	no error

*All circuits are tested as cable distances in 7dB loss

The probe is electrically very reliable for data communication, but connecting terminals one by one to send tone signals, is inefficient. Contact must be made to many telecommunication circuits on terminal blocks at once for better efficiency. Photo 2 shows the new probing device. The head of the device has as many spring probes as there are terminals on the terminating blocks. The probes have the same arrangement as the terminals. There are multiple types of accessing device. The device in photo 2 is for 75 terminals and this device is connected to a terminal block as shown in photo 1.

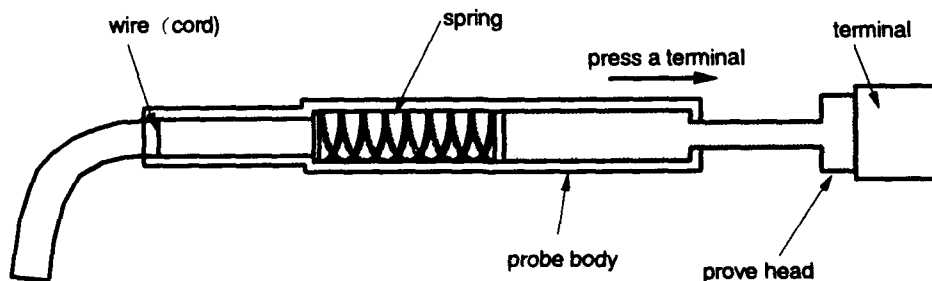
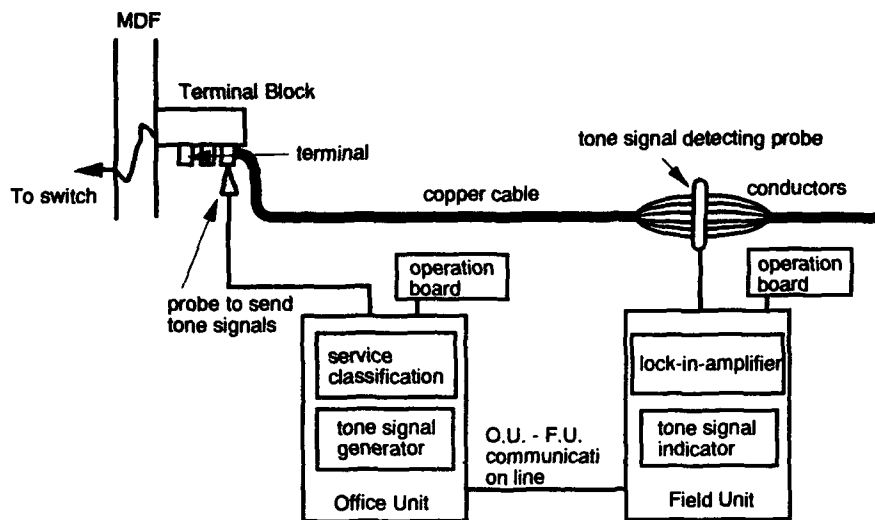
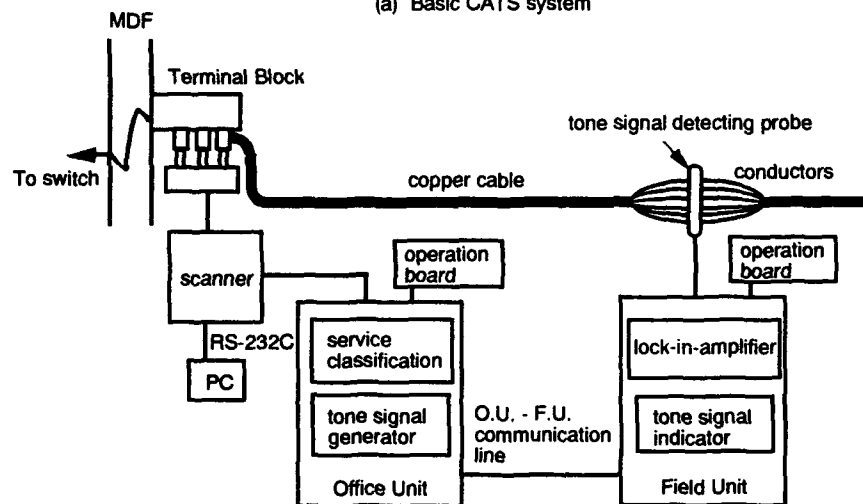


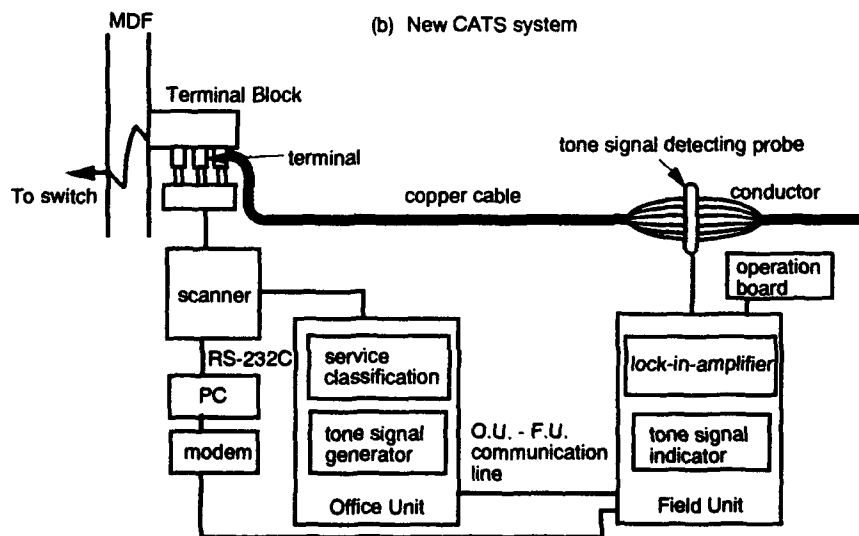
Fig. 2 Contact probe for terminals



(a) Basic CATS system



(b) New CATS system



(c) Remote controlled CATS system

Fig. 3 CATS system in pair identification

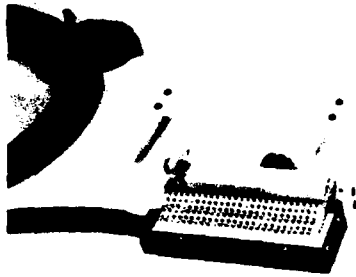


Photo 2 Access device head

The accessing devices make possible to access hundreds of data circuits at terminating blocks at the MDF very efficiently, while sending tone signals for pair identification without interrupting services.

3. Pair Identification without Interrupting Data Services

3.1 CATS System

The CATS (Cable Transfer Splicing) System allows pair identification and cable splicing with no interruption to data services, including 9600b/s analog modem communication, 64kb/s digital communication and ISDN 2B+D. The main features of the pair identification mechanism in CATS are listed below.

- a) very low level tone signals for pair identification (less than -60dBm) do not interfere with data transmission
- b) lock-in amplifier ²) is used to detect low level tone signals with high sensitivity
- c) CPU in the FU (Field Unit) of the system classifies service types of circuits and uses appropriate receiving circuits to detect tone signals
- d) two conductors of a pair are identified at once

Figure 3 (a) illustrates this system. The basic system has OU which is used at the MDF room to send tone signals and FUs which are used at the pair identification site in the field. As an interface between the OU and terminal blocks on the MDF, the accessing device discussed above and scanning units are used to send tone signals efficiently. Figure 3 (b) shows this system.

4. remote-controlled CATS System

As described above, the new CATS has been improved in the point of accessing services at terminal blocks. Hundreds of data communication lines can be connected with the new accessing device and scanners. In the new version, not only pair identification but also accessing to data circuits in use, can be performed without any interruption to data services.

However, the system still needs a person at each work site. Therefore, three persons are required in cable splicing, in which pair identification is unavoidable. To economize pair identification work, remote controlled OU is adopted.

This new-version CATS is shown in figure 3 (c). Connections for accessing the pairs to be identified are made with the accessing devices and chosen with remote controlled scanning units. Thus in this version, there is no need for workers to operate OUs without preparing them at the MDF, making more efficient. The CATS controlling office units such as scanners and OU are based on MODEM communication through RS-232C interfaces. Remote controlling is not limited to any distance for pair identification. Operating the system in telephone offices for pair identification is almost completely eliminated and the work-force is reduced one-third of that required by the previous system.

5. conclusion

Pair identification on copper cables should be performed without interrupting data services. This can provide better data circuits to users for reliable services in which there is no disconnection or data errors in data communication at all. It also provides many benefits to the telephone company, allowing cable splicing and pair identification at any time. In this respect, pair identification and accessing devices must be designed so as not to have any effect on data circuits. For this purpose, the remote-controlled CATS system is introduced in this paper. The system functions without interrupting data services such as ISDN provided over copper cables and without causing data communication errors. Telephone companies can use this technology to provide better data communication services to users and survive in the competitive telecommunication business. Apparently data communication lines with computers will continue to increase in the future, and this technology should contribute much.

The OU of the CATS system can now be controlled remotely from the fields, so the telephone company can economize on manpower in pair identification.

The accessing and pair identification method described in this paper is very useful in the preservation of copper cables, which still remain as the infrastructure of the telecommunication for most users. Economizing pair identification for cable splicing with CATS technology, it could be a positive way and provide a firm bridge between copper cable and optical fiber.

References

1)H. Kubozono, Y. Tsuchiya, M. Hirata, T. Shimomura
"Cable Transfer System Without Disturbing Integrity of
Information On Pair" Proc. of 37th I.W.C.S. p. 692-
697(1989)

2)S. Asakawa, T. Sakaguchi, S. Matsushashi "Advanced
Pair Identification to Eliminate Interference in Data
Services with Automatic Classification" Proc. of 42th
I.W.C.S p.78-85 (1991)



Shuji Asakawa
NTT Telecommunication
Field Systems R&D Center
1-7-1 Hanabatake, Tsukuba,
Ibaraki, 305, Japan

Shuji Asakawa received his M.E. degree in electronics engineering from Ehime University in 1989. He joined NTT in 1989. He is engaged in the development of copper cables at NTT Telecommunication Field Systems R&D Center, Japan.



Koji Ishikawa
NTT Telecommunication
Field Systems R&D Center
1-7-1 Hanabatake, Tsukuba,
Ibaraki, 305, Japan

Koji Ishikawa received his B.E. degree in management engineering from Osaka Electro-communication University in 1990. He joined NTT in 1990. He is engaged in the development of cable splicing technique at NTT Telecommunication Field Systems R&D Center, Japan.



Takafumi Sakaguchi
NTT Customer Systems
Development Department
1-6 Nakase, Mihama, Chiba,
261 Japan

Takafumi Sakaguchi is an Engineer at NTT Customer Systems Development Department, Japan. He received his B.E. degree in mechanical engineering from Kyusyu University in 1987. He joined NTT in 1987. He is engaged in the development of cables and splicing technique.



Satoshi Matsushashi
NTT Telecommunication
Field Systems R&D Center
1-7-1 Hanabatake, Tsukuba,
Ibaraki, 305 Japan

Satoshi Matsushashi is a senior engineer at NTT Telecommunication Field Systems R&D Center. He received his B.E. degree in electronics engineering from Hokkaido University in 1981. He joined NTT in 1981. He is engaged in the development of aerial cable installation technique and cable splicing technique at NTT. He is a member of the Institute of Electronics, Information and Communication Engineers of Japan.

"Improved Cure Test Techniques for Controlling Wire and Cable Compound Consistency"

Joseph A Jerdonek

Monsanto Company

ABSTRACT

Many curemeters can test wire and cable compounds to evaluate processing. A curemeter's sensitivity to compound changes and its signal-to-noise ratio demonstrates the potential usefulness of that curemeter for control testing.

This poster compares a MDR rotorless curemeter to a traditional R 100 oscillating disc curemeter when testing a EPDM wire and cable compound. The rotorless curemeter showed 1.4 to 15 times greater sensitivity than the R 100 curemeter when testing at 350°F. The MDR at 390°F had sensitivity better than or comparable to the R 100 at 350°F.

The test results show the productivity advantages of the MDR versus the R 100 curemeter. For example, the EPDM control compound has a recommended MDR test time at 350°F of 3 minutes versus 12 minutes for the R 100 at 350°F.

INTRODUCTION

Curemeters measure the batch-to-batch consistency of wire and cable compounds. The type of instrument and the test conditions can affect the quality of information. With improved cure testing information, more consistent production processing is possible.

A number of curemeter variables can effect the quality of cure testing information. A higher strain or angle of oscillation generally increases the torque or magnitude of the signal. If the strain is excessive, slippage can occur between the rubber sample and die surfaces. Slippage generally increases the variability or magnitude of noise in a test. Other variable that can affect the quality of cure testing are die design, temperature uniformity, and measurement precision.

The oscillating disk curemeter typically monitors the consistency of rubber compounds used for wire and cable applications. Higher test temperatures reduce testing time and increase testing throughput. Sensitivity to compound differences is normally reduced at higher testing temperatures. The rotor in the die cavity of the oscillating disk rheometer causes significant thermal lag, temperature variability, and longer cure times than constant temperature cures.

Rotorless curemeters have minimal thermal lag and more uniform sample temperature as compared to oscillating disc curemeters. Other improvements in the MDR curemeter die design reduce test variation or noise to improve the quality of information.

With minimal thermal lag, the rotorless rheometer can reduce testing time and increase testing throughput as compared to the oscillating disc rheometer.

An experiment with wire and cable compounds examines the effect of curemeter testing conditions on sensitivity to compound differences. It compares the oscillating disc curemeter with the rotorless curemeter. Testing conditions such as temperature and degree of oscillation arc are compared for sensitivity.

MAIN BODY

Testing

The comparative testing for curemeter type and conditions used a Nordel 2722 EPDM compound. This polymer is widely used in medium to high voltage cable insulations.

A designed experiment for published compound (DuPont Bulletin ER-340.1) has the 9 variations shown in Table 1. The design examines the effects of changes in clay, silane, and paraffinic oil on processability and cure characteristics.

1ST PASS

MATERIAL	Control	1	2	3	4	5	6	7	8	9
Nordel 2722	100.0	100.0	100.0	100.0	100.0	100.0	100.0	100.0	100.0	100.0
Polyethylene Homopolymer	5.0	5.0	5.0	5.0	5.0	5.0	5.0	5.0	5.0	5.0
Zinc Oxide	5.0	5.0	5.0	5.0	5.0	5.0	5.0	5.0	5.0	5.0
Red Lead (TRD-90)	5.0	5.0	5.0	5.0	5.0	5.0	5.0	5.0	5.0	5.0
Flectol H	1.5	1.5	1.5	1.5	1.5	1.5	1.5	1.5	1.5	1.5
Paraffin Wax	4.0	3.0	5.0	3.0	5.0	3.0	5.0	4.0	5.0	3.0
Translink 37 Clay	60.0	80.0	40.0	40.0	80.0	80.0	40.0	60.0	80.0	40.0
Sunpar 2280 Paraffinic Oil	0.0	0.0	0.0	0.0	10.0	10.0	10.0	5.0	0.0	10.0
TOTAL	180.5	199.5	161.5	159.5	211.5	209.5	171.5	185.5	201.5	169.5
SP. GRAV.	1.19	1.24	1.13	1.10	1.25	1.22	1.11	1.18	1.27	1.08

2ND PASS

1ST PASS BASE	180.5	199.5	161.5	159.5	211.5	209.5	171.5	185.5	201.5	169.5
Dicup R	2.6	2.6	2.6	2.6	2.6	2.6	2.6	2.6	2.6	2.6
Silane A-172/50% Wax	2.0	4.0	0.0	4.0	0.0	4.0	0.0	2.0	0.0	4.0
TOTAL	185.1	206.1	164.1	166.1	214.1	216.1	174.1	190.1	204.1	176.1
SP. GRAV.	1.18	1.23	1.13	1.09	1.24	1.21	1.11	1.17	1.27	1.08

Table 1

The experiment used an upside down mixing procedure. Filler, minor solids, and the EPDM on top were put into a BR banbury in the first stage. A sweep down @ 225°F and dump @ 275°F followed. The second stage added the peroxide/Silane and then dumped below 225°F. The batches were milled into sheets below 225°F and refrigerated until testing began.

The curemeter types and test conditions are as follows:

Curemeter Type	Test Temperature	Degree of Arc	Test Time
MDR 2000 (rotorless)	350°F	0.5	12 min
	390°F	0.5	6 min
R 100 (oscillating disc)	350°F	5	12 min
	390°F	5	6 min
	350°F	1	12 min
	390°F	1	6 min

One sample of each compound from the control through 9 was tested for each curemeter type and condition. Two replicate tests followed in the same sequence. A total of three samples per compound for each curemeter type and condition were tested in the same time period.

Control Compound Results

Rheographs: Figures 1 through 4 show the control compound rheographs for the MDR @ 0.5° arc and the R 100 @ 5° arc. The faster temperature recovery of the MDR rotorless curemeter results in shorter cure times. Shorter cure times make shorter test times possible.

Increasing the testing temperature also reduces cure times and makes shorter test times possible. For example, a 10-12 minute test time at 350°F can decrease to 3-4 minutes at 390°F.

The arc of 1° reduces the torque level of the R 100 approximately 50% as compared to the R 100 @ 5° of arc.

The maximum torque of the MDR @ 0.5 ° oscillation arc is approximately one tenth of the maximum torque of the R 100 @ 5 ° arc. But the MDR has ten times greater resolution for torque values. And the noise or variation in the torque from a curemeter test is as important as the magnitude of the torque or signal for control testing. The MDR 2000 also reports loss modulus (S") which is not available on the R 100 curemeter.

Effect of Compound Changes

Higher clay levels increased M_L , M_H , and decreased scorch safety and cure times. Oil addition decreased M_L , M_H , and increased scorch safety and cure times.

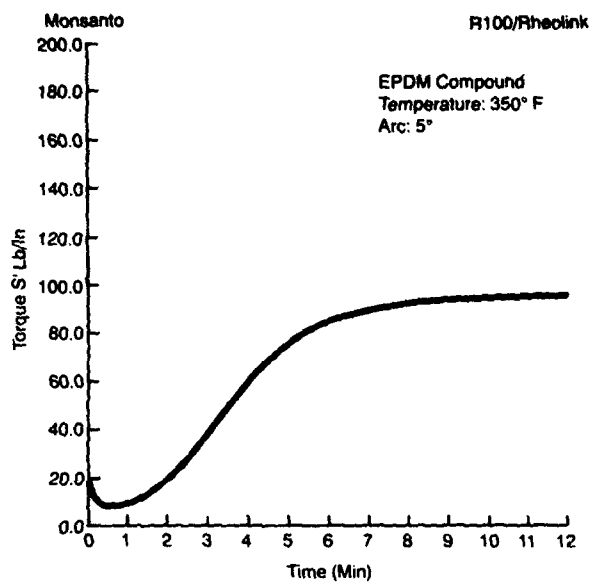


Figure 1—R100 @ 350° F

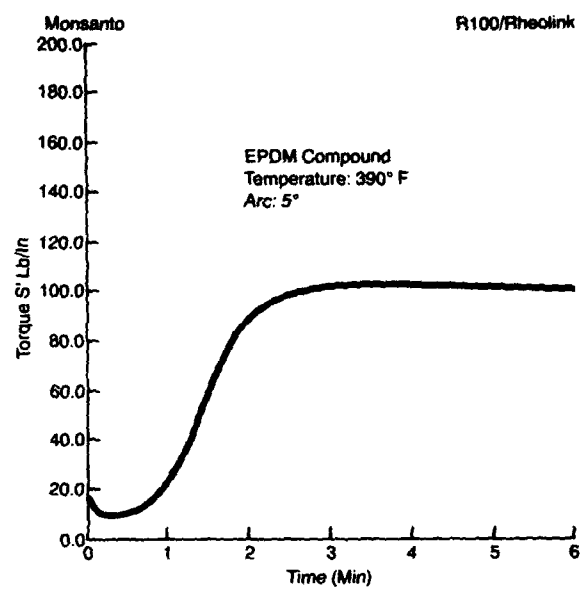


Figure 3—R100 @ 390° F

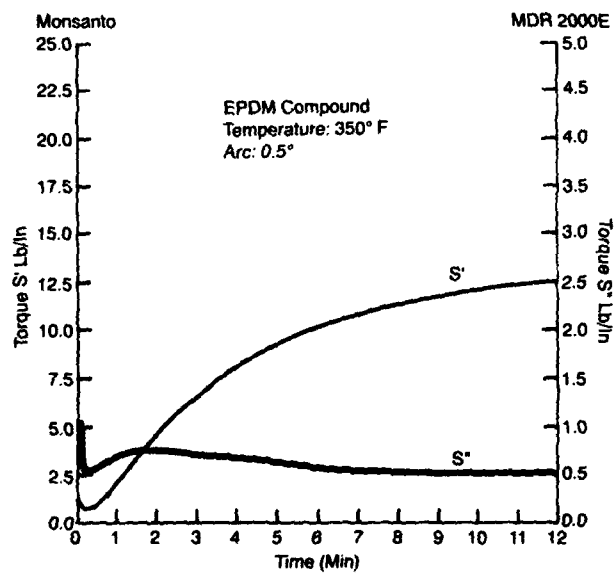


Figure 2—MDR 2000 @ 350° F

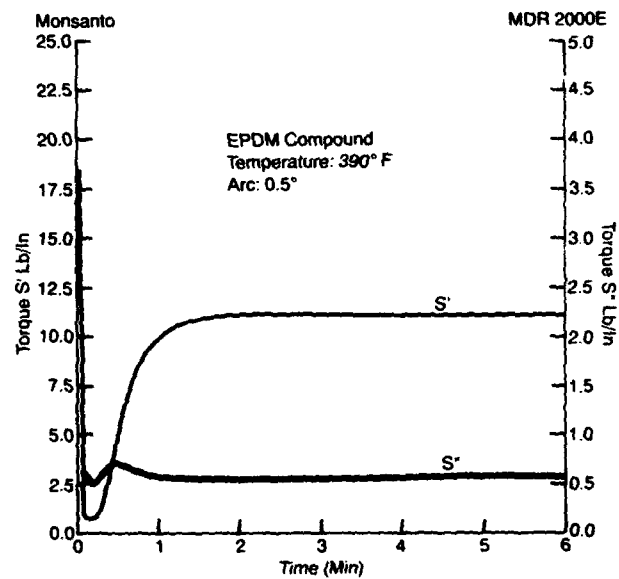


Figure 4—MDR 2000 @ 390° F

Curemeter Results:

Sensitivity: Detecting compound differences that can affect product quality requires good sensitivity in a curemeter test. A more sensitive test can prevent scrap or rework.

Sensitivity is the signal-to-noise ratio of the curemeter test. A higher value for the signal-to-noise ratio improves the capability of a curemeter test to detect compound differences. The signal is the difference between the maximum and minimum of the test result averages (\bar{x}) for all compound variations. The noise is the pooled standard deviation (S_p) of the replications of tests for each compound. The sensitivity follows from:

$$\text{Sensitivity} = (\text{Max } \bar{x} - \text{Min } \bar{x}) / S_p$$

Table 2 shows a typical sensitivity calculation for M_H results from the MDR rotorless curemeter.

Table 3 shows the sensitivity results for MDR and R 100 curemeter conditions. When testing at 350°F, the MDR rotorless curemeter had 1.4 to 15 times higher sensitivity than the R 100. The MDR showed approximately equal or higher sensitivity values for all data points and test conditions than the R 100.

New loss modulus information ($S''/\text{Tan } \delta$) from the MDR also showed potentially useful sensitivity values.

Curemeter sensitivity generally decreases as testing temperature increases. This was not statistically shown for R 100 scorch (t_{sx}) and cure times (t_x). These exceptions are believed to result from a combination of the slower recovery of the R 100 and the fast cure times of the compounds.

COMPOUND	1	2	3	4	5	6	7	8	9	0
MDR1	15.480	11.140	11.060	9.450	9.350	6.790	10.530	15.770	6.800	12.220
MDR2	15.810	11.290	11.260	9.550	9.460	6.810	10.480	15.940	6.950	12.260
MDR3	15.750	11.400	11.140	9.390	9.350	6.730	10.520	15.790	6.800	12.230
MPG	15.74667	11.27667	11.15333	9.46333	9.38667	6.77333	10.51	15.83333	6.87667	12.24
STD	0.053125	0.106562	0.082192	0.065997	0.051854	0.032990	0.021602	0.075865	0.061283	0.014142
VAR	0.002822	0.011356	0.006756	0.004356	0.002689	0.001089	0.000467	0.005756	0.003756	0.0002
MAX MPG	15.83333									
MIN MPG	6.773333									
MAX-MIN	9.06									
MPG VAR	0.003924									
Sp	0.062645									
S/N	144.6236									

Table 2

Signal/Noise Ratio EPDM Cable Compound

Data Pt	MDR @0.5 degrees		R 100@5 degrees	
	350 F	390 F	350 F	390 F
ML	90.5	80.6	24.2	5.1
MH	144.6	102.4	104.9	33.2
ts1	54.8	28.3	3.9	14.7
ts2	65.2	18.3	4	20.9
S'@ML	64.5	66		
S'@MH	42.2	28.2		
Tan d @ML	19.3	7.8		
Tan d @MH	47.6	33.5		
t10	159.2	10.8	16	14.6
t50	287.7	12.4	18	16.4
t90	31.3	9	13.9	16.4

Data Pt	MDR @0.5 degrees		R 100@1 degree	
	350 F	390 F	350 F	390 F
ML	90.5	80.6	4.7	8
MH	144.6	102.4	91	106.5
ts1	54.8	28.3	30	18.3
ts2	65.2	18.3	38	18.4
S'@ML	64.5	66		
S'@MH	42.2	28.2		
Tan d @ML	19.3	7.8		
Tan d @MH	47.6	33.5		
t10	159.2	10.8	15.6	6.9
t50	287.7	12.4	15.5	3.2
t90	31.3	9	4.7	9.2

Table 3

A second analysis of the curemeter results used ECHIP software for significance testing. Figures 5, 6, 7, and 8 show how well the MDR rotorless curemeter and the R 100 curemeter detected filler, oil, and silane changes in the EPDM compounds.

The MDR detected the changes in clay for all data points except t_{10} and t_{50} at 350°F. The R 100 detected the changes in clay only for M_L and t_{s2} at 350°F. For oil, the MDR again exceeded the detection level of the R 100. Neither instrument could detect changes in silane at the levels used in the experiment.

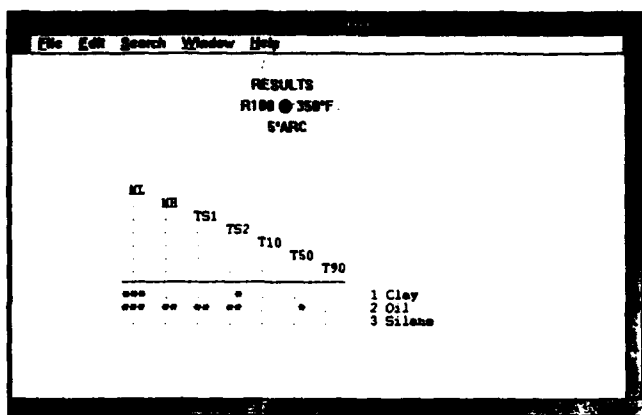


Figure 5: R 100 Test Results @ 350 F
Confidence Levels for Detecting Clay, Oil, Silane
* = 5% ** = 1% *** = 0.1%

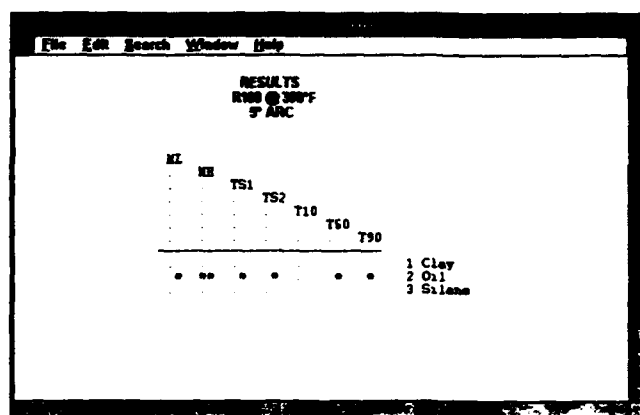


Figure 7: R 100 Test Results @ 390 F
Confidence Levels for Detecting Clay, Oil, Silane
* = 5% ** = 1% *** = 0.1%

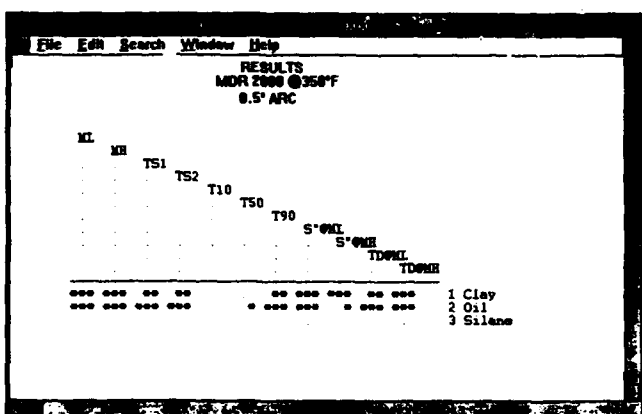


Figure 6: MDR Test Results @ 350 F
Confidence Levels for Detecting Clay, Oil, Silane
* = 5% ** = 1% *** = 0.1%

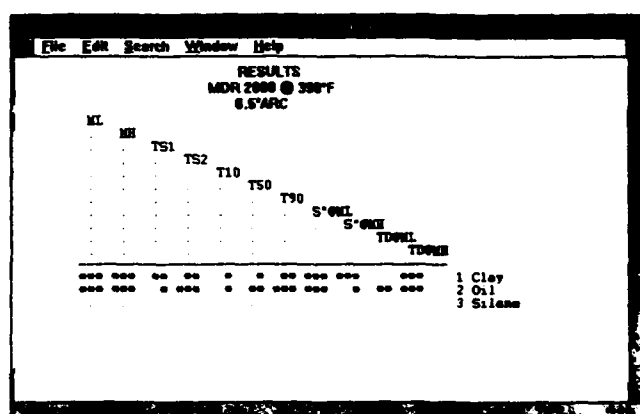


Figure 8: MDR Test Results @ 390 F
Confidence Levels for Detecting Clay, Oil, Silane
* = 5% ** = 1% *** = 0.1%

CONCLUSIONS

A MDR rotorless curemeter showed much greater sensitivity to EPDM compound variations than a R100 oscillating disc curemeter. The rotorless curemeter showed 1.4 to 15 times greater sensitivity than the R 100 curemeter when testing at 350°F. Sensitivity of the MDR at 390°F was better than or comparable to the R 100 at 350°F.

It is likely that slippage at the higher strains of R 100 testing at 1° and 3° of arc causes the decreased sensitivity as compared to the MDR curemeter.

ECHIP analysis confirmed the greater sensitivity of the MDR rotorless curemeter as compared to the R 100 curemeter for detecting compound changes.

ACKNOWLEDGEMENT

Jerry Rose of BICC Cables Corporation, Indianapolis, IN for advice, experimental design, ECHIP analysis, and compounding materials



Joseph A Jerdonek
Monsanto Company
Akron, OH

Joe Jerdonek has spent the past 15 years with Monsanto's Instruments Group. He is the Product Manager and is responsible for the Marketing Technical Services function.

Joe is a member of ASTM, ACS Rubber Division, and the Akron Rubber Group. He has a bachelor's of engineering science from Cleveland State University and an MBA from Case Western Reserve University.

Modern Wire and Cable Factory Automation: An Integrated Solution

Gregory E. Smith

Comm/Scope, Inc.
Claremont, NC 28610

Abstract

With the need for sharing and communicating data among the different areas of manufacturing, users are requiring a more efficient method of obtaining this data. This paper provides an overview of an implementation of an integrated automated factory control system within a cable manufacturing facility. The paper will discuss such issues as traceability, network architecture, and data analysis. A brief discussion of computer integrated manufacturing (CIM) is also given. By using programmable logic controllers to handle the necessary line controls and a workstation to act as the operator interface in concert with a company wide LAN, a very effective system can be produced.

Background

Computer integrated manufacturing (CIM) is a system, that links all aspects of a manufacturing facility together through the use of computers. CIM is often mistaken for factory automation, in which communication may be limited. In reality, however, CIM goes far beyond factory

automation. In CIM, all computers including the corporate mainframe computer, departmental mini computers, individual personal computers, and controllers on the factory floor are tied together by a communication network. This allows for the free flow of information between various departments such as marketing, production, engineering, shipping, and corporate planning.

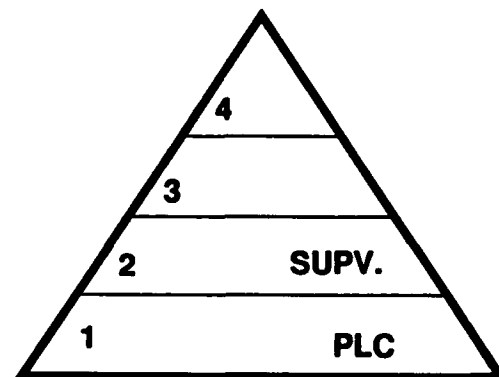


Figure 1: CIM Levels

A pyramid is often used to illustrate the four distinct levels of CIM (Figure 1). Level 1 represents the manufacturing process control. Here, various control devices monitor the different tasks that make up the entire process. It is placed at the base

because it has the largest number of communicating devices.

Level 2 represents process management and supervision. It gathers information from all the Level 1 devices in order to evaluate the process. One of its functions includes sending information back down to Level 1 in order to make adjustments in the process. It can also send data up to the higher levels. Level 2 is the beginning of a transition from a real-time environment into a transactional environment.

Levels 3 and 4, plant management and corporate management respectively, make up the transactional environment. They represent traditional business activities such as production scheduling, sales, marketing and maintenance scheduling. In CIM, they rely on the information they receive from Level 2 in order to make accurate decisions.

One of the major problems with many CIM systems is the lack of a smooth transition from the real-time environment into the transactional environment. This problem represents a restriction in the flow of manufacturing data into the accurate and timely information needed by plant and corporate management.

In a manufacturing facility such as a cable plant, this transition can prove to be very critical. Programmable logic controllers (PLCs) are used at the Level 1 stage to monitor data from the production lines. This data includes

items such as line speed, diameters, pressures and other process indications. A method of reporting this information back to the line operator as well as sending this data to the upper levels is needed.

Implementation

In order to accomplish this task, a solution has been developed that reports the Level 1 information to the line operator in a real time manner. It allows the operator to obtain the information needed in a quick and concise manner so as to reduce any decision making process. At the same time, this information is sent to a central database where it can be retrieved by engineers, or sent to a scheduling system for tracking purposes.

A key factor in the design of this system is that it operates in an 'open system' environment. This allows it to take advantage of several important standards that are supported in industry. Some of these standards include the Unix operating system, MIT X-Windows, IEEE 802.3 network, and the structured query language (SQL) for relative database operations. This use of accepted industrial standards help to protect this system against premature obsolescence of technology. These standards also make it possible for different vendor's products to work together, allowing the exporting of data to other applications on the network. These applications may be some form of specialized analysis or an MRP tracking system.

Architecture

The basic architecture for this control system is easily illustrated. A PLC is installed at each manufacturing line to control the process. This PLC is controlling such variables as temperature, line speeds, pressures and other process variables. At the same time, it acquires data from non-control parameters such as capacitance, sparker faults and eccentricity. A workstation is also installed at each line to act as the operator interface. This workstation is connected via a RS232 cable to the PLC. Through a series of unsolicited interrupts, the PLC sends information to the workstation on the different parameters being monitored. The software running on the workstation collects this data, and reports it to the operator. These reports can either be in the form of graphs and charts or by updating variables. This software is user configurable, which allows for program changes to be made easily as the process is enhanced. By using a centralized operator interface, the need for having a distributed array of control displays along the manufacturing line is eliminated.

Figures 2 and 3 give examples of the information available to the operator from the monitoring software. The first screen is an example of an overview of the manufacturing line. Such information as diameter values, line speed, pressures, as well as footage data is readily available to the

operator in one quick glance. Also any alarm conditions will also be indicated on this screen. The second screen is an example of some of the statistical data available to the operator. It shows an X-bar chart for diameter data that has been sampled at five seconds intervals over an hour period. By sampling the data at a higher, real time rate, the operator is able to track changes occurring in the product over time.

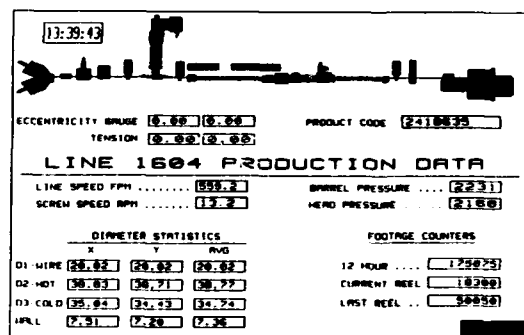


Figure 2: Overview Screen

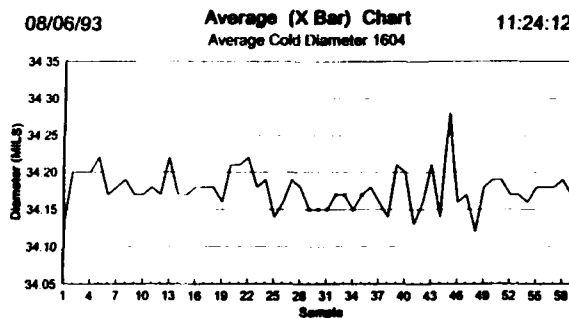


Figure 3: X-bar Diameter Chart

By operating in an UNIX environment, the workstations are true multi-tasking machines. In this manner they can constantly update data to and from the PLC, while at the same time displaying information and statistics for the operator

to run the manufacturing line.

These workstations are networked to a central server over an ethernet cable (Figure 4). As information is collected on each reel of cable run, a file is sent to the server to be read into the database. This file consists of information pertaining to the reel such as product code, material information, footage information, diameter statistics, as well as temperature setpoints, control chart setpoints, along with a date and time stamp. By saving this information, an historical record can be kept of when a cable is made. This is very useful in tracking schedules and orders, as well as creating a log of how a product was manufactured over time.

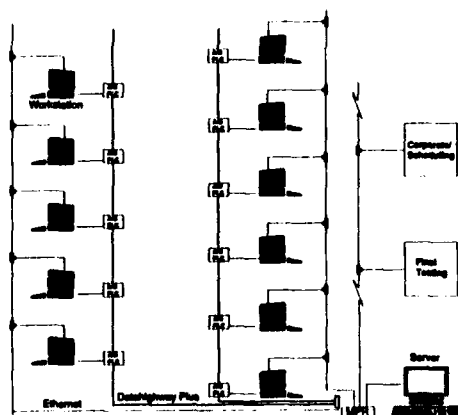


Figure 4: Process Network

Final Testing

The next area where an integrated communication environment proves to be beneficial is in final inspection and testing. The testing of the finished product is just as important

as the manufacturing process. By having this area automated, time and labor is greatly reduced. It is equally valuable for the reduction in testing errors. Testing of products is done by using an array of various electrical and optical test instruments that are controlled from UNIX workstations. After a reel has been connected to the test set, the inspector will enter information associated with the reel being tested into the workstation. The workstation then, through a series of program steps, will cause the test set to perform a variety of electrical or optical measurements on the reel of cable. These measurements may be such parameters as attenuation, structural return loss, nearend crosstalk, impedance and capacitance. The tested data is then saved into a file along with a header containing the reel information. This information is then sent over the network to the central database where it is logged along with other test data. In this manner, the information can be analyzed for consistency in production along with compliance to the accepted specifications.

Conclusion

The idea behind computer integrated manufacturing is simply as an environment for data, an environment which allows the user to learn more about a process, an environment which must change easily so as to benefit from the new knowledge obtained. An automated factory control system, integrating all aspects of

manufacturing from process to quality control to corporate planning has proven to be very beneficial. By combining the use of programmable logic controllers (PLCs) with workstations operating on an 'open systems' platform, a system has been designed that provides the operator and engineer with the critical information needed to demonstrate a statistically controlled process. At the same time, this information is saved into a database for historical analysis of the processes and equipment. Integration is not the goal of CIM. Knowledge is. Knowledge in the hands of those who can make a difference is the only way that automation will lead to profit improvement.

Acknowledgements

The author wishes to thank Vincent P. Stulginski and Martin D. Merholz for their contributions to the work described in this paper.

References

1. *Local Area Networks*, James Martin, copyright 1989 by Prentice Hall
2. "Local and Metropolitan Area Networks", ANSI/IEEE Standard 802.3-1990 Edition
3. *Toward Open Systems*., copyright 1989 by Hewlett Packard Company



Gregory E. Smith

Comm/Scope, Inc.
Claremont, NC 28610

Greg received his B.S. degree in Physics from Middle Tennessee State University and his M.S. degree in Electrical Engineering from Virginia Polytechnical Institute. Before joining Comm/Scope, he was employed by Siecor Corporation as a process control engineer. He is presently a Sr. Systems Engineer with the Network Cable Division of Comm/Scope where his duties include process automation, network design and systems administration.

ADDRESSING CURRENT AND FUTURE GLOBAL REQUIREMENTS FOR ENVIRONMENTALLY SEALED TELECOMMUNICATIONS TERMINAL SYSTEMS

Jim Pinyan, Mike Grice, Dan Swan

Raychem Corporation, Fuquay-Varina, North Carolina

Abstract

Requirements for telecommunications service wire connections are presented from a global perspective with insight as to the effects of future deployment of fiber optics in the distribution system of the outside plant. Critical in the discussion is the system architecture which is employed in the outside plant, the extremes in operating environment, and the broad range of applicable service wires.

A novel universal insulation displacement technology is presented which, when coupled with gel sealing technology, provides the necessary level of performance for meeting stringent industry requirements for environmental sealing and electrical stability. Integrated electrical surge protection is described which allows this system to be used as a platform to address all service wire connection applications.

An overview of various applications is presented, supporting the conclusion that a universal solution for service wire connections has been achieved.

Background

Distribution terminals are in the process of seeing the last evolutionary step for some time, maybe forever. The focus on fiber technology has changed the way operating companies re-focus on new technologies and new services.

Some companies are pushing technology advances to economically deploy fiber systems for multiple services, including video. Others are driven to provide services first, and let technology follow. The most recent trend is toward quick deployment of Coax/Copper (translate: Video/POTS) networks which offer an interim (maybe even long term) means of providing video services.

Whether focused on fiber, coax, or combinations of the two, operating companies are currently having difficulty spending time and effort on copper plant. However, it is hard to ignore that in almost all likely system architectures, a distribution terminal for service wire termination will remain part of the system. Both RBOCs and

Independents are faced with a need to provide staff support for distribution terminals at a time when they want to focus support on new technologies. The compromise seems to be an attitude that they will provide one more round of support to approve a terminal technology that will meet both today's POTS needs, and be suitable for their evolving needs.

What features are needed to service the current and evolving needs? First, a terminal connection should be as universal in its ability to connect to different service wires as a binding post, and do it without having to strip the service wire. What most of us think of as a normal tuning fork style IDC connection cannot handle the variety of service wires present. Unlike a binding post, however, the terminal connection should also be environmentally protected to provide an electrically stable connection. This reduces POTS service affecting troubles and provides a system capable of higher bandwidth applications. In addition, as electronics work their way into the outside plant, the need to provide serviceable electrical protection and to keep hands out of the electronics arises. A terminal design should be economically adapted to provide electrical protection with the same stable performance as for the connection. Finally, a design which accomplishes the previous requirements should be versatile enough to see its way into a variety of outside plant applications.

Service Wire Connection Applications

Service wire (often referred to as 'drop wire' in the United States) is used as the final link between high capacity distribution cable and the subscriber. It must therefore be terminated in discrete increments depending on the equivalent pair count of the distribution cable and the number of subscribers at each end destination. Historically, terminal blocks with pre-connectorized cable stubs have been spliced to the distribution cable and have, for the most part, not incorporated electrical surge protection to protect the installed cable. This

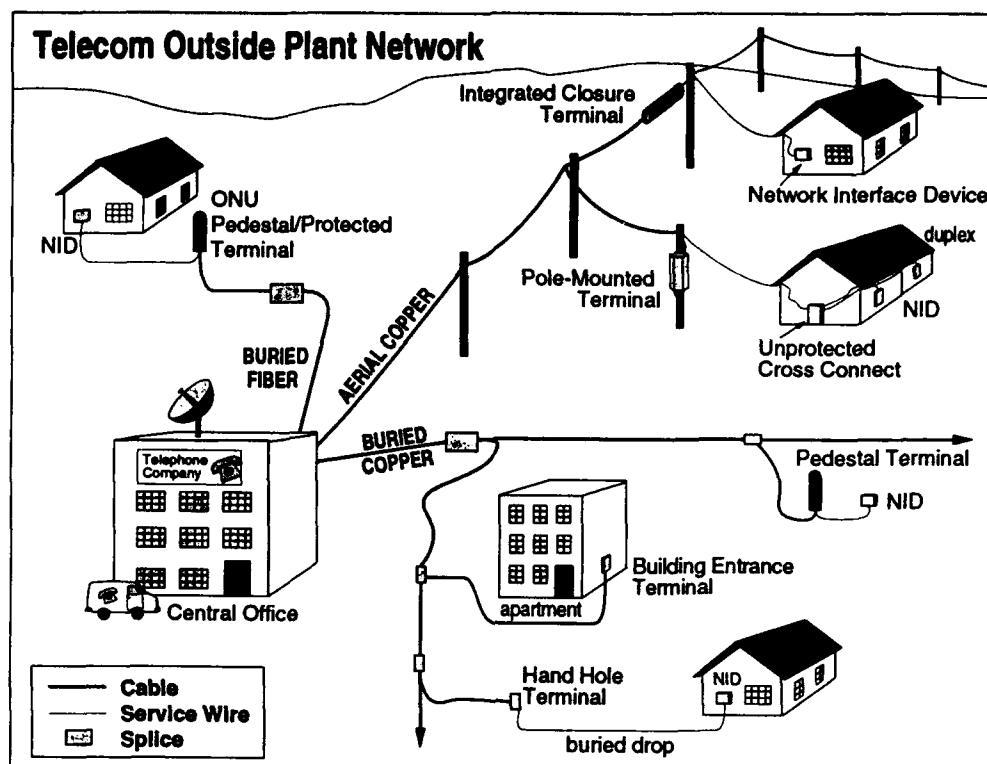


Figure 1

contrasts with the subscriber interface connection (which in the U.S. is located outside and is referred to as the Network Interface Device, or NID) and includes electrical protection to isolate the station equipment and, thus, the subscriber from bodily harm. A pictorial of service wire connection outside plant network is included in Figure 1.

Terminal Blocks

Terminal blocks can be located in many places in the outside plant. Aerial applications include pole mounted and strand mounted terminals. These aerial applications require the use of service wire which can withstand heavy abrasion and tensile loading. Buried applications include pedestal mounted terminals and hand hole terminals. Buried service wire must be resistant to moisture penetration and abrasion as well as rodent attack. All of these terminal blocks are in housings which shield them from harsh mechanical abuse but not necessarily environmental abuse such as insects, airborne contaminants, salt fog, condensation, etc. They are generally spliced to the distribution cable in a separate splice closure except for the strand mount terminal, which may incorporate an internal splice chamber.

Many countries outside the United States use site termination in lieu of preconnectorized cable stubs. In these applications, the terminal is used to connect the service wire directly to the distribution cable in an integrated splice compartment.

Subscriber Connection

The subscriber connection is carried out by a station protector or Network Interface Device generally located on the outside of the subscriber's dwelling. This unit connects the service wire to the inside house wire and is also used as a location for testing of the circuit by the subscriber or the telephone company technician. Electrical surge protection is always present in these devices in the United States. Electronic devices may be added for maintenance or multiplexing of circuits. Large dwellings requiring multiple line service employ building entrance terminals which can be located just outside the dwelling or in a basement.

The vast array of needs for connecting the subscriber with the distribution loop have generated a wide variety of service wires used in the outside plant and a family of products to terminate these service wires at each end.

Universal Service Wire Connection

Proliferation into several products is possible because of the flexibility of the electrical connection. This connection is made using an IDC type design called the Inverted Insulation Displacement Connector (IIDC). The design was driven by two key needs:

1. Must terminate all wire and re-terminate with gauge change.
2. Must perform in harsh outdoor environments.

In order to terminate the wires used in the outside plant of the telephone companies, a system was needed that would prevent the wire from destroying the contact or the contact from destroying the wire. At first, we attempted to find a correlation between the outer diameter of a wire and the true size of the metal conductor. By using this correlation, two independent slots could be designed to limit the amount of displacement required by one contact. This is referred to as the two-hole method. The two holes can either be two external holes or one external hole with a second in-line hole. The in-line design would limit the depth of insertion based on the outer diameter of the wire.

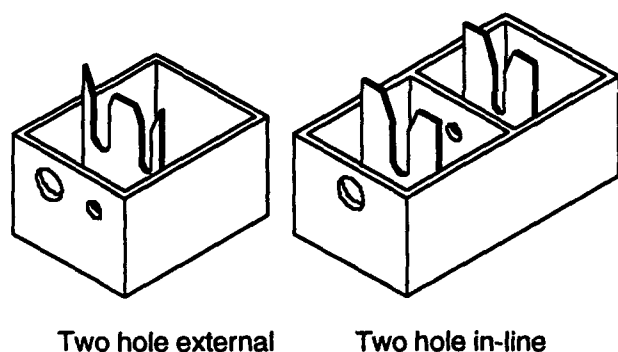


Figure 2 Hole Limiter Concepts

After studying the different types of wire, we found wires whose outer diameters were small, yet contained a sufficiently large inner core to damage standard IDCs. This discovery made the two-hole in-line concept unattractive. The in-line concept also required that the smallest of the wires be completely inserted past one contact to the next to ensure a good connection. The external two-hole concept was rejected due to the sensitivity of misapplication by the end-user, its unreliability, and the fact that it is not a true universal contact.

The IIDC eliminates the need for service wire identification through the combination of high strength alloys and a unique bi-spring interaction to reduce the stresses

created by inserting larger wires into contact slots small enough for finer gauge wires. As shown in Figure 3, the IIDC will deflect both inner and primary springs to make the connection with the larger gauge.

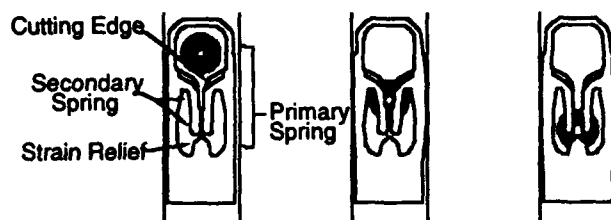


Figure 3 IIDC Illustrating Heavy Insulated Conductor Connection

In the case of smaller gauge termination, only the secondary springs are used, allowing for the proper amount of contact pressure to prevent wire damage.

In addition to the connection requirements, the IIDC must be able to penetrate the insulation of all service wires in an outside environment. In some areas, the terminal could be used to terminate drops in temperatures as low as -20°C . Under these conditions, the PVC insulation, common in the F-drop, becomes very hard; making damage to IDC systems more likely. A design solution to satisfy the functional needs under these extreme conditions was developed through the use of finite element analysis. As shown in Figure 3, the IIDC accommodates the force associated with heavily insulated drops by providing an aggressive internal cutting edge and strengthening ribs along the primary springs. These design features allow for multiple re-entries with F-drop and protect the integrity of the contact.

The current design currently meets or exceeds the industry standards. Some standards are a requirement for stress relaxation and thermal cycling, both of which require a change in contact resistance to be less than two milliohms. The stress relaxation exposes terminated connections to 118°C for a period of thirty (30) days. The temperature cycling includes:

- 1000 cycles of -40°C to 60°C — [twelve cycles / day] without gauge change
- 200 cycles of -40°C to 60°C — [twelve cycles / day] with gauge change
- 300 cycles of 4.4°C to 60°C — [two cycles / day] in 95% relative humidity

Temperature extremes are just one example of the harsh conditions the IDC must function in. The contact must also resist corrosive effects and be insulated from the other connections. This sealing is accomplished through the use of Gelguard™ sealant.

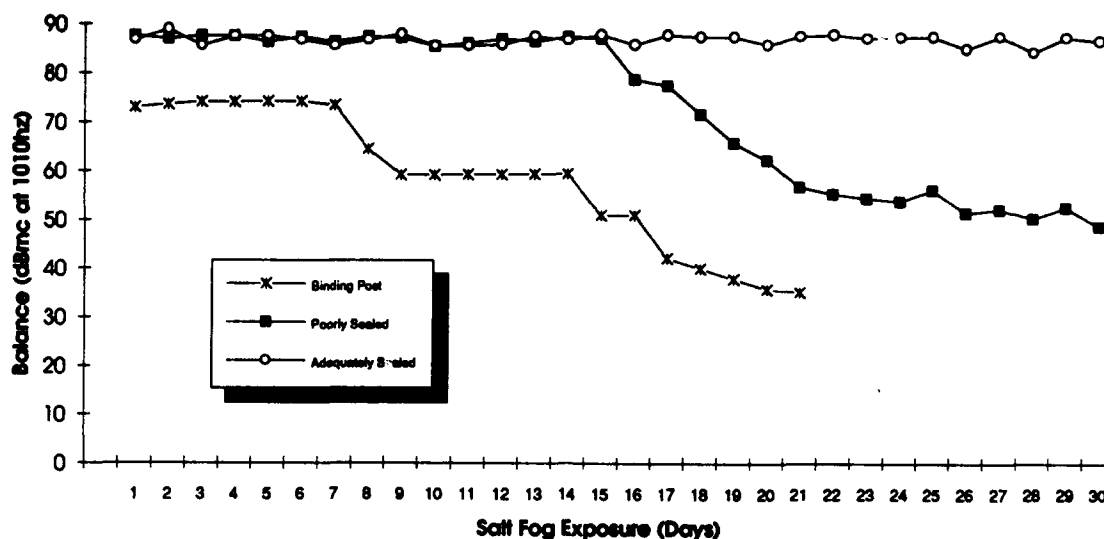


Figure #4 Environmental Effects on Transmission Balance

Environmental Sealing

The need to seal copper connections in the outside plant is well known to the construction and maintenance departments of telephone operating companies. Environmental sealing of terminal blocks and the advantages of Gelguard™ Sealant as a sealant material have been discussed by DeBruycker et. al. in the thirty-eighth IWCS proceedings. Environmental effects on transmission performance have now been correlated relative to commonly measured parameters such as insulation resistance.

The need for good quality of a telephone circuit has been driven by customers and their tolerance to audible noise. Data transmission is less tolerant to high frequency static and popping in that vital information may be lost. A measure of the quality of a telephone circuit is *Balance* which is measured in dB mc and is derived as follows:

$$\text{Balance} = \text{Power Influence} - \text{Noise}$$

The acceptable minimum level of balance is 60 dB mc. If balance drops below this level, there is physical trouble on the circuit which can cause problems for voice or data communications. The insulation resistance which corresponds to this level of balance is approximately 1×10^6 . Figure 4 shows a comparison of terminal systems exposed to a salt fog environment. A well sealed system can provide a circuit which exceeds this minimum level of balance whereas systems which have no environmental sealing or which are not adequately sealed can not.

During environmental simulation testing, the blocks were conditioned prior to salt fog exposure. The blocks were subjected to 50 thermal cycles (-40 degrees C to 60 degrees C, 3 cycles/day) and were then re-entered five times with service wire. This pre-conditioning is very important in predicting the performance of a product in the outside plant over a twenty-year life.

Integrated Electrical Protection

As electronics migrate to the distribution terminal location via Fiber to the Curb, multiplexing systems for copper relief, and devices provided for enhanced services, the need arises to protect these devices from lightening and power line induced surges. Existing protected terminal designs were large, complex, expensive to manufacture, and difficult to environmentally seal. Environmental sealing is an important consideration for the typical U.S. application of gas tubes with vent safe air gap back-up devices. These devices are extremely sensitive to humidity (and other contaminants which affect dielectric properties).

The solution to this emerging need for protection was to integrate the surge protector into the basic design of the service wire connector. A cross section of the newly designed system is shown in Figure 4.

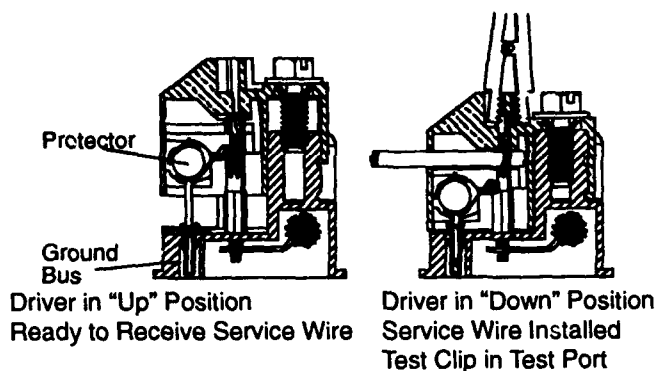


Figure 5 Service Wire Connector with Integrated Electrical Protection

This compact design utilizes the same molded base for unprotected as well as protected applications. A protected unit contains a ground strip bus and protected modules. This system is flexible and may be upgraded in the field simply by changing modules. The advantage of having the protector device in the driver module is that the protector is environmentally sealed and this is the only component filled with Gelguard™ sealant.

This design offers the advantage of balanced electrical protection by employing a three element gas discharge tube. This ensures that both tip and ring are simultaneously grounded during a surge on either line. The physical design ensures that the protector is in the circuit when the service wire is connected and that removal of the protector requires that the service wire be disconnected.

Conclusions

The emerging technologies for communications in the distribution loop will not immediately displace the embedded copper twisted pair network. The need for a new service wire connection system which meets the needs of the copper network and also functions with these emerging technologies has been addressed. The product which meets these needs employs universal insulation displacement connectors for reliable electrical connections, Gelguard™ sealant for environmental sealing, and integrated electrical protection to isolate electronics. It can be configured for distribution terminal applications as well as subscriber network interface devices.

Acknowledgments

The authors wish to thank Bill Curry and Ken Fien for transmission test data they provided and Linda Rogosich for publication support.

References

1. Tokarz, R., "Balance: The Ultimate Test for Noisy Lines" Outside Plant, March, 1991.
2. DeBruycker, E., et al, "An Environmentally Sealed Terminal Block with Rotary Connection", proceedings of the 38th International Wire and Cable Symposium, 1989, p.513.



Jim Pinyan is the Continuation Engineering Manager in Raychem's Transmission Electronics Group and was the Project Development Manager responsible for the work presented here. He holds B.S. and M.S. degrees in Mechanical Engineering from North Carolina State University, and has worked for Raychem for six years.



Michael E. Grice has been in the Telecom Division of Raychem for five years. Mr. Grice received his Bachelor's degree in Mechanical Engineering from North Carolina State University.



Dan Swan has been with Raychem for 11 years, and is currently Technical Marketing Manager. He holds a BSEE from Iowa State University, and graduate credits from the Florida Institute of Technology.

COST-EFFECTIVE CABLES FOR LAN- AND FTTH-APPLICATIONS

Brigitta Behr, Peter Brehm, Frank Brode, Michael Emmerich, Hans-Ulrich Müller

KWO Kabel GmbH
Berlin, Germany
Member of the BICC Group

Abstract

This paper describes new cost effective cables for LAN- and FTTH-applications offering economical and good installation features. The manufacture of these cables is possible with a minimum of production steps, reducing the manufacturing costs.

The characteristical properties of these cables are presented and their suitability for application in the subscriber network shown.

1. Introduction

Prognoses of the development of the fibre optics market [1] show a significant growth of the LAN and FTTH-cable segment in the next years.

The rapid increase of optical fibre cables in the subscriber network market depends on the competitive pricing for the cables, its installation and the transmission system.

In this article new cable types for the inhouse installation are presented. These cables are designed to give:

- * reduced manufacturing costs by reducing the number of production processes
- * a simple and quick installation by using a new "break out" technology.

The cable design must be regarded in connection with the network configuration. Present thinking suggests, that a passive network based on optical fibre cables with maximum of 10 fibres is the preferred version [2].

2. Cable Constructions

For the inhouse installation the customer needs cables with different designs depending on the proposed use.

For data transmissions over longer distances inside of a building, e.g. between different floors, low cost distribution cables with up to 10 fibres are necessary.

For the branching to the single "communication stations" easy handled break-out cables are preferred. These cables typically have 2 - 8 optical fibres.

2.1. Distribution Cable

Fig.1 shows two versions of distribution cables. The manufacturing process is very simple and can be carried out in a single step.

The flat tensile strength members enable a non problematic branching of these cables. The tubes of the cables can contain multimode as well as single mode fibres, tight buffered fibres, ribbons, copper or other cable elements.

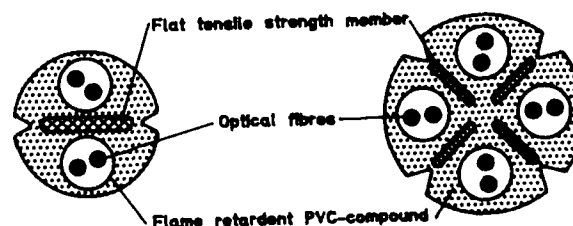


Fig.1 Distribution Cable Constructions

Because the cable elements are not stranded during the production process it was necessary to optimize the relation between the tensile-strain behaviour of the strength member and the overlength of the fibres in the tubes to guarantee their stress free storage up to the maximum allowed tensile force in the full operational temperature range. Investigations showed, that a fibre tension could only be observed for tensile forces larger than 1500 N (Fig. 2).

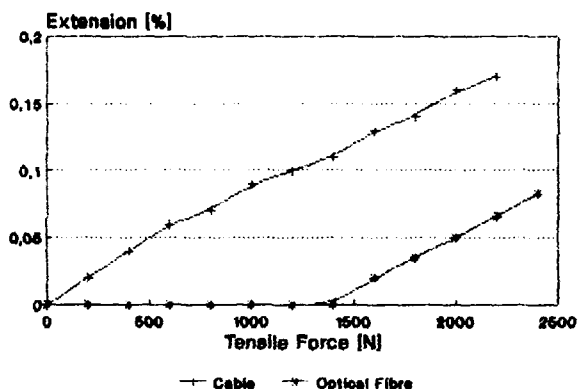


Fig. 2 Extension of the Cable and the Optical Fibre during Tensile strength Performance of a Distribution Cable

Typical attributes of these cables are:

Optical Fibres

Dimensions: 62.5/125 μm

Attenuation/Bandwidth: FDDI quality

Operational Properties

Maximum loss increase at 1300 nm in the temperature range from -10 °C to +70°C

$\Delta\alpha(1300\text{nm}) < 0.05 \text{ dB/km}$.

Fig. 3 shows the loss dependence on the temperature.

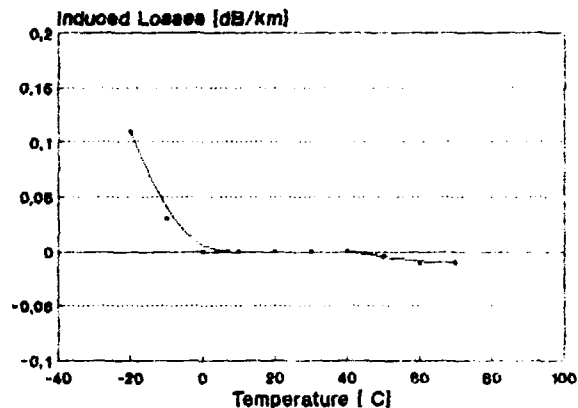


Fig. 3 Induced Losses in Dependence on the Temperature

The cable is made with a low cost version of a low smoke, flame retardent PVC-compound.

Mechanical Properties

The max. tensile force is 1500 N. The induced losses at this force are less than 0.05 dB/km. The dependence of the induced losses from the tensile strength is shown in Fig. 4.

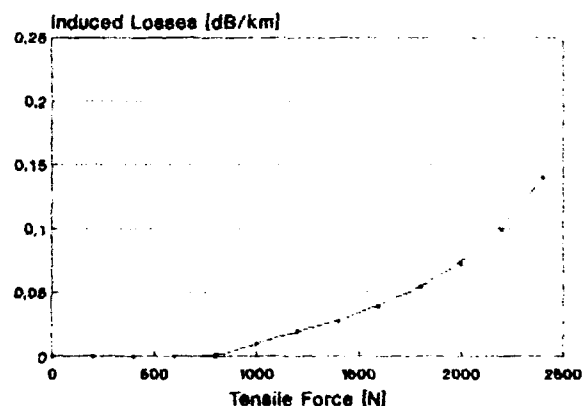


Fig. 4 Loss Increase of a Distribution Cable during Tensile Strength Performance

The cable shows only a little sensitivity against crush. At 700 N/cm the reversible loss increase is 0.15 dB.

2.2 Break Out Cable

In the Fig.5 are shown two types of break out cable consisting of four and eight single fibre cables. These cables can be made in one production step less than normal break out cables.

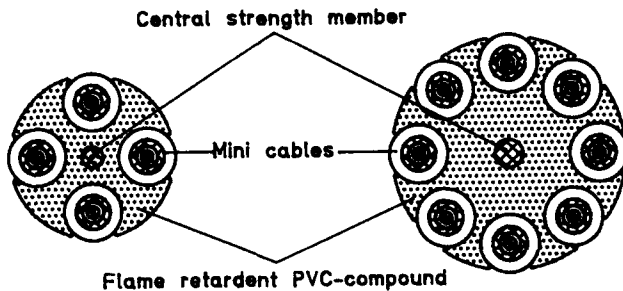


Fig. 5 Break Out Cable Constructions

The second advantage of this cable is the direct use of the single fibre cables without removing the cable sheath. This enables a cost effective installation technology.

The single fibre cables contain a strength member and can be connected with optical plugs.

If the strength member is not necessary it is also possible to produce cables with single tight buffered fibres. In this case higher count cables can be offered. The optical properties of this cable type are the same as the characteristics of the distribution cable.

The operational and mechanical properties of this cable are:

- * In the temperature range - 25 °C to 70°C no excess loss could be measured.
- * Up to the allowed tensile force of 2500 N no loss increase could be observed.
- * The cable construction shows a good resistance against mechanical damages such as crush, impact and torsion
The crush test with 1000 N/cm shows a reversible loss increase of only 0,03 dB.
After 100 impacts with 5 Nm there were no excess loss measured.
A torsion load with 25 turns over a length of 1 m shows a reversible induced loss of 0,05 dB

The slots in the cable construction are designed so that easy branching of the single cable elements is possible without a loss in its mechanical performance.

3. Economical Aspects

The manufacturing process of the distribution cables is very cost effective. The whole cable can be made in one step only. The comparison of the standard production time for a distribution cable and the new one, shows a time reduction of two thirds. Additionally the costs for the set up can also be reduced.

As stated earlier the break out cables can be made with one production step less than normal break out cables. But the greatest advantage of these cables is the easier handling during the installation because of the cable design concept that enables a single mini cable to be connected without removing the sheath. If it is necessary the mini cable can be subsequently replaced in the break out cable.

The installation behaviour of the presented cable constructions were tested in different inhouse projects for computer networks. The connection of the cables were made with commercially available enclosures.

The installation was more cost effective and less time consuming.

6. Summary

The cables presented in this article show good optical and mechanical properties. Because of their lower production and installation costs these cables are an effective solution especially for the LAN applications.

4. References

- [1] Markt & Technik Nr. 9 Feb. 93
- [2] LWL-Verkabelungskonzept für Daten-netzwerke (unpublished results), KWO 1993

Brigitta Behr, received her Ing.-degree from the Ingenieur-Fachhochschule Berlin. She is working in KWO Kabel since 1963. In the last years she is engaged in the field of optical fibre cable construction.



Michael Emmerich (36) received his diploma in electrical engineering from the Technische Universität Dresden. 1982 he joined KWO Kabel. He is engaged in the development of optical fibre cables and optical measurement techniques.



Peter Brehm (54), studied at the Technical University of Dresden and gained his Ph. D. in engineering 1981. He is working on the field of optical cable development since 1977 and is specialized on the field of material development for optical cables.



Hans Ulrich Müller (39), studied Physics at the Humboldt University of Berlin and joined KWO Kabel in 1972. He is a specialist for the development and design of optical fibre cables.



Frank Brode (38), is the head of the Development Group for optical fibre cables. He studied at Humboldt University Berlin physics and gained his Ph. D. in Physics 1985. Since 1977 he has been working on the field of the optical cable development.



Development of a Jointing/Repair Facility for High Reliability Submarine Cables

S.C. Beech

R. Maxted

STC Submarine Systems Limited, Southampton

ABSTRACT

To take advantage of short-haul unrepeaters cable opportunities the concept of modular marine installation has been developed. This is a significant change from the use of dedicated cable-laying ships to the use of 'vessels of convenience' that are converted for cable-laying with the provision of separate, transferable units. In many circumstances this approach has large cost-savings against conventional installation techniques.

As part of this approach a modular unit has been developed to provide a controlled environment for the manufacture of system joints at the dockside or on board the vessel. The nature of optical submarine cables requires that at all times the quality of the joint must be maintained for the system to perform throughout its projected life span. To achieve this all the necessary equipment has been incorporated into container units to provide a self-contained work area for use in remote regions and in climatic extremes.

This paper describes the design considerations, implementation and performance of the jointing/repair unit.

BACKGROUND

Historically a large proportion of the total unrepeaters submarine system purchase price covers the costs of installation which is carried out by ships, constructed specifically for cable-laying. As these ships are specialised, the corresponding daily charter rate required to cover their costs is high. The number of charter days required for cable installation is therefore not only for deployment but also for cable loading and transit to and from the cable-laying ground. Thus the total system cost may be greatly increased.

This conventional method of installation has meant that the submarine fibre optic cable system is fully assembled on the site of cable manufacture where it is tested both optically and electrically before it is transferred to the dedicated cable-laying ship. This can cause logistic problems at the manufacturing site because entire systems need to be stored with other cable systems awaiting shipment. This is compounded by the increasing number of short-haul systems, especially for unrepeaters applications.

To reduce the incurred installation cost, the philosophy for unrepeaters cable system deployment has been changed from the use of dedicated cable-laying ships to the use of 'vessels of convenience'^[1]. Furthermore, a cable specifically for unrepeaters systems has been developed^[2] which minimises metal content as it is not subject to the same current carrying requirement as that of a repeaters system. The physical size of the cable is also reduced as the maximum seabed depth between landing points that can be spanned by an unrepeaters cable (currently 300km) will not exceed 4km, approximately half that of maximum design depth for repeaters cables, and so the strength required for laying and recovery is reduced. The reduced cable diameter permits the cable to be coiled within a volume that can be fitted into a standard freight container in mini-creels or on drums. The cable can then be shipped to the nearest freight terminal at the cable-laying ground and then transferred to the dockside for assembly. Following assembly it is transferred to the cable-laying vessel hence saving the charter costs of ship loading and transit.



Plate 1 Vessel undergoing conversion

To improve the efficiency of conversion a complete suite of containerised equipment has been developed. The containerised units are organised into five groups to cover all eventualities. These are:

- 1) *Ship manoeuvrability*. The vessel used must be highly manoeuvrable so that it can closely follow a pre-

determined route in difficult sea conditions. To achieve this, items such as bow thrusters are installed.

2) **Cable handling.** The marine cable must be deployed in a controlled manner from the vessel. Containerised are the cable engines, bow sheaths, etc., which are necessary to control the deployment.

3) **Cable protection.** The most cost-effective means of cable protection in high risk areas, such as fish trawling grounds, is by direct burial using a submersible plough. This is deployed from the cable-laying vessel and pulled over the sea-bed, burying the cable into the sea-bed up to a metre depth. For this a lightweight plough^[3] and associated lifting 'A' frame for deployment is made available.

4) **People** As the crew compliment of a converted vessel is greatly increased, extra provision is made to the accommodation, office facilities, etc..

5) **Cable assembly.** During system installation consideration must be given to the need for unplanned jointing, as result of bad weather, and for the completion of planned joints such as final system linkage at sea. For this a jointing/repair facility is necessary.

Of these groups the jointing/repair facility performs a central role not only on the cable-laying vessel but also during the initial assembly of the system at the dockside. Here the facility has to function independently in remote areas, in varied climatic conditions and allow a team of jointers to work in an environment which is conducive to the joints being manufactured to the same high standard achievable at the site of cable manufacture.

The jointing requirements for marine cables are fundamentally different from land cable jointing because the cable is to be deployed, and remain operational, at 4 km depths. Hence resistance to water pressure (42 Mpa at full system depth), tensile strength to support its own suspended weight during deployment and recovery, and cable handling resistance must be considered.

The basic unrepeated cable^[4] is shown in FIGURE 1. The functional elements of the cable are the twelve optical fibres, currently being uprated to 48 fibres^[5], encapsulated in a protective elastomeric buffering material, which is surrounded by a butted steel 'C' tube. This acts as the pressure-resisting medium for cable deployment to 4 km sea depth. Around this a single layer of helically wound wires is stranded to provided the tensile strength required for 4 km deployment. All these elements are sealed within a continuously welded copper tube, forming a barrier against hydrogen and water ingress over the service life of the cable. Covering the copper is a high-density polyethylene layer which allows the metallic components of the cable to be used for fault location in the event of damage. The remaining two layers provide light armouring to give protection against abrasion, cable handling, etc. To provide greater protection, in

areas such as fish trawling grounds, the outer two layers are replaced with galvanised steel wires in various combinations to provide armoured cable types.

These considerations necessitate a more sophisticated joint, with a more involved manufacturing process, requiring a number of purpose made jigs and fixtures. The opposite is true for the design of land cable joints where the emphasis is on the ease of assembly and less on maintaining the cable strength. Should faults occur in land cable joints they can be repaired relatively quickly and cheaply. Marine failures however are lengthy and very costly to repair. The principal design requirements are therefore for lifetime reliability, ease of assembly and minimal optical loss whilst maintaining the tensile strength performance of the cable.

This report details how the jointing/repair facility has been constructed to fit within the overall philosophy of the use of 'vessels of convenience'.

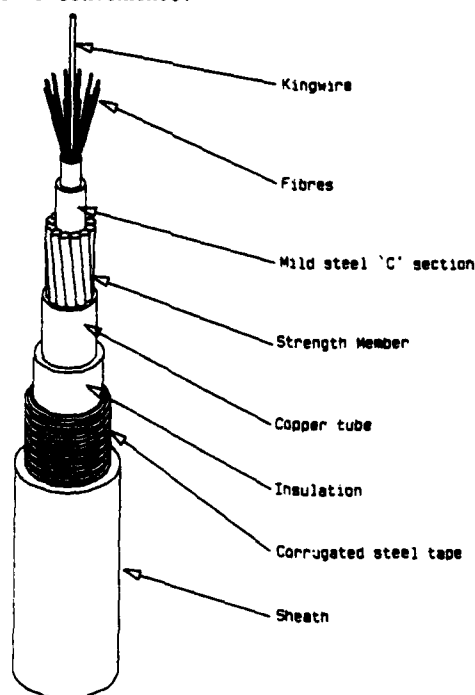


FIGURE 1 UNREPEATED MARINE CABLE

DESIGN CONSIDERATIONS

There are several requirements which the jointing unit must fulfil:-

1) **Self-contained** The system assembly is to be completed in an area, typically a dock side, which is not likely to provide the necessary facilities. This requires that the jointing unit must be totally self-sufficient. Thus it must have its own power supplies, carry sufficient spares and hold detailed technical information on equipment maintenance and repair.

2)Working environment To ensure that the reliability of a completed joint is maintained, the assembly area must be isolated from the outside environment. Thus the working space must not only be shielded from weather but also kept clean on the dockside and at sea on the cable-laying vessel. The unit must also be fully secure while it is being transported to the assembly site by sea or road.

The environment within the container also needs to be controlled so that the jointers can work in some comfort. Hence lighting, temperature, humidity, fume extraction, working space and ease of tool access need to be considered.

The size of the working space will be in conflict with the requirement for storage space and this must be managed so that all the necessary jointing equipment, spares, power and supplies can be contained.

3)Transportation The methods of transportation most likely to be available are the use of a container ship to the nearest terminal and then by road to the system assembly site. The most common container sizes are 20 ft and 40 ft. The maximum weight that can be carried in a 40 ft container is 38 tonnes. The containers are designed to be stacked up to a maximum of nine high, and so the unit must have sufficient strength to support this potential load.

4)Maintenance Due to the possible remoteness of the cable system assembly and whilst on board the cable vessel the equipment used needs to be of a simple and robust design which do not require sophisticated repair. The equipment should also, ideally, be of universally understood design principles. Spares, if required, should be available at the nearest local distributor. Where this is unlikely spares should be carried in the jointing container.

CONTAINER LAYOUT

Container size The shell of the jointing unit has been taken from a 30 ft container. This size was chosen, even though it falls between the two standard lengths, because a 20ft container was considered too small to provide the desired volume for storage whilst a 40 ft container would take up too much of the limited deck space available on the cable-laying vessel. This size is not a problem for road transport but for container ships the 30 ft container needs to be placed on a 40 ft rack. The rack is essentially a flat bed with end supports to allow stacking.

Joint access It can be seen from FIGURE 2 that major modifications have been made to the container construction. The largest of these is the provision of a flap, providing an opening along three-quarters of the container length. This is to permit the joint once assembled to be passed from within

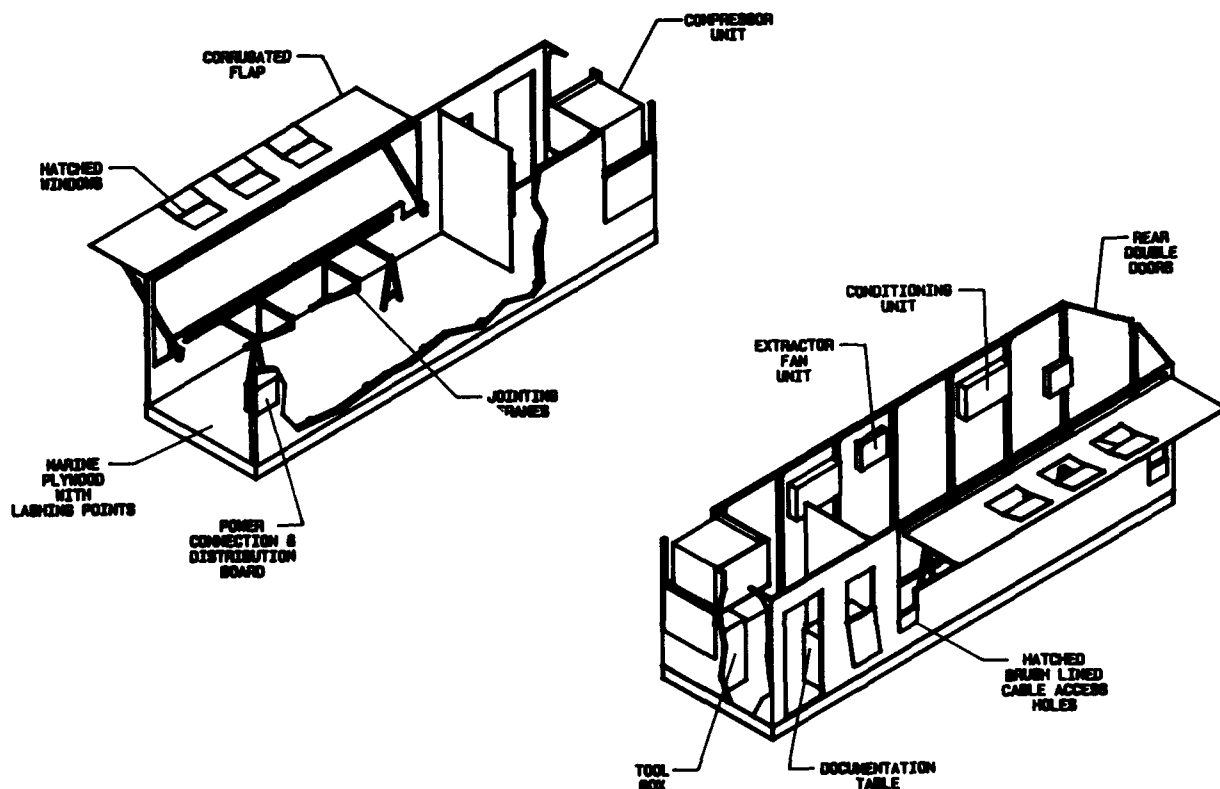


FIG.2 - ISOMETRIC VIEWS OF JOINTING CONTAINER

the jointing area to the cable storage area, which is generally a pre-fabricated cable creel. Around the edge of the opening is a sealing rubber gasket. The seal is broken for flap opening by use of a vertically mounted standard container door-locking mechanism.

Cable access In addition to the large flap two smaller access holes are provided in the bottom corners of the flap window. These allow unjointed cable ends to be brought within the container whilst the flap is closed. The holes are brushed lined to keep out draughts and water. They also have covering hatches to seal holes during container transportation and adverse weather on the cable-laying vessel.



Plate 2 View of the jointing container

Jointing frame On the inside of the container, just below the joint access flap seal, runs a rectangular steel section fixed to the container wall. From this steel section four triangular legs are supported. The legs are capable of being positioned anywhere along the length of the rectangular tube to accommodate various pieces of jointing equipment.

The method of tooling interchange is continuous from cable end preparation, the fitting of a table top for fibre splicing and up to the addition of cable stands for the application of heat-shrinkable cross-linked polymer sleeves which are applied using a propane flame torch. This layer seals the joint from water ingress.

With the interchanging of jointing rigs and tools on the jointing framework the potentially hazardous manoeuvring of exposed fibres in a confined space is avoided. In this way a lightweight joint, that is without external armouring layers, can be assembled entirely on the framework.

Joints in armoured cable are conducted on the frame up to the point of joint closure when it is transferred to separate jointing stands. This prevents the transfer of a tar compound, used to inhibit corrosion of the armouring wires, onto the jointing surfaces.

Power supply Two power supplies are provided for, electrical and a compressed air supply. A diesel driven 110 Volt 125 Amp generator and a diesel driven 140 psi Hydrovane

are situated on a stand-alone trailer. When the container is in use the trailer is situated outside the unit and the connection is made through an inlet in the container wall next to the rear double doors. The electrical distribution board is also located here, inside the container.

During transportation the trailer is stored within the jointing container. Behind the rear double doors ramps are provided for access and loading is assisted by a cable winch assembled across the centre of the container.

With the generators mounted on a manoeuvrable trailer they can be used after the cable system has been assembled and the jointing container has been transferred to the cable-laying vessel. Whilst the container is on board, the vessel's power supply can be used through an additional transformer, supplied as part of the container inventory. This transformer can also be used during system assembly if a nearby mains supply is available. The trailer, now available for other jointing activities, can be towed along the coast-line to the cable landing point, or points in the case of festoon systems, where it can provide the power supply for beach joint manufacture.

Temperature and humidity control Within the container the temperature and humidity is controlled with an air conditioning unit. The compressor unit is recessed into the corner of the container opposite the rear double doors allowing the unit to be mounted outside, but still maintaining the rectangular shape of the container. The compressor is externally fitted, not only to reduce the generated sound levels within the container, but also to dissipate the generated heat. The compressor feeds two slim width conditioning units fitted along the rear wall.

The air conditioning is configured with two compressor units so that failure of one does not affect the other. The conditioning units are also capable of generating heat if required.

Additional cooling of the container is provided by the erection of a canopy over the container, this alone can reduce the temperature within the container by 5°C.

Fume extraction An air extractor is located between the two air-conditioning units. An overhead hood is connected and this is positioned over the jointing frame during the fibre buffering, stripping and heatshrinking operations. Although a small risk, fumes can be outgassed if the materials are excessively heated and in such a small area as the container these fumes would potentially be hazardous.

Health and safety Although the potential risks within the container are small, fire extinguishers and first aid kits are provided.

Tool and documentation storage A small area, inside the container next to the air-conditioning compressor, is the partitioned mini-office. It is here that the jointing hand tools, equipment spares and the jointing and equipment documentation are stored. The documentation is held in

drawers built underneath a table top, which provides for a desktop. The hand tools and equipment spares are held in a large tool box secured in the space below the air compressor. Each tool is given a precise location in the foam lined drawers so that the tool inventory can be quickly checked and any missing tools identified.

Container lining The floor and lower half of the container walls are lined with varnished marine plywood enabling the surfaces to be kept clean. Should boards become damaged they can be easily replaced. Fitted into the boards are cargo strap rings for lashing down equipment during transit. Lashing points are also integrated into the wall reinforcement struts. The lashing points also provide fixing points for shelving which is invaluable for keeping tools and documents to hand during the jointing operation.

Storage The entire jointing inventory can be stored within the container and is easily unloaded on site.

PERFORMANCE

To date three jointing containers have been manufactured.

The first of the containers has been used during the recent installation of a festoon system in the Gulf of Thailand^[6]. The cable was transported to a dockside on drums where it was transferred from the drums to temporary cable storage creels and then assembled using the jointing container. After system test the cable was transferred to the a converted oil platform service vessel "Ibis". The modularisation of "Ibis" was completed when the jointing container was transferred on-board following the system assembly on the dockside. The 100 km of cable was then successfully installed in ten coastal loops around the Gulf of Thailand.

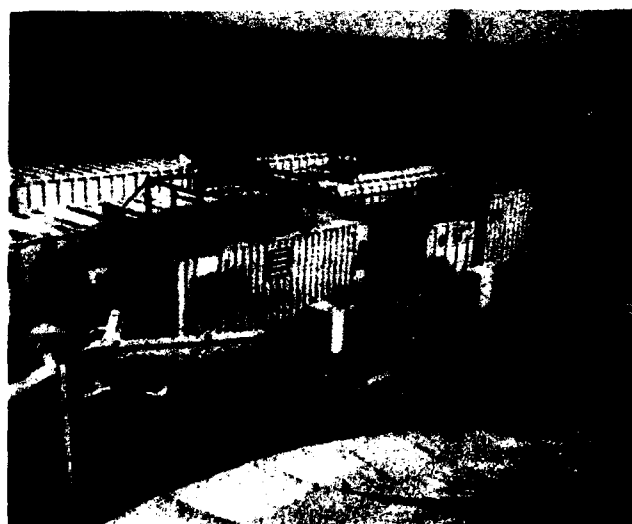


Plate 3 *Layout of the container modules*

The second and third jointing modules have been constructed with minor modifications to the fixtures and fittings. In particular, attention was made to the rust-proofing of equipment against humidity experienced in Thailand as the destination of the third container is to an inter-island system in the Mariana Islands north of New Guinea with similar climatic conditions. The second jointing container has been incorporated onto a converted trailer for the Thailand system which will remain on standby as a repair facility.

CONCLUSION

A containerised jointing environment has been successfully developed for use both on the dock-side and as a modular component of the 'vessel of convenience' philosophy. It has been successfully commissioned in the Gulf of Thailand where the conditions have been climatically and geographically harsh.

REFERENCES

- [1] A.J. Macleod
"Unrepeated Systems"
Proc. of Suboptic 1993, p 249-253
- [2] C.J. Rochester et al.
"Cable Design for Unrepeated Single Span Systems" Proc. of the IWCS 1990, p. 29-35
- [3] J.S. Merrett et al.
"Cable Protection: A Cost Effective Small Plough for Unrepeated Domestic Systems"
Proc. of Suboptic 1993, p 127-130
- [4] Beech S.C. et al.
"New repeated cable design testing, methodology and results"
Proc. of the IWCS, 1992, p 349-354
- [5] I.M. Boardman
"High Fibre Density Cable Systems for the Unrepeated Market"
Proc. of Suboptic 1993 p 309-312
- [6] D.R. Dean
"A Novel means of adding an Underwater Communications Network - Build, Transfer, Operate (BTO)"
Proc. of Suboptic, 1993, p 463-465

ACKNOWLEDGEMENTS

The authors would like to thank J.N. Russell for the use of his photographs and I. Roles for his time in producing the line drawings.

PMD CHARACTERIZATION OF PRODUCTION CABLES FOR CRITICAL LIGHTWAVE SYSTEMS

A. F. Judy, W. T. Greene and J. B. Haber

AT&T Bell Laboratories
2000 Northeast Expressway, Norcross GA 30071

ABSTRACT

We report recent results in measuring the polarization mode dispersion (PMD) of production fibers and cables. Beginning with a review of measurement principles, we compare two test methods on a sample of fibers and find agreement within the expected uncertainty. Using one of these methods we present results on production dispersion-shifted fiber showing low PMD levels that are stable when cabled. Further testing on conventional single-mode fiber cables shows no measurable PMD increase upon installation. Finally, temperature cycling of a variety of fibers and cables shows stable PMD at high temperatures but, for some fiber types, a small PMD increase at low temperatures.

INTRODUCTION

PMD is becoming an important parameter to specify for optical fiber cables. If excessive, it can affect a wide range of transmission systems including ASK digital,^[1] analog-video^[2] and coherent^[3] systems. Characterizing PMD can be difficult because random mode-mixing converts it into a stochastic parameter which varies randomly with wavelength, temperature and cable orientation. Thus, unlike chromatic dispersion, PMD has no deterministic wavelength dependence and no fixed zero-dispersion wavelength. Also it cannot be reliably derived by secondary parameters, such as fiber ovality.^[4] Consequently its characterization requires broadband testing and statistical evaluation. In this paper we compare measurement methods and present the PMD values of production fibers and their variations with temperature, cabling and cable installation.

MEASUREMENT METHODS

PMD is the length-normalized group delay difference between a fiber's two principle polarization modes. Like any dispersion term, it can be measured in either the time or wavelength (frequency) domains. The wavelength

domain appears the easiest to implement because of the ready availability of tunable, wideband optical sources and detectors. The PMD measurement then consists of detecting changes in transmitted polarization with a change in wavelength. We will compare two methods for detecting the polarization change which we designate as the polarization state analyzer (PSA) and fixed-polarizer (FP) methods.



Figure 1a. PSA Method

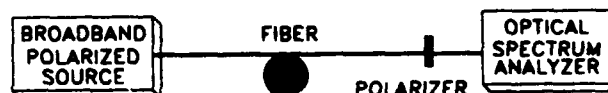


Figure 1b. FP Methods

PSA Measurement Method

The PSA method (Figure 1a) measures the actual output polarization state, for example using Stokes parameters, and derives PMD as a function of wavelength, $PMD(\lambda)$.^[5] It is an accurate but somewhat costly method, due to the expense of the required polarimeter. Its ability to measure the exact PMD at each wavelength is often less advantageous than one would expect. The reason is $PMD(\lambda)$ usually depends on extrinsic parameters such as the fiber's orientation, temperature, and cabling matrix. Thus $PMD(\lambda)$ can change dramatically and randomly with small environmental perturbations and can only be characterized statistically. Fortunately, in the case of a long fiber with random mode-coupling, $PMD(\lambda)$ should have a wavelength independent, Maxwellian probability distribution.^[6] Since a Maxwellian is determined by a single parameter, only its mean need be determined. Other

parameters can be derived from it, for example the standard deviation (σ) is 0.428 times the mean. We will demonstrate that the mean PMD ($\langle PMD \rangle$) is a robust parameter, varying relatively little with wavelength and environmental changes.

Using the PSA method, one finds $\langle PMD \rangle$ by measuring $PMD(\lambda)$ over a range, λ_1 to λ_2 with equal increments of $\delta\lambda$, and calculating the average:

$$\langle PMD \rangle_{PSA} = \frac{\delta\lambda}{\lambda_2 - \lambda_1} \sum_{\lambda_i=\lambda_1}^{\lambda_2} PMD(\lambda_i).$$

There is a fundamental uncertainty in this calculation caused by the finite wavelength range. Since the sum is effectively an average of a finite number N of independent samples from a Maxwellian distribution, the estimated mean will have an uncertainty of $\sigma_{Maxwell}/\sqrt{N} = 0.428 \langle PMD \rangle / \sqrt{N}$. As shown in Ref. (6), if $\delta\lambda$ is small N depends on the autocorrelation of $PMD(f)$ and is proportional to $\langle \Delta\tau \rangle \Delta f$ where $\langle \Delta\tau \rangle$ is the mean group delay difference (i.e. $\langle PMD \rangle / \sqrt{L}$), Δf is the frequency span ($c/\lambda_1 - c/\lambda_2$), and c is the light velocity. Thus the uncertainty in $\langle PMD \rangle_{PSA}$ is:

$$\sigma_{PSA} \approx 0.4 \sqrt{\frac{\langle \Delta\tau \rangle}{\Delta f L}}. \quad (1)$$

Here the coefficient 0.4 is estimated by Monte-Carlo computer simulation of long fibers with random mode-coupling. Also, we are assuming $\langle \Delta\tau \rangle$ increases with the square-root of length.

FP Measurement Method

The FP method provides a simpler means of estimating $\langle PMD \rangle$. It uses a fixed, linear polarizer at the fiber's output (Figure 1b) and measures the detected power versus wavelength.^[7] As the wavelength is swept, the power will oscillate with each maximum to minimum variation indicating a π phase shift between the two polarization states. One can estimate

$$\langle PMD \rangle_{FP} = K M \Delta f,$$

where M is the number of cycles (twice the number of extrema) between λ_1 and λ_2 . The parameter K ($K \leq 1$) accounts for some power fluctuations not being caused by group delay differences when mode-coupling occurs. In the case of strong, random mode-coupling, numeric simulations show $K=0.82$.^[8] If the polarization modes are not coupled at all, then $K=1$.

Similar to the PSA method, the value of $\langle PMD \rangle_{FP}$ will have a random error caused by the finite wavelength range that limits the number of independent samples in the average. Computer simulations show this to be:

$$\sigma_{FP} \approx 0.5 \sqrt{\frac{\langle \Delta\tau \rangle}{\Delta f L}}. \quad (2)$$

We note from equations (1) and (2) that if the measurement span Δf is the same for both methods, their fundamental uncertainty is comparable. The reason is Δf limits the number of independent samples of $PMD(\lambda)$ in both methods. This conclusion is not even strongly dependent on the PMD being Maxwellian distributed. When we simulate shorter fibers with weak mode-coupling the numeric coefficients in both equations decrease, but their ratio remains comparable. Thus, the inherent uncertainty of $\langle PMD \rangle$ is best improved by widening the wavelength span rather than using a different detection technique.

Finally, we note that two other error sources can limit the FP's accuracy. First, noise or trace ambiguity may cause errors in counting M . Second, K may be larger than 0.82 if a fiber has weak mode-coupling. Neither effect would limit the PSA's accuracy.

Experimental Comparison of PSA and FP Methods

We compared the two measurement methods on fifteen 71-km spools of dispersion shifted fiber. The long lengths, plus the fact that each spool comprises at least three spliced fibers, should assure random mode-coupling. For both the PSA and FP methods we used a tunable laser to sweep between 1480 and 1565 nm. The PSA method used a HP8509 for determining $PMD(\lambda)$ while the FP method used a fixed, linear polarizer and a HP8153A power meter.

When K is set to one, we observed (Figure 2) that, as expected, the $\langle PMD \rangle_{PSA}$ was always smaller than $\langle PMD \rangle_{FP}$. The value of K can be estimated from the ratio. This is 0.86 (with a 95% confidence interval of $\pm .04$) which is not different, at this significance level, from the theoretical K of 0.82. Also, we note that computer simulations of randomly coupled waveplates show the ratio of the two measurements will have a σ similar to Figure 2.

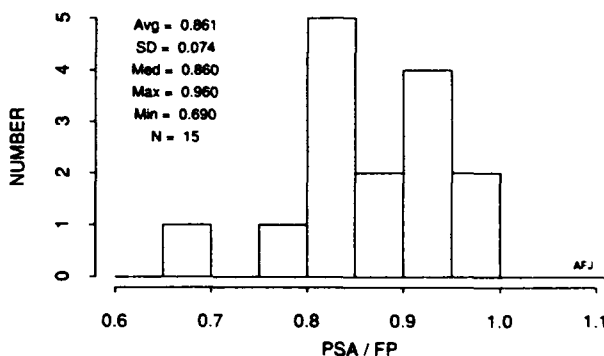


Figure 2. PMD Ratio of PSA and FP Methods

PMD MEASUREMENTS ON PRODUCTION FIBER AND CABLES

In the past year we have measured a variety of production fibers and cables using the FP measurement method. We report here recent results on the PMD statistics of dispersion shifted fibers, plus the evaluation of cabling effects, temperature variations, and installation effects on dispersion-shifted and conventional fiber optic cables.

Statistics for Dispersion Shifted Fiber

Optically amplified undersea cable systems present the most stringent PMD requirements for optical fibers. Not only do the amplifiers allow PMD effects to accumulate over the entire system length, but they also require dispersion-shifted (DS) fiber whose larger internal glass stress generally leads to higher PMD than conventional single-mode fibers. So the ability to make low PMD, DS fiber is essential for state-of-the-art manufacturers.

We have recently measured 113 71-km spools of MCVD DS fibers using a wavelength span from 1510 to 1610 nm. The spools were wound under low tension to minimize extraneous mode-mixing which might artificially reduce PMD. The results (Figure 3) show a mean level of 0.08 ps/√km. This would introduce only 8 ps of PMD in a 10,000 km system, meeting the requirements of a 5 Gbit/s digital transmission system.

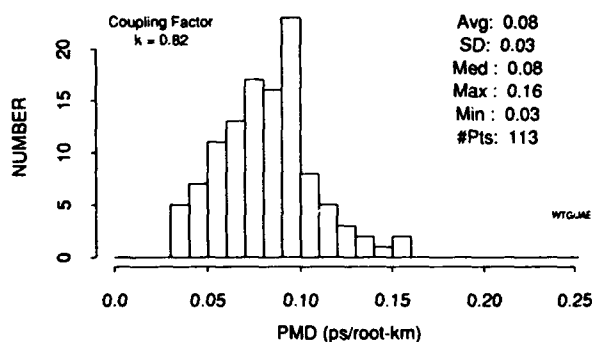


Figure 3. PMD Distribution of Dispersion Shifted Fiber

PMD Stability from Spools to Cables

For some fibers and some winding conditions, the PMD of a spooled fiber may change when cabled. If the spool is wound tightly the PMD may increase as the packaging induced mode-coupling is eliminated. If wound loosely, the PMD may decrease if the cable introduces mode-coupling. To evaluate this we measured forty-five 20-km spooled fibers, then cabled them into two central-tube cables, one 5-km and one 10-km. We measured the

spooled fibers with a wavelength span of 1200 to 1600 nm. Because of factory testing logistics, the finished cables were measured on a different PMD set with a wavelength span of 1525 to 1575 nm. The results (Figures 4 and 5) show no average change from spools to cables. Note that the variation observed for individual fibers agrees with that expected from Equation (2). That is, the σ of the 20-km spools, 5-km and 10-km cables should be 0.01, 0.03 and 0.04 ps/√km, respectively. So the σ of the change will be the root-sum-square of the spool's σ and the cable's σ which corresponds closely to the σ of 0.039 ps/√km shown in Figure 5.

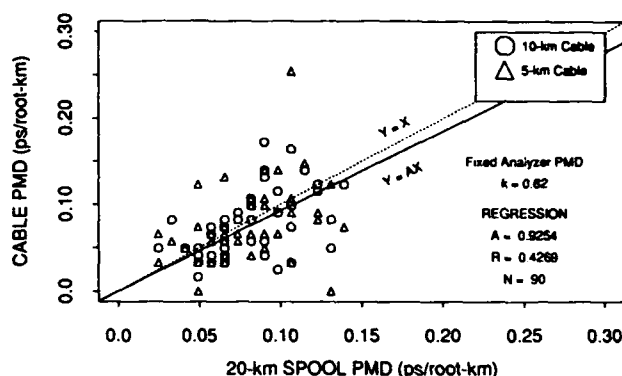


Figure 4. Cable PMD versus Spool PMD

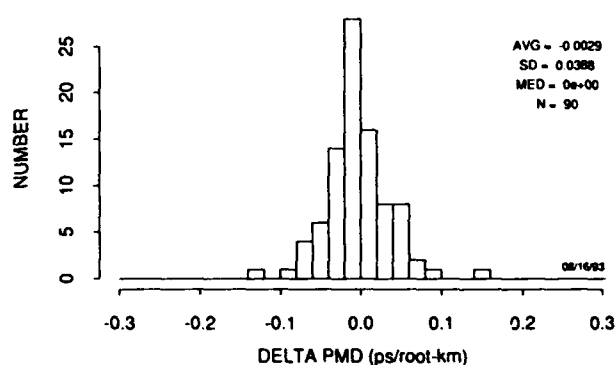


Figure 5. PMD Change from Spool to Cable

PMD Variations with Temperature

As described above, temperature variations will usually perturb the extrinsic stresses on a cabled fiber and cause $PMD(\lambda)$ to vary randomly over its Maxwellian probability distribution. Whether this also changes $\langle PMD \rangle$ must be determined experimentally. Using a wavelength span from 1200 to 1600 nm, we recently measured the $\langle PMD \rangle$ versus temperature on three different sets of cabled fibers:

Cable Type	Fiber Type
Central tube	Depressed Clad
Central tube	Dispersion Shifted
Loose tube	Matched Clad

The results (Figures 6-8) show that the $\langle \text{PMD} \rangle$ stability depends on the fiber type. The DS fiber showed no measurable temperature dependence. The mean of the

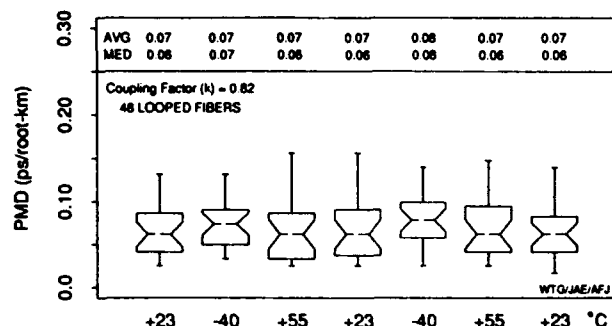


Figure 6. Temperature Cycle Results for Dispersion Shifted Fiber in Central Tube Cable

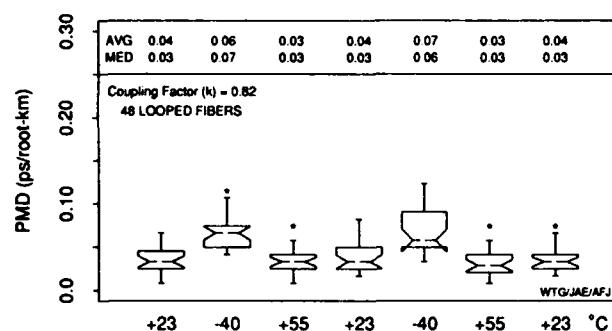


Figure 7. Temperature Cycle Results for Depressed Clad Fiber in Central Tube Cable

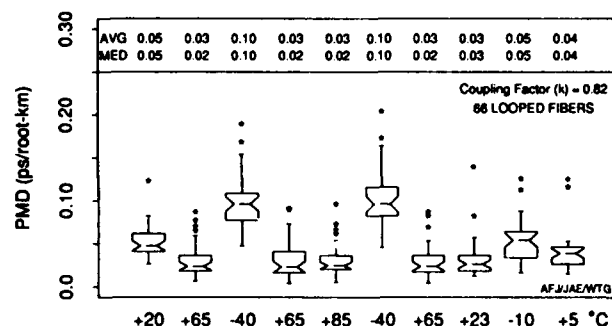


Figure 8. Temperature Cycle Results for Matched Clad Fiber in Loose Tube Cable

depressed-clad, conventional fibers almost doubled from 0.04 to 0.07 ps/ $\sqrt{\text{km}}$ at -40°C , and the matched-clad fibers tripled (from 0.03 to 0.10). The matched-clad data includes fibers made with both OVD and VAD processes, both of which showed the same temperature behavior. For the last set only, we measured at temperatures between -40°C and 20°C and detected a continuous PMD increase beginning at about 5°C .

These are, we believe, the first reported results of an increase in PMD at low temperature. The effect is small and should not be system affecting. Further testing is required to determine if the low temperature increase is inherent to the fibers or is caused by the cable structure.

Installation Effects

Finally, it is necessary to characterize the stability of PMD with cable installation. We studied this by measuring thirteen cables before and after installation in an aerial CATV system. The cables, containing different counts of current production, MCVD depressed-clad, conventional single-mode fiber, were initially measured in the factory in the $1.3\text{-}\mu\text{m}$ window. They were then installed and spliced into 40 fiber paths ranging in length between 5.5 and 19.7 km. Several months later, the PMD of the completed paths was measured, this time in the $1.5\text{-}\mu\text{m}$ window because of the test instrument's greater dynamic range. For each path, we calculated the root-sum-square of the factory data and compared it to the measured path. It is seen (Figure 9) that the statistics of the two are the same. Thus there is no measurable change with installation or with wavelength. Note that the mean in both cases is an extremely low 0.03 ps/ $\sqrt{\text{km}}$.

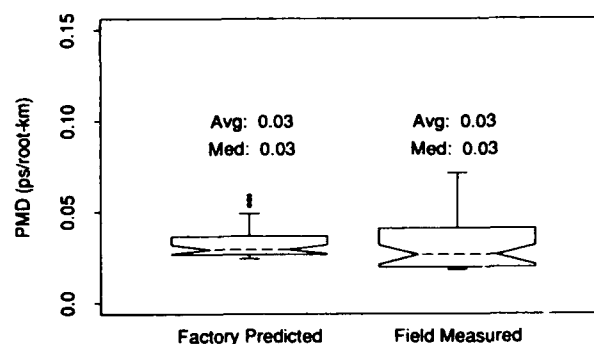


Figure 9. Factory Predicted and Field Measured PMD for 40 Paths

CONCLUSIONS

We have demonstrated that PMD can be routinely measured on production fibers and cables, that low PMD is attainable in dispersion shifted fiber, that it is possible to cable fibers without any measurable PMD increase, and this stability is maintained upon cable installation. We also note the unexpected result that the PMD of some cabled fibers increased at low temperatures. The increase is small, not system limiting, and requires further study to determine the cause.

ACKNOWLEDGEMENTS

We gratefully acknowledge the assistance and contributions of J. R. Edmonston, R. B. Kummer, H. O. Lindstrom, C. D. Poole, J. J. Refi, and R. E. Saltik.

REFERENCES

1. C. D. Poole, R. W. Tkach, A. R. Chraplyvy and D. A. Fishman, "Fading in Lightwave Systems Due to Polarization-mode Dispersion." *Photon Tech. Lett.*, vol. 3, pp.68-70, 1991.
2. T. E. Darcie and C.D. Poole, CED, May 1992.
3. M. S. Kao and J. Wu, "Effect of Polarization Mode Dispersion on a Coherent Optical System with Pilot Carrier." *J. Lightwave Technology*, vol.11, no.2, pp. 303-308, 1993.
4. A. F. Judy, et al., "PMD Characterization of Production Cables for Evolving Lightwave Systems." *OFC'93, Postdeadline Papers*, PD20-1.
5. B. L. Heffner, "Automated Measurement of Polarization Mode Dispersion Using Jones Matrix Eigenanalysis." *IEEE Photon. Tech. Lett.*, vol.4, no.9, pp.1066-1069, 1992.
6. C.D. Poole, J.H. Winters, and J.A. Nagel, "Dynamical Equation for Polarization Dispersion." *Optics Lett.*, vol.16, no. 6, p.372, 1991.
7. C.D. Poole, "Measurement of Polarization-mode Dispersion in Single-mode Fibers with Random Mode Coupling." *Optics Lett.*, vol.14, pp.523-525, 1989.
8. C. D. Poole and D. L. Favin, "Polarization-mode Dispersion Measurements Based on Transmission Spectra Through a Polarizer." To be published.

BIOGRAPHIES



Arthur F. Judy is a Distinguished Member of the Technical Staff in the Fiber Optic Systems Engineering Group. In his 23 years at AT&T Bell Laboratories he has worked and published on the theory, measurement and modeling of optical fibers as well as metallic

media. He has a BSEE from the University of Maryland, a MSEE from the University of Michigan, a MS in Physics from Georgia Tech and is currently pursuing a PhD in physics.



William T. Greene III is a Member of Technical Staff in the Fiber Optic Systems Engineering Group at AT&T Bell Laboratories, Norcross, Georgia. He joined the Glass Technology Group at Bell Labs in 1981 working with lightguide fabrication and

testing. From 1988 to the present, he has been working on outside plant component and media characterization testing. He holds a BET-EET degree from Southern Technical Institute and a MS degree from Georgia Institute of Technology.



Janice Haber joined AT&T Bell Laboratories in 1985. She was Technical Manager of the Fiber Optic Systems Engineering Group for Network Cable Systems from 1989 to 1993. During that time she worked with long haul, loop, and CATV network design, engineering and technical support. In 1993,

she joined the Network Systems Visual/Multimedia Communications organization where she works as a Market Manager for Local Exchange Carrier visual multimedia broadband systems. Janice holds an MSEE degree from the Georgia Institute of Technology and a BSEE from the University of Maryland.

RELATION BETWEEN POLARIZATION MODE DISPERSION AND FIBER CORE OVALITY IN LONG DSF

K. Kashihara, S. Aoyagi, H. Nakamura and O. Aso

The Furukawa Electric Co., Ltd.
6, Yawata - Kaigandori, Ichihara, Chiba 290 Japan

Abstract

Relation between the fiber core ovality and polarization mode dispersion (PMD) of long dispersion-shifted fiber (DSF) is studied experimentally for slightly oval core fiber (ovality < 3%). We confirmed that PMD is proportional to the core ovality.

According to our result and recent report¹⁾, we guess that the homogeneous propagation constant distribution of the optical fiber is violated during the optical fiber production process.

However in this theory, it is assumed that the propagation constant change due to optical fiber birefringence is independent from longitudinal distance and treated as usual function. If this assumption is plausible and if core ovality can be approximately represented as core ellipticity, PMD should be proportional to the fiber core ovality because the following relation has been confirmed by many authors¹⁾:

$$\frac{\partial(\Delta\beta)}{\partial\omega} \propto \text{core ovality.}$$

1. Introduction

Polarization mode dispersion is one of the most important characteristics for designing the ultra long and high bit rate amplified undersea communication system. In 1970s' many authors have studied the relation between the origins of birefringence and group delay difference for short single-mode optical fiber (in the case of negligible mode-coupling), e.g., ovality (ellipticity) of fiber core, stress, twist and so on²⁾.

Recently Poole developed a statistical treatment of polarization dispersion³⁾ by making use of the first-order approximation scheme⁴⁾ and coupled mode equation. In this paper, he showed the square root length dependence of expected PMD value for long fiber (extensive mode coupling limit) as

$$\sqrt{\langle \Delta\tau^2 \rangle} = \left| \frac{\partial(\Delta\beta)}{\partial\omega} \right| \sqrt{\frac{z}{h}} \quad (1)$$

In equation (1), $\Delta\beta$ is the propagation constant difference of the two principal states of polarization, ω is the angular frequency of light and h is defined as shown below

$$h = \int_{-\infty}^{\infty} du \langle \kappa^*(u) \kappa(z-u) \rangle \exp[i\Delta\beta u] \quad (2)$$

where κ is the coupling constant and treated as a probability function in order to describe the random-mode coupling. Thus $1/h$ represents a mean coupling length.

However most recently, Judy and his collaborators found that cabled fiber PMD is poorly related to the fiber core ovality and estimated the correlation coefficient between the PMD and fiber core ovality to be 0.15⁵⁾.

In this paper, we will study the relation between the PMD and the fiber core ovality of the uncabled DSF by making use of a frequency domain PMD measurement method: the wavelength scanning method^{6,7)}.

2. Experiment

(a) PMD Measurement Setup

In this experiment, PMD is measured using the wavelength scanning method^{8,9)}. Configuration of the experimental setup is shown in Figure 1. Tungsten lamp was used as white light source and all optical fibers under test were wound onto a 280mm diameter drum at 20gf tension. Length of DSF: z are in the region of $5\text{km} < z < 35\text{ km}$.

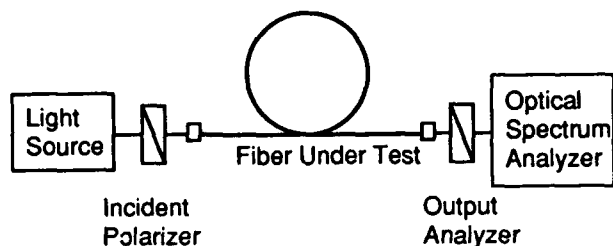


Figure 1 Experimental setup for wavelength scanning PMD measurement method.

It is assumed that the wavelength dependence of optical fiber birefringence is negligible (first order approximation^[4] is adopted). Typical wave form including N numbers of amplitude cycles in a finite wavelength span is shown in Figure 2 ($N = 3$).

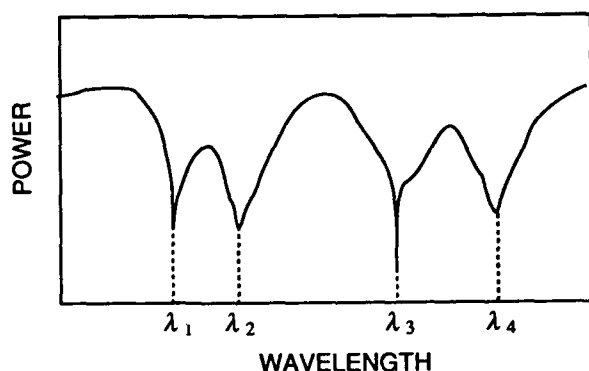


Figure 2 Typical waveform measured by the optical spectrum analyzer ($N = 3$).

From the output waveform, PMD value $\Delta\tau$ is calculated using the width of each cycle as

$$\Delta\tau_i = \frac{1}{c \left(\frac{1}{\lambda_i} - \frac{1}{\lambda_{i+1}} \right)}, \quad (i = 1, 2, \dots, N) \quad (3)$$

From the above assumption, the averaged PMD value in the wavelength domain

$$\langle \Delta\tau \rangle = \frac{1}{N} \sum_{i=1}^N \Delta\tau_i, \quad (4)$$

is equivalent to the averaged value of N times measurement in the case of the time domain method^[1]. Hence the statistical characteristics come from random mode coupling are averaged over in finite wavelength scan^[1].

(b) Fiber Core Ovality Measurement Setup

In order to measure the fiber core ovality, the FE - SEM(Field Emission Scanning Electron Microscope) system was used in this study. Resolving power of this system is shown 20 nm. Magnification of this microscope was corrected using the 1.0 μ m and 0.5 μ m pitch diffraction grating respectively. Thus, the accuracy of this microscope was achieved as +3%. Cross section of the optical fibers were etched by 25% HF included solution. After these procedures, cross section of optical fibers were observed with 5000 times magnification.

The above fiber core ovality measurements were supported by TORAY Research Center Co., Ltd.^[7].

3. Results and Discussions

The experimental result is shown in Figure 3. All DSFs under measurement are made by VAD method and their average diameter is 125 μ m. Figure 3 indicates the dependence of fiber core ovality on PMD for 8 DSFs. It is shown that PMD is proportional to the ovality. Because of the effect of other birefringence, PMD is not equal to zero when the ovality is zero. Correlation coefficient is calculated to be 0.81 .

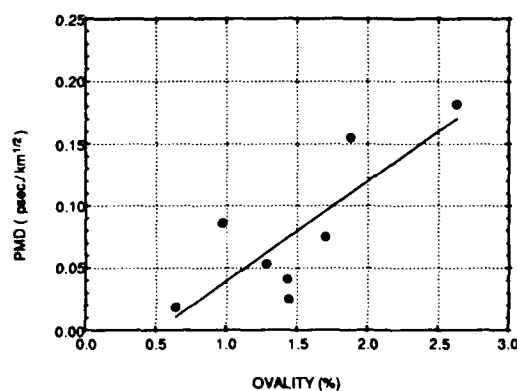


Figure 3. Ovality dependence of PMD for fiber on a 280mm drum with linear least squares fit . Correlation coefficient is 0.81.

Combining this result and the recent Judy *et. al.*'s result^[1], it could be considered that Poole's assumption of the statistical PMD theory seems is violated. In the case of fiber ovality, the above opinion suggests that the shape of DSF strand is changed randomly by some external force during the cable production process.

Furthermore recent experiments^[7] indicate the PMD change for each step during the cable production. From these results, it seems apparent that the PMD change due to external force occurs randomly.

However, Emig and his corroborators' recent report^[8] indicates that even the 1km short cabled single-mode fiber conserves the proportional relation between the PMD and fiber core ovality. So it is necessary to confirm whether the proportional relation is really violated or not in the process of cable production.

Thus from the above discussions, it is necessary to know whether the propagation constant change the constant value for the random probability function and to know when it changes, if it occurs, during the cable production process. We consider that this problem is important to study the PMD effect on the future communication system.

4. Conclusions

In this study, we confirmed that the PMD is proportional to the core ovality for long uncabled DSF. Comparing our result with other reports, we pointed out the importance of PMD change (propagation constant change) due to the process of optical fiber cable production.

We will study the above PMD change precisely in order to make the optical transmission lines more reliably.

Acknowledgement

We would like to thank Dr. Y. Namihiro of KDD R&D Laboratories for his important advices and fruitful discussions. We also would like to thank TORAY Research Co., Ltd. for their technical support. Last but not at least, we want to thank Mr. T. Takabayashi and Mr. H. Ogoshi of Furukawa Electric Co. Ltd. for their continuous encouragement.

References

- [1] A. F. Judy, J. B. Haber, W. B. Gardner, W. T. Greene, A. J. Ritger and K. L. Walker,
"PMD Characterization of Production Cables for Evolving Lightwave Systems,"
OFC-93, PD20 - 1 (1993) 83.
- J. J. Refi, T. E. Darcie, A. F. Judy and C. D. Poole,
" Polarization Mode Dispersion and Its Effect on Optical Transmission",
NCTA Technical Papers, (1993) 116.
- [2] see e.g., S. C. Rashleigh,
" Origins and Control of Polarization Effects in Single-Mode Fibers. ",
IEEE J. Lightwave Technol., LT - 1 (1983) and references there in.
- [3] C. D. Poole,
" Statistical Treatment of Polarization Dispersion in Single-Mode Fiber ",
Opt. Lett. 13 (1988) 687.
- [4] C. D. Poole and R. E. Wagner,
" Phenomenological Approach to Polarization Dispersion in Long Single-Mode Fibers ",
Electron. Lett. 22 (1988) 1029.
- [5] Y. Namihiro and J. Maeda,
" Comparison of Various Polarization Mode Dispersion Measurement Methods in Optical Fibres ",
Electron. Lett., 28 (1992) 2265.
- Y. Namihiro and J. Maeda,
" Polarization Mode Measurements in Optical Fibers ",
Symp. Optical Fiber Measurement, invited paper, NIST BOULDER - U.S.A., (1992) 145.
- [6] M. Saeda, private communications.
- [7] Y. Namihiro, private communications.
- [8] K. A. Emig, R. A. Westwig and D. E. Wolfe,
" The Impact and Importance of Polarization Mode Dispersion on Cable TV System Performance",
NCTA Technical Papers, (1993) 112.



Kazuhisa Kashihara

Furukawa Electric
Co., Ltd.

6, Yawata-Kaigandori
Ichihara, Chiba, 290,
Japan

Mr. Kashihara received B.E. and M.E. degree in mechanical engineering from Osaka Institute of Technology in 1983 and 1985 respectively.

He joined Furukawa Electric Co., Ltd., in 1985, and has been engaged in production engineering of optical fiber.

Now he is an assistant manager of Submarine Cable Section, Optical Fiber Production Department.



Hiroshi Nakamura

Furukawa Electric
Co., Ltd.

6, Yawata-Kaigandori
Ichihara, Chiba, 290,
Japan

Mr. Nakamura received B.E. degree in electrical engineering from Tokyo University in 1992 and joined Furukawa Electric Co., Ltd.

He has been engaged in optical fiber transmission research section.



Shigeru Aoyagi

Furukawa Electric
Co., Ltd.

6, Yawata-Kaigandori
Ichihara, Chiba, 290,
Japan

Mr. Aoyagi received B.E. and M.E. degree in chemical engineering from Yamagata University in 1989 and 1991 respectively and joined Furukawa Electric Co., Ltd. in 1991. He has been engaged in research of polarization mode dispersion of optical fibers as a submarine cable engineer.

Now he belongs to reliability engineering section of quality assurance department.



Osamu Aso

Furukawa Electric
Co., Ltd.

6, Yawata-Kaigandori
Ichihara, Chiba, 290,
Japan

Mr. Aso received B.E. degree in engineering physics from University of Electro-Communications in 1989 and M.S. degree by theoretical cosmology from Hirosaki University in 1991.

In 1991 he joined Furukawa Electric Co., Ltd. and has been engaged in optical fiber transmission research section.

POLARISATION MODE DISPERSION MEASUREMENTS AND RELEVANT THEORETICAL EVALUATIONS ON OPTICAL FIBRE RIBBON CABLES

G. Carones, F. Donazzi, R. Gaspari, A. Ginocchio

PIRELLI CAVI S.p.A. - DIVISIONE ITALIA - MILANO, ITALY

Abstract

The foreseen use of optical fibre ribbon cables in long distance links requires an accurate analysis of the Polarisation Mode Dispersion (PMD) phenomenon in order to establish if it is the limiting factor of transmission capability. We have compared the PMD measurements and the theoretical mechanical stresses due to ribbon to ribbon contact and/or contact between the ribbon and the cable structure. This comparison shows the correlations trend between PMD values and mechanical stresses. The theoretical development of the PMD phenomenon due to mechanical stresses is revisited. The conclusions highlight how the optical fibre ribbon cable can be utilised both in the distribution network or in high speed long distance links.

Introduction

In view of the increasing transmission rates in the optical systems, it is essential to characterise the optical cables with regard to the Polarisation Mode Dispersion (PMD). In fact it is necessary to guarantee that the PMD is not a limiting factor of the system capability in terms of bit-rate.

Worldwide the most commonly used optical cables are of loose designs; in such cables the optical fibres are not stressed and the PMD is negligible, due only to the design fibre bending.

The increasing utilisation of optical fibres in the distribution network and the necessity for more compact cable designs with a greater number of fibres has led to the development of optical fibre ribbon cables. The type of cables here considered, currently used in the Italian distribution network, is composed of a central core with five rectangular helicoidal slots. Into each slot a stack of five 4-fibre ribbons is cabled. The core is then taped and plastic sheathed (see Fig. 1). In such cables thermo-mechanical stresses on the ribbons are caused by mutual ribbon contact, or contact with the core slot by thermal cycling. These non uniform stresses may give rise to an increase in PMD. In Pirelli Cavi it has been carried out, on ribbon cables, a PMD measurement programme. To identify the possible

correlations between the strain and stresses of optical fibre ribbons and the consequent PMD values, a numerical analysis of the stress field in variously loaded ribbons has been performed by means of the Finite Elements Method (FEM). The theoretical results have been compared to the PMD measures on ribbon specimens subjected, on a dedicated equipment (the "expandable bobbin"), to the selected loads.

Theoretical background

The theoretical study main task is to identify the relevant parameters affecting the Polarisation Mode Dispersion (PMD) in optical fibres. At the present study level, the theoretical results are mainly qualitative and not directly used to quantify the PMD values.

In order to study the PMD in single mode optical fibres, it is worth recalling that single mode optical fibres must actually be considered two-mode ones since the fibre presents two possible degenerate modes that, in an ideal fibre, have the same propagation constants. However any real single mode fibre presents geometric, dielectric imperfections and strains that are due to bending, twisting or lateral contact as well as temperature changes. All the above phenomena cause birefringence.

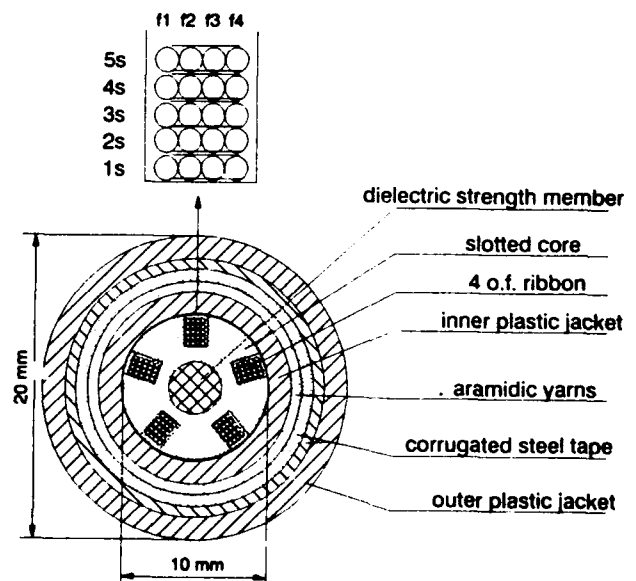


Fig. 1: 100-fibre slotted core ribbon cable.

i.e. a difference in the phase velocities of the two orthogonally polarised normal modes. Therefore the fibre becomes a real two-mode medium and may exhibit mode dispersion. The present work deals with the birefringence and consequent PMD caused by the mechanical stresses and geometrical deformations of the ribbon fibre core. The birefringence is therefore generated by:

- ribbon to ribbon contact, and/or contact between the ribbons and the core slots;
- ribbon bending;
- fibre core ellipticity, due to the above mechanical deformations.

In addition to that, when the core is elliptical, the twisting of the fibre generates an additional rate of birefringence.

Birefringence evaluation

In order to evaluate the overall mechanical birefringence of the fibres into a ribbon the single effects are separately evaluated and then superposed.

The mechanical deformation of a crystal is related to its optical behaviour by means of the tensorial elasto-optical relation¹. The components of the relative dielectric permeability tensor are related to the refractive indexes of a crystal; when a strain field is applied to the crystal, the variation of the permeability tensor coefficients are given by (in tensorial form):

$$\delta B_i = p_{ij} \epsilon_j \quad (1)$$

with:

$$\delta B_i = \delta \left(\frac{1}{n_i^2} \right) \quad (2)$$

and where:

n_i is the i-direction refractive index;
 p_{ij} is the crystal elasto-optical tensor;
 ϵ_j is the strain tensor.

For an isotropic material, like the fused silica, the tensor is given by¹:

$$p_{ij} = \begin{pmatrix} p_{11} & p_{12} & p_{12} & 0 & 0 & 0 \\ p_{12} & p_{11} & p_{12} & 0 & 0 & 0 \\ p_{12} & p_{12} & p_{11} & 0 & 0 & 0 \\ 0 & 0 & 0 & p_{44} & 0 & 0 \\ 0 & 0 & 0 & 0 & p_{44} & 0 \\ 0 & 0 & 0 & 0 & 0 & p_{44} \end{pmatrix} \quad (3)$$

p_{11} of the fused silica is equal to 0.121;
 p_{12} of the fused silica is equal to 0.270;
 p_{44} is equal to $(p_{11} - p_{12})/2$.

From:

$$\delta B_i = \delta \left(\frac{1}{n_i^2} \right) \quad (4)$$

it is:

$$\delta B_i = - \frac{2}{n_i^3} \delta n_i \quad (5)$$

or, since $n_i = n_0$:

$$\delta B_i = - \frac{2}{n_0^3} \delta n_i \quad (6)$$

From (1) and (6) finally it is derived:

$$\delta n_i = - \frac{n_0^3}{2} p_{ij} \epsilon_j \quad (7)$$

The birefringence, if the z axis is assumed coincident with the fibre axis can be evaluated as:

$$\delta \beta = k_x - k_y = k (\delta n_x - \delta n_y) \quad (8)$$

where:

k is the wave number $2\pi c/\lambda$;

n_x and n_y are the refractive indexes associated with the two orthogonal principal polarisation directions.

Birefringence due to bending

The birefringence caused by bending is due to the stresses acting into the normal section of the fibre and generated by the bending itself. The stress along the axis of the fibre, that is considered parallel to the z axis of the strain tensor, do not affect the birefringence of the two orthogonally polarised normal modes. Neglecting the very small strains in the binormal direction, the value of the fibre birefringence is given¹ by:

$$\delta \beta_b = - \frac{1}{4} k n_0^3 (p_{11} - p_{12}) (1 + \nu) \frac{r^2}{R^2} \quad (9)$$

with:

ν is the Poisson's ratio;
r is the fibre fused silica radius;
R is the bending radius.

Birefringence due to side pressure

As in the case of the bending, also in the event that a side pressure is applied, the birefringence due to side pressure is caused by the normal section strains and stresses.

A formula⁴ similar to that of the bending applies; the birefringence expressed in terms of the stresses along the normal (x axis) and binormal (y axis) of the bent fibre is:

$$\delta\beta_b = -\frac{1}{4} k n_0^2 (p_{11} - p_{12}) \frac{(1+\nu)}{E} (\sigma_x - \sigma_y) \quad (10)$$

where:

E is the Young's modulus of the fused silica;
 ν is the Poisson's ratio;

σ_x is the normal direction stress;

σ_y is the binormal direction stress.

Birefringence due to core ellipticity

On a weakly guiding fibre, with very small ellipticity and very small difference between the core and cladding refractive index, the birefringence can be expressed as:

$$\Delta\beta_c = \frac{e^2 (2\Delta)^{\frac{3}{2}}}{8a} \frac{N^2}{V^2} \left[U^2 + (U^2 + N^2) \left(\frac{J_0(U)}{J_1(U)} \right)^2 + U N^2 \left(\frac{J_0(U)}{J_1(U)} \right)^2 \right] \quad (11)$$

where:

e is the core ellipticity, given by:

$$\sqrt{[(a^2 - b^2)/a^2]};$$

a is the core semimajor axis;

b is the core semiminor axis;

Δ is the relative refractive index difference $(n_1 - n_2)/n_1$;

n_1 is the core refractive index;

n_2 is the cladding refractive index;

V is the normalised frequency:

$$V = k a n_1 \sqrt{2\Delta} \quad (12)$$

U and W are given by:

$$U = a \sqrt{n_1^2 k^2 - n_0^2} \quad (13)$$

$$W = a \sqrt{n_0^2 - k^2 n_2^2} \quad (14)$$

n_0 is the unperturbed refractive index.

For the frequency used in the tests the above formula is approximated with:

$$\Delta\beta_c = \frac{e^2 (2\Delta)^{\frac{3}{2}}}{8a} \quad (15)$$

The fast axis of the birefringence is parallel to the minor axis of the elliptical core.

Birefringence due to twisting of a fibre with an elliptical core

The twisting of a perfectly round fibre, i.e. of a fibre with round core produces birefringence of identical amount and sign on both the linearly polarised modes, i.e. generates optical activity without PMD. The birefringence generated by twisting such a fibre is given

by:

$$\delta\beta_t = 2 G \Gamma \frac{\phi_t}{n_1} \quad (16)$$

where:

G is the shear modulus of the fused silica;

Γ is the photoelastic constant;

ϕ_t is the twist angle per unit length.

When a fibre with elliptical core is twisted the overall effect can be summarised as a combination of the ellipticity birefringence and core twisting birefringence. Therefore it is given by:

$$\delta\beta_{ec} = \sqrt{\left(\frac{e^2 (2\Delta)^{3/2}}{8a} \right)^2 + \left[2\phi_t \left(1 - \frac{G\Gamma}{n_1} \right) \right]^2} \quad (17)$$

Polarisation Mode Dispersion as a function of the birefringence

The magnitude of the PMD depends on the derivative of the birefringence.

Since the propagation constants are expressed by:

$$k_i = \frac{n_i \omega}{c} \quad (18)$$

being:

c the vacuum light speed.

The PMD per fibre unit length is:

$$\delta\tau = \left| \frac{\partial(k_x - k_y)}{\partial\omega} \right| = \frac{|n_x - n_y|}{c} + \frac{\omega}{c} |n'_x - n'_y| \quad (19)$$

where the derivation with respect to ω is indicated by the prime. The second term indicates the dispersion of the medium and, since in weakly guiding silica fibres in near infra-red it is:

$$\frac{|n_x - n_y|}{\omega} > |n'_x - n'_y| \quad (20)$$

For a first order evaluation the PMD per unit length can be approximated with:

$$\delta\tau = \left| \frac{\partial(k_x - k_y)}{\partial\omega} \right| = \frac{|k_x - k_y|}{\omega} = \frac{\delta\beta}{\omega} \quad (21)$$

It has been demonstrated⁹ that the PMD for long fibres is correlated to that of short fibres by a Maxwellian distribution:

$$P(\delta\tau, x) = \frac{2\delta\tau^2}{\sqrt{2\pi}q^2} \exp\left(1 - \frac{\delta\tau^2}{2q^2}\right) \quad (22)$$

where q^2 is the variance.

By applying such a distribution the PMD for very long fibres is given by:

$$\delta\tau = \sqrt{\frac{8L_c}{\pi}} \sqrt{L} \delta\tau \quad (23)$$

where L_c is the correlation length, i.e. the length where, if a single linearly polarised mode is injected into the fibre, half of its power has been transferred to the orthogonal mode. For a number N_0 of fibres joined together a similar formula¹⁰ applies:

$$\delta\tau = \sqrt{\frac{8N}{\pi}} \delta\tau \quad (24)$$

Stresses and strains evaluation

In order to evaluate the PMD due to mechanical stresses and strains operating on a four fibres ribbon, a numerical evaluation has been applied by using the Finite Element Method. Half a ribbon (to take advantage of the stress field symmetry) has been discretised into a plane mesh made up with triangular elements. Distributed loads were applied accordingly to the test loading conditions.

The pressure and curvature taken into account in the evaluation were therefore identical to those applied to the ribbon when it has been tested on the "expandable bobbin".

The "expandable bobbin" is a piece of equipment used to test the performances of optical elements (fibres and ribbons)¹¹.

This apparatus is basically composed by a metallic drum, with several sectors, whose radial expansion can be monitored and controlled by a personal computer. The specimen to be tested is wound on the drum and the optical behaviour is monitored by means of dedicated instruments.

In the set-up used in the present experiments the sectors were provided with a metallic helical slot with contiguous pitch.

Into the slot a stack of five ribbons is wound with controlled pull tension so that the side pressure among the elements is known.

The stresses and strains of the silica core of the fibres can therefore be evaluated.

By expanding the drum the side pressure acting on the ribbons can be varied, and by applying the above formulae the PMD can be calculated and compared to the measured values.

PMD measurement

The PMD of the ribbon fibres has been measured using a commercial bench (HP 8509B Lightwave Polarisation Analyser). The measuring technique is based on a frequency domain method, i.e. on the evolution of the states of polarisation (SOPs) of the output signal as a function of the light source wavelength.

The PMD can be seen as the Differential Group Delay (DGD) $\delta\tau$ between the principal SOPs¹², and it is calculated by using the Jones-matrix eigenanalysis technique¹³. From a geometrical

point of view the evolution of polarisation, due to a variation in frequency (wavelength) of the input signal, can be represented as a trajectory of a point P on the Poincaré sphere (see Fig. 2).

The DGD $\delta\tau$ is then given by¹⁴:

$$\delta\tau = \frac{\phi}{2\pi} \frac{1}{\Delta f} = \frac{\phi}{2\pi} \frac{\lambda_1 \lambda_2}{c \Delta\lambda} \quad (25)$$

where ϕ is the angle between the Stokes vectors at λ_1 and λ_2 .

All the measures were carried out using a temperature tunable DFB laser source. The tuning range was 1314±1315 nm in 0.5 nm (= 58 GHz) steps, corresponding to a temperature variation between 18° and 32°C.

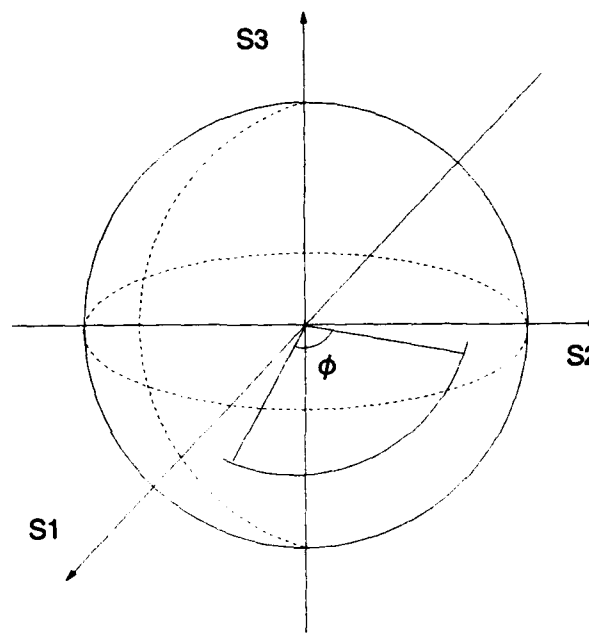


Fig. 2: Evolution of the State of Polarisation on the Poincaré sphere due to a variation in wavelength.

With this experimental set-up the maximum DGD, that can be measured into a 180 degrees arc on the Poincaré sphere, turns out to be 5.6 ps. The minimum measurable DGD, i.e. the instrumental uncertainty, is less than 0.05 ps.

Since a temperature controlled DFB laser, due to its small tunability, does not allow statistics of DGD to be obtained with sufficient accuracy¹¹, measurements on each fibre were repeated at different time (at least 5 times per fibre). In any case the measuring and data acquisition time, for a single fibre, was about 2 minutes, a value well below the threshold time (20 min, over which fluctuations of the SOP, for a fixed input signal, generally fall outside the corresponding experimental error bar of the measuring set-up¹⁵). The same equipment was then used to measure

the PMD performances of a 100 optical fibre (SMR type) ribbon cable, 3.1 Km long, in which all ribbons were spliced together, according to their position in the slots, to form an optical length of 15.5 Km for each fibre (see Fig. 3). This fibre concatenation was adopted so as to have a better measurement accuracy and, on the other hand, to have the possibility of measuring all ribbon fibres in function of their position in slot.

Since fluctuations in temperature strongly affect PMD values¹⁵, the cable, wound on its drum (2 m diameter), was kept at constant tem

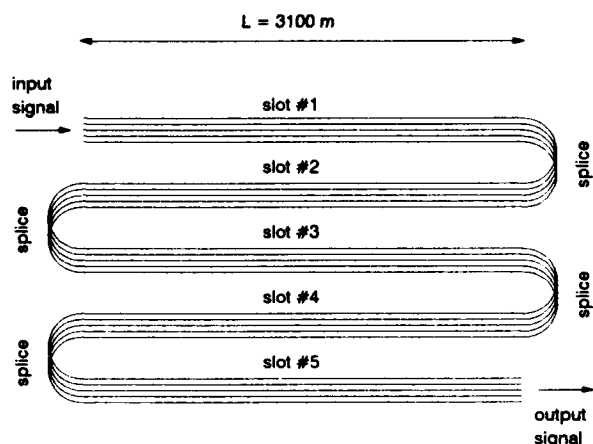


Fig. 3: Ribbon splicing sequence for cables PMD measurements.

perature ($T=18^{\circ}\text{C}$) for all the time required to perform all measures.

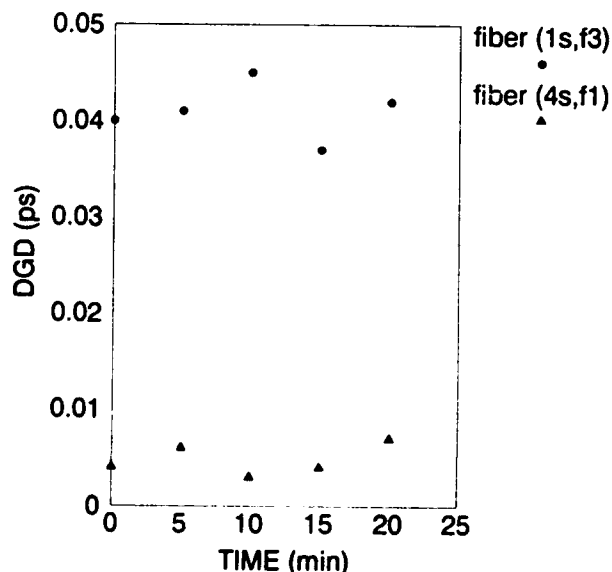


Fig. 4 : PMD stability measurement.

All fibre attenuation in the cable where previously measured (OTDR at 1550 nm): no attenuation increases were detected, except those due to the above mentioned splices. Previously measured (OTDR at 1550 nm): no attenuation increases were detected, except those due to the above mentioned splices. In order to check the uncertainty of this experimental set-up, a short time stability test was initially performed on all fibres by measuring, for a fixed wavelength input signal, the residual fluctuations in PMD values: each fibre was measured 5 times in 20 minutes, waiting 5 minutes between two consecutive measures. Fig. 4 shows the time behaviour of the worst and the best found case, that is fibres (1s,f3) and (4s,f1) (Fig. 1) respectively.

Part of these fluctuations can be due to:

- stress micro-fluctuations in the cable;
- micro-variations in temperature, probably in those parts of the cable lengths which were not temperature conditioned (i.e. the input and output heads);
- imperfections in the fibre joints to the polarisation analyzer (FC connectors were used).

It can be noticed, however, that the measured DGDs always fall below 0.05 ps; this value can therefore be assumed as an estimate of the experimental uncertainty.

Analysis of the results

The formulae derived in the Theoretical Background cannot take into account the intrinsic birefringence of the unstressed fibre due to dielectric imperfections of the core and/or intrinsic ellipticity of the core itself.

Besides, for what concerns the comparison between the expandable bobbin measurements and the theoretical results, it is necessary to disregard the twisting effect since, on the bobbin drum, the coils are wound with very short lay length and the twisting is negligible.

The theoretical results are moreover correlated to some constants that, for the tested fibres, are not completely known:

- the elasto-optical tensor components of doped silica;
- the fibre correlation length L_c ;
- the doped silica photoelastic constant Γ .

In order to better understand the correlations between PMD values and the strain field, it has been therefore preferred to compare the normalised theoretical and experimental results. When calculating the PMD as a function of birefringence, it has been taken into account the contributions of bending, side pressure and strain induced ellipticity.

In the case of the ribbon stack wound on the bobbin, the birefringence due to bending (Eq. 9) is nearly identical for any fibre into the stack since the radiuses of curvature of the fibres differs only by 10^{-3} terms.

The FEM analysis provides also the silica strain

field. The fibres core deformations and ellipticities are then easily derived from the calculated strain values.

The analysis of the theoretical results obtained, within the above considerations, for a stack of 5 ribbons stressed as on the "expandable bobbin" drum, indicates that the theoretical PMD is lower for the underlying ribbons while, for the top ribbon, the PMD is maximum (see Fig. 5).

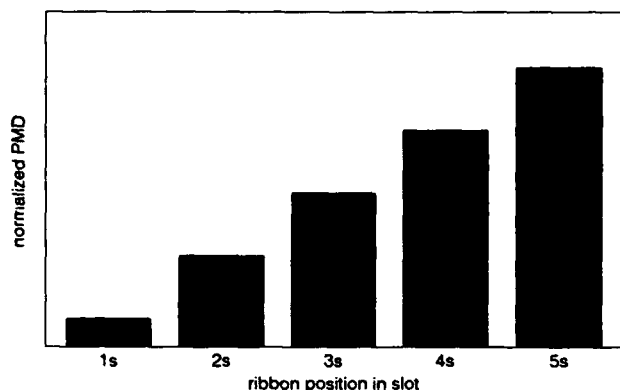


Fig. 5: Normalised theoretical PMD values for a ribbon stack.

The same trend has been obtained when measuring the PMD on the corresponding stack wound on the "expandable bobbin"; the PMD measurement obtained on cables confirms such a behaviour (Fig. 6). In fact the analysis of the

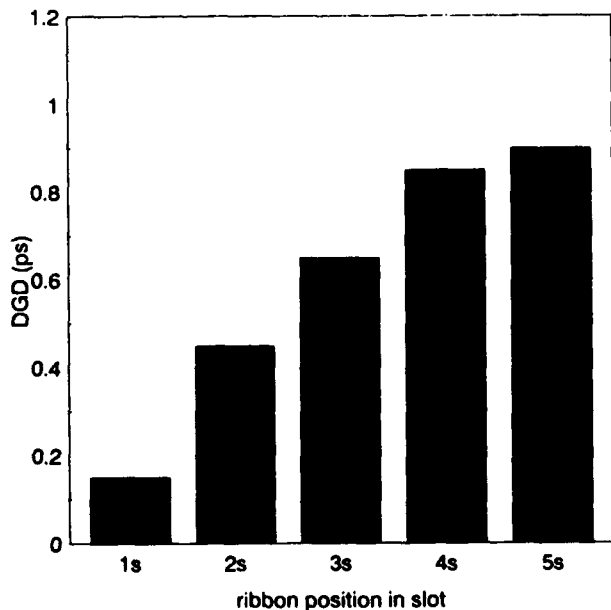


Fig. 6: PMD measured values on a 15.5 Km length of a 100-fibre ribbon cable.

FEM stress field indicates that, for the bottom ribbon, this stress field is, into the silica, roughly an hydrostatic one. In such an instance the "side pressure" birefringence is minimal, being minimal the difference between the σ_x and σ_y stresses; thus the corresponding PMD reaches a minimum. The DGD of the top ribbon (5s in Fig. 6) does not exactly follow the linear trend, but the similarity is, on the whole, satisfactory.

For what concerns the absolute PMD values, between measured and calculated data there is one order of magnitude of difference if the formulas are directly applied to the cables case.

This, as already mentioned, can be explained by the unknown multiplying coefficients used in the theoretical evaluation.

The value of the correlation length L_c and those of the other unknown constants have a relevant effect on the calculated PMD values; for instance if we consider that, for ribbon fibres, L_c can be considerably larger than the normally credited values, even the above mentioned difference can be explained.

Effect of PMD on the transmission length

It is possible to say, from the PMD values obtained from cables, that even in the worst case, the PMD is not a limiting factor of a system supplied with optical fibres ribbons.

In fact the permissible bit-rate for an optical link (being PMD the only limiting factor) is roughly given by:

$$B \leq \frac{1}{4 D_0 \sqrt{L}} \quad (26)$$

where:

B is the bit rate (bit s^{-1});
 D_0 is the link PMD (s Km^{-1});
 L is the link length (Km).

Considering a future very high bit-rate of 10 Gbit/s, from Eq. 26 it is possible to estimate the maximum optical link length when the only limiting factor is the PMD.

In the worst case of our experimental results (0.22 ps Km^{-1}), said length turns out to be over 10000 Km.

For connections of shorter length and lower bit-rate, as in the case of distribution network, the above considerations apply *a fortiori*.

Conclusions

A theoretical model of the opto-mechanical PMD behaviour in optical fibres has been discussed. The model has then been applied to evaluate the theoretical behaviour of optical fibre ribbons subjected to selected load conditions.

The theoretical results, obtained by means of a FEM analysis of the strain/stress field into the fibres silica cores, have been compared to the measured experimental results.

A first order comparison shows a correlation

between the theoretical computed results and the experimental ones. To conclude, from the experimental and theoretical results, it is possible to establish that, for optical fibre ribbon cables, the PMD is not the limiting factor for what concerns the cable capability, even for very long distance links.

Acknowledgements

The authors wish to thank the management of Pirelli Cavi-Divisione Italia for the authorization to publish this paper.

References

- 1 Nye J.F. : "Physical Properties of Crystals", Clarendon Press, Oxford 1985
- 2 Yariv A., Yeh P. : "Optical Waves in Crystals", Wiley and Sons 1984
- 3 Ulrich R. et Al. : "Bending-induced Birefringence in Single Mode Fibers", Opt. Lett. 5,6 (1980)
- 4 Eickoff W. et Al. : "Wavelength Dependence of Birefringence in Single Mode Fibers", Appl. Opt. 20,19 (1981)
- 5 Love J.D. et Al. : "Birefringence in Elliptically Deformed Optical Fibres", Electron. Lett. 15,20 (1979)
- 6 Smith A.M. : "Birefringence Induced by Bends and Twists in Single Mode Optical Fibers", Appl. Opt. 19,15 (1980)
- 7 Sakay J.-I. et Al. : "Birefringence and Polarisation Characteristics of Single Mode Optical Fibers under Elastic Deformations", IEEE Jour. Quant. Electron. 17,6 (1981)
- 8 Rashleigh S.C. et Al. : "Polarisation Mode Dispersion in Single Mode Fibers", Opt. Lett. 3,2 (1978)
- 9 Curti F. et Al. : "Statistical Treatment of the Evolution of the Principal States of Polarisation in Single-Mode Fibers", J. Lightwave Technol. 8,8 (1990)
- 10 Andresciani D. et Al. : "La Polarizzazione e la Dispersione nelle Fibre Ottiche Single-Mode", La Comunicazione 1/(1992)
- 11 Donazzi F. et Al. : "Problems Related to the Design and Manufacture of Optical Fibre Ribbons", EFOC-LAN Proc. 1991
- 12 Gisin N. et Al. : "Experimental Comparison Between Two Different Methods for Measuring Polarisation mode Dispersion in Single Mode Fibres", Electron. Lett. 27,24 (1991)
- 13 "Polarisation Measurements of Signals and Components", Product Note 8509-1 Hewlett Packard (1992)
- 14 Namihira Y. et Al. : "Comparison of Various Polarisation Mode Dispersion Measurements Methods in Optical Fibres", Electron. Lett. 28,25 (1992)
- 15 De Angelis C. et Al. : "Time Evolution of Polarisation Mode Dispersion in Long Terrestrial Links", J. Lightwave Technol. 10,5 (1992)



G. Carones
Pirelli Cavi - Divisione
Italia
Milano, ITALY

Mr. Carones was born in Milan in 1961. He graduated in Nuclear Engineering from Politecnico di Milano in 1987 and joined Pirelli Cavi in 1990, where he has been engaged in research and development of telecommunication Cables, dealing mostly with environmental tests on optical fibres/cables and measurement techniques.



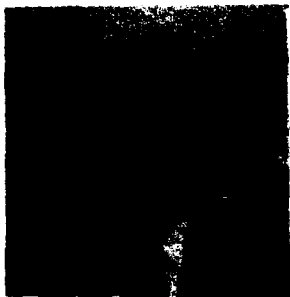
F. Donazzi
Pirelli Cavi - Divisione
Italia
Milano, ITALY

Mr. Donazzi was born in Piacenza, Italy, in 1946. He graduated in Mathematics from Università Statale degli Studi di Milano in 1971 and joined Pirelli Cavi in 1971, where he has been engaged in Research and Development Mathematical and Statistical Studies Centre. Since 1992 he has been responsible of the Applied Mathematics and Modelling Centre. He is a member of AICA.



R. Gaspari
Pirelli Cavi - Divisione
Italia
Milano, ITALY

Mr. Gaspari was born in Milan in 1963. He graduated in Aerospace Systems Engineering from Politecnico di Milano in 1988 and joined Pirelli Cavi in 1990, where he has been engaged in The Research and Development Dept.. He deals in mathematical modelling and measuring techniques development in the Applied Mathematics and Modelling Centre of the R&D Dept.. He is a member of Euroavia and AIDAA.



A. Ginocchio
Pirelli Cavi - Divisione
Italia
Milano, ITALY

Mr. Ginocchio was born in Milan in 1947. He graduated in Electrical Engineering from Politecnico di Milano in 1972 and joined Pirelli in 1974, where he was engaged in the research and development on submarine cables. Since 1987 he has been responsible for the technological development of optical fibre cables in Pirelli Cavi - Divisione Italia.

EXTRINSIC STRESS EFFECTS ON POLARIZATION MODE DISPERSION IN OPTICAL FIBER CABLES

Scott Grindstaff, Joseph Hill, Omid Daneshvar

AT&T Fitel Company
P.O. Box 486
Carrollton, Georgia 30117

Abstract

Polarization mode dispersion (PMD) of standard non-dispersion shifted single mode fibers at various stages of cable manufacturing is investigated. Also, the effects of external factors which may be present during the service life of the cable are simulated and analyzed. We report that general correlations exist between the fiber's intrinsic PMD and the effects of external stresses due to temperature and macrobending. The fiber's reaction to these external stresses are found to be quite different for various levels of intrinsic PMD. However, for recently published PMD levels, the average PMD changes are found to be small during the service life of the cable. Also, the test results show that at very low intrinsic birefringence levels, the external factors can become the dominant cause of PMD.

Background

As analog video communication has become the de-facto standard for lightwave common antenna TV (CATV) transport systems, polarization mode dispersion (PMD) is gaining more attention as one of the possible limitations to communication bandwidth. PMD is present to some extent in all single mode fibers. This dispersive phenomenon can be the result of extrinsic stresses caused by the fiber's surrounding environment, or

by mechanisms which are intrinsic to the fiber itself. The fiber's geometrical irregularities and stresses, whether intrinsic or extrinsic, set up a condition known as birefringence in the fiber. Due to birefringence slight changes occur between the effective refractive index of the two orthogonal polarization modes which propagate through a single mode fiber. If the propagation delay between the two modes is coupled with the effects of laser chirp and polarization dependent devices, in extreme cases, can cause increased bit-error rates in digital systems and higher order distortion effects in analog communications.^{[1][2]}

Two basic theories exist which are used to explain the PMD behavior in conventional single mode fibers. The two theories are very different in that they apply to fibers with different levels of intrinsic birefringence, and predict very opposite reactions to external bending and stresses. The first theory involves externally induced birefringence due to bending of the fiber. Many theoretical models have been developed which demonstrate that the fiber's bending birefringence (B_b), and thus induced PMD, is inversely proportional to the square of the fiber's bending radius (r) as shown in the following equation:^[3]

$$B_b = 0.25n^3(p_{11} - p_{12})(1 + \mu)(b/r)^2 \quad (1)$$

where n is the refractive index of the core, p_{11} and p_{12} are strain-optic coefficients, μ is Poisson's ratio for silica glass, b is fiber's outer radius, and r is the bend radius. It has been shown^[4] that, for fibers a few meters in length, the induced PMD due to bending can be approximated by:

$$PMD_b \approx \frac{B_b}{C} \quad (2)$$

where C is the speed of light. This relationship implies that PMD increases dramatically as the fiber experiences smaller bending radii. This effect is currently used in many fiber sensor applications. However, it is suspected that for long length fibers, the linear length relationship of PMD to length suggested by equations 1 and 2 will no longer be valid. This is due to the increased occurrence of coupling between the polarization modes.

The second theory deals with the effects of random external disturbances on fibers which have some low level of intrinsic birefringence. This theory concludes that Random extrinsic stresses along the length of the fiber result in increased coupling among the polarization modes. This increased random mode coupling interacts with the fiber's intrinsic birefringence and serves to decrease the fiber's PMD.^{[5][6]}

Experiments were performed on both cabled and uncabled fibers to investigate the influence of the fiber's environment on PMD. In particular, we investigated the effects of the cabling process and service life testing of the cabled fibers. One of the goals of our testing was to establish experimentally the level of birefringence where these two theories converge for cabled fibers so that the correct theoretical model could be applied.

Experiment

Measurement Method

PMD tests were performed using the wavelength scanning method.



Figure 1. PMD Test Configuration.

The measurement equipment (Figure 1) consisted of a 1310 nm edge emitting LED with a -3 dB spectral width of 70 nm. The light was then passed through a linear polarizer before being coupled into the single mode test fiber. At the output end of the test fiber the light is passed through a second polarizer and then coupled to the input of an optical spectrum analyzer (OSA). The OSA is used to measure the periodicity (n) of the polarization dependent output power versus wavelength. Equation 3 is used to calculate the average PMD between the two wavelengths λ_1 and λ_2 . For all of the tests a mode coupling factor (k) of 1 was used.

$$PMD = \frac{kn\lambda_1\lambda_2}{(\lambda_2 - \lambda_1)C} \quad (3)$$

A broad spectral width source was selected to achieve a higher resolution measurement. The source provided a measurement spectrum of 400 nm, which provides a time delay measurement ability down to approximately 0.03 picoseconds. This measurement method is currently under consideration by the Telecommunications Industries Association (TIA) as a standard test method for low birefringent single mode fibers.^[7]

Length Dependency

Many papers have demonstrated that PMD does not scale linearly with length. Instead, PMD tends to increase with the square root of fiber length.^[5] Tests were performed to determine if the square root length dependence could still be used for fibers wound on a shipping spool in order to make normalized comparisons throughout the various cabling processes.

To verify this relationship, we measured the PMD of two fibers which were wound on 162 mm diameter shipping spools under 50 grams of tension. Both fibers were initially 25 km in length, and were then cut and remeasured at approximately 5 km intervals. The results are shown in Figure 2.

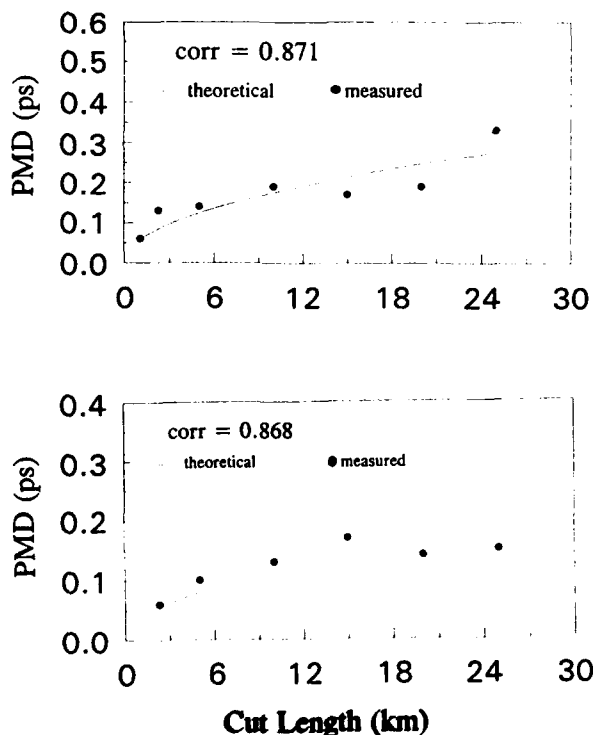


Figure 2. Theoretical vs. Measured Length Dependency.

A square root function was fit through the measured data and the correlation factor determined. When the variability due to measurement repeatability and the handling effects of removing fiber was considered, we found the square root dependency to length to be valid for fibers on a shipping spool.

Cabling

To determine the effects of the cabling process on PMD, a cable was manufactured with various fiber types. For the experiment, 48 fibers were selected from four fiber manufacturers representing MCVD, OVD, and VAD manufacturing methods. The fibers were selected to represent a range of PMD levels. The experimental cable was a 48 fiber, loose tube cable having 12 fibers per buffer tube, and a length of 1.5 km. The buffer tubes were stranded around a strength member using the reverse oscillating lay (ROL) method. Since the theoretical bending strain applied to the fiber is lowest just after the buffering process, the PMD measurement at buffering is considered to more closely represent the fiber's intrinsic state of birefringence and was, therefore, used as the reference point for comparing the various levels of PMD.

For the test, the PMD of each fiber was measured on the shipping spool, after buffering, and after stranding. After reviewing the test data it was evident that, although the changes were small, the fibers exhibited very different responses when subjected to the various degrees of stress associated with cabling. It appears that the direction of change is dependent upon the birefringence level of the fiber. This dependency on intrinsic birefringence is demonstrated in Figure 3 which shows the

different behavior observed after removing the fibers from the shipping spools and placing them into a buffer tube. The fibers above the 45° reference line exhibited higher PMD on the shipping spool, whereas the fibers below the reference line exhibited the opposite effect. The behavioral transition region appears to be between the buffering PMD levels of 0.10 ps/√km to 0.20 ps/√km.

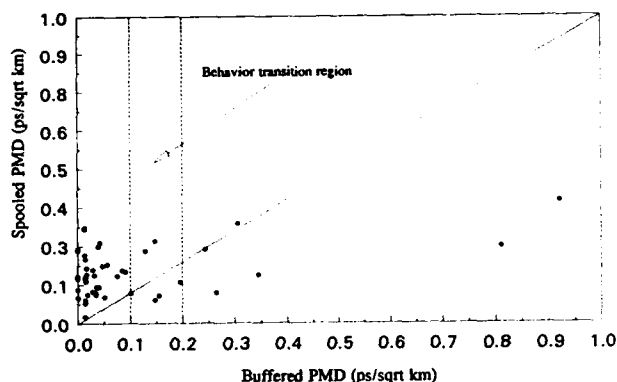


Figure 3. PMD Change from Spooled to Buffered States.

Fibers with PMD less than approximately 0.10 ps/√km after buffering demonstrate a significant decrease in PMD after being removed from the higher bending strain associated with the shipping spools. This data is consistent with the theory of induced birefringence due to strain. However, the fibers with higher levels of intrinsic birefringence typically increase in PMD during the transition from shipping spool to buffer tube. The data for these higher birefringent fibers seems to exhibit behavior consistent with the theory of decreased PMD due to increased random mode coupling. It is apparent that, in general, both theoretical responses to bending strain are applicable to the cabling process. Therefore, based on the fibers' different responses to strain, the data was segregated into two groups for further analysis. One group consisted of fibers with buffering PMD greater than 0.10

ps/√km, the fibers in the other group all had PMD values below this level.

For the final part of the cabling process the buffer tubes are stranded around a strength member. The bending strain on the fiber slightly increases after this process due to the helical bending of the buffer tube. After this process we noticed no change in the median PMD values, but a slight change in the distribution occurs as denoted by the box plots in Figure 4. From bottom to top the horizontal lines of each box represent the minimum data point, the 10, 25, 50, 75, and 90 percentiles, and the maximum value.

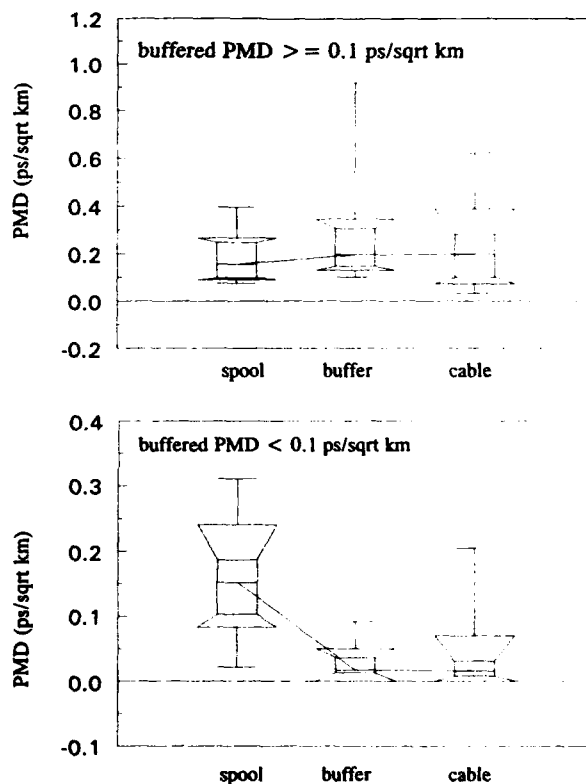


Figure 4. PMD Change During Cabling

The fact that the median PMD levels did not change significantly from buffering to the stranding process, despite the increase in bending strain, is probably due to the fact that the actual bending strains associated

with these processes are more random in nature than would exist on a spool. For example, the interaction among the fibers in each buffer tube, the fiber-to-tube length ratio, and the cyclical effects of the ROL stranding process are all combined to constitute the resultant stresses on the fiber. These stresses deviate slightly from fiber to fiber.

Service Life Tests

To determine the effects of service life testing on PMD, the trial cable was wound on a reel with a 71 cm drum diameter and placed in an environmental test chamber. The cable was cycled between its extreme operating temperatures of -40°C and $+70^{\circ}\text{C}$. The PMD of each fiber was measured at the extreme temperatures and compared to room temperature measurements. In addition, the cable was put through accelerated aging to determine the variation in PMD that could be expected during the service life of the cable. For this test the environmental chamber was held at $+85^{\circ}\text{C}$ for 7 days. After aging, the cable was again cycled between temperature extremes for measurement comparisons.

For analysis purposes the fibers were segregated into three groups based on their room temperature PMD levels. Figures 5, 6, and 7 show box plots of the cable's PMD distribution at each temperature.

The data indicates that with extraneous sources of sudden change such as wind and vibration not present, the effects of temperature cycling on PMD are fairly repeatable. In addition, when we examine the data in more detail, changes in PMD once again appear to be dependent upon the intrinsic level of birefringence within the

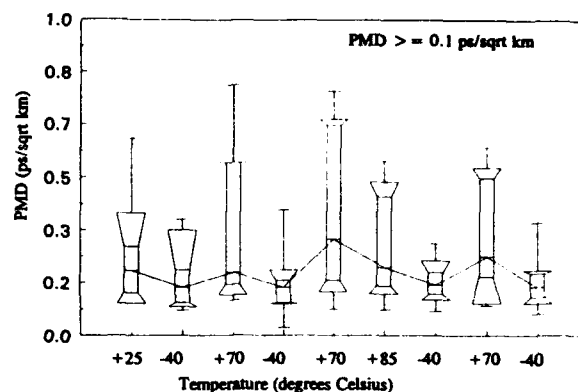


Figure 5. Cabled Fiber Response to Temperature Cycling and Accelerated Aging for Fibers Above 0.10 ps/ $\sqrt{\text{km}}$ at 25°C .

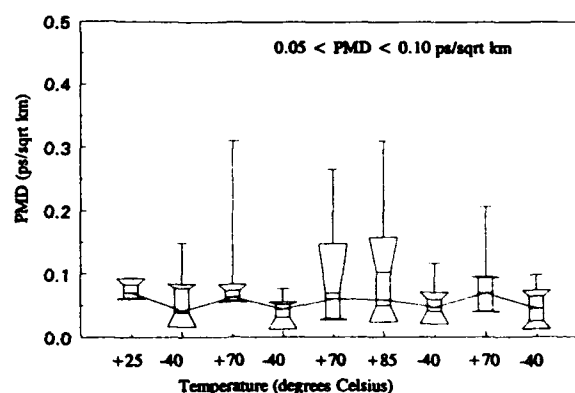


Figure 6. Cabled Fiber Response to Temperature Cycling and Accelerated Aging for Fibers Between 0.05 and 0.10 ps/ $\sqrt{\text{km}}$ at 25°C .

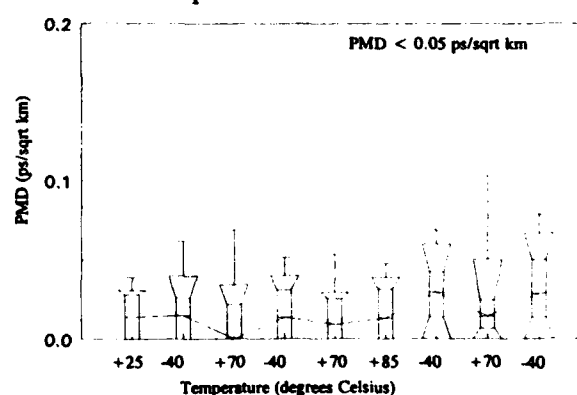


Figure 7. Cabled Fiber Response to Temperature Cycling and Accelerated Aging for Fibers below 0.05 ps/ $\sqrt{\text{km}}$ at 25°C .

fiber with higher birefringent fibers exhibiting more sensitivity to changes in their environment. For room temperature PMD levels $> 0.05 \text{ ps}/\sqrt{\text{km}}$ the median value of PMD generally decreases at -40°C where the stresses on the cabled fiber is typically greater, and increases with higher temperatures as the fiber experiences a more relaxed state. When analyzing the very low birefringent fibers we see that they have very little response to large temperature changes. Based on recently published production data, today's conventional single mode fibers typically have PMD levels below $0.05 \text{ ps}/\sqrt{\text{km}}$.^[8] This low level of birefringence would indicate a fairly stable PMD response throughout the operating temperatures of the cable.

The behavior of the fibers during temperature cycling agrees with that seen during the cabling process in that a slight behavioral change in PMD versus strain seems to occur at levels below $0.10 \text{ ps}/\sqrt{\text{km}}$. For service life testing, the behavioral change in PMD occurred at a slightly lower value ($0.05 \text{ ps}/\sqrt{\text{km}}$) than for the cabling process. This means that only the very low birefringent fibers experience increased birefringence induced by external stresses. It is felt that this is due to the much lower levels of applied stress during temperature cycling as opposed to the cabling process.

The $+85^\circ\text{C}$ measurements were made after aging the cable for 7 days at that temperature. Typically the results of this test cause some small amounts of shrinkage in the various components of the cable. The test data seems to indicate only a slight increase in the median values for very low birefringent fibers possibly due to the residual external stresses. The environmental test results indicate no

significant increases in PMD over the lifetime of the cable.

PMD versus uniform bending strain

The cabled fiber experiments apparently confirmed the existence of two distinctly different reactions of PMD to bending strain. However, the calculated bending strain in buffered and stranded states are typically based on an average theoretical strain calculation. Since the effective cabled bending strain is probably somewhat more random in nature than would be indicated by the calculated values, an attempt was made to verify the results of our test by measuring fibers under more uniform bending conditions.

For the experiment, four fibers were selected which would provide a range of PMD levels. The fibers were wound under 50 grams of tension onto various size spools ranging from 89 mm to 220 mm in diameter. The PMD level of each fiber was measured on each spool to determine its response to bending strain. The four fibers were then manufactured into a loose tube cable of the same design used in the previous experiment. The fibers' PMD at the buffering stage was then used to approximate their intrinsic PMD level.

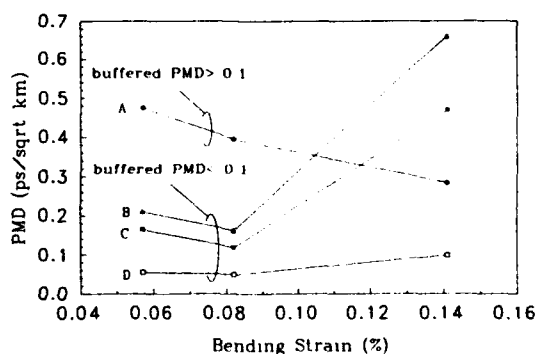


Figure 8. PMD vs. Bending Strain for Fibers Wound at Various Diameters.

As shown in Figure 8, the test data verifies the results found in the previous cabling experiment. Three of the experimental fibers exhibited a general increase in PMD with increased bending strain, and were all less than 0.10 ps/√km after being placed into a buffer tube. The fourth fiber experienced decreased PMD with increasing strain, and had a post buffering PMD level greater than 0.10 ps/√km. However, the levels of PMD found in the buffered and stranded states do not compare well with those on the various size spools, although the theoretical bending strains are in a comparable range. This difference is mostly due to the more uniform strain associated with the spools as opposed to the cabling process.

Conclusion

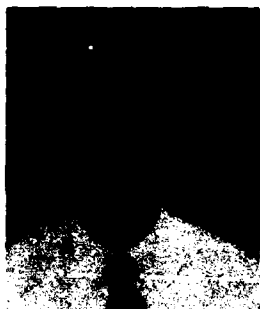
The effects of extrinsic stresses on cabled fiber PMD levels have been investigated. The test results indicate that the different levels of external stress associated with loose tube cable manufacturing serve to slightly change the effective birefringence of fibers from one process to the next. For the manufacturing processes, the data indicates that the theory of stress induced birefringence generally applies to fibers with PMD less than about 0.1 ps/√km. PMD levels greater than 0.1 ps/√km exhibit characteristics consistent with the theory of induced mode coupling which predicts reduced PMD due to random external stresses. In particular, it was found that single mode fibers experience artificially high or low levels of birefringence while on a shipping spool. Therefore, to obtain accurate measurements, the PMD performance of cabled single mode fibers must be measured after completing the cabling process.

Based on the low levels of PMD recently published for cabled single mode fibers^[8], the service life tests indicate that the typical fiber would experience only small changes in PMD with temperature. With the average cabled PMD values being 0.04 ps/√km or less, our test data indicates the majority of fibers would remain well below 0.1 ps/√km throughout the operating temperature range of the cable. Additionally, the accelerated aging test indicated no significant increase in PMD levels over the lifetime of the cable.

References

1. T.E. Darcie, C.D. Poole, "Polarization-induced performance variables," *Communications Engineering and Design (CED)*, May 1992, pp.50-58.
2. C.D. Poole et. al., "Fading in Lightwave Systems Due to Polarization Mode Dispersion," *IEEE Photonics Technology Letters*, Vol.3, No.1, January 1991.
3. R. Ulrich, S.C. Rashleigh, W. Eickhoff, "Bending-induced birefringence in single-mode fibers," *Optics Letters*, Vol.5, No.6, June 1980.
4. Nori Shibata et. al., "Polarization mode dispersion in a coil of single-mode fiber," *Optics Letters*, Vol.10, No.2, February 1985.
5. C.D. Poole, "Measurement of polarization-mode dispersion in single-mode fibers with random mode coupling," *Optics Letters*, Vol.14, No.10, May 1989.
6. C.D. Poole, J.H. Winters, and J.A. Nagel, "Dynamical equation for polarization dispersion," *Optics Letters*, Vol.16, No.6, March 1991.

7. "Polarization Mode Dispersion Measurement for Single-mode Optical Fibers by Wavelength Scanning," *FOTP-113*, submitted to *TIA/EIA FO-6.6.5*, January 26, 1993.
8. J.J. Refi et. al., "Polarization Mode Dispersion and It's Effect on Optical Transmission," *NCTA*, 1993.



Scott E. Grindstaff
AT&T Fitel Company
Carrollton, Georgia

Scott Grindstaff is Instrumentation Engineer at AT&T Fitel Company. He received a B. Sc. degree in Electrical Engineering Technology from Southern College of Technology in 1990. Since joining AT&T Fitel's Research and Development department in 1990, he has been responsible for the development of automation of measurement systems for optical fibers, cables and components. Mr. Grindstaff is a member of the Institute of Electronics and Electrical Engineers (IEEE).



Joseph A. Hill
AT&T Fitel Company
Carrollton, Georgia

Joseph A. Hill holds the position of Product Development Engineer at AT&T Fitel Company. He was granted a B. Sc. degree in Ceramic Engineering from Clemson University in 1989. He joined AT&T Fitel

in 1990, having the responsibilities of material and cable development. Mr. Hill is a member of the American Ceramic Society (ACerS) and the National Institute of Ceramic Engineers (NICE).



Omid Daneshvar
AT&T Fitel Company
Carrollton, Georgia

Omid Daneshvar is Research and Development Manager at AT&T Fitel Company. He holds B. Sc. and M. Sc. degrees in Electrical Engineering from Georgia Institute of Technology. He joined AT&T Fitel in 1985 and has since had responsibilities in the development of fiber optic cables and measurement systems. Mr. Daneshvar is a member of the Optical Society of America (OSA).

PMD REDUCTION OF OPTICAL FIBER CABLES FOR TRANSOCEANIC OPTICAL AMPLIFIER SUBMARINE CABLE SYSTEMS

Y. NAMIHIRA(*), T. KAWAZAWA(*), and N. NORIMATSU(**)

(*) KDD R&D Laboratories, 2-1-15, Ohara, Kamifukuoka, Saitama 356, Japan

(**) KDD CO. LTD., 2-3-2, Nishishinjuku, Shinjuku-Ku, Tokyo 163-03, Japan

ABSTRACT

This paper presents the development of two fully automated PMD (polarization mode dispersion) measurement systems, an interferometric method for short-length fibers and cables, and a fixed analyzer method for long-length product cabled fibers. Using the two kinds of the newly developed fully automated PMD measurement systems, the PMD reduction process of the cabled fibers for transoceanic optical amplifier submarine cable systems are also described.

The PMD increase of the cabled fibers resulted mainly from the intrinsic core ovality of the bare fibers. A low-PMD of less than $0.1 \text{ ps}/\sqrt{\text{km}}$ has been successfully achieved in 33 km-long cabled fibers. The PMD variations of these cabled fibers were found to be less than $0.01 \text{ ps}/\sqrt{\text{km}}$ under the 8000 m deep sea environmental conditions.

1. INTRODUCTION

In the conventional single-mode optical fibers (SMFs), there exists a modal birefringence due to external stress [1]-[4], geometrical core deformation (elliptical core) [4],[5] and thermal stress [6],[7] which give rise to polarization mode dispersion (PMD).

Especially, in the high bit rate ultra-long haul optical fiber amplifier systems, where the chromatic dispersion effects become very small by tuning the signal wavelength near the zero-dispersion wavelength, optical pulse broadening due to the PMD can become a major impairment if no effort is made to keep it within practical limits. Therefore, it is very important to measure accurately the PMD of the active EDFAs, the fiber optic devices and the long optical fibers and cables.

So far, the fading in lightwave transmission analog systems has been demonstrated [8] in a 1.7 Gbit/s IM-DD system using highly birefringence dispersion shifted fibers (DSFs) in which PMD was induced from the random polarization mode coupling

[9]. The PMD in the long-length optical fiber cables is complicated by the random polarization mode coupling that results from small variations in the birefringence along the fiber length. In the ultra-long and high bit rate transoceanic transmission systems using optical amplifiers, the PMD has turned out to be one of the more important parameters to degrade the BER (bit error rate) characteristics.

Therefore, it is very important : (1) to reduce of the PMD of the long-length cabled fibers, (2) to measure the PMD values accurately, and (3) to evaluate the magnitude of PMD variations of the cabled fibers due to being placed on under seafloor environmental conditions.

To make highly accurate PMD measurement in the low-PMD cabled fibers, we have already developed [10],[11] four kinds of PMD measurement methods such as : (1) interferometric method [10]-[12], (2) fixed analyzer (wavelength scanning) method [10],[11],[13], (3) Poincare sphere method [10],[11] and (4) SOP method [10],[11],[13]. However, in this paper we focus our attention on the two kinds of the newly developed fully automated PMD measurement systems [14] such as the interferometric method for short-length fibers and cables, and the fixed analyzer method for long-length product cabled fibers. Using the two kinds of the PMD measurement systems, the PMD reduction process of the cabled fibers for transoceanic optical amplifier submarine cable systems is presented.

The relationship between the PMD of the coated fibers and intrinsic PMD of the bare fibers, and the relationship between PMD variation and polarization mode coupling are also described.

2. PMD MEASUREMENT METHODS FOR OPTICAL FIBERS AND CABLES

2. 1 Interferometric PMD Method

Fig.1 shows a block diagram of the highly accurate and fully automated interferometric PMD measurement system [14], and the photograph is shown in Fig.2. In the fully automated interferometric PMD measurement system, the optical path is

modulated by actuating a corner cube with a piezoelectric transducer (PZT) at several tens Hz sinusoidal AC modulation instead of using an optical chopper to locate and identify the interference point in a short time [10]-[12]. The principle of the measurement is based on the Michelson interferometer [15]. The interferenced output optical powers (visibility curves) can be obtained if the group-delay difference (or PMD τ) between the two orthogonal polarized waves is within the coherence time of the optical source.

The averaged PMD τ is given by [10]-[12];

$$\tau = 2d/c \quad (1)$$

where, $2d$ and c are the optical path length ($= 2d$; twice the moving path length of the optical delay line, d) and the light velocity in free space, respectively. The measurement accuracy and dynamic range are strongly depending on the optical sources. The specifications of the fully automated interferometric PMD measuring equipment is shown in Table 1.

The examples of the interferometric PMD measurement of the polarization maintaining fiber [16] (PMF, $L \approx 0.85$ m) and the dispersion shifted fiber (DSF, $L \approx 16$ km) are shown in Figs.3-(a) and (b), respectively. In Fig.3, it is found that there is great difference between the two visibility curves of the PMF and the DSF. Many interference points in the visibility pattern of the DSF are interpreted as a results of the random polarization mode couplings [9],[14] along the fiber length. A comparison of the interferometric PMD method [10]-[12] with the fixed analyzer method [10],[11] is shown in Table 2. From Table 2, it was found that in the case of the strong random polarization mode coupling, the PMD value obtained from the peak to peak power definition was smaller than that of other PMD methods.

The definition of the PMD for the interferometric PMD method is shown in Fig.3 (b). In Fig.3 (b), the definition of (#1) is a half of the peak to peak powers of two visibility curves

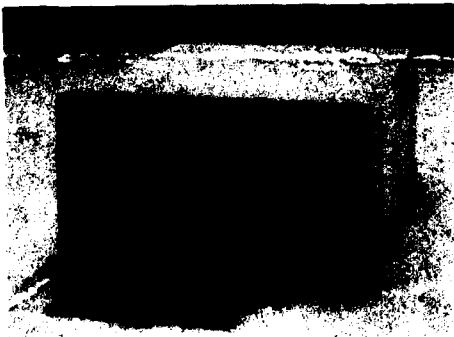


Fig.2 Photograph of fully automated interferometric PMD measurement system

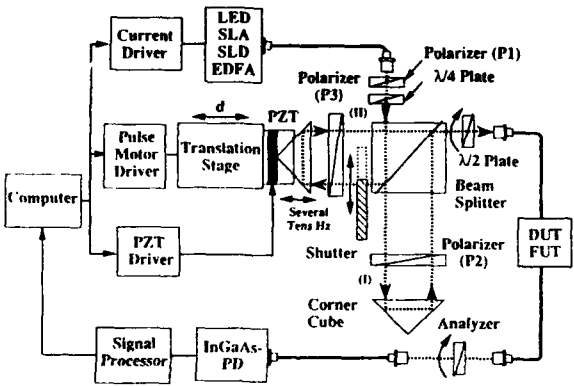


Fig.1 Block diagram of fully automated interferometric PMD measurement system

Table 1 Specification of interferometric PMD measurement system

Optical Source	LED	SLA	SLD	EDFA
Center Wavelength, λ_0	~ 1561 nm	~ 1565 nm	~ 1589 nm	~ 1540 nm
Spectral Width, $\Delta\lambda$	~ 89 nm	~ 83 nm	~ 53 nm	~ 22 nm
Coherence Time	~ 0.045 ps	~ 0.114 ps	~ 0.040 ps	~ 0.351 ps
Output Power of Optical Fiber	Light Source	~ -18 dBm	~ -19 dBm	~ -10 dBm
	System	~ -40 dBm	~ -40 dBm	~ -30 dBm
Dynamic Range	~ 30 dB	~ 30 dB	~ 40 dB	~ 50 dB
Measurement Resolution (Polarization Mode Coupling)	~ 0.002 ps (~ 0.05 ps)	~ 0.002 ps (~ 0.10 ps)	~ 0.002 ps (~ 0.05 ps)	~ 0.002 ps (~ 0.30 ps)
Measurement Time	~ 7 minutes			

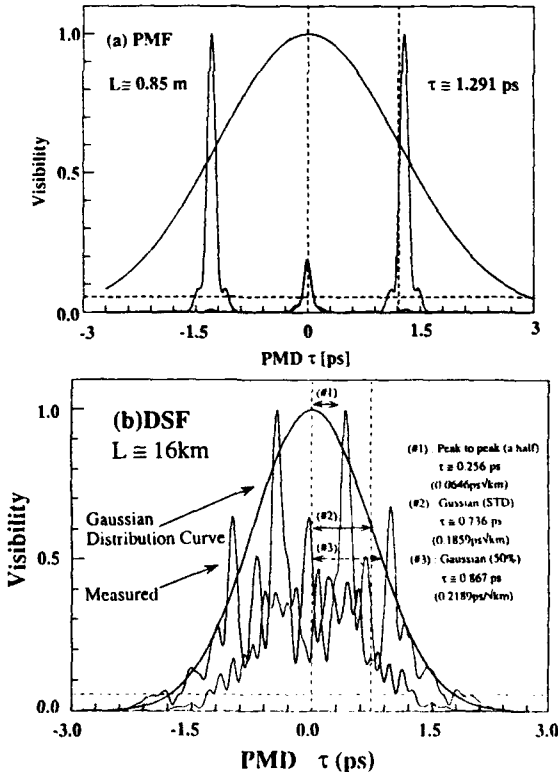


Fig.3 Example of interferometric PMD measurement results
(a) Polarization maintaining fiber (PMF ($L \approx 0.85$ m))
(b) Dispersion shifted fiber (DSF ($L \approx 16$ km))

(slow and fast birefringent waves) [10]-[12]. The definition of (#2) represents standard deviation (STD) of Gaussian fitting of the two visibility curves [14],[17]. Meanwhile, the definition of (#3) indicates a half of FWHM (Full Width Half Maximum, 50%) of Gaussian distribution of two visibility curves [14],[18]. From Table 2, it was confirmed that the definition of (#1) can be used in the case of the birefringence fiber optic devices such as PMFs. However, in the case of long optical fibers having the random polarization mode coupling, the PMD definitions of (#2) and/or (#3) are more appropriate for the PMD measurements than that of (#1) [14]. However, a further study as for PMD definitions for the interferometric PMD method will be needed.

2.2 Fixed Analyzer PMD Measurement Method

Fig. 4 shows a block diagram of the fully automated fixed analyzer (wavelength scanning) PMD measurement system [10],[11] using optical spectrum analyzer (OSA), and the photograph is shown in Fig.5. The measurement accuracy and dynamic range are depending on the optical sources. The specifications of the fully automated fixed analyzer PMD measurement system is shown in Table 3.

The examples of the PMD measurement of the PMF ($L \approx 0.85$ m) and the DSF ($L \approx 100$ km) are shown in Fig.6-(a) and (b), respectively. In the conventional fixed analyzer method, the interval of the peak to peak powers is equivalent to a phase difference of 2π (one beat length). However, in this paper, in order to avoid measuring error and to improve measuring accuracy, a newly fixed analyzer PMD measuring algorithm was used. In Fig.6, two curves represent the case of the fixed analyzer angle of 0 degree and 90 degree, respectively. Accordingly, the interval of the valley (peak) power of the curve of 0 degree (λ_1) to the valley (peak) power of 90 degree (λ_2) is equivalent to a phase difference of π (a half beat length).

The averaged PMD τ is expressed as ;

$$\tau \approx k / (2c n) \sum_{i=1}^n [\lambda_i + 1 \lambda_i / (\lambda_i + 1 - \lambda_i)] \quad (2)$$

where, $k (\leq 1)$, $i (= 1, 2, 3 \dots n-1, n)$, and c represent the polarization mode coupling factor, the numbers from peak at λ_i to the peak at λ_{i+1} , and the light velocity in the free space, respectively. Here, the odd number ($i = 1, 3, 5, \dots$) and the even number ($i = 2, 4, 6, \dots$) represent the case of the fixed analyzer angle of 0 degree and 90 degree, respectively.

The PMD of the PMF (Fig.6-a) shows almost periodic curve, meanwhile the curve of the DSF (Fig.6-b) indicates somewhat irregular periods because of the random polarization mode

Table 2 Comparison of interferometric PMD method with fixed analyzer PMD method

PMD Measurement Methods	Interferometric Method			Fixed Analyzer Method ($k \approx 0.84$)
	Peak to peak (#1)	Gaussian (STD) (#2)	Gaussian (50%) (#3)	
PMF ($L \approx 0.85$ m)	1.291 ps (1.519 ps/m)	1.213 ps (1.422 ps/m)	1.428 ps (1.680 ps/m)	1.286 ps (1.513 ps/m)
SMF ($L \approx 11$ km) (-4 dB)	0.045 ps (0.014 ps/√km)	0.142 ps (0.042 ps/√km)	0.167 ps (0.050 ps/√km)	0.181 ps (0.055 ps/√km)
DSF ($L \approx 1.6$ km) (-6 dB)	0.291 ps (0.074 ps/√km)	0.698 ps (0.151 ps/√km)	0.704 ps (0.178 ps/√km)	0.697 ps (0.175 ps/√km)
CSF 1 ($L \approx 50$ km) (-10 dB)	0.150 ps (0.021 ps/√km)	0.417 ps (0.056 ps/√km)	0.491 ps (0.069 ps/√km)	0.463 ps (0.108 ps/√km)
CSF 2 ($L \approx 150$ km) (-20 dB)	0.068 ps (0.007 ps/√km)	0.591 ps (0.059 ps/√km)	0.700 ps (0.070 ps/√km)	0.714 ps (0.071 ps/√km)
CSF 3 ($L \approx 150$ km) (-30 dB)	0.074 ps (0.006 ps/√km)	0.825 ps (0.075 ps/√km)	1.089 ps (0.089 ps/√km)	0.981 ps (0.080 ps/√km)

PMF : Polarization Maintaining Fiber, k : Polarization Mode Coupling Factor
SMF : 1.31 μ m Standard Single Mode Fiber (ITU-T G. 652 Fiber)
DSF : 1.55 μ m Dispersion Shifted Fiber (ITU-T G.653 Fiber)
CSF : 1.55 μ m Cutoff Shifted Fiber (ITU-T G.654 Fiber)

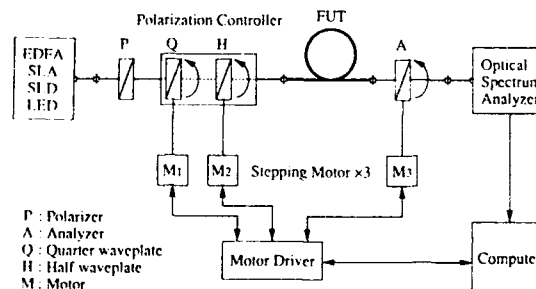


Fig.4 Block diagram of fully automated fixed analyzer PMD measurement system

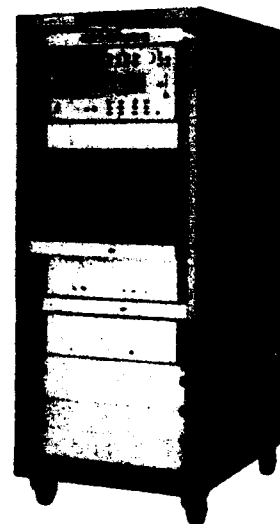


Fig.5 Photograph of fully automated fixed analyzer PMD measurement system

Table 3 Specification of fixed analyzer PMD measurement system

Optical Source	LED	SLA	SLD	EDFA
Center Wavelength, λ_0 [nm]	~ 1561	~ 1565	~ 1589	~ 1544
Spectral Width, $\Delta\lambda$ [nm]	~ 89	~ 83	~ 53	~ 30
Coherence Time [ps]	~ 0.045	~ 0.114	~ 0.040	~ 0.351
Output Power of Light Source [dBm]	~ -18	~ -19	~ -10	~ -3
Dynamic Range [dB]	~ 40	~ 40	~ 50	~ 60
Measurement Resolution [ps]	~ 0.05	~ 0.08	~ 0.08	~ 0.10
Measurement Time	~ 2.5 minutes			

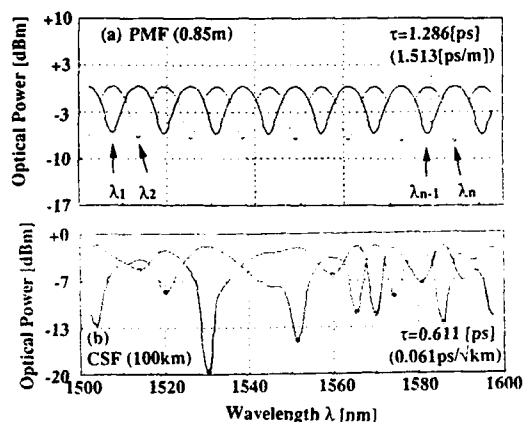


Fig. 6 Example of fixed analyzer PMD measurement results
 (a) Polarization maintaining fiber {PMF ($L \approx 0.85$ m)}
 (b) Dispersion shifted fiber {DSF ($L \approx 100$ km)}

coupling. The other PMD measurements results are summarized in Table 2 [14].

3. PMD MEASUREMENTS IN OPTICAL FIBER SUBMARINE CABLES

The PMD measurement in the 50 km long cable fabricating process is shown in Fig. 7. The PMD was measured using the fixed analyzer (wavelength scanning) method [10],[11],[13]. In Fig. 7, A, B, C and D refer to the three fiber makers and one cable maker, respectively.

Fig. 8 shows the cross sectional view of the transoceanic lightweight (LW) optical fiber submarine cable structure. The cable consists of an optical fiber unit with six (6) or four (4) DSFs, a water pressure resistance layer composed of a three divided steel pipe, high-tensile steel strands, a copper tube, and a layer of polyethylene insulation with an external polyethylene jacket [19]. In the LW cable, the three kinds of Fibers (DSFs) A, B and C of the VAD fabricating method were used, and these refractive index profiles are shown in Fig. 9 (a), (b) and (c), respectively. In Fig. 7, the Cables-A, B and C consist of the Fibers A, B and C, and the Units A, B and C, respectively.

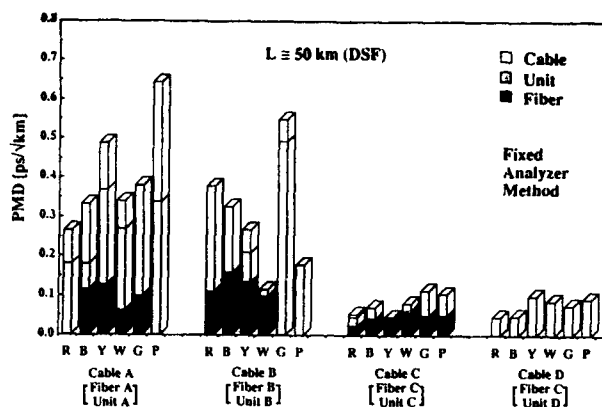


Fig. 7 Histogram of PMD variation in the cable fabricating process (Before PMD reduction)

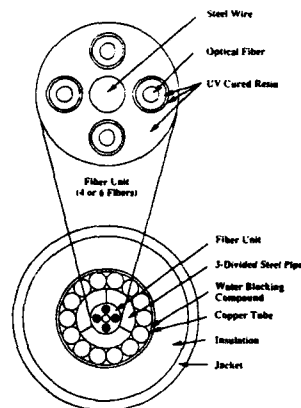


Fig. 8 Lightweight optical submarine cable structure

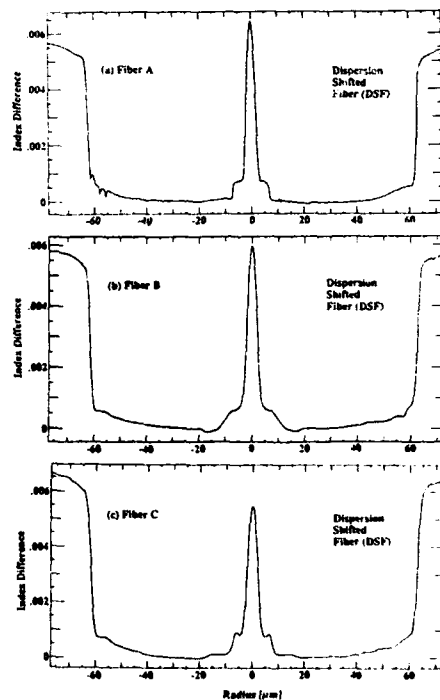


Fig. 9 Refractive index profiles of (a) Fiber A, (b) Fiber B and (c) Fiber C

However, the Unit D consists of the Fiber C. In addition, all Cables A, B and C were fabricated by the same cable maker D.

From Fig.7, the following results were confirmed ;

- (1) In case of the Cable A, the PMD increased rapidly in the cable fabricating process.
- (2) In case of the Cable B, the PMD violently varied in the cable fabricating process.
- (3) In case of the Cable C, the PMD was almost unchanged in the cable fabricating process.
- (4) In case of the Unit D, the PMD was almost unchanged in the cable fabricating process, which indicates the same behavior as the Cable C.

Fig.10 shows the PMD variation of the Cables A, B and C. The Fig.10 measurement is the same as in Fig.7, but described from a different viewpoint. From Fig.7 and Fig.10, it is found that after cabling process, the PMD of Cable A is much higher than that of the Cable B and Cable C.

In Fig.7, in the case of the Cable C and Unit D, the Fiber C is the same, but the Unit is different. However, the PMD of the Cable C and the Unit D show almost the same behavior. Therefore, it is conjectured that the PMD increase is mainly due to the fiber core ovality. The effects of the fiber fabricating process, external stress and other factors [21] on the PMD increase is considered to be very small. Then, the PMD variation is mainly due to the intrinsic PMD of bare fibers.

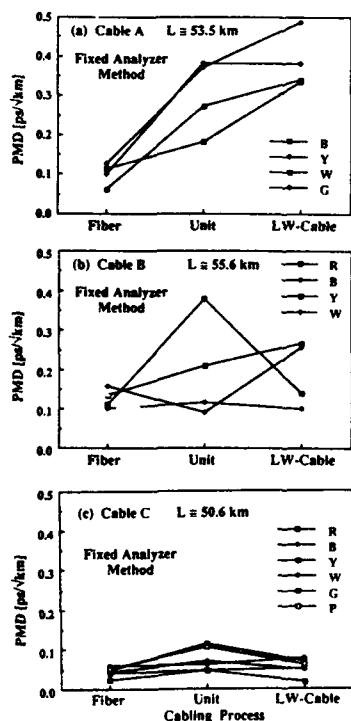


Fig.10 PMD variation in the cable fabricating process (a) Cable A, (b) Cable B, (c) Cable C

4. INTRINSIC PMD OF OPTICAL BARE FIBERS

In order to determine the intrinsic PMD, measurements of the PMD before and after the coating removal were carried out on loosely coiled ~ 300 m long each of the VAD Fibers A, B and C. The loosely coiled DSFs were soaked in concentrated sulfuric acid (H_2SO_4) to completely remove the fiber coating as shown in Fig.11 [20]. Then the intrinsic PMD was measured using the interferometric method [10]-[12], and the measurements of the PMD before and after fiber coating removal are shown in Fig.12. From Fig. 12, it was found that the PMD of the Fiber A was significantly increased after the fiber coating removal. The intrinsic PMD of the bare Fiber A is larger than that of the coated Fiber A.

Figs.13 - 15, shows the interferometric visibility pattern of the Fibers A, B and C, respectively. In Figs. 13 - 15, (a) and (b) indicate the PMD measurements in the case of before and after fiber coating removal.

Especially in Fiber A, it was observed from Fig. 13 (b) that random polarization mode coupling occurred. However, the polarization mode coupling was not observed in the Fiber B and Fiber C.

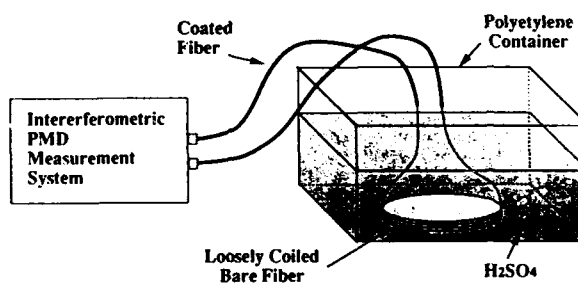


Fig.11 Experimental set up for measuring the intrinsic PMD of bare fiber

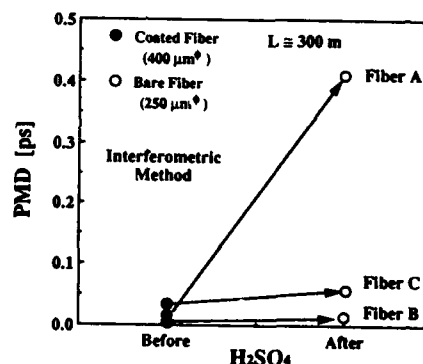


Fig.12 PMD of coated fibers and intrinsic PMD of bare fibers

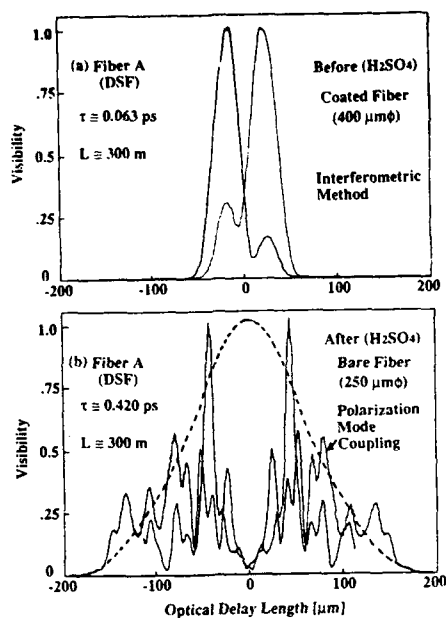


Fig.13 Interferometric PMD measurements in (a) coated fiber A and (b) intrinsic PMD in bare fiber A

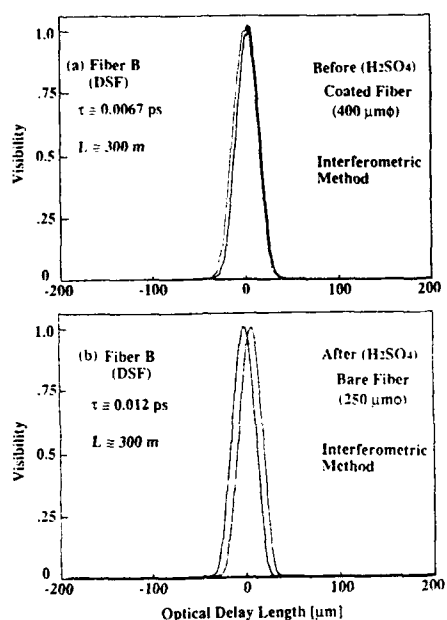


Fig.14 Interferometric PMD measurements in (a) coated fiber B and (b) intrinsic PMD in bare fiber B

5. PMD REDUCTION IN OPTICAL SUBMARINE CABLES

Therefore, we have developed the PMD reduction cable from the point of view of the fiber core ovality.

Fig.16 shows the PMD variation measurement using interferometric method [10] - [12] in the cable fabricating process of the first trial PMD reduction a short 2.5 km LW Cable A.

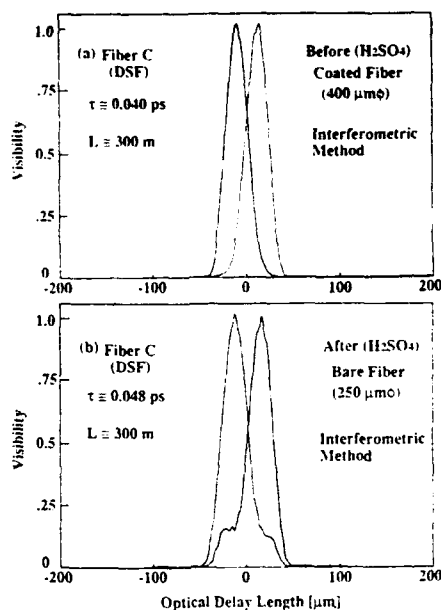


Fig.15 Interferometric PMD measurements in (a) coated fiber C and (b) intrinsic PMD in bare fiber C

Comparing Fig.10 (a) with Fig.16, it was found that the PMD of Cable A was drastically reduced by minimizing the fiber core ovality [20].

Fig.17 shows the interferometric visibility pattern of the Cable A after the cable fabricating process. It was found from Fig.17 that there was almost no polarization mode coupling in the Cable A after cabling process. The low PMD cable of 0.042 ps/sqrt(km) has been successfully achieved.

The PMD of the product ~ 33 km long transoceanic optical submarine cables was measured during the cable fabricating process such as fibers, fiber units, and cables by the fully automated fixed analyzer measurement system [10],[11]. The PMD variation of the Cables A, B and C in the cable fabricating process is shown in Figs.18 (a), (b) and (c), respectively.

With optimal fabricating conditions of the bare fibers, a low-PMD of less than 0.1 ps/sqrt(km) has been successfully achieved in ~ 33 km long transoceanic optical fiber submarine cables.

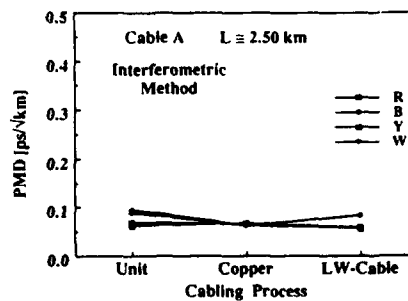


Fig.16 PMD variation of 2.5 km long cable A in the cable fabricating process (First PMD reduction)

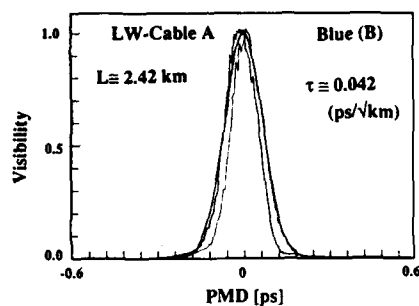


Fig. 17 Interferometric PMD measurement in Cable A

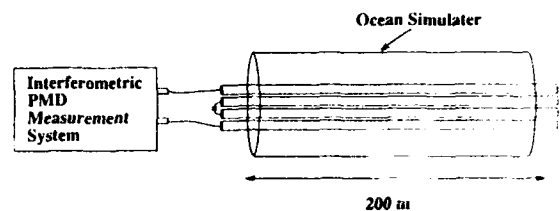


Fig. 19 Experimental set up for PMD variation of optical fiber submarine cable under deep sea environmental conditions

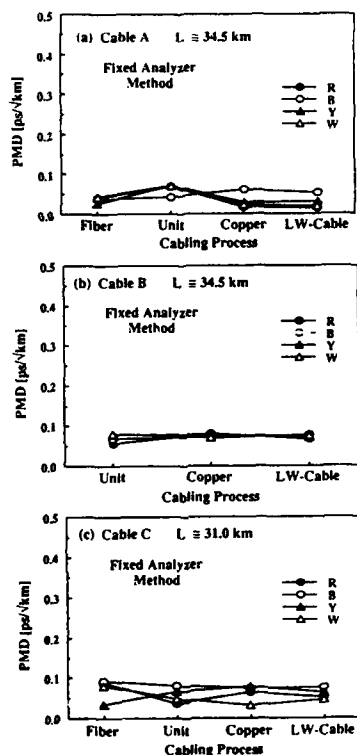
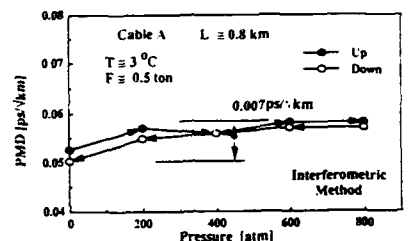


Fig. 18 PMD variation of ~ 33 km long cable in the cable fabricating process (Second PMD reduction)
(a) Cable A, (b) Cable B, and (c) Cable C

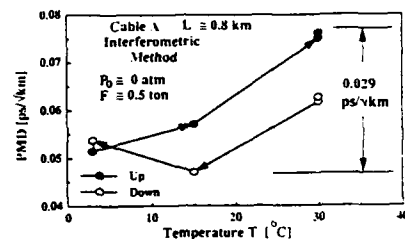
6. PMD EVALUATION TEST UNDER DEEP SEA ENVIRONMENTAL CONDITIONS

Fig. 19 shows the PMD variation measurement system for the transoceanic optical fiber submarine cable characteristics under 8000 m deep sea environmental conditions using a 200 m-long ocean simulator [19] and highly accurate fully automated interferometric measurement system [10]-[12], [14]. The PMD stability was within 0.002 ps [14].

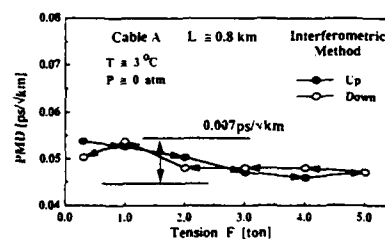
The test LW cable is a part of the ~ 33 km-long transoceanic optical fiber submarine Cable A, and it is composed of four (4) DSFs. These fibers were looped back in the termination, and the total fiber length was around 0.8 km.



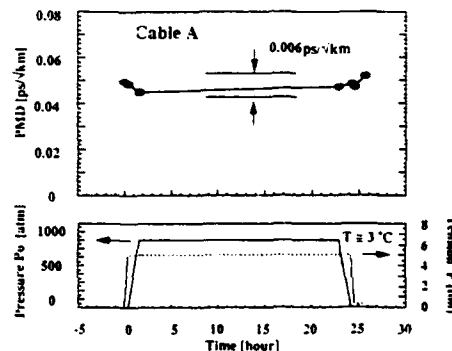
(a) Pressure



(b) Temperature



(c) Tension



(d) Composite stress states

Fig. 20 PMD variation under deep sea environmental conditions

The PMD measurement results of the Cable A under hydraulic pressure (0 - 800 atm), temperature (3 - 30°C), tension (0.3 - 5 ton), and composite stress (3°C, 800 atm, 5 ton) are shown in Figs. 20 (a), (b), (c) and (d), respectively.

From Fig.20, it was found that PMD variation of less than $0.007 \text{ ps} / \sqrt{\text{km}}$ was very small except for temperature-induced variation of $0.029 \text{ ps} / \sqrt{\text{km}}$. Therefore, it was confirmed that low and stable PMD transoceanic optical fiber submarine cable has been successfully achieved.

7. CONCLUSION

This paper presents PMD reduction process of the cabled fibers for transoceanic optical submarine cable systems using optical amplifiers, and the development of newly two kinds automated PMD measurement systems. The PMD of the product cables was measured during the cable fabricating process such as fibers, fiber units, and cables by the fixed analyzer measurement system. The mechanism of increase in PMD was clarified by investigating the relation between PMD values and the thickness of the fiber coating which was gradually removed in concentrated H_2SO_4 . The PMD measurement of the short-length (~300 m) coated fibers was carried out using the interferometric measurement system.

The PMD values of the intrinsic high-PMD coated fibers were increased after removing the fiber coating using the concentrated H_2SO_4 , while that of the intrinsic low-PMD coated fibers almost did not change after removing the fiber coating. From these experimental results, it was confirmed that the PMD of the cabled fibers was primarily caused by the intrinsic core ovality of the bare fiber rather than external stress and other factors [21].

With optimal fabricating conditions of the bare fibers, a low-PMD of less than $0.1 \text{ ps} / \sqrt{\text{km}}$ has been successfully achieved in ~ 33 km long product optical fiber submarine cables. The PMD variations were interferometrically measured using a 200 m-long ocean simulator under 8000 m deep sea environmental conditions of hydraulic pressure (0 - 800 atm), temperature (3 - 30°C), tension (0.3 - 5 ton), and composite stress (3°C, 800 atm, 5 ton).

It was found that PMD variation of less than $0.007 \text{ ps} / \sqrt{\text{km}}$ was very small except for temperature-induced variation of $0.029 \text{ ps} / \sqrt{\text{km}}$. Therefore, it was confirmed that low and stable PMD transoceanic optical fiber submarine cable has been successfully achieved.

ACKNOWLEDGEMENT

The authors wish to thank Dr. Y. Urano, Dr. K. Sakai and Dr. S. Akiba of KDD R&D Labs. and Mr. H. Wakabayashi, Mr. H. Yamamoto and Mr. M. Tanaka of KDD Headquarters for their encouragement, and Mr. K. Furusawa and Dr. K. Utaka of KDD R&D Labs. for their cooperation in experiment. We also wish to thank Sumitomo Electric Industries Co. Ltd., Fujikura Co. Ltd, Furukawa Electric Co. Ltd., and Ocean Cable Co. Ltd, for their manufacturing of optical fibers, fiber units and cables, and wish to thank Santec Corporation and Oyokoden Lab. Co. Ltd. for developing fully automated Interferometric and Fixed analyzer PMD measurement systems, respectively. We also thank Mr. J. Maeda, Mr. K. Nakajima, Mr. N. Tanahashi, Mr. A. Miyata, and Mr. K. Saitome for their cooperation.

REFERENCES

- [1] Y. Namihiro et al., "Effect of mechanical stress on the transmission characteristics of optical fibers (in Japanese)," IEICE Japan, vol.J60-C, no.7, pp.391-38, 1977.
- [2] Y. Namihiro : "Optoelastic constant in single mode optical fibers," IEEE, JLT, vol.LT-3, no.5, pp.1078-1083, 1985.
- [3] S. C. Rashleigh et al., "Polarization mode dispersion in single-mode fibers," Opt. Lett., vol.3, pp.60-62, 1978.
- [4] J. Sakai et al., "Birefringence and polarization characteristics of single-mode optical fibers under elastic deformations," IEEE, JQE, vol.QE-17, no.6, p.1041, 1981.
- [5] N. Shibata et al., "Polarization mode dispersion measurement in elliptical core single-mode fibers by a spatial technique," IEEE, JQE, vol.1, pp.53-58, 1982.
- [6] J. Sakai : "Thermal-stress-induced birefringence characteristics in elliptical core optical fibers (in Japanese)," IEICE Japan, Technical Report, OQE82-21, pp.17-24, 1982.
- [7] N. Shibata et al., "Birefringence and Polarization mode dispersion caused by thermal stress in single-mode fibers with various core ellipticities," IEEE, JQE, vol.1, pp.53-58, 1982.
- [8] C. D. Poole et al., "Fading in lightwave systems due to polarization-mode dispersion," IEEE, Photonics Technology Letters, vol.3, no.1, pp.68-70, 1991.
- [9] C. D. Poole : "Measurement of polarization mode dispersion in single mode fibers with random mode coupling," Opt. Lett., vol. 14, p.523, 1989.
- [10] Y. Namihiro et al., "Polarization mode dispersion measurements in optical fibers ", Symposium on Optical Fiber Measurements, NIST , Boulder, Co., pp.145-150, Sept. 1992.

- [11] Y. Namihiro et al., : "Comparison of various polarisation mode dispersion measurement methods in optical fibres", *Electron. Lett.*, vol.28, no.25, pp.2265-2266, 1992.
- [12] Y. Namihiro et al.,: "Fiber length dependence of polarization mode dispersion measurements in long-length optical fibres and installed optical submarine cables," *Journal of Optical Communications*, vol.12, no.1, pp.1-8, 1991.
- [13] Y. Namihiro et al., : "Spectral response measurements on polarisation splitting ratio of fused taper single-mode fibre couplers," *Electron. Lett.*, vol.23, no.23, pp.1204-1206, 1987.
- [14] Y. Namihiro et al., : "Fully automated interferometric PMD measurements for active EDFAs, fiber optic devices and optical fibers," *OFMC'93*, Torino, Italy, 1993.
- [15] K. Mochizuki et al., : "Polarization mode dispersion measurement in long single-mode fibres," *Electron. Lett.*, vol.17, no.4, pp.153-154, 1981.
- [16] Y. Namihiro et al., : "Birefringence in elliptical-cladding single-polarisation fibres," *Electron. Lett.*, vol.18, no.2, pp.89-91, 1982.
- [17] N. Gisin, et al.,: "Polarization mode dispersion of short and long single-mode fibers", *IEEE, JLT*, vol.9, no.7, pp.821-827, 1991.
- [18] F. Bruyere et al.,: "Polarization dispersion in a 1000 km Er-Doped fiber amplified link", *ECOC'92*, Berlin, Germany, pp.61-64, 1992.
- [19] Y. Namihiro et al.,: "Design considerations for 1.55 μm loss minimized 1.3 μm zero-dispersion single-mode optical fiber submarine cables," *Journal of Optical Communications*, vol.13, no.2, pp.1-11, 1992.
- [20] Y. Suetsugu et al., : "Polarization mode dispersion in dispersion shifted single mode fiber," *ECOC'93*, Montreux, Switzerland, We 28, 1993.
- [21] A. F. Judy et al.,: "PMD characterization of production cables for evolving lightwave systems," *OFC'93*, PD20, 1993.

BIOGRAPHY



Yoshinori Namihiro

**KDD R&D Laboratories
Lightwave Communication
Systems Group
Saitama, Japan**

Yoshinori Namihiro was born in Okinawa, Japan, on October 23 1949. He received the B. S. degree from Ryukyu University, Okinawa, Japan in 1973, and the M. S. and Ph. D. degrees, both in electrical communication engineering from Tohoku University, Sendai, Japan, in 1976 and 1979, respectively.

In 1979, he joined the KDD R & D Laboratories, Tokyo, Japan. He has been engaged in research on transmission characteristics, polarization fluctuation characteristics and polarization mode dispersion measurement techniques etc., in single mode optical fibers and optical fiber submarine cables.

He was awarded an *Electronics Letters Premium* from IEE in England in 1984, and the Best Paper Awards of *OEC'90* (Opto Electronics Conference) and *OEC'92* in Japan in 1990 and 1992, respectively. Also, he was responsible for Special Rapporteur of ITU-T (CCITT) SG. 15 Q.13 (Optical submarine cable systems) during 1989-1992 Study Period.

Dr. Y. Namihiro is a member of the Institute of Electronics, Information, and Communication Engineers (IEICE) of Japan, and IEEE, respectively.



Toshio Kawazawa

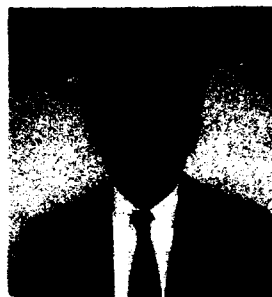
**KDD R&D Laboratories
Lightwave Communication
Systems Group
Saitama, Japan**

Toshio Kawazawa was born in Tokyo, Japan, on July 2, 1965. He received the B. S. and M. S. degrees, both in Electronics Engineering from Nihon University, Tokyo, Japan in 1988 and 1990, respectively.

He joined KDD Chikura cable landing station in 1990. He was transferred to KDD R&D Laboratories in 1991, and he has been engaged in research on optical fiber and optical fiber submarine cable characteristics.

He was awarded the Best Paper Award of *OEC'92* (Opto Electronics Conference) in Japan in 1992.

Mr. Toshio Kawazawa is a member of the Institute of Electronics, Information, and Communication Engineers (IEICE) of Japan.



Naoki Norimatsu

**KDD Headquarters
Submarine Cable
Systems Department
Tokyo, Japan**

Naoki Norimatsu was born in Fukuoka, Japan, on December 27, 1960. He received the B. S. and M. S. degrees, both in Electrical Engineering from Kyushu University, Fukuoka, Japan in 1981 and 1983, respectively.

He joined KDD R&D Laboratories in 1985. He was transferred to KDD Headquarters in 1989, and he has been engaged in the development and construction of optical fiber submarine cable system.

Mr. Naoki Norimatsu is a member of the Institute of Electronics, Information, and Communication Engineers (IEICE) of Japan.

**NEW DEVELOPMENTS IN ULTRA-VIOLET CURABLE OPTICAL FIBER COATINGS
BASED ON VINYL ETHER TECHNOLOGY**

J.R.Snyder¹, G.D.Green¹, R.J.Swedo¹, C.M.Srivastava²,
A.C.Levy³, R.J.Kovac³, P.R.Foy⁴

- 1 - AlliedSignal Inc, Des Plaines, IL
- 2 - AlliedSignal Inc, Morristown, NJ
- 3 - Alvin Levy & Assoc., Chamblee, GA
- 4 - Rutgers University, Piscataway, NJ

ABSTRACT

Coatings are applied to optical fibers to preserve fiber strength and to prevent microbending induced optical loss. The primary coating, which contacts the glass fiber, is a low Tg material that acts as a buffer to prevent microbending. The secondary coating, or outer coating, is a high modulus material that provides mechanical protection.¹ Commercial coating systems are based on ultra-violet curable acrylate materials. During the early stages of optical fiber development acrylate chemistry was well suited for this application. But with the advent of faster draw tower line speed requirements, the acrylate based coating formulations are limited. We previously reported the use of vinyl ether based formulations as coating systems for optical fibers.² This paper discusses new developments in the use of vinyl ethers as optical fiber coatings. Of particular interest is the observed thermal dependence on cure rate for vinyl ether based formulations.

INTRODUCTION

Recent advances have been made with vinyl ether based optical fiber coatings. New materials have been developed that improve physical properties and cure rate response. In addition to new material structures, a temperature related phenomena has been

utilized which allows one to achieve extremely fast rates of polymerization, i.e., cure response. Due to this phenomenon, other benefits have been observed, eg., reduced hydrogen generation and increased thermal stability.

Vinyl ethers polymerize by a cationic mechanism. The kinetics of this chemistry are greatly influenced by the temperature of the system. As the temperature of the system increases, the rate of polymerization also increases.³ This phenomenon translates into an increase in cure response, i.e., a lower dose to achieve optimal film properties. In summary, the line speeds on commercial draw towers can be increased.

This paper discusses new developments in the use of vinyl ether based coatings as applied to their use with optical fibers. Due to the difference in the vinyl ether reactive group through which polymerization and crosslinking occurs, certain advantages are observed. Vinyl ether groups possess inherently low steric hindrance, and hence exhibit a high degree flexibility and rotational freedom. As a result, polymerization or crosslinking through these functional groups imparts certain unique advantages to cured systems. Among these are low modulus at -40°C. In addition to very low temperature properties, one observes very high cure response.

A summary of data will be given for coatings based on this new technology. These data will include viscosity, thermomechanical, hydrogen generation and cure response.

EXPERIMENTAL

Materials - The monomers and oligomers used in this study were vinyl ether functionalized ester and urethane materials. A comprehensive discussion of these materials can be found in the literature.^{4,5} The photoinitiators and additives used in this study are commercially available materials. Formulation A is the secondary formulation that was reported in the IWCS'92 conference proceedings. Formulations B and C are improved secondary and primary formulations.

Radiation Curing - All films were cured by using either a RPC model QC-1202 ultraviolet processor (H bulbs by Aetek) or a Fusion System MC-6N conveyor with a P300 power supply (H bulbs by Fusion). The films were cured under a nitrogen atmosphere to simulate production conditions.

Tensile Testing - For film properties, all formulations were coated onto glass plates. The cured films were cut into 0.5 inch wide by 3.0 inch long strips. These strips were removed from the glass plates as free films. Tensile properties were measured using an Instron apparatus Model 4502 or a Thwing-Albert Intellect 500 apparatus. The modulus was measured at 1% elongation according to ASTM D882.

Tg Determination - The Tg of films were determined by Dynamic Mechanical Thermal Analysis using a Rheometrics Solids Analyzer RSA II. The strain rate was 0.003.

Hydrogen Generation - Film samples were sealed in septa vials in an air atmosphere. The samples were heated at 100°C for 24 hours. The vials head space was sampled and evaluated on a Hewlett Packard Gas Chromatograph, Model 5890 Series II using a TCD detector. The test was run at 35°C

with an Alltech molecular sieve column.

Onset of Oxidation - Thermal gravimetric analysis was performed using a Perkin-Elmer TGS-2. The test was conducted in air with a delta T is 10°C/min.

Viscosity - The viscosity verses temperature profiles for both primary and secondary formulations was evaluated using a Brookfield Viscometer model LDT with a Thermocell attachment.

THERMAL EFFECTS ON TENSILE PROPERTIES

We have previously reported the fast cure response of vinyl ether based coatings. This characteristic is further enhanced by increasing the temperature of the coating when it is cured.

Figure 1 shows modulus verses dose at room temperature (27°C) for Formulations A and B. Figure 2 shows modulus verses dose at elevated temperature (60°C) for Formulations A and B. The data from Figure 1 clearly indicates that the secondary coating formulations achieve optimum properties with low dose. Figure 2 shows the advantageous affect elevated temperature has on achieving optimal properties for vinyl ether based coating formulations. Similar effects are seen with vinyl ether based primary coatings.

Figure 3 shows the modulus vs dose of Formulation B at 80°C. As can be observe from this data, the cure dose required for optimal modulus has been further reduced. The dose requirement is between 0.025 and 0.050 J/cm². As one would expect, there is a linear response between dose and temperature to achieve full cure. This phenomenon offers some very exciting possibilities for UV curable vinyl ether coatings.

PHYSICAL PROPERTIES OF COATINGS

Typical properties for vinyl ether based coating systems are given in the following discussion. Tensile properties, glass transition, viscosity, water absorption and extractables will be discussed.

TENSILE PROPERTIES

The tensile properties of vinyl ether based primary(C) and secondary(B) formulations are shown in Table 1. The data indicate that these formulations are comparable to commercial acrylate based coating formulations

Table 1

	Primary	Secondary
Modulus (MPa)	1.5	970
Break Strength (MPa)	1.0	45
Elongation (%)	100	14

The films were cured at 0.20 J/cm² and 60°C. The samples were tested at 50% RH and 25°C.

MECHANICAL ANALYSIS

The ether linkage in vinyl ether based coatings allows one to achieve primary coating with very low Tg's without sacrificing the cure speed. The data in Table 2 shows the low Tg's of Formulation B and C that can be obtained.

Table 2

Glass Trans. Temp. (°C) (by DMTA)	Primary	Secondary
Start of Transition	-35	50
Tan Delta Max	-20	73

VISCOSITY

Due to the increase in the temperature

at which we can cure the vinyl ether coatings, the viscosities of the two formulations must remain at appropriate levels. The data given below in Table 3 shows the viscosity verses temperature for Formulations B and C.

Table 3

Temperature (°C)	Viscosity(cps)	
	Primary	Secondary
40	8250	5250
45	6000	3850
50	4200	2500
60	2200	1100
70	1320	520

WATER ABSORPTION AND EXTRACTABLES

The water absorption data below in Table 4 indicate that vinyl ether based coating formulations are not susceptible to water uptake. This is to be expected considering the chemistry of these systems. The fact that vinyl ether coatings have very low water absorption is important since the brittle fatigue failure of glass is accelerated by the presence of moisture.

Table 4

Coating Type	Water Absorption	Extractables
Primary(C)	0.75%	0.95%
Secondary(B)	1.10%	1.10%

ENVIRONMENTAL STABILITY

HUMIDITY EFFECTS

As previously reported, the tensile modulus of a coating is strongly affected by the moisture content, for both vinyl ether and acrylate secondary coatings. Recent advances in the secondary formulation have made

this phenomenon less of an issue. Table 5 below shows the change in film modulus as a function of relative humidity for Formulations B and C. For both coating types, modulus values remained within acceptable limits over the entire range of humidity evaluated. Figure 5 compares an improved secondary formulation (B) with one previously reported (A).

Table 5

Tensile Properties vs. Relative Humidity
(cured at 250 mj/cm² and 60°C)

Coating Type	Rel. Hum (% at 25°C)	Modulus (MPa)
Primary	0	2.51
Primary	53	1.47
Primary	95	1.51
Secondary	0	1213
Secondary	55	1048
Secondary	95	648

HYDROGEN GENERATION

The production of hydrogen gas by the protective coatings is detrimental to the performance of optical fibers. The hydrogen gas can diffuse through the coatings and chemically react with the glass fiber, causing signal loss. Samples of primary and secondary formulations were tested for hydrogen generation. The results are given below in Table 6. We have successfully reduced hydrogen generation to below 1.0 ul/gram of coating. The results also indicate that the amount of hydrogen gas produced is dose dependent. As the dose requirements decrease, the amount of hydrogen gas produced decreases.

Table 6

Hydrogen Generation (uL/g) (24 hrs at 100°C)	Primary	Secondary
cured @ 50mj/cm ² /60°C	0.35	0.66
cured @ 100mj/cm ² /60°C	2.00	1.65
cured @ 200mj/cm ² /RT	7.30	3.34

ONSET OF OXIDATION AND WEIGHT LOSS

The onset of oxidation and weight loss at 125°C are given below in Table 7. These results are comparable to what can be obtained with commercial coating systems.

Table 7

Property	Primary	Secondary
Onset of Oxidation (TGA @ 5 C/min, air)	260°C	275°C
Weight Loss @ 125°C (% by Weight)		
1 day	3.4	3.4
7 days	5.5	4.9
11 days	6.5	5.8

FIBER COATING STUDY

We have obtained samples of optical fiber coated with our vinyl ether based formulations. The coating adhesion was evaluated using the fiber coating pullout test. The tensile strength of the fiber was also determined. The data is given in Table 8 below. The results show that our coating systems performs well on fiber.

Table 8

Fiber Pullout Test (Per FOTP-105)	95% R.H.	Ambient (33%)
FR930401	1.6 lb	1.6 lb
Fiber Strength	Break Strength	Elongation
FR930401	13.8 lb	11.7%

CONCLUSIONS

We have made significant improvements with many of the coating properties of our vinyl ether based optical fiber formulations. The increased cure response with increasing temperature is of

particular interest. This phenomenon allows the coatings to reach optimal film properties at extremely low doses. This, in turn, gives us the ability to achieve lower levels of hydrogen generation. The most important result of this thermal affect is that these low dose requirements translate into faster line speeds.

REFERENCES

1. L.L. Blyler, Jr., and C.J. Aliosio in R.W. Tess and G.W. Poele, eds., Applied Polymer Science, 2nd ed., The American Chemical Society, Washington, D.C., 1984, Chapt. 38.
2. G.D. Green, J.R. Snyder, A.C. Levy, R.J. Kovac, P.R. Foy, International Wire and Cable Symposium conference proceedings, p. 253, 1992.
3. E.V. Sitzmann, R.L. Haynes, D.K. Barnes, C.M. Srivastava, G.D. Green, J.J. Swedo, J.J. Krajewski, Rapid Prototyping and Manufacturing conference proceedings, University of Nottingham, p. 338, 1993.
4. S.C. Lapin, RadTech '88: Conference Proceedings, p. 395, RadTech International, 1988.
5. S.C. Lapin, J.R. Snyder, RadTech '90: Conference Proceedings, p. 410, RadTech International, 1990.

Figure 1
Modulus vs Dose
Room Temperature

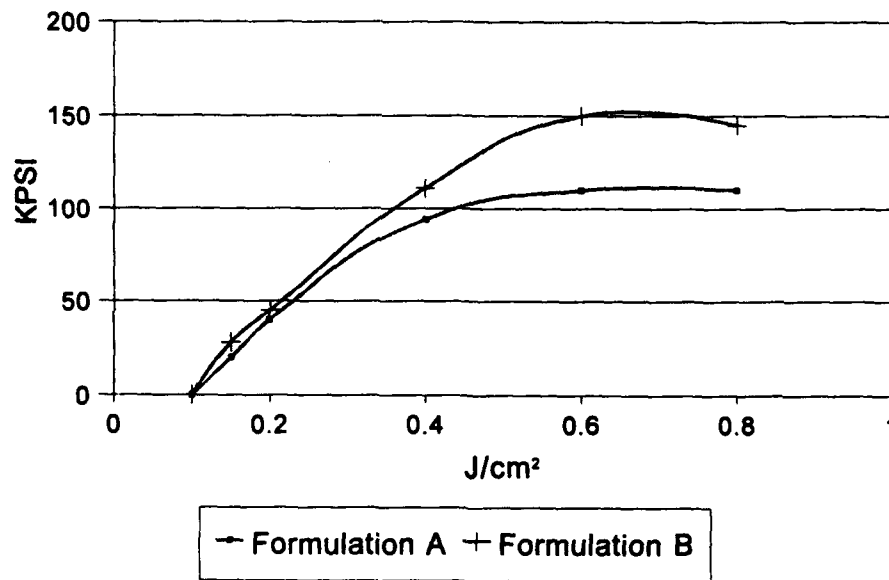


Figure 2
Modulus vs Dose
60°C

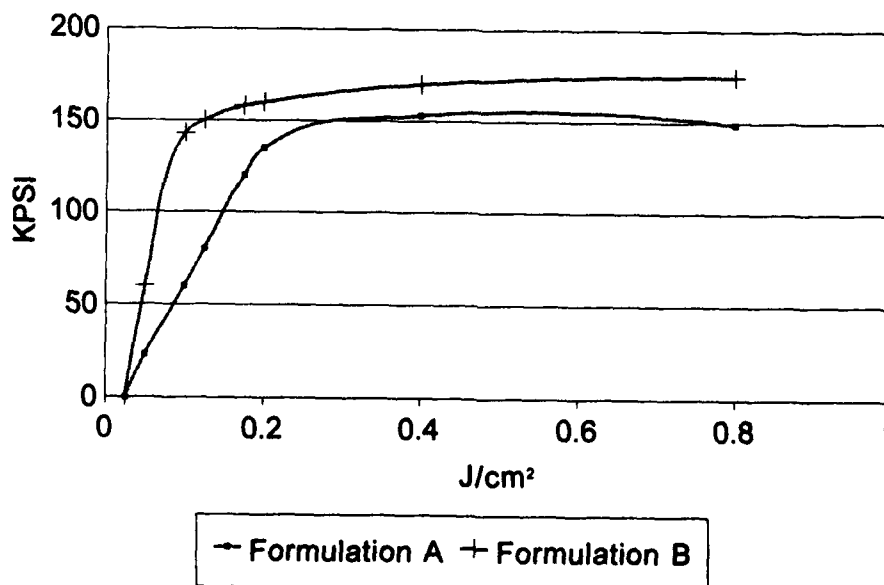


Figure 3
Modulus vs Dose
80°C

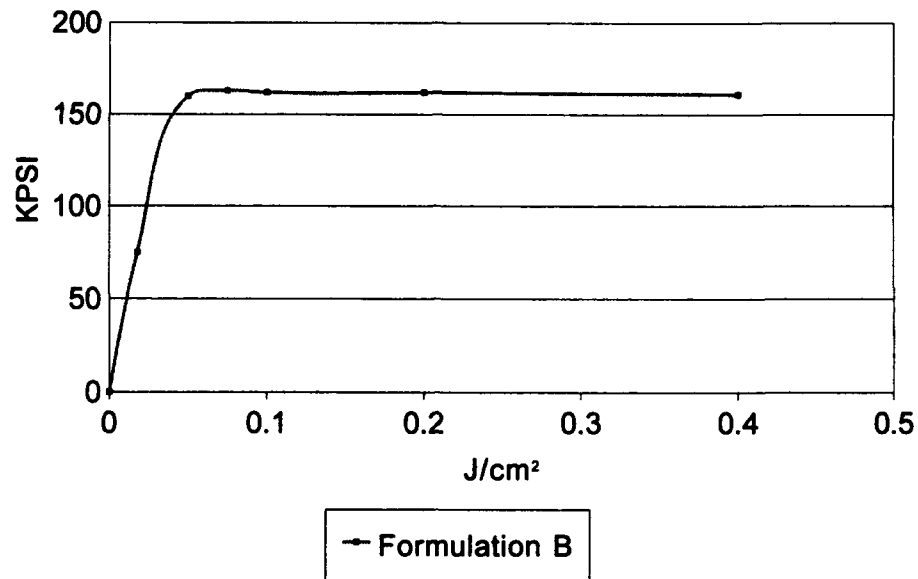
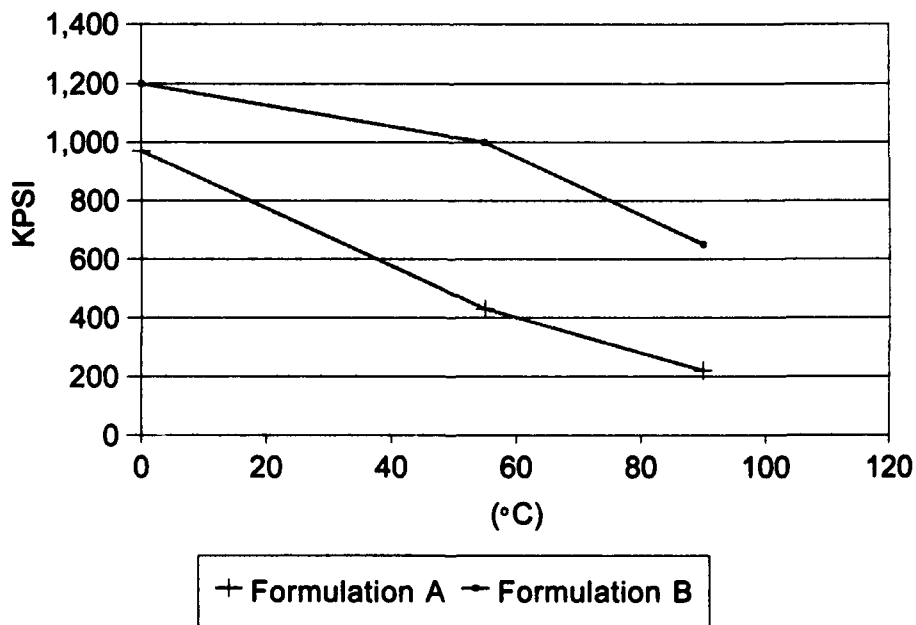


Figure 4
Modulus vs Rel. Hum.





James R. Snyder received his B.S. from the University of Illinois - Urbana/Champaign. Since 1988, he has been a research chemist at the AlliedSignal corporate laboratory in Chicago. His experience has been primarily in material research and product development, especially within cationic polymerizable systems. Mr. Snyder has nine patents and publications in conjunction with this work.



G. David Green received his Ph.D. in organic chemistry from the University of Arizona. Since joining AlliedSignal in 1986, he has been involved in synthetic polymer research. His experience includes the development of barrier coating for fibrous substrates, radiation effects on polymer substrates, high temperature thermosetting resins and more recently radiation curable coatings. He has over 15 publications and presentations ranging from nonlinear optical effects in polymers to radiation curable resins for stereolithography.



Raymond J. Swedo received his Ph.D. in organic chemistry from the University of Arizona. Since joining AlliedSignal in 1979, he has been involved in synthetic organic and polymer research. His experience includes the development of surfactants, membranes for RO, UF, and gas separations, polymeric reagents and catalysts, high temperature thermosetting resins, and radiation curable resin systems. He has 30 patents and 13 publications and presentations covering this research.



Alvin C. Levy received his Ph.D. in physical chemistry from the Georgia Institute of Technology. Since 1987 he has been president of Alvin C. Levy & Associates, a R&D laboratory specializing in the development of adhesives, coatings and sealants. His prior work experience includes product development with AT&T Bell Laboratories and E.I. Du Pont. Dr. Levy holds patents on coatings for optical fiber and filling compounds for both copper and optical fiber cable.



Raymond J. Kovac is a research engineer with Alvin C. Levy & Associates. He received his B.S. in Chemical Engineering from Drexel University. He has experience in R&D, manufacturing, product development and process economics. He worked previously for Georgia Tech Research Institute; Witco and AMAX.



Paul R. Foy is the Laboratory Supervisor of the Fiber Optic Materials Research Program at Rutgers University in Piscataway, New Jersey. He received a B.S. in Ceramic Engineering from Rutgers University in 1982. Mr. Foy worked for AFG Industries as a production engineer in their float glass operation until 1986. Since that time Mr. Foy has been involved in the research and development of fiber optic materials for Rutgers University. He has continued his education by completing a Masters in Ceramic Engineering in 1990 and is presently pursuing a Ph.D. in Ceramic Engineering from Rutgers University.

BLEND S BASED ON THERMOTROPIC LIQUID CRYSTALLINE POLYMERS (TLCP) AS PRIMARY COATING OF OPTICAL FIBERS

F.Cocchini*, I.Ferri*, G.Sabbato* and A.Apicella⁺

* Fos - Fibre Ottiche Sud, Battipaglia, Italy

⁺ University of Naples, Naples, Italy

ABSTRACT

Blends of a liquid crystalline copolymer with thermoplastic flexible polymers have been considered as second layer of the primary coating of optical fibers. This class of materials presents outstanding properties which suggest applications in harsh environments.

Compression type dies have been adopted for the melt application. The self-centering forces arising in this type of applicators avoid any damage to the fiber due to contact in the nipple. The process parameters and the die geometries have been studied to reduce the tensile stress on the fiber during drawing. High drawing speeds have been experienced. Surface quality has been studied and the relevant process and material parameters have been analyzed.

Good performances of the blend-coated fibers have been obtained

1. INTRODUCTION

The properties of TLCP's are quite interesting. They have high chemical resistance, good hydrolytic stability, high thermal stability and inherent flame resistance, and, depending on the degree of molecular orientation, very high modulus and small or even negative thermal expansion coefficient. These features suggested their application in cable manufacturing^{1,2}, but make them also suitable for primary coating of optical fibers for special applications (e.g. high temperature, corrosive environments) and even large scale applications where harsh environments can be encountered (e.g. LAN and FTTH)

However, the poor transverse properties, due to the highly fibrillate structure of TLCP's, are a critical item in their layers for primary coating. Blending of TLCP's with flexible technopolymers has been considered to

overcome this problem, by the inclusion of the fibrillate structure in an isotropic matrix.

The work of Isayev and Swaminathan³ shows how such a case can be obtained even at large TLCP percentage. In this work, blends of up to 70% of Hydroxybenzoic acid-Hydroxynaphthoic acid (HBA-HNA) 73-27 in polyetherimide (PEI) or in a silicone-polyimide copolymer (silicone PI) have been considered.

The above mentioned thermoplastic blends have low viscosity and low shrinkage on cooling, which have allowed relatively easy melt processing directly as primary coating on-line with the fiber drawing.

The work is divided into three main sections dealing with the materials, with the application process of the blends on the optical fibers, and with the final properties of the blend-coated fibers.

2. THE MATERIALS

A classical double layer structure has been considered. Tests without the first layer have been also performed. Standard UV-curing acrylates have been used as first layer in this preliminary experimental analysis which was mainly intended to state the applicability of TLCP blends in primary coating.

Three blends have been considered as second layer, see table I.

Blend	Composition
1	TLCP 70% + PEI 30 %
2	TLCP 70% + Silicone PI 30 %
3	TLCP 50% + Silicone PI 50 %

Table I - Blend Compositions.

The blends have been prepared in a twin screw extruder at 330 °C.

Some properties of the TLCP and PEI have been reported in table II, and compared to standard values of acrylic resins.

The viscosity of the blends is strongly non-newtonian and little higher than that of the base TLCP⁴. It can be easily controlled by changing melt temperature, and at high shear rates (above 10^4 sec^{-1}) it is comparable to the newtonian viscosity of standard acrylic resins (2–10 Pas).

Property	TLCP		PEI	Acrylate
	longi- tudinal	trans- verse		
shrinkage on process	.002 ⁺	.003 ⁺	0.007 ⁺	0.05–0.07 [*]
thermal expansion coefficient ($10^{-6}/^{\circ}\text{C}$)	–5	75	56	100–200
max water absorption (%)	0.02		1.25	1–2

+ Mould shrinkage on cooling (m/m)

* Shrinkage on curing ($\text{m}^3/\text{Kg}/\text{m}^3/\text{Kg}$)

Table II – Material Properties.

3. THE PROCESS

3.1 EQUIPMENT

A single screw extruder by Gimac has been mounted on a drawing tower, as in fig.1.

Pressure and melt temperature are measured just before the cross-head.

Two types of cross-head dies has been considered, see fig.2 and table III.

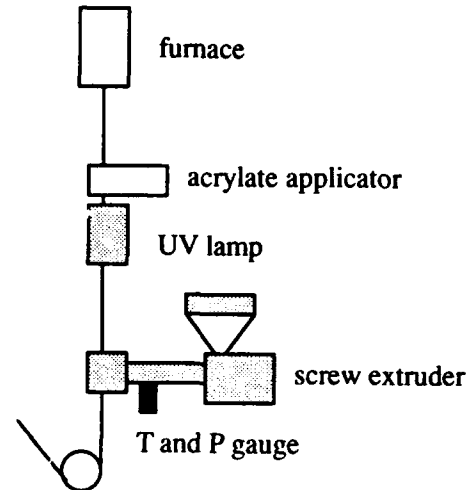


Figure 1 – Drawing tower layout.

Die type	Inner diameter (μm)	angle
A	350	7 °
B	340–360	12 °

Table III – Die Sizes and Geometries.

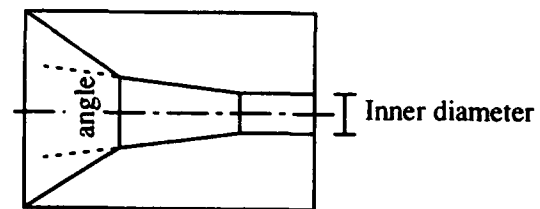


Figure 2 – Die geometry (schematic).

Both of them are pressure type as usually used to apply acrylic resins. This fact gives the advantage of the fiber self-centering, avoiding any scratch on the soft primary or on the glass itself, due to the contact with the nipple. This is essential for a good fiber manufacturing. Avoiding the elongational flow occurring in the tube type die², less extreme performances are obtained, but

also more isotropic and stable properties.

3.2 PROCESS PARAMETERS

As said before, the tensional force on the glass fiber is of great concern in the application.

To better understand how to optimize the process, the die has been modeled⁵ as a tube of length L and inner radius R . Inside, a fluid of viscosity η undergoes a pressure gradient ΔP and the drag force due to a fiber of radius kR ($k < 1$) running at a speed V .

In terms of the adimensional parameter

$$W = \frac{\Delta P R^2}{4 \eta L V} \quad (1)$$

the complete flow can be expressed in an analytic form as superposition of the pressure driven flow and of the drag flow. The stress at the die wall is

$$\tau_w = \eta \frac{V}{R} \left[\frac{1}{\ln k} - W \left(2 + \frac{1 - k^2}{\ln k} \right) \right] \quad (2)$$

The stress on the fiber is

$$\tau_f = \eta \frac{V}{R} \left[\frac{1}{k \ln k} - W \left(2k + \frac{1 - k^2}{k \ln k} \right) \right] \quad (3)$$

The volumetric throughput is

$$Q = \frac{\pi R^2 V}{2} \times \left[-\frac{1 - k^2}{\ln k} - 2k^2 + W \left(1 - k^2 + \frac{(1 - k^2)^2}{\ln k} \right) \right] \quad (4)$$

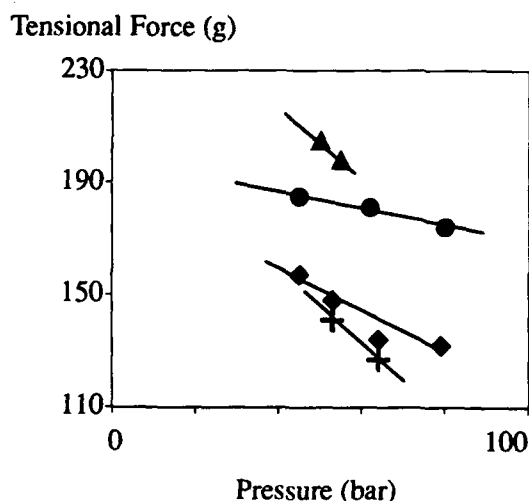
and the radius of the coated fiber is

$$R_{coated} = R \sqrt{k^2 + \frac{Q}{\pi R^2 V}} \quad (5)$$

The complex geometry of the die can be taken into account with an effective length L and an effective radius R rather than with the actual size⁵.

The non-Newtonian behavior of the blends modifies the quantitative results but not the qualitative trends. In particular from eqn.(3) it comes out that it is necessary to reduce the viscosity η , the speed V and the effective length L and to increase the pressure gradient ΔP in or-

der to reduce the tensional force on the fiber. Quantitative relationships have been obtained experimentally for the die A. The tensional forces on the fiber vs pressure at different melt temperatures and drawing speed are reported in fig.3. As can be seen, the tensional forces can be maintained at low values by a suitable control of the process parameters.

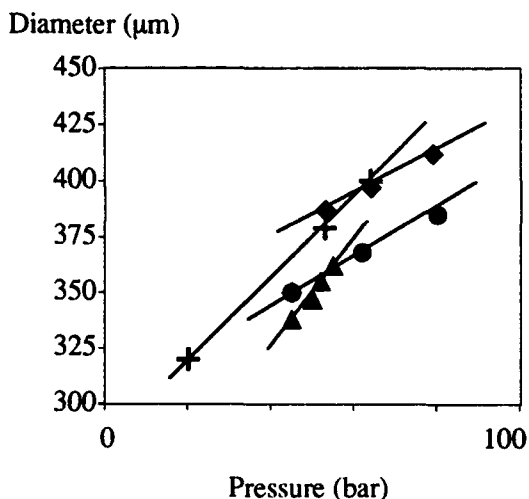


- + V=0.5 m/s, T=340 °C, without 1st layer
- ♦ V=0.5 m/s, T=340 °C, 200 µm diameter 1st layer
- V=0.5 m/s, T=330 °C, 200 µm diameter 1st layer
- ▲ V=1.0 m/s, T=340 °C, 200 µm diameter 1st layer

Figure 3 – Tensional Force vs Pressure in die A with blend 3.

The final diameters of the coated fiber vs pressure are reported in fig.4, again for the die A.

Surface finishing has been another problem in the blend application. In fig.5 and 6 the SEM photograph of two samples of blend-coated fiber are reported. The estimated stress at the wall in the die during process is about 5 and 15 MPa respectively. The sample in fig.6, obtained at the higher stress, has a better finishing, both in terms of waviness and fibrils at the surface, but still not optimized.



- + V=0.5 m/s, T=340 °C, without 1st layer
- ◆ V=0.5 m/s, T=340 °C, 200 μm diameter 1st layer
- V=0.5 m/s, T=330 °C, 200 μm diameter 1st layer
- ▲ V=1.0 m/s, T=340 °C, 200 μm diameter 1st layer

Figure 4 – Fiber Diameter vs Pressure in die A with blend 3.

Blend 2 was the worst in term of fibrils at the surface, probably because the silicon-PI is not as able as PEI to include the TLCP in large percentage. Therefore only blend 1 and 3 have been furtherly considered.

It is known that TLCP can show flow instabilities at low stress⁶, and a critical value of the stress at the wall of about 100 MPa at 340 °C is reported for a TLCP similar to the one used in this work. This critical value is expected to be lower in a blend. Nonetheless, stresses at the wall higher than those obtained for the samples of fig.5 and 6 seemed necessary to achieve a good surface finishing. As can be easily obtained from eqn.2, this can be achieved by changing the process parameters, i.e. increasing the viscosity, the drawing speed and the pressure or by changing the geometry, i.e. the effective length and the effective diameter of the die.



Figure 5 – SEM photograph of a blend-coated fiber with a stress at the wall of about 5 MPa.



Figure 6 – SEM photograph of a blend-coated fiber with a stress at the wall of about 15 MPa.

However increasing the pressure could cause flow out from the nipple, which has to be avoided.

Moreover, increasing the viscosity (i.e. decreasing the temperature) or the drawing speed will produce an intolerable increase of the tensional forces on the fiber (see fig.3 and eqn.3).

To avoid these occurrences, a different die (die B) has been adopted. This die, essentially, has effective length

and diameter lower than those of die A. The results of the following section all refer to experiments with die B, with the process parameters in the range reported in table IV.

Parameter	Range	Unit
T_{melt}	330–350	$^{\circ}\text{C}$
Pressure	10–30	bar
V_{draw}	1–7	m/s

Table IV – Process Parameters used with die B.

High drawing speeds have been experienced, but the small extruder available for the experimentation has not allowed to span a significant pressure range. As a matter of fact, the surface finishing, while satisfactory, was not yet comparable to acrylic coated fibers.

4. FIBERS CHARACTERIZATION

Several Km's of fibers have been continuously produced and coated with blend 1 and blend 3. The sample made with blend 1 present slightly better performances, while blend 3 is easier processable, allowing a greater efficiency of the extruder. Therefore higher drawing speed and pressure have been experienced with blend 3.

In table IV the main results have been summarized for both blends.

The added loss vs temperature measured with an OTDR for fibers coated with blend 1 and 3 are shown in fig.7. The samples are covered with a soft acrylate with low T_g as first layer. The added losses are small both for blend 1 and blend 3.

Property	Range	Units
Inner diameter	200	μm
Outer diameter	300–320	μm
Tensile Modulus at 0.5% strain	10–20	GPa
Attenuation @ 1550 nm	0.2–0.4	dB/Km
Strippability force	< 250	g

Table IV – Fiber Properties obtained with die B.

Added loss (dB/Km)

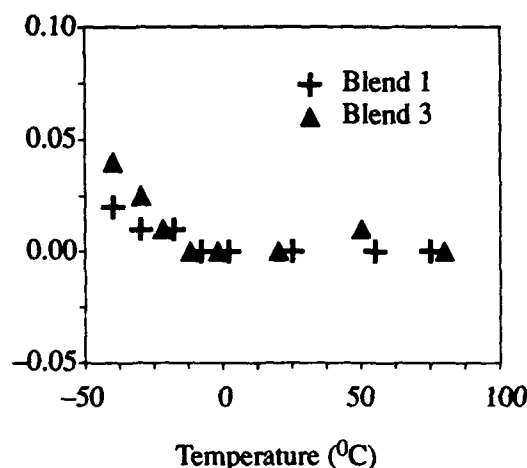


Figure 7 – Added Losses vs Temperature at 1550 nm for blend 1 and 3.

Added loss upon changes of the moisture (R.H.) are none or limited to few hundredth of dB/Km's, and completely reversible, depending on the acrylate used as first layer.

To better understand these features, measurements of the expansion of samples embedded in 100% R.H. have been carried out with a TMA⁷. The longitudinal dimensional changes of both blends are < 0.1%, with respect to about 1% for a standard acrylic resin.

Thus, considering both the hygroelastic behavior and the thermal behavior (tab.II), the thermoplastic blends result far more stable than acrylic resins. Therefore the small, but not zero, added losses found in the thermal and moisture cycling should arise from the lateral pressure exerted by the first acrylic layer which would expand between the constrain of the glass and of the outer blend coating. Further work on the optimal choice for the first layer of the coating is necessary.

The mechanical behaviour of the blend-coated fibers has been also analyzed. In fig.8 a typical force-strain curve is reported. It is evident the breaking of the coating at strain larger than about 3%, which is the typical elongation to break of the TLCP and of blends based on it⁸.

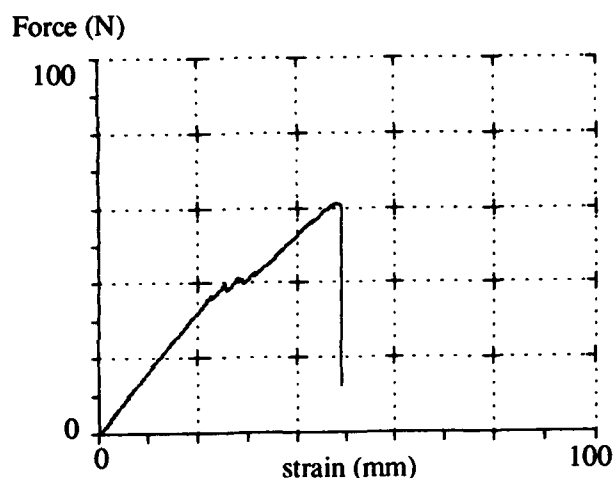


Figure 8 – Force vs Strain of a blend-coated fiber.

The long term reliability of a fiber with broken coating will be strongly reduced.

On the other hand a blend-coated fiber below the 3% limit could be more reliable than a standard fiber since a relevant part (up to 50%) of the applied load can be substained by the coating rather than by the glass, thus reducing the stress corrosion of the glass itself. This should be checked with long term static tests. On the contrary, dynamic measurements of the stress corrosion susceptibility factor n will be affected by the premature breakage of the coating at large strain and they cannot be used to estimate the fiber lifetime.

It is worthwhile to be noticed that blend-coated fiber without the first layer have significant lower strength. The elongation to failure is, in this case, almost similar to that of the blend coating, probably because of the cracks caused by the breakage of the coating on the un-protected glass.

5. CONCLUSIONS

Standard step index optical fibers for telecommunications have been primary coated with a first soft layer and a second hard layer of about 50 μm thickness, made with TLC_P's based blends. Good performances of the blend-coated fibers have been obtained, namely standard attenuation (e.g. about 0.2 dB/Km at 1550 nm) and

negligible added losses vs temperature and relative humidity. These preliminary results suggest how to optimize the process and the choice of the materials in view of applications in harsh environments.

ACKNOWLEDGEMENTS

The authors gratefully acknowledge the R&D Department of Pirelli Cavi and the Technical Group of FOS for assistance in this work, and the Management of FOS for the permission to publish the paper.

REFERENCES

- [1] F.Yamamoto Mol.Cryst.Liq.Cryst. **153**(1987)423.
- [2] D.J.Kenny and B.A.Cranfield PIT VI Proc. (1992) paper 20.
- [3] A.Isayev and S.Swaminathan US Patent 4,835,047 (1989).
- [4] L.Incarnato,M.R.Nobile and D.Acierno Makromol.Chem. Macrom.Symp. **68**(1993)277
- [5] K.Chida, S.Sakaguchi, M.Wagatsuma and T.Kimura Elect.Lett **18**(1982)713.
K.Chida,T.Kimura and M.Wagatsuma Rev.El.Comm.Lab. **32**(1984)425.
- [6] W.R.Krigbaum,C.K.Liu and D.K.Yang J.Polym.Sci B:Polym.Phys. **26**(1988)1711.
- [7] I.Ferri,F.Cocchini,A.Apicella and L.Nicolais PIT VI Proc. (1992) paper 18.
- [8] G.Kiss Polym.Eng.Sci. **27**(1987)410.

Liquid crystal polymer coated fibers with thermally stable delay time characteristics

A.Sano, A.Mogi, K.Suzuki and M.Miyamoto

Fujikura Ltd. Opto-electronics Laboratory
1440 Mutsuzaki Sakura Chiba 285 Japan

ABSTRACT

LCP coated fiber with a low thermal expansion coefficient has been realized. The mechanisms of stability of the thermal expansion coefficient are discussed in relation to the comonomer in polymerization, extrusion conditions and heat treatment. The thermal characteristics of the fabricated LCP coated fibers were examined. LCP fibers without delay time changes have been realized by cancelling the thermal coefficient of the optical fiber without the LCP coating. The delay time change was reduced to 0.1ps/km/°C or less for the range of 0°C to 30°C. The thermal characteristics of the cabled fiber are demonstrated. The performance of transmission loss and fiber strain showed sufficient stability for the normal range of temperatures.

INTRODUCTION

In the case of synchronized networks such as a phase array antenna system or synchronous computer control system, the delay time of the transmission lines must be kept constant for synchronization. In general, the environmental temperature is controlled to achieve this since the transmission lines have a nonzero thermal expansion coefficient. This becomes costly as the line becomes longer. Since LCP materials have a negative thermal expansion coefficient, they may be used to construct zero thermal expansion transmission lines. LCP coated fiber with a zero thermal expansion coefficient has been fabricated and studied. It was reported that LCP have a

negative thermal expansion in selective mold conditions. This method has been used in some applications. In this report, another approach is introduced to achieve repeatability and controllability of the thermal expansion coefficient of LCP coated fiber. The molecular structure of LCP is controlled by means of the selection of a comonomer for copolymerization. The crystal structure is also controlled by means of the limitation of molding parameters such as draw down ratio, draft ratio, R.T., etc.

STRUCTURE OF LCP COATED FIBER

Fig. 1 shows the structure of an LCP coated fiber. It has a silicone-coated optical fiber, 0.4 mm in diameter, at its center and an LCP coating as its outermost layer. Silicone is used because of adhesion to LCP resin. Table 1 shows the parameters of the optical fiber. The diameter of the LCP coating was made variable, i.e., it was made to vary with the kind of LCP and molding conditions.

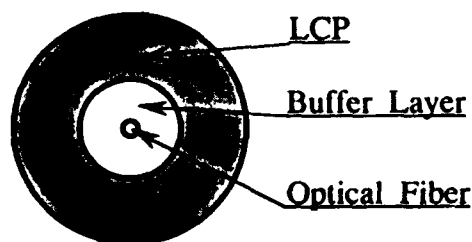


Fig.1 Structure of LCP Coated Fiber

Table.1

Kind	SM Fiber	MFD	9.5 μ m
Fiber Diameter	125 μ m	Cut-off Wavelength	1.25 μ m
Optical fiber Diameter	0.4 mm	LCP coating Diameter	Variable

Thermal properties of LCP fibers were investigated precisely by following equipments.

(1) Thermal Expansion Coefficient

Fig. 2 shows the principle of measuring thermal expansion coefficient. The measuring method uses a piece of quartz glass as reference sample and measures the thermal expansion of a fiber sample by detecting its longitudinal elongation by a differential transformer. Use of a horizontal dilatometer minimizes the effect of gravity, and the adoption of differential detection permits cancellation of the thermal expansion of the probe, which has been a problem in the past. As a result, it has become possible to measure the thermal expansion coefficient of the optical fiber with high accuracy of the order of 10^{-7} .

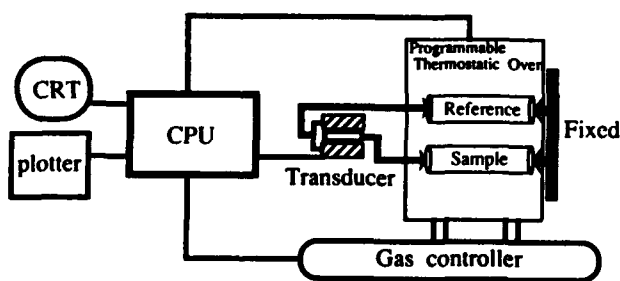


Fig.2 Device for Measuring Thermal Expansion Coefficient

(2) Thermal Delay Time Change

The measuring device is shown in Fig. 3. The signal from the synthesizer is converted by the E/O converter, passes through the fiber in the test tank and enters the O/E converter where the signal is converted again to an electric signal. This signal, along with with the reference signal from the generator, goes to the vector voltmeter, where the phase difference between the two signals is measured. From the phase difference, the delay time change is calculated by the following equation.

$$\Delta \tau = \frac{\Delta \Theta}{2 \pi f L}$$

$\Delta \tau$: Delay Time Change

$\Delta \Theta$: Phase Change

f : Synthesizer frequency

L : Fiber Length

Transmission Loss was measured by OTDR at 1.55 μ m wavelength.

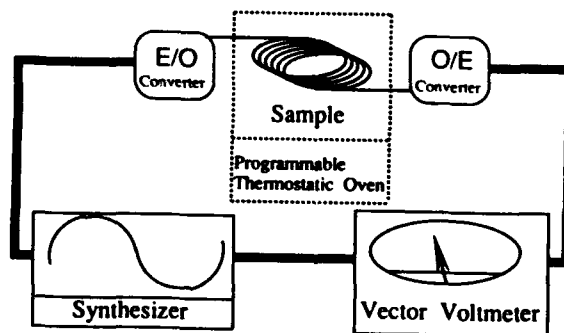


Fig.3 Device for Measuring Delay Time Change

SELECTION OF LCP COMONOMER

There are many kinds of LCPs containing various composites. We prepared three kinds of LCPs with different comonomers and coated them on silicone coated fibers with an outer diameter of 0.4mm. The fabricated LCP fibers were investigated for Young's modulus, thermal expansion coefficient, and delay time. The Young's modulus of the three LCP fibers are not dependent on the kinds of comonomers but seems affected by the kind of reinforcing material added to the base LCP. From the viewpoint of the extrusion process, the fusion point of LCPs is important. The LCP having the highest fusion point was difficult to mold. Figure 4 shows the relation between the fusion point and the thermal expansion coefficient in three LCPs with different comonomers (sample A,B, and C). It is noted that the fusion point and thermal expansion coefficient are greatly affected by the kind of comonomers. Sample A has low fusion point and small thermal expansion coefficient and is good for the control of thermal expansion coefficient by molding conditions. Next, the two samples found able to be molded were measured for delay time change. Fig. 5 shows the relation between thermal expansion coefficient and delay time change. The delay time change varies greatly as a liner function of the thermal expansion coefficient.

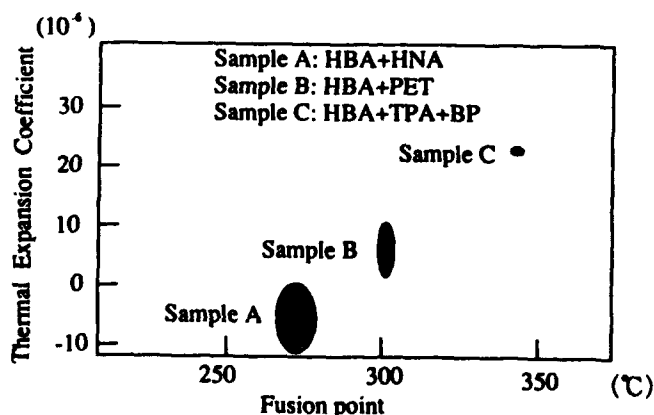


Fig.4 Thermal Expansion Coefficient by LCP comonomer type

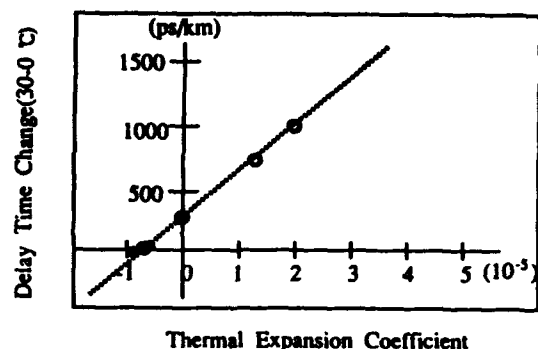


Fig.5 Dependence of Delay Time Change on Thermal Expansion Coefficient

CONTROL OF THERMAL EXPANSION COEFFICIENT BY MOLDING CONDITIONS

Thermal characteristics of LCP is considered to be affected by molding conditions. Using a low fusion point, low thermal expansion LCP, some samples were prepared with varying resin temperatures, Draw Down Ratios (DDR), draft ratios, and fiber back tensions. They were then measured for temperature dependence of transmission loss, thermal expansion coefficient and delay time change.

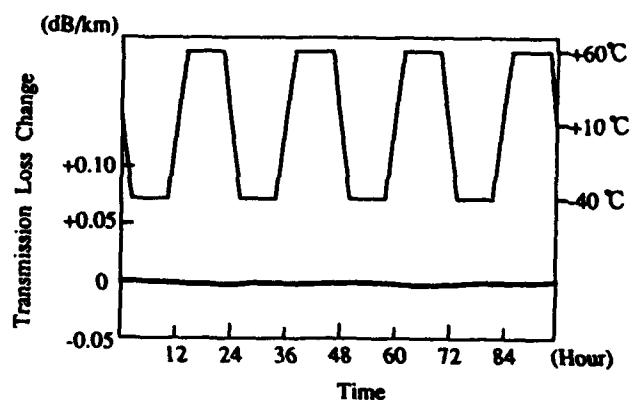


Fig.6 Temperature Dependence of Transmission Loss by LCP coated Fiber

EXPERIMENTAL RESULTS

a) Transmission Loss

Fig. 6 shows the temperature dependence of transmission loss. All of the trial samples, prepared with varying resin temperatures, DDRs, draft ratios and fiber back tensions, exhibited no change in transmission loss.

b) Resin Temperature

The value of thermal expansion becomes smaller with lower resin temperature, but this results in considerable degradation in moldability.

c) DDR and Draft Ratio

Fig. 7 shows the temperature dependence of thermal expansion coefficient. The LCP coated samples exhibit a negative thermal expansion coefficient at normal working temperatures. The contraction that is specific to crystalline polymer materials occurs in the "-" direction, so it can be seen that they are different from ordinal polymer materials. Moreover, this is not a simple phenomenon of orientation relaxation because a certain level of repeatability is obtainable during repeated heat cycles. Furthermore, the change in draft ratio exerts a greater influence than the change in DDR.

d) Repeatability

Fig. 8 shows the temperature dependence of delay time change. The delay time change varies greatly with initial temperature rise but begins to stabilize at the 2nd cycle.

From these results, it has been found that the thermal expansion coefficient can be controlled to some extent through the control of the molding conditions.

A low delay time change of less than $0.1 \text{ ps/km/}^\circ\text{C}$ has been obtained within the normal range of temperature.

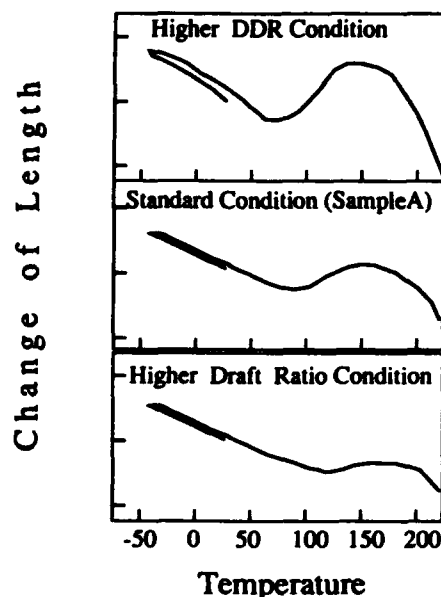


Fig.7 Thermal Expansion Behavior of LCP coated Fiber

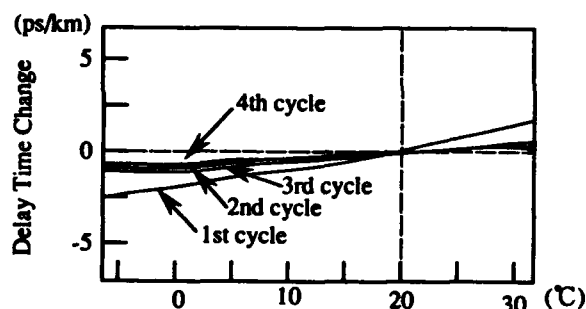


Fig.8 Temperature Dependence of Delay Time Change

APPLICATION FOR CABLE

We obtained LCP coated fiber having a controlled thermal expansion coefficient. However, the thermal expansion coefficient of cabled fiber is influenced by other cable components with different thermal expansion. In particular, the total thermal expansion coefficient of cable is dominated by the

thermal characteristic of the tension member. On the other hand, LCP has a high Young's modulus and, is expected to be usable as a central member for cables. The possibility of controlling cable elongation was investigated, as well as the control of thermal expansion of the LCP coated fiber.

CABLE STRUCTURE

Using a 1.6 mm single steel wire, 2.0 mm \varnothing single-stranded support fibers of G-FRP and K-FRP, and a single-stranded LCP coated fiber, each as a central member, 5-slot spacers about 6 mm in outside diameter were made and used for this experiment. LCP coated fibers were stranded around the central member, and the stranded assembly was wrapped with a tape and sheathed with polyethylene. The final outer diameter of the obtained cable was about 10 mm.

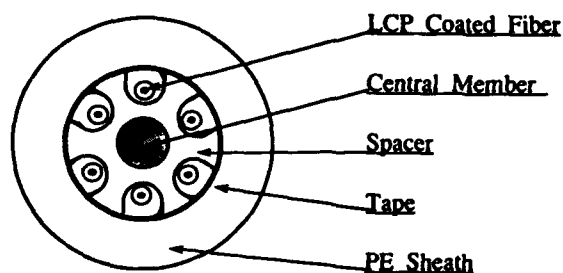


Fig.9 Cross Section Structure of Optical Fiber Cable

STRUCTURE OF LCP COATED FIBER

Table 2 shows the structure and parameters of the LCP coated fiber.

Table.2

Kind	SM Fiber	MFD	9.5 μ m
Fiber Diameter	125 μ m	Cut-off Wavelength	1.25 μ m
Optical fiber Diameter	0.4 mm	LCP coating Diameter	0.8 mm

IN-PROCESS VARIATION IN TRANSMISSION LOSS

The variation in transmission loss produced in each process of cabling and that was caused by the change in environmental temperature were measured by the OTDR method at a wavelength of 1.55 μ m. There was no clear difference due to the kind of central member, and the variation in transmission loss was within the limits of measuring error.

IN-PROCESS VARIATION THERMAL EXPANSION COEFFICIENT

The thermal expansion measuring device shown in Fig.2 was used for measuring the expansion at the end of each process. In addition, the thermal expansion at end of the repeated heat cycle was also measured to ensure the reliability of measurement. It was confirmed that both the aramid FRP type and the LCP type exhibit a negative thermal expansion coefficient at the initial stages of cabling, that is, in sheath process, but the former exhibits a positive thermal expansion coefficient at the end of the heat cycle. Furthermore, the steel wire type and the G-FRP type already exhibit a greater difference in thermal expansion than the LCP coated fiber at the initial stages of cabling. Therefore, when designing cables, it is necessary to investigate the design with due consideration for the working environment.

Cables using the LCP coated fiber as a central member were confirmed to exhibit thermal expansion coefficient stability with good repeatability compared with the steel wire, G-FRP and K-FRP types. The LCP coated fiber is expected to be useful in many new applications, not only for use in the control of cable length but for other uses as well.

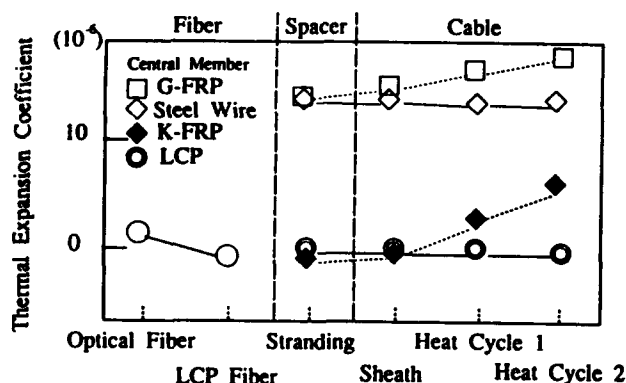


Fig.10 In-process Variation in Thermal Expansion Coefficient

CONCLUSION

The low delay time change of less than 0.1 ps/km/°C has been obtained by coating the optical fibers with liquid crystal polymer. The negative thermal coefficient of LCP was controlled by the introduction of an appropriate comonomer and optimizing the molding conditions such as resin temperature, DDR, and draft ratio. The obtained LCP coated fiber showed stable thermal stability and repeatability for heat cycles of normal temperature range. The performance of delay time change in cables with LCP fibers was also evaluated applying different materials for the central tension member. The LCP material has also been applied as a tension member for a slotted rod cable. This cable structure has shown the lowest thermal expansion coefficient. The LCP coated fibers and cables are promising as control cables with thermally stable delay time in some synchronous systems.

REFERENCES

- [1] W.J. Jackson, Jr., H.F. Kuhfuss, J. Polym. Sci. Polym. Chem. Ed, 14, 2043 (1976)
- [2] L.G. Cohen and J.W. Fleming, "Effect of temperature on transmission in lightguides", BSTJ. Vol. 58, (1979) pp. 945-951
- [3] E.F. Andersen, "Differential propagation delay in optical multifiber cables", Electron Lett. Vol. 16 No. 10, (1980) pp. 389-391.
- [4] L.A. Bergman, S.T. Eng, and A.R. Jhonston "Temperature stability of transit time delay for a single mode fiber in a loose tube cable", Electron Lett. Vol. 19 No. 21, (1983) pp. 865-866.
- [5] R. Kashyap, S. Hornung, M.H. Reeve, and S.A. Cassidy, "Temperature desensitisation of delay in optical fibers for sensor applications", Electron Lett. Vol. 19 No. 24, (1983) pp. 1039-1040
- [6] S. Yamakawa, Y. Shuto, F. Yamamoto, Proc. 9th European Conference on Optical Communication (ECOC), p. 227 (1983)
- [7] Y. Shuto, Y. Takeuchi, F. Yamamoto, Trans. IEICE, E70, 14 (1987)
- [8] G.F. Lutes, L.E. Primas, "State of the art fiber optics for reference frequency distribution over short distances", in Proc. 20th PTTI (1988)



Akira Sano
 Opto-Electronics
 Laboratory
 Fujikura Ltd.
 1440 Mutsuzaki
 Sakura-shi, Chiba-ken
 285 Japan

Akira Sano was born in 1960. He joined Fujikura Ltd. after his graduation from Kyoto University with a B.E. in 1983 and has been engaged in research and development of cable materials. He is an engineer of the Telecommunication Cable Section and a member of IEICE of Japan.



Akio Mogi
 Opto-Electronics
 Laboratory
 Fujikura Ltd.
 1440 Mutsuzaki
 Sakura-shi, Chiba-ken
 285 Japan

Akio Mogi was born in 1946. He joined Fujikura Ltd. after his graduation from Haneda Institute High School in 1967 and has been engaged in research and development of the metallic cables and optical cables. He is now the manager of the telecommunication line department and a member of IEICE of Japan.



Kazunari Suzuki
 Opto-Electronics
 Laboratory
 Fujikura Ltd.
 1440 Mutsuzaki
 Sakura-shi, Chiba-ken
 285 Japan

Kazunari Suzuki was born in 1971. He joined Fujikura Ltd. after his graduation from Hachinohe College of Technology in 1991 and has been engaged in research and development of optical fiber cables. He is an engineer of the Telecommunication Cable Section and a member of IEICE of Japan.



Matsuhiro Miyamoto
 Opto-Electronics
 Laboratory
 Fujikura Ltd.
 1440 Mutsuzaki
 Sakura-shi, Chiba-ken
 285 Japan

Matsuhiro Miyamoto was born in 1953. He received the M.S. degree from the Tokyo Institute of Technology in 1978. He joined Fujikura Ltd. and has been engaged in research and development of optical fibers and cables. He is now the manager of the Telecommunication Cable Section and a member of IEICE of Japan.

COATING DESIGN OF THIN COATED FIBER FOR ULTRA-HIGH-COUNT OPTICAL FIBER CABLE

*Kazumasa OISHI, Wataru KATSURASHIMA, Tatsuya KAKUTA,
Yasuo MATSUDA, and Shigeru TANAKA*

SUMITOMO ELECTRIC INDUSTRIES, LTD.
YOKOHAMA, JAPAN

Abstract - Thin coated optical fibers for the ultra-high-count optical fiber cable were fabricated and their mechanical and optical characteristics were evaluated.

Concerning mechanical characteristics, a new method has been developed to evaluate the abrasion resistance of the coating layers. It was clarified that the mechanical durability of the coated optical fiber mainly depends on the thickness and Young's modulus of secondary coating layer. Especially, the minimum thickness of secondary coating layer proved to be about a half of the roughness that the coated optical fiber might encounter during the fabrication process in order to maintain the mechanical strength.

We also investigated the optical characteristic against microbending. It was concluded that thickening of layer and decrease of Young's modulus of primary coating are advantageous in improving the microbending characteristics of the thin coated optical fiber.

1. INTRODUCTION

On the basis of the FTTH (Fiber-To-The-Home) conception ⁽¹⁾ expressed by NTT in Japan, the ultra-high-count and pre-connectorized optical fiber cable, which has more than 1000-fibers in the almost same diameter as the conventional high-count optical fiber cable, is recently discussed ⁽²⁾. To realize the cable with high optical fiber density, it is essential to develop the thin coated optical fiber, the multi-count fiber ribbon, and the modified cable construction. However, the coating structure of optical fibers is closely related to the mechanical and optical characteristics. Thinning of the coating layers may cause deterioration of the fiber strength during the

manufacturing processes of the cable and optical performance against microbending ⁽³⁾. In order to reduce the thickness of the coating layers, therefore, it is necessary to clarify the optimum coating design that does not reduce the mechanical and optical characteristics. However the relationship between the coating design and the characteristics of thin coated optical fiber has not been clarified completely.

Therefore, we have investigated the characteristics of thin coated optical fibers from the view point of the coating design.

2. COATED OPTICAL FIBER

In order to protect from abrasion damage and to maintain optical properties, optical glass fiber is generally coated with polymer layers.

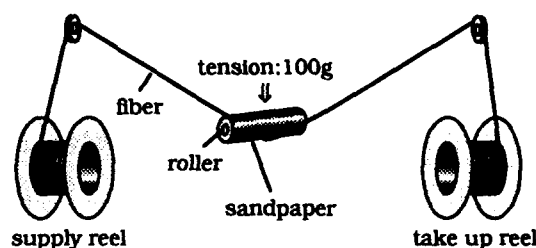
To investigate the optimum coating structure of fibers for the ultra-high-count optical cable, we prepared several optical fibers with two-layer coatings of UV curable urethan acrylate resin. The optical glass fiber is a normal single-mode type with a diameter of 125 μ m. The thicknesses and Young's moduli of the primary and secondary coating layers are shown in Table 1. The mechanical durability and the optical characteristics against microbending for these fibers were evaluated.

Table 1 Structure of thin coated optical fibers

fiber sample No.	primary coating layer / secondary coating layer		
	coating diameter (μm)	Young's modulus (kg/mm^2)	coating thickness (μm)
1	150/180	0.07/170	12.5/15.0
2	160/180	0.07/170	17.5/10.0
3	170/180	0.07/170	22.5/5.0
4	150/190	0.07/170	12.5/20.0
5	160/190	0.07/170	17.5/15.0
6	150/200	0.07/170	12.5/25.0
7	160/200	0.07/170	17.5/20.0
8	170/200	0.07/170	22.5/15.0
9	180/220	0.07/170	27.5/20.0
10	180/240	0.07/170	27.5/30.0
11	150/180	0.07/60	12.5/15.0
12	150/180	0.07/70	12.5/15.0
13	150/180	0.07/150	12.5/15.0
14	150/180	0.06/170	12.5/15.0
15	150/180	0.13/170	12.5/15.0
16	180/240	0.13/60	27.5/30.0

Table 2 Abrasive particle size of sandpaper

grade of sandpaper (#)	average diameter of particle (μm)
320	40
400	30
600	20
800	14
1000	11.5

**Figure 1** Abrasion Resistance Test

3. MECHANICAL DURABILITY

Generally, it is considered that the strength of fibers is mainly determined by original flaws existed on the optical glass fiber, or secondary flaws induced on the surface of the optical glass fiber by damages of the coating layers. Especially for fibers with thin coating layer, the major factor of strength is expected to be the secondary flaws. If the coating layer of the optical fiber is too thin to protect the glass surface from a foreign matter, the strength of the fiber is seriously degraded. To improve the mechanical strength of thin coated optical fiber, therefore, it is necessary to clarify the optimum coating structure and material that minimize the reduction of durability of the coating layers against a foreign matter (abrasive particle).

To assure strength of optical fiber, weak points in the optical fiber are usually eliminated by loading a tension for the entire length. This test is called the screening test. However screening test requires long length of test fibers and

long time for evaluation. Moreover, it is very difficult to discriminate between the original flaw and the secondary flaw in screening test.

For quantitative investigation of the abrasion resistance for the coating layers, therefore, a new evaluation method (Abrasion Resistance Test) was developed.

3-1 ABRASION RESISTANCE TEST

Using a fiber rewinding machine, first, thin coated optical fibers shown in Table 1 were uniformly abraded by passing through a roller wrapped with sandpapers of several grades with a tension of 100g, as shown in Figure 1. In Table 2, average diameter of abrasive particles on the sandpapers is listed (according to Japanese Industrial Standard). The diameter of the roller is 11mm. Next, the tensile strength of the original and abraded fibers was measured at gage length of 300mm with 100mm/min of strain rate.

A parameter expressing the abrasion resistance, R_s , was defined by equation (1).

$$R_s = S_A / S_0 \text{ -----(1)}$$

Where S_A and S_0 represent the average failure strength of abraded fiber and original fiber respectively. This test requires short length fiber and less time and removes the influence of original flaws.

3-2 ABRASION RESISTANCE FACTOR

The followings are the factors which seem to effect abrasion resistance of coating layers :

- 1° thickness of total coating layers,
- 2° thickness of primary coating layer,
- 3° thickness of secondary coating layer,
- 4° mechanical properties of primary coating layer,
- 5° mechanical properties of secondary coating layer,
- 6° abrasive particle size, and
- 7° stress pressed by abrasive particles.

In this paper, we discuss these factors except for 7°. In mechanical properties of primary(4°) and secondary(5°) coating layer, we took notice of Young's modulus.

3-3 DEPENDENCE OF COATING STRUCTURE

The relation between the thickness of the coating layers and abrasion resistance was investigated. As a result, it was clarified that the abrasion resistance of the coating layers mainly depends on the thickness of secondary coating layer (T_s), as shown in Figure 2. Circle means that R_s is almost 100% and triangle is under 98%. Cross means fiber break during winding.

We also found the critical thickness of secondary coating layer is closely related to the diameter of abrasive particle (D_A), and the size D_A of

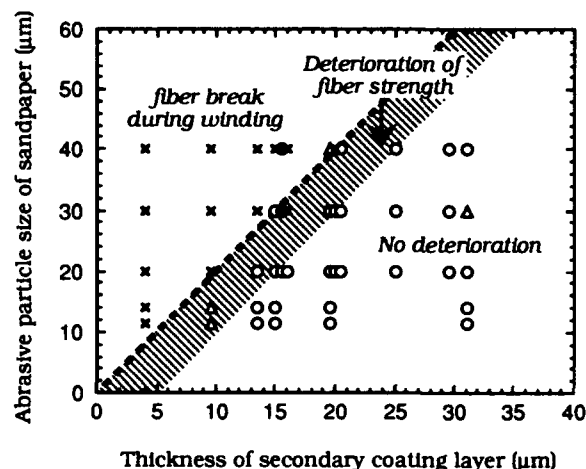


Figure 2 Dependence of the thickness of secondary coating layer and abrasive particle size on average failure strength

particle which causes the break of fiber is expressed by the equation (2).

$$D_A > 2 T_s \text{ -----(2)}$$

To maintain the mechanical strength of coated optical fiber, it is estimated that the thickness of secondary coating layer should be more than a half of the roughness (size of abrasive particle) which the coated optical fiber might encounter during the manufacturing processes of the cable.

We must know the size D_A of particle in the actual manufacturing environment to determine the minimum thickness T_s of secondary coating layer for thin coated optical fiber.

3-4 DEPENDENCE OF COATING MATERIAL

The relation between the Young's modulus of coating layers and abrasion resistance was investigated. Figure 3 shows Young's modulus of secondary coating layer also influences the abrasion resistance of thin coated optical fiber.

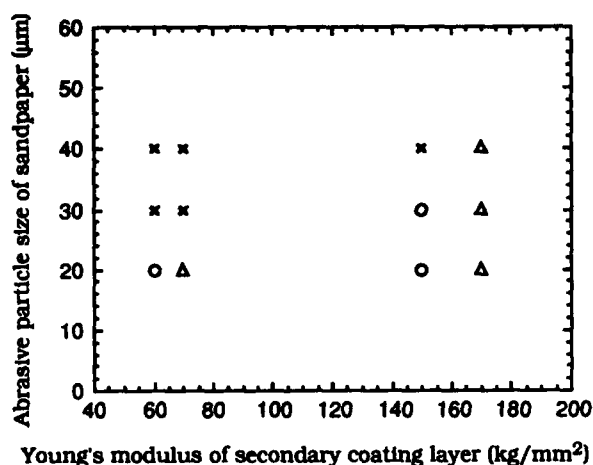


Figure 3 Dependence of Young's modulus of secondary coating layer and abrasive particle size on average failure strength

To maintain the mechanical strength, Young's modulus of the secondary coating layer should be surely higher than conventional secondary coating material.

We must also evaluate other subjects which effect on abrasion resistance such as elongation in mechanical properties of coating layers.

4. OPTICAL CHARACTERISTICS AGAINST MICROBENDING

4-1 EVALUATION METHOD

To investigate the optical characteristics against microbending, Long Span Winding Test (Figure 4) was applied ⁽³⁾. The fiber was wound in one layer with a tension of 100g on a reel wrapped with a sandpaper of #1000 (according to Japanese Industrial Standard).

Chromatic loss spectrum was measured before and after winding test and we got a increase of loss by subtraction of these values.

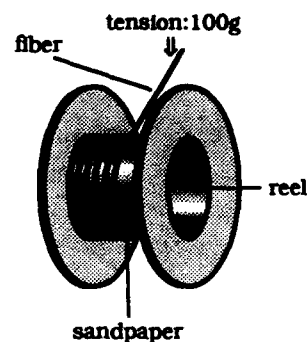


Figure 4 Long Span Winding Test

4-2 PRESUMED MICROBENDING LOSS (PML)

It is well known that microbending loss depends on the parameters of fiber. Therefore, in the actual experiment, it is rather difficult to compare the detected loss increase of individual fiber with different parameters of fiber. To overcome this problem, we introduced presumed microbending loss (PML) method ⁽⁴⁾.

By fitting the measured data to microbending formula, we get the correlation length L_c and average bending radius R . These parameters are assumed to be inherent to the bending condition and not to be influenced by parameters of fiber. Therefore the effect of parameters of fiber on the increase of induced loss is compensated. Substituting L_c and R again into the equation presuming standard fiber whose mode-field-diameter is $9.5\mu\text{m}$ and effective cut-off wavelength is $1.25\mu\text{m}$, we get presumed microbending loss (PML).

4-3 DEPENDENCE OF COATING STRUCTURE

The relation between the thickness of the coating layers and PML was investigated. Figure 5 shows the experimental result. The microbending characteristic of the thin coated optical fibers

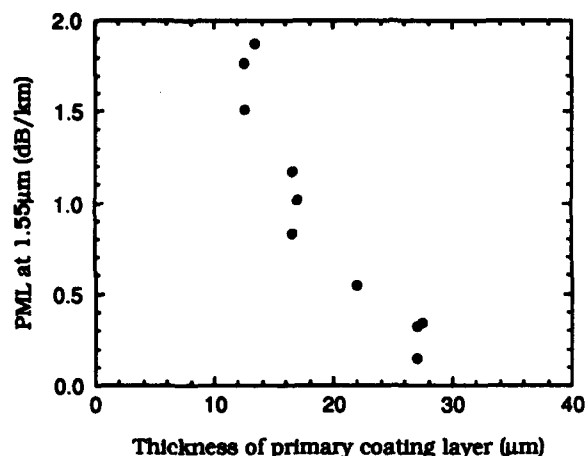


Figure 5 Dependence of the thickness of primary coating layer and PML

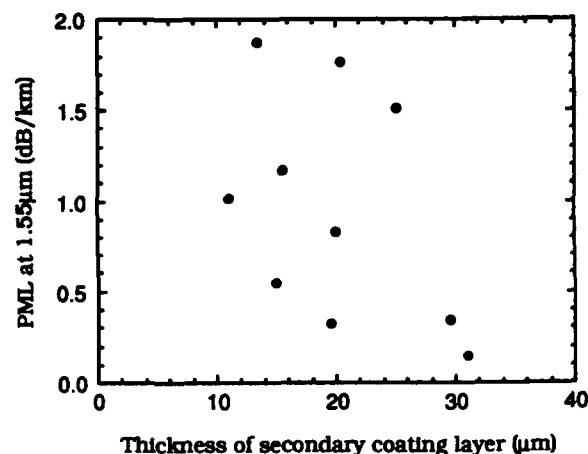


Figure 7 Dependence of the thickness of secondary coating layer and PML

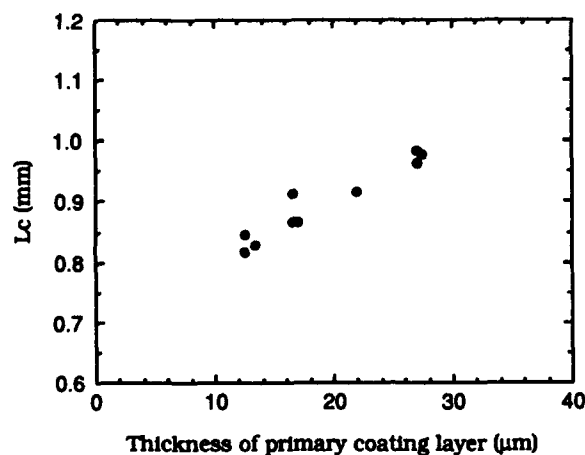


Figure 6 Dependence of thickness of primary coating layer and correlation length L_c

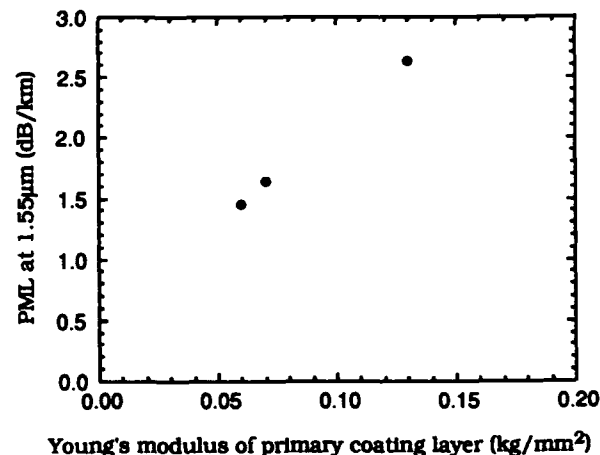


Figure 8 Dependence of the Young's modulus of primary coating layer and PML

proved to mainly depend on the thickness of primary coating layer. Thinning of primary coating layer results in a larger loss increase. Also, correlation length L_c has dependence on the thickness of primary coating layer (Figure 6).

On the contrary, the influence of thickness of the secondary coating layer on microbending characteristics is very little (Figure 7).

4-4 DEPENDENCE OF COATING MATERIAL

The relation between Young's modulus of the coating layers and PML was investigated. Figure 8 shows the experimental result and indicates the PML of thin coated optical fiber is almost proportional to the Young's modulus of primary coating layer. Lower Young's modulus of primary coating layer results in a smaller loss increase.

5. CONCLUSION

To realize the ultra-high-count optical fiber cable, thin coated optical fiber with excellent mechanical and optical characteristics is indispensable. For this reason, we have investigated the optimum coating structure and material for the thin coated optical fiber.

First, a new method (Abrasion Resistance Test) has been developed to evaluate the abrasion resistance of the thin coating layers. Using this method, it was clarified that the mechanical durability of the coated optical fiber depends on thickness and Young's modulus of secondary coating layer. To conclude for mechanical durability of thin coated optical fiber, thicker secondary coating with higher Young's modulus is favorable.

Next, using Long Span Winding Test, it was clarified that optical performance against microbending of the coated optical fiber depends on thickness and Young's modulus of primary coating layer. To conclude for optical properties of thin coated optical fiber, thicker primary coating with lower Young's modulus is favorable.

REFERENCES

- (1) T.UENOYA, "The Optical Fiber Loop 21 Plan" OEC'90 (1990).
- (2) S.TOMITA et al., "Preliminary Research into Ultra High Density and High Count Optical Fiber Cables" IWCS'91 (1991).
- (3) M.HARA et al., "Design of Downsized Coated Optical Fibers to Minimize Microbending Loss" IWCS'92 (1992).
- (4) W.KATSURASHIMA et al., "Microbending Loss of Thin Coating Single Mode Fiber for Ultra-High-Count Cable" IWCS'92 (1992).



Kazumasa OISHI

Sumitomo Electric Industries, Ltd.

*1, Taya-cho, Sakae-ku
Yokohama, Japan*

Kazumasa Oishi received his M.S. degree in Geochemistry from Tsukuba University in 1991. He joined Sumitomo Electric Industries, Ltd. in 1991, and has been engaged in research and development of optical fiber and cables. He is a member of Transmission Media Department in Yokohama Research Laboratories.

Wataru KATSURASHIMA

Sumitomo Electric Industries, Ltd.

*1, Taya-cho, Sakae-ku
Yokohama, Japan*



Wataru Katsurashima graduated from Tokyo University in 1987. He joined Sumitomo Electric Industries, Ltd. in 1987, and has been engaged in research and development of optical fiber and cables. He is a member of Communication Department in Yokohama Research Laboratories and a member of Institute of Electronics and Communication Engineers of Japan.



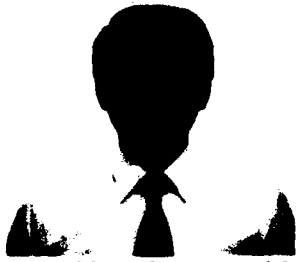
Tatsuya KAKUTA

Sumitomo Electric Industries, Ltd.

*1, Taya-cho, Sakae-ku
Yokohama, Japan*

Tatsuya Kakuta received his M.E. degree in Applied Chemistry from Osaka University in 1985. He joined Sumitomo Electric Industries, Ltd. in 1985, and has been engaged in research and development of optical fiber and cables. He is a member of Transmission Media Department in Yokohama Research Laboratories and a member of Institute of Electronics and Communication Engineers of Japan.

Yasuo MATSUDA



*Sumitomo Electric
Industries, Ltd.*

*1, Taya-cho, Sakae-ku
Yokohama, Japan*

Yasuo Matsuda received his M.E. degree in Chemistry from Tokyo University in 1978. He joined Sumitomo Electric Industries, Ltd. in 1978, and has been engaged in research and development of optical fiber and cables. He is a chief research associate of Transmission Media Department in Yokohama Research Laboratories.

Shigeru TANAKA

*Sumitomo Electric
Industries, Ltd.*

*1, Taya-cho, Sakae-ku
Yokohama, Japan*

Shigeru Tanaka received his M.E. and Ph.D. degree from Tokyo University in 1976 and 1989. He joined Sumitomo Electric Industries, Ltd. in 1976, and has been engaged in research and development of optical fiber and cables. He is a chief associate of Communication Department in Yokohama Research Laboratories and a member of Institute of Electronics and Communication Engineers of Japan.

DEVELOPMENT AND CHARACTERIZATION OF NOVEL UV-CURABLE OPTICAL FIBER COATINGS

Chander P. Chawla and Erwin S. Poklacki

DSM Desotech Inc.
1122 St. Charles Street, Elgin, IL 60120

ABSTRACT

UV curable acrylate systems have been used during the last decade for the protection of optical fiber for telecommunications. These systems are cured by a free radical mechanism and have the advantage of rapid cure speed and excellent composite properties. The radiation cure industry has been evaluating a number of alternative systems which have performance properties equivalent to the acrylate systems but do not have their potential toxicity/sensitization. One of the alternative chemistries is vinyl ether based systems which are cured by a cationic polymerization process. These systems tend to significantly change their mechanical properties after cure due to post cure phenomena. Another alternative chemistry is the free radical copolymerization of vinyl ether and maleate components. Both of these components are difficult to homopolymerize free radically. Vinyl ether and maleate components form an alternating copolymer and can give a wide range of properties. In this paper we describe the use of modified vinyl ether - maleate technology in developing potentially lower toxicity UV curable optical fiber coatings. These coating compositions contain a very small amount of a high molecular weight acrylate component. The cure speeds of these systems were found to be equivalent to the conventional acrylate systems. The mechanical properties of these systems were also comparable to those of the acrylate systems. In general, most of the properties required for optical fiber coating were similar for acrylate and acrylate oligomer modified vinyl ether-maleate coatings. The aging behavior of these coatings was also studied. It was concluded that lower toxicity vinyl ether-maleate based compositions could be useful as optical fiber coatings.

INTRODUCTION

UV curable acrylate systems have been used during the last decade, for the protection of telecommunication optical fiber. These systems are cured by a free radical mechanism and have the advantage of rapid cure speed and excellent composite properties. The radiation cure industry has been evaluating a number of alternative systems which have properties similar to acrylate systems, but have the potential for reduced toxicity and sensitization. One of the alternative chemistries explored consists of vinyl ether based systems, which are photopolymerized by a cationic mechanism¹. These systems tend to significantly change their mechanical properties due to a post cure phenomenon. Another alternative chemistry is the free radical photocopolymerization of vinyl ether and maleate components^{2,3}. Each of these components do not undergo efficient free radical homopolymerization. However, vinyl ether and maleate functional components readily form an alternating copolymer which can provide a wide range of properties. The cure speed of these systems can be enhanced by the addition of acrylate functional components. In this paper we describe the

use of vinyl ether - maleate technology in developing potentially lower toxicity UV curable optical fiber coatings. These coatings are free of acrylate monomers. A small amount of high molecular weight (MW) acrylate component is included to improve the cure speed of the system. This should not affect the potential toxicity of these coatings due to the high MW of the acrylate oligomer.

EXPERIMENTAL

Film Preparation

All coatings were drawn down on clean 23 cm x 30 cm glass plates using a Pacific Scientific Automatic Drawdown Apparatus. Either a 75 or a 150 micrometer Bird Film Applicator was used. These films were then cured at an appropriate dose using "D" and/or "H" lamps in a Fusion Curing Unit (Model K523/2). The dose was measured by an International Light Inc. "Light Bug" IL 390.

Film Aging

The elevated temperature aging at 125°C was conducted using convection ovens. The hydrolytic aging was carried out in an electric pressure steam sterilizer (120°C/100%RH). The Q-UV aging was conducted in a chamber under ambient temperature and humidity, with 2 UVB lamps, 6 inches away from the samples.

Peak Water Absorption and Percent Extractables

These were measured by a dynamic water sensitivity test method⁴ under ambient laboratory conditions in glass bottles.

Dynamic Mechanical Analysis (DMA)

A Rheometrics Solids Analyzer RSA II was used to run the dynamic mechanical analysis on the aged and unaged samples. The sample dimensions were 12 mm X 23 mm. The frequency was set at 1.0 radian/second. Before starting a sweep, the sample was preheated to 80°C for a minimum of five minutes in a dry nitrogen

atmosphere of the rheometer's environmental chamber, to remove any water that may be present, which could act as a plasticizer.

Weight Change Measurements

Free films (3X3 cm) were used for weight change measurements. They were preconditioned at 60°C for one hour before aging, cooled in the desiccator for 15 minutes, and weighed. After aging at 125°C, or under Q-UV light, the samples were postconditioned in the desiccator for 15 minutes before reweighing to determine the weight loss.

Viscosity

Viscosity measurement was conducted using a Brookfield viscometer with spindle #15 at 50 rpm, at 25°C.

Refractive Index

Refractive Index was measured using an Abbe-3L refractometer.

Tensile Properties

Tensile properties were measured using an Instron model #4201 at 23°C/50%RH. The sample dimensions were 5.08 cm X 1.27 cm and the strain rate was 50%/minute.

Hydrogen Generation

Hydrogen generation was measured using the Key-Med Exhaled Hydrogen Monitor. About 4-6 grams of sample was placed in a 120 ml bottle, flushed with argon, and then sealed. The sample was heated at 80°C for 24 hours, cooled to room temperature, and the hydrogen concentration measured.

Oxidation Induction Temperature (OIT)

OIT was determined using a DuPont 912 Differential Scanning Calorimeter. A sample was heated in an oxygen environment from 90°C to 300°C at a heating rate of 10°C/minute.

Thermogravimetric (TG) Weight Loss

The weight loss was measured using a DuPont 951 TG Analyzer. A known weight of the sample was heated isothermally at 200°C, for 40 minutes. The air flow rate was 70 mL/minute.

Adhesion

Nominal 75 micrometer films were cured on cleaned, polished glass plates. These films were aged at 23°C/50%RH for seven days, at which time a 180 degree peel test was run on part of the sample using an Instron (model TTD) to determine the 50% RH adhesion (2.54 cm wide specimen; strain rate=25.4cm/minute). The films were additionally aged at 95%RH for one day and the peel test was run on the remaining samples to determine the 95%RH adhesion.

Coefficient of Thermal Expansion (COE)

The COE was measured using a DuPont 934 Thermomechanical Analyzer. The sample was cryogenically cooled using liquid nitrogen and then heated at a rate of 5°C/minute to about 80°C. An expansion probe was used with a 2 gram load. The nitrogen flow rate was 50mL/minute.

Coefficient of Friction (COF)

The COF was determined on an Instron (model TTD) using a three point contact sled weighing ~100 grams, with a 25.4 cm/ minute strain rate.

Photocalorimetry Studies

Photocalorimetry studies were conducted using the Perkin Elmer DSC 7, with a DPA 7 accessory attached. A 450 watt Xenon lamp was used as the light source.

RESULTS AND DISCUSSION

Photocalorimetry Studies on Monomer Systems

Figures 1 and 2 show the photopolymerization exotherms of a maleate (diethyl maleate or DEM) and a vinyl ether (triethylene glycol divinyl ether or DVE-3) monomer, respectively, in an air atmosphere at 50°C. Both of these contain two percent of a photoinitiator used for free radical polymerization. The rate of polymerization, as expected, was extremely slow for both vinyl ether and maleate components since these monomers do not homopolymerize free radically.

Figure 3 shows the photopolymerization exotherm (in air) of a 1:1 equivalent mixture of the same two monomers in the presence of two percent of the same free radical photoinitiator at 50°C. The mixture of these two monomers, as expected, polymerized rapidly.

Figure 4 shows the photopolymerization exotherms for a monofunctional acrylate monomer (cyclohexyl acrylate)

and for a mixture of the same acrylate monomer and DVE-3 (in a nitrogen atmosphere) at 50°C. The acrylate monomer polymerized at a reasonable rate. The photopolymerization of the mixture proceeded at a fast rate since the acrylate monomer could also copolymerize with the vinyl ether monomer.

Figure 5 shows some photopolymerization exotherms for mixtures of vinyl ether, maleate, and acrylate monomers (vinyl ether equivalents = maleate + acrylate equivalents) using one percent of a free radical type photoinitiator at 30°C. The three samples vary in the type of vinyl ether monomer used. Samples with phenoxy ethyl vinyl ether (PEVE) and tetrahydrofurfuryl vinyl ether (THFVE) gave faster rates of polymerization compared to the sample with propenyl ether of propylene carbonate (PEPC). The photopolymerization, in general, proceeded at a fast rate since both acrylate and maleate components copolymerize with the vinyl ether component.

Comparison of Acrylate Coating Properties with the Acrylate Oligomer Modified Vinyl Ether-Maleate Coatings

Tables I and II show the property comparison of acrylate inner (coating 1) and outer (coating 3) primary coatings with acrylate oligomer modified vinyl ether-maleate inner (coating 2) and outer (coating 4) coatings.

Liquid Coating Properties: It is possible to prepare acrylate oligomer modified vinyl ether-maleate coatings with viscosities suitable for processing (~3000-11000 mPa.s). The refractive index and viscosity can be optimized by varying the coating composition.

Cured Film Properties: One of the required properties of UV curable optical fiber coatings is the rapid development of ultimate mechanical properties as a function of cure dose. Inner primary coating 2 developed 95% of its ultimate modulus at 0.2 J/cm² (Figure 6) which is faster than coating 1 as well as other commercial acrylate coating systems. The cure speeds of the two outer primary coatings were essentially the same. The tensile strength, elongation, and tensile modulus properties for acrylate oligomer modified vinyl ether-maleate inner and outer primary coatings were comparable to those of the acrylate oligomer coatings. The dynamic mechanical analysis curves for the inner primary coating 2 and outer primary coating 4 are shown in Figures 7 and 8 respectively. A wide range of glass transition temperatures are achievable through the proper choice of monomer and oligomer combinations. These properties were again comparable to the acrylate coatings. The inner primary coating 2 had excellent retention of adhesion in a wet environment. Maintaining constant adhesion in diverse environments is critical for

fiber performance. Both inner and outer primary coatings were thermo-oxidatively stable as shown by oxidation induction temperatures and thermogravimetric weight losses. Hydrogen generation was higher for both inner (coating 2) and outer primary (coating 4) coatings compared to the acrylate coatings. The peak water absorption values of coatings 2 and 4 were comparable to the acrylate coatings. The percent extractable content for inner primary coating 2 was higher than desired. The balanced COE values of outer primary coating 4 above and below the coating's T_g may be advantageous in minimizing microbending losses during temperature cycling. The COF values of the two outer primary coatings are quite similar.

Environmental Stability of Vinyl Ether-Maleate-Acrylate Oligomer Based Coatings

Tables III and IV show some aging data on inner primary coating 2 and outer primary coating 4. On aging at 125°C for one week, the equilibrium modulus (E_0) for the inner primary coating 2 remained unchanged. This means that the crosslink density has not changed and the polymer is not undergoing any degradation either through chain scission or additional crosslinking. There were some increases in the T_g measures of $E' = 1000\text{MPa}$, $E' = 100\text{MPa}$ and $\tan \delta$ peak, possibly due to loss of some volatile, uncrosslinked materials. After 3 weeks aging at 125°C, outer primary coating 4 shows minor changes in the position of the $\tan \delta$ peak and the equilibrium modulus. The weight loss after eight weeks @ 125°, is only 5.7%, which is very comparable to the acrylate coatings.

Aging at 120°C/100%RH, for up to two weeks, leads to some increase in the $\tan \delta$ peak value and a decrease of the equilibrium modulus of inner primary coating 2. Under these conditions, the $\tan \delta$ peak did not change for the outer primary coating 4, however the equilibrium modulus dropped. The drop in modulus may be due to hydrolysis which results in chain scission. The hydrolysis resistance of these coatings can be improved through an optimal oligomer/monomer selection. A number of acrylate coatings studied in the past have shown poorer performance under these conditions. It should also be pointed out that there are several acrylate coatings in commerce, which perform better under these aging conditions.

The weight loss of outer primary coating 4 under Q-UV light for eight weeks was 2.4%, which again is very low.

CONCLUSIONS

This study demonstrates that, it is possible to prepare free radically curable (using UV light) optical fiber coatings that do not contain acrylate monomers. Many of the properties and aging behavior of the acrylate oligomer modified vinyl ether-maleate coatings are similar to the existing acrylate coatings. There are a few properties (e.g. hydrogen generation and percent extractable for the inner primary coating) which require optimization. The toxicity testing of these type of coatings is under investigation.

Table I. Property Comparison of Acrylate and Acrylate Oligomer Modified Vinyl Ether-Maleate Inner Primary Coatings

Coating Property	Inner Primary 1	Inner Primary 2
<u>Liquid Coating</u>		
Viscosity, mPa.s	10,000	4,450
Refractive Index	1.49	1.47
<u>Cured Film</u>		
Tensile Properties Tensile Strength, MPa	4.1	3.2
Elongation, %	200	220
Modulus, MPa	2.6	2.55
Cure Speed(Dose @95% Modulus), J/cm ²	1.0	0.2
Dynamic Mechanical Properties E' = 1000MPa, °C	-11.5	-7
E' = 100MPa, °C	13	7
Tan δ Peak, °C	24.3	12.5
E ₀ , MPa	2.0	2.8
Adhesion, g. force @50% RH	540	390
@95% RH	215	290
Water Sensitivity Peak Water Absorption, %	2.7	0.8
Extractables (3wk soak), %	3.5	5.1
COE X 10 ⁻⁸ , cm/cm °C Below T _g	90	<100
Above T _g	260	590
OIT, °C	202	252
TG Weight Loss, %	NA	4.6
H ₂ Generation, μ L/g	0.3	1.7

Table II. Property Comparison of Acrylate and Acrylate Oligomer Modified Vinyl Ether-Maleate Outer Primary Coatings

Coating Property	Outer Primary 3	Outer Primary 4
<u>Liquid Coating</u>		
Viscosity, mPa.s	5,000	3,240
Refractive Index	1.51	1.47
<u>Cured Film</u>		
Tensile Properties Tensile Strength, MPa	26	30
Elongation, %	16	11
Modulus, MPa	690	760
Cure Speed(Dose @95% Modulus), J/cm ²	1.5	1.1
Dynamic Mechanical Properties E' = 1000MPa, °C	31	29
E' = 100MPa, °C	62	59
Tan δ Peak, °C	59	56.5
E ₀ , MPa	36	34
COF Film to Stainless Steel	0.4	0.9
Water Sensitivity Peak Water Absorption, %	3.5	2.2
Extractables(3w k soak), %	0.5	1.5
COE X 10 ⁻⁸ , cm/cm °C Below T _g	210	<100
Above T _g	910	170
OIT, °C	210	263
TG Weight Loss, %	4.2	3.4
H ₂ Generation, μ L/g	0.5	1.3

Table III. Environmental Stability of Acrylate Oligomer Modified Vinyl Ether-Maleate Inner Primary Coating

Pretreatment	E' = 1000MPa, °C	E' = 100MPa, °C	Tan δ Peak, °C	E _o , MPa
Control	-7	7	12.5	2.8
1wk @ 125°C	-3	13.5	24.5	2.7
1wk @ 120°C/100%RH	-6	11	26.5	0.8
2wk @ 120°C/100%RH	-7.5	6	16.5	0.8

Table IV Environmental Stability of Acrylate Oligomer Modified Vinyl Ether-Maleate Outer Primary Coating

Pretreatment	E' = 1000MPa, °C	E' = 100MPa, °C	Tan δ Peak, °C	E _o , MPa
Control	29	59	56.5	34
1wk @ 125°C	41	70	66	41
2wk @ 125°C	39.5	69	60	37
3wk @ 125°C	40	69	68	37
1wk @ 120°C/100%RH	32	54	56.5	17
2wk @ 120°C/100%RH	32	53.5	56	14
Pretreatment		Weight Loss, %		
8 weeks at 125°C		6.8		
8 weeks under Q-UV light		2.4		

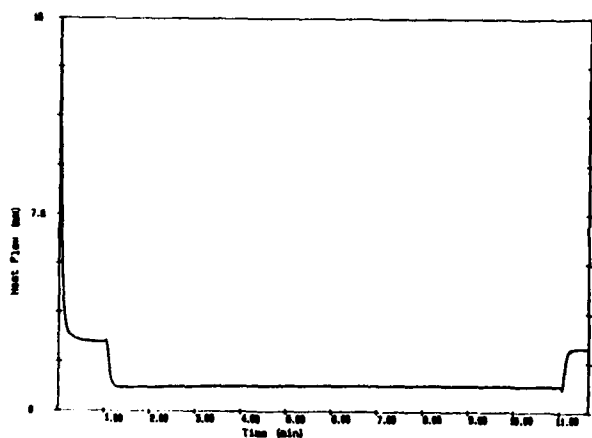


Figure 1 Photopolymerization exotherm of diethyl maleate (DEM).

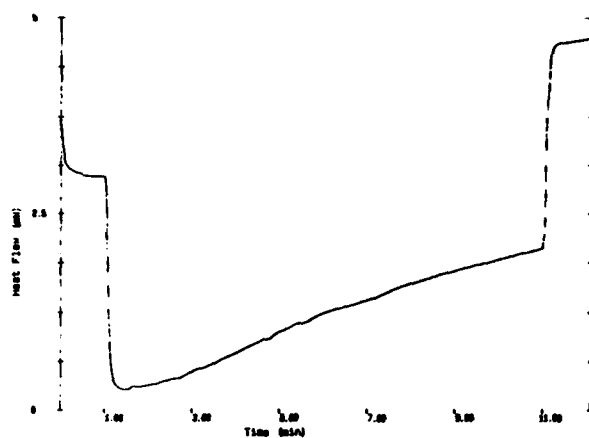


Figure 2 Photopolymerization exotherm of DVE-3.

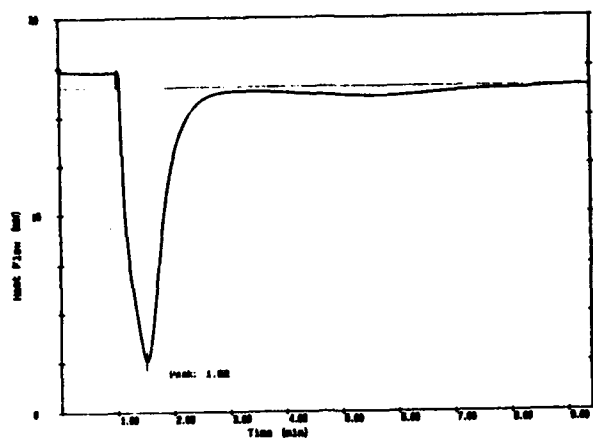


Figure 3 Photopolymerization exotherm of a 1:1 mixture of DVE-3 and DEM.

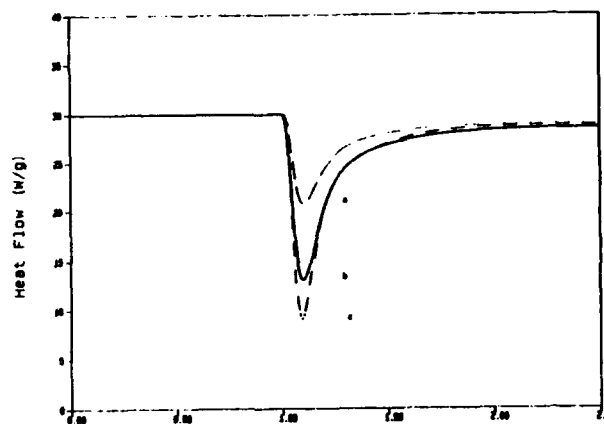


Figure 5 Photopolymerization exotherms of a mixture of maleate, acrylate, and vinyl ether monomers (vinyl ether equivalents = acrylate + maleate equivalents): with (a) PEPC, (b) PEVE, and (c) THFVE.

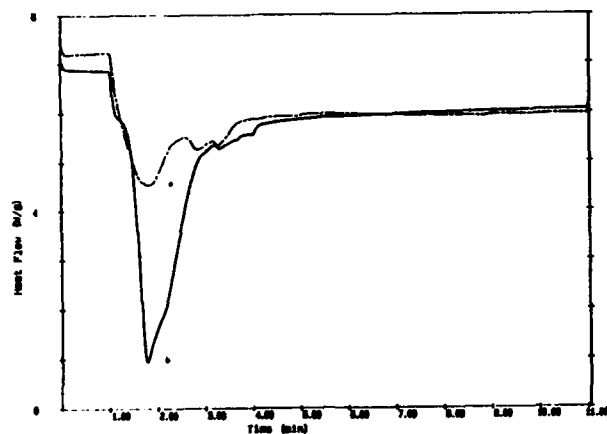


Figure 4 Photopolymerization exotherms of (a) cyclohexyl acrylate and (b) a 1:1 mixture of DVE-3 and cyclohexyl acrylate.

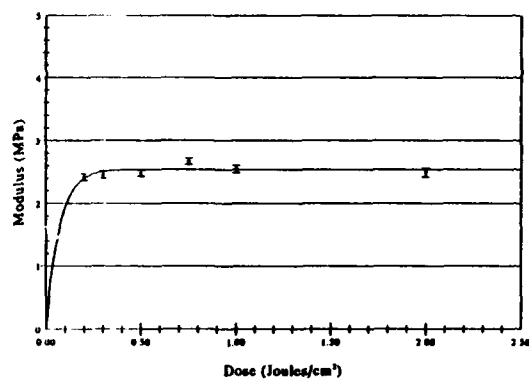


Figure 6 Dose versus modulus for the acrylate oligomer modified vinyl ether-maleate inner primary coating 2.

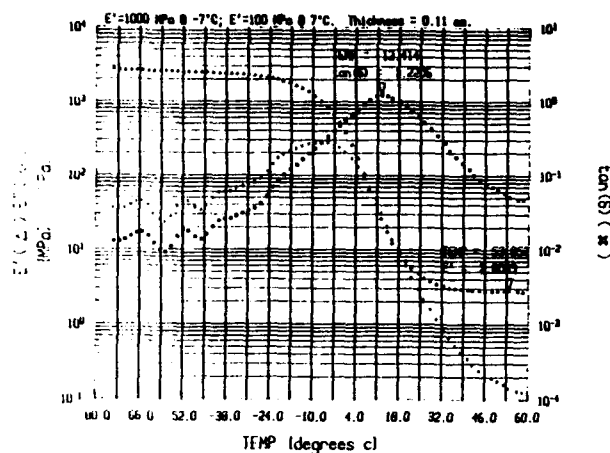


Figure 7 Dynamic mechanical curve for the acrylate oligomer modified vinyl ether-maleate inner primary coating 2.

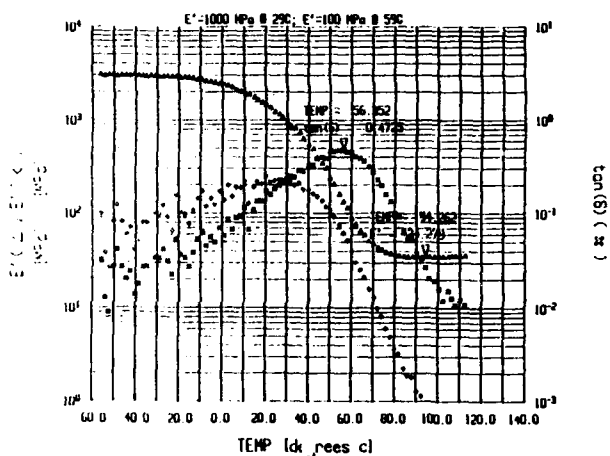


Figure 8 Dynamic mechanical curve for the acrylate oligomer modified vinyl ether-maleate outer primary coating 4.

ACKNOWLEDGEMENTS

The authors would like to acknowledge Michael G. Sullivan for his help in preparing the samples, DSM Desotech's analytical group for testing of the samples, and Steven R. Schmid for helpful suggestions.

REFERENCES

1. S. C. Lapin, "Radiation Curing, Science and Technology", S. P. Pappas, ed. Plenum Press, New York, 1992, p. 241.
2. S. C. Lapin, J. J. Schouten, G. K. Noren, E. J. Moschovis, RadTech Europe 1993, Conference Proceedings, p. 502.
3. J. J. Schouten, G. K. Noren, and S. C. Lapin, Radtech'92 North America Conference Proceedings, Vol. 1, p. 167.
4. C. P. Chawla, T. E. Bishop, D. M. Szum, and K. P. Murray, Optical Engineering Vol. 30 Number 6, p. 763.



Chander P. Chawla received his Ph.D. in polymer science from the University of Southern Mississippi in May 1990. He obtained a master's degree in polymer science and technology from the Indian Institute of Technology, New Delhi, in 1984, and a master's degree in chemistry from the University of Delhi, New Delhi, in 1982. He has been working in the area of fiber optic coatings since October 1989. He is currently a senior research chemist in the optical Fiber coatings group of DSM Desotech Inc., 1122 St. Charles St., Elgin, IL 60120.



Erwin S. Poklacki received his Ph.D. in Organic Chemistry from Northwestern University in 1961, after receiving his bachelor's degree from Loyola University of Chicago in 1957. He has been working in polymer chemistry in synthetic rubber, plastics and coatings. He is currently a senior research associate in the Optical Fiber Materials Group of DSM Desotech Inc., 1122 St. Charles St., Elgin, IL 60120.

DESIGNING AN OPTICAL FIBER DUAL COATING SYSTEM FOR LOOSE TUBE AND RIBBON CABLE LONG LINE AND LOCAL LOOP APPLICATIONS

Robert J. Overton
Adolphe R. Lopez
Alcatel Telecommunications Cable
Roanoke, Virginia

Henri-Marc Michaud
Alcatel Fibres Optiques
Bezons, France

Claude Lasne
Alcatel Alsthom Recherche
Marcoussis, France

Ronald G. Sommer
KABEL RHEYDT AG
Moenchengladbach, Germany

ABSTRACT

A new optical fiber dual coating system is introduced. The new coatings have been developed from the principles of correlating individual material properties with the resulting on-fiber performance in a number of handling and environmental issues. By this method, the new coatings have been tailored to meet the demands of loose-tube as well as ribbon cable designs, exceeding the requirements for handling and reliability in both.

INTRODUCTION

Optical fiber has now largely replaced copper conductors in long line telecommunications cable and is widely used for data transmission as well. The next step is large-scale introduction into local loop telephone and cable TV service, and this is expected in the relatively near future. Fiber networks will allow unprecedented quality and economy in video delivery and will bring similar benefits for the home in voice and data communications. These fiber-in-the-loop (FITL) applications are now made economically feasible through innovative couplers, splitters, and mass splicing techniques along with improved control of fiber geometries¹.

Along with improvements in fiber geometric precision and in coupling technology, deployment of FITL in addition to the already established applications of fiber optics demands better performance from the other material components of such systems in protection against environmental hazards. Optical fiber coatings, in particular, will have to be versatile in resistance to dangers which are much more common in FITL applications than in the comparatively hermetic conditions in long distance cables, where fiber exposure points are far fewer and more sheltered. A vastly larger number of splices per fiber kilometer with FITL strengthens the demand for easy and reliable mechanical stripping as well as increasing the risk of accidental exposures to common solvents such as acetone and propanol, which can damage the ability of the coatings to offer protection. The more frequent exposure of fibers to very low temperatures will continue to test the ability of coating systems to buffer against microbending-induced added loss. Neighborhood pedestals are not sealed, and insects and animals have

access. Wasp sprays are routinely used on entering a pedestal for work, and optical fibers are exposed to the petroleum-based carrier solvents and to the chemical poisons themselves. Temperature and humidity extremes will also be encountered in climates such as found in the West and subtropical South in the United States. The danger is that the effectiveness of optical fiber coatings as protection in these environments can be severely diminished through oxidative or hydrolytic degradation mechanisms^{2,3}. A substantial percentage of fiber optic cables will find installation in the vicinity of steam lines, where there are risks to the coatings from thermal damage, alone and in combination with high humidity, to say nothing of direct steam impingement⁴.

Besides the necessity to weather adverse conditions, fiber optic coatings must now be enormously versatile in packaging possibilities as well. Coatings are challenged by the rising popularity of ribbon structures for optical fibers, where the need to strip (usually with a heat stripping tool) coating and ribbon matrix cleanly in a single motion can require different characteristics of the coatings than does mechanically stripping a single fiber. For a coating system to be accepted in ribbon in the worldwide marketplace, it must succeed in meeting the wide variety of testing required in Europe and other regions where ribboned fiber is well-established. The odds are that ribbon structures as well as loose tube cables will be utilized in FITL installations, and the fiber manufacturer's production economies demand a coating system that is able to perform in both applications.

This paper introduces a New Coating System which meets the challenges for versatility and reliability extant in today's applications. The authors present some of the methodology behind the coating development and performance results in testing to meet the specifications of both North American and European markets. The data is sometimes compared to the previous system used in Alcatel's North American unit as well as to several other commercially used coating systems in the market today.

STRIPPABILITY

Mechanical Stripping

For splicing and terminations, the coatings must be removed from optical fiber ends, an operation currently done with mechanical stripping tools in the case of single fibers or with heated stripping apparatus for opening ribbon structures. Strippability is a subjectively judged attribute of a dual coating system, although there is a procedure specified in the Bellcore requirements document TR-NTW-000020 to quantify strip force. In general, a craftsman wants the coatings to remove cleanly with a single pass of the stripping tool while tolerating a few stray coating crumbs left behind if these can be removed with a single wipe of a towelette. It is thought that the strippability is influenced by

1. the adhesion of the primary to the glass
2. the coefficients of expansion (CTE's) of the coatings
3. the modulus, ultimate mechanical properties and toughness of the coatings

The configuration of the coating apparatus also must play a part, but that will not be considered here. The contributions from the factors listed above have not to date been thoroughly modeled, but the development technique followed here led to tailoring the secondary coating to have a relatively high glass transition temperature (so that it exhibits a glassy behavior in the mechanical stripping operation), a high degree of toughness but low ultimate elongation. The primary coating is designed with a decreased level of mechanical adhesion to the glass (through a deliberate choice of cure shrinkage allowed and properly combining the primary and secondary coating CTE's) and a very low glass transition temperature so that it behaves as a soft rubber during the stripping exercise.

The coefficient of thermal expansion is important because of the state of stress that results in the coatings after the cure process. Consider the case in which the primary coating is applied and cured prior to the application of the secondary coating. The effect of an expansion coefficient differential has been well-treated in the past^{5,6} and will not be re-derived in detail here. It is sufficient to observe that

a) the coatings are at an elevated temperature as the secondary is cured,

b) due to the difference between temperature at cure and room temperature, there will be a radial stress exerted by the coatings, acting on the surface of the glass, and

c) the magnitude and direction of the stress will be dependent on the ratio $\frac{\alpha_{\text{primary}}}{\alpha_{\text{secondary}}}$, where α is the thermal expansion coefficient. Tables I and II show the ratios for the rubbery regions and the stripping performance for the New System, the previous coating system and another widely used commercial system (Commercial A).

TABLE I. EXPANSION COEFFICIENT RATIOS AND STRIP FORCE OF SEVERAL COATING SYSTEMS

SYSTEM	$\frac{\alpha_{\text{primary}}}{\alpha_{\text{secondary}}}$	STRIP FORCE*, 1
New System	0.87	1.00
Previous System	0.39	0.90
Commercial A System	0.29	0.75

* per EIA/TIA 455-178

TABLE II. MECHANICAL STRIPPABILITY OF THE COATING SYSTEMS

SYSTEM	STRIPPABILITY
New System	Excellent
Previous System	Fair
Commercial A	Fair

A "Strippability" judgment was made based on reports from a number of expert craftspeople who were given the fibers in blind tests in which the Miller tool was used. The participants looked for ease and smoothness of the stripping movement and for a minimum of crumbs left to be wiped off. The New System stripped smoothly with one pass and required little additional work to clean off crumbs. The other two systems usually took two or more passes with the tool before the craftspeople stopped to wipe the fiber, and the crumbs were more persistently adhered to the fiber.

While the strip force itself does not differ radically among the three coating systems, the perceived strippability is quite different. A larger coefficient of expansion of the primary (relative to the secondary) reduces the mechanical adhesion of the coatings after the coatings cool following the cure process and eases mechanical stripping.

Stripping Ribbon Structures

There are no standard procedures at present to define ribboned fiber strippability, but heated stripping tools are commonly in use in the industry. A heated tool was used to compare strippability of colored fibers with several of the coating systems, packaged in 12-fiber, edge-bonded ribbon structures all with the same matrix material. The tool was designed to remove ribbon matrix and fiber coatings in one pass. It was heated to 105°C, and the ribbon end was placed in the tool for 5 seconds before accomplishing the stripping. The goal was complete and clean removal of ribbon matrix and fiber coatings in a single pass. Table III lists the results for several coating systems examined (including a Commercial B system available in ribbon structures).

TABLE III. FIBER OPTIC COATINGS AND HEAT STRIPPABILITY OF EDGE-BONDED RIBBON STRUCTURES.

COATING SYSTEM	RANK	COMMENTS
New System	1-2	clean, complete strip in one pass
Commercial B	1-2	clean, complete strip in one pass
Commercial A	3	smear residue after first pass, several passes required plus wiping
Previous System	4	difficult to strip, smear residue requiring several passes and wiping to remove

Commercial A and the Previous system both have primaries with very high adhesion to glass achieved through both chemical and mechanical effects. The new primary coating relies on a careful balance of sufficient adhesion to glass to preclude delamination under handling or environmental exposure while maintaining excellent heat strippability properties. For both the New system and the Commercial B system, the matrix and coatings come off as a unit, leaving clean, bare fiber ready for splicing.

Effects of Aging

Fibers with the New System were aged in a number of aggressive environment, comprising

- 85°C/85% RH - 30 days
- 85°C dry - 30 days
- 85°C water - 30 days
- exposure to wasp spray per TR-NTW-000020

and the strip force was followed with aging/exposure. The results are shown in Figures 1 through 4, along with the results on three commercial fibers utilizing coating systems A and B already introduced, and Commercial C. In each case strip force is essentially unchanged by the aging or by exposure to wasp spray.

FIGURE 1. Strip force with time in aging at 85°C/85% RH.

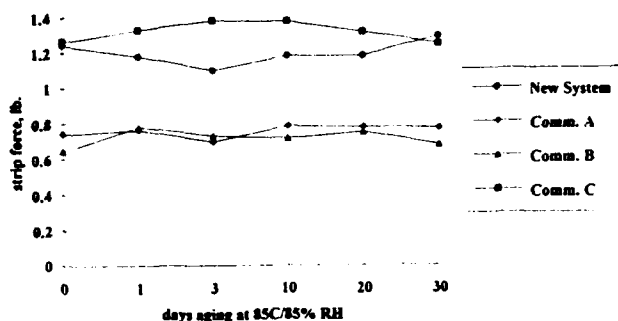


FIGURE 2. Strip force with time in aging at 85°C dry.

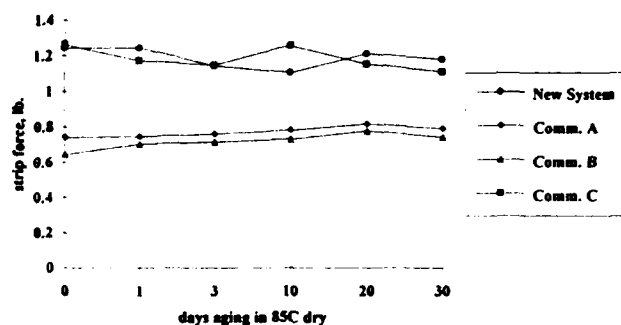


FIGURE 3. Strip force with time aging in 85°C water.

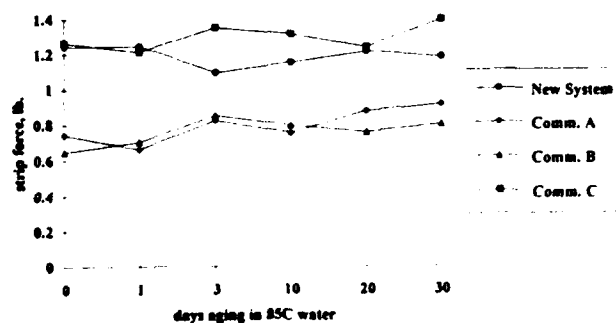
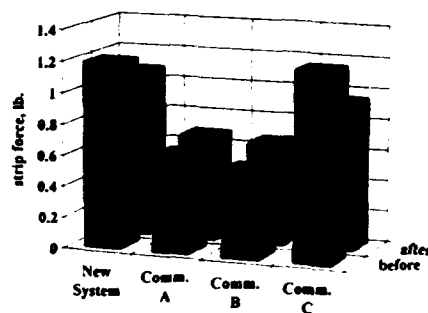
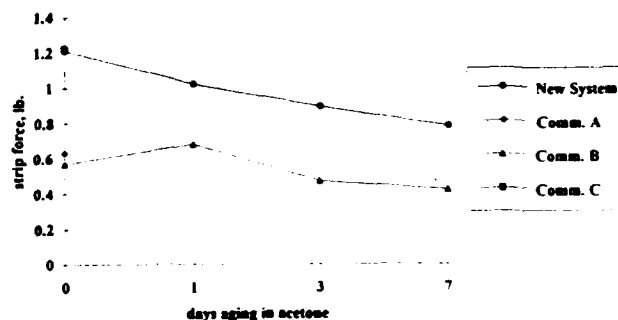


FIGURE 4. Strip force before and after exposure to petroleum-based wasp spray.



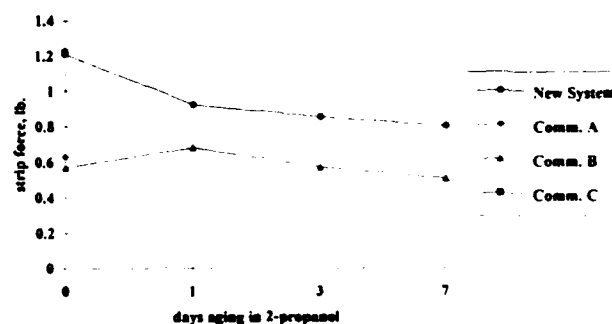
Exposure to common solvents is a hazard which will be encountered more and more frequently as fiber is deployed in the local loop environment due to the higher number of splices and terminations. The New System along with Commercial A, B and C fibers were immersed for seven days in acetone, in 2-propanol, and in a 30 percent ammonia solution, examining the strip force at intervals in the test. Figures 5 through 7 show the results. Commercial A and Commercial C coated fibers completely lost their coatings early in the exposures to acetone and 2-propanol while the New System and Commercial B fiber maintain in-specification strip force.

FIGURE 5. Strip force with time immersed in acetone.



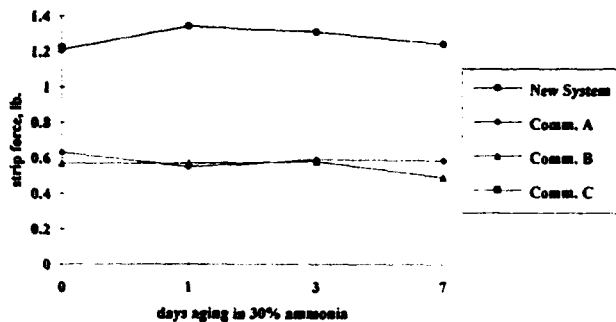
note: The Commercial A and Commercial C coatings spontaneously delaminated from the glass.

FIGURE 6. Strip force with time immersed in 2-Propanol.



note: The Commercial A and Commercial C coatings spontaneously delaminated from the glass.

FIGURE 7. Strip force with time immersed in 30% ammonia.



LOW TEMPERATURE ATTENUATION

In the more extreme climates of the North, optical fiber will be exposed to very low temperatures during the winter months. Especially inside cable, an individual fiber may be subjected to lateral forces due to thermal shrinkage of the coatings⁷ and to point stresses from crossovers and bumps inside jackets. These forces can result in microbending-induced added loss if the primary coating fails to buffer the fiber adequately, e.g. if the primary becomes too stiff to absorb the stress through deformation and instead transfers the stress through to the fiber. To aid in our understanding of the relationship between the primary coating mechanical properties and microbending-induced loss at low temperature, the mechanical characteristics of several primary coatings, including the New primary, were investigated via dynamic mechanical spectrometry and thermal mechanical analysis.

A Rheometrics Solids Analyzer was utilized to determine the storage and loss components, E' and E'' respectively, of the dynamic tensile modulus, E^* , isothermally through a range of oscillatory frequencies from 0.1 to 100 radians/second. Typically, these "frequency sweeps" were obtained at each of a number of temperatures from about 40°C down to -60°C, changing the temperature in 5 to 10°C increments between measurements. The primary coatings were cured at 1.0 J/cm² in a film thickness of approximately 250 microns. Rectangular strips of about 5 mm width were cut from each material for the measurements. Care was taken to maintain a small, static strain in the samples at each temperature, such that the samples remained in tension as the dynamic strain oscillated about the static strain level.

The frequency sweeps for each material were shifted on the frequency axis, applying the principles of time-temperature superposition⁸, to form smooth curves (usually termed "master curves") of E' and E'' vs reduced frequency. Master curves are shown in Figure 8 for the New System primary coating and in Figure 9 for the primary coating used in both the Commercial A and C systems, where the reference temperature is 25°C for each curve.

The dynamic modulus may be converted to stress relaxation vs time at any temperature within the bounds of experimentation by first shifting the master curve to the temperature of interest via the temperature dependent frequency shift factors, then calculating the transformation via the following relation⁹,

$$E(t) = E'(\omega) - 0.40E''(0.40\omega) + 0.014E''(10\omega) \quad (1)$$

where ω is the dynamic oscillatory frequency. Figure 10 shows $E(t)$ with time at -40°C for this example of the two primary coatings. The data quantifies how the stress in each coating decreases with time under a constant strain such as might be caused by a point load on the fiber. Note that a stress induced by a strain in the New primary relaxes to near the equilibrium (rubbery) modulus within about 30 hours, while similar relaxation in the other material requires several

orders of magnitude longer time at -40°C.

FIGURE 8. Master curve of tensile storage and loss modulus, E' and E'' , for the New primary coating.

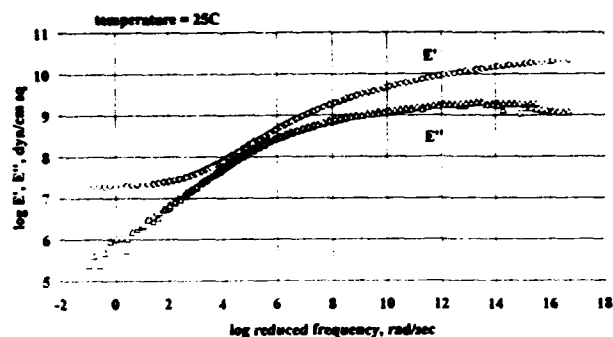


FIGURE 9. Master curve of tensile storage and loss modulus, E' and E'' , for the Commercial A and C primary coating.

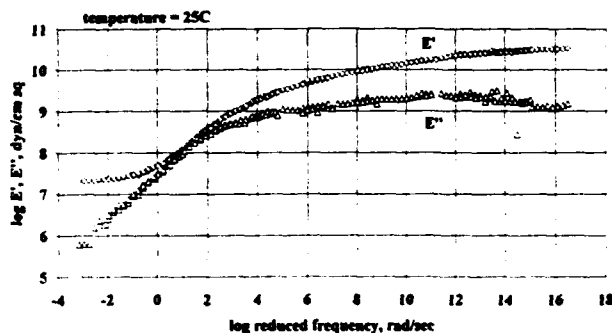
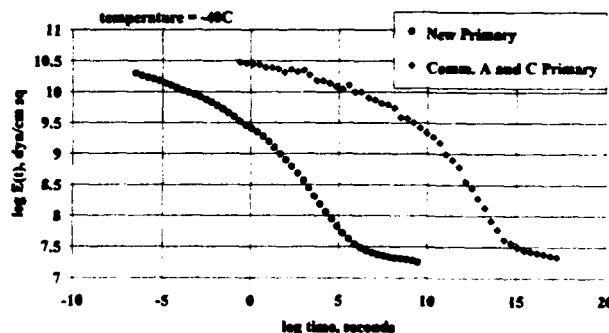


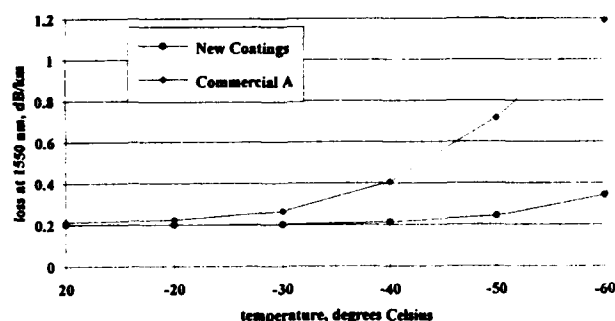
FIGURE 10. Tensile stress relaxation modulus $E(t)$ vs time for the New primary coating and the Commercial A and C primary coating. The temperature is references to -40°C.



To relate this information to on-fiber data, we employed a fiber packaging technique, sometimes referred to as a "basketweave" wind, on a quartz spool. Approximately two kilometers each of fiber with the New System and with Commercial A were wound on a spool under 50 grams tension with the traverse, or lay, set to 1.0 cm per turn on the spool. This introduces many crossovers in the fibers which act as

point loads on the coatings, creating a very microbend-aggressive configuration. Coated fibers were chosen for the winding such that the mode field diameters were similar along with the coating thicknesses. The loss was measured at room temperature, and then the fibers were cycled in a temperature chamber in 10°C increments down to -60°C, holding the temperature at each increment for 24 hours and measuring the attenuation in the fibers. Figure 11 shows the added loss relative to the room temperature, after-basketweave measurement at each low temperature for the two coating systems. The benefit of a primary coating which relaxes rapidly at low temperature is obvious.

FIGURE 11. Low temperature attenuation at 1550 nm for fibers with the New System and with the Commercial A system wound on a quartz spool in a basketweave configuration.



RELIABILITY

Heat and Humidity Effects

The deleterious effects of environments of high humidity and/or temperature can impact both optical fiber lifetime and handling characteristics. (The effects on strippability have already been discussed.) Such environments are found in the Southwest and Southeast geographical extremes in the U.S., and in underground installations in cities where, for instance, the fiber might be in proximity to leaky steam pipes. Here, lifetime is examined via static fatigue test in two-point bending, per the EIA/TIA 455-97 procedure, in an environment of 85°C/85% relative humidity. Precision bore silica tubes, ranging in size from 0.1574 inch to 0.2457 inch in inside diameter, were used to achieve stresses from 1.81 GPa to 2.89 GPa. For every coating system examined, at least three sets of 20 fiber specimens were tested at each stress level. The results are given in Figure 12 for the New Coatings, the previous coatings, and Commercial A and Commercial B fiber.

FIGURE 12. Static fatigue stress corrosion factors for the New System and several commercial systems. The fiber environment is 85°C/85% relative humidity.

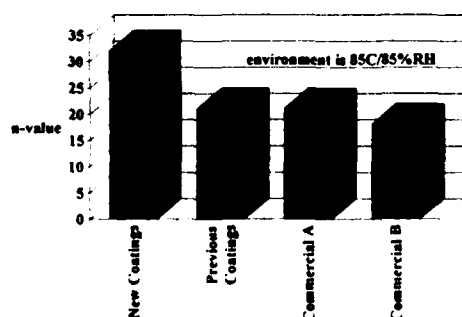


Table IV gives measurements of the moisture permeability of several secondary coatings, including that used by the Commercial A system. (The Commercial B and C secondaries are proprietary and unavailable for film testing.)

TABLE IV. WATER VAPOR PERMEABILITY MEASURED ON FILMS OF SECONDARY COATING

COATING	COEFFICIENT P*
New Secondary	0.0170
Previous Secondary	0.0290
Comm. A Secondary	0.0330

*The coefficient is lower for lower permeability, and is given in units of metric perm-centimeter.

Note that the New System secondary is the least permeable to moisture. Based on the results to date, the New System is the most protective against heat and humidity induced fatigue. These results carry over into dynamic strength tests, where 30 day, 85°C/85% RH aging of fiber coated with the New System typically results in a 5 to 10 percent increase in median strength over unaged fiber while maintaining a passing value for the Weibull slope parameter, m. Tables V and VI give typical 0.5 meter dynamic strength test results for the New System, Commercial A, Commercial B and Commercial C fiber, before and after the aging.

TABLE V. TYPICAL WEIBULL MEDIAN STRENGTH (A) BEFORE AGING AND (B) AFTER AGING AT 85°C/85% RH

COATINGS	(A) KPSI	(B) KPSI
New System	675	725
Commercial A	690	590
Commercial B	625	620
Commercial C	690	600

TABLE VI. WEIBULL SLOPE PARAMETER, m, (A) BEFORE AGING AND (B) AFTER AGING AT 85°C/85% RH

COATINGS	(A) m	(B) m
New System	140	45
Commercial A	142	10
Commercial B	76	19
Commercial C	144	23

LOOSE TUBE CABLE PERFORMANCE

The New System has passed the Bellcore cable qualification test program in several loose tube cable designs including armored and non-armored constructions using the full range of colors for the fiber. To highlight the test results:

- on average, zero added loss at 1310 or 1550 nm on cabling
- on the second temperature cycle to -40°C, the average added loss at 1550 nm was 0.01 dB/km with a maximum loss of 0.05 dB/km
- on the second temperature cycle to -40°C after 168 hours at 85°C, the average added loss at 1550 nm was 0.04 dB/km with a maximum loss of 0.08 dB/km
- in the cable freeze test, the average loss of power was 0.01 dB at 1550 nm with a maximum loss of power of 0.05 dB
- after 30 days in filling gels at 85°C and 85% RH, the fiber strip force exhibits negligible change from the unaged performance

PERFORMANCE IN RIBBON STRUCTURES

The New System has undergone extensive testing for fiber ribbon application, particularly in the European market where demands on coating performance can be especially rigorous. At this writing, some of the testing is incomplete, but in these the ribbon structures made with the New System are so far performing well where most other systems failed early on.

Tests performed in three different European units agree with the strippability results reported above, in that in both encapsulated and edge-bonded ribbon structures heat stripping a ribbon results in the clean removal of the desired portion of coating/ink/matrix as a unit leaving the fiber ends clean and bare for splicing.

Fiber breakout is excellent, with no transfer of color (noting that only UV-curable inks have been used to date).

In temperature cycling tests from +85°C to -60°C the maximum loss occurred at -60°C with added loss of 0.012 dB/km at 1310 nm and 0.018 dB/km at 1550 nm. In the 21 day, 20°C water sink test, the maximum loss at 1310 nm was at 9 days with 0.03 dB/km added loss for one fiber, and at 1550 nm the fibers exhibited "added" loss of less than zero with one fiber showing 0.01 dB/km added loss at 22 days.

In the 60°C water sink test, approximately 300 hours of the required 670 hours are complete as of this writing. The requirement under consideration presently is that no fiber exhibit 1.0 dB/km added loss during the test. Several commercial systems included in the test have already failed. The New System with two different inking systems are currently showing a maximum added loss of 0.23 dB/km with one ink and 0.1 dB/km with the other ink system.

SUMMARY

A new coating system has been introduced to meet the rigorous demands of both loose tube and ribbon applications in tomorrow's long lines and local loop markets. The introduction is the result of a careful study to correlate the material properties of fiber optic coatings with the on-fiber performance, which has been followed by this new coating design that successfully addresses the broadening performance challenges in the world's markets and environments.

Alcatel remains committed to continuing product improvement. The authors are maintaining a program to increase the understanding of the coating material properties/performance relationships. As better models are developed to describe the immensely complex interactions of the fiber and its two coatings, still further improvements in the coating systems are expected.

¹D. B. Keck, *Photonics Spectra*, pp 93-94, January, 1993.

²D. A. Simoff, M. G. Chan, J. T. Chapin, B. J. Overton, *Polymer Engineering and Science*, Vol. 29, 1177, 1989.

³D. S. Szum, C. P. Chawla, T. E. Bishop, K. P. Murray, J. M. Zimmerman, *Proceedings of the 39th International Wire and Cable Symposium*, p 703, 1990.

⁴N. E. Hardwick, III, K. Kathiresan, J. G. Hartley, *Proceedings of the 41st International Wire and Cable Symposium*, pp 158-167, 1992.

⁵S-T Shive, S. Lee, *Journal of Applied Physics*, Vol. 72, no. 1, pp18 - 23, July, 1992.

⁶P. C. P. Bouten, D. J. Broer, C. M. G. Jochem, T. P. M. Meuwissen, *Polymer Engineering and Science*, Vol. 29, no. 17, pp 1172 - 1176, 1989.

⁷S. T. Shive, *IEEE Photonics Technology Letters*, Vol. 4, No. 7, pp746-748, July 1992.

⁸see, for example, J. D. Ferry, *Viscoelastic Properties of Polymers*, 3rd edition, p 271 (1980, Wiley & Sons, New York).

⁹K. Ninomiya, J. D. Ferry, *Journal of Colloidal Science*, Vol. 14, p 36, 1959.



Bob J. Overton is a Senior Principal Scientist in the Fiber Development Group at Alcatel Telecommunications Cable in Roanoke, Virginia. He received a B.S. in Chemistry from Mercer University in Atlanta, GA and the M.S. in Polymers from the Georgia Institute of Technology. After 14 years with AT&T Bell Laboratories working in fiber optic coatings and cable materials, he joined Alcatel in 1991 and is at present responsible for the development of coatings and fiber strength improvement. He holds five patents in various areas of fiber optics materials science and processing and has a number of publications on fiber optic materials and processes in journals and symposia proceedings.

Adolphe R. Lopez is a Visiting Scientist with the Alcatel Telecommunications Cable Fiber Development Group in Roanoke, VA. He received a Ph. D. in Materials Chemistry from the University of Rennes in 1991, where he focused on specialty glasses for optical fibers and novel methods for fabricating very high purity glass. Since then he has worked in materials development at Alcatel Alsthom Recherche in Marcoussis, France, and in coatings development in the U. S. His work has been published in *Annals of Chemistry: Materials Science*, the proceedings of the "High Temperature Material Properties Symposium", and the proceedings of the SPIE Optical Fiber materials and Devices Symposium.



Henri-Marc Michaud joined Alcatel Fibres Optiques in Bezons, France, as a Process Engineer after receiving his Ph. D. in Materials Science and Engineering from the Institut National Polytechnique de Grenoble in 1991, where his research focused on determining the mechanisms of inter-granular deformation within bi-crystals of germanium. His current responsibilities include the development of new equipment and processes for optical fiber fabrication. He has authored a number of papers on the application of X-ray diffraction and electron microscopy to the study of the microstructure and deformation of crystals.



Ronald G. Sommer is Manager for Fiber Optic Development at KABEL RHEYDT AG (formerly AEG KABEL AG). He received a Ph. D in Physical Chemistry from the University of Iowa in 1974 and has since worked continually in the area of optical fibers. He joined AEG KABEL in 1987 after working previously in the United States and the United Kingdom.



Claude Lasne is a Research Engineer with the Materials and Characterization Group of Alcatel Alsthom Recherche in Marcoussis, France, having joined Alcatel after graduating from Dijon University (France). He worked in the development of new technology materials for electrotechnique applications, then turned to analytical activities, particularly the mass spectrometry of solids. He is now dealing with polymer characterization by thermal and infrared techniques as applied to the development of polymer coatings. He has authored several papers on sodium-sulfur electrochemical batteries, analysis of solids by spark source mass spectrometry, and hydrogen generation from structural materials of fiber optic telecommunications cables.

Development of a 100-fiber submarine cable

Nobuyuki YOSHIKAWA and Tadatoshi TANIFUJI

NTT Telecommunication Field Systems R&D Center
Tokai-Mura, Naka-Gun, Ibaraki-ken, 319-11, Japan

Abstract

NTT has developed a 100-fiber submarine cable. This is the first submarine cable with a fiber ribbon and "air-core" structure. The fiber ribbons are packed into slots arranged helically on a polyethylene rod which is installed in stranded steel wires covered with a pressure resistant copper pipe. A new absorbent tape prevents water from penetrating in the cable. Experimental results revealed its excellent watertightness. The compact structure facilitates fibre identification and fiber splicing and reduces cost. A sea trial was conducted at a depth of 3000m and confirmed that the overall performance was excellent.

1. Introduction

NTT has been developing original submarine optical fiber cables and related technologies since the 70s as shown in Fig.1, and research on prototype submarine cable using graded index fiber began in 1977[1][2]. In March 1980, sea trials were first conducted on burying armored cable at Takehara, Hiroshima. The structure of the shallow sea cable composed of Si-Ny coated fibers, a single copper pipe, and torque-balanced two-layered armor[3]. In 1982, we developed our first commercial cable with single-mode fibers and a strong pressure-resistant structure of tension wires sandwiched between inner and outer copper pipes. Water was prevented from penetrating the cable by jointing boxes[4] connected to the cable every 5 kms. The coated fiber diameter was 0.9mm. A deep sea cable for use at depths of up to 8000m[5] and which is itself watertight was developed in 1985[6]. A fiber coated with UV curable resins and 0.4mm in diameter and a watertight optical unit were developed. A high-strength fusion splice

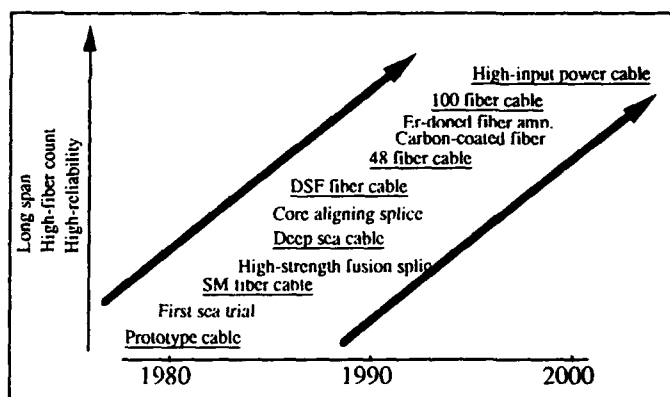


Fig.1 Recent cable development at NTT

technology and core aligning fusion splice technology[7] were developed and the cable unit length increased to more than 40km. In 1986, a dispersion shifted fiber for 1.55 μ m wavelength usage was used in cables, extending the non-repeated transmission span to 120km[8]. The expansion of optical networks created a need for the development of multi-fiber submarine cables. In 1989, a 48-fiber cable using coated-fibers 0.25mm in diameter was developed[9].

The recent development of carbon-coated fibers (CCF) has greatly improved the long-term reliability of mechanical and transmission characteristics, and we have improved on their initial strength for practical application[10][11]. The development of Er-doped fiber amplifiers has extended the transmission distance of cables and has promoted a need for a non-repeated system. The system is flexible, economical, as well as highly-reliable. The expansion of optical networks also required submarine cables to be compatible with land cables in the number of fibers. Consequently, we developed a 100-fiber cable[12].

2. Fundamental design

The cross section of the newly developed 100-fiber cable is shown in Fig.2. Five 4-fiber ribbons are packed tightly into slots arranged helically on a polyethylene rod. This is the first submarine cable which uses ribbon fibers. Also, this is the first "air-core" type submarine cable in the world. A sea water absorbent tape is arranged around the slots to prevent water from penetrating in the cable. A slight strain is intentionally retained in the fiber during the cabling process to prevent fiber slippage during laying and recovery. The cable structure is very simple and is basically different from the conventional cable structure.

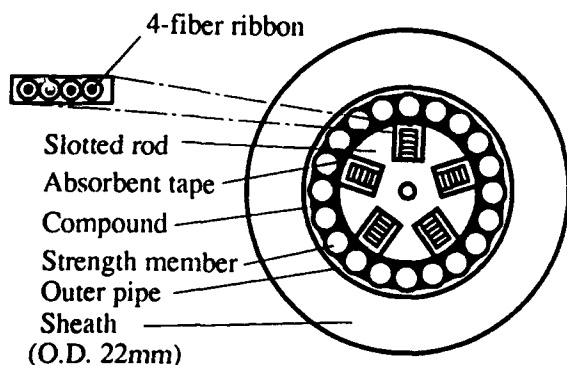
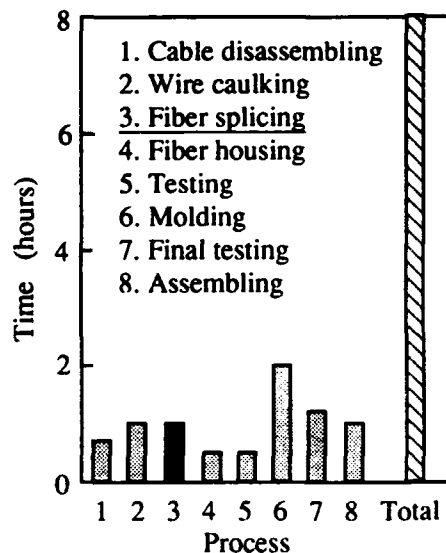
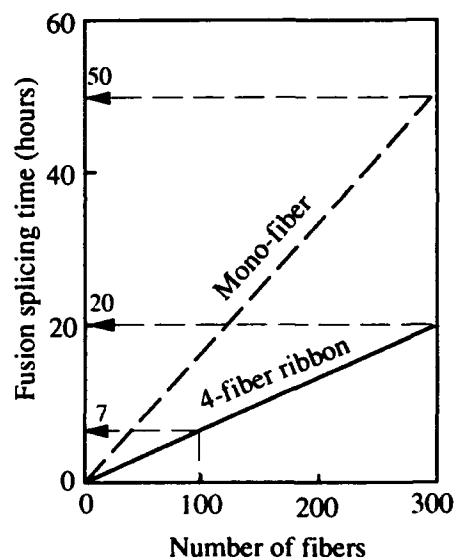


Fig.2 Cross-section of a 100-fiber cable.

The new structure satisfies many requirements, resulting from the increase in the number of fibers used in cables. Since ocean weather conditions can quickly change, the repair of submarine optical fiber cables must be performed within 24 hours. Splicing a 100-fiber cable one fiber at a time, however, is simply too time consuming. Figure 3(A) shows a typical histogram of cable repair time on cable ship. Cable jointing procedure after cable recovery is an 8-step process. A 6-fiber cable takes 8 hours to repair. Figure 3(B) shows calculated fusion splicing time versus number of fibers. It takes about 10 minutes for fusion splicing of a conventional mono-fiber. For a 4-fiber ribbon, it is about 16 minutes. Calculated results indicate the possibility of 300-fiber splices within 20 hours for a 4-fiber ribbon.



(A)



(B)

Fig.3 Time histogram of cable jointing.

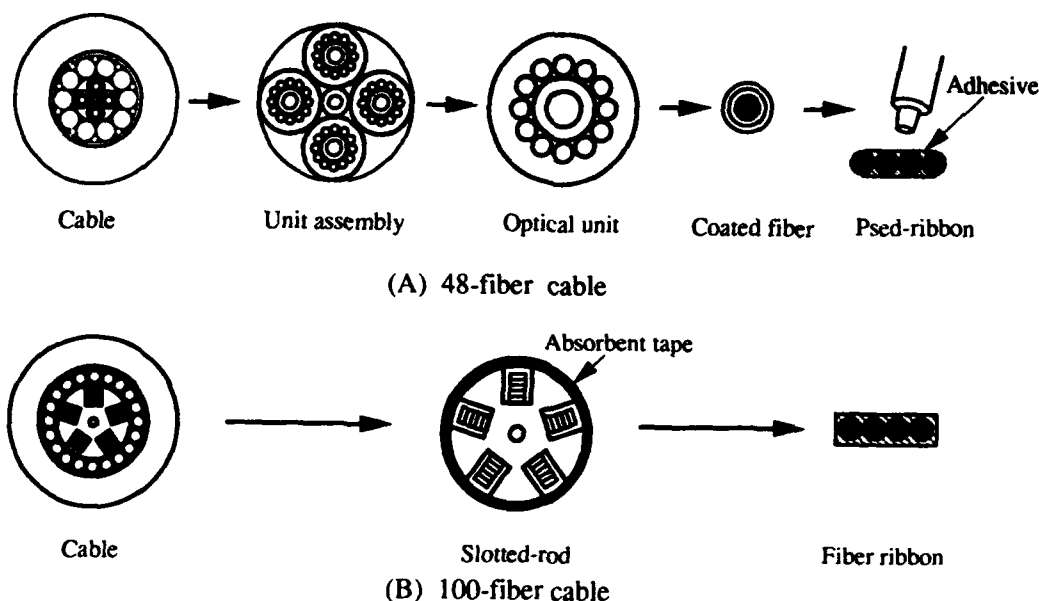


Fig.4 Cable disassembling process.

Figure 4 shows the disassembling process of a cable. In a conventional 48-fiber cable, all fibers are coated with uv-curable resins in order to form a watertight optical unit. Separating fiber from the optical unit is very delicate process, requiring skill and patience. Unintentional fiber breakage means starting over. For practical purposes, 48 is the maximum number of fiber for this type of structure. In a 100-fiber cable, however, fibers are much easier to separate and require less technical skills. This is possible because of the "air-core" structure which has proven itself in land cables. The "air-core" structure can prevent strain increase caused by cable bending. Because of these merits, we decided to use a 4-fiber ribbon and "air-core" structure in a submarine cable. In order to reduce mass-fusion splice loss, we are developing compact mass axis alignment splicing equipment using micro robotics[13]. Figure 5 shows a comparison of the cabling process of a conventional 48-fiber[9] cable and the 100-fiber cable. The new cable structure is simple and economical. Assembling four 12-fiber optical units in the 48-fiber cable is a five-step process. The 25 4-fiber ribbons of the 100-fiber cable, however, are packed into the slots

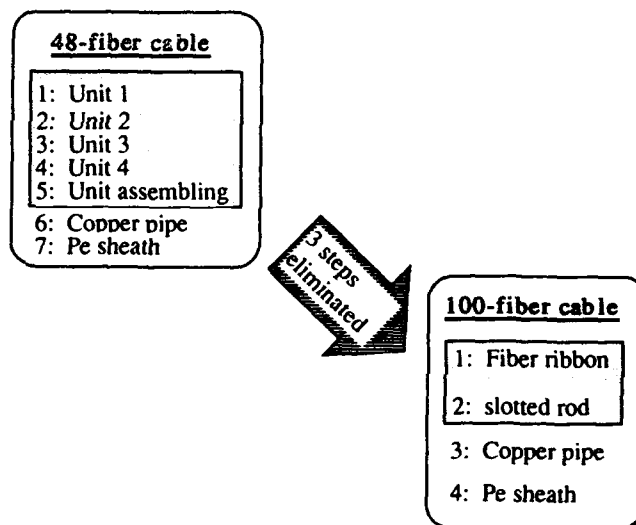


Fig.5 Cabling process

in a one-step process. This significantly reduces the cost. The compact structure also makes it easier to identify fibers, and it may make it possible to increase the number of fibers in the future.

3. Cable characteristics

The structure using ribbon fibers and a slotted rod was originally designed for land cables. To adopt this structure for submarine cables, we had to cope with many requirements that are particular for submarine cables. The requirements include mechanical strength, optical loss stability, water-tightness, and high reliability. Figure 6 shows the relationship between load applied to the outer pipe and its ellipticity. We applied lateral load to the outer pipe without a polyethylene sheath, and without a slotted rod, the applied load deforms the wire array and the shell effect decreases. The dash-dotted line shows the calculated copper pipe deformation ignoring the shell effect of the stranded wires. The solid dots show measured values with a slotted rod. The experimental results confirm that the structure is sufficiently strong. The slotted rod helps maintain the wire assembly array and thus its rigidity. The slotted rod also prevents the outer pipe from buckling under hydraulic pressure. The maximum application depth of the 100-fiber cable is 3000 m. Figure 7 shows the characteristics of the water absorbent tape developed for the 100-fiber cable. Drops of sea water applied on the 0.3 mm thick absorbent tape and its height change versus time were measured. The volume quickly expands and shuts off the water path in the cable. The water blocking abilities of the cable were measured.

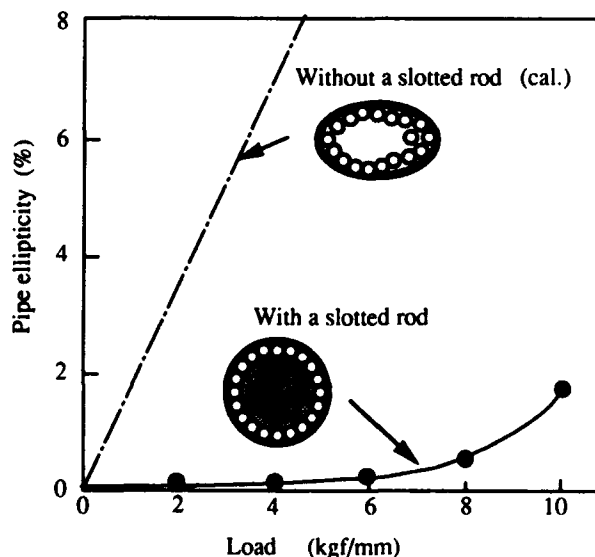


Fig.6 Relationship between lateral load and pipe ellipticity.

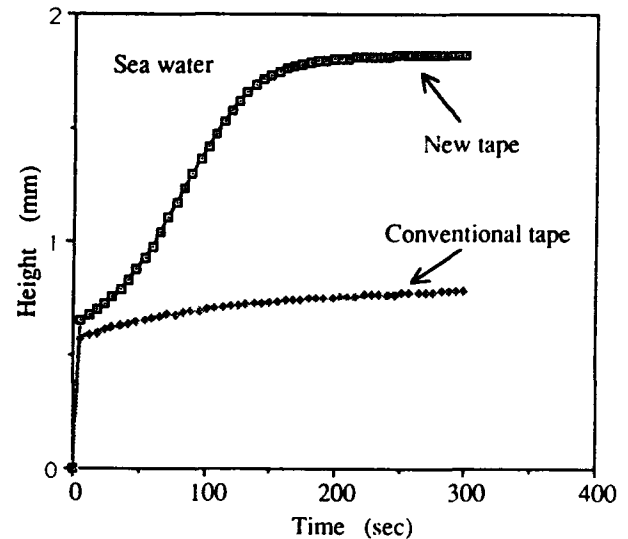


Fig.7 Water absorption characteristics of absorbent tape for submarine cable.

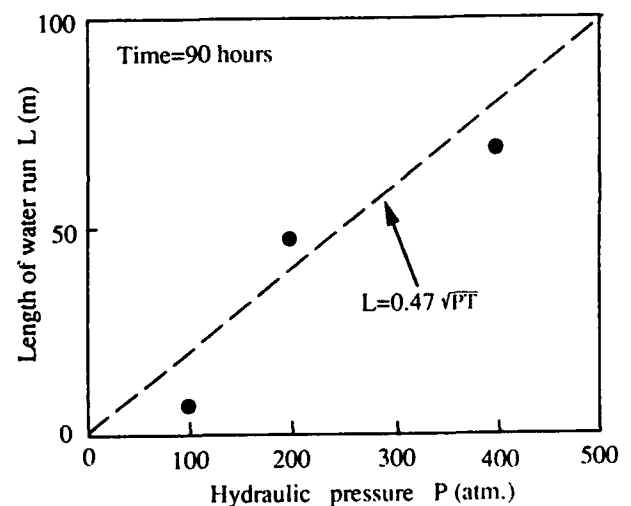


Fig.8 Relationship between hydraulic pressure and length of water run.

Figure 8 shows the relationship between hydraulic pressure and length of water run in a cable. Hydraulic pressure using artificial sea water was suddenly applied to one end of a 100m cable, and we measured the time it took for the sea water to come out the other end of the cable. After 90 hours, however, we observed no water. We disassembled the cable

and measured the length of water run in the cable. In spite of the "air-core" structure, length of water run was 68 m at a pressure of 400 atms. The value is smaller than that of a conventional deep-sea cable[6]. Assuming that the length of water run L is in proportion to the square root of the hydraulic pressure P and time T , we obtain $L=0.47\sqrt{PT}$. Length of water run for two weeks at a depth of 3000m is calculated at only 150 m. The absorbent tape also works as a dryer. When a submarine cable is laid on the sea bottom, cable temperature decreases and the humidity in the cable's air turns to dew. In this case, the absorbent powder captures the humidity and dew in the cable, keeping the fibers dry. Figure 9 shows the relationship between relative humidity and the increase in saturation weight of absorbent tape. Temperature dependence of the absorbent tape is low. Assuming the weight increase of absorbent tape during cable manufacturing at 25°C is 10%, relative humidity in the cable at the sea bottom of 5 °C becomes about 43%. This dry condition helps maintain the long term reliability of the fiber.

The use of carbon coating on silica fiber can greatly improve fiber reliability by preventing both mechanical fatigue and hydrogen induced loss increase[14][15]. In the early stages of development, we found that surface roughness of carbon-coated fiber (CCF) has a certain relationship with its initial strength. We proposed and demonstrated for the first time in this field that a scanning tunneling microscope (STM) can be used to measure the roughness[10]. This fact indicated a way to improve the strength. As a result, we developed a CCF whose initial strength is as large as that of non-hermetic fibers which also has a high n -value (fatigue resistance parameter) and maintains resistance to hydrogen-induced optical loss. We have already carried out a field test on CCF[16] and decided to apply them practically to 100-fiber submarine cable. The required proof strain is derived from a proof theory[17] and takes into account the residual fiber strain after cable laying[18]. Figure 10 shows the calculated relationship between allowable strain over a 20-year period and n -value for cases with proof strain levels of 1% and 2%. For a conventional fiber with $n=20$, the allowable strain is 0.5% for 2% proof strain. In contrast, the value is about

0.8% even for 1% proof strain, because of its high n -value of 150. Low-proof strain CCFs are less expensive than conventional high-proof strain fibers, despite the added cost of carbon-coating.

Table 1 summarizes main features of the 100-fiber cable. Cable diameter and weight are nearly the same as those of a conventional deep-sea cable[9][19].

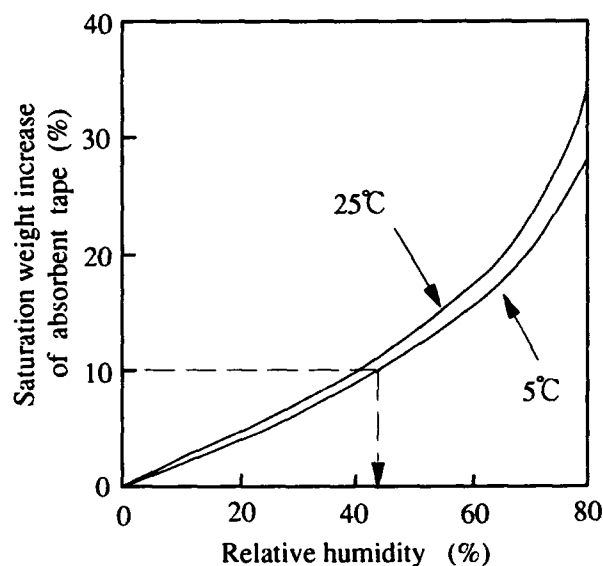


Fig. 9 Humidity absorption characteristics of absorbent tape.

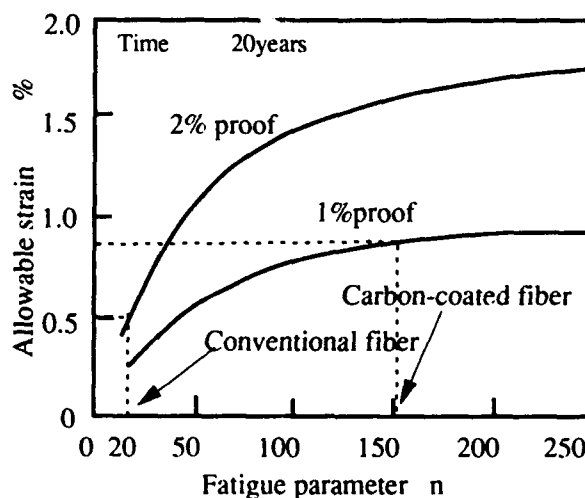


Fig.10 Required proof strain for conventional fiber and carbon-coated fiber.

Table Outline of 100-fiber cable

Number of fiber	Less than 120
Fiber type	4-fiber ribbon
System type	Non-repeated
Application depth	3000 m
Break tension	10000kg
Allowable load	100 kg/cm
Cable weight	1kg/m in air 0.5kg/m in water
Cable diameter	22.5 mm
Watertightness	Excellent
AC signal supply	Possible

4. Sea trial results

A sea laying and recovery test was performed on 5500 m of a prototype 100-fiber cable using the Kuroshio-maru cable ship. The test was performed in the area of Bousou-oki having an average ocean depth of 3000 m. Two pieces of the cable were connected at a joint box, and fibers were spliced at an end box and formed 11000 m of loop configurations. Pay-out was performed from the bow of the ship using a drum engine, and laying proceeded at two knots. The ship was then brought to a stop for 2 hours followed by cable recovery at about two knots. The maximum cable tension during recovery was less than 3 tons. The optical loss change of 6 loops during the sea trial are shown in Fig. 11. Measured fibers were single-mode for 1.3-micron usage and the light-source wavelength was 1.3-micron. In respect to cable laying, a maximum increase of 30 mdB occurred for the 11000m of loop. Converting these figures to km, we obtained a maximum increase of less than 3 mdB/km, which is small, verifying that the cable is stable. The loss returned to the initial value after cable recovery. The fiber length change during the sea trial is shown in Fig. 12. The length change

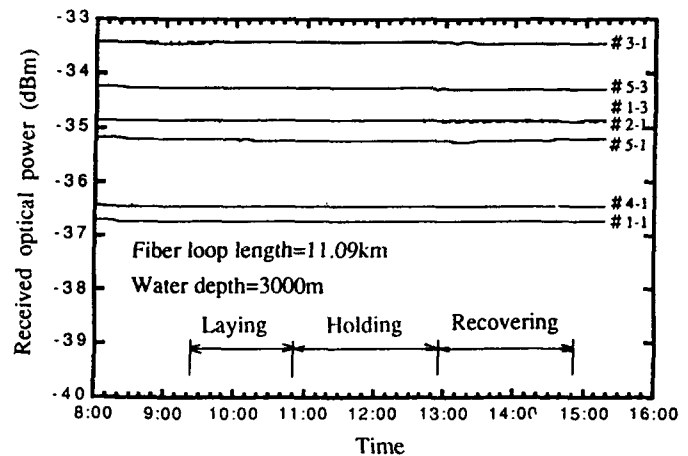


Fig 11. Optical loss change during sea trial.

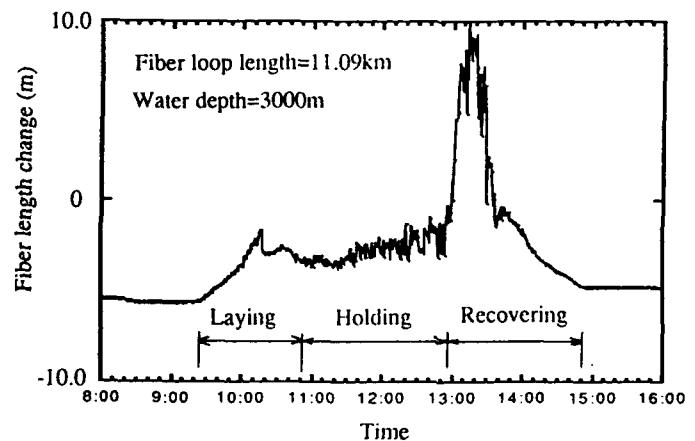


Fig.12 Fiber length change during sea trial.

was measured by the pulse-phase method and the results include the effect of temperature change. Since the vertical axis in the figure indicates the change in length of a fiber loop, cable elongation should be taken as half of these values. The length change showed good agreement with the cable tension change. The residual elongation before cable laying and after recovery is about 1 m. Converting this value to residual strain, we obtained 0.02% because pay-outted cable length was 5000 m. The results indicate that all ribbon fibers in the slotted rod are tightly held, and no slippage occurs between the ribbon fibers and the slotted rod during laying and recovery. Figure 13 shows the wavelength dependence of

optical-loss measured in the cable ship. Three lines in the figure indicate the characteristics before laying, during holding, and after recovery, respectively. Measured differences are within the level of measuring accuracy. This fact indicates that no change occurred in the bending radius of the fibers along the 5000 m of cable during the sea trial.

All these results indicate the stable transmission characteristics of the newly developed "air-core" submarine cable.

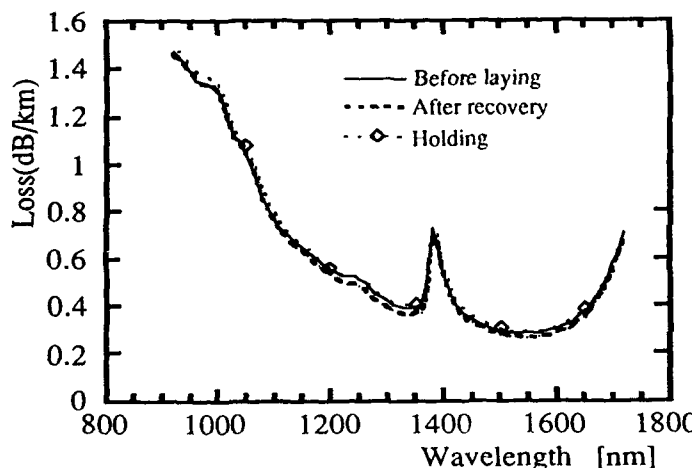


Fig.13 Wavelength dependence of optical loss during sea trial.

Summary

NTT developed a 100-fiber submarine cable. This is a unique submarine cable because it adopts 4-fiber ribbons and "air-core" structure for the first time for submarine cable. Many merits such as easiness of fiber identification, time saving in splicing, compactness, and low price, were derived from the new structure. Development of a new absorbent-tape for sea water enabled to establish this structure.

This cable, together with carbon-coated fibers, will be introduced into the two sections between Wakayama and Tokushima (18 km), and between Matsuyama and Ohita (60 km) this autumn.

Acknowledge

The authors would like to thank Dr. M. Kawase for his valuable advice and suggestions. The authors also thank the staff members of the NTT Submarine Cable Engineering Center for their support during the sea trial.

References

- [1] N. Kojima, T. Yabuta, Y. Negishi, K. Iwabuchi, O. Kawata, K. Yamashita, Y. Miyajima and N. Yoshizawa, "Submarine optical fiber cable development and laying results", *Applied Optics*, Vol.21, No.5, pp. 815-821, 1982.
- [2] K. Yamashita, Y. Murakami, K. Ishihara, Y. Negishi and N. Kojima, "Design of a submarine optical-fiber cable using graded-index multimode fibers", *IEEE J. Lightwave Technol.*, Vol. LT-1, No.2, pp. 346-353, June 1983.
- [3] T. Yabuta, N. Yoshizawa and N. Kojima, "Cable kink analysis: cable loop stability under tension", *ASME, J. Applied Mechanics*, Vol.104, pp. 584-588, 1982.
- [4] S. Furukawa, O. Kawata, K. Ishihara and Y. Negishi, "Structural design and sea trial results for a submarine optical-fiber cable joint box", *IEEE J. Lightwave Technol.*, Vol. LT-2, No. 4, pp. 550-558, August 1984.
- [5] Y. Negishi, K. Ishihara, Y. Murakami and N. Yoshizawa, "Design of deep-sea submarine optical fiber cable", *IEEE J. Lightwave technol.*, Vol. LT-2, No. 6, PP. 839-845, 1984.
- [6] N. Yoshizawa, M. Ohnishi, K. Ishihara and Y. Negishi, "Water propagation blocking properties of submarine optical fiber cable", *IEE Electronic Lett.*, Vol.21, No.18, pp.796-798, 1985.
- [7] O. Kawata, K. Hoshino and K. Ishihara, "Core-axis-alignment method to achieve ultra-low-loss fusion splicing for single-mode optical fibers", *Optics Letters*, Vol.9, pp. 255-256, June 1984.
- [8] Y. Negishi, Y. Murakami, O. Kawata and N. Yoshizawa, "First sea trial of 1.5 μ m submarine optical fiber cable", *IEEE J. Lightwave technol.*, Vol. 6, No. 2, pp. 281-286, February 1988.
- [9] N. Yoshizawa, T. Yada, T. Horiguchi and T. Kurashima, "Design and sea trial results of a 48-fiber submarine optical fiber cable", *Trans. IEICE*, Vol. J71-B-I, No. 6, pp. 495-503, June 1991. (in Japanese)
- [10] N. Yoshizawa, H. Tada and Y. Katsuyama, "Strength improvement and fusion splicing for carbon-coated optical fiber", *IEEE J. Lightwave Technol.*, Vol. 9, No. 4, pp. 417-421, April 1991.

[11] N. Yoshizawa, Y. Miyajima and Y. Katsuyama, "A one-hundred-fiber submarine cable composed of hermetically-coated fiber ribbons inserted into slots", Proceedings of IWCS, 1989, pp. 603-610

[12] N. Yoshizawa and T. Tanifuji, "Advanced submarine optical fiber cable technologies at NTT", 2nd International Conference on Optical Fiber Submarine Telecommunication Systems, pp. 290-295, March, 1993

[13] S. Aoshima, N. Yoshizawa and T. Yabuta, "Compact mass axis alignment device with piezoelements for optical fibers", IEEE Photonics Technol. Lett., Vol. 4, No. 5, pp. 462-464, May, 1992.

[14] M. Ohnishi, N. Yoshizawa, Y. Miyajima, O. Kawata and Y. Negishi, "Loss stability assurance against hydrogen for submarine optical fiber cable", IEEE J. Lightwave Technol., Vol. 6, No. 2, February 1988.

[15] K. Noguchi, N. Shibata, N. Uesugi and Y. Negishi, "Loss increase for optical fibers exposed to hydrogen atmosphere", IEEE J. Lightwave Technol., Vol. LT-3, pp. 236-243, 1985.

[16] Y. Katsuyama, N. Yoshizawa and T. Yashiro, "Field evaluation result on hermetically coated optical fiber cables for practical application", IEEE J. Lightwave Technol. Vol. 9, NO. 9, pp. 1041-1046, September 1991.

[17] Y. Miyajima, M. Ohnishi, O. Kawata, K. Ishihara and Y. Negishi, "Fiber strength assurance for deep-submarine optical-fiber cable using the proof-testing method", IEEE J. Lightwave Technol., Vol. LT-3, No. 2, pp. 248-255, April 1985.

[18] T. Kurashima, T. Horiguchi, N. Yoshizawa, H. Tada and M. Tateda, "Measurement of distributed strain due to laying and recovery of submarine optical fiber cable", Applied Optics, Vol. 30, No. 3, January 1991.

[19] K. Ishihara, O. Kawata and N. Yoshizawa, "Design and characteristics of submarine optical fiber cable", Review of ECL, Vol. 33, No. 6, pp. 911-916, 1985.

Nobuyuki Yoshizawa NTT

Telecommunication
Field Systems Research
& Development Center
Tokai, Ibaraki,
319-11, JAPAN



Nobuyuki Yoshizawa is a senior research engineer. He was born in 1954. He received B.E. and M.E. degrees in mechanical engineering from Waseda University in 1977 and 1979, respectively. In 1979, he joined NTT where he has been engaged in research on submarine optical fiber cables and carbon-coated fibers. His current interest includes suppression of stimulated Brillouin scattering. Dr. Yoshizawa is a senior member of IEEE.

Tadatosahi TANIFUJI NTT

Telecommunication
Field Systems Research
& Development Center
Tokai, Ibaraki,
319-11, JAPAN



Tadatosahi Tanifuji is the leader of high count optical cable research group. He was born in 1949. He received B.E. and M.E. degrees in electronics engineering from Hokkaido University in 1972 and 1974, respectively. He joined NTT in 1974. Since 1991, he has been engaged in research on a 100-fiber submarine cable and a high-density and pre-connectorized optical fiber cable. Dr. Tanifuji is a member of IEEE.

DISPERSION MANAGEMENT IN LONG-HAUL OPTICALLY AMPLIFIED SUBMARINE SYSTEMS

J. N. Russell * N. H. Taylor** K. C. Byron*** I. J. Blewett****

* STC Submarine Systems Limited, Southampton SO9 4YZ, UK

*** BNR Europe Limited, Harlow CM17 9NA, UK

** STC Submarine Systems Limited, London SE10 0AG, UK

**** Heriot Watt University, Edinburgh, UK

ABSTRACT

Long-haul optically amplified systems require tight control of the fibre chromatic dispersion. Why this is, and how it can be achieved practically, are examined in this paper. Experimental results are presented on the variation of fibre chromatic dispersion due to environmental effects. These show that the effect of temperature in particular needs to be taken into account in planning the dispersion management of the system. Experience is reported on the chromatic dispersion measurement limitations encountered in building a 6300 km test bed.

BACKGROUND

In conventional repeated systems any degradation in the optical signal is effectively removed by the re-timing that occurs in every regenerator. This is not the case for optically amplified systems where imperfections in the transmitted optical signal accumulate along the whole length of the system. The designer of an optically amplified system has to control a number of parameters simultaneously, these include:

- Maintaining an adequate signal level
- Ensuring the noise accumulation is within specified limits
- Ensuring that the signal bits do not interfere with each other

The first two of these effects arise because of the fibre loss and amplifier noise, further details of their control can be found in the literature [1],[2]. This paper will concentrate upon the third effect, how in a practical system the design can ensure that the inter symbol interference (ISI) is small. It will consider the main causes of ISI, namely fibre chromatic dispersion and non-linearity and discuss how these need to be controlled in a practical system using dispersion management schemes. The effects of polarisation mode dispersion will not be considered as these are the result of a stochastic process which cannot be equalised.

An important consideration in these schemes is the additional contribution to dispersion arising from environmental effects on the fibre characteristics.

To provide this additional information in the management scheme, measurements have been carried out on the effects of pressure, temperature, strain and bending on the fibre chromatic dispersion characteristics. The results of these measurements and their impact on dispersion management are discussed in this paper.

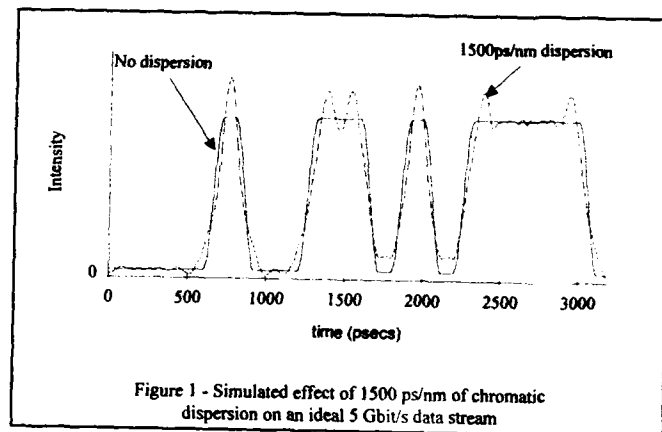


Figure 1 - Simulated effect of 1500 ps/nm of chromatic dispersion on an ideal 5 Gbit/s data stream

THE EFFECT OF CHROMATIC DISPERSION ON SYSTEM PERFORMANCE

This section will consider the mechanisms by which fibre dispersion and non-linearity can affect the overall system performance. It is assumed that the systems are not solitonic and that they will be operated in the 1550 nm window. This offers the lowest fibre loss and allows erbium doped fibre amplification.

Chromatic dispersion

In an optical fibre different wavelengths travel at differing velocities. The optical signal inevitably contains a range of wavelengths and this results in a broadening of the optical pulses causing ISI. Figure 1 shows the effect of chromatic dispersion on a data stream, the pulses are seen to have been broadened by the dispersion such that there is significant interference between them.

In order to minimise the effects of chromatic dispersion the system should be operated with the signal wavelength at the zero dispersion wavelength λ_0 of the fibre. It has been shown, however, [3] that if every fibre was to have exactly this dispersion zero, then large spectral broadening of the signal due to fibre non-linearity would occur. Fortunately, to reduce the effects of pulse broadening, it is only necessary to ensure that the average dispersion over the entire system is zero. One way of achieving this is to use a mixture of DSF (dispersion shifted fibre) and NDSF (non dispersion shifted fibre). The DSF is chosen to have a slightly negative dispersion at the signal wavelength and is used for the majority of the system, its dispersion is compensated for by short lengths of NDSF fibre which have a very large positive dispersion per unit length. This technique will be described in more detail in following sections.

The distortion caused by chromatic dispersion is proportional to the bandwidth of the signal itself. By the choice of suitable transmitter technology this will approach the spectral width of the modulating signal which, for a 5 Gbit/s system is approximately 0.04 nm. Chromatic dispersion by itself does not broaden the signal spectrum it only changes the relative phase delay between the different components.

Fibre non-linearity

The spectral width of the transmitted signal is so narrow that if chromatic dispersion was the only effect then this could be relatively easily overcome. This is demonstrated by the fact that commercially available systems operating at 2.5 Gbit/s are available that can tolerate up to 1500 ps/nm dispersion on NDSF fibre. A second effect however that must be taken into account on long-haul optically amplified systems is that of the spectral broadening of the signal caused by the fibre non-linearity.

The refractive index $n(t)$ of glass can be written as

$$n(t) = n_0 + n_2 \cdot I(t)$$

where n_0 and n_2 are the linear and non-linear parts respectively and $I(t)$ is the optical intensity at time t . The greater the intensity the greater the refractive index and the slower the light travels. Additional frequency components are generated as inter modulation products. This mechanism is variously known as self phase modulation or four wave mixing dependant upon the components involved.

Self phase modulation (SPM) is the broadening of the signal optical spectrum by the non-linearity. As the light intensity rises during the beginning of the pulse it undergoes an increasing phase shift since $n(t)$ increases and it travels slower. The rate of change of phase is equivalent to frequency therefore, during the rising and falling edges of the pulse, new frequencies are generated.

Four wave mixing is the inter modulation between the amplifier noise and the signal or between the noise components themselves. It is deleterious in that it is a mechanism that sucks power from the signal and converts it into noise.

The fibre non-linearities can cause large spectral broadening of the signal on very long systems as shown in figure 2. In order to be able to identify the received signal all of these wavelengths must travel at approximately the same velocity. Thus the effect of fibre non-linearity is to significantly tighten the required dispersion specification.

The effects of fibre non-linearity can be reduced by decreasing the optical intensity $I(t)$. This intensity is related to the power in the fibre $P(t)$ by

$$I(t) = \frac{P(t)}{A_{eff}}$$

where A_{eff} is the effective area of the fibre. This will become a key fibre parameter in future systems as an increase in A_{eff} will allow more power to be launched into the fibre for the same non-linearity. This in turn will lead to greater repeater spacing.

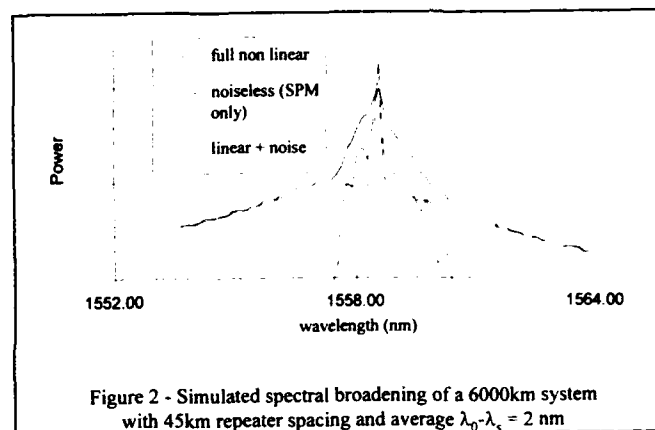


Figure 2 - Simulated spectral broadening of a 6000km system with 45km repeater spacing and average $\lambda_0 - \lambda_s = 2$ nm

Phase matching in fibres

Although fibre non-linearity will always lead to signal spectral broadening due to SPM and four wave mixing, these processes can be made less efficient by the choice of a suitable dispersion management scheme.

Efficient build-up of non-linear products occurs when there is a fixed phase relationship between spectral components over a significant length of fibre. Fortunately dispersion can reduce this. Consider a sharply rising pulse edge launched into the fibre. Initially, the large rate of change of intensity will give rise to sizeable spectral broadening. However, as the pulse propagates through the fibre, dispersion acts to slow the pulse edges and hence reduces this effect. Note; if the signal is always at exactly the λ_0 of the fibre this will not be the case which is why this condition must be avoided.

PRACTICAL SYSTEM DESIGN

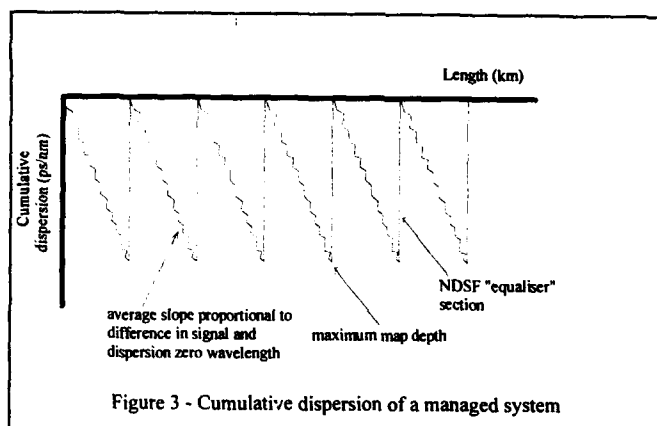
The fundamental mechanisms that affect the inter symbol interference were discussed in the previous section. The ways in which these affect a practical system design will now be covered and an example given of a possible method of managing the system dispersion.

Specifying the fibre chromatic dispersion

On current regenerative systems operating at up to 2.5 Gbit/s a loose dispersion zero specification of approximately 1535 nm to 1560 nm is all that is necessary. This is wide enough to make routine production measurements of dispersion unnecessary.

Long-haul optically amplified systems will require very much tighter specification of each fibre dispersion zero in order that the average value comes out very close to zero. This requirement must be met whilst allowing as much of the production fibre as possible to be used in order to reduce costs. It must also be met over the range of environmental conditions that the system will see during its life.

As discussed in the section on chromatic dispersion the use of slightly negative dispersion fibre with short sections of high positive dispersion NDSF allows a system to operate with close to zero chromatic dispersion whilst avoiding severe pulse broadening problems. Typically the NDSF cable will comprise less than 1% of the total. This allows some relaxation of the DSF specification as the exact length of NDSF can be selected to "equalise" the actual dispersion measured on the manufactured DSF cable.



Although the dispersion of individual fibres can be allowed to vary by several nanometres the average dispersion needs to be controlled to better than 1 nm. The control of average limits over a batch of fibres rather than hard go/no-go limits on every fibre represents a major change from current practice. It impacts upon the fibre procurement specification and on the control systems necessary within the cable factory to cater for possible reallocation of cable sections during manufacture.

Practical dispersion management using NDSF equalisers

The cumulative dispersion obtained using the chromatic dispersion management scheme discussed for a long-haul optically amplified system is shown in figure 3. The slope of the cumulative dispersion is proportional to the average offset of the DSF cabled fibre λ_0 and the signal wavelength.

If the cumulative dispersion is allowed to become too large then the rising and falling edges of the pulses become very slow and significantly interfere with each other. Self phase modulation therefore spreads not only the high frequency energy in the pulse edges which carry no information, but also the lower frequencies which do. This means that the ideal manufacturing situation of performing all the equalisation at the ends of the system may not be possible and intermediate NDSF fibre equalisers are required along the route.

Where intermediate NDSF equalisers are used then these will compensate several kilometres of fibre. By adding an additional constraint, that all fibres within the multi-fibre cable require the same degree of equalisation, then this could be provided by manufacturing "equalising" cable which is cut to the required length during system assembly.

Allowance for measurement inaccuracy on incoming fibre lengths

Long-haul optically amplified systems are among the first application of fibre optics that require chromatic dispersion to be measured to a high degree of accuracy. Dispersion zero differences of up to 2 nm have been reported on a round robin fibre measured by a number of laboratories. [4]. An internal study by STC and BNR(E) has shown that whilst this variability can be reduced to around 0.5 nm it will still be significant.

In order to ensure that the fibre dispersion zero wavelength does not approach that of the signal the average λ_0 must be specified to be longer by the measurement uncertainty than would otherwise be required.

ENVIRONMENTAL EFFECTS

Measurements

Measurements of environmental effects on primary coated dispersion shifted fibres have been carried out to identify the dominant influences on system bandwidth in the installed submarine cables.

Investigations have been carried out on the effects of temperature, pressure, strain and bend radius on the fibre dispersion as described below. All measurements of dispersion were made using an EG&G CD3 chromatic dispersion kit.

Temperature: The fibre under test was wound under low tension on to a glass bobbin and placed in an oven. Measurements of the dispersion characteristic were taken in steps of 20° from -20° to 80°C and then back again to -20°. At each temperature 2 hours elapsed before the measurement was taken in order to allow the fibre to reach thermal equilibrium.

Pressure: For these measurements the glass bobbin was placed in a high pressure water tank used for oceanic simulations of cable performance. The pressure was increased in steps of 1000 psi (6.89 MPa) from atmospheric pressure to 12,000 psi corresponding to an ocean depth of 8 km.

Strain: To measure the strain dependence a fibre was passed several times over the end pulleys of a long cable straining test apparatus. This consisted of a fixed pulley and a moveable pulley some 150 metres distant. The moveable pulley is attached to a winch and is used to strain the fibre by a controllable amount.

Bend Radius: The fibre was initially wound on to a drum with a bend radius of 155 mm and the dispersion characteristic measured. The fibre was then off-wound onto successively smaller drums always at the same winding tension of 100g. Between each smaller radius winding, the fibre was rewound onto the original drum to check for induced changes in its original dispersion.

Results

It was observed in all the investigations that there were no measurable changes in the dispersion slope over the wavelength range of interest (1530-1560 nm) and no hysteresis was observed in the dispersion characteristics. The effects on the dispersion characteristic may then be summarised by referring to the wavelength of minimum dispersion as a function of the environmental measurand. For the temperature, pressure and strain measurements, a straight line characteristic was obtained and the results are summarised in table 1 below.

Measurand	Measurement Range	Slope
Temperature	-20° to +80° C	0.030 nm/°C
Pressure	0 - 80 MPa	0.0076 nm/MPa
Strain	0 - 1.8 %	1.7 nm/%

Table 1 - Environmental effects on dispersion zero

It must be noted that these results were obtained on uncabled fibre. For a cabled fibre, the design of the cable can mask the effects of strain and pressure and these results probably indicate a worst case. The effects of temperature however are unlikely to be affected by cable design so allowance for this can be made at an early stage in system design without recourse to further measurements on the cabled fibre.

The effect of the bend radius on chromatic dispersion shows a change of 0.05 ps/nm/km corresponding to a shift in zero dispersion of about 0.6 nm for a bend radius of 40 mm. This is unlikely to have any noticeable impact on system design since only short lengths of fibre are wound on small radii reels in the repeaters. However, theoretical studies of the effect on bend for increasing index difference shows that for an index difference of 0.030 and a core diameter of 3.0 μm , the shift in zero dispersion wavelength is a few tens of nanometres [5]. Since the fibre for erbium amplifiers has a large index difference, the effect of bends may have some impact on system dispersion particularly in long amplified systems.

System implications of environmental effects

Cabled fibre is largely protected from the effects of pressure, strain and bending reported and hence the effect of these on the overall chromatic dispersion is likely to be small. Of more importance is the temperature dependence. Except for the continental shelves, most long amplified systems will be in very deep water where the temperature is relatively stable at approximately 2°C. This means that the dispersion zero of the cabled fibre will decrease by approximately 0.6 nm on laying. To compensate for this the equalisation cable added in the cable factory, where the temperature will be approximately 20°C, will need to under compensate for the measured dispersion. Fine tuning of the equalisation in the terminal stations will probably also be needed to optimise the system for the exact dispersion as laid.

MEASUREMENT OF CHROMATIC DISPERSION

The tight specification placed upon the dispersion of the fibres in a cable used for long-haul optically amplified systems makes it essential that accurate measurement techniques are available. We have built a 6300 km optically amplified test bed for which chromatic dispersion measurements were made of every constituent fibre. We found that, whilst commercially available dispersion sets provided the necessary repeatability, accurate calibration against a standard fibre calibrated by the National Physical Laboratories in London was necessary. Additionally, the dispersion of the concatenated system was measured as it was built up in order to provide accurate information on which to base the system equalisation.

The amplifier noise and relatively small optical bandwidth at the end of a long system precluded the use of commercially available chromatic dispersion measurement equipment for long system measurements. In order to make the accurate phase delay measurements necessary to determine the chromatic dispersion we found it necessary to use two laser sources which were combined and then modulated using an acousto-optic device. After passing through the system the two signals were separated using optical filters and the relative delay measured using lock-in techniques. This method was found to give good results whose accuracy is largely determined by the wavelength measurement of the source lasers. The effects of the amplifier noise at the output, combined with some polarisation mode dispersion, did however make the measurement a time-consuming operation requiring operator skill. Further developments will be needed before it can be considered robust enough to be viable on board a cableship.

SUMMARY

Long-haul optically amplified systems require accurate control of the fibre chromatic dispersion. Although the majority of the cable for these systems will utilise dispersion shifted fibre, short lengths of unshifted "equalising" sections may also be required to set the dispersion zero of the overall system accurately. Environmental effects, particularly that of the temperature change when the system is laid, need to be taken into account in order to achieve the desired dispersion profile with length.

ACKNOWLEDGEMENTS

The authors would like to acknowledge the contributions of D. Butler and V. Syngal of STC Submarine Systems Limited and Nigel Jolley of BNR Europe Limited in developing the technique for measuring dispersion on long-haul systems. We would also like to thank the directors of STC for permission to publish this work.

REFERENCES

- [1] C.Giles and E.Desurvire : "Propagation of signal and noise in concatenated erbium-doped fiber optical amplifiers", Journal of Lightwave Technology vol 9 no 2 pp 147-153
- [2] N.Taylor : "Power budgets for long-haul optically amplified systems" 4th IEE Conference on Telecommunications, Manchester 18-21 April 1993
- [3] D. Marcuse : "Single channel operation in very long nonlinear fibers with optical amplifiers at zero dispersion", Journal of Lightwave technology vol 9 no 3 pp 356-361
- [4] "Cost 217 inter comparison of chromatic dispersion measurements on single mode fibres", EFOC 92
- [5] I. J. Blewett : "Effect of bending on the chromatic dispersion of single -mode optical fibres", to be published.

BIOGRAPHIES

John Russell was born in 1954 in Birmingham, England. He graduated in Applied Physics from University College, London in 1975. On leaving college he joined STC with the Transmission Products Division. Later he moved to the new optical fibre unit where he worked on measurements, installation and cable design for land based systems. In 1982 Mr Russell moved to STC Submarine Systems where he is in charge of a group working on the design of submarine cables.

Nigel Taylor was born in 1954 in Mansfield, England. He received a BSc in Electronic Engineering from Birmingham University in 1976. He joined STC Submarine Systems on graduating and has worked on the design of coaxial analogue and optically regenerated digital systems. His current interests are in the system design of ultra-long amplified systems. He obtained an MSc from Imperial College, London in 1991 in Communications and Signal Processing.

Kevin Byron is a Senior Principal Research Engineer at BNR Europe Limited. He graduated from the University of Salford in 1970 with a degree in electronics, and from the University of Hull with a doctorate in applied physics. He joined STL (now BNR Europe) in 1974 where he has been engaged in research on a number of areas of optical fibre communication. He is a visiting lecturer at the University of Glasgow, a visiting fellow at the University of Salford and a Fellow of the Institute of Physics.

Ian Blewett graduated from Imperial College, London with a BSc in Physics in 1983. He completed an MSc in Optoelectronics and Laser Devices at Heriot Watt University in 1992 and is currently undertaking research in non-linear effects in II-VI materials at Heriot Watt University

The Design and Manufacture of Fiber and Cable for Undersea Optical Amplifier Systems

Robert E. Frantz, Kwang S. Kim, Louis J. Marra, Dan L. Philen*, Marsha Spalding Stix, and Raymond D. Tuminaro

AT&T Bell Laboratories, Holmdel, NJ; *AT&T Bell Laboratories, Norcross, GA

Abstract

In contrast to the regenerators of existing transoceanic fiber optic cable systems, the next generation of systems will utilize optical amplifiers to realize all optical transmission. These new systems present challenging performance objectives, derived from analytical simulation and tested experimentation, regarding the management of chromatic dispersion, polarization mode dispersion, optical attenuation, and non-linear effects over the length of a cost-effective and robust, long-haul undersea link. The combined requirements of performance, cost, and reliability necessitate state-of-the-art manufacturing, as well as measurement techniques and section assembly algorithms. In addition, extensive characterization and qualification of cabled fibers with respect to environmental effects, such as temperature, pressure, and tension, ensures the transmission performance of installed AT&T SL2000 optical amplifier systems.

Background

The projected growth of international telecommunication volume through the next century has created a market for very high capacity undersea transmission systems. The technological revolution of all optical transmission employing optical amplifiers provides the capability of using digital optical pulses by combining the best characteristics of previous regenerated optical and amplified coaxial systems.

At the highest level, an undersea optical amplifier system can be subdivided into shore equipment (transmission lasers/detectors, power feed and system monitoring equipment, terminals to interface with the terrestrial network, etc.) and undersea equipment (mechanical pressure vessels, optical amplifiers, cables and joints, etc.).

Optical amplifier systems are similar to optical regenerated systems in that digital optical pulses are transmitted between terminal stations, often thousands of kilometers apart, using cabled optical fibers. Unlike optical regenerative systems, optical amplifier systems use: dispersion shifted fibers and operate at the system minimum dispersion wavelength to

control dispersion accumulation; and utilize gain from erbium doped fiber amplifiers to balance optical attenuation introduced by the cabled fiber and components in the transmission path. The use of optical amplifiers also improves system reliability by eliminating bit-rate specific high speed electronics from the undersea plant.

Optical amplifier systems resemble coaxial systems since they: provide signal amplification at regular intervals along the system length but only transmit and detect the signals at the terminals; and require occasional equalization along the transmission path to maintain optimal performance. But unlike earlier lower capacity coaxial systems, optical amplifier systems provide digital transmission at multi-gigabit transmission rates.

The advantages of amplifier systems over previous architectures (including the elimination of bit-rate specific high speed electronics from the undersea plant) offset the additional system complexity of managing system performance over multiple optical parameters.

Optical Performance and Measurement

Amplifier-based, undersea cable systems, designed to transmit signals over distances of thousands of kilometers, require cabled fibers that have been optimized for four transmission parameters: (1) chromatic dispersion, (2) polarization mode dispersion, (3) non-linearity, and (4) loss. Each of these parameters will be discussed below.

Chromatic Dispersion

In the case of chromatic dispersion, it is essential that the average zero dispersion wavelength of each of the fiber transmission paths be aligned with the narrow-band (1 to 2 nm) gain peak that results when hundreds of amplifiers are cascaded in an iterative cable-repeater chain extending over the full system length, which for a transoceanic systems can be as long as 9,000 km. Precise control of the average in-situ zero dispersion wavelength requires the imposition of demanding fiber manufacturing tolerances and record keeping, as well as an ability to periodically interpose short special cabled fiber segments aimed at precisely adjusting the accumulated dispersion to its prescribed value. In

practice, we use cables containing dispersion shifted fibers having average zero dispersion wavelengths of about 1,561 nm for most of the cable path; at intervals of hundreds of kilometers, dispersion compensating cable segments, containing fibers having average zero dispersion wavelengths of 1,310 nm, are introduced with the objective of achieving an average composite zero dispersion wavelength of 1,558.5 nm at the projected deep sea operating temperature of 3° C. The achievement of the desired chromatic dispersion properties at ocean bottom temperatures requires that we apply a correction to room temperature fiber characterizations to reflect the known sensitivity of zero dispersion wavelength to changes in temperature.

Measurements of chromatic dispersion with high accuracy are carried out with modified commercial test sets, which provide multi-wavelength group delay data. From this data, zero dispersion wavelength and dispersion slope are extracted. Key features in AT&T's measurement of zero dispersion wavelength include: use of a modulated tunable laser encompassing a wide range of wavelengths above and below the zero dispersion wavelength of the fiber being measured, inclusion of a wave meter in the test instrumentation to establish the precise operating wavelength of the laser source, and the use of precisely calibrated long length fiber reference standards of known zero dispersion wavelength at the fiber and cable manufacturing facilities.

Polarization Mode Dispersion (PMD)

Fibers with perfect circular symmetry can propagate two orthogonal HE_{11} modes over a given distance with identical transit times. Practical fibers, however, have cores that are slightly elliptical and contain stress in the optical guiding region of the fibers. These imperfections break the degeneracy of the orthomodes, giving rise to birefringent effects that result in the differences in group delays of the two modes referred to as PMD. The fact that a signal can be carried by two modes having different transit times can lead to serious system impairment, where the amount of impairment is related to bit rate, system length, PMD characteristics of the fiber path, as well as interaction with other impairments such as fiber non-linearity.

Practical fiber guiding systems are subject to distributed coupling between the propagating modes, causing an exchange of energy between the modes; this coupling, or exchange of energy between modes, is due to a combination of factors, some of which are intrinsic to the as-manufactured fiber and some of which are imposed by external factors such as loading on a bobbin, cabling effects, etc. This coupling between modes can be beneficial from a system operating point of view, since the end-to-end dispersive effects are lessened in the presence of coupling. The beneficial effects

of fiber paths with mode coupling, however, are difficult to characterize and represent since they are statistical in nature; from a system transmission point of view, the statistical nature of the PMD parameter contributes to performance variability, a variability that is not easy to accurately capture without long time system operation.

The PMD's of fibers have been characterized by a variety of techniques, including the Stokes parameter, Fiber Fabry-Perot (FFP), and wavelength scanning methodologies. The Stokes parameter method has been used to obtain the statistical PMD distribution of a long fiber, which is Maxwellian,

$$P(\tau) = \frac{2\tau^2}{\sqrt{2\pi}\sigma^3} \exp\left[-\left(\frac{\tau^2}{2\sigma^2}\right)\right],$$

where $P(\tau)$, τ , and σ^2 are the probability function, PMD, and variance, respectively. Both the σ of the PMD distribution and the mean PMD value are important parameters to predict the system performance. The wavelength scanning method has been used when only the average value of PMD is required. The FFP technique has been used to measure the PMD of a short fiber without significant mode coupling. This technique gives us PMD values that do not depend on fiber configurations, such as winding conditions, bobbin sizes, and other effects that introduce coupling between the eigen modes.

In our development program, we have measured PMD of fibers on bobbins; on long straight paths without having been cabled; in partial and finished cables; in cables that were subject to seabottom pressures; and in cables, before and after long term viscoelastic relaxation. Our current cabled fibers have been found to have extremely low PMD's, typical of that shown in Table 1.

Non-linearity

The refractive index profiles of silica-based media are most often represented by simple numerical values corresponding to the core and cladding regions of the fiber. This representation is usually adequate for describing first order propagation behavior, which comprises low signal level transmission over propagation distances that are not too long. However, in the case of amplifier based systems, thousands of kilometers in length, it is not sufficient to use the simple index of refraction representation. The refractive index of fiber in the long system is affected by the optical power level of the transmission signal. Although the change of refractive index is small, the cumulative effect over a long optical path can contribute to system performance degradation, due to changes in the optical spectrum and the signal pulse shape. As a measure of this non-linear effect, n_2/A_{eff} has been used, where the following definitions apply:

$$n(\omega, P) = n_0(\omega) + n_2 \frac{P}{A_{\text{eff}}},$$

$$A_{\text{eff}} = \frac{2\pi \int E^2(r) r dr}{\int E^4(r) r dr}.$$

where n_0 is the power independent part of the refractive index and ω is the optical frequency in radians. Generally speaking, a large effective area is desirable for long amplifier based systems using the Non Return to Zero (NRZ) signal format. The challenge is to achieve this high effective area in dispersion shifted fibers, while simultaneously achieving the target zero dispersion wavelength and acceptable transmission performance in bends.

The non-linear properties of dispersion shifted fibers have been inferred and verified by a variety of different techniques, including: self phase modulation measurements on sample lengths of 200 to 500 m using a mode locked 1319 nm YAG laser (scaled to the signal band wavelength of 1,558.5 nm); measurements of refractive index profiles, coupled with calculations relating to electric field distributions; long fiber (10 km) Raman gain measurements of fibers excited with very high power optical sources, etc. Reasonable consistency was found with the various techniques. We find typical values for n_2 and A_{eff} to be $2.6 \times 10^{-20} \text{ m}^2/\text{W}$ and $50 \mu\text{m}^2$, respectively.

Typical Cabled Fiber Optical Performance	
Fiber Type	Dispersion shifted
Coating Structure	Dual: high/low modulus 250 μm
Identification	color coating
Mode Field Diameter (Peterson II)	8.4 μm
Effective area	$> 50 \mu\text{m}^2$
n_2	$2.6 \times 10^{-20} \text{ m}^2/\text{W}$
Average λ_0	1,561 nm
PMD (in cable)	$< 0.1 \text{ ps}/\sqrt{\text{km}}$
Loss in undrawn cable environment	0.21 dB/km
Proof test strength	200 kpsi
Static fatigue n-factor	> 18
Aging (all causes)	$< 0.01 \text{ dB}/\text{km}$

Table 1

Loss

The loss of dispersion shifted fibers tends to be somewhat higher than that of conventional fibers due to increased Rayleigh scattering resulting from higher levels of GeO_2 dopant incorporated in the fiber core. When in an as-drawn and unspliced state, average losses typically range from 0.20 to 0.21 dB/km. With cabling, and associated splicing and joining, we have found that we can expect installed losses of 0.21 dB/km. Loss measurements are carried out with standard cutback measuring techniques.

Typical Cabled Fiber Performance Summary

Table 1 contains a summary of the typical optical performance values associated with cabled SL dispersion shifted fibers. As can be observed, all parameters have values consistent with demanding long system performance.

Fiber Design and Manufacture

In order to realize these aggressive optical properties, attention has been devoted to every stage of the design and manufacture of the fiber. Synthetic quartz preforms are carefully processed for uniformity of thickness, concentricity, and ovality. The fiber is drawn to give long lengths of high strength (1.4 GPa) fiber to meet the existing requirements for system reliability. The fiber is then coated with two layers of acrylate coating and subjected to rigorous testing and measurements to ensure that all of the fiber properties meet the requirements for ocean cable product.

This fiber has also been optimized for the special requirements of the system. The zero dispersion wavelength has been moved to a wavelength where the fiber zero dispersion wavelength and the spectral gain peak of the amplifiers complement each other. The distribution of the zero dispersion wavelength around the target wavelength is closely controlled in manufacture, producing fibers having a narrow range around the median.

In an optical amplifier system, any light that is generated in the fiber by effects other than the primary laser transmission process will also be amplified. One source of such light generation is by nonlinear effects caused by high power densities in the fiber core. SL2000 fibers have been designed to have slightly higher mode field diameters than those found in other dispersion shifted fibers while still meeting the requirement for low bend sensitivity. This makes the "effective area" of the fiber core larger, which reduces the power density, and minimizes the effects of nonlinear power generation.

One very important parameter to control in the SL2000 fiber is the Polarization Mode Dispersion. Several fiber properties (core ovality, etc.) can cause the PMD to be large. At AT&T, SL2000 fibers are manufactured using special feedback controls to ensure low ovality of the fiber core. Other processing techniques are used to reduce the PMD still further. The SL2000 fiber made in this way has PMD less than 0.1 ps/ $\sqrt{\text{km}}$ when manufactured and after cabling, and has set a new world class level for low PMD in cabled fiber.

Once the design criteria, such as minimizing the nonlinear effect, minimizing the PMD, and controlling the target for the zero dispersion wavelength are known, the fiber design is fixed, and production started. The fiber that is produced is

then selected for cabling using very sophisticated select routines to retrieve the fiber from the existing inventory. These routines must balance the distribution in zero dispersion wavelength, the PMD, and any differences in attenuation between fibers in a given group of fibers going into a cable. The attenuations must be matched so that there is minimal variation in attenuation between fibers in a group. "Running averages" are compiled and monitored to assure that the final design requirements on attenuation and dispersion will meet the completed system requirement.

Finally, the fibers are assembled into groups or "sets". Individual as-drawn and proof tested fiber lengths are spliced together to make up a long length of fiber, usually about 70 km. Several long lengths of fiber having matched attenuation and zero dispersion wavelength are then grouped together to form a "set". Each fiber in the set may then be color coded aid in fiber identification during splicing and cable assembly. This set is then shipped to the cable factory for processing into the final cable.

Cable Design, Processing, and Qualification

The undersea cable includes fibers and an electrical conductor to provide both the transmission and power paths for the amplifier system. Cables are designed to isolate the fibers and electrical conductor from the ocean environment and to provide a range of levels of mechanical protection from known and unexpected hazards. The cable manufacturing process must reliably maintain the optical performance of the fibers at minimum cost.

The degree to which cables must be protected varies with depth of water, since shallow continental shelves are significantly more hazardous than deep abyssal plains. Deep water cables have no additional protection external to the electrical insulation and provide a robust, cost effective solution for the majority of most systems. Protected/Armored cables consist of a "transmission core" and externally applied armor (typically tapes or wires). Different levels of protection can be provided by varying the armor thickness and material, or using multiple layers of armor.

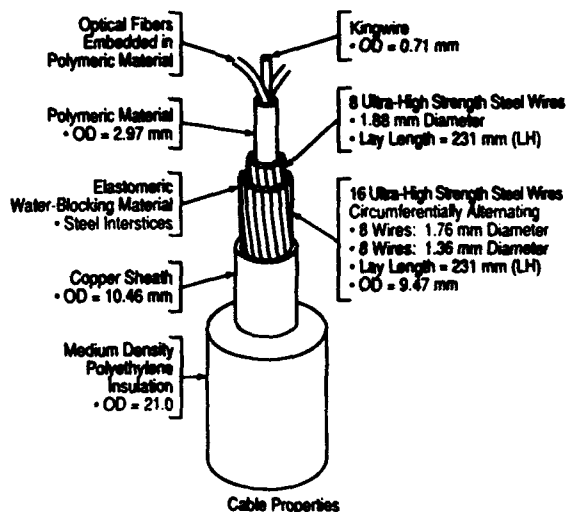
Cables for SL2000 systems draw upon AT&T's proven SL design technology and world class manufacturing processes. SL cable is manufactured in four processing steps: (1) Unit Fiber Structure (UFS), (2) composite power conductor, (3) polyethylene insulation, and (4) armor/protection application. The modular nature of all SL2000 cable processes allows for flexibility in cable manufacture.

UFS

The UFS is the lightguide core of SL2000 cables. In SL2000 UFS manufacture, up to 6 fiber pairs are embedded in an elastomer around a central kingwire. This tight buffer design ensures that fiber properties are consistent from the time of manufacture throughout the system life.

Power Conductor

Stranded strength members, waterblocking material, and continuously welded copper sheath are then applied around the UFS to form the composite conductor. This conductor provides the power path for the amplifiers during system operation and a fault locating path for system repair. The stranded strength members form an internal cage which provides a protective pressure vessel around the fibers to minimize environmental effects on the fiber optical parameters. The welded copper sheath forms a hermetic seal to prevent moisture penetration into the UFS and fibers during normal operation.



Cable Properties

Minimum Cable Tensile Strength	107 kN
Maximum Operating Tensile Strength	81 kN
Weight in Air	8.3 kN/km
Weight in Seawater	4.8 kN/km
Cable Hydrodynamic Constant	43 Degree-Knots
Cable Modulus	22.4 km

Deep Water Cable (DW)

Figure 1

Insulation

The conductor is then passed through an extrusion line where a medium density polyethylene insulation layer is applied with a thin adhesive interfacial layer to complete SL Deep Water (DW) cable manufacture. DW cable (see Figure 1) is typically used in deep ocean areas such as abyssal plains and constitutes most of the cable used in a transoceanic system.

Protection Application

When required, SL Deep Water cable can be converted into SL Special Applications (SPA) cable by applying a longitudinal steel tape and high density polyethylene jacket over the insulation. SL-SPA is often used in areas with more aggressive ocean bottom conditions (continental slopes, etc.), areas with known or suspected bottom hazards, and at locations of planned cable handling such as initial/final joint and interconnection points.

Armoring

SL armored cables utilize layers of armor wires over the SL deep water cable to provide additional protection as required for each system. These cables are used in areas with higher risk of external aggression (trawlers, rock outcroppings, etc.). SL armored cables include: Light Wire Armor (LWA) - one layer of armor wires; Single Armor (SA) - one layer of heavier armor wires; Double Armor (DA) - two layers of armor wires; Rock Armor (RA) - a second layer of heavy wires applied at a short lay length over SL-LWA cable; and custom cable types to meet special system needs. Sketches of common SL cables are shown in Figure 2.

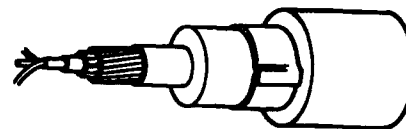
Characterization, Qualification, and Verification Testing

Prototypes and final design and production samples are tested to ensure that SL cables will meet system performance requirements after installation. Mechanical and optical tests range from simple elongation tests of armor wires to combined temperature/pressure/tension testing of finished cables to simulate ocean deployment and recovery conditions. Tests are performed on completed cable as well as constituent materials and partially processed cable.

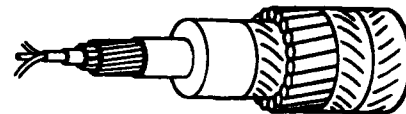
Cable prototype characterization tests allow us to evaluate mechanical robustness and variations in the optical parameters of PMD, loss, and chromatic dispersion as a function of environmental stresses (such as tension, bending, torsion, temperature, pressure, radiation, chemical exposure, etc.). Since the final design may change slightly from development prototypes, characterization tests involve a wide range of different stresses but generally are generally limited in stress combinations and test duration.

Qualification involves validation of the final cable design and materials and therefore, qualification tests concentrate on proving compliance to functional requirements and supporting specific customer requirements in RFQs. Qualification tests include extensive cyclic load tests and combined stress tests (reverse bend/tension, flexure/temperature, tension/temperature/pressure, etc.).

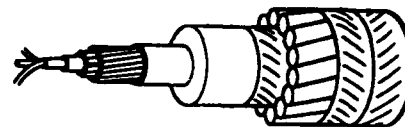
Verification tests are performed periodically on cable product to verify continued conformance to product



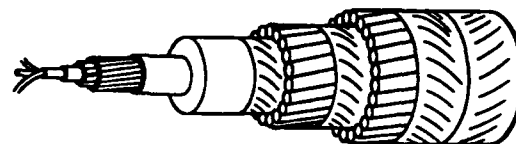
Special Applications Cable (SPA)



Light-Wire Armored Cable (LWA)



Single-Armored Cable (SA)



Double-Armored Cable (DA)

Figure 2

requirements. These tests typically involve a few tests selected to monitor critical or process/material sensitive parameters. In addition, sea trials are performed as necessary to verify performance and deployment/handling/repair assumptions.

Section Assembly

Section assembly is the final stage of cable processing prior to system assembly. This process configures the inventory of manufactured cable sub-sections to meet the requirements for the cable repeater sections. Optical amplifier technology requires an enhanced functionality for this process over that of regenerative systems.

For regenerative systems, the requirements for the section assembly process are, in order of priority:

1. Achievement of the bulk loss requirements for each fiber path in each individual section;
2. Maximum utilization of the cable inventory cleared for system use;

3. Achievement of the nominal section length. (This requirement has a lower priority because it is not critical to system performance, and the repeater to cable cost ratio shows that it is beneficial to lower the nominal section length to utilize higher-loss cable, at the expense of an additional repeater.)

In regenerative systems, these requirements can be realized through the construction of individual sections in a sequential manner. During the construction, achieving the section's bulk loss target is the single design consideration. The properties of the sections already built or to be built need not be considered.

The requirements for section assembly in an optically amplified system, listed below, are more complex: (Items 1 to 5 have equal priority)

1. Achievement of the bulk loss requirements for each fiber path in each individual section;
2. Achievement of the bulk loss requirements for each fiber path over the entire system;
3. Achievement of an average system section length above a specified minimum level;
4. Achievement of the required map of chromatic dispersion along the system length;
5. Achievement of an average polarization mode dispersion (PMD) for each fiber path in the system below a specified maximum level;
6. Maximum utilization of the cable inventory cleared for system use. (This requirement has a lower priority for amplified systems because average section length and PMD are critical to system performance and therefore inventories which adversely affect these averages may not be used.

These requirements are achieved by a number of sub-processes executed during the section assembly phase: screening and binning of the incoming inventory; construction of the sections; and adjustment of certain transmission parameters.

Screening is necessary to achieve the average system PMD and section length requirements (the latter requirement is, in effect, a requirement regarding the average attenuation, in dB/km, of the system). Both of these properties are intrinsic to the cable and cannot be altered by their configuration.

Binning of the inventory ensures the maximum utilization of the inventory. The average attenuation requirements are more severe for long-distance, high-capacity systems. Thus, cables which are screened-out for these systems may be

acceptable for others.

During construction of the sections, consideration must be given to the losses of individual section fiber paths as well as the loss of each fiber path over the system length.

Given the possibility of loss variation between paths, the section assembly process must periodically make adjustments to the loss of one or more fiber paths to achieve the requirements over the system length. The adjustments will be made through the insertion of planned splice losses.

After cables have been selected for repeater sections, they are joined together using cable-to-cable joints. To minimize development expense and maximize reliability, SL2000 systems utilize the same proven Type 11 joints used in current SL560 systems.

System Assembly

System assembly is the integration of assembled cable sections to repeaters to form a continuous system segment. The Type 11 coupling hardware used to connect SL2000 cables to repeaters is similar to the cable-to-cable joints used in section assembly with the exception that a pigtail termination is substituted for one of the cable terminations. The pigtail provides a protected path for the fibers and insulated electrical path from the splice box to the repeater body.

Chromatic dispersion management, which started during fiber manufacture, continues through system assembly to ensure the needed dispersion configuration, or "map", in the finished system. To accomplish the needed map, periodic adjustments are made to bring the cumulative chromatic dispersion to the specified window. These adjustments involve the periodic insertion of cabled non-dispersion shifted (low zero dispersion wavelength) fiber into selected repeater spans.

Conclusion

Undersea optical amplified systems place tight requirements on a number of transmission performance parameters and require a detailed understanding of the environmental effects on those parameters. AT&T SL2000 systems provide a reliable and cost-effective integration of proven design technology, state-of-the-art manufacturing methods and new testing and assembly processes to realize the performance advantages of the next generation in long-haul undersea links.

Robert E. Frantz

(101 Crawfords Corner Rd., P.O. Box 3030, Holmdel, NJ 07733-3030) is a Member of Technical Staff in the Undersea Cable Development Group at AT&T Bell Laboratories. He is responsible for optically amplified cable design and qualification. Bob received his B.S. degree in Mechanical Engineering from Case Western Reserve University in 1985 and joined AT&T Bell Laboratories in the same year. He received his M.S. degree in Mechanical Engineering from Stanford University in 1986 and N.J. Professional Engineer's License in 1991. At Bell Labs, he has been involved in the analysis of undersea cable mechanics and dynamics, cable reliability, and shipboard handling methods.



Kwang S. Kim

(101 Crawfords Corner Rd., P.O. Box 3030, Holmdel, NJ 07733-3030) is a Member of the Technical Staff in the Undersea Lightguide Repeater Components Group at AT&T Bell Laboratories. He joined Bell Laboratories in 1983 and is currently responsible for characterization of optical fibers and cables for optical amplifier transmission systems. He received his M.S. and Ph.D. degrees in physics from New York University in 1975 and 1982, respectively, and is a member of the American Physical Society.



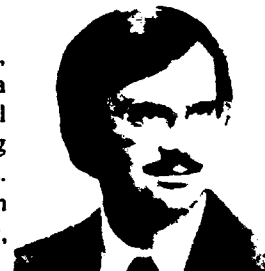
Louis J. Marra

(101 Crawfords Corner Rd., P.O. Box 3030, Holmdel, NJ 07733-3030) is a Member of Technical Staff in the Undersea Cable Product Realization Group at AT&T Bell Laboratories. He is responsible for the development and implementation of the section assembly algorithm. Mr. Marra has received a B.E. degree from the Cooper Union for the Advancement of Science and Arts and a M.S. degree from Stanford University, both in Mechanical Engineering. He has been with AT&T since 1981.



Dan L. Philen

(2000 Northeast Expressway., Norcross, GA 30071) is a Distinguished Member of Technical Staff in the Systems Engineering group at AT&T Bell Laboratories. He received a B.S. degree in chemistry from Auburn University, Auburn, AL, in 1968, and a Ph.D. degree in physical chemistry from Texas A&M University, College Station, TX, in 1975. He was a Robert A. Welch Postdoctoral Fellow in electrical engineering in 1975 at Rice University, Houston, TX. From 1976 to 1979 he was with Georgia Institute of Technology, Atlanta, Ga., engaged in measurements of trace pollutants in the upper atmosphere by laser induced fluorescence. Since 1979 he has been with AT&T Bell Laboratories, Atlanta, Ga., and is the author of numerous publications on measurements of optical fiber properties and holds patents in fiber measurements and cable design. He is listed in "Who's Who In Optical Science And Engineering", "Who's Who In Technology Today", "Who's Who In The South and Southwest", and "Men of Achievement". He is a member of The American Chemical Society, The Optical Society of America, Sigma Xi - The Research Society of North America, Sigma Pi Sigma - Physics Honorary, and Phi Lambda Upsilon - Chemistry Honorary.



Marsha Spalding Stix

(101 Crawford Corner Rd., P.O. Box 3030, Holmdel, NJ 07733-3030) is Technical Manager of the Undersea Lightguide Cable Development Group at AT&T Bell Laboratories. She received her B.S. in Mechanical Engineering from California State University Fresno and her M.S. in Mechanical Engineering from Stanford University. Before joining AT&T, she worked at Sandia Laboratories in Albuquerque, N.M. in the area of mechanical design. She is currently responsible for the development of new SL cable designs and cabling of new fiber types, as well as physical and optical characterization of undersea cables. She holds two patents in the areas of cable design and inspection.



Raymond D. Tuminaro

(101 Crawford Corner Rd., P.O. Box 3030, Holmdel, NJ 07733-3030) is Technical Manager of the Undersea Lightguide Repeater Components Group at AT&T Bell Laboratories. He received his B.S.E.E. and M.S.E.E. degrees from New York University in 1957 and 1959. His pre-Bell Laboratories work experience included microwave component, antenna, and radar system design. Since joining Bell Labs in 1966, he has been involved in assessing the vulnerability of telecommunications facilities to electromagnetic pulses generated by nuclear bursts, the design of waveguide media for millimetric wave transmission systems, performance modeling of long, repeatered coaxial cable systems, the design of satellite earth stations, and the development of optical fiber transmission systems. The last assignment has, since 1980, included the development and characterization of fibers, cables, and optical components for deployment in long haul undersea lightguide systems.



EXPENDABLE MINIATURE FIBER OPTIC CABLE FOR UNDERWATER COMMUNICATIONS

Jack Rosko

Gerry Lochfelm

Kenneth Cotton

Berk-Tek, Inc.
Fuquay-Varina, North Carolina

ABSTRACT

As new Fiber Optic Systems have developed for underwater applications, a need was demonstrated for an Expendable Miniature Fiber Optic Cable Interlink (EMFOC). The application demanded that a length of 20 Km be manufactured in an extremely small size to optimize the handling and pay-out requirements. Additionally the cable must be able to withstand high underwater pressures and exhibit very low attenuation ($< .45$ dB/Km).

This paper addresses the evolution of the design and processing steps taken to manufacture a Miniature Underwater Fiber Optic Cable. Pressure, temperature dependence, tensile, cut-thru, hockling and kinking test results are reviewed.

INTRODUCTION

As the communications link for unmanned undersea vehicles (UV) becomes more demanding both the United States Navy and Commercial Companies have turned to Fiber Optic Cables to fulfill their requirements. Advanced UV's are being used for search, recovery, salvage, inspection and observation missions. The heavy coaxial communication cables are being replaced by Fiber Optic Cables with a fraction of the weight and vastly increased bandwidth. This paper reviews the development of a low loss, long length, Expendable Miniature Fiber Optic Cable.

DESIGN CONSIDERATIONS

The scope of this project was to develop a Miniature, One Fiber, Single-Mode, Fiber Optic Cable that would meet the following requirements :

- * Simple, reliable, low cost design
- * Loss: < 0.45 Db/Km @ 1300NM & < 0.30 dB/Km @ 1550 NM
- * Operating Temp. range: -40° to $+70^{\circ}$ C
- * Weight: 2.3 Lbs/Kft
- * Cross Sectional Area < 0.0030 IN²
- * Working tensile strength: 42 Lbs at 0.7% strain
- * Max working depth: 23,000 ft (10,000 psi)
- * Length: = 20,000 meters

- * Exposed to ocean floor environment for an operational life time of 30 days
- * Hockle resistant
- * Geometry and jacket material compatible with pack adhesives.
- * Specific gravity of 1.48

TEST/TRIAL PROCEDURE

The development of this cable started in 1989. The final design was a $0.033'' \times 0.079''$ rectangular cable, with a cross sectional areas of 0.0026 IN², using one dispersion shifted single-mode fiber, between two parallel $0.011''$ steel wires. A semirigid PVC was employed as the jacketing material.

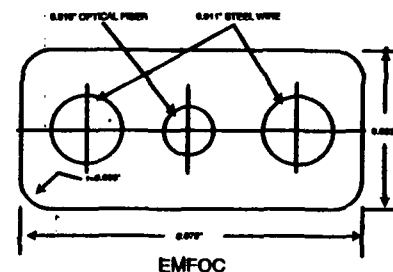


Fig. 1

Fig 1 shows the cross-section area of the EMFOC. The optical fiber used is a commercial grade 100kpsi, dispersion shifted, single-mode, having a 250 um UV - cured Acrylate coating. The strength member used is a specially coated $0.011''$ steel wire. A solid extruded jacket of a semirigid PVC provided the protection from mechanical elements such as abrasion, cut through and kinking.

a.) HYDROSTATIC PRESSURE TESTING

Reference Standard: EIA-455-102

A one kilometer length of cable was wound around a mandrel and pressure tested to 10,000 PSIG. A diagram of the test set-up is shown in Figure 2. The cable sample was cycled twice, with the first cycle having an overnight soak at 10,000 PSIG. The sample was measured with an OTDR and measurements were recorded at 1,000 PSIG intervals during both pressurization and depressurization. There was no significant transmission loss observed during this test. Test results are shown in Figure 3.

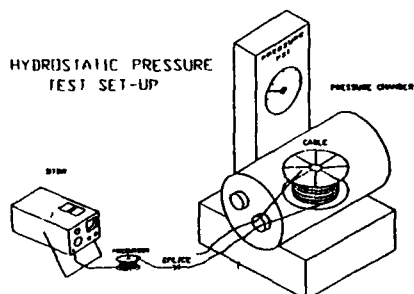
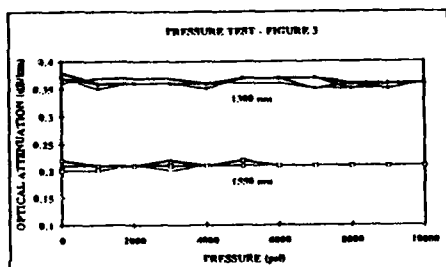


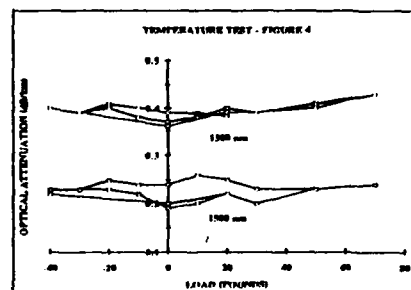
Fig. 2



b.) TEMPERATURE TESTING

Reference Standard: EIA-455-52

The cable specimen used in this test was one kilometer in length. The purpose of this test was to simulate storage and transportation temperatures as well as sea floor temperatures to which the cable might be exposed. The sample was temperature cycled between -40° and $+70^{\circ}$ C. A stabilized power meter was used in conjunction with a Macintosh PCPC II for automatic cycling and recording of data. The test results are shown below in Figure 4.



The transmission loss observed during the test showed a slight increase in attenuation at the temperature extremes. An increase of approximately 0.05 dB/Km at 1300 nm and 0.02 dB/Km at 1550 nm was observed.

c.) KINK TEST

Reference Standard: EIA-455-88

The kink test was designed to simulate the hazards posed by various physical sea floor obstacles. The test measures the optical loss as a function of the load applied to the cable when it is bent around an edge. A 1550 nm power meter was used to measure the optical loss. The kink fixture consists of a plate with a 0.75" radius edge and a cable clamp located 1.2 inches away from the cable edge. Please see Figure 5. One end of the sample is wrapped around a mandrel and clamped. The other end is clamped to the test fixture with the cable going over the test edge. Figure 6 shows the test results.

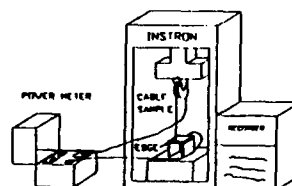
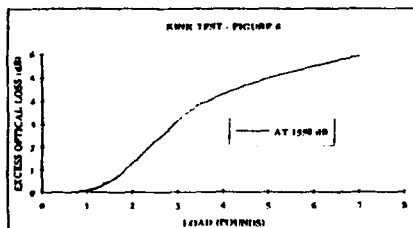


Fig. 5



The test results indicate that the cable starts to experience additional transmission loss at approximately a one pound load.

d.) CUT TEST

Again this mechanical test was performed to simulate the hazards that the cable might be exposed to on the sea floor. The cut test used a 0.007" radius cutter fixed in an Instron Tensile Tester. See Figure 7. A 1550 NM power meter was used to measure the optical loss. The test results are shown in Figure 8.

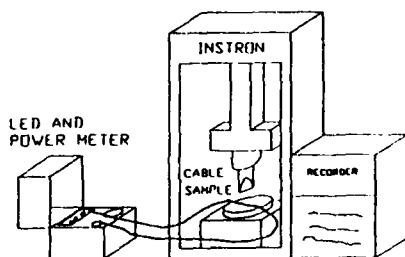
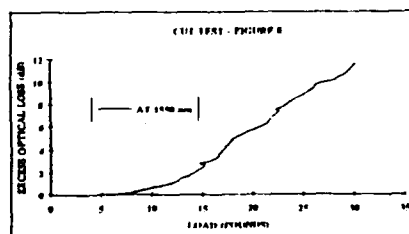


Fig. 7



The cut test results indicate that the cable starts to experience additional transmission loss at approximately six to seven pounds of load.

e.) TENSILE TEST

Reference Standard: EIA-455-33

Approximately 800 meters of cable were tensioned during this test. The attenuation was measured for a baseline reading. The cable was then tensioned to its working load. At the working design load of 42 Lbs, no attenuation increase was noted. See Figure 9 for the test setup.

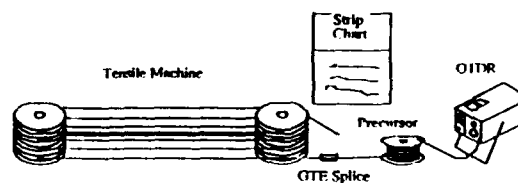


Fig. 9

The cable was also tested with a short gage sample on an Instron tensile tester. Figure 10 shows the results of this test.

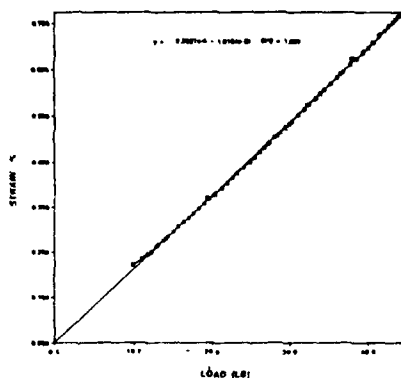


Fig. 10

As can be seen from the tensile test results the cable is at approximately 0.70% strain at the design working load of 42 Lbs. There was no additional power loss observed during this test.

f.) HOCKLING TEST

Hockling occurs when a cable is twisted, allowed to go slack such that a loop forms and then retensioned. With a sufficient number of twists the loop in the cable will not "POP" out but continually decrease in size until the cable kinks. The hockling test was designed to measure the number of twists in a given length of cable required to make the cable hockle. The test set-up shown in Figure 11 consists of two drill chucks to hold the ends of the cable. One end of the cable is attached to a fixed post and the other on a sliding bracket which moved in line with the post. The chuck on the sliding bracket had a handle to allow the cable sample to be twisted in either direction. Each sample was twisted once, allowed to go slack and retensioned. This was repeated with successively more twists until a hockle formed. A tension meter was attached to the sliding chuck to measure the tension required to pull the cable into a hockle. Samples were tested in each twist direction, clockwise and counterclockwise.

The hockle test results for this cable were 10 twists at 3 Lbs.

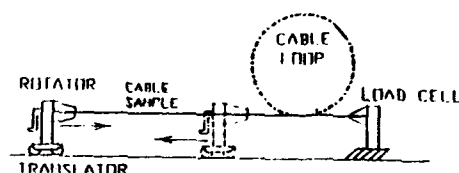


Fig. 11

MANUFACTURING

The key to manufacturing this Miniature Underwater Fiber Optic Cable was in the tooling design. Early designs encountered problems with poor performance in the pressure testing. Major improvements in this area centered around changes to the tooling designs. Solid extrusion was essential to the final cable designs excellent pressure performance.

A major factor in the coilability of this cable was the uniformity of the dimensions. The cable is manufactured to a tolerance of $\pm 0.001"$ over a 20 kilometer length. Currently the cable is in production in lengths exceeding 20 kilometers.

CONCLUSIONS

The test results of this Fiber Optic Cable have clearly indicated that a Long-Length Expendable Miniature Fiber optic Cable can be produced meeting the severe requirements of underwater applications.

Through design, process and material experimentation this cable has exceeded the required specifications for size, handling characteristics and loss for the Fiber Optic Cable Interlink.

Future activities will include further research of materials as well as process modifications to firmly establish manufacturing conditions.

ACKNOWLEDGEMENTS

The authors wish to acknowledge the assistance and cooperation of the Naval Command Control and Ocean Surveillance Center San Diego Ca. for permission to publish and present this paper. In particular, we would like to thank Mr. Chris Young, Mr. Andy Estabrook and Mr. Peter Jung for performing the majority of the qualification tests.



Gerry Loehfelm

Berk-Tek, Inc.
EOP Division
100 technology Park Ln.
Fuquay-Varina, NC 27526

Gerry Loehfelm received his B.S. Degree in Physics from the college of Charleston, Charleston, S.C. He joined Berk-Tek Inc. in 1986 and has been involved in research and development of Miniature Underwater Cables for the past five years. After six years in the United States Navy Submarine Service Mr. Loehfelm worked for DUPONT and Sumitomo Electric. He is currently working as the Vice President of the Electro Optics Division of Berk-Tek Inc.



Jack Rosko

Berk-Tek, Inc.
EOP Division
100 Technology Park Ln.
Fuquay-Varina, NC 27526

Jack Rosko received his BSEE Degree from Union College in Schenectady, NY. He has worked for Berk-Tek since 1991 and is now the Engineering Manager. Mr. Rosko has been involved in Fiber Optic Cable design and development since 1979. His previous work experience has been with Siecor, Phalo OSD, and Sumitomo Electric.



Kenneth B. Cotton

Berk-Tek, Inc.
EOP Division
100 Technology Park Lane
Fuquay-Varina, NC 27526

Kenneth Cotton received a B.S. from the University of North Carolina at Chapel Hill. After serving in the U.S. Marine Corps, Mr. Cotton worked for Buckeye Gas Products Co. and E-Z-Go Div. of Textron, Inc. he studied electrical engineering at Wake Technical College. Mr. Cotton joined Berk-Tek in Jan, 1990 where he has advanced to the position of Process Engineering Specialist.

INVESTIGATION OF CABLE BEHAVIOUR IN WATER DURING LAYING OF FIBEROPTIC SUBMARINE CABLES.

Svend Hopland

Norwegian Telecom

Technology Department, Cable Division, Oslo, NORWAY

ABSTRACT:

We have investigated the behaviour of our submarine cables in water by studying the shape of towed cable lengths. The shape of the cables are calculated based on position readings of hydroacoustic transponders attached to the submerged cables. We have found that a straight line configuration is a good approximation to steady state towing. Our heavy armoured cables are more stable than our light armoured cables. We have determined experimentally the hydrodynamic constants. Finally, we have studied transient towed cable geometries when the ship's speed is "abruptly" changed.

1. INTRODUCTION

Norwegian Telecom is installing a substantial amount of fiberoptic submarine cables along the Norwegian coast as parts of our junction and trunk network. The bottom topography along our cable routes is generally very rugged with underwater mountain formations, sharp and high ridges, leads and troughs. Optimal cable routes are selected based on detailed topography maps provided by a comprehensive multibeam echosounder survey, and uphill and downhill slopes of 30-60 degrees may often be encountered. We have earlier presented a concept for installation of fiberoptic submarine cables in such terrain ¹.

During laying of our submarine cables, little or no real time information is available about the actual shape of the curve formed by the cable length submerged in water. According to theory, a straight line configuration should be valid during steady state cable laying. However, the validity of this assumption has not been experimentally investigated in detail on cable lengths of practical interest. Moreover, during laying, the cable ship may for some reason increase or decrease its speed, and the steady state condition will thus be temporarily violated. For laying of light and vulnerable fiberoptic submarine cables in rugged terrain, the margins to failure are small, and a well controlled laying method ¹ and detailed information of the cable behaviour in water, is necessary. As a result, we have investigated the behaviour of our cables during typical installation conditions. Here, we present the results of a towed cable experiment giving valuable

information about the behaviour of our fiberoptic submarine cables in water. Both steady state and transient cable behaviour is investigated.

2. CABLE CHARACTERISTICS

Our standard submarine cable constructions are light armoured (LA) with one layer of armour, or heavy armoured (HA) with two layers of armour. The cables have outer sheaths consisting of high density polyethylene with a smooth outer surface. The cable parameters are shown in Table 1.

Cable type	Weight in air/sea (kg/m)	Outer diameter (mm)	Outer sheath
LLA	1.08/0.67	22.5	HDPE
LA	1.64/1.08	26.4	HDPE
HA1	2.70/1.81	33.2	HDPE
HA2	3.10/2.05	36.0	HDPE

Table 1: Fiberoptic submarine cable parameters.

The LLA cable has an extra light armour, and is only installed in fresh water (lakes), while LA, HA1 and HA2 are used for sea water installations.

3. CABLE TOWING EXPERIMENT

According to cable laying theory, stationary or steady state deployment conditions are obtained when the cable ship is sailing at constant horizontal speed, the cable pay out rate is constant, and the bottom tension of the cable is zero ². In this case the cable will form a straight line configuration from the cable ship down to the sea bottom. The angle of the cable with the horizontal (laying angle α) is then given by the hydrodynamic constant of the cable (H) and the horizontal velocity of the cable ship (V), as shown later in Equation (1) of Ch. 4.1.3.

Only the normal drag force acting on the cable will determine the laying angle α . Also, the tangential water resistance (skin friction) is negligible for our cable types at normal laying speeds. We can therefore investigate cable behaviour in water during cable laying by studying the behaviour of towed cable lengths. Specifically, at steady state towing the hydrodynamic constants can be experimentally determined.

3.1 Equipment

In the towing experiments, small size and low weight cylindrical hydroacoustic transponders were attached to the cable. Mechanical and electrical data for the mini transponders are shown in Table 2. The cable length interval between two neighbouring transponders was typically 75-100 meters, and four transponders were used simultaneously on each towed cable. The far end transponder was attached 25 meters from the cable end in order to avoid end effects.

On board the ship, a hydroacoustic transducer unit collected positional data from the submerged transponders once every five seconds and the position of each transponder relative to the ship was accordingly calculated with high accuracy. During towing, the transponder positions are continuously monitored, and the actual shape of the towed cable length can be calculated.

Comparing transponder sizes and weights and spacing with the cable parameters given in Table 1, we may assume that the transponders do not affect the towed cable geometries.

Transponder	Length (mm)	Diam. (mm)	Weight air/sea (kg)	Range (m)	Accuracy (m)
A	262	68	1.6/0.6	600	± 2
B	314	68	2.1/0.9	1000	± 2

Table 2: Data for mini transponders A and B.

The towing ship used differential GPS navigation equipment, which monitored accurately the ship's position, velocity and course. The ship's horizontal speed was calculated as the average velocity based on time and positions readings during the last 60 seconds; updating values every 1.0 seconds. Velocity readings from the ship's speed log was also noted.

3.2 Towing procedures

The towing was performed in a typical Norwegian fjord at a sea depth of approximately 500 meters. The towed cable lengths were typically 300-600 meters in order to maintain safe distance between the far end transponder and the sea bottom. Also, in this case the lengths of the towed cables are

of the same length as in our practical laying situations. The transponder spacing was 75-100 meters giving a satisfactory resolution of the towed cable geometry. All towing were programmed to take place along straight lines. Two modes of towing were applied: Steady state towing and variable speed towing.

During steady state towing the ship speed was kept constant at different speeds ranging from zero knots to 3.5 knots; thus well exceeding our typical laying speed range of 1.5-2.0 knots.

In the variable speed towing mode the velocity of the ship was changed "abruptly" from a high value of steady state towing to a low value and vice versa.

4. RESULTS

Generally during towing, we found all transponder positions to be very close to the vertical plane defined by the straight horizontal line followed by the ship. Thus, the coordinates of interest were the transponder depth and the transponder layback behind the ship.

During the towing experiments, the ship's speed log showed higher or lower values than those measured by the DGPS navigator, thus suggesting that some surface current was present; the value of which was observed to vary within the range 0-0.8 knots. However, this surface current did not affect the towed cable geometries, as shown later in Ch. 4.1.

4.1 Steady towing mode

In this towing mode each cable was allowed to stabilize for 15-20 min. at each towing speed in order to obtain stationary towing conditions. Then followed a 10-15 min. logging period of transponder positions.

4.1.1 Straight line approximation

In Fig. 1 and Fig. 2 are shown towed cable geometries for light armoured cable (LA) and heavy armoured cable (HA2), respectively, at different steady state towing velocities. A representative logging period of approximately 4 minutes, including four consecutive geometries with a time spacing of 75 seconds, is shown at each towing velocity.

We note that both the LA cable and the HA2 cable are very nearly in vertical positions when the ground speed (DGPS-speed) is zero. This shows that the surface current has no noticeable influence on the towed cable geometries. It also shows that there are no major sea currents in the water column in the fjord trial area that affects the cable geometries significantly.

LIGHT ARMoured CABLE (LA)

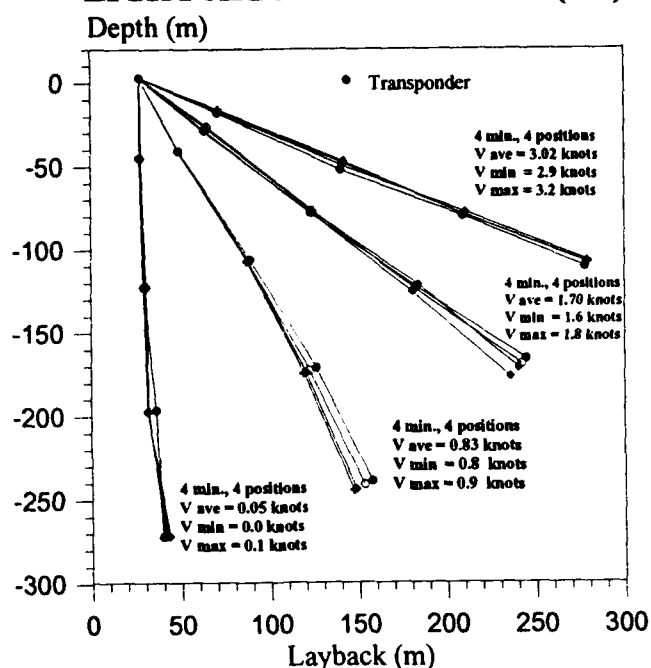


Figure 1: Towed cable geometries for LA cable at different steady state velocities.

HEAVY ARMoured CABLE (HA2)

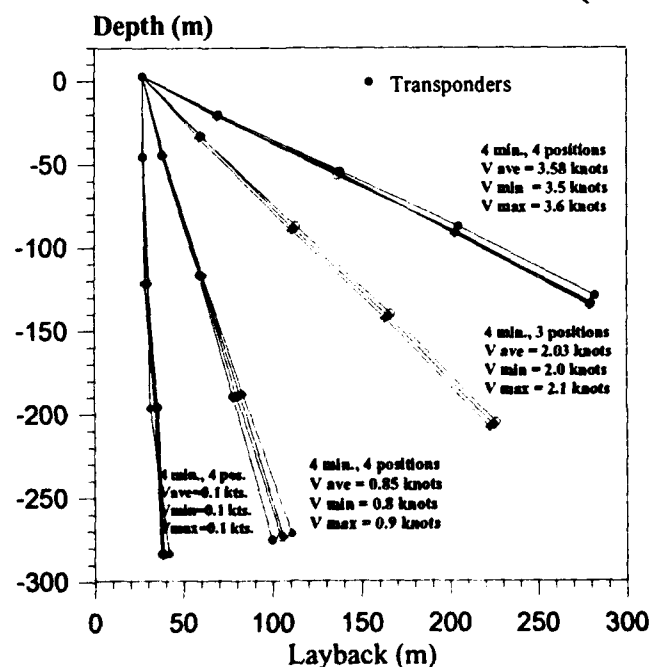


Figure 2: Towed cable geometries for HA2 cable at different steady state velocities.

From Fig. 1 and Fig. 2, it can be seen that the towed cable geometries in general are close to straight lines at the different constant towing speeds.

However, some minor buckling or curved cable geometries have been observed. In these cases, the cable geometry near the ship was often not representative for the total towed geometry.

There was evidence that our heavy armoured cables (HA1 and HA2) are more stable and less prone to buckling/ curved geometries than our light armoured cables (LLA and LA).

Obviously, during steady towing, small variations in towing velocity are inevitable due to factors such as varying surface currents and winds. Variable towing speed may easily cause small movements or buckling of the cables, as will be visualized later in Ch. 4.2. Local variations in sea currents in the water column may also have had some influence on the cable geometry.

In conclusion, we have here shown that a straight line cable configuration at steady state is a good approximation for our cables at typical installation conditions.

4.1.2 Towed cable length dependence

We have checked if the towed cable length has any influence on the steady state cable geometry. For the LA cable, we payed out 300 m additionally cable length in steps of 100 m while keeping the towing velocity constant. The results are shown in Fig. 3.

We observe that, independent of the towed length, cable geometry remains a straight line with approximately the same angle with the horizontal. With reference to typical variations of geometries observed at steady state (see Ch. 4.1.1), we may conclude that cable geometry and angle α is not affected by the different towed cable lengths used in this investigation.

4.1.3 Hydrodynamic constants

According to our observations, we can conclude that each steady state towing condition can, with good approximation, be characterized with an average straight line cable geometry with angle α with the horizontal, and its corresponding average towing velocity (V_{ave}).

From theory, the angle α at steady state towing is given by Equation (1):

$$(1) \quad \cos \alpha = \sqrt{1 + \frac{1}{4} \left(\frac{H}{V} \right)^4} - \frac{1}{2} \left(\frac{H}{V} \right)^2$$

where H is the hydrodynamic constant of the cable, and V is the towing velocity.

LIGHT ARMoured CABLE (LA)

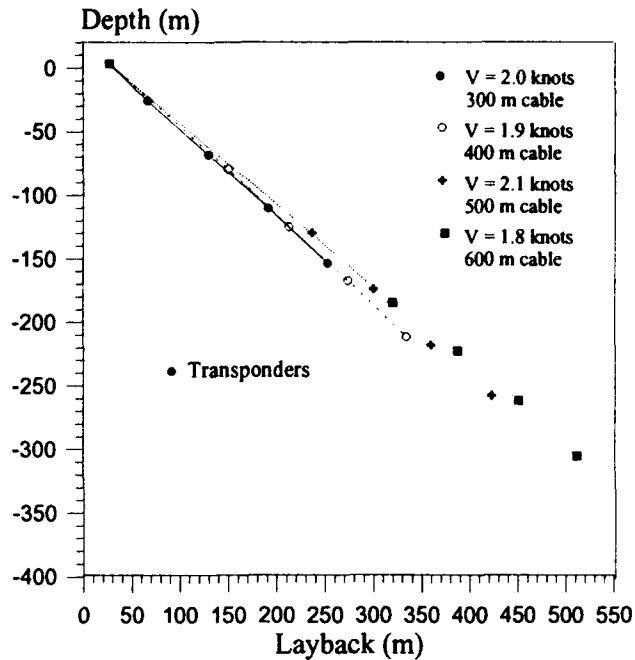


Figure 3: Towed LA cable geometry at constant towing velocity and different towed cable lengths.

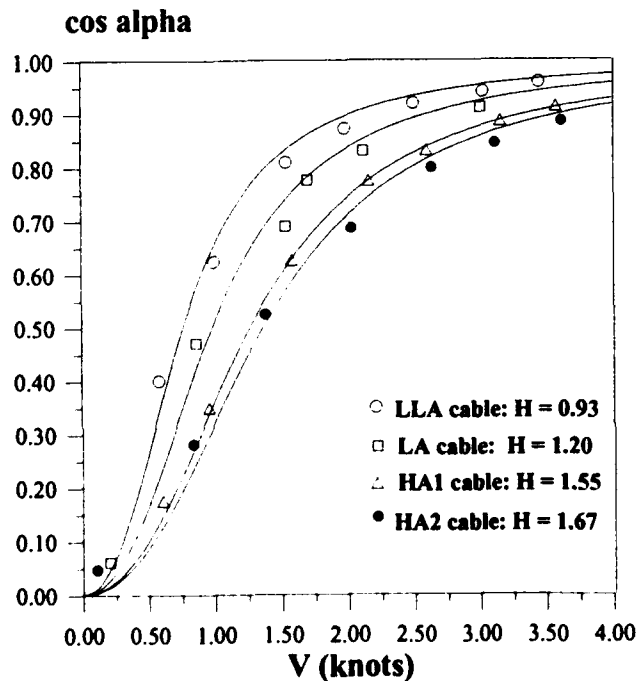


Figure 4: Experimental and theoretical variation of angle α with towing speed V for LLA, LA, HA1 and HA2 cables.

We have measured the angle α and the corresponding average speed V_{ave} for our cables and curve fitted the data to Eq. (1) by the least square method. The results are shown in Fig. 4.

The hydrodynamic constants determined for our cables are listed in Table 3.

Cable type	Hydrodynamic constant	
	Radian-knots	Degree-knots
LLA	0.93	53.3
LA	1.20	68.8
HA1	1.55	88.6
HA2	1.67	95.7

Table 3: Experimentally determined hydrodynamic constants.

These values are lower than those predicted theoretically by ref. 2 for smooth cables. We note, however, that the predicted values are valid only at high towing speed values ($\cos \alpha \approx 1$), whereas in our calculations we have used the range of towing speed values relevant for our fiberoptic cables (low, medium and high speeds).

It is important to include low and medium speed values, since a practical laying situation may occasionally require low laying speeds. The hydrodynamic constants determined by this method describe relevant steady state laying conditions for our cables, and are used for determining the laying angles during laying¹.

4.2 Variable speed towing mode

In this towing mode the ship's speed was changed as quickly as possible from one steady state velocity to another, within our laying speed range, in order to study the transient cable behaviour. Transponder positions were logged throughout the period.

Readings of the ship's speed log were used to measure the time used for a speed change. Typically, the towing speed had reached its new value within 45-60 seconds.

Fig. 5 and Fig. 6 show the transient LA and HA1 cable configurations, respectively, when the ship's speed is increased rapidly. The time slot between each shown cable geometry is 60 seconds.

LIGHT ARMoured CABLE (LA)

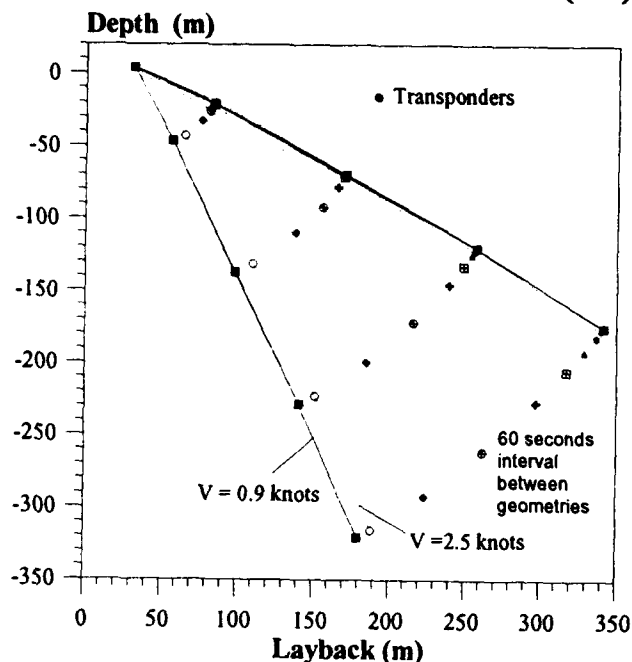


Figure 5: Transient LA cable geometries when towing velocity is increased "abruptly".

HEAVY ARMoured CABLE (HA1)

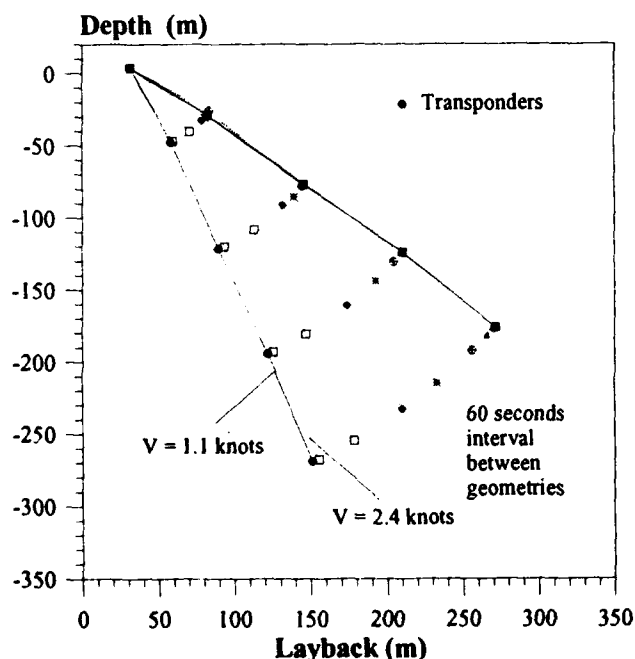


Figure 6: Transient HA1 cable geometries when towing velocity is increased "abruptly".

We note that the cable geometry close to the ship changes after a short time. Here, the cable soon reaches the straight line configuration corresponding to the new steady state condition. After that, an increasingly longer cable length reaches the new straight line configuration. We find that the length of cable reaching its final configuration increases roughly proportionally with time.

For an LA cable length of 360 m, the transition time is measured to approximately 420 seconds. For an HA1 cable length of 300 meters, the transition time is measured to approximately 360 seconds.

In Fig. 7 and Fig. 8 are shown the transient LA and HA1 cable geometries, respectively, when the ship's speed is *decreased* rapidly. The time slot between each shown cable geometry is 60 seconds.

LIGHT ARMoured CABLE (LA)

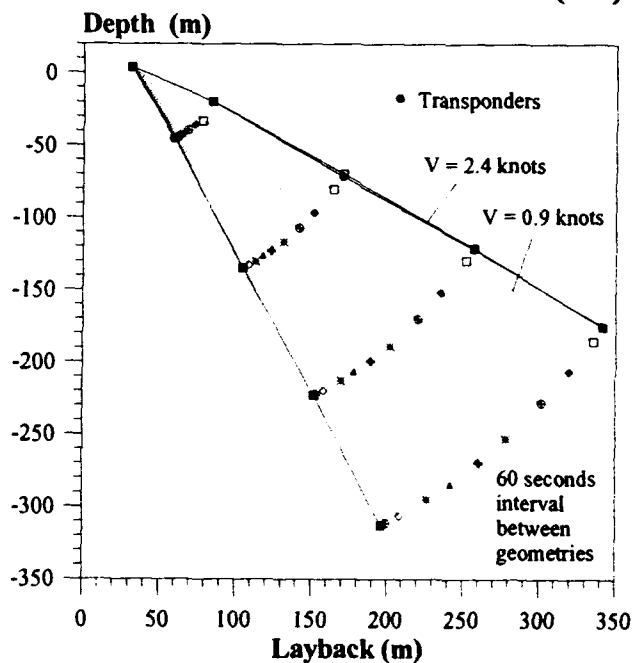


Figure 7: Transient LA cable geometries when towing velocity is *decreased* "abruptly".

Here, the curvature of the cable is more uniformly distributed along the cable length and the transition proceed more slowly. The total transition times for the LA cable and the HA1 cable has been measured to be approximately 540 seconds and 480 seconds, respectively.

In ref. 3, the time necessary for the cable to settle when the laying speed is *decreased*, is approximately given as:

$$(2) \quad T = h/U$$

, where h is the water depth and U is the vertical sinking rate or hydrodynamic constant for the cable.

HEAVY ARMoured CABLE (HA1)

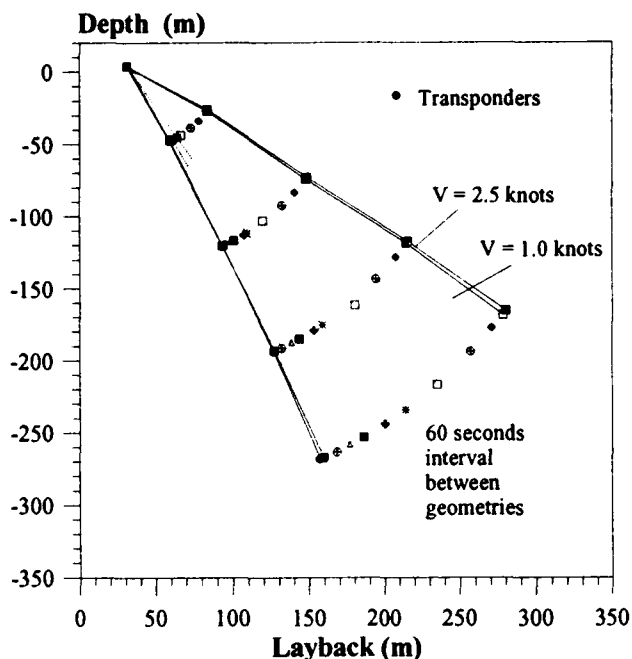


Figure 8: Transient HA1 cable geometries when towing velocity is *decreased* "abruptly".

In our case; using (2) and the values of H from Table 3 and the depth corresponding to the towed cable length, the transition time T is estimated to be 515 seconds and 350 seconds for the LA cable and the HA1 cable, respectively. Thus, Eq. (2) has underestimated the transition times in our case.

We have here clearly seen that variations in the ship's speed during towing, will cause deviations from the straight line. Specifically, the cable geometries near the ship will be quickly affected, and is therefore not indicative for the situation as a whole. During cable laying, if the ship's speed varies, this effect may be significant. Therefore, suitable parameters should be used for cable laying control¹.

5. CONCLUSIONS

We have investigated the behaviour of our fiberoptic submarine cables during laying by studying towed cable geometries under conditions that are nearly identical to our practical laying situations. Hydroacoustic mini-transponders attached at regular intervals along the submerged cables have made possible a detailed experimental study of steady state and variable speed towed cable behaviour. We have confirmed that a straight line cable configuration is a good approximation for steady state towing, as predicted by theory. However, minor buckling/curvature has been observed, and the cable configuration near the ship is not always representative for the

whole towed cable length. Evidence have shown that our heavy armoured cables are more stable than our light armoured cables. Surface currents have not affected towed cable geometries. The length of towed cable has not affected cable geometry or towing angle at steady state. We have determined the hydrodynamic constants for our cables by curve fitting data of towing angle versus towing speed in the speed range relevant for laying of our cables. When the towing speed is "abruptly" changed, the cable geometry is altered in a characteristic manner. Specifically, the cable geometry near the ship's bow is easily affected by speed changes. The transition times for our cables are measured and compared with a simple theoretical model. In summary, this study has given relevant and important information about the behaviour of our cables in sea water.

6. ACKNOWLEDGEMENT

The author wishes to thank Emil Marhaug and his crew of Norwegian Telecom, for supplying mechanical equipment and assistance with the deployment of the cables during the fjord trials. Thanks to Lars Hafskjær, Norwegian Telecom; for assistance with curve fitting the data. Also thanks to Martin Dukefoss, Geoteam A/S, for supplying ship, mini transponders and navigation equipment.

7. REFERENCES

1. S. Hopland and Albert Klykken: "Installation of Submarine Fiberoptic Cables in Rugged Coastal Terrain". IWCS 1992, pp. 492-496
2. E. E. Zajac: "Dynamics and Kinematics of the Laying and Recovery of Submarine Cable". Bell System Technical Journal, September 1957, pp. 1129-1207.
3. S. Shimura: "International Submarine Cable Systems". KDD Engineering and Consulting, Inc., Publication 1984, Page 321.

Svend Hopland

Norwegian Telecom,
Technology Department,
Cables Division,
P.box. 6701, St. Olavs Plass
Oslo, NORWAY



Svend Hopland graduated from the Norwegian Institute of Technology in 1985 with a Ph. D. on optical fibers. In 1986 he joined Norwegian Telecom, where he is presently a senior engineer on fiberoptic cables

PLOUGH - TOWING ANALYSIS IN SUBMARINE CABLE LAYING

J. Fang and J. A. Witz

Department of Mechanical Engineering, University College London,
London, U.K.

Abstract

A numerical solution to the steady state governing equation for plough towing is developed. This analysis takes into account the effect of ship forward speed, and can handle multiple-element tow lines. For a range of soil resistances which the plough might encounter, the length of tow wire and the layback of the plough relative to ship are obtained to satisfy the maximum tow wire angle requirement at the plough. These two parameters are then used to calculate the configuration of the cable, meeting criteria such as cable tension and angle at the plough, length of cable on the seabed and the cable touch-down point ahead of the plough. Guide tubes have to be employed if any of these criteria cannot be satisfied.

1 Introduction

There is an increasing demand to lay and bury marine cables in deeper waters in order to avoid damage from fishing boards or dragging anchors. In the recent past 200 m was once regarded as the maximum water depth for burial of marine cables. These days this is no longer the case and cables are now being buried in water depths exceeding 500m. Some industry observers foresee the need to bury cables in water depths beyond 1000m. These water depths present significant operational challenges. In order to support these operations reliable analysis methods are needed to predict the operational parameters in the planning stages.

Figure 1 illustrates the towing operation of sea plough. The basic principle is to tow the plough from the stern of the lay vessel. In parallel, cable is paid out from the stern, passed through the plough and buried in the trench dug by the plough. Typical rates of advance are around 0.5 m/s (1 knot). The bottom angle of the tow wire needs to be kept below approximately 15 degrees in order not to destabilise the plough. The tow wire bottom tension depends on the encountered soil conditions. The cable tension at the plough also needs to be low in order to ensure that the cable remains buried after the plough. Typical cable bottom tensions are around 0.5 tonnes with a limiting maximum value of around 2 tonnes. Some tension is often required in order to suppress any tendency the cable has to form loops at the plough. In the ideal situation the cable is maintained in suspension between the lay vessel and the plough. In relatively shallow water and for light cables this is feasible. Often this is not the case and guide tubes are deployed in order to guide the cable down the tow wire catenary. These guide tubes consist of intermittent rings separated by spacers running down the complete length of the tow wire. Deployment of guide tubes adds significant costs to an already expensive operation and therefore there is a need for a reliable computer based planning and operations tool to establish whether or not it is necessary to use guide tubes.

This paper is concerned with presenting a numerical solution to the static catenary equations of the tow wire and the marine cable which includes the fluid drag force. Thus, this analysis takes into account the effect of ship

forward speed, and can handle multiple-element tow lines. For the range of soil resistances which the plough might encounter, the length of the tow wire and the layback of the plough relative to ship are obtained to satisfy the maximum tow wire angle requirement at the plough. These two parameters are then used to calculate the configuration of the cable, meeting criteria such as cable tension and angle at the plough, length of cable on the seabed and the cable touch-down point ahead of the plough. Guide tubes have to be employed if any of these criteria cannot be satisfied. This numerical solution has been used in burial operations and agreement between predictions and field measurements are shown to be good.

2 Theoretical analysis

2.1 Tow line analysis

Governing equation: Starting at the plough let s be the arc length along the stationary configuration. We define s to be positive in the direction away from the plough. We let θ be the angle between the positive s direction and the direction of the ship velocity, as indicated in Figure 1.

Figure 2 shows the forces acting on an element of tow line, with tension at the point s being denoted by T . The normal drag force per unit length D_N is given by:

$$D_N = C_D \frac{1}{2} \rho V^2 d \sin \theta |\sin \theta| \quad (1)$$

where ρ is the mass density of water; d is the diameter; V is the ship speed; and the modulus ensures that the drag force maintains the correct direction for all θ .

The drag coefficient C_D in equation (1) is essentially constant for the range of velocities encountered here. However, the corresponding coefficient for a skin friction force associated with V_c the component of flow along the tow line, is not constant. For the tow line of smooth exterior, the expression:

$$D_T = C_f \frac{1}{2} \rho V_T^2 \pi d \quad (2)$$

with $C_f = 0.055/(N_R)^{0.14}$ was found to give good agreement with the experimental data, as is shown by Zajac¹. Here D_T is the skin friction or tangential drag force per unit length; and N_R is the Reynolds number defined as $N_R = V_T L / \nu$, where ν is the kinematic viscosity of water; V_T is the relative velocity of the water with respect to a tow line element given by $V_T = V \cos \theta$.

Summing the forces acting on the tow line element shown in Figure 2 in the tangential and normal directions, dividing by Δs and sending Δs to zero, gives:

$$T \frac{d\theta}{ds} + D_N - w \cos \theta = 0 \quad (3)$$

$$\frac{dT}{ds} - D_T - w \sin \theta = 0 \quad (4)$$

where w is the weight per unit length of the tow line element in the fluid medium under consideration i.e. air or water.

Numerical solution: Equations (3) and (4) form a set of first order ordinary differential equations. It is an initial value problem with known values of tension and angle at the plough i.e. $T = T_0$ and $\theta = \theta_0$ at $s = 0$.

The basis of the solution method is described as follows. The infinitesimal term ds in equations (3) and (4) is replaced by a finite incremental arc length Δs . The equations are then multiplied by this finite step Δs . This gives algebraic formulae for the changes in the functions T and θ when the independent variable s is incremental by one stepsize Δs . In the limit of making the stepsize very small, a good approximation to the underlying differential equations is achieved.

The detailed steps used in the iterative solution of equations (3) and (4) are described as follows.

- (1) Select a stepsize Δs .

- (2) For a tow line element of length Δs , the first estimates of the tension and angle in the middle of this element are given by the known values of tension and angle at one of its two ends:

$$T = T_i \quad \text{and} \quad \theta = \theta_i$$

- (3) Calculate the increments in tension and angle between the two ends of this element, by rearranging equations (3) and (4):

$$\Delta T = (w \sin \theta + D_T) \Delta s$$

$$\text{and} \quad \Delta \theta = (w \cos \theta - D_N) \Delta s / T$$

- (4) The values of tension and angle in the middle of the element are then updated:

$$T = T_i + \Delta T / 2 \quad \text{and} \quad \theta = \theta_i + \Delta \theta / 2$$

- (5) Repeat steps (3) and (4) until the differences in ΔT and $\Delta \theta$ from two consecutive iteration cycles are within a preset tolerance level. The solution is then obtained.

- (6) The tension and angle at the other end of the element are now given by

$$T_j = T_i + \Delta T \quad \text{and} \quad \theta_j = \theta_i + \Delta \theta$$

and the horizontal and vertical distances between the two ends are:

$$\Delta x = \Delta s \cos \theta \quad \text{and} \quad \Delta y = \Delta s \sin \theta$$

- (7) Repeat steps (2) to (6) until the whole length of a tow line is stepped through.

This solution method is simple and efficient, although it is not as robust as some of the more sophisticated numerical methods available. However, since T and θ are very smooth functions of arc length s owing to the nature of the problem, no real difficulties are presented with the above calculation method and it is therefore considered adequate.

Multiple-element tow line: As shown in Figure 1, a typical tow line is comprised of four components with different physical properties: a bridle, a joint, the tow wire in water and the tow wire above the mean water level.

The calculation method outlined in the previous section is applied to each of the three components of the tow line assembly which are submerged in water. Since the tension and inclination angle at lower end of the bridle are known, its configuration and the tension and angle at the upper end of the bridle can be obtained by using the solution method. By the condition of continuity at the node adjoining the bridle and the joint, these tension and angle values are passed on to the lower end of the joint. Similarly, the configuration, end tensions and end angles are determined for the joint and the part of the tow wire submerged in water.

The configuration of the tow wire in the air from the mean water level to the stern sheave is calculated by the elastic catenary formulae, Peyrot and Goulois²:

$$H = F_1 \left(\frac{L_u}{EA} + \frac{1}{w} \log_{10} \frac{F_4 + T_j}{T_i - F_2} \right) \quad (5)$$

$$V = \frac{1}{2EAw} (F_1^2 - T_i^2) + \frac{T_j - T_i}{w} \quad (6)$$

$$L = L_u + \frac{1}{2EAw} (F_1 T_j - F_2 T_i + F_1^2 \log_{10} \frac{F_4 + T_j}{T_i - F_2}) \quad (7)$$

$$\text{where} \quad \begin{aligned} F_1 &= T_i \cos \theta_i & F_2 &= T_i \sin \theta_i; \\ F_3 &= -F_1 & F_4 &= -F_2 + wL_u; \\ F_5 &= T_j \cos \theta_j & F_6 &= T_j \sin \theta_j. \end{aligned}$$

In the above equation, w is the weight per unit length; EA is the axial stiffness; L_u and L are the unstretched and stretched lengths; H and V are the horizontal and vertical distances between the two ends; T_i and T_j are the tensions, and θ_i and θ_j are the angles to horizontal at catenary ends i and j respectively. F_1 and F_3 are the horizontal components, and F_2 and F_4 are the vertical components of T_i and T_j respectively. All the parameters are illustrated in Figure 3.

The total layback of plough relative to vessel is then obtained along with tow wire top tension, top angle and the required tow wire length. If fluid drag is not an issue then the above elastic catenary formulae can also be used for the tow wire in the water.

2.2 Cable analysis

There are a number of requirements placed on the cable bottom tension and angle in order to prevent possible damage to the cable. The cable bottom angle needs to be horizontal or negative so that it does not interfere with the tow line. The bottom tension is usually kept between 0.5 to 2.0 tonnes to prevent it from throwing loops in front of plough under low tension or from causing deburial problems under high tension.

A cable may take any one of the three configurations shown in Figure 1, depending on the layback of the plough relative to the vessel for a given water depth. As the layback is increased, the cable bottom angle will go from the horizontal to a negative inclination until it touches the seabed. As the layback is further increased, the length of cable resting on seabed is also increased. A step by step routine is developed to determine the cable configuration.

First, the cable bottom angle is taken as zero. Then the bottom tension is varied to match the layback set by the tow line, using the elastic catenary formulae described previously. If the layback is matched and the bottom tension is within the bands set by the operator, then the configuration is found to be the first case labelled A in Figure 1. Otherwise, one proceeds to the next stage.

Second, the cable bottom tension takes the required value, and the bottom angle is varied to match the layback from the tow line analysis. If the layback is matched while the bottom angle is within the required bands and the cable is off the seabed, the cable takes configuration B in Figure 1. Otherwise, one proceeds to the next stage.

Third, a part of the cable will rest on the seabed. An iterative method is developed to determine the length of cable on the seabed. The aim of the iteration is to meet the continuity in tension for the whole cable, taking into account of the seabed friction force. Again, the elastic catenary formulae previously described is used to model the suspended cable lengths adjacent to the plough and to the vessel. With a very large layback, the amount of cable on the seabed can be unacceptably long. In this case, guide tubes have to be used.

2.3 Plough towing with guide tubes

The guide tubes are assembled on board the vessel and added on to the tow wire as the water gets deeper. They are supported by the tow wire and extend from the bridle to the vessel. The cable runs through the guide tubes and it will not touch the seabed or throw loops if a certain amount of tension is maintained.

A simplified analysis is adopted where the fluid drag force is neglected, and the elastic catenary formulae are used with the weight per unit length being the combined weight of the tow wire, guide tubes and cable. As the advance speed is around a maximum of 0.5m/s (1 knot) in ploughing operations, this omission of drag force will introduce an error of 1% at most. This error level is considered acceptable bearing in mind the measurement noise induced by the vessel's motions in waves.

3 Examples and discussions

3.1 Ploughing without guide tubes

The configuration of a cable, as mentioned in the foregoing, is a function of the following parameters: tow wire bottom tension, tow wire bottom angle, water depth and the type of cable being laid. The effects of these parameters are examined in the following examples. The properties of the components in a tow line and two example cables used here are listed in Table 1.

Water depth: A reference case is chosen as a basis for comparison in which the light cable is laid under a tow wire bottom tension of 10 tonnes, and tow wire bottom angle of 10 degrees to the horizontal. A drag coefficient C_D of 1.0 is used in the analysis. The analysis results are shown in Table 2 for the water depths ranging from 20 m to 500 m. As can be seen in Table 2, in shallow waters the top tension of the cable can be controlled such that the cable bottom angle prior to the plough is horizontal whilst its bottom tension is less than the set upper limit of 1 tonne. As the water depth increases, the cable bottom tension can no longer be kept horizontal without exceeding the bottom tension limit of 1 tonne. The bottom angle is then negative and the cable sags but is still clear of the sea bed. As the water depth increases further, the sag point touches the seabed and the length of cable on the seabed increases with the water depth.

Tow wire bottom tension: When a harder soil is encountered, the towing tension is increased. Shown in Table 3 are the results for a bottom tension of 20 tonnes, while the values of the other parameters remain the same as in the reference case. It is obvious that under higher towing tensions, the layback of the plough relative to the vessel is larger. As a result, the cable touches the seabed at a shallower water depth, and a longer length of cable rests on the seabed for the same water depth.

Tow wire bottom angle: The effect of an increased tow wire bottom angle of 15 degrees is studied. The rest of the parameters are the same as those in the reference case. The analysis results are shown in Table 4. It is seen by comparing Table 4 with Table 2, that an increase in the bottom tow wire angle reduces the layback of the plough relative to the vessel. Consequently, this increase in the tow wire bottom angle results in the cable touching the seabed at a larger water depth and there is a shorter length of cable on the seabed for the same water depth.

Cable self-weight: A much heavier cable is used for comparison with the light cable to examine the influence of the cable self-weight on the cable configurations. The results with the heavy cable are shown in Table 5. Since the tow wire bottom tension and angle are unchanged compared with the reference case, the layback of the plough relative to the vessel remain the same. A heavier cable, when suspended, generates higher tensions at the two ends. Therefore, a larger amount of cable rests on the seabed so that its self-weight is supported by the seabed and the maximum bottom tension requirement is satisfied. For the same reason, the heavy cable will touch the seabed at a shallower water depth.

3.2 Comparison with field measurements

Measurements of tow wire top tension, plough layback and total tow wire catenary length have been made in a number of burial operations. The range of measured tow wire catenary lengths against water depth is plotted in Figure 4. Also shown in the same figure are the predicted catenary lengths with a tow wire bottom tension of 5 tonnes and a bottom angle of 15 degrees. The agreement between the analysis and the measurements is considered to be good.

3.3 Ploughing with guide tubes

In some circumstances, a combination of unfavourable parameters may put the cable under risk of being damaged. For instance, it can be seen in Table 5 that the heavy cable will have a very large amount of cable on the seabed in water depths exceeding 500 m, which is undesirable. Another undesirable condition is when the plough end cable touch down point is too close to the plough. In these cases, guide tubes have to be used. The relevant data of an example guide tube is listed in Table 1, and the analysis results are given in Table 6. Note that the length of a guide tube section is 1 m.

4 Conclusions

A numerical solution to the static catenary equation incorporating the fluid drag force and its implementation on desktop computer provides a useful and economical package for both planning and field operation of ploughing. Agreement between predictions and field measurements are shown to be good.

The water depth, tow wire bottom tension and bottom angle, and the cable self-weight are important parameters in ploughing. The requirements on cable bottom tension and angle can be easily achieved for light cables, low towing tensions, high tow line angles and in shallow water depths. At the other extreme, one must resort to the use of guide tubes for heavy cables, high towing tensions (i.e. hard soils), or in very deep water.

References

- 1 E. E. Zajac, "Dynamics and kinematics of the laying and recovery of submarine cable", Bell System Technical Journal, Vol. XXXVI, No. 5, September, 1957.
- 2 A H Peyrot and A M Goulois, "Analysis of cable structures", Computer and Structures, Vol 10, pp 805-813, 1979.

Dr. J. Fang and Dr. J. A. Witz are both of the Department of Mechanical Engineering, University College London, Torrington Place, London WC1E 7JE, U.K.

Jie Fang is a research fellow in Offshore Engineering. Joel Witz is a lecturer in Ocean Engineering, and is active as an engineering consultant to the offshore hydrocarbons and marine telecommunication industries.

Table 1. Data of components of a tow line, cables and guide tubes

	Diameter (mm)	Weight per unit length in air (kg/m)	Weight per unit length in water (kg/m)	Axial stiffness (MN)
Bridle	50.9	-	9.9	200.0
Joint	100.0	-	125.0	770.0
Tow wire	36.0	5.9	4.85	100.0
Light cable	38.1	2.9	1.75	63.2
Heavy cable	55.5	9.3	6.8	90.0
Guide tubes	-	4.31	3.75	-

Table 2. Ploughing without guide tubes, towing tension: 10 ton, towing angle: 10 deg, light cable

TOW WIRE					CABLE							
BOTTOM TENSION: 10.0 TON					BOTTOM TENSION (MAXIMUM): 1.0 TON							
BOTTOM ANGLE: 10.0 DEG												
WATER DEPTH	LAYBACK	CATENARY	TOP TENSION	TOP ANGLE	BOTTOM ANGLE	PLOUGH LAYBACK	LENGTH ON SEABED	SHIP LAYBACK	TOP TENSION	TOP ANGLE	CATENARY LENGTH	BOTTOM TENSION
(m)	(m)	(m)	(ton)	(deg)	(deg)	(m)	(m)	(m)	(ton)	(deg)	(m)	(ton)
20.0	104.9	101.8	10.13	13.4	0.0	0.0	0.0	0.0	0.49	24.2	107.9	0.45
50.0	218.2	219.1	10.27	16.4	0.0	0.0	0.0	0.0	0.91	26.5	226.2	0.82
100.0	368.7	377.8	10.51	20.4	-3.1	0.0	0.0	0.0	1.18	32.4	388.7	1.00
200.0	600.5	630.3	11.00	26.3	-4.8	47.7	70.5	482.2	1.41	41.9	653.8	1.00
300.0	784.7	840.0	11.49	30.7	-4.8	47.7	139.5	597.6	1.64	47.7	877.6	1.00
400.0	941.7	1026.1	11.97	34.3	-4.8	47.7	197.6	696.5	1.86	51.8	1078.9	1.00
500.0	1080.4	1197.1	12.46	37.3	-4.8	47.7	248.1	784.6	2.08	55.0	1265.5	1.00

Table 3. Ploughing without guide tubes, towing tension: 20 ton, towing angle: 10 deg, light cable

TOW WIRE					CABLE							
BOTTOM TENSION: 20.0 TON					BOTTOM TENSION (MAXIMUM): 1.0 TON							
BOTTOM ANGLE: 10.0 DEG												
WATER DEPTH	LAYBACK	CATENARY	TOP TENSION	TOP ANGLE	BOTTOM ANGLE	PLOUGH LAYBACK	LENGTH ON SEABED	SHIP LAYBACK	TOP TENSION	TOP ANGLE	CATENARY LENGTH	BOTTOM TENSION
(m)	(m)	(m)	(ton)	(deg)	(deg)	(m)	(m)	(m)	(ton)	(deg)	(m)	(ton)
20.0	113.3	110.1	20.12	11.8	0.0	0.0	0.0	0.0	0.56	22.6	116.1	0.52
50.0	246.6	246.8	20.27	13.6	-0.5	0.0	0.0	0.0	1.10	24.1	253.9	1.00
100.0	434.9	441.6	20.51	16.2	-4.8	47.7	42.3	344.9	1.22	32.2	455.0	1.00
200.0	739.5	762.2	21.00	20.2	-4.8	47.7	187.7	504.0	1.51	40.5	790.8	1.00
300.0	989.4	1031.5	21.49	23.4	-4.8	47.7	307.2	634.5	1.77	45.8	1077.8	1.00
400.0	1206.1	1270.2	21.97	26.1	-4.8	47.7	409.3	749.2	2.03	49.5	1335.6	1.00
500.0	1399.8	1488.1	22.46	28.5	-4.8	47.7	499.0	853.1	2.28	52.4	1573.4	1.00

Table 4. Ploughing without guide tubes, towing tension: 10 ton, towing angle: 15 deg, light cable

TOW WIRE					CABLE							
BOTTOM TENSION: 10.0 TON					BOTTOM TENSION (MAXIMUM): 1.0 TON							
BOTTOM ANGLE: 15.0 DEG												
WATER DEPTH	LAYBACK	CATENARY LENGTH	TOP TENSION	TOP ANGLE	BOTTOM ANGLE	PLOUGH LAYBACK	LENGTH ON SEABED	SHIP LAYBACK	TOP TENSION	TOP ANGLE	CATENARY LENGTH	BOTTOM TENSION
(m)	(m)	(m)	(ton)	(deg)	(deg)	(m)	(m)	(m)	(ton)	(deg)	(m)	(ton)
20.0	74.7	72.6	10.13	17.5	0.0	0.0	0.0	0.0	0.27	32.7	78.9	0.23
50.0	163.6	166.4	10.28	19.9	0.0	0.0	0.0	0.0	0.56	33.9	174.1	0.47
100.0	290.4	302.7	10.52	23.2	0.0	0.0	0.0	0.0	0.93	36.5	313.0	0.75
200.0	496.9	532.3	11.01	28.4	-2.9	0.0	0.0	0.0	1.36	42.7	551.0	1.00
300.0	666.9	729.5	11.49	32.5	-4.8	47.7	43.7	575.4	1.57	48.9	762.7	1.00
400.0	814.1	907.5	11.98	35.9	-4.8	47.7	96.5	669.9	1.78	53.0	955.6	1.00
500.0	945.5	1072.6	12.46	38.7	-4.8	47.7	143.6	754.2	2.00	56.2	1136.2	1.00

Table 5. Ploughing without guide tubes, towing tension: 10 ton, towing angle: 10 deg, heavy cable

TOW WIRE					CABLE							
BOTTOM TENSION: 10.0 TON					BOTTOM TENSION (MAXIMUM): 1.0 TON							
BOTTOM ANGLE: 10.0 DEG												
WATER DEPTH	LAYBACK	CATENARY LENGTH	TOP TENSION	TOP ANGLE	BOTTOM ANGLE	PLOUGH LAYBACK	LENGTH ON SEABED	SHIP LAYBACK	TOP TENSION	TOP ANGLE	CATENARY LENGTH	BOTTOM TENSION
(m)	(m)	(m)	(ton)	(deg)	(deg)	(m)	(m)	(m)	(ton)	(deg)	(m)	(ton)
20.0	104.9	101.8	10.13	13.4	-9.0	0.0	0.0	0.0	1.16	31.6	109.4	1.00
50.0	218.2	219.1	10.27	16.4	-9.5	24.1	61.0	133.1	1.55	40.8	231.9	1.00
100.0	368.7	377.8	10.51	20.4	-9.5	24.1	143.6	201.0	2.14	48.3	401.1	1.00
200.0	600.5	630.3	11.00	26.3	-9.5	24.1	265.9	310.5	3.20	55.7	676.8	1.00
300.0	784.7	840.0	11.49	30.7	-9.5	24.1	358.5	402.2	4.16	59.9	910.5	1.00
400.0	941.7	1026.1	11.97	34.3	-9.5	24.1	434.5	483.1	5.07	62.8	1120.7	1.00
500.0	1080.4	1197.1	12.46	37.3	-9.5	24.1	499.6	556.7	5.95	65.0	1315.4	1.00

Table 6. Ploughing with guide tubes, towing tension: 10 ton, towing angle: 10 deg, light cable

TOW WIRE BOTTOM TENSION: 10.0 TON						
TOW WIRE BOTTOM ANGLE: 10.0 DEG						
CABLE BOTTOM TENSION: 1.0 TON						
WATER DEPTH	LAYBACK	CATENARY	TOW WIRE	TOP	CABLE TOP	NUMBER OF
(m)	(m)	LENGTH	TENSION	ANGLE	TENSION	GUIDETUBES
		(m)	(ton)	(deg)	(ton)	
20.0	94.6	91.8	10.2	16.0	1.04	92
50.0	184.7	186.6	10.6	21.1	1.09	187
100.0	296.5	309.0	11.1	27.2	1.18	310
200.0	460.1	500.7	12.1	35.6	1.36	501
300.0	585.6	661.1	13.1	41.5	1.53	662
400.0	690.1	805.6	14.2	46.0	1.71	806
500.0	780.7	940.3	15.2	49.6	1.88	941

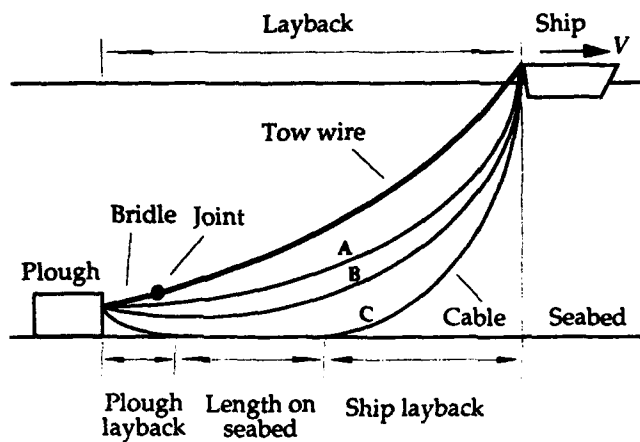


Figure 1 Ploughing operation, showing three possible cable configurations A, B and C

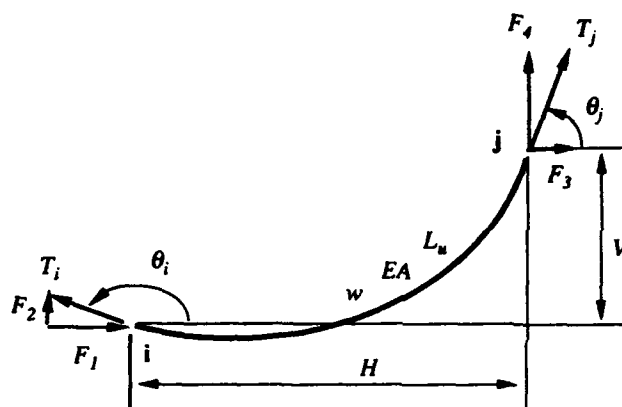


Figure 3. Plane catenary element

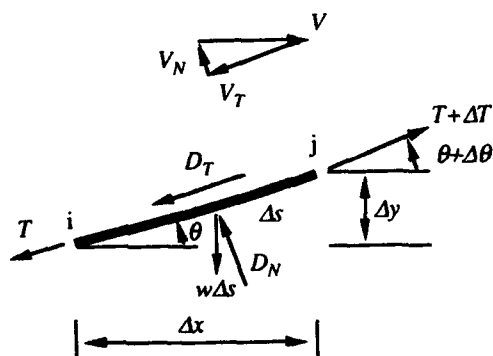


Figure 2. Forces acting on a tow line element

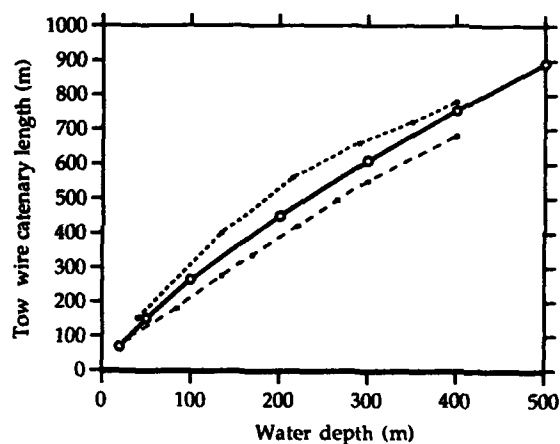


Figure 4. Comparison between predictions and measurements

- measured, lower band;
- ... measured, upper band;
- predictions, light cable,
towing tension = 5 tonnes,
towing angle = 15 degrees.

DEVELOPMENT OF FIBER SPLICING METHOD FOR OPTICAL SUBMARINE CABLE

Tatsuya Shimobachi, Shigeru Suzuki, Hidemitsu Hisata
Yuzo Tokumaru*, Toru Yanagi*, Ken Kashima*

Ocean Cable Co., Ltd.

*Sumitomo Electric Industries, Ltd.

1. ABSTRACT

We developed an optical fiber splicing method which provides a simple mechanism, efficient splicing procedure and high reliability for land installation.

The advantage of this new splicing method is as follows,

1) It is possible to splice optical fibers, proof test and reinforce the spliced portion using this fusion splicer.

2) It is possible to remove the coating of fibers without injurious chemicals.

3) As the anti-twisting mechanism is equipped with the fusion splicer, it is possible to obtain high reliability fiber spliced portion for minimizing the residual strain of twisting and bending during fiber splicing operation.

From the above-mentioned advantages, the long reliability is guaranteed for 25 years with the newly developed fiber splicing method. This allows the splicing time to be reduced to 1/4 as compared to the conventional optical fiber splicing method for the submarine cable systems.

2. INTRODUCTION

Lately, the installation of the optical submarine cable systems has been quickly advanced in communication networks of the information-oriented age and thus there has been a strong demand for enhancing efficient fiber splicing operations depending on the number of fiber splicing points increase.

Since the optical submarine cables are used for long-distance transmission, low loss and high reliability are required at their spliced portions.

Currently, it can be said that the technology for high reliability fiber splicing methods has almost been established (1), but all the methods are adopted to use the injurious chemicals at the primary coating removal procedure or the restoring of surface scratch of the optical fiber after splicing operation.

However, it is difficult to apply such methods in restricted circumstance such as manholes.

Therefore, we targeted the following items of development as a new optical fiber splicing method:

1) A compact equipment and simple process which is applicable to jointing work necessary in a manhole.

2) A safe method which does not use any injurious chemicals.

3) The failure probability of 10^{-5} or less per splicing for 25 years.

This paper reports on the theory of the developed method and the processes of its practical use.

3. THEORY

The thermal strain arising from a temperature change and mechanical strain which are caused by twisting, bending and tension strain while the handling of optical fiber splicing operation are applied to the spliced portion. (2)

The theory of reliability for optical fiber spliced portion of the land joint is shown as follows.

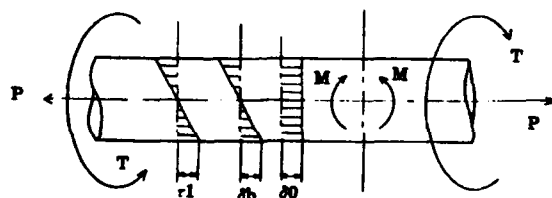


Figure 3.1
Model of Composite Stress Applied to
Optical Fiber

In this case, the value σ_1 and value σ_2 of the maximum main stress are expressed by the following equation (1):

$$\left. \begin{matrix} \sigma_1 \\ \sigma_2 \end{matrix} \right\} = \frac{1}{2} (\sigma_b + \sigma_0) \pm \frac{1}{2} \sqrt{(\sigma_b + \sigma_0)^2 + 4\tau_1^2}$$

$$= \frac{1}{Z} \left[\frac{1}{2} \left\{ M + \frac{P}{A} Z \pm \sqrt{\left(M + \frac{P}{A} Z \right)^2 + T^2} \right\} \right]$$

$$= \frac{16}{\pi d^3} \left[\left(M + \frac{Pd}{8} \right) \pm \sqrt{\left(M + \frac{Pd}{8} \right)^2 + T^2} \right] \dots\dots\dots \textcircled{1}$$

Therefore, the maximum principal strain applied to the optical fiber is expressed by equation ②:

$$\epsilon_{\max} = (\sigma_1 + \nu \sigma_2) / E \dots\dots\dots \textcircled{2}$$

where,

T: Twisting moment ($= G \cdot \theta \cdot J$, θ = Twisting angle (RAD/mm))

M: Bending moment ($= EI/R$, R = Radius of curvature)

Z: Coefficient of bent cross section

A: Cross sectional area

τ_1 : Maximum twisting force of T ($= T/Z_p$)

Z_p : Coefficient of twisted cross section ($= Z/2$)

σ_b : Bending stress at outer edge of M ($= M/Z$)

σ_0 : Vertical stress of lateral cross section of P ($= P/A$)

d: Diameter of optical fiber

E: Young's modulus of glass

G: Twisting rigidity ($= E/2(1 + \nu)$)

ν : Poisson's ratio of glass

J: Polar moment of interior of area of glass ($= \pi d^4/32$)

I: Moment of interior of area ($= \pi d^4/64$)

P: Tension ($= E \cdot \epsilon \cdot \pi d^2/4$)

Then ϵ is the thermal strain corresponding to the temperature change of thermal shrink tube used to reinforce the spliced portion. This ϵ is calculated with follows equation ③ and the material specifications of thermal shrink tube listed in Table 3.1 (1)

$$\epsilon = \frac{A_1 \cdot E_1 \cdot \alpha_1 + A_2 \cdot E_2 \cdot \alpha_2 + A_3 \cdot E_3 \cdot \alpha_3}{A_1 \cdot E_1 + A_2 \cdot E_2 + A_3 \cdot E_3} - \alpha_1 \times \Delta T \quad \textcircled{3}$$

Table 3.1
Material Specifications of Thermal Shrink

	Optical fiber (i=1)	EVA(i=2)	Steel wire (i=3)
Cross section A_i	0.0123mm ²	1.037mm ²	1.767mm ²
Y o u n g ' s modulus E_i	7300kg/mm ²	5kg/mm ²	20000 kg/mm ²
Coefficient of linear expansion α_i	$5.5 \times 10^{-7}/(^{\circ}\text{C})$	$2 \times 10^{-4}/(^{\circ}\text{C})$	$2 \times 10^{-5}/(^{\circ}\text{C})$

The temperature change ΔT is assumed as 40°C ($20^{\circ}\text{C} \rightarrow 60^{\circ}\text{C}$), above ϵ is calculated as follows,
 $\epsilon = 7.77 \times 10^{-4}$

On the other hand, the failure probability F of the spliced portion when the value ϵ_{max} of the maximum principal strain is applied to the spliced portion can be obtained from equation (4) (2).

$$F = 1 - \text{EXP}[-N_p \times m / (n-2) \times (\epsilon_{\text{max}} / \epsilon_p)^n \times t_s / t_p] \quad (4)$$

where,

N_p : Failure probability by proof test.

m : Weibull distribution parameter

n : Fatigue coefficient

ϵ_{max} : Applied load strain

ϵ_p : Proof strain

t_s : Load time

t_p : Proof time

Figure 3.2 shows the failure probability F VS proof strain ϵ_p depending on applied load strain ϵ_{max} , where $N_p=0.5$, $m=4$, $n=21$, $t_s=7.88 \times 10^8$ (25 years), $t_p=1$ d=0.125 mm, $E=7300$ and $\nu=0.17$.

For example, in order to achieve the failure probability of 10^{-5} for spliced portion more than 25 years, it is required to minimize ϵ_{max} with less than 0.0012 when ϵ_p is 5×10^{-3} .

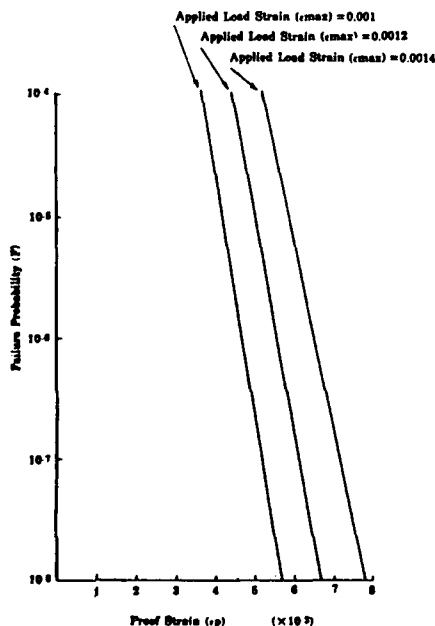


Figure 3.2
Failure Probability VS Proof Strain

4. SPLICING METHOD AND EQUIPMENT

The development of the new splicing method is targeted at minimizing bending, twisting and tension of the optical fiber. Figure 4.1 shows the process flow of the fiber splicing method.

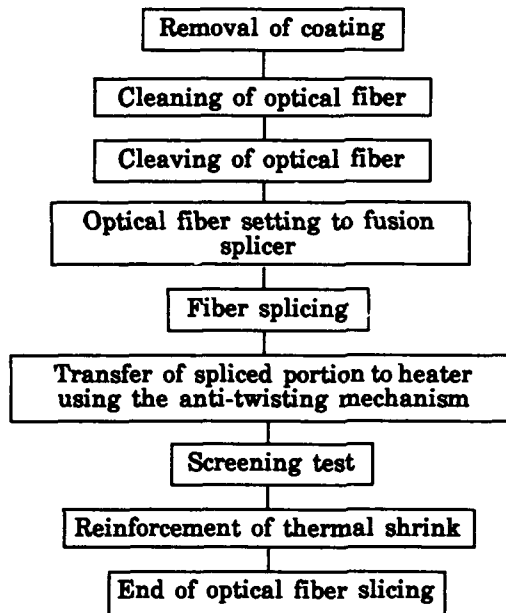


Figure 4.1 Splicing Process Flow

The fiber splicing method has the following features:

4.1 Method of Removal for Optical Fiber Coating

The coating of the optical fiber is removed by the heating remover without using injurious chemicals.

4.2 Method of Cleaving of Optical Fiber

The optical fiber cleaving length is 3mm which is the minimum value of naked optical fiber required for discharge this fusion splicing.

This cleaving length provides higher accuracy of axial alignment of the optical fiber core and lower splicing loss. In this process, the fiber cutter is designed so that it does not come into direct contact with the naked fiber and cause damage, thus providing higher splicing strength.

4.3 Versatility of Optical Fiber Clamp of Fusion Splicer

The fusion splicer is a core monitor type of fusion splicer modified to clamp the coating of the optical fiber in the V groove and allows alignment of the fiber core automatically. Consequently, this prevents damage of the naked optical fiber and provides higher splicing strength. For installation versatility, the V groove was improved to cover some types of diameters.

4.4 Equipping of Anti-Twisting Mechanism

The fusion splicer is equipped the anti-twisting mechanism for preventing twisting of the fiber spliced portion. Consequently, after fiber splicing operation, it is possible to transfer the fiber spliced portion to the heater with holding the both ends of fiber using anti-twisting mechanism.

The processes which are fiber splicing, proof test and reinforcement can be done with a single fusion splicer. Furthermore the load cell which is equipped with the fusion splicer can record the applied proof value.

Device improvement and process simplification provide a fiber splicing time of about 5 minutes. This is about a quarter of our conventional fiber splicing time.

The splicing length of 6mm allows the Thermal shrink tube to be reduced to 32mm which is approximately a half of the conventional length of 60mm (3) (4).

Figures 4.2, 4.3 and 4.4 show the outer view of the fusion splicer with the anti-twisting mechanism, the operation of the anti-twisting mechanism and the dimensions of the thermal shrink tube, respectively.

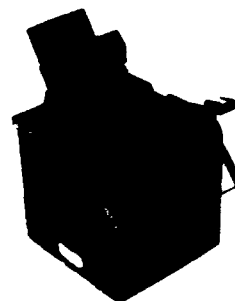


Figure 4.2 Outer View of Fusion Splicer with Anti-Twisting Mechanism

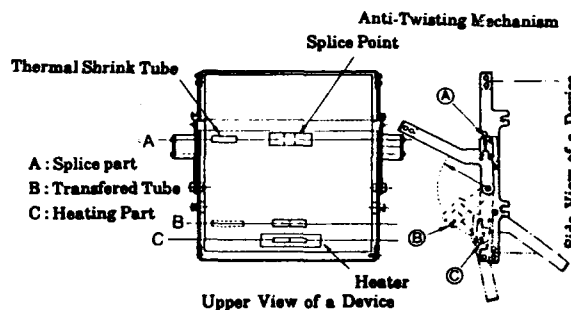


Figure 4.3 Operation of Anti-Twisting Mechanism

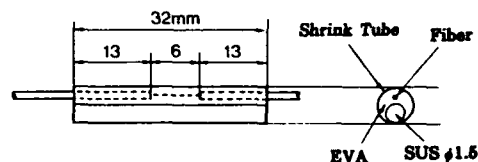


Figure 4.4 Dimensions of Thermal Shrink Tube

5. EXPERIMENT

5.1 Checking Twist-Preventing Effects at The Spliced Portion

The following are two possible causes of twisting at the spliced portion: We measured the twisting angle of the spliced portion with following two possible causes.

① When holding the optical fiber spliced portion in the anti-twisting mechanism after splicing operation.

② While the end of the above operation until the transfer to the heater.

As a result of our experiment of $n=10$, ① was 10 degrees/100mm (span of anti-twisting mechanism) at maximum and ② was zero degree. Therefore, maximum twisting angle is calculated with 0.175 RAD/100 mm.

5.2 Checking Bend-Preventing Effects at The Spliced Portion

We measured 10 spliced samples of optical fiber in a thermal shrink tube with a microscope and a Video Micro Analyzer. Measurements showed that a bend per spliced portion of 6mm long was at most 0.01mm. Therefore radius of curvature becomes $R=450$ mm.

5.3 Splicing Loss

The estimated loss of the optical fiber is image-processed and displayed by the fusion splicer. Figure 5.1 shows an example of the splicing loss characteristics of the optical fiber with the two different diameters of $\phi 0.25$ mm and $\phi 0.6$ mm.

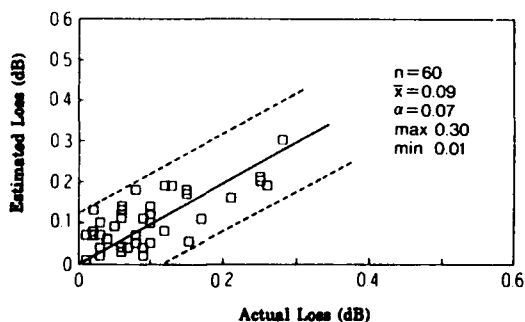


Figure 5.1
Splicing Loss Characteristics of Optical Fiber with Diameters of $\phi 0.25$ mm and $\phi 0.6$ mm

The splicing loss characteristics of fibers of $\phi 0.4$ mm and other similar diameters are approximately equal to or better than those plotted in Figure 5.1.

For the coating clamping method, attention should be paid to the dispersion of the coating diameter and the elastic deformation of the coating when fixing is performed in the V groove. For this method with a short cleaving length of 3mm, improving the V groove and allowing proper discharge conditions provides 0.13dB of an error between the actual loss and the estimated loss, 0.09dB on the average and 0.3dB at maximum.

5.4 Splicing Loss Variation

We prepared the 30 samples which are spliced and reinforced sequentially. Then the samples are applied to the test for 125 heat cycles (-20°C to $+60^{\circ}\text{C}/4$ hrs/cycle) and for high temperature and humidity (60°C , 95%RH) for 900 hours. The results of the measured loss variation during testing are shown in Figures 5.2 and 5.3. The loss variation in each test was smaller than 0.01dB per splice.

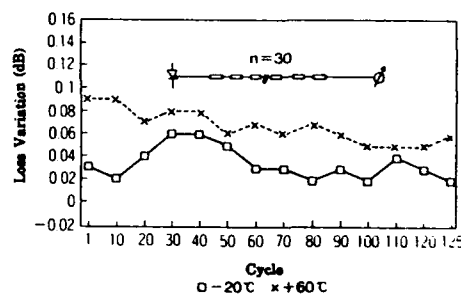


Figure 5.2
Loss Variation in Heat Cycle Test

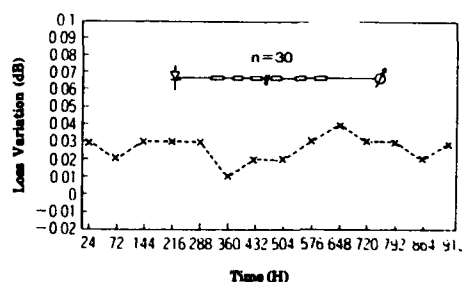


Figure 5.3
Loss variation in High Temperature and Humidity Test

5.5 Splicing Strength

5.5.1 Strength of optical fiber splicing

Figure 5.4 shows an example of the distribution characteristics of tensile strength before and after reinforcing the thermal shrink tube at the optical fiber spliced portion after a 0.5% proof test.

The strength distribution after splicing shows a gradient of 2kg at the maximum and 600g at the minimum, but after the thermal shrink tube reinforcement, the low strength distribution (below 1kg) shows a tendency for the strength to approximately double.

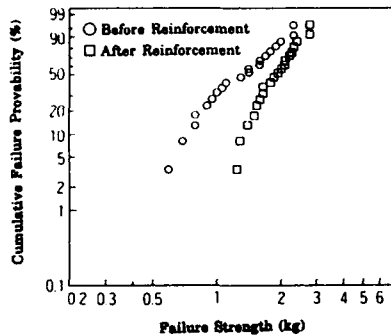


Figure 5.4

Distribution Characteristic of Tensile Strength Before and After Reinforcing Thermal Shrink Tube at The Spliced Portion

5.5.2 Measurement of fatigue coefficient n at the spliced portion

We performed a dynamic fatigue test of $n=20$ under the strain rate conditions of $2.5\% \text{min}^{-1}$, $25\% \text{min}^{-1}$ and $250\% \text{min}^{-1}$ to measure the value n at the spliced portion in this method.

Figure 5.5 shows the results of the measurements. We obtained approximately 22 as value n .

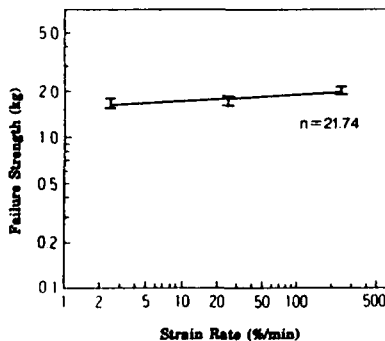


Figure 5.5

Dynamic Fatigue Test

5.5.3 Yield in 0.5% proof test

We applied a 0.5% proof test to about 600 spliced portion and found that the yield efficiency was more than 99%.

5.5.4 Strength after environmental test at the spliced portion

We applied a heat cycle test and a high temperature and humidity test as an accelerated deterioration test to the reinforced fiber spliced portion to measure the tensile strength.

Figure 5.6 shows the tensile strength distribution before and after the heat cycle test under the condition of twisted 4π per 1000mm on both sides of the spliced and reinforced portion, and Figure 5.7 shows the tensile strength distribution before and after the high temperature and humidity test under the same twisted condition.

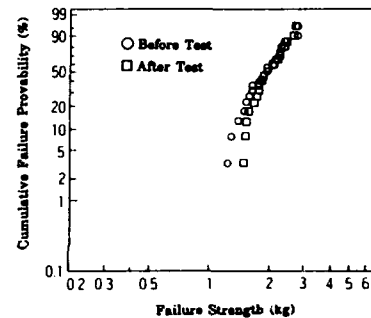


Figure 5.6

Tensile Strength Before and After Heat Cycle Test by Twisting

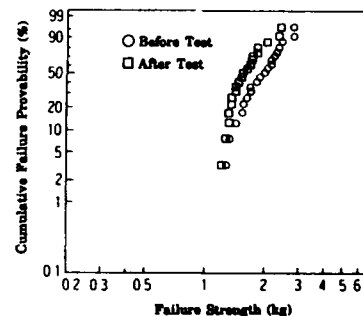


Figure 5.7

Tensile Strength Before and After High Temperature and Humidity Test by Twisting

The maximum twist which is generated with the optical fiber winding bobbin is $2\pi/2m$. Assuming that this twist propagate to the spliced and reinforced portion, we performed a heat cycle test with the spliced and reinforced portion wound around the real fiber winding bobbin.

Figure 5.8 shows the tensile strength distribution before and after the heat cycle test, and Figure 5.9 shows the tensile strength distribution before and after the high temperature and humidity test.

Although the distribution is slightly dispersed, the strength deterioration was not recognized before and after each testing. No twisting stress propagate to any fiber spliced portion even when applied from outside for a long time, and the initial strength was maintained.

We confirmed the long-term reliability of the spliced and reinforced portion with the thermal shrink tube.

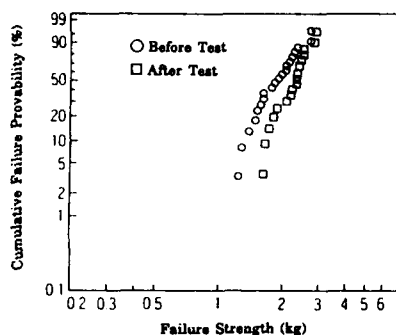


Figure 5.8
Tensile Strength Distribution Before and After Fiber Winding Bobbin Heat Cycle Test

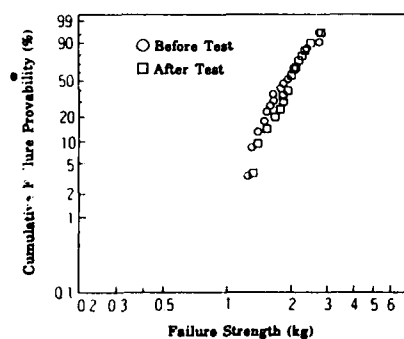


Figure 5.9
Tensile Strength Distribution Before and After Fiber Winding Bobbin High Temperature and Humidity Test

6. CONCLUSION

Taking the special environments of optical fiber submarine cable system into consideration, we have developed the new splicing method which is simplified mechanism, guaranteed safe operation and efficiency, theoretically and experimentally.

We have got the result using this method that the maximum principal strain ϵ_{max} is;

$$\epsilon_{max} = 0.00102$$

On the other hand failure probability F for more than 25 years is calculated equation ③ at Section 3.

$$N_p = 0.5$$

(In the experiment, the yield on a 0.5% proof level is more than 99% but in this calculation, a yield of 50% was used strictly).

$$m = 4$$

$$n = 22$$

$$\epsilon_p = 0.005$$

$$t_s = 7.88 \times 10^{-8} \text{ sec. (25 years)}$$

$$t_p = 1 \text{ sec.}$$

Then failure probability is calculated by substituting above parameter and $\epsilon_{max} = 0.00102$. Consequently, F is calculated with an order of 10^{-7} .

This new fiber slicing method proved to have high reliability for a long term.

Basing of above result, this new method was put into practical use and has been applied to the installation of our optical submarine cable systems.

7. ACKNOWLEDGEMENTS

The authors would like to acknowledge the assistance and co-operation of all parties involved in the development.

References

- (1) Matsumoto et al., "Long-Term Reliability Assurance for Arc-Fusion Spliced Fiber", (in Japanese) Trans. IECE Japan Vol. J 67-B, pp 521 ~ 528, 1984
- (2) Matsumoto et al., "Reliability of Arc-Fusion Spliced Fiber with Reinforcement Element", (in Japanese) Trans. IECE Japan Vol. J 66-B, pp 523 ~ 530, 1983
- (3) Matsumoto et al., "Arc-Fusion Splice of Optical Fiber and Reliability in Field", 31st IWCS, pp169 ~ 178
- (4) Tokumaru et al., "A New Reinforcement Method for Fiber-Optic Connection Parts", Sumitomo Electric Technical Review No. 22, pp140 ~ 150, 1983



Tatsuya Shimobachi
Ocean Cable Co., Ltd.
3-12-1,
Shin-Yamashita,
Naka-ku Yokohama,
Japan

Tatsuya Shimobachi was born in 1957. He graduated from Tokyo Denki University with a B. E. degree in 1982. He joined Ocean Cable Co., Ltd. and he has been engaged in research and development of optical submarine cables. He is now a senior engineer of submarine cable division.



Yuzo Tokumaru
Sumitomo Electric
Industries, Ltd.
1, Taya-cho, Sakae-ku
Yokohama, Japan

Yuzo Tokumaru was born in 1949. He graduated from Oita Technical College in 1970. He joined Sumitomo Electric Industries, Ltd. in 1970 and he has been engaged in the development of splicing technology for telecommunication cable.



Shigeru Suzuki
Ocean Cable Co., Ltd.
3-12-1,
Shin-Yamashita,
Naka-ku Yokohama,
Japan

Shigeru Suzuki was born in 1956. He graduated from Tokyo Metropolitan University with a B. E. degree in 1979. He joined Ocean Cable Co., Ltd. and he has been engaged in research and development of optical fiber submarine cables. He is now an assistant manager of submarine cable division and a member of IEICE of Japan.



Toru Yanagi
Sumitomo Electric
Industries, Ltd.
1, Taya-cho, Sakae-ku
Yokohama, Japan

Toru Yanagi was born in 1939. He joined Sumitomo Electric Industries, Ltd. in 1964 and he has been engaged in research and development of fusion splicer technology.



Hidemitsu Hisata
Ocean Cable Co., Ltd.
3-12-1,
Shin-Yamashita,
Naka-ku Yokohama,
Japan

Hidemitsu Hisata was born in 1967. He graduated from Tokai University with a B. E. degree in 1990. He joined Ocean Cable Co., Ltd. and he has been engaged in development of submarine cable. He is now a engineer of submarine cable division.



Ken Kashima
Sumitomo Electric
Industries, Ltd.
1, Taya-cho, Sakae-ku
Yokohama, Japan

Ken Kashima was born in 1969. He graduated from Shinsyu University with a B. E. degree in 1992. He joined Sumitomo Electric Industries, Ltd. in 1992 and he has been engaged in the development of splicing technology for telecommunication cable.

LOW FIRE HAZARD CABLES - THE EUROPEAN EXPERIENCE

J Richard Barker,

D Elizabeth M Ness

BICC Cables (NA) Indianapolis IN, BICC Energy Cables (UK) Prescott UK

Abstract

This paper highlights the growth of Low Fire Hazard cables in the European marketplace. It examines three differing applications for Low Fire Hazard cables; The Channel Tunnel, European Rolling Stock, and Fire Survival cables in Germany. The associated advances in both cable design and material technology needed to meet these new customer requirements are discussed.

The possible future developments in fire testing are discussed, where the testing of complete systems, as opposed to materials or single cables, is gaining recognition world wide.

In this paper, particular emphasis is given to the German DIN 4102 Pt.12¹ Fire test as being an example of the future of fire testing for electrotechnical systems.

1.0 Introduction

Reduced fire hazard cables are still a growing part of the European cable manufacturers' portfolio.

The ubiquitous "electrical fault" is often given as the cause of many fires (e.g. UK Home office survey) and major disasters lead to tightening of regulations on a broad front.

The loss of HMS Sheffield during the Falklands conflict led to a review of all cable specifications by the UK Ministry of Defence (Navy). Similarly, the aftermath of the Kings Cross transit fire caused transit authorities world wide to review and tighten cable specifications.

The initial impetus came in the early 1970's from loss of the La Spezia power station in Italy where power cables utilizing traditional PVC compounds caused transmission of the fire throughout the structure. This event led to CESI (Centro Elettrotecnico Sperimentale Italiano) developing the vertical ladder propagation test for cables which has now developed into IEC 332-3², IEEE 383³, CSA FT4⁴ and the proposed IEEE 1202⁵ range of propagation test.

The evolution of the cable fire propagation test to include smoke emission, rate of heat release, and measurement of effluent as in UL 1202 reflects the maturing of fire testing of cables to encompass all potentially hazardous aspects of fire.

As fire testing has developed, so in response have market needs. Consequently the European cable engineer has had to develop both materials and cable designs to meet ever more exacting customer requirements.

This paper examines three different cable applications, and reviews the developments in technology required to meet advanced reduced fire hazard specifications.

2.0 Low Smoke and Fume Jacket Materials

In the early 1980's London Underground banned the use of halogenated materials for cables. The first zero halogen cables had poor mechanical and physical properties: tensile strength less than 700 psi, tear strength less than 20 lb/in, and very poor resistance to water.

Using statistical experimental techniques, formulations have been developed which surpass even the established PVC jacketing materials in mechanical and physical properties.

Each candidate component of the new low smoke and fume (LSF) jackets are subjected to rigorous examination alone and in combination with each other.

This total mapping has allowed selection of an optimum formulation for each customer application.

A conservative estimate for the total number of possible combinations from Table I that can be examined is several million. However, the use of statistical methods reduces experimental trials to less than 100 and maximizes the information that can be gained.

VARIABLE NAME	CATEGORIZED VARIABLE	CONTINUOUS VARIABLE
POLYMER	Homopolymer Copolymer/Terpolymer Polymer Blend	Melt Index / Mooney Viscosity Copolymer Content Blend Ratio
FILLER	Chemical Type Morphology Ionic Purity	Particle Size Concentration
FILLER TREATMENT	Chemical Type	Concentration
STABILIZER	Chemical type Lone Synergistic	Concentration
APPLICATION	Thermoplastic Thermoset	Degree of x-linking
CURE SYSTEM	Peroxide Type Co-agent Type E-Beam Promoter	Concentration Dosage
SPECIAL ADDITIVES	Flame Retardants Hydrophobicity Promoters Process Aids Light Stabilizers	Concentration

Table I: Experimental Variables

PROPERTY	CONSIDERATION
COST	Price vs Performance
RHEOLOGY	Viscosity Temperature Melt Fracture
PHYSICAL PROPERTIES	Tensile Strength Elongation Tear Abrasion Etc.
HEAT AGEING	Retained Physical Property Temperature Time
FLUID RESISTANCE	Retained Physical Property Swell/Uptake Temperature Time
COLD TEMPERATURE PERFORMANCE	Brittleness Temperature Cold Bend Impact
FIRE PROPERTIES	LOI & Temperature Index Smoke Emission Small Scale Fire Performance (VW-1) Large Scale Fire Performance (IEEE 383)
AESTHETICS	Smoothness/Coefficient of Friction Strippability Color Printability

Table II: Experimental Responses

One of the most onerous applications for the new generation of LSF jackets was the UK/France Channel Tunnel (Figures Two & Three). Enhanced moisture and salt spray resistance were essential, and, as the cables are unarmored, the jacket has to be exceptionally tough.

The cable was specially designed to pass Category A of the IEC 332-3 propagation test, which is the most severe at a loading on the ladder of 7 litres/metre non-metallic cable volume.

Table III shows properties of the developed LSF jacket in comparison with a reduced propagation PVC jacket.

This type of enhanced LSF formulation has also been used in new power station constructions and is approved by London Underground, as well as surpassing the requirements of the British Standard for Low Smoke and Fume Armored Cables, BS6724⁶.

PROPERTY	REDUCED PROPAGATION PVC	NEW ENHANCED LSF	UNITS
<u>MECHANICAL PROPERTIES</u>			
Tensile Strength at Break	> 12.5 >1775	> 13 >1850	MPa psi
Tear Resistance	8 45	11 63	N/mm Lb/in
Elongation at Break	≥ 150	145	%
<u>REACTION TO MOISTURE</u>			
Water vapor permeation rate (1mm thick plaque)	3.2	1.3	g/m ² /24hr
7 days, 70°C in water, 1mm plaque % water uptake	2.1	1.2	%
<u>REACTION TO FIRE</u>			
	Armored	Unarmored	
IEC 332-3 Cat A Propagation	Pass	Pass	
IEC 1034 ¹¹ Smoke Emission Channel Tunnel requirements	Fail	Pass	

Table III: Properties of Enhanced Low Smoke and Fume (LSF) Jacket

3.0 The Channel Tunnel Rolling Stock Cables

The main market needs in Mass Transit revolve around the efficient movement of a large number of people through confined spaces in safety and comfort. In addition, the modern mass transit system will be high technology, often employing air conditioning with forced air circulation.

Many trains and trams are designed to move both in the open and in tunnels. Thus, all the key safety features of the highest technology low fire hazard cables are needed.

For the Channel Tunnel, cable for both Shuttle

and Through-Train applications required enhanced levels of toughness, flexibility, temperature range, thermal ageing, fluid/acid/alkali resistance, reduced fire propagation and low smoke and fume.

These cables also must contain zero halogen content.

Variations of the Channel Tunnel (TransManche Link, TML⁷) specifications can be found across Europe, (the closest are the French standards) but as yet this remains the most challenging specification.

Table IV shows the advance in cable specification.

PROPERTY	FORMER REQUIREMENTS	NEW REQUIREMENTS FOR THE CHANNEL TUNNEL
Service Life at Operating Temperature	Unspecified	Up to 100,000 hours
Fluid Resistance	ASTM No. 2 Oil	ASTM No.2 Oil ASTM No.3 Oil Ester Based Oils (e.g. Midel)
Flame Retardancy	IEC 332-1 (single cable)	IEC 332-1 ⁸ (Single Cable) IEC 332-3 (Large Scale cable bunch) NF C 32 070 ⁹ - bunched cables.
Smoke Emission	None	NBS Smoke Chamber (ASTM E662 ¹⁰) IEC 1034 ¹¹ (3m Cube)
Fire Effluent Tests		IEC 754-1 ¹² IEC 754-2 ¹³ NF C 20 454 ¹⁴

Table IV: Advances in Mass Transit Rolling Stock Cable Specifications.

4.0 Fire Survival in Germany

Fire survival cables, one example being the well known mineral insulated, copper clad products are widely used for systems which must operate during and after fire. The IEC test for continued operation (IEC 331) exposes a single cable to a flame of specified temperature (650°C) and measures time to electrical failure. Three hours is the maximum test time.

The British Standard, BS 6387¹⁵, extends this concept to temperatures up to 950°C and includes the effects of impact and water spray.

The German authorities have taken a further step, and insist that all fire survival cables systems are tested as an entity according to DIN 4102 Pt.12, therefore cables are tested with a nominated make of accessories; ladders, trays, ceiling holders and ceiling clips.

Cables are installed into the test room as they would be in a real installation, including cleats and bends. The test room is built around the cables for each test. When installed, the cables are energized at rated voltage, and continuity monitored throughout the test. The cables are exposed to gas flames, and the temperature of test chamber rises according to the ISO curve to reach 1000°C after 90 minutes (Figure One).

Survival ratings are for 30, 60 and 90 minutes for at least two identical samples. In practice, only the 30 and 90 minute ratings are user specified: E30, E90.

To pass the test, cables must be designed with fire survival as the prime objective, although the

products must also meet the complete zero halogen specification VDE 0266¹⁶.

Typically, to meet the lowest E30 rating, fire protection tapes are utilized. To meet E90 requirements, a much more robust construction is essential, requiring special insulation and several protective tape layers.

To gain qualification, the test must be carried out with each make of cable accessory. Cables are marked with their test certificate numbers, and must be sold as a system.

The test itself costs in the region of \$10,000, with the additional cost of ancillary equipment, and manpower for the time required to construct the test enclosure (approximately one full week).

This new generation of fire survival cables will be specified in all essential circuits (fire alarm, smoke/heat extraction, emergency lighting, etc) by the German Länder through State Building Regulations.

5.0 Summary

These three recent advances in reduced fire hazard cable technology for the Channel Tunnel, European Rolling Stock and the German Fire Survival cables are typical of the ever advancing European customer requirements.

The move to testing complete cable systems in Germany has been echoed in Australia, with a similar testing regime (AS 3013¹⁷) and must represent the future need to test representative electrotechnical systems in realistic fire scenarios.

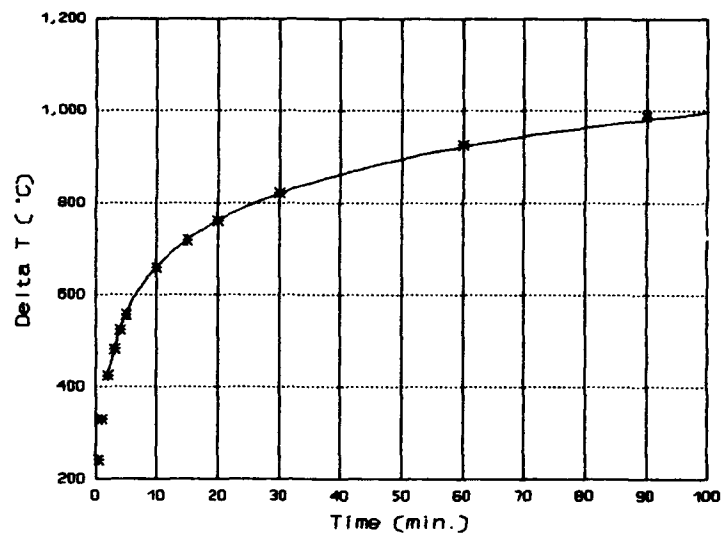


Figure 1 ISO Curve

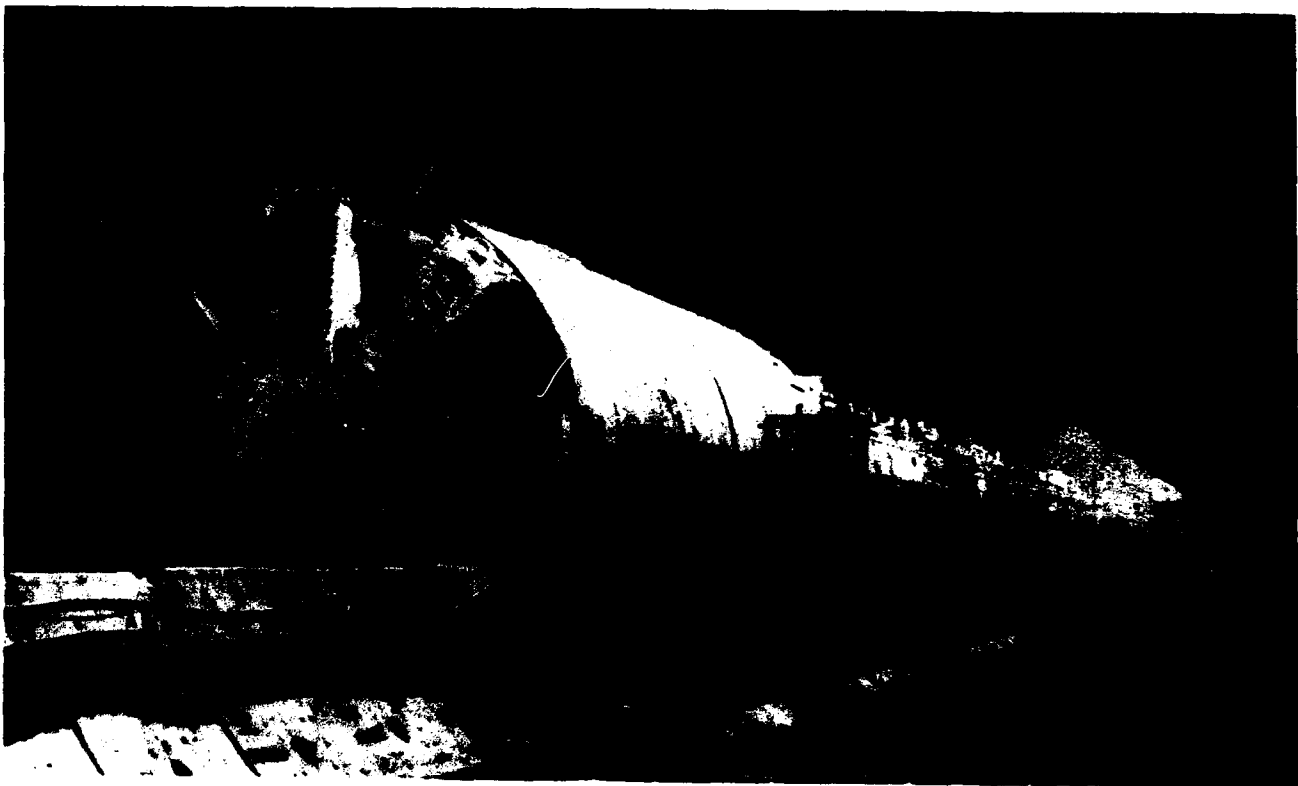


Figure 2 Channel Tunnel Boring Machine

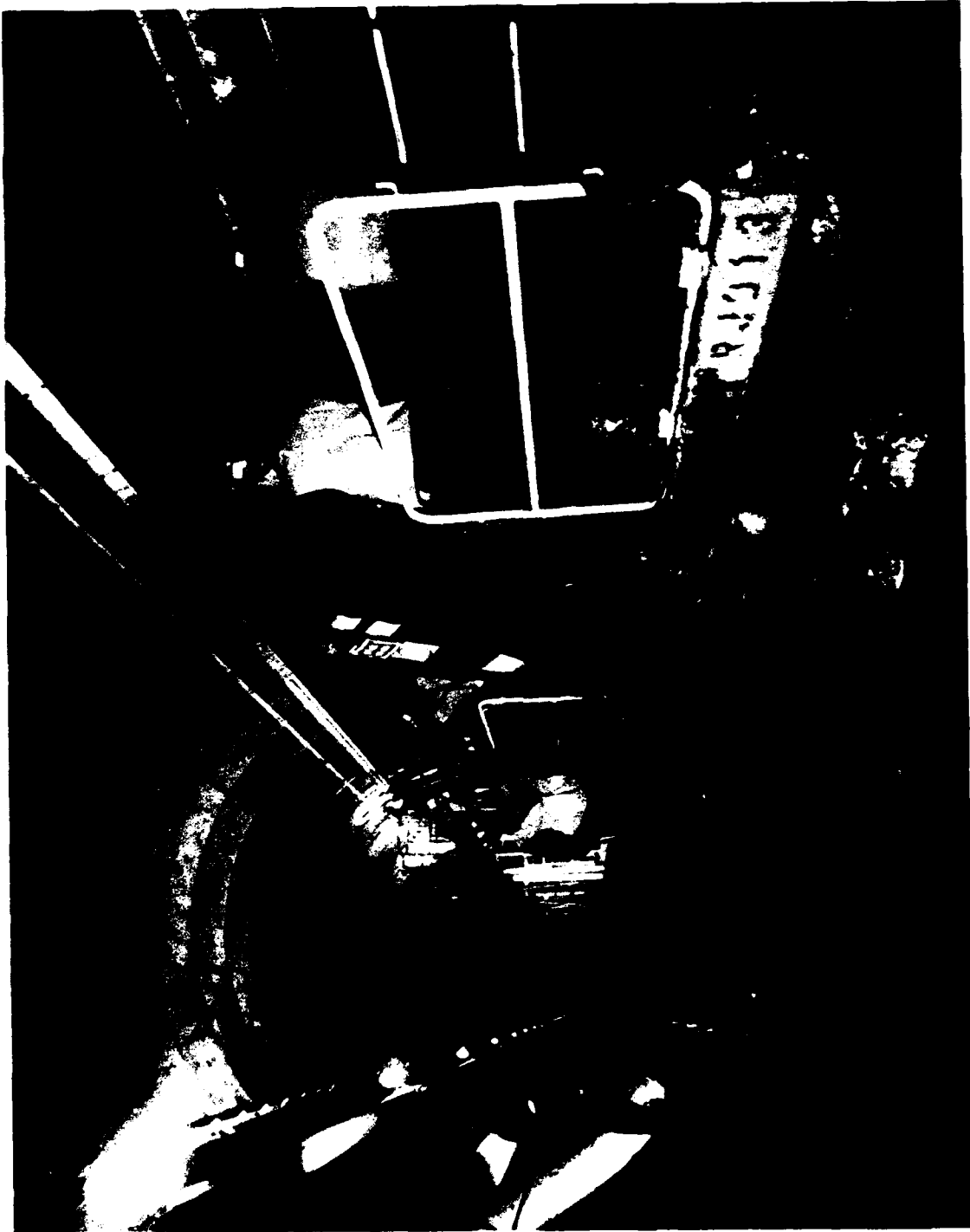


Figure 3 Installation of Zero Halogen Cable in the UK/France Channel Tunnel

References

1. DIN 4102 pt12 Fire Behavior of building materials and components. 1991.
2. IEC 332-3 Vertical fire test on a cable bunch. 1989.
3. IEEE 383 Vertical Tray flame test (UL 1581)
4. CSA FT4 C22.2 # 0.3-M1985 Test methods for electrical wires and cables
5. IEEE 1202 IEEE Standard for flame testing of cables for use in cable tray in Industrial and Commercial occupancies 1991.
6. BS6724 Armored cables for electricity supply having thermosetting insulation with low emission of smoke and corrosive gases when affected by fire 1990.
7. TML Specs:

TM 1-04 Technical specification for cable & wires with thin wall insulation for control and monitoring circuits 1990.

TM 1-05 Technical specifications for cables and conductors of Power circuits 1990.

TM 1-06 Technical specifications for special cables and conductors 1990.
8. IEC 331 Fire resisting characteristics of Electric cables 1970.
9. NF C 32 070 Fire testing of bunched cables.
10. ASTM E662 Standard test method for Specific optical density of smoke generated by solid materials 1983.
11. IEC 1034 Measurement of smoke density of electric cables burning under defined conditions, pt 1:1990, pt 2:1991.
12. IEC 754-1 Determination of the amount of Halogen acid gas evolved during the combustion of polymer material taken from cables 1982.
13. IEC 754-2 Determination of the degree of acidity of gases evolved during the combustion of polymer material taken from electric cables by measuring pH and conductivity 1982.
14. NF C 20 454 Analysis and titration of gases evolved by pyrolysis or combustion of materials used in electrotechnics 1984.
15. BS 6387 Performance requirements for cables required to maintain circuit integrity under fire conditions 1983.
16. VDE 0266 Cables with improved characteristics in cases of fire (Draft) 1993.
17. AS 3013 Electrical installations - Wiring systems for specific applications 1990.

Acknowledgements

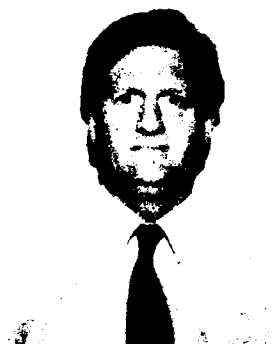
L. Tingle, H Tipping, G Roberts, T Jones
BICC Energy Cables (UK)

J Richard Barker

Richard Barker is a graduate in Polymer Science and Technology from Manchester Polytechnic (UK) and is a member of the Institute of Electrical & Electronic Engineers and the Plastics and Rubber Institute (UK).

Richard joined BICC at its' Elastomeric cables facility in Leigh (UK) in 1973, and worked for several years in polymeric formulations for elastomeric cable applications including reduced fire hazard materials. In early 1987 he transferred to the newly formed Technology Centre at Wrexham (UK) and worked with Dr Ness on fire testing and low fire hazard cables.

In 1991 he moved, with his family, to Indianapolis (USA) as the R&D Manager for Industrial Products at the Indianapolis Technology Center BICC NA.



D Elizabeth M Ness

Dr. Ness is a graduate in Chemistry, and obtained her doctorate on the photo-degradation of polymers. This was followed by post-doctoral research into emulsion polymerization. She is a Chartered Chemist, Member of the Royal Institute of Chemistry, and member of the Plastics and Rubber Institute.

Elizabeth joined BICC at its' Research and Engineering Centre in 1978, and has been involved for many years in the development of new cable materials, particularly those with reduced fire hazard properties. She was Manager of the Polymer Materials Department of the new BICC Cables Wrexham Technology Centre, and is now Business Development Manager of BICC Cables Energy Division at Prescott, Merseyside, UK.

Dr Ness is a member of several British Standards Committees dealing with reaction -to-fire tests, and is secretary of the IEC TC89 Working group 7, dealing with Toxic Hazards from fire involving Electrotechnical Products.



CONE CORROSIMETER TESTING OF FIRE RETARDANT AND OTHER POLYMERIC MATERIALS FOR WIRE AND CABLE APPLICATIONS

Diana S. Malin

Quantum Chemical Corporation, USI Division

ABSTRACT

In the past, materials have been specified into applications requiring flame retardant properties, based on the chemical composition of the product, not necessarily based on the material's fire performance in the application.

The Polyolefins Fire Performance Council of the Society of the Plastics Industry, Inc., studied 23 different, commercially available materials using the Cone Corrosimeter as proposed by ASTM D 09.21.04. Combustion property data on each material was collected, including ignition time, heat release rate, total heat released, heat of combustion, and smoke.

In this paper, the results for the various materials tested are reported and compared. These data indicate that the perceived advantages and disadvantages of specific materials are not always confirmed from the results of Cone Corrosimeter testing. These results confirm the need for specifications to be based on performance and not on material composition.

The results also indicate that all material combustion properties relevant to the specific application should be considered when evaluating the potential hazard of a material in a fire situation.

1.0 INTRODUCTION

The Polyolefins Fire Performance Council (PFPC), an operating unit of the Society of the Plastics Industry, Inc. (SPI), has published data comparing four test methods on 23 materials for determination of smoke corrosivity.¹⁻⁶

One of the methods evaluated in these studies was "Fire Response Standard for Determining the Corrosive Effect of Combustion Products Using a Cone Corrosimeter", proposed by ASTM D 09.21.04. In this method, a Cone Calorimeter as described in ASTM E 1354, "Standard Test Method for Heat and Visible Smoke Release Rates for Materials and Products Using an Oxygen Consumption Calorimeter", with the addition of a gas sampling system, is used to determine corrosivity. During the tests, data relating to the combustion properties of the materials were generated, in addition to corrosion measurements. The purpose of this work was to examine the available combustion data generated by the Cone Corrosimeter of the test materials.

The polymeric materials evaluated included several different wire and cable coating materials, including polyolefins with mineral fillers, polyolefins with halogen flame retardants, halogenated polymers, high temperature thermoplastics, intumescent polypropylene, polyolefin base resins, nylon base resin, and a Douglas fir reference material.

All of the experiments were performed at the Underwriters Laboratory at Northbrook, Illinois under the direction of Dr. Pravinray Gandhi.

2.0 MATERIALS EVALUATED

Table I lists the 23 polymeric materials evaluated in the PFPC Cone Corrosimeter study⁴. These resins and compounds represent a broad sampling of polymeric materials that are used in wire and cable jacketing and insulation applications. They are all commercially available.

The study included polymeric materials that retard flame spread by several means. Samples 1 - 8 composed of hydrated mineral fillers compounded with polyolefin resins or resin blends. They retard flame spread by the endothermic release of water-of-hydration.

Sample 9 is an intumescent polypropylene compound containing a phosphorus flame retardant additive. This material retards flame spread by formation of a char barrier. Its flaming characteristics are different from most of the others studied.

There are two types of halogenated flame retardant materials included. Samples 10 and 11 contain halogenated additives. Samples 12 - 16 have halogen chemically bonded to the polymer backbones. Brominated and chlorinated materials deter flame spread by halogen radical release and subsequent formation of flame poisoning radicals. They act in the vapor phase to extinguish flame, often through the synergistic action of the halogenated species with antimony oxide. Fluoropolymers are halogenated materials that have a very high limiting oxygen index and retard flame spread by resisting ignition.

Included are three high temperature thermoplastic materials. Sample 17 is a polymer alloy containing a phosphorus flame retardant additive. Sample 18 is an unfilled Polyetherimide (PEI) resin. Sample 19 is a PEI/siloxane copolymer that resists flame spread by the formation of a char barrier. Samples 18 and 19 are also difficult to ignite and retard flame spread by resisting ignition.

Samples 20, 21 and 22, three unfilled base resins from different suppliers are included to compare filled versus unfilled resins.

Finally, Sample 23, Douglas fir, was included as a standard as it is widely used as a control in flame testing of materials for the building industry.

3.0 EXPERIMENTAL

3.1 APPARATUS

The Cone Calorimeter, as described in ASTM E 1354-90, was developed by the National Institute of Standards and Technology (NIST). The test was designed to measure the response of a material to controlled levels of radiant heat with or without a spark ignition source. The test provides combustion data such as ignitability, heat release, mass loss, and smoke release of specimens under a range of heat flux conditions. The Cone Calorimeter also has the capability of measuring the CO and CO₂ content of combustion gases.

A Cone Corrosimeter, as described in proposed method ASTM D 09.21.04, is a Cone Calorimeter with a gas sampling apparatus. The gas sampling apparatus enables the Cone Corrosimeter to measure the corrosivity of the test material's combustion products, in addition to combustion data. The gas sampling apparatus removes a portion of the gases from the exhaust stream, which could effect the results of the combustion data measurements of heat and smoke release. The gas sampling apparatus would not be expected to effect the measurement of ignitability of the specimen.

Figure 1 shows the Cone Corrosimeter apparatus. The apparatus consists of a conical heater, a temperature controller, an exhaust system, a load cell, a specimen holder, an ignition circuit, a smoke obscuration measuring system, a gas sampling system and a corrosion target.

The gas sampling system consists of a conical funnel, stainless steel gas sampling tip, stainless steel tubing, electrical heating tape, silicone rubber tubing, flowmeter, exposure chamber, target support stand and a pump. The exposure chamber is shown in Figure 2.

For corrosion testing, two targets, available from Rohrbach Cosasco Systems, were used during each test at each heat flux. Model 610 is a double loop copper film on a glass substrate, mounted to a plastic strip with a copper film thickness of 2500 Å. Model 030788-S0.35-8061 is a double loop copper film encapsulated in a plastic substrate with a copper film thickness of 45,000 Å.

3.2 TEST PROCEDURE

The Cone Corrosimeter protocol to develop corrosion data as described in the proposed ASTM D 09.21.04 method was followed⁴. In addition to corrosion data, combustion data was also collected. ASTM E 1354-90 describes the methodology behind collection of the combustion data. The specimens tested were 100 x 100 x 6.3 mm molded plaques.

The test protocol does not specify the heat flux to be used. The proposed ASTM D 09.21.04 method suggests heat fluxes of 25 and 50 kW/m² in the Nonmandatory Appendix. In this study, heat fluxes of 25 and 50 kW/m² were used to simulate two different fire scenarios, although bench tests cannot duplicate actual fire conditions.⁴ These heat fluxes are also suggested in the Nonmandatory Appendix of ASTM E 1354-90.

Some materials, such as compounds with mineral fillers, do not lose 100% of their mass when burned. The Cone Corrosimeter method is run until the sample loses 70% of its total combustible mass, or one hour, whichever is a shorter time.

In order to determine the 70% mass loss, prior to conducting the corrosion tests, two mass loss determination tests were conducted on each material to establish the total mass loss at the designated heat flux. From an average of this data, 70% mass loss of each material is calculated. These mass loss determination tests are run using the same procedure as the corrosion determinations, but without corrosion gas sampling.

For each corrosion determination test, the following procedure was followed.

After setting the exhaust flow rate, the heat flux and load cell were calibrated. The initial mass of the specimen was recorded. The specimen was mounted in the specimen holder, backed with aluminum foil and topped with a grid to prevent spark igniter fouling with samples that intumesce. The specimen was placed on the load cell and exposed to radiant heat at the chosen heat flux. A spark igniter was used to ignite combustible vapors released by the specimen under the heat flux. The time until ignition was recorded.

After ignition, the sample was allowed to burn. Heat release rate and sample weight loss were monitored continuously during the combustion process. The combustion gases from the specimen were drawn past a laser detector which measured visible smoke generation (specific extinction cross-section area). CO and CO₂ content of the combustion gases was not determined for all materials, therefore the data will not be discussed.

A portion of the combustion gases were drawn into the corrosion gas sampling apparatus. The sampling flow was stopped when the specimen lost 70% of the total mass loss determined previously, or 60 minutes elapsed after the start of the test. The inlet and outlet lines of the exposure chamber were sealed to allow the combustion products to react with the target for one hour from the start of the test. The targets were removed from the exposure chamber and placed in an environmental chamber with a dry bulb temperature of 23°C and 75% relative humidity. After 24 hours of conditioning in the environmental chamber, the resistance of the corrosion target was measured from which metal loss was calculated⁴.

3.3 RECORDED DATA

The following combustion data was recorded during each of the initial mass loss and corrosion tests: sample identification and composition, date, room temperature and relative humidity, specimen thickness and mass, radiant heat flux, corrosion target span and identification, volumetric sampling rate, time to sustained flaming, mass loss data, heat release, visible smoke generation and time of test start. CO and CO₂ content of combustion gases was determined on some of the materials.

For determination of corrosion potential, the following information was collected: corrosion exposure chamber temperature, sampling time and corrosimeter values of the targets at the start of the test, at the end of the one hour combustion products exposure and at the end of the 24 hours of post-exposure in the environmental chamber.

4.0 DISCUSSION OF RESULTS

4.1 SUMMARY OF DATA

Time to ignition is not affected by gas sampling. Therefore the data from all specimen tests, including the initial 70% mass loss determinations, were analyzed for time to ignition.

The gas sampling for corrosion testing removes some combustion products from the exhaust stream, which may effect the data collected for maximum heat release, average effective heat of combustion and smoke generation. Therefore, the data used in the analysis of these properties were limited only to the data from the corrosion determination tests. The data collected from the initial 70% mass loss determinations were not included in the analyses of maximum heat release, average effective heat of combustion and smoke generation.

Several of the specimens did not ignite or were not tested at a heat flux of 25 kW/m², therefore, only data at 50 kW/m² was evaluated.

Corrosion data discussed will be limited to the data developed using the 45,000 Å target, as many of the 2,500 Å target results went off-scale for several of the materials⁴. In addition, the 45,000 Å target resulted in the broadest differentiation of the materials tested⁵.

For Samples 9 (Intumescent PP), 15 (PTFE), 20 (PE homopolymer) and 21 (EVA) only time to ignition is discussed. These materials melted over the edges of the sample pan and dripped from the load cell onto the bottom of the combustion chamber. When this occurred, the mass loss determinations became invalid, as did the heat release, visible smoke generation and corrosion results.

The time to ignition data for each test at a heat flux of 50 kW/m² are shown in Table II. The mass loss, maximum heat release, total heat release, average effective heat of combustion, smoke generation and corrosion data for each corrosion test at a heat flux of 50 kW/m² and 45,000 Å target are shown in Table III. Data for time to ignition, maximum heat release rate, specific extinction cross-section area and corrosion were statistically analyzed, using the Studentized Maximum Modulus Test⁷. This test groups the samples statistically. Results for samples in the same group are considered statistically indistinguishable from each other, based on this data. The results of this analysis are shown in Table IV.

Calculations for determination of average maximum heat release rate, average effective heat of combustion, and average specific extinction cross-section area are shown in Appendix A.

4.2 SAMPLES WHICH ARE DIFFICULT TO IGNITE

Sample 14 (PVDF) pyrolyzed during the test at 50 kW/m². As noted in Table II, Sample 14 lost weight during the test, however, it did not burn in a manner similar to the other materials tested, because it is very difficult to ignite. Since weight loss took place during the pyrolysis, measurements of heat release, smoke and corrosion were possible.

4.3 IGNITION TIME

The measurement of ignition time gives an indication of the speed at which a sample can be ignited under the conditions of this test, in which the material is exposed to a spark ignition source while under a 50 kW/m² heat flux. Ignition results are shown in Figure 3.

Samples 14 (PVDF) and 15 (PTFE) had the longest ignition times of all the samples, confirming the difficulty in igniting these fluoropolymer materials.

As a group, the high temperature thermoplastic compounds (Samples 17, 18 and 19) were not significantly different in performance than the mineral filled polyolefin compounds.

As a group, the mineral filled polyolefin compounds (Samples 1-8) had longer ignition times than the intumescent polypropylene sample (Sample 9).

Mineral filled polyolefins compounds had a longer time to ignition than polyolefin base resins, as shown by a comparison of Samples 1 - 8 as a group with Samples 20 and 21 as a group.

Time to ignition of polyolefins with halogenated flame retardant additives was not significantly different from time to ignition of polyolefin base resins, as shown by a comparison of Samples 12 and 13 as a group with Samples 20 and 21 as a group.

4.4 MAXIMUM HEAT RELEASE RATE

Maximum heat release rate is the peak heat release rate per unit sample area. The peak heat release rate is the maximum point on the heat release vs. time curve. The calculation for maximum heat release rate is shown in Appendix A. Maximum heat release rate results are shown in Figure 4.

Sample 22 (Nylon) had the highest maximum heat release rate of the materials tested followed by Sample 17 (high temperature thermoplastic compound) and Sample 10 (crosslinked polyethylene copolymer with chlorinated additive).

Sample 14 (PVDF) had the lowest maximum heat release rate.

4.5 TOTAL HEAT RELEASE

Total heat release is the summation of the heat release rate over the entire test time. Total heat release results are shown in Figure 5.

Sample 10 (crosslinked polyethylene copolymer with chlorinated additive) had the highest total heat release of the samples tested. Sample 16 (PVC) had the lowest total heat release.

4.6 EFFECTIVE HEAT OF COMBUSTION

Effective heat of combustion is a calculated value indicating the heat release per unit specimen consumed during combustion. The calculation used to determine effective heat of combustion from the Cone Calorimeter measurements is shown in Appendix A. Effective heat of combustion data are shown in Figure 6.

Samples 14 (PVDF) and 16 (PVC) had the lowest average effective heat of combustion under the heat flux conditions of this test.

4.7 SPECIFIC EXTINCTION CROSS-SECTION AREA

Specific extinction cross-section area is a value derived from a measurement of smoke obscuration taken by a laser optical system located in the exhaust system. The calculation for specific extinction cross-section area is shown Appendix A. Specific extinction cross-section area results are shown in Figure 7.

Sample 17 (high temperature thermoplastic) produced the most smoke of the materials tested.

The mineral filled polyolefin compounds (Samples 1 - 8) as a group produced less smoke in this test than halogenated polyolefin compounds (Samples 10 - 13).

Halogenated polyolefin compounds (Samples 10 - 13) as a group produced more smoke in this test than Samples 14 (PVDF) and 16 (PVC).

Samples 17 and 19, high temperature thermoplastic compounds, produced more smoke in this test than the mineral filled polyolefin compounds (Samples 1 - 8).

4.8 CORROSION

Corrosion measures the corrosive potential of combustion gases⁴. A 45,000 Å probe was used for the data reported. Corrosion results are shown in Figure 8.

Samples 16 (PVC) and 12 (halogenated polyolefin compound) produced the highest level of corrosion of the samples tested.

The mineral filled polyolefin samples (Samples 1 - 8), as a group produced lower corrosion than halogenated samples (10, 12, 13, 14, and 16).

Sample 11 (crosslinked polyethylene copolymer with brominated additive) did not significantly differ in corrosion performance when compared with the mineral filled polyolefin compounds.

Samples 17 and 19, high temperature thermoplastic compounds did not significantly differ in corrosion performance when compared with mineral filled polyolefin samples (Samples 1 - 8).

4.9 USE OF CONE CORROSIMETER DATA FOR HAZARD ASSESSMENT

The search for an easy way to classify materials according to their hazard in fire situations has been ongoing for many years. Some have proposed the creation of a "hazard index" by combining the heat release, visible smoke, ignitability, toxicity and corrosivity to rate the expected combustion behavior of a material or finished product. The Cone Corrosimeter, when comprised of a Cone Calorimeter and gas sampling apparatus, can provide a measure of heat release rate, visible smoke generation, ignitability, corrosivity and CO and CO₂ emissions. The information presented in Table IV shows that a material can perform well in one combustion parameter, but not so well in another.

For example, the data developed by PFPC show that some materials, such as Sample 14, are difficult to ignite with the energy available in some fires. However, Sample 14 pyrolyzed as evidenced by the weight loss and caused corrosion of the targets. The difficulty in igniting these types of materials may be outweighed by the corrosive potential of the material in certain situations, such as in electronic installations. However, the same material may be beneficial in some applications because it has a longer ignition time and low visible smoke while smoldering.

Another aspect of hazard assessment is the specification of materials for applications based solely on chemical composition. Some of the common perceptions about performance of materials based solely on composition are not borne out by the test results. For example, Sample 4, a crosslinked polyethylene copolymer with brominated additive, performed similarly to the mineral filled polyolefin samples in corrosivity testing. Also, the PVDF sample (Sample 14) was among the lowest visible smoke producers because it pyrolyzed at the heat flux of 50 kW/m².

Selection of materials should be done on the basis of application and after considering all relevant combustion parameters.

Possible alternatives to a single "hazard index" exist. One possible alternative would be devising a hazard index for each different application, weighing the various parameters according to their importance in the application. Another option would be rating a material's combustion properties separately, similar to the National Fire Protection Association's (NFPA) health, flammability and reactivity rating system for materials.⁶ In the NFPA system, a material can be classified on a scale of 0 - 4 for each relevant parameter. A similar system could be devised for rating the combustion properties of materials.

4.10 DISADVANTAGES OF THE CONE CALORIMETER AND CONE CORROSIMETER

4.10.1 Sample Holder

The sample holder used in the Cone Corrosimeter and Cone Calorimeter has limitations in design that restrict the usefulness of the apparatus for testing certain materials.

Materials which become very fluid during combustion, such as thermoplastic polyethylene or ethylene vinylacetate copolymers, may flow out of the sample holder and drip. The dripping is a problem because the measurement of weight loss is affected as the material drips off the load cell. Also, in some cases, the molten polymer can seep underneath the foil backing and soak into the glass wool behind the foil. Material which drips or seeps away is not available for combustion, which will affect the other combustion data as well.

Some modification of the sample holder is needed to enable the Cone Corrosimeter and Cone Calorimeter to be useful for a wider range of materials. One possible modification is to place the specimen in a heat resistant glass or metal dish designed with the same cross-sectional area as the current sample holder. Such a dish could be designed with sides that would contain molten polymer during combustion. Such a system would also eliminate the possibility of material from seeping into a glass wool backing.

4.10.2 Sampling Technique for Corrosion Testing

The sampling method in the proposed ASTM D 09.21.04 standard test method for measuring corrosion with a Cone Corrosimeter continually withdraws a fraction of the combustion gases (4 l/m) and passes them through an 11.4 l chamber containing the corrosion target. Therefore, the time required for gas to pass through the system is always 2.85 minutes. The chamber is closed after 70% of the combustible specimen weight is lost. The target remains in the environment at the time the sampling flow was stopped for the balance of an hour from the time the specimen was exposed to the heat. This time can be 40 to 50 minutes. Therefore, most target exposure is to the gases that evolve during the three minutes of combustion prior to closing the chamber.

If the combustion gas species are constant throughout the test period, this sampling procedure is satisfactory. Combustion gas species would be expected to be constant for

- 1) homogeneous materials that do not contain significant amounts of easily volatilized corrosive components,
- 2) composite or multi-layer samples of the same material which meet criteria 1.

The sampling method may produce significant discrepancies from real world corrosion composite or multi-layer samples of two or more materials. A practical case would be a cable with a non-halogen jacket and PVC insulation.

The deficiencies in the sampling system could be improved, but not eliminated by increasing the time required for gas to pass through the system by using a lower sampling rate and a larger target chamber. A better system would be the use of a syringe type sampling apparatus which would draw a gas sample at a rate proportional to the specimen burning rate. A third solution would be to bleed a sample stream into an evacuated chamber at a rate which would approximately fill it during the combustion period.

5.0 CONCLUSIONS

The Cone Corrosimeter apparatus, comprised of a Cone Calorimeter with a gas sampling apparatus, has the capability to evaluate many different combustion properties of a material at one time.

Changes to the sample holder design, such as using glass or metal dish, would increase the number of materials that could be tested using the Cone Corrosimeter and Cone Calorimeter by eliminating sample dripping that occurs with the current sample holder design.

Changes to the gas sampling design for corrosion testing would allow the probe to be exposed to a representation of all of the gases evolved during the combustion process, after the exposure chamber is closed.

When selecting materials for an application, the selection of materials should be based on the requirements of the specific application and each material's individual combustion parameter performance. A single, overall "hazard index" may not provide enough information for material specifiers to select the proper material for a particular situation.

6.0 ACKNOWLEDGEMENTS

The Polyolefins Fire Performance Council (PFPC) has been an operating unit of the Society of the Plastics Industry, Inc. since 1989. At the time this data developed, PFPC consisted of following member companies: BP Chemicals, Dow Chemical Company, GE Plastics, Himont Inc., J.M. Huber Corporation, Solem Division, Lonza, Inc., Quantum Chemical Corporation, USI Division and Union Carbide Corporation. Carl F. Tripp is Managing Director of the PFPC.

PFPC wishes to thank Dr. Pravinray Gandhi, Robert G. Backstrom, Gary Gardell, John Donovan and Dan Plyman of Underwriters Laboratories, Northbrook, Illinois for their contributions in obtaining the test results. The author would also like to thank Dr. Michael Benson of Quantum Chemical Corporation, USI Division, for his assistance with the statistical analysis of the data, and Dr. Steve Kessel for his assistance with understanding the previous PFPC work.

7.0 REFERENCES

1. Kessel, S. L., Bennett, J. G., Jr., Rogers, C. E., *Corrosivity Test Methods for Polymeric Materials, Proceedings of the 40th International Wire and Cable Symposium*, p 348, 1991.
2. Rogers, C.E., Kessel, S. L., and Bennett, J. G., Jr., *Corrosivity Test Methods for Polymeric Materials Part 2 - CNET Test Method, Proceedings of the Seventeenth International Conference on Fire Safety*, p 392, January 1992.
3. Bennett, J. G., Jr., Kessel, S. L., Rogers, E. E., *Corrosivity Test Methods for Polymeric Materials Part 3 - Modified DIN Test Method, Proceedings of the Fire Retardant Chemicals Association Meeting*, p 79, April 1992.
4. Bennett, J. G., Jr., Kessel, S. L., Rogers, C. E., *Corrosivity Test Methods for Polymeric Materials Part 4 - Cone Corrosimeter Test Method, Proceedings of the Fire Retardant Chemicals Association Meeting*, p 1, October 1992.
5. Kessel, S. L., Rogers, C. E., Bennett, J. G., Jr., *Corrosivity Test Methods for Polymeric Materials Part 5 - A Comparison of Four Test Methods, Proceedings of the 18th International Conference on Fire Safety*, January 1993.
6. NFPA Standard 704, *Identification of the Fire Hazards of Materials*, NFPA, Boston, 1980.
7. SAS/ASSIST® Software, SAS® Institute, Inc., Cary, North Carolina, 1992.



Diana S. Malin received her B.S. degree in Chemical Engineering from the University of Missouri-Rolla in 1983. She joined Quantum Chemical Corporation, USI Division in 1983 as a Technical Service Engineer, working in several application areas. Currently, she holds the position of Section Leader, Wire and Cable Technical Service and Product Development.

Table I. Polymeric Materials Evaluated

<u>No</u>	<u>Company</u>	<u>Product Designation</u>	<u>Material Description</u>	<u>PPPC Nos. 1-5</u>
1	BP	EXP 839	XL olefin elastomer with metal hydrate filler	1
2	EXXON	EX-FR-100	EVA polyolefin with ATH filler	4
3	UCC	UNIGARD TM RE DFDA-1736NT	Polyolefin copolymer with mineral filler	10
4	UCC	UNIGARD TM RE HFDA-1393BK	XL polyolefin copolymer with mineral filler	11
5	QUANTUM	PETROTHENE [®] XL 7403	XL polyolefin copolymer with ATH filler	12
6	QUANTUM	PETROTHENE [®] YR 19535	XL polyolefin copolymer with ATH filler	13
7	QUANTUM	PETROTHENE [®] YR 19543	EVA polyolefin with mineral filler	14
8	UCC	UCARSIL [®] FR-7920NT	Polyolefin with mineral filler	15
9	HIMONT	EXP 127-32-6	Intumescent polypropylene	8
10	BP	POLYCURE TM 798	XL polyethylene copolymer with chlorinated additive	16
11	UCC	UNIGARD TM HP HFDA-6522NT	XL polyethylene copolymer with brominated additive	25
12	DOW	5435-30-11	Blend of HDPE and chlorinated PE elastomer	2
13	DOW	5348-40-1	Chlorinated PE with fillers	3
14	COMMERCIAL SAMPLE		A polyvinylidene fluoride material	17
15	COMMERCIAL SAMPLE		A polytetrafluoroethylene material	18
16	COMMERCIAL SAMPLE		A PVC material	19
17	GEP	NORYL [®] PX1766	Polyphenylene oxide/polystyrene blend	5
18	GEP	ULTEM [®] 1000	Polyetherimide	6
19	GEP	SILTEM [®] STM1500	Polyetherimide/siloxane copolymer	7
20	UCC	DGDK-3364NT	Polyethylene homopolymer	21
21	QUANTUM	ULTRATHENE [®] UE 631	EVA polyolefin copolymer	23
22	NYLET	P50	Nylon 6,6	24
23			Douglas fir	22

Table II - Time to Ignition for All Specimens*

Tests Run at Heat Flux of 50kW/m²

SAMPLE	TIME TO IGNITION (sec)
1A	93
1B	95
1C	91
1D	86
1E	90
1 Average	91
1 Standard Dev.	3.4
2A	90
2B	87
2C	86
2D	88
2E	86
2 Average	87
2 Standard Dev.	1.7
3A	95
3B	125
3C	131
3D	127
3E	128
3 Average	121
3 Standard Dev.	3.4
4A	115
4B	119
4C	123
4D	122
4E	115
4 Average	119
4 Standard Dev.	3.8
5A	149
5B	120
5C	139
5D	138
5E	160
5 Average	141
5 Standard Dev.	15
6A	70
6B	73
6C	70
6D	74
6E	67
6 Average	71
6 Standard Dev.	2.8
7A	57
7B	62
7C	65
7D	45
7E	63
7 Average	58
7 Standard Dev.	8
8A	92
8B	90
8C	86
8D	91
8E	88
8 Average	89
8 Standard Dev.	2.4

Table II - Time to Ignition for All Specimens*

Tests Run at Heat Flux of 50kW/m² (Continued)

SAMPLE	TIME TO IGNITION (sec)
9A	24
9B	25
9C	27
9D	24
9E	24
9 Average	25
9 Standard Dev.	1.3
10A	83
10B	82
10C	83
10D	61
10E	75
10 Average	77
10 Standard Dev.	9.4
11A	104
11B	112
11C	89
11D	93
11E	114
11F	116
11 Average	105
11 Standard Dev.	11
12A	51
12B	51
12C	54
12D	49
12E	50
12 Average	51
12 Standard Dev.	3.7
13A	36
13B	31
13C	38
13D	38
13E	39
13 Average	36
13 Standard Dev.	8.8
14A**	766
14B	891
14C	803
14 Average	820
14 Standard Dev.	64
15A	227
15B	226
15C	204
15D	212
15 Average	217
15 Standard Dev.	11
16A	33
16B	29
16C	33
16D	41
16E	39
16 Average	35
16 Standard Dev.	4.9

*Includes data from two initial 70% mass loss determinations and corrosion tests.

**Sample pyrolyzed during test.

Table II - Time to Ignition for All Specimens*

Tests Run at Heat Flux of 50kW/m² (Continued)

<u>SAMPLE</u>	<u>TIME TO IGNITION (sec)</u>	<u>SAMPLE</u>	<u>TIME TO IGNITION (sec)</u>
17A	61	20A	56
17B	58	20B	56
17C	55	20C	67
17D	55	20D	61
17E	55	20 Average	60
17 Average	57	20 Standard Dev.	5.2
17 Standard Dev.	2.7		
18A	206	21A	49
18B	176	21B	55
18C	108	21C	47
18D	124	21D	49
18E	138	21E	56
18F	135	21 Average	51
18G	134	21 Standard Dev.	4.0
18 Average	146		
18 Standard Dev.	23	22A	79
		22B	81
19A	77	22C	114
19B	69	22D	70
19C	66	22E	96
19D	80	22 Average	88
19E	74	22 Standard Dev.	17.3
19 Average	73		
19 Standard Dev.	5.7	23A	25
		23B	19
		23C	29
		23D	27
		23E	29
		23 Average	26
		23 Standard Dev.	4.1

*Includes data from two initial 70% mass loss determinations and corrosion tests.

Table III - Combustion and Corrosion Data for Specimens Tested For Corrosion*

Test Run at Heat Flux of 50kW/m² with 45000 Angstrom Probe

<u>SAMPLE</u>	<u>PRETEST SAMPLE WEIGHT(g)</u>	<u>SAMPLE WT LOSS(g)</u>	<u>MAX HEAT RELEASE RATE (kW/m²)</u>	<u>TOTAL HEAT RELEASED (kJ)</u>	<u>AVERAGE HEAT OF COMBUSTION (kJ/g)</u>	<u>AVG. SPEC. EXTIN. CROSS-SECT. AREA (m²/g)</u>	<u>CORROSION** WEIGHT LOSS (Ang)</u>
1C	117.39	65.0	105.0	1136.5	17.5	0.178	608
1D	113.06	62.5	108.5	1107.6	17.7	0.234	450
1E	115.76	62.5	107.2	1270.1	20.3	0.209	743
1 Average	115.4	63.3	106.9	1171	18.5	0.207	600
1 Std. Dev.	2.2	1.4	1.8	87	1.6	0.028	147
2C	93.77	59.3	168.0	1350.0	22.8	0.288	428
2D	91.82	55.0	151.6	1316.3	23.9	0.327	450
2E	93.06	57.5	139.6	1202.6	20.9	0.279	315
2 Average	92.9	57.3	153.1	1290	22.5	0.298	398
2 Std. Dev.	1.0	2.1	14.2	77	1.5	0.02	72.4
3C	93.62	52.5	122.0	1194.7	22.8	0.075	608
3D	93.65	55.0	113.2	1609.6	29.3	0.124	563
3E	95.32	52.5	116.8	1204.8	22.9	0.095	675
3 Average	94.2	53.3	117.3	1336	25.0	0.098	615
3 Std. Dev.	1.0	1.4	4.4	237	3.7	0.02	56

* Includes data from corrosion determinations only.

** 45,000 Angstrom Probe

Table III - Combustion and Corrosion Data for Specimens Tested For Corrosion*

Test Run at Heat Flux of 50kW/m² with 45000 Angstrom Probe (Continued)

SAMPLE	PRETEST SAMPLE WEIGHT(g)	SAMPLE WT LOSS(g)	MAX HEAT RELEASE RATE (kW/m ²)	TOTAL HEAT RELEASED (kJ)	AVERAGE HEAT OF COMBUSTION (kJ/g)	AVG. SPEC. EXTIM. CROSS-SECT. AREA (m ² /g)	CORROSION** WEIGHT LOSS (ABg)
4C	89.52	53.1	123.6	1113.6	21.0	0.149	563
4D	94.09	55.0	127.4	1117.9	20.3	0.278	473
4E	93.36	52.5	136.9	1147.1	21.8	0.157	810
4 Average	92.3	53.5	129.3	1126	21.0	0.195	615
4 Std. Dev.	2.4	1.3	6.8	18.2	0.7	0.07	174
5C	92.64	63.1	298.8	1582.1	25.1	0.376	90
5D	92.29	63.7	253.5	1557.3	24.4	0.286	0
5E	93.61	62.5	332.7	1602.4	25.6	0.371	135
5 Average	92.8	63.1	295.0	1581	25.0	0.344	75.0
5 Std. Dev.	0.7	0.6	40	22.6	0.6	0.05	69
6C	93.17	59.4	192.3	1541.5	26.0	0.225	518
6D	92.56	59.4	239.7	1510.6	25.4	0.249	653
6E	89.95	56.3	186.1	1505.3	26.7	0.260	765
6 Average	91.9	58.4	206.0	1519	26.0	0.245	645
6 Std. Dev.	1.7	1.8	29	19.5	0.6	0.02	124
7C	87.12	56.3	376.9	1659.0	29.5	0.194	473
7D	87.13	57.5	291.7	1464.0	25.5	0.237	495
7E	91.03	55.7	215.0	1369.2	24.6	0.294	518
7 Average	88.4	56.5	294.5	1497	26.5	0.242	495
7 Std. Dev.	2.2	0.9	81	147	2.6	0.05	22
8C	86.63	51.9	110.7	1366.8	26.3	0.119	630
8D	86.53	50.0	117.6	1393.9	27.9	0.063	450
8E	86.55	48.1	120.6	1334.0	27.7	0.069	608
8 Average	86.6	50.0	116.3	1365	27.3	0.084	563
8 Std. Dev.	0.05	1.9	5.1	30.0	0.9	0.03	98
10C	83.32	64.3	491.1	1797.2	28.0	0.874	1845
10D	82.52	65.6	403.8	1836.1	28.0	0.904	1485
10E	82.68	64.4	497.7	1856.1	28.8	0.912	2565
10 Average	82.8	64.7	464.2	1829	28.3	0.897	1965
10 Std. Dev.	0.4	0.7	52	30.0	0.5	0.02	550
11C	79.04	56.9	392.7	1040.6	18.3	0.830	450
11D	82.69	56.8	328.1	1026.3	18.1	0.925	315
11E	81.37	61.8	434.4	1174.5	19.0	0.959	540
11F	82.07	58.7	416.1	1180.7	20.1	0.940	675
11 Average	81.3	58.5	392.8	1105	18.9	0.913	495
11 Std. Dev.	1.6	2.3	46.4	83.0	0.9	0.05	151
12C	76.98	61.3	163.5	1509.8	24.6	1.012	4095
12D	75.12	60.0	182.7	1526.2	25.4	0.981	4320
12E	75.70	58.8	183.8	1563.9	26.6	1.030	5738
12 Average	75.9	60.0	176.7	1533	25.5	1.01	4718
12 Std. Dev.	0.9	1.2	11.4	28	1.0	0.025	891
13C	97.89	61.8	100.9	1170.8	18.9	0.633	4905
13D	96.40	56.3	106.3	1193.7	21.2	0.720	1350
13E	95.58	55.6	110.0	1135.2	20.4	0.546	189
13 Average	96.6	57.9	105.7	1166	20.2	0.633	2148
13 Std. Dev.	1.2	3.4	4.6	29	1.2	0.087	2457
14A***	102.14	98.2	29.7	753.1	7.7	0.196	2925
14B	102.97	88.8	27.6	528.6	6.0	0.050	2385
14C	99.54	90.0	29	567.1	6.3	0.046	2048
14 Average	101.5	92.3	28.9	616	6.7	0.097	2453
14 Std. Dev.	1.8	5.1	1.1	120	0.9	0.08	442

* Includes data from corrosion determinations only.

** 45,000 Angstrom Probe

Table III - Combustion and Corrosion Data for Specimens Tested For Corrosion*

Test Run at Heat Flux of 50kW/m² with 45000 Angstrom Probe (Continued)

SAMPLE	PRETEST SAMPLE WEIGHT(g)	SAMPLE WT LOSS(g)	MAX HEAT RELEASE RATE (kW/m ²)	TOTAL HEAT RELEASED (kJ)	AVERAGE HEAT OF COMBUSTION (kJ/g)	AVG. SPEC. EXTIN. CROSS-SECT. AREA (m ² /g)	CORROSION** WEIGHT LOSS (Ang)
16C	103.94	58.8	51.9	391.1	6.7	0.161	2903
16D	103.03	63.7	54.0	424.5	6.7	0.152	5760
16E	103.00	61.3	55.3	412.5	6.7	0.126	6953
16 Average	103	61.3	53.7	409	6.7	0.146	5205
16 Std. Dev.	0.5	2.4	1.7	17.0	0	0.02	2081
17C	65.25	59.4	467.4	1267.3	21.3	1.298	405
17D	65.90	60.0	515.3	1295.8	21.6	1.302	405
17E	65.82	60.0	490.6	1296.1	21.6	1.322	630
17 Average	65.6	59.8	491.1	1286	21.5	1.31	480
17 Std. Dev.	0.3	0.3	23.9	16	0.2	0.01	130
18C	78.61	43.8	158.5	854.6	19.5	0.305	360
18D	78.50	35.0	98.5	594.9	17.0	0.335	248
18E	80.11	36.2	105.1	653.2	18.0	0.354	0
18 Average	79.1	38.3	121.0	701	18.2	0.33	203
18 Std. Dev.	0.9	4.8	32.9	136	1.2	0.02	184
19C	73.33	54.4	177.6	1122.3	20.6	0.926	585
19D	73.24	38.1	147.0	741.7	19.5	1.120	653
19E	73.31	53.7	167.2	1005.7	18.7	0.896	383
19 Average	73.3	48.7	164.0	957	19.6	0.981	540
19 Std. Dev.	0.05	9.2	15.5	195	0.9	0.12	140
22C	61.60	53.1	992.2	1547.9	29.2	0.209	878
22D	61.66	55.7	967.0	1562.7	28.1	0.198	878
22E	61.30	50.6	690.5	1222.0	24.2	0.181	3375
22 Average	61.5	53.1	883.2	1444	27.2	0.196	1710
22 Std. Dev.	0.2	2.5	167.0	192	2.6	0.01	1442
23B	128.00	109.4	137.0	1417.0	13.0	0.025	585
23C	106.42	86.9	180.8	1166.4	13.4	0.025	698
23D	134.00	113.8	149.7	1293.3	11.4	0.055	383
23 Average	123	103.0	155.8	1292	12.6	0.035	555
23 Std. Dev.	14.5	14.0	22.5	125	1.0	0.02	159

* Includes data from corrosion determinations only.

** 45,000 Angstrom Probe

*** Sample 14 pyrolyzed during test

Table IV - Studentized Maximum Modulus (SMM)⁷

Test Ranking And Grouping of Materials

Average Time to Ignition (ranked in decreasing order ->)

Sample No.	14	15	18	5	3	4	11	1	8	22	2	10	19	6	20	7	17	21	12	13	16	23	9
SMM	A	B	C	C	C	C		G	G	G	G	G	G	G	G	G	G						
Groupings			D	D	D	D	D	H	H	H	H	H	H	H	H	H	H	H	H				
				E	E	E	E	E	E	E	E	F	F	J	J	J	J	J	J	K	K	K	K
							F	F	F	F	F	I	I	I	I	I	I	I	I				

Average Maximum Heat Release Rate (ranked in increasing order ->)

Sample No.	14	16	13	1	8	3	18	4	2	23	19	12	6	7	5	11	10	17	22
SMM		E	E	E	E	E	E	E	E	E	E	E	E			B	B	B	A
Groupings	F	F	F	F	F	F	F	F	D	D	D	D	D	C	C	C			

Average Specific Extinction Cross Section Area (ranked in increasing order ->)

Sample No.	23	8	14	3	16	4	22	1	7	6	2	18	5	13	10	11	19	12	17
SMM						D	D	D	D	D	D	D	D	C	B	B	B	B	A
Groupings		F	F	F	F	F	F	F	F	F	E								
	G	G	G	G	G	G	G												

Average Corrosion (ranked in increasing order ->)

Sample No.	5	18	2	11	17	7	19	23	8	1	3	4	6	22	10	13	14	12	16
SMM ⁵	C	C	C	C	C	C	C	C	C	C	C	C	C	C	C	C	A	A	A
Groupings															B	B	B		

Samples within the same group are considered statistically indistinguishable.

FIGURE 1
CONE CORROSIMETER

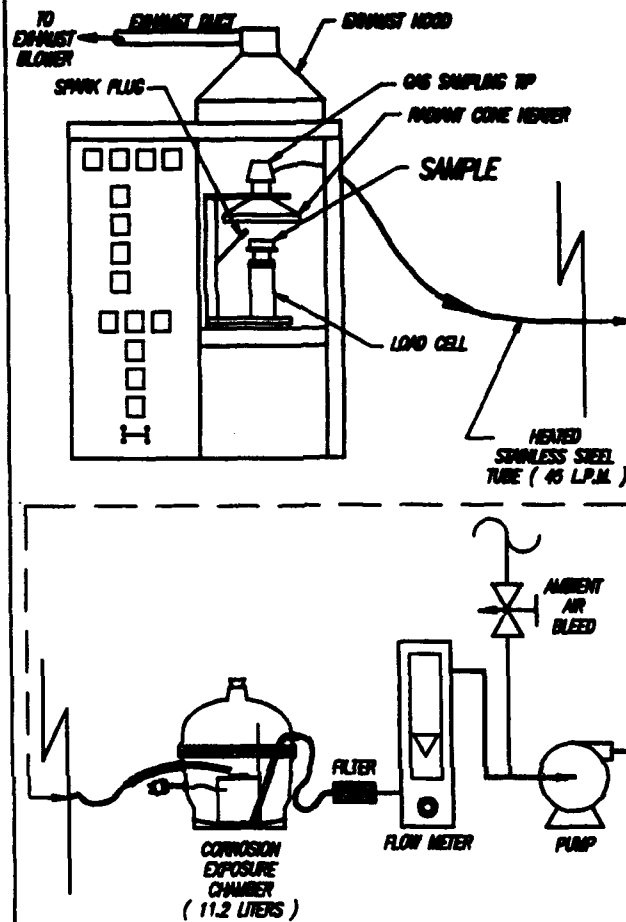


FIGURE 2
CORROSION EXPOSURE CHAMBER

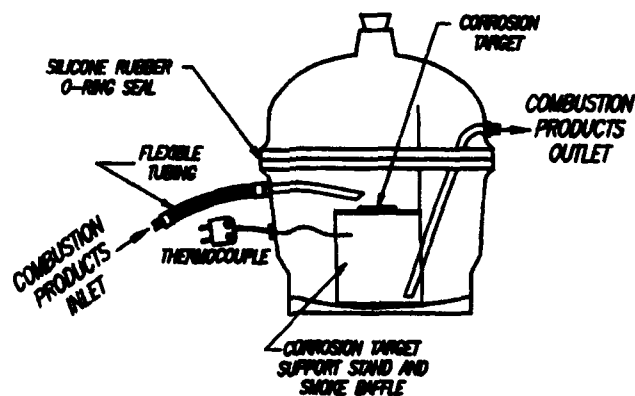


Figure 3. Time to Ignition
50 kW/m² Heat Flux

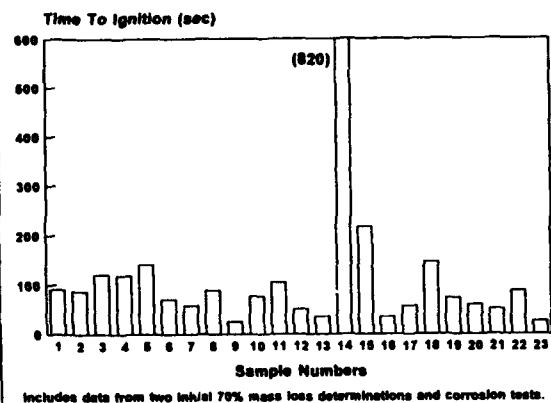


Figure 6. Average Heat of Combustion
50 kW/m² Heat Flux

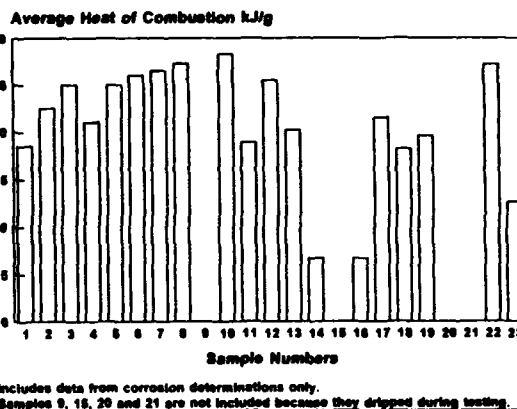


Figure 4. Maximum Heat Release Rate
50 kW/m² Heat Flux

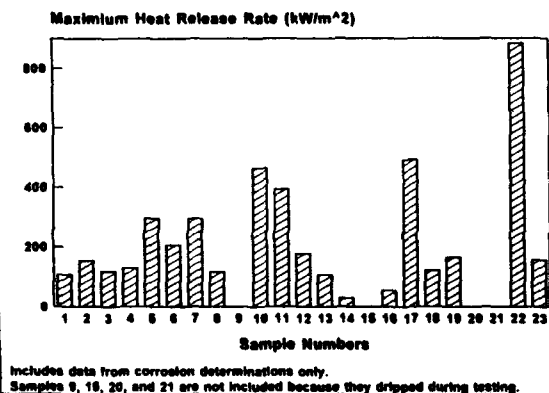


Figure 7. Average Specific Extinction
Cross-Section Area

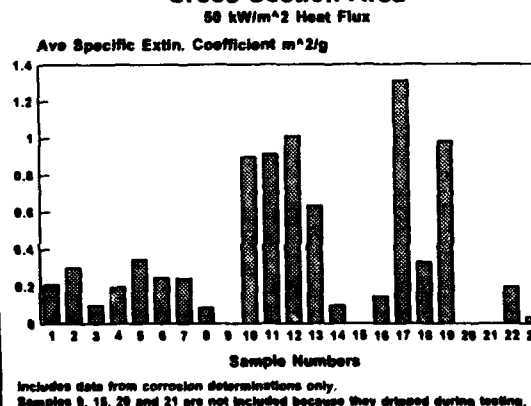


Figure 5. Total Heat Released
50 kW/m² Heat Flux

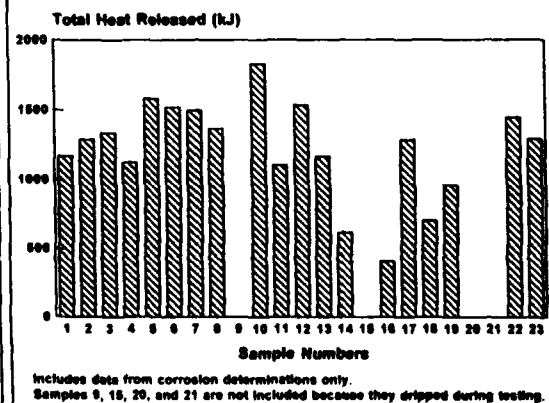
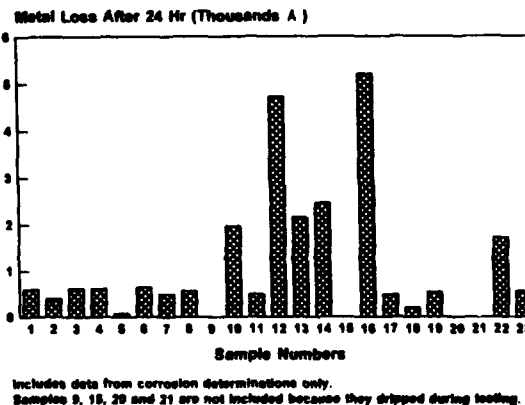


Figure 8. Corrosion Results
50 kW/m² Heat Flux, 45,000 Probe



APPENDIX A

CONE CALORIMETER CALCULATIONS

Maximum Heat Release Rate

$$\text{Maximum Heat Release Rate} = \frac{\text{Peak Heat Release Rate (kW)}}{\text{Sample Area (m}^2\text{)}}$$

where sample area = 0.01 m²

Average Effective Heat of Combustion

$$\text{Average Effective Heat of Combustion} = \frac{\int_{t_0}^{t_{\text{end}}} \text{HRR } dt}{\text{Weight Loss}}$$

where t_{end} is the test time in seconds
and weight loss is measured in grams

Average Specific Extinction Cross-Section Area

$$\text{Average specific extinction cross-section area} = \frac{\int_{t_0}^{t_{\text{end}}} (k)V dt}{\text{Weight Loss}}$$

where (k) is the extinction coefficient measured by the laser
optical system (1/m)
V is volumetric flow rate (m³/s)

NON-HALOGEN, LOW SMOKE INSULATION FOR LOW VOLTAGE TELECOMMUNICATIONS POWER WIRE APPLICATIONS

F. F. Makan

AT&T - Power Systems, 3000 Skyline Drive, Mesquite (Dallas), Texas 75149

ABSTRACT

The development of non-halogen, low smoke, low voltage DC power wires for use on cable trays in telecommunications central offices and other applications is presented from the standpoint of a customer of an insulation manufacturer/compounder and a wire manufacturer. Primary new requirements included low smoke corrosivity and low smoke toxicity. The insulation was designed to exceed all the applicable requirements of UL 44, UL 1581 and UL 1685 which include requirements for limited smoke (LS), flame retardancy and high long term wet insulation resistance.

INTRODUCTION

Electrical fires in many countries in telecommunications facilities, on board ships, in subways and elsewhere, seem to have given birth to the so called non-halogen movement because halogenated insulation was implicated in the effects of the fires. Besides fatalities and injuries due to smoke inhalation, electronic equipment was extensively damaged by the effects of smoke. In telecommunication central office fires, the latter was a major effect due primarily to wires installed on open cable trays. Although the wires available at the time were flame retardant, additional requirements were identified to address smoke related problems. AT&T Power Systems collaborated with Union Carbide to develop a power wire which retained all the desirable properties of the DC distribution power wires being used at the time while reducing significantly the smoke emitted during combustion. This development resulted in a wire which exceeds the applicable requirements.

PURPOSE OF PAPER

The purpose of this paper is to describe the successful application of the first limited smoke, non-halogen, crosslinked polyolefin insulated wire for use in power applications in telephone central offices from a customer viewpoint. The paper will cover the development of requirements and the insulation.

BACKGROUND

The part of the telecommunications industry involved with telephones and related products uses DC powered equipment extensively to take advantage of the high back up reliability offered by batteries charged by rectifiers (battery chargers). The overriding requirement these wires must satisfy is to provide uninterrupted service for years and years in the specified environment. The most common method of distributing this DC power from the power source to the load equipment is via insulated single conductor building wire. This wire is also used for wiring among the power source equipment. Some equipment uses this wire as hook up wire within it. Voltages range from nominal 24 to 140 volts DC. Sizes of the wire range from 14 AWG to 750 kcmil. The wires are used in pairs referred to as battery and return. The wire is also used for grounding and lightning protection purposes. Prior to the introduction of this wire the insulation of choice was chlorosulphonated polyethylene with flame retardant properties but poor cut-through resistance. The chlorosulphonated polyethylene was introduced in the 1970's to supersede EPDM and SBR because of its superior oxygen index (28%) and flame retardancy (IEEE 383 Vertical Tray Flame Test). As with the former insulation the non-halogen wire was required to meet the requirements associated with the National Electrical Code RHH-RHW designation as reflected in UL 44 and UL 1581. Almost contemporaneously at the time of development NEC had introduced the LS (Limited Smoke) designation and subsequently UL introduced UL 1685. Higher cut-through resistance has been achieved successfully. A natural consequence of this has been the wire requires greater effort to strip.

The 1990 National Electrical Code introduced a limited smoke designation reflected by the suffix LS. UL standard 1685 was introduced to include the limited smoke property. The insulation uses a polyolefin resin filled with hydrated mineral fillers to achieve the low smoke property.

CONSTRUCTION OF WIRE

For DC distribution, telephone central offices most commonly use American Wire Gauge (AWG) sizes

14, 12, 10, 8, 6, 4, 2, 1/0, 2/0, 4/0, and 350 kcmil, 500 kcmil and 750 kcmil.

Two constructions of the wire in the above referenced sizes were developed to correspond to constructions being used at the time of development. The difference between the two is in the type of stranding of the conductor provided. One construction uses Class B concentric lay stranding per ASTM B 8; the other uses Class I rope lay stranding having bunch stranded members per ASTM B 172.

The individual conductor strands are soft or annealed, tinned or lead-alloy plated, copper meeting all the electrical and mechanical requirements of ASTM B 33 or ASTM B 189.

The insulation is separated from the conductor by a helically wound polyester film separator wrapped over the conductor prior to extruding the insulation. The separator is intended to prevent the insulation from adhering to the conductor.

A single cotton braid covering is applied over the insulation on all wire sizes. The cotton braid is of the woven type as specified in UL Standard 44. The cotton braid is intended to protect the insulation from abrasion and cutting forces, especially when chlorosulphonated polyethylene is the insulating material.

On wire sizes 6 AWG and larger, a polyester film is helically wrapped over the insulation prior to applying the cotton braid covering.

The cotton braid is saturated with a heat and moisture resistant flame retardant compound. A finish is applied over the saturated cotton braid to obtain a uniform color (grey, red, blue and green).

ENVIRONMENT

The telephone central office environment is normally controlled and the ambient temperature can be considered to be at a nominal 30°C. The cable trays supporting the wire are most often mounted close to the ceiling thereby exposing the outer wires to fluorescent lights, and to water in the event of accidental operation of water sprinklers. The lower layers of wires in a tray are subjected to the weight of the wires above them. The wires rest on the rungs of the cable trays or the weight is more uniformly distributed if the rungs are covered by solid plate type covers. There might be areas of local stress concentration in transition areas, for example, where trays change levels and/or direction or where wires bend to make connections at equipment below the trays. The wires might be exposed to the heat exhausted from the equipment under the cable trays. There are occasions where the wire might be used outdoors, for example, between equipment housed temporarily in trucks. In this case the wires are exposed to the elements.

APPLICATION

Most power distribution from the DC power plant to telecommunications switching and transport equipment in telephone central offices is at nominal 48 volts DC (normally, the actual voltage is 52.08 volts) in the United States. The medium for distribution is 600 V rated building wire, National Electrical Code designated as RHH-RHW. The wire is supported on cable trays, also referred to as cable racks.

The distribution wires from the DC power plant to the load equipment are almost always single conductor RHH-RHW designated building wire. These wires are generally large in size because the low distribution voltage necessitates large load currents. The length of these conductors may extend from a few feet to several hundred feet if, for example, the distribution extends from the power plant in the basement of the central office to several stories up to the load equipment. Several large conductors may need to be connected in parallel to control voltage drop across them. Even for short conductors, when voltage drop is very low, large conductors are preferred so that the wire operating temperature due to conductor resistance heat losses are low.

Several layers of these wires are supported in open horizontal and vertical cable trays. The wires are tied securely at frequent intervals to the cable trays by twine. If the wire is not covered by a cotton braid, then it is wrapped with strips of vulcanized fiber at the point where it is tied down or where it rests on sharp edges. This is to prevent the twine or sharp edge from cutting through the insulation. Poor cut-through susceptibility is a serious problem with chlorosulphonated polyethylene insulation. The new non-halogen wire, with its high cut-through resistance, presents the opportunity for eliminating the cotton braid cover.

At the start of the project, after considering a number of alternatives, it was decided that the program objectives were to develop an insulation material capable of meeting or exceeding the following design targets:

- Oxygen index (OI) > 28%
- UL/CSA safety agency approval
- Pass UL RHH-RHW tests
- Low smoke toxicity
- Flame retardance
- Low smoke corrosiveness
- Non-halogenated insulation.

Three new areas of tests were not covered by UL for the type of insulation under consideration at that time. A decision had to be made as to which tests to use for measuring success in meeting design objectives. The three types of tests are:

- Smoke density tests
- Corrosivity tests
- Toxicity tests.

It is acknowledged that there is much difference of opinion among experts in the field as to which are the proper tests to assess the effects of smoke. Availability of test facilities and legislative requirements helped to decide on the following tests:

- ASTM E-662 for smoke emission (Standard Test Method for Specific Optical Density of Smoke Generated by Solid Materials).
- US Navy acid gas generation test for smoke corrosivity.
- The University of Pittsburgh Protocol is required when marketing insulation in New York State. The State of New York does not have any pass or fail requirements.
- Flame retardancy is addressed by meeting the UL1581 and IEEE 383.
- Vertical Tray Flame Test to permit the use on cable trays.
- UL 44 and UL 1581 for Class XL insulation provides requirements and tests for the application described above.

(Therefore, the wire, although a new development, was treated as an enhancement of the existing design of RHH-RHW).

The following tests although not required by UL 44 for RHH-RHW insulation were specified by AT&T:

- Crushing test,
- Dielectric breakdown after glancing impact test,
- Dielectric breakdown after scoring test.
- Vertical tray flame test for sizes from 14 AWG through 2 AWG.

DEVELOPMENT

After a development period of about two years, an insulation was developed which met all the requirements of UL 44 and UL 1581 and was listed accordingly. Concurrently, because of the uncertainties of being able to meet each and every requirement, a dual core insulation was also developed. The inner core was 10 mils of polyethylene and the outer core was non-halogenated crosslinked polyolefin of the same composition as the single core construction. The dual core wire was successfully listed, however, further development was abandoned because this wire was more difficult to flex than the single construction and was less economical to manufacture because of dual or tandem extrusion of two layers. When UL 1685 was published, the single core non-halogen insulation was successfully resubmitted for UL approval.

CONCLUSION

This wire has been marketed for the last two years for use in telephone central offices and other applications in two versions. One with class B stranding and the other with class I stranding. The only reported problems from

installers are the insulation is more difficult to strip and more difficult to bend in the larger sizes compared to chlorosulphonated polyethylene.

ACKNOWLEDGEMENTS

The author thanks S. Ramachandran of Union Carbide for his constructive comments in the preparation of this paper.

REFERENCES

1. Ramachandran, S., Jow, J., Keogh, M. J., Nesgood, P. J., "Improved Processability in Reduced Emission Wire and Cable Materials for the Telecommunication Industry." Proceedings of the 39th International Wire and Cable Symposium, November, 1990.
2. UL44 Underwriters Laboratories Inc. Standard for Rubber-Insulated Wires and Cables.
3. UL1581 Underwriters Laboratories Inc. Reference Standard for Electrical Wires, Cables and Flexible Cords.
4. UL1685 Underwriters Laboratories Inc. Vertical Tray Fire Propagation and Smoke Release Test for Electrical and Optical Fiber Cables.

Author

(Photo not available).

Frank Makan graduated from the University of Roorkee, Roorkee, India with a degree in Bachelor of Engineering (Electrical). He has been with AT&T since 1968 in various engineering assignments which included dc power distribution, application of power wires, systems grounding, lightning protection and design and development of power systems. Currently, he is a Member of the Technical Staff at Bell Laboratories in AT&T-Energy Systems in the Purchased Products Development and Engineering group.

NONTHERMAL DAMAGE ASSOCIATED WITH WIRE AND CABLE FIRES

A.Tewarson

Factory Mutual Research Corporation
Norwood, MA 02062

ABSTRACT

Various small-scale (Factory Mutual Research Corporation, [FMRC], ASTM and DIN) and large-scale (FMRC) test methods to measure corrosion due to fire products are reviewed. An attempt has been made to combine the results with ignition, flame spread, generation of heat and fire products for wires and cables. A corrosion parameter has been identified for use in models to assess nonthermal damage due to corrosion. Minimum concentration of halogenated fire products has been identified for corrosion damage.

Restriction of fire propagation within the ignition zone for materials is one of the ways of reducing the impact of nonthermal damage. In the paper thus pass/fail criteria of fire propagation tests, such as CSA-FT4, ICEA, UL-1581, and UL-910, have been correlated with the group classification of cables following the Fire Propagation Index (FPI) relationship from the FMRC cable specification standard, class No. 3972.

INTRODUCTION

The damage to life and property in fires is identified as: 1) thermal damage due to release of heat, and 2) nonthermal damage due to release of smoke, toxic, corrosive and odorous products and/or due to decomposed and un-decomposed fire extinguishing agents. Nonthermal damage to property includes corrosion, electrical malfunctions, discoloration, unpleasant odors, etc. Most industries are susceptible to nonthermal fire damage.

There is a potential of nonthermal damage from the fire products of wires and cables due to the chemical make-up of the insulation and jacket materials. For example, in the following fires involving wire and cables, there was nonthermal damage due to smoke contamination and corrosion due to halogenated acids²:

1) Fire at the Telephone Central Office at Hinsdale, Illinois (1988)

Fire started in an electrical cable tray involving polyvinylchloride jacketed cables, damaging expensive equipment and causing far-reaching phone outages.

2) Fire at the New York Telecommunication Center (1987)

Fire started in the main frame, near the ceiling, on the first floor. There was extensive nonthermal damage to electronic switching systems.

3) Fire at the New York Telephone Exchange (1973)

Fire started in the cable vault and spread vertically through the cable penetrations, to the main distribution frame and switching equipment in the two floors above. Large quantities of smoke and corrosive products were generated from the

intense fire involving PVC and other cables resulting in extensive nonthermal property damage.

4) Fire at the Telephone Exchange Building, Barcelona, Spain (1973)

A fire started in the sixth floor, spreading to seventh and eighth floors. The upward fire spread involving PVC cables was very rapid, spreading through cable penetrations. There was extensive nonthermal property damage.

5) Fire at the Zurich-Hottingen Telephone Exchange (1969)

There was extensive nonthermal property damage due to smoke and HCl generated from PVC cable fires.

6) Fire at the Telephone Exchange in Canberra, Australia.

There was extensive nonthermal property damage.

Because of the need to evaluate the nonthermal damage potential of fire products of wires and cables, test methods have been developed to determine flame spread behavior of wires and cables, generation rates of fire products and their corrosive nature and damaging effects of smoke¹.

The most common methods used to determine the flame spread behavior of wires and cables are based on the visual determination of charring or surface damage length, and/or heat release rate and/or ignition characteristics. The smoke generation characteristics are determined from smoke optical density. The corrosive nature of the fire products is determined by the loss of metal exposed to the products. The metal loss is quantified either directly using a precision balance or by measuring change in the resistance. The smoke damage is determined by its color, odor, charge, adsorbed species, and ease of removal from surfaces by solvents such as water.

The general principles of the methods used to determine flame spread behavior of wires and cables and the resulting damaging effects of the fire products are discussed in this paper.

TECHNICAL BACKGROUND

Ignition and flame spread

When a material is exposed to external heat flux, generally identified as an ignition source, it absorbs heat at a rate dependent on the material's thickness, ignition temperature, thermal conductivity, specific heat and density. The ignition temperature above ambient, thermal conductivity, specific heat, and density are combined together and defined as the *Thermal Response Parameter (TRP)* of the material³. The higher the TRP value, the longer it takes for material to heat up and ignite and slower is the spread of flame on the surface. The region where material is heated by internal or external heat sources resulting in ignition is defined as the ignition zone.

All electrical wires and cables are expected to burn in the ignition zone. Beyond the ignition zone, the surface is heated by the heat flux provided by the flames of wires and cables burning in the ignition zone. Over-heating of wire and cables and other burning materials also provide additional heat flux beyond the ignition zone. Once the heat flux from the flame and other sources satisfy the TRP requirement, the flame moves beyond the ignition zone. The rate of movement of the flame on the surface, defined as surface flame spread rate, depends on the magnitude of the heat release rate from the burning wires and cables, TRP value of the material, and additional heat fluxes and heat losses from the surface. For generalized representation of the flame spread characteristics of the wires and cables, chemical heat release rate and TRP values are combined and defined as the *Fire Propagation Index (FPI)*⁴:

$$FPI = 1000 \times (0.40 \dot{Q}'_{ch})^{1/3} / TRP \quad (1)$$

where \dot{Q}'_{ch} is the chemical heat release rate per unit cable tray width or circumference of the cable (kW/m), TRP is in kW-s^{1/2}/m². Flame spreads very rapidly beyond the ignition zone for cables for which FPI values are equal to or greater than 20, but relatively slowly for cables with FPI values equal to or greater than 10 but less than 20. Flame spread decelerates or there is no flame spread beyond the ignition zone for cables with FPI values less than 10.

Numerous tests are used to assess the flame spread beyond the ignition zone for wires and cables.

Flame spread tests- small exposed surfaces:

Examples of tests are Vertical Wire Flame test (VW-1) and ASTM-D2863-70 Oxygen Index test. In these tests ignition source strength is weak.

Flame spread tests- large exposed surfaces:

Examples of tests are UL-910, IEEE-1202, CSA-FT4, IEEE-383, UL-1581, ICEA, and FMRC Class No. 3972 (large-exposed surfaces simulated by enhanced oxygen concentration).

Figure 1 shows a generalized correlation between pass/fail test criteria of CSA-FT4, ICEA, UL-1581, and UL-910 tests and group classification of cables determined from Eq. (1). For the construction of this figure, damage length and heat release rate measured in the CSA-FT4, ICEA, UL-1581, and UL-910 and time to ignition measured in the Cone Calorimeter, as reported in Refs. 6 and 7, were used. Measured flame tip distance in the UL-910 test was taken as the damage length. In Fig. 1, the numbers 1, 2, and 3 are the FMRC criterion of group classification of cables⁸, 4 is the acceptance criterion in the UL-910 test⁷, and 5 is the acceptance criterion in the CSA-FT4⁶.

The data in Fig. 1 show that fluorinated cables which pass the UL-910 test acceptance criterion are generally Group 1 cables. Some of the cables which pass the CSA-FT4 test acceptance criterion are Group 2 cables, while others are Group 3 cables. There is thus a need to resolve the inconsistencies in the CSA-FT4 test results, possibly through additional pass/fail criteria of flame length/ damage length less than or equal to 1.5 and/or chemical heat release less than 300 kW/m, and/or TRP greater than 300 kW-s^{1/2}/m².

Generation of Heat, Smoke and Corrosive Products:

Flame spread represents mass loss of insulation/jacket materials as they burn and generate heat and products. For each gram of insulation/jacket material burned, certain amounts of energy and products are generated. Energy generated during flame spread per unit mass of the

insulation/jacket material burned is defined as the *chemical heat of combustion (kJ/g)*. Mass of a product generated during flame spread per unit mass of the insulation/jacket material burned is defined as the *yield of the product (g/g)*. Each generic type of insulation/ jacket material has characteristic values for the chemical heat of combustion and yields of fire products, such as shown in Table 1, where data are taken from Ref. 9. The data were measured in FMRC⁹ Flammability Apparatus (50 kW-Scale), shown in Fig. 2. This Apparatus is a standard test apparatus for the FMRC cable specification standard class no. 3972⁸. For similar mass loss rates, the higher are the values for the chemical heat of combustion and yields of products, the higher are the chemical heat release rates and generation rates of products.

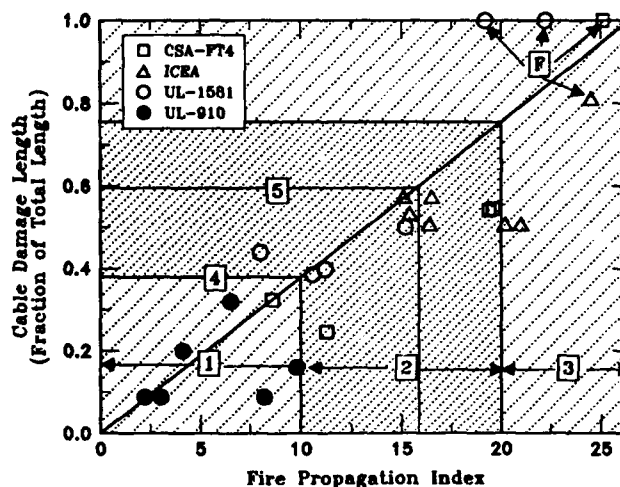


Figure 1. Cable Damage Length Versus the Fire Propagation Index for CSA-FT4, ICEA, UL-1581, and UL-910 Tests. Values in the Figure are Calculated from the Data Reported in Refs. 6 and 7. F: Failed the Test Criterion.

Table 1
Chemical Heat of Combustion and Yields of Fire Products for Selected Electrical Wires and Cables^a

Insulation/ jacket	CHC ^b (kJ/g)	CO ₂	Yield (g/g) CO	Smoke
<u>Polyethylene (PE) / polyvinylchloride (PVC)</u>				
1	31.3	2.08	0.100	0.076
2	20.9	1.29	0.147	0.136
<u>PVC-Nylon/PVC-nylon</u>				
1	10.2	0.63	0.084	ND
2	9.2	0.49	0.082	0.115
<u>PE, polypropylene / chlorosulfonated PE</u>				
1	29.6	1.95	0.072	ND
2	13.9	0.89	0.121	0.164
<u>Cross-linked polyethylene (XLPE)/XLPE</u>				
1	28.3	1.78	0.114	0.120
2	12.5	0.83	0.110	0.120
<u>XLPE/Neoprene</u>				
1	12.6	0.68	0.122	ND
2	10.3	0.63	0.082	0.175
<u>Silicone/PVC</u>				
1	10.0	0.76	0.110	0.111
2	15.6	1.19	0.065	0.119
<u>Polytetrafluoroethylene (PTFE)/ PTFE</u>				
1	3.2	0.18	0.091	0.011
2	5.7	0.383	0.103	0.005

^a: Data taken from Ref. 9; ^b:CHC-chemical heat of combustion; ND: not determined.

The yields of products generated in fires cannot exceed the

maximum stoichiometric yield, which is the yield when all the fuel atoms are converted to the product. The maximum stoichiometric yields for selected halogenated materials, some of which are used as insulation and jacket materials, are listed in Table 2, taken from Ref. 10. The abbreviations in the table are: PE: polyethylene; PVC: polyvinylchloride; PVF: polyvinyl fluoride (Teflon[®]); PVDF: polyvinylidene fluoride (Kynar[®]); TFE: tetrafluoroethylene (Teflon[®]); ETFE: PE and TFE copolymer, (Tefzel[®]); CTFE: chloro trifluoroethylene; ECTFE: PE and CTFE copolymer (Halar[®]); PFA: perfluoroalkoxy (Teflon[®]); FEP: fluorinated PE and polypropylene (Teflon[®]); PVDC: polyvinylidene chloride.

Table 2
Maximum Stoichiometric Yields of Water, Smoke, HCl and HF for Fluoro- and Chloropolymers^a

Insulation/ Jacket	Maximum Stoichiometric yield (g/g)			
	Water	Smoke	HF	HCl
Fluoropolymer				
PVF	0.59	0.52	0.44	0
PVDF	0.28	0.38	0.63	0
ETFE	0.29	0.38	0.62	0
ECTFE	0.25	0.33	0.42	0.25
PFA	0	0.28	0	0
FEP	0	0.26	0	0
TFE	0	0.24	0	0
CTFE	0	0.21	0	0
Chloropolymers				
PE-0 % Cl	1.29	0.86	0	0
PE-25%Cl	0.97	0.65	0	0.25
PE-36%Cl	0.83	0.55	0	0.36
Neoprene	0.51	0.55	0	0.41
PE-42%Cl	0.75	0.50	0	0.43
PE-48%Cl	0.68	0.45	0	0.49
PVC	0.44	0.39	0	0.58
PVDC	0.19	0.25	0	0.75

^a: Data from Ref. 10.

The data in Table 2 provide insight into the corrosion behavior of the fire products of wires and cables. Halogen acids (HF and HCl) and water are the dominant products responsible for corrosion. For PE, no halogen acid is generated and thus no corrosion is expected. For PFA, FEP, TFE, and CTFE, no water and halogen acids are generated as there is no hydrogen in the structure and thus corrosion from the combustion products of these materials would depend on the amount of water available in the environment and extent of hydrolysis of the organo-fluorinated products. For ETFE, ECTFE, PVF, and PVDF, and the chlorinated materials, both water and halogen acids are generated and thus corrosion would be expected from the combustion products of these materials even if the environment is completely dry.

NONTHERMAL DAMAGE ASSESSMENT: TECHNIQUES AND APPARATUSES

The nonthermal damage in fires is assessed in terms of corrosion and smoke damage. For the assessment of corrosion, two types of techniques are used: 1) gas phase corrosion technique, and 2) solution phase corrosion technique. The smoke damage is assessed in terms of color, odor, charge, adsorbed species, and staining.

The Gas Phase Corrosion Technique

In this technique, a high sensitivity atmospheric corrosion probe (model P610-TF50-C11000, Rohrbach Cosasco [RC])^{1,12-15} or a CNET corrosion probe^{13,16-18} is exposed to gaseous fire products.

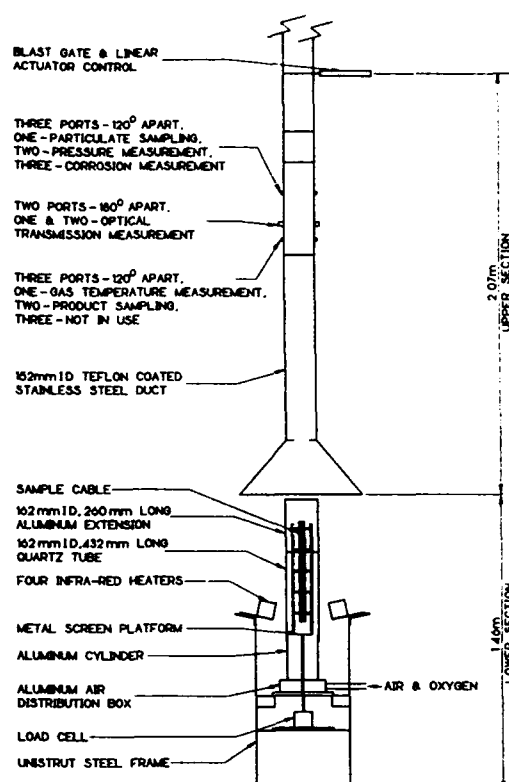


Figure 2. The FMRC Flammability Apparatus (50 kW-Scale).

The RC probe consists of two strips embedded in an epoxy-fiber glass plate. One strip is coated and acts as a reference and the other non coated strip acts as a sensor. As the sensor strip corrodes and loses its thickness, its resistance changes. The change in resistance, representing extent of corrosion of the metal, is measured by the difference in the resistance between the two strips by a Corrosometer (Model 4208, Rohrbach Cosasco). The probe readings remain reliable up to about half the thickness of the metal strip.

The gas phase corrosion is generally measured every minute for the first hour and then every hour for 24 to 48 hours. The corrosion rate, r_{corr} , is calculated from the following relationship:

$$r_{corr} = (d_1 - d_2) / (t_2 - t_1) \quad (2)$$

where r_{corr} is in A°/min , d_1 is the metal thickness (A°) at time $t_1(s)$, d_2 is the metal thickness (A°) at time $t_2(s)$. Corrosion rate normalized by the average fire products concentration is defined as the gas phase corrosion parameter, $(A^\circ/min)/(g/m^3)^{10}$. Average fire products concentration is the ratio of the mass loss rate to total volumetric flow rate of fire product-air mixture.

The RC 2,500 A° copper probe with a metal thickness of 5,000 A° is one of the most suitable probe for assessing corrosion due to fire products. The probe is manufactured by vacuum deposition technique to obtain an open matrix with little resistance to in-depth diffusion of products, resulting in rapid corrosion. It is designed to monitor short term corrosion (24 to 48 hours) for environments with small concentrations of corrosive products. The 2,500 A° copper probe is used in the FMRC test methods^{1,10,12}, in the ASTM E05.21.70 Radiation Combustion/Exposure test method^{13,15} and in the ASTM

D09.21.04 Cone Corrosometer test method^{13,14}.

The ASTM E05.21.70 and D09.21.04 test methods¹³ also use a 45,000 A° copper probe with a metal thickness of 90,000 A° for highly halogenated materials. The 45,000 A° probe is made of thin metal foil with a compact crystalline structure which offers resistance to in-depth product diffusion and corrosion is slow. The probe is not as sensitive as the 2,500 A° probe. This is shown by the data in Fig. 3, taken from Ref. 13. The corrosion rates were measured by the 2,500 and 45,000 A° probes, exposed side-by-side to same environments and exposure conditions. As expected, the corrosion rate measured by the 45,000 A° probe is about a third the rate measured by the 2,500 A° probe.

The CNET probe consists of an epoxy-fiber glass plate embedded with about 170,000 A° thick copper conductors. The probe is maintained at 40°C by water circulating under the probe. The change in the resistance of the probe is recorded at the beginning and at the end of the test to determine the extent of corrosion. The extent of corrosion is defined in terms of percent corrosivity factor, determined from the percent change in the resistance, normalized by the standard board resistance of 8 ohm. The probe is used in the CNET^{13,16,17} and the DIN¹⁸ test methods.

The Solution Phase Technique

The technique is used in the DIN^{13,18} test and in the FMRC test methods^{1,10,12,19,20}. In the technique used at FMRC, a mild steel corrosion probe (model 1032-S4-G10100-0, Rohrback Cosasco) is exposed to the water solution of the fire products. The probe consists of a mild steel loop attached to an epoxy-fiber glass rod, with a built-in reference. The mild steel loop acts a sensor. As the sensor loop corrodes and loses its thickness, its resistance changes. The extent of corrosion is measured by the difference in the resistance between the loop and the reference by the Corrosometer (Model 4208, Rohrback Cosasco) and corrosion rate is determined from Eq. (2).

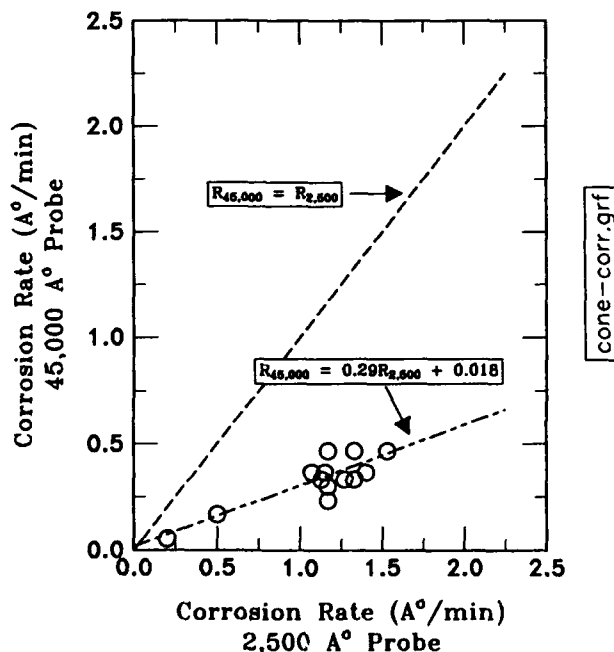


Figure 3. Average Corrosion Rates Calculated from the Data Reported in Ref. 13 for RC 2,500 and 45,000 A° Copper Probes in the ASTM D09.21.04 Test.

In this technique fire products are either bubbled directly into known volumes of water or are collected in the gas phase on cellulose based filter papers of known area. After the test, the color, odor, and mass of the products deposited on the filter papers are determined. The fire products are extracted with 100 ml of distilled water.

The solution phase corrosion is measured every hour for 24 to 48 hours. In some cases, concentrations of corrosive ions such as chloride, bromide, and fluoride, are also determined using selective ion electrodes.

In the DIN 57 472 test standard, pH and conductivity of the solution are measured.

Test Apparatuses

In the tests, small- to large-scale apparatuses and enclosures are used.

The FMRC test methods^{1,3-5,8,10,12,19,20}

In the test methods, three test apparatuses and an enclosure are used to assess the nonthermal damage due to smoke and corrosive fire products. The apparatuses used in the tests are: a 50 kW-scale apparatus, shown in Fig. 2, a 500 kW-scale apparatus, which is very similar to the 50 kW-scale apparatus, except for larger sample sizes, and a 10,000 kW-Scale Apparatus (Fire Products Collector), shown in Fig. 4. The enclosure used in the tests is 13.4 m long, 12.2 m wide and 6.1 m high with a volume of 997 m³ (Figure 5).

In the 50 and 500 kW-Scale Apparatus, about 0.10 m x 0.10m horizontal and 0.10m wide and 0.61 m high vertical wire and cable samples inside quartz tubes are used. In the 10,000 kW-Scale apparatus and the 997 m³ enclosure, single and multiple cable trays are used. The general cable tray dimensions are 2.4 m long, 0.46 m wide, and 80 mm deep.

In the 50- and 500-kW-Scale Apparatuses, air is introduced at the bottom of the Apparatuses with oxygen concentrations in the range of 0 to 11% for nonflaming fires, and in the range of 12 to 50 % for flaming fires. In the tests, samples are exposed to external heat fluxes, applied by four infrared heaters, in the range of 0 to 65 kW/m². In the 10,000-kW Scale Apparatus and the 997 m³ enclosure, tests are performed under natural air flow conditions.

In all three apparatuses, the fire products-air mixture is captured in the sampling duct, where measurements are made for chemical, convective, and radiative heat release rates, generation rates of fire products, smoke characteristics (optical transmission, electrical charges, color, odor, adsorbed species, and stain), and extent of corrosion using the 2,500 A° copper probes located in the sampling ducts and above the fire as shown in Figs. 2 and 4. For solution phase corrosion, filter paper and water bubblers located in the gas analysis sampling lines are used.

Only limited number of tests are performed in the 997 m³ enclosure. In the tests, filter papers, to monitor contamination levels and smoke characteristics, and 2,500 A° copper probes, to monitor corrosion, are placed at four levels about 0.30, 2.1, 4.0, and 5.8 m below the ceiling, each level having eight locations (five locations, 1.5 m from each other and three locations at right angles, 1.5 m away from each other). Thus a total of 32 locations are monitored in the tests.

The ASTM E05.21.70 Radiant Combustion-Exposure standard test method^{13,15}

In the test, 25 x 50 mm sample contained inside a 320 mm long and 30 mm I.D. quartz tube, sealed at one end, is exposed to 25 and 50 kW/m² of external heat flux. The fire products are

exhausted into a closed 200 liter chamber. Humidity is introduced by heating water in an aluminum beaker by a hot plate inside the chamber. Gas phase corrosion is measured by six RC copper 2500 A° (and 45,000 A°) corrosion probes. The probes are exposed for 60 minutes in the chamber with a 24 hour post exposure at 75 % relative humidity. Sample mass loss rate and concentrations of various fire products in the exposure chamber are measured.

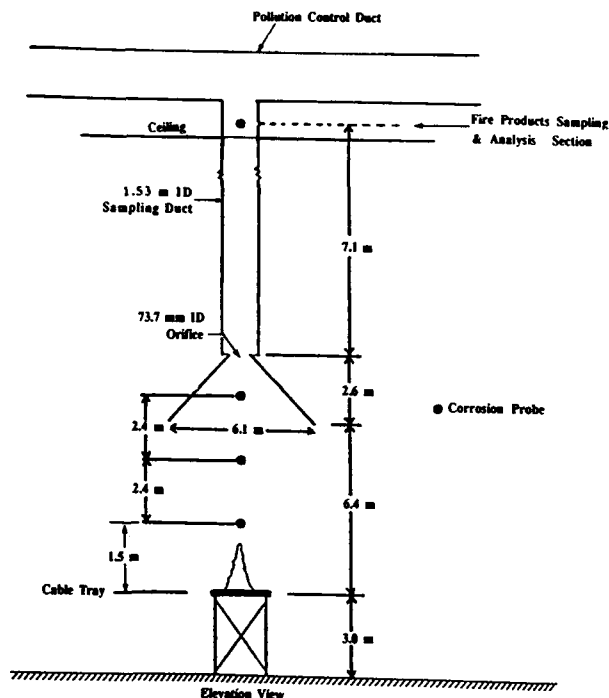


Figure 4. The FMRC 10,000 kW-Scale Flammability Apparatus (the Fire Products Collector).

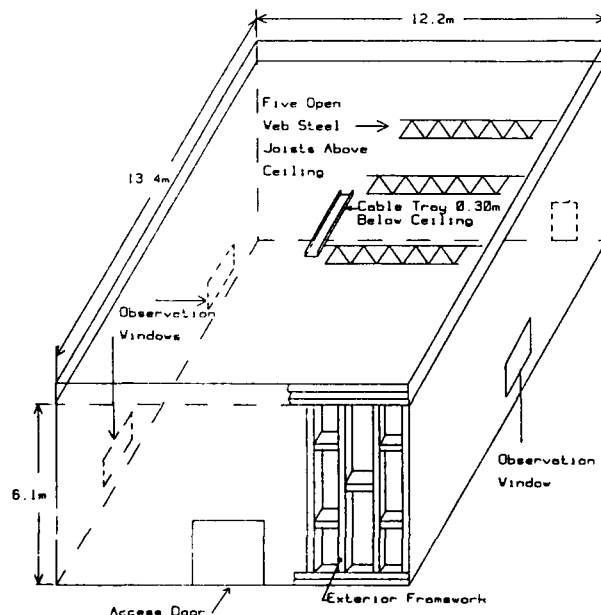


Figure 5. The FMRC 997 m³ Nonthermal Damage Test Enclosure.

The D09.21.04 Cone Corrosometer test method^{13,14}

Corrosion tests are performed using fire products generated from 100 x 100 mm horizontal samples, exposed to external heat flux values up to 100 kW/m². The samples are exposed to external heat flux until 70 % of the mass is lost. The products mixed with air are collected in a 11.2 liter exposure chamber at a rate of 2.38 volume change per minute during the test and sealed after the test. The corrosion is monitored by the RC copper 2500 A° probe (and 45,000 A°) during the test and one additional hour, after which the probe is placed in a chamber at 75 % relative humidity and 23 °C for 24 hours.

The CNET test method^{13,16,17}

In the test, 600 mg of the sample mixed with 100 mg of polyethylene are burned for 2 minute and 30 seconds in a Plexiglas cylinder (concentration = 35 g/ m³). Water is injected inside the chamber to achieve the desired humidity. The sample is ignited with an electrical coil heated to 800 °C. The water cooled CNET corrosion probe, maintained at 40 °C, is located on the floor. The probe is exposed to combustion products during the test and one hour after the test.

The DIN test method^{13,18}

In the test, samples are heated in a 0.11 m long quartz tube by a variable-temperature annular oven that moves along the tube at 10 mm/min in a direction opposite to the air flow. The samples are cylindrical of equal volume or weight per unit length. The fire products are swept out of the tube by a 100 l/min air stream. Near the exit of the quartz tube, 75 mm x 20 mm x 1 mm thick sheets of iron, steel, copper, aluminum and zinc are located for assessing the gas phase corrosion¹⁸. The fire product-air mixture exiting from the tube flows through a 7 liter glass cylinder, where a CNET corrosion probe is located to monitor gas phase corrosion¹⁸ or is bubbled through water traps to measure solution phase corrosion¹³.

NONTHERMAL DAMAGE ASSESSMENT: TEST RESULTS

In fires involving halogenated materials, chloride ion contamination levels in the range of about 5 to 900 microgram/cm² have been measured²¹. As a general rule, equipment with contamination levels below about 30 microgram/cm² can be easily restored to service with very little impact on long-term reliability²¹. Equipment with exposure levels from 30 to 90 microgram/cm² can also be restored to service as long as no unusual corrosion problems arise and the environment is strictly controlled soon after the fire²¹. As the contamination level rises above 90 microgram/cm², the effectiveness of cleaning dwindles and the cost of cleaning quickly approaches the replacement cost of the equipment²¹.

The nonthermal damage assessment tests are performed in small to large-scale apparatuses and enclosures to determine contamination levels of smoke and corrosive products and the resulting damage and effectiveness of protection.

Small-Scale Tests

Small-scale tests are performed to provide pertinent data for the assessment of nonthermal damage and effectiveness of protection. The assessments are performed through simple or complex models. Some of the key parameters that are needed for the models are: 1) contamination levels on surfaces in terms of microgram/cm², 2) smoke characteristics-optical transmission, color, smell, adsorbed species, electrical charges, and staining, and 3) gas and solution phase corrosion parameters. Currently, these parameters are being quantified in the small-scale tests such as in the FMRC 50-

and 500 kW-Scale Flammability Apparatus, in the ASTM E05.21.70 and D09.21.04, CNET and DIN test apparatuses. Examples of the type of data being measured are given in Tables 3 and 4. The data show that:

- 1) products of non-halogenated materials and fire retardants show negligible corrosion and the values of the gas phase corrosion parameter is equal to or less than about 0.007 (A°/min)/(g/m³),
- 2) fire retardation of non-halogenated materials increases extent of corrosion with values of the gas phase corrosion parameter between 0.011 to 0.046 (A°/min)/(g/m³). These values are about 1/10th the values for the halogenated materials,
- 3) for halogenated materials, the gas phase corrosion parameter values are greater than 0.14 (A°/min)/(g/m³),
- 4) the increase in the extent of corrosion due to the presence of water is not significant for materials with hydrogen atom in the structure (Table 2 and associated discussion),
- 5) increase in the oxygen concentration in the environment increases the extent of corrosion,
- 6) the difference between the gas phase corrosion parameters of PVC and Teflon by a factor of seven is probably due to the inefficiency of hydrolysis process for the conversion of fluorocarbon products generated from Teflon to HF and high water solubility of HCl generated from PVC.

The solution phase corrosion parameter values measured in the FMRC Flammability Apparatus show that they are comparable for all the halogenated materials and are significantly higher than the values for the gas phase.

Table 3
Corrosion Parameter in (A°/min)/(g/m³) for Flaming and Non-Flaming Fires at Various Oxygen Concentration

Polymer	O ₂ (%)	F/NF ^a	Water	Corrosion Parameter	
				FMRC	E05.21.70 ^b
EVA	21	F	no	nd	0.001
EVA-FR1	21	F	no	nd	0.021
PE	21	F	no	nd	0.002
PE-FR1	21	F	no	nd	0.024
PE-FR1	21	F	yes	nd	0.036
PE-FR2	21	F	no	nd	0.022
PE-FR2	21	F	yes	nd	0.024
PE-FR2	21	F	no	nd	0.014
PE-FR2	21	F	yes	nd	0.016
PE/25 %Cl	10	NF	yes	0.14	nd
PE/36 % Cl	10	NF	yes	0.15	nd
PE/48 % Cl	10	NF	yes	0.19	nd
PVC	10	NF	yes	0.15	nd
	21	NF	no	nd	0.027
	21	F	yes	0.12	0.087
	21	F	yes	1.0	nd
TFE	0	NF	yes	0.0036	nd
	10	NF	yes	0.011	nd
	40	NF	yes	0.035	nd
	21	F	yes	0.42	nd

^a: F: flaming, NF: non-flaming; ^b: 1500 minute average, data from Ref. 15; FR-1: red phosphorus fire retardant; FR-2: bromine fire retardant; EVA: ethylene-vinyl acetate copolymer; PE: polyethylene.; nd: not determined.

Table 4
Gas Phase Corrosion Parameter for Various Plastics
Calculated from the Data Measured in the E05.21.70 Test^a

Sample	Description	Corrosion Parameter ^b (A°/min)/(g/m ³)
1	Crosslinked polyolefin (XLPO) + metal hydrate	0.007
2	HD polyethylene (PE) & Chlorinated PE blend	>0.098
3	Chlorinated PE + fillers	>0.098
4	Ethylvinylacetate (EVA) PO +ATH filler	0.012
5	Polyphenylene oxide/ polystyrene (PS) blend	0.005
6	Polyetherimide	0.002
7	Polyetherimide/siloxane copolymer	0.005
8	Intumescent polypropylene (PP)	0.025
9	Nylon + mineral filler	-
10	Polyolefin copolymer + mineral filler	0.046
11	XLPO + mineral filler	0.011
12	XLPO + ATH	0.003
13	XLPO + ATH	0.007
14	EVA PO + mineral filler	0.013
15	PO + mineral filler	0.016
16	CLPE + chlorinated additive	>0.098
17	Polyvinylidene fluoride	>0.098
18	Polytetrafluoroethylene	>0.098
19	Polyvinylchloride (PVC)	>0.098
20	PVC wire	>0.098
21	PE homopolymer	0.006
22	Douglas fir	0.006
23	EVA PO copolymer	0.003
24	Nylon 6,6	0.008
25	XLPE copolymer + brominated additives	0.091

^a: from Reference 13; ^b: average concentration assumed to be 17.0 g/m³ based on the data reported in Ref. 15.

Large-Scale Tests

Large-scale tests are performed to validate small-scale test results and to determine distribution pattern of the products. At FMRC, large-scale tests are performed in the 10,000 kW-Scale Flammability Apparatus (Fire Products Collector), shown in Fig. 4 and in the 997 m³ enclosure, shown in Fig. 5.

The FMRC 10,000 kW-Scale Apparatus

Tests were performed using 3 layers of PE/PVC cables in a horizontal cable tray (2.4 m long, 0.46 m wide and 0.08 m deep); details are described in Ref. 22. The tray was located about 3 m above the floor. Tests were performed with and without coating the cables. Cables were ignited electrically. Gas phase corrosion was measured at various heights above the cable tray, as shown in Fig. 4. In addition, heat release rate and generation rates of fire products were also measured. Figure 6 taken from Ref. 22, shows the data for the corrosion rate at various heights.

Since the gas phase corrosion parameter for the cable is about 1.0 (A°/min)/(g/m³), the decrease in the corrosion rate with height is an indication of the dilution of the products by air entrainment. The decrease in the corrosion rate due to coating is primarily due to decrease in the extent of fire propagation or decrease in the FPI value and secondarily due to neutralization of HCl generated from the cable by the alkaline coating.

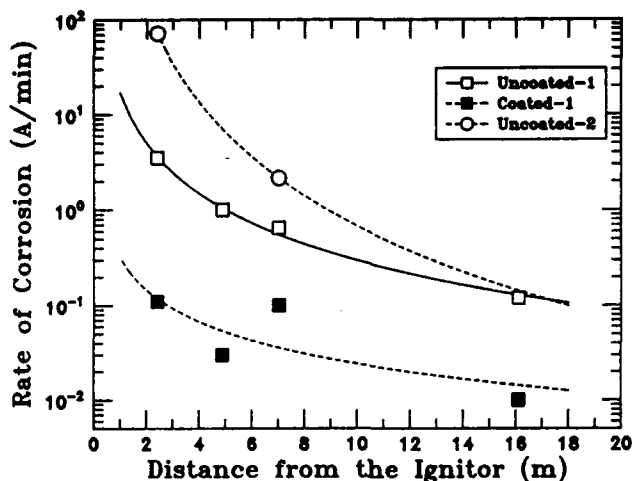


Figure 6. Average Gas Phase Corrosion Rates at Various Heights above the Ignition Source for the Non-Flaming Fires of Coated and Un-coated Polyethylene-Polyvinylchloride Cable in a Horizontal Cable Tray. Figure Taken from Ref. 22.

These data suggest that quantification of corrosion parameter in small-scale tests is useful. Materials with high values of corrosion parameter would require higher protection in terms of limiting the extent of fire propagation and/or increasing the dilution of the products with air. For cables with similar values of the corrosion parameter, Group 1 cables are expected to provide better protection from nonthermal damage than the Group 3 cables.

The FMRC 997 m³ Enclosure

In the tests, horizontal and vertical cable trays with three layers of PE/PVC cables (cable outer diameter: about 19 mm; linear density: 345 gm/m) were used; details are described in Ref. 22. The cable tray was 2.4 m long, 0.46 m wide and 0.08 m deep. The cable tray was located in the center of the enclosure (about 0.30 m below the ceiling for horizontal cable tray test). For vertical cable tray test, the tray was located on the floor at the center of the enclosure. Electrical overheating and arcing were used for fire initiation. Chloride ion contamination and corrosion were monitored at 32 locations.

In both horizontal and vertical tray fire tests, fire propagation was limited and the tests were basically nonflaming fire tests. The average concentrations of the fire products in the horizontal and vertical tests were 3 and 6 gm/m³ respectively²². The chloride ion contaminations in microgram/cm² at various locations in horizontal and vertical cable tray fire tests, taken from Ref. 22, are shown in Fig. 7 and 8 respectively.

The data in Fig. 7 show that for an average fire products concentration of 3 g/m³ in the horizontal test, the chloride ion contamination level at all locations did not exceed 20 microgram/cm². With this contamination level, equipment can be easily restored to service with very little impact on long-term reliability²¹. Thus 3 g/m³ may be considered as the lower level for the average fire products concentration for limiting nonthermal damage to equipment²².

The data in Fig. 8 show that for an average fire products concentration of 6 g/m³ in the vertical test, the chloride ion contamination level at all locations exceeded the 30 microgram/cm². Coating of the cable, however, kept the contamination level below the 30 microgram/cm² level²².

These results suggest the importance of the Fire Propagation Index to limit extent of fire propagation by coating and

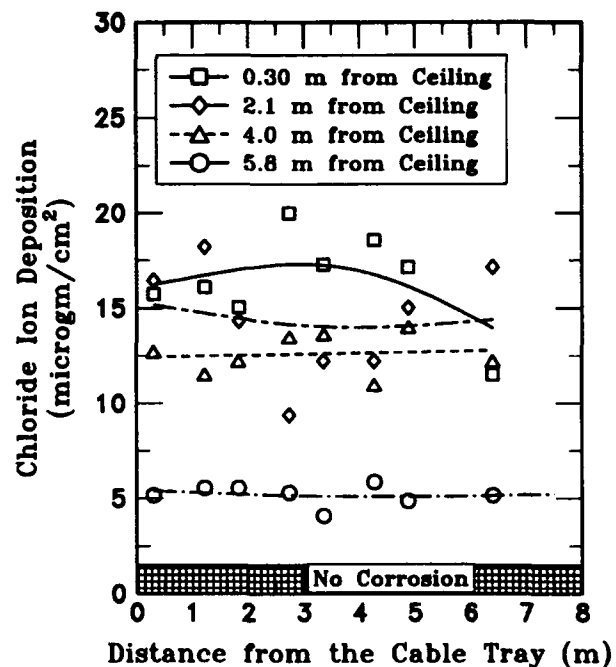


Figure 7. Chloride Ion Contamination at Various Locations for an Average Fire Products Concentration of 3 gm/m³ Inside the FMRC 997 m³ Enclosure for Nonflaming Fire of Horizontal Polyethylene-Polyvinylchloride Cable Tray. Figure taken from Ref. 22.

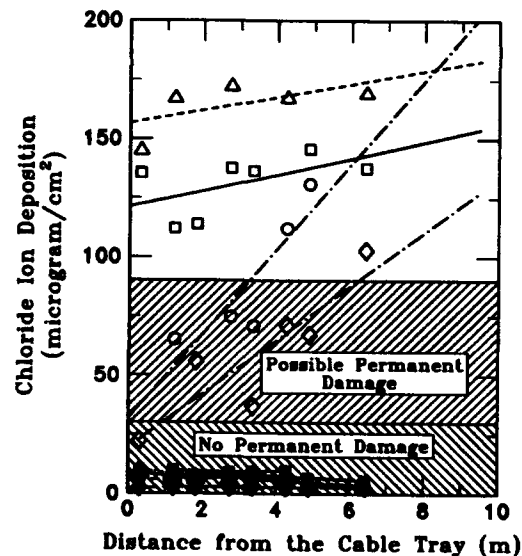


Figure 8. Chloride Ion Contamination at Various Locations for an Average Fire Products Concentration of 6 gm/m³ Inside the FMRC 997 m³ Enclosure for Nonflaming Fire of Vertical Polyethylene-Polyvinylchloride Cable Tray. Figure taken from Ref. 22.

product dilution. Use of materials with low values of the gas phase corrosion parameter would have provided information on an alternate protection means.

Since several factors need to be considered in order to assess nonthermal damage, models become useful tools.

At FMRC, the FSG model has been developed to predict flame spread behavior of materials including wires and cables^{23,24}. The ultimate objective is to use this model to predict fire propagation and generation of smoke and corrosive products and combine the results of smoke and corrosion measurements to assess nonthermal damage in various fires involving wires and cables as well as other materials.

SUMMARY

1) Halogenated materials and halogenated additives have higher corrosion rates than non-halogenated materials and additives. Halogenated material with no hydrogen in the structure, however, are weakly corrosive in the gas phase. Corrosion in the solution phase is much faster than in the gas phase;

1) several small-scale tests have been developed to quantify extent of corrosion in the gas phase and in the solution phase. The results expressed in terms of corrosion parameter are expected to be helpful to assess nonthermal damage with the help of models;

2) Protection from nonthermal damage is possible by limiting the extent of fire propagation and dilution of products. Reduction in the extent of fire propagation can be achieved by reducing the Group classification of wires and cables from 3 to 2 to 1 by changes in the materials, coatings, and other methods;

3) Use of materials with very low values of corrosion parameter provides an alternate means of protection from nonthermal damage.

REFERENCE

1. Tewarson, A., "Nonthermal Fire Damage", *J. Fire Science*, 10, 188, 1992.
2. Karydas, D.M. "A Probabilistic Methodology for the Fire Smoke Hazards Analysis of Electronic Equipment" Ph.D. Thesis in Industrial Engineering, Northeastern University, Boston, Mass. May 30, 1990.
3. Tewarson, A., and Khan, M.M., "Flame Propagation for Polymers in a Cylindrical Configuration and Vertical Orientation", *Twenty-Second Symposium (International) on Combustion*, p.1231. The Combustion Institute, Pittsburgh, Pa. 1988.
4. Tewarson, A., and Khan, M.M., "A New Standard Test for the Quantification of Fire Propagation Behavior of Electrical Cables Using Factory Mutual Research Corporation's Small Scale Flammability Apparatus", *Fire Technology*, 28, 125, 1992.
5. Tewarson, A., "Surface Flame Spread", Document Prepared for the IEC TC89 WG8, April 1993.
6. Hirschler, M.M., "Survey of Fire Testing of Electrical Cables", *Fire and Materials*, 16, 107, 1992.
7. Clarke, F., Hoover, J.H., Caudill, L., Fine, A., Parnell, A., and Butcher, G., "Characterizing Fire Hazard of Unprotected Cables in Over-Ceiling Voids Used for Ventilation", p.100, *Interflame 1993*. Interscience Communications Limited, London, UK 1993.
8. Specification Standard for Cable Fire Propagation, Class No.3972. Factory Mutual Research Corporation, Norwood, MA. 02062 (1989).
9. Tewarson, A. "Generation of Heat and Chemical Compounds in Fires", Section 1, Chapter 13, pp. 1-179 in

The SFPE Handbook of Fire Protection Engineering (P.J. DiNenno, Ed.), National Fire Protection Association Press, Quincy, MA, 1988.

10. Tewarson, A., Chu, F., and Ziang, F.H., "Combustion of Halogenated Polymers" submitted to the *Fourth International Symposium of the Fire Safety Science*, May 1994.

11. Handbook of Plastics and Elastomers, Harper, C.A. (Editor-in-Chief), McGraw-Hill Book Company, New York, N.Y., 1975.

12. Chu, F.L., "Development and Application of Nonthermal Damage Assessment Techniques", Factory Mutual Research Corporation, Norwood, MA. Technical Report J.I. OV1J1.RC, October, 1992.

13. Kessel, S.L., Rogers, C.E., and Bennett, J.G., "Corrosive Test Methods for Polymeric Materials Part 5- A Comparison for Four Test Methods", *Eighteenth International Conference on Fire Safety*, Product Safety Corporation, Sunnyvale, CA, January, 1993.

14. Dickinson, P.R., "Evolving Fire Retardant Material Issues: A Cable Manufacturer's Perspective", *Fire Technology*, November, 345, 1992.

15. Grand, A.F., "Evaluation of the Corrosivity of Smoke Using A Laboratory Radiant Combustion Exposure Apparatus", *J. Fire Sciences*, 10, 72, 1992.

16. Rio, P., "Presentation de l'essai "Corrosivite" mis au point au CNET-Lab-SER/ENV Centre National d'Etudes des Telecommunications", 1983.

17. Bottin, M.F., "The ISO Static Test Method for Measuring Smoke Corrosivity", *J. Fire Science*, 10, 160, 1992.

18. Barth, E., Muller, B., Prager, F.H., and Wittbecker, F., "Corrosive Effects of Smoke: Decomposition with the DIN Tube According to DIN 53436", *J. Fire Sciences*, 10, 432, 1992.

19. Tewarson, A., Khan, M.M., and Steciak, J.S., "Combustibility of Electrical Wire and Cable for Rail Rapid Transit Systems, Vol.1. Flammability", U.S. Department of Transportation Technical Report DOT-TSC-UMTA-83-4.1, National Technical Information Service, Springfield, VA (April 1982).

20. Tewarson, A., and Khan, M.M. "Generation of Smoke from Electrical Cables" p.100 in *Proceedings of the ASTM Symposium on Characterization and Toxicity of Smoke*, Hasegawa, H.K. (Editor), ASTM STP 1082. The American Society of Testing and Materials, Philadelphia, PA., 1988.

21. Reagor, B.T., "Smoke Corrosivity: Generation, Impact, Detection, and Protection", *J. Fire Sciences*, 10, 169, 1992.

22. Tewarson, A., Chu, F., and Hill, J.P., "Quantification of Fire Characteristics for Assessment of Nonthermal Fire Damage", *Fire Technology* (submitted).

23. Delichatsios, M.M., Mathews, M.K., and Delichatsios, M.A., "An Upward Fire Spread and Growth Simulation", *Fire Safety Science, Proceedings of the Third International Symposium*, pp. 207, Elsevier Science Publishers, Ltd., London, 1991.

24. Wu, P., "The Fire Spread and Growth Program", Interoffice Correspondence, to A. Tewarson, Factory Mutual Research Corporation, Norwood, MA, March 26, 1993.

The author received his Ph.D. degree in Fuel Science/Physical Chemistry in 1969 from the Pennsylvania State University. Currently he is the manager of the Flammability Section and holds the position of senior research specialist at the Factory Mutual Research Corporation. He is internationally recognized for his research and has over 100 papers and publications. His research interests are chemical kinetics, flammability, and nonthermal damage. One of the areas examined in great detail in his research is the fire behavior of wires and cables.

PERFORMANCE CHARACTERISTICS OF LOW SMOKE/ZERO HALOGEN CABLES

Bobby C. Gentry, Tye Cene, Jerry M. Hesterlee

Southwire Company, Carrollton, Georgia

ABSTRACT

This paper presents test results comparing standard Type TC with Zero Halogen Type TC.

Standard Type TC utilized Type THHN/THWN PVC insulated, nylon jacketed conductors (nine conductors of AWG 12 copper) with a PVC jacket over the assembly. Zero Halogen Type TC is constructed the same except the PVC is replaced with a Non Halogen Polyolefin material for both insulation and jacket.

The test results show the positive influence Zero Halogen insulating and jacketing materials have on performance properties of heat release, ignition time, smoke obscuration, weight loss, corrosion, flame travel, total smoke release, peak smoke release, CO emission and toxicity.

INTRODUCTION

Conductor insulating and jacketing materials containing halogens have been used for many years. The halogens found in these materials are: Chlorine, Bromine and Fluorine.

Halogens improve certain properties such as flame, chemical and oil resistance, but also have some negative effects.

Gasses produced during combustion of halogenated materials react with moisture to produce halogen acids; for example, Hydrogen Chloride (HCL) and Hydrogen Bromide (HBr).

The most common halogenated insulating and jacketing material for electrical wire and cable is Polyvinyl Chloride (PVC).

Southwire Company has worked to develop several zero halogen polyolefin-based insulating and jacketing materials as an alternate to PVC.

FIRE RETARDING ZERO HALOGEN MATERIALS

PVC is normally treated with Antimony or Bromine (both release toxins when burned) to enhance fire retardency of the PVC, compounding the toxic potential in a fire.

The fire retarding effect of polyolefin-based reduced emission compounds is brought about through the use of hydrated mineral fillers.

Up to 30% of these fillers is hydrated water that is released in a fire situation. When exposed to flame, available heat is used to volatilize the water of hydration, thus cooling the flame and slowing decomposition. The water vapors will block the oxygen supply from the fuel, and the fire may be extinguished or its progress retarded.

PRODUCT DEVELOPMENT

Products developed to date using zero halogen polyolefin-based insulating and jacketing materials are: NM-B, THHN, SIS, TC (jacket only), and MC (jacket only). TC, MV-90 (jacket only) and THWN are presently under development. The initial products developed are described below:

NM-B

NM-B (see Figure 1) is primarily used in residential wiring as branch circuits for outlets, switches and other loads. NM-B meets or exceeds UL Standards 83 and 719. Conductor is rated for 600 V., 60°C. operation.

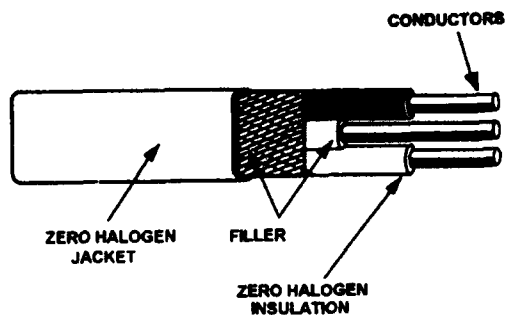


Figure 1
NM-B

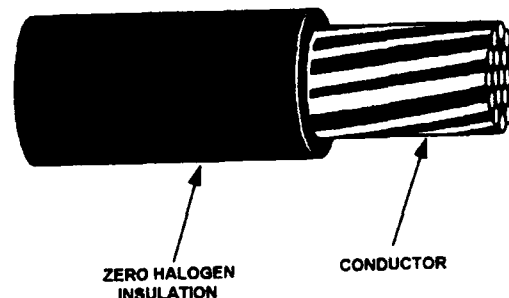


Figure 3
SIS

THHN

THHN conductors (see Figure 2) are primarily used for power and control circuits in commercial and industrial applications. THHN meets or exceeds UL Standard 83. Conductors are rated for 600 V, 90°C operation in dry locations. Product is oil, gasoline, and abrasion resistant.

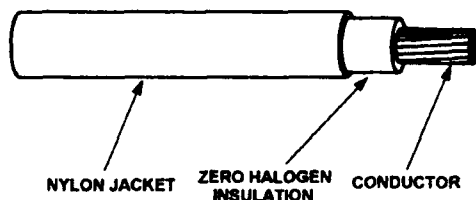


Figure 2
THHN

MC (Metal Clad Cable)

Type MC (see Figure 4) is used for services, feeders and branch circuits for power, lighting, control and signal circuits per Article 334 of the National Electrical Code. MC cable meets or exceeds UL Standards 44, 83 and 1277. The cable is rated according to the conductor Types used in the core assembly.

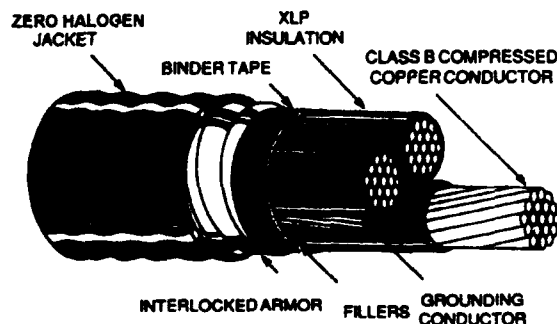


Figure 4
MC

SIS (Switchboard Wiring)

Type SIS (see Figure 3) is used in switchboards, panelboards and distribution boards installed for the control of light and power circuits, and battery-charging panels supplied from light or power circuits. SIS meets or exceeds UL Standard 44. Conductor is rated for 90°C. operation.

MV-90 (Medium Voltage Cable)

Type MV (see Figure 5) is a single or multiconductor solid dielectric insulated cable rated 2001 volts to 35,000 volts. Type MV is used on power systems in wet or dry locations, in raceways, cable trays, direct buried and in messenger supported wiring per Article 326 of the NEC.

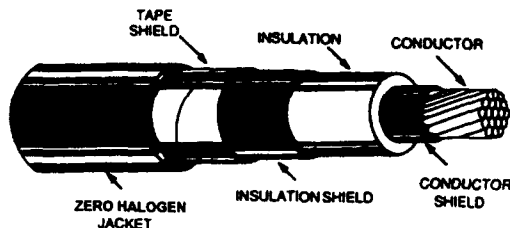


Figure 5
MV

TC (Power and Control Tray Cable)

Type TC (see Figure 6) is used for power, lighting, control, and signal circuits. In cable trays, raceways or where supported in outdoor locations by a messenger wire per Article 340 in the National Electrical Code.

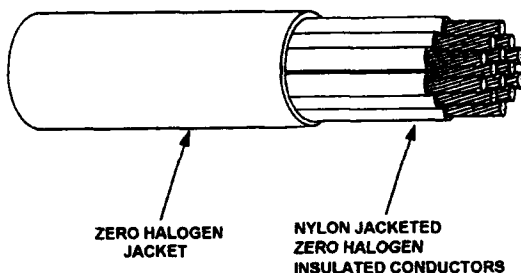


Figure 6
TC

This paper reviews the performance characteristics of Low Smoke/Zero Halogen Power and Control Tray Cable, Type TC.

TEST SPECIMENS

Properties and performance characteristics were determined using Low Smoke/Zero Halogen and PVC Power and Control Tray Cable test specimens as described below:

AWG 12 Conductors (9)
Conductors Type THHN/THWN
Insulation thickness .015"
Nylon thickness .004"
Jacket thickness .045"

PHYSICAL PROPERTIES

Typical physical properties of the zero halogen insulation and jacket materials used in the power and control tray cable comparison are shown in Appendix 1. This data shows the insulation and jacket meet or exceed accepted industry requirements.

EMISSION CHARACTERISTICS

Cone calorimeter, vertical tray flame test and the University of Pittsburgh Toxicity tests were used to compare the emissions characteristics of the Zero Halogen and PVC power and control tray cable specimens.

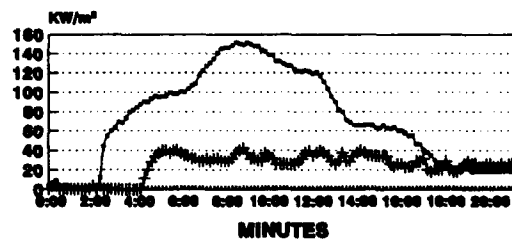
CONE CALORIMETER

The cone calorimeter tests were conducted in accordance with ASTM E1354. Each sample was tested in a horizontal orientation at an external radiant flux level of 25 KW/m² with a spark pilot ignition source and an initial exhaust mass flow rate of 30 g/s.

The data obtained included: heat release, ignition time, smoke obscuration, weight loss and corrosion.

Cone calorimeter results are shown in the following figures 7, 8, 9 and 10.

CONE CALORIMETER 9 COND.#12 AWG CONTROL CABLE (STD vs RE)



— PVC CON/PVC JKT + RE COND/RE JKT

(Avg. PVC Cable Ignition: 2.3 min)
(Avg. RE Cable Ignition: 4.3 min)

Figure 7
HEAT RELEASE

CONE CALORIMETER 9 COND. #12 AWG CONTROL CABLE COROSOMETER TESTS

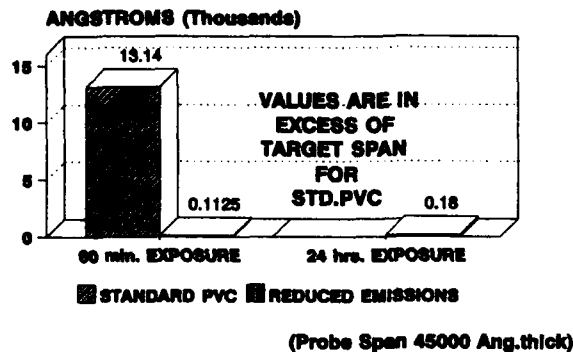
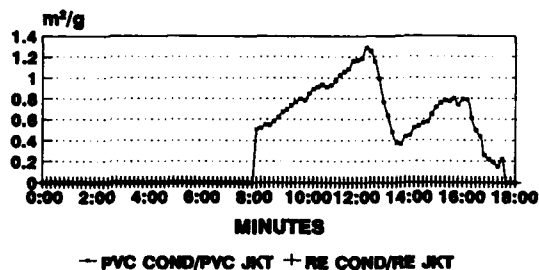


Figure 8
CORROSION

CONE CALORIMETER 9 CON.#12 AWG CONTROL CABLE (STD vs RE)



(RE cables did not show appreciable smoke values)

Figure 9
SMOKE OBSCURATION

CONE CALORIMETER 9 COND.#12 AWG CONTROL CABLE (STD vs RE)

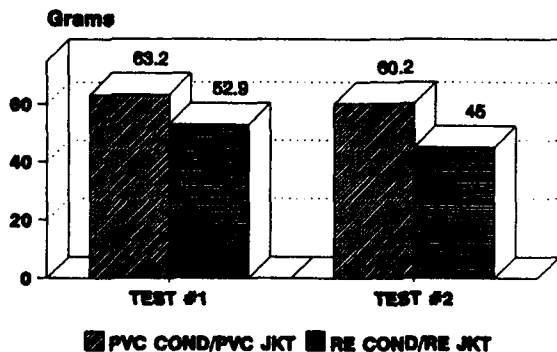


Figure 10
TOTAL WEIGHT LOSS

VERTICAL TRAY FLAME TEST

The UL 1685 Vertical Tray Flame test was conducted on both the PVC and zero halogen constructions. Data obtained included flame height vs. time, total smoke release, and peak smoke release. Results are shown in figures 11, 12 and 13.

VERTICAL TRAY FLAME TEST 9 COND.#12 AWG CONTROL CABLE (STD vs RE)

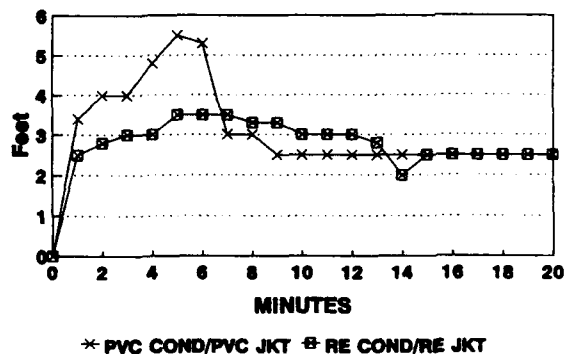


Figure 11
FLAME HEIGHT

VERTICAL TRAY FLAME TEST 9 COND.# 12 AWG CONTROL CABLE (STD vs RE)

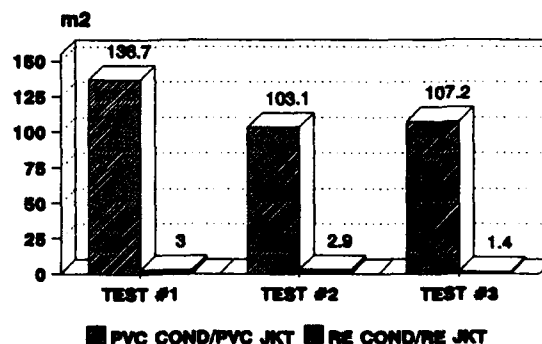


Figure 12
TOTAL SMOKE RELEASE

VERTICAL TRAY FLAME TEST 9 COND.#12 AWG CONTROL CABLE (STD vs RE)

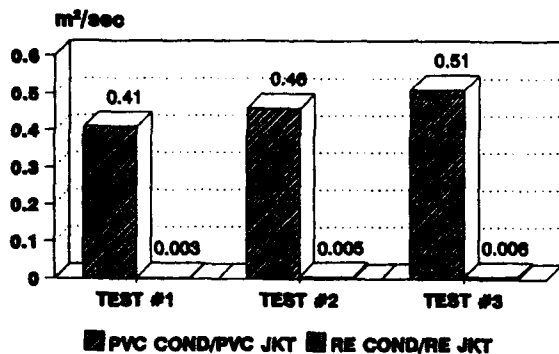


Figure 13
PEAK SMOKE RELEASE

TOXICITY TEST

The University of Pittsburgh toxicity test was used to evaluate toxicity of the gasses produced during thermal decomposition. The weight of material tested which causes death of 50% of the test animals is referred to as the LC₅₀ value of that material.

The severity of the toxicity is measured from a LC₅₀ value of zero to one hundred, zero representing the most toxic level. As the (LC₅₀) value increases, the toxicity level decreases.

As a benchmark, wood has a LC₅₀ value of 70.

In this test, materials were heated at 20°C/minute and two levels of testing were conducted. The first series of the tests were done as the protocol directed; a 30 minute exposure followed by a ten minute recovery period. The second series extended the recovery period from ten minutes to two weeks. See figure 14 for results.

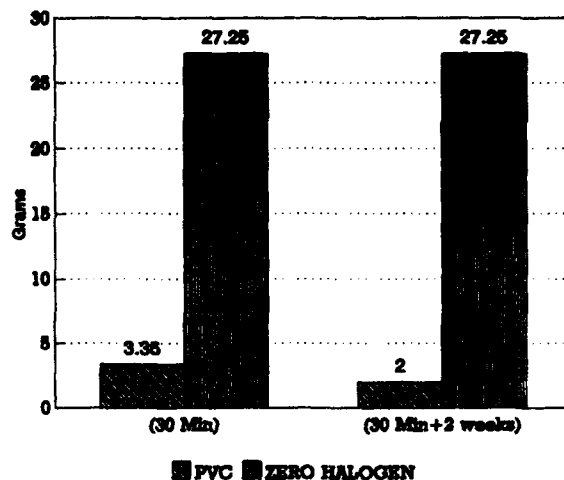


Figure 14
LC₅₀ VALUES

Carbon monoxide emission levels also showed drastic improvement when compared to standard cables (see figure 15). The reason for the lower carbon monoxide levels is related to the type fire retardant used.

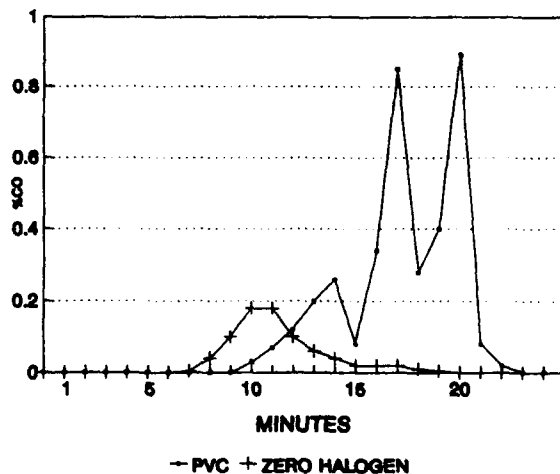


Figure 15
GAS ANALYSIS (CO%)

CONCLUSIONS

Analysis of the results obtained from testing conducted to compare the emission characteristics of zero halogen and PVC power and control tray cable reveals that zero halogen insulated and jacketed cable:

- * Low smoke/zero halogen power and control tray cable meets or exceeds accepted industry requirements.
- * Has a characteristic of delayed ignition.
- * Emits less dense smoke and less total smoke.
- * Is significantly less corrosive than standard PVC cable, based on cone calorimeter results.
- * Is less toxic than PVC cable according to LC₅₀ values from the University of Pittsburgh toxicity test.
- * Has significantly lower carbon monoxide emission levels.

APPLICATION POSSIBILITIES

Potential applications for low smoke/zero halogen insulated and jacketed cables include:

- * Commercial buildings.
- * Computer rooms.
- * Telecommunications.
- * High risk buildings.
(Hospitals, nursing homes, theaters, hotels).
- * Industrial application.
(Control centers).
- * Subways.
- * Shipboard.
- * High-population public assembly areas i.e., sports arenas and shopping malls.

APPENDIX I
TYPICAL PROPERTIES
ZERO HALOGEN TYPE TC CABLE

PROPERTY	INSULATION			JACKET		
	TEST METHOD	REQUIREMENT	RESULT	TEST METHOD	REQUIREMENT	RESULT
Limited Oxygen Index	ASTM D2863	None	34	ASTM D2863	None	40
Density	ASTM D1505	None	1.39	ASTM D1505	None	1.48
Tensile (PSI)	UL 1581	Min. 2000	3100	UL 1581	N/A	2000
Elong. (%)	UL 1581	Min. 150	250	UL 1581	N/A	160
Aged Tensile Ret.-%	UL 1581	Min. 75	98*	UL 1581	N/A	145*
Aged Elong. Ret.-%	UL 1581	Min. 65	90*	UL 1581	N/A	75*
Def.-% @121 C.	UL 83	Max. 30	30	UL 1277	Max. 50	N/A
Low Temp. Flex.	UL 83	No Cracks -25 C.	Pass	UL 1277	No Cracks -25 C.	Pass
Flame Test	UL 83	All-Wires	Pass	UL 1277	Vert. Tray	Pass

Note: N/A=Not yet available, *=7days at 121°C.

AUTHORS:

Bobby C. Gentry, Development Manager, Southwire (Presenter)
Jerry M. Hesterlee, A.V.P. Wire & Cable Technology, Southwire
Tye Cene, Senior Development Engineer, Southwire

1625 nm MONITORING SYSTEM DESIGN FOR THE PREVENTIVE MAINTENANCE OF FIBER OPTICS PLANTS

E. COTTINO, D. DELLERA, S. DE PAOLI

AET Telecomunicazioni, Laboratorio Tecnologie Ottiche
Via G. RE 47, 10146 TORINO, ITALY

ABSTRACT

A monitoring system of optical fiber cable plants called VDO designed by AET that is able to supply all the necessary information to evaluate the performances offered by optical bearer links is presented.

The main feature of VDO system is to be fully transparent to transmission system, in other words it doesn't alter the performances. This is obtained by the monitoring of the optical bearer at a different wavelength from the operating one by means of a suitably designed laser working at 1625 nm.

The advantage of using a source of 1625 nm is given by the greater fiber sensitivity to stresses and bendings occurring at this wavelength. In this way it's possible to prevent the eventual degradation of the fibers

1. INTRODUCTION

The present fiber optics transmission systems only foresee controls on the quality of the signal received based on error rates established by the CCITT, while a bearer supervision is not provided for.

Therefore, should the system exceed such limits, it is necessary to verify whether this is due to the transmission systems or to the optical bearers. That means a double research before being able to go back to the origin of the problem.

Such system designed by AET for the monitoring and evaluation of the fiber optics plants degradation is integrated in the service support systems of the network transmission and supplies all the information necessary to evaluate the performance conditions offered by the optical bearer links.

It specifically allows to detect the loss variations of fibres, splices and optical connectors inside a plant which cause the links deterioration and may subsequently lead to a service inefficiency.

2. PROJECT OPTIMIZATION

The Italian optical bearer telecommunications network is realized with two types of fibres: the "standard" monomode and "dispersion shifted" monomode. The first one is particularly suitable to work in second optical window, that is at 1300 nm, while the second is suitable for the third optical window at 1550 nm. Therefore, it is necessary to search for a higher wavelength laser source so as not to interfere with the systems working in the above mentioned optical windows.

The advantage deriving from the use of an OTDR at a wavelength superior to 1600 nm is bound to the greater fibres sensitivity to stresses and bendings in such spectrum part. In such a way it is possible to prevent the degradation of the fibre itself.

On the grounds of these considerations, the choice made foresees the use of an OTDR able to send a control signal at a wavelength of 1625 nm (figure 1). The identification of this value has been carried out in order to guarantee a good compromise between the fibre loss (too high at superior wavelengths) and the separation from the service signal transmitted at 1550 nm.

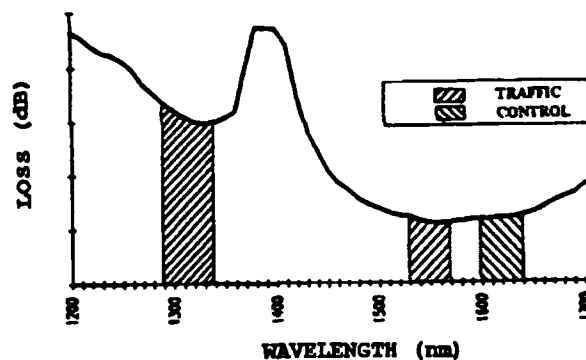


Fig. 1 : loss wavelength trace

3. FIBRE SURVEY

A special importance in the system improvement is given to the measurements carried out in laboratory and on field in order to analyze the fibres behaviour as regards loss and sensitivity to bendings, at a wavelength different from the "optical windows" being used until today.

Therefore a series of spectral loss measurements have been carried out on fibres of recent and old production with a special attention to the value of 1625 nm constituting the wavelength assumed in the line monitoring.

Picture number one shows the loss trace depending on the wavelength of a standard fibre. Note how the loss coefficient reaches a value very close to 1550 nm in the band assigned to maintenance (1600 - 1640 nm).

The spectral loss traces in picture n. 2 and 3 concerning respectively SM and SM-DS fibres of recent production, underline how, at about 1600 nm, their loss coefficient is almost the same as their respective coefficient at 1550 nm.

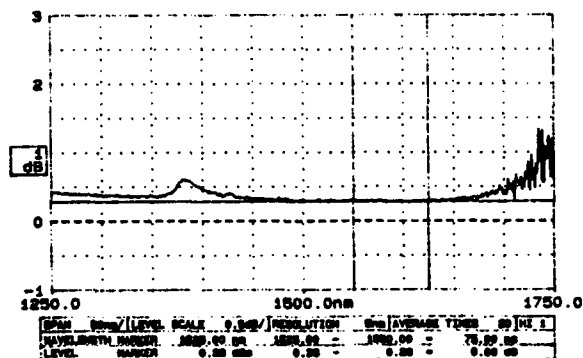


Fig. 2 : SM loss comparison 1550/1625 nm

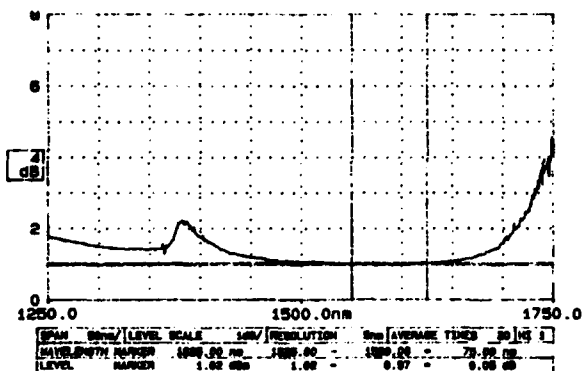
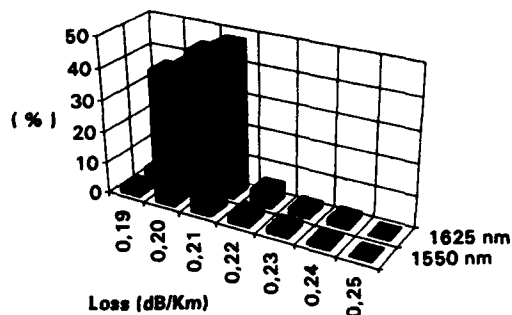


Fig. 3 : SM-DS loss comparison 1550/1625 nm

As a verification of the results previously shown, loss measurements have been carried out on a sample of 600 dispersion shifted fibres by means of the backscattering technique using an OTDR equipped with a 1627 nm wavelength shifted laser source.

The results are shown in picture n.4



(%)	1550 nm (dB/Km)	1625 nm (dB/Km)	(%)
2	0,19	0,19	3
42	0,20	0,20	48
50	0,21	0,21	48
3	0,22	0,22	5
2	0,23	0,23	2
1	0,24	0,24	2
0	0,25	0,25	0

Fig. 4 : SM DS loss comparison

4. SOURCE CHARACTERIZATION AT 1625 nm

The source used by the control device (OTDR) in the monitoring system is a class 1 laser with an emission wavelength of 1625 nm with a tolerance of ± 5 nm.

Picture n.5 shows the laser source spectrum.

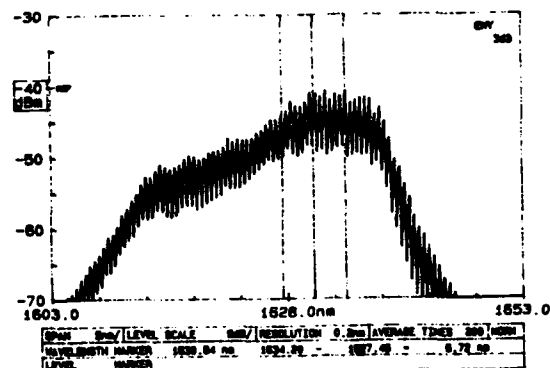


Fig. 5 : 1625 nm laser source spectrum

5. BENDING SENSITIVITY

Normal matched cladding type monomode fibres and step index type show a bending sensitivity directly proportional to the wavelength.

There are different data concerning this kind of behaviour obtained with the analysis of a great number of samples.

On plants, the bending effect could be more evident in the cable termination racks or in the splicing closures where an incorrect cabling could give origin to loss concentrated increases. The use of a 1625 nm wavelength will be more selective because of the increase, at such wavelength, of the fibres sensitivity to the micro and macrobendings.

Tests have shown evidence of such a phenomenon passing from 1550 to 1625 nm.

In the following pictures 6 and 7, you can see the results of bendings sensitivity tests carried out in laboratory.

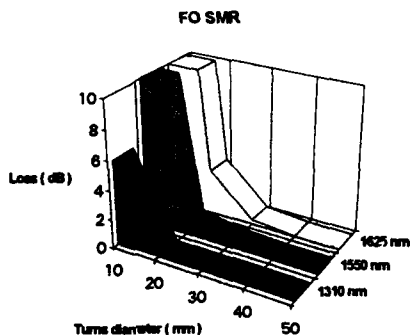


Fig. 6 : SMR fiber bending sensitivity

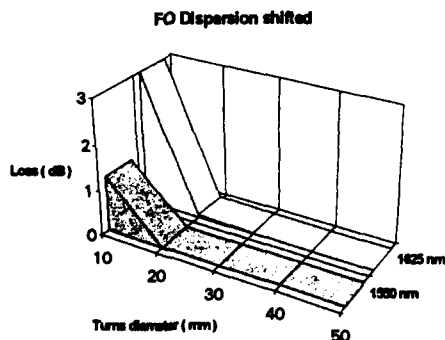


Fig. 7 : SM DS fiber bending sensitivity

To confirm the laboratory results are been performed test measurement on field, related to several plants equipped with singlemode dispersion shifted fibers. The results about this test are shown in the histogram of picture n. 7, is possible see that difference between the mean value at 1550 and 1625 nm, on an example of 1746 champs, is only 0,0022 dB.

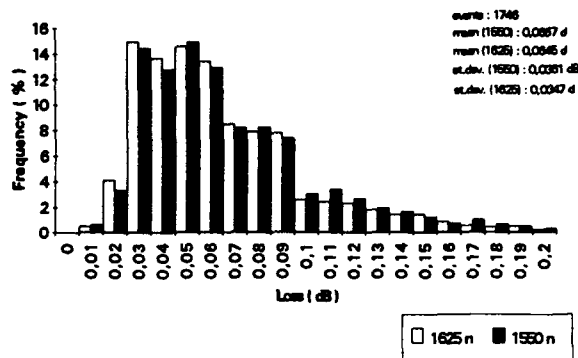


Fig. 7 : splice loss comparison 1550/1625 nm

6. OPTICAL BRANCHES

Optical branches constitute the interface point between the monitoring system and the line allowing the separation or recombination of the two signals (control and traffic) present in fibre.

An optical branch is essentially a device in which the wavelength dependence of the optical power has been duly checked under the project phase. Furthermore, this component must ensure the least insertion loss in order not to weigh excessively on the power budget of the transmission systems.

The WDM fusion technology is adopted to obtain the optical branches.

Pictures n.8 and 9 show the respective tranfer traces for 1550 and 1625 nm outputs concerning the traffic and control signal.

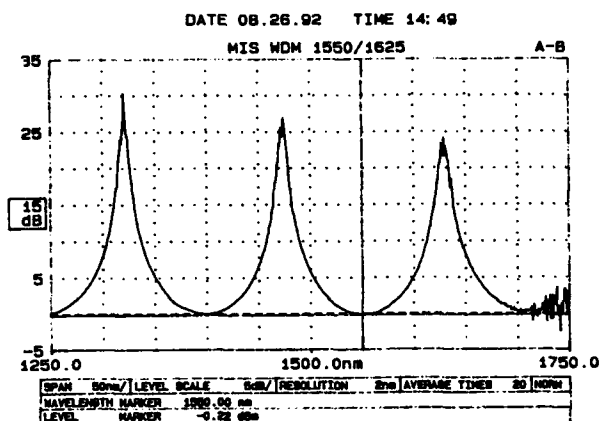


Fig. 8 : output 1550 nm

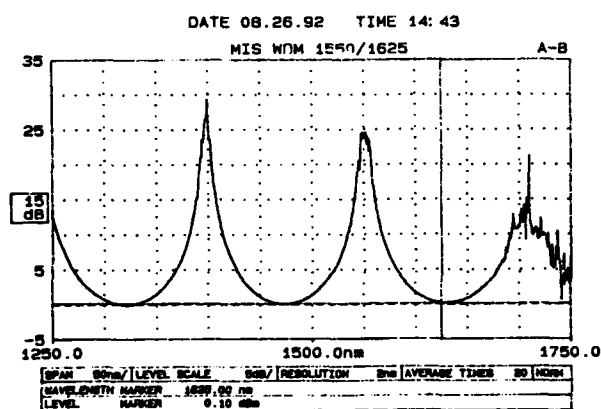


Fig. 9 : output 1625 nm

7. SYSTEM STRUCTURE

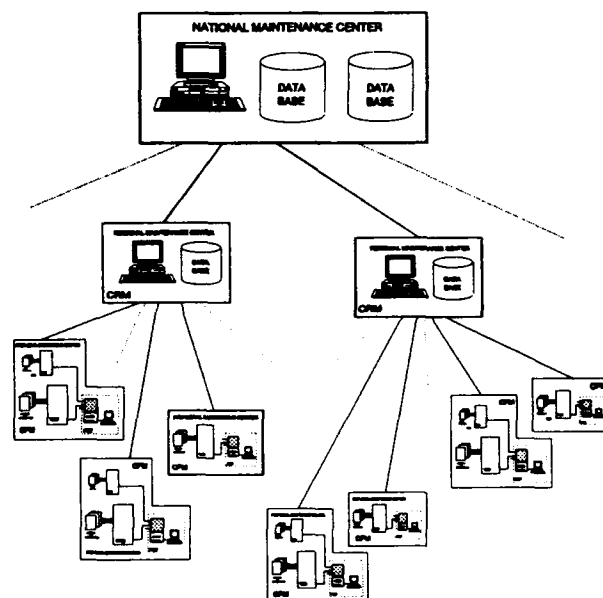
VDO system has a three levels structure, as below described:

- CPM Peripheral Monitoring Center, one each peripheral site of the system
- CRM Regional Maintenance Center, one each maintenance team site
- CNG National Maintenance Center

The CPM is the peripheral part of VDO system, basically consisting of :

- an optical supervisory rack, called TMO, where plant optical fibers and WDMs are terminated and optical switch is housed
- a supervising site, called PCT, capable to control one or more TMOs. Functions like measurement, data processing, display, configuration, local storage and interfacing to the wearest Local Maintenance Center (CLM) are here performed. PCT can include operator site consisting of one PC with graphic monitor

Data communication network also allows to send acquired data to the CNM.



CPM : PERIPHERAL MONITORING CENTER
CRM : REGIONAL MAINTENANCE CENTER
CNM : NATIONAL MAINTENANCE CENTER
TMO : OPTICAL MONITORING RACK COMPONENTS
PCT : LOCAL SYSTEM CONTROLLER

Fig. 10 : System structure

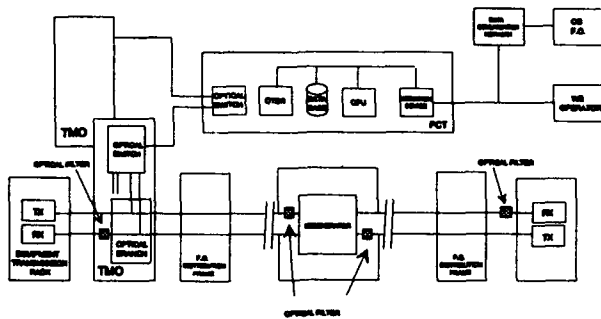


Fig. 11 : System application

8. TESTS ON FIELD

The verifications carried out on field substantially consist in monitoring the error rate of devices with the presence in line of the monitoring signal. In codirectional configuration the monitoring signal may influence negatively the transmission systems, especially on short and medium distance links; in such cases it is absolutely necessary to equip the receiver with a special filter. Many tests have been made with transmission systems working 34, 140, 565 Mbit/s and 2.5 Gbit/s. Trials consisted essentially to evaluate receiver sensibility with monitoring. Measurements have been performed using optical fibers with lengths as we could find in optical plants. In fact from length depends the pulse widening due to the chromatic dispersion. Next pictures show test results and measurement configurations.

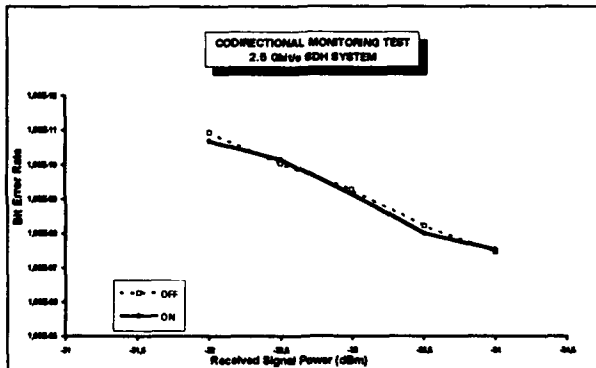


Fig. 12 : Codirectional test

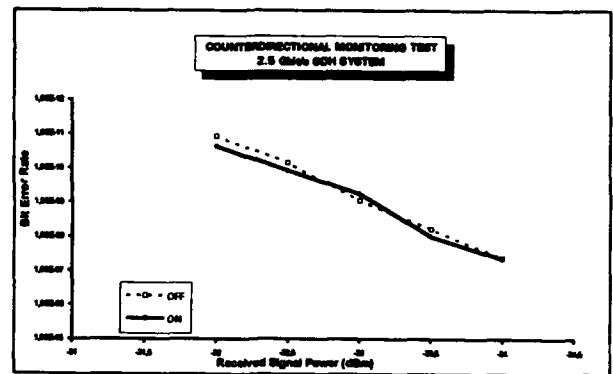


Fig. 13 : Counterdirectional test

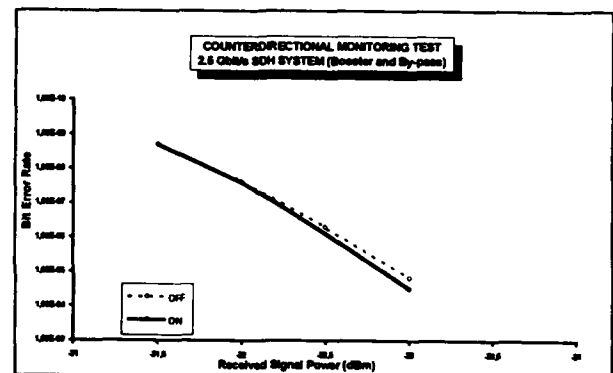
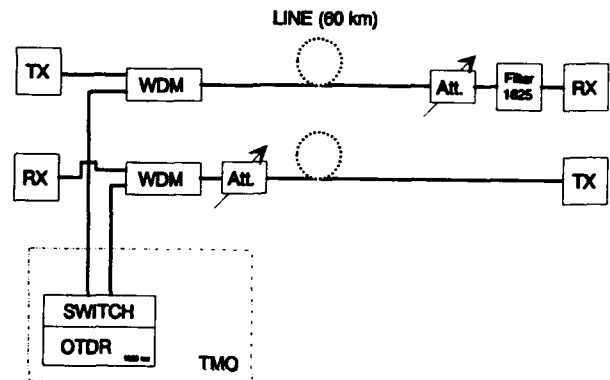
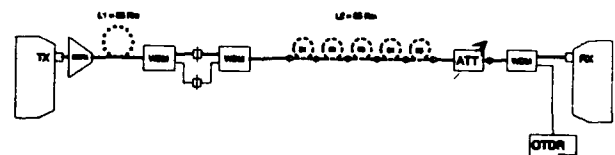


Fig. 14 : Booster and by-pass test



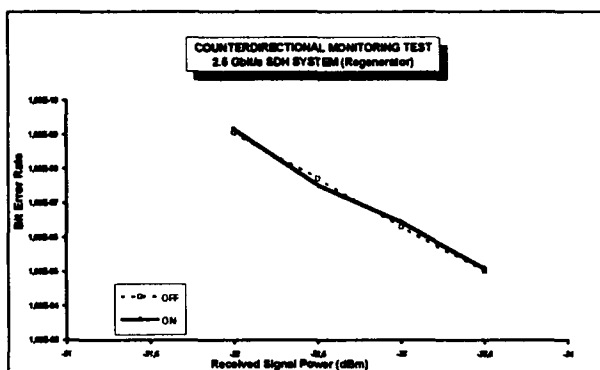
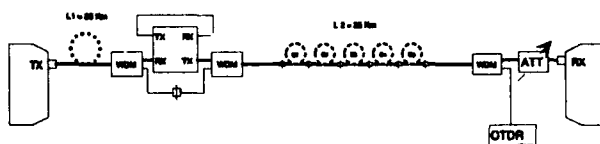


Fig. 15 : Regenerator test



Tests carried out have shown good results; the error rate of transmission systems has not increased in a significant way by introducing the control signal.

8. CONCLUSIONS

The progressive introduction of fibre optics lines in the telecommunications network, has determined an increasing interest towards those control systems which are able to guarantee a preventive maintenance of the plant.

On this purpose, tests carried out by AET Telecomunicazioni both in laboratory and on field have shown the importance of using a shifted wavelength laser.

At present, the VDO system has been installed both on long distance plants and subscriber network in Italy and tests are being carried out.

REFERENCES

- T. Uenoya, et al., "Operation, administration and maintenance systems of the optical fiber loop", Proceedings of Globecom, pp. 1493-1497, (1990).
- H. Takasugi, et al., "Design and evaluation of automatic optical fiber operation support system", Proceedings of 39th I.W.C.S., pp. 623-629, (1990).
- H. Matsumoto, et al., "Cable transfer and supervisory system for trunk optical fiber cables", Proceedings of 40th I.W.C.S., pp. 787-792, (1991).



Edoardo Cottino received his degree of electronic engineering from the Politecnico di Torino, Italy, in 1982. He is currently the Director of AET Telecomunicazioni Optical Technology Laboratory and the project leader of VDO Monitoring System for the preventive maintenance of fiber optics plants. He is a member of SPIE, CCITT, IEC.

Increasing Productivity Of Single and Mass Optical Fiber Splicing When Testing With One-Way OTDR

William E. Beasley

Sumitomo Electric Fiber Optics Corp.
78 Alexander Drive, Research Triangle Park, NC 27709

ABSTRACT

Numerical analysis and Monte-Carlo simulations have been used to correlate optimization of the system power budget to splicing productivity in the field. This analysis has been accomplished through properly choosing the maximum allowable splice loss and utilizing knowledge about splicer performance, mode field diameter (MFD) distributions, and maximum allowable splice loss. Based on these results, a conservative acceptance criteria for one-way OTDR measurements can be chosen to improve the productivity for a variety of splicers, either single or mass, fusion or mechanical.

INTRODUCTION

With the large Single-Mode (SM) fiber base that is already installed in communications infrastructures, and the increasing number of installations of fiber from different manufacturers, it is becoming ever more difficult to evaluate the system loss budget by measuring splice losses.^{1,2}

The traditional method for measuring link loss is by an end-to-end power meter measurement. The optical time domain reflectometer (OTDR), used for fault location and trouble shooting, has also become a popular tool for evaluating individual splice losses in striving to minimize the overall link loss.

The OTDR is a powerful tool that is often misunderstood and misused. The basic backscattering principle of its operation makes the OTDR very sensitive to fibers' MFD dependent light-coupling properties. Different fibers will intrinsically capture more or less backscattered light resulting in varying signal levels back to the OTDR. When two fibers with different MFD values are joined and measured with an OTDR, either an apparent loss or "gainer" appears at the interface. This commonly known phenomenon is an artifact of the one-way OTDR measurement. The error component of measured loss is governed by the following equation.³

$$\alpha_{OTDR} = 10 \cdot \text{Log} \left(\frac{W_2}{W_1} \right) \quad (1)$$

W_1 is the mode field radius, MFR, for the first (upstream) fiber and W_2 is the MFR for the second (downstream) fiber. This apparent loss does not have an effect on the system loss budget and should not be considered as splice loss. MFD differences do add a minimal additional loss to the splice but can be typically ignored due to their small order of magnitude. Equation 2 defines the actual loss contributed by the different MFDs.^{4,5}

$$\alpha_{MFD} = -20 \cdot \text{Log} \left(\frac{2 \cdot W_1 \cdot W_2}{W_1^2 + W_2^2} \right) \quad (2)$$

Equation 3 shows each loss contributor of the one-way OTDR measured loss where $\alpha_{splice\ loss}$ includes attenuation due to core to core offset, tilt, and other loss mechanisms.

$$\alpha_{measured} = [\alpha_{splice\ loss} + \alpha_{MFD}]_{actual} + \alpha_{OTDR} \quad (3)$$

The most effective way of overcoming this measurement error is by taking bidirectional OTDR measurements. The average of the splice loss measured in both directions cancels out α_{OTDR} , leaving only actual splice loss, α_{actual} .⁶

Bidirectional measurements, though, are not always feasible in the field due to location and access restraints. If one-way OTDR measurements are to be used for splice loss evaluation, corrections based on the MFDs of each fiber must be used to offset the effect of α_{OTDR} .

ANALYSIS

MFD Distributions

Traditionally, evaluations of dissimilar fiber splices with one-way OTDR include a correction value based on only the nominal MFD values and Equation 1. This correction value is added to the splice loss acceptance criteria. For example, a fiber from one vendor, which comes from a MFD distribution of $8.8 \pm 0.5 \mu\text{m}$, is spliced to another vendor's fiber with MFD distribution of $9.3 \pm 0.5 \mu\text{m}$. Assume the splice crew's goal is to make a splice with loss less than 0.20 dB. If the splice crew had access to only the 8.8 μm MFD fiber for testing, they would add 0.24 dB (from

Equation 1) to 0.20 dB to get the new acceptance criteria of 0.44 dB. From the other direction, they would add -0.24 dB to the maximum allowed loss and would use -0.04 dB as the acceptance criteria.

The nominal MFD values are the root cause for problems with one-way OTDR splice loss predictions but the distributions (assumed gaussian) make predictions practically impossible. Even when splicing fibers of the same type together, the distribution of MFD values about the nominal value can cause measurement errors. Currently, the US industry specifies a $\pm 0.5 \mu\text{m}$ MFD distribution. Elsewhere in the world, it can vary even more. Below are some of the MFD ranges for some currently available SM fiber.

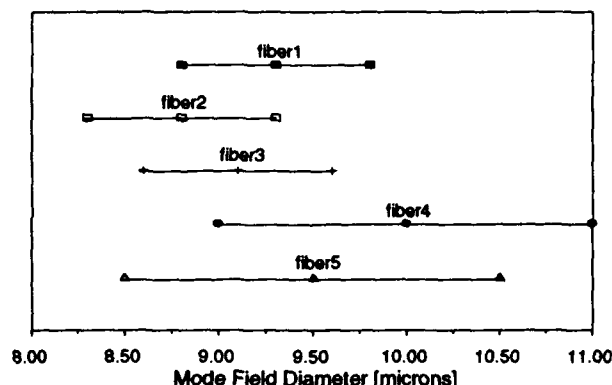


Figure 1. MFD Ranges for several currently available SM fiber types.

When two fiber distributions are combined using Equation 1, the resulting one-way OTDR apparent loss can have a distribution similar to the ones shown in Figure 2.

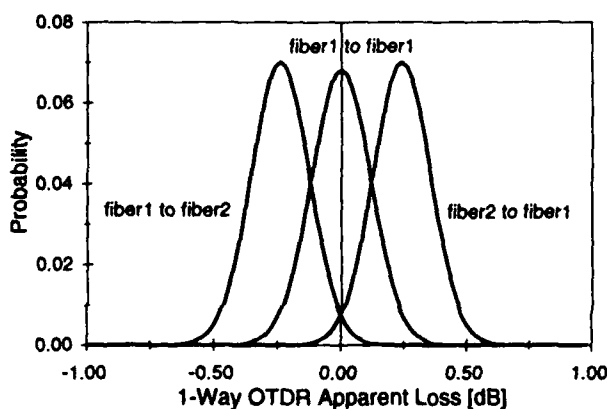


Figure 2. α_{OTDR} probabilities.

In the above figure, either a positive or negative shift will occur to the measurement depending on the direction of the measurement. Note that even a similar fiber splice (fiber₁ to fiber₁) can show an erroneous added loss or gain. Variations in the standard deviations of either fiber MFD distribution will shrink or stretch the curves accordingly.⁶

Based on the MFD distributions alone, the nominal MFD value still seems to be a good choice for a correction factor. However, there are other variables that we have access to that also contribute to the splice loss, such as the loss distribution generated by a particular type of splicer.

Splicer Loss Distribution

The most obvious effect on the overall splicer performance in the field is the performance of the splicing machine or splice itself. A good working single fiber splicer will produce a loss distribution with a low average and tight standard deviation, while mass fiber splicers typically have higher nominal losses and greater spreads. Figure 3 below shows distributions for various splicer types. "Great", "Good", and "Poor" splicers reflect three different general splicer performances. A log-normal distribution is assumed for each curve.

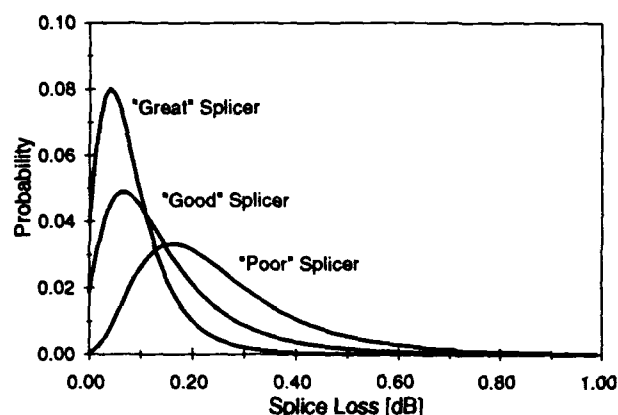


Figure 3. Individual splicer performance curves.

If we combine the probability distributions from each of the contributing factors as shown in Equation 3, the resulting one-way OTDR apparent splice loss distribution can be plotted. In Figure 4 below, splicer performance data for a "Great" splicer was used with $8.8 \pm 0.5 \mu\text{m}$ and $9.3 \pm 0.5 \mu\text{m}$ MFD distributions (9.3 μm distribution fiber is downstream of 8.8 μm distribution fiber).

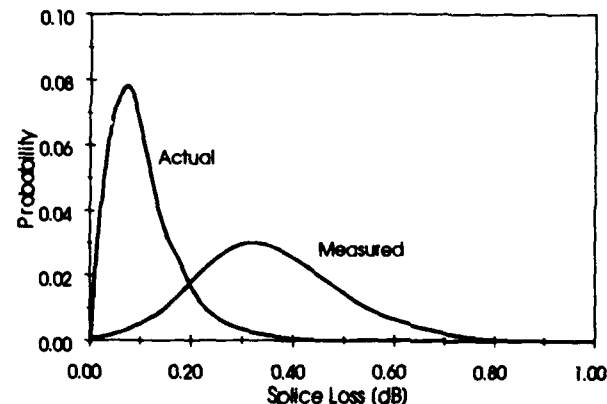


Figure 4. Actual and one-way OTDR measured splice loss.

Because there is no control in picking fibers from their original MFD distributions and actual splice loss is nominally independent of OTDR error, the actual splice loss and the measured loss is uncorrelated. This lack of correlation is one reason why the simple shift based on the nominal MFD values is not optimum.

Methods

To explore the effect of different acceptance criteria on fiber splicing, numerical analysis is performed to look at each possible combination of splice losses and MFD values. For each combination, the actual loss, measured one-way loss, and the probability is calculated and compared against an arbitrary acceptance criteria.

The goal is to increase splicing productivity by improving the predictability of splice losses. Productivity can be influenced by both requiring good splices be respliced and accepting bad splices. Thus *TotalPoor%* is defined in Equation 4.

$$\text{TotalPoor\%} = \text{GoodRejection\%} + \text{BadAcceptance\%} \quad (4)$$

From the analysis, plotting *GoodRejection%* and *BadAcceptance%* versus the acceptance criteria used, we see that too low of a criteria will reject all of the good splices while a high acceptance criteria will accept more bad splices.

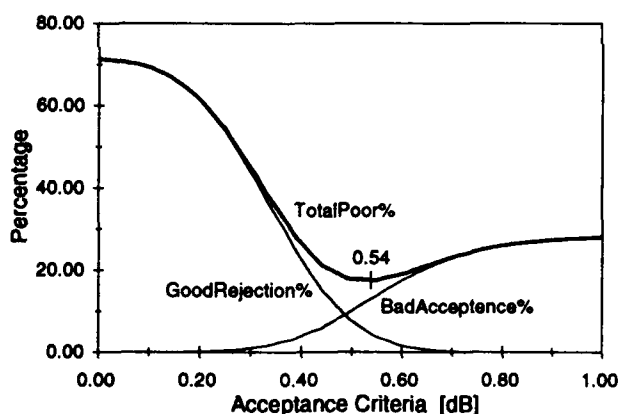


Figure 5. Percentage of poor splice loss predictions versus splice loss acceptance criteria used for "Good" Splicer.

Because the goal in testing of splices is to minimize the number of poorly categorized splices, an optimum acceptance criteria value can be resolved from Figure 5 for a particular splicer and fiber types. In the above example, an $8.8 \pm 0.5 \mu\text{m}$ MFD fiber is spliced to an $9.3 \pm 0.5 \mu\text{m}$ fiber. If the maximum allowed splice loss of 0.20 dB was used as an acceptance criteria, 62% of the splices made would be falsely predicted as good or bad. With the nominal shifted criteria of 0.44 dB, 21% of the splices are falsely categorized. Using the optimum criteria of 0.54 dB, false decisions are reduced to 17%.

These curves are heavily weighted based on the performance of the splicing machine. A good working splicer will shift the resultant curve to a higher acceptance criteria in order to reduce the number of good splices being thrown away. Figure 6 below shows the total poor prediction percentage curves for the three different splicer performances of Figure 3.

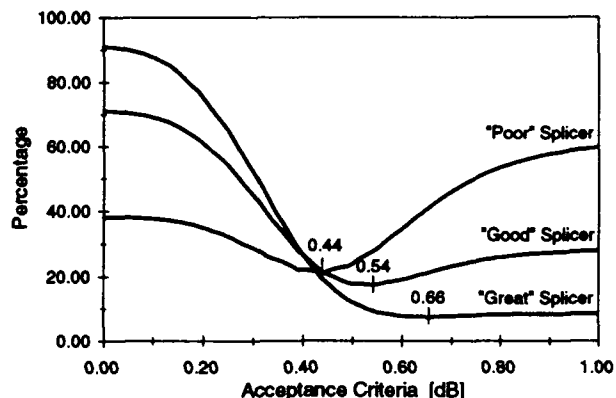


Figure 6. Productivity Optimized acceptance criteria curves for various splicer types.

The mass splicers inherently have somewhat lower splice performances than single fiber splicers simply due to the splicing of 12 fibers at a time. The effect of 12 fiber mass splicers can thus be modeled into the analysis through splicer performance. The optimized criteria for "Good" and "Poor" splicers, with the higher percentage of bad splices (greater than 0.20 dB), approach the traditional correction based on only the nominal MFD values. This result is expected because the nominal shift assumes a non weighted, 50/50 chance of good and bad splice losses. The "Great" splicer, which produces more good splices than bad ones, causes the optimum criteria to shift higher in order to accept more of the good splices. Bad splices are not a threat as there are fewer of them.

For a range of fiber types and splicer performances, Table 1 summarizes the optimum acceptance criteria values generated from the numerical analysis.

Table 1. *Productivity Optimized acceptance criteria for various splicer and fiber configurations.*

Fiber ₁ MFD [μm]	Fiber ₂ MFD [μm]	Customer Specified Maximum Allowed Loss [dB]	Traditional Nominal Adjusted Acceptance Criteria [dB]	Optimized Acceptance Criteria [dB]		
				"Great" Splicer	"Good" Splicer	"Poor" Splicer
8.8 ± 0.5	9.3 ± 0.5	0.20	0.44	0.66	0.54	0.44
9.3 ± 0.5	8.8 ± 0.5	0.20	-0.04	0.12	0.06	-0.04
9.3 ± 0.5	9.3 ± 0.5	0.20	0.20	0.41	0.30	0.19
9.1 ± 0.5	9.3 ± 0.5	0.20	0.29	0.50	0.40	0.29
9.3 ± 0.5	9.1 ± 0.5	0.20	0.11	0.29	0.21	0.10

RESULTS

To evaluate the splicing results using the newly obtained acceptance criteria, Monte-Carlo simulations were performed. A database of fiber MFD values was set up for each fiber type distribution and was randomly picked from for each simulated splice. Below, Table 2 shows the parameters used in obtaining all of the results from the Monte-Carlo testing.

Table 2. *Parameters used for Monte-Carlo simulations.*

Variable	Value
MFD ₁ Nominal / Sigma	8.8 / 0.167 μm
MFD ₂ Nominal / Sigma	9.3 / 0.167 μm

First the "great" working splicer from Figure 3 was evaluated. The actual splice loss was randomly drawn from the diagrammed distributions and the one-way OTDR measured splice loss was calculated for each splice. Then the splice was accepted or rejected based on the acceptance criteria and determined to be a good or bad splice based on a customer specified maximum allowed loss of 0.20 dB. In order to achieve convergence, 5000 splices were made for each test.

Total Poor Prediction % is the percentage of the 5000 splices that were incorrectly evaluated using the one-way OTDR and the acceptance criteria. *Maximum* and *Average Actual Splice Losses* reflect the splices that were categorized as good and kept.

An acceptance criteria of 0.66 dB improves the splicing productivity through a lower poor prediction rate but allows for a few higher loss splices to get through. Breaking and resplicing a fiber several times might never pass the tighter acceptance criteria solely due to the MFD differences of the two fibers. Therefore, reducing the *Good Splice Rejection* is very important.

At this point, the trade off between the user's maximum allowed loss and productivity becomes important. By slightly increasing the maximum allowed splice loss, the productivity can be significantly increased without greatly jeopardizing the actual splice losses. In Table 4 below, this is accomplished because of the splicer's excellent performance and the relatively few number of bad splices. This productivity improvement is also evident for the poorer performing splicers with only a slight increase in the maximum actual splice loss.

Table 3. *Monte-Carlo results from splicing with the "Great" splicer.*

Maximum Allowed Splice Loss	Criteria	Prediction Percentages			Actual Splices			
		Good Splice Rejection	Bad Splice Acceptance	Total Poor Prediction	% Splices Kept	Maximum Loss	Average Loss	% Above Maximum Allowed
0.20 dB	0.20 dB	75.6%	0.1%	75.7%	15.8%	0.21 dB	0.05 dB	0.4%
0.20 dB	0.44 dB	16.9%	2.1%	19.0%	76.5%	0.33 dB	0.08 dB	2.7%
0.20 dB	0.66 dB	0.7%	7.3%	8.0%	97.9%	0.46 dB	0.10 dB	7.4%

Table 4. *Effect of maximum allowed splice loss on splices made with the "Great" splicer.*

Maximum Allowed Splice Loss	Criteria	Prediction Percentages			Actual Splices			
		Good Splice Rejection	Bad Splice Acceptance	Total Poor Prediction	% Splices Kept	Maximum Loss	Average Loss	% Above Maximum Allowed
0.20 dB	0.66 dB	0.7%	7.3%	8.0%	97.9%	0.46 dB	0.10 dB	7.4%
0.30 dB	0.76 dB	0.3%	1.5%	1.8%	99.6%	0.47 dB	0.10 dB	1.5%
0.40 dB	0.86 dB	0.0%	0.3%	0.3%	99.9%	0.47 dB	0.10 dB	0.3%

Table 5. *Effect of mass splicing on the "Good" splicer.*

Mass Splice	Criteria	Prediction Percentages			Actual Splices			
		Good Splice Rejection	Bad Splice Acceptance	Total Poor Prediction	% Splices Kept	Maximum Loss	Average Loss	% Above Maximum Allowed
1 fiber	0.54 dB	4.0%	13.4%	17.4%	80.9%	0.52 dB	0.13 dB	16.5%
6 fibers	0.54 dB	46.5%	4.2%	50.7%	29.2%	0.52 dB	0.12 dB	14.5%
12 fibers	0.54 dB	64.9%	1.1%	66.0%	7.7%	0.50 dB	0.12 dB	13.8%

Table 6. *Effect of maximum allowed splice loss on 12 fiber mass splices.*

Maximum Allowed Splice Loss	Criteria	Prediction Percentages			Actual Splices			
		Good Splice Rejection	Bad Splice Acceptance	Total Poor Prediction	% Splices Kept	Maximum Loss	Average Loss	% Above Maximum Allowed
0.20 dB	0.54 dB	64.9%	1.1%	66.0%	7.7%	0.50 dB	0.12 dB	13.8%
0.30 dB	0.65 dB	52.5%	2.3%	54.8%	37.7%	0.57 dB	0.14 dB	6.0%
0.40 dB	0.75 dB	30.2%	1.5%	31.7%	66.1%	0.57 dB	0.15 dB	2.3%

Mass splicing techniques were simulated within the Monte-Carlo evaluation through splicing multiple fibers at a time before judging whether or not to accept the splice. If one fiber in the splice did not meet the acceptance criteria, the entire splice was rejected. For the results in Table 5, the "Good" splicer distribution was used to simulate the slightly higher losses which might be seen with mass splicers. A maximum allowed splice loss of 0.20 dB was used along with the optimized criteria of 0.54 dB.

The increase in *good splice rejection* % comes from all of the good splices that are thrown away due to a single high loss within the same mass splice. Realistically, this poor prediction rate is offset by the actual increase in productivity achieved by splicing 12 or 6 fibers at a time. Similar to the single fiber splicing, the mass splicing benefits greatly from an increase in the customer specified maximum allowed splice loss without penalty to the achieved splice losses as shown in Table 6.

CONCLUSIONS

Numerical optimization was used to determine an optimized acceptance criteria for evaluating splices with one-way OTDR measurements. This new criteria minimizes the poor prediction rate by reducing the number of miscategorized splices which depend on the mode field diameter distributions of each fiber type being spliced, the type of splicer, and the customer specified maximum allowed splice loss.

Shifting the splice loss acceptance criteria improves productivity in the field with only a slight compromise of the resulting maximum accepted splice loss distribution. This trade-off is important for both the engineers relying on one-way OTDR measurements for system power budgets and for splice crews in the field breaking and resplicing fibers unnecessarily. Proper choice of the maximum allowed splice loss and the acceptance criteria can benefit both splicing productivity and the knowledge about the actual splice loss.

Mass splicing techniques can withstand lower prediction performance due to the existing inherent increase in productivity from splicing multiple fibers. Evaluation of mass splices can also benefit from the optimized acceptance criteria. By relaxing the maximum allowed splice loss and using the optimized acceptance criteria, rejection of good spliced fibers is reduced by half for 12 fiber mass splices.

ACKNOWLEDGMENTS

The author thanks Eric Buckland for his time and effort in helping prepare this study.

REFERENCES

1. J. Schiestle, M. Stammer, "Fishing for the Perfect Splice," TE&M, pp. 31-36, February 1, 1993.
2. J. Denny, "Practical Considerations of Joining Fiber from Different Vendors," Outside Plant, pp. 34-36, November, 1992.
3. F. Kapron, C. Kozikowski, T. Olson, "Novel OTDR Effects in Determining Losses of Single-Mode Fibers and Splices," Proceedings of 35th IWCS, p. 338, November, 1986.
4. D. Marcuse, "Loss Analysis of Single-Mode Fiber Splices," B.S.T.J., Vol. 56, p. 703, May - June 1977.
5. S. Nemoto, T. Makimoto, "Analysis of Splice Loss in Single-Mode Fibers Using a Gaussian Field Approximation," Optical and Quantum Electronics, Vol. 11, p. 447, 1979.
6. S. Mettler, "Monte-Carlo Analysis of the Effect of Mode Field Diameter Mismatch on Single-Mode Fiber Splices," Proceedings of 8th NFOEC, pp. 647-663, April, 1992.

William E. Beasley graduated from Duke University in 1990 where he received a B.S.E. in Mechanical Engineering and a B.A. in Mathematics. He joined Sumitomo Electric Fiber Optics Corp. in 1990 as a Product Design Engineer supervising the Lightwave Laboratories and is now an Applications Engineer for outside plant cables. William



is a member of the Optical Society of America, the American Society for Mechanical Engineers, the International Society for Optical Engineering, and is actively involved with the Telecommunications Industry Association standards committees.

Low-coherence reflectometer using multimode light source and elastic optical-fiber delay line for testing optical-fiber connectors

Masaru Kobayashi, Nobuo Kuwaki, and Koji Yoshida

NTT Technical Assistance and Support Center
Tokyo, Japan

Abstract

A proposed low-coherence reflectometer for testing optical-fiber connectors can measure return losses as high as 90 dB. It uses an optical adjustment-free interferometer that includes a multimode Fabry-Perot laser diode and an optical-fiber delay line, which utilizes the elasticity in optical fiber. A prototype is compact and tests connectors quickly and easily.

Introduction

High-return-loss optical-fiber connectors are being developed for high-speed digital transmission systems, optical analog transmission systems, such as cable television, and so on. Physical contact and angled surface connectors have return losses of over 40 and 60 dB, respectively (1), (2). Conventional return-loss measurement is done by launching continuous wave light and measuring the reflected optical power by direct detection. Measurable return loss is therefore limited by Rayleigh backscattering in the optical fiber. The Rayleigh backscattering relative power is about -70 dB/m in a conventional single-mode optical fiber and is proportional to the optical fiber length, so the measurable limit is under 40 dB in an optical-fiber cable longer than 1 km.

Low-coherence reflectometry (3) is expected to enable high-return-loss measurement. It uses a low coherent light source and a two-beam interferometer. It can measure the reflectional distribution in optical waveguides to a spatial resolution of under 100 μm . The Rayleigh backscattering relative power in this spatial resolution is under -110 dB. However, the spatial optical delay line in the interferometer makes low-coherence reflectometry difficult to use, because it needs precise optical-axis adjustment.

We have developed a low-coherence reflectometer that does not require optical-axis adjustment. The reflectometer changes the optical path length by slightly stretching the optical fiber, without spatially propagating the light. The small optical path length change is supplemented by the unique coherency of the multimode light source which indicates multiple peaks.

This paper describes the layout and measurement principle of the proposed reflectometer. A measurable return loss of over 90 dB is experimentally indicated. A compact prototype that can quickly and easily test connectors is also presented.

Layout

The proposed reflectometer uses an optical-fiber Michelson interferometer, composed of a multimode Fabry-Perot laser diode (FP-LD), an a master connector line, an optical-fiber delay line, and a PIN-photodiode (PIN-PD), which are optically coupled with an optical-fiber coupler (Fig. 1). The connector to be tested is connected to the master connector. The FP-LD has a wavelength of 1.3 μm and output power of about 1 mW. The delay-line optical fiber is stretched at a constant speed by a mechanical stage. A reflector is connected to the end of the delay line.

The FP-LD continuous wave output is divided in two by the coupler; the two lights are then launched into the delay line and the master connector line. These signal and reference lights are reflected by the test connector surface and the reflector, and then re-coupled by the optical coupler and launched into the PIN-PD. The beat signal envelope, which is generated by changing reference-light optical path length, is detected by a selective level meter.

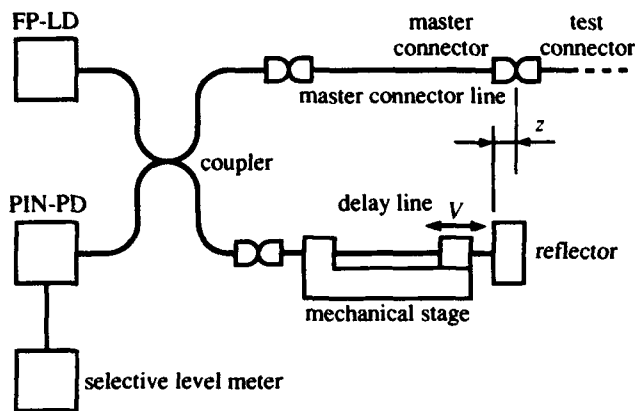


Fig. 1 Low-coherence reflectometer using multimode laser diode and elastic optical-fiber delay line

FP-LD: Fabry-Perot laser diode

PIN-PD: PIN photodiode

Measurement principle

In a two-beam interferometer, the complex amplitudes of the signal and reference lights, $E_{sig}(t)$ and $E_{ref}(t)$, and the beat signal, $I(t)$, are expressed as

$$E_{sig}(t) = k_1 r \int_{-\infty}^{\infty} E(v) \exp j\{2\pi(v+v_c)t\} dv, \text{ and } (1)$$

$$E_{ref}(t) = k_2 \int_{-\infty}^{\infty} E(v) \exp j\{2\pi(v+v_c)(t+\tau)\} dv, (2)$$

$$\text{where } \tau = \frac{2n_g(z-Vt)}{c}, \text{ and } (3)$$

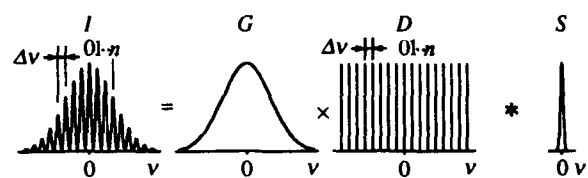
$$I(t) = 2 \operatorname{Re}[E_{sig}^* \cdot E_{ref}] = k_3 r \cos(2\pi f_c t) \gamma(\tau), (4)$$

$$\text{where } \gamma(\tau) = \int_{-\infty}^{\infty} I(v) \exp j(2\pi v\tau) dv, (5)$$

$$f_c = v_c \frac{2n_g V}{c} = \frac{2n_g V}{\lambda_c}, (6)$$

r is the reflection coefficient of the test surface, v_c is the center frequency of the FP-LD output, v is the optical frequency from v_c , τ is the delay time between the signal and reference light, z is the difference in optical fiber length between signal and reference line, V is the optical fiber stretching speed, n_g is the group refractive index of the optical fiber, $E(v)$ and $I(v)$ are the Fourier amplitude and the optical power spectrum of the FP-LD output, c is the speed of light, and k_n is

$$(a) I(v) = (G \cdot D * S)(v)$$



$$(b) \gamma(\tau) = (g * d \cdot s)(\tau)$$

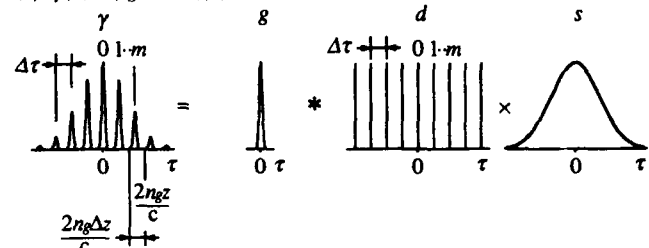


Fig. 2 Model of (a) optical power spectrum and (b) degree of coherence of Fabry-Perot laser diode

a constant. Equation (4) indicates that the beat signal, which is proportional to the reflection coefficient r , has a carrier frequency of f_c and that the envelope is $\gamma(\tau)$; $\gamma(\tau)$ is a Fourier transform pair of $I(v)$ and equals the degree of coherence.

$I(v)$ of the FP-LD output is described as follows, using gain spectrum $G(v)$, longitudinal mode spectrum $S(v)$, and the delta function series $D(v)$ that has intervals of longitudinal mode Δv , as shown in Fig. 2 (a),

$$I(v) = (G \cdot D * S)(v), \text{ with } (7)$$

$$D(v) = \sum_n \delta(n\Delta v), (8)$$

where $*$ indicates a convolution, and n is an integer. Substituting Eq. (7) into Eq. (5) and using the convolution theorem of the Fourier transformation, we get

$$\gamma(\tau) = (g * d \cdot s)(\tau), \text{ with } (9)$$

$$\left. \begin{aligned} g(\tau) &\Leftrightarrow G(v), & \Delta g(\tau) \Delta G(v) &\sim 1, \\ s(\tau) &\Leftrightarrow S(v), & \Delta s(\tau) \Delta S(v) &\sim 1, \\ d(\tau) &= \sum_m \delta(m\Delta\tau) \Leftrightarrow D(v), & \Delta\tau \Delta v &= 1, \end{aligned} \right\} (10)$$

where \Leftrightarrow indicates that the functions at both ends are Fourier transform pairs, m is an integer, $\Delta\tau$ is the

interval of the delta function in the time domain, and Δg , ΔG , Δs , and ΔS are the width of each function. Generally, the Fourier spectrum and the coherency are nearly reciprocal to each other, as expressed in Eq. (10).

As indicated in Eq. (9), the degree of coherence has multiple peaks with interval $\Delta\tau$ (Fig. 2 (b)). One peak therefore can certainly be measured by stretching the optical fiber Δz for $2n_g\Delta z/c \geq \Delta\tau$, even though z is not zero. The peak, I_{peak} , is expressed as

$$I_{peak} = k_4 r \gamma(m\Delta\tau) = k_4 r s(m\Delta\tau) \quad , \text{ with} \quad (11)$$

$$\frac{2n_g(z - \Delta z)}{c} \leq m\Delta\tau \leq \frac{2n_g z}{c} \quad (12)$$

Since I_{peak} is proportional to r , return loss Γ of the test surface can be estimated by

$$\Gamma = -20 \log \frac{I_{peak}}{I_{peak,ref}} + \Gamma_{ref} \quad (\text{dB}), \quad (13)$$

utilizing the measured result, $I_{peak,ref}$, for a standard surface that has known reflectivity Γ_{ref} . In this paper, an opened optical-fiber connector surface ($\Gamma = 14.7$ dB) is used as a standard surface.

Light source characteristics and design

Our proposed reflectometer is based on the measurement principle described in the previous section. The design parameters are the optical-fiber stretching length in the delay line, Δz , and the allowable difference z between the signal and reference line.

We measured the optical power spectrum and the coherency of the FP-LD output with an optical spectrum analyzer and a bulk-type Michelson interferometer. The optical spectrum indicates that the wavelength interval of the longitudinal mode, $\Delta\lambda$, is 0.85 nm and that the bandwidth of each longitudinal mode is under the 0.1-nm measurement resolution of the optical spectrum analyzer (Fig. 3). The coherency indicates that the peak interval, $n_g\Delta z$, is 1.1 mm and that the peaks decrease 10 dB at a delay of about $\Delta s/2 = 12.5$ mm (Fig. 4). The optical fiber must therefore be stretched more than 0.75 mm and the allowable optical fiber length difference z must be under 9 mm,

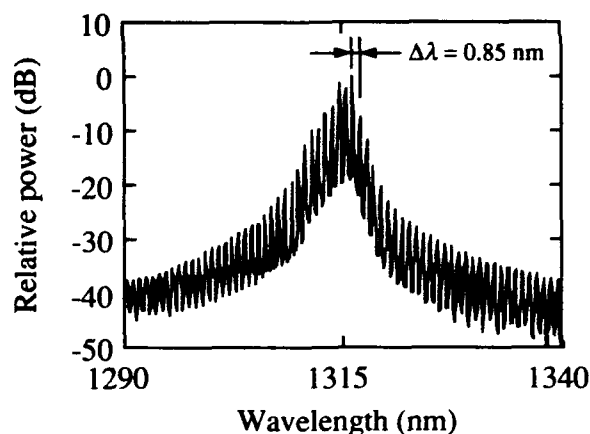


Fig.3 Optical power spectrum of Fabry-Perot laser diode output

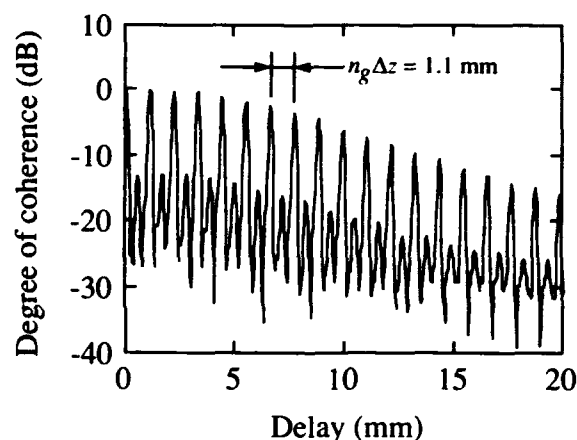


Fig.4 Degree of coherence of Fabry-Perot laser diode output

considering the relation $n_g z \leq \Delta s/2$.

Since the relation between $\Delta\lambda$ and Δz is described well by Eq. (10), the stretching length of the optical fiber can be designed based on the optical power spectrum. We can thus avoid measuring the coherency with a Michelson interferometer, which is not a conventional instrument. On the other hand, it is difficult to estimate the coherence length from the optical spectrum because the longitudinal bandwidth is below the measurement resolution of the optical spectrum analyzer. When the bandwidth is 0.1 nm, the resolution of a conventional optical spectrum analyzer, the allowable difference is estimated to be about 5 mm. The measurable return loss is therefore not reduced much when the allowable difference is 5

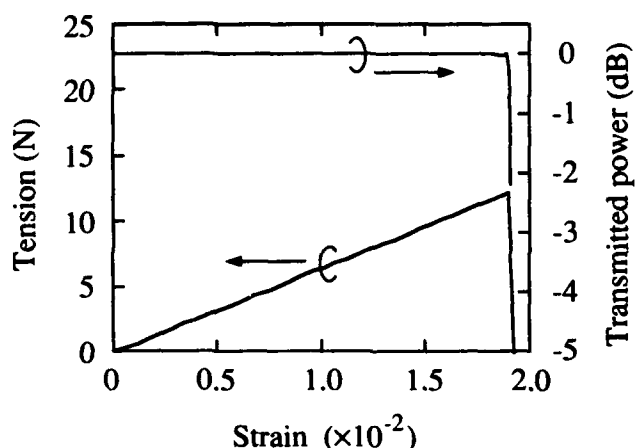


Fig. 5 Strain dependence of tension and insertion loss of single mode fiber

mm, which is the practically attainable precision in optical-fiber length adjustment.

We next measured the strain dependence of tension and transmitted optical power of conventional single-mode fiber. The tension-strain relation is linear and Young's modulus calculated from the slope is 52.2 GPa (Fig. 5). The cleaved tension and strain are about 12 N and about 2%, respectively. The transmitted optical power does not change. From these results and the FP-LD characteristics, an optical fiber 1 meter long is designed to be stretched with a maximum tension of about 2 N to attain an optical path length change of 1 mm under a 0.1% strain.

Experimental results

Signal waveforms, detectable return loss, and measurement accuracy were measured for a cleaved optical-fiber surface in several refractive index liquids, instead of for the master connector surface. The optical-fiber length difference was adjusted to within 1 mm and the delay of the signal light to the reference light was almost zero, so the maximum peak in the coherency waveform could be measured. The speed of the optical path length change was 65 $\mu\text{m/s}$ and the carrier frequency of the beat signal was 100 Hz. The signal power was measured with a selective level meter with a bandwidth of 20 Hz.

We measured the signal waveforms under four conditions (Fig. 6): (a) the optical fiber end was open so the signal level could be calibrated with the

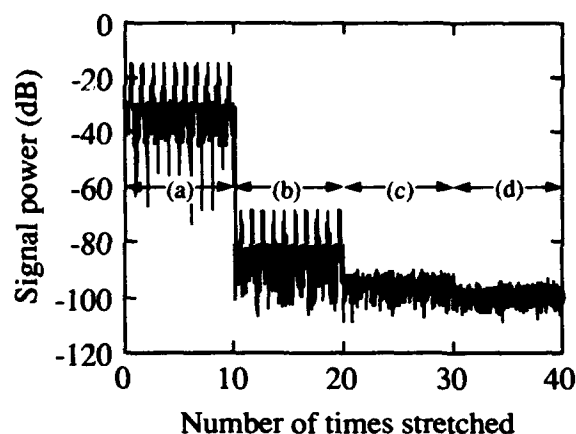


Fig. 6 Measured signal waveforms

- (a) with optical fiber end open: reference level
- (b) in refractive index liquid $n_g = 1.4517$
- (c) long optical fiber: Rayleigh backscattering level
- (d) no optical fiber: optical intensity noise level

standard surface; (b) the optical fiber end was immersed in a refractive index liquid with $n_g = 1.4517$, which simulates measuring a test connector; (c) the long optical fiber was connected to the optical coupler instead of the master connector to measure the Rayleigh backscattering level; and (d) the master fiber was removed so the optical intensity noise level could be measured without an interference signal.

The peak average in waveform (a) was calibrated to -14.7 dB. The peaks indicate reflectivity, which has the opposite sign of the return loss. Waveform (b) shows that a return loss of over 60 dB can be measured stably with a standard deviation of 0.1 dB. Waveform (c) is the Rayleigh backscattering level and is measurable reflectivity. The level is about -90 dB and corresponds to the Rayleigh backscattering relative power Γ_R calculated by

$$\Gamma_R = 10 \log \{ S \alpha \Delta s(\tau) \} \quad (\text{dB}) \quad (14)$$

with the Rayleigh scattering coefficient $\alpha = 69 \times 10^{-5}$, the backscattering capture ratio $S = 1.3 \times 10^{-3}$ for an 1.3- μm single-mode fiber (4), and the coherence length of the FP-LD output $\Delta s(\tau) = 13 \text{ mm}$. Waveform (d) shows that the optical intensity noise level is -94 dB with a detection bandwidth of 20 Hz. Waveforms (c) and (d) indicate that, to further increase the

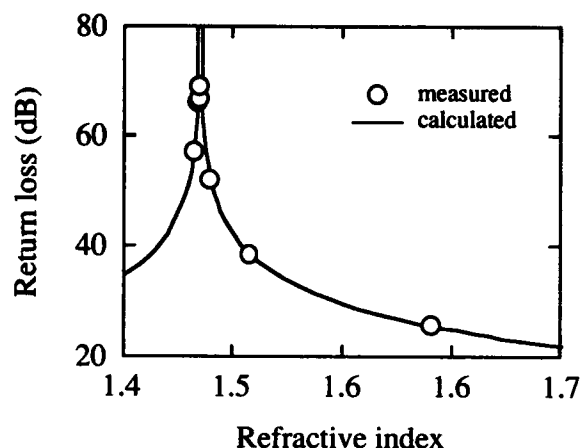


Fig. 7 Return loss of cleaved optical-fiber surface in refractive index liquid

measurable return loss, it is necessary to use an FP-LD that has a smaller coherence length and to further narrow the detection bandwidth. However, the small coherence length requires precise adjustment of the optical fiber length.

The measured return loss of a cleaved optical-fiber surface in several refractive-index liquids is shown in Fig. 7. The line is calculated using a Fresnel equation with a group refractive index of both the liquids n_g and the optical fiber of 1.452,

$$\Gamma = -20 \log \left(\frac{1.452 - n_g}{1.452 + n_g} \right) \text{ (dB)}. \quad (15)$$

The results correspond with calculation and results measured conventionally with an optical power meter with a range maximum of 50 dB. The measurement accuracy of the proposed reflectometer is therefore confirmed.

Prototype

We developed a prototype based on the above described design (Fig. 8). The 1-m optical fiber in the delay line is rolled to reduce space requirements (Fig. 9). The optical fiber is attached to a speaker by a bar, which moves back and forth at a speed of 1 mm/s. We can thus measure the return loss within about 1 second. The measurable return loss is 70 dB, determined by the intensity noise of the FP-LD output with detection bandwidth of 1 kHz. The bandwidth is

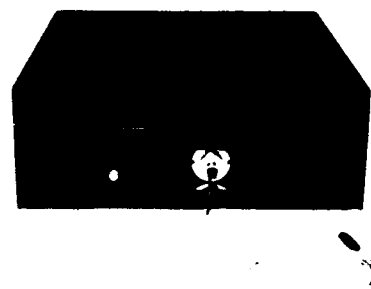


Fig. 8 Prototype of proposed low-coherence reflectometer
400 × 120 × 420 (w × h × d) (mm)

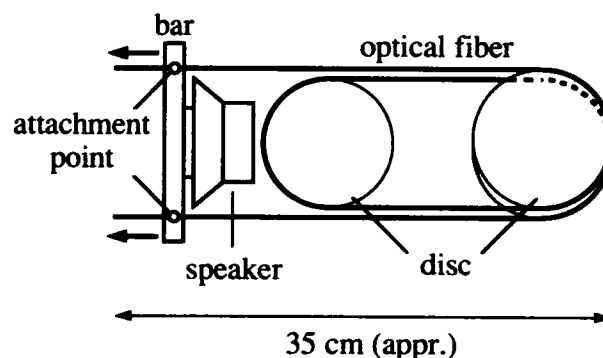


Fig. 9 Optical-fiber delay line in prototype

wide because the beat signal frequency is high according to the optical-fiber stretching speed. It is possible to achieve a measurable return loss of 90 dB by stretching the optical fiber more smoothly and narrowing the detection bandwidth. Operation is very easy. The reference measurement is done automatically and the return loss is measured immediately after connecting the test connector to the master connector.

Conclusion

We proposed and demonstrated a low-coherence reflectometer that does not require optical adjustment. It uses a multimode Fabry-Perot laser diode (FP-LD) and an elastic optical-fiber delay line. Measurement is done by stretching the optical fiber less than 1 mm; the stretching length is determined by the longitudinal

mode interval of the FP-LD output. The proposed reflectometer can measure return losses as high as 90 dB, which is the level determined by Rayleigh backscattering in the coherence length of the FP-LD output. The prototype is very compact and measures return losses as high as 70 dB quickly and easily.

References

- (1) K. Kanayama, R. Nagase, Y. Ando, and K. Matsunaga, "Advanced PC optical fiber connectors," 1990 Autumn National Convention Record, The Institute of Electronics, Information and Communication Engineers, C-283 (1990) (in Japanese).
- (2) R. Rao, J.S. Cook, "High return loss connector design without using fiber contact or index matching," Electron. Letter, Vol. 22, No. 14, p. 731 (1986).
- (3) K. Takada, I. Yokohama, K. Chida, and J. Noda, "New measurement system for fault location in optical waveguide devices based on an interferometric technique," Appl. Opt. Vol. 26, p. 1603 (1987).
- (4) S.D. Personick, "Photon probe- An optical-fiber time-domain reflectometer," Bell Syst. Tech. J., Vol. 56, p. 335 (1977).



Masaru Kobayashi

NTT
Technical Assistance
and Support Center
Midori-cho
Musashino-shi
Tokyo, 180 Japan

Masaru Kobayashi was born in 1963 and received B.E. and M.E. degrees in mechanical engineering from Nagoya University, Japan, in 1986 and 1988.

He joined NTT Opto-electronics Laboratories in 1988. He was engaged in research on high-resolution optical reflectometry for optical fiber and optical waveguide devices characterization. Since 1991, he has been engaged in development of optical components evaluation tool at Technical Assistance and Support center.

He is a member of IEICE of Japan.



Nobuo Kuwaki

NTT
Technical Assistance
and Support Center
Midori-cho
Musashino-shi
Tokyo, 180 Japan

Nobuo Kuwaki was born in 1958 and received B.E. and D.E. degrees in electric engineering from Chiba University, Japan, in 1980 and 1991.

He joined Musashino Electrical Communications Laboratories, Nippon Telegraph and Telephone Public Corporation in 1980. He was engaged in research on the balanced pair cable design and the dispersion-modified optical fiber design. Since 1989, he has been engaged in research of evaluation for optical fiber and device transmission characteristics at Technical Assistance and Support center.

He is a member of IEICE of Japan.



Koji Yoshida

NTT
Technical Assistance
and Support Center
Midori-cho
Musashino-shi
Tokyo, 180 Japan

Koji Yoshida was born in 1950 and received B.E. in communication engineering from Osaka University, Japan, in 1973.

He joined Ibaraki Electrical Communications Laboratories, Nippon Telegraph and Telephone Public Corporation in 1973. He has been engaged in research on millimeter waveguide, evaluation of optical fiber, and measures against induced voltage on metallic cable.

He is now a group leader in Technical Assistance and Support center and a member of IEICE of Japan.

NEW TECHNIQUE FOR OPTICAL FIBER OUTSIDE DIAMETER MEASUREMENT AND CALIBRATION

*Claude BREHM, *Philippe DARBON, *Benoit MINVIELLE, DFP,
**Henri GAGNAIRE,

*Alcatel Alsthom Recherche, Route de Nozay, 91460 Marcoussis, FRANCE
**Université de St-Etienne, 23, rue du Docteur P. Michelon, 42023 Saint-Etienne, FRANCE

ABSTRACT

- A new interferometric device has been built and is able to measure diameter variations of close to $0.1 \mu\text{m}$ at a high speed of approximately 100 kHz (i.e. a measurement every $170 \mu\text{m}$ at a drawing speed of 1000 m/min).

Validation has been made with low speed, off-line, measurement of the same stripped fiber.

- A similar new interferometric device can be used, in static, to make a convenient absolute measurement on fiber outside diameter. It can also evaluate elliptical effects.

A comparison is being made with primary calibration obtained by optomechanical technics such as contact interferometric microscopy which are advocated by Standard Laboratories.

- These equipments allow a precise control of fiber characteristics during drawing process, therefore they are very useful to improve fiber drawing conditions and increase the quality of the end product.

INTRODUCTION

- Reduced fluctuations on fiber outside diameter is needed for efficient, easy and cheap connection in single-mode optical fiber. Fiber outside diameter measurements can be made on-line during fiber drawing.

Classical on-line measurements are too slow for present drawing speeds. The equipments typically used in fiber producing units are laser scanning fiber shadow measuring devices. These are very reliable and convenient for a close-loop control on capstan speed during fiber drawing. In this case measurement averaging improves efficiency. Nevertheless they show two main drawbacks :

- limited measurement frequency : 4 Hz with a good repeatability measurements close to $0.2 \mu\text{m}$ and 500 Hz but with not so good a repeatability. At the drawing speed of 1000 m/min, frequency of 4 Hz or 500 Hz translates into a measurement at respectively every 4 m or every 3 cm of fiber length.

- calibration is made with metallic wires which are known with a limited accuracy ($125 \pm 0.2 \mu\text{m}$).

- Earlier studies^{1,2,3} have shown that the ability of forward light scattering pattern analysis to determine the diameter of an optical fiber. The fiber is illuminated by a light beam perpendicular to the fiber

axis. The forward pattern is made of interference fringes of varying intensity in an angular range from 5° to 90° in the plane perpendicular to fiber axis. Changes in fiber diameter causes both movement of the fringes and variation in the number of fringes displayed in a particular angle range.

Such systems⁴ can be calibrated optically, they have a good measurement repeatability of $\pm 0.25 \mu\text{m}$, they use an electronically scanned diode array for fringe pattern analysis at a limited rate of 1 kHz.

- A new process of this forward scattering pattern phenomenon has been split into two separate equipments :

- the first one is based on the analysis of interference fringe shifting in a particular scattering direction angle. As it uses a photodetector array to detect directly the motion of one interfringe as the fiber diameter is varying, it has a very high measurement rate close to 100 kHz. This is more and more useful for on-line fiber diameter measurement as drawing speed increases⁵.

- the second equipment, by contrast gives a very accurate and absolute measurement of fiber diameter, off line, by counting on a static fiber the number of fringes in a wide angle range. This may be used to process standard fibers and to calibrate laser scanning fiber shadow measuring devices⁶.

FIBER SCATTERING PATTERN FROM A SIDE-ILLUMINATED GLASS FIBER

- As the scattering angle θ increases from incident direction in the range of 0 to 180° :

- a first angular field, between 0 and 10° , is related to the scattering of incident ray by the fiber

- a second angular field, between 10° and 80° , is characterized by successive bright and dark fringes, the contrast is the highest for polarized light and it can be related to interferences as described below.

Various secondary rays from the same incident ray are shown on figure 1 : R_e reflected, T, R_1 and R_2 refracted in the fiber. The angular deviation of these rays versus value of the incident angle ($X = \sin i$) is plotted on figure 2. When the angular deviation is less than 80° , only two rays are involved, R_e reflected at the fiber surface and T refracted into the fiber. As shown in figure 3, these two rays do not have the same incident angle i , therefore interference appears.

If D is the fiber diameter and n the refractive index of the fiber, the optical path difference between the two rays is :

$$\delta = D \cdot f(n, \theta) = D \cdot (\sin \theta/2 + (n^2 - 1 - 2n \cos \theta/2)^{1/2})$$

Between two scattering angles the number of interference fringes is only dependent on the fiber refractive index and on the fiber diameter. This gives a direct measurement of the fiber diameter if the fiber index is known.

For single-mode fibers the core diameter is less than one tenth of the fiber outside diameter and the core-cladding index difference is small. Therefore core effect is not significant.

On the other hand, the shifting of interference fringes, in a given scattering direction, can be directly related to fiber diameter fluctuations, without any fringe counting.

• Two equipments, for fiber diameter measurement, based on this scattering phenomenon have been studied at Saint Etienne University, the first one is for high accuracy absolute measurement of fiber diameter in static, the second one is for high speed relative measurement of fiber diameter in dynamic.

STATIC INTERFEROMETRY, FOR CALIBRATION OF FIBER DIAMETER MEASUREMENTS

The figure 4 shows a schematic layout of the measuring equipment. The beam of polarized He-Ne laser is focused on the fiber which is placed at the center of a goniometer. Polarization and fiber axis have the same direction. The scattering pattern is focused on the photodetector which is set on a motor-driven rotation stage. A crossed polarizer is placed in front of the photodetector to avoid saturation in the direction of incident ray. Measurement is made on a fiber height of 100 μm . Power data are collected every 0.01° for the determination of fringe pattern limits and every 0.03° for fringe counting. Averaging is done on 2000 sample points at 20kHz. Measurement accuracy then would be better than 0.1 μm . First measurements have been made on a typical single-mode fiber:

- with fiber rotation on its axis, one measurement after each 60° rotation

\emptyset (μm) : 125.16 (0°), 125.23 (60°), 125.07 (120°), 125.16 (180°), 125.24 (240°), 125.12 (300°), 125.16 (360°)

a slight ellipticity is pointed out on the fiber cross section

- with fiber translation along 1mm of its axis, one measurement every 100 μm .

\emptyset (μm): 125.16, 125.16, 125.16, 125.16, 125.16, 125.16, 125.16, 125.16, 125.16, 125.16,

This equipment is being certified by the French National Standard Laboratory (L.N.E.) by comparison with optomechanical technics such as contact interferometric microscopy. Our goal is to set such equipment as secondary standard maker for easy calibration of various fiber diameter measurement devices, like laser scanning shadow type.

DYNAMIC INTERFEROMETRY, FOR HIGH SPEED MEASUREMENT OF FIBER DIAMETER FLUCTUATIONS

The other equipment based on the same forward scattering pattern analysis is described in figure 5. It follows the shift of one interference fringe as the fiber diameter is varying, this is done in a scattering direction close to 70°. The optical system is such as fringe position is not affected by fiber vibration along its axis and involves 100 μm of fiber length. The detector is a photodiode with 20 separate elements. One bright interfringe illuminates 4 diodes. Fringe shifting is analysed in real time with a resolution of a quarter of interfringe which is close to 0.1 μm . Measurement speed is only limited by the signal amplifier bandwidth which is close to 100 kHz. Best paper plotters are limited to 10 kHz, so it is necessary to use computer and hard disk, for data storage and process, able to work at 1 MHz.

This equipment has been tested on-line during fiber drawing at 450m/min, together with a classical laser scanning shadow measuring device which averages diameter fluctuations on a 2 m fiber length, figure 6. Fiber diameter variations close to $\pm 0.4 \mu\text{m}$ are shown on few meters of fiber length, these are smoothed by the laser scanning shadow device.

More accurate comparison of fiber diameter data can be done off-line with the equipment described on figure 7. After continuous coating stripping, the fiber is moved in front of fiber diameter measuring devices at a speed of 20 mm per minute. Laser scanning shadow measurement has then minimum spatial limitation, close to 100 μm . Comparison of data is shown in figure 8, diameter variations, recorded on a 120 mm fiber length by both equipments, are very similar. Measurement averaging (256 per second) with the laser scanning shadow measuring device gives a smoother variation of fiber diameter.

CONCLUSION

New techniques based on well-known fiber scattering phenomenon have been tested for outside diameter optical fiber measurement.

The first device is for a static measurement of bare fiber by counting the number of interference fringe in a wide angular range

It has a high accuracy better than 0.1 μm for fiber diameter and can also give information on fiber ellipticity and conicity. This can be used for calibration of other measuring equipments after validation in comparison with optomechanical interferometry measurements

The second device is for high speed measurement during fiber drawing process. It is able to measure fiber outside diameter variations close to 0.1 μm at a high speed approximately 100 kHz. Validation has been made with low-speed off-line measurement of the same stripped fiber.

These equipments allow a precise control of fiber characteristics during drawing process, therefore they are very useful to improve fiber drawing condition and increase the quality of the end product.

ACKNOWLEDGEMENTS

The authors would like to thanks G. Orcel of Alcatel Fibres Optiques for helpful discussion.

REFERENCES

- [1] K.C. Kao, T.W. Davies, R. Worthington, Radio and Electronic Engineer, 39, 105-111, (1970)
- [2] H.M. Presby, J. Opt. Soc. Am., 64, 280-284, (1974)
- [3] L.S. Watkins, J. Opt. Soc. Am., 64, 767-772, (1974)
- [4] D. H. Smithgall, Applied Optics, vol 16, N° 9., 2395-2402, (1977)
- [5] H.Gagnaire, Opto 81., 36-37, (1981)
- [6] H.Gagnaire, B. U. P. , 744, (1992)

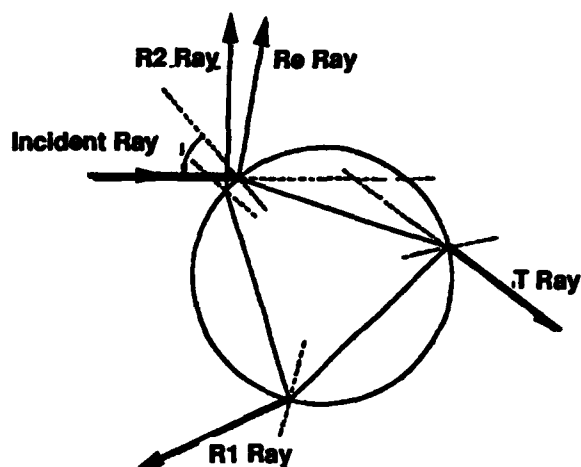
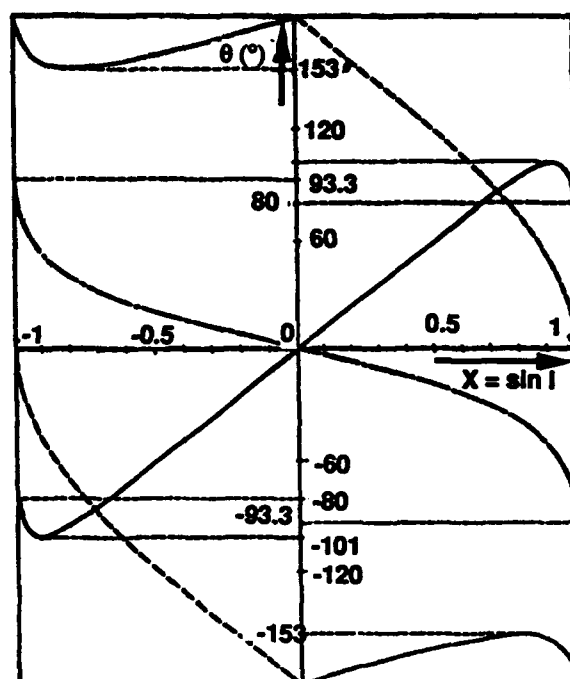


Figure 1 : Fiber cross-section :
4 rays are issued from the same incident ray



--- Re Ray -.-.- T Ray
 R1 Ray — R2 Ray

Figure 2 : Scattering angle of various rays
versus sinus of incident angle

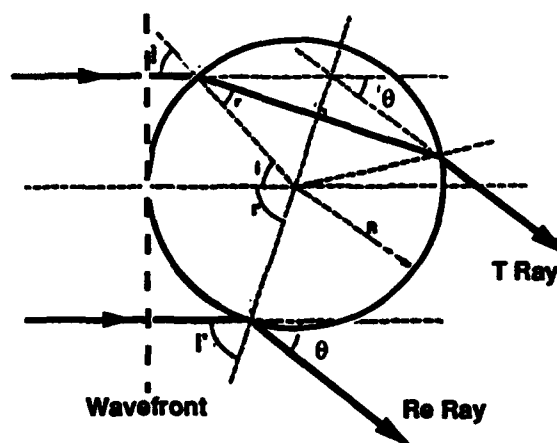


Figure 3 :
Fiber cross-section : optical path difference
between two rays Re and T scattered
in the same direction

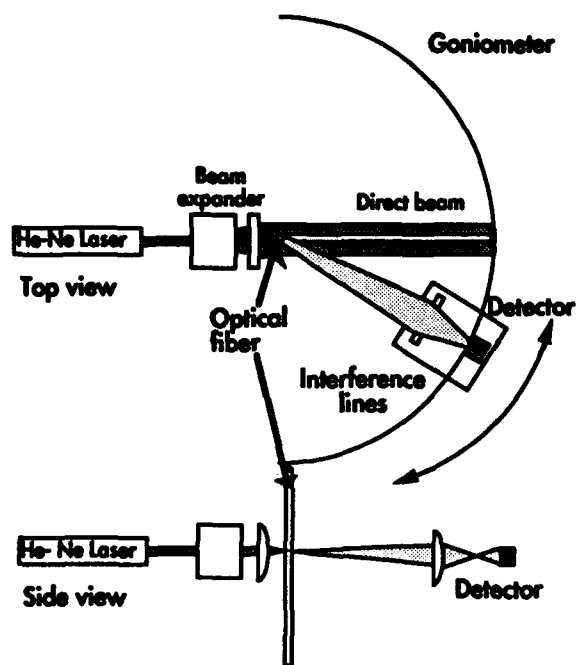


Figure 4 : Fiber O. D. Static measuring device based interference analysis

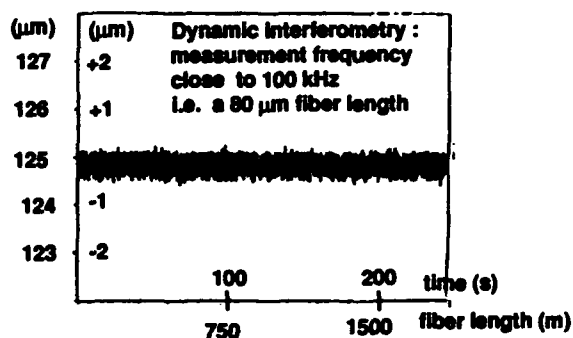
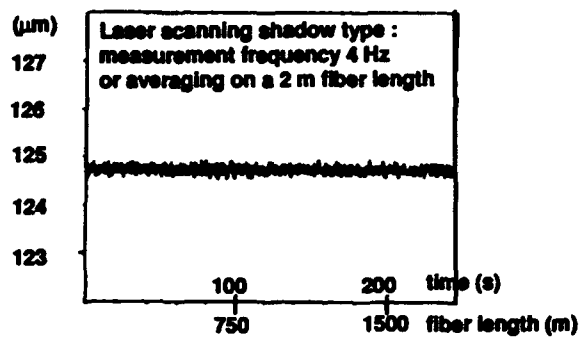


Figure 6 : Comparison of fiber diameter measurement data from laser scanning shadow and from dynamic interferometry, on-line during fiber drawing at 450 m/min

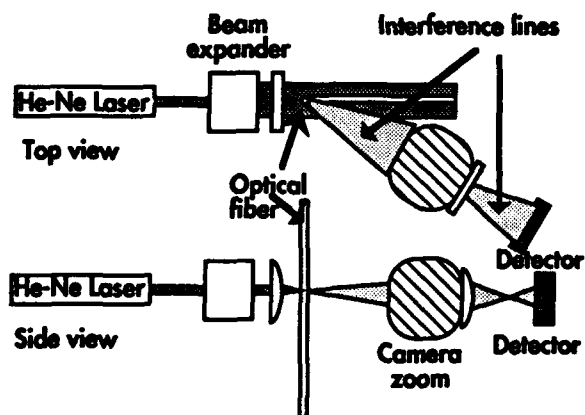


Figure 5 :
Fiber O. D. dynamic measuring device based interference analysis

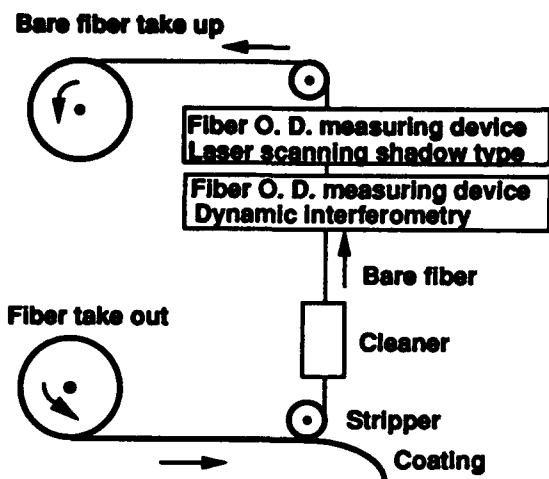


Figure 7 : Off-line low speed fiber diameter measurement

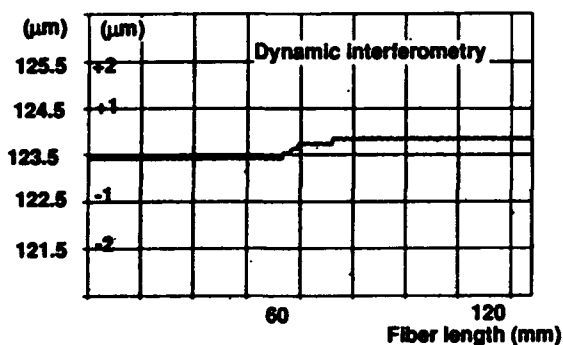
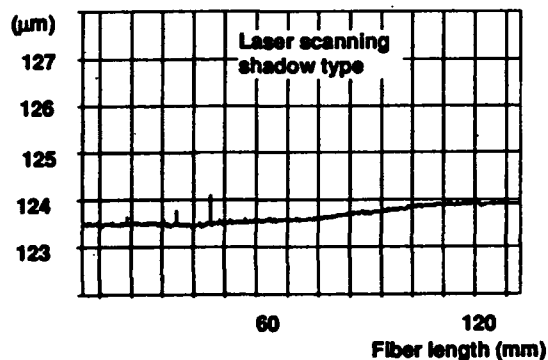


Figure 8 : Comparison of fiber diameter measurement data from laser scanning shadow and dynamic Interferometry, off-line (20 mm/min) after plastic coating stripping



Claude Brehm was born in France on January 1941. He received the Engineer diploma from Ecole Nationale Supérieure de Chimie de Paris in 1964 and Ph. D. degree from Paris University in 1969. He joined Alcatel Alsthom Recherche, and is presently in the Fiber and Photonic Department leader of the optical fiber group involved in fiber drawing. He is member of OSA and of the French Optical Society.



Philippe Darbon was born in France on July 1956. He received the Ph. D. degree in Material Science from the University of Bordeaux, France in 1981. At present he is Research Engineer at Alcatel Alsthom Recherche in the Fiber and Photonic Department. His current fields of interest are optical fiber manufacture and microdimensional metrology. He is member of the French Optical Society.

Benoit Minvielle was born in France on June 1966. He was graduate in chemical and physical instrumentation in 1990. He joined Alcatel Alsthom Recherche in the Fiber and Photonic Department, his fields of interest are sensor and metrology.

MEASURING THE ENDURANCE OF OPTICAL FIBERS

Z. Pasturczyk, M. Ruiz-Vidal & C. Saravanos

Optical Cable Plant, Northern Telecom Canada Ltd.
Saskatoon, Saskatchewan, CANADA

ABSTRACT

The endurance of optical fibers has been determined in order to address the handling and workability of fibers in the field. The performance of several fiber coating types have been compared. Based on observed trends in these test results, a set of requirements are specified to obtain a coating with the best possible endurance.

INTRODUCTION

Despite the fragile nature of glass optical fibers they are expected to survive the cabling process and, without the need for special treatment, offer years of service in the field while subject to routine handling. This wouldn't be possible without the protective coating applied during the fiber drawing process. The primary function of optical fiber coatings is to separate the glass surface from external abrasive elements that could initiate extrinsic flaws, leading to catastrophic failures in the field. This coating must offer protection against aging and mechanical damage. Currently there is no reliable test method to evaluate the coating in that respect. The test procedure described in FOTP-66 "Abrasion resistance of optical fiber" [1] is no longer recommended by North American standards because of poor repeatability. This paper describes a test method to evaluate the endurance (robustness associated with hardness, strength, and coefficient of friction) of optical fiber coatings. The proposed test method reflects what can happen to the fiber as it goes through the cabling process or in the field during cable installation or maintenance.

The endurance test method was applied as a development tool in evaluation of optical fiber coatings. Different coating materials, the effect of the aging process, and various coloring inks were investigated.

TEST METHOD

The endurance test station layout is shown in Figure 1. The fiber under test is stretched between a fixed mandrel (5) and a rotating mandrel (1). The fixed mandrel (5) is attached to

a loadcell which measures the fiber tension. The scoring blade (3) mounted on the translation stage (4) contacts the fiber at the shallow angle of 3° . The blade is shaped as shown in enlarged part of Figure 1. The blade is made of super hard tungsten/cobalt alloy capable of scoring a pure silica glass surface. The stationary vertical post (2) controls the angle of the fiber on the other side of the blade. This approximately 90° angle must be consistent to achieve acceptable measurement repeatability. The post (2) makes this angle independent of how the fiber is placed on the mandrel (1). The mandrel (1) rotates in the direction of the arrow and is used to stretch the fiber to an initial tension of 250 grams. Upon reaching 250 gram tension the mandrel (1) stops rotating and the translation stage (4) starts moving in the direction of the arrow. The movement of the scoring blade (3) along the fiber does not change the angle of the fiber to the loadcell. The part of the fiber between the blade and the fixed mandrel (5) is always perpendicular to the loadcell axis to ensure accurate readings of the fiber tension.

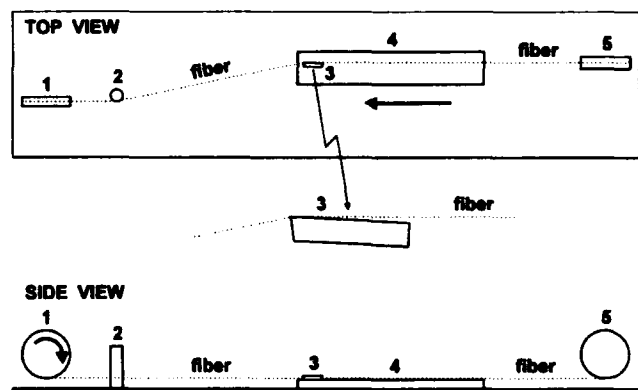


Figure 1. Endurance test station diagram showing top view, side view, and the blade detail.

The blade sliding along the fiber increases the tension above 250 grams. The fiber tension is continuously monitored. At some point the pressure of the blade on the fiber is sufficiently high so that the blade starts scraping the coating from the fiber. As soon as the blade touches the glass surface, the fiber breaks due to the

externally induced surface flaw. The highest tension recorded is indicative of coating endurance. The numbers reported for a given fiber are based on the measurement of ten samples, and include the average value and standard deviation. The repeatability of this test method, estimated as a ratio of the standard deviation to the average value, is better than 6%.

TEST RESULTS

The endurance of several commercially available fibers, representing current industry standard, dual coating, as well as its predecessor, single coating, were measured. Dual coating employs an inner layer of very soft material with a Young modulus around 2 MPa and an outer layer of very hard material with a Young modulus often exceeding 1.5 GPa. The inner layer protects the glass fiber from microbending by absorbing external stresses through elastic deformation while the outer layer provides structural protection against external forces. Single coatings use a material with a Young modulus around 100 MPa, which is a compromise between microbend protection and mechanical protection.

The endurance of the above fibers is compared in Figure 2. As one can see, single coated fibers offer significantly better endurance than dual coated ones. The differences among various manufacturers within each group are minor.

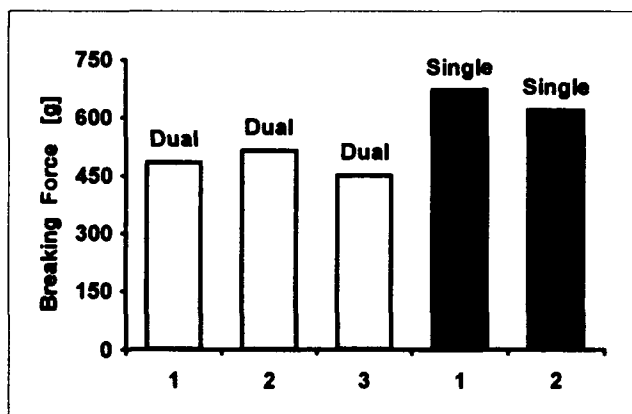


Figure 2. Endurance of several fibers available commercially.

Dual coated fibers rely on a relatively thin outer layer of very hard coating as a protection against mechanical damage. Once this layer is gone, the blade penetrates through the inner layer of very soft coating almost instantly. Evidently single coatings with a thick layer of medium hard

material takes longer to scrape from the fiber and demonstrate better endurance.

The effect of the aging process on endurance was investigated using fibers with different coating materials. The aging was done in 85% humidity at 85°C for 30 days. The results are shown in Fig. 3.

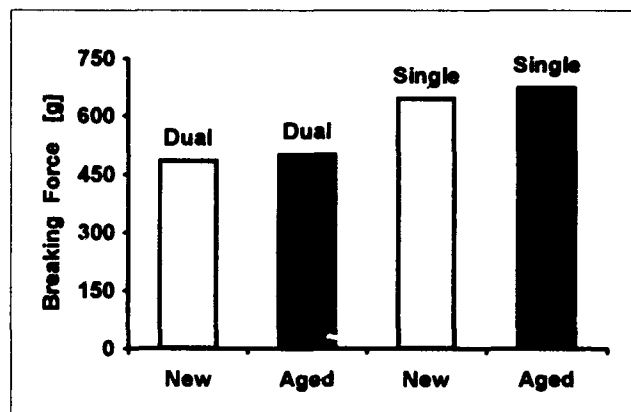


Figure 3. Comparison of fiber endurance before and after accelerated aging.

All coating materials show a slight improvement in endurance due to aging. The coatings become harder to scrape from the fiber for two possible reasons: an increase in the Young's modulus of the coating material and increased coating adhesion to the glass fiber.

The above results were obtained using uncolored fiber. The fiber in the field, where it is most likely to get abused, is all colored. The effect of different coloring inks, and colors, on endurance was studied. The results are shown in Figure 4.

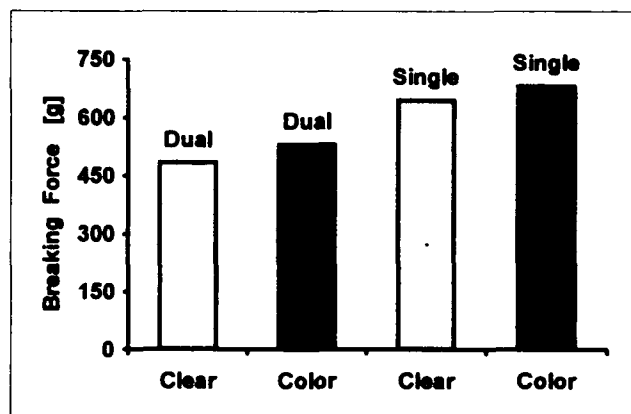


Figure 4. Comparison of fiber endurance before and after coloring.

There was no difference in endurance from one color to another, nor was there a difference between different ink manufacturers. All colored fibers, however, performed better than uncolored ones. The improvement is due to the additional layer of material the blade has to go through before reaching the fiber. An interesting distinction was observed while testing colored fibers. As soon as the blade starts moving, it scrapes the ink layer. In the case of uncolored fibers the blade initially just slides along the coating surface and does not penetrate into coating until half way towards the fiber break point. This difference indicates that the ink layer is not optimized for strength; it is just there for color identification. The layer of ink is relatively thin (i.e. $\sim 5\mu\text{m}$) and since it is always applied on fully cured coatings it doesn't bond strongly to the substrate. As a result it doesn't take much to damage the coloring ink.

CONCLUSIONS

An improved test method for the evaluation of optical fiber endurance has been proposed and examined. In this method, the coated fibers are subjected to treatment representative of actual field conditions. The measurement repeatability is better than 6%.

The endurance of all dual coated fibers falls short of the endurance of single coated fibers. The aging process improves endurance of all coatings tested. Fiber coloring has a similar effect. The improvement comes from the addition of the ink layer. There was no differentiation in performance among different colors. The layer of ink is much easier to damage than the fiber coating.

REFERENCES

- [1] FOTP-66 "Abrasion resistance of optical fiber", ANSI/EIA-455-66-1990.



Zygmunt Pasturczyk
Northern Telecom
Canada Ltd.
Optical Cable Plant
Saskatoon,
Saskatchewan,
CANADA

Zygmunt Pasturczyk received the M.Sc. degree in physics from the Warsaw Technical University in 1976. In 1977, at the Warsaw Technical University, he was engaged in optical waveguides and integrated optics research. He joined SED Systems in 1982, where he was involved with optical instrumentation for upper atmosphere research. Since 1988 he has been a Research Scientist with Northern Telecom Optical Cable Plant, working initially in development of installation products then moving into the area of fiber drawing and focusing on improvements of fiber coating.

PICTURE

NOT

AVAILABLE

Marles Ruiz-Vidal
Northern Telecom
Canada Ltd.
Optical Cable Plant
Saskatoon,
Saskatchewan,
CANADA

Marles Ruiz-Vidal joined Northern Telecom in 1983. She has worked in manufacturing aspects of optical fiber and cable production. In 1990 she accepted a position in fiber R&D where she is actively involved in evaluating new fiber designs, improvements of fiber reliability including new test methods for reliability testing, and advancements of fiber drawing processes.



Costas Saravanos
Northern Telecom
Canada Ltd.

Optical Cable Plant
Saskatoon,
Saskatchewan,
CANADA

Costas Saravanos graduated from the University of Athens, Greece, with a B.Sc. degree in Physics in 1973. He received his M.Sc degree in Solid State Physics from the South Dakota School of Mines and Technology and is currently completing his Ph.D. degree in Electrical Engineering from University of Ottawa.

Following a year with the Digital Transmission Division of Northern Telecom, he joined the Optical Systems Division in 1982 where he was engaged in the fiber process optimization. Since 1985 he has been an R&D Manager responsible for the fiber design optimization and the design and development of optical fiberconnectors. In 1991 he became Manager of Northern Telecom's Fiber R&D team.

Improvement of the Support System for Subscriber Optical Fiber Cable Operations

Takeshi ISOMURA, Hideki SUZUKI, Masahito ARII, and Naoyuki ATOBE

NTT Customer Systems Development Department, 6
Nakase 1-chome, Mihama-ku, Chiba-shi 261 Japan

Abstract

An improved support system for subscriber optical-fiber cable operations and a new premises distribution (PD) cabinet have been developed. The standard support system, which is capable of automatic remote testing without interrupting service, is too expensive to use in offices that do not have a large number of optical fibers. The improved system is economical enough for wide distribution. In Japan, NTCE have recently been liberalized. An improved fault identification method and simplified optical interfaces in the PD cabinet have been developed to distinguish carriers' facilities from customers' facilities. Evaluation of the new system's functions on a system prototype show excellent performance.

1. Introduction

It is expected that customers' needs for telecommunication services will grow and diversify as we move into the 21st century. Carriers must therefore develop facilities and networks that can meet these needs in a timely manner. Current transmission networks, composed mainly of metallic cables, do not provide enough capacity to meet customers' needs. Carriers are therefore developing optical subscriber networks. NTT is introducing optical-fiber cables into subscriber networks in two stages: fiber-to-the-office (FTTO) and fiber-to-the-home (FTTH). To introduce optical fiber facilities soon, it is necessary to design optical subscriber networks that can also supply current telecommunication services. During the current FTTO stage, NTT is introducing nation-wide central terminal/remote terminal systems which provide basic plain old telephone service and ISDN services(1). Already, many optical-fiber cables have been

installed in subscriber networks. With this installation, however, we are facing increasing problems related to the operation and maintenance of fiber-cable facilities. In particular,

- There has been an increase in the time required to test and maintain optical-fiber cables due to the manual processes used.
- Faults in fiber lines are distinguished from those in transmission equipment manually, which is a slow process, making the system less reliable for customers.
- Since there is no administration system for the optical-loop networks, the increase in the number of fibers is causing the paperwork needed to administratively control the fibers to increase and approach its limit.

A few years ago we developed the AURORA (automatic optical fiber operations support system) to efficiently support testing and administration during construction and maintenance of subscriber optical-fiber cables and transmission equipment. This system has four functional units(2)(3):

- An optical time domain reflectometer (OTDR) whose waveform shows fiber losses, splice losses, reflection values, and fault location.
- Filter-embedded connectors (FE connectors) which transmit 1.31 μ m light, but interrupt 1.55 μ m test light.
- Optical couplers insensitive to wavelength.
- Workstations, a test controller, and fiber selectors.

Table 1 shows the automatic remote control tests which can be carried out using this system.

Table 1 Automatic remote control tests with AURORA

tests		wavelength(μm)
OTDR tests	cable construction tests	1.31
	maintenance tests on in-service fibers	1.55
	fault identification tests	1.55
optical loss tests		1.31
fiber identification		1.55

AURORA was introduced in the Tokyo, Kansai, and Kyushu areas for commercial use in 1990 and has operated successfully. For example, testing time during cable construction has decreased by 75%.

Since, it is difficult to determine the scale of the optical-fiber networks that will ultimately be needed, because the demand for optical fiber is not yet clear, and since AURORA is too expensive to allow it to be used in offices with a lesser number of optical fibers, we have developed a more economical AURORA system.

In Japan, NTCE has recently been liberalized. Accordingly, from the viewpoints of improving maintenance efficiency and service reliability, the improved operation support system has been studied to identify faults correctly and decrease repair time using the automatic remote testing. A new premises distribution (PD) cabinet was developed which has physical interfaces between carriers' facilities and customers' facilities.

This paper describes the design and performance evaluation of the improved AURORA and the new PD cabinet. The configuration of the improved subscriber optical-fiber cable system is shown in Figure 1.

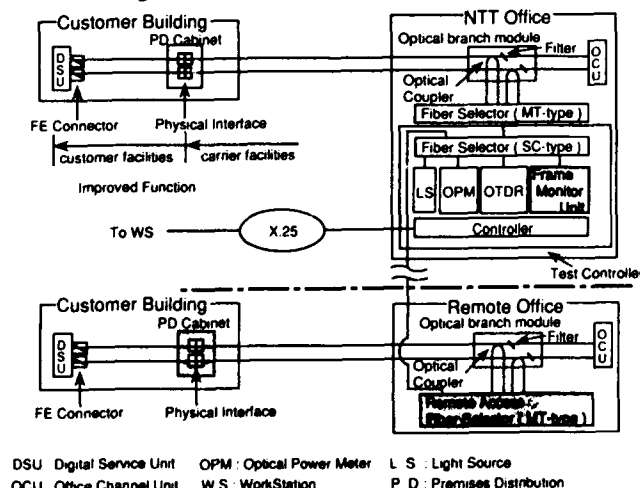


Figure 1 Improved Subscriber Optical-fiber Cable System

2. Improved AURORA

2.1 Remote Access Fiber Selector

The test controller and fiber selectors in the standard AURORA must be located in the same central office. This makes the system expensive and, as a result, it can only be used in offices with a large number of installed optical fibers. A remote access (RA) fiber selector was developed that can be installed in our other offices and connected to the test controller. It is optically stable as well. The configuration of the optical fiber connection between the test controller and the RA fiber selector is shown in Figure 2. Testing light radiated from the test controller is inserted into an optical fiber via an optical test fiber (OTF), the RA fiber selector, and an optical coupler. The OTF consists of two optical fibers. One is used to conduct various optical tests, and the other is used to measure optical connecting loss in this system.

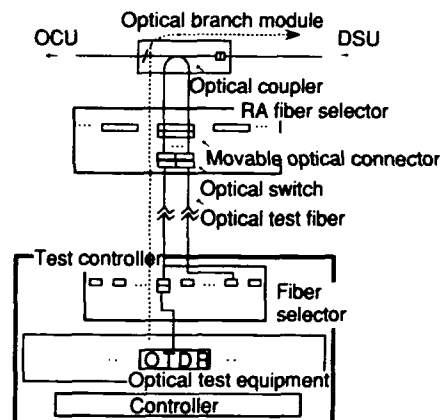


Figure 2 Schematic View of New System

There are several difficulties, however, in applying the RA fiber selector. The OTDR measures the combination of back scattering waveforms transmitted through the optical fiber and the OTF. As a result, the waveform transmitted by only the optical fiber cannot be measured. To eliminate this problem, an optical switch is used in the RA fiber selector. This switch engages during OTDR tests and eliminates back scattering light from the OTF (Figure 3). In addition, the optical switch reduces the number of optical-fiber lines between the test controller and the RA fiber selector, i.e. a normal fiber selector needs eight optical fibers, whereas an RA fiber selector needs only two.

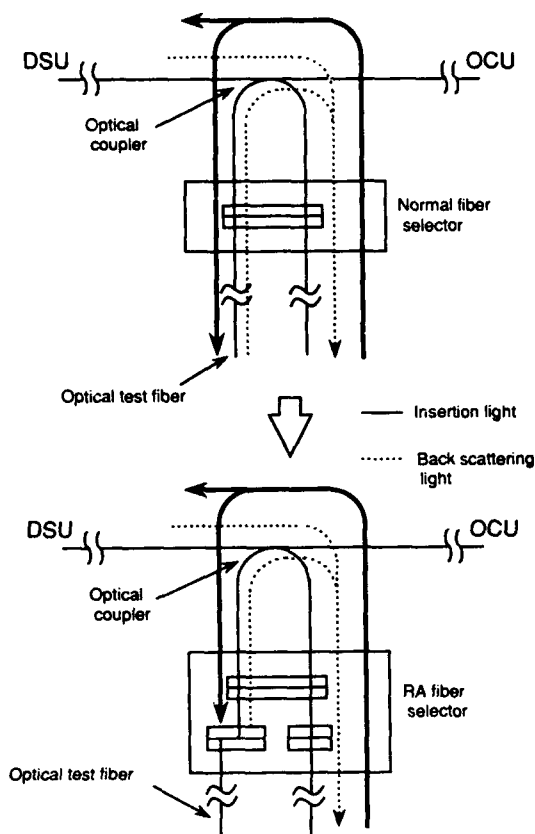


Figure 3 Fiber Selector Action for OTDR Test

To evaluate the optical stability of the RA fiber selector, loss fluctuation in the optical switch was examined in a repeated switching test (up to 50,000 times). The results are shown in Figure 4. Loss fluctuation was found to be less than ± 0.12 dB and it remains consistent after repeated switching. Since the RA fiber selector makes this system inexpensive, it can be used in small offices. As shown in Figure 5, more than 95% of the subscriber optical fiber cable plant we experimented with could be tested economically by the new AURORA.

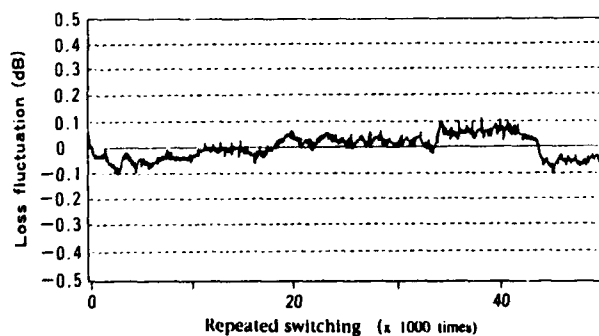


Figure 4 Fluctuation of Connection Loss for Repeated Switching

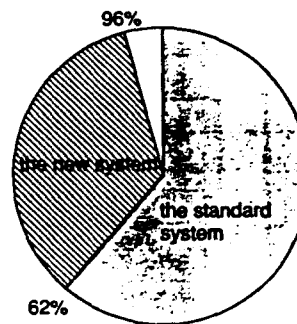


Figure 5 Expansion of the System Introduction

3. New Functions for the Liberalization of Digital Service Unit (DSU) and Premise Telecommunication Facilities

3.1 Improved Fault Identification

Conventional fault identification methods for fiber-optics subscriber systems comprise the loop 1 and loop 2 tests used in transmission operation systems and the optical-line fault identification method used in the standard AURORA. Unfortunately, faults in optical devices in the office channel unit (OCU) and intra-building optical-fiber cables cannot be detected by using these methods.

To ensure high service reliability and maintenance efficiency, we evaluated these potential fault identification methods: an optical-level monitor test, a frame monitor test, and another loop test (Table 2). The frame monitor test was judged to be best, and was the one we implemented. This method enables perfect fault identification. Figure 6 shows the measurement principle for the frame monitor test.

Table 2 Evaluation of Potential Fault Identification Methods

Item	Optical-Level Monitor Test 1)	Frame Monitor Test	Another Loop Test 2)
fault identification accuracy	X	O	O
time to identify fault	Δ	Δ	O
technical difficulty	O	O	X
cost	O	Δ	X
overall evaluation	X	O	Δ

1) Fault identification method which measures the optical level with the OPM in the test controller.

2) Fault identification method which adds a loop-back function to the fiber selector (SC-type) and loops the light from the OCU LD to the OCU PD. (see Fig 7)

O : good
Δ : average
X : poor

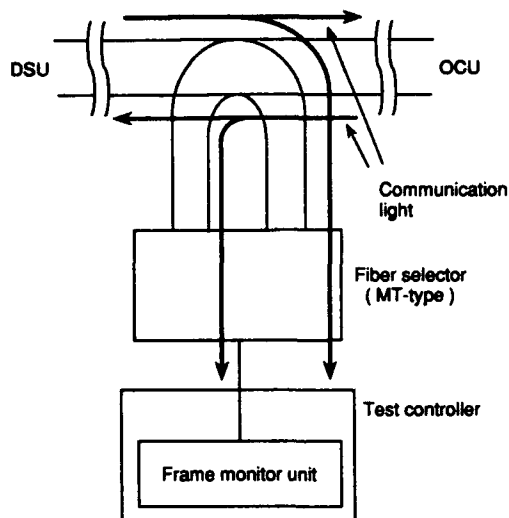


Figure 6 Measurement Principle for Frame Monitor Test

The frame monitor unit mounted in the test controller is capable of detecting the frame signal between the OCU and the DSU through an optical coupler and fiber selectors. The loss of frame alignment, a remote-end alarm signal, or a CRC error is detected by the unit, indicating that a fault has occurred between an optical device in the OCU and an intra-building optical-fiber cable, or that a DSU fault has occurred.

Figure 7 shows how faults are located with the standard method and with the new method. In the standard method, the loop 2 test identifies data termination equipment (DTE) faults, the loop 1 test identifies electrical circuit faults in the OCU, and the optical-line fault identification method identifies DSU faults and subscriber line faults. In the new AURORA, the frame monitor test function identifies faults in optical devices in the OCU and in the optical fiber. Faults in subscriber fiber-optic systems can thus be automatically identified.

The improved fault identification function was evaluated through the use of a prototype (Table 3). For each of the four tested fault locations, the correct alarm was given for each trial.

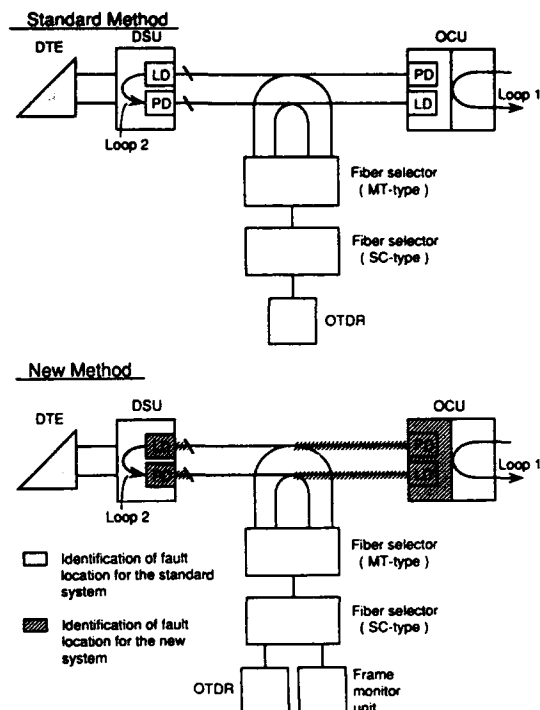


Figure 7 Identification of Fault Location using the Standard Method and the New Method

Table 3 Frame Monitor Test Evaluation

fault location	expected alarm		result			
	from DSU	from OCU	from DSU	correct alarm / trials	from OCU	correct alarm / trials
optical source connector at DSU	loss of incoming signal	remote-end alarm signal	loss of incoming signal	5/5	remote-end alarm signal	5/5
optical receiver connector at DSU	remote-end alarm signal	none	remote-end alarm signal	5/5	none	5/5
optical source connector at OCU	remote-end alarm signal	loss of incoming signal	remote-end alarm signal	5/5	loss of incoming signal	5/5
optical receiver connector at OCU	none	remote-end alarm signal	nothing	5/5	remote-end alarm signal	5/5

3.2 New Premises Distribution Cabinet

To physically separate the customer telecommunication facilities from the carrier facilities, a physical interface was needed. The requirements for this physical interface were:

- (1) provide an equal footing for all physical interfaces,
- (2) allow easy connection and disconnection of the fibers, and
- (3) not affect in-service fibers in the PD cabinet when accessing other fibers.

Since standard cabinets did not provide these functions, we developed a new PD cabinet that did. We did this by improving the standard cabinet. To facilitate connections compactly and economically, we used the 2 multi-pass push on (MPO) connector (Figure 8), which is generally used. This connector consists of two fibers which are a telecommunication unit. Since the connector is obliquely cut, it does not need a coat of oil to prevent reflection. It can thus be connected by simply pushing it together. The 2 MPO connectors can therefore be simultaneously and easily connected and disconnected to the physical interfaces. To prevent accidental touching of the carrier facilities, they are located behind an inner door. In-service fibers are therefore not affected when workers/customers access other fibers. In addition, the cabinet is made of plastic to make it economical and light. Figure 9 shows an overview of the new PD cabinet; its main characteristics are shown in Table 4.

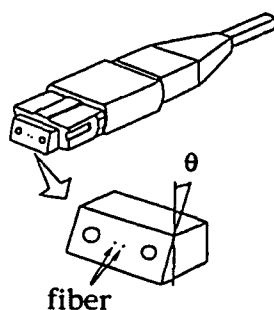


Figure 8 2 MPO Connector

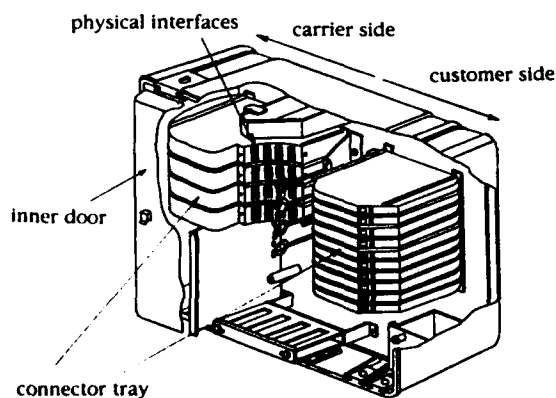


Figure 9 New PD Cabinet

Table 4 New PD Cabinet

maximum number of fibers to be accommodated	size (H×W×D) [mm]	weight [kg]	number of cables for network side	number of cables for premises side
8	265×330×80	2.0	1	1
32	360×450×205	6.5	2	4
100	760×360×215	18	4	8
200	1455×705×205	60	4	18

An evaluation of the loss fluctuation of the in-service fibers when workers accessed the other fibers showed that there was very little loss fluctuation (Figure 10). This cabinet is expected to provide the following advantages.

- A distinct physical interface between the carriers' facilities and the customers' facilities.
- Fibers can be connected and disconnected without interrupting in-service fibers.

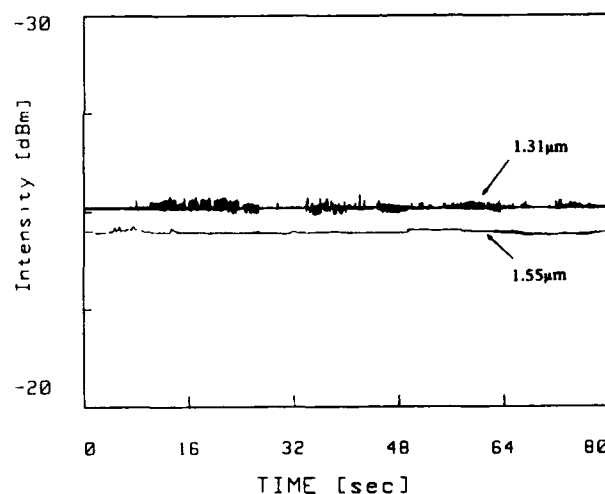


Figure 10 Loss Fluctuation of In-service Fibers in the New Cabinet

4. Conclusion

To promote the effective operation and maintenance of optical-fiber subscriber loops, we improved the AURORA and evaluated its performance. A prototype system achieved an expanded application area for the system and improved telecommunication services. It also made it easy to distinguish between faults in a fiber line and faults in the transmission equipment.

The new AURORA is a cost-effective and time-saving way to construct and maintain fiber-optical subscriber networks; it has been available nationwide since April 1993.

Furthermore, to be liberalize premises telecommunication facilities, we developed a new PD cabinet which is economical and compact, and provides physical interfaces between the carriers' facilities and the customers' facilities. This cabinet was introduced in April 1992.

References

1. Y. Shibata, T. Yoshihara and A. Shirai, 'Evolution of Fiber-optic Subscriber Loop Systems in NTT', Issls 91, pp. 263-269.
2. H. Takasugi, N. Tomita, T. Uenoya, I. Nakamura and Y. Yokoo, 'Design and evaluation of automatic optical fiber operation support system', International Wire & Cable Symposium Proceedings 1990, pp. 623-628.
3. N. Tomita, H. Takasugi, H. Suzuki and T. Uenoya, 'An automatic maintenance test system for optical subscriber loops', Proceedings E-FOC 91, pp. 130-134.



Takeshi Isomura; Takeshi Isomura received B.E. degree in fine measurement and M.E. degree in systems engineering both from Nagoya Institute of Technology in 1988 and 1990, respectively. He joined NTT in 1990. Since 1991, he has been engaged in the development of operation & maintenance systems for optical subscriber lines.



Hideki Suzuki; Hideki Suzuki received B.E. and M.E. degrees in mechanical engineering from Ibaraki University in 1986 and 1988. He joined NTT in 1988. Since 1989, he has been engaged in the development of operation & maintenance systems for optical subscriber lines.



Masahito Arit; Masahito Arit received his M.S degree in Computer Science from Tokyo Institute of Technology in 1985. He joined NTT in 1985. He was engaged in the development of telecommunications cable systems from 1985 to 1989, and the development of support system for optical fiber cable operations from 1991 to 1993. From 1989 to 1991, he worked in Telecommunications Development Bureau of International Telecommunications Union in Geneva, Switzerland. He is a manager in Outside Plant Engineering Division in NTT Plant Planning Department. He is a member of the Institute of Electronics, Information and Communication engineers of Japan.



Naoyuki Atobe; Naoyuki Atobe received the B.S. degree in electrical engineering from Kyushu University in 1979. After joining the Engineering Bureau, Nippon Telegram Telephone Public Corporation, in 1979, he worked on research and development of communication cables and splicing technologies. He had worked on planning and investment of telecommunication plants at Hokuriku regional head quarter in 1986. He is a Senior Manager of NTT Network Systems Development Center, Fiber Optics Local Network Systems Project Group, and is currently engaged in development of testing system for fiber optics local network systems, and fiber termination systems.

Mr. Atobe is a member of the Institute of electronics, information and communication engineers of Japan.

FIBER OPTIC MEASUREMENT TECHNIQUES FOR IMPROVED PRODUCT AND SYSTEM QUALITY CONTROL

Richard G. Gravely III, Stephen R. Stokes, Eric L. Buckland

Sumitomo Electric Fiber Optics Corp.
78 Alexander Drive, Research Triangle Park, NC 27709

ABSTRACT

As specifications for optical performance become more stringent, institution of fiber measurement and analysis techniques that are more accurate, efficient, and consistent is essential. This paper investigates fiber attenuation calculation, fiber fault characterization, and fiber attenuation uniformity algorithms. In addition to product analysis, measurement test system quality is monitored. The result is a total integrated quality system for rapid assessment of process, product, and test system performance and improvements.

INTRODUCTION

Efficient and accurate optical testing of fiber characteristics is necessary for rapid product assessment and information feedback for process control. This challenge means that current measurement techniques need improvement while developing and evaluating new techniques to fully characterize optical performance. Four algorithms to compute the attenuation coefficient are examined with selection based on technical correctness, speed, and simplicity. Fiber fault location and characterization is essential for fiber performance evaluations. Four techniques are compared based on performance characteristics including noise rejection capabilities, resolution, sensitivity, and accuracy. Beyond these specific parameters, a generalized quality indicator is desirable to allow prediction of loss for internal segments and improve information feedback through the process. Fiber attenuation uniformity algorithms are compared and evaluated.

ATTENUATION CALCULATION

Nominal fiber attenuation has typically been characterized using a least squares linear fit. This approach has potential for errors and inaccuracies in non linear fiber OTDR signatures (See Figure 1).

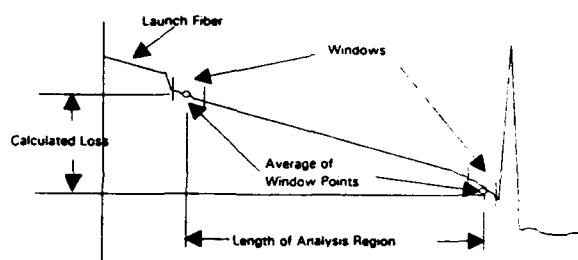


Figure 1: Attenuation Error Due to Least Squares

The possibility of error prompts an evaluation of attenuation calculation techniques including least squares, simple two point, two point with averaged end points, and two point with least squares fitted end points. Simple two point calculation of attenuation coefficient is susceptible to noise even after averaging the signal. The two point with averaged end points uses a window of determined length at either end of the fiber trace and calculates an average value of the data points. The window length is determined by the point resolution of the machine and/or the length of the test fiber. Typically, a minimum of 4 and a maximum of 20 data points is used for the calculation. Simple two point subtraction is used and the result is then divided by the length less the length of a window. Figure 2 illustrates this technique.

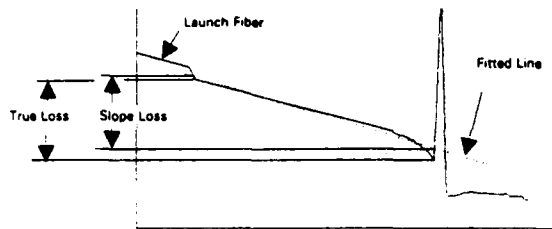


Figure 2: Averaged End Points

Note that the Calculated end-to-end loss is less than the actual loss. However, when dividing by the length of the analysis region, the attenuation coefficient is adjusted appropriately.

The two point with least squares fitted end points technique also uses a window approach. A linear fit is calculated and the equations are regressed to the start and end point of the fiber. Simple two point subtraction is used and divided by the total length of the fiber (See Figure 3).

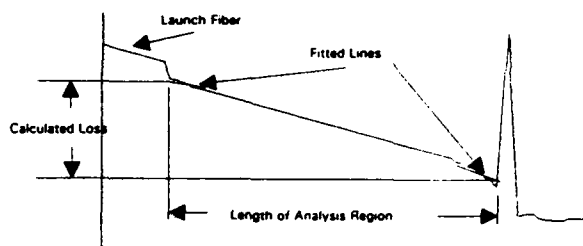


Figure 3: Least Squares on End Windows
(Fitted Lines Exaggerated For Clarity)

The results of these two approaches are virtually identical (See Figure 4) with the least squares fitted end points performing slightly better on fiber signatures with severe drops at the beginning or end of the fiber. However, the windows of the least squares fitted end points technique is dependent on the number of data points. This can cause calculation problems at large pulse widths.

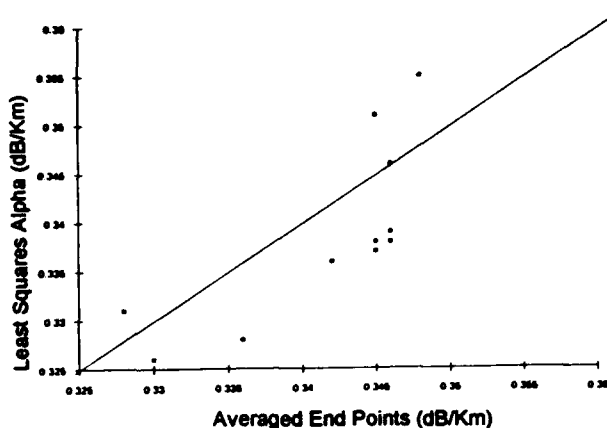


Figure 4: Least Squares vs Averaged End Points

Since both methods offer virtually identical results, the two point loss method utilizing averaged end points is chosen for its simplicity and accuracy.

FIBER FAULT LOCATION

Of specific importance is the ability to recognize, locate, and characterize faults in the fiber signature. To employ a measurement system capable of automatically assessing fiber faults offers many advantages. Specifically, more reliable and consistent fault reporting and a large reduction in operator intervention.

A comparison of four fault location techniques is presented in this paper. Candidates are eliminated from consideration when failing to meet certain requirements such as noise rejection and sensitivity capabilities. The four techniques are: First Derivative analysis, Second Derivative analysis, Step Function convoluted with First Derivative, and Difference of Gaussians convoluted with the First Derivative.

For reference throughout this paper, Figure 5 contains an OTDR trace that contains several faults with a zero noise level and the resulting first and second derivative.

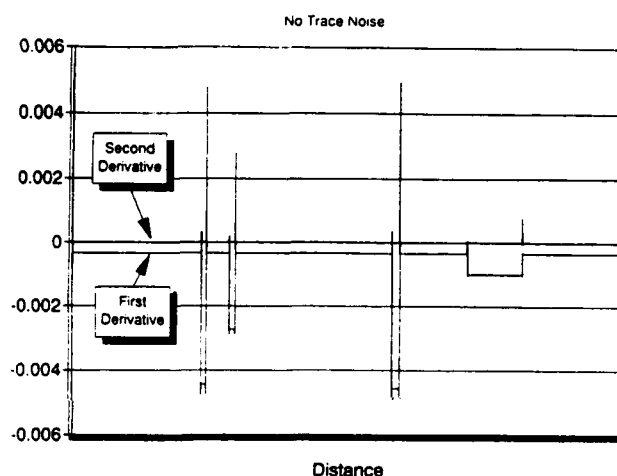
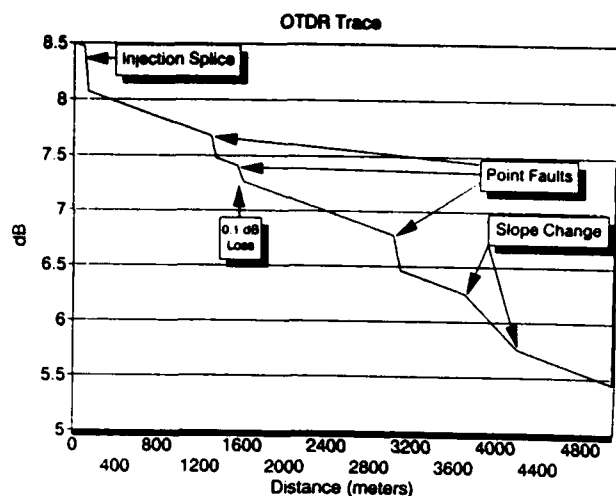


Figure 5: Noise Free Trace and the First and Second Derivative

Noise rejection capability is necessary when relying on data received from an OTDR. Invariably, the data will contain some level of noise depending on machine characteristics. It is precisely the lack of noise rejection capabilities that allows us to eliminate the Second Derivative analysis, the First Derivative, and when combined with sensitivity performance eliminates the Step Function with First Derivative. Figure 6 demonstrates the resulting first derivative on the OTDR trace contained in figure 5 with a noise level of 0.005 dB. Note that the result would be difficult to analyze and that the second derivative is not shown as it simply magnifies the noise level in the first derivative trace.

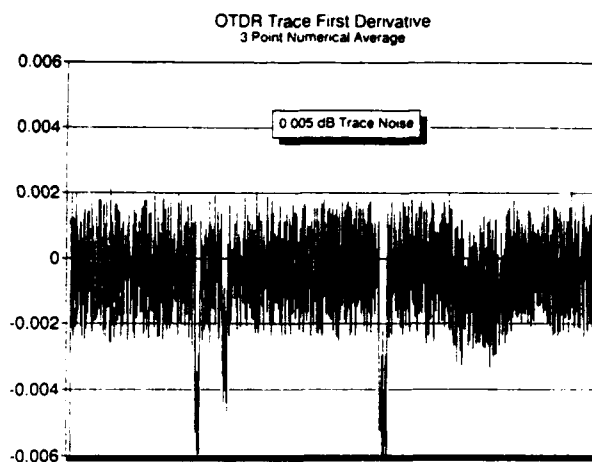


Figure 6: First Derivative of Trace with 0.005 dB Noise Level

First and Second Derivative analysis of the OTDR signature does not require detailed explanation as these mathematical functions are straight forward. Simply, the derivative of the OTDR trace is calculated and is analyzed for excursions that fall outside of an established threshold. Clarification of the Step on First Derivative technique and Difference of Gaussians technique, however, is appropriate. A detailed explanation of the Step Function with First Derivative and the Difference of Gaussians techniques is presented.

The Step Function with First Derivative is a simple function which is convoluted with the first derivative of the OTDR trace. Localized slope changes in the OTDR trace will form steps within the first derivative. The step function is applied as a filter on a point by point basis along the first derivative array. Figure 7 illustrates the step function.

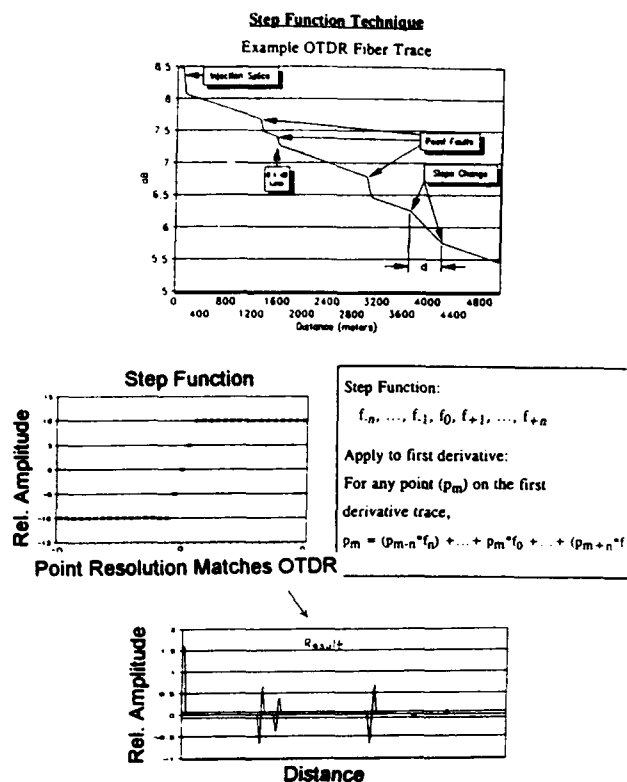


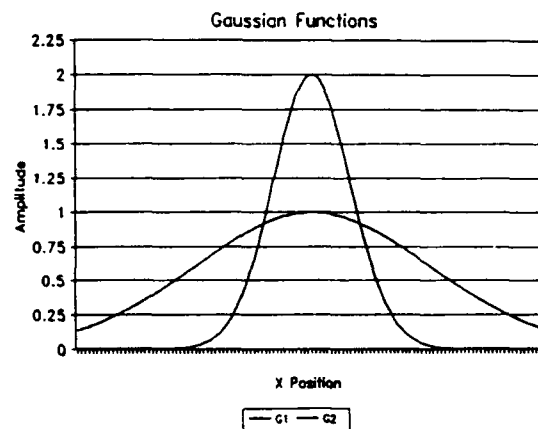
Figure 7: Step Function

The step function is a linear array which is used to operate on the first derivative array. This function also provides a smoothing effect by operating on multiple points of the first derivative array to reduce noise influence. The number of points used, $2 \cdot n$, will control the amount of smoothing but must be balanced with execution speed and resolution. While the OTDR trace slope remains constant, the resulting function, p_m , will be zero when the step function is applied to the first derivative of the OTDR trace. When a change in slope occurs, p_m will deviate from zero at the slope change inflection point. From Figure 5, the maximum and minimum peaks in the resulting step function correspond to the slope change inflection points of the OTDR trace. A simple filter function is passed along the trace to locate the abrupt changes, identifying fault locations.

This technique performs exceptionally well with a noise free trace. However, the nature of the step as a "build up" function becomes problematic with the introduction of noise. Briefly, increasing and decreasing edges of the spikes, seen in Figure 7 (Result Trace), are results of "build up" from the leading and trailing ends of the step. As noise is introduced, the fault spikes become indiscernible from noise spikes. To minimize the influence of noise, the number of points in the leading and trailing edge of the step must be increased. However, increasing the number of points reduces the sensitivity of the step to identify faults, the fault spikes almost disappear due to the weighting of the surrounding points. Therefore, there is a trade off between noise rejection and resolution. From experience with this function, satisfactory results are difficult to obtain.

In order to improve sensitivity, a technique using a central weighted function needs to be applied. The Difference of Gaussians technique is employed offering exceptional noise rejection and high sensitivity. Figure 8 illustrates the conception of the Difference of Gaussians function.

Fault Location Techniques: Difference of Gaussians Analysis



Gaussian Functions:

$$G1 = G_01 (\exp\{-r^2/2w_1^2\})$$

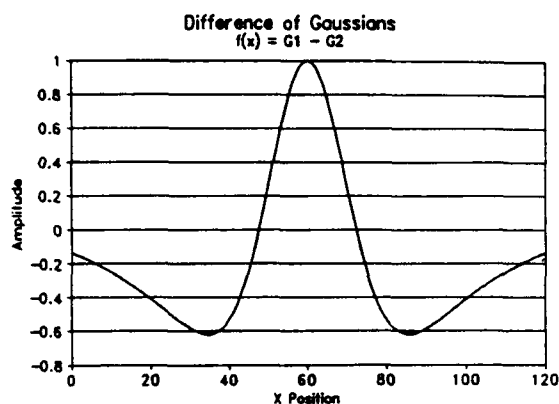
$$G2 = G_02 (\exp\{-r^2/2w_2^2\})$$

where:

G_01 & G_02 are constants which set maximum amplitude of each function. The ratio of amplitudes will control the integral of the resulting difference function.

w_1 & w_2 control the Gaussian envelope width. The width will control the algorithm's location ability with respect to fault shape and the spatial resolution of the function.

Resulting Gaussian Difference Function:



- * The function is applied to the discrete points of the trace or its derivative.
- * Typically used in boundary detection.
- * Good noise immunity.

Figure 8: Conception of Difference of Gaussians

The width of this function controls the algorithm's fault location ability, while the negative tails influence noise rejection capabilities. The resultant function is constrained such that its integral is zero. Therefore, the function may be optimized for specific fault size ranges and equipment noise levels. As the Difference of Gaussians function is convoluted with the first derivative trace in a manner identical to application of the step function as described above, the position and negative areas of the function cancel out in regions of constant slope. When encountering an inflection point, the high magnitude of the center point of the Difference of Gaussians function magnifies this inflection significantly, forming a spike. Figure 9 demonstrates the resulting function of the Difference of Gaussian when applied to the trace in Figure 5.

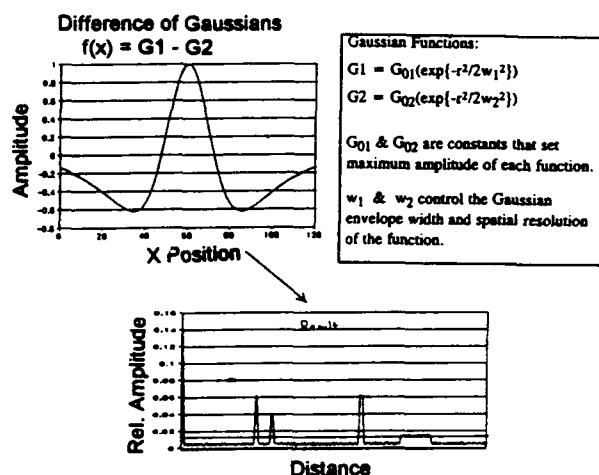
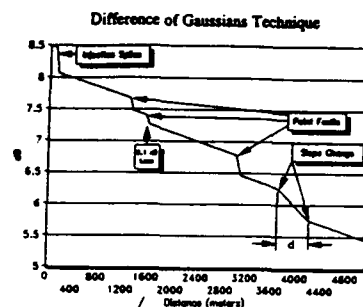


Figure 9: Difference of Gaussians Function

In practice, the function is approximated by an integer array (See Figure 10) for computational simplicity. When optimized, the Difference of Gaussian function offers good noise rejection and sensitivity.

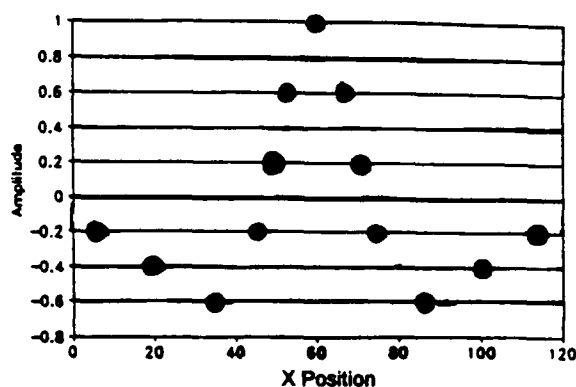


Figure 10: Integer Array Equivalent of Difference of Gaussians Function

Analysis of the result is performed using a two pass filtering technique use to identify potential fault locations. The first pass filter is determined by calculating the standard deviation of the points and multiplying this by a predetermined rejection factor to identify boundaries. This filter is then passed along the array of points and any data points that fall outside of the band are recorded as potential faults. These points are then eliminated from the function and the standard deviation is re-calculated for the remaining points. Again, this standard deviation is multiplied by a new rejection factor to determine the upper and lower limits for the second pass filter. The process of potential fault location for the second pass filter is the same as the first pass filter.

Initially, potential fault locations that are within a specified distance, typically 150 meters, of each other are combined to form one fault location. The specified distance is a function of the pulse width and resolution requirements. Once start and end points have been determined for potential faults, analysis of fault size is performed. This analysis takes the classical approach of operating on the original OTDR trace by fitting a line to the left of the start point and to right of the point of each potential fault. The right line is regressed back to the knee location and the vertical drop is measured. Figure 11 diagrams the technique.

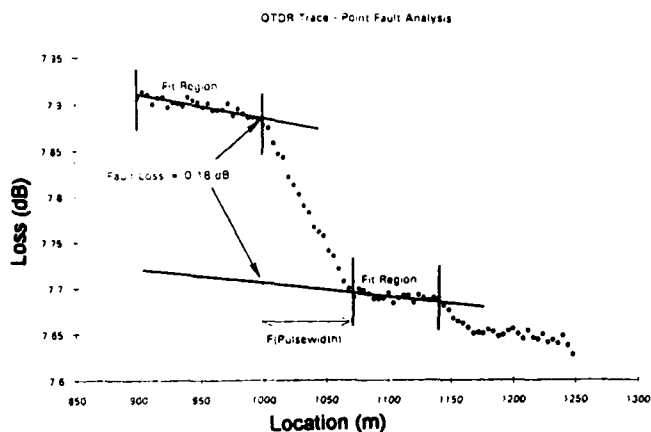


Figure 11: Fault Analysis

Once the size of the potential fault has been calculated, a comparison to a specified minimum fault loss is made to determine whether or not to classify the anomaly as a confirmed fault. The specified minimum fault loss value indicates to the system to assess anomalies as faults if their resulting loss is greater than or equal to the specified value.

For information feedback, fault size and location as well as the attenuation coefficient of regions between faults is reported. After fault location and identification has completed, the system performs further analysis in the form of the generalized quality parameter of non-uniformity.

Motivation for Non-Uniformity Parameter

Current industry specifications refer to an end-to-end attenuation coefficient coupled with a maximum allowable local point defect. Attenuation coefficient is measured utilizing the cut-back or OTDR techniques as described in FOTP 78 and FOTP 61 respectively. Point defect measurements are defined in FOTP 59 and are most accurately identified through the above described technique. This assessment of fiber quality is an important tool towards establishing effective corrective action programs for optical fiber and cable quality improvements. However, a more generalized measure (non-uniformity parameter) of quality fluctuations along the fiber length is desirable to fully depict product performance.

As system lengths approach the supplied lengths from the cable manufacturer, internal optical fluctuations have not been shown to have an effect on system performance, and this generalized non-uniformity parameter has little impact. For short length applications, small fluctuations in attenuation coefficient (dB/Km) do not translate into significant accumulation of power loss (dB) or detriment to the system power budget. However, with fiber manufactures drawing fiber lengths greater than 25 Km, it is not unusual for internal segments to have attenuation coefficients greater than or less than the end-to-end coefficient. Therefore, as users buy master lengths of fiber or cable and assign shorter lengths to product or system, there is a need to calculate the loss of internal segments with precision so that adverse effects on yields and cost can be avoided.

Although both the cable manufacturer and user are affected, the cable manufacturer absorbs the majority of the impact created by internal variations of fiber quality. For the cable manufacturer, who is typically supplied with long lengths of fiber, optimum utilization of fiber into the manufacture of cables with significantly varying lengths requires some technique to accurately predict internal segment attenuation. The ability to precisely assign the available fiber distribution into cable production runs effects yields, manufacturing costs, and ultimately the cost of product to the end user. For both the fiber and cable manufacturer, a generalized defect parameter has the potential to provide a useful feedback tool for improving both product and measurement system quality.

International Standards

Primarily motivated by the need for a universally accepted parameter to promote fair description and trade of optical fiber product, international standards bodies are reviewing methods to provide a general measure of internal segment quality. A number of methods continue to be discussed and are briefly mentioned here for completeness, with the remaining discussion devoted to the "Excess Loss" method as proposed and revised by P. Lovely, T. Hanson and D. Pregibon in TIA F.O. 6.6.5.1.

Three categories of the non-uniformity definition are proposed:

- [1] Maximum internal segment coefficient.
- [2] "Tram-track" upper and lower backscatter control limits.
- [3] Excess Loss

The maximum segment coefficient [1] approach involves the measurement and specification of the maximum attenuation coefficient of internal segment lengths above some minimum length, generally one or two kilometers. Several versions of this method exist, however, one must measure every segment length above the specified minimum length for the results to be technically correct. Depending on the point resolution of the machine and the length of the fiber, measurement of every segment length can be extremely time consuming and taxing on the system. Not only is there an issue with computation execution time, there is a significant discussion as to the appropriate minimum length. As minimum length decreases, measured results will be increasingly equipment dependent.

The "tram-track" [2] technique places control limits on the backscatter trace by superimposing a line on the trace with a slope equal to a defined target or the nominal attenuation coefficient. This line is then bordered with parallel lines of a specified distance from the center line. Any actual data points existing outside of this border results in a failure of that product to meet the set expectation. On single direction OTDR traces, this method has the potential to significantly penalize fiber since the OTDR records captured backscattered illumination and is thus only an indirect measure of attenuation in the fiber. When applied to Bi-Directional OTDR traces, this method can penalize good fibers which happen to have regions of exceptionally low attenuation that fall outside of the upper limit.

The Excess Loss technique [3] takes a different approach. This method compares the difference between the actual power throughput of internal segments to the expected power based on the nominal attenuation. Fiber non-uniformity is recorded only if the power throughput is lower than expectation so that penalties on superior regions are avoided. Additionally, the use of this approach provides a parameter in units of absolute power (dB) as opposed to a length normalized coefficient (dB/Km) which may be used in a manner more consistent with end use. More specifically, this approach more accurately depicts the products effect on power budgets and may suffice to replace point discontinuity specification in favor of a truly generalized parameter.

Procedure for Calculating Excess Loss [Parameter]

This technique must be applied to the combined Bi-Directional OTDR trace so that the influence of unidirectional backscatter non-uniformity caused by fiber geometric properties will be avoided. The Excess Loss equation is a two parameter curve of the following form:

$$\alpha_{\max}(L) = \alpha_{\text{ref}} + N/L \quad \text{Equation 1}$$

α_{ref} is the reference coefficient (dB/Km), which may or may not be the end-to-end coefficient, N is the non-uniformity parameter (dB), and both are determined by the algorithm. The Excess Loss algorithm determines these values such that Eqn. 1 forms a curve that completely bounds the maximum attenuation for all possible segment lengths while minimizing the error over a discrete length range. Figure 12 shows the maximum attenuation coefficient for every possible segment length. The discrete data points are the actual coefficient for all segments of length L_i and the solid line is the result of Equation 1.

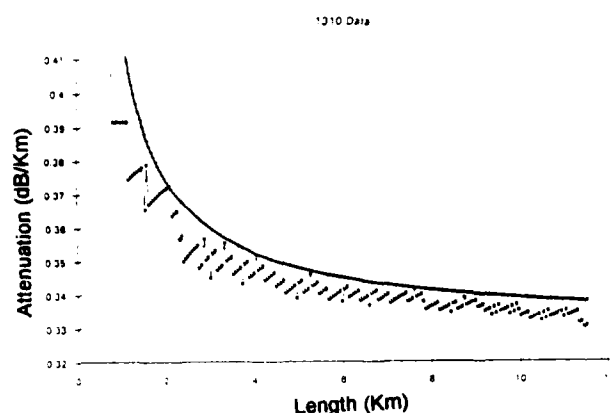


Figure 12: Segment Loss (Data) with Nonuniformity (Solid Curve) Curve

Note that the curve intersects a minimum of two of the data points, at least one of which will fall in the 1 Km to 3.5 Km range, thus minimizing the error over this length range. The harmonic mean, calculated as the reciprocal of the average of the reciprocals of the lengths in this range, allows this technique to "anchor" the resulting curve to two of the actual data points.

This technique does not require that the maximum attenuation coefficient be calculated for every possible segment, a step that would be far too time consuming. An algorithm developed by Hanson and under consideration as an FOTP, efficiently calculates the output values α_{ref} and N , by which the maximum segment attenuations are completely bounded.

Specification of Non-Uniformity

The development of this specification around $\alpha_{max}(L)$, α_{ref} , and N is a necessary step toward commercial utilization.

Current specification standards reference end-to-end attenuation coefficient and a maximum allowable discontinuity. Various specification methodologies utilizing the non-uniformity parameter are envisioned, namely:

- [1] Specifying maximum internal segment attenuation coefficient above a minimum length L_0 .

$$\alpha_{max} = \alpha_{ref} + N/L; \quad L \geq L_0$$

- [2] Specifying α_{ref} together with a maximum non-uniformity N .

Specifications of the first type are related to the use of stepped or sliding window attenuation measurement techniques for segment attenuation specifications mentioned earlier. This specification procedure has numerous difficulties. Technically, specification of L_0 remains an issue, as obviously the value for α_{max} explodes rapidly as the length decreases. Similarly, N , even for the highest quality fiber, has a lower bound determined by instrument noise. This gives a false implication that internal segment attenuation coefficients may be higher than actual. This is motivation for employing pre- or post data acquisition filtering techniques, but currently no post data acquisition techniques are widely applied, especially in field situations. The last problem is the use of the appropriate α_{ref} . In general, use of such a specification procedure requires significant re-thinking of the usage of fiber attenuation information in commerce and design.

Perhaps the second method proposal is the simpler, and most straightforward approach. N then becomes a generalized replacement for the point discontinuity specification currently employed. N remains bounded by measurement noise, basically in the same fashion as the discontinuity analyses described above. The choice of reference α in equation 3 is simplified by using the end-to-end attenuation for calculations of internal segment attenuation since the difference between the two parameters α_{ref} and $\alpha_{end-end}$ is not significant. That is, α_{ref} is an intermediate result used in the computation of N . In this way internal segments may still be approximated by a system

designer using equation 3 and substituting $\alpha_{\text{end-end}}$ for α_{ref} . Figure 13 illustrates that the difference between α_{ref} and $\alpha_{\text{end-end}}$ is minimal for fiber lengths ranging from 1.7 to 12 Km.

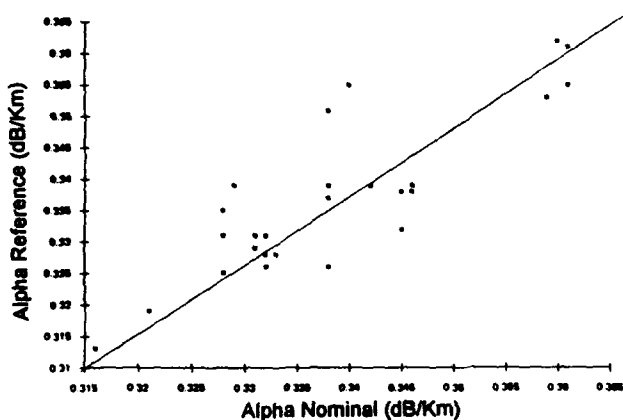


Figure 13: Alpha Reference vs Alpha Nominal

Thus, by modifying current product specification procedures to reference:

$$\frac{\alpha_{\text{end-to-end}} \text{ (dB/Km)}}{N \text{ (dB)}}$$

it is possible to minimize the impact on current customs and practices, generalize the concept of discontinuity or OTDR defect, and enhance the fiber users' (cabler or end user) ability to predict internal segment or cut-length product performance.

Quality Control Through Non-Uniformity

For quality control, it is instructive to view the wavelength dependent performance of non-uniformity. Figure 14 shows the relationship between non-uniformity at 1310 nm and 1550 nm for 10 fibers of length 12 Km. For this set, 1-way OTDR values are used, rather than the combined trace, for illustration only.

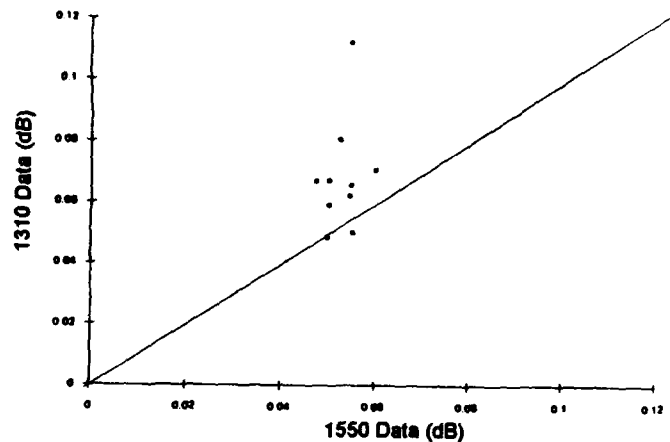


Figure 14: 1310 nm vs 1550 nm Data

As can be seen the 1310 nm values tend to be higher in the single direction trace. This is reasonable in light of higher Rayleigh scattering at this wavelength, and greater sensitivity of backscatter capture fluctuations at this wavelength. As fiber attenuation continues to approach the Rayleigh limit, minor longitudinal fluctuations may become more visible. In any case, this wavelength dependent non-uniformity should provide valuable feedback to fiber manufacturing for continued glass improvement, and to the cable manufacturer for continued process improvement.

Another valuable feature of this non-uniformity technique is to evaluate instrument operation. Specifically because N is lower bound by system noise, machine performance can be compared. As seen in figure 15, differences across machines is visible.

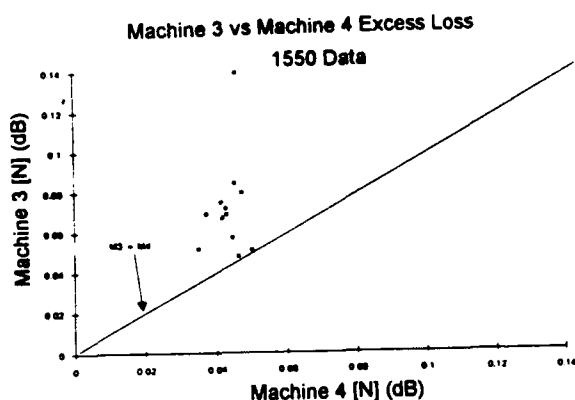
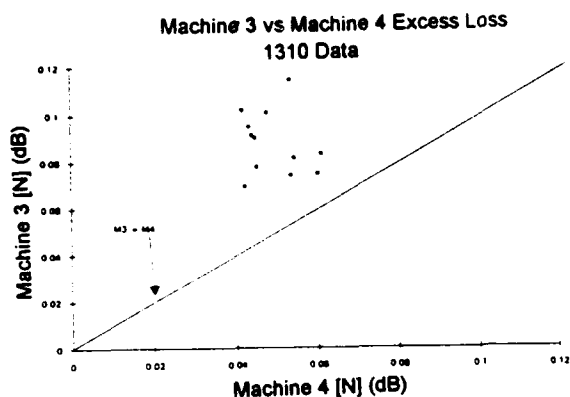


Figure 15: Machine Comparison

As a statistical quality control tool, monitoring non-uniformity, either through reference fiber tests or through pooled product statistics provides a new tool for measurement system improvements.

Conclusions

As the demands on today's fiber optic products increase, the development of measurement systems that offer advanced analysis techniques is imperative. A PC based fiber optic OTDR measurement system incorporating a revised nominal attenuation coefficient, automated fault analysis techniques, and a fiber attenuation uniformity measurement is introduced. The analysis tools offered by this system provide a means to more accurately and more reliably depict optical performance while minimizing operator intervention. Investigations into data filtering techniques as well as fiber non-uniformity evaluations are being pursued.

Richard G. Gravely III received his B.S. degree in Electrical Engineering from North Carolina State University in 1991. He joined Sumitomo Electric Fiber Optics Corp. in 1992 as a Product Design Engineer responsible for measurement system development. Richard is a member of the Institute of Electrical and Electronics Engineers, Inc.

Stephen R. Stokes obtained a B.S. degree in Electrical Engineering from Virginia Polytechnic Institute and State University in 1988. He was employed by ITT Electro Optical Products Division and, subsequently, Alcatel Cable Systems from 1980 to 1990 in the development of fiber optic measurement systems. From 1990 to 1991 he was employed by Galileo Electro-Optics Corporation as a Design Engineer in the development of light guide and imagescope products. He has been employed by Sumitomo Electric Fiber Optics Corp. since 1991 in the development of fiber optic cables and as supervisor of the Lightwave Laboratories. He is currently manager of Product Design Engineering.

Eric L. Buckland obtained his B.S. degree (1985) and M.S. degree (1992) in Physics from North Carolina State University. Employed at Sumitomo Electric Fiber Optics Corp. since 1985, he has been engaged in the research and development of optical fibers and cables. He is currently pursuing a Ph.D. at the University of Rochester Institute of Optics. Mr. Buckland is a member of the Optical Society of America.

THE EFFECTS OF ENVIRONMENT ON ULTRA-VIOLET CURABLE OPTICAL FIBRE COATINGS

E.CRESSAN, P.ANDRE, D.CRESPEL, O.FOURNIER, A.MORGAND, A.PERAUDEAU,
Y.RUELLO

LABORATOIRE DE CARACTERISATION DES MATERIAUX
FRANCE TELECOM - CNET LAA/ELR/CSD
BP 40, 22301 LANNION CEDEX
FRANCE

Abstract

An inquiry has been made into the compatibility of various filling compound and water with the UV-curable coatings of optical fibres. To study these coatings it is important to use suitable methods. FTIR (Fourier Transform Infrared Spectroscopy) is a suitable test for determining the degree of cure of the coatings and TMA (Thermo Mechanical Analysis) can be used to study the effects of the environment. These two methods are described in this paper and results on both free films and fibres itself are exposed.

1. Introduction

Single mode optical fibre has become a standard in optical communications. Most of the fibres used are coated with two layers of UV-curable acrylate.

These coatings must present good reliability, minimal ageing effect in different environments, such as filling compounds and water. In fact, important changes in coating aspect on some fibres extracted from cable have been observed.

To understand what's happened, it is important to have suitable methods to study fibre coatings. A search is being made for a method of determining first the cure of the coating and secondly the effects of environment.

After exposing the various methods used to study both films and fibres, a choice of the most versatile one will be made to study the ageing of coatings.

2. Tests methods used for films characterisation

The film preparation is as follows: each liquid coating (outer and inner) is placed in a Teflon mould. Coatings are then cured to different levels using a fusion system model 450, equipped with a D-lamp. The UV-dose is measured using the UVIMAP apparatus. We obtain films that are uniformly cured as well as of uniform thickness (about 100 µm).

2.1. MEK extraction test

This test enables extraction of all the coating material which is not polymerised⁽¹⁾. About 5 grams of cured film is weighed and extracted for 12 hours with MEK (Methyl Ethyl Ketone) in a Soxhlet extractor. The gel fraction percentages (%GF) are calculated by the following equation:

$$\%GF = \frac{\text{Weight of the sample after extraction}}{\text{Weight of sample before extraction}} \times 100 \quad (1)$$

The degree of cure is then obtained:

$$\text{Degree of cure \%} = \frac{\%GF \text{ sample}}{\%GF \text{ fully cured coating}} \times 100 \quad (2)$$

We consider that a coating is fully cured when repeated exposure to UV light does not result in significant decreases in extractable content. Two overcured samples are used to insure an accurate baseline for full cure. Figure 1, below, shows the degree of cure for inner and outer coating.

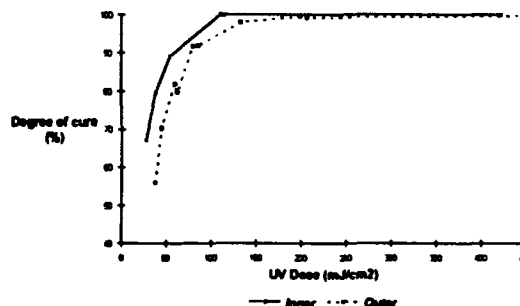


Fig. 1: Degree of cure versus UV-Dose

We can note that the primary coating cure is faster than the secondary coating one. This is expected because the cross link density in the soft primary layer is much smaller than in the hard one.

To access to the degree of cure of a coating, Soxhlet extraction is an economical method, but takes about one day and is a destructive test. Therefore, it is necessary to find a faster technique.

2.2. Fourier Transform Infrared Spectroscopy (FTIR)

The FTIR method is based on the visibility of acrylic double bonds in the infrared spectra. During the polymerisation the amount of acrylic groups decreases as they react to form the polymer network.

Coatings with different degree of cure are placed on both side of an ATR(Attenuated Total Reflectance) KRS5 crystal. The equipment used for the tests is Nicolet FTIR model 510P.

For the outer coating, the 810cm^{-1} peak (C-H deformation vibration on the acrylate double bond) is used to follow the degree of cure of a coating. Figure 2, shows the change in intensity of the C-H peak as the material is cured. To normalise any variations in the level of sample/crystal contact, the 830cm^{-1} peak, which is not affected by the curing reaction (figure 2), can be used⁽²⁾.

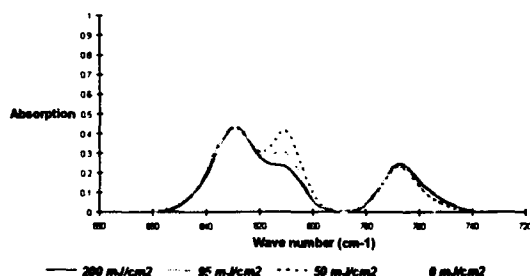


Fig. 2: Outer coating spectra for different UV-Dose

The state of cure is calculated as a percentage using the following equation:

$$\% \text{ Cure} = \frac{\text{SR}(\text{uncured}) - \text{SR}(\text{sample})}{\text{SR}(\text{uncured})} \times 100 \quad (3)$$

where SR is the surface ratio of 810cm^{-1} peak and 830cm^{-1} peak.

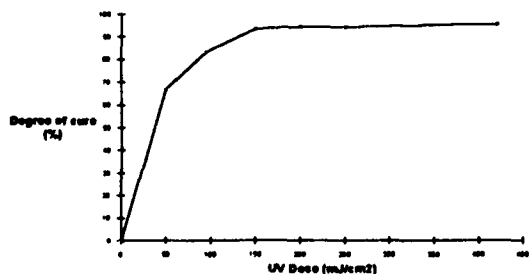


Fig. 3: Degree of cure versus UV-Dose for the outer layer

The figure 3 shows the degree of cure of the outer coating versus the UV-Dose.

For the inner coating, the same peak at 810cm^{-1} is used. Figure 4, shows the change in intensity of the C-H peak as the material is cured. The peak used to normalise any variations in sample/crystal contact, is the 755cm^{-1} peak.

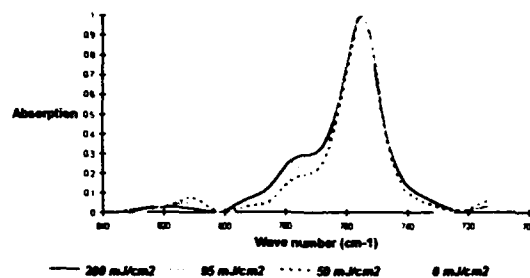


Fig. 4: Inner coating spectra for different UV-dose

The state of cure is then calculated with the same equation used for the outer coating (equation 3), and the curve of degree of cure versus UV-Dose is obtained:

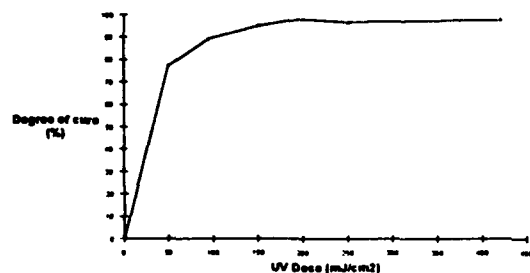


Fig. 5: Degree of cure versus UV-Dose for the inner layer.

We can note like the MEK extraction, that the primary coating cure is faster than the secondary coating one. In fact, to have a degree of 90% , the UV-dose for the inner layer is 105 mJ/cm² and for the outer one, 130 mJ/cm²

FTIR technique, which gives not only better resolution but also is non-destructive and fast, is preferable to the MEK extraction method.

2.3. Thermomechanical analysis (TMA)

TMA measures the change in dimension of a sample as it is heated. TMA is performed with the Perkin-Elmer TMA7 with a quartz probe for compression measurements.

Free films are placed under the probe and heated from 50°C to 150°C with a rate of 5°C/min.

For the outer coating, the force applied is 2000 mN and for the inner one, 500 mN. We obtain curve of penetration versus temperature (figure 6). A change of

slope occurs at the T_g which can be easily determined as it can be seen in figure 6.

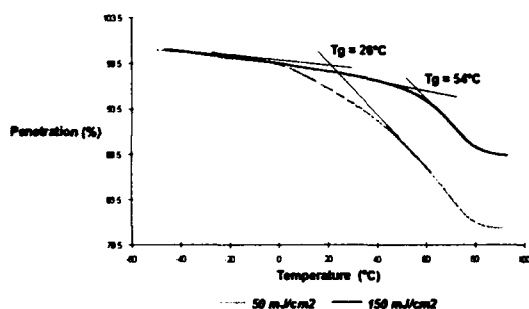


Fig. 6: TMA curves for two different outer coatings

T_g measurements of inner and outer coatings are summarised in table 1:

UV-Dose mJ/cm ²	Inner coating T_g (°C)	Outer coating T_g (°C)
50	17	27
95	18	51
150	18	54
200	19	55
250	20	57
420	20	56

The repeatability is $\pm 2^\circ\text{C}$

Table 1: T_g values of inner and outer coatings

We can note that there are no significant variations in T_g values for the inner layer and for the outer one excepting for the less cured coating which T_g decreases. Thermal analysis can be used to verify that a coating is not undercured, but it is an unsuitable method to precisely determine a degree of cure.

Some measurements in dynamic mechanical analysis (DMA7) have been performed on the same coatings studied with TMA7. For experimental reasons (it is difficult to study the coatings of fibres in extension mode) it is preferable to use the TMA7, which is suitable to follow glass transition changes.

3. Description of tests methods used for fibres characterisation

In the preceding paragraph we have studied different methods to characterise the cure and the physical state of free films.

Two methods are suitable, the FTIR one to study the degree of cure and TMA to follow glass transition. These two techniques will be used to study the coatings on a fibre.

3.1. FTIR

The principle of measurement for free films exposed in the preceding paragraph is used to study fibres.

The sample is prepared by cutting the fibres into 36 pieces of about 150 mm. These pieces are then aligned with an apparatus elaborated in our laboratory and transferred on a rectified steel substrate. They are maintained with an adhesive (figure 7).

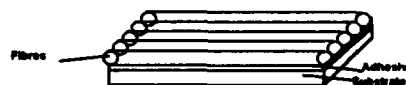


Fig. 7: sample for infrared measurements

This array of 36 fibres correctly aligned is then placed on one side of the crystal of the FTIR spectrometer. To increase the reproducibility of the measure we use a dynamometric screwdriver. It is then possible to determine the degree of cure of different fibres with a good repeatability ($\pm 1\%$). Figure 8 represents spectra obtained for different fibres.

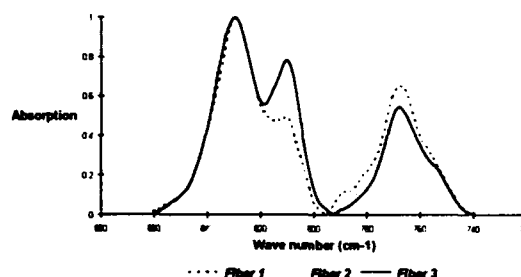


Fig. 8: FTIR spectra for different fibres

Degree of cure, calculated with equation (3), are for fibre 1: 95%, fibre 2: 90% and fibre 3: 78%.

FTIR technique is a good one to determine the degree of cure but only measure the outer surface (about $3\mu\text{m}$ thick) of the coating. Therefore, by performing an abrasion of the array of fibres (figure 9) we can see if the cure is the same after removing some micrometers of the coating.

The abrasion system is described in figure 9. It consists of putting the sample in translation under a weight and to guide it in a groove. At each pass, the abrasive is replaced to avoid glazing the sample. The choice of the abrasive is very important, it is preferable to use a very fine one, not to tear off the polymer.

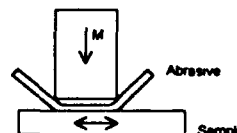


Fig. 9: Abrasion system

This method allows the outer coating to be removed after some passes and to give access to the inner layer of the fibre. The precision of the removed thickness is $\pm 5 \mu\text{m}$.

Figure 10, shows the infrared spectra obtained for different abrasions (removed thicknesses vary from $0 \mu\text{m}$ to $51 \mu\text{m}$).

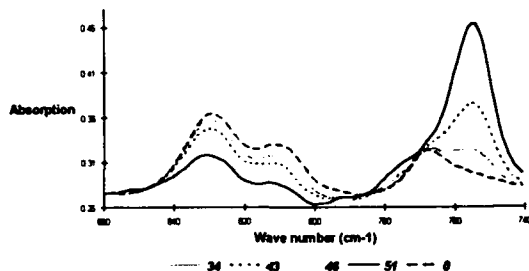


Fig. 10: infrared spectra for different abrasion.

The more the sample is abraded, the more the intensity of the 830 cm^{-1} peak (referred to the outer layer) decreases and the intensity of the 755 cm^{-1} peak (related to the inner layer) increases.

The abrasion method cannot be used to determine the degree of cure of the inner layer because infrared bands used to quantify inner and outer coatings are the same (810 cm^{-1}).

On the other hand, this method can be used to verify the good bulk-cure of the outer coating. Some experiments have been done and show there is no significant changes of the degree of cure when $15 \mu\text{m}$ of outer layer are removed.

Another interest of the abrasion method, is that it can be used to remove the coloured coating on fibres extracted from a cable.

Figure 11, shows the spectra of a coloured fibre before and after abrasion.

Before abrasion, it is impossible to determine the degree of cure because the infrared bands of the colorant mask the bands used to quantify the outer coating. After removing about $15 \mu\text{m}$, effects of the coloured coating become negligible and the degree of cure can be calculated (89% for the fibre represented in figure 11)

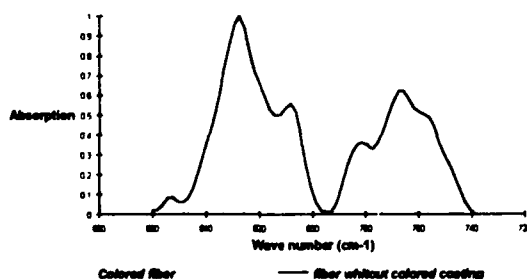


Fig. 11: spectra of a coloured fibre

FTIR method is a suitable one to measure the cure of a fibre; abrasion method allows analysis of the polymerisation inside the materials.

3.2. Thermomechanical analysis

The principle to measure thermomechanical properties of fibres is as follows: a piece of fibre of about 10 mm length is placed under the quartz probe of the TMA7 instrument. The sample is then heated from -50°C to 150°C with a rate of $5^\circ\text{C}/\text{min}$. The force applied is 100 mN. We obtain curve of penetration versus temperature like the one illustrated in figure 12.

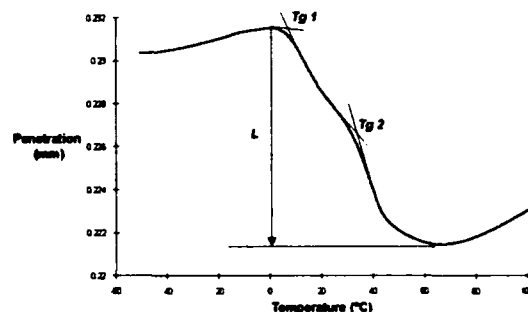


Fig. 12: typical TMA curve

After an expansion of the sample, we note two changes of slope which correspond to the glass transitions of the primary ($Tg1$) and the secondary ($Tg2$) coatings. L parameter represents the dimensional variation of the coating during the glass transition.

This test has a good repeatability on condition that sample preparation is performed with great care. Standard deviation for the glass transitions determination is lower than 3°C .

The same fibres represented in figure 8 have been studied with TMA7 instrument (figure 13).

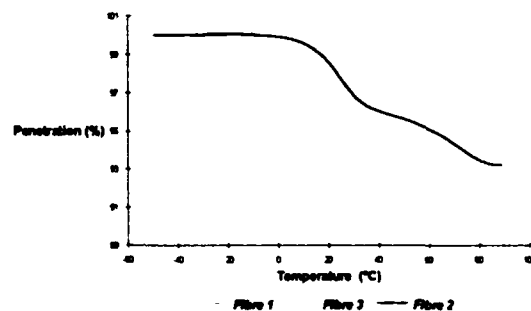


Fig. 13: TMA curves of different fibres

The different parameters are listed in the table 2.

	Fibre 3	Fibre 2	Fibre 1
Tg1 (°C)	10	14	15
Tg2 (°C)	/	57	58
L (%)	10,2	6,8	4,9
% Cure (FTIR)	78	90	95

Table 2: TMA data for three different fibres

The glass transitions temperature can not be used to see the difference of cure except for fibre 1 where we just note one transition (corresponding to the inner layer), the second one does not appear, probably because it is too close to the first temperature, which reveals an uncured system (confirmed with the infrared measurements). On the other hand, the dimensional parameter (L) seems to be a good parameter to compare the cure of different fibres. In fact, important penetration of the probe, reveals that the coating is softer.

4. Ageing in different environments

The actual design of optical cables requires the fibres to be embedded in an hydrophobic gel to avoid water infiltration. Jelly filled compounds actually used are composed of silicone or hydrocarbon oil, the jellification is obtained with pyrogenic silica treated to be hydrophobic. It is important to verify that both filling compounds and water do not affect the properties of the coatings. TMA and FTIR will be used to follow the coatings properties after ageing.

4.1. Ageing on free films

Outer and inner resins are cured to different levels and their mechanical properties (TMA) are studied after immersion in two filling compounds, A and B which are respectively hydrocarbon and silicon products, and in water during a few days at 23°C. The degree of cure of these samples are calculated with FTIR method. Results of Tg measurements for outer coatings are summarised in table 3:

% of cure		67	94
Reference Tg		27	57
Ageing in water	Tg	16	24
	ΔTg	-11	-23
Ageing in A	Tg	37	47
	ΔTg	+10	-10
Ageing in B	Tg	38	56
	ΔTg	+11	-1

Table 3: TMA results after ageing for outer coating

Uncured coating presents after ageing in filling compounds an increase in the Tg of about 10°C, which can be explained by the presence of a large amount of extractable materials⁽³⁾. In water, the Tg decreases, there is an affinity between water and coating which provokes a swelling of the coating. Correct cured coating presents also a swelling in contact with water and hydrocarbon filling compound. On the other hand, the silicon gel does not affect mechanical properties of correct cured coating.

Tg measurements for inner coatings after ageing are summarised in table 4.

% of cure		88	98
Reference Tg		18	19
Ageing in water	Tg	20	20
	ΔTg	+2	+1
Ageing in A	Tg	26	20
	ΔTg	+8	+1
Ageing in B	Tg	28	21
	ΔTg	+10	+2

Table 4: TMA results after ageing for inner coating

Inner uncured coating exhibits the same behaviour as the outer uncured coating after ageing in filling compounds: increase in the Tg value probably due to the extractable content. On the other hand water for both uncured and correct cured coating does not change the Tg value.

Correct inner cured coating presents no significant change after ageing in different compounds, in comparison with the outer coating which presents swelling in hydrocarbon gel and in water.

TMA data shows that the outer layer presents a larger affinity for water and hydrocarbon compound than the inner one and that the effects of environment vary with the cure of the coating.

4.2. Ageing on fibres

A lot of ageing tests have been done on correctly cured fibres, results are summarised in table 5:

Ageing	Tg1 change (°C)	Tg2 change (°C)	L change (%)
water	-3	-12	-1
A	-1	-13	-2
B	0	-1	0

Table 5: TMA variations after ageing

In contact with hydrocarbon jelly, a decrease in Tg2 and L values has been observed. The outer layer swells in

contact with this compound. On the other hand, the characteristics of the inner layer does not change. In silicon filling compound, no change occurs. This product presents a good compatibility with the coatings. Results on fibres are correlated with free films one for a correct cure. The ageing in different environment of undercured fibres is actually studied.

Figure 14 represents the effect of the water on a fibre.

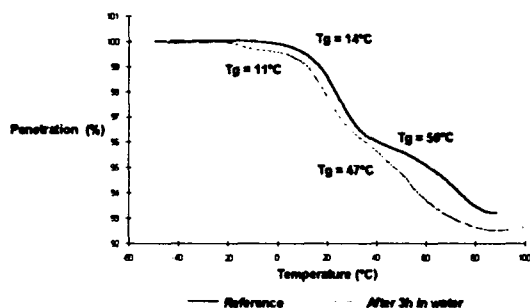


Fig. 14: TMA curves before and after ageing

We can note no significant change in Tg1 value after ageing in water. On the other hand there is a decrease of about 10°C of Tg2 which means the outer coating swells in contact with water. The dimensional parameter L increase after ageing, the coating becomes softer.

Some measurements of the coating stripping forces have been performed and show a decrease of the stripping force after ageing in water and hydrocarbon filling compound⁽⁴⁾. The results of thermal analysis allow us to say that this decrease is probably due to the swelling of the outer layer.

5. Conclusion

This study shows that UV-curable coatings of fibres can be sensitive to some environments such as hydrocarbon filling compound and water when they present a correct curing and when they are undercured their properties change not only in these products but also in silicon filling compound. Therefore it is really important to measure the degree of cure of fibres. The FTIR technique is a good one to calculate this parameter on fibre with or without a coloured coating.

The thermomechanical analysis allows the verification of no critical changes of the glass transition after ageing in various compounds. Results exposed in this paper show that the outer layer is less resistant to different environments, with which it can come into contact, than the inner layer which presents better behaviour for correct cured fibres.

6. References

- (1) Coating stripping force measurement: a new and quick test method for the determination of the degree of curing for optical fibre coating
H.Marsman, R. Wauben, G.Kuyt / IWCS 1991
- (2) The measurement of cure in optical fibres coatings
E F L D' Souza / British Telecommunications
- (3) Effect of chemical environments on UV curable optical fibre coatings
Chawla, Szum / IWCS 1991
- (4) Etude de la compatibilité des revêtements de fibres optiques avec différents produits de remplissage par analyse thermomécanique / comparaison avec les méthodes de dénudage
Y.Ruello, P.André, D.Crespel, E.Cressan, O.Fournier, A.Morgand, A.Peraudeau / OPTO 93

Acknowledgements

The authors thank M. Poulain, professor at the University of Rennes in France for his helpful criticism, and A. Le Pollès, O. Guyomard for the measures they had performed during their laboratory course.



Emmanuelle Cressan was born in France, in 1967. She received in 1991 her **MAGISTERE MATERIAUX** degree (physics and chemistry of materials) and **DEA degree** (Diplome d' Etudes Approfondies) in solid chemistry from the university of Rennes, France. In 1991, she joined the laboratory of the CNET to prepare her Ph.D. degree.



Patrick André received his thermal technician degree in 1987. He joined CNET in 1988 where he was involved in specifications and tests studies for materials used in optical cables and accessories.



Alain Peraudeau received his chemical technician degree in 1977. He joined CNET in 1982 where he was involved in specifications and tests studies for materials used in optical cables and accessories.



Daniel Crespel received his mechanical technician degree in 1965. He joined CNET in 1966; he has been participating in several studies such as copper and fibre wave guide, optical fibre splices and connectors.



Yves Ruello received his engineering degree from Ecole d'Application des Hauts Polymères of Strasbourg in 1981 and joined CNET in 1983. He is in charge of Splicing and Materials group where responsibilities consist in studying new materials and splicing technics, performing tests and establishing specifications.



Odile Fournier was born in France in 1957. She received in 1981 her diploma of engineer in science of materials from Montpellier, France. She joined the CNET in 1982 to study telecommunications cables and cables materials.



Annie Morgand, born in Lannion, France, in 1968, is specialised in Physics and Chemistry of Materials. She joined CNET to study optical cable materials after obtain her diploma of Engineer in science of materials in 1991.

THE EFFECTS OF AGING ON THE DISCERNIBILITY OF THE COLOR IDENTIFICATION OF OPTICAL FIBERS

Rolf A. Frantz* and Irene M. Plitz†

*Bellcore, Morristown, NJ; †Bellcore, Red Bank, NJ

ABSTRACT

Optical fibers in cables are identified using standard color codes specified by the Electronic Industries and Telecommunications Industry Associations. These are intended to ensure that each fiber color from any cable supplier can be easily matched to the same fiber color from any other supplier, throughout the cable service life. However, the defined tolerances on these standard colors are so broad that each color can be visibly different among suppliers. Cable manufacturers choose from a variety of ink types, suppliers, and application techniques. Additional variability is added by the fiber coating material (and for ribbons, the matrix material). Transparent inks, formulated for use with fiber-contacting devices, further expand the range of visual differences. Finally, all colors undergo changes due to aging. This paper explores the variability and discernibility of fiber colors and how they are affected by various aging conditions.

INTRODUCTION

Color coding inks are applied to the outer surface of polymer-coated optical fibers to identify them when they are grouped together in cables. These inks may be solvent-based and cured by heat, or they may be totally reactive and cured by exposure to ultraviolet (UV) light. They may be formulated to be opaque or transparent; the latter are particularly desirable for use with light injection/detection devices, fiber identifiers, and similar fiber-contacting instruments. An ink may bond strongly to the outer surface of the fiber coating, or it can form a separate layer that may not adhere well. This bond governs how easily the ink can be removed from the fiber, either intentionally (e.g., to connect a fiber identifier) or unintentionally (while handling fibers to separate them for individual connection or splicing).

Cable manufacturers typically buy uncolored fiber and color code it as needed for ongoing cable production. The choice of the inking technology (solvent-based or UV-cured, transparent or opaque) rests with, and varies among, cable manufacturers. Regardless of the technology used, however, color coding must ensure distinct identification of each fiber by its own unique color throughout the service life of the cable. As fiber ages, not only can the ink color change, but so can the color of the underlying polymer coating and, in the case of ribbon fiber, the color of the ribbon matrix material (edge-bonding or encapsulating). This can cause problems in identifying specific fibers in an older splice case or pedestal. In addition, the conditions under which the fibers are seen in the field—for example, the lighting, the background, and the possible presence of a residual film of buffer tube gel—introduce additional biases into the perception of each fiber color. Reports coming to Bellcore suggest that field personnel usually do an excellent job of identifying each fiber; however, small departures from the norm in any of the factors affecting the perceived fiber colors can quickly cause problems when two or more fibers cannot be uniquely identified by their colors.

Twelve colors, listed in Table 1, have been defined for coding optical fibers. The first ten were defined by the Electronic Industries Association (EIA) over thirty years ago for color coding electronic components and copper wire and cable insulation. EIA Standard RS-359A, "EIA Standard Colors for Color Identification and Coding," gives detailed specifications for these colors.^[1] The last two colors were recently added to address the need to identify optical fibers bundled in multiples of 12 fibers. EIA/TIA (Telecommunications Industry Association) Standard EIA/TIA-598, "Color Coding of Fiber Optic Cables," gives specifications for these colors.^[1] All colors are specified by centroid or "target" values and by allowable tolerances about these values. The intent of these standards is to ensure that all manufacturers use the same colors to identify fibers in their cables.

Subsequent sections of this paper discuss ways of describing colors and the use of color measuring instruments to address perceptual problems that have limited previous attempts to define allowable color changes. We examine the variability of the initial colors of color-coded fibers and quantify the color changes that occur during aging under various conditions. We present thermal stability data that correlate with the chemical changes accompanying discoloration. Finally, we explore how large color changes can be yet still maintain the discernibility of different colors after aging.

COLOR DESCRIPTION AND MEASUREMENT

Color description and measurement mix art and science. The Munsell notation used by engineers to communicate common specifications for color^[2] was developed by the American artist A. H. Munsell. The perceived color of an object is biased by the light source, as anyone who has looked at the same article of clothing under fluorescent light, incandescent light, and sunlight can attest. Also, the color perception of individuals differs; color blindness is only the most obvious of a variety of color perception deficiencies. Even limiting attention to the object itself, the perceived color depends upon its surface gloss and its transparency, as well as on its inherent color.

Color Spaces

Color has three attributes: *lightness*—how black or white it is; *hue*—whether it is "red," "yellow," "green," "blue," etc.; and *chroma*—how vivid it is. Color can thus be described in a three-dimensional space as shown in Figure 1. *Lightness* ranges from black to white along the z-axis; *hue* and *chroma* locate a color in an x-y plane. Munsell notation describes the location of a color in this space. *Lightness* has a scale of 1 (black) to 10 (white). *Hue* (the angular location in the x-y plane) is described as being Red, Yellow-Red, Yellow, Green-Yellow, Green, Blue-Green, Blue, Purple-Blue, Purple, or Red-Purple. Within each hue family there are ten steps. *Chroma* describes how far a color is radially from the z axis; 0 chroma is neutral ("N") white, gray, or black. Munsell notation gives the hue first, followed by

TABLE 1. EIA CENTROID COLORS FOR OPTICAL FIBER COLOR CODING

COLOR NAME	ABBREVIATION	MUNSELL DESCRIPTION	L*, C*, h COORDINATES	L*, a*, b* COORDINATES
Red	RD	2.5R 4/12	41.22, 54.89, 16.67°	41.22, 52.59, 15.74
Orange	OR	2.5YR 6/14	61.70, 79.31, 58.57°	61.70, 41.37, 67.67
Brown	BR	2.5YR 3.5/6	35.98, 34.30, 50.09°	35.98, 22.01, 26.30
Yellow	YL	5Y 8.5/12	86.21, 86.78, 93.20°	86.21, -4.87, 86.62
Green	GR	2.5G 5/12	51.58, 69.56, 155.42°	51.58, -63.26, 28.93
Blue	BL	2.5PB 4/10	41.22, 40.92, 267.13°	41.22, -2.06, -40.86
Violet (Purple)	VI	2.5P 4/10	41.22, 45.11, 310.86°	41.22, 29.52, -34.11
White	WH	N 9/	91.08, 0, —	91.08, 0, 0
Slate (Gray)	SL	N 5/	50.94, 0, —	50.94, 0, 0
Black	BK	N 2/	20.56, 0, —	20.56, 0, 0
Rose	RS	10RP 8/6	81.35, 24.62, 14.55°	81.35, 23.83, 6.18
Aqua	AQ	10B 8/6	81.35, 27.22, 245.74°	81.35, -11.19, -24.81

the lightness (called "value"), a slash, and the chroma. For example, 2.5R 4/12 is a Red color tending slightly toward Red-Purple, fairly dark (4/10 of the way from black to white), and quite vivid (maximum chroma varies with hue, but never exceeds 16). Munsell notations for the EIA centroid colors are given in Table 1. Tolerances on the hue, value, and chroma attributes for wire and cable products are shown in Table 2.

Other notations may be used to describe this same color space. In L^*C^*h coordinates, shown in Figure 1, L^* is the lightness (on a scale of 0–100), C^* is the chroma (again varying with hue, but rarely exceeding 100), and h is the hue angle (with red at 0°, yellow at 90°, green at 180°, and blue at 270°). $L^*a^*b^*$ notation uses an xyz coordinate system: L^* is again lightness, while a^* and b^* define the x and y axes as shown in Figure 1. Values of $a^*<0$ imply a green quality, while $a^*>0$ implies red; similarly, $b^*<0$ implies blue, while $b^*>0$ implies yellow. L^*C^*h and $L^*a^*b^*$ descriptions of the EIA centroid colors are also given in Table 1.

Color Measurement

The accepted industry technique for assessing the colors of coded optical fibers is visual matching to samples of the Munsell standard centroid and tolerance colors. The use of a standard lighting source, viewing angle, background or environment, and color-matching swatches, together with trained observers, have refined this technique so that it is largely successful. Nonetheless, color matching involves subjective judgments that are open to disagreements.^[3] In addition, Bellcore documents allow no discernible changes in color during product qualification aging tests^[4]; any change must be too small to be determined reliably by Munsell matching. Since field personnel identify fiber colors visually, Munsell matching should be the final authority for the acceptance of color-coded fiber. However, colorimetry offers advantages for batch-to-batch quality control and for the measurement of color changes during aging. Long-term comparison studies have shown that colorimeters accurately and reproducibly report differences between samples.^[5] These differences may be smaller than those perceptible by eye.

Modern colorimeters often allow the user to control the spectral distribution of the light source and the color space in which the data are presented, and to calibrate using color reference chips. Available light spectra include International Commission on Illumination (CIE) standards C and D₆₅ for daylight. By using illuminant C for all measurements, we obtained Munsell coordinates from the colorimeter, which enabled us to reference the EIA/TIA standards and perform confirmation matches against Munsell color chips. We used $L^*a^*b^*$ coordinates to express color differences because of the simplicity of the calculations. Finally, we used Munsell color chips of the EIA/TIA centroid colors as calibration references for the meter.

Meter illumination/viewing geometry is usually 45°/0° or diffuse/8°. In the former, light is directed at either a 45° angle or a 0° angle to the surface, with the detector positioned at the complementary angle to avoid specular (mirrorlike) reflection from glossy surfaces. This can also be accomplished using diffuse illumination, in which the light comes from all angles within a white reflecting sphere and the detector is placed 8° (typically) off the vertical from the surface. All measurements in this paper used a 45°/0° colorimeter. Confirmation checks were made by repeating some measurements with a diffuse/8° meter.

INITIAL COLOR VARIABILITY

Color coded fibers from different manufacturers can differ significantly in their renditions of the standard colors. Table 2 summarizes the results of colorimeter measurements on samples of colored fiber from five suppliers. For all measurements reported in this paper, the samples consisted of double layers of colored fiber orthogonal to each other. A white background was chosen because some colors were relatively transparent and the light reflected from the white surface back through the fibers enhanced the hue and chroma readings. Three measurement locations were selected at random over the 1/4"-square sample area; the meter averaged three readings at each location. Meter repeatability at any one location was within 0.02 units for L^* , a^* , and b^* . Each data point thus is the average of nine individual measurements. An advantage of the $L^*a^*b^*$ (and L^*C^*h) color space is that such mathematical averaging can be done; the Munsell averages reported in Table 2 could only be determined by converting the $L^*a^*b^*$ averages reported by the colorimeter.

FIGURE 1. THREE-DIMENSIONAL DESCRIPTIONS OF COLOR SPACE

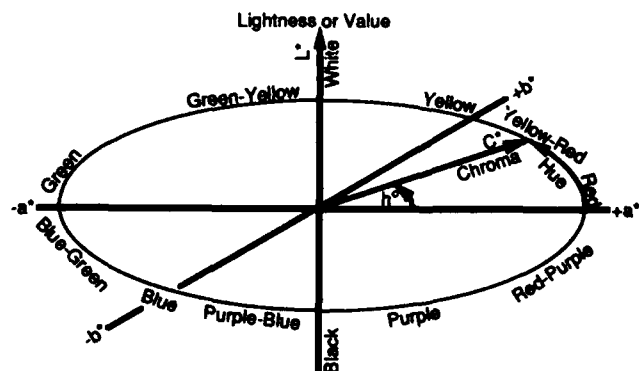


TABLE 2. VARIATIONS IN FIBER COLORS AMONG SUPPLIERS

COLOR	TOLERANCE RANGE	SUPPLIER 1	SUPPLIER 2	SUPPLIER 3	SUPPLIER 4	SUPPLIER 5
Red	10RP-5.5R 3.5-5.2±10	0.7R 3.7/11.0	1.4R 3.9/13.1	0.1R 3.4/11.0	4.4R 2.4/7.0	6.8R 4.4/12.8
Orange	10R-5 YR 5-7±10	2.2YR 5.9/13.4	1.7YR 5.9/12.9	9.4R 5.8/14.3	9.5R 5.0/14.0	1.5YR 5.6/11.1
Brown	7.5R-7.5YR 2.5-4.5/4.5-8	0.2YR 3.8/7.8	2.5YR 3.2/4.5	3.9YR 3.8/3.7	4.4YR 2.3/2.4	0.2YR 3.4/6.6
Yellow	1.25Y-8.75Y ≥7.5/≥8	4.4Y 7.8/12.5	6.2Y 8.0/12.4	2.1Y 8.0/13.2	2.6Y 7.3/14.4	5.4Y 8.0/13.0
Green	9GY-5G 4-6/≥8	2.8G 4.0/8.8	2.6G 4.7/9.8	3.2G 4.6/7.6	8.2G 3.9/9.6	0.2G 5.1/10.2
Blue	7.5B-5PB 3-5.2/≥8	1.6PB 3.3/7.6	3.2PB 3.8/10.2	4.9PB 3.6/10.2	5.7PB 2.4/10.0	1.9PB 4.2/11.1
Violet	10PB-5P 3-5.5/≥5.5	4.7P 4.2/5.8	3.7P 3.6/8.2	3.0P 4.5/9.4	1.8P 2.0/8.8	3.3P 3.9/6.2
White	N ≥8.75/0-0.5 or 1	0.3GY 8.6/0.8	6.4Y 8.6/0.9	6.6Y 9.0/0.6	4.0GY 8.5/1.0	6.4Y 8.9/1.2
Slate	N 4.5-6/0-0.5	8.9B 5.6/0.4	8.2B 4.6/0.8	0.6Y 4.2/0.0	2.8G 4.2/2.2	6.7BG 4.4/0.2
Black	N ≤2.3/0-0.5	1.2GY 1.8/0.2	N 1.8/0.0	6.1Y 1.9/0.0	4.9Y 1.7/0.2	7.6PB 1.6/0.2
Rose	7.5RP-2.5R 7-(8)/4-(6)	1.9R 7.3/5.0	9.5RP 6.6/7.2	3.1R 6.9/7.4	6.6RP 5.2/12.8	3.7R 5.5/7.4
Aqua	(10B)-2.5PB 7-(8)/4-(6)	8.6B 7.2/4.7	8.6G 6.2/4.2	6.4B 7.0/6.7	4.1B 5.2/8.3	2.5BG 6.8/6.0

The tolerance ranges in Table 2 are those allowed for wire and cable products in EIA/TIA standards 359A and 598. The italicized numbers in parentheses for Rose and Aqua estimate tolerances as yet unspecified; the numbers are comparable to the tolerances for other non-neutral colors.

The colorimeter measurements correlate to fractional Munsell numbers that cannot be matched using a standard set of Munsell color chips. However, by interpolating between standard chips, we were able to confirm the correlation for a few fibers from each supplier.

The bold-faced italicized numbers for various fibers indicate attributes that lie outside the defined tolerance ranges. At least three colors from each manufacturer fail to meet one or more specified tolerances; in some cases two or even all three attributes are outside these tolerances.

Rose and Aqua are clearly troublesome. Part of this is that they are relatively new colors and manufacturers have had limited experience with them. In addition, Aqua has been the subject of some controversy in its interpretation: the specification in EIA/TIA-598 is a pale blue, while many people interpret the term "Aqua" to imply a blue-green hue. Agreement on a revised definition of Aqua appears imminent, so this problem should be eased. The variations in Rose that are apparent in Table 2 suggest that it may also be desirable to further refine this color.

Even when an attribute of a color is within tolerance for all manufacturers, the colors supplied can be quite different. Of particular concern are the hue ranges for Red and Yellow, which are both greater than four units. While differences in chroma and value are often psychologically accepted as "brighter," "darker," or "lighter" versions of a single color, human perception is relatively intolerant of hue differences. All of these colored fibers are individually discernible and identifiable by name as Red, Orange, Brown, etc.; however, problems arise when cables from more than one manufacturer are terminated at a common location.

COLOR CHANGES DURING AGING

The discernibility of fiber colors is adversely affected by aging. The amount of discoloration depends upon time, temperature, and the immediate environment (e.g., dry air, humidity, buffer tube gel) around the fibers. The extent to which coating discoloration shows through the ink depends upon the thickness and opacity of the ink layer. We aged samples under a variety of conditions to assess the impact of these factors.

Color changes are reported as ΔE s—the linear distances between two colors, in this case the initial and aged colors. ΔE is calculated from the differences in the orthogonal $L^*a^*b^*$ dimensions:

$$\Delta E = \sqrt{(\Delta L^*)^2 + (\Delta a^*)^2 + (\Delta b^*)^2}$$

$\Delta E=1$ represents the smallest change that most people can detect in a pastel color (Rose, Aqua); for light, bright colors (Yellow, Orange), a ΔE of 2-3 may be just discernible, while for dark colors (Blue, Violet), ΔE must be ≥5 to be discernible. Large ΔE s should be viewed in the context of the tolerances and separations of the EIA/TIA standard colors. The tolerances in Table 2 represent ΔE s from the centroid colors of roughly 10-12 in chroma and value. ΔE s for hue vary, since the distance depends upon the hue change (angle) and the chroma (radius); the numbers generally range from 10-15, but are as small as 5 (Violet) and as large as 28 (Green). The distances between centroid colors are typically >50, although for certain color pairs (Red-Brown, Slate-Black, Blue-Violet), ΔE is just over 30.

Fiber Samples

We measured the color changes of fibers in Table 2 after aging in 85°C dry air for a month. We also measured samples from two suppliers after aging in cables or in buffer tubes where they were surrounded by gel. One of these aging tests was conducted in the laboratory, the other at a field site near Mesa, AZ.

TABLE 3. COLOR CHANGES (ΔE) FOR FIBERS IN TABLE 2 AFTER AGING 1 MONTH AT 85°C

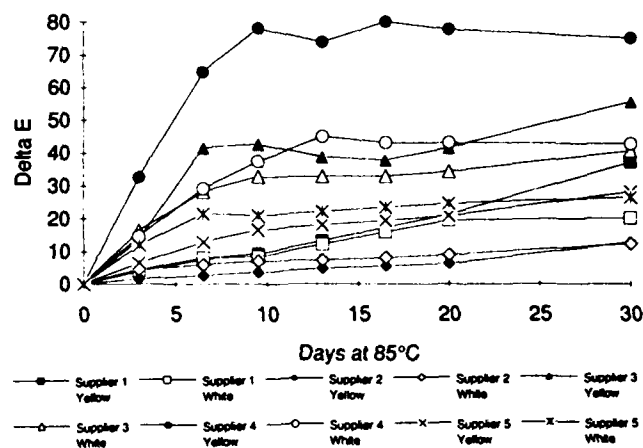
COLOR	SUPPLIER 1	SUPPLIER 2	SUPPLIER 3	SUPPLIER 4	SUPPLIER 5
Red	3.78	3.71	4.71	3.53	7.12
Orange	13.34	5.89	17.50	34.68	18.03
Brown	3.77	1.17	14.47	5.03	3.77
Yellow	36.92	12.57	55.51	74.92	28.03
Green	6.10	4.52	17.81	32.20	20.79
Blue	12.24	12.65	11.47	35.17	31.52
Violet	14.30	4.67	15.08	37.70	13.92
White	20.05	12.22	40.45	42.57	26.31
Slate	0.92	0.44	8.10	26.13	5.53
Black	1.01	0.43	4.19	1.26	2.07
Rose	6.08	4.12	15.39	33.07	18.77
Aqua	17.19	3.46	26.81	44.35	21.03

The color changes due to 85°C aging in air are summarized in Table 3. The most stable colors were those from supplier 2: the color changes in the Red, Brown, Green, Violet, Slate, and Black samples were very difficult to detect by eye. At the other extreme were the samples from supplier 4: only the Red, Brown, and Black samples were minimally changed, while the Yellow and White samples changed so much that they were almost impossible to identify visually. All of the changes in the Rose and Aqua samples were readily

discernible by comparison to the unaged fibers; however, except for supplier 4, these colors were easily identifiable after aging. Supplier 4, in an effort to develop colors that facilitate the use of fiber-contacting devices, used inks that were noticeably transparent compared to the other four suppliers. The colors from suppliers 1, 3, and 5 lie between the extremes; the dark colors (Brown, Slate, Black) showed relatively small changes, whether gauged by meter or by eye, while the lightest colors (Yellow, White) showed distinct color changes after aging.

The color changes in these Yellow and White fibers are plotted in Figure 2 as a function of aging time. Plots for other colors from each supplier are similar in shape, but generally with smaller ΔE s. The fibers from suppliers 1 and 2 show a slow but steady increase in their discoloration over time, while the fibers from suppliers 3, 4, and 5 experience most of their color change in the first week and are relatively stable after that time. Given sufficient aging time, the discoloration of the former fibers may match or even exceed the discoloration of the latter fibers. This emphasizes that color discernibility should only be assessed after aging under conditions and for a time period that appropriately simulate the effects and duration of the service life of the fibers.

FIGURE 2. DISCOLORATION OF SELECTED FIBERS DURING AGING



We also removed the ink from sample fibers from each of the five suppliers after aging them at 85°C for one month. Table 4 lists the resulting color changes, which are generally consistent with the results in Figure 2. Fibers from suppliers 1 and 2 showed little color change in either the de-inked or colored state; fibers from supplier 4 showed large changes in both cases. The large ΔE of the de-inked fiber from supplier 5 is apparently well masked by many of the ink colors, as shown by the small ΔE s in the last column of Table 3.

TABLE 4. COLOR CHANGES (ΔE s) FOR DE-INKED FIBERS AGED ONE MONTH AT 85°C

SUPPLIER	ΔE
1	2.05
2	3.33
3	7.95
4	12.12
5	14.05

Cables from supplier 3 were stored outdoors in Mesa, AZ. The color changes after 17 months of aging are summarized in Table 5. The "Bare" fiber data are for the bare sections of the Orange striped and Blue striped fibers used prior to the adoption

of Rose and Aqua. Not surprisingly, the ΔE for Yellow is large, while the ΔE s for Slate and Black are small. Even with a ΔE of almost 17, the Yellow fiber was discernible as Yellow, albeit a dark, dull shade that was perceived as degraded. The large ΔE s for the Orange and Brown fibers are due in part to a loss of color resulting from flaking and peeling of the ink when the samples were removed from the buffer tube and the excess gel was wiped off. Although only observed with these fibers, this raises another aspect of discernibility: inks must remain on the fibers to be effective for identification. The changes in the remaining colors, while visible and measurable, did not significantly affect their discernibility.

TABLE 5. COLOR CHANGES (ΔE s) FOR FIBERS AGED IN CABLE FOR 17 MONTHS IN MESA, AZ

COLOR	ΔE
Bare	8.78
Red	4.29
Orange	13.65
Brown	7.05
Yellow	16.94
Green	4.12
Blue	6.13
Violet	3.48
White	6.64
Slate	2.06
Black	2.83

The last aging tests were done with samples from supplier 5 both in air and in buffer tube gel for 14 days at 85°C. As shown in Table 6, there were noticeable differences in the discolorations under these conditions. The second column gives the ΔE s for fibers that were removed from the buffer tubes and wiped clean of gel. The ΔE s in the third column are for fibers that were removed from the buffer tube but aged without wiping off any gel. The fourth column represents fibers aged in the gel inside the buffer tube. For all colors, leaving the gel on the fibers significantly increased the color change. Enclosing the fibers in the buffer tube resulted in even greater color changes for eight of the ten colors. These results suggest that the gel interacts with the inks and/or the coating. This is substantiated by comparison to the last column in Table 3: nine of the ten fibers had larger ΔE s after 14 days of aging in buffer tubes than after a month of aging in air. We observed similar discolorations in a previous study of the interaction between fiber coatings and buffer tube gels.⁽⁶⁾ This interaction is another aspect of color stability and emphasizes the need to perform aging tests under different conditions to represent all field service environments (cables, sealed closures, breathable pedestals, etc.).

TABLE 6. EFFECTS OF GEL ON COLOR CHANGES (ΔE s) AFTER TWO WEEKS AGING AT 85°C

COLOR	GEL WIPED OFF	RESIDUAL GEL LAYER	AGED IN BUFFER TUBE
Red	5.70	10.40	23.64
Orange	8.18	17.66	30.67
Brown	8.26	24.57	16.88
Yellow	26.03	35.09	48.43
Green	13.93	23.04	41.41
Blue	8.20	11.63	24.93
Violet	8.19	12.69	23.85
White	22.93	26.12	38.16
Slate	2.26	5.06	9.08
Black	4.36	6.12	2.78

Film Samples

One difficulty with testing fibers is that, while the ink can usually be removed to measure the discoloration of the coating, the coating cannot be removed from the ink to isolate the changes in the ink alone. We have started a program of testing that will involve films of secondary coatings, films of secondary coatings with different inks applied, and eventually films of inks alone. Our first test involved aging a set of films representing the ten original color codes in EIA/TIA-359A. These films were made of a 150 μm thick layer of a standard secondary coating with an approximately 5 μm thick layer of UV-curable ink applied to one surface. The films were aged in 85°C dry air, in an 85°C/85% RH environment, and also immersed in two different buffer tube gels (polypropylene glycol based and paraffin based) in closed containers in an 85°C oven. The color changes resulting from these aging conditions are summarized in Table 7.

TABLE 7. COLOR CHANGES (ΔE s) FOR FILM SAMPLES AFTER 28 DAYS AT 85°C IN VARIOUS AGING ENVIRONMENTS

COLOR	DRY AIR	85% RH	PARAFFIN GEL	
			GEL	GEL
Red	0.69	10.65	1.96	9.72
Orange	2.55	3.26	1.07	0.85
Brown	3.18	7.88	2.91	*
Yellow	4.20	9.67	3.07	6.60
Green	2.95	2.87	4.11	12.75
Blue	2.79	2.41	1.69	2.21
Violet	3.57	4.44	1.27	2.42
White	5.12	6.61	8.62	10.10
Slate	0.84	5.15	2.26	4.41
Black	1.31	1.06	4.97	4.61

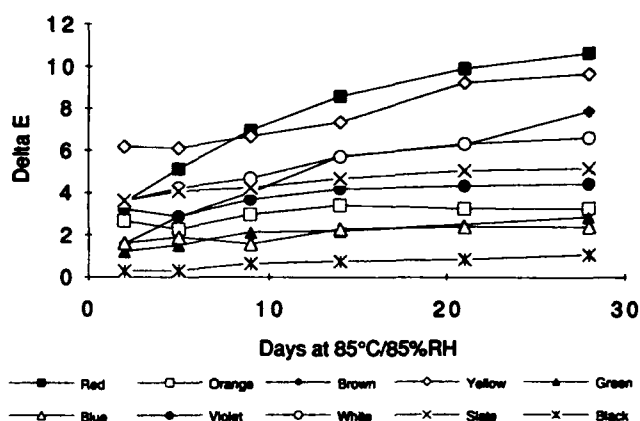
*Sample removed from aging after 14 days when ΔE reached 26.5.

For most colors, aging in the 85% RH environment caused greater color changes than aging in dry air. Similarly, aging in the polypropylene glycol gel usually caused greater color changes than in the paraffin gel. The former gel took on a yellowish tint around the Brown, Yellow, and Green film samples after the first week of aging, suggesting it was dissolving these inks. The Brown sample, in fact, rapidly changed color, becoming lighter (partly through loss of ink) and tending toward an olive drab color. When it was removed from aging after two weeks, its ΔE was over 26, and it was no longer identifiable as Brown. Fibers exposed to this gel in our previous study⁽⁶⁾ did not show such an effect; the reaction is apparently specific to this ink formulation. All of the other samples, including those with ΔE s of 10–13, were readily identifiable as their original colors after 28 days of aging in each environment.

As with the fiber samples from suppliers 3–5, these films experienced most of their color change during the first week to ten days, except when aged in the 85% RH environment. As Figure 3 shows, this environment caused many of the colors to continue to change throughout the 28-day exposure. Although not all colors show the large rate of change displayed by Red and Yellow, a slow increase in ΔE indicates that some degradation is continuing to occur. The differences may be due to differences in the formulation of the individual ink colors, for example, the choice of pigment binder, the pigment concentration, the "wetting power" of the ink on the coating surface, the thickness and opacity of the final ink layer, etc. These results again emphasize the need to test all inks in all service environments to fully understand the potential for color changes.

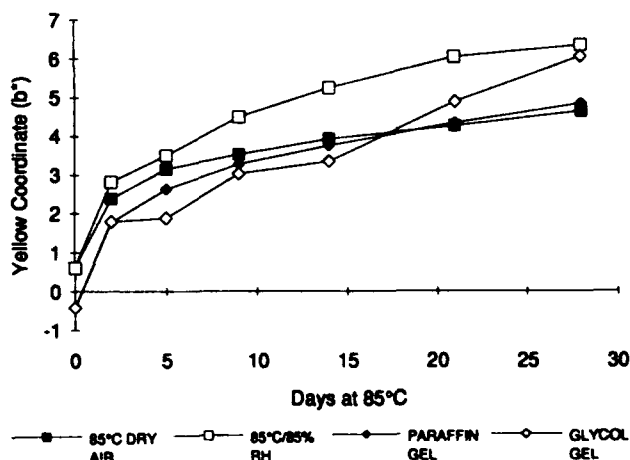
It is important to understand the direction of the color change as well as its magnitude. In all cases, these ink films showed a

FIGURE 3. COLOR CHANGES FOR FILM SAMPLES DURING 85% RH AGING



tendency to yellow. Figure 4 shows this increase in yellowness, as measured by the change in the b^* coordinate, for the White films aged in all four environments. Not all films were as well behaved in demonstrating a monotonic increase over time, but the end results were generally similar. In this figure, we have plotted the actual b^* coordinate of the color, rather than the change in color as in the previous plots. The two different starting coordinates reflect the differences between samples taken from different parts of the ink/coating sheet; the fact that such differences occur is again an argument for measuring color differences rather than absolute colors to track the aging and discoloration. The final b^* values (roughly 4–6) are not large, considering that b^* exceeds 100 for the bright Yellow ink film, but they are large enough to be perceived as a noticeable dulling of the White ink due to the aging.

FIGURE 4. YELLOWING OF WHITE FILM UNDER VARIOUS AGING CONDITIONS



THERMAL STABILITY EFFECTS

Thermal oxidative degradation is one mechanism that may cause optical fiber coatings to yellow.⁽⁷⁾ If the ink layer is not thick or opaque enough to mask this yellowing, the fiber coating can contribute to the color changes we observed during aging.

We monitored the oxidative stability of the coating by measuring the onset temperature for oxidation while heating the sample in a differential thermal analyzer under an oxygen environment. Approximately 15–20 mg of fiber was heated from 35°C to 300°C at a rate of 10°C/min. under a constant oxygen flow. The oxygen onset temperature was recorded as the temperature at which oxidation began. Multiple measurements were reproducible to within $\pm 1\%$.

Table 8 presents the oxygen onset data for unaged fibers and for fibers aged one month in dry air at 85°C. The data for the unaged fibers show that suppliers 1 and 2 used fiber coatings that are more thermally stable than the others. For the fibers from suppliers 3–5, the oxygen onset temperatures decreased after aging, while the coatings used by suppliers 1 and 2 retained their higher stability. This is consistent with the results in Table 3, where the ΔE s for fibers from suppliers 3–5 are typically much larger than those for suppliers 1 and 2. The largest decrease in oxygen onset temperature occurred for the uninked fiber from supplier 5. This is consistent with the large ΔE reported in Table 4 for this fiber with the ink removed.

TABLE 8. OXYGEN ONSET TEMPERATURES (°C) FOR UNINKED, DE-INKED, AND SELECTED COLORED FIBERS

SUPPLIER	COLOR	BEFORE AGING	1 MONTH AT 85°C
1	Uninked	242	240
	De-Inked	—	240
	Aqua	234	229
2	De-Inked	—	238
	Yellow	—	232
	Blue	242	239
3	De-Inked	—	181
	Rose	182	169
	Aqua	187	178
4	De-Inked	—	167
	Violet	195	190
5	Uninked	205	189
	De-Inked	—	173
	Blue	178	178
	Rose	183	177

Table 9 summarizes the results for the fibers aged in gels. The data for supplier 3 are consistent with the ΔE measurements in Table 5. However, the data for supplier 5 suggest either that a different coating or inking process was used or that the color of the ink has a significant effect, since the oxygen onset temperatures for these unaged samples are about 12% higher than for the inked uncabled samples in Table 8. The changes in the onset temperatures after aging show about the same extent of degradation.

TABLE 9. OXYGEN ONSET TEMPERATURES (°C) FOR FIBERS AGED IN GEL

SUPPLIER	COLOR	UNAGED	AGED
3	Bare	170	172
	Orange	181	172
	Brown	182	174
	Yellow	209	—
5	Orange	208	190
	Yellow	206	—
	White	202	180

The data for the film samples are given in Table 10. The oxygen onset temperatures for the unaged samples indicate that the thermal stability of this coating is comparable to that of the fiber coatings used by suppliers 1 and 2. The only aged sample to show a visually significant color change was Brown; part of this change is due to ink removal by the gel. However, the discoloration is also consistent with the large decrease in the oxygen onset temperature, which is larger than that for any of the fibers from suppliers 1 and 2.

TABLE 10. OXYGEN ONSET TEMPERATURES (°C) FOR FILMS

COLOR	UNAGED	AGED
Brown	243	227*
Yellow	239	—
Violet	243	—
White	249	—
Black	240	—

* After 14 days at 85°C in polypropylene glycol gel.

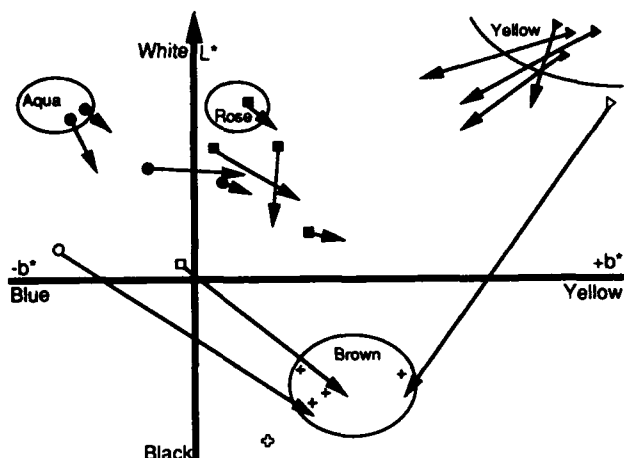
ALLOWABLE COLOR CHANGES

Fiber colors can and will change during the service life of a cable, but they must remain distinct and identifiable. A bright Yellow can be allowed to age to a darker, less vivid color provided that color can be easily recognized as "Yellow" when the fiber is bundled with other aged and discolored fibers. In practice, such identifications can be made even when the aged colors lie outside the EIA/TIA standard tolerance ranges. However, it is not sufficient that two colors simply be "different" (e.g., a light and a dark brown); each aged color must be readily traced to its original color. This means that no aged color can overlap into the space of another aged color. For well-separated colors such as Green and Blue, this is unlikely to be a problem. For closely-spaced colors such as Red, Orange, and Brown, however, an overlap might occur. Thus the restriction on allowed color changes during aging is that aged Red must remain visibly redder than aged Orange and aged Brown, while aged Brown must remain darker than any aged Orange, etc.

Examination of the color tolerances in EIA/TIA 359A and 598 suggests that an aged, end-of-life color could be at most one Munsell unit outside the tolerance limits on hue, value, or chroma. This avoids overlaps among aged colors except for Orange and Brown, which overlap in hue and are close in value initially. To keep these colors distinct, the value cannot get lighter for Brown or darker for Orange than the tolerance limits given in EIA/TIA 359A. Since one Munsell unit corresponds to a ΔE of about five, the total allowable change of three to four Munsell units (from the centroid to the tolerance limit and one unit beyond) corresponds to a ΔE of about 15–20. In practice, colors in Tables 3–7 with ΔE s >20 were visually quite changed by aging.

The aged colors are perceived as darker, duller, and browner. Figure 5 illustrates a cross-section of color space through the L^*b^* plane. The projections onto this plane of the allowed tolerance ranges for Yellow, Rose, Aqua, and Brown are shown. The arrows indicate how the L^* and b^* coordinates of the Yellow, Rose and Aqua fibers from the five suppliers moved toward Brown during one month of aging at 85°C. The transparent Yellow, Rose, and Aqua, represented by the open symbols, all moved into the tolerance range for Brown. The coordinates of the unaged Brown fibers, including the transparent Brown (open cross), are shown for reference. When intermixed, short lengths of the aged Yellow, Rose, and Aqua fibers and of the various unaged Brown fibers, while discernibly different, could not be readily identified as to

FIGURE 5. COLOR CHANGES OF SELECTED FIBERS
PROJECTED ON THE L*b* PLANE



supplier and original color. Thus, not only the magnitude of the color change, ΔE , but its *direction* should be known to ensure that the aged color remains distinct and identifiable.

SUMMARY

The series of measurements and tests described in this paper have shown that:

1. Colorimeters are useful tools for quantifying color differences and color changes. The numeric results agree with visual observations and psychological reactions to aged colors as "faded," "dull," "dark," "brownish," and often difficult to distinguish from each other.
2. A single fiber color from different suppliers can be visually quite different, even within the EIA/TIA tolerances, and initial colors do not always meet these tolerances.
3. Color changes can occur in coded fibers due to discoloration of the ink layer, the underlying coating, or both.
4. Color changes correlate with decreased thermal stability of the coatings, as evidenced by the decreases in the oxygen onset temperatures.
5. In some cases, the color change may be exacerbated because of flaking or peeling of the ink or because of an incompatibility with the environment—in particular, with the buffer tube gel.
6. Aging tests should include cable, closure, and pedestal environments, since the color changes that occur differ among these environments and all of them may be encountered in service.
7. ΔE is a useful quantifying measure of discoloration. It is a vector quantity, whose components of hue, value, and chroma clarify the nature of the color change. ΔE s of up to 20 from the centroid color may be acceptable except for Orange and Brown.
8. The ΔE allowed for any aging test depends upon the position of the original color relative to the centroid, the direction of the color change, and the duration and severity of the aging.

ACKNOWLEDGMENTS

We gratefully acknowledge the patience of John Parisi and David Dolinoy in making many of the color measurements.

REFERENCES

1. EIA/TIA standards are available from the Electronic Industries Association, Engineering Department, 2001 Eye Street, N.W., Washington, D.C. 20006.
2. *The Measurement of Appearance*, by Richard S. Hunter and Richard W. Harold, Wiley-Interscience, New York, Second Edition, 1987.
3. Private communications from Bellcore quality inspectors and telephone company personnel.
4. "Generic Requirements for Optical Fiber and Optical Fiber Cable", TR-NWT-000020, Bell Communications Research, Morristown, NJ, Issue 5, 1992.
5. "Standard Test Method for Calculation of Color Differences from Instrumentally Measured Color Coordinates," ASTM Standard D-2244-89, American Society for Testing and Materials, 1916 Race Street, Philadelphia, PA 19103, 1989.
6. "Fiber Coating Interactions with Buffer Tube Gels," by R. A. Frantz and I. M. Plitz, *Optical Engineering*, Vol. 30, No. 6, p. 767, June 1991.
7. "Thermo-Oxidative Aging of a Primary Lightguide Coating in Films and Dual-Coated Fibers," by D. A. Simoff, M. G. Chan, J. T. Chapin, and B. J. Overton, *Polymer Engineering and Science*, Vol. 29, No. 17, p. 1177, September 1989.

Rolf A. Frantz is a Distinguished Member of Technical Staff in the Fiber Distribution and Reliability Research Group at Bellcore. He holds BS and MEng degrees from Cornell University and received his PhD at Brown University. He spent eleven years at Bell Laboratories, working principally on applications problems of dielectric materials, and he continued working in this area when he came to Bellcore in 1983. Since 1988, he has been concerned with the applications and reliability problems of fiber coatings, adhesives, coloring inks, gels, and related materials used in manufacturing optical fibers, cables, connectors and splices.



Irene M. Plitz is a Member of Technical Staff in Bellcore's Plastics and Rubber Research Group. She graduated from Morgan State University in 1970 with a BS in chemistry and then joined AT&T Bell Laboratories. Since becoming part of Bellcore in 1983, Irene's interests have centered around the degradation, characterization, and reliability of polymeric materials used in the telecommunications industry.



THE MECHANICAL PERFORMANCE OF AGED DUAL-COATED FIBERS WITH VARYING EXTENTS OF COATING CURE

Hakan H. Yuce*, Rolf A. Frantz*, Osman S. Gebizlioglu†, Irene M. Plitz†, Tarja T. Volotinen‡

*Bellcore, Morristown, NJ, USA; †Bellcore, Red Bank, NJ, USA

‡Ericsson Cable, AB, Hudiksvall, Sweden

ABSTRACT

Polymer coatings are applied to optical fibers to provide protection against mechanical and environmental stresses. The protection afforded by a coating depends in part upon how well cured that coating is. Previous work on single-coated fibers has shown that lower extents of cure can lead to reduced fiber strength and poorer fatigue resistance. However, because the test fibers did not use dual-layer coatings, they were not representative of fibers typically installed in field service. In this paper, we extend our previous work to dual-coated fibers and demonstrate that our earlier conclusions about the effects of incomplete cure and of aging on fiber mechanical performance are directly applicable. The techniques used previously to measure the extent of cure of single-layer coatings are shown to be applicable to dual-layer coatings. Changes in glass surface morphology during aging are shown to correlate with the degradation of both the coating and the fiber strength.

INTRODUCTION

Improvements in the mechanical behavior of fibers have resulted from reductions in the size of flaws, such as surface abrasions and microcracks that are present in all glass fibers. This is achieved in turn by minimizing damage to the fiber during drawing and by applying protective polymeric coatings immediately after drawing. The initial strength of a fiber is determined by the size of the largest flaw present; the long-term strength is controlled by the slow growth of flaws in the fiber in the presence of stress and/or a corroding species in the environment. This latter process is known as fatigue (static and dynamic) in the literature on glass and as stress corrosion in other fields. High strength fused silica optical fibers, with strengths on the order of 800 kpsi, are characterized by a unimodal Weibull parameter m (~100) in short gage lengths. Nevertheless, these high measured strengths are less than half the theoretical strength of silica glass (~2000 kpsi), which can only be measured in inert environments. The lower measured strength of pristine fibers has been attributed to fatigue, i.e., flaw initiation and crack growth in the presence of chemical species in the test environment. Since polymer coatings are normally applied to protect the optical fiber against mechanical damage which degrades its intrinsic strength, the presence of chemical species on the fiber (glass) surface will be significantly affected by the properties of the coating. The influence of different polymer coatings on the mechanical characteristics of silica fibers has been extensively reported.^[1-11] In particular, the water absorption and adhesion to glass of the polymer coating were found to correlate with fiber strength and fatigue behavior^[6], and the coating chemistry was found to correlate with aging behavior.^[9]

Typical coatings are comprised of two layers: a soft inner layer that cushions the fiber against mechanical forces, and a stiffer, stronger outer layer that provides environmental protection and helps to distribute localized mechanical loads. In previous studies we examined the effects of different extents of cure in single-layer coatings representative of each of these two coating types.^[1, 12-13] The data showed that the strip force, strength, and fatigue characteristics of a fiber are degraded when such single-layer protective coatings are inadequately cured.

In the present work, we connect these avenues of investigation: the effects of different dual-layer coatings and the effects of extent of cure on the mechanical reliability of optical fibers. To accomplish this, we have extended our previous work to dual-coated fibers with varying extents of cure in both of the coating layers. The results summarized in this paper demonstrate that dual-layer coatings experience performance degradations similar to the single-layer coatings studied previously. The median strength of the uncured fiber is reduced, increasing the potential for mechanical failure during installation. Poorer fatigue resistance heightens the susceptibility of the fiber to long-term failure in service. In addition, the techniques used previously to analyze the extent of cure of single-layer coatings are shown to be directly applicable to the more typical dual-layer structure. Finally, analyses of the aged coating and glass demonstrate that the extent of the changes in the coating (e.g., loss of residual curing and extraction of unreacted material) and in the glass surface morphology correlate with the initial extent of coating cure. These correlations suggest how the deterioration of the protection afforded by the coating during aging leads to degradation in the strength and fatigue resistance of the glass.

SAMPLE PREPARATION AND AGING

Three test fibers were drawn in lengths of approximately 2500m from a standard fused silica preform. Three different sets of conditions were used to obtain varying extents of cure. The normally-cured fiber was drawn at 200 m/min; three ultraviolet (UV) lamps were used to provide the curing dosage for the polyurethane acrylate coating. The under-cured fiber was also drawn at 200 m/min, but only one UV curing lamp was used; this coating thus received approximately $1/3$ as much UV radiation as the coating on the normally-cured fiber. The over-cured fiber was drawn using all three UV lamps, but the drawing speed was reduced to 100 m/min; this coating thus received approximately twice as much UV radiation as the normally-cured coating. In the remainder of this paper, we will frequently refer to the under-cured, normally-cured, and over-cured *fibers* as a simple identification of these fibers with differing extents of coating cure.

Each fiber sample was divided into four lengths, one of which was tested in the unaged condition as a reference. We aged the remaining lengths of all three fibers in three environments:

- In an 85°C "dry" oven. The temperature was controlled to within $\pm 1^\circ\text{C}$. The humidity was uncontrolled, but was typically less than 30% RH throughout the aging time.
- In 85°C deionized (DI) water. The temperature was controlled to within $\pm 0.5^\circ\text{C}$. The pH of the water was maintained at 7.0 ± 0.5 using a buffering solution.
- In an 85°C/85% RH environment. The temperature was controlled to within $\pm 1^\circ\text{C}$ and the humidity to within $\pm 4\%$ RH. Deionized water of pH 7 was used to maintain the humidity.

All samples were aged as loose coils to provide "zero-stress" aging conditions. Samples were removed from the aging environments after one day, seven days, and 30 days of aging.

INITIAL COATING CURE

To ensure that the three fiber coatings had different extents of cure, we analyzed them using several different techniques that we evaluated previously.^[12, 13] Differential photocalorimetry (DPC), evaporative rate analysis (ERA), Fourier transform infrared spectroscopy (FTIR), and dynamic mechanical thermal analysis (DMTA) each provide different insights into the extent of cure and the effects of aging.

The results, shown in Table 1, confirmed that each of the coatings did indeed have a different extent of cure. The DPC data show that a large residual reaction occurred in the under-cured fiber, while no reaction was detected in the over-cured fiber, indicating an essentially complete cure. The ERA cure index data substantiate this result; small values of the index indicate a large absorption and retention of solvent, while large values indicate a tightly cross-linked coating that absorbs only a minimal amount of solvent. Similarly, the FTIR data show that more unreacted acrylate was present in the under-cured coating than in the normally-cured coating, while none was detected in the over-cured coating. Finally, the increasing T_g values indicate that more cross-linking occurred as the UV curing dosage was increased from under-cured to over-cured.

Table 1. Relative Extents of Cure of Test Fibers

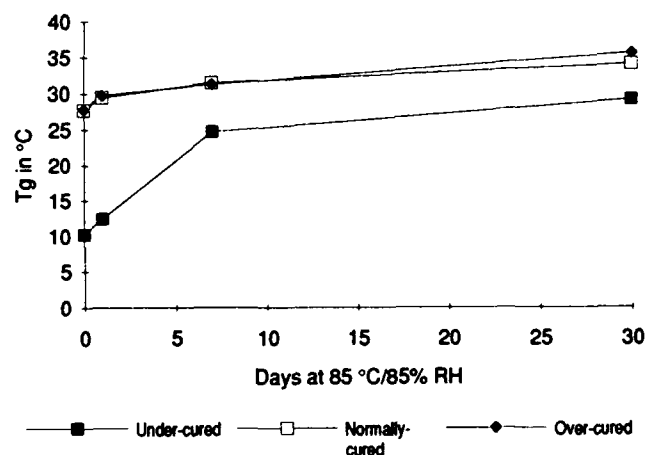
	Under-cured Fiber	Normally-cured Fiber	Over-cured Fiber
DPC Residual Cure	7.5 J/g	2.1 J/g	—
ERA Cure Index	209	454	944
FTIR Reacted Acrylate	1.3	0.8	—
DMTA 1-Hz T_g	10.2 °C	27.7 °C	27.8 °C

The data indicate that these techniques can be extended to dual-coated fibers. The DPC test detects the heat of the residual reaction, without identifying whether it is generated in the inner or outer layer of the coating (or both). In the ERA test, the solvent was applied to the ends of the fiber samples as well as the sides, in order to promote its penetration into the more absorbent inner layer. The FTIR test probes only the outer coating layer; however, the differences in the measured extents of cure are smaller than in the DPC and ERA tests. This suggests that the DPC and ERA results are indicative of an incomplete cure in both coating layers. Finally, the DMTA results suggest that under-curing the coating may have a more significant effect on the mechanical properties of the coating than over-curing.

EFFECTS OF EXTENT OF CURE ON COATING AGING

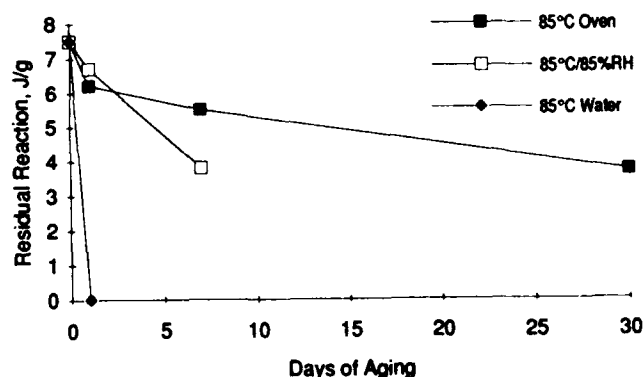
In all cases, the under-cured coating was more affected by aging than the normally-cured and over-cured coatings. Figure 1 shows how the T_g of each coating increased during aging in the 85 °C/85% RH environment. The increase for the under-cured coating was 2 1/2 times that of the normally-cured or over-cured coatings. This suggests that the under-cured fiber could experience greater changes in its strength and fatigue properties due to aging than the normally-cured and over-cured fibers.

Figure 1. Effects of 85 °C/85% RH Aging on T_g



As we have observed in previous tests,^[13] the 85 °C deionized water was a more severe aging environment for all three coatings than the 85 °C/85% RH environment, which in turn was more severe than the 85 °C dry oven. Figure 2 shows the effects of all three environments on the residual cure of the under-cured coating. While some residual curing can still be measured in the coating when it is exposed to UV light after 30 days of aging in a dry oven, no residual curing is observed after only one day in 85 °C deionized water. In the 85 °C/85% RH environment, some residual curing occurs after seven days of aging, but this disappears sometime before the end of the 30-day exposure. This behavior suggests that the mechanical properties of the fibers might experience larger changes after aging at 85 °C/85% RH than after dry aging, and even larger changes after aging in 85°C water.

Figure 2. Effect of Aging on Residual Cure Reaction in Under-cured Fiber



The DMTA data confirm the relative severity of the different aging environments, as shown in Table 2. Increases in T_g can indicate either an increasing cross-link density or densification and stiffening of the coating. A higher cross-link density is a direct consequence of a further curing reaction. However, densification and consequent stiffening might also result from the loss of volatile and/or soluble materials from the original coating formulation. The changes in the loss tangent ($\tan \delta$) in Table 2 are consistent with degradation (and densification) of the coating, rather than with the development of additional cross-linking. Optical microscopy confirmed that the under-cured coating had become embrittled and had begun to shrink and crack.

Table 2. DMTA Data for Unaged and 30-Day Aged Fibers

Fiber	Aging	T_g , °C	$\tan \delta$
Under-cured	Unaged	10.2	1.42
	85 °C Dry	29.3	0.14
	85 °C/85% RH	29.1	0.14
	85 °C Water	54.4	0.15
Normally-cured	Unaged	27.7	0.12
	85 °C Dry	32.0	0.12
	85 °C/85% RH	34.0	0.13
	85 °C Water	35.4	0.13
Over-cured	Unaged	27.8	0.09
	85 °C Dry	33.8	0.11
	85 °C/85% RH	35.5	0.13
	85 °C Water	35.3	0.12

The data suggest that most of the changes in the coatings are due to the extraction (by water or water vapor) of unreacted photoinitiator, monomer, and oligomers. The residual DPC reaction ceases to occur, implying that either cross-linking is completed or unreacted photoinitiator and/or other reactants are being lost; the change is more rapid in the water and RH environments, which are more aggressive in extracting material from the coating.^[13, 14] The FTIR data show that some potential reaction sites continue to exist; that further curing does not occur can thus be attributed to a loss of initiator or other reactant. The T_g and $\tan \delta$ changes are together consistent with extraction and degradation, rather than cross-linking.

The fatigue resistance and strength retention of the glass are directly related to the ability of the coating to keep contaminants away from the glass surface. If material is extracted from the coating, it can become more permeable, allowing water to more easily penetrate toward the glass surface. If the adhesion of the coating to the glass is diminished, moisture can more easily react at surface defect sites and increase the vulnerability of the fiber to additional degradation.

MECHANICAL TESTS

We conducted dynamic tensile strength experiments on each of the fibers, both as received and after aging in the various environments indicated above. The tests were conducted at a strain rate of 5%/min in a laboratory ambient environment of 23 °C and a relative humidity of 50%.

We also used an atomic force microscope (AFM) to examine the surfaces of the unaged and aged fibers. The polymer coating on the fibers was removed before the examination by dipping the fibers into hot (~200 °C) H_2SO_4 and rinsing in deionized water.

In addition to the dynamic strength experiments, we tested the unaged fibers in static tension and in two-point bending, using an 85 °C deionized water environment. In the static tension

test,^[2] a length of fiber was gripped at each end and pulled in tension using weights. In this test, it is usually inconvenient to immerse the grips in the test environment; therefore the fiber was threaded through an environmental chamber before being gripped and loaded. In the two-point bending test, used for studying fiber fatigue, short lengths of fiber are bent double and inserted into precision bore glass tubes.^[15] Fracture of the fibers is monitored acoustically. The maximum tensile stress that occurs on the fiber surface is given by

$$\sigma = 2.396E \frac{r}{D-d}$$

where D is the internal diameter of the tube, E is the Young's modulus of the silica fiber, r is its radius, and d is the total fiber diameter including the protective coating.

MECHANICAL CHARACTERIZATION

The dynamic tensile strengths of the fibers with each of the three different extents of cure fell onto a straight line when plotted on Weibull coordinate axes, as shown in Figure 3. This indicates that the failure distribution for each fiber can be approximated by a Weibull cumulative probability distribution of the form:

$$F = 1 - 2 \left(\frac{\sigma}{\sigma_{50}} \right)^m$$

where F is the cumulative probability of failure at a stress less than or equal to σ , and σ_{50} is the median strength. The parameter m is the slope of the curve in the Weibull plot and provides a measure of the breadth of the strength distribution, with large values of m associated with narrow distributions. The relative breadth of the strength distribution can be calculated from this equation as:

$$\frac{\sigma_{90} - \sigma_{10}}{\sigma_{50}} = \left(3.32 \frac{1}{m} - 0.152 \frac{1}{m} \right)$$

where σ_{90} , σ_{50} , and σ_{10} are the 90th, 50th, and 10th percentile strength values, respectively.

Figure 3. Tensile Strength Distributions for Unaged Fibers

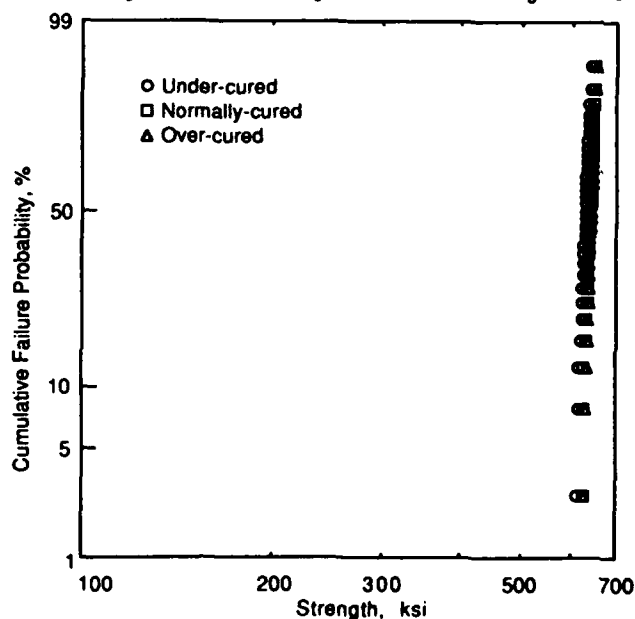


Table 3. Fiber Tensile Strengths after Aging in an 85 °C Dry Oven

Aging Time (days)	Under-cured Fiber			Normally-cured Fiber			Over-cured Fiber		
	σ_{90} (ksi)	m	$\sigma_{90} - \sigma_{10}$ (ksi)	σ_{90} (ksi)	m	$\sigma_{90} - \sigma_{10}$ (ksi)	σ_{90} (ksi)	m	$\sigma_{90} - \sigma_{10}$ (ksi)
Unaged	627	110	18	637	118	17	639	139	14
7	663	43	47	671	120	17	674	75	28
30	691	50	42	689	101	21	677	94	22

Table 4. Fiber Tensile Strengths after Aging at 85 °C/85% RH

Aging Time (days)	Under-cured Fiber			Normally-cured Fiber			Over-cured Fiber		
	σ_{90} (ksi)	m	$\sigma_{90} - \sigma_{10}$ (ksi)	σ_{90} (ksi)	m	$\sigma_{90} - \sigma_{10}$ (ksi)	σ_{90} (ksi)	m	$\sigma_{90} - \sigma_{10}$ (ksi)
Unaged	627	110	18	637	118	17	639	139	14
1	292	7	124	322	15	65	392	10	117
7	310	7	131	299	9	99	386	9	128
30	282	13	65	304	11	83	375	20	57

Table 5. Fiber Tensile Strengths after Aging in 85 °C Water (pH 7±0.5)

Aging Time (days)	Under-cured Fiber			Normally-cured Fiber			Over-cured Fiber		
	σ_{90} (ksi)	m	$\sigma_{90} - \sigma_{10}$ (ksi)	σ_{90} (ksi)	m	$\sigma_{90} - \sigma_{10}$ (ksi)	σ_{90} (ksi)	m	$\sigma_{90} - \sigma_{10}$ (ksi)
Unaged	627	110	18	637	118	17	639	139	14
1	310	31	31	341	33	32	368	70	16
7	258	33	24	247	42	18	263	55	15
30	82	2	118	256	40	20	258	58	14

As shown in Figure 3, the tensile strengths of the unaged fibers fit a Weibull distribution very well. Tables 3–5 summarize the median strengths and the breadths of the strength distributions, ($\sigma_{90} - \sigma_{10}$), obtained for the unaged and aged fibers in the tensile experiments. In general, the under-cured unaged fiber was about 10 ksi weaker than the normally-cured and over-cured fibers and it exhibited a slightly broader strength distribution. For all three curing conditions, there was a slight increase in strength in the dry aging environment as the aging time increased (Table 3). However, the median strength of all fibers decreased with increasing aging time in the wet aging environments, and the decrease was more dramatic in liquid water than in high humidity (compare Tables 4 and 5). The under-cured fiber experienced more severe aging, as shown in Figure 4. The breadth of the strength distribution for the aged under-cured fiber is somewhat larger than that for the other two curing conditions and again the aging effect was more dramatic in liquid water. These results are generally consistent with the changes that occurred in the coatings during aging in these environments.

These strength results are consistent with the surface roughnesses of these fibers as measured with the AFM. Surface profiles of an unaged fiber and of fibers aged for one month in deionized water are shown in Figure 5. Note that the vertical scale for the unaged fiber profile is twice as sensitive as that for the aged normally-cured and over-cured fibers, and four times as sensitive as that for the aged under-cured fiber. The under-cured fiber experienced more severe aging, just as more severe aging was seen in its coating. The roughened surface showed an increase in both the amplitude and the wavelength of the surface contours with increasing aging time, consistent with earlier predictions^[16] and findings.^[17] These qualitative observations on the relative surface roughness can be put on a more quantitative basis by considering the maximum values of the roughness heights obtained from the AFM and given in Table 6.

Table 6. AFM Roughness Height for Unaged and Aged Fibers

Fiber	Roughness Height, nm
Unaged, all fibers	~1.3
Aged†, under-cured	33.6
Aged†, normally-cured	17.8
Aged†, over-cured	14.5

†Aging condition: 1 month in deionized water at 85 °C.

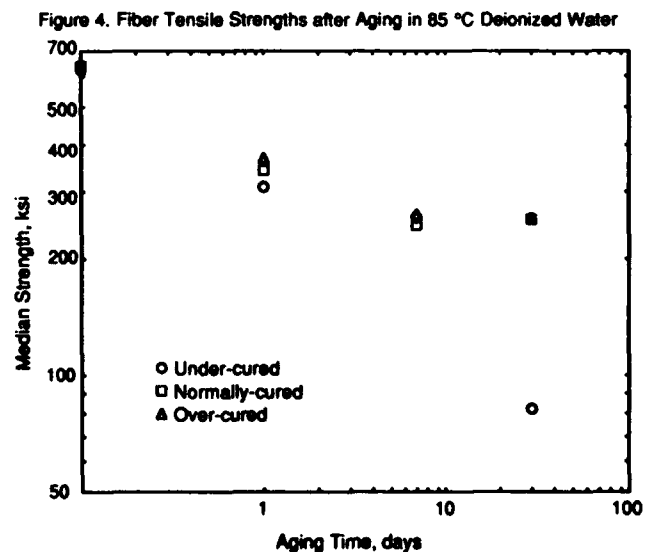
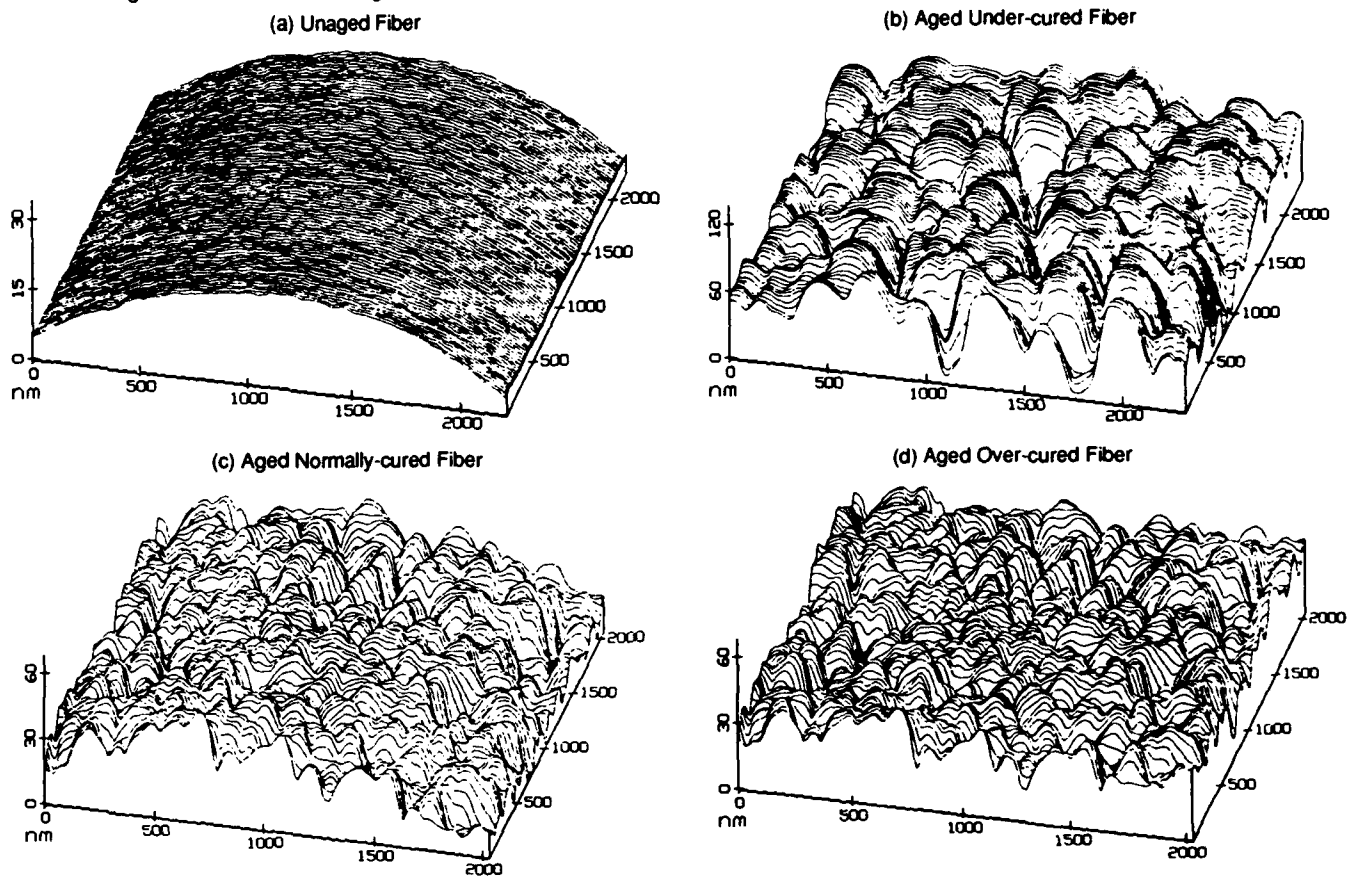


Figure 5. Unfiltered AFM Images of the Glass Surface of Unaged Fiber and of Fibers Aged One Month in 85 °C Deionized Water



The tensile static fatigue results obtained by testing unaged fibers with different extents of cure in an 85 °C deionized water environment are shown in Figure 6. If it is assumed that the initial strengths of these fibers fit a Weibull distribution, and if the power law dependence for the crack growth rate is assumed, it can be shown^[18] that the median time-to-failure, t_f , at constant stress, σ , is given by:

$$t_f = C\sigma^{-n_s}$$

where C is a parameter independent of both σ and t_f , and n_s is the static crack growth exponent. The values of n_s for the different fibers can be obtained by fitting this equation to the data for time to failure versus applied stress, which should plot as a straight line in log-log coordinates. As seen in Figure 6, the data for these fibers can best be fit by two straight lines. This so-called knee or transition in the static fatigue data has been observed by several workers.^[19] The values of n_s obtained from these data are given in Table 7.

Table 7. Values of n_s Calculated from Tension Test Data

Fiber	n_s
Under-cured	15.2, 2.93
Normally-cured	20.8, 3.26
Over-cured	21.2, 4.1

In this table, the two values of n_s listed for each fiber are for the high stress and low stress regions, respectively. Note that n_s increases with an increased extent of cure. This increase in the

n_s value means a decrease in the rate of crack growth. The effect of a change in n_s on the rate of crack growth can be estimated by considering a more general form of the equation for the time to failure in static fatigue than that used above, namely^[20]:

$$t_f = \frac{A \left(\frac{K_o}{K_c} \right)^n S^{n-2}}{(n-2)\sigma_a^n}$$

where K_o , K_c , A are constants for a given glass and are independent of n , S is the strength, σ_a is the applied stress, and n is the crack growth exponent. The ratio of the time to failure at a stress, σ , for two fibers of differing strengths, S , and differing values of n is given by:

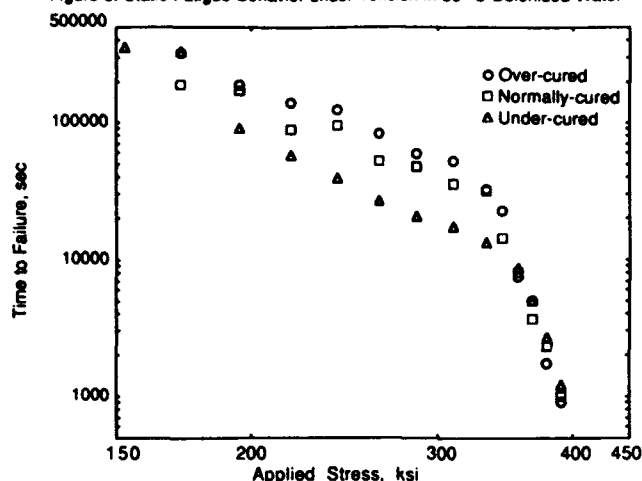
$$\frac{t_1}{t_2} = \left(\frac{K_o}{K_c} \right)^{(n_1-n_2)} \left(\frac{n_2-2}{n_1-2} \right) \frac{\sigma^{(n_2-n_1)} S_1^{(n_1-2)}}{S_2^{(n_2-2)}}$$

Letting the subscript 1 refer to the normally-cured fiber, the subscript 2 refer to the under-cured fiber and the subscript 3 refer to the over-cured fiber, the values of n , S , and σ given in Table 8 can be used.

Table 8. Strength Parameters for Test Fibers

Parameter	(1) Under-cured	(2) Normally-cured	(3) Over-cured
n	15.2	20.8	21.2
S , ksi	627	637	639
σ , ksi	50	50	50

Figure 6. Static Fatigue Behavior under Tension in 85 °C Deionized Water



Using values of $K_0 = 0.371 \text{ ksi(in)}^{1/2}$ and $K_c = 0.72 \text{ ksi(in)}^{1/2}$ (see [20]) the ratio of $t_{\text{normally-cured}}$ to $t_{\text{under-cured}}$ is 32,500 and the ratio of $t_{\text{over-cured}}$ to $t_{\text{normally-cured}}$ is 50. The normally-cured and over-cured fibers therefore have far better fatigue resistance and life expectancy than the under-cured fiber. The relative improvements from under-cured to normally-cured to over-cured (32,500:50) are similar to the changes measured using DMTA (T_g , 17.5:0.1; $\tan \delta$, 1.30:0.03).

CONCLUSIONS

The mechanical characteristics of dual-coated fibers with different extents of coating cure have been compared both before and after aging in several environments. In addition, the effects of cure on coating behavior and aging have been characterized and correlated with fiber mechanical behavior.

The lower the extent of cure, the more susceptible the coating is to extraction of unreacted material and to degradation in all aging environments. Degradation increases permeability and decreases adhesion to glass, both of which make the glass more vulnerable to attack by the aging environment.

The tensile strength data for the unaged fibers regardless of extent of cure could be fit well by a Weibull distribution. The over-cured fiber had the tightest strength distribution, while the under-cured fiber had the broadest distribution.

The median strength of the unaged under-cured fiber was lower than that of the normally-cured and over-cured fibers. This is consistent with the lower crack growth exponent, n , determined in the static fatigue tests, and with the greater susceptibility to degradation of the under-cured coating.

The fiber strengths decreased with increasing aging time in wet aging environments, and this decrease was more dramatic in liquid water than in high humidity. The under-cured fiber experienced more severe aging of both the glass and the coating.

Because the under-cured fiber has a lower n value, crack growth is faster at a given applied stress than for the normally-cured or over-cured fibers. Fiber coatings must be fully cured to protect the glass fiber and ensure a robust and durable fiber network.

Atomic force microscopy of the glass surface confirmed that the surface degradation (i.e., the formation and growth of strength-reducing flaws) correlated with both the extent of cure of the coating and its resultant aging behavior.

REFERENCES

1. H. H. Yuce, I. M. Plitz, R. A. Frantz, and M. Andrejco, Proc. 39th Int. Wire and Cable Symp. (1990), p. 715.
2. J. T. Krause, J. Non-Cryst. Solids, **38 & 39** (1980), p. 497.
3. J. E. Ritter, Jr., K. Jakus, and D. S. Cook, Proc. 2nd Int. Conf. Environ. Degrad. Eng. Mater. Aggr. Envir. (1981), p. 565.
4. J. T. Krause, C. R. Kurkjian, and M. J. Matthewson, Ext. Abst., 87th Ann. Mtg. Amer. Ceram. Soc. (1985), p. 145.
5. T. Wei, Adv. Ceram. Mater., **1** (1986), p. 237.
6. B. J. Skutnik, B. D. Munsey, and C. T. Brucker, Mater. Res. Soc. Symp. Proc., **88** (1987), p. 27.
7. T. Wei and B. J. Skutnik, J. Non-Cryst. Solids, **102** (1988), p. 100.
8. H. H. Yuce, A. D. Hasse, P. L. Key, and M. J. Andrejco, Proc. 37th Int. Wire and Cable Symp. (1988), p. 732.
9. H. H. Yuce, J. P. Varachi, Jr., J. P. Kilmer, C. R. Kurkjian, and M. J. Matthewson, OFC '92, postdeadline paper, PD21 (1992), p. 395.
10. H. C. Chandan, J. R. Petisce, J. W. Shea, C. R. Taylor, L. L. Blyler, D. Innis, and L. Shepherd, Proc. 41st Int. Wire and Cable Symp. (1992), p. 239.
11. M. J. Matthewson, H. H. Yuce, V. V. Rondinella, P. R. Foy, and J. R. Hamblin, OFC '93, postdeadline paper, PD21 (1993).
12. R. A. Frantz, I. M. Plitz, and S. R. Schmid, Proc. 40th Int. Wire and Cable Symp. (1991), p. 134.
13. R. A. Frantz, I. M. Plitz, H. H. Yuce, and O. Gebizlioglu, Proc. 41st Int. Wire and Cable Symp. (1992), p. 279.
14. J. Julian and C. P. Chawla, RadTech '92 No. Amer. UV/EB Conf. Proc. (1992), p. 315.
15. S. F. Cowap and S. D. Brown, Amer. Ceram. Soc. Bull., **63** [3] (1984), p. 495.
16. M. J. Matthewson and C. R. Kurkjian, J. Amer. Ceram. Soc., **71** (1988), p. 177.
17. R. S. Robinson and H. H. Yuce, J. Amer. Ceram. Soc., **74** [4] (1991), p. 814.
18. F. P. Kapron and H. H. Yuce, J. Optical Engineering, **30** [6] (1991), p. 700.
19. H. C. Chandan and D. Kalish, J. Amer. Ceram. Soc., **65** [3] (1982), p. 171.
20. P. L. Key et al, J. Non-Cryst. Solids, **38 & 39** (1980), p. 463.

Hakan H. Yuce is Director of the Fiber Distribution and Reliability Research group at Bellcore, with responsibility for research in the areas of optical fiber and fiber-optic component reliability and new low-cost installation methods for fiber-in-the-loop deployment. He plays an active role in the establishment of US and international standards for optical fiber test procedures to assure reliability. He has a BS in Mechanical Engineering from the Technical University of Istanbul, an MS in Mechanical Engineering from MIT, and a PhD in Mechanical Engineering and Materials Science from Stanford University. He was a 1992 recipient of *Telephony's* Ray Blain Outside Plant Achievement Award.



Rolf A. Frantz is a Distinguished Member of Technical Staff in the Fiber Distribution and Reliability Research Group at Bellcore. He holds BS and MEng degrees from Cornell University and received his PhD at Brown University. He spent eleven years at Bell Laboratories, working principally on applications problems of dielectric materials, and he continued working in this area when he came to Bellcore in 1983. Since 1988, he has been concerned with the applications and reliability problems of fiber coatings, adhesives, coloring inks, gels, and related materials used in optical fibers, cables, connectors and splices.



Osman S. Gebizlioglu is a Member of Technical Staff in the Plastics and Rubber Research Group at Bellcore. He holds BSc and MSc degrees in Chemical Engineering from the Middle East Technical University in Ankara, Turkey. After receiving his PhD in the Polymer Materials Program of the Chemical Engineering Department at Princeton University, he did postdoctoral research as a Monsanto Fellow in the Department of Mechanical Engineering at MIT. Since he joined Bellcore in 1987, he has conducted research on the mechanical reliability of polymeric materials in fiber optic cables, optical devices, and connectors.



Irene M. Plitz is a Member of Technical Staff in the Plastics and Rubber Research Group at Bellcore. She graduated from Morgan State University in 1970 with a BS degree in chemistry and then joined AT&T Bell Laboratories. Since becoming part of Bellcore in 1983, her interests have centered around the degradation, characterization, and reliability of polymeric materials used in the telecommunications industry.



Tarja T. Volotinen is a Specialist in optical fibers in the Telecom Cables Division of Ericsson Cables AB. She received her MSc from the University of Helsinki in 1978 and worked for Nokia Cables in Finland on measurement techniques for optical fibers and cables. Since joining Ericsson in 1986, she has focused particularly on the performance and mechanical reliability of optical fibers. She received her PhD in Physics from the University of Helsinki in 1991. In 1992-1993, she was a visiting scientist in the Fiber Distribution and Reliability Group at Bellcore, working on mechanical reliability issues affecting optical fibers and cables.



SOLVENT SWELLING OF OPTICAL FIBER COATINGS AS A DIAGNOSTIC MEASURE OF CROSSLINKING

P. Wiltzius, E. Helfand, D. Tull[†], D. A. Simoff

AT&T Bell Laboratories
Murray Hill, New Jersey

ABSTRACT

The degree of cure of optical fiber coatings determines many performance properties, but can be difficult to assess *in situ*. We evaluate a solvent swelling technique as a tool for assessing the cure state of the primary (inner) coating. The coating on an optical fiber that is immersed in a good solvent swells as it absorbs the solvent, reaching an equilibrium value. Measuring the unswollen and swollen dimensions of the coatings allows us to determine the polymerization index or crosslink density of the polymeric network. Advantages of the swelling test over mechanical *in situ* tests include ease of operation and the possibility for assessing the cure state of the secondary coating as well as that of the primary one.

INTRODUCTION

Silica optical fibers are typically coated with two polymeric coatings: a soft, rubbery primary (inner) coating to cushion against microbending losses, and a hard secondary (outer) coating to provide abrasion resistance to the primary.^[1] Most commonly these are urethane acrylate formulations that are applied as viscous solventless prepolymers during fiber drawing. They are cured via free radical polymerization upon exposure to intense UV lamps for only a fraction of a second.

The completeness of cure for the primary coating is critical to the mechanical integrity of the fiber, affecting properties such as coating/glass adhesion^[2] and fiber strength.^[3] One test that reflects the cure of the primary coating is the "pullout" test,^[4] which measures the force necessary to pull 1 cm of glass out of its coating. The relationship between pullout force and UV dose is illustrated in Figure 1 for a set of fibers that we describe in detail later. Note, we define

$$\text{dose factor} = (\text{number of UV lamps})/(\text{draw speed, m/s})$$

While these and earlier^[2] data show that pullout force increases with degree of cure, the test was devised to measure adhesion and can be affected by factors other than cure. A more direct diagnostic for coating cure is the *in situ* modulus test.^[4] This uses a similar geometry to the pullout test to measure low-strain shear modulus of the primary coating, which is theoretically proportional to its crosslink density.^[6] Other methods that have been proposed for analyzing the cure of fiber coatings include photocalorimetry, infrared spectroscopy, strip force, solvent extraction, evaporation rate analyses and high pressure liquid chromatography.^{[7] [8] [9]}

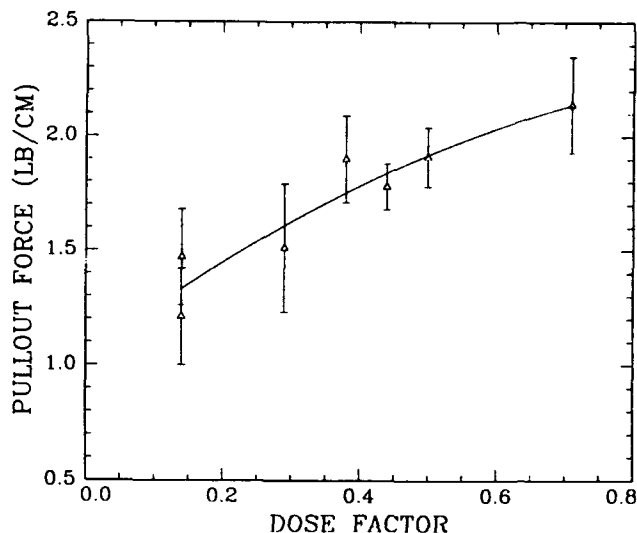


Figure 1. Relationship between pullout force and UV dose factor.

In this paper we evaluate a solvent swelling technique as an alternate method for assessing the cure state of the primary coating. We try to establish a relationship between the degree of swelling that the primary coating experiences when immersed in a good solvent and the measured values of pullout force and *in situ* modulus. This swelling test is simpler and/or less time-consuming than most of the tests mentioned above, and offers the possibility of measuring degree of cure for the secondary coating independently from that of the primary. In principle, it is non-destructive in that the fiber can be returned to near normal after testing by allowing the solvent to evaporate.

This study further serves to build a foundation for understanding swelling behavior of the coatings in various liquids that a fiber might encounter, such as cleaning fluids or cable filling compounds.

EXPERIMENTAL

Fibers.

Four sets totaling 26 different fibers dual-coated with UV-curable coatings were studied. The same primary and secondary coating formulations were used on all 26 fibers. Fibers 1-9 were drawn such that the amount of UV exposure was adjusted by controlling the draw speed and the number of lamps as listed in Table 1. Fibers 10-14 were drawn with varying levels of UV transmission as measured through a quartz center tube. Fibers 15-18 and 19-26 are two sets that were drawn under conditions selected to give a wide range of pullout values. Except for fiber 14 the pullout values had been measured and are listed in Table 1. For fiber 14 we assume a pullout value equal to the value of fiber 13, since they were of similar origin. The pullout measurements were performed at ambient temperature and humidity except for fibers 16 and 17, which were measured at 25°C / 95% RH. For these latter fibers, the difference in test humidity is not expected to affect the pullout value greatly. Since the various fibers have quite different origins we code the results in Figures 4, 5, 7 and 8 with the following symbols: circles (fibers 1-9), triangles (10-14), diamonds (15-18), stars (19-26).

Solvent Swelling Measurements.

The swelling measurements were performed at room temperature on 5 cm long pieces of fiber that were immersed in toluene between spaced microscope slides. Prior to testing, the fibers had been stored in the dark at room temperature and lab ambient humidity. Toluene was chosen because it was found to be a good solvent for this and other optical fiber coatings.^[2] The ends of the fiber were not allowed to be in contact with the solvent in order to prevent delamination. The fiber was viewed with a Zeiss microscope equipped with a UD 16 objective. A Pulnix CCD camera was attached to the microscope. With a Data Translation high resolution frame grabber board DT2851 in a personal computer we acquired, analyzed and stored pictures of the swelling fiber as a function of time.

The image processing which yielded the various dimensions of the fiber involved a number of steps. Noise reduction was achieved through averaging cross-sections of the fiber parallel to the fiber axis. In a second step a one-dimensional Laplacian^[10] was performed, followed by a search for minima in the transformed data corresponding to the interfaces between glass/primary coating, primary coating/secondary coating, secondary coating/toluene. The dimensions were normalized by using an internal calibration assuming a glass diameter of 125 μm . The combination of microscope objective and CCD pixel size used gave a resolution of 1.1 μm .

RESULTS and DISCUSSION

Figures 2a and 2b show a typical set of dimensions measured on the swelling fiber #3. The various symbols denote the secondary coating diameter (o), the primary coating diameter (+), the glass diameter (Δ), the primary coating thickness (diamonds) and the secondary coating thickness (X). The secondary coating begins swelling immediately after

Table 1. List of Fibers

#	Pullout (lb/cm)	Comments
1	1.47 \pm 0.21	draw speed 7 m/s, 1 UV lamp
2	1.51 \pm 0.28	draw speed 7 m/s, 2 UV lamp
3	2.14 \pm 0.21	draw speed 7 m/s, 5 UV lamp
4	1.78 \pm 0.10	draw speed 9 m/s, 4 UV lamp
5	1.90 \pm 0.19	draw speed 8 m/s, 3 UV lamp
6	1.21 \pm 0.21	draw speed 7 m/s, 1 UV lamp
7	1.51 \pm 0.28	draw speed 7 m/s, 2 UV lamp
8	1.91 \pm 0.13	draw speed 8 m/s, 4 UV lamp
9	1.90 \pm 0.19	draw speed 8 m/s, 3 UV lamp
10	1.46 \pm n.a.	UV transmission 21%
11	1.67 \pm 0.10	UV transmission 36%
12	1.67 \pm 0.10	UV transmission 51%
13	1.93 \pm 0.08	UV transmission 80%
14	n.a.	see text
15	1.45 \pm n.a.	"
16	3.18 \pm n.a.	"
17	3.34 \pm n.a.	"
18	1.48 \pm n.a.	"
19	2.71 \pm 0.12	"
20	1.69 \pm 0.06	"
21	3.25 \pm n.a.	"
22	3.05 \pm 0.18	"
23	3.02 \pm 0.15	"
24	2.72 \pm 0.15	"
25	3.35 \pm n.a.	"
26	2.72 \pm 0.18	"

immersion in toluene at time 0. Its average thickness increases from 25 μm to 30 μm (20%) and then decreases during the remainder of the experiment to about 27 μm . This decrease occurs when the underlying primary coating begins to swell, stretching the secondary coating circumferentially and thinning it radially. At no point does the volume of the secondary coating decrease, however. A plot of the volume of the secondary coating normalized to unity at time 0, as shown in Figure 3 (o), reveals that it swells to about 1.4 times its initial value.

The primary coating does not change during the first 200 seconds. It takes this long for the solvent to diffuse through the secondary coating. After this lag time it swells radially by a factor of 1.95 for this particular fiber. This corresponds to a volume change of 2.34x, as indicated by crosses in Figure 3. The difference in swelling between primary and secondary coating is due to the smaller crosslink density in the primary coating.

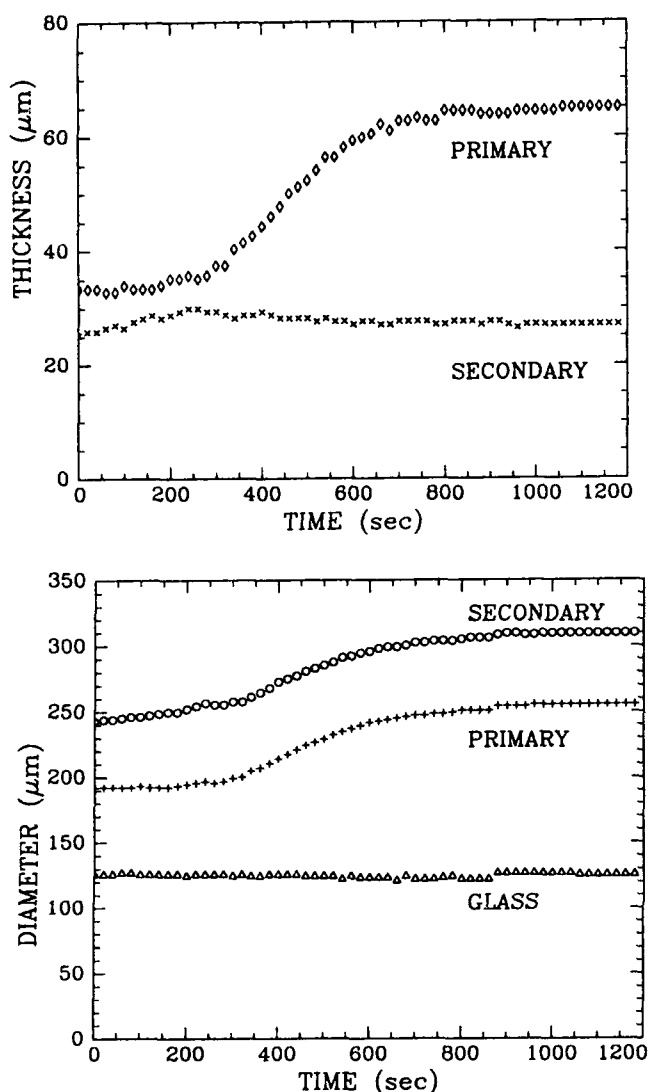


Figure 2. Time-dependent dimensions measured on swelling fiber: a) secondary coating diameter (o), primary coating diameter (+), glass diameter (Δ); b) primary coating thickness (diamonds), secondary coating thickness (X).

Figures 4a and 4b show the unswollen primary and secondary coating diameters of the various fibers. The data points are averages over 3 to 6 fiber samples and have an uncertainty of typically $\pm 2 \mu\text{m}$.

In this memo we are not interested in the time dependence of the swelling process although it contains potentially useful kinetic information. We are only going to analyze the dependence of the swollen radii in the equilibrium state ($t \rightarrow \infty$) on coating properties. From data as shown in Figure 2 we obtain the radii of the coatings normalized to the glass radius. Dimensions at $t = 20$ minutes were assumed to represent equilibrium values. These values, with subscript 1 for primary and 2 for secondary coating and a prime for the swollen state, are tabulated in Table 2 together with the pullout data.

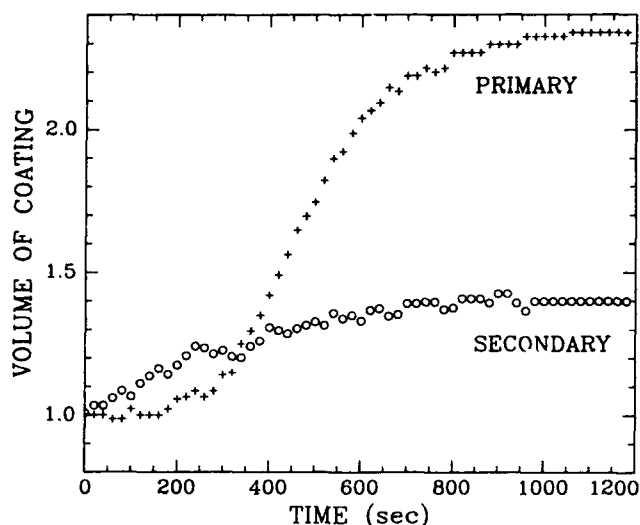


Figure 3. Time-dependent volume changes of secondary (o) and primary (+) coatings swelling in toluene, normalized to unity at time 0.

From data as shown in Table 2 we calculate the ratio of the primary radius in the swollen state at long times (20 minutes) to the initial unswollen radius. This simplest measure of swelling is plotted in Figure 5. There is an inverse relationship between this ratio and the pullout value. This is expected, since a large swelling ratio indicates a low crosslink density and thus a low degree of cure and low pullout value.

In the case of an isotropic, unrestricted rubber it would be possible to deduce the crosslink density directly from the swelling ratio. It is clear, however, that for our particular geometry — a two layer cylindrical polymer coating on an unswellable core — a more sophisticated data analysis is required. This is the subject of the next section.

Swelling of a Cylindrical Fiber Coating.

We have combined elastic and thermodynamic theories to produce differential equations describing the relationship between swelling and crosslinking. These equations are discussed briefly in the Appendix. A polymer gel immersed in a good solvent swells under two competing effects. The gain in entropy of mixing favors as much solvent as possible inside the polymer network. When the polymer is diluted with solvent, however, it stretches the crosslinked network, which costs elastic free energy. The balance of these two effects leads to an equilibrium swollen network. This problem was originally solved by Flory and Rehner^[11] for an isotropic, unrestricted network.

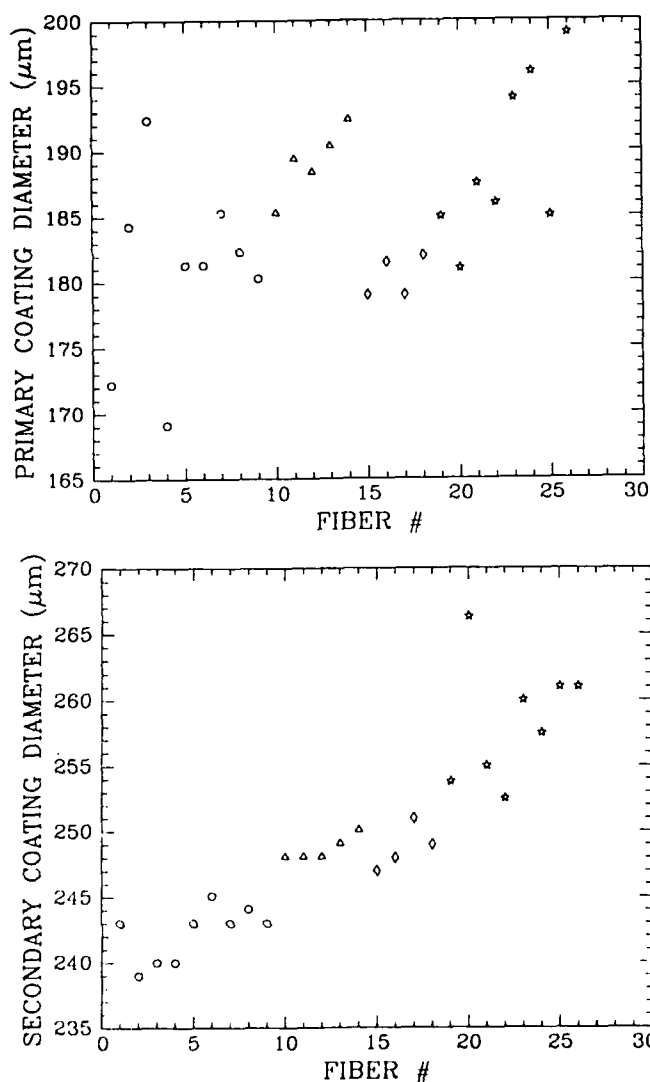


Figure 4. Unswollen coating diameters for the fibers in this study:

- a. Primary coatings
- b. Secondary coatings

The fibers are coded as follows: circles (fibers 1-9), triangles (10-14), diamonds (15-18), stars (19-26).

Table 2. Swelling Results							
#	Pullout	R_1	R_2	R'_1	R'_2	N_{e1}	N_{e2}
1	1.47	1.38	1.94	1.82	2.43	320	16
2	1.51	1.47	1.91	1.94	2.42	190	16
3	2.14	1.54	1.92	2.05	2.47	150	18
4	1.78	1.35	1.92	1.74	2.39	200	19
5	1.90	1.45	1.94	1.91	2.46	180	18
6	1.21	1.45	1.96	1.94	2.50	250	18
7	1.51	1.48	1.94	1.95	2.45	180	16
8	1.91	1.46	1.95	1.91	2.46	150	18
9	1.90	1.44	1.94	1.90	2.44	240	16
10	1.46	1.48	1.98	1.95	2.48	220	14
11	1.67	1.52	1.98	1.96	2.48	120	18
12	1.67	1.51	1.98	1.96	2.47	140	15
13	1.93	1.52	1.99	1.98	2.48	170	14
14	1.95	1.54	2.00	2.00	2.47	180	12
15	1.45	1.43	1.98	1.83	2.37	500	10
16	3.18	1.45	1.98	1.80	2.37	100	14
17	3.34	1.43	2.01	1.79	2.45	100	18
18	1.48	1.46	1.99	1.88	2.44	180	14
19	2.71	1.48	2.03	1.88	2.46	140	13
20	1.69	1.45	2.13	1.85	2.58	170	14
21	3.25	1.50	2.04	1.91	2.52	100	18
22	3.05	1.49	2.02	1.89	2.46	120	14
23	3.02	1.55	2.08	1.92	2.46	90	10
24	2.72	1.57	2.06	2.03	2.53	160	12
25	3.35	1.48	2.09	1.85	2.56	80	19
26	2.72	1.59	2.09	1.96	2.50	70	14

Here the same ideas were exploited, but for the polymer network geometry relevant to polymer coated optical fibers. The assumptions made were: 1) the primary and secondary coatings are concentric; 2) the primary coating is attached to the glass fiber; 3) the primary and secondary coating are connected to each other via chemical crosslinks; 4) the solvent-polymer interaction parameter χ is the same for both coatings; 5) both coatings are above the glass temperature. [Note, although the secondary coating is somewhat glassy at room temperature, it becomes rubbery during plasticization by solvent.]

Two coupled differential equations have been derived, which describe the swelling of the coatings as a function of radius (in cylindrical coordinates) in the equilibrium state. The goal is to compute the polymerization index, N_e , for both the primary and the secondary coating from the swelling data. The polymerization index is defined as the average number of

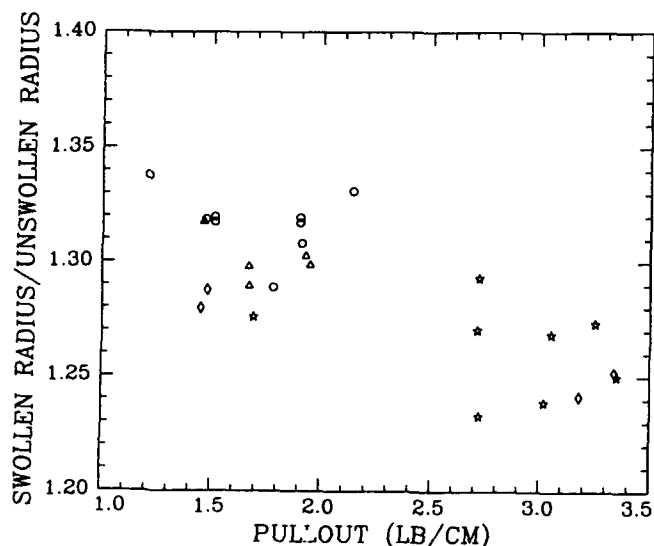


Figure 5. Relationship between swelling ratio of the primary coating (R'_1/R_1) and pullout force.

monomers between crosslinks in the polymer network. The equations have to be solved numerically for a given set of parameters, i.e. initial unswollen radii of primary and secondary coating, χ parameter, and a ratio of monomer to solvent molecular volume, v_r .

Since the system of equations contains only ratios of radii we normalized all dimensions to the diameter of the glass fiber, which is tightly monitored during production and remains constant during the test. The solvent-polymer interaction parameter will be fixed at a value of $\chi = 0.0$, i.e. the tendency to swell the polymer is driven by entropy. v_r will be taken to be 0.1. The values for χ and v_r should be determined experimentally for each given solvent-polymer pair. The values chosen here are reasonable and a different set of values would affect the results only quantitatively.

In Figure 6 we show the calculations for fiber # 2 as a representative example. R'_1 and R'_2 are the normalized swollen radii of the primary and secondary coatings, respectively. The polymerization index of the primary coating N_{e1} is the parameter annotating the calculated lines on the upper figure, whereas it is the polymerization index of the secondary coating N_{e2} which annotates the lines on the lower figure. The measured values of R'_1 and R'_2 from the swelling experiments are indicated by the cross-in-circle symbol. Note that a unique set of contours for N_{e1} and N_{e2} is generated for each fiber, depending upon the particular starting dimensions of its coatings. Figure 6 allows us to determine the values of N_{e1} and N_{e2} such as those compiled in the two last columns of Table 2.

The values of N_{e1} are typically 15 times larger than the values of N_{e2} . This is consistent with the secondary coating being more tightly crosslinked than the primary, and with the equilibrium modulus of the secondary coating being ~15 times larger than the modulus of the primary network.

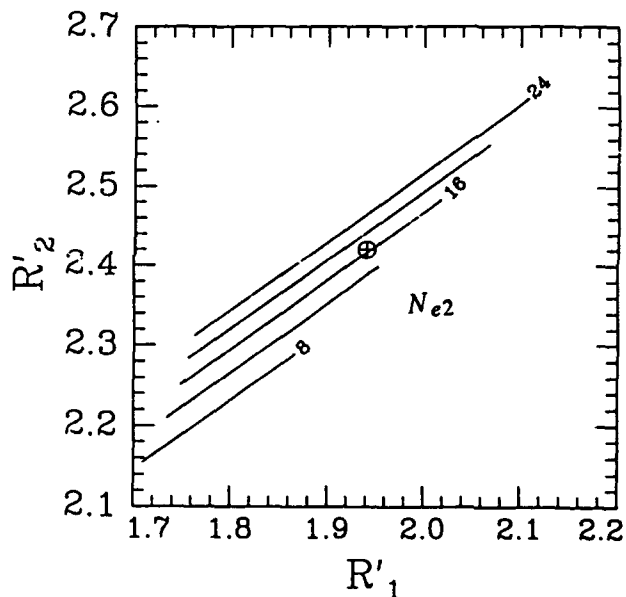
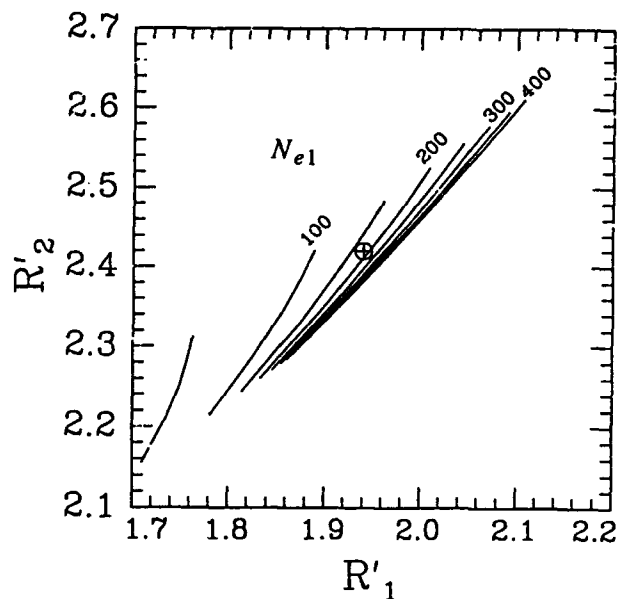


Figure 6. Numerically computed grids for determining polymerization indices of primary (N_{e1}) and secondary (N_{e2}) coatings. The example is for fiber #2.

The accuracy with which N_{e1} and N_{e2} can be determined is limited by the accuracy of R'_i . This error is of the size of the symbol in Figure 6 and is used for the error bars in Figure 7. We judge these error bars to be conservative.

The correlation between the polymerization indices and the pullout values for primary and secondary coatings are shown in Figures 7 and 8. Except for a few outlying points there is a strong correlation between N_{e1} and the pullout values. Qualitatively the trend is as expected. A fiber with a large

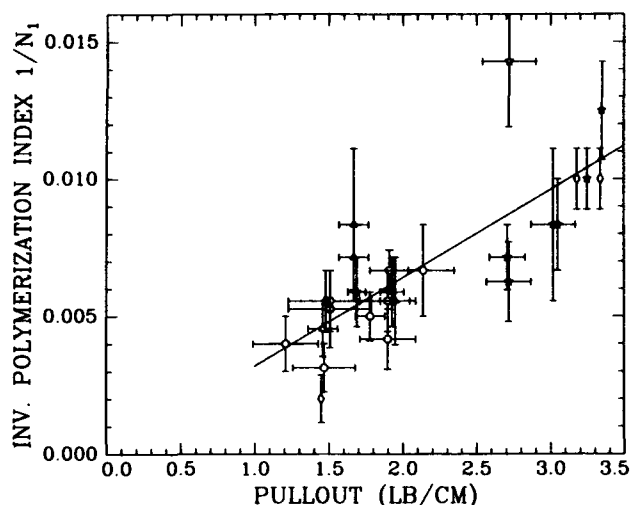


Figure 7. Relationship between inverse polymerization index of the primary coating ($1/N_{e1}$) and pullout force.

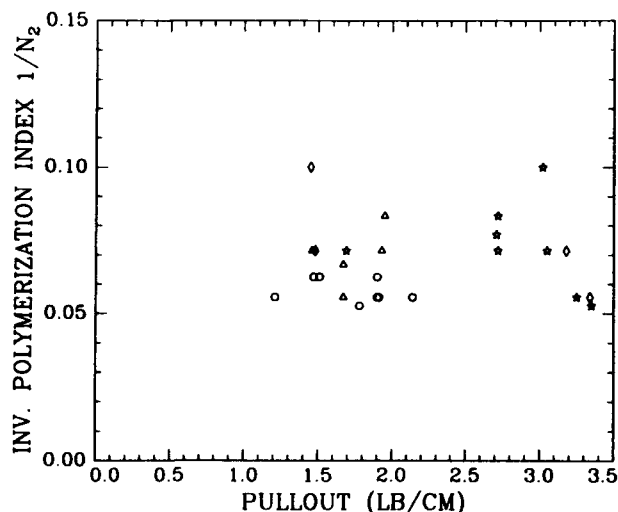


Figure 8. Relationship between inverse polymerization index of the secondary coating ($1/N_{e2}$) and pullout force.

value of N_{e1} (loosely crosslinked polymer network) has a small pullout value and vice-versa. The straight line is a linear fit through the data and extrapolates reasonably well to zero pullout for infinite N_{e1} (no crosslinking). The correlation between pullout values and N_{e2} is virtually non-existent. This again is reasonable since the pullout test does not examine the cure level of the secondary coating.

As mentioned earlier, a more appropriate (though more time-consuming) mechanical test than pullout for assessing cure is the *in situ* modulus test. We observed a roughly linear relationship between $1/N_{e1}$ and *in situ* modulus for limited data that were available (Figure 9).

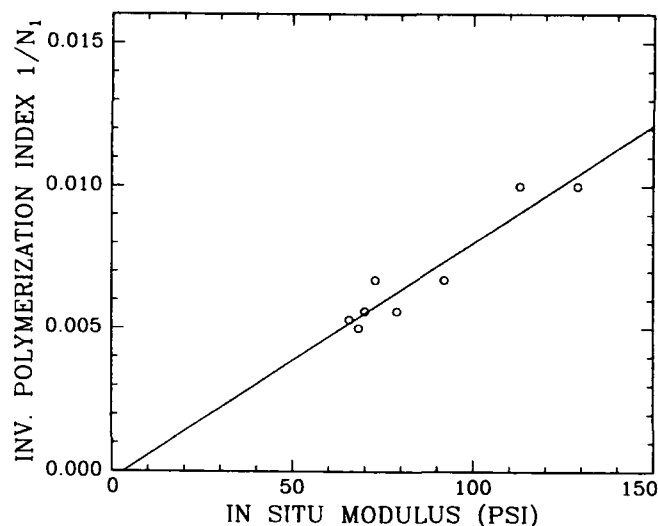


Figure 9. Relationship between $1/N_{e1}$ and *in situ* modulus.

SUMMARY

Solvent swelling of the polymer coatings on optical fibers proves to be an interesting technique for the assessment of the cure level of the polymer network. We developed techniques to obtain the polymerization index, which is related to the crosslink density, from the unswollen and swollen radii of the coatings. There is a clear correlation between the polymerization index of the primary coating with the pullout values. The index of polymerization of the secondary coating and the pullout values are uncorrelated, as expected. At this point it is not clear what the major causes of the scatter in Figure 6 are. Possibilities are, 1) uncertainty in the determination of the radii, 2) uncertainty in the pullout values, 3) deficiencies in the model.

We would like to emphasize that although we used a sophisticated setup with CCD-camera, framegrabber, PC with elaborate software, these are not necessary. If kinetic information is not important, as in this study, the unswollen and swollen radii can be obtained from photographs taken with a microscope.

Perhaps the strongest argument in favor of this technique is its ease of operation and independence of operator skills. The solvent swelling technique is very simple to perform and can be easily automated.

ACKNOWLEDGEMENTS

We would like to thank R. C. Moore, J. W. Shea and A. Hale for providing the optical fibers used in this study, and for providing many of the pullout and *in situ* modulus data. We also thank L. L. Blyler, Jr. for helpful discussions and encouragement.

REFERENCES

1. L. L. Blyler, Jr. and C. J. Aloisio, *CHEMTECH*, **17**, 680-684 (1987).
2. H. C. Chandan, J. R. Petisce, J. W. Shea, C. R. Taylor, L. L. Blyler, D. Inniss, L. Shepherd *Proceedings of the 41st International Wire and Cable Symposium* 239 (1992).
3. H. H. Yuce, I. M. Plitz, R. A. Frantz, M. Andrejco *Proceedings of the 39th International Wire and Cable Symposium* 715 (1990).
4. C. R. Taylor, *Meeting Digest of OFC*, Optical Society of America, Washington D.C., 20 (1985). A revised test is currently used.
5. B. J. Overton and C. R. Taylor *Polym. Engr. Sci.*, **29**(17), 1169 (1989).
6. See, for example: J. D. Ferry *Viscoelastic Properties of Polymers*, 3rd Ed., John Wiley and Sons, New York, 234 (1980).
7. R. A. Frantz, I. M. Plitz, S. R. Schmid *Proceedings of the 40th International Wire and Cable Symposium*, 134 (1991).
8. I. M. Plitz, R. A. Frantz *Radtech '92 North America, Conference Proceedings*, V1, 308 (1992).
9. J. L. Jostan, R. G. Sommer, M. Hoffart *Proceedings of the 41st International Wire and Cable Symposium* 267 (1992).
10. R. C. Gonzalez and P. Wintz *Digital Image Processing*, Addison-Wesley, Reading, MA, 338 (1987).
11. P. J. Flory and J. Rehner, Jr., *J. Chem. Phys.* **11**, 521 (1943).

APPENDIX: Equations Describing the Swelling

In this Appendix we will present briefly the equations that describe the equilibrium swollen state of the dual-coated fiber. In the unswollen state the system consists of: i) a glass fiber of radius ρ_0 ; ii) a primary coating with outer radius ρ_1 ; and iii) a secondary coating of outer radius ρ_2 . Position in the coatings will be specified by the cylindrical variables (ρ , ϕ , and z), such that $\mathbf{x} = \rho \hat{\mathbf{e}}_\rho + z \hat{\mathbf{e}}_z$ locates points in the unswollen system. In the swollen state the polymer at point \mathbf{x} goes to \mathbf{x}' . We define a function α such that

$$\mathbf{x}' = \alpha(\rho) \rho \hat{\mathbf{e}}_\rho + z \hat{\mathbf{e}}_z$$

We have assumed that the system is constrained by the inner glass fiber such that no deformation in the z direction occurs, so all variables are functions of ρ only.

It is best to use as independent variables the coordinates, \mathbf{x} , of the unswollen coating. This is convenient because one knows where points of the unswollen polymer (such as ρ_2) are, but where they end up is what one is trying to determine. The concentration ϕ_p is the concentration of polymer at ρ' , but, as we just said, one should write ϕ_p as a function of ρ , i.e., $\phi_p(\rho'(\rho))$. To simplify the notation let us introduce the variable $\psi(\rho) = \phi_p(\rho'(\rho))$.

Standard elasticity theory enables one to write an expression for the ratio of the volume of a polymer element in the swollen state to the volume of that element unswollen. This volume ratio is also equal to the inverse of the polymer volume fraction in the swollen state. On this basis one gets as the first equation describing the swollen state

$$\frac{d\alpha}{d\rho} = \frac{1}{\rho \alpha \psi} - \frac{\alpha}{\rho}$$

A second differential equation arises from the fact that chemical potentials must be constant after the swelling has reached equilibrium, i.e., the derivatives of the chemical potentials with respect to position must be zero. Note that the chemical potentials must contain both a thermodynamic term, as if the system were similar to that of an uncrosslinked polymer solution at the local concentration, $\psi(\rho)$; and a term arising from the elastic free energy of the polymer. The resulting equation is

$$\rho \frac{d\psi}{d\rho} = - \frac{[1 - 1/(\alpha^2 \psi)]^2}{v_r N_e \psi [1/(1 - \psi) - 2\chi] + 1/(\alpha^2 \psi^2)}$$

These differential equations hold in both coatings, but two joining conditions are required to go from one region to the next. One condition is that the function α is continuous across the boundary separating the layers. The second condition, related to the constancy of the chemical potentials, is that the function defined by

$$h(\rho) = v_r \{ \log[1 - \psi(\rho)] + \psi(\rho) + \chi \psi^2(\rho) \} + \frac{1}{N_e(\rho) \alpha^2(\rho) \psi(\rho)}$$

is also continuous.

Two boundary conditions are needed. The first, arising from the adhesion of the coatings to the glass, is that $\alpha(\rho_0) = 1$. The second, related to chemical potentials, is that $h(\rho_2) = 0$.

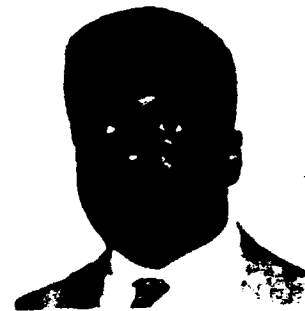
Dimensional analysis of the equations shows that the solutions depend only on the reduced distance variable, $R = \rho/\rho_0$. For given R_1 , R_2 , N_{e1} , and N_{e2} one can solve the equations and extract the swollen reduced radii of the two coatings, R_1' and R_2' . Different pairs (R_1' , R_2') are found as N_{e2} is varied. Plotting these pairs of points gives the constant N_{e1} curves of Figure 5. Similarly the constant N_{e2} curves are determined.

AT&T Bell Laboratories
600 Mountain Avenue
Murray Hill, NJ



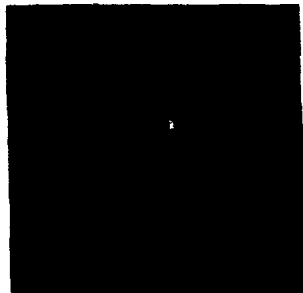
Pierre Wiltzius attended the E.T.H. in Zurich, Switzerland where he received the degree of Diplomphysiker in 1976 and the degree of Dr. sc. nat. in 1981. He was a postdoctoral fellow in the Physics Department at the University of California between 1982 and 1984. He joined AT&T Bell Laboratories in 1984 where he currently is the head of the Condensed Matter Physics Research Department. His research interests include phase transitions and non-equilibrium phenomena in soft condensed matter systems.

Northwestern University
Dept. of Electrical Engr.
Evanston, IL



Damon Tull received a BS in Electrical Engineering (1991) from Rensselaer Polytechnic Institute. He has worked with Mobil Corp. as a co-op intern, and as a summer student at AT&T Bell Laboratories. He is the recipient of an AT&T Corporate Research Fellowship Program award, and is currently pursuing an MS/PhD in Signal Processing in the Electrical Engineering Dept., Northwestern University Technological Institute, Evanston, IL.

AT&T Bell Laboratories
600 Mountain Avenue
Murray Hill, NJ



Eugene Helfand is a Distinguished Member of Technical Staff at AT&T Bell Laboratories. His research interests are in the area of polymer theory, and include studies of block copolymers, interfaces, conformational dynamics, rheology, and polymers in strong shear fields. He received a BS in Chemistry (1955) from the Polytechnic Institute of Brooklyn and an MS (1957) and PhD (1958) from Yale University. In 1988 he was awarded the American Physical Society High Polymer Physics Prize, and he was the recipient of a John Simon Guggenheim Memorial Foundation Fellowship in 1970.

AT&T Bell Laboratories
600 Mountain Avenue
Murray Hill, NJ



Debra Simoff received a BS in Chemical Engineering and a BA in Chemistry (1977) from the University of Iowa. She worked 3 years as a product development engineer with Monsanto Plastics Co., then earned an MS in Polymer Engineering and Science (1983) from the University of Massachusetts, Amherst. She joined AT&T Bell Laboratories in 1982 as a Member of Technical Staff, where she studies accelerated aging behavior and structure/property relationships of optical fiber coatings and other cable materials.

Toward a Zero Loss Change Outside Plant Cable

Stephen R. Stokes, Paul E. Neveux, Jr, Richard G. Gravely, Eric L. Buckland

Sumitomo Electric Fiber Optics Corp.
78 Alexander Drive, Research Triangle Park, NC 27709

Abstract

Identification and elimination of the contributors to low level loss increases in fiber optic cable has become necessary to meet today's increasingly stringent performance specifications. To this end, a study of intrinsic and extrinsic characteristics of the coating and ink system was conducted for product optimization as aggressive steps toward a zero loss increase outside plant cable. This paper outlines characteristics of these systems that are shown to affect optical performance. From these results, proper selection of materials as well as strict process control is crucial in minimization of low level loss increases.

I. INTRODUCTION

With the introduction of Bellcore TR-TSY-000020, Generic Requirements for Optical Fiber and Optical Fiber Cable, Issue 5, the in-service performance requirements were reduced by one-half as compared to the previous Issue 4. Although not explicitly stated, the implied objective is a zero dB attenuation increase level throughout cable manufacturing and subsequent mechanical and environmental testing. Sources of attenuation increases in the 0.1 dB/Km and above range can be typically attributed to cable design parameters including loose tube design, rigid strength element selection, stranding or relative fiber-to-cable length and cable thermal expansion coefficient, among others. These cable design elements have been optimized in our current stranded loose tube and single tube outside plant cable designs to afford virtually zero attenuation increase.

In any cable design, the optical fiber is the fundamental element of signal transmission quality. An in depth investigation of the role of UV acrylate coating systems and ink coating systems on optical fibers was conducted so that proper materials could be selected. With tightening performance requirements of fiber optic cable standards, it is imperative that sources of very low level attenuation increases be identified, evaluated and resolved so that a true zero loss change cable may be developed. In this paper, the interactions of the UV acrylate and solvent ink fiber coating systems are studied as fundamental contributors to attenuation increases of ≤ 0.05 dB/Km through process and environmental testing of optical fiber cables. These low level attenuation increases are typically a result of microbending and may be caused by intrinsic coating material properties and/or by extrinsic or externally applied pressures. This paper presents test plans and methods of analysis that offer criteria for the

optimal combination of fiber coating systems. Through careful selection of coating materials and strict control of the solvent inking process low level attenuation increases may be eliminated.

II. OPTICAL FIBER UV ACRYLATE COATING SYSTEMS

To separate the effects that UV acrylates and solvent inks have on the performance of optical fibers, the basic characteristics of the UV acrylate layer with respect to environmental changes must first be assessed. In this manner, the limitations of the UV acrylate coated fiber can be determined, and, the additional effects of overcoating the fiber with a solvent ink may be isolated.

A. Basic Coating Characteristics

The standard UV acrylate optical fiber coating system is a careful balance of materials and dimensions whose performance is designed to resist microbending over a variety of temperatures and humidity.¹ The typical telecommunications grade optical fiber coating system includes a relatively low modulus acrylate layer surrounded by a higher modulus outer shell. The soft inner material deforms more readily than the fiber and allows the fiber to remain relatively straight, inhibiting microbending. Protecting the soft inner layer is a hard outer coating material which not only resists abrasion and cutting, but adds a small amount of bend resistance as well. Attenuation increases will be experienced when external forces, an ill-behaving ink for example, exceed the design limitations of the coating system and fiber.

Further details on acrylate coating design parameters are beyond the scope of this paper and are not reviewed here. However, for reference, Table 1 lists ranges of typical values.

Table 1. Typical UV Acrylate Coating Values

Coating Layer	Inner Diameter [μm]	Outer Diameter [μm]	Modulus [kg/mm ²]
Primary	125 ± 1	187 ± 20	0.1 - 1
Secondary	187 ± 20	245 ± 10	50 - 100

B. Effect of Temperature on Basic Performance

Given the designed coating systems, comparisons of uncabled fiber at low temperature offer relative insight to the quality of the coating design. Intrinsically, the polymeric coating has a higher thermal expansion coefficient than the glass. As the high modulus outer shell contracts at low temperatures, the system contracts until the relative energy in the fiber is overcome by the deformation energy in the primary coating and the fiber buckles within the coating structure. The resultant optical radiant loss is characterized by a strong temperature dependence relative to the material parameters, and by a microbend-like, wavelength independent spectral attenuation curve. Various extrinsic deficiencies such as nonuniform adhesion of the primary acrylate coating to the glass, air bubbles in the coatings or coating dimension eccentricities may also cause a characteristic microbend-like loss structure with a relatively smooth temperature dependence.

The high quality of current single-mode optical fibers allows temperature cycling to be performed across the range of -60°C to $+70^{\circ}\text{C}$. Figures 1 - 4 show the results of temperature cycling tests of three different coatings, labeled "A", "B" and "C" which were applied to fiber of identical designs. The coated fibers were wound into coils of approximately 1000 meters each and loosely placed around a large diameter acrylate tube to suspend them inside of a temperature chamber. The fibers were selected at random from commercial lots and constitute a cross section of optical properties. The coils were measured for attenuation using an OTDR at 1310 nm and 1550 nm. The temperature chamber was cycled through -60°C and $+70^{\circ}\text{C}$ while measuring the attenuation at each temperature extreme for two cycles. The fibers were then aged at 85°C for 120 hours and then put through two more $-60^{\circ}\text{C}/+70^{\circ}\text{C}$ cycles.

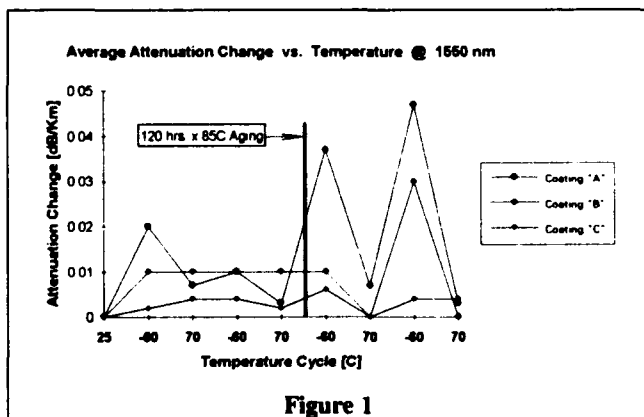


Figure 1

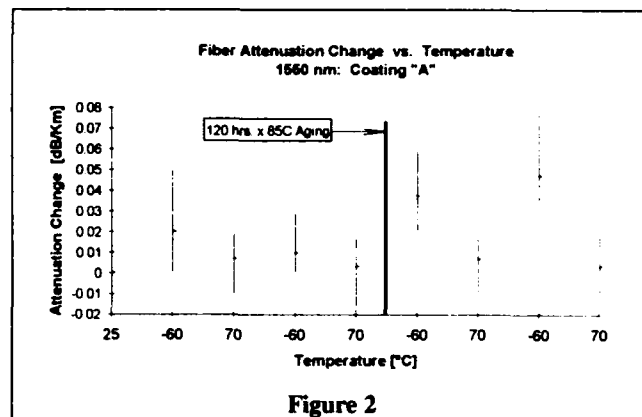


Figure 2

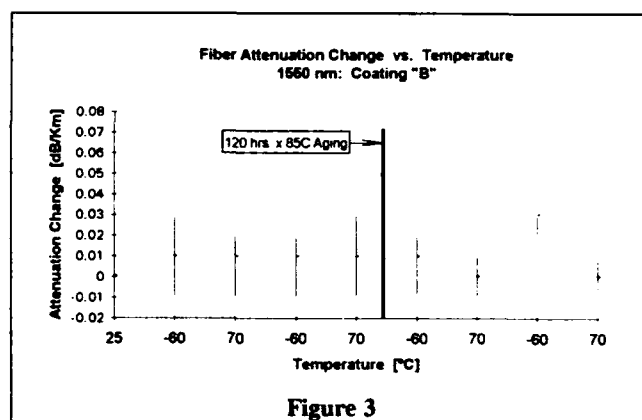


Figure 3

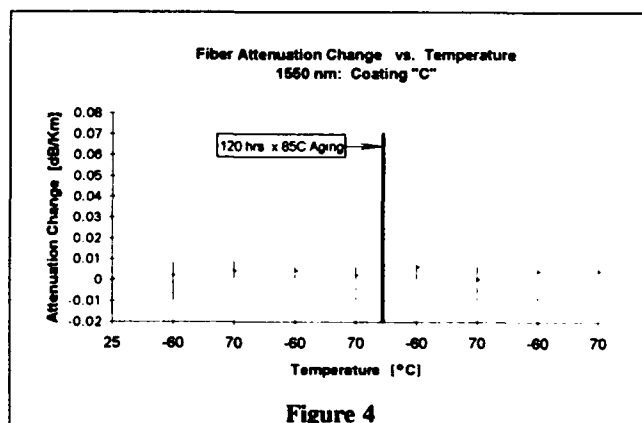


Figure 4

Coating "A" was an early optical fiber coating which is no longer in use. Coatings "B" and "C" are current varieties of dual UV acrylate coatings. The attenuation increases were due primarily to intrinsic microbending effects, *i.e.* those which are

dependent on the optical fiber coating properties. The graphs illustrate two interpretations of the data, the average increase and the range of individual fiber attenuation increases. While coating "A" is obviously the poorest performer, the differences between coatings "B" and "C" are more subtle. However, when individual fiber increases are illustrated as ranges, as shown in Figures 3 and 4, the differences are discernible indicating that coating "C" offers better temperature stability than its competitors.

C. The Effect of Humidity on Basic Performance

Moisture dependence of the acrylate coating material modulus is an important consideration since moisture is a plasticizing agent. It is particularly important to prevent softening of the coating as the fiber goes through inking and cabling processes if there is no humidity control. If the effect of moisture on the coating materials is pronounced and the fiber is subjected to nonuniform external forces, bending losses may be experienced. If the fiber attenuation is to remain unaffected, the acrylate coating layer must maintain its physical characteristics through environmental changes. Two areas of coating response, the effect of humidity on coating modulus and moisture sorption rates of the coating materials, were investigated to verify environmental stability.

1. Moisture Concentration

To determine the effect of moisture concentration on coating modulus, samples of each coating type were obtained by using acetone to remove the entire coating from the fiber as a "tube". The tensile modulus was measured as a function of humidity at constant temperature by testing the sample inside an environmental chamber mounted on a tensiometer. The results, given in Table 2, show a reduction in modulus for coating "A" of 56% whereas for coatings "B" and "C", the modulus decreased by only 5% and 11%, respectively. Since the change in modulus is due mostly to the secondary coating, a fiber with coating "A" is more susceptible to microbending and coating damage during processing in high humidity environments.

TABLE 2. 2.5% Secant Coating Modulus vs. Humidity

Coating Type	0% RH Modulus [Kg/mm ²]	100% RH Modulus [Kg/mm ²]	Percent Change [%]
"A"	75.0	33.1	- 56
"B"	74.2	70.3	- 5
"C"	71.9	63.7	- 11

2. Rate of Moisture Sorption

To determine the rate of moisture sorption, approximately 100 meter coils of "B" and "C" coated optical fiber were

desiccated for over 24 hours under a dry nitrogen purge for the absorption runs and soaked in a 100% RH (23°C) desiccator for the desorption runs. The samples were timed as they were quickly removed from the desiccator and weighed on an analytical balance. The actual starting weight at time zero was obtained by extrapolation. The coils were allowed to come to equilibrium humidity at room temperature. Typical desorption and absorption curves are shown in Figure 5 for Coating "B" fiber (coating "C" fibers experienced a similar response). The sorption rates start out fast, then slow as they asymptotically reach ambient moisture content.

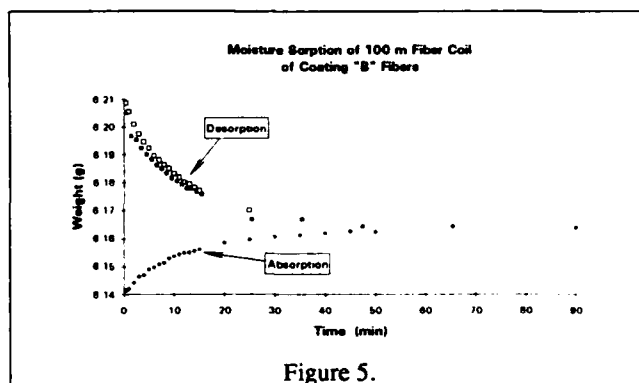


Figure 5.

All conditions (geometry, etc.) being constant, the ratio of the mass at time, t , to the mass at infinite time is proportional to the square root of the time:²

$$\frac{M_i - M_t}{M_i - M_\infty} \propto t^{1/2}$$

where

M_i is the initial mass,

M_t is the mass at any time,

M_∞ is the mass at infinity.

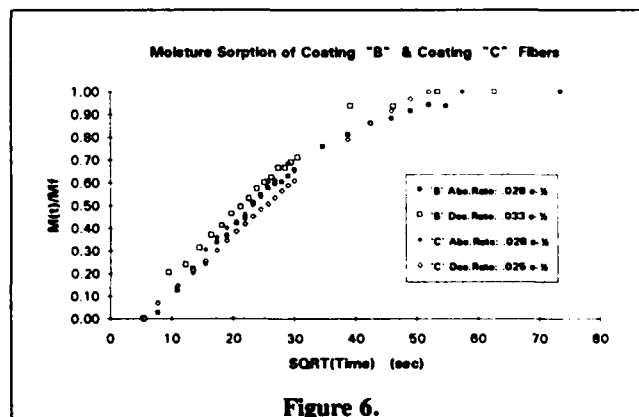


Figure 6.

The results of this analysis, shown in Figure 6, reveal that the moisture content has reached 90% of the saturated value within 42 minutes, a relatively quick response requiring careful consideration of the environment during processing. Note that the desorption and absorption curves have the same rates. This means that the rate of moisture sorption is not dependent on the concentration of water in the polymer. Both coating types "B" and "C" were found to have essentially the same rate as shown in Figure 6 and in Table 2.

What distinguishes coatings "B" and "C" is the total amount of moisture which can be absorbed into the coating. Shown in Table 2 are the results of the percent weight gain and loss after desiccation for fiber coils of the two coatings. maximum percent moisture was calculated as follows:

Max. % Moisture = $100 \times (W_{100\% RH} - W_{0\% RH}) / W_{0\% RH}$
where W represents the respective weights of the fiber.

Table 2. Sorption Rates & Max. % Moisture Content for Coils

Coating Type	Run Type	Sorption Rates (sec ^{-1/2})	Starting Weights	Calc. Max. % Moisture
"B"	Desorption	0.0333	6.2108 g	1.15%
	Absorption	0.0283	6.1404 g	
"C"	Desorption	0.0282	6.5826 g	1.99%
	Absorption	0.0247	6.4543 g	

As can be seen in Table 2, coating "C" absorbs nearly twice as much moisture as coating "B", although from this experiment it was not possible to determine what layer (primary or secondary) was responsible for the difference. It should be noted, however, that, while moisture can cause corrosion of the glass fiber, coating "C" fiber retains its median tensile strength after aging at 85°C and 85% RH much longer than coating "B" fiber.³ While these two facts seem at odds with each other, more dominant mechanisms may be in control. In any case, the amount of moisture absorption of the individual acrylate layers must be examined before any conclusions can be reached. With additional qualification testing, and careful analysis of results to determine significance levels, the optimal coating material may be selected.

III. SOLVENT INK SYSTEMS

The acrylate coated fiber is covered with a solvent ink whose sole purpose is to provide identification of fibers in cables. It follows that a stable, coating compatible and consistent ink must be introduced. While there are two types of inking systems available, UV and solvent, this paper focuses on the latter. Evaluation of the solvent ink system is based on performance testing of individual fibers and cabled fibers. Solvent ink systems are composed primarily of carrier solvent,

binder resin and pigment. Therefore, how the solvent ink is formulated will greatly determine whether or not application of the ink on the fiber will cause added loss in the cable. In this case, simple fiber coil experiments can screen poorly performing inks. However, in most, if not all, of these formulations, the binder resin has a relatively low temperature softening point. Therefore, the propensity of the ink to cause fiber to fiber or fiber to tube adhesion, as a result of the high temperatures seen at extrusion, must be evaluated to ensure stable conditions for processing. Additionally, process parameters such as ink application, line speeds, and oven temperatures, must be determined and controlled to facilitate proper ink adhesion, ink layer thickness, and uniformity.

Three inks, designated as inks "A", "B" and "C", were selected for further evaluation from a variety of candidates. UV acrylate coating "C" was selected for inking due to its low level of moisture and temperature dependence. The optimal ink composition was identified through results of qualification testing, including surface tack, ink adhesion, processing issues, and ultimately cabled fiber performance at low temperature after aging.

A. Surface Tack

It is crucial that the chosen ink maintain physical characteristics when exposed to high temperature extremes during tube extrusion. Surface tack, manifested as ink sticking, is potentially affected by both intrinsic and extrinsic characteristics such as ink components and the amount of residual solvent remaining in the ink after processing. Although subjective, a relative assessment of the potential to stick can be made. The test method consists of one meter samples of each color twisted together in a bundle and then coiled. The coils are then hung in an environmental chamber where they are exposed to high temperatures for 5 to 15 minutes. The samples are removed from the chamber, uncoiled, and evaluated. The twisted bundle should separate readily without any evidence of fiber to fiber adhesion. The three inks performed similarly with little or no surface tack while other ink candidates exhibited high levels of sticking thereby eliminating them from consideration.

B. Ink Adhesion

Adequate ink adhesion is necessary from both a processing and customer point of view. The ink should adhere sufficiently to meet processing requirements and survive the rigors of cleaning by craftspersons in the field. The "wipe" and boiling water immersion tests were performed to ensure that the ink layer integrity was maintained throughout the cable manufacturing process and into the field. Since loss of adhesion of the ink to fiber surface may cause localized bending forces that affect the fiber structure, a measurement of ink adhesion was expected to

yield some predictive ability of attenuation loss in cables. However, initial attempts to establish a correlation were inconclusive. Nonetheless, these two tests are relative indicators of the quality of the inks and process.

Adhesion can be affected by the ink selection and/or process conditions. Thick ink layers or insufficient drying of the solvent may allow the presence of residual solvents to decrease the ink to acrylate bond. A subjective go - no go test using dry and alcohol soaked gauze were utilized to characterize adhesion of the ink. Any ink removal that occurs after 10 wipes was considered poor and the severity was recorded. All three inks performed adequately, however, as will be explained in the cabled fiber section, the inks performed dissimilarly.

C. Ink Reliability

Once an ink has shown to have acceptable performance after inking, its reliability must be assessed to determine its long term effect on attenuation. Shown in Table 4 are the results of aging three fiber coils colored with ink "C" at 85°C for up to 60 days. Attenuation was measured at 25°C (room temperature) and -40°C. As can be seen, ink "C" does not adversely affect the attenuation of the fiber even after 60 days of aging. Note also that there is no color dependence to the results.

Table 4. Attenuation Change during Temperature Cycling vs. 25°C Attenuation at 1.55 μm

Temp./Days@ 85°C/85% RH	Blue Fiber (dB/km)	Brown Fiber (dB/km)	Aqua Fiber (dB/km)
+25°C/7	0.00	0.00	-0.01
-40°C/7	-0.01	0.00	-0.01
+25°C/15	0.00	0.01	0.00
-40°C/15	-0.02	-0.01	-0.02
+25°C/30	-0.01	-0.01	-0.01
-40°C/30	-0.01	0.00	-0.02
+25°C/60	-0.01	0.00	-0.01
-40°C/60	-0.01	0.00	-0.02

D. Processing

The primary problem experienced through the tubing process is fiber-to-fiber or fiber-to-tube adhesion resulting from high temperatures during extrusion. This problem may be exacerbated by moisture which acts as a plasticizer for many solvent inks. Severe fiber-to-fiber adhesion is typically identified at inspection after tubing. More subtle occurrences of fiber point sticking may only show up after tube stranding where differential movement of the fibers in the tube may result in attenuation increases.

To determine whether an ink may cause a problem in process or in finished cable, the ink must be tested for worst case situations. For example, to determine what effect moisture may have in the fiber, trials were conducted where the fibers were subjected to 100% RH at room temperature for 24 hours prior to inking and subsequently tubed in production without dehumidification. Shown in Table 3 are the attenuation changes for fibers processed with solvent ink "C" and coating "C" under normal conditions and worst case conditions, as described above.

Table 3. Attenuation Change for Fibers Processed with Ink "C" and Coating "C" under Normal & Worst Case Situations

Process	Process Condition	λ (nm)	Avg. $\Delta\alpha$ (dB/km)	Max. $\Delta\alpha$ (dB/km)
Fiber-Tube	Normal	1310	+0.013	+0.02
		1550	+0.012	+0.02
	Worst Case	1310	+0.015	+0.02
		1550	+0.010	+0.02
Tube-Core	Normal	1310	-0.012	+0.01
		1550	-0.009	+0.03
	Worst Case	1310	-0.018	+0.00
		1550	-0.009	+0.03
Cable: @ 2nd -40°C after 85°C Aging	Normal	1310	0.00	+0.01
		1550	+0.02	+0.03
		1650	-0.06	-0.03
	Worst Case	1310	-0.01	0.00
		1550	0.0	+0.03
		1650	-0.08	-0.03

As can be seen from the table, ink "C" is unaffected by the loose tube extrusion process and the presence of humidity. Stranding the tubes into the cable core was unaffected optical performance. This indicates that there is little, if any, presence of fiber-to-fiber adhesion. The -40°C after aging temperature cycle results support this conclusion.

IV. CABLED FIBER

Not all ink problems can be anticipated by testing fiber coils. The true test of a fiber ink is in a cable structure. Testing within a cable structure is more severe as fibers are grouped together in a jelly filled buffer tube and experience the effects of cable component expansion at high temperatures and contraction at low temperature extremes. Therefore, the final acceptance test for the fiber and ink combination must be an environmental and accelerated aging test within the cable. The test may be performed to Bellcore's TR-20.

Shown in Table 4 is a comparison of the three ink types which were applied to fibers of the same design using the same process conditions. Twelve standard solid colors of each ink type were processed into three separate jelly filled buffer tubes. The tubes were stranded into a dielectric, ROL, plain sheath cable. The cable was temperature cycled through two -40°C to +70°C cycles, aging at 85°C for 168 hours and two more -40°C to +70°C cycles. As can be seen in Table 4, Ink "B" has a problem at 1550 nm, Ink "A" is borderline, and Ink "C" performs well within specification.

Table 4. Attenuation Change as Cable:
Second -40°C after 7 Days of 85°C Aging

Ink Type	λ (nm)	Average $\Delta\alpha$ (dB/km)	Maximum $\Delta\alpha$ (dB/km)
Ink A	1310	0.0	+0.01
	1550	+0.03	+0.05
	1650	-0.06	-0.04
Ink B	1310	+0.03	+0.06
	1550	+0.05	+0.11
	1650	-0.03	+0.09
Ink C	1310	0.0	+0.01
	1550	+0.02	+0.03
	1650	-0.06	-0.03

Figures 7 and 8 show the temperature cycling data at 1550 nm and 1650 nm respectively. Each data point indicates the average attenuation change of the 12 fibers with respect to the initial 25°C measurement.

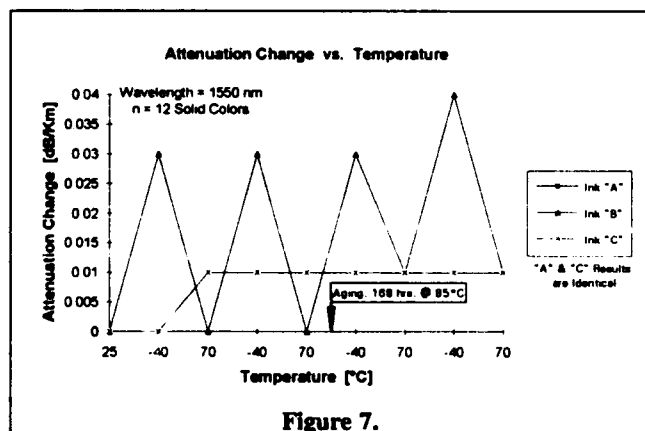


Figure 7.

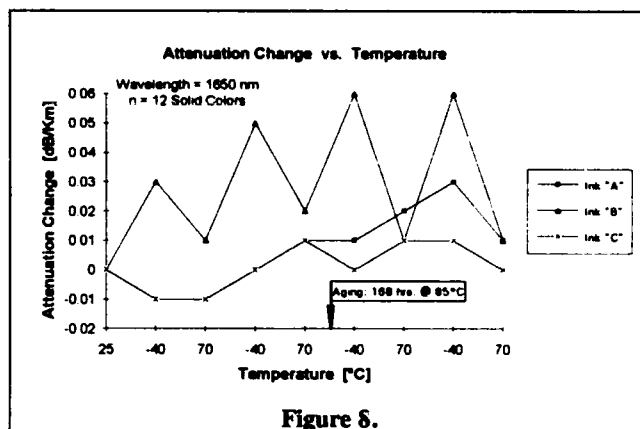


Figure 8.

From the 1550 nm results, it is evident that ink "B" falls out of the selection process as it shows poor performance at low temperatures. Inks "A" and "C" perform comparably when analyzing the average performances. Bending characteristics are more pronounced at longer wavelengths and examination of performance at 1650 nm aids in differentiation between the two inks. Ink "C" showed significantly better low temperature performance after aging. The following graph shows the range of attenuation increase at temperature extremes for ink "C". Based on the 1550 nm and 1650 nm data, ink "C" is clearly superior to ink "A" with respect to bending performance at temperature extremes.

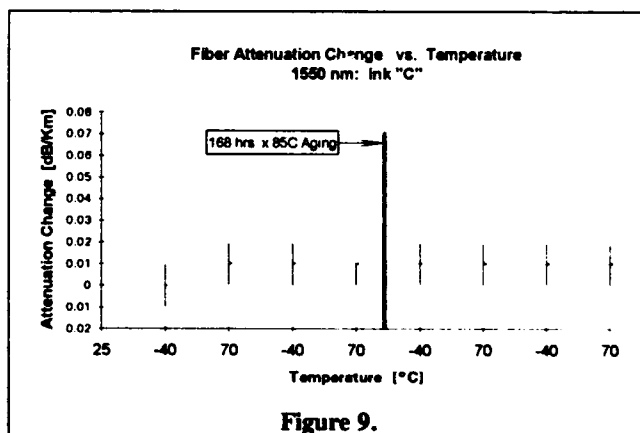


Figure 9.

V. SUMMARY

Test procedures have been developed such that contributors of low level loss increases due to solvent ink - UV acrylate coating interactions could be identified, evaluated, and resolved. These

investigations have revealed characteristics of both the coating and the ink structure that are necessary to optimize optical performance of the cable. The foundation for a resilient system begins with a well designed UV acrylate coated fiber. Through rigorous testing, the optimal acrylate coating was selected from the available choices supplied by the fiber manufacturers. Once the performance of the coated optical fiber was characterized, fiber coated with various solvent inks were evaluated for ink adhesion and surface tack in addition to the low temperature and humidity aging tests performed on the uninked fibers. Using the most accurate optical testing equipment and analytical methods available, e.g. fiber attenuation uniformity algorithms,⁴ the most stable ink system was chosen. As testing methods become more sensitive, further progress may be made in identifying other sources of low level attenuation increases. As a result, a "zero loss" increase cable may be achieved.

Acknowledgments

The authors would like to thank the members of the Lightwave and Materials Laboratory for conducting the experiments and special thanks to Mr. Ron Smith for compiling test data.

- ¹ Grasso, G.; Meli, F.; "Microbending Losses of Cabled single Mode Fibres," ECOC 1988. Gloge, D.; *Optical-Fiber Packaging and Its Influences on Fiber Straightness and Loss*, " Bell System Technical Journal, Volume 54(2), February 1975, p.p. 245-262.
- ² Comyn, J., ed., "Polymer Permeability," Elsevier Applied Science Publishers, LTD., Belfast, 1985
- ³ Neveux, Paul E., unpublished results; obtained via short gauge tensile strength tests.
- ⁴ Gravely, R.; Stokes, R.; Buckland, E.; "Fiber Optic Measurement Techniques for Improved Product and System Quality Control," 42nd IWCS Proceedings, 1993.

Stephen R. Stokes obtained a B.S. degree in Electrical Engineering from Virginia Polytechnic Institute and State University in 1988. He was employed by ITT Electro Optical Products Division and, subsequently Alcatel Cable Systems from 1980 to 1990 in the development of fiber optic measurement systems. From 1990 to 1991 he was employed by Galileo Electro-Optics Corporation as a Design Engineer in the development of light guide and imagescope products. He has been employed by Sumitomo Electric Fiber Optics Corp. since 1991 in the development of fiber optic cables and as supervisor of the Lightwave Laboratories. He is currently Manager of Product Design Engineering.

Richard G. Gravely III received his B.S. degree in Electrical Engineering from North Carolina State University in 1991. He joined Sumitomo Electric Fiber Optics Corp. in 1992 as a Product Design Engineer responsible for optical measurement system development. Richard is a member of the Institute of Electrical and Electronics Engineers, Inc.

Paul E. Neveux, Jr. obtained his double B.S. in Chemistry and Biology in 1979 from Antioch College, Yellow Springs, Ohio. After completing his Doctorate in Inorganic Photochemistry at the University of North Carolina in Chapel Hill, he held a post-doctoral fellowship position investigating conducting liquid crystal polymers at Duke University in Durham, North Carolina. In 1986, he joined Sumitomo Electric Fiber Optics Corp. and currently supervises the Materials Testing & Reliability Laboratory. Dr. Neveux is an active member in the Telecommunications Industry Association and American Chemical Society.

Eric L. Buckland obtained his B.S. degree (1985) and M.S. (1992) in Physics from North Carolina State University. Employed at Sumitomo Electric Fiber Optics Corp. since 1985, he has been engaged in the research and development of optical fibers and cables. He is currently pursuing a Ph.D. at the University of Rochester Institute of Optics. Mr. Buckland is a member of the Optics Society of America.

AUTHORS INDEX

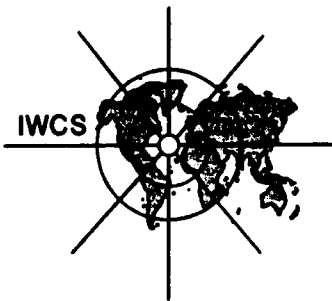
Name	Page	Name	Page
ABERSON, J. A.	536	CHOJETZKI, CH.	270
ACHBACHER, D. G.	400	COBB, G. S.	496, 502
AIKAWA, H.	374	COCCHINI, F.	674
AKIYAMA, M.	250	CORTINES, C. G.	42
ALAVI, A.	365	COTTINO, E.	799
ALLEGRETTO, A. E.	381	COTTON, K.	729
ALLS, G. E.	189	CRESPER, D.	843
ANDRE, P.	843	CRESSAN, E.	843
AOYAGI, S.	635	DAHL, R.	87
APICELLA, A.	674	DANESHVAR, O.	647
ARAKI, S.	386	DANZUKA, T.	374
ARII, M.	826	DARBON, P.	817
ASAKAWA, M.	155	DAVIS, L. E.	451
ASAKAWA, S.	601	DE PAOLI, S.	799
ASANO, K.	250	DEAN, JR., D. L.	231
ASO, O.	635	DEBSKA, A.	547
ATOBE, N.	826	DELLERA, D.	799
BABOIAN, R.	458	DELOMEL, J. C.	42
BALDAUF, J.	386, 596	DEVLIN, B. T.	562
BANFI, A.	182	DOMINIK, H.	353
BARKER, B. D.	463	DONAZZI, F.	639
BARKER, J. R.	757	DOUGHERTY, T.	126
BEASLEY, W. E.	805	DRAKE, W. O.	77
BEECH, S. C.	625	ECKARD, A.	547
BEHR, B.	621	EICKHOLT, J.	476
BENSEL, W. H.	502	EKROTH, C.-G.	404
BENSINK, J. J.	487	EMMERICH, M.	621
BIJKER, TH.	487	ENAMI, T.	557
BLACK, W. Z.	148	ENDO, S.	591
BLEWETT, I. J.	716	FANG, J.	740
BOES, P.	117	FANN, D.-M.	578
BONICEL, J. P.	42	FARGAHI, A.	182
BOTELHO, J. W.	566	FERRELL, M. R.	189
BREHM, C.	817	FERRI, I.	674
BREHM, P.	621	FCURNIER, O.	843
BRODE, F.	621	FOY, P. R.	665
BROWN, C. J.	463	FRAGALE, A.	164
BROWN, R. J.	20	FRANTZ, R. A.	256, 850, 857
BUCKLAND, E. L.	833, 872	FRANTZ, R. E.	721
BUCZMA, E.	164	FUJITA, I.	374
BYRON, K. C.	716	FURUMIYA, T.	194
CAMPS, S.	174	GAGNAIRE, H.	817
CARONES, G.	639	GASPARI, R.	639
CARR, J. J.	394	GEBIZLIOGLU, O. S.	509, 857
CAVIGLIA, F.	36	GENNO, S.	194
CENE, T.	792	GENTRY, B. C.	792
CHANG, T.-C.	578	GINOCCHIO, A.	639
CHAWLA, C. P.	694	GLEW, C. A.	435
CHEN, K.-y.	578	GRAVELY, R. G.	872
CHEN, W.-J.	578	GRAVELY III, R. G.	833
CHENG, L. P.	541	GREEN, G. D.	665

Name	Page	Name	Page
GREENE, W. T.	630	KOBAYASHI, K.	386
GRICE, M.	616	KOBAYASHI, M.	811
GRIFFIOEN, W.	471	KOMATSUDA, H.	557
GRINDSTAFF, S.	647	KOMIYA, Z.	531
GRISWOLD, G. N.	48	KONDO, E.	339
GROSSO, P.	479	KOVAC, R. J.	665
GURNEY, E.	126	KROUPA, K. M.	20
HABER, J. B.	630	KUMAKURA, T.	570
HAGMANN, H.	182	KUWAKI, N.	811
HAH, J. Y.	71	LACHMANN, D.	516
HARDY, I.	479	LASNE, C.	701
HARRIS, D. O.	231	LATOSZYNSKI, P.	117
HARRISON, D. F.	202	LE DROUMAGUET, D.	479
HASLØV, P.	65	LE NOANE, G.	479
HATTORI, T.	591	LEHAN, K.	97
HAYASHI, Y.	265	LEVY, A. C.	665
HAYES, T. M.	106	LIESE, W.	353
HAYNES, G.	458	LIN, Y.-c.	578
HELFAND, E.	864	LINDSTROM, H. O.	502
HESTERLEE, J. M.	792	LOEHFELM, G.	729
HILL, J.	647	LOPEZ, A. R.	701
HIRAO, H.	238	MADDALI, P. S. V.	283
HISATA, H.	749	MAKAN, F. F.	780
HÖG, G.	42	MÄLHAMMAR, G.	404
HOLLEY, D. W.	296	MALIN, D. S.	765
HOPLAND, S.	734	MALONEY, J. E.	113
HOSOYA, H.	250	MALTZ, G. D.	270
HSIAO, J.-M.	578	MARKEZICH, R. L.	400
IDE, T.	591	MARRA, L. J.	721
INOUE, N.	491	MATSUDA, Y.	687
ISHIDA, H.	244	MATSUHASHI, S.	339, 601
ISHIDA, K.	386	MATSUMOTO, M.	5
ISHIKAWA, H.	374	MATSUURA, H.	491
ISHIKAWA, K.	601	MAXTED, R.	625
ISOMURA, T.	826	McGURK, G.	463
JACKSON, K. W.	20, 28	McWHORTER, B. B.	148
JENZER, B.	586	MERCIER, D.	283
JERDONEK, J. A.	606	MERRIKEN, J. R.	231
JONES, W. W.	496	MEYER, J.	346
JUDY, A. F.	630	MICHAUD, H.-M.	701
KAKII, T.	244	MINVIELLE, B.	817
KAKUTA, T.	687	MIYAMOTO, M.	386, 521, 596, 680
KANAI, K.	225	MOGI, A.	680
KANZAKI, H.	430	MONTALTI, F.	36
KASHIHARA, K.	635	MORGAND, A.	843
KASHIMA, K.	749	MOROOKA, M.	212
KATSURASHIMA, W.	687	MORRISON, T.	591
KAWAKAMI, H.	155	MÜLLER, H.-U.	621
KAWASAKI, H.	212	NAGASAWA, S.	5
KAWAZAWA, T.	655	NÄGELE, W.	182
KHAN, M. J.	310	NAIDU, H.	265
KIKUCHI, Y.	238	NAKAMURA, H.	635
KIM, K. S.	721	NAKAMURA, M.	374
KIM, Y. S.	71	NAKAYAMA, T.	339
KINARD, M. D.	552	NAMIHIRA, Y.	655
KISH, P.	283	NANNI, F.	36

Name	Page	Name	Page
NESS, D. E. M.	757	SCHONFELD, H.	353
NEVEUX, JR., P. E.	872	SCHULTE, J.	270
NOMURA, Y.	238, 265	SEKI, T.	491
NORIMATSU, N.	655	SEMBER, R. G.	536
NUDD, H. R.	141	SERAFINI, E.	218
OGAWA, K.	596	SHIFLETT, E. O.	189
OH, B. D.	71	SHIGEMATSU, T.	225
OHNUMA, T.	557	SHIMIZU, S.	430
OISHI, K.	687	SHIMOBACHI, T.	749
OKABAYASHI, H.	339	SHIONO, T.	491
OKADA, N.	386, 521	SIDDIQUI, S.	552
OKAGAWA, S.	16	SIGMON, N. A.	304
OLOFSSON, H.	346	SIMOFF, D. A.	864
OLSZEWSKI, J. A.	174	SKOVGAARD, N. H.	65
OSAWA, S.	155	SMITH, G. E.	611
OSORIO, C.	174	SNYDER, J. R.	665
OTAKE, A.	430	SOLLENBERGER, N. W.	20, 28
OVERTON, R. J.	701	SOMMER, R. G.	701
OZAWA, Y.	155	SPALDING STIX, M.	721
PARKER, T. L.	28	SPARKS, G. L.	329
PARRY, M. J.	202	SRIVASTAVA, C. M.	665
PASTURCZYK, Z.	527, 822	ST. CYR, K.	323
PATERNACK, G.	531	STOKES, S. R.	833, 872
PAUQUET, J. R.	77	SUINO, D.	36
PERAUDEAU, A.	843	SUZUKI, H.	826
PETISCE, J. R.	28, 552	SUZUKI, I.	212
PHILEN, D. L.	721	SUZUKI, K.	680
PIFFARETTI, J.	586	SUZUKI, N.	570
PINYAN, J.	616	SUZUKI, S.	749
PLITZ, I. M.	256, 509, 850, 857	SUZUKI, Y.	596
POKLACKI, E. S.	694	SWAN, D.	616
POUILLY, S.	42	SWEDO, R. J.	665
PRESTON, J.	541	SZENTESI, O. I.	231
RAMPALLI, S.	410	TAKAOKA, S.	570
REES, D.	56	TAKASUGI, Y.	531
REICHERT, W.	323	TANAKA, S.	570, 687
REITH, L. A.	256	TANIFUJI, T.	5, 708
RICHTER, S.	97	TATARKA, D.	189
RÖDDER, T.	516	TATAT, O.	42
ROGESTEDT, M.	87	TAYLOR, C.	552
ROMAN, R. C.	189	TAYLOR, C. R.	28
ROSKO, J.	729	TAYLOR, J.	541
RUELLO, Y.	843	TAYLOR, N. H.	716
RUIZ-VIDAL, M.	822	TEWARSON, A.	783
RUSSELL, J. N.	716	THALMAN, W. J.	547
SABBATO, G.	674	THEODOSSI, C.	182
SAITO, M.	16	THOMAS, P. M.	502
SAKAGUCHI, T.	601	THOMSON, C. J. W.	202
SANO, A.	680	TODESCO, R. V.	77
SANO, H.	570	TOKUMARU, Y.	749
SANTANA, M. R.	20	TOMITA, S.	5
SARAVANOS, C.	527, 822	TRACEY, C.	557
SAWANO, H.	521	TSUCHIYA, I.	244
SAWYER, D.	541	TULL, D.	864
SCHICK, G.	446	TUMINARO, R. D.	721
SCHOEPKE, D.	182	TUZZOLO, M. R.	381

Name	Page
UEDA, T.	244
UKACHI, T.	531
URRUTI, E. H.	381
VASQUEZ, R.	174
VELA, H.	113
VERBICH, O.	135
VERDENHALVEN, G.	270
VERLANDE, K.	270
VOLOTINEN, T. T.	857
WAKINOSONO, T.	591
WALLING, J.-H.	283
WALSH, F. C.	463
WALTERS, D. L.	202
WATANABE, K.	596
WATSON, V. E.	56
WEAVER, J. A.	547
WEBB, S. H.	20
WEI, T.	562
WENSKI, W.	353
WHITE, G.	56
WILTZIUS, P.	864

Name	Page
WITZ, J. A.	740
WOOD, W. W.	256
YAMADA, H.	225
YAMAGUCHI, S.	194
YAMAKAWA, J.	225
YAMAMOTO, T.	557
YAMANAKA, M.	521
YAMANISHI, T.	244
YAMAZAKI, S.	155
YANAGASE, H.	225
YANAGI, T.	749
YOKOSUKA, H.	238, 250, 265
YOSHIDA, K.	811
YOSHIDA, Y.	155
YOSHINAGA, H.	557
YOSHINUMA, M.	212
YOSHIZAWA, N.	708
YUCE, H. H.	857
ZAMZOW, P. E.	42
ZEHNDER, C.	182
ZIMMERMANN, H.	182



43rd International Wire and Cable Symposium (IWCS)

Atlanta Hilton Hotel

Atlanta, Georgia

November 14-17, 1994



REQUESTS FOR ABSTRACTS

TECHNICAL SESSIONS

Candidate papers for technical sessions should cover subjects of interest to the wire and cable industry. The industry typically consists of manufacturers, suppliers, OEM's and users who are involved with telecommunication (inside building, outside plant, submarine), control and signaling, quality control, processes, process control, manufacturing systems, interconnections, computers, electronic wiring, digital data systems, local area networks, data links, utilities for electrical power transmission and distribution. Papers are solicited covering both copper and fiber optic cable technology.

TRACK 1 - FIBER OPTIC CABLES

Papers in these sessions should involve areas such as: optical wave-guides, buffering techniques, cable designs, processing improvements, fiber coatings, new materials, fire considerations, installation, splicing developments, and field experience.

TRACK 2 - COPPER CABLES

As in the past, the IWCS will give special attention to advances in the design and manufacturing of copper cables. Papers in these sessions should involve areas such as: new developments in wire and cable design, shielding, wire harnesses, cable assemblies, connectorized cables, splicing and terminating techniques; new and improved materials, fire considerations, installation experience, cost reduction programs, and quality improvement programs; manufacturing techniques and use of copper cable network for higher level services, e.g. use of symmetrical copper network for data and high frequency applications.

POSTER SESSION

Papers in this session generally focus on developments in materials, measurement techniques, test procedures, installation practices or results of other brief investigations for both copper and fiber optic cables. Presentation of a paper in a Poster Session provides an opportunity for effective one-to-one communication and display of your material. Poster Session papers will be printed in the IWCS Proceedings and should not exceed five pages.

RELATED INTEREST SUBJECTS

Subjects of interest in these sessions include: global marketing strategies, domestic and international market surveys, future network plans, future industry needs and experience surveys.

Papers in the previously described areas are solicited. The listing below shows some typical categories for guidance purposes only and are not limited to these categories:

Applications and Field Evaluation

Future requirements in electronic systems, transmission characteristics, environmental performance, electromagnetic compatibility and interconnections; terminations, splices and couplers

Process and Manufacturing

Insulating, shielding and sheathing; twisting, stranding, cabling, filling, taping, marking and automation; armouring and water blocking; round, flat and composite cables; quality-control methods

Disposal, Recycling and Reutilization of Copper Cables

National regulations, environmental considerations, disposal techniques, separation of cable materials, physical/chemical analysis techniques, reutilization of materials

Systems

Integration of wire, cables, fiber optics and other components, data cables, local area networks, inter- and intra-facility data distribution and management systems, computer and peripheral equipment wires, interconnections, optical waveguides and cable considerations, EMI and RFI considerations, testing and test procedures

Design and Testing

Unique cable constructions, new measuring techniques, quality assurance and field tests

Military Applications

Fixed plant, tactical communications, aircraft, shipboard, undersea applications and rapid deployment

Power and Industrial Cables

Low, medium and high voltage a.c. and d.c. cables and accessories, joints and terminations, materials, processing, flame and radiation resistance, design, testing, installation, service restoration and experience, aerial and underground applications in transmission and distribution

Cost Reduction and Quality Improvement Programs

Manufacturing equipment and processes improvements, maintenance programs, scrap reduction programs, supplier relationships, quality control practices and quality assurance testing

Related Interest

Domestic and International marketing, surveys, future network and technological planning

Author's Name(s) & Association _____

Contact for Correspondence _____

Company _____

Address _____

City _____ State _____ ZIP _____

Country _____

Telephone _____ Fax _____

Check the appropriate session:

-- Fiber Technical

-- Copper Technical

-- Poster

Mail 25 copies before March 11, 1994 to:
International Wire and Cable Symposium, Inc.
174 Main St
Eatontown, NJ 07724
USA

AUTHOR'S SCHEDULE

Abstracts Due:	March 11, 1994
Acceptance Notification:	April 29, 1994
Complete Manuscript Due:	August 12, 1994
Symposium:	November 13-16, 1994

To submit a technical or poster session paper, prepare a comprehensive abstract using the format below:

1. TITLE OF PAPER: _____

2. PRIMARY CONCLUSION OR RESULT (One Paragraph):

3. BACKGROUND - WHY WAS WORK UNDERTAKEN? (One Paragraph)

4. ABSTRACT (Use additional pages as needed. See Note Below)

NOTE: Items 2, 3 and 4 should not be less than 300 words nor more than 500 words total in order to be considered by the Committee. The substance of submitted papers shall not have been previously published or presented and must satisfy the Committee's criteria for content, originality and minimal commercial content.

Acceptance by the Committee will be based on the abstract. Notification of acceptance will be mailed by April 29, 1994. The full manuscript will be required by August 12, 1994. The committee reserves the right to reject any final paper manuscript, if in its judgement, it does not comply with the guidelines on content, originality and minimal commercial content.